TRANSPORT PHENOMENA FOR CHEMICAL REACTOR DESIGN

TRANSPORT PHENOMENA FOR CHEMICAL REACTOR DESIGN

Laurence A. Belfiore
Department of Chemical Engineering
Colorado State University
Fort Collins, CO

A JOHN WILEY & SONS, INC., PUBLICATION

Copyright © 2003 by John Wiley & Sons, Inc. All rights reserved.

Published by John Wiley & Sons, Inc., Hoboken, New Jersey.
Published simultaneously in Canada.

No part of this publication may be reproduced, stored in a retrieval system or transmitted in any form or by any means, electronic, mechanical, photocopying, recording, scanning, or otherwise, except as permitted under Section 107 or 108 of the 1976 United States Copyright Act, without either the prior written permission of the Publisher, or authorization through payment of the appropriate per-copy fee to the Copyright Clearance Center, Inc., 222 Rosewood Drive, Danvers, MA 01923, 978-750-8400, fax 978-750-4470, or on the web at www.copyright.com. Requests to the Publisher for permission should be addressed to the Permissions Department, John Wiley & Sons, Inc., 111 River Street, Hoboken, NJ 07030, (201) 748-6011, fax (201) 748-6008, e-mail: permreq@wiley.com.

Limit of Liability/Disclaimer of Warranty: While the publisher and author have used their best efforts in preparing this book, they make no representations or warranties with respect to the accuracy or completeness of the contents of this book and specifically disclaim any implied warranties of merchantability or fitness for a particular purpose. No warranty may be created or extended by sales representatives or written sales materials. The advice and strategies contained herein may not be suitable for your situation. You should consult with a professional where appropriate. Neither the publisher nor author shall be liable for any loss of profit or any other commercial damages, including but not limited to special, incidental, consequential, or other damages.

For general information on our other products and services please contact our Customer Care Department within the U.S. at 877-762-2974, outside the U.S. at 317-572-3993 or fax 317-572-4002.

Wiley also publishes its books in a variety of electronic formats. Some content that appears in print, however, may not be available in electronic format.

Library of Congress Cataloging-in-Publication Data:

Belfiore, Laurence A.
Transport phenomena for chemical reactor design / Laurence A. Belfiore.
p. cm.
ISBN 0-471-20275-4 (cloth : alk. paper)
1. Transport theory. 2. Chemical reactors–Fluid dynamics. I. Tittle.

TP156.T7 B45 2002
660′.2832–dc21

2002028832

Printed in the United States of America

10 9 8 7 6 5 4 3 2 1

This book is dedicated to Alphonse and all the women in my life: Olivia, Carol, Lorraine, Jenny, Sarah, and Sally. Buddy and Pookie were also inspirational. It is an environmentally friendly book because all proceeds will be used to support motorless motion in Colorado's clean air above 10,000 feet, particularly the ascent of Mount Evans at 14,260 feet from Bergen Park (i.e., the highest paved road on the planet), which, along with col de la Bonette at 2830 meters northwest of St. Etienne de Tinee and southeast of Barcelonnette (i.e., the highest paved road in Europe), is one of the most awesome bike rides on the planet.

CONTENTS

PREFACE **xix**

PART I ELEMENTARY TOPICS IN CHEMICAL REACTOR DESIGN **1**

1 Multiple Chemical Reactions in Plug Flow Tubular Reactors and Continuous Stirred Tank Reactors **3**

1-1 Gas-Phase Plug-Flow Tubular Reactors That Produce Triethanolamine from Ethylene Oxide and Ammonia, 3

1-2 Multiple Chemical Reactions in a Liquid-Phase CSTR, 11

1-3 Multiple Chemical Reactions in a CSTR Train, 19

Problems, 26

2 Start Up Behavior of a Series Configuration of Continuous Stirred Tank Reactors **33**

2-1 Analysis of Multiple Reactions in Two CSTRs: Illustrative Problem, 34

2-2 Analysis of a Train of Five CSTRs: Illustrative Problem, 38

Problems, 46

3 Adiabatic Plug-Flow Tubular Reactor That Produces Methanol Reversibly in the Gas Phase from Carbon Monoxide and Hydrogen 47

3-1 Temperature-Averaged Specific Heats, 48

3-2 Conversion Dependence of Mass Fraction and Heat Capacity of the Mixture, 50

3-3 Plug-Flow Mass Balance in Terms of CO Conversion, 51

3-4 Thermal Energy Balance for a Differential Reactor, 52

3-5 Thermodynamics of Multicomponent Mixtures, 53

3-6 Coupled Heat and Mass Transfer, 55

3-7 Kinetics and Thermodynamics of Elementary Reversible Reactions in the Gas Phase, 56

3-8 Integration of the Nonisothermal PFR Design Equation, 60

Problems, 62

4 Coupled Heat and Mass Transfer in Nonisothermal Liquid-Phase Tubular Reactors with Strongly Exothermic Chemical Reactions 65

4-1 Strategies to Control Thermal Runaway, 65

4-2 Parametric Sensitivity Analysis, 83

4-3 Endothermic Reactions in a Cocurrent Cooling Fluid, 87

4-4 Countercurrent Cooling in Tubular Reactors with Exothermic Chemical Reactions, 95

4-5 Manipulating the Inlet/Outlet Temperature of a Countercurrent Cooling Fluid: Multiple Stationary-State Behavior in Exothermic PFRs, 97

Problems, 104

5 Multiple Stationary States in Continuous Stirred Tank Reactors 105

5-1 Mass Balance, 106

5-2 Chemical Kinetics, 106

5-3 Thermal Energy Balance, 107

5-4 Multiple Stationary States, 110

5-5 Endothermic Chemical Reactions, 115

Problems, 117

6 Coupled Heat and Mass Transfer with Chemical Reaction in Batch Reactors 123

6-1 Isothermal Analysis of Experimental Rate Data, 123

6-2 Formalism for Multiple Reactions, 129

6-3 Adiabatic Operation, 130

6-4 Nonisothermal Analysis of a Constant-Volume Batch Reactor, 131

Problems, 136

7 Total Pressure Method of Reaction-Rate Data Analysis 139

7-1 Elementary Reversible Gas-Phase Reactions in a Constant-Volume Flask, 139

7-2 Generalized Linear Least-Squares Analysis for a Second-Order Polynomial with One Independent Variable, 142

Problems, 145

PART II TRANSPORT PHENOMENA: FUNDAMENTALS AND APPLICATIONS 153

8 Applications of the Equations of Change in Fluid Dynamics 155

8-1 Important Variables, 155

8-2 Physical Properties in Fluid Dynamics, 156

8-3 Fundamental Balance in Momentum Transport, 158

8-4 Equation of Motion, 167

8-5 Exact Differentials, 173

8-6 Low-Reynolds-Number Hydrodynamics, 175

8-7 Potential Flow Theory, 205

Problems, 222

9 Derivation of the Mass Transfer Equation 253

9-1 Accumulation Rate Process, 253

9-2 Rate Processes Due to Mass Flux Across the Surface That Bounds the Control Volume, 254

9-3 Rate Processes Due to Multiple Chemical Reactions, 255

9-4 Constructing Integral and Microscopic Descriptions of the Mass Transfer Equation, 256

9-5 Diffusional Fluxes in Multicomponent Mixtures, 257

9-6 Diffusional Fluxes and Linear Transport Laws in Binary and Pseudo-Binary Mixtures, 260

9-7 Simplification of the Mass Transfer Equation for Pseudo-Binary Incompressible Mixtures with Constant Physical Properties, 261

10 Dimensional Analysis of the Mass Transfer Equation 265

10-1 Dimensional Scaling Factors for the Mass Transfer Rate Processes, 265

10-2 Dimensionless Form of the Generalized Mass Transfer Equation with Unsteady-State Convection, Diffusion, and Chemical Reaction, 266

10-3 Functional Dependence of the Molar Density of Species i Via Dimensional Analysis, 269

10-4 Maximum Number of Dimensionless Groups That Can Be Calculated for a Generic Mass Transfer Problem, 271

Problems, 272

11 Laminar Boundary Layer Mass Transfer around Solid Spheres, Gas Bubbles, and Other Submerged Objects 275

11-1 Boundary Layer Mass Transfer Analysis, 275

11-2 Tangential Velocity Component v_θ Within the Mass Transfer Boundary Layer, 284

11-3 Boundary Layer Solution of the Mass Transfer Equation, 287

11-4 Interphase Mass Transfer at the Solid–Liquid Interface, 298

11-5 Laminar Boundary Layer Mass Transfer Across a Spherical Gas–Liquid Interface, 303

11-6 Boundary Layer Solution of the Mass Transfer Equation Around a Gas Bubble, 306

11-7 Interphase Mass Transfer at the Gas–Liquid Interface, 313

Problems, 328

12 Dimensional Analysis of the Equations of Change for Fluid Dynamics Within the Mass Transfer Boundary Layer 361

12-1 Generalized Dimensionless Form of the Equation of Motion for Incompressible Fluids Undergoing Laminar Flow, 362

12-2 Incompressible Newtonian Fluids in the Creeping Flow Regime, 362

12-3 Locally Flat Momentum Boundary Layer Problem for Laminar Flow Around Solid Spheres, 363

12-4 Renormalization of the Dimensionless Variables Reveals Explicit Dependence of g^* on Re, 365

13 Diffusion and Chemical Reaction Across Spherical Gas–Liquid Interfaces 369

13-1 Molar Density Profile, 369

13-2 Molar Flux Analysis, 372

PART III KINETICS AND ELEMENTARY SURFACE SCIENCE 381

14 Kinetic Mechanisms and Rate Expressions for Heterogeneous Surface-Catalyzed Chemical Reactions 383

14-1 Converting Reactants to Products, 383

14-2 Isotherms, 384

14-3 Single-Site Adsorption of Each Component in a Multicomponent Mixture, 392

14-4 Dual-Site Adsorption of Submolecular Fragments, 394

14-5 Summary of Adsorption Isotherms for Pure Gases, 397

14-6 Hougen–Watson Kinetic Models, 399

14-7 Pressure Dependence of the Kinetic Rate Constant Via Elements of Transition State Theory, 420

14-8 Interpretation of Heterogeneous Kinetic Rate Data Via Hougen–Watson Models, 424

Problems, 428

PART IV MASS TRANSFER AND CHEMICAL REACTION IN ISOTHERMAL CATALYTIC PELLETS 447

15 Diffusion and Heterogeneous Chemical Reaction in Isothermal Catalytic Pellets 449

15-1 Complex Problem Descriptions Without Invoking Any Assumptions, 449

15-2 Diffusion and Pseudo-Homogeneous Chemical Reactions in Isothermal Catalytic Pellets, 452

15-3 Pseudo-First-Order Kinetic Rate Expressions That Can Replace Hougen–Watson Models and Generate Linearized Ordinary Differential Equations for the Mass Balance, 453

15-4 Diffusion and Heterogeneous Chemical Reactions in Isothermal Catalytic Pellets, 458

Problem, 459

16 Complete Analytical Solutions for Diffusion and Zeroth-Order Chemical Reactions in Isothermal Catalytic Pellets 461

16-1 Catalytic Pellets with Rectangular Symmetry, 461

16-2 Long, Cylindrically Shaped Catalysts, 464

16-3 Spherical Pellets, 466

16-4 Redefining the Intrapellet Damkohler Number So That Its Critical Value Might Be the Same for All Pellet Geometries, 468

Problems, 470

17 Complete Analytical Solutions for Diffusion and First-Order Chemical Reactions in Isothermal Catalytic Pellets 473

17-1 Catalytic Pellets with Rectangular Symmetry, 473

17-2 Long, Cylindrically Shaped Catalysts, 475

17-3 Spherical Pellets, 476

Problems, 480

18 Numerical Solutions for Diffusion and *n*th-Order Chemical Reactions in Isothermal Catalytic Pellets 483

18-1 Kinetic Rate Law and Diffusional Flux, 483

18-2 Mass Transfer Equation in Three Coordinate Systems, 484

18-3 Numerical Results for Second-Order Irreversible Chemical Kinetics, 487

18-4 Equivalent Examples with Different Characteristic Length Scales, 488

19 Numerical Solutions for Diffusion and Hougen–Watson Chemical Kinetics in Isothermal Catalytic Pellets 491

19-1 Dimensionless Kinetic Rate Law, 491

19-2 Mass Balance for Reactant A, 493

19-3 Dimensionless Correlation for the Effectiveness Factor in Terms of the Intrapellet Damkohler Number, 497

19-4 Dimensionless Correlation for Porous Wafers with Rectangular Symmetry, 500

19-5 Numerical Results for $A_2 + B \rightarrow C + D$ in Flat-Slab Wafers with Rectangular Symmetry, 501

Problems, 505

20 Internal Mass Transfer Limitations in Isothermal Catalytic Pellets 509

20-1 Reactor Design Strategy, 509

20-2 Correlations for Catalysts with Different Macroscopic Symmetry, 512

20-3 Effectiveness Factors, 515

20-4 Dimensionless Correlation between the Effectiveness Factor and the Intrapellet Damkohler Number, 521

Problems, 527

21 Diffusion Coefficients and Damkohler Numbers Within the Internal Pores of Catalytic Pellets 539

21-1 Dependence of Intrapellet Pore Diffusion on Molecular Size, 539

21-2 Knudsen Diffusion in Straight Cylindrical Pores, 543

21-3 Ordinary Molecular Diffusion in Binary and Pseudo-Binary Mixtures, 544

21-4 Estimating Tortuosity Factors and Intrapellet Porosity Based on the Distribution in Orientation and Size of Catalytic Pores Via the Parallel-Pore Model, 553

Problems, 558

PART V ISOTHERMAL CHEMICAL REACTOR DESIGN 561

22 Isothermal Design of Heterogeneous Packed Catalytic Reactors 563

22-1 Simplification of the Generalized Mass Transfer Equation for a One-Dimensional Plug Flow Model, 564

22-2 Differential Form of the Design Equation for Ideal Packed Catalytic Tubular Reactors Without Interpellet Axial Dispersion, 567

22-3 Design of a Packed Catalytic Tubular Reactor for the Production of Methanol from Carbon Monoxide and Hydrogen, 573

22-4 Design of Non-Ideal Heterogeneous Packed Catalytic Reactors with Interpellet Axial Dispersion, 579

22-5 Mass Transfer Peclet Numbers Based on Interpellet Axial Dispersion in Packed Catalytic Tubular Reactors, 592

22-6 Applications to a Packed Chromatographic or Ion-Exchange Column, 596

22-7 Factors That Must Be Considered in the Design of a Packed Catalytic Tubular Reactor, 597

Problems, 601

23 Heterogeneous Catalytic Reactors with Metal Catalyst Coated on the Inner Walls of the Flow Channels 611

23-1 Convective Diffusion in Catalytic Reactors of Noncircular Cross Section and Nonuniform Catalyst Activity, 611

23-2 Fully Developed Fluid Velocity Profiles in Regular Polygon Ducts, 614

23-3 Mass Transfer Equation, 619

23-4 Details of the Numerical Algorithm, 624

23-5 Second-Order Correct Finite-Difference Expressions for First Derivatives on the Boundary of the Flow Cross Section, 627

23-6 Viscous Flow, 632

Problems, 645

24 Designing a Multicomponent Isothermal Gas–Liquid CSTR for the Chlorination of Benzene to Produce Monochlorobenzene 655

24-1 Strategy to Solve This Problem, 656

24-2 Gas-Phase Mass Balances with Interphase Mass Transfer, 658

24-3 Liquid-Phase Mass Balances with Chemical Reaction, Interphase Transport, and Reaction-Enhanced Mass Transfer Coefficients, 659

24-4 Interfacial Equilibrium and Equality of Interfacial Fluxes, 665

24-5 Molecular Diffusion in Liquids, 671

24-6 Nonlinear Equation Solver Program, 673

Problems, 681

PART VI THERMODYNAMICS AND NONISOTHERMAL REACTOR DESIGN 685

25 Classical Irreversible Thermodynamics of Multicomponent Mixtures 687

25-1 Strategy to Analyze Nonequilibrium Systems, 688

25-2 Microscopic Equation of Change for Kinetic Energy, 689

25-3 Re-Expressed Equation of Change for Kinetic Energy, 690

25-4 Microscopic Equation of Change for Internal Energy Via the First Law of Thermodynamics, 692

25-5 Microscopic Equation of Change for Total Energy, 693

25-6 Identification of the Molecular Flux of Thermal Energy in the Equation of Change for Total Energy, 695

25-7 Equation of Change for Entropy, 696

25-8 Rate of Entropy Production in Multicomponent Systems with Chemical Reaction, 697

25-9 Linear Relations Between Fluxes and Forces That Obey the Curie Restriction, 701

25-10 Coupling Between Diffusional Mass Flux and Molecular Flux of Thermal Energy in Binary Mixtures: The Onsager Reciprocal Relations, 703

25-11 Identification of Fourier's Law in the Molecular Flux of Thermal Energy and the Requirement That Thermal Conductivities Are Positive, 705

25-12 Complete Expression for the Diffusional Mass Flux of Component A in a Binary Mixture, 706

25-13 Thermodynamic Evaluation of $(\partial\varphi_A/\partial\omega_A)_{T,p}$ in Binary Mixtures, 708

25-14 Connection between Transport Phenomena and Thermodynamics for Diffusional Mass Fluxes and Diffusivities in Binary Mixtures, 709

25-15 Liquid-Phase Diffusivities and the Stokes–Einstein Diffusion Equation for Binary Mixtures, 710

Problems, 712

26 Molecular Flux of Thermal Energy in Binary and Multicomponent Mixtures Via the Formalism of Nonequilibrium Thermodynamics 717

26-1 Three Contributions to **q** in Binary Systems, 717

26-2 Thermodynamic Analysis of $\varphi_A - T(\partial\varphi_A/\partial T)_{p,\omega_A}$, 719

26-3 Analysis of the Interdiffusional Flux of Thermal Energy in Binary Mixtures and Generalization to Multicomponent Mixtures, 723

Problems, 724

27 Thermal Energy Balance in Multicomponent Mixtures and Nonisothermal Effectiveness Factors Via Coupled Heat and Mass Transfer in Porous Catalysts 727

27-1 Equation of Change for Specific Internal Energy That Satisfies the First Law of Thermodynamics, 727

27-2 Multicomponent Transport in Porous Catalysts, 731

27-3 Nonisothermal Effectiveness Factors in Porous Catalysts, 733

27-4 Physicochemical Properties of Gases Within Catalytic Pellets, 737

27-5 Estimates of the Maximum Temperature Rise Within Catalytic Pellets for Exothermic Chemical Reactions, 740

27-6 Design of a Nonisothermal Packed Catalytic Tubular Reactor, 745

Problems, 748

28 Statistical Thermodynamics of Ideal Gases 757

28-1 Generalized Postulates, 757

28-2 Introduction to Quantum Statistical Mechanics, 758

28-3 The Ergodic Problem, 760

28-4 $\mathscr{H}$ Theorem of Statistical Thermodynamics, 761

28-5 Consistency with Classical Thermodynamics, 763

28-6 Internal Energy and Heat Capacity of Monatomic Ideal Gases, 768

28-7 Diatomic Gases, 768

28-8 Entropy and Chemical Potential, 776

Problems, 780

29 Thermodynamic Stability Criteria for Single-Phase Homogeneous Mixtures 785

29-1 Energy Representation of the Fundamental Equation and Exact Differentials, 785

29-2 Legendre Transformations, 787

29-3 Euler's Integral Theorem for Homogeneous Functions of Order m, 790

29-4 Gibbs–Duhem Equation, 794

29-5 Analysis of Partial Derivatives Via Jacobian Transformations, 795

29-6 Thermodynamic Stability Relations, 798

30 Coupled Heat and Mass Transfer in Packed Catalytic Tubular Reactors That Account for External Transport Limitations 821

30-1 Intrapellet and Bulk Species Concentrations, 823

30-2 Intrapellet and Bulk Gas Temperature, 825

30-3 Evaluation of $C_{A,\,surface}$ Via the Effectiveness Factor: Complete Strategy for Packed Catalytic Tubular Reactors, 830

30-4 Reactor Design, 835

30-5 Maximum Conversion in Non-Ideal Packed Catalytic Tubular Reactors Under Isothermal Conditions, 842

30-6 Analysis of First-Order Irreversible Chemical Kinetics in Ideal Packed Catalytic Tubular Reactors When The External Resistances to Heat and Mass Transfer Cannot Be Neglected, 845

Problems, 852

References **861**

Index **865**

PREFACE

In this book, the design of chemical reactors is approached from microscopic heat and mass transfer principles. The content is influenced heavily by my training at Stevens Institute of Technology, Yale University, and the University of Wisconsin. Several ideas presented herein crystallized out of thin air, just like snowflakes, in the Colorado high country above 10,000 feet, where phones, faxes, e-mail, junk mail, and all other media disturbances were nonexistent. A few problems were synthesized in les hautes Alpes, where the ascent of any premiere col with 42×24 low gearing is a test of strength and perseverance. Isothermal design strategies begin with the microscopic mass transfer equation, and assumptions are invoked until a one-dimensional mass balance can be integrated to produce macroscopic results. We focus on packed catalytic tubular reactors in which reactant gases must diffuse into the pores of the pellets and adsorb on active catalytic sites before chemical reaction occurs. Hence, Langmuir adsorption isotherms, Langmuir–Hinshelwood mechanisms, and Hougen–Watson kinetic rate expressions are employed to design heterogeneous catalytic reactors. Once the kinetics are understood and rate laws can be generated, isolated catalytic pellets are analyzed in terms of pseudo-homogeneous models with diffusion and chemical reaction. This section of the book treats zeroth-order, first-order, *n*th-order, and Hougen–Watson chemical kinetics with the overall goal of generating dimensionless correlations between the effectiveness factor and the intrapellet Damkohler number. Quantitative methods are described to estimate effective intrapellet diffusivities as well as axial dispersion coefficients in packed beds. Effective intrapellet diffusion coefficients appear in the denominator of the intrapellet Damkohler number, and axial dispersion coefficients are required to calculate the mass transfer Peclet number and the interpellet Damkohler number when convection, axial dispersion, and chemical reaction are operative in non-ideal packed catalytic

tubular reactors. Nonisothermal effects in isolated pellets are addressed within the framework of classical irreversible thermodynamics. The complete expression for the molecular flux of thermal energy in multicomponent systems, excluding the Dufour effect, is used to predict intrapellet temperature profiles that are coupled to reactant concentration profiles within the catalyst. Complete details are provided to calculate nonisothermal effectiveness factors, and examples are discussed which illustrate key dimensionless parameters that exhibit strong influence on the effectiveness factor. The complete design of a heterogeneous catalytic tubular reactor combines all the previous information when nonisothermal effects are important and the external resistances to heat and mass transfer cannot be neglected. Convective diffusion in regular polygon channels with expensive metal catalyst coated on the inner walls of the flow channel is described and compared with packed reactors. Optimal catalyst deposition strategies are incorporated into a three-dimensional mass transfer model.

In an attempt to broaden the scope of the book, several examples of heat and mass transfer with multiple chemical reactions in continuous stirred tanks and plug-flow reactors, including start up behavior, adiabatic operation, and gas–liquid dispersed systems, are discussed primarily in the introductory section (i.e., Part I). Novel examples of multiple stationary states in exothermic tubular reactors with countercurrent cooling are presented quantitatively and compared with similar phenomena in continuous-stirred tanks. Thermal energy effects in batch reactors are also discussed. Most problems and examples require numerical methods to obtain quantitative results. The appropriate software is employed to solve coupled ordinary differential equations, in some cases with split boundary conditions, and results are presented graphically or in tabular form. Various segments of this book can be incorporated into several chemical engineering courses at both the graduate and undergraduate levels. Complementary topics in transport phenomena and thermodynamics that provide support for chemical reactor analysis are included for completeness. These are (1) fluid dynamics in the creeping and potential flow regimes around solid spheres and gas bubbles, (2) the corresponding mass transfer problems that employ velocity profiles derived in the fluid dynamics section to calculate interphase heat and mass transfer coefficients, (3) heat capacities of ideal gases via statistical thermodynamics to calculate Prandtl numbers, and (4) thermodynamic stability criteria for homogeneous mixtures which reveal that binary molecular diffusion coefficients must be positive. Topics 1 and 2 are based on information from Professor Ed Lightfoot's intermediate transport phenomena course at the University of Wisconsin. Complementary topic 3 was extracted from a statistical mechanics course in the chemistry department at Wisconsin taught by Professor Charles F. Curtiss, and the information in topic 4 was presented by Professor Curtiss in a chemical thermodynamics course. The primary use of the entire treatise follows a complete year of graduate courses in transport phenomena and chemical reactor design. In this mode, Part I works well as a review of the required undergraduate reactor design course, and topics 1 through 4, described briefly above, provide useful information that complements the main focus of this book.

There are a few instructors from my undergraduate and graduate education that I must thank personally, because they introduced me to the topics discussed in this book and provided me with the tools to address these issues. Professor George B. DeLancey at Stevens Institute of Technology presented most of the material in the introductory review section when I was a senior in his chemical reactor design course in 1975. These problems were intriguing, with practical implications, and they required numerical analysis via Newton–Raphson root finding or Runge–Kutta–Gill integration of coupled ordinary differential equations. In 1975, it was necessary to write Fortran code on punchcards or at remote teletypes to obtain numerical solutions. Most of these problems in the introductory section have been modified and reworked via Engineering Equation Solver or Polymath. One of the most versatile problems discussed by Professor DeLancey was the chlorination of benzene in a gas–liquid continuous-stirred tank. This material is presented in Chapter 24. These results can be used to analyze the effect of interphase mass transfer on the design of a gas–liquid CSTR. Without algebraic equation solvers, Professor DeLancey presented an elaborate substitution approach which involved nonlinear analysis due to second-order irreversible chemical reaction between benzene and dissolved chlorine in the liquid phase. More recently, the solution is obtained with much less tedium via nonlinear algebraic equation solvers. The solution to the first review problem on multiple chemical reactions in gas-phase plug-flow tubular reactors in Chapter 1 was developed in its entirety by undergraduate student Terrence Pikul at Colorado State University during the 2.5-hour chemical reactor final exam in December 1994. While I was grading Terrence's exam, it was immediately obvious that his solution was much better than mine. So I swallowed my ego, gave him 10 or 20 points extra credit, and adopted his approach. At the University of Wisconsin, Professor Bob Bird presented Laplace transform and matrix analyses of the start up behavior of a CSTR train with first-order irreversible chemical reaction in a 1977 fall semester course offering of mathematical methods in chemical engineering. This review problem has been extended to multiple chemical reactions in Chapter 2, and it also appeared on a reactor design final exam at Colorado State University. Professor Stuart W. Churchill at the University of Pennsylvania is acknowledged for reviewing the multiple-stationary-states introductory problem in plug-flow tubular reactors with countercurrent cooling. Professor Churchill convinced me that, indeed, multiple steady states are possible in tubular reactors.

Professor Stanley H. Langer's personal notes on Langmuir adsorption, Langmuir–Hinshelwood mechanisms, and Hougen–Watson kinetic models were extremely helpful. I obtained this information from a 1976 fall semester graduate course on kinetics and catalysis at the University of Wisconsin. In a 1978 spring semester graduate course offering of physicochemical hydrodynamics presented by Professor Bird, I learned the fundamentals of irreversible thermodynamics in binary mixtures with chemical reaction. After extending this information to multicomponent mixtures, I employed the results to analyze nonisothermal effectiveness factors via the complete expression for the molecular flux of thermal

energy, which includes Fourier's law, the Dufour effect (this was neglected), and the interdiffusional flux. Laurent Simon, a graduate student in advanced mass transfer at Colorado State, is acknowledged for checking some of my numerical results on this topic, which require the solution of three coupled first-order ordinary differential equations with split boundary conditions. Professor Lightfoot is acknowledged for introducing me to boundary layer heat and mass transfer around solid spheres and gas bubbles in a 1976 graduate course in intermediate transport phenomena. This information provides the general scaling behavior of Nusselt and Sherwood numbers in terms of the Reynolds and Prandtl or Schmidt numbers when the thermal and concentration boundary layers are thin. Heat and mass transfer coefficients based on these correlations are used to estimate external transport resistances between catalytic pellets and the bulk fluid phase moving through a packed catalytic tubular reactor. Correlations for flow around gas bubbles are employed to estimate the magnitude of mass transfer coefficients in gas–liquid dispersed systems for the chlorination of benzene in Chapter 24.

In the summers of 1975 and 1976, I participated in an undergraduate research program at Yale University hosted by its Department of Engineering and Applied Science. Professor Daniel E. Rosner of Yale's Chemical Engineering Department chose me to work on a simulation-based project focusing on convection, diffusion, and heterogeneous chemical reaction in flow channels with noncircular cross section and metal catalyst coated on the inner walls. This "tube-wall" reactor problem is described in detail in Chapter 23. I used some of the methodology presented by Professor DeLancey for tray-by-tray calculations in multicomponent distillation columns and employed the Thomas algorithm to solve a partial differential mass balance using linear algebraic finite-difference equations characterized by a tridiagonal coefficient matrix. When the flow cross section is annular, the inner cylindrical wall is catalytically active, and the outer wall is inert, numerical simulations were performed in parallel with nitrogen atom recombination experiments on a metal wire. The overall objective of this research was to understand thermal energy transfer to the heat shield of the Space Shuttle upon re-entry into the Earth's atmosphere. Most of the numerical results in Chapter 23 were extracted from the 1988 M.S. thesis of Seong Young Lee at Colorado State University, entitled "Convective Diffusion in Heterogeneous Catalytic Reactors with Rectangular Cross Section and Nonuniform Catalyst Activity."

Diffusion and zeroth-order chemical reaction in porous catalysts are presented in detail for pellets with rectangular, cylindrical, and spherical symmetry. These effectiveness factor problems represent a logical extension of Section 18.7 in Bird, Stewart, and Lightfoot's *Transport Phenomena*, Second Edition (pp. 563–567). However, with no guiding light, I stumbled several times before correcting all of my mistakes. I must acknowledge Mark Heinrich, a student in graduate reactor design at Colorado State during the spring of 1994, for informing me that my initial approach to diffusion and zeroth-order chemical reaction produced effectiveness factor vs. intrapellet Damkohler number, correlations that intersected curves for other reaction orders instead of defining the asymptotes at large and small Damkohler numbers. Then Brandon Vail, a senior in transport phenomena at Colorado State during the

spring of 1997, refined my definition of the critical spatial coordinate in porous catalysts below which reactants do not penetrate when the intrapellet Damkohler number is larger than its critical value. This crutch is required for zeroth-order kinetics because there is no automatic method of "turning off" the rate of reactant consumption when the central core of the catalyst is starved of reactants. Zeroth-order chemical kinetics generate mathematically simple problem definitions, but these problems are conceptually challenging. Diffusion and Hougen–Watson chemical kinetics posed another stumbling block because the rate law contains molar densities of several reactants and products, and I couldn't relate all of these molar densities within the pores of the catalyst. Coupled solution of several second-order ODEs with split boundary conditions was not the preferred approach because trial and error was required for each ODE via the "shooting" method. Hence, a modification of stoichiometry and the steady-state mass balance with convection and chemical reaction was required because, now, diffusion and chemical reaction were important. Professor DeLancey's notes from a 1976 graduate course in mass transfer provided the solution to this bottleneck moments before the graduate reactor design class at Colorado State was scheduled to meet one morning in the spring of 1994.

Finally, I must thank students and colleagues in Colorado State's Department of Chemical Engineering for their assistance. Professor David B. McWhorter introduced me to a porous media approach to estimate axial dispersion coefficients. These are required to calculate mass transfer Peclet numbers and interpellet Damkohler numbers, and to compare ideal and non-ideal simulations in packed catalytic tubular reactors. Jeremiah J. Way's M.S. thesis in 2003 under my guidance, entitled "Interpellet Axial Dispersion and External Mass Transfer Resistance in Heterogeneous Packed Catalytic Tubular Reactors: A Simulation-Based Study," has identified the critical value of the mass transfer Peclet number above which packed catalytic tubular reactors perform ideally. Jeremiah's correlations and tabular data reveal that the critical value of the mass transfer Peclet number depends on the interpellet Damkohler number, the effectiveness factor, and the catalyst filling factor for a packed bed. These results are summarized in Chapter 22. Of particular importance, correlations are presented that allow one to predict deviations from ideal reactor performance when one operates at subcritical mass transfer Peclet numbers. Jeremiah is also acknowledged for clarifying some intrapellet diffusion concepts about the orientation part of the distribution function and the corresponding tortuosity factors in the parallel-pore model. Professor Ranil Wickramasinghe provided useful information about commercial chromatographic separation columns and maximum filling factors for spherically shaped catalysts (i.e., 66 to 74%) in packed beds. Professor Terry G. Lenz provided thermodynamic comments on the nonisothermal batch and adiabatic tubular reactor introductory problems in Part I which employ a reversible reaction scheme for the production of methanol from carbon monoxide and hydrogen. Professor Lenz was extremely helpful in his identification of energy changes for chemical reaction in the thermal energy balance, based on partial molar properties instead of pure-component molar properties. Professor Naz Karim provided assistance with

the matrix analysis of start up behavior for multiple tanks (i.e., CSTRs) in series. Professors Vince Murphy, Jim Linden, and Ken Reardon fine-tuned a biochemical engineering cell culture problem based on principles discussed in Chapter 24, which focuses on gas–liquid continuous-stirred tanks. Professors Vince Murphy and David Dandy are acknowledged for providing reference material and answering my "off-the-wall" questions, whenever asked. Professor Dandy supports my choice of boundary conditions at the inlet to a packed catalytic tubular reactor with significant interpellet axial dispersion. In other words, the dimensionless molar density of reactant A at the tube inlet is, by definition, unity. This boundary condition is appropriate in the design of an ideal tubular reactor in which axial dispersion is negligible at high mass transfer Peclet numbers. However, I also employ this boundary condition to simulate non-ideal reactor performance, whereas most of the chemical reactor community has settled on a modification of this boundary condition because axial dispersion is important beyond the inlet plane, but absent prior to the inlet plane. Professors Branka Ladanyi and Marshall Fixman of the Colorado State Chemistry Department and Professor Vince Murphy are acknowledged for helping me analyze the pressure dependence of kinetic rate constants in terms of the volume of activation, which is described best as a difference between partial molar volumes of the activated complex and all the reactants. As a senior at Colorado State, Mark Heinrich was enrolled in an undergraduate transport phenomena course in the fall of 1991 when he suggested that the finite-difference formula for first and second derivatives, presented in Chapter 23, should be developed in general for non-equispaced data points. Mark Heinrich and Tony Rainsberger, in the same class, suggested that coupled heat and mass transfer in nonisothermal tubular reactors in Chapter 4 should be analyzed with cocurrent cooling fluids. Then, in the spring of 1994, as a graduate student in advanced reactor design at Colorado State, Mark Heinrich helped me finalize an approximate method to estimate multicomponent diffusivities and resistances in porous catalysts. Dimensionless correlations between the effectiveness factor and the intrapellet Damkohler number in various shaped catalysts were prepared by graduate students Chris Cannizzaro, Bill Nagle, David Oelschlager, and Ken Tunnicliff in the spring of 1994. Bill Nagle suggested a modification of the Danckwerts boundary condition in the exit stream of a non-ideal plug-flow tubular reactor such that ideal and non-ideal reactors satisfy the same boundary conditions in the inlet and exit streams. This idea is described in detail in Chapter 22. When David John Phillips was enrolled in undergraduate chemical reactor design at Colorado State in the fall of 1999, he generated the idea for Problem 5-3. In other words, he questioned the number of steady states that exist in a nonisothermal CSTR when the rate of thermal energy removal vs. temperature coincides with the steepest section of the rate of thermal energy generation such that there is essentially a continuum of operating points that are common to both curves. Graduate student Neema Saxena corrected some mathematical errors in Chapter 27 by replacing total derivatives with partial derivatives when the "dot" product of unit normal vectors with temperature and concentration gradients is constructed. Neema also clarified one of the momentum boundary conditions

at gas–liquid interfaces, where continuity of the velocity vector is imposed. In other words, "perfect slip" is more appropriate than "no slip," and the velocity component tangential to the interface in the liquid phase induces circulation within bubbles. Graduate student Anthony Tartaglione helped me generate ideal and non-ideal reactor simulations when the external resistance to mass transfer cannot be neglected. Jeremiah Way completed the analysis of external mass transfer resistance in packed catalytic tubular reactors and discovered the following simulation-based phenomena: (1) Higher conversion of reactants to products is achieved at shorter residence times, over a restricted range of mass transfer Peclet numbers; and (2) non-ideal reactors perform better than ideal reactors, based on the conditions required to achieve maximum conversion of reactants to products, because the ideal simulations are not valid when the mass transfer Peclet number is smaller than its critical value. These nontraditional results are attributed to the interplay between external mass transfer resistance and average residence-time effects in packed catalytic tubular reactors. Graduate student Eric M. Indra deserves a special thanks for proofreading a major portion of the manuscript during the "early years," and Dr. Pronab Das and Dr. Mary Pat McCurdie also read various chapters. It gives me great pleasure to express sincere appreciation for many fruitful discussions with two colleagues, Drs. Rajiv Bhadra and Allen Rakow, who knew about, but are no longer here to witness the impact of, this textbook. Their intellectual enthusiasm and sense of humor are greatly missed. I apologize to anyone else, who provided assistance directly or indirectly, whose name was forgotten.

Fort Collins, Colorado L.A.B.
November 22, 2002
belfiore@engr.colostate.edu

Transport Phenomena for Chemical Reactor Design. Laurence A. Belfiore
Copyright © 2003 John Wiley & Sons, Inc.
ISBN: 0-471-20275-4

PART I

ELEMENTARY TOPICS IN CHEMICAL REACTOR DESIGN

Transport Phenomena for Chemical Reactor Design. Laurence A. Belfiore
Copyright © 2003 John Wiley & Sons, Inc.
ISBN: 0-471-20275-4

1

MULTIPLE CHEMICAL REACTIONS IN PLUG FLOW TUBULAR REACTORS AND CONTINUOUS STIRRED TANK REACTORS

1-1 GAS-PHASE PLUG-FLOW TUBULAR REACTORS THAT PRODUCE TRIETHANOLAMINE FROM ETHYLENE OXIDE AND AMMONIA

Triethanolamine is produced from ethylene oxide and ammonia at 5 atm total pressure via three consecutive elementary chemical reactions in a gas-phase plug-flow tubular reactor (PFR) that is not insulated from the surroundings. Ethylene oxide must react with the products from the first and second reactions before triethanolamine is formed in the third elementary step. The reaction scheme is described below via equations (1-1) to (1-3). All reactions are elementary, irreversible, and occur in the gas phase. In the first reaction, ethylene oxide, which is a cyclic ether, and ammonia combine to form monoethanolamine:

$$CH_2CH_2O + NH_3 \longrightarrow HOCH_2CH_2NH_2 \qquad (1\text{-}1)$$

At 325 K, the kinetic rate constant for the first reaction is 5 L/g mol·min. In the second reaction, ethylene oxide and monoethanolamine combine to form diethanolamine:

$$CH_2CH_2O + HOCH_2CH_2NH_2 \longrightarrow (HOCH_2CH_2)_2NH \qquad (1\text{-}2)$$

At 325 K, the kinetic rate constant for the second reaction is 10 L/g mol·min. In the third reaction, ethylene oxide reacts with diethanolamine to generate triethanolamine:

$$CH_2CH_2O + (HOCH_2CH_2)_2NH \longrightarrow (HOCH_2CH_2)_3N \qquad (1\text{-}3)$$

At 325 K, the kinetic rate constant for the third reaction is 7 L/g mol·min. Coupled mass and thermal energy transport with multiple reactions in a plug-flow reactor suggests that the temperature of the reactive mixture changes by about 4 °C from inlet (323 K) to outlet (327 K).

The overall objective is to produce triethanolamine, which is featured in the third reaction. Which of the following alternatives is more desirable: a stoichiometric (1 : 1) feed of ethylene oxide and ammonia enters the reactor; or a 3 : 1 molar ratio of ethylene oxide to ammonia enters the reactor? Provide support for your answer by calculating the reactor volume in liters and the outlet molar flow rate of triethanolamine that correspond to your design.

1-1.1 Strategy to Solve This Problem

The solution to this problem requires an analysis of multiple gas-phase reactions in a differential plug-flow tubular reactor. Two different solution strategies are described here. In both cases, it is important to write mass balances in terms of molar flow rates and reactor volume. Molar densities and residence time are not appropriate for the convective mass-transfer-rate process because one cannot assume that the total volumetric flow rate is constant in the gas phase, particularly when the total number of moles is not conserved. In each reaction, 2 mol of reactants generates 1 mol of product. Furthermore, an overall mass balance suggests that the volumetric flow rate is constant only when the overall mass density does not change. This is a reasonable assumption for liquid-phase reactors but not for gas-phase problems when the total volume is not restricted. The exception is a constant-volume batch reactor.

A few comments are in order about the fact that the reactor does not operate isothermally and that there is at least a 4 K difference between the temperatures of the inlet and outlet streams. Since the wall of the reactor is not insulated, interactions with the surroundings will provide a heating or cooling mechanism to offset the endothermic or exothermic nature of the chemical reaction. In an adiabatically enclosed reactor, the bulk temperature will increase or decrease continuously for reactions that are exothermic or endothermic, respectively. In the absence of thermodynamic data for enthalpies of formation at 298 K and heat transfer coefficient information, it seems reasonable to neglect thermal effects as a first approximation. The problem statement indicates that the outlet temperature of the reactive mixture is 4 K higher than the inlet temperature. However, no information is provided about the actual temperature profile from inlet to outlet, and more information is required to predict the bulk temperature within the reactor as a function of reactor volume or axial coordinate. It could be incorrect to conclude that the maximum temperature of the mixture is 327 K at the outlet of the reactor. Consider the following scenario. If the sum of all three heats of reaction suggests that the multiple reaction scheme is exothermic, strong temperature increases within the reactor could trigger the phenomenon of thermal runaway, where the reaction rates increase dramatically. For irreversible chemical reactions, thermal runaway depletes the reactants rather quickly at high temperatures. Under these conditions, all reactions are essentially completed and

heat is no longer generated far upstream from the reactor outlet. The remainder of the reactor functions as a heat exchanger to decrease the bulk temperature to 327 K, which is slightly higher than the inlet temperature. The solution strategies neglect temperature variation within the reactor and use the kinetic rate constants at 325 K as provided in the problem description.

When multiple reactions occur in the gas phase, the mass balance for component i is written for an ideal tubular reactor at high mass transfer Peclet numbers in the following form, and each term has units of moles per volume per time:

$$\frac{dF_i}{dV} = \sum_j \nu_{ij} \mathfrak{R}_j \tag{1-4}$$

where F_i is the molar flow rate of component i, dV the differential reactor volume, ν_{ij} the stoichiometric coefficient of component i in reaction j, and $\mathfrak{R}_j$ the intrinsic rate law for reaction j. There are three elementary irreversible chemical reactions, and the units of the kinetic rate constants suggest that each second-order rate law should be constructed in terms of molar densities. Partial pressures and mole fractions can be introduced via the ideal gas law and Dalton's law as follows:

$$C_i = \frac{N_i}{V_{\text{total}}} = y_i \frac{p}{RT} \tag{1-5}$$

Finally, the mole fraction of component i is written as its molar flow rate divided by the total molar flow rate. The differential mass balance is written for each component in the mixture: A = ethylene oxide, B = ammonia, C = monoethanolamine, D = diethanolamine and E = triethanolamine. The matrix of stoichiometric coefficients is summarized as follows for five components that participate in three independent chemical reactions:

	Component				
Reaction	A	B	C	D	E
First	−1	−1	+1	0	0
Second	−1	0	−1	+1	0
Third	−1	0	0	−1	+1

Five coupled ordinary differential equations (ODEs) can be written for the five unknowns F_i, where i = A, B, C, D, E:

$$\frac{dF_A}{dV} = -\mathfrak{R}_1 - \mathfrak{R}_2 - \mathfrak{R}_3$$

$$\frac{dF_B}{dV} = -\mathfrak{R}_1$$

$$\frac{dF_C}{dV} = +\mathfrak{R}_1 - \mathfrak{R}_2$$

$$\frac{dF_D}{dV} = +\mathfrak{R}_2 - \mathfrak{R}_3$$
$$\frac{dF_E}{dV} = +\mathfrak{R}_3 \tag{1-6}$$

The kinetic rate law for each elementary irreversible chemical reaction is written in terms of gas-phase molar densities (A, B, C, D, where $A = C_A$, etc.) as follows:

$$\mathfrak{R}_1 = k_1 AB$$
$$\mathfrak{R}_2 = k_2 AC \tag{1-7}$$
$$\mathfrak{R}_3 = k_3 AD$$

The relation between gas-phase molar density and molar flow rates for ideal gases is obtained via equation (1-5):

$$C_i = \frac{pF_i}{RT\sum_j F_j} \tag{1-8}$$

where the sum of molar flow rates in the denominator includes all components and represents the total molar flow rate. Five boundary conditions are required at $V = 0$ to define a unique solution of these highly coupled ODEs. For a stoichiometric (1 : 1) feed of ethylene oxide and ammonia at the reactor inlet, $F_A = F_B = 1$ g mol/min and $F_i = 0$ for the three products C, D, and E. For a 3 : 1 molar ratio of ethylene oxide to ammonia, $F_A/3 = F_B = 1$ g mol/min and all other $F_i = 0$. Since triethanolamine is the product desired, it is important to monitor its molar flow rate F_E as a function of reactor volume in each case. The reactor design strategy must consider both alternatives [i.e., a stoichiometric (1 : 1) feed vs. a 3 : 1 feed ratio of ethylene oxide to ammonia]. The final decision should address the need for a costly separation process to extract the desired product, triethanolamine, from the gas mixture, if necessary. Qualitatively, one must also consider the initial cost to build the reactor, the operating cost to supply ethylene oxide, and the rate of production of triethanolamine.

The solution strategy described above is based on writing a differential plug-flow reactor mass balance for each component in the mixture, and five coupled ODEs are solved directly for the five molar flow rates. The solution strategy described below is based on the *extent of reaction* for independent chemical reactions, and three coupled ODEs are solved for the three extents of reaction. Molar flow rates are calculated from the extents of reaction. The starting point is the same as before. The mass balance is written for component i based on molar flow rate and differential reactor volume in the presence of multiple chemical reactions:

$$\frac{dF_i}{dV} = \sum_j \nu_{ij}\mathfrak{R}_j \tag{1-4}$$

However, the similarities end here. The differential change in the molar flow rate of component i, dF_i, is written as follows:

$$dF_i = \sum_j (dF_i)_{\text{cfRj}} \tag{1-9}$$

where the acronym "cfRj" represents the contribution from reaction j. Hence, $(dF_i)_{\text{cfRj}}$ represents the differential change in the molar flow rate of component i due to the jth chemical reaction. The differential mass balance becomes

$$\frac{dF_i}{dV} = \sum_j \left(\frac{dF_i}{dV}\right)_{\text{cfRj}} = \sum_j \nu_{ij}\mathfrak{R}_j \tag{1-10}$$

When all terms are grouped on the left-hand side of equation (1-10), the rearranged mass balance for component i,

$$\sum_j \left[\left(\frac{dF_i}{dV}\right)_{\text{cfRj}} - \nu_{ij}\mathfrak{R}_j\right] = 0 \tag{1-11}$$

can be written in standard form as

$$\sum_j \psi_j = 0 \tag{1-12}$$

$$\psi_j = \left(\frac{dF_i}{dV}\right)_{\text{cfRj}} - \nu_{ij}\mathfrak{R}_j \tag{1-13}$$

Now it is necessary to introduce the concept of *independent chemical reactions*. A reaction is classified as *independent* if it cannot be synthesized from a linear combination of the other chemical reactions. In other words, the backward reaction for a reversible scheme is not independent of the forward reaction because it is only necessary to multiply the forward step by (-1) to obtain the backward step. Hence, a reversible chemical reaction represents only one independent step, and consequently, only one extent of reaction is defined for a reversible sequence. The theorem states that "if all chemical reactions are independent, $\Sigma_j \psi_j = 0$ if and only if each $\psi_j = 0$ for all values of j." The differential mass balance for component i focuses on the contribution from reaction j, and if reaction j is independent,

$$\psi_j = \left(\frac{dF_i}{dV}\right)_{\text{cfRj}} - \nu_{ij}\mathfrak{R}_j = 0 \tag{1-14}$$

This relation is rearranged such that all terms which involve component i are grouped together. The result is

$$\frac{(dF_i)_{\text{cfRj}}}{\nu_{ij}} = R_j\,dV = d\xi_j = \text{same for every component in reaction } j \tag{1-15}$$

where $d\xi_j$ is the differential extent of the jth independent chemical reaction, with units of molar flow rate. Hence, the design equation for multiple chemical reactions in a gas-phase differential tubular reactor at high mass transfer Peclet numbers is

$$\frac{d\xi_j}{dV} = \mathfrak{R}_j \tag{1-16}$$

and this design equation is written once for each independent chemical reaction, which is consistent with the fact that a different extent ξ is defined for each independent chemical reaction. For three independent reactions involving ethylene oxide in the gas phase, the following set of coupled ODEs must be solved:

$$\begin{aligned} \frac{d\xi_1}{dV} &= k_1 \mathrm{AB} \\ \frac{d\xi_2}{dV} &= k_2 \mathrm{AC} \\ \frac{d\xi_3}{dV} &= k_3 \mathrm{AD} \end{aligned} \tag{1-17}$$

where the molar density of component A is written as $C_\mathrm{A} = \mathrm{A}$, and so on. Three boundary conditions are required to define a unique solution to these ODEs. By definition, each extent of reaction is zero at the inlet to the reactor, where $V = 0$. The similarities between the two approaches return when one relates molar densities, partial pressures, and mole fractions as

$$C_i = y_i \frac{p}{RT} \tag{1-5}$$

and the mole fraction of component i is

$$y_i = \frac{F_i}{\sum_j F_j} \qquad 1 \le j \le \text{ total number of components} \tag{1-18}$$

The final task, before solving the coupled ODEs for the extents of reaction ξ_1, ξ_2, and ξ_3 is to express component molar flow rates in terms of the extents of reaction.

Based on the definition of the differential extent of the jth chemical reaction via equation (1-15), and the fact that

$$dF_i = \sum_j (dF_i)_{\mathrm{cfRj}} \tag{1-9}$$

$$\frac{(dF_i)_{\mathrm{cfRj}}}{\nu_{ij}} = \mathfrak{R}_j \, dV = d\xi_j \tag{1-15}$$

it follows that the differential of the total molar flow rate of component i can be expressed as

$$dF_i = \sum_j \nu_{ij}\, d\xi_j \tag{1-19}$$

When (1-19) is integrated from the reactor inlet, where $V = 0$, $F_i = F_{i0}$, and $\xi_j = 0$ for each independent chemical reaction ($j = 1, 2, 3$ for this particular problem) to any arbitrary position downstream from the inlet, one obtains the desired relation between a component molar flow rate and the extents of reaction:

$$F_i = F_{i0} + \sum_j \nu_{ij}\xi_j \qquad 1 \le j \le \text{ total number of independent reactions} \tag{1-20}$$

This equation is written for each of the five components in the gas-phase reactor. Given the matrix of stoichiometric coefficients for the five gas-phase components in three chemical reactions (see page 5),

$$\begin{aligned} F_A &= F_{A0} - \xi_1 - \xi_2 - \xi_3 \\ F_B &= F_{B0} - \xi_1 \\ F_C &= \xi_1 - \xi_2 \\ F_D &= \xi_2 - \xi_3 \\ F_E &= \xi_3 \end{aligned} \tag{1-21}$$

The molar densities in the rate laws are expressed in terms of mole fractions for ideal gas behavior via

$$C_i = y_i \frac{p}{RT} \tag{1-5}$$

and the mole fraction of component i is written in terms of the extents of reaction via molar flow rates:

$$y_i = \frac{F_i}{\sum_j F_j} \qquad 1 \le j \le \text{total number of components} \tag{1-18}$$

One differential design equation,

$$\frac{d\xi_j}{dV} = \mathfrak{R}_j \tag{1-16}$$

is written for each independent chemical reaction, and it is now possible to solve three coupled ODEs in terms of three unknowns: ξ_1, ξ_2, and ξ_3. Of course, both methods of solution produce the same final answers.

Verify the claim that both methods of solution produce the same final answers, and hence the same reactor design strategy, when the two alternatives [i.e., stoichiometric (1 : 1) feed vs. the 3 : 1 feed ratio] are considered. A more rigorous addendum to both approaches employs the Hagen–Poiseuille equation for laminar flow or the Ergun equation if the tubular reactor is packed with porous solid catalysts to calculate the pressure drop through the reactor instead of assuming that $p =$ constant from inlet to outlet.

1-1.2 Computer-Aided Solution

Since triethanolamine is the desired product, it is important to monitor its molar flow rate F_E as a function of reactor volume in each case. Most differential equation solver software packages will integrate five coupled ODEs quickly and easily to generate the following results. The stoichiometric (1 : 1) feed in case 1 requires a 25- to 30-L reactor to produce 0.1 mol of triethanolamine per minute. If the reactor operates in this fashion, simulations indicate that the outlet molar flow rate of ethylene oxide is essentially zero. Furthermore, ammonia (B) and the three products (C > D > E) exit the reactor in measurable quantities. Hence, a costly separation process is required to extract the desired product, triethanolamine (E), from the gas mixture. The upper limit of F_E is 0.113 g mol/min if the reactor volume is increased significantly. For the stoichiometric (1 : 1) feed, the outlet molar flow rate of triethanolamine is always smallest, excluding, of course, ethylene oxide. The 3 : 1 feed ratio in case 2 generates the predictions of reactor performance in terms of the molar flow rate of triethanolamine that are listed in Table 1-1.

Hence, a 3 : 1 molar feed ratio of ethylene oxide to ammonia seems to be advantageous with a corresponding reactor volume between 75 and 100 L. The

TABLE 1-1 Effect of Reactor Volume on the Outlet Molar Flow Rate of Triethanolamine in an Isothermal Gas-Phase PFR Operating at 325 K[a]

Reactor Volume (L)	Molar Flow Rate of Triethanolamine (g mol/min)
25	0.13
50	0.49
75	0.75
100	0.87
125	0.92
150	0.94
175	0.95
200	0.96

[a] The feed stream contains a 3 : 1 molar flow rate ratio of ethylene oxide to ammonia.

production rate of triethanolamine is between seven- and eight-fold larger than in case 1 with a stoichiometric (1 : 1) feed. The initial cost to build the reactor will be approximately three- or four-fold larger and the operating cost to supply ethylene oxide will be three-fold larger relative to the stoichiometric (1 : 1) feed. However, the increased rate of production of triethanolamine could be worth the larger capital investments for initial and operating costs. This decision strategy is qualitative in the absence of cost data, but one should weigh the factor of 3 to 4 from an investment viewpoint against the factor of 7 to 8 in terms of product revenue. Furthermore, when the reactor volume is greater than ≈70 L with a 3 : 1 molar feed ratio of ethylene oxide to ammonia, the outlet molar flow rate of triethanolamine is largest, and the cost of separating the desired product should be much smaller relative to the stoichiometric (1 : 1) feed. For example, the outlet mole fraction of triethanolamine is 93% when the reactor volume is 250 L. Once again, cost data are required to determine if this exceedingly large reactor is cost-effective with respect to the separation process required, which should be rather inexpensive.

1-2 MULTIPLE CHEMICAL REACTIONS IN A LIQUID-PHASE CSTR

1-2.1 Steady-State Analysis Based on Extents of Reaction

If component i participates in several chemical reactions in a well-mixed continuous-stirred tank reactor (CSTR) with volume V_{CSTR}, then the macroscopic mass balance at large mass transfer Peclet numbers is

$$\frac{dN_i}{dt} = F_{i,\,\text{inlet}} - F_{i,\,\text{outlet}} + V_{\text{CSTR}} \sum_j \nu_{ij} \mathfrak{R}_j \tag{1-22}$$

where N_i represents the moles of component i and the other notation is the same as described earlier on page 5. Since the left side of (1-22) vanishes at steady state, rates of convective mass transfer (i.e., $F_{i,\,\text{outlet}} - F_{i,\,\text{inlet}}$) are balanced by the production of component i in all the reactions (i.e., $V_{\text{CSTR}} \sum_j \nu_{ij} \mathfrak{R}_j$). As illustrated in the liquid-phase problem below, it is possible to:

1. Express the molar flow rate of component i as a product of total volumetric flow rate q_{total} and molar density C_i (i.e., $F_i = q_{\text{total}} C_i$).
2. Invoke a steady-state macroscopic mass balance for each component in the reactive mixture.
3. Use chemical kinetic principles to write the rate law for each reaction in terms of molar densities.
4. Solve coupled algebraic equations for all molar densities in the CSTR exit stream.

Our objective in this section is to introduce a complementary method of solution based on extents of reaction ξ_j, which have units of molar density. To initiate

this approach, one manipulates the convective mass transfer terms for component i as follows:

$$F_{i,\,\text{inlet}} - F_{i,\,\text{outlet}} = \sum_j (F_{i,\,\text{inlet}} - F_{i,\,\text{outlet}})_{\text{cfRj}} = q_{\text{total}} \sum_j (C_{i,\,\text{inlet}} - C_{i,\,\text{outlet}})_{\text{cfRj}} \tag{1-23}$$

Now the steady-state mass balance for component i can be written as a sum of contributions from each chemical reaction:

$$F_{i,\,\text{inlet}} - F_{i,\,\text{outlet}} + V_{\text{CSTR}} \sum_j \nu_{ij} \mathfrak{R}_j$$

$$= \sum_j [q_{\text{total}} (C_{i,\,\text{inlet}} - C_{i,\,\text{outlet}})_{\text{cfRj}} + V_{\text{CSTR}} \nu_{ij} \mathfrak{R}_j] = 0 \tag{1-24}$$

Division by q_{total} and identification of residence time $\tau = V_{\text{CSTR}}/q_{\text{total}}$ yields the final form of the complete mass balance for component i:

$$\sum_j [(C_{i,\,\text{inlet}} - C_{i,\,\text{outlet}})_{\text{cfRj}} + \tau \nu_{ij} \mathfrak{R}_j] = 0 \tag{1-25}$$

If each step in the multiple reaction sequence is independent and cannot be synthesized from a linear combination of the other reactions, each kinetic rate law $\mathfrak{R}_j$ is unique and

$$(C_{i,\,\text{inlet}} - C_{i,\,\text{outlet}})_{\text{cfRj}} + \tau \nu_{ij} \mathfrak{R}_j = 0 \tag{1-26}$$

The previous statement based on the contribution from reaction j obviously satisfies the complete mass balance for component i. It is written for each independent reaction. Furthermore, one applies stoichiometry to the contribution from reaction j and groups all quantities that are specific to component i. For example,

$$\frac{(C_{i,\,\text{outlet}} - C_{i,\,\text{inlet}})_{\text{cfRj}}}{\nu_{ij}} = \tau \mathfrak{R}_j \tag{1-27}$$

Since each side of (1-27) is the same for each component in the mixture but unique to reaction j, one defines the extent of the jth chemical reaction ξ_j such that:

1. $\tau \mathfrak{R}_j = \xi_j$
2. $(C_{i,\,\text{outlet}} - C_{i,\,\text{inlet}})_{\text{cfRj}} = \nu_{ij} \xi_j$

Expression 1 represents the CSTR design equation for steady-state analysis in the presence of multiple chemical reactions. This design equation is written for each independent reaction. If there is only one chemical reaction and subscript j is not required, the extent of reaction ξ is analogous to $\chi C_{\text{A,inlet}}$, where χ

represents the conversion of reactant A based on molar flow rates, in general, and molar densities for liquid-phase reactions. Expression 2 is used to calculate molar densities in terms of the extents of reaction. For example,

$$F_{i,\,\text{outlet}} - F_{i,\,\text{inlet}} = q_{\text{total}}(C_{i,\,\text{outlet}} - C_{i,\,\text{inlet}})$$
$$= q_{\text{total}} \sum_j (C_{i,\,\text{outlet}} - C_{i,\,\text{inlet}})_{\text{cfRj}} = q_{\text{total}} \sum_j \nu_{ij}\xi_j \tag{1-28}$$

Hence, molar densities are calculated as follows:

$$C_{i,\,\text{outlet}} = C_{i,\,\text{inlet}} + \sum_j \nu_{ij}\xi_j \tag{1-29}$$

1-2.2 Chlorination of Benzene

We apply the concepts discussed above to design a CSTR that operates at 55 °C for the chlorination of benzene in the liquid phase. It is necessary to account for all three chlorination reactions. Chlorine gas is bubbled through the liquid mixture in the CSTR and it must diffuse across the gas–liquid interface before any of the reactions can occur. For this particular problem, it is reasonable to assume that chlorine is present as a solubilized liquid-phase component, and its molar density in the inlet liquid stream is given as a fraction ε of the inlet molar density of pure liquid benzene. In a subsequent example discussed in Chapter 24, a two-phase gas–liquid CSTR analysis is presented which accounts for the realistic fact that benzene enters the reactor in an undiluted liquid stream, and chlorine is actually bubbled through as a gas. It is sufficient to consider that the fraction $\varepsilon = 0.25$ remains constant for all simulations. In the first chlorination step, benzene reacts irreversibly with dissolved chlorine to produce monochlorobenzene and hydrogen chloride:

$$C_6H_6 + Cl_2 \longrightarrow C_6H_5Cl + HCl \tag{1-30}$$

The inlet molar density of benzene is $C_{\text{benzene, inlet}} = 11.28$ g mol/L, and the kinetic rate constant for the first reaction is $k_1 = 8.84 \times 10^{-3}$ L/mol·s at 55 °C. The overall objective is to design a CSTR that will maximize the rate of production of monochlorobenzene. Economics should be considered from a qualitative viewpoint. In the second reaction, the desired product, monochlorobenzene, reacts irreversibly with dissolved chlorine to produce dichlorobenzene and hydrogen chloride:

$$C_6H_5Cl + Cl_2 \longrightarrow C_6H_4Cl_2 + HCl \tag{1-31}$$

The kinetic rate constant for the second reaction is a factor of 8 smaller than the kinetic rate constant for the first reaction at 55 °C. In the third reaction, dichlorobenzene reacts irreversibly with dissolved chlorine to generate trichlorobenzene and hydrogen chloride:

$$C_6H_4Cl_3 + Cl_2 \longrightarrow C_6H_3Cl_3 + HCl \tag{1-32}$$

The kinetic rate constant for the third reaction is a factor of 30 smaller than the kinetic rate constant for the second reaction at 55 °C.

Illustrative Problem. Generate a CSTR performance curve for the molar density of the desired product, monochlorobenzene, in the outlet stream of the reactor vs. $\log \tau k_1$, where τ is the average residence time for convective mass transfer and k_1 is the kinetic rate constant for the first chlorination step. Identify your operating point on the CSTR performance curve. Design the CSTR by calculating the volume associated with this operating point if the volumetric flow rate is 50 L/min (i.e., ≈12 to 13 gallons/min). Solve this problem by two different methods: (a) using extents of reaction ξ_j, and (b) using only molar densities C_i without introducing ξ_j's.

SOLUTION. (a) Molar density of pure liquid benzene (g mol/L):

$$C_{\text{benzene, inlet}} = 11.28$$

Ratio of kinetic rate constants for the first and second chlorination reactions at 55 °C:

$$\frac{k_2}{k_1} = \frac{1}{8}$$

Ratio of kinetic rate constants for the second and third chlorination reactions at 55 °C:

$$\frac{k_3}{k_2} = \frac{1}{30}$$

Ratio of dissolved chlorine to benzene on a molar basis in the inlet stream:

$$\varepsilon = 0.25$$

Inlet molar density of chlorine dissolved in the liquid phase:

$$C_{\text{chlorine, inlet}} = \varepsilon C_{\text{benzene, inlet}}$$

Matrix of stoichiometric coefficients:

		Component					
Reaction	Extent ξ_j	C_6H_6	Cl_2	HCl	C_6H_5Cl	$C_6H_4Cl_2$	$C_6H_3Cl_3$
First chlorination	ξ_1	−1	−1	+1	+1	0	0
Second chlorination	ξ_2	0	−1	+1	−1	+1	0
Third chlorination	ξ_3	0	−1	+1	0	−1	+1

Molar density of benzene in the CSTR exit stream (g mol/L):

$$C_{\text{benzene, outlet}} = C_{\text{benzene, inlet}} - \xi_1$$

Molar density of monochlorobenzene in the CSTR exit stream (g mol/L):

$$C_{\text{monochlorobenzene, outlet}} = \xi_1 - \xi_2$$

Molar density of dichlorobenzene in the CSTR exit stream (g mol/L):

$$C_{\text{dichlorobenzene, outlet}} = \xi_2 - \xi_3$$

Molar density of dissolved chlorine in the CSTR exit stream (g mol/L):

$$C_{\text{chlorine, outlet}} = C_{\text{chlorine, inlet}} - \xi_1 - \xi_2 - \xi_3$$

Kinetic rate laws, excluding rate constants, for the three chlorination reactions:

$$\mathfrak{R}_1 = C_{\text{benzene, outlet}} C_{\text{chlorine, outlet}}$$
$$\mathfrak{R}_2 = C_{\text{monochlorobenzene, outlet}} C_{\text{chlorine, outlet}}$$
$$\mathfrak{R}_3 = C_{\text{dichlorobenzene, outlet}} C_{\text{chlorine, outlet}}$$

CSTR design equations with multiple chemical reactions and τk_1 as a parameter:

$$\xi_1 = (\tau k_1)\mathfrak{R}_1$$
$$\xi_2 = (\tau k_1)\frac{k_2}{k_1}\mathfrak{R}_2$$
$$\xi_3 = (\tau k_1)\frac{k_2}{k_1}\frac{k_3}{k_2}\mathfrak{R}_3$$

Volumetric flow rate (L/min):

$$q_{\text{total}} = 50$$

Kinetic rate constant for the first chlorination step at 55 °C (L/mol·min):

$$k_1 = 0.00884 \times 60$$

CSTR volume (L):

$$V_{\text{CSTR}} = \frac{(\tau k_1) q_{\text{total}}}{k_1}$$

(b) Without introducing the extents for each independent chemical reaction, we have the following steady-state mass balance for each component (accumulation = input − output + rate of production = 0):

C_6H_6:

$$0 = C_{\text{benzene, inlet}} - C_{\text{benzene, outlet}} - (\tau k_1)\mathfrak{R}_1$$

Cl_2:

$$0 = C_{\text{chlorine, inlet}} - C_{\text{chlorine, outlet}} - (\tau k_1)\mathfrak{R}_1 - (\tau k_1)\frac{k_2}{k_1}\mathfrak{R}_2 - (\tau k_1)\frac{k_2}{k_1}\frac{k_3}{k_2}\mathfrak{R}_3$$

C_6H_5Cl:

$$0 = 0 - C_{\text{monochlorobenzene, outlet}} + (\tau k_1)\mathfrak{R}_1 - (\tau k_1)\frac{k_2}{k_1}\mathfrak{R}_2$$

$C_6H_4Cl_2$:

$$0 = 0 - C_{\text{dichlorobenzene, outlet}} + (\tau k_1)\frac{k_2}{k_1}\mathfrak{R}_2 - (\tau k_1)\frac{k_2}{k_1}\frac{k_3}{k_2}\mathfrak{R}_3$$

$C_6H_3Cl_3$:

$$0 = 0 - C_{\text{trichlorobenzene, outlet}} + (\tau k_1)\frac{k_2}{k_1}\frac{k_3}{k_2}\mathfrak{R}_3$$

HCl:

$$0 = 0 - C_{\text{hydrogen chloride}} + (\tau k_1)\mathfrak{R}_1 + (\tau k_1)\frac{k_2}{k_1}\mathfrak{R}_2 + (\tau k_1)\frac{k_2}{k_1}\frac{k_3}{k_2}\mathfrak{R}_3$$

The performance curve for the desired product, monochlorobenzene, and the CSTR volume required are presented in Figure 1-1 as a function of $\log(\tau k_1)$. The

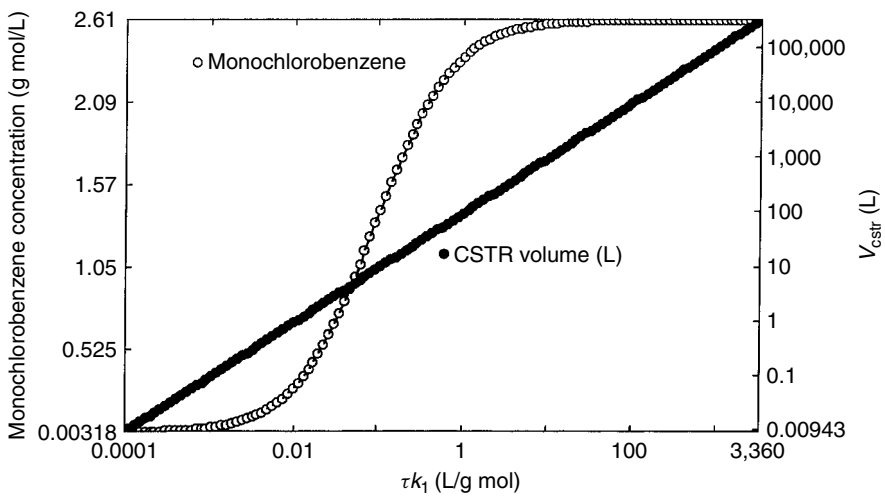

Figure 1-1 CSTR performance curve for the production of monochlorobenzene from chlorine and benzene in a gas–liquid continuous-stirred tank reactor, and the corresponding total reactor volume required to achieve these outlet molar densities of C_6H_5Cl.

two methodologies generate the same results, as expected. A reasonable design that considers economics qualitatively is as follows;

$$10^{-1} < \tau k_1 \text{ (L/g mol)} < 10^{0}$$

$$1.42 < C_{\text{monochlorobenzene, outlet}} \text{ (g mol/L)} < 2.38$$

$$10 < V_{\text{CSTR}} \text{ (L)} < 96$$

Problem. The following sequence of elementary irreversible reactions occurs in a liquid-phase CSTR with a feed stream that contains only reactant A.

$$2\text{A} \xrightarrow{k_1(T)} \text{B} + \text{C} \qquad \text{A} + \text{C} \xrightarrow{k_2(T)} \text{D}$$

All components exhibit relatively low vapor pressures below 90 °C. The activation energy for the first reaction is 15 kcal/mol, and the activation energy for the second reaction is 14 kcal/mol. The steady-state molar density ratio of reactive intermediate C to reactant A in the CSTR exit stream and in the well-mixed reactor is

$$\frac{\text{C}}{\text{A}} = \frac{\tau k_1 \text{A}}{1 + \tau k_2 \text{A}}$$

(a) Are the two elementary steps independent?
(b) Calculate the selectivity of the final product D relative to the intermediate product B.

$$S_{\text{D/B}} \equiv \frac{F_{\text{D, outlet}} - F_{\text{D, inlet}}}{F_{\text{B, outlet}} - F_{\text{B, inlet}}} = \frac{\text{D}}{\text{B}}$$

where F_i is the molar flow rate of component i.

If component D is the desired product:

(c) Is it better to operate the CSTR at 30 °C or 55 °C?
(d) Is it advantageous to dilute the feed of reactant A with an inert solvent?
(e) Is it advantageous to increase the reactor volume?
(f) Is it advantageous to increase the volumetric flow rate?

If component B is the desired product:

(g) Is it better to operate the CSTR at 30 °C or 55 °C?
(h) Is it advantageous to dilute the feed of reactant A with an inert solvent?
(i) Is it advantageous to increase the reactor volume?
(j) Is it advantageous to increase the volumetric flow rate?

SOLUTION. *Answer (b) and verification of the molar density ratio, C/A.* Stoichiometric coefficients, extents of reaction, and kinetic rate laws are summarized

below. Four components participate in two independent elementary reactions. Hence, two extents of reaction are required.

Reaction	Extent ξ_j	Component A	B	C	D	Rate Law
$2A \rightarrow B + C$	ξ_1	-2	$+1$	$+1$	0	k_1A^2
$A + C \rightarrow D$	ξ_2	-1	0	-1	$+1$	k_2AC

Application of the CSTR design equation for each independent chemical reaction yields

$$\xi_1 = \tau \mathfrak{R}_1 = \tau k_1 A^2$$
$$\xi_2 = \tau \mathfrak{R}_2 = \tau k_2 AC$$

The molar density of each component is expressed in terms of extents of reaction as

$$A = A_0 - 2\xi_1 - \xi_2$$
$$B = \xi_1$$
$$C = \xi_1 - \xi_2$$
$$D = \xi_2$$

If one combines the two design equations with the expression for the molar density of reactive intermediate C, it is possible to verify the molar density ratio, C/A, which is given in the problem statement.

$$C = \xi_1 - \xi_2 = \tau k_1 A^2 - \tau k_2 AC$$
$$C + \tau k_2 AC = C(1 + \tau k_2 A) = \tau k_1 A^2$$

Hence,

$$\frac{C}{A} = \frac{\tau k_1 A}{1 + \tau k_2 A}$$

This intermediate result is employed to calculate the selectivity of final product D relative to intermediate product B, and its inverse if B is the desired product. For example:

$$S_{D/B} = \frac{D}{B} = \frac{\xi_2}{\xi_1} = \frac{\tau k_2 AC}{\tau k_1 A^2} = \frac{k_2}{k_1}\frac{C}{A} = \frac{\tau k_2 A}{1 + \tau k_2 A}$$
$$S_{B/D} = \frac{B}{D} = \frac{1}{S_{D/B}} = 1 + \frac{1}{\tau k_2 A}$$

Answers (c) through (j). Answers to parts (c) through (f) are based on analysis of $S_{D/B}$. Answers to parts (g) through (j) are based on analysis of $S_{B/D}$. Since the kinetic rate constant k_1 does not affect either selectivity, comparison of activation energies for the two reactions is not an important consideration in the final design. Final product D is favored at (1) higher temperature, (2) higher concentrations of reactant A in the exit stream, (3) larger reactor volume, and (4) slower volumetric flow rate. Intermediate product B is favored at (1) lower temperature, (2) lower concentration of reactant A in the CSTR exit stream, (3) smaller reactor volume, and (4) larger volumetric flow rate.

1-3 MULTIPLE CHEMICAL REACTIONS IN A CSTR TRAIN

1-3.1 Generalized Steady-State Analysis

Sequential application of the steady-state design equations is required when multiple chemical reactions occur in a series configuration of well-mixed tanks. If temperature, residence time, kinetic rate laws, and the characteristics of the feed to the first reactor are known, then it is possible to predict molar densities in the exit stream of the first reactor, which represent the feed to the second reactor, and so on. Subscripts are required to monitor:

Components	i
Independent chemical reactions	j
Reactors in series	k

For example,

C_{ik} molar density of component i in the exit stream of the kth tank

ν_{ij} stoichiometric coefficient of component i in the jth reaction. If the reaction scheme is modified by catalysts, etc., that differ in each tank, then subscript k is required

$\mathfrak{R}_{jk}$ rate of the jth chemical reaction using conditions in the exit stream of the kth tank

ξ_{jk} extent of the jth chemical reaction in the kth tank

τ_k residence time for the kth reactor

T_k operating temperature in the kth reactor

The CSTR design equation

$$\xi_{jk} = \tau_k \mathfrak{R}_{jk}$$

is written for each independent chemical reaction in each tank. If all reactions are nth-order and irreversible, the generic form of each rate law is

$$\mathfrak{R}_{jk} = k_{j\infty} \exp\left(-\frac{E_{\text{act},j}}{RT_k}\right) \prod_{i \text{ reactants}} (C_{ik})^{-\nu_{ij}}$$

Molar densities in the kinetic rate laws are expressed in terms of extents of reaction as follows:

$$C_{ik} = C_{i,k-1} + \sum_j \nu_{ij}\xi_{jk}$$

1-3.2 Unrestricted Optimization of the Yield of a Reactive Intermediate

Consider the following generic complex multiple reaction scheme that occurs isothermally in a liquid-phase CSTR train. Both reactors operate at the same temperature. In the first elementary step, 1 mol of reactant A and 2 mol of reactant B reversibly produce intermediate product D, which is the desired product:

$$\mathrm{A} + 2\mathrm{B} \longleftrightarrow \mathrm{D}$$

The equilibrium constant for the first reaction, based on molar densities, is

$$K_{\mathrm{eq,\,C/1}} = \frac{k_{\mathrm{forward\ 1}}}{k_{\mathrm{backward\ 1}}} = 10\ (\mathrm{L/mol})^2$$

The third-order forward kinetic rate constant for the first reaction is

$$k_{\mathrm{forward\ 1}} = 0.05(\mathrm{L/mol})^2/\mathrm{min}$$

In the second elementary step, 1 mol of reactant B and 1 mol of intermediate product D irreversibly generate intermediate product E:

$$\mathrm{B} + \mathrm{D} \longrightarrow \mathrm{E}$$

via the second-order kinetic rate constant

$$k_2 = 0.01\ \mathrm{L/mol{\cdot}min}$$

In the third elementary step, 1 mol each of intermediate products D and E irreversibly generate the final product F:

$$\mathrm{D} + \mathrm{E} \longrightarrow \mathrm{F}$$

with the second-order kinetic rate constant

$$k_3 = 0.02\ \mathrm{L/mol{\cdot}min}$$

The feed stream to the first CSTR contains stoichiometric proportions (i.e., 1 : 2) of reactants A and B, and the molar density of reactant A in this inlet stream is

$$C_{\mathrm{A,\,inlet}} = 0.5\ \mathrm{g\ mol/L}$$

Illustrative Problem. As a reactor design engineer, your task is to design a train of two CSTRs in series that operate at the same temperature, which will maximize the yield of intermediate product D in the exit stream of the second reactor. What yield is expected for intermediate product D in the exit stream of the second CSTR? The yield of intermediate product D is defined as

$$\text{yield}(\text{D}_2) \equiv \frac{F_{\text{D2}} - F_{\text{D, inlet}}}{F_{\text{A, inlet}}} = \frac{C_{\text{D2}} - C_{\text{D, inlet}}}{C_{\text{A, inlet}}}$$

where F_{ik} is the molar flow rate of component i in the exit stream of the kth reactor.

Helpful hints. Use the conjugate gradient method of optimization with 2 degrees of freedom. In other words, you should develop a set of n equations in terms of $n + 2$ variables that describe the steady-state operation of three independent chemical reactions in a train of two chemical reactors. Maximization algorithms implicitly use two additional equations to determine optimum performance of the CSTR train:

$$\frac{\partial[\text{yield}(D_2)]}{\partial \tau_1} = 0 \qquad \text{at constant } \tau_2$$

$$\frac{\partial[\text{yield}(D_2)]}{\partial \tau_2} = 0 \qquad \text{at constant } \tau_1$$

These two additional restrictions are implemented numerically. Identify two key independent design variables and provide realistic upper and lower bounds for these variables to assist the maximization algorithm in finding the best answer. The conjugate gradient optimization method should converge in approximately 20 iterations.

Matrix of stoichiometric coefficients. Five components participate in three independent elementary reactions. Hence, three extents of reaction are required. The kinetic rate law for each elementary step is included in the following table.

		Component					
Reaction	Extent ξ_j	A	B	D	E	F	Rate Law
$\text{A} + 2\text{B} \leftrightarrow \text{D}$	ξ_1	-1	-2	$+1$	0	0	$k_1(\text{AB}^2 - \text{D}/K_{\text{eq}})$
$\text{B} + \text{D} \rightarrow \text{E}$	ξ_2	0	-1	-1	$+1$	0	$k_2\text{BD}$
$\text{D} + \text{E} \rightarrow \text{F}$	ξ_3	0	0	-1	-1	$+1$	$k_3\text{DE}$

SOLUTION. Concentrations $C_{i, \text{inlet}}$ of the five reactive species in the inlet stream to the first reactor, in units of g mol/L:

$$\text{A}_{\text{inlet}} = 0.5$$

$$\text{B}_{\text{inlet}} = \Theta_{\text{B}}\text{A}_{\text{inlet}} \qquad \Theta_{\text{B}} = 2$$

$$\text{D}_{\text{inlet}} = \text{E}_{\text{inlet}} = \text{F}_{\text{inlet}} = 0$$

Concentrations C_{i1} of the five reactive species in the exit stream of the first reactor, in terms of the extents of reaction ξ_{j1} in the first CSTR:

$$\begin{aligned}
\mathrm{A}_1 &= \mathrm{A}_{\text{inlet}} - \xi_{11} \\
\mathrm{B}_1 &= \mathrm{B}_{\text{inlet}} - 2\xi_{11} - \xi_{21} \\
\mathrm{D}_1 &= \mathrm{D}_{\text{inlet}} + \xi_{11} - \xi_{21} - \xi_{31} \\
\mathrm{E}_1 &= \mathrm{E}_{\text{inlet}} + \xi_{21} - \xi_{31} \\
\mathrm{F}_1 &= \mathrm{F}_{\text{inlet}} + \xi_{31}
\end{aligned}$$

Kinetic rate laws $\mathfrak{R}_{j1}$ for three independent elementary reactions in the first CSTR:

$$\begin{aligned}
\mathfrak{R}_{11} &= k_{\text{forward }1}(T_1)\left[\mathrm{A}_1(\mathrm{B}_1)^2 - \frac{\mathrm{D}_1}{K_{\text{eq, C}/1}(T_1)}\right] \\
\mathfrak{R}_{21} &= k_2(T_1)\mathrm{B}_1\mathrm{D}_1 \\
\mathfrak{R}_{31} &= k_3(T_1)\mathrm{D}_1\mathrm{E}_1
\end{aligned}$$

CSTR design equations, $\xi_{j1} = \tau_1\mathfrak{R}_{j1}$, for three independent reactions in the first reactor:

$$\begin{aligned}
\xi_{11} &= \tau_1\mathfrak{R}_{11} \\
\xi_{21} &= \tau_1\mathfrak{R}_{21} \\
\xi_{31} &= \tau_1\mathfrak{R}_{31}
\end{aligned}$$

Concentrations C_{i2} of the five reactive species in the exit stream of the second reactor, in terms of the extents of reaction ξ_{j2} in the second CSTR:

$$\begin{aligned}
\mathrm{A}_2 &= \mathrm{A}_1 - \xi_{12} \\
\mathrm{B}_2 &= \mathrm{B}_1 - 2\xi_{12} - \xi_{22} \\
\mathrm{D}_2 &= \mathrm{D}_1 + \xi_{12} - \xi_{22} - \xi_{32} \\
\mathrm{E}_2 &= \mathrm{E}_1 + \xi_{22} - \xi_{32} \\
\mathrm{F}_2 &= \mathrm{F}_1 + \xi_{32}
\end{aligned}$$

Kinetic rate laws $\mathfrak{R}_{j2}$ for three independent elementary reactions in the second CSTR:

$$\begin{aligned}
\mathfrak{R}_{12} &= k_{\text{forward }1}(T_2)\left[\mathrm{A}_2(\mathrm{B}_2)^2 - \frac{\mathrm{D}_2}{K_{\text{eq, C}/1}(T_2)}\right] \\
\mathfrak{R}_{22} &= k_2(T_2)\mathrm{B}_2\mathrm{D}_2 \\
\mathfrak{R}_{32} &= k_3(T_2)\mathrm{D}_2\mathrm{E}_2
\end{aligned}$$

CSTR design equations, $\xi_{j2} = \tau_2 \mathfrak{R}_{j2}$, for three independent reactions in the second reactor:

$$\xi_{12} = \tau_2 \mathfrak{R}_{12}$$

$$\xi_{22} = \tau_2 \mathfrak{R}_{22}$$

$$\xi_{32} = \tau_2 \mathfrak{R}_{32}$$

There are 2 degrees of freedom, τ_1 and τ_2, in this unrestricted optimization problem. The yield of intermediate product D in the exit stream of the second CSTR achieves a maximum of 35.4% when $\tau_1 = 26.9$ min and $\tau_2 = 27$ min.

1-3.3 CSTR Design Strategies

Four CSTR design strategies are summarized below when simple third-order irreversible chemical kinetics convert reactants to products.

1. It is advantageous to employ a longer residence time for the last reactor in series. This claim is justified by the following results, which have been generated by the supporting numerical algorithms.

   a. Two CSTRs in series (see Figure 1-2 and Table 1-2). The sequence of equations on page 24 calculates the conversion of reactant A in both exit streams for two CSTRs in series. The kinetics are *n*th-order irreversible and depend only on the molar density of reactant A. Both reactors operate at the same temperature, so that the *n*th-order kinetic rate constant is the same in both CSTRs. Furthermore, the characteristic chemical reaction

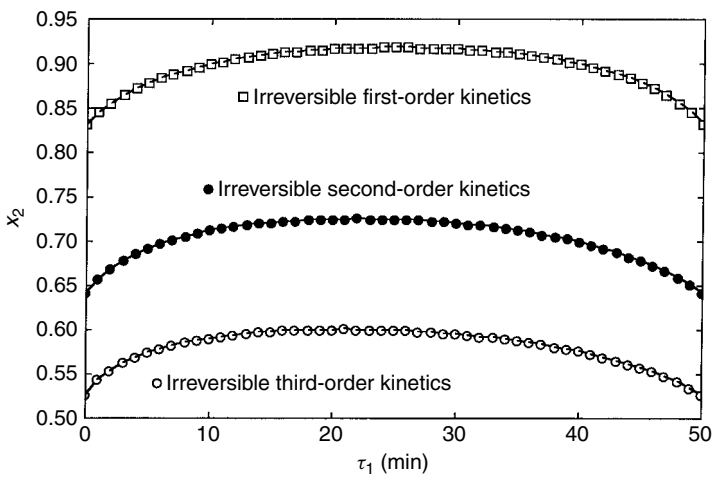

Figure 1-2 Example of restricted isothermal optimization for two CSTRs in series. This graph illustrates the effect of residence time in the first reactor on the outlet conversion from the second reactor in series for simple *n*th-order kinetics, where $n = 1, 2, 3$.

TABLE 1-2 Restricted Residence-Time Optimization for Two CSTRs in Series Operating at the Same Temperature[a]

Reaction Order	Residence Time (min)		Conversion (%)	
	τ_1	τ_2	χ_1	χ_2
1	25	25	71	92
1.5	23	27	59	81
2	22	28	52	73
3	21	29	42	60
4	20	30	35	52
5	20	30	31	46
6	20	30	28	41
7	19	31	25	37
8	19	31	23	34
9	19	31	22	32
10	19	31	20	30

[a]Includes the effect of reaction order n for simple nth-order chemical kinetics on optimum residence times and outlet reactant conversions in each CSTR. $k(T_1) = k(T_2) = 0.1$ (L/mol)$^{n-1}$/min; $\tau_1 + \tau_2 \approx 50$ min; $C_{A,\,inlet} = 1$ mol/L.

time constant λ is the same in both CSTRs when they operate at the same temperature. When the kinetics are first order, the optimum strategy requires that both reactors be of equal size. For higher-order kinetics where $n > 1$, the optimum strategy suggests that the first reactor should be slightly smaller. *Note*: There is only one independent variable, τ_1 or τ_2, due to the restricted optimization nature of this formulation.

$\tau_1 \mathfrak{R}_1 - C_{A0}(x_1 - x_0) = 0$ design equation for the first CSTR

$\tau_2 \mathfrak{R}_2 - C_{A0}(x_2 - x_1) = 0$ design equation for the second CSTR in series

$\tau_1 + \tau_2 = 50$ example of restricted optimization, residence times are in minutes

$\mathfrak{R}_1 = k_{forward}(T_1)[C_{A0}(1 - x_1)]^n$
nth-order rate law in the first CSTR

$\mathfrak{R}_2 = k_{forward}(T_2)[C_{A0}(1 - x_2)]^n$
nth-order rate law in the second CSTR in series

$k_{forward}(T_1) = k_{forward}(T_2)$ units depend on n, time units are in minutes

$k_{forward}(T_1) = 0.1$ λ is 10 min

$x_0 = 0$ conversion of reactant A in the inlet stream to the first CSTR

$C_{A0} = 1$ molar density of reactant A in the inlet stream to the first CSTR, moles per volume

TABLE 1-3 Restricted Residence-Time Optimization for Three CSTRs in Series Operating at the Same Temperature[a]

Reaction Order	Residence Time (min)			Conversion (%)		
	τ_1	τ_2	τ_3	χ_1	χ_2	χ_3
1	33	33	33	77	95	99
1.5	28	36	36	63	85	92
2	26	37	37	54	76	85
3	24	38	38	43	63	72
4	23	38	38	37	54	62
5	22	39	39	32	47	55
6	22	39	39	29	43	49
7	21	39	39	26	39	45
8	21	39	39	24	36	41
9	20	39	39	22	33	38
10	20	39	39	21	31	36

[a]Includes the effect of reaction order n for simple nth-order chemical kinetics on the optimum residence times and outlet reactant conversions in each CSTR. $k(T_1) = k(T_2) = k(T_3) = 0.1$ (L/mol)$^{n-1}$/min; $\tau_1 + \tau_2 + \tau_3 \approx 99$ to 100 min; $C_{A,\,inlet} = 1$ mol/L.

b. Three CSTRs in series (see Table 1-3). This strategy can be extended rather easily to a longer train of reactors, all of which operate at the same temperature. For higher-order kinetics where $n > 1$ in a train of three well-mixed reactors, the optimum strategy suggests that the last two reactors in the train should be larger than the first. Numerical results from this restricted optimization are summarized in Table 1-3. *Note*: This is an example of restricted optimization because the sum of all three residence times is fixed, but there are two independent variables, or 2 degrees of freedom, in the numerical algorithm.

2. The same reactant conversion can be achieved in the exit stream of the last reactor in series when the total volume of a CSTR train is less than the volume of the one-CSTR setup.
3. If the total volume of a CSTR train is the same as the volume of the one-CSTR setup, the final conversion in the exit stream of the last reactor in the train is greater than the final conversion in the exit stream of the one-CSTR setup.
4. When two CSTRs in series operate at different temperatures, it is advantageous to employ a longer residence time for the higher-temperature reactor. This strategy should be employed for reversible exothermic reactions, even though the equilibrium conversion decreases at higher temperature, because most reactors do not operate in the "near-equilibrium" regime (see Problem 1-7).

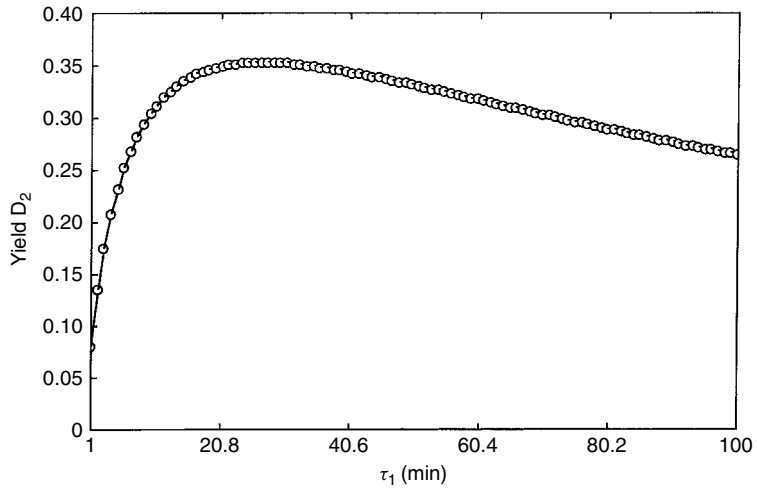

Figure 1-3 Example of unrestricted optimization in a train of two CSTRs that operate at the same temperature. This graph illustrates the effect of residence time for each reactor (i.e., $\tau_1 = \tau_2$) on the yield of intermediate product D in the exit stream of the second reactor.

Let's revisit the previous unrestricted optimization problem described on pages 20–23 in two CSTRs with 2 degrees of freedom and apply strategy 4. Since both reactors operate at the same temperature (i.e., $T_1 = T_2$), it might seem reasonable that an optimum design should keep the mixture in each CSTR for the same amount of time, on average. Hence, $\tau_1 = \tau_2$. Now, this problem conforms to unrestricted optimization with 1 degree of freedom (i.e., either τ_1 or τ_2). The behavior of the system of equations that describe the yield of intermediate product D in the exit stream of the second CSTR can be analyzed as a function of residence time. Optimum performance is obvious in Figure 1-3 when the reactive mixture remains in each CSTR for 25 to 29 min.

PROBLEMS

1-1. Draw the flow configuration for two CSTRs in series when the chemical kinetics are third order and irreversible. The objective is to maximize reactant conversion in the exit stream of the last CSTR. One CSTR operates at 75°C and the other CSTR operates at 30°C. Which reactor should be larger? Which reactor should be first in the train?

1-2. For a particular liquid-phase chemical reaction, the kinetic rate law is zeroth order:

$$\mathfrak{R} = k_\infty \exp\left(-\frac{E_{\text{act}}}{RT}\right)$$

In other words, $\mathfrak{R}$ is not a function of conversion or molar densities. The characteristic chemical reaction time constant is 25 min. The temperature is the same in each case. The following reactor configurations are employed.

(1) One CSTR: $V_1 = 50$ L, $q = 5$ L/min

(2) One CSTR: $V_1 = 100$ L, $q = 5$ L/min

(3) Two CSTRs in series: $V_1 + V_2 = 50$ L, $q = 5$ L/min

(4) Two CSTRs in series: $V_1 + V_2 = 100$ L, $q = 5$ L/min

From highest to lowest, rank the conversion of reactant A to products in the CSTR exit stream for the four configurations described above.

1-3. One liquid-phase chemical reaction occurs in an isothermal configuration of PFRs. The chemical kinetics are second order and irreversible [i.e., $\mathfrak{R} = k_2(C_A)^2$], and the characteristic chemical reaction time constant λ is 5 min. Rank the configurations listed in Table P1-3 from highest final conversion of reactant A in the exit stream of the last PFR in series to lowest final conversion in the exit stream of the last PFR. In each case, the volumetric flow rate is 10 L/min and $C_{A,\,inlet}$ is the same. Calculate the final conversion of reactant A in the exit stream of the third PFR in series for case 7.

TABLE P1-3 Ten Series Configurations of Plug-Flow Reactors and Corresponding Reactor Volumes

Case	No. PFRs in Series	Volume (L)		
		V_1	V_2	V_3
1	1	60		
2	1	45		
3	2	30	30	
4	2	40	20	
5	2	20	40	
6	2	45	45	
7	3	20	20	20
8	3	15	15	15
9	3	30	30	30
10	3	20	30	40

1-4. Three components (A,B,C) participate in two independent elementary chemical reactions:

$$A \longrightarrow B \longrightarrow C$$

in isothermal liquid-phase reactors. The kinetic rate constant for the first irreversible chemical reaction ($A \rightarrow B$) is $k_1 = 0.15$ min^{-1}. The kinetic rate constant for the second irreversible chemical reaction ($B \rightarrow C$) is $k_2 = 0.05$ min^{-1}. The feed stream contains only 1 mol of reactant A per litre.

All reactors operate at the same temperature. The reactor types and configurations are described below. Notice that the total residence time for each configuration is 1 min, whereas the chemical reaction time constants are ≈7 minutes for the first reaction and 20 min for the second reaction.

(1) One CSTR with a reactor volume of 10 L. The flow rate is 10 L/min.

(2) Two CSTRs in series. The volume of each reactor is 5 L and the volumetric flow rate is 10 L/min.

(3) Two CSTRs in parallel. The volume of each reactor is 5 L and the volumetric flow rate in each reactor is 5 L/min.

(4) One PFR with a volume of 10 L and a volumetric flow rate of 10 L/min.

(5) Two PFRs in series. The volume of each reactor is 5 L and the volumetric flow rate is 10 L/min.

The rate of production of intermediate product B in the final exit stream of each configuration has been calculated for the five cases described above. When two CSTRs are arranged in parallel, both exit streams contribute to the overall rate of production. In units of moles of B per minute, five correct answers and two incorrect answer for $q_{\text{total}}C_{\text{B}}$ are

$$1.42 \quad 1.36 \quad 1.36 \quad 1.30 \quad 1.24 \quad 1.24 \quad 1.18$$

Associate a numerical answer for the rate of production of intermediate product B with each of the five configurations and reactor types described above.

1-5. The following multiple-reaction scheme converts reactants A and B to final product E via intermediate D in the liquid phase. Each reaction represents an elementary step. The feed contains a 1 : 1 molar ratio of reactants A and B. The kinetic rate constant is indicated for each step in the chemical reaction.

Step 1. $\text{A} + \text{B} \rightarrow \text{D}$ via $k_1(T)$
Step 2. $\text{D} \rightarrow \text{A} + \text{B}$ via $k_2(T)$
Step 3. $\text{B} + \text{D} \rightarrow \text{E}$ via $k_3(T)$

(a) How many independent chemical reactions occur?

(b) Use one graph and sketch the molar density of each component vs. time in a constant-volume batch reactor. Put four curves on one graph and label each curve.

(c) Use the pseudo-steady-state approximation (PSSA) to obtain an expression for the molar density of reactive intermediate D.

(d) Elementary step 3 is the slowest one in the mechanism. Use your answer to part (c) and express the rate law in terms of measurable quantities for the rate of conversion of reactants to products.

(e) Use the extents of reaction ξ_j and write all of the equations that must be solved to design a liquid-phase CSTR based on the three-step mechanism described above.

(f) Use the extents of reaction ξ_j and write an expression for the selectivity of intermediate product D with respect to final product E in a CSTR. $S_{D/E} = ?$

(g) Write all of the equations that must be solved, including the initial conditions, to analyze the startup behavior of one CSTR based on the three-step mechanism described above.

1-6. **(a)** Use the extents of reaction ξ_j and write all eight equations that must be solved to design an ideal gas-phase PFR in which the following three independent elementary reactions occur.

Step 1. $A + 2B \rightarrow D$ via $k_1(T)$, (volume/mol)^2/time
Step 2. $D \rightarrow A + 2B$ via $k_2(T)$, 1/time
Step 3. $A + 2D \rightarrow E$ via $k_3(T)$, (volume/mol)^2/time
Step 4. $2A + E \rightarrow F$ via $k_4(T)$, (volume/mol)^2/time

The feed stream contains a 1 : 2 molar flow rate ratio of reactants A and B. The overall objective is to identify the PFR volume that maximizes the molar flow rate of intermediate product E.

(b) Use only one set of axes and sketch the molar flow rates of intermediate product E and final product F as a function of reactor volume V_{PFR}. Qualitatively identify the optimum reactor volume (i.e., $V_{PFR,\,optimum}$) on the horizontal axis of your graph.

1-7. This exercise deals with the restricted optimization of a train of two CSTRs with variable temperature options when the chemical reaction is reversible and exothermic. Consider the following third-order non-elementary reversible chemical reaction, which occurs in a train of two liquid-phase CSTRs:

$$2A \longleftrightarrow B$$

The catalyst is most effective when the reactors operate between 350 and 370 K. Under these conditions, the forward kinetic rate constant is described by a preexponential factor of 1×10^9 (L/mol)^2/min and an activation energy of 17,000 cal/mol. The feed stream to the first CSTR contains reactant A at a molar density of 0.4 mol/L. Economic considerations restrict the total residence time of both reactors to be 10^3 min or less. The temperature dependence of the dimensionless equilibrium constant is modeled as follows (see pages 57–60):

$$K_{\text{equilibrium},C} = \exp\left(\text{A} + \frac{\text{B}}{T}\right)$$

$$\text{A} = \frac{\Delta S^{\circ}_{\text{Rx, 298 K}}}{R}$$

$$\text{B} = -\frac{\Delta H^{\circ}_{\text{Rx, 298 K}}}{R}$$

The reaction is exothermic because a chemical bond is formed and thermal energy is liberated when 2 molecules of reactant A combine to produce 1 molecule of product B. The entropy change is negative due to the reduction in total moles as the reaction proceeds. Hence, the following thermodynamic data are applicable when the stoichiometric coefficient of reactant A is -1;

$$\Delta H^{\circ}_{\text{Rx, 298 K}} = -9000 \text{ cal/mol}$$
$$\Delta S^{\circ}_{\text{Rx, 298 K}} = -15 \text{ cal/mol·K}$$

Design the CSTR train by specifying the residence time τ in minutes and the temperature T in Kelvin for each reactor that maximize the conversion of reactant A in the exit stream of the second CSTR. The gas constant R is 1.987 cal/mol·K.

1-8. Calculate the CSTR operating temperature that maximizes the yield of a reactive intermediate. Consider the following multiple reaction scheme that occurs in one liquid-phase CSTR:

$$\text{A} \longrightarrow \text{B} \longrightarrow \text{C}$$

The overall objective is to determine the CSTR operating temperature that maximizes the yield of intermediate product B. The pre-exponential factor and Arrhenius activation energy for each reaction are:

$\text{A} \longrightarrow \text{B}$: $\quad k_{1\infty} = 1 \times 10^7 \text{ (L/mol)}^{n-1}/\text{s} \quad E_{\text{act, 1}} = 15 \text{ kcal/mol}$

$\text{B} \longrightarrow \text{C}$: $\quad k_{2\infty} = 4 \times 10^6 \text{ (L/mol)}^{n-1}/\text{s} \quad E_{\text{act, 2}} = 12 \text{ kcal/mol}$

The feed stream contains reactant A at a total mass flow rate of 250 g/s. The reactor volume is 100 L, and the overall density of the reactive mixture is 1 g/cm^3 or 1 kg/L.

(a) Identify the operating temperature that maximizes the yield of intermediate product B if both reactions represent elementary steps and

(i) $C_{\text{A, inlet}} = 1$ mol/L

(ii) $C_{\text{A, inlet}} = 2$ mol/L

(b) Identify the operating temperature that maximizes the yield of intermediate product B if both reactions follow second-order irreversible kinetics, and

(i) $C_{A,\,inlet} = 1$ mol/L

(ii) $C_{A,\,inlet} = 2$ mol/L

(c) Identify the operating temperature that maximizes the yield of intermediate product B if both reactions follow second-order irreversible kinetics, the total mass flow rate is reduced to 100 g/s, and $C_{A,\,inlet} = 1$ mol/L.

Transport Phenomena for Chemical Reactor Design. Laurence A. Belfiore
Copyright © 2003 John Wiley & Sons, Inc.
ISBN: 0-471-20275-4

2

START UP BEHAVIOR OF A SERIES CONFIGURATION OF CONTINUOUS STIRRED TANK REACTORS

This analysis begins with the unsteady-state mass balance for component i in the k^{th} well-mixed reactor. At high-mass-transfer Peclet numbers, which are primarily a function of volumetric flow rate q, the rate processes of interest are accumulation, convective mass transfer, and multiple chemical reactions. Generic subscripts are

i	designates components in the mixture
j	identifies the chemical reaction
k	denotes the tank in series

For liquid-phase reactions in a constant-volume CSTR, the mass balance for component i in tank k is written with units of moles per time, analogous to equation (1-22). The control volume is the entire contents of the kth tank, V_k:

$$\text{accumulation} = \text{input} - \text{output} + \text{rate of production} \tag{2-1a}$$

$$\frac{dN_{ik}}{dt} = \frac{d(V_k C_{ik})}{dt} = qC_{i,\,k-1} - qC_{ik} + V_k \sum_j \nu_{ij} \mathfrak{R}_{jk} \tag{2-1b}$$

where N represents moles, C is molar density, ν_{ij} the stoichiometric coefficient of component i in reaction j, and $\mathfrak{R}_{jk}$ the intrinsic kinetic rate law for the jth chemical reaction evaluated at conditions in the kth tank. Division by the volume of the kth reactor and identification of the residence time in this tank, $\tau_k = V_k/q$,

leads to the final form of the unsteady-state mass balance:

$$\frac{d}{dt}C_{ik} = \frac{1}{\tau_k}\{C_{i,k-1} - C_{ik}\} + \sum_j \nu_{ij}\mathfrak{R}_{jk} \tag{2-2}$$

which should be written for each component in each CSTR. If each reactor initially contains an inert mixture, and reactants are injected into the first tank at $t = 0$, then the initial conditions in the exit streams are $C_{ik} = 0$ at $t = 0$, $k \geq 1$. The inlet molar density of reactant i in the feed stream of the first tank (i.e., $C_{i,\text{inlet}}$) is based on the characteristics of the feed, which probably does not contain reactive intermediates or products.

2-1 ANALYSIS OF MULTIPLE REACTIONS IN TWO CSTRs: ILLUSTRATIVE PROBLEM

Analyze the transient startup behavior of a train of two liquid-phase CSTRs that operate isothermally at the same temperature. Four components participate in two independent chemical reactions. In the first independent elementary reaction, 1 mol of reactant A and 2 mol of reactant B reversibly produce 1 mol of intermediate product D:

$$\text{A} + 2\text{B} \longleftrightarrow \text{D} \tag{2-3}$$

via forward kinetic rate constant k_1 (i.e., 0.5 $\text{L}^2/\text{mol}^2 \cdot \text{min}$) and an equilibrium constant based on molar densities, $K_{\text{eq.C}} = k_1/k_2$ (i.e., 10 L^2/mol^2). In the second independent elementary step, 1 mol each of reactant A and intermediate product D irreversibly produce 1 mol of final product E:

$$\text{A} + \text{D} \longrightarrow \text{E} \tag{2-4}$$

with kinetic rate constant k_3 (i.e., 0.2 $\text{L}/\text{mol} \cdot \text{min}$). The feed stream to the first reactor contains stoichiometric proportions of reactants A and B (i.e., 1 : 2 molar flow rate ratio of A to B). The average residence times are 15 min for the first CSTR and 10 min for the second CSTR.

1. How many residence times (i.e., based on $\tau_1 = 15$ min) are required to achieve a steady-state response in the exit stream of the first CSTR?
   [*Ans.*: 4 or 5.]
2. How many residence times (i.e., based on $\tau_2 = 10$ min) are required to achieve a steady-state response in the exit stream of the second CSTR?
   [*Ans.*: ≈ 8.]

3. Do any of the transient molar density profiles exhibit overshoot with respect to their steady-state values? [*Ans.*: Yes, reactant A in both CSTRs.]

Solution. Four unsteady-state mass balances are written and solved numerically to characterize the composition of the exit stream for each reactor. Initially, all of the parameters are declared. The average residence times are $\tau_1 = 15$ min and $\tau_2 = 10$ min. The third-order kinetic rate constant for the forward step in the first independent elementary reaction is $k_1 = 0.5\ \mathrm{L}^2/\mathrm{mol}^2 \cdot \mathrm{min}$. The equilibrium constant, based on molar densities, for the first independent elementary reaction is $K_{\mathrm{eq.C}} = 10\ \mathrm{L}^2/\mathrm{mol}^2$. The second-order kinetic rate constant for the second independent elementary reaction is $k_3 = 0.2\ \mathrm{L}/\mathrm{mol} \cdot \mathrm{min}$. The molar densities of all four components in the inlet stream to the first CSTR, for a stoichiometric feed of reactants A and B, are

$$\begin{aligned} C_{\mathrm{A,\,inlet}} &= 1\ \mathrm{mol/L} \\ C_{\mathrm{B,\,inlet}} &= \Theta_{\mathrm{B}} C_{\mathrm{A,\,inlet}} \qquad (\Theta_{\mathrm{B}} = 2) \\ C_{\mathrm{D,\,inlet}} &= 0 \\ C_{\mathrm{E,\,inlet}} &= 0 \end{aligned} \tag{2-5}$$

The molar densities of all four reactive components in the exit stream of the first CSTR at $t = 0$ are

$$\begin{aligned} C_{\mathrm{A1}}(t=0) &= 0 \\ C_{\mathrm{B1}}(t=0) &= 0 \\ C_{\mathrm{D1}}(t=0) &= 0 \\ C_{\mathrm{E1}}(t=0) &= 0 \end{aligned} \tag{2-6}$$

The matrix of stoichiometric coefficients (ν_{ij}) that accounts for all four components in both independent chemical reactions is as follows:

	Component i			
Reaction	A	B	D	E
1. $\mathrm{A} + 2\mathrm{B} \longleftrightarrow \mathrm{D}$	−1	−2	+1	0
2. $\mathrm{A} + \mathrm{D} \longrightarrow \mathrm{E}$	−1	0	−1	+1

The kinetic rate laws for both independent elementary reactions in the first CSTR that operates at temperature T_1 are

$$\begin{aligned} \mathfrak{R}_{11} &= k_1(T_1)\left\{C_{\mathrm{A1}}(C_{\mathrm{B1}})^2 - \frac{C_{\mathrm{D1}}}{K_{\mathrm{eq.C}}(T_1)}\right\} \\ \mathfrak{R}_{21} &= k_3(T_1) C_{\mathrm{A1}} C_{\mathrm{D1}} \end{aligned} \tag{2-7}$$

Unsteady-state mass balances for all four components in the first CSTR are

$$\begin{aligned}
\frac{dC_{A1}}{dt} &= \frac{C_{A,\,inlet} - C_{A1}}{\tau_1} - \mathfrak{R}_{11} - \mathfrak{R}_{21} \\
\frac{dC_{B1}}{dt} &= \frac{C_{B,\,inlet} - C_{B1}}{\tau_1} - 2\mathfrak{R}_{11} \\
\frac{dC_{D1}}{dt} &= \frac{C_{D,\,inlet} - C_{D1}}{\tau_1} + \mathfrak{R}_{11} - \mathfrak{R}_{21} \\
\frac{dC_{E1}}{dt} &= \frac{C_{E,\,inlet} - C_{E1}}{\tau_1} + \mathfrak{R}_{21}
\end{aligned} \tag{2-8}$$

Numerical methods are required to integrate these coupled ordinary differential equations and to calculate the time-dependent molar density of each component in the exit stream of the first CSTR. Generic integral expressions are illustrated below. The Runge–Kutta–Gill fourth-order correct algorithm is useful to perform this task.

$$\begin{aligned}
C_{A1}(t) &= C_{A1}(t=0) + \int_{t'=0}^{t} \frac{dC_{A1}}{dt'}\,dt' \\
C_{B1}(t) &= C_{B1}(t=0) + \int_{t'=0}^{t} \frac{dC_{B1}}{dt'}\,dt' \\
C_{D1}(t) &= C_{D1}(t=0) + \int_{t'=0}^{t} \frac{dC_{D1}}{dt'}\,dt' \\
C_{E1}(t) &= C_{E1}(t=0) + \int_{t'=0}^{t} \frac{dC_{E1}}{dt'}\,dt'
\end{aligned} \tag{2-9}$$

Results for the first CSTR are illustrated in Figure 2-1.

The molar densities of all four reactive components in the exit stream of the second CSTR at $t = 0$ are

$$\begin{aligned}
C_{A2}(t=0) &= 0 \\
C_{B2}(t=0) &= 0 \\
C_{D2}(t=0) &= 0 \\
C_{E2}(t=0) &= 0
\end{aligned} \tag{2-10}$$

The kinetic rate laws for both independent elementary reactions in the second CSTR that operates at temperature $T_2 = T_1$ are represented by equation (2-11). Hence, the kinetic rate constants and the equilibrium constant are the same in both reactors:

$$\begin{aligned}
\mathfrak{R}_{12} &= k_1(T_2)\left\{C_{A2}(C_{B2})^2 - \frac{C_{D2}}{K_{eq.\,C}(T_2)}\right\} \\
\mathfrak{R}_{22} &= k_3(T_2)C_{A2}C_{D2}
\end{aligned} \tag{2-11}$$

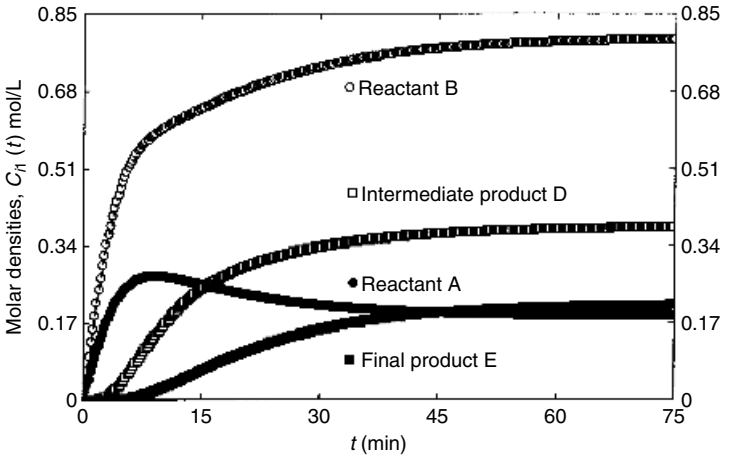

Figure 2-1 Multiple chemical reactions in a CSTR train: transient molar density response in the exit stream of the first reactor. Approximately $4\tau_1$ or $5\tau_1$ is required to achieve steady-state behavior in the first reactor, where τ_1 is 15 min.

In the unsteady-state mass balances for all four components in the second CSTR, the input terms due to convective mass transfer are based on the unsteady-state solutions in the exit stream of the first CSTR [i.e., $C_{i1}(t)$]:

$$\begin{aligned}
\frac{dC_{\mathrm{A2}}}{dt} &= \frac{C_{\mathrm{A1}} - C_{\mathrm{A2}}}{\tau_2} - \mathfrak{R}_{12} - \mathfrak{R}_{22} \\
\frac{dC_{\mathrm{B2}}}{dt} &= \frac{C_{\mathrm{B1}} - C_{\mathrm{B2}}}{\tau_2} - 2\mathfrak{R}_{12} \\
\frac{dC_{\mathrm{D2}}}{dt} &= \frac{C_{\mathrm{D1}} - C_{\mathrm{D2}}}{\tau_2} + \mathfrak{R}_{12} - \mathfrak{R}_{22} \\
\frac{dC_{\mathrm{E2}}}{dt} &= \frac{C_{\mathrm{E1}} - C_{\mathrm{E2}}}{\tau_2} + \mathfrak{R}_{22}
\end{aligned} \tag{2-12}$$

Numerical methods are required to integrate these coupled ordinary differential equations, which are also coupled to the ODEs from the first CSTR, and calculate the time-dependent molar density of each component in the exit stream of the second CSTR:

$$C_{\mathrm{A2}}(t) = C_{\mathrm{A2}}(t=0) + \int_{t'=0}^{t} \frac{dC_{\mathrm{A2}}}{dt'}\, dt'$$

$$C_{\mathrm{B2}}(t) = C_{\mathrm{B2}}(t=0) + \int_{t'=0}^{t} \frac{dC_{\mathrm{B2}}}{dt'}\, dt'$$

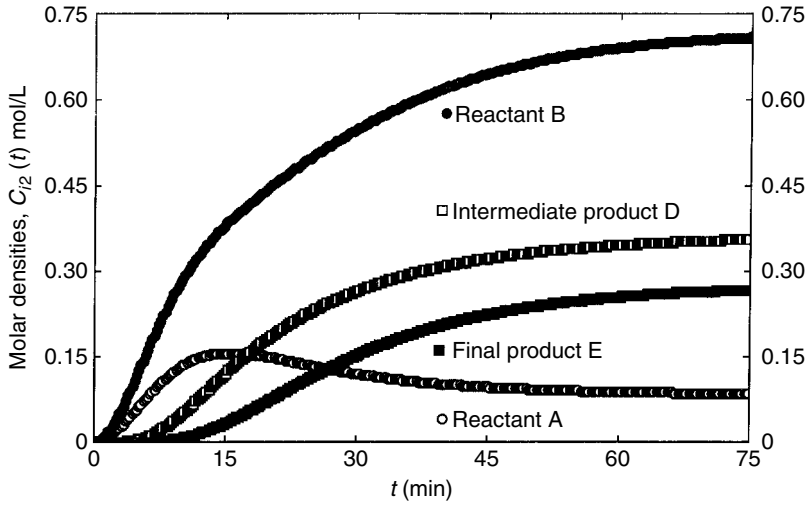

Figure 2-2 Multiple chemical reactions in a CSTR train: transient molar density response in the exit stream of the second reactor. Approximately $8\tau_2$ is required to achieve steady-state behavior in the second reactor, where τ_2 is 10 min.

$$C_{D2}(t) = C_{D2}(t=0) + \int_{t'=0}^{t} \frac{dC_{D2}}{dt'}\, dt'$$
$$C_{E2}(t) = C_{E2}(t=0) + \int_{t'=0}^{t} \frac{dC_{E2}}{dt'}\, dt' \qquad (2\text{-}13)$$

Results for the second CSTR are illustrated in Figure 2-2.

2-2 ANALYSIS OF A TRAIN OF FIVE CSTRs: ILLUSTRATIVE PROBLEM

Consider a train of five CSTRs in series that have the same volume and operate at the same temperature. One first-order irreversible chemical reaction occurs in each CSTR where reactant A decomposes to products. Two mass-transfer-rate processes are operative in each reactor. The time constant for convective mass transfer across the inlet and outlet planes of each CSTR is designated by the residence time $\tau = V/q$. The time constant for a first-order irreversible chemical reaction is given by $\lambda = 1/k_1$. The ratio of these two time constants,

$$\beta = \frac{\tau}{\lambda} = \frac{Vk_1}{q} = 0.5 \qquad (2\text{-}14)$$

is the same in each CSTR. Analyze the startup behavior of the CSTR train. The molar density of reactant A (i.e., C_{A0}) is 1 mol/L in the inlet stream to the first reactor.

(a) Generate one graph that contains five curves. Each curve represents the molar density of reactant A in the exit stream of each of the five CSTRs as a function of t/τ, where t is variable time and τ is the average residence time for each reactor.

(b) Prove that the exact analytical solution for the transient behavior of reactant A in the exit stream of each CSTR is given by equation (2-15) for first-order irreversible chemical kinetics in equisized reactors that operate at the same temperature.

$$C_{Ak}\left(\frac{t}{\tau}\right) = \frac{C_{A0}}{(1+\beta)^k}\left\{1 - \exp\left[-(1+\beta)\frac{t}{\tau}\right]\sum_{\alpha=0}^{k-1}\frac{[(1+\beta)t/\tau]^\alpha}{\alpha!}\right\} \tag{2-15}$$

(c) Develop a correlation that allows one to determine the number of residence times required to achieve steady-state concentrations in the exit stream of the kth CSTR.

Solution (a). The generic unsteady-state mass balance with one chemical reaction (i.e., $j = 1$) is written for reactant A in each CSTR:

$$\frac{d}{dt}C_{Ak} = \frac{1}{\tau_k}\{C_{A,k-1} - C_{Ak}\} + \nu_{A1}\mathfrak{R}_{1k} \tag{2-16}$$

$$\mathfrak{R}_{1k} = \frac{C_{Ak}}{\lambda(T_k)} \tag{2-17}$$

Multiplication by residence time τ_k yields (i.e., with $\nu_{A1} = -1$)

$$\tau_k\frac{d}{dt}C_{Ak} = \frac{dC_{Ak}}{d(t/\tau_k)} = C_{A,k-1} - C_{Ak} - \frac{\tau_k}{\lambda(T_k)}C_{Ak} \tag{2-18}$$

$$\frac{dC_{Ak}}{d(t/\tau_k)} = C_{A,k-1} - (1+\beta)C_{Ak} \tag{2-19}$$

This equation is written in each of the five CSTRs:

$$\begin{aligned}
&\text{First CSTR:} && \frac{dC_{A1}}{d(t/\tau)} = C_{A0} - (1+\beta)C_{A1}\\
&\text{Second CSTR:} && \frac{dC_{A2}}{d(t/\tau)} = C_{A1} - (1+\beta)C_{A2}\\
&\text{Third CSTR:} && \frac{dC_{A3}}{d(t/\tau)} = C_{A2} - (1+\beta)C_{A3}\\
&\text{Fourth CSTR:} && \frac{dC_{A4}}{d(t/\tau)} = C_{A3} - (1+\beta)C_{A4}\\
&\text{Fifth CSTR:} && \frac{dC_{A5}}{d(t/\tau)} = C_{A4} - (1+\beta)C_{A5}
\end{aligned} \tag{2-20}$$

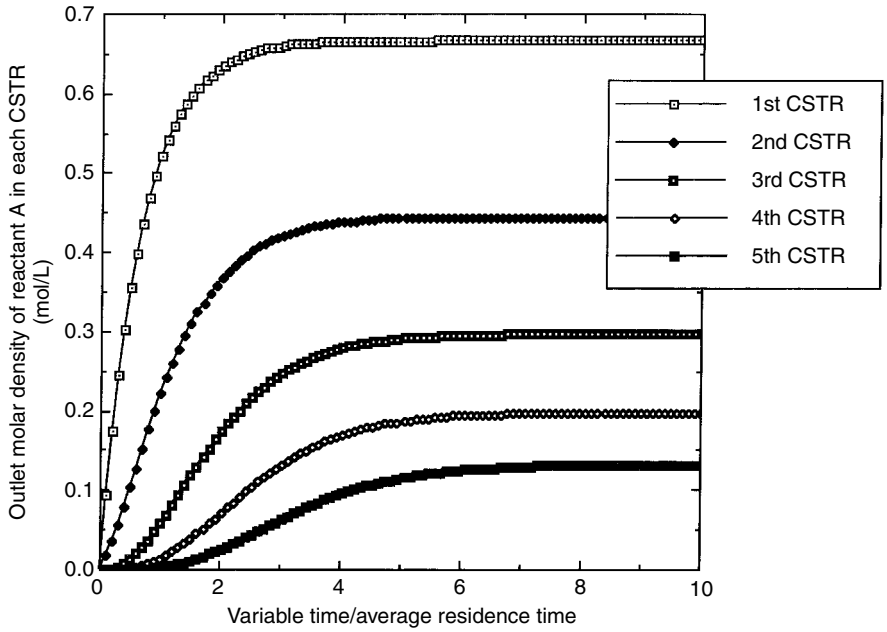

Figure 2-3 Transient molar density response for reactant A in a series configuration of five equisized CSTRs that operate at the same temperature, with simple first-order chemical kinetics.

The numerical solution of these five coupled ODEs is illustrated in Figure 2-3.

Solution (b)

Steady-State Solution. The steady-state response for each CSTR is obtained by neglecting the accumulation term in the generic mass balance from part (a):

$$\frac{dC_{Ak}}{d(t/\tau_k)} = C_{A,k-1} - (1+\beta)C_{Ak} = 0 \tag{2-21}$$

Hence, the steady-state recurrence formula is

$$C_{Ak} = \frac{C_{A,k-1}}{1+\beta} \tag{2-22}$$

which suggests that C_{Ak} should be of the following form:

$$C_{Ak} = \sigma\,\Xi^k = \frac{\sigma\,\Xi^{k-1}}{1+\beta} \tag{2-23}$$

$$\Xi = \frac{1}{1+\beta} \tag{2-24}$$

The constant σ is determined from the molar density of reactant A in the feed stream to the first reactor:

$$C_{A0} = \sigma \Xi^{\circ} = \sigma \tag{2-25}$$

The steady-state solution is

$$(C_{Ak})_{\text{steady state}} = \frac{C_{A0}}{(1+\beta)^k} \tag{2-26}$$

Laplace Transform Analysis. Transient response in the exit stream of the kth CSTR is obtained via Laplace transform analysis of the mass balance that was developed in part (a):

$$\frac{dC_{Ak}}{d(t/\tau)} = \frac{dC_{Ak}}{d\omega} = C_{A,\,k-1} - (1+\beta)C_{Ak} \tag{2-27}$$

$$C_{Ak} = 0 \text{ at } \omega = t/\tau = 0 \qquad \text{for } k \geq 1 \tag{2-28}$$

Hence, the ordinary differential equation for $C_{Ak}(\omega)$ in the time domain is transformed into the Laplace domain and solved for $C_{Ak}(s)$ (Wylie, 1975, pp. 264–265, theorem 2):

$$sC_{Ak}(s) - C_{Ak}(\omega = 0) = C_{A,\,k-1}(s) - (1+\beta)C_{Ak}(s) \tag{2-29}$$

where s is the transformed time variable. The recurrence formula is

$$C_{Ak}(s) = \frac{C_{A,k-1}(s)}{s + (1+\beta)} \tag{2-30}$$

The molar density of reactant A in the inlet stream of the first CSTR is C_{A0}/s in the Laplace domain. Hence, when the recurrence formula (2-30) is applied to the first reactor (i.e., $k = 1$),

$$C_{A1}(s) = \frac{C_{A0}(s)}{s + (1+\beta)} = \frac{C_{A0}/s}{s + (1+\beta)} \tag{2-31}$$

The final solution for the kth reactor in the Laplace domain is

$$C_{Ak}(s) = \frac{C_{A0}}{s} \frac{1}{[s + (1+\beta)]^k} \tag{2-32}$$

The convolution theorem is useful to invert the final result for $C_{Ak}(s)$ in the Laplace domain and recover $C_{Ak}(\omega)$ in the time domain. The appropriate inverse Laplace transforms are (Wylie, 1975, p. 268, formula 5; p. 278, formula 3)

$$\mathfrak{L}^{-1} \frac{C_{A0}}{s} = C_{A0} \tag{2-33}$$

$$\mathfrak{L}^{-1} \frac{1}{[s + (1+\beta)]^{\mathrm{k}}} = \frac{\omega^{k-1} \exp[-(1+\beta)\omega]}{(k-1)!} \tag{2-34}$$

Application of the convolution theorem yields (Wylie, 1975, p. 309, theorem 1)

$$C_{Ak}(\omega) = C_{Ak}(t/\tau) = \frac{C_{A0}}{(k-1)!}\int_0^{\omega} x^{k-1}\exp[-(1+\beta)x]\,dx \tag{2-35}$$

This integral expression is equivalent to equation (2-15) when $\omega = t/\tau$.

Matrix Analysis. Startup behavior of a series of n CSTRs in series with first-order irreversible chemical reaction is described by n coupled ODEs. These equations:

$$\begin{aligned}
&\text{First CSTR:} && \frac{dC_{A1}}{d(t/\tau)} = C_{A0} - (1+\beta)C_{A1}\\
&\text{Second CSTR:} && \frac{dC_{A2}}{d(t/\tau)} = C_{A1} - (1+\beta)C_{A2}\\
&n\text{th CSTR:} && \frac{dC_{An}}{d(t/\tau)} = C_{A,n-1} - (1+\beta)C_{An}
\end{aligned} \tag{2-36}$$

can be presented in matrix form as

$$\frac{d\mathbf{C}}{d\omega} + \mathbf{A}\cdot\mathbf{C} = \mathbf{C}_{\text{inlet}} \tag{2-37}$$

$$\mathbf{C}(\omega = 0) = \mathbf{C}_{\text{initial}} = \mathbf{0} \tag{2-38}$$

where $\mathbf{C}$ is an $n \times 1$ column vector that contains the time-dependent molar density of reactant A in the exit stream of each CSTR (i.e., C_{Ak}, $1 \le k \le n$). $\omega = t/\tau$ contains the independent time variable divided by the average residence time τ, which is the same for each CSTR because all reactors have the same volume. $\mathbf{A}$ is an $n \times n$ square bidiagonal coefficient matrix (see equation 2-53). The main diagonal contains n identical elements (i.e., $1+\beta$). Convective mass transfer in the outlet stream of each CSTR accounts for 1, and first-order irreversible chemical reaction is responsible for β. The diagonal just below the main diagonal contains $n-1$ identical elements (i.e., -1), which account for convective mass transfer in the inlet stream of each CSTR. $\mathbf{C}_{\text{inlet}}$ is an $n \times 1$ column vector that contains only one nonzero constant in the first row (i.e., C_{A0}). This is characteristic of the feed stream to the first CSTR. All other entries are zero because convective mass transfer in the inlet stream of the other reactors is variable, not constant. Hence, this variable contribution to the inlet stream of all reactors, except the first, is accounted for by -1 along the diagonal below the main diagonal in $\mathbf{A}$ described above.

As a preliminary to the solution of (2-37) it is instructive to solve a similar inhomogeneous ODE for $x(\omega)$ without matrices:

$$\frac{dx}{d\omega} + ax = x_{\text{inlet}} \tag{2-39}$$

$$x(\omega = 0) = x_{\text{initial}} \tag{2-40}$$

where x_{inlet} and x_{initial} are constants. The homogeneous solution is obtained by ignoring x_{inlet} and solving

$$\frac{dx}{d\omega} + ax = 0 \tag{2-41}$$

which has the following solution via separation of variables:

$$\frac{dx}{x} = -a\, d\omega \tag{2-42}$$

$$x(\omega)_{\text{homogeneous}} = (\text{constant}) \exp(-a\omega) \tag{2-43}$$

Since x_{inlet} is constant, the particular solution is obtained by choosing a constant for $x_{\text{particular}}$. This constant is determined via substitution in the original ODE;

$$x(\omega)_{\text{particular}} = \frac{x_{\text{inlet}}}{a} \tag{2-44}$$

The complete solution to (2-39) is obtained by adding the homogeneous and particular solutions, given by (2-43) and (2-44), respectively:

$$x(\omega) = x(\omega)_{\text{homogeneous}} + x(\omega)_{\text{particular}} = \text{constant} \cdot \exp(-a\omega) + \frac{x_{\text{inlet}}}{a} \tag{2-45}$$

Application of the initial condition at $\omega = 0$ allows one to determine the integration constant:

$$x(\omega = 0) = \text{constant} + \frac{x_{\text{inlet}}}{a} = x_{\text{initial}} \tag{2-46}$$

The final solution is

$$x(\omega) = \left(x_{\text{initial}} - \frac{x_{\text{inlet}}}{a}\right) \exp(-a\omega) + \frac{x_{\text{inlet}}}{a} \tag{2-47}$$

By analogy, preserving the order of matrix multiplication, which is not commutative, the solution to the following matrix differential equation for the CSTR startup response,

$$\frac{d\mathbf{C}}{d\omega} + \mathbf{A} \cdot \mathbf{C} = \mathbf{C}_{\text{inlet}} \tag{2-48}$$

$$\mathbf{C}(\omega = 0) = \mathbf{C}_{\text{initial}} = \mathbf{0} \tag{2-49}$$

is

$$\mathbf{C}(\omega) = \exp(-\mathbf{A}\omega) \cdot (\mathbf{C}_{\text{initial}} - \mathbf{A}^{-1} \cdot \mathbf{C}_{\text{inlet}}) + \mathbf{A}^{-1} \cdot \mathbf{C}_{\text{inlet}} \tag{2-50}$$

The inverse of $\mathbf{A}$ (i.e., $\mathbf{A}^{-1}$) is calculated from the adjoint matrix of $\mathbf{A}$ divided by the determinant of $\mathbf{A}$ (see Wylie, 1975, pp. 483–484, definitions 1 and 2). Hence,

$$\mathbf{A}^{-1} = \frac{\operatorname{adj} \mathbf{A}}{\det \mathbf{A}} \tag{2-51}$$

where $\det \mathbf{A} = (1+\beta)^n$, and the adjoint of $\mathbf{A}$ is the transpose of the cofactor matrix. If there are four CSTRs in series (i.e., $n = 4$), then the adjoint matrix of $\mathbf{A}$ is

$$\operatorname{adj} \mathbf{A} = \begin{matrix} (1+\beta)^3 & 0 & 0 & 0 \\ (1+\beta)^2 & (1+\beta)^3 & 0 & 0 \\ 1+\beta & (1+\beta)^2 & (1+\beta)^3 & 0 \\ 1 & 1+\beta & (1+\beta)^2 & (1+\beta)^3 \end{matrix} \tag{2-52}$$

because

$$\mathbf{A} = \begin{matrix} 1+\beta & 0 & 0 & 0 \\ -1 & 1+\beta & 0 & 0 \\ 0 & -1 & 1+\beta & 0 \\ 0 & 0 & -1 & 1+\beta \end{matrix} \tag{2-53}$$

Matrix multiplication yields the following 4×1 column vector result when $n = 4$:

$$\begin{aligned} \mathbf{A}^{-1} \cdot \mathbf{C}_{\text{inlet}} &= \frac{1}{\det \mathbf{A}} \operatorname{adj} \mathbf{A} \cdot \mathbf{C}_{\text{inlet}} \\ &= \frac{C_{\text{A0}}}{(1+\beta)^4} \cdot \begin{matrix} (1+\beta)^3 \\ (1+\beta)^2 \\ 1+\beta \\ 1 \end{matrix} \end{aligned} \tag{2-54}$$

Analogous to the Taylor series expansion of an exponential function, if a matrix appears as the argument of an exponential operator, then the function is expanded as follows:

$$\exp(-\mathbf{A}\omega) = \mathbf{1} - \mathbf{A}\omega + \frac{\mathbf{A}^2\omega^2}{2!} - \frac{\mathbf{A}^3\omega^3}{3!} + \frac{\mathbf{A}^4\omega^4}{4!} - \cdots \tag{2-55}$$

where $\mathbf{1}$ is the identity matrix of the same rank as $\mathbf{A}$ (i.e., n), $\mathbf{A}^2 = \mathbf{A} \cdot \mathbf{A}$, $\mathbf{A}^3 = (\mathbf{A} \cdot \mathbf{A}) \cdot \mathbf{A}$, and so on. The $n \times 1$ column vector represented by $\mathbf{C}_{\text{initial}}$ contains all zero elements because startup requires that the molar density of reactant A in the exit stream of each reactor vanish at $\omega = 0$. Hence, the transient behavior of n CSTRs in series, given by (2-50), can be written in matrix form as

$$\mathbf{C}(\omega) = [\mathbf{1} - \exp(-\mathbf{A}\omega)] \cdot (\mathbf{A}^{-1} \cdot \mathbf{C}_{\text{inlet}}) \tag{2-56}$$

and expansion of the exponential yields the final solution:

$$\mathbf{C}(\omega) = \left(\mathbf{A}\omega - \frac{\mathbf{A}^2\omega^2}{2!} + \frac{\mathbf{A}^3\omega^3}{3!} - \frac{\mathbf{A}^4\omega^4}{4!} + \cdots\right) \cdot (\mathbf{A}^{-1} \cdot \mathbf{C}_{\text{inlet}}) \tag{2-57}$$

One should compare the analytical solution given by equation (2-15) with the Laplace transform and matrix results for startup behavior of a series of n CSTRs with first-order irreversible chemical reaction. The three solutions are equivalent. An alternative proof of the analytical solution that does not require mathematical rigor is based on graphical comparison of the numerical results in Figure 2-3 with the solution given by equation (2-15). The numerical and analytical solutions are indistinguishable.

Solution (c). Explicit evaluation of equation (2-15) yields:

$$\frac{C_{Ak}(t/\tau)}{(C_{Ak})_{\text{steady state}}} = 1 - \Phi_k \exp(-\alpha) \tag{2-58}$$

$$(C_{Ak})_{\text{steady state}} = \frac{C_{A0}}{(1+\beta)^k} \tag{2-59}$$

$$\alpha = \frac{(1+\beta)t}{\tau} \tag{2-60}$$

$$\begin{aligned}
\Phi_1 &= 1 \\
\Phi_2 &= 1 + \alpha \\
\Phi_3 &= 1 + \alpha + \frac{\alpha^2}{2!} \\
\Phi_4 &= 1 + \alpha + \frac{\alpha^2}{2!} + \frac{\alpha^3}{3!} \\
\Phi_5 &= 1 + \alpha + \frac{\alpha^2}{2!} + \frac{\alpha^3}{3!} + \frac{\alpha^4}{4!}
\end{aligned} \tag{2-61}$$

The number of residence times required to achieve steady-state conditions in the exit stream of each CSTR for a series configuration of five equisized reactors that operate at the same temperature, with simple first-order chemical kinetics, is

kth CSTR in the Train	t/τ Such That, $1 - \Phi_k \exp(-\alpha) \approx 1$ When $\beta = 0.5$
1	9.5
2	11.5
3	13.1
4	14.6
5	16.0

PROBLEM

2-1. You have designed the following tracer experiment to determine whether your continuous flow reactor for pilot-scale study is perfectly mixed, like an ideal CSTR. At time $t = 0$, you inject 100 g of an inert tracer into the 100 L reactor after establishing a feed flow rate of 25 L per min. Your technician measures the tracer concentration in the outlet stream for a few minutes and provides you with the following data:

Time (sec)	Tracer Concentration (g/L)
20	0.94
50	0.84
100	0.53
200	0.30
400	0.15

(a) Develop an unsteady state macroscopic mass balance on the nonreactive tracer, assuming that the continuous flow reactor is perfectly mixed. After $t = 0$, there is no tracer input to the reactor via convective mass transfer. Hence, use the "spike" input at $t = 0$ as an intial condition for your unsteady state mass balance.

(b) Obtain an analytical solution to your unsteady state macroscopic mass balance from part (a).

(c) Obtain a numerical solution to your unsteady state macroscopic mass balance from part (a).

(d) Is the reactor perfectly mixed? Explain your answer.

Transport Phenomena for Chemical Reactor Design. Laurence A. Belfiore
Copyright © 2003 John Wiley & Sons, Inc.
ISBN: 0-471-20275-4

3

ADIABATIC PLUG-FLOW TUBULAR REACTOR THAT PRODUCES METHANOL REVERSIBLY IN THE GAS PHASE FROM CARBON MONOXIDE AND HYDROGEN

A stoichiometric feed of carbon monoxide (CO) and hydrogen (H_2) enters a 2-cm-inner-diameter tubular reactor at 340 K and 1 atm total pressure. The wall of the tube is well insulated from the surroundings, and the pressure drop throughout the reactor is negligible. The forward rate constant for this elementary gas-phase reversible reaction is characterized by a pre-exponential factor of 2×10^4 mol/cm^3·min·atm^3 and an Arrhenius activation energy of 5000(R), where R is the universal gas constant. Based on equilibrium thermodynamic data for the species in this particular reaction, kinetic and equilibrium relations between temperature and conversion can be generated and plotted on the same graph. The two curves intersect at an equilibrium conversion of $\approx$9% based on the molar flow rate of carbon monoxide. This is the hypothetical maximum conversion (i.e., $\approx$9%) that can be achieved in one adiabatic tubular reactor, based on the inlet conditions described above, if the volume is infinitely large. Your task as a chemical reactor design engineer is to calculate the required length of a PFR that will convert 8% of the inlet carbon monoxide to methanol in the exit stream of the first reactor when the overall mass flow rate is 1 kg/min. The physical property data are listed in Table 3-1.

This problem requires an analysis of coupled thermal energy and mass transport in a differential tubular reactor. In other words, the mass and energy balances should be expressed as coupled ordinary differential equations (ODEs). Since 3 mol of reactants produces 1 mol of product, the total number of moles is not conserved. Hence, this problem corresponds to a variable-volume gas-phase flow reactor and it is important to use reactor volume as the independent variable. Don't introduce average residence time because the gas-phase volumetric flow rate is not constant. If heat transfer across the wall of the reactor is neglected in the thermal energy balance for adiabatic operation, it

TABLE 3-1 Pure-Component Gas-Phase Thermodynamic Properties for CO, H_2, and CH_3OH

Physical Property	Carbon Monoxide	Hydrogen	Methanol
Enthalpy of formation (cal/mol), at 298 K	−26,416	0	−48,100
Free energy of formation (cal/mol), at 298 K	−32,808	0	−38,700
Molecular weight	28	2	32
C_p (cal/mol·K) $= a + bT(\mathrm{K}) + c[T(\mathrm{K})]^{-2}$, at 298 K $\leq T \leq$ 2500 K			
a	6.79	6.52	
b	0.98×10^{-3}	0.78×10^{-3}	
c	-0.11×10^{5}	0.12×10^{5}	
C_p(cal/mol·K) $= \alpha + \beta T(\mathrm{K}) + \gamma[T(\mathrm{K})]^2$, at 298 K $\leq T \leq$ 1500 K			
α			4.394
β			24.274×10^{-3}
γ			-6.855×10^{-6}

is possible to combine the mass and energy balances to obtain an analytical expression for temperature as a function of conversion when the following assumptions are invoked.

3-1 TEMPERATURE-AVERAGED SPECIFIC HEATS

The heat capacity term in the thermal energy balance represents the heat capacity of the mixture, and it is a function of temperature and conversion. There are a few methods to calculate this heat capacity. Weighting factors are required to account for the fact that there are three components in the mixture. Mole fractions y_i are the appropriate weighting factors when the molar heat capacity of each component, with units of cal/mol·K, is used. Mass fractions ω_i represent the weighting factors when the specific heat of each component, with units of cal/g·K, is used. Stoichiometric coefficients ν_i are not required, except for their appearance in the expressions for mass or mole fractions. A simplified approach that eliminates the temperature dependence of the heat capacities is to perform a temperature average of each pure-component heat capacity before performing the appropriate weighted average based on mass or mole fractions. Since the reaction is exothermic and heat is liberated, the inlet temperature to the reactor is a good choice for the lower-temperature limit (i.e., $T_{\text{lower}} = 340$ K) in the integral expression for the temperature-averaged heat capacity. At this stage in the problem solution, it is necessary to estimate the upper temperature limit of integration (i.e., $T_{\text{upper}} \approx 400$ K). This estimate is not much different from

the temperature at the reactor outlet (i.e., ≈423 K), which corresponds to 8% conversion of carbon monoxide. If the temperature polynomial for each pure-component heat capacity is

$$C_{p,\,\text{component}\,i} = a_i + b_i T + \frac{c_i}{T^2} \tag{3-1}$$

then the temperature-averaged heat capacity is

$$\begin{aligned}\langle C_{p,\,\text{component}\,i}\rangle &\equiv \frac{1}{(T_{\text{upper}} - T_{\text{lower}})}\int_{T_{\text{lower}}}^{T_{\text{upper}}}\left\{a_i + b_i T + \frac{c_i}{T^2}\right\} dT \\ &= a_i + \frac{1}{2}b_i(T_{\text{upper}} + T_{\text{lower}}) + \frac{c_i}{T_{\text{upper}}T_{\text{lower}}}\end{aligned} \tag{3-2}$$

If the temperature polynomial for each pure-component heat capacity is

$$C_{p,\,\text{component}\,i} = \alpha_i + \beta_i T + \gamma_i T^2 \tag{3-3}$$

then the temperature-averaged heat capacity is

$$\begin{aligned}\langle C_{p,\,\text{component}\,i}\rangle &\equiv \frac{1}{(T_{\text{upper}} - T_{\text{lower}})}\int_{T_{\text{lower}}}^{T_{\text{upper}}}\{\alpha_i + \beta_i T + \gamma_i T^2\}\, dT \\ &= \alpha_i + \frac{1}{2}\beta_i(T_{\text{upper}} + T_{\text{lower}}) + \frac{1}{3}\frac{\gamma_i[(T_{\text{upper}})^3 - (T_{\text{lower}})^3]}{(T_{\text{upper}} - T_{\text{lower}})}\end{aligned} \tag{3-4}$$

The results shown in Table 3-2 are obtained for the three gas-phase components in the reactor.

Now that the pure-component heat capacities have been averaged over the temperature range of operation, it is necessary to focus on the conversion dependence of mass fractions and mole fractions.

TABLE 3-2 Temperature-Averaged Pure-Component Heat Capacities for CO, H_2, and CH_3OH

	$\langle C_{p,\,\text{component}\,i}\rangle$	
Component	cal/mol·K	cal/g·K
CO	7.07	0.25
H_2	6.90	3.45
CH_3OH	12.44	0.39

3-2 CONVERSION DEPENDENCE OF MASS FRACTION AND HEAT CAPACITY OF THE MIXTURE

For gas-phase flow reactors, conversion of the key-limiting reactant (i.e., CO) is typically defined in terms of its molar flow rate (i.e., F_A):

$$\chi \equiv \frac{F_{A,\,\text{inlet}} - F_A}{F_{A,\,\text{inlet}}} \tag{3-5}$$

Hence, molar flow rates are linear functions of conversion because dF_i/ν_i is the same for all components, based on stoichiometry and the mass balance with convection and one chemical reaction (see equation 3-15):

$$\frac{dF_i}{\nu_i} = \frac{dF_A}{\nu_A} \tag{3-6}$$

$$\frac{F_i - F_{i,\,\text{inlet}}}{\nu_i} = \frac{F_A - F_{A,\,\text{inlet}}}{\nu_A} \tag{3-7}$$

$$F_i = F_{i,\,\text{inlet}} + \nu_i F_{A,\,\text{inlet}}\chi \tag{3-8}$$

Since the molar flow rate of component i (F_i) is defined as the product of total mass flow rate (i.e., ρq) and component i's mass fraction (ω_i) divided by its molecular weight MW_i,

$$F_i = \frac{\omega_i \rho q}{\text{MW}_i} \tag{3-9}$$

it follows directly that component mass fractions are linear functions of conversion:

$$\omega_i = \omega_{i,\,\text{inlet}} + \frac{\nu_i(\text{MW}_i)\omega_{A,\,\text{inlet}}}{\text{MW}_A}\chi \tag{3-10}$$

This result does not depend on whether the total number of moles is conserved. In other words, it is not necessary that the sum of stoichiometric coefficients for all reactants and products vanish. In contrast, the gas-phase mole fraction of component i is defined as the molar flow rate of component i divided by the total molar flow rate:

$$y_i = \frac{F_i}{\sum_j F_j} \qquad 1 \le j \le N \tag{3-11}$$

In general, mole fractions are not linear functions of conversion because the total number of moles and the total molar flow rate are not constant when $\delta = \sum_i \nu_i \neq 0$. For this particular problem, $\delta = -2$. In summary, the easiest approach to performing a weighted average of heat capacities of all components in the mixture is to use a mass-fraction-weighted sum of the temperature-averaged specific heat of each pure component. Hence,

$$\langle C_{p,\,\text{mixture}}\rangle = \sum_i \omega_i \langle C_{p,\,\text{component}\,i}\rangle \qquad 1 \le i \le N \tag{3-12}$$

Now, the heat capacity of the mixture is a linear function of conversion, and the temperature dependence has been averaged. The final result for the heat capacity of the mixture in units of cal/g·K is

$$\langle C_{p,\,\text{mixture}}\rangle = \sum_i \omega_{i,\,\text{inlet}}\langle C_{p,\,\text{component}\,i}\rangle + \frac{\chi\,\omega_{\text{A, inlet}}}{\text{MW}_\text{A}}\sum_i \nu_i(\text{MW}_i)\langle C_{p,\,\text{component}\,i}\rangle \tag{3-13}$$

The feed stream to the reactor is based on a 2 : 1 molar flow rate ratio of hydrogen to carbon monoxide. This corresponds to an inlet CO mass fraction of $\omega_{\text{A, inlet}} = 0.875$. The heat capacity of the mixture for this specific problem reduces to

$$\langle C_{p,\,\text{mixture}}\rangle = 0.65 - 0.26\ \chi \qquad \text{(cal/g·K)} \tag{3-14}$$

Since the maximum conversion required to design the reactor and allowed by equilibrium constraints is on the order of 10% (i.e., $\chi \approx 0.10$), the conversion-dependent term contributes ≈0.03 cal/g·K, which is less than 5% of the total heat capacity near the reactor outlet and much less near the inlet. Hence, it seems reasonable to neglect the conversion dependence of $\langle C_{p,\,\text{mixture}}\rangle$ and use 0.65 cal/g·K throughout the adiabatic tubular reactor.

3-3 PLUG-FLOW MASS BALANCE IN TERMS OF CO CONVERSION

Now, the coupled mass and thermal energy balances can be combined and integrated analytically to obtain a linear relation between temperature and conversion under nonequilibrium (i.e., kinetic) conditions because it is not necessary to consider the temperature and conversion dependence of $\langle C_{p,\,\text{mixture}}\rangle$. At high-mass-transfer Peclet numbers, axial diffusion can be neglected relative to convective mass transfer, and the mass balance is expressed in terms of molar flow rate F_i and differential volume dV for a gas-phase tubular reactor with one chemical reaction:

$$\frac{dF_i}{dV} = \nu_i \mathfrak{R} \tag{3-15}$$

where the intrinsic rate law $\mathfrak{R}$ has units of moles per volume per time for homogeneous kinetics. Hence, it is obvious that dF_i/ν_i is independent of component i, which leads to stoichiometric relations for molar flow rate (3-8), mole fraction, and mass fraction (3-10). At the differential level, molar flow rate and mass fraction are linearly related when the total mass flow rate (i.e., ρq) is constant. Equation (3-9) yields:

$$dF_i = \frac{d(\omega_i \rho q)}{\text{MW}_i} = \rho q \frac{d\omega_i}{\text{MW}_i} \tag{3-16}$$

which is reasonable at steady state with one inlet stream and one outlet stream. Hence,

$$\rho q \frac{d\omega_i}{dV} = \nu_i(\text{MW}_i)\mathfrak{R} \tag{3-17}$$

The final form of the mass balance is written in terms of the conversion of CO by invoking the linear relation between ω_i and χ. Hence, equation (3-10) yields:

$$d\omega_i = \frac{\nu_i(\mathrm{MW}_i)\omega_{\mathrm{A,\,inlet}}}{\mathrm{MW_A}}\,d\chi \tag{3-18}$$

and

$$\omega_{\mathrm{A,\,inlet}}\rho q\frac{d\chi}{dV} = (\mathrm{MW_A})\mathfrak{R} \tag{3-19}$$

This equation is integrated numerically to determine the reactor volume that corresponds to 8% conversion of CO. However, this task cannot be accomplished until one employs kinetics, thermodynamics, and stoichiometry to express the rate law in terms of temperature, pressure, and conversion. Temperature can also be expressed in terms of conversion upon consideration of the thermal energy balance at high-heat-transfer Peclet numbers.

3-4 THERMAL ENERGY BALANCE FOR A DIFFERENTIAL REACTOR

The first law of thermodynamics for an open system at steady state that performs no work on the surroundings other than pV work across the inlet and outlet planes of a differential control volume is written with units of energy per volume per time:

$$\rho q\frac{dh}{dV} = \frac{dQ}{dV} \tag{3-20}$$

where h is the specific enthalpy of the reactive mixture, which contains several components, and Q is the rate at which thermal energy enters the control volume across the lateral surface. The right-hand side of this thermal energy balance vanishes for adiabatic operation. Under nonadiabatic conditions, the differential rate of conductive heat transfer at the reactor wall (dQ) with units of energy per time is expressed in terms of an appropriate heat transfer coefficient, an instantaneous temperature difference, and the differential lateral surface area. Specific enthalpy conveniently includes contributions from both internal energy and pV work. Heat effects due to the endothermic or exothermic nature of the chemical reaction are accounted for by the total differential of specific enthalpy for a multicomponent mixture. For single-phase behavior of a mixture of N components in which the chemical reactions have not reached equilibrium, the phase rule suggests that $N + 1$ independent variables are required to describe an intensive thermodynamic property, such as specific enthalpy. By choosing temperature T, pressure p, and $N - 1$ mass fractions ω_i (i.e., $1 \le i \le N - 1$), one is assured that the thermal energy balance will be expressed in terms of

temperature and the specific heat of the mixture at constant pressure, $\langle C_{p,\,\text{mixture}}\rangle$. Hence, the objectives are to (1) calculate the total differential of specific enthalpy, (2) apply the first law of thermodynamics for open systems, and (3) generate temperature profiles for nonisothermal reactor performance.

3-5 THERMODYNAMICS OF MULTICOMPONENT MIXTURES

In agreement with the phase rule for single-phase behavior, if

$$h = h(T,\, p,\, \omega_1,\, \omega_2,\, \ldots,\, \omega_{N-1}) \tag{3-21}$$

then the total differential of specific enthalpy is expressed as follows:

$$dh = \left(\frac{\partial h}{\partial T}\right)_{p,\,\text{composition}} dT + \left(\frac{\partial h}{\partial p}\right)_{T,\,\text{composition}} dp + \sum_i \left(\frac{\partial h}{\partial \omega_i}\right)_{T,p,\ \text{all}\ \omega_{j[j\neq i,N]}} d\omega_i \tag{3-22}$$

where the summation includes the first $N-1$ components in the mixture. The temperature coefficient of specific enthalpy at constant pressure and composition is identified as the heat capacity of the mixture. Hence,

$$\langle C_{p,\,\text{mixture}}\rangle = \left(\frac{\partial h}{\partial T}\right)_{p,\,\text{composition}} \tag{3-23}$$

Standard thermodynamic formalism for the total differential of specific enthalpy in terms of its natural variables (i.e., via Legendre transformation, see equations 29-20 and 29-24*b*) allows one to calculate the pressure coefficient of specific enthalpy via a Maxwell relation and the definition of the coefficient of thermal expansion, α.

$$dh = T\,ds + v\,dp + \text{terms that account for variations in composition} \tag{3-24}$$

$$\left(\frac{\partial h}{\partial p}\right)_{T,\,\text{composition}} = T\left(\frac{\partial s}{\partial p}\right)_{T,\,\text{composition}} + v \tag{3-25}$$

$$\left(\frac{\partial s}{\partial p}\right)_{T,\,\text{composition}} = -\left(\frac{\partial v}{\partial T}\right)_{p,\,\text{composition}} \qquad \text{(Maxwell relation)} \tag{3-26}$$

$$\left(\frac{\partial v}{\partial T}\right)_{p,\,\text{composition}} \equiv v\alpha \tag{3-27}$$

$$\left(\frac{\partial h}{\partial p}\right)_{T,\,\text{composition}} = v(1-\alpha T) \tag{3-28}$$

The pressure coefficient of specific enthalpy is identically zero for ideal gases, but the thermal energy balance must include a pressure contribution for other fluids. The partial derivative of h in the summation of (3-22), $(\partial h/\partial \omega_i)_{T,p,\ \text{all}\ \omega_{j[j\neq i,N]}}$,

resembles a partial molar quantity because temperature, pressure, and composition of 'almost' all of the other species are held constant. It is not possible to vary the mass fraction of component i while all other mass fractions remain constant because the necessary restriction that all mass fractions must sum to unity would be violated. In other words, at least two mass fractions must change, ω_i and ω_N. Changes in ω_N are not independent. They are equal and opposite to those of ω_i to guarantee that all mass fractions sum to unity. If specific enthalpy is replaced by extensive enthalpy H and mass fraction is replaced by mole numbers N_i, then one defines the partial molar enthalpy of component i (i.e., $\mathfrak{h}_i$) as

$$\left(\frac{\partial H}{\partial N_i}\right)_{T,\, p,\ \text{all}\ N_{j[j\neq i]}} = \mathfrak{h}_i \tag{3-29}$$

The partial derivative of interest, $(\partial h/\partial \omega_i)_{T,\, p,\ \text{all}\ \omega_{j[j\neq i,N]}}$, is written in terms of partial molar enthalpies, $\mathfrak{h}_i$. Derivation of the exact expression can be found in Section 26-2 (see equations 26-30 and 26-31). The total differential of specific enthalpy is written in terms of temperature, pressure, and compositional variations as

$$dh = \langle C_{p,\,\text{mixture}} \rangle\, dT + v(1-\alpha T)\, dp + \sum_i \left(\frac{\mathfrak{h}_i}{\text{MW}_i} - \frac{\mathfrak{h}_N}{\text{MW}_N}\right) d\omega_i \tag{3-30}$$

where MW is molecular weight and the summation in (3-30) includes the first $N-1$ components. One invokes the restriction that all mass fractions must sum to unity (i.e., a constant) and differential changes in all mass fractions must sum to zero. Hence, the summation in equation (3-30) is simplified as follows:

$$\sum_i d\omega_i = -d\omega_N \qquad 1 \le i \le N-1 \tag{3-31}$$

$$\begin{aligned}\sum_{i=1}^{N-1} \left(\frac{\mathfrak{h}_i}{\text{MW}_i} - \frac{\mathfrak{h}_N}{\text{MW}_N}\right) d\omega_i &= \sum_{i=1}^{N-1} \frac{\mathfrak{h}_i}{\text{MW}_i}\, d\omega_i - \frac{\mathfrak{h}_N}{\text{MW}_N} \sum_{i=1}^{N-1} d\omega_i \\ &= \sum_{i=1}^{N} \frac{\mathfrak{h}_i}{\text{MW}_i}\, d\omega_i \end{aligned} \tag{3-32}$$

The mass balance for a differential plug-flow reactor (equation 3-17) that operates at high-mass-transfer Peclet numbers allows one to replace $d\omega_i$ in (3-32):

$$d\omega_i = \nu_i (\text{MW}_i) \mathfrak{R} \frac{dV}{\rho q} \tag{3-33}$$

Now the total differential of specific enthalpy contains a chemical reaction contribution via the kinetic rate law $\mathfrak{R}$:

$$dh = \langle C_{p,\,\text{mixture}} \rangle\, dT + v(1-\alpha T)\, dp + \left(\sum_{i=1}^{N} \nu_i \mathfrak{h}_i\right) \mathfrak{R} \frac{dV}{\rho q} \tag{3-34}$$

The summation in (3-34) represents an exact expression for the molar enthalpy change due to chemical reaction, ΔH_{Rx} (see Tester and Modell, 1997, pp. 769–770):

$$\Delta H_{\mathrm{Rx}} = \sum_{i=1}^{N} \nu_i \mathfrak{h}_i \tag{3-35}$$

In practice, pure-component molar enthalpies are employed to approximate ΔH_{Rx}. This approximation is exact for ideal solutions only, when partial molar properties reduce to pure-component molar properties. In general, one accounts for more than the making and breaking of chemical bonds in (3-35). Nonidealities such as heats of solution and ionic interactions are also accounted for when partial molar enthalpies are employed. Now, the first law of thermodynamics for open systems, which contains the total differential of specific enthalpy, is written in a form that allows one to calculate temperature profiles in a tubular reactor:

$$\rho q \frac{dh}{dV} = \rho q \langle C_{p,\,\mathrm{mixture}} \rangle \frac{dT}{dV} + q(1 - \alpha T)\frac{dp}{dV} + (\Delta H_{\mathrm{Rx}})\mathfrak{R} = \frac{dQ}{dV} \tag{3-36}$$

The final form of the differential thermal energy balance for a generic plug-flow reactor that operates at high-mass and high-heat-transfer Peclet numbers allows one to predict temperature as a function of reactor volume:

$$\rho q \langle C_{p,\,\mathrm{mixture}} \rangle \frac{dT}{dV} = \frac{dQ}{dV} - q(1 - \alpha T)\frac{dp}{dV} + (-\Delta H_{\mathrm{Rx}})\mathfrak{R} \tag{3-37}$$

It should be obvious from the discussion above that thermodynamics plays a major role in the development of reactor design formulas when heat effects due to chemical reaction are important.

3-6 COUPLED HEAT AND MASS TRANSFER

For adiabatic performance of a variable-volume gas-phase tubular reactor, the first term on the right-hand side of (3-37) is identically zero, and the second term vanishes if the gas mixture behaves ideally. Hence, the coupled plug-flow mass and thermal energy balances are

$$\omega_{\mathrm{A,\,inlet}} \rho q \frac{d\chi}{dV} = (\mathrm{MW_A})\mathfrak{R} \tag{3-38}$$

$$\rho q \langle C_{p,\,\mathrm{mixture}} \rangle \frac{dT}{dV} = (-\Delta H_{\mathrm{Rx}})\mathfrak{R} \tag{3-39}$$

These coupled first-order ODEs allow one to generate conversion and temperature profiles as a function of reactor volume. It is not appropriate to introduce average residence time unless the fluid is incompressible. If one combines these balances

and eliminates the kinetic rate law $\mathfrak{R}$, which could be rather complex for reversible reactions, then conversion and temperature obey the following simple relation under nonequilibrium conditions:

$$\omega_{\mathrm{A,\,inlet}}(-\Delta H_{\mathrm{Rx}})\frac{d\chi}{dV} = \mathrm{MW_A}\langle C_{p,\,\mathrm{mixture}}\rangle\frac{dT}{dV} \tag{3-40}$$

Integration from the reactor inlet where $V = 0$, $\chi = 0$, and $T = T_{\mathrm{inlet}}$ to any position downstream allows one to estimate analytically the reactor temperature in terms of conversion if the heat capacity of the mixture is averaged over the operating temperature range and its dependence on conversion is neglected. The desired relation is

$$T = T_{\mathrm{inlet}} + \frac{\chi(-\Delta H_{\mathrm{Rx}})\omega_{\mathrm{A,\,inlet}}}{\mathrm{MW_A}\langle C_{p,\,\mathrm{mixture}}\rangle} \tag{3-41}$$

For the production of methanol from a stoichiometric feed of CO and H_2, the final expression for nonequilibrium reactor temperature is

$$T(K) = 340 + 1042.5\chi \tag{3-42}$$

The temperature-dependent physical constants in the mass balance (i.e., the kinetic rate constant and the equilibrium constant) are expressed in terms of nonequilibrium conversion χ using the linear relation (3-42). The concept of local equilibrium allows one to rationalize the definition of temperature and calculate an equilibrium constant when the system is influenced strongly by kinetic changes. In this manner, the mass balance is written with nonequilibrium conversion of CO as the only dependent variable, and the problem can be solved by integrating only one ordinary differential equation for χ as a function of reactor volume.

3-7 KINETICS AND THERMODYNAMICS OF ELEMENTARY REVERSIBLE REACTIONS IN THE GAS PHASE

It is necessary to focus on details of the rate law $\mathfrak{R}$ before the mass balance,

$$\omega_{\mathrm{A,\,inlet}}\rho q\frac{d\chi}{dV} = (\mathrm{MW_A})\mathfrak{R} \tag{3-43}$$

can be integrated to calculate the required reactor volume that corresponds to 8% conversion of CO (i.e., $\chi = 0.08$). This is an elementary reversible reaction in the gas phase where the equilibrium constant is employed to write the kinetic rate law for the backward step. The reaction rate is third order in the forward direction and first order in the backward direction. This implies that the forward and backward kinetic rate constants have different units (i.e., mol/vol·time·atm^n) and that the equilibrium constant based on gas-phase partial pressures, $K_p = \prod_{i=1}^{N}(p_i)^{\nu_i}$, is

not dimensionless, in general. Based on the units of the pre-exponential factor for the forward kinetic rate constant (mol/cm^3·min·atm^3), it should be obvious that the rate law must be constructed in terms of gas-phase partial pressures instead of molar densities. Hence,

$$\mathfrak{R} = k_{\text{forward}}(T)\, p_{\text{CO}} (p_{\text{H}_2})^2 - k_{\text{backward}}(T)\, p_{\text{CH}_3\text{OH}} \tag{3-44}$$

The principle of microscopic reversibility allows one to express the backward rate constant in terms of the forward rate constant divided by K_p, which is the equilibrium constant based on gas-phase partial pressures. K_p has units of pressure to the power δ, where δ is the sum of the stoichiometric coefficients (i.e., $\delta = -2$ for this problem). Handbook values for standard-state free energies of formation at 298 K are used to calculate the Gibbs free-energy change for reaction at 298 K (i.e., $\Delta G^\circ_{\text{Rx, 298}}$), and this is used to calculate a dimensionless equilibrium constant, $K_{\text{equilibrium, } f}$ at 298 K, based on fugacity ratios or activities. The temperature dependence of this equilibrium constant is given by (3-61) and (3-65). Chemical equilibrium for a generic chemical reaction implies that

$$\sum_{i \text{ components}} \nu_i \mu_i (T,\ p,\ \text{composition}) = 0 \tag{3-45}$$

where ν_i and μ_i are the stoichiometric coefficient and chemical potential of component i, respectively. One expresses μ_i in the reactive mixture at equilibrium in terms of $[\mu_{i,\text{ pure}}(T)]^\circ$, the latter of which is based on a pure-component reference state where the fugacity is 1 atm. Hence,

$$\mu_i(T,\ p,\ \text{composition}) = [\mu_{i,\text{ pure}}(T)]^\circ + RT \ln \frac{f_{i,\text{ mixture}}}{f_{i,\text{ pure}}} \tag{3-46}$$

where $f_{i,\text{ mixture}}$ and $f_{i,\text{ pure}}$ represent the fugacity of component i in the reactive mixture and in the pure-component reference state, respectively. The statement of chemical equilibrium yields

$$\begin{aligned} \sum_{i \text{ components}} \nu_i [\mu_{i,\text{ pure}}(T)]^\circ &= -RT \sum_{i \text{ components}} \nu_i \ln \frac{f_{i,\text{ mixture}}}{f_{i,\text{ pure}}} \\ &= -RT \ln \prod_{i \text{ components}} \left(\frac{f_{i,\text{ mixture}}}{f_{i,\text{ pure}}} \right)^{\nu_i} \end{aligned} \tag{3-47}$$

One identifies the stoichiometric-coefficient-weighted sum of pure-component chemical potentials in the reference states, at unit fugacity, with the standard-state free-energy change for chemical reaction, since $[\mu_{i,\text{ pure}}(T)]^\circ$ is equivalent to the molar Gibbs free energy of pure component i in this reference state. Hence,

$$\sum_{i \text{ components}} \nu_i [\mu_{i,\text{ pure}}(T)]^\circ = \Delta G^\circ_{\text{Rx}}(T) \tag{3-48}$$

The equilibrium constant from thermodynamics is defined as follows in terms of fugacity ratios:

$$K_{\text{equilibrium, } f} \equiv \prod_{i \text{ components}} \left(\frac{f_{i,\text{ mixture}}}{f_{i,\text{ pure}}} \right)^{\nu_i} \tag{3-49}$$

Now, the statement of chemical equilibrium reduces to

$$\Delta G^{\circ}_{\text{Rx}}(T) = -RT \ln K_{\text{equilibrium, } f} \tag{3-50}$$

If the gas-phase reactive mixture behaves ideally at low to moderate pressures, all fugacity coefficients are very close to unity and the fugacity of each component in the mixture can be approximated by its partial pressure. Hence,

$$K_{\text{equilibrium, } f} = \prod_{i \text{ components}} (p_i / f_{i,\text{ pure}})^{\nu_i} = \frac{K_p}{K^{\circ}_{\text{standard state}}} = \exp\left[-\frac{\Delta G^{\circ}_{\text{Rx}}(T)}{RT} \right] \tag{3-51}$$

where $K^{\circ}_{\text{standard state}}$ is the equilibrium constant for the chemical reaction using a standard-state fugacity (i.e., $f_{i,\text{ pure}}$) of 1 atm for each component. As illustrated above in (3-46), these standard-state fugacities define the pure-component reference state about which the concentration dependence of the chemical potential is expanded, and they identify the standard state for calculation of $\Delta G^{\circ}_{\text{Rx}}$ via (3-48). Hence, $K^{\circ}_{\text{standard state}}$ always has a value of unity when standard-state fugacities are defined as 1 atm. Most important, this standard-state equilibrium constant has units of atmospheres to the power δ, which match the units of K_p. In other words, at any temperature,

$$K_p(T) = K^{\circ}_{\text{standard state}} \exp\left[-\frac{\Delta G^{\circ}_{\text{Rx}}(T)}{RT} \right] [=] (\text{atm})^{\delta} \tag{3-52}$$

and all partial pressures in the rate law must be expressed in atmospheres. The homogeneous kinetic rate law with units of moles per volume per time is

$$\mathfrak{R} = k_{\text{forward}}(T) \left\{ p_{\text{CO}} (p_{\text{H}_2})^2 - \frac{p_{\text{CH}_3\text{OH}}}{K_p(T)} \right\} \tag{3-53}$$

Dalton's law for ideal gas mixtures is used to express partial pressures as a product of total pressure in atmospheres and mole fraction y_i. Based on the definition of CO conversion χ in terms of molar flow rate for gas-phase flow reactors and the fact that the mole fraction of component i is equal to its molar flow rate divided by the total molar flow rate, the following expression is obtained for the mole fraction of component i:

$$F_i = F_{i,\text{ inlet}} + \nu_i F_{\text{A, inlet}} \chi \tag{3-54}$$

$$y_i = \frac{F_i}{\Sigma_j F_j} = \frac{\Theta_i + \nu_i \chi}{\delta \chi + \Sigma_j \Theta_j} \qquad 1 \le j \le N \tag{3-55}$$

where ν_i is the stoichiometric coefficient, δ the sum of stoichiometric coefficients, and Θ_i the inlet molar flow rate ratio of component i with respect to key limiting reactant A:

$$\Theta_i = \frac{F_{i,\,\text{inlet}}}{F_{\text{A},\,\text{inlet}}} \tag{3-56}$$

Hence, $\Theta_{\text{A}} = 1$, by definition. In summary, all partial pressures in the rate law should be written as a product of total pressure and mole fraction. Then, mole fractions can be expressed in terms of the conversion of CO. Alternatively, the ideal gas law can be used to express partial pressures p_i as $C_i RT$, and the conversion dependence of molar density C_i is tabulated by Fogler (1999, p. 96) for variable-volume gas-phase flow reactors. It should be emphasized that $y_i p_{\text{total}}$ and $C_i RT$ generate the same function of conversion when the ε parameter in Fogler's expressions is written as

$$\varepsilon = \frac{\delta}{\Sigma_j \Theta_j} \qquad 1 \le j \le N \tag{3-57}$$

The factor of T in the molar density expressions for nonisothermal problems cancels with RT when partial pressures are calculated via $C_i RT$.

The temperature dependence of the dimensionless equilibrium constant from thermodynamics, $K_{\text{equilibrium},\,f}(T)$, is obtained quantitatively by differentiating equation (3-50):

$$-\frac{d \ln K_{\text{equilibrium},\,f}}{dT} = \frac{d(\Delta G^\circ_{\text{Rx}}/RT)}{dT} = \frac{1}{RT}\frac{d(\Delta G^\circ_{\text{Rx}})}{dT} - \frac{\Delta G^\circ_{\text{Rx}}}{RT^2} \tag{3-58}$$

The temperature dependence of ΔG is given by $-\Delta S$ at constant pressure and composition because

$$dG = -S\,dT + V\,dp + \sum_i \mu_i\,dN_i \qquad 1 \le i \le N \tag{3-59}$$

Hence, the final result, which allows one to calculate $K_{\text{equilibrium},\,f}$ at any temperature, is

$$\frac{d \ln K_{\text{equilibrium},\,f}}{dT} = \frac{\Delta S^\circ_{\text{Rx}}}{RT} + \frac{\Delta G^\circ_{\text{Rx}}}{RT^2} = \frac{\Delta H^\circ_{\text{Rx}}}{RT^2} \tag{3-60}$$

which is a classic expression in any thermodynamics text (see Smith and Van Ness, 1987, p. 508; Tester and Modell, 1997, p. 765). Equation (3-60) is typically integrated with respect to temperature under the assumption that the enthalpy change for reaction is not a function of temperature. Hence, $\Delta H^\circ_{\text{Rx}}$ is calculated from enthalpies of formation at 298 K, which are obtained from calorimetry and tabulated in handbooks. Upon integration from 298 K to temperature T, one obtains

$$\ln K_{\text{equilibrium},\,f} = A + \frac{B}{T} \tag{3-61}$$

$$A = \frac{\Delta S^{\circ}_{\mathrm{Rx},\,298}}{R} = -26.7 \tag{3-62}$$

$$B = -\frac{\Delta H^{\circ}_{\mathrm{Rx},\,298}}{R} = 10{,}913\ \mathrm{K} \tag{3-63}$$

for the production of methanol from CO and H_2.

This is exactly the same as the final result that one obtains if the temperature dependence of $\Delta G^{\circ}_{\mathrm{Rx}}$ is approximated as

$$\Delta G^{\circ}_{\mathrm{Rx}} = \Delta H^{\circ}_{\mathrm{Rx},\,298} - T\,\Delta S^{\circ}_{\mathrm{Rx},\,298} \tag{3-64}$$

and the dimensionless equilibrium constant $K_{\mathrm{equilibrium},\,f}$ is calculated from equation (3-50):

$$\ln K_{\mathrm{equilibrium},\,f} = -\frac{\Delta G^{\circ}_{\mathrm{Rx}}}{RT} = -\frac{\Delta H^{\circ}_{\mathrm{Rx},\,298} - T\,\Delta S^{\circ}_{\mathrm{Rx},\,298}}{RT} \tag{3-65}$$

For the synthesis of methanol from CO and H_2, $A < 0$ because there is a decrease in the number of gas-phase moles upon reaction [i.e., $\Sigma_i(\nu_i) < 0$], and $B > 0$ because the reaction is exothermic. The final form of the rate law for the production of methanol is

$$\mathfrak{R} = k_{f,\,p\infty} \exp\left(\frac{-E_{\mathrm{act},\,p}}{RT}\right)[p(\mathrm{atm})]^3 \left\{ y_{\mathrm{CO}} y_{\mathrm{H_2}}^2 - \frac{[p(\mathrm{atm})]^{-2} y_{\mathrm{CH_3OH}}}{\exp(A + B/T)} \right\} \tag{3-66}$$

where

$$T = T_{\mathrm{inlet}} + \frac{\chi(-\Delta H_{\mathrm{Rx}})\omega_{\mathrm{A,\,inlet}}}{\mathrm{MW_A}\langle C_{p,\,\mathrm{mixture}}\rangle} = 340 + 1042.5\chi\,(\mathrm{K})$$

$$y_i = \frac{\Theta_i + \nu_i \chi}{\delta\chi + \sum_j \Theta_j} \qquad 1 \le j \le N$$

$$\delta = -2,\ \Theta_{\mathrm{CO}} = 1,\ \Theta_{\mathrm{H_2}} = 2,\ \Theta_{\mathrm{CH_3OH}} = 0,\ \text{and}\ \sum_{j=1}^{N} \Theta_j = 3.$$

3-8 INTEGRATION OF THE NONISOTHERMAL PFR DESIGN EQUATION

Now, it is possible to integrate the plug-flow differential mass balance for conversion as a function of reactor volume:

$$\omega_{\mathrm{A,\,inlet}} \rho q \frac{d\chi}{dV} = (\mathrm{MW_A})\mathfrak{R} \tag{3-67}$$

If the mass flow rate is expressed in grams per minute, the pre-exponential factor for the forward kinetic rate constant has units of mol/cm^3·min·atm^3, and the total pressure is expressed in atmospheres, then the reactor volume has units of cubic centimeters. The problem is solved in terms of an arbitrary mass flow rate as follows:

$$\omega_{\mathrm{A,\,inlet}} \frac{d\chi}{d(V/\rho q)} = (\mathrm{MW_A})\Re \tag{3-68}$$

where the independent variable is reactor volume V divided by total mass flow rate. This rearrangement is valid for both gas- and liquid-phase flow reactors because the total mass flow rate is constant unless material escapes across a permeable wall, such as in blood capillaries and hollow-fiber membranes. The ideal plug-flow differential mass balance is solved using a fourth-order correct Runge–Kutta–Gill numerical integration scheme. The truncation error that accumulates with each step is monitored, and integration should cease if this error becomes too large. If one increments $V/\rho q$ from 0 at the reactor inlet to 1 cm^3·min/g in 100 steps, then the conversion of CO achieves an asymptotic value of 0.089, as illustrated in Figure 3-1. Alternatively, one could increment CO conversion from $\chi = 0$ at the inlet to slightly less than 0.089 (i.e., 176 steps)

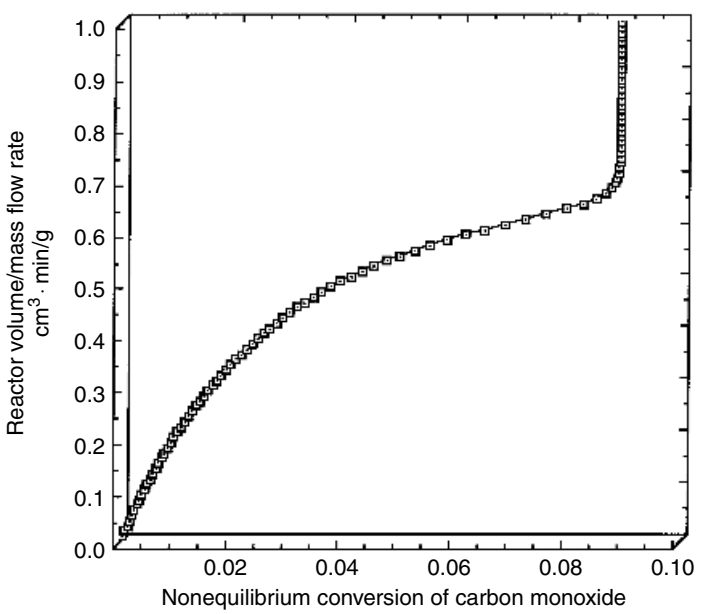

Figure 3-1 Reactor volume vs. nonequilibrium conversion of CO in a single-stage adiabatic plug-flow reactor that produces methanol from CO and H_2. The steep increase in reactor volume near 9% CO conversion is a consequence of near-equilibrium conditions when the feed enters at 340 K.

and calculate $V/\rho q$ via numerical integration. The desired conversion of 8% corresponds to

$$\frac{V}{\rho q} = 0.64 \text{ cm}^3\cdot\text{min/g} \qquad \text{at } \chi = 0.08 \tag{3-69}$$

Hence, reactor volume $V = \pi R^2 L = 640$ cm^3 and the reactor length L is about 204 cm when the total mass flow rate is 1000 g/min. These results are valid at high-mass and heat-transfer Peclet numbers.

PROBLEMS

3-1. Benzene is hydrogenated to cyclohexane in a series of two gas-phase tubular reactors. A stoichiometric feed of benzene and hydrogen enters the first reactor. The reversible elementary chemical reaction is

$$C_6H_6(g) + 3H_2(g) \rightleftharpoons C_6H_{12}(g)$$

and a catalyst is not required. The appropriate gas-phase thermodynamic data are provided in Table 3-3.

(a) At 5 atm total pressure, calculate the equilibrium temperature when the equilibrium conversion of the key reactant, benzene, is 75%. Remember that the reactor is thermally insulated from the surroundings.

(b) Obtain an expression for the homogeneous kinetic rate law for this elementary reversible reaction that should be used in the appropriate mass balance to design the size of the first tubular reactor in series. This rate law depends on temperature, pressure, and conversion of benzene. Remember that a stoichiometric feed of benzene and hydrogen enters the first reactor on a molar-flow-rate basis.

TABLE 3-3 Pure-Component Gas-Phase Thermodynamic Properties at 298 K for C_6H_6, H_2, and C_6H_{12} (cal/g mol)

Property	Benzene (C_6H_6)	Hydrogen (H_2)	Cyclohexane (C_6H_{12})
$\Delta G^\circ_{\text{formation}}$	30,989	0	7,590
$\Delta H^\circ_{\text{formation}}$	19,820	0	−29,430
Molecular weight	78	2	84
Inlet mole fraction[a]	0.25	0.75	0
Inlet mass fraction[a]	0.93	0.07	0

[a] Characteristics of the feed stream to a gas-phase plug-flow reactor are provided for both reactants

(c) Sketch the temperature profile as a function of reactor length. Based on a consideration of the residence time for convective mass transfer through the reactor and the time constant for reversible chemical reaction, it is estimated that equilibrium conditions are almost achieved when the length of the reactor is 10 m. Be sure to sketch the temperature profile from $z = 0$ to 15 m, and indicate the effect that near-equilibrium conditions will have on the temperature in this first adiabatically enclosed reactor in series.

(d) Calculate a numerical value for the adiabatic temperature rise (Kelvin) in the first ideal plug-flow tubular reactor when the conversion of benzene is 30% based on molar flow rates. A 1 : 3 molar ratio of benzene to hydrogen enters the reactor, and the temperature-averaged specific heat is 0.85 cal/g·K.

(e) Is your answer to part (d) larger, smaller, the same, or too complex to evaluate relative to the adiabatic temperature rise in one well-mixed CSTR when the feed streams are identical and the final conversion of benzene is 30%?

(f) Is your answer to part (d) larger, smaller, the same, or too complex to evaluate relative to the adiabatic temperature rise in one well-mixed CSTR if the feed streams are identical and both reactors have the same volume $V_{CSTR} = V_{PFR}$, and the same residence time, $\tau_{CSTR} = \tau_{PFR}$?

(g) Should the reactive gas-phase mixture be heated or cooled prior to entering the second adiabatic tubular reactor in series to obtain higher conversion of benzene to cyclohexane? Provide support for your answer.

(h) What equations must be solved to calculate the length of a double-pipe heat exchanger between each reactor if the liquid-phase cooling fluid in the annular region moves countercurrent to the gas-phase mixture of benzene, hydrogen, and cyclohexane in the inner tube. The overall objective is to obtain a temperature of 400 K for the reactive fluid in the inlet stream to all the tubular reactors in series. Be sure to include boundary conditions in your final answer.

(i) Should the second PFR in series operate at higher total pressure, lower total pressure, or the same total pressure relative to the first reactor? The overall objective is to obtain the highest possible conversion of benzene to cyclohexane.

3-2. Use Figure 3-1 as a starting point and sketch the relation between reactor volume and nonequilibrium conversion of carbon monoxide if the insulation that covers the wall of the tubular reactor is removed. Think about the effect that heat transfer across the wall of the reactor has on the temperature of the reactive fluid. Then, consider the effect of temperature on the kinetics of the reaction, and the effect of chemical kinetics on the reactor volume required to achieve a specified conversion. Finally, consider the effect of temperature

on the equilibrium conversion for an exothermic reaction via Le Châtelier's principle. You must illustrate differences in both kinetic and equilibrium conditions for your graph when the insulation is removed relative to the one in Figure 3-1. Include two graphs of reactor volume vs. CO conversion on one set of axes, where one of the graphs is exactly the same as the one in Figure 3-1 for adiabatic operation.

Transport Phenomena for Chemical Reactor Design. Laurence A. Belfiore
Copyright © 2003 John Wiley & Sons, Inc.
ISBN: 0-471-20275-4

4

COUPLED HEAT AND MASS TRANSFER IN NONISOTHERMAL LIQUID-PHASE TUBULAR REACTORS WITH STRONGLY EXOTHERMIC CHEMICAL REACTIONS

4-1 STRATEGIES TO CONTROL THERMAL RUNAWAY

When exothermic chemical reactions are characterized by large enthalpy changes, a design strategy must be implemented to remove the heat and minimize the temperature rise within the reactive fluid. Thermal runaway is identified by upward curvature and a steep increase in temperature vs. average residence time τ that will generate charred products which are not very useful. Six possible solutions are described below to prevent the phenomenon of thermal runaway from occurring. These successful strategies are summarized here for tubular reactors with the flexibility to implement cocurrent or countercurrent cooling in a concentric double-pipe configuration.

1. Lower the inlet temperature of the reactive fluid.
2. Reduce the outer wall temperature of the reactor.
3. Increase the surface-to-volume ratio of the reactor.
4. Increase the flow rate of a cocurrent cooling fluid.
5. Employ a cooling fluid that undergoes a strongly endothermic reaction.
6. Reduce the inlet temperature of a countercurrent cooling fluid.

4-1.1 Plug-Flow Mass Balance That Neglects Axial Diffusion

At high-mass-transfer Peclet numbers, the steady-state mass balance for component i, with units of moles per time, is expressed in terms of its molar flow rate F_i and differential volume $dV = \pi R^2 \, dz$ for a tubular reactor. If species i

participates in j reactions, then:

rate of convective input + rate of production = rate of convective output (4-1)

$$\begin{aligned} \left(F_{i,z}\right)_{\text{inlet}} + \sum_j \nu_{ij} \mathfrak{R}_j \, dV &= \left(F_{i,z+dz}\right)_{\text{outlet}} \\ dF_i = \left(F_{i,z+dz}\right)_{\text{outlet}} - \left(F_{i,z}\right)_{\text{inlet}} &= \sum_j \nu_{ij} \mathfrak{R}_j \, dV \end{aligned} \tag{4-2}$$

where z represents the primary flow direction in cylindrical coordinates, ν_{ij} the stoichiometric coefficient of species i in reaction j, and the intrinsic rate law for the j^{th} chemical reaction $\mathfrak{R}_j$ has units of moles per volume per time for homogeneous kinetics. The molar flow rate of component i (F_i) is defined as the product of total mass flow rate (i.e., $q\rho_{\text{total}}$) and component mass fraction (ω_i) divided by its molecular weight MW_i:

$$F_i = \frac{\omega_i q \rho_{\text{total}}}{\text{MW}_i} \tag{4-3}$$

where q represents volumetric flow rate and ρ_{total} is the overall mass density of the reactive mixture. If there is one inlet stream and one outlet stream, then the total mass flow rate through the tubular reactor remains constant and the differential mass balance allows one to predict changes in mass fraction for each species:

$$d\omega_i = \text{MW}_i \sum_j \nu_{ij} \mathfrak{R}_j \frac{dV}{q\rho_{\text{total}}} \tag{4-4}$$

This result will be employed in conjunction with the thermal energy balance for reactive systems. If there is only one chemical reaction, then subscript j is not required and dF_i/ν_i is independent of component i:

$$\frac{dF_i}{\nu_i} = \frac{dF_{\text{A}}}{\nu_{\text{A}}} = \mathfrak{R} \, dV \tag{4-5}$$

which leads to stoichiometric relations for molar flow rate, mole fraction, and mass fraction via the mass balance with convection and chemical reaction. Integration of (4-5) from the reactor inlet to any position downstream produces the following macroscopic flow rate relation:

$$\frac{F_i - F_{i,\,\text{inlet}}}{\nu_i} = \frac{F_{\text{A}} - F_{\text{A,\,inlet}}}{\nu_{\text{A}}} \tag{4-6}$$

For flow reactors, the conversion of key-limiting reactant A is typically defined in terms of its molar flow rate (i.e., F_{A}):

$$\chi \equiv \frac{F_{\text{A,\,inlet}} - F_{\text{A}}}{F_{\text{A,\,inlet}}} \tag{4-7}$$

Hence, stoichiometry reveals that all molar flow rates are linear functions of conversion. This is obvious when $F_A - F_{A,\,inlet}$ in the macroscopic flow rate relation (4-6) is replaced by $-\chi F_{A,\,inlet}$:

$$F_i = F_{i,\,inlet} + \nu_i F_{A,\,inlet}\chi \tag{4-8}$$

and $\nu_A = -1$ for reactant A. The macroscopic stoichiometric flow rate relation also reveals that component mass fractions are linear functions of conversion via (4-3) and (4-8):

$$\omega_i = \omega_{i,\,inlet} + \frac{\nu_i(\mathrm{MW}_i)\omega_{A,\,inlet}}{\mathrm{MW}_A}\,\chi \tag{4-9}$$

when the total mass flow rate through the reactor is constant. This is reasonable at steady state with one inlet stream and one outlet stream. One must exercise caution when applying the results in this chapter if, for example, material escapes across the lateral wall of a hollow-fiber ultrafiltration membrane because the overall mass flow rate through the fiber decreases continuously. The stoichiometric relation for mass fractions (i.e., 4-9) does not rely on conservation of total moles. In other words, it is not necessary that the sum of stoichiometric coefficients for all reactants and products must vanish. In contrast, the gas-phase mole fraction of component i is defined as the molar flow rate of component i divided by the total molar flow rate:

$$y_i = \frac{F_i}{\sum_{j=1}^{N} F_j} \tag{4-10}$$

In general, mole fractions are not linear functions of conversion because the total number of moles and the total molar flow rate are not constant when $\delta = \sum_{i=1}^{N} \nu_i \neq 0$. The thermal energy balance described below requires a weighted average of heat capacities for all components in the mixture. The easiest approach to perform this average is to use a mass-fraction-weighted sum of temperature-averaged specific heats of each pure component. Hence,

$$\langle C_{p,\,mixture}\rangle = \sum_{i=1}^{N} \omega_i \langle C_{p,\,component\ i}\rangle \tag{4-11}$$

Now the heat capacity of the mixture is a linear function of conversion, and the temperature dependence of each $C_{p,\,component\ i}$ has been averaged. The final result for $\langle C_{p,\,mixture}\rangle$ in units of cal/g·K, which employs (4-9), is

$$\langle C_{p,\,mixture}\rangle = \sum_{i=1}^{N} \omega_{i,\,inlet}\langle C_{p,\,component\,i}\rangle + \frac{\chi\omega_{A,\,inlet}}{\mathrm{MW}_A}\sum_{i=1}^{N} \nu_i \mathrm{MW}_i \langle C_{p,\,component\,i}\rangle \tag{4-12}$$

At the differential level, molar flow rate and mass fraction are linearly related when the total mass flow rate (i.e., $q\rho_{total}$) is constant at steady state with one inlet

stream and one outlet stream. Differentiating (4-3) with one chemical reaction yields:

$$dF_i = q\rho_{\text{total}} \frac{d\omega_i}{\text{MW}_i} = \nu_i \mathfrak{R}\, dV \tag{4-13}$$

Hence,

$$q\rho_{\text{total}} \frac{d\omega_i}{dV} = \nu_i (\text{MW}_i)\mathfrak{R} \tag{4-14}$$

The final form of the mass balance is written in terms of conversion χ for one chemical reaction by invoking the linear relation between ω_i and χ (see equation 4-9). Hence,

$$d\omega_i = \frac{\nu_i (\text{MW}_i)\omega_{\text{A, inlet}}}{\text{MW}_\text{A}} d\chi \tag{4-15}$$

and

$$\left(\frac{\omega_{\text{A, inlet}}\, \rho_{\text{total}}}{\text{MW}_\text{A}}\right) \frac{d\chi}{d\tau} = \mathfrak{R} \tag{4-16}$$

where the average residence time τ for liquid-phase flow reactors is V/q and the term in parentheses in (4-16) represents the inlet molar density of reactant A.

4-1.2 Thermal Energy Balance for a Differential Reactor

The first law of thermodynamics for an open system at steady state that performs no work on the surroundings other than pV work across the inlet and outlet planes of a differential control volume is written with units of energy per volume per time:

$$q\rho_{\text{total}} \frac{dh}{dV} = \frac{dQ}{dV} \tag{4-17}$$

where h is the specific enthalpy of the reactive mixture, which contains several components, and Q is the rate at which thermal energy enters the control volume across the lateral surface. The differential rate of conductive heat transfer at the reactor wall (dQ) with units of energy per time is expressed in terms of an appropriate heat transfer coefficient, an instantaneous temperature difference and the differential lateral surface area. Specific enthalpy conveniently includes contributions from both internal energy and pV work. Heat effects due to the endothermic or exothermic nature of the chemical reaction are accounted for by the total differential of specific enthalpy for a multicomponent mixture, as illustrated in Section 4-1.3. For single-phase behavior of a mixture of N components in which the chemical reactions have not reached equilibrium, the phase rule suggests that $N + 1$ independent variables are required to describe an intensive thermodynamic property, such as specific enthalpy. By choosing temperature T, pressure p, and $N - 1$ mass fractions ω_i (i.e., $1 \leq i \leq N - 1$), one is assured

that the thermal energy balance will be expressed in terms of temperature and the specific heat of the mixture at constant pressure, $\langle C_{p,\,\text{mixture}}\rangle$. Hence, the objectives are to (1) calculate the total differential of specific enthalpy, (2) apply the first law of thermodynamics for open systems, and (3) generate temperature profiles for nonisothermal reactor performance.

4-1.3 Thermodynamics of Multicomponent Mixtures

In agreement with the phase rule for single-phase behavior, if

$$h = h(T,\, p,\, \omega_1,\, \omega_2,\, \ldots,\, \omega_{N-1}) \tag{4-18}$$

then the total differential of specific enthalpy is expressed as

$$dh = \left(\frac{\partial h}{\partial T}\right)_{p,\,\text{composition}} dT + \left(\frac{\partial h}{\partial p}\right)_{T,\,\text{composition}} dp + \sum_i \left(\frac{\partial h}{\partial \omega_i}\right)_{T,\,p,\,\text{all}\,\omega_{j[j\neq i,N]}} d\omega_i \tag{4-19}$$

where the summation includes the first $N-1$ components in the mixture. The temperature coefficient of specific enthalpy at constant pressure and composition is identified as the heat capacity of the mixture. Hence,

$$\langle C_{p,\,\text{mixture}}\rangle = \left(\frac{\partial h}{\partial T}\right)_{p,\,\text{composition}} \tag{4-20}$$

Standard thermodynamic formalism for the total differential of specific enthalpy in terms of its natural variables (i.e., via Legendre transformation, see equations 29-20 and 29-24*b*) allows one to calculate the pressure coefficient of specific enthalpy via a Maxwell relation and the definition of the coefficient of thermal expansion, α.

$$dh = T\,ds + v\,dp + \text{terms that account for variations in composition} \tag{4-21}$$

$$\left(\frac{\partial h}{\partial p}\right)_{T,\,\text{composition}} = T\left(\frac{\partial s}{\partial p}\right)_{T,\,\text{composition}} + v \tag{4-22}$$

$$\left(\frac{\partial s}{\partial p}\right)_{T,\,\text{composition}} = -\left(\frac{\partial v}{\partial T}\right)_{p,\,\text{composition}} \qquad \text{(Maxwell relation)} \tag{4-23}$$

$$\left(\frac{\partial v}{\partial T}\right)_{p,\,\text{composition}} \equiv v\,\alpha \tag{4-24}$$

$$\left(\frac{\partial h}{\partial p}\right)_{T,\,\text{composition}} = v(1-\alpha T) \tag{4-25}$$

The pressure coefficient of specific enthalpy is identically zero for ideal gases, but the thermal energy balance must include a pressure contribution for other fluids. The partial derivative of h in the summation of (4-19), $(\partial h/\partial \omega_i)_{T,\,p,\,\text{all}\,\omega_{j[j\neq i,N]}}$,

resembles a partial molar quantity because temperature, pressure, and composition of almost all of the other species are held constant. It is not possible to vary the mass fraction of component i while all other mass fractions remain constant because the necessary restriction that all mass fractions must sum to unity would be violated. In other words, at least two mass fractions must change, ω_i and ω_N. Changes in ω_N are not independent. They are equal and opposite to those of ω_i to guarantee that all mass fractions sum to unity. If specific enthalpy is replaced by extensive enthalpy H and mass fraction is replaced by mole numbers N_i, one defines the partial molar enthalpy of component i (i.e., $\mathfrak{h}_i$) as follows:

$$\left(\frac{\partial H}{\partial N_i}\right)_{T,\, p,\, \text{all } N_{j[j\neq i]}} = \mathfrak{h}_i \tag{4-26}$$

The partial derivative of interest, $(\partial h/\partial \omega_i)_{T,\, p,\, \text{all } \omega_{j[j\neq i,N]}}$, is written in terms of partial molar enthalpies, $\mathfrak{h}_i$. Derivation of the exact expression can be found in Section 26-2 (see equations 26-30 and 26-31). The total differential of specific enthalpy is written in terms of temperature, pressure, and compositional variations as follows:

$$dh = \langle C_{p,\,\text{mixture}} \rangle\, dT + v(1-\alpha T)\, dp + \sum_{i=1}^{N-1} \left(\frac{\mathfrak{h}_i}{\text{MW}_i} - \frac{\mathfrak{h}_N}{\text{MW}_N}\right) d\omega_i \tag{4-27}$$

where MW is the molecular weight and the summation in (4-27) includes the first $N-1$ components. One invokes the restriction that all mass fractions must sum to unity (i.e., a constant) and differential changes in all mass fractions must sum to zero. Hence, the summation in (4-27) is simplified as follows:

$$\sum_{i=1}^{N-1} d\omega_i = -d\omega_N \tag{4-28}$$

$$\sum_{i=1}^{N-1} \left(\frac{\mathfrak{h}_i}{\text{MW}_i} - \frac{\mathfrak{h}_N}{\text{MW}_N}\right) d\omega_i = \sum_{i=1}^{N-1} \frac{\mathfrak{h}_i}{\text{MW}_i}\, d\omega_i - \frac{\mathfrak{h}_N}{\text{MW}_N} \sum_{i=1}^{N-1} d\omega_i$$

$$= \sum_{i=1}^{N} \frac{\mathfrak{h}_i}{\text{MW}_i}\, d\omega_i \tag{4-29}$$

The mass balance for a differential plug-flow reactor with multiple chemical reactions that operates at high-mass-transfer Peclet numbers allows one to replace $d\omega_i$ in (4-29):

$$d\omega_i = (\text{MW}_i) \sum_j \nu_{ij} \mathfrak{R}_j \frac{dV}{q\rho_{\text{total}}} \tag{4-30}$$

Now the total differential of specific enthalpy contains a chemical reaction contribution via the kinetic rate law $\mathfrak{R}_j$ for each reaction:

$$dh = \langle C_{p,\,\text{mixture}} \rangle\, dT + v(1-\alpha T)\, dp + \sum_j \mathfrak{R}_j \left(\sum_{i=1}^{N} \nu_{ij} \mathfrak{h}_i\right) \frac{dV}{q\rho_{\text{total}}} \tag{4-31}$$

The summation over all N components in (4-31) is an exact representation of the molar enthalpy change for the j^{th} chemical reaction, $\Delta H_{\text{Rx},j}$ (Tester and Modell, 1997, pp. 769–770). In other words,

$$\Delta H_{\text{Rx},j} \equiv \sum_{i=1}^{N} \nu_{ij} \mathfrak{h}_i \tag{4-32}$$

which accounts for nonidealities such as heats of mixing and ionic interactions, as well as the making and breaking of chemical bonds. Typically, one employs pure-component molar enthalpies to calculate $\Delta H_{\text{Rx},j}$. This approximation is exact for ideal solutions only, because partial molar properties reduce to pure-component molar properties. Now, the first law of thermodynamics for open systems, which contains the total differential of specific enthalpy, is written in a form that allows one to calculate temperature profiles in a tubular reactor with multiple chemical reactions:

$$q\rho_{\text{total}} \frac{dh}{dV} = q\rho_{\text{total}} \langle C_{p,\,\text{mixture}} \rangle \frac{dT}{dV} + q(1 - \alpha T)\frac{dp}{dV} + \sum_j \Delta H_{\text{Rx},j} \mathfrak{R}_j = \frac{dQ}{dV} \tag{4-33}$$

The final form of the differential thermal energy balance for a generic liquid-phase plug-flow reactor that operates at high-mass and high-heat-transfer Peclet numbers allows one to predict temperature as a function of the average residence time $\tau = V/q$:

$$\rho_{\text{total}} \langle C_{p,\,\text{mixture}} \rangle \frac{dT}{d\tau} = \frac{dQ}{dV} - (1 - \alpha T)\frac{dp}{d\tau} + \sum_j (-\Delta H_{\text{Rx},j}) \mathfrak{R}_j \tag{4-34}$$

It should be obvious from the discussion above that thermodynamics plays a major role in the development of reactor design formulas when heat effects due to chemical reaction are important.

4-1.4 Conductive Heat Transfer across the Lateral Surface: Forms for dQ/dV

The instantaneous rate of thermal energy transport into the reactive fluid across the wall at radius R is given by dQ/dV in (4-34), with units of energy per volume per time. The differential control volume of interest that contains the reactive fluid is $dV = \pi R^2 dz$, where z is the spatial coordinate that increases in the primary flow direction. Four possibilities allow one to determine this rate of conductive heat transfer across the lateral surface of the reactor:

1. Adiabatically enclosed reactors where the outer wall is insulated completely from the surroundings
2. Reactors that maintain constant heat flux across the wall at radius R
3. Reactors that maintain constant wall temperature on the outside of the tube, analogous to steam condensation heat exchangers
4. Cocurrent or countercurrent cooling fluids in the annular region of a concentric double-pipe configuration

Adiabatic Reactors. These reactors operate such that $dQ/dV = 0$. Hence, there is no heat transfer across the lateral surface and all the thermal energy generated via exothermic chemical reaction remains within the reactor. Temperature profiles within the tube are predicted from the simplified thermal energy balance when only one chemical reaction occurs:

$$\rho_{\text{total}}\langle C_{p,\,\text{mixture}}\rangle \frac{dT}{d\tau} = -(1-\alpha T)\frac{dp}{d\tau} + (-\Delta H_{\text{Rx}})\mathfrak{R} \tag{4-35}$$

where the second term on the right side of (4-35) is primarily responsible for an increase or decrease in temperature when the chemical reaction is exothermic or endothermic, respectively. Usually, the pressure contribution is neglected and the thermal energy balance,

$$\rho_{\text{total}}\langle C_{p,\,\text{mixture}}\rangle \frac{dT}{d\tau} = (-\Delta H_{\text{Rx}})\mathfrak{R} \tag{4-36}$$

is combined analytically with the mass balance (see equation 4-16):

$$\frac{\omega_{\text{A, inlet}}\,\rho_{\text{total}}}{\text{MW}_{\text{A}}}\frac{d\chi}{d\tau} = \mathfrak{R} \tag{4-37}$$

to predict adiabatic temperature changes as follows:

$$\rho_{\text{total}}\langle C_{p,\,\text{mixture}}\rangle \frac{dT}{d\tau} = (-\Delta H_{\text{Rx}})\frac{\omega_{\text{A, inlet}}\,\rho_{\text{total}}}{\text{MW}_{\text{A}}}\,\frac{d\chi}{d\tau} \tag{4-38}$$

Hence,

$$\frac{dT}{d\chi} = \frac{(-\Delta H_{\text{Rx}})\omega_{\text{A, inlet}}}{\text{MW}_{\text{A}}\langle C_{p,\,\text{mixture}}\rangle} \tag{4-39}$$

under nonequilibrium conditions. For exothermic chemical reactions where the temperature dependence of the specific heat of the mixture has been averaged and the effect of conversion on $\langle C_{p,\,\text{mixture}}\rangle$ is negligible, (4-39) is integrated from the reactor inlet (i.e., $\chi = 0$, $T = T_{\text{inlet}}$) to final conditions downstream where $\chi = \chi_{\text{final}}$ and $T = T_{\text{maximum}}$. The adiabatic temperature rise is predicted from the following nonequilibrium relation between temperature and conversion:

$$\Delta T_{\text{adiabatic}} = T_{\text{maximum}} - T_{\text{inlet}} = \frac{(-\Delta H_{\text{Rx}})\omega_{\text{A, inlet}}\chi_{\text{final}}}{\text{MW}_{\text{A}}\langle C_{p,\,\text{mixture}}\rangle} \tag{4-40}$$

This temperature rise can be reduced by diluting reactant A with an inert solvent so that the mass fraction of A in the inlet stream (i.e., $\omega_{\text{A, inlet}}$) decreases. This strategy is more attractive if the inert solvent exhibits an exceedingly large specific heat, which contributes significantly to $\langle C_{p,\,\text{mixture}}\rangle$.

Constant Heat Flux across the Lateral Surface. This condition is described quantitatively by expressing the differential rate of thermal energy transport dQ

into the reactor as a product of the constant flux , with units of energy per area per time, and the differential lateral surface area. Hence,

$$dQ = 2\pi R dz \tag{4-41}$$

and the quantity of interest in the thermal energy balance, with units of energy per volume per time, is

$$\frac{dQ}{dV} = \frac{1}{\pi R^2}\frac{dQ}{dz} = \frac{2}{R} = \text{constant} \tag{4-42}$$

To develop a well-behaved temperature profile throughout the reactor, the constant heat flux must be negative for exothermic reactions. If the pressure contribution to specific enthalpy is neglected, one simulates temperature profiles via the following form of the thermal energy balance when only one chemical reaction occurs:

$$\rho_{\text{total}}\langle C_{p,\,\text{mixture}}\rangle\frac{dT}{d\tau} = \frac{2}{R} + (-\Delta H_{\text{Rx}})\,\mathfrak{R} \tag{4-43}$$

together with the plug-flow mass balance:

$$\frac{\omega_{\text{A, inlet}}\,\rho_{\text{total}}}{\text{MW}_{\text{A}}}\,\frac{d\chi}{d\tau} = \mathfrak{R} \tag{4-44}$$

Numerical integration of these two coupled first-order ODEs (i.e., equations 4-43 and 4-44) is initiated at the reactor inlet, where $\chi(\tau = 0) \equiv 0$ and $T(\tau = 0) = T_{\text{inlet}}$.

Constant Outer Wall Temperature. If the chemical reaction is exothermic and the outer wall temperature of the reactor is lower than the temperature of the reactive fluid, then conductive heat transfer across the lateral surface will provide the necessary cooling. This condition is required to prevent thermal runaway. The differential rate of thermal energy transport dQ into the reactor across the lateral surface is given by the product of (1) an overall heat transfer coefficient that accounts for resistances in the thermal boundary layer within the reactive fluid, as well as the tube wall itself; (2) an instantaneous temperature difference $T_{\text{wall}} - T$, where T is the bulk temperature of the reactive fluid at axial position z; and (3) the differential lateral surface area, $2\pi R\,dz$. Hence,

$$dQ = U_{\text{overall}}[T_{\text{wall}} - T(z)]2\pi R dz \tag{4-45}$$

with units of energy per time. Rates of heat transfer across the lateral surface of the control volume, with units of energy per volume per time, are calculated as follows:

$$\frac{dQ}{dV} = \frac{1}{\pi R^2}\frac{dQ}{dz} = \frac{2U_{\text{overall}}}{R}\,[T_{\text{wall}} - T(z)] \tag{4-46}$$

Hence, conversion and temperature profiles in a plug-flow tubular reactor with constant outer wall temperature are simulated by solving two coupled first-order ODEs that represent mass and thermal energy balances at high Peclet numbers. They are summarized here for completeness in terms of a generic rate law $\mathfrak{R}$ when only one chemical reaction occurs:

$$\frac{\omega_{\mathrm{A,\,inlet}}\,\rho_{\mathrm{total}}}{\mathrm{MW_A}}\,\frac{d\chi}{d\tau} = \mathfrak{R} \tag{4-47}$$

$$\rho_{\mathrm{total}}\langle C_{p,\,\mathrm{mixture}}\rangle\frac{dT}{d\tau} = -\frac{2U_{\mathrm{overall}}}{R}\,(T - T_{\mathrm{wall}}) + (-\Delta H_{\mathrm{Rx}})\,\mathfrak{R} \tag{4-48}$$

where

$$\tau = \frac{V}{q} = \frac{z}{\langle v_z\rangle} \qquad \chi(\tau = 0) \equiv 0 \qquad T(\tau = 0) = T_{\mathrm{inlet}}$$

Numerical methods such as the Runge–Kutta–Gill fourth-order correct integration algorithm are required to simulate the performance of a nonisothermal tubular reactor. In the following sections, the effects of key design parameters on temperature and conversion profiles illustrate important strategies to prevent thermal runaway.

Manipulating the Outer Wall Temperature. Reactant A is converted irreversibly and exothermically to products in a tubular reactor with constant outer wall temperature. The inlet temperature of the reactive mixture is 340 K. The overall objective of this design problem is to observe thermal runaway and identify the critical outer wall temperature which represents the crossover from a thermally well-behaved reactor to one that exhibits thermal runaway. When this condition is identified, a reactor design strategy can be formulated to prevent the strong temperature changes characteristic of thermal runaway from occurring. Since the chemical reaction is strongly exothermic, heat is liberated and the following group of terms is negative:

$$\frac{C_{\mathrm{A0}}\Delta H_{\mathrm{Rx}}}{\rho_{\mathrm{total}}\langle C_{p,\,\mathrm{mixture}}\rangle} = -146\ K \tag{4-49}$$

where

$$C_{\mathrm{A0}} = \frac{\omega_{\mathrm{A,\,inlet}}\,\rho_{\mathrm{total}}}{\mathrm{MW_A}}$$

is the inlet molar density of reactant A. Heat transfer via radial conduction across the wall at radius R, enhanced by axial convection of thermal energy in the primary flow direction, provides a cooling mechanism. The time constant for heat transfer is defined by the following group of terms:

$$\frac{\rho_{\mathrm{total}}\langle C_{p,\,\mathrm{mixture}}\rangle R}{2U_{\mathrm{overall}}} = 5\ \mathrm{s} \tag{4-50}$$

The Arrhenius kinetic rate constant is described by an activation energy (i.e., E_{act}) of 22.5 kcal/mol and a pre-exponential factor (i.e., k_∞) of 3.94×10^{12} s^{-1}. Hence,

$$k_{forward}(T) = k_\infty \exp\left(-\frac{E_{act}}{RT}\right) [=] \ s^{-1} \tag{4-51}$$

Identify the critical outer wall temperature which represents the crossover from a thermally well-behaved reactor to one that exhibits thermal runaway. Qualitatively, how should the reactor design engineer manipulate the constant outer wall temperature to prevent thermal runaway? (See Figures 4-1 and 4-2.)

Manipulating the Surface-to-Volume Ratio of the Reactor. As illustrated in Figures 4-1 and 4-2, thermal runaway occurs when the inlet temperature of the reactive mixture is 340 K and the constant outer wall temperature is $\geq$336 K. Since the homogeneous chemical reaction is strongly exothermic, heat is generated volumetrically throughout the entire reactor. The cooling mechanism is provided by heat transfer across the wall, and this process is a surface-related phenomenon. Identify the critical surface-to-volume ratio of the reactor which represents the crossover from a thermally well-behaved system to one that exhibits thermal runaway when $T_{inlet} = T_{wall} = 340$ K. It is not acceptable to prevent thermal runaway by changing the inlet and/or outer wall temperatures. It is also not acceptable to modify the overall heat transfer coefficient $U_{overall}$.

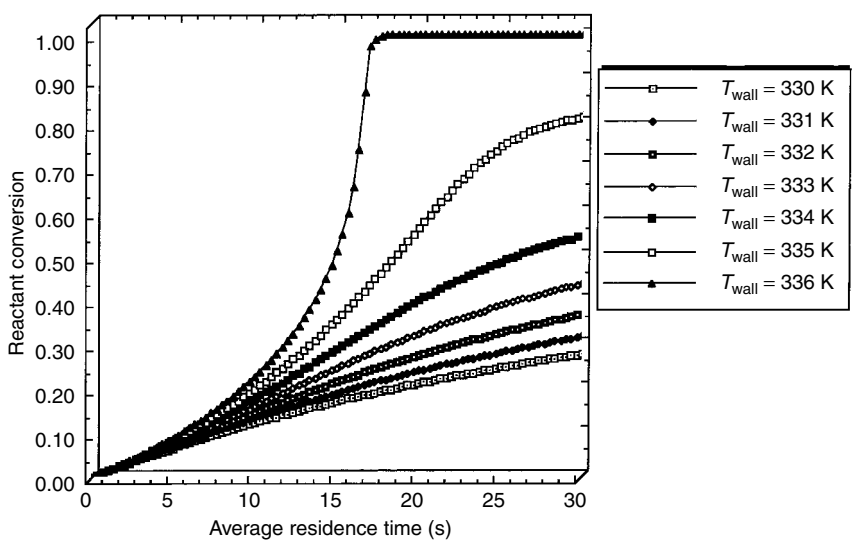

Figure 4-1 Sensitivity of reactant conversion to changes in the wall temperature for nonisothermal plug-flow tubular reactors with exothermic chemical reaction. The reactive fluid enters at 340 K.

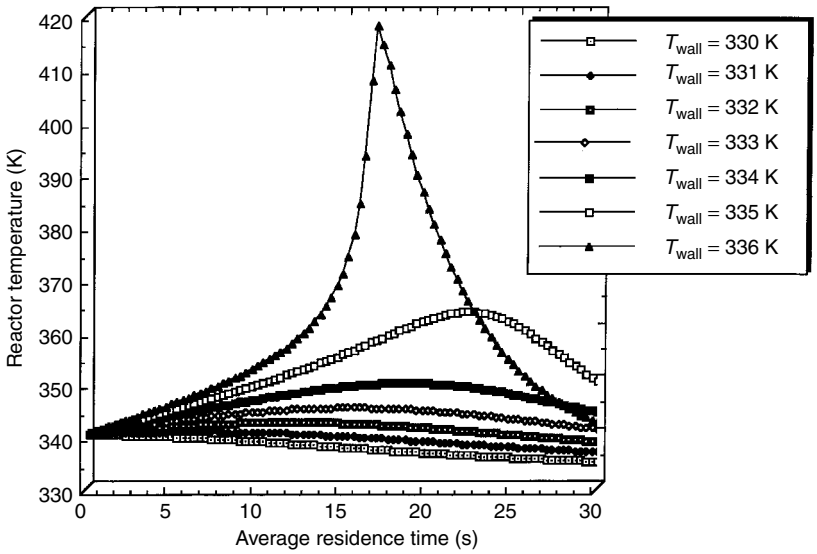

Figure 4-2 Sensitivity of reactor temperature to changes in the wall temperature for nonisothermal plug-flow tubular reactors with exothermic chemical reaction. The reactive fluid enters at 340 K.

Qualitatively, how should the design engineer manipulate the surface-to-volume ratio of the reactor to prevent thermal runaway? (See Figures 4-3 and 4-4.)

Coupled Heat and Mass Transfer with Cocurrent Cooling in a Concentric Double-Pipe Configuration. Now the differential rate of thermal energy transport into the reactive fluid across the inner wall at radius R_{inside} is adopted from equation (4-46) by replacing T_{wall} with T_{cool}, where T_{cool} is the bulk temperature of the cooling fluid, and wall radius R with inner wall radius R_{inside}. Hence,

$$\frac{dQ}{dV} = \frac{1}{\pi R_{\text{inside}}^2}\frac{dQ}{dz} = -\frac{2U_{\text{overall}}}{R_{\text{inside}}}\,[T_{\text{Rx}}(z) - T_{\text{cool}}(z)] \tag{4-52}$$

where T_{Rx} is the bulk temperature of the reactive fluid. The overall heat transfer coefficient in (4-52) accounts for three resistances in series: the thermal boundary layers in each fluid, and the wall itself. It is not possible to simulate the performance of this reactor with cocurrent cooling until an additional thermal energy balance is constructed for the cooling fluid, because T_{cool} is not constant. The differential control volume for the cooling fluid on the shell side of the double-pipe heat exchanger is

$$dV_{\text{cool}} = \pi(R_{\text{outside}}^2 - R_{\text{inside}}^2)\,dz \tag{4-53}$$

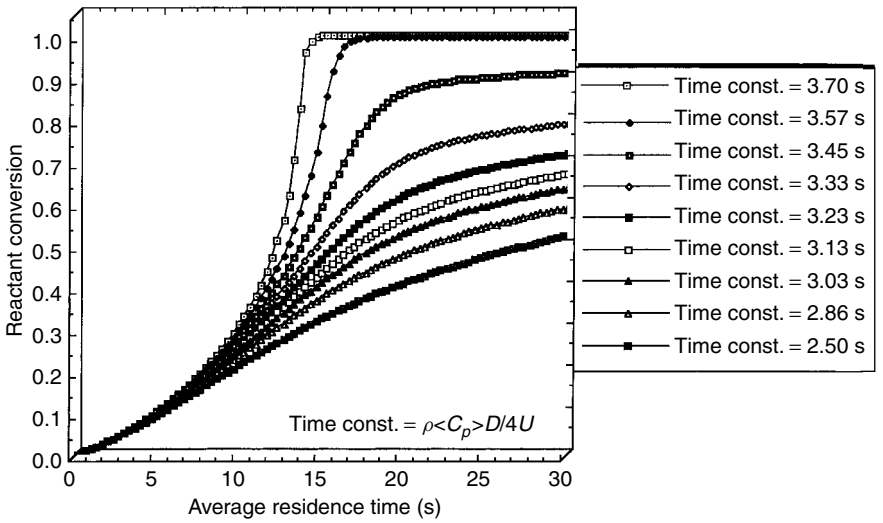

Figure 4-3 Sensitivity of reactant conversion to changes in the lateral heat transfer time constant for nonisothermal plug-flow tubular reactors with exothermic chemical reaction. The inlet and constant wall temperatures are 340 K.

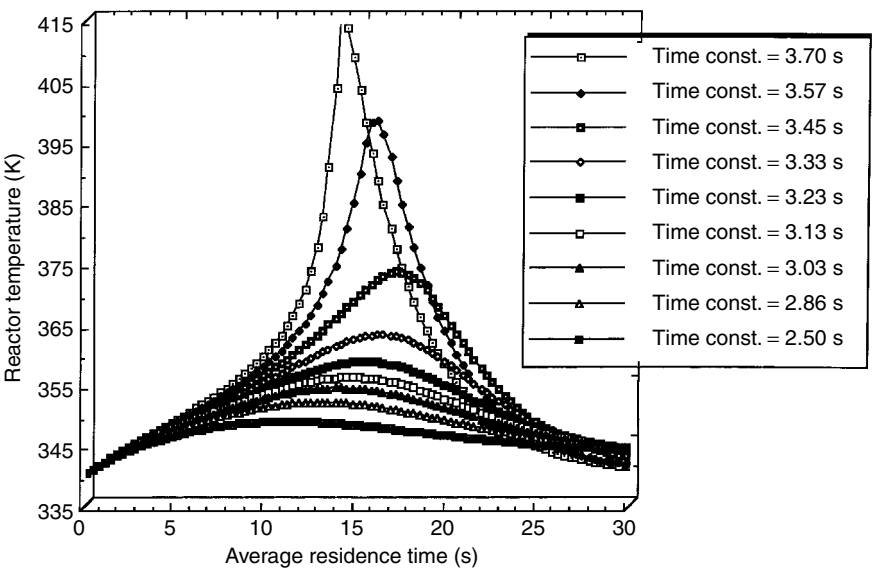

Figure 4-4 Sensitivity of reactor temperature to changes in the lateral heat transfer time constant for nonisothermal plug-flow tubular reactors with exothermic chemical reaction. The inlet and constant wall temperatures are 340 K.

where R_{outside} is the radius of the outer tube and z is the spatial coordinate that increases in the direction of flow of both fluids. If the outer wall of the double-pipe configuration is completely insulated from the surroundings, then the steady-state differential thermal energy balance, with units of energy per time, is

$$\begin{aligned}\text{convective input at } z = \text{conductive output at } R_{\text{inside}} \\ + \text{convective output at } z + dz\end{aligned} \tag{4-54}$$

$$(\rho_{\text{cool}} q_{\text{cool}} h_{\text{cool}})_z = dQ + (\rho_{\text{cool}} q_{\text{cool}} h_{\text{cool}})_{z+dz} \tag{4-55}$$

where ρ_{cool} is the overall mass density, q_{cool} the volumetric flow rate, h_{cool} the specific enthalpy, the subscript "cool" identifies properties of the cooling fluid, and the differential rate of conductive heat transfer dQ out of the cooling fluid at radius R_{inside} is exactly the same as the rate of conductive heat transfer into the reactive fluid. Hence,

$$dQ = U_{\text{overall}}\ [T_{\text{cool}}(z) - T_{\text{Rx}}(z)] 2\pi R_{\text{inside}}\, dz \tag{4-56}$$

At steady state, the overall mass flow rate of the cooling fluid (i.e., $\rho_{\text{cool}} q_{\text{cool}}$) is constant because there are only one inlet stream and one outlet stream, with no mass transfer across either wall at R_{inside} or R_{outside}. Under these conditions, the thermal energy balance is equivalent to the first law of thermodynamics for open systems, as stated in equation (4-17):

$$\begin{aligned}\rho_{\text{cool}} q_{\text{cool}}[(h_{\text{cool}})_{z+dz} - (h_{\text{cool}})_z] = \rho_{\text{cool}} q_{\text{cool}}\, dh_{\text{cool}} = -dQ \\ = U_{\text{overall}}[T_{\text{Rx}}(z) - T_{\text{cool}}(z)] 2\pi R_{\text{inside}}\, dz\end{aligned} \tag{4-57}$$

Thermodynamics is required to express the total differential of specific enthalpy for the cooling fluid in terms of temperature, pressure, and composition. One adopts a previous result from the thermodynamics of multicomponent mixtures (i.e., see equation 4-31), which allows for the possibility that a single chemical reaction might occur in the annular region of the double-pipe configuration. The generalized result is

$$dh_{\text{cool}} = \langle C_{p,\,\text{cool}} \rangle\, dT_{\text{cool}} + v_{\text{cool}}(1 - \alpha_{\text{cool}} T_{\text{cool}})\, dp + \frac{\Delta H_{\text{cool}} \mathfrak{R}_{\text{cool}}\, dV_{\text{cool}}}{\rho_{\text{cool}} q_{\text{cool}}} \tag{4-58}$$

where $\mathfrak{R}_{\text{cool}}$ is the kinetic rate law and ΔH_{cool} the enthalpy change for chemical reaction, v_{cool} the specific volume, and α_{cool} the thermal expansion coefficient, all within the cooling fluid. Once again, the pressure contribution to specific enthalpy is neglected for liquids, and the thermal energy balance is written in terms of the cooling fluid temperature:

$$\begin{aligned}\rho_{\text{cool}} q_{\text{cool}} \frac{dh_{\text{cool}}}{dz} = \rho_{\text{cool}} q_{\text{cool}} \langle C_{p,\text{cool}} \rangle \frac{dT_{\text{cool}}}{dz} + \Delta H_{\text{cool}} \mathfrak{R}_{\text{cool}} \frac{dV_{\text{cool}}}{dz} \\ = 2\pi R_{\text{inside}} U_{\text{overall}}[T_{\text{Rx}}(z) - T_{\text{cool}}(z)]\end{aligned} \tag{4-59}$$

Since

$$\frac{dV_{\text{cool}}}{dz} = \pi(R_{\text{outside}}^2 - R_{\text{inside}}^2) \tag{4-60}$$

one simulates temperature profiles within the cooling fluid by solving the following first-order ODE for $T_{\text{cool}}(z)$:

$$\rho_{\text{cool}} q_{\text{cool}} \langle C_{p,\text{cool}} \rangle \frac{dT_{\text{cool}}}{dz} = 2\pi R_{\text{inside}} U_{\text{overall}} [T_{\text{Rx}}(z) - T_{\text{cool}}(z)] + (-\Delta H_{\text{cool}}) \mathfrak{R}_{\text{cool}} \pi (R_{\text{outside}}^2 - R_{\text{inside}}^2) \tag{4-61}$$

Obviously, this thermal energy balance is coupled to the mass balance on the cooling fluid if chemical reaction occurs in the annular region, and it is also coupled to the mass and thermal energy balances for the reactive fluid within the inner tube because $T_{\text{Rx}}(z)$ is required to calculate the rate of conductive heat transfer across the inner wall. In most cases, the cooling fluid is a pure liquid, such as water or glycol, which experiences no chemical reaction. Hence, $\mathfrak{R}_{\text{cool}} \to 0$ and three coupled first-order ODEs are required to simulate the performance of tubular reactors with cocurrent cooling in a double-pipe configuration:

$$\frac{\omega_{\text{A, inlet}} \rho_{\text{Rx}}}{\text{MW}_{\text{A}}} \frac{d\chi}{d\tau_{\text{Rx}}} = \mathfrak{R}(T_{\text{Rx}}, \chi) \tag{4-62}$$

$$\rho_{\text{Rx}} \langle C_{p,\text{Rx}} \rangle \frac{dT_{\text{Rx}}}{d\tau_{\text{Rx}}} = -\frac{2U_{\text{overall}}}{R_{\text{inside}}} (T_{\text{Rx}} - T_{\text{cool}}) + (-\Delta H_{\text{Rx}}) \mathfrak{R}(T_{\text{Rx}}, \chi) \tag{4-63}$$

$$\rho_{\text{cool}} q_{\text{cool}} \langle C_{p,\text{cool}} \rangle \frac{dT_{\text{cool}}}{dz} = 2\pi R_{\text{inside}} U_{\text{overall}} (T_{\text{Rx}} - T_{\text{cool}}) \tag{4-64}$$

where

$$\tau_{\text{Rx}} = \frac{V_{\text{Rx}}}{q_{\text{Rx}}} = \frac{z}{\langle v_z \rangle_{\text{Rx}}} \qquad \chi(z=0) \equiv 0$$

$$T_{\text{Rx}}(z=0) = T_{\text{Rx, inlet}} \qquad T_{\text{cool}}(z=0) = T_{\text{cool, inlet}}$$

Properties of the reactive fluid within the inner tube are identified by the subscript Rx, and $\mathfrak{R}$ represents the kinetic rate law that converts reactant A to products. Only one independent variable is required to simulate reactor performance because axial coordinate z and average residence time for the reactive fluid τ_{Rx} are related by the average velocity of the reactive fluid $\langle v_z \rangle_{\text{Rx}}$. In comparison with the single-pipe reactor discussed earlier, the double-pipe reactor contains two additional design parameters that can be manipulated to control thermal runaway; radius ratio κ and average velocity ratio ψ, defined as follows:

$$\kappa \equiv \frac{R_{\text{inside}}}{R_{\text{outside}}} \tag{4-65}$$

$$\psi \equiv \frac{\langle v_z \rangle_{\text{cool}}}{\langle v_z \rangle_{\text{Rx}}} \tag{4-66}$$

One expresses the thermal energy balance for the cooling fluid in terms of the average residence time of the reactive fluid as follows:

Step 1. Write the volumetric flow rate of the cooling fluid in terms of its average velocity and flow cross section:

$$q_{\text{cool}} = \langle v_z \rangle_{\text{cool}} \pi (R^2_{\text{outside}} - R^2_{\text{inside}}) \tag{4-67}$$

Step 2. Manipulate the spatial derivative of the cooling fluid temperature to obtain T_{cool} as a function of τ_{Rx}:

$$\begin{aligned} q_{\text{cool}} \frac{dT_{\text{cool}}}{dz} &= \langle v_z \rangle_{\text{cool}} \pi (R^2_{\text{outside}} - R^2_{\text{inside}}) \frac{dT_{\text{cool}}}{d(\tau_{\text{Rx}} \langle v_z \rangle_{\text{Rx}})} \\ &= \pi (R^2_{\text{outside}} - R^2_{\text{inside}}) \psi \frac{dT_{\text{cool}}}{d\tau_{\text{Rx}}} \end{aligned} \tag{4-68}$$

Step 3. Divide the entire thermal energy balance of the cooling fluid by the flow cross-sectional area of the annulus, $\pi (R^2_{\text{outside}} - R^2_{\text{inside}})$.

Step 4. Express the following geometric factor in terms of the radius ratio κ, which accounts for the lateral heat transfer area relative to the flow cross section of the cooling fluid:

$$\frac{2\pi R_{\text{inside}}}{\pi (R^2_{\text{outside}} - R^2_{\text{inside}})} = \frac{2}{R_{\text{inside}}} \frac{\kappa^2}{1 - \kappa^2} \tag{4-69}$$

Hence, design parameters κ and ψ appear in the final form of the cooling fluid's thermal energy balance:

$$\rho_{\text{cool}} \langle C_{p,\,\text{cool}} \rangle \psi \frac{dT_{\text{cool}}}{d\tau_{\text{Rx}}} = \frac{2U_{\text{overall}}}{R_{\text{inside}}} \frac{\kappa^2}{1 - \kappa^2} (T_{\text{Rx}} - T_{\text{cool}}) \tag{4-70}$$

The cooling fluid experiences a smaller temperature increase from inlet to outlet when ψ is larger, because the residence time of the cooling fluid is shorter. In fact, the flow rate ratio parameter ψ, which was defined above as a ratio of average velocities, also represents a ratio of average residence times. For example, the average residence time of the cooling fluid is defined as

$$\begin{aligned} \tau_{\text{cool}} \equiv \frac{V_{\text{cool}}}{q_{\text{cool}}} &= \frac{\pi (R^2_{\text{outside}} - R^2_{\text{inside}}) z}{\pi (R^2_{\text{outside}} - R^2_{\text{inside}})\ \langle v_z \rangle_{\text{cool}}} \\ &= \frac{z}{\langle v_z \rangle_{\text{cool}}} = \frac{z}{\psi \langle v_z \rangle_{\text{Rx}}} = \frac{\tau_{\text{Rx}}}{\psi} \end{aligned} \tag{4-71}$$

Hence,

$$\psi \equiv \frac{\langle v_z \rangle_{\text{cool}}}{\langle v_z \rangle_{\text{Rx}}} = \frac{\tau_{\text{Rx}}}{\tau_{\text{cool}}} \tag{4-72}$$

The thermal energy balance (4-70) predicts no change in the cooling fluid's temperature when $\kappa = 0$ and an infinite increase in T_{cool} when $\kappa \to 1$. This suggests that the probability of experiencing thermal runaway can be reduced if the radius ratio is smaller, because T_{cool} will not increase too much. When the outer radius of the double-pipe configuration is fixed, smaller values of κ correspond to a larger surface-to-volume ratio for the reactive fluid in the inner tube:

$$\left(\frac{\text{surface}}{\text{volume}}\right)_{\text{inner tube}} = \frac{2}{\kappa R_{\text{outside}}} \tag{4-73}$$

and to a smaller exposed surface-to-volume ratio for the cooling fluid in the annular region:

$$\left(\frac{\text{heat transfer surface}}{\text{volume}}\right)_{\text{annular region}} = \frac{2}{R_{\text{outside}}} \frac{\kappa}{1-\kappa^2} \tag{4-74}$$

This is advantageous for a well-behaved double-pipe reactor because the volumetric generation of thermal energy in the inner tube has a feasible escape route across the wall at R_{inside}, whereas larger volumes of cooling fluid reduce the increase in T_{cool}.

Manipulating the Flow Rate of a Cocurrent Cooling Fluid. Reactant A is converted irreversibly and exothermically to products in a tubular reactor. The reactive mixture in the inner pipe is cooled using a concentric double-pipe heat exchanger. The cooling fluid in the annular region flows cocurrently with respect to the reactive fluid. The radius ratio κ of the double-pipe configuration is 0.5, the inlet temperature of the reactive fluid is 340 K, and the inlet temperature of the cooling fluid is 335 K. The heat transfer time constant across the inner wall of the double-pipe configuration for the cooling fluid is

$$\frac{\rho_{\text{cool}} \langle C_{p,\,\text{cool}} \rangle R_{\text{inside}}}{2U_{\text{overall}}} = 5 \text{ s} \tag{4-75}$$

The outer wall of the double-pipe configuration at radius R_{outside} is thermally insulated from the surroundings. These conditions, together with the parametric values defined earlier in this chapter on page 74, could produce thermal runaway. Identify the critical ratio of average velocities, $\psi = \langle v_z \rangle_{\text{cool}} / \langle v_z \rangle_{\text{Rx}}$, which represents the crossover from a thermally well behaved reactor to one that exhibits thermal runaway. It is not acceptable to prevent thermal runaway by changing the inlet temperature of either fluid. Also, do no change the overall heat transfer coefficient U_{overall} or the radius ratio κ. Qualitatively, how should the reactor design engineer manipulate the flow rate of the cocurrent cooling fluid to prevent thermal runaway? (See Figures 4-5 to 4-7.)

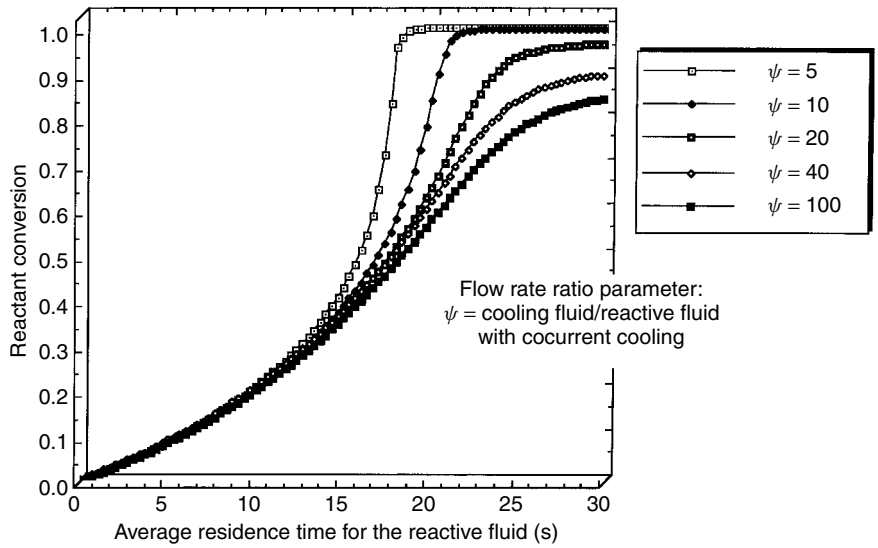

Figure 4-5 Sensitivity of reactant conversion to changes in flow rate ratio for nonisothermal plug-flow tubular reactors with exothermic chemical reaction and cocurrent cooling in a concentric double-pipe configuration with radius ratio $\kappa = 0.5$. The inlet temperatures are 340 K for the reactive fluid and 335 K for the cooling fluid.

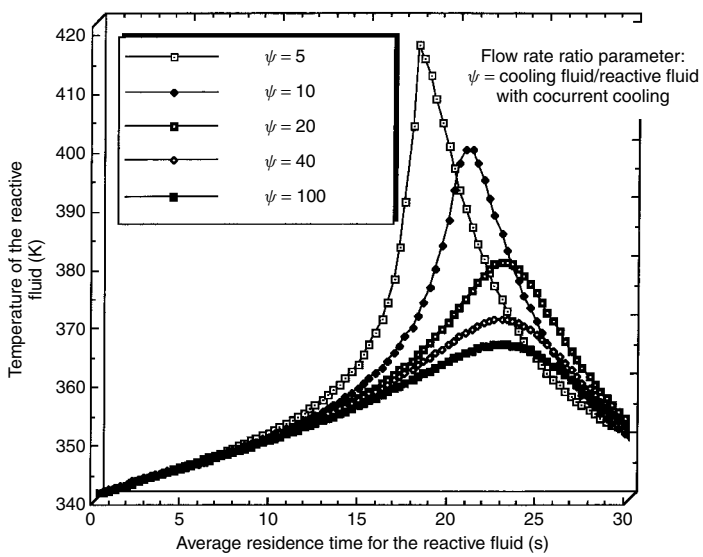

Figure 4-6 Sensitivity of reactive fluid temperature to changes in flow rate ratio for nonisothermal plug-flow tubular reactors with exothermic chemical reaction and cocurrent cooling in a concentric double-pipe configuration with radius ratio $\kappa = 0.5$. The inlet temperatures are 340 K for the reactive fluid and 335 K for the cooling fluid.

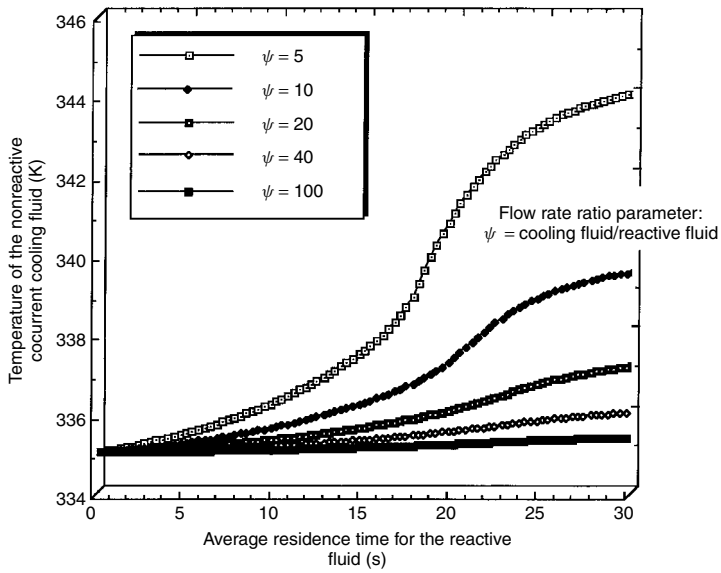

Figure 4-7 Sensitivity of cooling fluid temperature to changes in flow rate ratio for nonisothermal plug-flow tubular reactors with exothermic chemical reaction and cocurrent cooling in a concentric double-pipe configuration with radius ratio $\kappa = 0.5$. The inlet temperatures are 340 K for the reactive fluid and 335 K for the cooling fluid.

4-2 PARAMETRIC SENSITIVITY ANALYSIS

Numerical simulations of reactor performance in this chapter illustrate that small changes in key design parameters have a significant influence on temperature and conversion profiles in plug-flow tubular reactors. This phenomenon is called *parametric sensitivity*. Detailed analysis of parametric sensitivity in nonisothermal tubular reactors enables the design engineer to control thermal runaway. Consider the following set of parameters for a single-pipe reactor with constant outside wall temperature in which one first-order irreversible, exothermic chemical reaction occurs:

$$T_{\text{inlet}} = 340 \text{ K}$$

$$k_\infty = 3.94 \times 10^{12} \text{ s}^{-1}$$

$$E_{\text{activation}} = 22.5 \text{ kcal/mol}$$

$$\frac{C_{\text{A0}} \Delta H_{\text{Rx}}}{\rho_{\text{Rx}} \langle C_{p,\text{Rx}} \rangle} = -146 \text{ K}$$

$$\frac{\rho_{\text{Rx}} \langle C_{p,\text{Rx}} \rangle R}{2U_{\text{overall}}} = 5 \text{ s}$$

$$0 \le \tau_{\text{Rx}} \le 30 \text{ s}$$

TABLE 4-1 Summary of Parametric Sensitivity Results for Nonisothermal Plug-Flow Tubular Reactors When the Feed Stream Enters at 340 K[a]

T_{wall} (K)	T_{max} (K)	χ_{max} at $\tau_{Rx} = 30$ s (%)
330	340	28
331	341	32
332	342	37
333	345	44
334	350	55
335	363	81
336	417	100 at $\tau_{Rx} = 18$ s

[a]Includes the effect of a constant wall temperature on the maximum temperature and reactant conversion that can be achieved. Thermal runaway occurs when χ_{max} is 100%.

Numerical results are summarized in Table 4-1 for seven different values of the outer wall temperature.

The reactor is rather well behaved when the outside wall temperature is 335 K, but thermal runaway occurs when $T_{wall} = 336$ K. Hence, T_{wall} exhibits a critical value between 335 and 336 K because thermal runaway occurs when $T_{wall} > (T_{wall})_{critical}$. Thermal runaway can be prevented when $T_{wall} = 340$ K if the surface-to-volume ratio of the reactor is increased by decreasing the tube radius R. This important design modification is accounted for by decreasing the time constant for heat transfer across the lateral surface. Numerical results are summarized in Table 4-2 for a single-pipe reactor with $T_{inlet} = T_{wall} = 340$ K at nine different values of the heat transfer time constant.

Based on the entries in Table 4-2, it is possible to control thermal runaway in the tubular reactor with constant outside wall temperature, described above, if the heat transfer time constant is ≤ 3.45 s. Difficulty in identifying the critical value of any key design parameter via comparison of temperature increases (i.e., $T_{max} - T_{inlet}$) is circumvented by analyzing the conversion profile also. For example, the last two entries in Table 4-2 indicate that 100% conversion of reactant A is achieved in the first half of the reactor because steep increases in temperature have occurred that are characteristic of thermal runaway. When a cocurrent cooling fluid is employed in the annular region of a concentric double-pipe configuration to remove heat generated by the reactive fluid in the inner tube, conversion and temperature profiles are influenced by the flow rate ratio ψ and the radius ratio κ. For example, both fluids exhibit the same time constant for heat transfer across the wall at R_{inside}, the outer wall at $R_{outside}$ is thermally insulated from the surroundings, and double-pipe reactor performance is simulated for the following set of parameters:

$$(T_{Rx})_{inlet} = 340 \text{ K}$$

TABLE 4-2 Summary of Parametric Sensitivity Results for Nonisothermal Plug-Flow Tubular Reactors When the Inlet and Constant Wall Temperatures Are 340 K[a]

$\rho_{Rx}\langle C_{p,Rx}\rangle R/2U_{overall}$ (s)	T_{max} (K)	χ_{max} at $\tau_{Rx} = 30$ s (%)
2.50	349	52
2.86	352	59
3.03	354	64
3.13	356	67
3.23	358	72
3.33	363	79
3.45	373	91
3.57	398	100 at $\tau_{Rx} = 20$ s
3.70	416	100 at $\tau_{Rx} = 15$ s

[a]Includes the effect of the lateral heat transfer time constant on the maximum temperature and reactant conversion that can be achieved. Thermal runaway occurs when χ_{max} is 100%.

$$(T_{cool})_{inlet} = 335 \text{ K}$$

$$\kappa = \frac{R_{inside}}{R_{outside}} = 0.5$$

$$\kappa_\infty = 3.94 \times 10^{12} \text{ s}^{-1}$$

$$E_{activation} = 22.5 \text{ kcal/mol}$$

$$\frac{C_{A0}\Delta H_{Rx}}{\rho_{Rx}\langle C_{p,Rx}\rangle} = -146 \text{ K}$$

$$\left(\frac{\rho\langle C_p\rangle R_{inside}}{2U_{overall}}\right)_{Rx/cool} = 5 \text{ s}$$

$$0 \le \tau_{Rx} \le 30 \text{ s}$$

Numerical results are listed in Table 4-3 for five values of ψ which illustrate that thermal runaway occurs when the flow rate ratio is less than approximately 20, but sensitivity to small changes in ψ is rather weak here.

Obviously, thermal runaway occurs in the previous example if the flow rate ratio is unity. However, it is possible to control a double-pipe reactor with $\psi = 1$ by decreasing the radius ratio. This is illustrated in Table 4-4 for conditions described in the previous example. Thermal runaway occurs when $\kappa \ge \kappa_{critical}$ and the critical radius ratio lies somewhere between 0.10 and 0.15.

Hence, the parametric sensitivity analysis outlined in this section identifies critical values, or a range of critical values, for (1) the outside wall temperature, (2) the heat transfer time constant, (3) the flow rate ratio ψ, and (4) the radius ratio κ, which delineates the boundary between well-behaved reactor performance and thermal runaway. Other parameters that exhibit critical values and

TABLE 4-3 Summary of Parametric Sensitivity Results for Nonisothermal Plug-Flow Tubular Reactors with Cocurrent Cooling in a Double-Pipe Configuration with Radius Ratio $\kappa = 0.5$[a]

ψ	$(T_{Rx})_{max}$ (K)	$(T_{cool})_{max}$ at $\tau_{Rx} = 30$ s (K)	χ_{max} at $\tau_{Rx} = 30$ s (%)
5	418	344	100 at $\tau_{Rx} = 19$ s
10	400	339.6	100 at $\tau_{Rx} = 23$ s
20	380	337	96
40	370	336	90
100	366	335.4	85

[a]Inlet temperatures are 340 K for the reactive fluid and 335 K for the cooling fluid. Includes the effect of the flow rate ratio parameter ψ on the maximum temperatures for both fluids and maximum reactant conversion. Thermal runaway occurs when χ_{max} is 100%.

TABLE 4-4 Summary of Parametric Sensitivity Results for Nonisothermal Plug-Flow Tubular Reactors with Cocurrent Cooling in a Double-Pipe Configuration[a]

κ	$(T_{Rx})_{max}$ (K)	$(T_{cool})_{max}$ at $\tau_{Rx} = 30$ s (K)	χ_{max} at $\tau_{Rx} = 30$ s (%)
0.02	363.6	335.0	82
0.04	364.4	335.2	83
0.06	365.8	335.4	85
0.08	368.1	335.7	88
0.10	371.8	336.2	91
0.11	374.2	336.5	93
0.12	377.0	336.9	95
0.13	380.3	337.2	97
0.14	384.2	337.6	98
0.15	387.6	338.1	99
0.16	392.0	338.5	100 at $\tau = 29$ s
0.18	398.7	339.6	100 at $\tau = 24$ s
0.20	404.1	340.7	100 at $\tau = 21$ s
0.25	416.8	344.0	100 at $\tau = 19$ s

[a]The flow rate ratio is unity, and the inlet temperatures are 340 K for the reactive fluid and 335 K for the cooling fluid. Includes the effect of the radius ratio κ on the maximum temperatures for both fluids and maximum reactant conversion. Thermal runaway occurs when χ_{max} is 100%.

TABLE 4-5 Reactor Design Strategies to Prevent the Phenomenon of Thermal Runaway in Plug-Flow Tubular Reactors

Design Parameter	Manipulation
1. Inlet temperature of the reactive fluid	Decrease
2. Inlet temperature of the cooling fluid	Decrease
3. Activation energy for the chemical reaction	Increase
4. Enthalpy change for the chemical reaction	Decrease
5. Inlet molar density of reactant A	Decrease

the appropriate manipulation of them to control thermal runaway are summarized in Table 4-5. The effect of a catalyst that reduces the potential energy of the activated complex in the transition state is accounted for in parameter 3, whereas dilution effects are described in parameter 5. Investigate design strategy 3 in Table 4-5 for a single-pipe reactor with constant wall temperature. Let $T_{\text{wall}} = 300$ K, $T_{\text{inlet}} = 330$ K, use a lateral heat transfer time constant of 3.57 s, and maintain all of the other parameters in this section. Then, compare temperature and conversion profiles which correspond to Arrhenius activation energies of 20.8 and 20.9 kcal/mol.

4-3 ENDOTHERMIC REACTIONS IN A COCURRENT COOLING FLUID

This novel design strategy to simulate and control thermal runaway in a double-pipe reactor requires the simultaneous solution of four coupled first-order ODEs to describe conversion and temperature profiles within the inner pipe and in the annular region. Mass and thermal energy balances for exothermic reaction within the inner pipe are exactly the same as those discussed above (see equations 4-62 and 4-63). Hence, for one exothermic reaction (i.e., A $\rightarrow$ products) in the inner pipe,

$$\frac{\omega_{\text{A, inlet}}\rho_{\text{Rx}}}{\text{MW}_{\text{A}}}\frac{d\chi_{\text{A}}}{d\tau_{\text{Rx}}} = \mathfrak{R}_{\text{A}}(T_{\text{Rx}}, \chi_{\text{A}}) \tag{4-76}$$

$$\rho_{\text{Rx}}\langle C_{p,\text{Rx}}\rangle\frac{dT_{\text{Rx}}}{d\tau_{\text{Rx}}} = -\frac{2U_{\text{overall}}}{R_{\text{inside}}}(T_{\text{Rx}} - T_{\text{cool}}) + (-\Delta H_{\text{Rx}})\mathfrak{R}_{\text{A}}(T_{\text{Rx}}, \chi_{\text{A}}) \tag{4-77}$$

$$\chi_{\text{A}}(z = 0) \equiv 0 \tag{4-78}$$

$$T_{\text{Rx}}(z = 0) = T_{\text{Rx, inlet}} \tag{4-79}$$

where χ_{A} represents the conversion of reactant A via exothermic chemical reaction in the inner pipe and $\mathfrak{R}_{\text{A}}$ is the corresponding rate law. Similarly, the thermal energy balance in the annular region, which includes flexibility for chemical reaction, has been discussed previously, and it remains unchanged if the wall at

R_{outside} is adiabatic. For one endothermic reaction (i.e., B $\rightarrow$ products) for the cooling fluid in the annular region, equation (4-61) yields:

$$\rho_{\text{cool}} q_{\text{cool}} \langle C_{p,\,\text{cool}} \rangle \frac{dT_{\text{cool}}}{dz} = 2\pi R_{\text{inside}} U_{\text{overall}} [T_{\text{Rx}}(z) - T_{\text{cool}}(z)] + (-\Delta H_{\text{cool}}) \mathfrak{R}_{\text{B}}(T_{\text{cool}}, \chi_{\text{B}}) \pi (R^2_{\text{outside}} - R^2_{\text{inside}}) \quad (4\text{-}80)$$

$$T_{\text{cool}}(z = 0) \equiv T_{\text{cool, inlet}} \quad (4\text{-}81)$$

where χ_{B} describes the conversion of reactant B to products via endothermic reaction in the annular region, and $\mathfrak{R}_{\text{B}}$ is the corresponding rate law. One introduces τ_{Rx} into the cooling fluid's thermal energy balance as follows:

Step 1. Write the volumetric flow rate q_{cool} as a product of the average velocity $\langle v_z \rangle_{\text{cool}}$ and the flow cross section $\pi(R^2_{\text{outside}} - R^2_{\text{inside}})$.

Step 2. Write $\langle v_z \rangle_{\text{cool}}$ as a product of ψ and $\langle v_z \rangle_{\text{Rx}}$.

Step 3. Identify the important independent variable as $\tau_{\text{Rx}} = z/\langle v_z \rangle_{\text{Rx}}$.

Step 4. Divide the entire thermal energy balance by the flow cross section in the annular region, $\pi(R^2_{\text{outside}} - R^2_{\text{inside}})$.

Step 5. Express $2\pi R_{\text{inside}}/\pi(R^2_{\text{outside}} - R^2_{\text{inside}})$ in terms of the radius ratio κ and R_{inside}.

The final result for the cooling fluid's thermal energy balance is similar to (4-70), however, with heat effects due to chemical reaction:

$$\rho_{\text{cool}} \langle C_{p,\,\text{cool}} \rangle \psi \frac{dT_{\text{cool}}}{d\tau_{\text{Rx}}} = \frac{2U_{\text{overall}}}{R_{\text{inside}}} \frac{\kappa^2}{1 - \kappa^2} (T_{\text{Rx}} - T_{\text{cool}}) + (-\Delta H_{\text{cool}}) \mathfrak{R}_{\text{B}}(T_{\text{cool}}, \chi_{\text{B}}) \quad (4\text{-}82)$$

The primary objective of this section is to add a mass balance for reactant B to the set of coupled ODEs required to simulate the performance of this double-pipe reactor. The simplest approach to accomplish this task is to adopt the mass balance at high Peclet numbers for reactant A within the inner pipe, replace subscript A with subscript B, and replace subscript "Rx" for the reactive fluid in the inner pipe with subscript "cool" for the reactive cooling fluid in the annular region. Hence, modification of (4-76) yields:

$$\frac{\omega_{\text{B, inlet}} \rho_{\text{cool}}}{\text{MW}_{\text{B}}} \frac{d\chi_{\text{B}}}{d\tau_{\text{cool}}} = \mathfrak{R}_{\text{B}}(T_{\text{cool}}, \chi_{\text{B}}) \quad (4\text{-}83)$$

$$\chi_{\text{B}}(z = 0) \equiv 0 \quad (4\text{-}84)$$

Since both residence times are related by the flow rate ratio (i.e., $\tau_{\text{cool}} = \tau_{\text{Rx}}/\psi$), one rewrites the cooling fluid's mass balance in terms of the residence time for

the reactive fluid within the inner pipe τ_{Rx} and includes the flow rate ratio ψ as a factor for convective mass transfer on the left side of the equation:

$$\frac{\omega_{B,\,inlet}\rho_{cool}}{MW_B}\psi\frac{d\chi_B}{d\tau_{Rx}} = \Re_B(T_{cool},\,\chi_B) \tag{4-85}$$

The Runge–Kutta–Gill fourth-order correct numerical integration algorithm for coupled ODEs is useful to simulate this double-pipe reactor after temperature- and conversion-dependent kinetic rate laws are introduced for both fluids. The generalized procedure is as follows:

Step 1. Use inlet conditions as a starting point to generate graphs of temperature and conversion as a function of axial position z, or τ_{Rx}.

Step 2. Use mass and thermal energy balances for both fluids to calculate the slope of conversion and temperature with respect to τ_{Rx} at conditions in the feed. The actual algorithm averages this slope at several positions within a small interval that represents discrete jumps in τ_{Rx}.

Step 3. Use the point-slope method to predict temperature and conversion at a small distance downstream in the primary flow direction.

Step 4. Be sure that the step size, or jump, in τ_{Rx} is small enough to avoid accumulating errors when temperature and conversion change abruptly.

Step 5. March through the reactor by incrementing τ_{Rx} from inlet to outlet. This is equivalent to repeating steps 1 to 3 numerous times in a computerized loop.

Step 6. Present the results graphically as a function of τ_{Rx}.

4-3.1 Cocurrent Cooling Fluid That Undergoes a Strongly Endothermic Chemical Reaction

Reactant A is converted irreversibly and exothermically to products in a 2-in.-inner-diameter tubular reactor (i.e., A $\rightarrow$ products) via first-order chemical kinetics. This reactive mixture in the inner tube is cooled using a concentric double-pipe heat exchanger. The cooling fluid in the annular region flows cocurrently with respect to the reactive fluid. The radius ratio of the double-pipe configuration is $\kappa = R_{inside}/R_{outside} = 0.5$, the inlet temperature of the reactive fluid in the inner tube is 340 K, and the inlet temperature of the cooling fluid in the annular region is also 340 K. Most important, the cooling fluid in the annular region undergoes a strongly endothermic chemical reaction (i.e., B $\rightarrow$ products) that represents a mirror image of the reactive fluid in the inner tube. In other words, the pre-exponential factor and activation energy for the kinetic rate constants are exactly the same for both fluids (see the examples in Section 4-2). However, the enthalpy changes for the chemical reactions are exactly opposite. The chemical reaction in the inner tube (A $\rightarrow$ products) is strongly exothermic ($\Delta H_{RxA} = -15$ kcal/mol) and heat is generated volumetrically throughout the inner tube. Hence, the following group of terms in the thermal energy balance

within the inner tube is negative:

$$\frac{C_{A0}\Delta H_{RxA}}{\rho_{Rx}\langle C_{p,\,Rx}\rangle} = -150 \text{ K} \tag{4-86}$$

The overall heat transfer coefficient across the inner wall of the double-pipe configuration is

$$U_{inside} = 10^4 \text{ kcal/m}^2\cdot\text{h}\cdot\text{K} \approx 0.3 \text{ cal/cm}^2.\text{s.K} \tag{4-87}$$

Hence, the time constant for heat transfer across the inner wall at radius R_{inside} is the same for the reactive fluid in the inner tube (subscript "Rx") and the reactive cooling fluid in the outer tube (subscript "cool"):

$$\frac{\rho_{Rx}\langle C_{p,\,Rx}\rangle R_{inside}}{2U_{inside}} = \frac{\rho_{cool}\langle C_{p,\,cool}\rangle R_{inside}}{2U_{inside}} = 5 \text{ s} \tag{4-88}$$

The outer wall of the double-pipe configuration at radius $R_{outside}$ is thermally insulated from the surroundings. Identify the acceptable range of the flow rate ratio parameter ψ that corresponds to a well-behaved novel reactive system which does not exhibit thermal runaway. The appropriate reactor design equations are summarized in Table 4-6.

TABLE 4-6 One-Dimensional Mass and Thermal Energy Balances for Plug-Flow Tubular Reactors with Cocurrent Cooling in a Concentric Double-Pipe Configuration[a]

nth-Order irreversible chemical kinetics: $\mathfrak{R}_A(T_{Rx}, \chi_A) = k_{Rx}(T_{Rx})[C_{A0}(1-\chi_A)]^n$

Irreversible kinetics, cooling fluid: $\mathfrak{R}_B(T_{cool}, \chi_B) = k_{cool}(T_{cool})[C_{B0}(1-\chi_B)]^n$

Arrhenius model for both fluids: $k_{Rx/cool}(T_{Rx/cool}) = k_\infty \exp\left(\dfrac{-E_{activation}}{RT_{Rx/cool}}\right)$

Mass balance for reactant A, inner tube: $C_{A0}\dfrac{d\chi_A}{d\tau_{Rx}} = \mathfrak{R}_A(T_{Rx}, \chi_A)$

Mass balance for reactant B, outer tube: $C_{B0}\psi\dfrac{d\chi_B}{d\tau_{Rx}} = \mathfrak{R}_B(T_{cool}, \chi_B)$

Thermal energy balance for the reactive fluid within the inner tube:

$$\rho_{Rx}\hat{C}_{pRx}\frac{dT_{Rx}}{d\tau_{Rx}} = \frac{2U_{inside}}{R_{inside}}(T_{cool} - T_{Rx}) + (-\Delta H_{Rx})\mathfrak{R}_A(T_{Rx}, \chi_A)$$

Thermal energy balance for the cocurrent reactive cooling fluid:

$$\rho_{cool}\hat{C}_{pcool}\psi\frac{dT_{cool}}{d\tau_{Rx}} = \frac{2U_{inside}}{R_{inside}}\frac{\kappa^2}{1-\kappa^2}(T_{Rx} - T_{cool}) + (-\Delta H_{cool})\mathfrak{R}_B(T_{cool}, \chi_B)$$

[a]The reactive fluid experiences exothermic chemical reaction. An endothermic chemical reaction occurs in the cooling fluid to enhance its potential to remove heat generated by the reactive fluid.

Illustrative Problem

(a) Describe qualitatively why thermal runaway occurs when the flow rate of the cocurrent endothermic cooling fluid is too high. In other words, thermal runaway occurs when $\psi > 0.65$. (See Figures 4-8 and 4-9.)
(b) Describe qualitatively why thermal runaway occurs when the flow rate of the cocurrent endothermic cooling fluid is too low. In other words, thermal runaway occurs when $\psi < 0.15$. (See Figures 4-10 and 4-11.)
(c) Generate graphs of temperature and conversion for both fluids vs. τ_{Rx} that illustrate thermal runaway at high and low values of ψ.

4-3.2 Concentric Double-Pipe Configurations That Are Not Insulated from the Surroundings

These reactors contain an additional conductive heat transfer mechanism across the outer wall at $R_{outside}$ that must be included in the cooling fluid's thermal energy balance. If one adopts equations (4-55), (4-57), and (4-58) for cocurrent cooling,

$$\rho_{cool} q_{cool}\, dh_{cool} \approx \rho_{cool} q_{cool} \langle C_{p,cool} \rangle\, dT_{cool} + \Delta H_{cool} \Re_{cool}\, dV_{cool} = -dQ \tag{4-89}$$

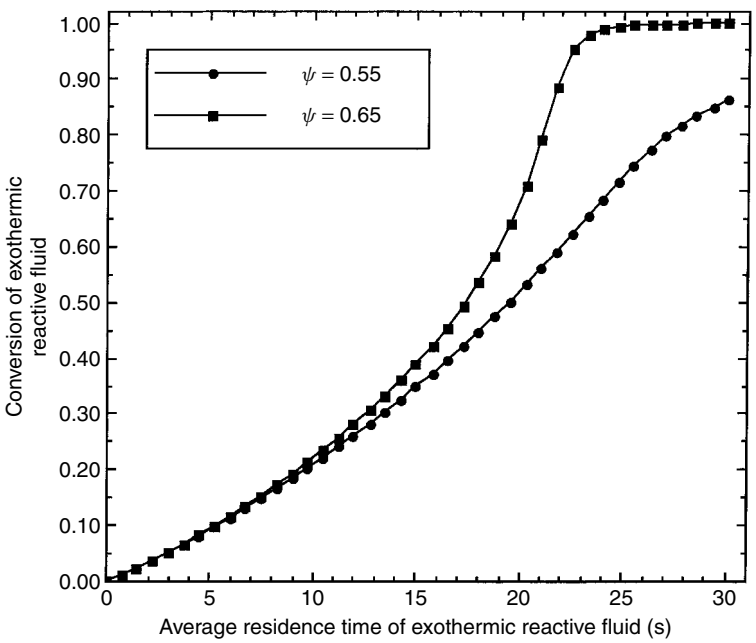

Figure 4-8 Effect of higher flow rate ratios on the conversion of an exothermic reactive fluid in a plug-flow reactor with endothermic cocurrent cooling in a concentric double-pipe configuration with radius ratio $\kappa = 0.5$. Both fluids enter the double-pipe reactor at 340 K.

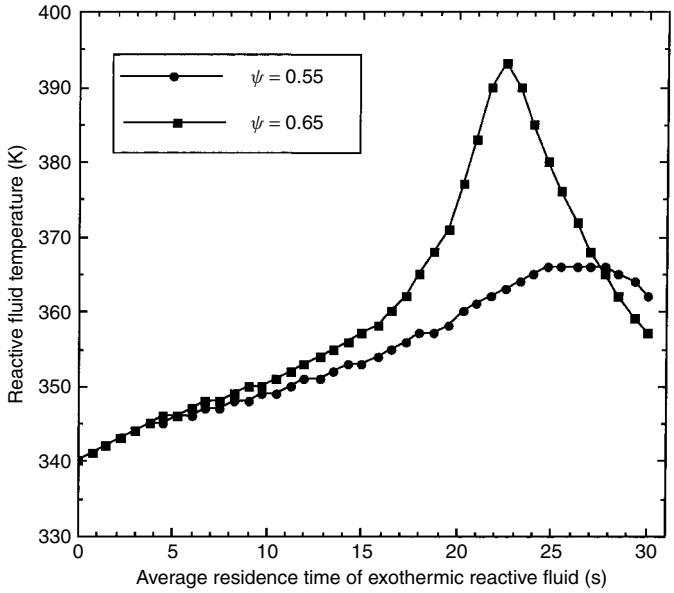

Figure 4-9 Effect of higher flow rate ratios on the temperature of an exothermic reactive fluid in a plug-flow reactor with endothermic cocurrent cooling in a concentric double-pipe configuration with radius ratio $\kappa = 0.5$. Both fluids enter the double-pipe reactor at 340 K.

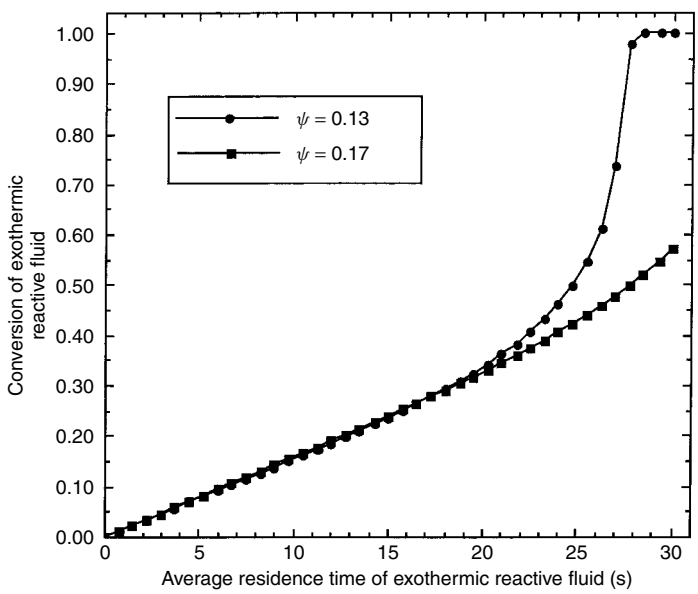

Figure 4-10 Effect of lower flow rate ratios on the conversion of an exothermic reactive fluid in a plug-flow reactor with endothermic cocurrent cooling in a concentric double-pipe configuration with radius ratio $\kappa = 0.5$. Both fluids enter the double-pipe reactor at 340 K.

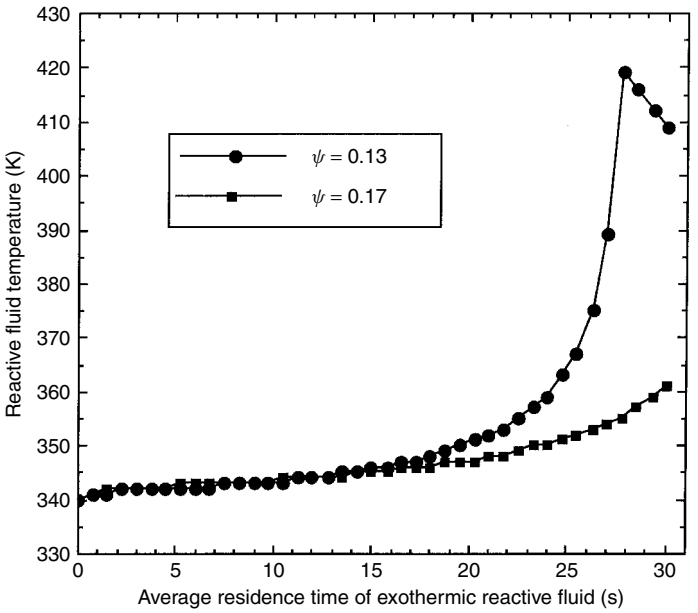

Figure 4-11 Effect of lower flow rate ratios on the temperature of an exothermic reactive fluid in a plug-flow reactor with endothermic cocurrent cooling in a concentric double-pipe configuration with radius ratio $\kappa = 0.5$. Both fluids enter the double-pipe reactor at 340 K.

then dQ represents the differential rate of conductive heat transfer out of the cooling fluid, with units of energy/time. Since both walls must be considered,

$$dQ = U_{\text{overall, inside}}(T_{\text{cool}} - T_{\text{Rx}})2\pi R_{\text{inside}}\, dz + U_{\text{overall, outside}}(T_{\text{cool}} - T_{\text{ambient}})2\pi R_{\text{outside}}\, dz \tag{4-90}$$

where T_{ambient} is the temperature of the surroundings and the overall heat transfer coefficients across the inside and outside walls at R_{inside} and R_{outside}, respectively, contain a sum of three resistances in series. $U_{\text{overall, inside}}$ accounts for thermal resistances in the liquid boundary layers on each side of the inner wall, as well as the wall itself. $U_{\text{overall, outside}}$ accounts for thermal resistances in the liquid boundary layer that hugs the inside of the outer wall, the gas-phase boundary layer adjacent to the outside of the outer wall, and the outside wall. In the absence of phase changes, thermal conductivities and heat transfer coefficients are much smaller for gases than their counterparts for liquids. Consequently, the gas-phase boundary layer adjacent to the outside of the outer wall provides the dominant contribution to $U_{\text{overall, outside}}$, which is much smaller than $U_{\text{overall, inside}}$. This is consistent with the fact that the time constant for heat transfer across the outer wall is much larger than its counterpart across the inner wall. Hence, the rate of heat transfer across the outer wall is of secondary importance. In general,

temperatures within the cooling fluid are calculated from the following first-order ODE, which is obtained by combining (4-89) and (4-90):

$$\rho_{\text{cool}} q_{\text{cool}} \langle C_{p,\text{cool}} \rangle \frac{dT_{\text{cool}}}{dz} = (-\Delta H_{\text{cool}}) \mathfrak{R}_{\text{cool}} \frac{dV_{\text{cool}}}{dz} + 2\pi R_{\text{inside}} U_{\text{overall, inside}} (T_{\text{Rx}} - T_{\text{cool}}) - 2\pi R_{\text{outside}} U_{\text{overall, outside}} (T_{\text{cool}} - T_{\text{ambient}}) \tag{4-91}$$

subject to the condition that $T_{\text{cool}} = T_{\text{cool, inlet}}$ at $z = 0$. This equation is simplified and manipulated for most applications, as follows:

1. In the absence of any chemical reaction within the cooling fluid, $\mathfrak{R}_{\text{cool}} \to 0$.
2. The volumetric flow rate q_{cool} is written as a product of $\langle v_z \rangle_{\text{cool}}$ and the annular flow cross section, $\pi(R_{\text{outside}}^2 - R_{\text{inside}}^2)$, the latter of which is equivalent to dV_{cool}/dz.
3. The average velocity in the annulus $\langle v_z \rangle_{\text{cool}}$ is written as a product of the flow rate ratio ψ and $\langle v_z \rangle_{\text{Rx}}$.
4. The independent variable z, which increases in the primary flow direction of both fluids, is rewritten in terms of the average residence time of the reactive fluid in the inner pipe, $\tau_{\text{Rx}} = z/\langle v_z \rangle_{\text{Rx}}$.
5. The entire thermal energy balance for the cooling fluid is divided by the annular flow cross sectional area.
6. The following ratios are expressed in terms of R_{inside} and the radius ratio κ:

$$\frac{2\pi R_{\text{inside}}}{\pi(R_{\text{outside}}^2 - R_{\text{inside}}^2)} = \frac{2}{R_{\text{inside}}} \frac{\kappa^2}{1 - \kappa^2} \tag{4-92}$$

$$\frac{2\pi R_{\text{outside}}}{\pi(R_{\text{outside}}^2 - R_{\text{inside}}^2)} = \frac{2}{R_{\text{inside}}} \frac{\kappa}{1 - \kappa^2} \tag{4-93}$$

Hence, one calculates T_{cool} as a function of τ_{Rx} via numerical a solution of

$$\rho_{\text{cool}} \langle C_{p,\text{cool}} \rangle \psi \frac{dT_{\text{cool}}}{d\tau_{\text{Rx}}} = \frac{2U_{\text{overall, inside}}}{R_{\text{inside}}} \frac{\kappa^2}{1 - \kappa^2} (T_{\text{Rx}} - T_{\text{cool}}) - \frac{2U_{\text{overall, outside}}}{R_{\text{inside}}} \frac{\kappa}{1 - \kappa^2} (T_{\text{cool}} - T_{\text{ambient}}) \tag{4-94}$$

Thought-Provoking Problem. Modify the thermal energy balance (i.e., equation 4-94) in the annular region if the cooling fluid flows countercurrently with respect to the reactive fluid in the inner pipe. No chemical reaction occurs in the cooling fluid.

An equivalent form of the nonreactive cooling fluid's thermal energy balance in terms of R_{outside} is

$$\rho_{\text{cool}}\langle C_{p,\,\text{cool}}\rangle\psi\frac{dT_{\text{cool}}}{d\tau_{\text{Rx}}} = \frac{2U_{\text{overall, inside}}}{R_{\text{outside}}}\frac{\kappa}{1-\kappa^2}(T_{\text{Rx}} - T_{\text{cool}}) - \frac{2U_{\text{overall, outside}}}{R_{\text{outside}}}\frac{1}{1-\kappa^2}(T_{\text{cool}} - T_{\text{ambient}}) \quad (4\text{-}95)$$

Equation (4-95) provides efficient rationalization of the cooling fluid's temperature profile in the limit as $\kappa \to 0$ at constant R_{outside}. This corresponds to pure heat exchange between the cooling fluid and the surroundings when the inner pipe does not exist. Hence, (4-95) reduces to:

$$\rho_{\text{cool}}\langle C_{p,\,\text{cool}}\rangle\psi\frac{dT_{\text{cool}}}{d\tau_{\text{Rx}}} = \rho_{\text{cool}}\langle C_{p,\,\text{cool}}\rangle\frac{dT_{\text{cool}}}{d\tau_{\text{cool}}} = -\frac{2U_{\text{overall, outside}}}{R_{\text{outside}}}(T_{\text{cool}} - T_{\text{ambient}}) \quad (4\text{-}96)$$

which agrees with the thermal energy balance for the reactive fluid in the inner pipe (i.e., see equation 4-77):

$$\rho_{\text{Rx}}\langle C_{p,\,\text{Rx}}\rangle\frac{dT_{\text{Rx}}}{d\tau_{\text{Rx}}} = -\frac{2U_{\text{overall, inside}}}{R_{\text{inside}}}(T_{\text{Rx}} - T_{\text{cool}}) + (-\Delta H_{\text{Rx}})\mathfrak{R}_{\text{A}}(T_{\text{Rx}},\,\chi_{\text{A}}) \quad (4\text{-}97)$$

if (1) no chemical reaction occurs, $\mathfrak{R}_{\text{A}}(T_{\text{Rx}},\,\chi_{\text{A}}) \to 0$; (2) the annular region does not exist; (3) T_{cool} is replaced by T_{ambient}; (4) the subscript "Rx" is replaced by the subscript "cool"; and (5) the subscript "inside" is replaced by the subscript "outside." If all of these restrictions are applicable, then one obtains the following analytical solution for the cooling fluid's temperature profile when T_{ambient} is constant:

$$T_{\text{cool}}(\tau_{\text{CMT}}) = T_{\text{ambient}} + (T_{\text{cool, inlet}} - T_{\text{ambient}})\exp\left(-\frac{\tau_{\text{CMT}}}{\tau_{\text{HT}}}\right) \quad (4\text{-}98)$$

where $\tau_{\text{CMT}} = \tau_{\text{cool}}$ is the time constant for convective mass transfer within the cooling fluid and τ_{HT} is the time constant for heat transfer across the wall at radius R_{outside} to the surroundings at temperature T_{ambient} (i.e., see equation 4-75).

4-4 COUNTERCURRENT COOLING IN TUBULAR REACTORS WITH EXOTHERMIC CHEMICAL REACTIONS

This is the most mathematically demanding situation because the inlet condition for the cooling fluid (i.e., $T_{\text{cool}} = T_{\text{cool, inlet}}$) is known at the far end of the double-pipe reactor at $z = L$, whereas the inlet conditions for the reactive fluid (i.e.,

$\chi = 0$, $T_{Rx} = T_{Rx,\,inlet}$) are available at $z = 0$. This is known classically as a *split boundary value problem*, and it is characteristic of countercurrent flow heat exchangers. When numerical methods are required to integrate coupled mass and thermal energy balances subjected to split boundary conditions, it is necessary to do the following:

Step 1. Guess the outlet temperature of the cooling fluid at $z = 0$.

Step 2. Solve the set of three coupled ODEs from $z = 0$ to $z = L$ via the appropriate Runge–Kutta–Gill algorithm.

Step 3. Compare the calculated inlet temperature of the cooling fluid with the known boundary condition at $z = L$.

Step 4. Iterate until the correct guess for $T_{cool,\,outlet}$ at $z = 0$ produces agreement with the actual boundary condition at $z = L$.

Alternatively, as illustrated in the next section:

Step 1. Choose an outlet temperature for the cooling fluid at $z = 0$.

Step 2. Solve the set of three coupled ODEs from $z = 0$ to $z = L$.

Step 3. Identify the final value of T_{cool} at $z = L$ as the inlet temperature of the cooling fluid that produces the chosen value of $T_{cool,\,outlet}$ at $z = 0$.

These strategies are required to solve countercurrent flow problems numerically because ODE algorithms expect the user to provide either initial conditions at the same time (i.e., typically $t = 0$) for transient analysis or all boundary conditions at one value of the independent spatial coordinate for steady-state analysis.

At steady state, the countercurrent cooling fluid's thermal energy balance is constructed from a differential control volume in the annular region:

$$dV_{cool} = \pi(R^2_{outside} - R^2_{inside})\,dz \tag{4-99}$$

where the independent spatial coordinate z increases in the direction of flow of the reactive fluid within the inner pipe. It is not necessary to introduce another spatial coordinate z_{cool} that increases in the direction of flow of the cooling fluid because

$$dz_{cool} = -dz \tag{4-100}$$

In other words, all mass and thermal energy balances are constructed in terms of one independent spatial coordinate (i.e., z) or one residence time (i.e., $\tau_{Rx} = z/\langle v_z\rangle_{Rx}$). The consequences of this choice are that convective transport of thermal energy enters the cooling fluid's control volume at $z + dz$ and exits at z. In contrast, convective transport of thermal energy enters the control volume (i.e., $dV = \pi R^2_{inside}\,dz$) of the reactive fluid within the inner pipe at z and exits at

$z + dz$. If the outer wall of the double-pipe configuration is not insulated from the surroundings, then one develops the countercurrent cooling fluid's thermal energy balance as follows:

$$\text{convective input at } z + dz = \text{conductive output/both walls} + \text{convective output at } z \tag{4-101}$$

$$(\rho_{\text{cool}} q_{\text{cool}} h_{\text{cool}})_{z+dz} = dQ + (\rho_{\text{cool}} q_{\text{cool}} h_{\text{cool}})_z \tag{4-102}$$

where each term has units of energy per time. The differential rate of conductive heat transfer out of the cooling fluid across both walls is the same as (4-90) for cocurrent flow:

$$dQ = U_{\text{overall, inside}}(T_{\text{cool}} - T_{\text{Rx}})2\pi R_{\text{inside}}\, dz + U_{\text{overall, outside}}(T_{\text{cool}} - T_{\text{ambient}})2\pi R_{\text{outside}}\, dz \tag{4-103}$$

Hence, equation (4-102) reduces to:

$$\rho_{\text{cool}} q_{\text{cool}}[(h_{\text{cool}})_{z+dz} - (h_{\text{cool}})_z] = \rho_{\text{cool}} q_{\text{cool}}\, dh_{\text{cool}} = dQ \tag{4-104}$$

which differs by a negative sign from the cooling fluid's thermal energy balance given in (4-57). This is a consequence of cocurrent vs. countercurrent flow. If the cooling fluid does not experience any chemical reaction, the final form of its thermal energy balance for countercurrent flow can be adopted from equation (4-94) by reversing the sign of each term on the right side of the balance:

$$\rho_{\text{cool}} \langle C_{p,\,\text{cool}} \rangle \psi \frac{dT_{\text{cool}}}{d\tau_{\text{Rx}}} = -\frac{2U_{\text{overall, inside}}}{R_{\text{inside}}} \frac{\kappa^2}{1-\kappa^2}(T_{\text{Rx}} - T_{\text{cool}}) + \frac{2U_{\text{overall, outside}}}{R_{\text{outside}}} \frac{1}{1-\kappa^2}(T_{\text{cool}} - T_{\text{ambient}}) \tag{4-105}$$

This ODE for $T_{\text{cool}}(\tau_{\text{Rx}})$ is analyzed in the next section together with mass and thermal energy balances for the reactive fluid within the inner pipe.

4-5 MANIPULATING THE INLET/OUTLET TEMPERATURE OF A COUNTERCURRENT COOLING FLUID: MULTIPLE STATIONARY-STATE BEHAVIOR IN EXOTHERMIC PFRs

Reactant A is converted irreversibly and exothermically to products in a 2-in.-inner-diameter tubular reactor via first-order chemical kinetics. The reactive mixture in the inner pipe is cooled using a concentric double-pipe heat exchanger. The nonreactive cooling fluid in the annular region flows countercurrently with respect to the reactive fluid. The radius ratio of the double-pipe configuration is $\kappa = R_{\text{inside}}/R_{\text{outside}} = 0.5$, the inlet temperature of the reactive fluid is 340 K,

and the average velocity of the cooling fluid is twofold larger than the average velocity of the reactive fluid (i.e., $\psi = 2$). The homogeneous chemical reaction is strongly exothermic ($\Delta H_{Rx} = -15$ kcal/mol) and heat is generated volumetrically throughout the inner pipe. Hence, the following group of terms in the thermal energy balance for the reactive fluid is negative:

$$\frac{C_{A0}\Delta H_{Rx}}{\rho_{Rx}\langle C_{p,\,Rx}\rangle} = -150 \text{ K} \tag{4-106}$$

TABLE 4-7 System of Equations That Must Be Analyzed to Prevent Thermal Runaway in a Plug-Flow Tubular Reactor with Countercurrent Cooling in a Concentric Double-Pipe Configuration That Is Not Insulated from the Surroundings[a]

nth-Order irreversible chemical kinetics: $\mathfrak{R}_A(T_{Rx}, \chi) = k_{Rx}(T_{Rx})[C_{A0}(1-\chi)]^n$

Arrhenius model/transition-state theory: $k_{Rx}(T_{Rx}) = k_\infty \exp\left(\dfrac{-E_{activation}}{RT_{Rx}}\right)$

Mass balance for reactant A: $C_{A0}\dfrac{d\chi}{d\tau_{Rx}} = \mathfrak{R}_A(T_{Rx}, \chi)$

Thermal energy balance for the reactive fluid within the inner pipe:

$$\rho_{Rx}\hat{C}_{p,\,Rx}\frac{dT_{Rx}}{d\tau_{Rx}} = \frac{2U_{inside}}{R_{inside}}(T_{cool} - T_{Rx}) + (-\Delta H_{Rx})\mathfrak{R}_A(T_{Rx}, \chi)$$

Thermal energy balance for the countercurrent cooling fluid:

$$\rho_{cool}\hat{C}_{p,\,cool}\psi\frac{dT_{cool}}{d\tau_{Rx}} = \frac{2U_{inside}}{R_{inside}}\frac{\kappa^2}{1-\kappa^2}(T_{cool} - T_{Rx}) + \frac{2U_{outside}}{R_{outside}}\frac{1}{1-\kappa^2}(T_{cool} - T_{ambient})$$

Boundary conditions at the inlet to the reactor, where $\tau_{Rx} = 0$:
Conversion of reactant A, $\chi = 0$
Inlet temperature of the reactive fluid, $T_{Rx} = 340$ K
Outlet temperature of the countercurrent cooling fluid, $T_{cool} =$ (guess)

Parameters defined in the problem statement:

$(\tau_{Rx})_{final} = 30$ s $\quad \kappa = 0.5 \quad \psi = 2 \quad T_{ambient} = 295$ K

$k_\infty = 3.94 \times 10^{12}$ s^{-1} $\quad n = 1 \quad E_{activation} = 22.5$ kcal/mol

$\Delta H_{Rx} = -15$ kcal/mol $\quad \dfrac{C_{A0}\Delta H_{Rx}}{\rho_{Rx}\hat{C}_{p,\,Rx}} = -150$ K

$U_{inside} = 10^4 \dfrac{\text{kcal}}{\text{m}^2\cdot\text{h}\cdot\text{K}} \quad \dfrac{\rho_{Rx}\hat{C}_{p,\,Rx}R_{inside}}{2U_{inside}} = \dfrac{\rho_{cool}\hat{C}_{p,\,cool}R_{inside}}{2U_{inside}} = 5$ s

$U_{outside} = 20\dfrac{\text{kcal}}{\text{m}^2\cdot\text{h}\cdot\text{K}} \quad \dfrac{\rho_{cool}\hat{C}_{p,\,cool}R_{outside}}{2U_{outside}} = 2500$ s

[a] Notice that the boundary conditions are split.

Heat transfer via radial conduction across the inner wall at radius R_{inside}, enhanced by axial convection of thermal energy in the primary flow directions, is characterized by the following overall heat transfer coefficient:

$$U_{\text{inside}} = 10^4 \text{ kcal/m}^2\cdot\text{h}\cdot\text{K} \tag{4-107}$$

The time constant for heat transfer across the inner wall of the double-pipe configuration is the same for the reactive fluid and the nonreactive cooling fluid:

$$\frac{\rho_{\text{Rx}}\langle C_{p,\text{Rx}}\rangle R_{\text{inside}}}{2U_{\text{inside}}} = \frac{\rho_{\text{cool}}\langle C_{p,\text{cool}}\rangle R_{\text{inside}}}{2U_{\text{inside}}} = 5 \text{ s} \tag{4-108}$$

The outer wall of the double-pipe configuration at radius R_{outside} is not thermally insulated from the surroundings and the overall outside heat transfer coefficient is

$$U_{\text{outside}} = 20 \text{ kcal/m}^2\cdot\text{h}\cdot\text{K} \tag{4-109}$$

TABLE 4-8 Correlation between the Inlet and Outlet Temperatures of a Countercurrent Cooling Fluid and the Maximum Conversion for an Exothermic Reactive Fluid in a Concentric Double-Pipe Configuration That Is Not Insulated from the Surroundings[a]

Temperature of Cooling Fluid (K)		Outlet Reactant Conversion at $\tau_{\text{Rx}} = 30$ s (%)
Inlet	Outlet	
308.8	337.5	100
312	**337**	**90 (thermal runaway)**
317	**336.8**	**71 (well-controlled)**
322	336	49
323.7	335	39
324.1	334	33
324.1	333	29
323.8	332	26
323.4	331	23
322.8	330	20
318.9	325	12
314	320	8
310.8	317	6.5
308.6	315	6
302.9	310	4
297.2	305	3
291.3	300	2.5
285.4	295	2
279.4	290	1.8

[a] A distinction is made between a thermally well-controlled tubular reactor and one that exhibits thermal runaway.

The time constant for heat transfer to the surroundings, across the outer wall, is

$$\frac{\rho_{\text{cool}}\langle C_{p,\,\text{cool}}\rangle R_{\text{outside}}}{2U_{\text{outside}}} = 2500 \text{ s} \tag{4-110}$$

and ambient temperature is constant at 295 K. Monitor the performance of this double-pipe reactor for the following range of average residence times τ_{Rx} of the reactive fluid: $0 \leq \tau_{\text{Rx}} \leq 30$ s. Then correlate the inlet and outlet temperatures of the cooling fluid with the outlet conversion of the reactive fluid, and identify the critical outlet temperature of the cooling fluid that represents the crossover from a thermally well-behaved reactor to one that exhibits thermal runaway. The appropriate reactor design equations are summarized in Table 4-7. As mentioned in Section 4-4, this split boundary value problem is solved numerically by choosing values of the cooling fluid's outlet temperature, and solving three coupled ODEs to determine $T_{\text{cool, inlet}}$ at $z = L$ which corresponds to the chosen value of $T_{\text{cool, outlet}}$ at $z = 0$. Results are presented in Figure 4-12 and Table 4-8.

Notice that the double-pipe reactor is well behaved when the outlet temperature of the cooling fluid is less than 337 K. On the other hand, if $T_{\text{cool, inlet}} \geq 324.5$ K,

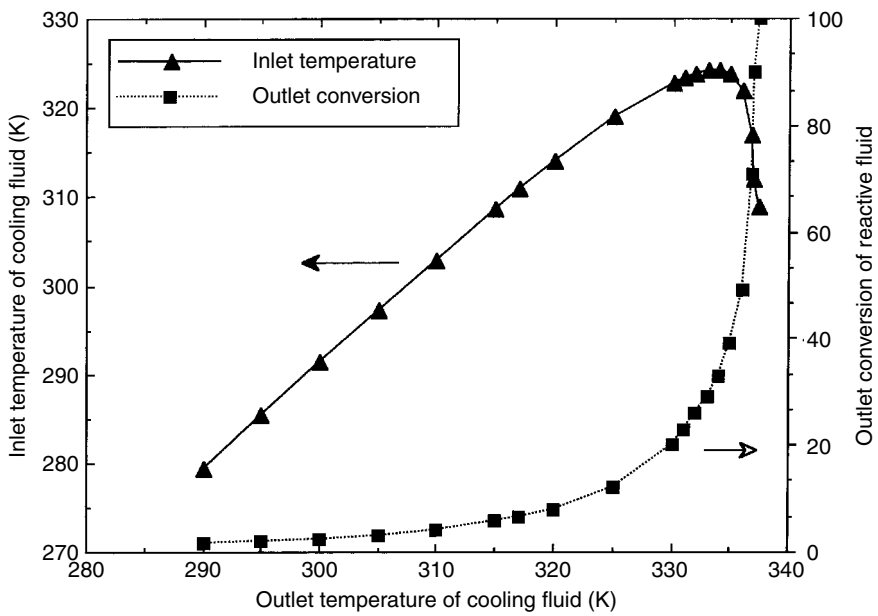

Figure 4-12 Correlation between the inlet and outlet temperatures of a countercurrent cooling fluid and the maximum conversion for an exothermic reactive fluid in a concentric double-pipe configuration with radius ratio $\kappa = 0.5$ that is not insulated from the surroundings. The exothermic reactive fluid enters at 340 K. Two different steady-state solutions exist when the inlet temperature of the cooling fluid is between 308 K and 324 K.

then thermal runaway is inevitable, and interestingly enough, no steady-state solution exists! The biggest surprise is that two steady-state solutions exist when 308 K $\leq T_{\text{cool, inlet}} \leq$ 324 K. For example, if $T_{\text{cool, inlet}} \approx 309$ K, then either

$$\text{(a) } T_{\text{cool, outlet}} = 315 \text{ K} \qquad \chi_{\text{final}} = 6\% \text{ at } \tau_{\text{Rx}} = 30 \text{ s}$$

or

$$\text{(b) } T_{\text{cool, outlet}} = 337.5 \text{ K} \qquad \chi_{\text{final}} = 100\% \text{ at } \tau_{\text{Rx}} = 30 \text{ s}$$

Obviously, (a) represents a well-behaved double-pipe reactor, whereas (b) is in the regime of thermal runaway (see Figure 4-13).

Consider a second example where $T_{\text{cool, inlet}} \approx 322$ K. Once again, the system must choose between two different paths (see Figure 4-14). Either

$$\text{(a) } T_{\text{cool, outlet}} = 329 \text{ K} \qquad \chi_{\text{final}} = 18\% \text{ at } \tau_{\text{Rx}} = 30 \text{ s}$$

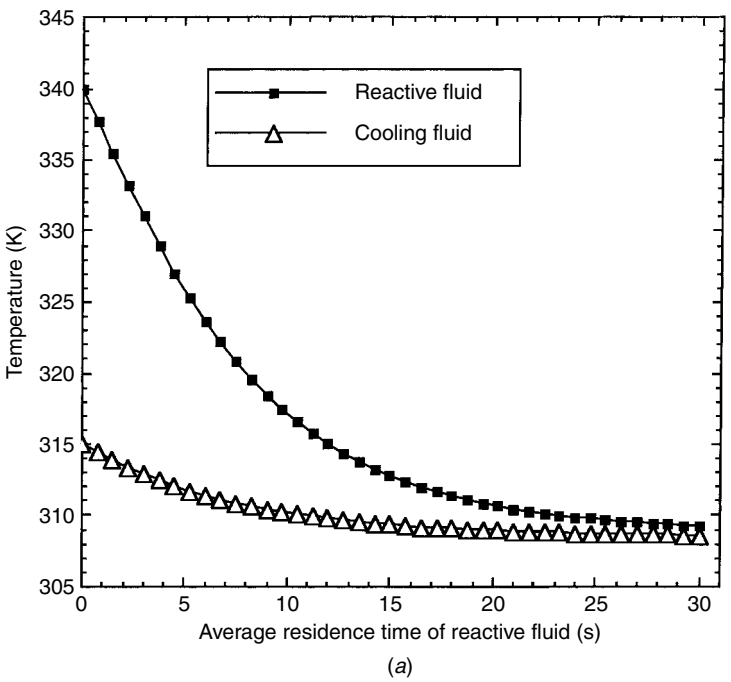

Figure 4-13 Examples of two different steady-state solutions for the reactive and cooling fluid temperature profiles in a countercurrent concentric double-pipe configuration with exothermic chemical reaction in the inner tube. In both cases, the inlet temperatures of the reactive and cooling fluids are 340 K and 309 K, respectively. (*a*) Thermally well-behaved reactor with only 6% outlet conversion of reactants to products. (*b*) Thermal runaway reactor with 100% outlet conversion of reactants to products.

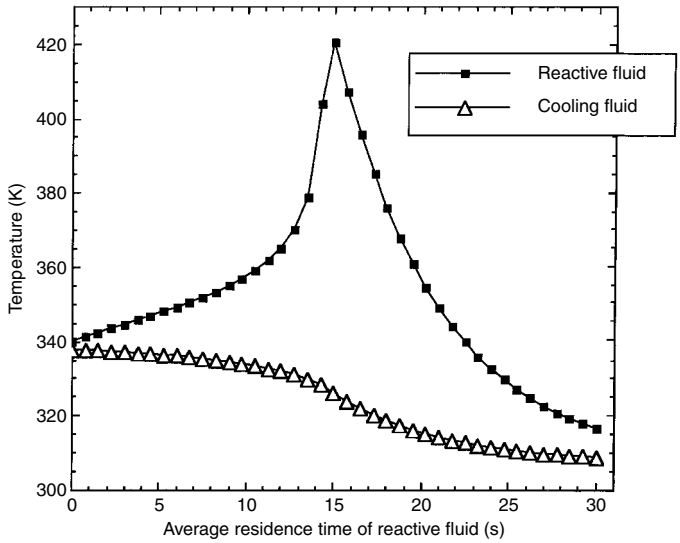

Figure 4-13 (*continued*)

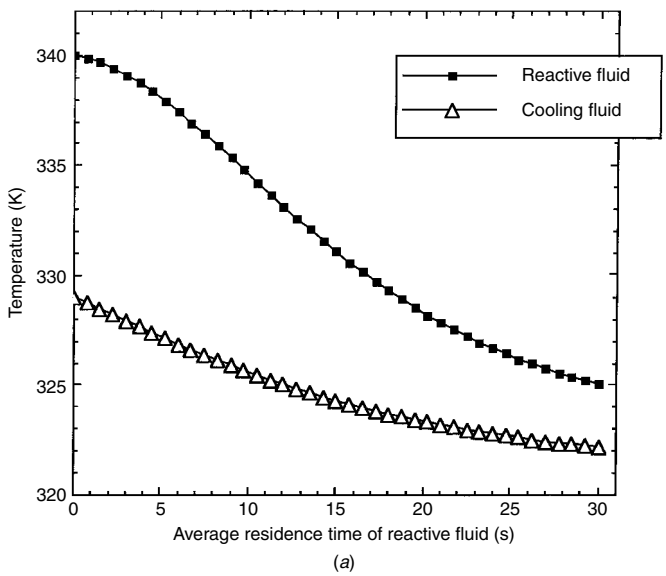

Figure 4-14 Examples of two different steady-state solutions for the reactive and cooling fluid temperature profiles in a countercurrent concentric double-pipe configuration with exothermic chemical reaction in the inner tube. In both cases, the inlet temperatures of the reactive and cooling fluids are 340 K and 322 K, respectively. (*a*) Thermally well-behaved reactor with 18% outlet conversion of reactants to products. (*b*) Thermally well-behaved reactor with 49% outlet conversion of reactants to products.

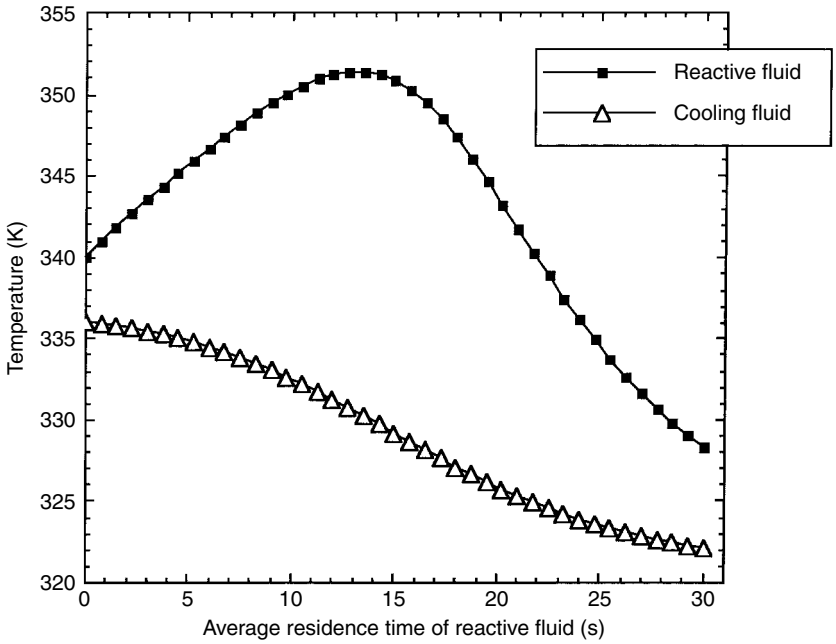

(*b*)

Figure 4-14 (*continued*)

or

$$\text{(b) } T_{\text{cool, outlet}} = 336 \text{ K} \qquad \chi_{\text{final}} = 49\% \text{ at } \tau_{\text{Rx}} = 30 \text{ s}$$

Stability analysis could prove to be useful for the identification of stable and unstable steady-state solutions. Obviously, the system will gravitate toward a stable steady-state operating point if there is a choice between stable and unstable steady states. If both steady-state solutions are stable, the actual path followed by the double-pipe reactor depends on the transient response prior to the achievement of steady state. Hill (1977, p. 509) and Churchill (1979a, p. 479; 1979b, p. 915; 1984; 1985) describe multiple steady-state behavior in nonisothermal plug-flow tubular reactors. Hence, the classic phenomenon of multiple stationary (steady) states in perfect backmix CSTRs should be extended to differential reactors (i.e., PFRs).

The classic landmark paper on parametric sensitivity in nonisothermal chemical reactors is by Bilous and Amundson (1956). A more recent example of multiple stationary states in packed catalytic tubular reactors is discussed by Pedernera *et al.* (1997).

PROBLEMS

4-1. Consider a liquid-phase plug-flow tubular reactor with irreversible nth-order endothermic chemical reaction. The reactive mixture is heated with a fluid that flows cocurrently in the annular region of a double-pipe configuration. The mass and heat transfer Peclet numbers are large for both fluids. All physical properties of both fluids are independent of temperature and conversion, and the inlet conditions at $z = 0$ are specified. What equations are required to investigate the phenomenon of parametric sensitivity in this system?

4-2. A complex exothermic chemical reaction occurs in a plug-flow tubular reactor with constant energy flux across the wall at radius R. All thermophysical properties of the reactive fluid are independent of temperature and conversion. Derive the relations between conversion χ, fluid temperature T, and reactor volume V_{PFR} at high-mass and high-heat-transfer Peclet numbers.

Transport Phenomena for Chemical Reactor Design. Laurence A. Belfiore
Copyright © 2003 John Wiley & Sons, Inc.
ISBN: 0-471-20275-4

5

MULTIPLE STATIONARY STATES IN CONTINUOUS STIRRED TANK REACTORS

Multiple steady-state behavior is a classic chemical engineering phenomenon in the analysis of nonisothermal continuous-stirred tank reactors. Inlet temperatures and flow rates of the reactive and cooling fluids represent key design parameters that determine the number of operating points allowed when coupled heat and mass transfer are addressed, and the chemical reaction is exothermic. One steady-state operating point is most common in CSTRs, and two steady states occur most infrequently. Three stationary states are also possible, and their analysis is most interesting because two of them are stable whereas the other operating point is unstable.

Nonisothermal operation of a liquid-phase CSTR with reversible exothermic nth-order chemical kinetics is the focus of this chapter. The reactor is well insulated from the surroundings, except for heat exchange across the cooling coil. The reaction scheme is

$$2A \longleftrightarrow B$$

Coupling of two molecules of reactant A liberates thermal energy, but the entropy change is negative. The equilibrium constant is expressed in terms of standard-state enthalpy and entropy changes for reaction at 298 K, and the temperature dependence of the forward kinetic rate constant is modeled by an Arrhenius function. Thermal energy is generated volumetrically due to the exothermic nature of the chemical reaction. As the temperature increases, the equilibrium constant decreases and Le Châtelier's principle shifts the reaction to the left, which favors reactant A. Hence, reactant conversion increases initially and then decreases at higher temperatures when the reactor operates in the near-equilibrium regime. Also at higher temperatures, the forward kinetic rate constant increases and the

characteristic time constant for chemical reaction decreases. For reversible nth-order reactions, the time constant for chemical reaction is defined in terms of the kinetic rate constant for the forward step:

$$\lambda = \frac{1}{k_{\text{forward}}(T)(C_{\text{A, inlet}})^{n-1}} \frac{K_{\text{equil}}}{1 + K_{\text{equil}}} \tag{5-1}$$

where $C_{\text{A, inlet}}$ is the inlet molar density of reactant A and K_{equil} is the dimensionless equilibrium constant. When the time constant for convective mass transfer through the CSTR (i.e., residence time τ) is much larger than λ, particularly at high temperatures, the reaction is equilibrium controlled. The conversion rate approaches zero when the reaction approaches equilibrium. This provides an explanation for the fact that the rate of heat generation increases initially and then decreases at very high temperatures. In each numerical example presented below, the residence time is 200 s and the reactor volume is 20 L.

5-1 MASS BALANCE

Coupled mass and thermal energy balances are required to analyze the nonisothermal response of a well-mixed continuous-stirred tank reactor. These balances can be obtained by employing a macroscopic control volume that includes the entire contents of the CSTR, or by integrating plug-flow balances for a differential reactor under the assumption that temperature and concentrations are not a function of spatial coordinates in the macroscopic CSTR. The macroscopic approach is used for the mass balance, and the differential approach is employed for the thermal energy balance. At high-mass-transfer Peclet numbers, the steady-state macroscopic mass balance on reactant A with axial convection and one chemical reaction, and units of moles per time, is

$$\text{convective input} + \text{rate of production} = \text{convective output} \tag{5-2}$$

$$q_{\text{Rx}} C_{\text{A, inlet}} + \nu_{\text{A}} \mathfrak{R} V_{\text{CSTR}} = q_{\text{Rx}} C_{\text{A, outlet}} \tag{5-3}$$

This reduces to

$$\tau \mathfrak{R} - C_{\text{A, inlet}} \chi = 0 \tag{5-4}$$

where $\nu_{\text{A}} = -1$ is the stoichiometric coefficient of reactant A (i.e., after division of the chemical reaction by 2), $\tau = V_{\text{CSTR}}/q_{\text{Rx}}$, and $\chi = 1 - C_{\text{A, outlet}}/C_{\text{A, inlet}}$ is the conversion of reactant A with respect to $C_{\text{A, inlet}}$.

5-2 CHEMICAL KINETICS

The reversible kinetic rate law for nth-order chemical reaction is

$$\mathfrak{R} = k_{\text{forward}}(C_{\text{A}})^n - k_{\text{backward}}(C_{\text{B}})^n = k_{\text{forward}} \left[C_A^n - \frac{C_B^n}{K_{\text{equil}}(T)} \right] \tag{5-5}$$

If the reactor is well stirred, then the molar densities of reactant A and product B in the kinetic rate law are expressed in terms of conversion χ via stoichiometry and the steady-state mass balance with convection and chemical reaction:

$$C_{\mathrm{A}} = C_{\mathrm{A,\,outlet}} = C_{\mathrm{A,\,inlet}}\,(1-\chi) \tag{5-6}$$

$$C_{\mathrm{B}} = C_{\mathrm{B,\,outlet}} = C_{\mathrm{B,\,inlet}} + C_{\mathrm{A,\,inlet}}\nu_{\mathrm{B}}\chi = C_{\mathrm{A,\,inlet}}(\Theta_{\mathrm{B}} + \nu_{\mathrm{B}}\chi) \tag{5-7}$$

where Θ_{B} is the inlet molar density ratio of product B relative to reactant A. The temperature dependence of the dimensionless equilibrium constant from thermodynamics is

$$K_{\mathrm{equil}}(T) = \exp\left(\mathrm{A} + \frac{\mathrm{B}}{T}\right) \tag{5-8}$$

$$\mathrm{A} = \frac{\Delta S^{0}_{\mathrm{Rx,\,298}}}{R_{\mathrm{gas}}} \tag{5-9}$$

$$\mathrm{B} = -\frac{\Delta H^{0}_{\mathrm{Rx,\,298}}}{R_{\mathrm{gas}}} \tag{5-10}$$

The Arrhenius expression for the kinetic rate constant is

$$k_{\mathrm{forward}}(T) = k_{\infty}\exp\left(-\frac{E_{\mathrm{activation}}}{R_{\mathrm{gas}}T}\right) \tag{5-11}$$

5-3 THERMAL ENERGY BALANCE

If one adopts a plug-flow thermal energy balance on the reactive fluid within a differential CSTR at high-heat-transfer Peclet numbers, then equation (3-37) yields:

$$\rho_{\mathrm{Rx}} q_{\mathrm{Rx}} \langle C_{p,\mathrm{Rx,\,feed}}\rangle \frac{dT_{\mathrm{CSTR}}}{dV_{\mathrm{CSTR}}} = \frac{dQ_{\mathrm{input}}}{dV_{\mathrm{CSTR}}} + (-\Delta H_{\mathrm{Rx}})\mathfrak{R} \tag{5-12}$$

where dQ_{input} represents the differential rate of thermal energy transfer into the CSTR across the wall of the cooling coil. There is no other heat exchange with the surroundings. Integration of this equation over the total volume of a well-mixed CSTR from inlet to outlet yields the following macroscopic thermal energy balance for the nonisothermal reactor:

$$\int \rho_{\mathrm{Rx}} q_{\mathrm{Rx}} \langle C_{p,\mathrm{Rx,\,feed}}\rangle\, dT_{\mathrm{CSTR}} - \int dQ_{\mathrm{input}} = \int (-\Delta H_{\mathrm{Rx}})\mathfrak{R}\, dV_{\mathrm{CSTR}} \tag{5-13}$$

If the kinetic rate law $\mathfrak{R}$ is not a function of position throughout the well-mixed reactor, and $d\aleph_{\mathrm{conduction}} = -dQ_{\mathrm{input}}$ is the differential rate of thermal energy

removal from the CSTR across the wall of the cooling coil via heat conduction, then the macroscopic thermal energy balance reduces to

$$\rho_{\mathrm{Rx}} q_{\mathrm{Rx}} \langle C_{p,\mathrm{Rx,\ feed}} \rangle (T_{\mathrm{CSTR}} - T_{\mathrm{Rx,\ inlet}}) + \aleph_{\mathrm{conduction}} = (-\Delta H_{\mathrm{Rx}}) \Re V_{\mathrm{CSTR}} \quad (5\text{-}14)$$

The rate of heat generation $G_{\mathrm{Rx}}(T)$ due to exothermic chemical reaction in the CSTR, with units of calories per second, is

$$G_{\mathrm{Rx}}(T) = -\Delta H^0_{\mathrm{Rx,\ 298}} \Re V_{\mathrm{CSTR}} \quad (5\text{-}15)$$

$$V_{\mathrm{CSTR}} = \tau q_{\mathrm{Rx}} \quad (5\text{-}16)$$

where $T = T_{\mathrm{CSTR}}$ is the temperature within the reactor and in the exit stream. The rate of heat removal from the CSTR, $\aleph(T)$, contains contributions from convection and conduction:

$$\aleph(T) = \aleph_{\mathrm{convection}}(T) + \aleph_{\mathrm{conduction}}(T) \quad (5\text{-}17)$$

Convective transport of thermal energy through the reactor is given by

$$\aleph_{\mathrm{convection}}(T) = \rho_{\mathrm{Rx}} q_{\mathrm{Rx}} \langle C_{p,\mathrm{Rx,\ feed}} \rangle (T - T_{\mathrm{Rx,\ inlet}}) \quad (5\text{-}18)$$

The rate of heat removal due to conduction across the cooling coil and into the cooling fluid is given by

$$\aleph_{\mathrm{conduction}}(T) = \rho_{\mathrm{cool}} q_{\mathrm{cool}} \langle C_{p,\mathrm{cool}} \rangle [1 - \exp(-\text{cool factor})](T - T_{\mathrm{cool,\ inlet}}) \quad (5\text{-}19)$$

$$\text{cool factor} = \frac{U_{\mathrm{overall}} \pi D_{\mathrm{cooling\ coil}} L_{\mathrm{cooling\ coil}}}{\rho_{\mathrm{cool}} q_{\mathrm{cool}} \langle C_{p,\mathrm{cool}} \rangle} \quad (5\text{-}20)$$

5-3.1 Thermal Energy Balance for the Cooling Fluid

The rate of thermal energy transport across the wall of the cooling coil, as summarized by (5-19) and (5-20), is calculated from a thermal energy balance on the nonreactive cooling fluid when the temperature of the surroundings (i.e., in the CSTR) is constant at $T_{\mathrm{CSTR}} = T$. At high-heat-transfer Peclet numbers, the quasi-macroscopic thermal energy balance over a differential control volume in the cooling fluid [i.e., $dV_{\mathrm{cooling\ fluid}} = \pi (D_{\mathrm{cooling\ coil}}/2)^2\, dz$] is adopted from equation (4-64):

$$\rho_{\mathrm{cool}} q_{\mathrm{cool}} \langle C_{p,\mathrm{\ cool}} \rangle\, dT_{\mathrm{cool}}/dz = \frac{d\aleph_{\mathrm{conduction}}}{dz} = \pi D_{\mathrm{cooling\ coil}} U_{\mathrm{overall}} (T_{\mathrm{CSTR}} - T_{\mathrm{cool}}) \quad (5\text{-}21)$$

where $d\aleph_{\mathrm{conduction}}$ represents the differential rate of heat removal from the CSTR, which enters the cooling fluid across the wall of the cooling coil. The calculation proceeds as follows:

1. Equation (5-21);

$$\rho_{\text{cool}} q_{\text{cool}} \langle C_{p,\,\text{cool}} \rangle \frac{dT_{\text{cool}}}{dz} = \pi D_{\text{cooling coil}} U_{\text{overall}} (T_{\text{CSTR}} - T_{\text{cool}}) \tag{5-22}$$

   is integrated to obtain an expression for the instantaneous temperature difference, $T_{\text{CSTR}} - T_{\text{cool}}$.
2. The rate of thermal energy removal from the CSTR across the wall of the cooling coil is obtained by integrating:

$$\frac{d\aleph_{\text{conduction}}}{dz} = \pi D_{\text{cooling coil}} U_{\text{overall}} (T_{\text{CSTR}} - T_{\text{cool}}) \tag{5-23}$$

   over the length of the cooling coil (i.e., $L_{\text{cooling coil}}$) after the temperature-difference profile is determined in step 1.

The temperature-difference profile is obtained from (5-22) via separation of variables:

$$\rho_{\text{cool}} q_{\text{cool}} \langle C_{p,\,\text{cool}} \rangle \frac{dT_{\text{cool}}}{T_{\text{CSTR}} - T_{\text{cool}}} = \pi D_{\text{cooling coil}} U_{\text{overall}}\, dz \tag{5-24}$$

Integration from $z = 0$, where $T_{\text{cool}} = T_{\text{cool, inlet}}$ at the inlet to the cooling coil, yields

$$\rho_{\text{cool}} q_{\text{cool}} \langle C_{p,\,\text{cool}} \rangle \ln \left[\frac{T_{\text{CSTR}} - T_{\text{cool, inlet}}}{T_{\text{CSTR}} - T_{\text{cool}}} \right] = \pi D_{\text{cooling coil}} U_{\text{overall}} z \tag{5-25}$$

Rearrangement of (5-25) yields the temperature-difference profile as a function of axial coordinate z, which increases in the primary flow direction:

$$T_{\text{CSTR}} - T_{\text{cool}} = (T_{\text{CSTR}} - T_{\text{cool, inlet}}) \exp \left(- \frac{\pi D_{\text{cooling coil}} U_{\text{overall}} z}{\rho_{\text{cool}} q_{\text{cool}} \langle C_{p,\,\text{cool}} \rangle} \right) \tag{5-26}$$

Now the macroscopic rate of thermal energy removal from the CSTR, across the cooling coil is calculated from (5-23) and (5-26):

$$\aleph_{\text{conduction}} \equiv \int d\aleph_{\text{conduction}} = \pi D_{\text{cooling coil}} U_{\text{overall}} \int_{z=0}^{L_{\text{cooling coil}}} (T_{\text{CSTR}} - T_{\text{cool}})\, dz \tag{5-27}$$

Hence,

$$\aleph_{\text{conduction}}(T) = \rho_{\text{cool}} q_{\text{cool}} \langle C_{p,\,\text{cool}} \rangle [1 - \exp(-\text{cool factor})](T - T_{\text{cool, inlet}}) \tag{5-28}$$

5-4 MULTIPLE STATIONARY STATES

The numerical example illustrated below in Figure 5-1 separately evaluates the rate of thermal energy generation $G_{Rx}(T)$ due to chemical reaction, and the total rate of heat removal from the CSTR, $\aleph(T)$, via convection and conduction, over the temperature range 200 K $\leq T \leq$ 600 K. The CSTR operates at temperature T_{CSTR} when

$$G_{Rx}(T_{CSTR}) = \aleph(T_{CSTR}) \tag{5-29}$$

as dictated by the steady-state macroscopic thermal energy balance given by (5-14). Under most conditions, one operating temperature is predicted because $G_{Rx}(T)$ and $\aleph(T)$ intersect at one point. For the particular set of physically realistic parameters defined below, the thermal energy balance is satisfied at the following temperatures and corresponding conversions of reactant A for the example problem illustrated in Figure 5-1:

T_{CSTR}	χ
$T_{lower} = 301$ K	1.4%
$T_{middle} = 399$ K	29%
$T_{upper} = 513$ K	62%

Hence, the reactor operates at one of these three temperatures. One must consider initial startup conditions and the effect of a fluctuating reactor temperature on

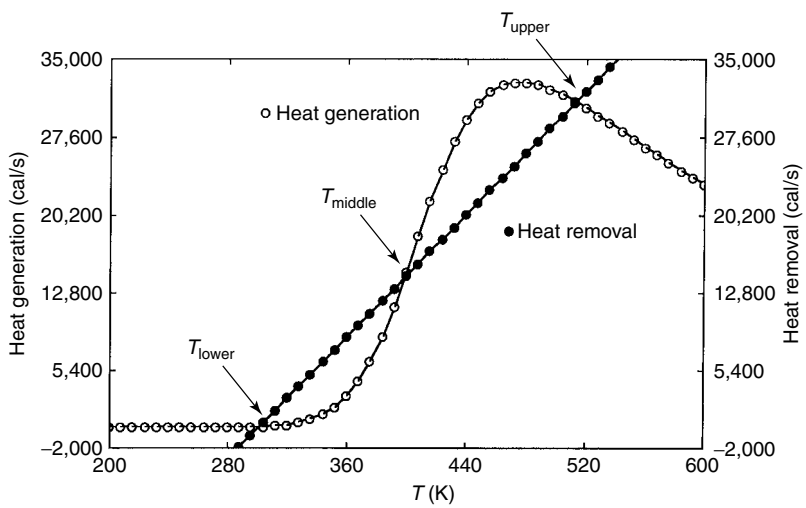

Figure 5-1 Numerical and graphical example for a nonisothermal CSTR with exothermic chemical reaction, illustrating the phenomenon of three steady-state operating points as dictated by three intersections of the rates of thermal energy generation and removal vs. temperature curves.

$G_{Rx}(T)$ and $\aleph(T)$ to determine which operating temperature is most favorable. The *parametric values* are as follows:

$C_{A,\,inlet} = 0.1$ mol/mL	$\Theta_B = 0$	$\nu_B = 0.5$
$\tau = 200$ s	$k_\infty = 10^5$ s^{-1}	$E_{activation} = 14{,}000$ cal/mol
$\Delta H^0_{Rx,\,298} = -5000$ cal/mol	$\Delta S^0_{Rx,\,298} = -10$ cal/mol·K	$\rho_{Rx} = 0.75$ g/mL
$q_{Rx} = 100$ mL/s	$T_{Rx,\,inlet} = 325$ K	$\rho_{cool} = 1$ g/mL
$q_{cool} = 250$ mL/s	$T_{cool,\,inlet} = 280$ K	$R_{gas} = 1.987$ cal/mol·K
$\langle C_{p,Rx,\,feed}\rangle = 0.9$ cal/g·K	$\langle C_{p,\,cool}\rangle = 1$ cal/g·K	$L_{cooling\ coil} = 200$ cm
$V_{CSTR} = 20$ L	$D_{cooling\ coil} = 1.5$ cm	$n = 1$
$U_{overall} = 3600$ kcal/m^2·h·K $= 0.1$ cal/cm^2·s·K		

5-4.1 Stable and Unstable Operating Points

If 293–298 K represents a plausible range of startup temperatures for the CSTR described in the previous section, then:

$$G_{Rx}(T) > \aleph(T) \qquad T < 301 \text{ K} \tag{5-30}$$

and the reactor temperature increases dynamically because the rate of thermal energy generation is larger than the rate of heat removal. At 301 K, steady state is achieved because $G_{Rx}(301\text{ K}) = \aleph(301\text{ K})$. T_{lower} is a *stable* operating point because small fluctuations in reactor temperature decrease in amplitude and the CSTR operating point returns to 301 K. This is rationalized as follows, based on the graphs in Figure 5-1:

If $T < T_{lower}$	$G_{Rx}(T) > \aleph(T)$	reactor temperature increases to T_{lower}
If $T_{lower} < T < T_{middle}$	$G_{Rx}(T) < \aleph(T)$	reactor temperature decreases to T_{lower}

However, operation of the CSTR at 301 K is not very attractive because the conversion of reactant A predicted is only 1.4%. Similar analysis reveals that T_{upper} is also a *stable* operating point because small changes in reactor temperature above or below T_{upper} produce an imbalance between $G_{Rx}(T)$ and $\aleph(T)$ that shifts the steady-state operating point back to T_{upper}. For example (see Figure 5-1):

If $T > T_{upper}$	$G_{Rx}(T) < \aleph(T)$	reactor temperature decreases to T_{upper}
If $T_{middle} < T < T_{upper}$	$G_{Rx}(T) > \aleph(T)$	reactor temperature increases to T_{upper}

It is difficult, if not impossible, to operate at T_{middle} without implementing external control of inlet temperatures and/or flow rates of either the reactive mixture or the cooling fluid. T_{middle} represents an *unstable* operating point because small fluctuations in reactor temperature grow until the CSTR gravitates toward one of the two stable operating points at T_{upper} or T_{lower}. For example (see Figure 5-1):

If $T_{middle} < T < T_{upper}$	$G_{Rx}(T) > \aleph(T)$	reactor temperature increases to T_{upper}
If $T_{lower} < T < T_{middle}$	$G_{Rx}(T) < \aleph(T)$	reactor temperature decreases to T_{lower}

5-4.2 Effect of $T_{cool,inlet}$ on Reactor Performance: Ignition

The rate of thermal energy removal vs. reactor temperature is illustrated in Figure 5-2 when the cooling fluid enters the cooling coil at 280, 300, 320, and 350 K. $T_{cool,\,inlet}$ affects the rate of thermal energy removal but not the rate of thermal energy generation in the CSTR. Based on equation (5-19), an increase in $T_{cool,\,inlet}$ shifts the linear heat removal curve $\aleph(T)$ to the right without perturbing its slope. As illustrated in Figure 5-2, reactor simulations at inlet cooling fluid temperatures of 280, 300, and 320 K predict three possible steady-state operating points (i.e., T_{lower}, T_{middle}, and T_{upper}), where T_{middle} is unstable and T_{lower} and T_{upper} are stable. If the CSTR operates at T_{lower} with rather low conversion and $T_{cool,\,inlet}$ increases continuously by preheating the cooling fluid, the temperature

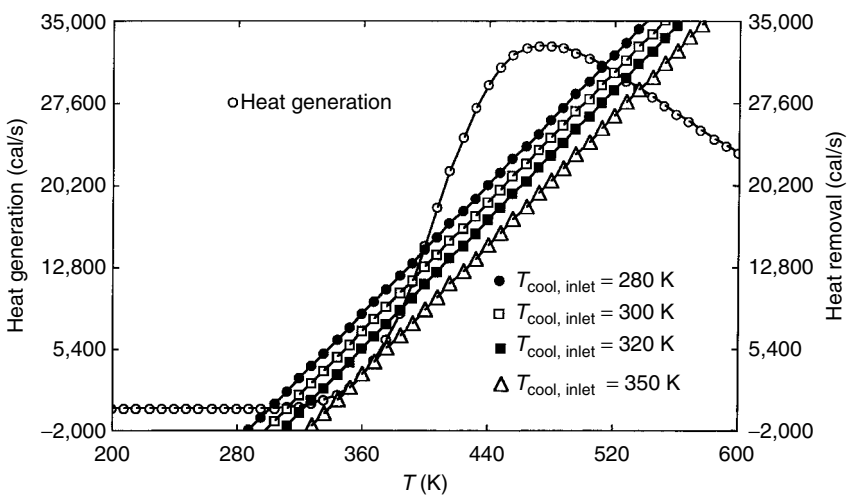

Figure 5-2 Effect of the inlet cooling fluid temperature on the rate of thermal energy removal and the number of allowed steady-state operating points for a nonisothermal CSTR with exothermic chemical reaction. All of the other parameters are the same as those in Figure 5-1.

of the reactor increases smoothly and follows the increase in T_{lower}. Notice how T_{lower} increases and T_{middle} decreases as $T_{\text{cool, inlet}}$ increases. These two steady-state operating points meet at 367 K and 8% conversion when $T_{\text{cool, inlet}} = 350$ K. Under these conditions, $\aleph(T)$ is tangent to the rate of thermal energy generation curve and there are only two possible steady-state operating points (i.e., at 367 K with 8% conversion and at 536 K with 58% conversion). A slight increase in $T_{\text{cool, inlet}}$ above 350 K produces a single CSTR operating point above 536 K. This nonisothermal CSTR phenomenon is called *ignition* because the reactor temperature exhibits parametric sensitivity with respect to $T_{\text{cool, inlet}}$. In other words, a slight increase in the inlet temperature of the cooling fluid produces a 169 K increase in the reactor operating temperature (i.e., from 367 to 536 K in Figure 5-2).

5-4.3 Effect of $T_{\text{cool, inlet}}$ on Reactor Performance: Hysteresis and Extinction

In a continuation of the preceding example, the CSTR operates slightly above 536 K with slightly less than 58% conversion. This is the equilibrium-controlled regime where Le Châtelier's principle dictates lower conversion at higher temperature for exothermic reactions. There is only one operating point when $T_{\text{cool, inlet}}$ is greater than 350 K. Of particular interest is the locus of CSTR operating points when the inlet temperature of the cooling fluid decreases continuously from above 350 K. Three steady states are possible when $T_{\text{cool, inlet}}$ is less than 350 K. When multiple stationary states are possible, the system gravitates toward the stable operating point that is closest to the preceding operating point. Hence, the system follows the highest-temperature operating point T_{upper}, which decreases at lower $T_{\text{cool, inlet}}$, as illustrated in Figure 5-2. Notice that the CSTR follows one sequence of operating temperatures when $T_{\text{cool, inlet}}$ increases from below 280 K, and a different sequence when $T_{\text{cool, inlet}}$ decreases from above 350 K. For example,

$T_{\text{CSTR}} = 316$ K conversion $= 0.4\%$ if $T_{\text{cool, inlet}}$ approaches 300 K from <280 K

$T_{\text{CSTR}} = 520$ K conversion $= 61\%$ if $T_{\text{cool, inlet}}$ approaches 300 K from >350 K

This is an example of *hysteresis*. In fact, a hysteresis loop is produced by mapping the locus of CSTR operating temperatures in response to cycling the inlet temperature of the cooling fluid from below 280 K to above 350 K. Hysteresis is observed over the range of $T_{\text{cool, inlet}}$ that corresponds to multiple-steady-state behavior. If the system follows the locus of highest-temperature operating points (i.e., T_{upper}) as the inlet temperature of the cooling fluid decreases from above 350 K to the lowest $T_{\text{cool, inlet}}$ that is consistent with multiple-steady-state behavior (i.e., on the edge of the hysteresis loop), a further decrease in $T_{\text{cool, inlet}}$ causes the operating temperature of the CSTR to drop precipitously. In reference to Figure 5-2, the reactor temperature decreases by more than 169 K. This phenomenon, called *extinction*, can be classified as another example of parametric sensitivity.

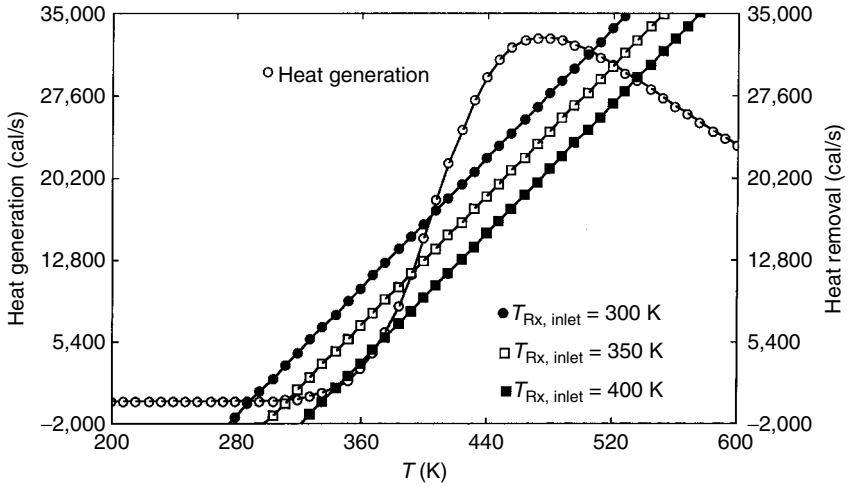

Figure 5-3 Effect of the inlet reactive fluid temperature on the rate of thermal energy removal and the number of allowed steady-state operating points for a nonisothermal CSTR with exothermic chemical reaction. See Figure 5-1 for all other parameters.

5-4.4 Effect of $T_{\text{Rx, inlet}}$ on Reactor Performance

The inlet temperature of the reactive fluid affects the rate of thermal energy removal $\aleph(T)$ via equation (5-18) but not the rate of thermal energy generation $G_{\text{Rx}}(T)$. Hence, ignition, extinction, and hysteresis loops are generated in response to cycling $T_{\text{Rx, inlet}}$. This behavior is similar to the discussion in the preceding two sections. An increase in $T_{\text{Rx, inlet}}$ shifts $\aleph(T)$ to the right without perturbing its slope. This is illustrated in Figure 5-3 for three different inlet temperatures of the reactive fluid (i.e., 300, 350, and 400 K) when the inlet temperature of the cooling fluid is 280 K. All other parameters are as summarized below Figure 5-1. If three stationary states are predicted for each reactor simulation, then an increase in $T_{\text{Rx, inlet}}$ affects the CSTR operating temperatures in the following manner:

1. T_{lower} increases.
2. T_{middle} decreases.
3. T_{upper} increases.

5-4.5 Effect of Flow Rate on Reactor Performance

The flow rate of either fluid affects the slope of $\aleph(T)$ via equation (5-18) or (5-19), but not $G_{\text{Rx}}(T)$ if the CSTR volume and residence time remain constant. Since the reactive fluid flow rate q_{Rx} cannot be changed without affecting either the CSTR volume or residence time, Figure 5-4 illustrates how the cooling fluid flow rate q_{cool} affects the steady-state operating points when all of the

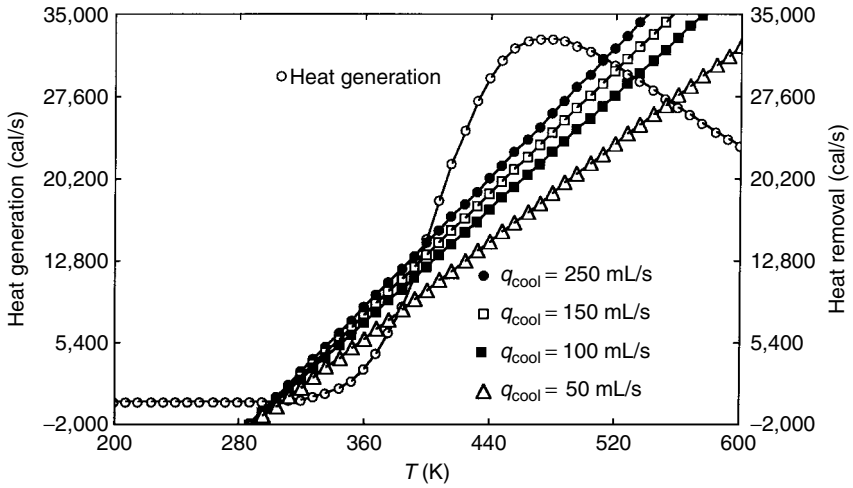

Figure 5-4 Effect of cooling fluid flow rate on the rate of thermal energy removal and the number of allowed steady-state operating points for a nonisothermal CSTR with exothermic chemical reaction. See Figure 5-1 for all other parameters.

other parameters are provided below Figure 5-1. As already noted, all numerical examples in this chapter pertain to a 20-L reactor with a residence time of 200 s. Lower cooling fluid flow rates decrease the slope of the thermal energy removal rate $\aleph(T)$, but the slope is always positive. Multiple-steady-state behavior is predicted at each of the four values of q_{cool}, from 50 to 250 mL/s. Lower-cooling-fluid flow rates perturb the three CSTR operating points as follows:

1. T_{lower} is essentially unaffected.
2. T_{middle} decreases.
3. T_{upper} increases.

5-5 ENDOTHERMIC CHEMICAL REACTIONS

Nonisothermal response of a well-insulated liquid-phase CSTR with reversible endothermic nth-order chemical kinetics is compared with earlier examples in this chapter, where the reaction was exothermic. Now the reaction scheme is

$$\text{A} \longleftrightarrow 2\text{B} \tag{5-31}$$

Dissociation of reactant A is an endothermic process in which the entropy change is positive. Consequently, the equilibrium constant increases at higher temperature via Le Châtelier's principle, which shifts the reaction to the right in favor of

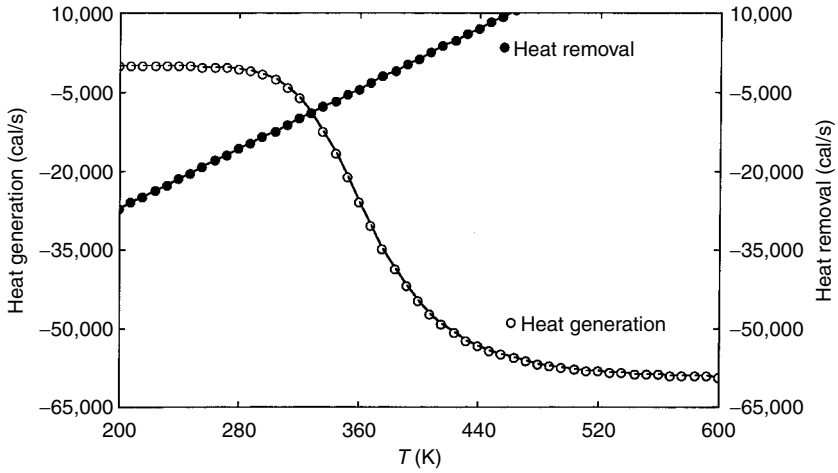

Figure 5-5 Numerical and graphical example of the operating point for a nonisothermal CSTR with endothermic chemical reaction. Multiple stationary-state phenomena do not occur. All parametric values are provided below.

product B. Hence, reactant conversion increases continuously at higher temperature. Thermal energy generation $G_{\mathrm{Rx}}(T)$, as defined by equation (5-15), is always negative, due to the endothermic nature of the chemical reaction. In fact, both $G_{\mathrm{Rx}}(T)$ and $\aleph(T)$ are negative at the CSTR operating point when the reaction is endothermic. In Figure 5-5, the CSTR operates at 328 K with 15% conversion of reactant A, and

$$G_{\mathrm{Rx}}(328\ \mathrm{K}) = \aleph(328\ \mathrm{K}) = -8.8\ \mathrm{kcal/s} \tag{5-32}$$

There is only one steady-state operating point. The endothermic reaction extracts heat from the fluid medium in the CSTR and lowers its temperature. To counterbalance this effect, the inlet temperature of the reactive fluid is higher in this example (i.e., 350 K instead of 325 K), and a heat transfer fluid that supplies thermal energy to the CSTR across the coil replaces the cooling fluid. The physical properties of the heat transfer fluid (i.e., q_{heat}, ρ_{heat}, $\langle C_{p,\,\mathrm{heat}}\rangle$, and $T_{\mathrm{heat,\,inlet}}$) replace the corresponding properties of the cooling fluid to obtain the desired thermal energy balance for the fluid that supplies thermal energy to the CSTR across the coil.

The parametric values are as follows:

$$C_{\mathrm{A,\,inlet}} = 0.1\ \mathrm{mol/mL} \qquad \Theta_{\mathrm{B}} = 0 \qquad \nu_{\mathrm{B}} = 2$$

$$\tau = 200\ \mathrm{s} \qquad k_{\infty} = 10^{5}\ \mathrm{s}^{-1} \qquad E_{\mathrm{activation}} = 12{,}000\ \mathrm{cal/mol}$$

$$\Delta H^{0}_{\mathrm{Rx,\,298}} = 6000\ \mathrm{cal/mol} \qquad \Delta S^{0}_{\mathrm{Rx,\,298}} = 20\ \mathrm{cal/mol{\cdot}K} \qquad \rho_{\mathrm{Rx}} = 0.75\ \mathrm{g/mL}$$

$$q_{\mathrm{Rx}} = 100\ \mathrm{mL/s} \qquad T_{\mathrm{Rx,\,inlet}} = 350\ \mathrm{K} \qquad \rho_{\mathrm{heat}} = 1\ \mathrm{g/mL}$$

$$q_{\text{heat}} = 200 \text{ mL/s} \qquad T_{\text{heat, inlet}} = 425 \text{ K} \qquad R_{\text{gas}} = 1.987 \text{ cal/mol·K}$$

$$\langle C_{p,\text{Rx, feed}} \rangle = 0.9 \text{ cal/g·K} \qquad \langle C_{p,\text{heat}} \rangle = 1 \text{ cal/g·K} \qquad L_{\text{cooling coil}} = 200 \text{ cm}$$

$$V_{\text{CSTR}} = 20 \text{ L} \qquad D_{\text{cooling coil}} = 1.5 \text{ cm} \qquad n = 1$$

$$U_{\text{overall}} = 3600 \text{ kcal/m}^2\text{·h·K} = 0.1 \text{ cal/cm}^2\text{·s·K}$$

Further inspection of $G_{\text{Rx}}(T)$ and $\aleph(T)$ in Figure 5-5 leads to the general conclusion that multiple stationary states do not occur when the chemical reaction is endothermic, because $d\aleph/dT$ is always positive. In other words, multiple intersections between $G_{\text{Rx}}(T)$ and $\aleph(T)$ are possible only if $d\aleph/dT$ is negative.

PROBLEMS

5-1. A nonisothermal CSTR with exothermic chemical reaction contains a cooling coil and exhibits three possible steady-state operating points. You want the reactor to operate at the stationary state (i.e., the middle one at T_{middle}) that is unstable. The temperature of the reactive fluid in the CSTR increases slightly. If you do not counterbalance this increase in temperature, it is not possible to operate at the unstable operating point because the reactor will shift toward the high-temperature operating point at T_{upper}. Identify three possible one-line strategies that must be implemented immediately (i.e., "on the fly") to counterbalance an increase in reactor temperature and allow continuous operation at the unstable operating point. *Note*: Each strategy represents a possible solution to this problem. It is not necessary to implement all three strategies simultaneously. Also, it is not possible to modify the dimensions of the reactor or the cooling coil immediately.

Answer: Increase the flow rate of the reactive fluid, increase the flow rate of the cooling fluid, and decrease the inlet temperature of the cooling fluid.

5-2. It is desired to operate a nonisothermal liquid-phase CSTR with exothermic chemical reaction at 440 K under steady-state conditions. The complete description of this reactor was discussed in this chapter via parametric values and the supporting equations. The reactor design engineer must specify the heat transfer area for the cooling coil that is immersed in the reactive mixture. For the conditions illustrated in Figure 5-1, the rate of thermal energy generation is greater than the rate of thermal energy removal at 440 K [i.e., $G_{\text{Rx}}(T) > \aleph(T)$]. You decide to use the following computer program, which generated the graphs of $G_{\text{Rx}}(T)$ and $\aleph(T)$ vs. T in Figure 5-1 to calculate the required heat transfer area, but your colleague correctly realizes that one equation must be deleted and three equations must be added before the program will provide the answers required. *Hint*: Do not change the diameter of the cooling coil or the inlet temperature and volumetric flow rate of either fluid.

This sequence of equations and supporting parameters analyzes the nonisothermal response of a liquid-phase CSTR with reversible exothermic nth-order chemical kinetics. The reaction scheme is $2A \Leftrightarrow B$, where 2 mol of reactant A reversibly produce 1 mol of product B. The equilibrium constant is expressed in terms of the standard state enthalpy and entropy changes for reaction at 298 K. The temperature dependence of the forward kinetic rate constant is modelled by an Arrhenius function. The time constant for convective mass transfer is 200 s and the reactor volume is 20 L. Thermal energy is generated volumetrically due to the exothermic nature of the chemical reaction. As temperature increases, the equilibrium constant decreases and Le Châtelier's principle shifts the reaction to the left, which favors reactant A. Hence, reactant conversion increases initially, and then decreases at higher temperature. Also, at higher temperatures, the forward kinetic rate constant increases and the characteristic time constant for chemical reaction decreases. Remember that for reversible reactions where the order of the forward and backward steps is the same, the time constant for chemical reaction λ is defined by

$$\lambda = \frac{1}{(k_{\text{forward}} + k_{\text{backward}})C_{\text{A0}}^{n-1}} = \frac{K_{\text{equil}}}{1 + K_{\text{equil}}}\left(\frac{1}{k_{\text{forward}}C_{\text{A0}}^{n-1}}\right)$$

Since residence time tau is much larger than lambda at high temperatures, the reaction is "equilibrium controlled". This means that the reaction approaches equilibrium and the rate of reaction approaches zero, which provides an explanation for the fact that the rate of thermal energy generation increases initially, and then decreases at very high temperatures.

Nonisothermal CSTR design equations:

$\tau\mathfrak{R} - C_{\text{A0}}\chi = 0$ (CSTR mass balance when there is only one chemical reaction)

$\mathfrak{R} = k_{\text{forward}}\left[C_{\text{A}}^{n} - \dfrac{C_{\text{B}}^{n}}{K_{\text{equil}}}\right]$ (Reversible kinetic rate law for nth-order reactions)

$C_{\text{A}} = C_{\text{A0}}(1 - \chi)$ (Definition of reactant conversion based on molar density of reactant A)

$C_{\text{B}} = C_{\text{A0}}(\Theta_{\text{B}} + \nu_{\text{B}}\chi)$ (Stoichiometry and the mass balance to calculate all molar densities)

$K_{\text{equil}} = \exp\left(\text{A} + \dfrac{\text{B}}{T_{\text{CSTR}}}\right)$ (Temperature dependence of the equilibrium constant, from thermodynamics)

$$A = \frac{\Delta S^0_{Rx}}{R_{gas}}$$ (Standard state entropy change for reaction at 298 K, divided by the gas constant)

$$B = -\frac{\Delta H^0_{Rx}}{R_{gas}}$$ (Standard state enthalpy change for reaction at 298 K, divided by the gas constant)

$$k_{forward} = k_\infty \exp\left[-\frac{E_{activation}}{R_{gas} T_{CSTR}}\right]$$ (Arrhenius kinetic rate constant for the forward reaction in terms of the activation energy)

$$heat_{generation} = -\Delta H^0_{Rx} \Re V_{CSTR}$$ (Rate of thermal energy generation due to chemical reaction, cal/sec)

$$V_{CSTR} = \tau q_{Rx}$$ (The classic expression for reactor volume)

$$heat_{removal} = heat_{convection} + heat_{conduction}$$ (2 contributions to the rate of thermal energy removal, cal/sec)

$$heat_{convection} = \rho_{Rx} q_{Rx} C_{p,\,Rx,\,feed}(T_{CSTR} - T_{CSTR,\,inlet})$$ (Rate of heat removal due to convective transport of thermal energy thru the reactor)

$$heat_{conduction} = \rho_{cool} q_{cool} C_{p,\,cool}\{1 - \exp(-\text{cool factor})\}(T_{CSTR} - T_{cool,\,inlet})$$ (Rate of thermal energy removal due to conduction across the cooling coil and into the cooling fluid)

$$\text{cool factor} = U_{overall} \pi D_{cooling\ coil} L_{cooling\ coil} / (\rho_{cool} q_{cool} C_{p,\,cool})$$

Parameters:

$C_{A0} = 0.1$ (Molar density of reactant A in the CSTR inlet stream in units of moles per mL)

$\Theta_B = 0$ (Inlet molar density ratio of product B to reactant A)

$\nu_B = 0.5$ (Stoichiometric coefficient of product B when $\nu_A = -1$)

$\tau = 200$ (Time constant for convective mass transfer (i.e., average residence time) in seconds)

$k_\infty = 10^5$ (Pre-exponential factor for the kinetic rate constant, units of inverse seconds)

$E_{activation} = 14000$ (Activation energy in calories per mole)

$\Delta H^0_{Rx} = -5000$ (Enthalpy change for the exothermic reaction at 298 K, units of calories per mole)

$\Delta S^0_{Rx} = -10$ (2 mol of A produce 1 mol of B, delta S at 298 K is negative, cal/mole-degree)

$q_{Rx} = 100$ (Volumetric flow rate of the reactive fluid, mL per second)

$q_{cool} = 250$ (Volumetric flow rate of the cooling fluid, mL per second)

$T_{CSTR,\,inlet} = 325$ (Inlet temperature of the reactive fluid, degrees Kelvin)

$T_{cool,\,inlet} = 280$ (Inlet temperature of the cooling fluid, degrees Kelvin)

$C_{p,\,Rx,\,feed} = 0.9$ (Specific heat of the feed stream to the CSTR, only reactant A, cal/gram-degree)

$C_{p,\,cool} = 1$ (Specific heat of the cooling fluid, which is most likely water, cal/gram-degree)

$\rho_{Rx} = 0.75$ (Average density of the hydrocarbon reactive mixture, gram/mL)

$\rho_{cool} = 1$ (Average density of the cooling fluid, which is most likely water, in gram/mL)

$D_{cooling\ coil} = 1.5$ (Diameter of the cooling coil, centimeters)

$L_{cooling\ coil} = 200$ (Length of the cooling along the direction of fluid flow, cm)

$U_{overall} = 0.1$ (Overall heat transfer coefficient across the cooling coil. A typical value for forced convection in coils with water as the cooling fluid is 3600 kcal per square meter-hour-degree Kelvin, which translates to 0.1 calorie per square centimeter-second-degree Kelvin)

$R_{gas} = 1.987$ (Universal gas constant, in units of calories per mole per degree Kelvin)

$n = 1$ (Order of the forward and backward chemical reactions)

(a) What parametric equation must be deleted?

Answer: $L_{cooling\ coil} = 200$ cm.

(b) Write the three equations that must be added to the nonisothermal CSTR design algorithm provided above. Three one-line answers are required.

Answer: $T_{CSTR} = 440$ K, $\text{heat}_{generation} = \text{heat}_{removal}$, and heat transfer area $= \pi \cdot D_{cooling\ coil} \cdot L_{cooling\ coil}$.

(c) Predict the outlet temperature in Kelvin for the cooling fluid.

Answer: $T_{cool,\ outlet} = 366$ K.

(d) Remove the cooling coil and calculate the adiabatic temperature rise in the CSTR.

5-3. Discuss the interesting situation where the linear rate of thermal energy removal vs. temperature is coincident with the steepest section of the rate-of-thermal-energy-generation curve for exothermic chemical reactions in a CSTR. Even though there is only one theoretical point of intersection of the two temperature-dependent functions, there could be a range of CSTR operating points where $G_{Rx}(T) \approx \aleph(T)$ within a reasonable tolerance. Consider ignition, extinction, hysterisis loops, stable and unstable operating points, and fluctuating reactor temperature in your analysis.

5-4. How do the following changes in a well-mixed CSTR with exothermic chemical reaction affect the rates of thermal energy generation G_{Rx} and removal $\aleph$ (i.e., increase, decrease, or no change)? Provide two answers for each part below, one for G_{Rx} and one for $\aleph$.

(a) The inlet temperature of the cooling fluid is increased.

(b) The mass flow rate of the cooling fluid is decreased.

(c) The enthalpy change for the chemical reaction is larger in absolute value.

(d) The activation energy for the chemical reaction is decreased by a catalyst.

(e) The inlet temperature of the reactive fluid is decreased.

(f) The length of the cooling coil is increased.

(g) The reactor operates at a higher temperature, but it has not reached the near-equilibrium regime.

5-5. (a) Use the data provided in Figure 5-4 and sketch the operating temperature of the reactor vs. the volumetric flow rate of the cooling fluid. Use arrows and indicate the path followed by the reactor in response to cycling the volumetric flow rate of the cooling fluid.

(b) Does ignition occur (i.e., a large increase in operating temperature) within the CSTR upon increasing or decreasing the volumetric flow rate of the cooling fluid?

(c) Does extinction occur (i.e., a large decrease in operating temperature) within the CSTR upon increasing or decreasing the volumetric flow rate of the cooling fluid?

Transport Phenomena for Chemical Reactor Design. Laurence A. Belfiore
Copyright © 2003 John Wiley & Sons, Inc.
ISBN: 0-471-20275-4

6

COUPLED HEAT AND MASS TRANSFER WITH CHEMICAL REACTION IN BATCH REACTORS

6-1 ISOTHERMAL ANALYSIS OF EXPERIMENTAL RATE DATA

If digital control is implemented to maintain isothermal operation of a batch reactor and an external source or sink of thermal energy is available to accomplish this task, then it is possible to analyze the rate of conversion of reactants to products via coupled heat and mass transfer. For exothermic reactions, the rate at which thermal energy is generated by chemical reaction must match the rate at which thermal energy is removed by heat transfer across the external wall. For example, a solid sample in an aluminum pan that is placed in a differential scanning calorimeter can be modeled as an isothermal batch reactor during kinetic measurements of the rate of reaction. The calorimeter operates in an isothermal mode and functions as a digital controller by monitoring the rate at which thermal energy must be added to or removed from the system to maintain constant temperature. Analysis begins by writing an unsteady-state total energy balance for a batch reactor with no exchange of mass between the system and the surroundings due to convective transport. The most general form of the total energy balance for a closed system that performs no mechanical work on the surroundings is

$$\frac{dE}{dt} = \left(\frac{dQ}{dt}\right)_{\text{input}} \tag{6-1}$$

where total energy E is the sum of kinetic, potential, and internal energies, and $(dQ/dt)_{\text{input}}$ is the rate of heat exchange between the surroundings (i.e., the calorimeter equipped with digital control) and the batch reactor. This is essentially the first law of thermodynamics in differential form. By convention, the rate of heat exchange is positive when the system receives heat from the surroundings. Since the

kinetic and potential energies of the system do not change with time, the unsteady-state total energy balance reduces to the following thermal energy balance:

$$\frac{dU}{dt} = \left(\frac{dQ}{dt}\right)_{\text{input}} \tag{6-2}$$

where U is the extensive internal energy of the system. Standard thermodynamic formalism is employed to express the total differential of internal energy in terms of temperature T, pressure p, and mole numbers N_i for a multicomponent system that contains r species:

$$dU = \left(\frac{\partial U}{\partial T}\right)_{p,\text{all } N_i} dT + \left(\frac{\partial U}{\partial p}\right)_{T,\text{all } N_i} dp + \sum_{i=1}^{r} \left(\frac{\partial U}{\partial N_i}\right)_{T,p,\text{all } N_j (j\neq i)} dN_i \tag{6-3}$$

The total time derivative of (6-3) yields

$$\frac{dU}{dt} = \left(\frac{\partial U}{\partial T}\right)_{p,\text{all } N_i} \frac{dT}{dt} + \left(\frac{\partial U}{\partial p}\right)_{T,\text{all } N_i} \frac{dp}{dt} + \sum_{i=1}^{r} \left(\frac{\partial U}{\partial N_i}\right)_{T,p,\text{all } N_j (j\neq i)} \frac{dN_i}{dt} \tag{6-4}$$

which is appropriate for this analysis of kinetic rate data. The coefficients of dT/dt and dp/dt in (6-4) are evaluated from the total differential expression for the extensive internal energy of a multicomponent system in terms of its natural variables S, V, and all N_i:

$$dU = T\,dS - p\,dV + \sum_{i=1}^{r} \mu_i\,dN_i \tag{6-5}$$

where μ_i is the chemical potential of species i, and V and S are the extensive volume and entropy, respectively, of the system (i.e., the batch reactor). This differential form of the first law for multicomponent systems (i.e., equation 6-5) is used in conjunction with a Maxwell relation and the definition of thermophysical properties like heat capacity C_p, thermal expansion coefficient α, and isothermal compressibility κ to calculate the temperature and pressure coefficients of the extensive internal energy. For example,

$$\left(\frac{\partial U}{\partial T}\right)_{p,\text{all } N_i} = T\left(\frac{\partial S}{\partial T}\right)_{p,\text{all } N_i} - p\left(\frac{\partial V}{\partial T}\right)_{p,\text{all } N_i} \equiv C_p - p\alpha V \tag{6-6}$$

$$\left(\frac{\partial U}{\partial p}\right)_{T,\text{all } N_i} = T\left(\frac{\partial S}{\partial p}\right)_{T,\text{all } N_i} - p\left(\frac{\partial V}{\partial p}\right)_{T,\text{all } N_i} \equiv V(\kappa p - \alpha T) \tag{6-7}$$

$$\left(\frac{\partial S}{\partial p}\right)_{T,\text{all } N_i} = -\left(\frac{\partial V}{\partial T}\right)_{p,\text{all } N_i} \tag{6-8}$$

where C_p is an extensive heat capacity with units of energy per Kelvin,

$$C_p \equiv \left(\frac{\partial H}{\partial T}\right)_{p,\text{all } N_i} = T\left(\frac{\partial S}{\partial T}\right)_{p,\text{all } N_i} \tag{6-9}$$

α is the coefficient of thermal expansion (i.e., $\approx 10^{-4}$ K^{-1} for liquids, $1/T$ for ideal gases),

$$\alpha \equiv \left(\frac{\partial \ln V}{\partial T}\right)_{p,\text{all } N_i} \tag{6-10}$$

and κ is the coefficient of isothermal compressibility (i.e., $\approx 10^{-6}$ atm^{-1} for liquids, $1/p$ for ideal gases),

$$\kappa \equiv -\left(\frac{\partial \ln V}{\partial p}\right)_{T,\text{all } N_i} \tag{6-11}$$

The coefficient of dN_i/dt in the summation of (6-4) is defined as the partial molar internal energy of species i, because differentiation with respect to mole numbers of component i is performed at constant T, p and mole numbers of all other species in the mixture. The unsteady-state mass balance for species i in a batch reactor,

$$\frac{dN_i}{dt} = \nu_i V \mathfrak{R} \tag{6-12}$$

describes the time dependence of the moles of species i due to one chemical reaction. In (6-12), $\mathfrak{R}$ is the intrinsic rate law with units of moles per volume per time for homogeneous kinetics, and ν_i is the stoichiometric coefficient of species i. Hence, (6-2), (6-4), and (6-12) adopt the following form when the mass and energy balances are combined:

$$\begin{aligned}\frac{dU}{dt} &= (C_p - p\alpha V)\frac{dT}{dt} + V(\kappa p - \alpha T)\frac{dp}{dt} \\ &\quad + V\mathfrak{R}\sum_{i=1}^{r}\nu_i\left(\frac{\partial U}{\partial N_i}\right)_{T,p,\text{all } N_j(j\neq i)} = \left(\frac{dQ}{dt}\right)_{\text{input}}\end{aligned} \tag{6-13}$$

When the product of ν_i and the partial molar internal energy of species i is summed over all components in the system, one obtains an exact expression for the molar internal energy change for the reaction (see Tester and Modell, 1997, pp. 769–770). In other words,

$$\Delta U_{\text{Rx}} \equiv \sum_{i=1}^{r}\nu_i\left(\frac{\partial U}{\partial N_i}\right)_{T,p,\text{all } N_j(j\neq i)} \tag{6-14}$$

even though pure component molar internal energies are typically employed in practice to calculate ΔU_{Rx}. When reactive mixtures behave ideally, the summation in (6-14) is simplified considerably, because partial molar properties reduce to pure component molar properties. In general, the summation in (6-14) also accounts for nonidealities and effects due to pressure and mixing. The unsteady-state thermal energy balance for a closed system with one chemical reaction is written in the following form when physical processes such as vaporization of volatile by-products do not occur:

$$\frac{dU}{dt} = (C_p - p\alpha V)\frac{dT}{dt} + V(\kappa p - \alpha T)\frac{dp}{dt} + V\mathfrak{R}(\Delta U_{\text{Rx}}) = \left(\frac{dQ}{dt}\right)_{\text{input}} \tag{6-15}$$

For isothermal operation of a constant-volume batch reactor, the closed-system thermal energy balance can be simplified as follows;

1. $dT/dt = 0$ for isothermal operation at steady state.
2. $V(\kappa p - \alpha T)\, dp/dt$ is negligible in magnitude relative to $V\mathfrak{R}\Delta U_{\text{Rx}}$ and $(dQ/dt)_{\text{input}}$ when pressure represents an additional degree of freedom at constant T and V for liquids.

Hence, the closed-system thermal energy balance reduces to

$$-\left(\frac{dQ}{dt}\right)_{\text{input}} = \left(\frac{dQ}{dt}\right)_{\text{removal}} \approx V\mathfrak{R}(-\Delta U_{\text{Rx}}) \tag{6-16}$$

where $(dQ/dt)_{\text{removal}}$ represents the rate at which thermal energy is removed from the reactor via heat transfer across the external wall, as specified by the digital control system to maintain isothermal operation. Equation (6-16) indicates that this rate of heat exchange must be balanced by the rate of thermal energy generation for exothermic reactions.

The unsteady-state mass balance for species i in a batch reactor with one chemical reaction was presented above as

$$\frac{dN_i}{dt} = \nu_i V\mathfrak{R} \tag{6-17}$$

One introduces the definition of reactant conversion χ in terms of the moles of key-limiting reactant A:

$$\chi \equiv \frac{N_{\text{A}}(t=0) - N_{\text{A}}(t)}{N_{\text{A}}(t=0)} \tag{6-18}$$

Furthermore, stoichiometry and the mass balance for a batch reactor via (6-17) reveal that

$$\frac{dN_i}{\nu_i} = \frac{dN_{\text{A}}}{\nu_{\text{A}}} = V\mathfrak{R}\, dt \qquad (\nu_{\text{A}} \equiv -1) \tag{6-19}$$

Hence,

$$\frac{dN_i}{dt} = -\nu_i \frac{dN_A}{dt} = \nu_i N_A(t=0)\frac{d\chi}{dt} \tag{6-20}$$

and the mass balance given by (6-17) can be re-expressed in terms of the time dependence of reactant conversion as

$$N_{A0}\frac{d\chi}{dt} = V\Re \tag{6-21}$$

where N_{A0} represents the initial number of moles of reactant A injected into the reactor at $t = 0$. A few comments are required here to analyze the time dependence of reactant conversion when the volume of the batch reactor increases. For gas-phase reactors, the ratio of reactor volume V to the initial number of moles of reactant A, N_{A0}, is $RT/[y_{A0}p_{total}(t=0)]$ if the gas mixture behaves ideally. y_{A0} is the initial mole fraction of reactant A at $t = 0$. Hence, if reactor volume is increased without introducing more moles of reactants, this effect is equivalent to decreasing total pressure at constant temperature. Under these conditions, V/N_{A0} increases, but this increase is offset by a decrease in $\Re$, which is proportional to p_{total} raised to the sum of the magnitudes of the stoichiometric coefficients of all the reactants for elementary reactions. When the kinetics are irreversible nth-order and $n > 1$, the time rate of increase of reactant conversion is smaller when the batch reactor volume increases without introducing more moles of reactants. For first-order kinetics, $d\chi/dt$ is unaffected by this increase in reactor volume because chemical reaction time constants are independent of molar density or partial pressure. If reactor volume is increased at constant temperature and pressure by increasing the number of moles of reactants, the ratio V/N_{A0} remains unchanged, $d\chi/dt$ is unaffected, and reactor volume does not influence the rate of conversion of reactants to products. For liquids, reactor volume does not appear explicitly in the unsteady-state macroscopic mass balance because N_{A0}/V is identified as the initial molar density of reactant A at $t = 0$. Since liquid-phase reactors operate approximately at constant density, an increase in reactor volume is proportional to an increase in the mole numbers of all components in the mixture. Hence, molar densities and $d\chi/dt$ are not affected by an increase in reactor volume under isothermal conditions.

When the steady-state thermal energy balance (6-16) is combined with the unsteady-state species mass balance (6-21), the time dependence of reactant conversion (i.e., $d\chi/dt$) can be calculated from the digital controller response, which monitors the rate of thermal energy removal across the outer wall of the reactor for exothermic chemical reactions:

$$\frac{d\chi}{dt} = \frac{(dQ/dt)_{removal}}{N_{A0}(-\Delta U_{Rx})} \tag{6-22}$$

where the numerator on the right side (6-22) is measured experimentally. The molar internal energy change for reaction, which can be approximated using

pure component enthalpies of formation at 298 K, specific heat data, and $H = U + pV$, (see Section 6-4), is based on a stoichiometric coefficient of -1 for the component used to define conversion χ. Hence, the denominator on the right side of (6-22) represents the total amount of thermal energy that should be liberated by an exothermic irreversible reaction that achieves 100% conversion of reactants to products. If the rate law is modeled empirically as an nth-order irreversible chemical reaction which depends only on the molar density of reactant A, then:

$$\mathfrak{R} = k_n(T)(C_A)^n = \frac{C_{A0}(1-\chi)^n}{\lambda(T)} \tag{6-23}$$

where $k_n(T)$ is a temperature-dependent nth-order kinetic rate constant with units of (volume/mol)$^{n-1}$ per time, $C_{A0} = N_{A0}/V$ is the initial molar density of reactant A, and $\lambda(T)$ is a characteristic time constant for nth-order irreversible chemical reaction, given by

$$\lambda(T) \equiv \frac{1}{k_n(T)(C_{A0})^{n-1}} \tag{6-24}$$

The parameters n and $\lambda(T)$ which characterize the rate law are evaluated via the differential method of reaction-rate data analysis based on the unsteady-state mass balance:

$$N_{A0}\frac{d\chi}{dt} = V\mathfrak{R} \tag{6-25}$$

Substitution for $\mathfrak{R}$ via (6-23) yields

$$\log\left(\frac{d\chi}{dt}\right) = n\log(1-\chi) - \log\lambda(T) \tag{6-26}$$

where conversion vs. time data are obtained experimentally from the transient response of a digital controller, which is required to maintain isothermal operation of the batch reactor. In other words, integration of equation (6-22) yields:

$$\chi(t) = \frac{\int_0^t (dQ/d\xi)_{\text{removal}}\, d\xi}{N_{A0}(-\Delta U_{Rx})} \tag{6-27}$$

Hence, one combines (6-22), (6-26), and (6-27) as follows:

$$\log\frac{(dQ/dt)_{\text{removal}}}{N_{A0}(-\Delta U_{Rx})} = n\log\frac{\int_t^\infty (dQ/d\xi)_{\text{removal}}\, d\xi}{N_{A0}(-\Delta U_{Rx})} - \log\lambda(T) \tag{6-28}$$

where $(dQ/dt)_{\text{removal}}$ is the experimental instantaneous rate of heat removal monitored by a digital controller. This analysis reveals that the parameters n and $\lambda(T)$ which characterize the kinetic rate law can be determined from isothermal experiments in a batch reactor with digital control. The empirical reaction order n represents the first-order coefficient (i.e., the slope), and the time constant $\log\lambda(T)$ is the zeroth-order coefficient (i.e., the intercept) of $d\chi/dt$ vs. $1-\chi$

on log-log coordinates when experimental data are matched to a first-order polynomial via linear least-squares analysis. If isothermal experiments are performed at several different temperatures and $\lambda(T)$ from each set of isothermal data is correlated with reciprocal absolute temperature, then an apparent activation energy for the forward reaction is obtained via linear least-squares analysis of $\ln\lambda$ vs. $1/T$, even if the empirical reaction order n exhibits weak dependence on temperature. It is not possible to analyze $\ln k_n(T)$ vs. $1/T$ and extract an activation energy if the empirical reaction order n varies with temperature because the units of k_n depend on the value of n, whereas the characteristic time constant for chemical reaction always has dimensions of time.

6-2 FORMALISM FOR MULTIPLE REACTIONS

If multiple chemical reactions occur, then the coupled mass and thermal energy balances for isothermal operation with negligible pressure effects are (see equations 6-2, 6-4, and 6-12):

$$\frac{dN_i}{dt} = V\sum_j \nu_{ij}\mathfrak{R}_j \qquad 1 \le i \le r \tag{6-29}$$

$$\sum_{i=1}^{r}\left(\frac{\partial U}{\partial N_i}\right)_{T,p,\text{all } N_j(j\neq i)}\frac{dN_i}{dt} \approx \left(\frac{dQ}{dt}\right)_{\text{input}} \tag{6-30}$$

where ν_{ij} is the stoichiometric coefficient of component i in reaction j and $\mathfrak{R}_j$ represents the kinetic rate law for the jth chemical reaction in the mechanism. Equations (6-29) and (6-30) can be combined as follows:

$$\begin{aligned}\sum_{i=1}^{r}\left(\frac{\partial U}{\partial N_i}\right)_{T,p,\text{all } N_j(j\neq i)}\frac{dN_i}{dt} &= V\sum_j \mathfrak{R}_j\sum_{i=1}^{r}\nu_{ij}\left(\frac{\partial U}{\partial N_i}\right)_{T,p,\text{all } N_j(j\neq i)}\\ &= V\sum_j \mathfrak{R}_j(\Delta U_{\text{Rx}})_j \approx \left(\frac{dQ}{dt}\right)_{\text{input}}\end{aligned} \tag{6-31}$$

where $(\Delta U_{\text{Rx}})_j$ is the molar internal energy change for the jth chemical reaction. As mentioned above, one usually replaces partial molar properties with pure-component molar properties to approximate the molar internal energy change for each chemical reaction. The analysis described in the previous section for one chemical reaction will yield useful results for a multiple-reaction sequence if it is possible to identify a rate-limiting step. If all steps occur on the same time scale and it is not possible to isolate one that is rate limiting, then the controller provides experimental information about the rate of heat transfer across the external wall to operate the reactor isothermally, but one cannot combine the mass and energy balances to obtain useful information about the extent of each reaction or the rate of conversion of reactants to products.

6-3 ADIABATIC OPERATION

If a batch reactor is completely insulated from the surroundings and there is only one chemical reaction, then the mass and thermal energy balances can be combined analytically to yield the maximum temperature rise for exothermic reactions. The same procedure provides an estimate of the maximum temperature drop if the reaction is endothermic. If pressure effects are negligible, in accord with the previous analyses, coupled heat and mass transfer yield (see equation 6-15):

$$\frac{dU}{dt} \approx (C_p - p\alpha V)\frac{dT}{dt} + V\mathfrak{R}(\Delta U_{\mathrm{Rx}}) = \left(\frac{dQ}{dt}\right)_{\mathrm{input}} = 0 \tag{6-32}$$

which allows one to predict temperature changes as follows:

$$(C_p - p\alpha V)\frac{dT}{dt} = V\mathfrak{R}(-\Delta U_{\mathrm{Rx}}) \tag{6-33}$$

The unsteady-state mass balance (6-21) is used to replace $V\mathfrak{R}$ in (6-33) so that temperature and reactant conversion can be related analytically at any time during the course of the reaction:

$$(C_p - p\alpha V)\frac{dT}{dt} = N_{\mathrm{A0}}(-\Delta U_{\mathrm{Rx}})\frac{d\chi}{dt} \tag{6-34}$$

If the concentration dependence of thermophysical properties is neglected and temperature-averaged properties are employed, then integration of (6-34) yields

$$(C_p - p\alpha V)[T - T(t=0)] = N_{\mathrm{A0}}(-\Delta U_{\mathrm{Rx}})[\chi - \chi(t=0)] \tag{6-35}$$

The maximum temperature rise or drop $\Delta T_{\max}$ in an adiabatic batch reactor occurs when equilibrium is achieved. By definition, there is no conversion of reactants to products at $t = 0$. Hence,

$$\Delta T_{\max} = T_{\mathrm{equilibrium}} - T(t=0) = \frac{N_{\mathrm{A0}}(-\Delta U_{\mathrm{Rx}})\chi_{\mathrm{equilibrium}}}{C_p - p\alpha V} \tag{6-36}$$

provides a conservative estimate (i.e., overestimate) of the maximum temperature change. The actual temperature change will be less than this prediction because sensible heat effects associated with the wall of the vessel have not been considered. It is interesting to note that the adiabatic temperature change predicted by (6-36) for batch reactors is slightly different than $\Delta T_{\max}$ for flow reactors (see equation 4-40). Continuous-stirred tanks and plug-flow reactors exhibit the same functional form for the adiabatic temperature change. However, plug-flow reactors will experience a larger actual $\Delta T_{\max}$ relative to CSTRs because, if all other design parameters are the same (i.e., particularly inlet temperature and residence time), PFRs yield higher conversion than CSTRs. Equation (6-36) reveals that $\Delta T_{\max}$ is linearly proportional to χ_{final} for all types of reactors.

6-4 NONISOTHERMAL ANALYSIS OF A CONSTANT-VOLUME BATCH REACTOR

The following sequence of equations and supporting parameters provides an analysis of the nonisothermal operation of a constant-volume cylindrical batch reactor. A stoichiometric feed of carbon monoxide and hydrogen is injected into the reactor via an inert carrier gas, such as argon, and the overall objective is to produce methanol. The reactor is insulated from the surroundings, but it contains a cooling coil to remove the thermal energy generated by the exothermic chemical reaction. It is necessary to integrate coupled mass and thermal energy balances to monitor temperature, conversion and pressure profiles as a function of time for unsteady-state operation. The gas mixture behaves ideally. The coefficient of thermal expansion α for ideal gases is $1/T$, which is about one order of magnitude larger than α for liquids. The coefficient of isothermal compressibility κ for ideal gases is $1/p$, which is about five or six orders of magnitude larger than κ for liquids. This is reasonable because gases are relatively easy to compress at ambient pressure, and liquids are essentially incompressible. The pressure contribution to the thermal energy balance,

$$V(\kappa p - \alpha T)\frac{dp}{dt} \tag{6-37}$$

vanishes identically for ideal gases, and the temperature coefficient of the extensive internal energy of the mixture,

$$\left(\frac{\partial U}{\partial T}\right)_{p,\text{all } N_i} \equiv C_p - p\alpha V = C_p - \frac{pV}{T} = C_p - N_{\text{total}}R \tag{6-38}$$

is essentially C_V.

$T_{\text{initial}} = 300$ K (initial temperature of the reactive gas mixture)

$p_{\text{initial}} = 100/760$ atm (initial pressure in atmospheres)

$\Theta_{\text{argon}} = 3$ (inlet molar ratio of the inert carrier gas, argon, relative to CO)

$\Theta_{\text{CO}} = 1$ (definition of the inlet molar ratio of CO, with respect to CO)

$\Theta_{\text{hydrogen}} = 2$ (stoichiometric feed of hydrogen, injected at $t = 0$ with CO and argon)

$\Theta_{\text{methanol}} = 0$ (no methanol is injected into the reactor at $t = 0$)

$\sum_{i=1}^{4} \Theta_i = \Theta_{\text{CO}} + \Theta_{\text{hydrogen}} + \Theta_{\text{methanol}} + \Theta_{\text{argon}}$ (inverse of the initial CO mole fraction)

$$\nu_{CO} = -1 \text{ (stoichiometric coefficient of CO)}$$

$$\nu_{hydrogen} = -2 \text{ (stoichiometric coefficient of hydrogen)}$$

$$\nu_{methanol} = 1 \text{ (stoichiometric coefficient of methanol)}$$

$$\delta = \sum_{i=1}^{4} \nu_i = \nu_{CO} + \nu_{hydrogen} + \nu_{methanol} \text{ (change in the total number of moles when 1 mol of CO reacts)}$$

$$\text{diameter}_{\text{batch reactor}} = 25 \text{ cm (diameter of the batch reactor)}$$

$$\text{height}_{\text{batch reactor}} = 50 \text{ cm (height of the batch reactor)}$$

$$\text{volume}_{\text{batch reactor}} = \frac{\pi}{4}(\text{diameter}_{\text{batch reactor}})^2 \, \text{height}_{\text{batch reactor}}$$

(batch reactor volume in mL)

$$R''_{gas} = 82 \text{ mL·atm/mol·K (gas constant)}$$

$$\text{gram}_{CO}(t=0) = \frac{28 p_{\text{initial}} \text{volume}_{\text{batch reactor}}}{\left(R''_{gas} T_{\text{initial}} \sum_{i=1}^{4} \Theta_i \right)}$$

(grams of CO injected into the batch reactor at $t = 0$)

$$N_{CO}(t=0) = \frac{\text{gram}_{CO}(t=0)}{28} \text{ (initial number of moles of CO injected into the reactor at } t = 0)$$

$$N_{\text{total}}(t) = N_{CO}(t=0)\left[\delta\chi(t) + \sum_{i=1}^{4} \Theta_i\right]$$

(time-dependent total number of moles in the reactor)

$$y_{CO}(\chi) = \frac{\Theta_{CO} + \nu_{CO}\chi}{\delta\chi + \sum_{i=1}^{4} \Theta_i} \text{ (mole fraction of CO)}$$

$$y_{hydrogen}(\chi) = \frac{\Theta_{hydrogen} + \nu_{hydrogen}\chi}{\delta\chi + \sum_{i=1}^{4} \Theta_i} \text{ (mole fraction of hydrogen)}$$

$$y_{methanol}(\chi) = \frac{\Theta_{methanol} + \nu_{methanol}\chi}{\delta\chi + \sum_{i=1}^{4} \Theta_i} \text{ (mole fraction of methanol)}$$

$$y_{argon}(\chi) = 1 - y_{CO}(\chi) - y_{hydrogen}(\chi) - y_{methanol}(\chi)$$

$$k_{p\infty} = 2 \times 10^4 \text{ g-mol/(mL·min·atm}^3\text{) (pre-exponential factor for kinetic rate constant)}$$

$$R_{gas} = 1.987 \text{ cal/mol·K (gas constant)}$$

$E_{\text{activation}}/R_{\text{gas}} = 5000$ K (activation energy divided by the gas constant)

$k_{p,\text{forward}}(T) = k_{p\infty} \exp\left(-\dfrac{E_{\text{activation}}}{R_{\text{gas}}T}\right)$ g-mol/mL·min·atm^3 (Arrhenius temperature dependence of the kinetic rate constant)

(Thermodynamic data to evaluate the temperature-dependent equilibrium constant)

$\Delta G^{\circ}_{\text{formation298,CO}} = -32{,}808$ cal/g-mol (free energy of formation of CO at 298 K)

$\Delta G^{\circ}_{\text{formation298,methanol}} = -38{,}700$ cal/g-mol (free energy of formation of CH_3OH at 298 K)

$$\Delta G^{\circ}_{\text{Rx,298}} = \sum_i \nu_i \Delta G^{\circ}_{\text{formation298},i} = \nu_{\text{CO}} \Delta G^{\circ}_{\text{formation298,CO}} + \nu_{\text{methanol}} \Delta G^{\circ}_{\text{formation298,methanol}}$$

(free-energy change for the chemical reaction at 298 K, cal/g-mol)

$\Delta H^{\circ}_{\text{formation298,CO}} = -26{,}416$ cal/g-mol (enthalpy of formation of CO at 298 K)

$\Delta H^{\circ}_{\text{formation298,methanol}} = -48{,}100$ cal/g-mol (enthalpy of formation of CH_3OH at 298 K)

$$\Delta H^{\circ}_{\text{Rx,298}} = \sum_i \nu_i \Delta H^{\circ}_{\text{formation298},i} = \nu_{\text{CO}} \Delta H^{\circ}_{\text{formation298,CO}} + \nu_{\text{methanol}} \Delta H^{\circ}_{\text{formation298,methanol}}$$

(enthalpy change for the chemical reaction at 298 K, cal/g-mol)

$\Delta S^{\circ}_{\text{Rx,298}} = \dfrac{\Delta H^{\circ}_{\text{Rx,298}} - \Delta G^{\circ}_{\text{Rx,298}}}{298}$ (entropy change for the chemical reaction at 298 K, cal/mol·K)

$A = \dfrac{\Delta S^{\circ}_{\text{Rx,298}}}{R_{\text{gas}}}$ (dimensionless entropy change for the chemical reaction at 298 K)

$B = -\dfrac{\Delta H^{\circ}_{\text{Rx,298}}}{R_{\text{gas}}}$, K

$K_{\text{eq.},p}(T) = \exp\left(A + \dfrac{B}{T}\right)$ (equilibrium constant for the chemical reaction based on partial pressures, atm$^{\delta}$)

$$p(t) = p_{\text{initial}} \frac{T}{T_{\text{initial}}} \frac{\delta\chi(t) + \sum_{i=1}^{4} \Theta_i}{\sum_{i=1}^{4} \Theta_i}$$ (time-dependent total pressure within the batch reactor, atm)

$$\mathfrak{R} = k_{p,\text{forward}}(T)[p(t)]^3 \left\{ y_{\text{CO}}(\chi)[y_{\text{hydrogen}}(\chi)]^2 - \frac{y_{\text{methanol}}(\chi)[p(t)]^{\delta}}{K_{\text{eq.,}\,p}(T)} \right\}$$ (reversible elementary kinetic rate law based on partial pressures, g-mol/mL·min)

$$N_{\text{CO}}(t=0)\frac{d\chi}{dt} = \mathfrak{R} \cdot \text{volume}_{\text{batch reactor}}$$ (time rate of change of CO conversion from the unsteady-state batch reactor mass balance, g-mol/min)

$$\chi_{\text{initial}} = 0 \text{ (initial CO conversion at } t = 0)$$

$$\chi(t) = \chi_{\text{initial}} + \frac{\text{volume}_{\text{batch reactor}}}{N_{\text{CO}}(t=0)} \int_0^t \mathfrak{R}\, dt$$ (time dependence of CO conversion)

If temperature T is chosen arbitrarily, the set of equations presented above will simulate the performance of an isothermal constant-volume batch reactor. See Figures 6-1 and 6-2 for CO conversion at various temperatures and initial pressures.

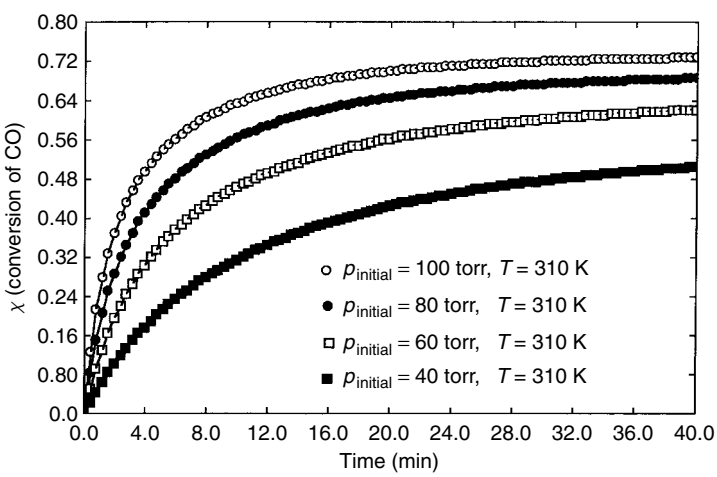

Figure 6-1 Effect of initial pressure on the time-dependent conversion of CO in a constant-volume batch reactor which operates isothermally at 310 K. Le Châtelier's principle predicts higher equilibrium conversion of CO to methanol when the pressure increases.

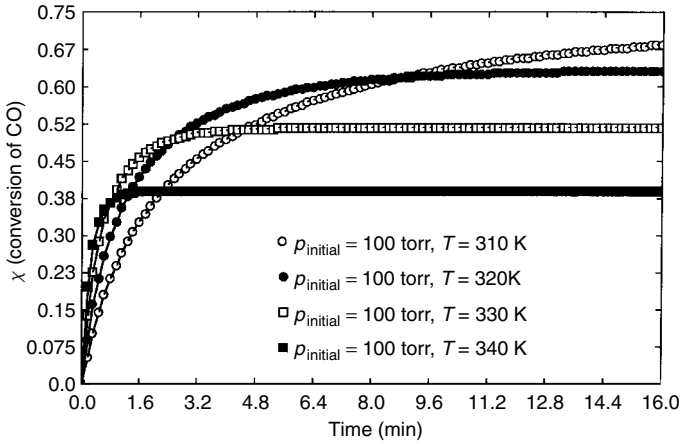

Figure 6-2 Effect of temperature on the time-dependent conversion of CO in a constant-volume batch reactor which operates initially at a total pressure of 100 torr. The initial rate of conversion of CO to methanol proceeds faster when the temperature increases, but Le Châtelier's principle predicts lower equilibrium conversion for exothermic chemical reactions at higher temperatures.

If thermal energy effects are important and the reactor does not operate isothermally, then the information described below is required to analyze reactor performance.

(temperature polynomials for pure-component molar heat capacities; T is in Kelvin and C_p is in cal/mol·K).

$$C_{p,\mathrm{CO}}(T) = 6.79 + 0.98 \times 10^{-3}T - 0.11 \times 10^{5}T^{-2}$$

$$C_{p,\mathrm{hydrogen}}(T) = 6.52 + 0.78 \times 10^{-3}T + 0.12 \times 10^{5}T^{-2}$$

$$C_{p,\mathrm{methanol}}(T) = 4.394 + 24.274 \times 10^{-3}T - 6.855 \times 10^{-6}T^{2}$$

$$C_{p,\mathrm{argon}} = \tfrac{5}{2}R_{\mathrm{gas}}, \text{ monatomic gases do not rotate or vibrate}$$

$$C_{p,\mathrm{mixture}}(T, \chi) = \sum_{i=1}^{4} y_i(\chi)C_{p,i}(T), \text{ including argon (mole-fraction-weighted molar heat capacity of the reactive mixture, cal/mol·K)}$$

$$\Delta C_{p,\mathrm{Rx}}(T) = \sum_{i=1}^{4} \nu_i C_{p,i}(T) = \nu_{\mathrm{CO}}C_{p,\mathrm{CO}}(T) + \nu_{\mathrm{hydrogen}}C_{p,\mathrm{hydrogen}}(T) + \nu_{\mathrm{methanol}}C_{p,\mathrm{methanol}}(T) \text{ (stoichiometric-coefficient-weighted } \Delta C_{p,\mathrm{Rx}} \text{ for the chemical reaction, cal/mol·K)}$$

$$\Delta H_{\mathrm{Rx}}(T) = \Delta H^{\circ}_{\mathrm{Rx},298} + \int_{298}^{T} \Delta C_{p,\mathrm{Rx}}(\xi)\, d\xi \quad \text{(temperature-dependent enthalpy change for the chemical reaction, cal/g-mol)}$$

$$\Delta U_{\mathrm{Rx}}(T) = \Delta H_{\mathrm{Rx}}(T) - \delta p \frac{V}{N_{\mathrm{total}}} \quad \text{(see, for example, Felder and Rousseau, 2000, p. 444)}$$

$$= \Delta H_{\mathrm{Rx}}(T) - \delta R_{\mathrm{gas}} T \quad \text{(temperature-dependent internal energy change for the chemical reaction, cal/g-mol)}$$

$$\left(\frac{dQ}{dt}\right)_{\mathrm{removal}} = \Phi_{\text{specified to prevent thermal runaway}} \quad \text{(rate of heat removal due to conduction across the cooling coil and into the cooling fluid, cal/min)}$$

$$\rho_{\mathrm{cool}} = 1 \text{ g/mL (average density of the cooling fluid, which is most likely water)}$$

$$q_{\mathrm{cool}} = 50 \text{ mL/s (volumetric flow rate of the cooling fluid)}$$

$$C_{p,\mathrm{cool}} = 1 \text{ cal/g·K (specific heat of the cooling fluid)}$$

$$T_{\mathrm{cool,\ inlet}} = 280 \text{ K (inlet temperature of the cooling fluid)}$$

Calculate the outlet temperature of the cooling fluid,

$$\left(\frac{dQ}{dt}\right)_{\mathrm{removal}} = 60\rho_{\mathrm{cool}} q_{\mathrm{cool}} C_{p,\,\mathrm{cool}} (T_{\mathrm{cool,\ outlet}} - T_{\mathrm{cool,\ inlet}})$$

$$\{N_{\mathrm{total}}(t)[C_{p,\mathrm{mixture}}(T, \chi) - R_{\mathrm{gas}}]\}\frac{dT}{dt} = -\left(\frac{dQ}{dt}\right)_{\mathrm{removal}} + \mathfrak{R} \cdot \mathrm{volume}_{\mathrm{batch\ \ reactor}}(-\Delta U_{\mathrm{Rx}})$$

(time rate of change of reactor temperature from the unsteady-state thermal energy balance, cal/min)

$$T(t) = T_{\mathrm{initial}} + \int_{t=0}^{t} \frac{-(dQ/dt)_{\mathrm{removal}} + \mathfrak{R} \cdot \mathrm{volume}_{\mathrm{batch\ \ reactor}}(-\Delta U_{\mathrm{Rx}})}{N_{\mathrm{total}}(t)[C_{p,\mathrm{mixture}}(T, \chi) - R_{\mathrm{gas}}]}\, dt$$

(time dependence of reactor temperature) (6-39)

PROBLEMS

6-1. One irreversible chemical reaction occurs in a constant-volume batch reactor. The reaction is exothermic and a digital controller removes thermal energy at an appropriate rate to maintain constant temperature throughout the course of the reaction. Sketch the time dependence of the rate of thermal energy removal, $(dQ/dt)_{\mathrm{removal}}$ vs. time, for isothermal operation when the rate law is described by:

(a) First-order irreversible chemical kinetics, $\mathfrak{R} = k_1 C_A$.

(b) Zeroth-order irreversible chemical kinetics, $\mathfrak{R} = k_0 \neq f(C_A)$.

6-2. (a) What equations must be solved to calculate the adiabatic temperature change in a constant-volume batch reactor when five components participate in three independent elementary reactions, as illustrated below?

$$\begin{aligned} A + 2B &\longleftrightarrow D \qquad \text{via } k_1(T) \text{ and } K_{eq.C}(T) \\ A + D &\longrightarrow E \qquad \text{via } k_2(T) \\ D + E &\longrightarrow F \qquad \text{via } k_3(T) \end{aligned}$$

All reactions occur on the same time scale, and the energetics of each reaction are similar.

Answer: The unsteady-state macroscopic mass balance for each component in a constant-volume batch reactor with multiple chemical reactions,

$$\frac{dN_i}{dt} = V \sum_j \nu_{ij} \mathfrak{R}_j \qquad 1 \leq i \leq r \text{ (i.e., } r = 5)$$

reduces to the batch reactor design equation in terms of molar densities C_i, where $C_i = N_i / V$:

$$\frac{dC_i}{dt} = \sum_j \nu_{ij} \mathfrak{R}_j \qquad 1 \leq i \leq r$$

These coupled ODEs describe the time dependence of molar density for each component in the reactive mixture. Specifically, for the problem of interest, the unsteady-state mass balances reduce to

$$\begin{aligned} \frac{dC_A}{dt} &= -\mathfrak{R}_1 - \mathfrak{R}_2 \\ \frac{dC_B}{dt} &= -2\mathfrak{R}_1 \\ \frac{dC_D}{dt} &= \mathfrak{R}_1 - \mathfrak{R}_2 - \mathfrak{R}_3 \\ \frac{dC_E}{dt} &= \mathfrak{R}_2 - \mathfrak{R}_3 \\ \frac{dC_F}{dt} &= \mathfrak{R}_3 \end{aligned}$$

and the corresponding kinetic rate laws for the three chemical reactions are

$$\mathfrak{R}_1 = k_1(T)\left[C_A(C_B)^2 - \frac{C_D}{K_{eq.C}(T)}\right]$$
$$\mathfrak{R}_2 = k_2(T)C_A C_D$$
$$\mathfrak{R}_3 = k_3(T)C_D C_E$$

Since the reactor does not operate isothermally, these five coupled mass balances must be solved in conjunction with the unsteady-state thermal energy balance for an adiabatic reactor, where $(dQ/dt)_{input} = 0$. If pressure effects are negligible,

$$\frac{dU}{dt} \approx (C_p - p\alpha V)\frac{dT}{dt} + \sum_{i=1}^{r}\left(\frac{\partial U}{\partial N_i}\right)_{T,p,\text{all } N_j(j\neq i)}\frac{dN_i}{dt}$$
$$\approx \left(\frac{dQ}{dt}\right)_{input} = 0$$

Coupled heat and mass transfer yield the following ODE for the time dependence of reactor temperature after substitution for dN_i/dt:

$$(C_p - p\alpha V)\frac{dT}{dt} = -V\sum_j \mathfrak{R}_j \sum_{i=1}^{r} \nu_{ij}\left(\frac{\partial U}{\partial N_i}\right)_{T,p,\text{all } N_j(j\neq i)}$$
$$= V\sum_j \mathfrak{R}_j(-\Delta U_{Rx})_j$$

where $\mathfrak{R}_j$ represents the kinetic rate law for the jth chemical reaction in the mechanism, and $(\Delta U_{Rx})_j$ is the internal energy change associated with the jth step, as defined by

$$(\Delta U_{Rx})_j \equiv \sum_{i=1}^{r} \nu_{ij}\left(\frac{\partial U}{\partial N_i}\right)_{T,p,\text{all } N_j(j\neq i)}$$

Hence, six coupled ODEs (i.e., five mass balances and one thermal energy balance) must be solved to calculate the adiabatic temperature change in this mixture of five components.

(b) Explain why kinetic and thermodynamic data are required for each chemical reaction to obtain a quantitative estimate of the adiabatic temperature change for a multiple-reaction scheme (in any type of reactor), whereas thermodynamic data are sufficient to calculate $\Delta T_{adiabatic}$ if only one reaction occurs.

Transport Phenomena for Chemical Reactor Design. Laurence A. Belfiore
Copyright © 2003 John Wiley & Sons, Inc.
ISBN: 0-471-20275-4

7

TOTAL PRESSURE METHOD OF REACTION-RATE DATA ANALYSIS

7-1 ELEMENTARY REVERSIBLE GAS-PHASE REACTIONS IN A CONSTANT-VOLUME FLASK

Consider the following generic reversible reaction that contains two reactants and two products:

$$\mathrm{A} + b\mathrm{B} \longleftrightarrow c\mathrm{C} + d\mathrm{D} \tag{7-1}$$

The four-component gas mixture behaves ideally at moderately low pressures, and the sum of stoichiometric coefficients ν_i is not zero. Hence,

$$\frac{dp_{\text{total}}}{dt} > 0 \qquad \text{if} \quad \delta = \sum_i \nu_i = c + d - b - 1 > 0 \tag{7-2a}$$

$$\frac{dp_{\text{total}}}{dt} < 0 \qquad \text{if} \quad \delta < 0 \tag{7-2b}$$

where p_{total} is the total pressure within the flask (i.e., batch reactor). The objective of this chapter is to analyze the time dependence of total system pressure and extract information about the kinetic rate constant for elementary reactions. The unsteady-state macroscopic mass balance with reversible chemical reaction is written for component i in a constant-volume flask. The accumulation rate process is balanced by the rate of production due to one chemical reaction. In units of moles per time,

$$\frac{dN_i}{dt} = \nu_i \int \mathfrak{R}\, dV_R = \nu_i \mathfrak{R} V_R \tag{7-3}$$

if the contents of the flask are well mixed such that the intrinsic rate law is not a function of position. N_i represents the moles of component i, ν_i is the stoichiometric coefficient of component i, $\mathfrak{R}$ represents the rate law, and V_R is the volume of the flask. The ideal gas law is written as

$$p_{\text{total}} V_R = N_{\text{total}} RT \tag{7-4}$$

$$p_{\text{total}} = \sum_i p_i \tag{7-5}$$

$$N_{\text{total}} = \sum_i N_i \tag{7-6}$$

where p_i is the partial pressure of component i in the mixture. The ideal gas law is written individually for each component in the mixture:

$$p_i V_R = N_i RT \tag{7-7}$$

which allows one to re-express the unsteady-state macroscopic mass balance in terms of p_i:

$$\frac{dN_i}{dt} = \frac{V_R}{RT}\frac{dp_i}{dt} = \nu_i \mathfrak{R} V_R \tag{7-8}$$

Stoichiometry and the unsteady-state mass balance with chemical reaction yield the following relation between component partial pressures:

$$\frac{dp_i}{\nu_i} = \frac{dp_{\text{A}}}{\nu_{\text{A}}} = RT\mathfrak{R}\,dt = \text{same for each component} \tag{7-9}$$

Integration of this stoichiometric relation (7-9) from $t = 0$, where $p_i = p_i(0)$, to variable time t and $p_i(t)$ produces the following result when the stoichiometric coefficient of reactant A is -1:

$$p_i(t) = p_i(0) + \nu_i[p_{\text{A}}(0) - p_{\text{A}}(t)] \tag{7-10}$$

Summation of (7-10) over all components in the mixture,

$$\sum_i p_i(t) = \sum_i p_i(0) + [p_{\text{A}}(0) - p_{\text{A}}(t)] \sum_i \nu_i \tag{7-11}$$

provides a relation between total pressure and the partial pressure of reactant A:

$$p_{\text{total}}(t) = p_{\text{total}}(0) + \delta[p_{\text{A}}(0) - p_{\text{A}}(t)] \tag{7-12}$$

This equation is rearranged to calculate $p_{\text{A}}(0) - p_{\text{A}}(t)$ in terms of total pressure:

$$p_{\text{A}}(0) - p_{\text{A}}(t) = \frac{p_{\text{total}}(t) - p_{\text{total}}(0)}{\delta} \tag{7-13}$$

which allows one to relate the partial pressure of any component in the mixture to total pressure via (7-10) and (7-13):

$$p_i(t) = p_i(0) + \frac{\nu_i}{\delta}[p_{\text{total}}(t) - p_{\text{total}}(0)] \tag{7-14}$$

Dalton's law is used to calculate the initial partial pressure of component i in terms of mole fraction y_i and total pressure. Hence,

$$p_i(0) = y_i(0)\, p_{\text{total}}(0) \tag{7-15}$$

Equations (7-14) and (7-15) are useful because it is customary to express the intrinsic rate law for gas-phase reactions in terms of partial pressures. For the elementary reversible reaction given by (7-1):

$$\mathfrak{R} = k_{\text{forward},\, p}(T)\left[p_{\text{A}} p_{\text{B}}^{b} - \frac{p_{\text{C}}^{c} p_{\text{D}}^{d}}{K_{\text{equil},\, p}(T)}\right] \tag{7-16}$$

where $k_{\text{forward},\, p}(T)$ is the temperature-dependent kinetic rate constant for the forward reaction, with units of moles/volume·time·pressure^{1+b}, and $K_{\text{equil},\, p}(T)$ is the temperature-dependent equilibrium constant based on partial pressures, with units of (pressure)$^{\delta}$. Now, each partial pressure in the rate law can be expressed in terms of total pressure via (7-14) and (7-15). This rate law is combined with the unsteady-state mass balance,

$$\frac{V_R}{RT}\frac{dp_i}{dt} = \nu_i \mathfrak{R} V_R \tag{7-17}$$

to analyze the time dependence of total pressure. This is achieved by summing equation (7-17) over all components in the mixture. The result is

$$\frac{dp_{\text{total}}}{dt} = \delta RT\mathfrak{R} \tag{7-18}$$

Now it is possible to develop a strategy for analyzing the time dependence of total pressure for gas-phase reactions when the sum of stoichiometric coefficients does not vanish. Since the order of the forward and backward reactions is known for elementary steps, linear least-squares analysis via the differential approach is useful to determine the forward kinetic rate constant if the equilibrium constant can be calculated from thermodynamics. The logical sequence of steps is as follows:

Step 1. Measure total pressure vs. time and generate two columns of data, t_i and $p_{\text{total},\, i}$.

Step 2. Numerically differentiate p_{total} vs. t to generate dp_{total}/dt via an nth-order-correct finite difference formula at each discrete data point.

Step 3. The data should be matched to the following model with one independent variable:

$$y = b'x + c' \tag{7-19}$$

with $c' = 0$.

Step 4. The dependent variable at each time step, with units of pressure/time, is

$$y_i = \left(\frac{d\,p_{\text{total}}}{dt}\right)_{t=t_i} \tag{7-20}$$

A central difference expression is appropriate to calculate the time rate of change of p_{total} at most points in the data set, but a forward difference is required for the initial point at $t = 0$, and a backward difference is necessary at the last data point.

Step 5. The independent variable at each time step, with units of (pressure)$^{1+b}$, is

$$x_i = p_{\text{A}}(t_i)[p_{\text{B}}(t_i)]^b - \frac{[p_{\text{C}}(t_i)]^c[p_{\text{D}}(t_i)]^d}{K_{\text{equil, }p}(T)} \tag{7-21}$$

$$p_i(t_i) = y_i(0)p_{\text{total}}(0) + \frac{\nu_i}{\delta}[p_{\text{total}}(t_i) - p_{\text{total}}(0)] \tag{7-22}$$

Step 6. Since the zeroth-order coefficient (i.e., the intercept c') is forced to be zero, the first-order coefficient from linear least-squares analysis is

$$b' = \frac{\sum_i x_i y_i}{\sum_i (x_i)^2} = \delta RT k_{\text{forward, }p}(T)[=](\text{time}\cdot\text{pressure}^b)^{-1} \tag{7-23}$$

which yields a forward kinetic rate constant with units of moles/volume·time·(pressure)$^{1+b}$. Details of the linear least-squares procedure are discussed below.

7-2 GENERALIZED LINEAR LEAST-SQUARES ANALYSIS FOR A SECOND-ORDER POLYNOMIAL WITH ONE INDEPENDENT VARIABLE

Experimental measurements yield N data pairs (i.e., x_i and y_i, $1 \le i \le N$), and it is desired to model the data with the following quadratic function:

$$y(x) = ax^2 + bx + c \tag{7-24}$$

The objective of this exercise is to use all the data pairs and determine the optimum values of the parameters a, b, and c in the second-order polynomial given

by (7-24). Even though the polynomial is not linear, the three parameters can be calculated from simultaneous solution of three linear algebraic equations. The nature of the model function determines whether linear or nonlinear analysis is required to determine the parameters. Sometimes, simple algebraic manipulation together with taking the logarithm of the entire equation reduces a nonlinear problem to one that requires linear analysis. The quadratic function $y(x)$ that best matches the discrete data pairs is determined by comparing $y(x_i)$ and y_i, $1 \leq i \leq N$. Since differences between $y(x_i)$ and y_i can be positive or negative, a very poor match between model and data might yield small overall differences when $y(x_i) - y_i$ is summed over all data pairs if some of the differences cancel fortuitously. To avoid this problem in the evaluation of any polynomial model, the error is constructed as follows:

$$\text{Error}(a, b, c) = \sum_{i=1}^{N} [y(x_i) - y_i]^2 = \sum_{i=1}^{N} [a(x_i)^2 + bx_i + c - y_i]^2 \tag{7-25}$$

so that all differences between model and data contribute to larger error. The same final result could be achieved by summing the absolute value of the difference between model and data over all points. If Error, as defined in (7-25), is plotted in four-dimensional space as a function of the three parameters, the best combination of a, b, and c produces a global minimum on this multidimensional surface. This condition is expressed mathematically as

$$\left(\frac{\partial \text{Error}}{\partial a}\right)_{b,c} = 2 \sum_{i=1}^{N} (x_i)^2 [a(x_i)^2 + bx_i + c - y_i] = 0 \tag{7-26a}$$

$$\left(\frac{\partial \text{Error}}{\partial b}\right)_{a,c} = 2 \sum_{i=1}^{N} x_i [a(x_i)^2 + bx_i + c - y_i] = 0 \tag{7-26b}$$

$$\left(\frac{\partial \text{Error}}{\partial c}\right)_{a,b} = 2 \sum_{i=1}^{N} [a(x_i)^2 + bx_i + c - y_i] = 0 \tag{7-26c}$$

Minimization is assured because there is no upper bound to the error. These three linear algebraic equations are rearranged into a canonical form that allows direct application of Cramer's rule to calculate a, b, and c:

$$a \sum_{i=1}^{N} (x_i)^4 + b \sum_{i=1}^{N} (x_i)^3 + c \sum_{i=1}^{N} (x_i)^2 = \sum_{i=1}^{N} (x_i)^2 y_i \tag{7-27a}$$

$$a \sum_{i=1}^{N} (x_i)^3 + b \sum_{i=1}^{N} (x_i)^2 + c \sum_{i=1}^{N} x_i = \sum_{i=1}^{N} x_i y_i \tag{7-27b}$$

$$a \sum_{i=1}^{N} (x_i)^2 + b \sum_{i=1}^{N} x_i + \sum_{i=1}^{N} c = \sum_{i=1}^{N} y_i \tag{7-27c}$$

The following summations over all of the $x_i - y_i$ data pairs are defined to simplify the final solution for the three parameters:

$$S_1 = \sum_{i=1}^{N} x_i \qquad S_2 = \sum_{i=1}^{N} (x_i)^2 \qquad S_3 = \sum_{i=1}^{N} (x_i)^3 \qquad S_4 = \sum_{i=1}^{N} (x_i)^4$$
$$S_5 = \sum_{i=1}^{N} y_i \qquad S_6 = \sum_{i=1}^{N} x_i y_i \qquad S_7 = \sum_{i=1}^{N} (x_i)^2 y_i \tag{7-28}$$

If one chooses to exclude one or more data points from the analysis, the seven summations defined above must be modified accordingly and N is reduced. Multivariable minimization of the error in equation (7-25) is accomplished by solving the following coupled linear equations:

$$aS_4 + bS_3 + cS_2 = S_7 \tag{7-29a}$$

$$aS_3 + bS_2 + cS_1 = S_6 \tag{7-29b}$$

$$aS_2 + bS_1 + cN = S_5 \tag{7-29c}$$

The determinant of the coefficient matrix is calculated from the left side of (7-29):

$$\det 1 = NS_2S_4 + S_1S_2S_3 + S_1S_2S_3 - (S_2)^3 - N(S_3)^2 - S_4(S_1)^2 \tag{7-30}$$

Cramer's rule yields the following solution for a, b, and c:

$$a = \frac{NS_2S_7 + S_1S_3S_5 + S_1S_2S_6 - S_5(S_2)^2 - NS_3S_6 - S_7(S_1)^2}{\det 1} \tag{7-31a}$$

$$b = \frac{NS_4S_6 + S_1S_2S_7 + S_2S_3S_5 - S_6(S_2)^2 - NS_3S_7 - S_1S_4S_5}{\det 1} \tag{7-31b}$$

$$c = \frac{S_2S_4S_5 + S_2S_3S_6 + S_1S_3S_7 - S_7(S_2)^2 - S_5(S_3)^2 - S_1S_4S_6}{\det 1} \tag{7-31c}$$

There are many situations where a linear model is desired (i.e., $y = bx + c$). The optimum values of the first-order coefficient b (i.e., slope) and the zeroth-order coefficient c (i.e., intercept) can be calculated from a subset of the information provided above for a second-order polynomial model. It is not necessary to minimize the error with respect to the second-order coefficient a. Furthermore, $a = 0$ in the other two linear equations. Hence, equations (7-29) reduce to:

$$bS_2 + cS_1 = S_6 \tag{7-32a}$$

$$bS_1 + cN = S_5 \tag{7-32b}$$

The determinant of the coefficient matrix is calculated from the left side of (7-32):

$$\det 2 = NS_2 - (S_1)^2 \tag{7-33}$$

Cramer's rule yields the following solution for b and c:

$$b = \frac{N S_6 - S_1 S_5}{\det 2} \tag{7-34a}$$

$$c = \frac{S_2 S_5 - S_1 S_6}{\det 2} \tag{7-34b}$$

If the linear polynomial has a known value of the intercept c, the linear least-squares procedure identifies the best slope via minimization of the error with respect to b. The value of b is obtained by solving the first of the two simultaneous linear equations for b and c. Equations (7-32) reduce to:

$$bS_2 + cS_1 = S_6 \tag{7-35}$$

Hence,

$$b = \frac{S_6 - cS_1}{S_2} \tag{7-36}$$

where the known value of c is used together with the appropriate summations to calculate b.

PROBLEMS

7-1. The irreversible decomposition of phosphine follows first-order kinetics at 650°C in a closed vessel:

$$PH_3(g) \longrightarrow \tfrac{1}{4}P_4(g) + \tfrac{3}{2}H_2(g)$$

Calculate the time dependence of **(a)** the total pressure and **(b)** the partial pressure of each component if the batch reactor is injected with 1 atm of pure PH_3 at $t = 0$.

Answer: The unsteady-state macroscopic mass balance describes the time dependence of total pressure in terms of the kinetic rate law, which is based on the partial pressure of phosphine for first-order irreversible kinetics:

$$\frac{d\,p_{\text{total}}}{dt} = \delta RT\mathfrak{R} = \frac{3}{4} RT k_{\text{forward},\,p}(T)\, p_{PH_3}$$

where $RTk_{\text{forward},\,p}(T) = k_{\text{forward},\,C}(T)$ is a first-order kinetic rate constant with dimensions of inverse time, and p_{PH_3} is the partial pressure of phosphine. Stoichiometry and the unsteady-state mass balance with chemical reaction for ideal gases allows one to relate $p_{PH_3}(t)$ and $p_{\text{total}}(t)$ via equations (7-14) and (7-15):

$$p_{PH_3}(t) = y_{PH_3}(t=0)\, p_{\text{total}}(t=0) - \tfrac{4}{3}[p_{\text{total}}(t) - p_{\text{total}}(t=0)]$$

Since the reactor is injected with pure phosphine, $y_{PH_3}(t=0)=1$ and

$$\frac{dp_{\text{total}}}{dt}=\frac{3}{4}k_{\text{forward, }C}(T)\left\{p_{\text{total}}(t=0)-\frac{4}{3}[p_{\text{total}}(t)-p_{\text{total}}(t=0)]\right\}$$
$$=\frac{1}{4}k_{\text{forward, }C}(T)[7p_{\text{total}}(t=0)-4p_{\text{total}}(t)]$$

Separation of variables yields

$$\frac{dp_{\text{total}}}{7p_{\text{total}}(t=0)-4p_{\text{total}}(t)}=\frac{1}{4}k_{\text{forward, }C}(T)\,dt$$

Integration from $t=0$ to variable time t provides the desired expression for the time dependence of total pressure:

$$-\frac{1}{4}\ln\frac{7p_{\text{total}}(t=0)-4p_{\text{total}}(t)}{3p_{\text{total}}(t=0)}=\frac{1}{4}k_{\text{forward, }C}(T)t$$
$$p_{\text{total}}(t)=\frac{1}{4}p_{\text{total}}(t=0)\{7-3\exp[-k_{\text{forward, }C}(T)t]\} \qquad (a)$$

The total pressure in the reactor asymptotically reaches $\frac{7}{4}p_{\text{total}}(t=0)$ after very long reaction times. The time dependence of the partial pressure of each component is obtained from stoichiometry and expression (a), which is rearranged below:

$$p_{\text{total}}(t)-p_{\text{total}}(t=0)=\tfrac{3}{4}p_{\text{total}}(t=0)\{1-\exp[-k_{\text{forward, }C}(T)t]\}$$

PH_3 : $p_{PH_3}(t)=p_{\text{total}}(t=0)-\frac{4}{3}[p_{\text{total}}(t)-p_{\text{total}}(t=0)]$

$p_{PH_3}(t)=p_{\text{total}}(t=0)\exp[-k_{\text{forward, }C}(T)t]$

P_4 : $p_{P_4}(t)=\frac{1}{3}[p_{\text{total}}(t)-p_{\text{total}}(t=0)]$

$p_{P_4}(t)=\frac{1}{4}p_{\text{total}}(t=0)\{1-\exp[-k_{\text{forward, }C}(T)t]\}$

H_2 : $p_{H_2}(t)=2[p_{\text{total}}(t)-p_{\text{total}}(t=0)]$

$p_{H_2}(t)=\frac{3}{2}p_{\text{total}}(t=0)\{1-\exp[-k_{\text{forward, }C}(T)t]\}$

7-2. Ammonia is produced from a stoichiometric feed of nitrogen and hydrogen via the following elementary reversible chemical reaction in the gas phase:

$$N_2(g)+3H_2(g)\longleftrightarrow 2NH_3(g)$$

A constant-volume batch reactor operates at 800 K and reactants are injected to a total initial pressure of 350 atm. Calculate the time dependence of total pressure in the reactor.

Answer: Let's begin with the kinetic rate law in terms of partial pressures and the temperature-dependent equilibrium constant from thermodynamics;

$$\mathfrak{R} = k_{\text{forward, } p}(T)\left[p_{N_2} p_{H_2}^3 - \frac{p_{NH_3}^2}{K_{\text{equil, } p}(T)}\right]$$

The forward kinetic rate constant $k_{\text{forward, } p}(T)$ exhibits Arrhenius temperature dependence and has dimensions of moles/volume·time·atm^4. The equilibrium constant based on gas phase partial pressures has dimensions of (atm)$^\delta$, where $\delta = -2$. Since N_2 and H_2 are present in their standard states, the enthalpy and free energy of formation for NH_3 at 298 K allow one to construct the temperature dependence of $K_{\text{equil, } p}$ as follows:

$$K_{\text{equil, } p}(T) = K^\circ_{\text{standard state}} \exp\left(\text{A} + \frac{\text{B}}{T}\right)$$

where T must be in Kelvin, and

$$\text{A} = \frac{\Delta S^\circ_{\text{Rx, 298}}}{R} = \frac{\Delta H^\circ_{\text{Rx, 298}} - \Delta G^\circ_{\text{Rx, 298}}}{298R}$$

$$\text{B} = -\frac{\Delta H^\circ_{\text{Rx, 298}}}{R}$$

$$\Delta H^\circ_{\text{Rx, 298}} = 2\Delta \text{H}^\circ_{\text{formation, NH}_3}(\text{at 298 K}) = 2(-11,040 \text{ cal/g-mol})$$

$$\Delta G^\circ_{\text{Rx, 298}} = 2\Delta G^\circ_{\text{formation, NH}_3}(\text{at 298 K}) = 2(-3976 \text{ cal/g-mol})$$

The appropriate bond energies that are consistent with these thermodynamic data are

N≡N(945 kJ/mol) H−H(436 kJ/mol) N−H(391 kJ/mol)

The unsteady-state macroscopic mass balance for a constant-volume batch reactor describes the time rate of change of total pressure:

$$\frac{dp_{\text{total}}}{dt} = \delta RT\mathfrak{R} = -2RT\mathfrak{R}$$

The partial pressure of each component in the kinetic rate law is evaluated in terms of total pressure via stoichiometry;

Nitrogen (N_2): $p_{N_2}(t) = y_{N_2}(t=0)p_{\text{total}}(t=0) + \frac{1}{2}[p_{\text{total}}(t) - p_{\text{total}}(0)]$

Hydrogen (H_2): $p_{H_2}(t) = y_{H_2}(t=0)p_{\text{total}}(t=0) + \frac{3}{2}[p_{\text{total}}(t) - p_{\text{total}}(0)]$

Ammonia (NH_3): $p_{NH_3}(t) = y_{NH_3}(t=0)p_{\text{total}}(t=0) - [p_{\text{total}}(t) - p_{\text{total}}(0)]$

For a stoichiometric feed of reactants,

$$y_{N_2}(t=0) = \tfrac{1}{4} \qquad y_{H_2}(t=0) = \tfrac{3}{4} \qquad y_{NH_3}(t=0) = 0$$

Hence, one must solve the following ordinary differential equation for the time dependence of total pressure:

$$\frac{dp_{\text{total}}}{dt} = -2RTk_{\text{forward, }p}(T)\left[p_{N_2}p_{H_2}^3 - \frac{p_{NH_3}^2}{K_{\text{equil, }p}(T)}\right]$$

subject to the initial condition that $p_{\text{total}}(t=0) = 350$ atm. If the gas mixture does not behave ideally at this high pressure, it might seem reasonable to replace partial pressures by fugacities in the kinetic rate law. For example,

$$f_{i,\text{ mixture}} = y_i\phi_i p_{\text{total}}$$

where y_i represents mole fraction and ϕ_i is the fugacity coefficient of component i in the mixture at the prevailing temperature and pressure. Critical constants are useful to evaluate ϕ_i for each component at 800 K and 350 atm. This exercise is performed for pure-component fugacity coefficients below to determine if non-ideal effects are important.

Gas	T_C (K)	T_r	p_C (atm)	p_r	$\phi_{\text{pure comp.}}$
H_2	33.1	24.2	12.8	27.3	$\approx$1.2
N_2	125.9	6.4	33.5	10.4	$\approx$1.2
NH_3	405.4	2.0	111.5	3.1	0.95

Ideality seems like a reasonable assumption for this gas mixture at the temperature and pressures of operation since each pure-component fugacity coefficient is not much different from unity. Total pressure will decrease below 350 atm during the course of the reaction because $\delta = -2$.

7-3. Simulate the time dependence of total pressure for the ammonia synthesis described in Problem 7-2 at 400 K. The constant-volume batch reactor is charged initially to a total pressure of 100 atm. The Arrhenius forward kinetic rate constant exhibits a pre-exponential factor of 1×10^5 mol cm^3·min·atm^4. Since the strongly energetic nitrogen–nitrogen triple bond (i.e., N≡N) must be broken to produce NH_3, the activation energy for this reaction (i.e., 30 kcal/mol) is quite large.

(a) Predict the total pressure in the batch reactor and the fractional conversion of N_2 to NH_3 after 2 h of operation.

(b) Predict the total pressure in atmospheres when equilibrium is achieved.

(c) Identify two strategies to increase the equilibrium conversion of N_2 to NH_3.

7-4. The gas-phase production of methanol from carbon monoxide and hydrogen is carried out in a small constant-volume batch reactor under isothermal conditions and the pilot-plant operator measures the total pressure within the reactor vs. time for subsequent reaction-rate data analysis. A stoichiometric feed of carbon monoxide and hydrogen is introduced to the reactor at time $t = 0$, and the total pressure is 3 atm. Sketch the raw data as total pressure vs. time. Be sure to indicate the appropriate equation that describes the shape of the curve.

7-5. (a) We plan to apply the integral method of reaction-rate data analysis for elementary reversible reactions. Neither you nor anyone else in your company remembers how to integrate or differentiate, but I claim that it is possible to prove whether

$$2\psi k_{\text{forward, }C} t = \ln \frac{C_A(t) + (1/2K_{\text{equil }C}) + \psi}{C_{A0} + (1/2K_{\text{equil }C}) + \psi} + \ln \frac{C_{A0} + (1/2K_{\text{equil }C}) - \psi}{C_A(t) + (1/2K_{\text{equil }C}) - \psi}$$

$$\psi = \sqrt{\frac{1}{4K_{\text{equil }C}^2} + \frac{C_{A0}}{K_{\text{equil }C}}}$$

represents the correct analytical solution to the following unsteady-state macroscopic mass balance for reactant A in a constant-volume flask:

$$-\frac{dC_A}{dt} = k_{\text{forward, }C}\left[C_A C_B - \frac{C_D}{K_{\text{equil }C}}\right]$$

The elementary reversible liquid-phase chemical reaction is

$$A + B \longleftrightarrow D$$

the initial molar density of reactant A is C_{A0}, stoichiometric amounts of A and B are introduced into the flask at $t = 0$, and $K_{\text{equil }C}$ is the equilibrium constant for the chemical reaction based on liquid-phase molar densities. Hence, $K_{\text{equil }C}$ has dimensions of inverse molar density. Is the analytical solution correct? Provide support for your answer. Remember that the economy is strong and everyone in your company is surfing the Internet to trade stocks during normal working hours. Consequently, they don't have time to review their math notes, which, luckily, they didn't discard after their course on ordinary differential equations was completed. Hence, no one knows how to perform analytical integration of the unsteady-state macroscopic mass balance for

a constant-volume batch reactor with reversible chemical kinetics. This fact was obvious after you asked everyone about their math skills at the company meeting yesterday.

(b) Your technician measures the molar density of reactant A vs. time for the liquid-phase elementary reversible reaction described in part (a). The equilibrium constant is calculated from thermodynamics. Use methods (i) and (ii) below, and identify the independent variable x and the dependent variable y from which linear least-squares analysis can be implemented in the form $y = ax + b$, to calculate the second-order forward kinetic rate constant from the first-order coefficient a (i.e., the slope) in the model. *Hint:* In both cases, $b = 0$.

(i) Differential method of reaction-rate data analysis.

(ii) Integral method of reaction-rate data analysis.

7-6. You are applying linear least-squares analysis to a set of 20 data pairs. The model is a linear first-order polynomial with slope b (i.e., the first-order coefficient) and intercept c (i.e., the zeroth-order coefficient). It is necessary to force the intercept c to be zero, analogous to some of your laboratory calibration curves. Hence, $c = 0$.

(a) Begin with the linear least-squares description (i.e., see equations 7-29) for a generalized second-order polynomial (i.e., $y = ax^2 + bx + c$) and identify the equation that must be solved to calculate the first-order coefficient b.

(b) Now calculate b from your equation in part (a) in terms of the appropriate summations that involve $x_i - y_i$ data pairs.

7-7. (a) Provide a detailed explanation of the linear least-squares analysis (LLSA) procedure to calculate the kinetic rate constant $k_r(T)$ for a stoichiometric feed of reactants A and B in a constant-volume batch reactor if the rate law is

$$\mathfrak{R} = k_r(T)C_A C_B$$

and the stoichiometrically balanced reaction is $A + B \rightarrow C + D$.

(b) For the irreversible chemical reaction described in part (a), data are available for the molar density of reactant A vs. time at two different temperatures. Use one set of axes and sketch the molar density of reactant A vs. time at higher temperature and lower temperature. Be sure to label the two curves.

(c) For the irreversible chemical reaction described in part (a), use one set of axes and sketch the rate of depletion of reactant A vs. time at higher temperature and lower temperature. Be sure to label the two curves.

7-8. Concentration–time data are available for an irreversible liquid-phase constant-volume reaction in which the rate law $\mathfrak{R}$ is a function of the molar

density of reactants A and B. The differential method of data analysis has been applied to determine the order of the reaction with respect to each reactant. Using this information, the integral method of data analysis generates the following model for the time dependence of the conversion of key-limiting reactant A:

$$\chi(t) = \frac{C_{A0} - C_A(t)}{C_{A0}} = 1 - \frac{1}{1 + k_n C_{A0} t}$$

By answering the questions below, describe a linear least-squares procedure that will allow you to process the raw data (t, C_A) and calculate the nth-order kinetic rate constant k_n.

(a) Identify the independent data column.

(b) Identify the dependent data column.

(c) What type of polynomial should be used to analyze the data?

(d) How does one calculate the kinetic rate constant k_n from the coefficients of the polynomial model?

7-9. Describe the linear least-squares analysis (LLSA) procedure that allows one to calculate the reaction order n from a set of discrete data points for reaction half-time $t_{1/2}$ vs. the initial concentration of reactant A, C_{A0}. The kinetics are irreversible and nth-order, and the rate law is only a function of the molar density of reactant A. Answer this question by providing the following information:

(a) Identify the independent variable, x_i.

(b) Identify the dependent variable, y_i.

(c) What type of polynomial model should be used to analyze the data?

(d) How does one calculate the reaction order n from the parameters that are obtained from linear least-squares analysis?

(e) For what value (or values) of the reaction order n is the reaction half-time independent of the initial concentration of reactant A?

7-10. What method of reaction-rate data analysis is most appropriate to calculate the order of the forward reaction via LLSA when the chemical reaction is nonelementary and reversible, and the equilibrium constant is not infinitely large? The constant-volume flask is charged initially with reactants A and B only, not products C and D.

7-11. Fourth-order-correct finite-difference expressions are much more accurate for calculating the rate of depletion of reactant A (i.e., $-dC_A/dt$) in a constant-volume flask via concentration–time data than are second-order-correct formulas.

(a) How many terms are required in the Taylor series prior to truncation to develop finite-difference expressions that are fourth-order-correct?

(b) At how many discrete points (t, C_A) must the Taylor series be evaluated to calculate all the unknowns (i.e., the coefficients) in the Taylor series if the finite-difference expressions are fourth-order-correct?

(c) If the data are nonequispaced on the time axis, how many different values of C_A (at most) appear in the final fourth-order-correct expression for the rate of depletion, $-dC_A/dt$?

7-12. How many experimental data triplets (t, C_A, C_B) are required to perform LLSA of the initial rate of reaction at $t = 0$ via the differential method in an isothermal constant-volume batch reactor if the following conditions are satisfied simultaneously:

(1) The rate law is $\mathfrak{R} = k_r(T)(C_{A0})^{\alpha}(C_{B0})^{\beta}$.

(2) All of the summations in the linear least-squares calculations contain 10 terms.

(3) All data points are included in the analysis.

(4) The initial rate of depletion of reactant A at $t = 0$ is calculated numerically via a second-order-correct finite-difference formula.

Transport Phenomena for Chemical Reactor Design. Laurence A. Belfiore
Copyright © 2003 John Wiley & Sons, Inc.
ISBN: 0-471-20275-4

PART II

TRANSPORT PHENOMENA: FUNDAMENTALS AND APPLICATIONS

Transport Phenomena for Chemical Reactor Design. Laurence A. Belfiore
Copyright © 2003 John Wiley & Sons, Inc.
ISBN: 0-471-20275-4

8

APPLICATIONS OF THE EQUATIONS OF CHANGE IN FLUID DYNAMICS

Most flow problems in fluid dynamics involve a fluid in motion adjacent to a stationary wall — the wall of a tube, for example — or a fluid that is set in motion by a moving surface; this is the case in a viscosity-measuring device. In general, the bulk fluid and the solid surface are moving at different relative speeds, and this generates viscous stress at the interface. Macroscopic correlations in fluid dynamics focus on the fluid–solid interface and calculate the force exerted by the fluid on the solid, or vice versa, via the fluid velocity gradient at the wall. These macroscopic momentum transport correlations contain the friction factor and the Reynolds number. Hence, one calculates the Reynolds number from the characteristics of the flow problem and uses these dimensionless correlations to determine the value of the friction factor. Frictional energy losses in straight sections of a tube are estimated from the friction factor. The size of a pump required to offset all the dissipative processes that reduce fluid pressure can be estimated from the non-ideal macroscopic mechanical energy balance (i.e., Bernoulli equation) that incorporates friction loss via the friction factor. In some cases, macroscopic momentum transfer correlations relate torque and angular velocity for the viscosity-measuring devices, allowing one to calculate the viscosities of Newtonian or non-Newtonian fluids from measurements of torque vs. angular velocity.

8-1 IMPORTANT VARIABLES

8-1.1 Velocity Vector

The fluid velocity vector is one of the most important variables in fluid dynamics. A *vector* can be described as a quantity that has magnitude and direction.

A more sophisticated description identifies a vector as a mathematical entity that associates a scalar with each coordinate direction in a particular coordinate system. Hence, there are three scalar velocity components that constitute the velocity vector, and they are typically written in the following manner in three different coordinate systems:

v_x	v_y	v_z	in rectangular Cartesian coordinates
v_r	v_θ	v_z	in cylindrical coordinates
v_r	v_θ	v_φ	in spherical coordinates

Each flow problem is solved in only one coordinate system (i.e., the coordinate system that best exploits the symmetry of the macroscopic boundaries).

8-1.2 Molecular Momentum Flux

Viscous stress is an extremely important variable, and this quantity is identified by the Greek letter τ. Viscous stress represents molecular transport of momentum, analogous to heat conduction and diffusion. All molecular transport mechanisms correspond to irreversible processes that generate entropy under realistic conditions. When fluids obey Newton's law of viscosity, there is a linear relation between viscous stress and velocity gradients. All fluids do not obey Newton's law of viscosity, but almost all gases and low-molecular-weight liquids are Newtonian.

8-1.3 Pressure

Fluid pressure is the third important variable, and it is designated by the letter p. Force balances contain fluid pressure because pressure forces are exerted across surfaces, and there are, at most, six surfaces that enclose fluid completely within a control volume. Pressure forces are operative under hydrodynamic and hydrostatic conditions. Force balances in this chapter typically apply to fluids in motion — hence, the name *fluid dynamics*. However, these balances are generic enough to describe the situation when fluids are at rest. In other words, the force balances will be applicable to describe hydrostatics when the velocity vector and τ vanish.

8-2 PHYSICAL PROPERTIES IN FLUID DYNAMICS

Physical properties of a fluid can be described within the context of transport analogies for all the transport processes. Numerical solutions to fluid dynamics problems require that the viscosity μ and the density ρ are known. Under isothermal conditions, if the fluid is Newtonian and incompressible, both of these physical properties are constants that depend only on the fluid, not the flow conditions. The viscosity μ is the molecular transport property that appears in the

linear constitutive relation that equates the molecular transport of momentum with velocity gradients. The ratio of viscosity to density is called the *kinematic viscosity*, $\nu = \mu/\rho$, or *momentum diffusivity*, with units of (length)^2/time.

8-2.1 Physical Properties for Heat Transfer

Numerical solutions to simple thermal energy transport problems in the absence of radiative mechanisms require that the viscosity μ, density ρ, specific heat C_p, and thermal conductivity k are known. Fourier's law of heat conduction states that the thermal conductivity is constant and independent of position for simple isotropic fluids. Hence, thermal conductivity is the molecular transport property that appears in the linear law that expresses molecular transport of thermal energy in terms of temperature gradients. The thermal diffusivity α is constructed from the ratio of k and ρC_p. Hence, $\alpha = k/\rho C_p$ characterizes diffusion of thermal energy and has units of length^2/time.

8-2.2 Physical Properties for Mass Transfer

The binary molecular diffusion coefficient, $\mathfrak{D}_{AB}$, has units of length^2/time and characterizes the microscopic motion of species A in solvent B, for example. $\mathfrak{D}_{AB}$ is also the molecular transport property that appears in the linear law that relates diffusional fluxes and concentration gradients. In this respect, the same quantity, $\mathfrak{D}_{AB}$, represents a molecular transport property for mass transfer and a diffusion coefficient. This is not the case for the other two transport processes.

8-2.3 Transport Analogies Based on Physical Properties

It is instructive to construct the ratio of the diffusivities for thermal energy transfer and mass transfer with respect to momentum transport. In doing so, one generates dimensionless numbers that appear in correlations for heat and mass transfer coefficients. The ratio of momentum diffusivity ν to thermal diffusivity α is equivalent to the Prandtl number, $\mathrm{Pr} = \nu/\alpha = \mu C_p/k$. The Prandtl number is simply a ratio of physical properties of a fluid. However, a very large value of the Prandtl number means that diffusion of thermal energy away from a hot surface, for example, is poor relative to the corresponding diffusion of momentum. This implies that the thermal boundary layer which contains all the temperature gradients will remain close to the surface when the fluid flow problem is fully developed. Convective transport parallel to a hot surface maintains thin thermal boundary layers by sweeping away any thermal energy that diffuses too far from the surface. Fully developed laminar flow in a straight tube of circular cross section means that the momentum boundary layer (containing all of the velocity gradients) next to the surface on one side of the tube has grown large enough to intersect the boundary layer from the surface on the other side of the tube. It should be no surprise that these boundary layers will meet in the center of the tube when fully developed flow is attained, and the thickness of the momentum

boundary layer is actually the radius of the tube. Hence, a very large Prandtl number means qualitatively that under fully developed laminar flow conditions when the momentum boundary layer has filled the cross section of the tube, the thermal energy or temperature boundary layer hugs the wall. As a consequence, high rates of heat transfer are prevalent because transport normal to a surface is inversely proportional to the thickness of the boundary layer adjacent to the surface in question. This boundary layer contains all the gradients that generate molecular transport.

Analogously, the ratio of momentum diffusivity ν to mass diffusivity $\mathfrak{D}_{AB}$ is equivalent to the Schmidt number, $\mathrm{Sc} = \nu/\mathfrak{D}_{AB} = \mu/\rho\mathfrak{D}_{AB}$. It follows directly from the discussion in the preceding paragraph that for very large values of the Schmidt number, mass transfer boundary layers remain close to the adjacent surface and high rates of mass transfer are obtained. Hence, the Schmidt number is the mass transfer analog of the Prandtl number. The momentum transport analog of the Schmidt or Prandtl numbers is 1, because one constructs the ratio of momentum diffusivity to momentum diffusivity. The consequence of this statement is that if a heat transfer correlation for the Nusselt number, which contains the Prandtl number, can be applied to an analogous momentum transport problem, then the Prandtl number should be replaced by 1 to calculate the momentum transfer coefficient (i.e., $\rho\langle v\rangle_{\text{average}} f/2$, where f is the friction factor) via the dimensionless correlation for $\frac{1}{2}f\cdot\mathrm{Re}$, where Re is the Reynolds number. Of course, if a heat transfer problem is completely analogous to a posed mass transfer problem, then the Prandtl number in the dimensionless Nusselt number correlation should be replaced by the Schmidt number to calculate the mass transfer coefficient via the dimensionless correlation for the Sherwood number.

8-3 FUNDAMENTAL BALANCE IN MOMENTUM TRANSPORT

In this section, concepts are discussed that one must understand to construct force balances based on momentum transfer rate processes. The fluid, the specific problem, and the coordinate system are generic at this stage of the development. If the discussion that follows seems quite vague, then perhaps it will become more concrete when specific problems are addressed. The best approach at present is to state the force balance in words and then focus on each type of momentum transfer rate process separately.

The strategy for solving fluid dynamics problems begins by putting a control volume within the fluid that matches the symmetry of the macroscopic boundaries, and balancing the forces that act on the system. The system is defined as the fluid that is contained within the control volume V, which is completely surrounded by surface S. Since a force is synonymous with the time rate of change of momentum as prescribed by Newton's laws of motion, the terms in the force balance are best viewed as momentum rate processes. The force balance for an open system is stated without proof as $\mathbf{1 = 2 + 3 + 4 + 5}$, where

1 is the rate of accumulation of fluid momentum within V
2 represents forces acting on the system across S due to convective momentum flux, or bulk fluid flow
3 represents viscous forces acting on the system across S due to molecular momentum transport
4 represents forces acting on the system across S due to fluid pressure
5 is the sum of all external forces that act on the fluid within V

It should be emphasized that force is a vector quantity and, hence, the force balance described qualitatively above is a vector equation. A vector equation implies that three scalar equations must be satisfied. This is a consequence of the fact that if two vectors are equal, then it must be true that they have the same x-component, the same y-component, and the same z-component, for example, in rectangular coordinates.

8-3.1 Accumulation Rate Process (i.e., 1)

It is necessary to associate mathematical quantities with each type of momentum transfer rate process that is contained in the vector force balance. The fluid momentum vector is expressed as $\rho\mathbf{v}$, which is equivalent to the overall mass flux vector. This is actually the momentum per unit volume of fluid because mass is replaced by density in the vectorial representation of fluid momentum. Mass is an extrinsic property that is typically a linear function of the size of the system. In this respect, $m\mathbf{v}$ is a fluid momentum vector that changes magnitude when the mass of the system increases or decreases. This change in fluid momentum is not as important as the change that occurs when the velocity vector is affected. On the other hand, fluid density is an intrinsic property, which means that it is independent of the size of the system. Hence, $\rho\mathbf{v}$ is the momentum vector per unit volume of fluid that is not affected when the system mass increases or decreases. The total fluid momentum within an arbitrarily chosen control volume V is

$$\int_V \rho\mathbf{v}\, dV \tag{8-1}$$

The rate of accumulation of fluid momentum within V involves the use of a total time derivative to detect changes in fluid momentum during a period of observation that is consistent with the time frame over which the solution to a specific problem is required. The mathematical representation of the accumulation term **1** with units of momentum per time (hence, rate of momentum) is

$$\frac{d}{dt}\int_V \rho\mathbf{v}\, dV = \int_V \frac{\partial(\rho\mathbf{v})}{\partial t}\, dV + \int_S \rho\mathbf{v}(\mathbf{v}_{\text{surface}} \cdot \mathbf{n})\, dS \tag{8-2}$$

where $\mathbf{n}$ is an outward-directed unit normal vector on the surface S that completely surrounds the control volume V, and $\mathbf{v}_{\text{surface}}$ is the local velocity of the surface. The previous expression represents the Leibnitz formula for differentiating

TABLE 8-1 Appropriate Time Derivative for the Accumulation Rate Process in the Equation of Motion[a]

Control Volume	$\mathbf{v}_{\text{surface}}$	Time Derivative
Stationary, $V \neq f(t)$	0	Partial, $\partial(\rho\mathbf{v})/\partial t$
Moving, $V(t)$	$\mathbf{v}_{\text{surface}} \neq v_{\text{fluid}}$	Total, $d(\rho\mathbf{v})/dt$
	$\mathbf{v}_{\text{fluid}} = \mathbf{v}$	Substantial, $D(\rho\mathbf{v})/Dt$

[a]The surface that completely surrounds the system within the control volume exhibits velocity $\mathbf{v}_{\text{surface}}$.

a three-dimensional integral, and it is also known as the Reynolds transport theorem. If the control volume is stationary, or fixed in space, then the spatial coordinates of V are not functions of time and $\mathbf{v}_{\text{surface}} = 0$. Hence, the total time derivative operator can be replaced by a partial time derivative:

$$\frac{d}{dt}\int_V \rho\mathbf{v}\,dV = \int_V \frac{\partial(\rho\mathbf{v})}{\partial t}\,dV \tag{8-3}$$

It should be obvious that this term is volumetric, which means that the accumulation rate process applies to the entire system contained within the control volume. The stipulation that the control volume be stationary simplifies the mathematics to some extent, but the final form of the force balance does not depend on details pertaining to the movement of the control volume. Possibilities for this motion and the appropriate time derivatives are summarized in Table 8-1. The substantial derivative operator

$$\frac{D(\rho\mathbf{v})}{Dt} = \frac{\partial(\rho\mathbf{v})}{\partial t} + \mathbf{v}\cdot\nabla\rho\mathbf{v} \tag{8-4}$$

is required if the control volume moves with a velocity at every point on its surface that matches the local fluid velocity.

8-3.2 Normal Forces and Shear Forces Due to Momentum Flux

Terms identified by **2, 3, and 4** in the force balance are unique because they are surface related and act across the surface S that bounds fluid within the control volume V. *Surface related* is a key terms here; it indicates that flux is operative. The units of momentum flux are momentum per area per time. There are three contributions to momentum flux that have units of momentum per area per time. Since the units of momentum flux are the same as force per unit area, one of the flux mechanisms is pressure. Recall that pressure is a scalar quantity, which means that there is no directional nature to fluid pressure. In other words, fluid pressure acts similarly in all coordinate directions. However, pressure forces are operative in a fluid, and they act perpendicular to any surface that contacts the fluid. These forces act along the direction of the unit normal vector

that characterizes the orientation of the surface, and for this reason, pressure forces are classified as normal forces. In general, a normal force is one that acts perpendicular to the surface across which the force is transmitted. Choose any well-defined simple surface in one of the coordinate systems mentioned above (rectangular, cylindrical, or spherical) and identify two orthogonal coordinate directions within the surface and one coordinate that is normal to the surface. Consider the walls, floor, or ceiling of a room in rectangular coordinates, for example. An alternative viewpoint is the following. As one moves on a simple surface, two coordinates change and one remains fixed. This simple surface is typically defined as one with a constant value of the coordinate that remains fixed in the surface. The coordinate that remains fixed is also in the direction of the unit normal vector. In summary, forces due to momentum flux act across surfaces and can be classified as normal forces or shear forces. Normal forces act perpendicular to a surface along the unit normal vector. Shear forces act parallel to the surface along one of the two coordinate directions that define the surface. Hence, momentum flux initially identifies a simple surface with a unit normal vector that is coincident with one of the unit vectors of an orthogonal coordinate system. Then momentum flux identifies a vector force per unit area that acts across this surface, and this vector force has three scalar components. One of these scalar force components acts colinear with the unit normal vector to the surface, and this force is designated as a normal force. The other two scalar force components act along coordinate directions within the surface itself, and these forces are called *shear forces* because the surface area across which the force acts is parallel to the direction of the force.

Forces Due to Bulk Fluid Flow (i.e., 2). Bulk fluid flow contributes significantly to momentum flux. This convective mechanism is designated $\rho\mathbf{vv}$. The mathematical form of convective momentum flux is understood best by initially constructing the total mass flux vector for a pure or multicomponent fluid and then generating the product of mass flux with momentum per unit mass. Mass flux is a vector quantity that has units of mass per area per time, and $\rho\mathbf{v}$ is the mathematical representation of the total mass flux vector. Of course, $\rho\mathbf{v}$ also represents the momentum vector per unit volume of fluid as introduced above for the accumulation rate process. The total mass flux vector represents an important contribution to the balance on overall fluid mass. If one accepts $\rho\mathbf{v}$ as the vector representation of convective flux of overall fluid mass, it is possible to construct the product of $\rho\mathbf{v}$ with the momentum vector per unit mass of fluid, the latter of which is analogous to the velocity vector $\mathbf{v}$. This product of $\rho\mathbf{v}$ and $\mathbf{v}$ is not the scalar ("dot") product or the vector ("cross") product from vector calculus. Convective momentum flux is a quantity that generates nine scalars. This should be obvious if one chooses the rectangular coordinate system for illustration and multiplies the three scalar components of the mass flux vector $(\rho v_x, \rho v_y, \rho v_z)$ by the three scalar components of the velocity vector (v_x, v_y, v_z). Using rigorous mathematical terminology, convective momentum flux $\rho\mathbf{vv}$ is a second-rank tensor that associates a vector with each coordinate direction. Since there are three orthogonal coordinate directions identified by the unit vectors of

a coordinate system, $\rho\mathbf{vv}$ identifies a vector with each of the three coordinate directions. Recall that a vector associates a scalar with each coordinate direction. Hence, there are nine scalars that one can generate from three distinct vectors, and these nine scalars constitute the state of a second-rank tensor such as convective momentum flux. It is instructive to write all nine scalars of $\rho\mathbf{vv}$ and comment about the subscripts on the scalar velocity components. Eight of the nine scalars of $\rho\mathbf{vv}$ are identically zero for a simple one-dimensional flow problem when the velocity vector is given by

$$\mathbf{v} = \delta_x v_x + \delta_y(0) + \delta_z(0) \tag{8-5}$$

If fluid motion is restricted to the x direction in rectangular coordinates as illustrated above, then the only nonvanishing scalar of convective momentum flux is $\rho v_x v_x$, which has units of momentum per time per area or force per unit area. Hence, $\rho\mathbf{vv}$ contains forces per unit area that are transmitted across the surfaces that bound fluid within the control volume, and terms of this nature due to convection motion of a fluid must be included in the force balance. One must construct the product of each of the nine scalars generated from this second-rank tensor with the surface area across which the force (or stress) is transmitted. Information about these surfaces and the coordinate direction in which the force acts is contained in the subscripts of the velocity components. For the most general type of fluid flow in rectangular coordinates, the nine scalars that one can generate from convective momentum flux are

$$\begin{array}{lll} \rho v_x v_x & \rho v_x v_y & \rho v_x v_z \\ \rho v_y v_x & \rho v_y v_y & \rho v_y v_z \\ \rho v_z v_x & \rho v_z v_y & \rho v_z v_z \end{array} \tag{8-6}$$

It should be obvious that these nine scalars for convective momentum flux fit nicely in a 3×3 matrix. All second-rank tensors generate nine scalars, and it is acceptable to represent the tensor by the matrix of scalars. If the matrix is symmetric, then the tensor is classified as a symmetric tensor. This is true for convective momentum flux because the product of two velocity components $v_i v_j$ does not change if the second component is written first. Another positive test for symmetry is obtained by interchanging the rows and columns of the 3×3 matrix to generate a second matrix that is indistinguishable from the original matrix. Notice that the matrix components on the main diagonal from upper left to lower right have the same two subscripts and can be written in general as $\rho(v_i)^2$. These forces satisfy the requirement for normal forces. Each acts in the ith coordinate direction (where $i = x$, y, or z) and the unit normal vector to the surface across which the force is transmitted is also in the ith direction. In summary, when momentum flux is expressed in matrix form, the main-diagonal entries represent forces per unit area that act along the direction of the normal vector to the surface across which the force is transmitted. The off-diagonal

elements represent shearing forces because these forces act in one of the two coordinate directions that define the surface across which the force is transmitted.

As an illustrative example, focus on the element in the first row and second column, $\rho v_x v_y$, for the matrix representation of the convective momentum flux tensor. The subscript x on the first velocity component indicates that $\rho v_x v_y$ is a force per unit area acting across a simple surface oriented with a unit normal vector in the $\pm x$ direction. The subscript y on the second velocity component reveals that this force acts in the y direction. If we perform this analysis for all nine components in the matrix (8-6) the three entries in the first row represent x, y, and z components, respectively, of the vector force per unit area that is transmitted across the simple surface defined by a constant value of the x coordinate, which means that the unit normal vector to the surface is colinear with the x direction. In vector-tensor notation, this is

$$\mathbf{n} \cdot \rho \mathbf{v}\mathbf{v} = \rho v_x \mathbf{v} \qquad \mathbf{n} = \delta_x \tag{8-7}$$

Similarly, the three entries in the second row of the matrix (8-6) represent x, y, and z components, respectively, of the vector force per unit area that is transmitted across the simple surface defined by a constant value of the y coordinate, which means that the unit normal vector to the surface is colinear with the y direction. This information can be condensed into vector-tensor notation as

$$\mathbf{n} \cdot \rho \mathbf{v}\mathbf{v} = \rho v_y \mathbf{v} \qquad \mathbf{n} = \delta_y \tag{8-8}$$

Finally, the three entries in the third row of the matrix (8-6) represent x, y, and z components, respectively, of the vector force per unit area that is transmitted across the simple surface defined by a constant value of the z coordinate, which means that the unit normal vector to the surface is colinear with the z direction. This information is equivalent to

$$\mathbf{n} \cdot \rho \mathbf{v}\mathbf{v} = \rho v_z \mathbf{v} \qquad \mathbf{n} = \delta_z \tag{8-9}$$

These vector forces per unit area are obtained by taking the dot product of a unit normal vector with the second-rank tensor due to convective momentum flux. Each force is transmitted across the surface in the direction of $\mathbf{n}$. If $\mathbf{n}$ represents an outward-directed unit normal vector on each differential element of surface dS that surrounds fluid within the control volume, then the vector force acting on the system due to convective momentum flux is

$$\int_S (-\mathbf{n} \cdot \rho \mathbf{v}\mathbf{v})\, dS \tag{8-10}$$

because it is desired to express the force transmitted in the direction of $-\mathbf{n}$.

Forces Due to Viscous Momentum Flux (i.e., 3). A molecular momentum flux mechanism exists which relates viscous stress to linear combinations of velocity gradients via Newton's law of viscosity if the fluid is Newtonian. Viscous

momentum flux τ is also a second-rank tensor that identifies a vector with each coordinate direction. In any orthogonal coordinate system,

$$\tau = \sum_i \delta_i \tau_i \tag{8-11}$$

where τ_i is a vector viscous force per unit area that acts across a simple surface with unit normal vector in the ith coordinate direction. Since τ_i is a vector, it can be expanded in summation notation such that τ_{ij} represents the jth scalar component of this vector. Hence,

$$\tau_i = \sum_j \delta_j \tau_{ij} \tag{8-12}$$

Expressions (8-11) and (8-12) can be combined to illustrate how a second-rank tensor such as τ, associates a scalar with each ordered pair of coordinate directions, $\delta_i \delta_j$:

$$\tau = \sum_{ij} \delta_i \delta_j \tau_{ij} \tag{8-13}$$

where τ_{ij} is the jth scalar component of a vector viscous force per unit area that acts across a simple surface with unit normal vector in the ith coordinate direction. Hence, nine scalars (i.e., τ_{ij}) are required to describe the complete state of viscous stress in a fluid. These forces, or stresses, that arise from τ are not due to inertia or bulk fluid motion like those that are generated from $\rho\mathbf{vv}$, but they are viewed best as frictional forces that arise when fluid parcels on adjacent streamlines slide past one another because they are moving at different relative speeds. A simple analogy of the shearing forces generated by viscous momentum flux is the action that one performs with a piece of sandpaper to make a wood surface smooth. The wood surface is analogous to the wall of a tube, for example, and the motion of the sandpaper is representative of the fluid layers that are adjacent to the wall. The surface forces under consideration definitely meet the requirements of shearing forces because the surface is oriented parallel to the direction of fluid motion, the latter of which coincides with the direction of the force. In polymer processing operations, if the fluid viscosity is large enough and the flow is fast enough, then thermal energy will be generated by frictional shear at the interface between the fluid and the wall. This is analogous to the fact that a wood surface is slightly warmer after it is sanded, and the surface temperature is higher when the sanding is performed more vigorously. As illustrated in (8-14), the matrix representation of viscous momentum flux τ is generated by assigning two subscripts to the letter τ to facilitate the row and column for each entry. Unlike the convective momentum flux tensor in (8-6) where a single subscript was assigned to each velocity component in the product $\rho\mathbf{vv}$, now it is necessary to put both subscripts on τ. One should analyze both subscripts on τ in the same manner that $\rho v_i v_j$ was analyzed above.

In rectangular coordinates, the matrix representation for viscous momentum flux is written as

$$\begin{matrix} \tau_{xx} & \tau_{xy} & \tau_{xz} \\ \tau_{yx} & \tau_{yy} & \tau_{yz} \\ \tau_{zx} & \tau_{zy} & \tau_{zz} \end{matrix} \tag{8-14}$$

with $\tau_{ij} = \tau_{ji}$. The interpretation of these nine scalars follows directly from the discussion of the nine scalars that are generated by $\rho\mathbf{vv}$. The only difference is that the forces result from a molecular mechanism that is analogous to heat conduction and mass diffusion rather than bulk fluid motion. For example, the second-row of scalars in (8-14) represents x, y, and z components, respectively, of the vector viscous force per unit area that is transmitted across the simple surface defined by a constant value of y, which means that the unit normal vector to the surface is colinear with the y direction. In vector-tensor notation, this is equivalent to

$$\mathbf{n} \cdot \tau = \mathbf{n} \cdot \sum_i \sum_j \delta_i \delta_j \tau_{ij} = \sum_j \delta_j \tau_{yj} \equiv \tau_y \qquad \mathbf{n} = \delta_y \tag{8-15}$$

In other words, $\mathbf{n} \cdot \tau$ represents a vector viscous force per unit area that acts across a surface with unit normal vector $\mathbf{n}$, and the force is transmitted in the direction of $\mathbf{n}$. Hence, if $\mathbf{n}$ is the outward-directed unit normal vector that emanates from each differential element of surface dS that surrounds fluid within V, then the vector viscous force acting on the system (i.e., transmitted in the direction of $-\mathbf{n}$) is

$$\int_S (-\mathbf{n} \cdot \tau)\, dS \tag{8-16}$$

Normal Forces Due to Pressure Stress (i.e., 4). Using the formalism described in the preceding two sections, it is also possible to represent the pressure contribution to momentum flux in matrix notation. However in this case, all the entries have the same magnitude (i.e., p) and they lie on the main diagonal from upper left to lower right. There are no off-diagonal components because fluid pressure generates surface forces that act in the direction of the unit normal vector to the surface across which the force or stress is transmitted — they are all normal forces. In each coordinate system, the matrix representation of the pressure contribution to momentum flux can be written in the following form:

$$\begin{matrix} p & 0 & 0 \\ 0 & p & 0 \\ 0 & 0 & p \end{matrix} \tag{8-17}$$

In vector-tensor notation, pressure stress is written as a second-rank tensor as

$$p \sum_i \sum_j \delta_i \delta_j \delta_{ij} = p \sum_i \delta_i \delta_i \tag{8-18}$$

where $\delta_i \delta_j$ is an ordered pair of unit vectors, better known as a *unit dyad* or the *dyadic product* of δ_i and δ_j, and δ_{ij} is the Kronecker delta, which has a value of unity when $i = j$ and zero when $i \neq j$. Pressure forces that act on the system across surface S with outward-directed unit normal vector $\mathbf{n}$ are expressed in vector-tensor notation as

$$\int_S \left(-\mathbf{n} \cdot p \sum_i \sum_j \delta_i \delta_j \delta_{ij} \right) dS = \int_S \left(-\mathbf{n} \cdot p \sum_i \delta_i \delta_i \right) dS = \int_S (-\mathbf{n} p)\, dS \tag{8-19}$$

The vector-tensor algebra in (8-19) is analogous to multiplying a 1×3 row matrix for $\mathbf{n}$ by a 3×3 identity matrix for the unit tensor, defined by $\sum_i \delta_i \delta_i$. If multiplication is allowed, then the product of any matrix with the identity matrix yields the original matrix.

Summary of Forces Due to Total Momentum Flux (i.e., 2, 3, and 4). In the preceding three sections, a total of 21 scalar quantities has been identified; nine from $\rho \mathbf{vv}$, nine from τ, and three from the pressure contribution to momentum flux. They represent all the possible surface force components that can be generated from the total momentum flux tensor. When each of these scalars is multiplied by the surface area across which the stress acts, a quantity with units of momentum per time is obtained. If $\mathbf{n}$ represents the outward-directed unit normal vector at every point on surface S that encloses the system within an arbitrary control volume V, then the total force acting on the system across S (i.e., in the direction of $-\mathbf{n}$) due to total momentum flux is given by

$$\int_S \left[-\mathbf{n} \cdot \left(\rho \mathbf{vv} + \tau + p \sum_i \delta_i \delta_i \right) \right] dS = \int_S [-\mathbf{n} \cdot (\rho \mathbf{vv} + \tau) - \mathbf{n} p]\, dS \tag{8-20}$$

The 21 scalar surface forces due to total momentum flux are distributed equally among the three scalar balances that constitute the total vector force balance.

8-3.3 Momentum Rate Processes Due to External Body Forces (i.e., 5)

All terms in the momentum balance have units of momentum per unit time, which is synonymous with the units of force. In this respect, it is necessary to account for external forces (i.e., sources) that act on the fluid within the control volume. In general, these forces are not surface related. They are called *body forces* because they act volumetrically like the accumulation rate process, which means that each fluid parcel within the system is affected by a body force. The

primary body force of interest is gravity. The external vector force due to gravity is written intrinsically via the fluid density in the following manner;

$$\int_V \rho \mathbf{g}\, dV \tag{8-21}$$

where **g** is the gravitational acceleration vector. The fluid density is employed instead of the total fluid mass within the system to ensure that the gravitational force does not have to be modified if the mass or size of the system changes. It is true that the size of the control volume V could change in response to an increase or decrease in system mass at constant density. However, one of the last steps in the development of all microscopic balances is division by the control volume, which generates a completely intrinsic equation that is independent of system size or mass.

8-3.4 Other External Forces

There are other types of external body forces in addition to gravity that should be included in a compete study of fluid dynamics. For example, fluid particles that have permanent electric dipoles will experience body forces in the presence of an electric field, and particles with magnetic moments experience forces and torques due to magnetic fields. These forces are important and must be considered in a study of ferrohydrodynamics and magnetohydrodynamics. Unlike gravity forces, electric and magnetic fields exert forces that are particle specific. Unfortunately, fluid flow in the presence of electric and magnetic fields is rarely covered in undergraduate and graduate courses because the complexity of the problems increases several fold, limiting discussion to the simplest examples for which exact solutions require the use of advanced mathematical techniques. Even though surface tension forces cannot be classified as body forces (i.e., they should be accounted for in the boundary conditions), they play an important role in the operation of viscosity-measuring devices such as parallel-plate and cone-and-plate viscometers, where a thin film of fluid is placed between two closely spaced horizontal surfaces. The lower surface is stationary and the upper one rotates at constant angular velocity. In the absence of surface tension, the test fluid would spread and completely wet the solid surfaces, in response to rotation which generates centrifugal forces. Then the fluid would "fall off the table" since there are no restraining walls. Of course, surface tension plays the role of restraining walls and keeps the fluid from exiting the viscometer if the rotational speeds are slow enough.

8-4 EQUATION OF MOTION

8-4.1 Generalized Vector-Tensor Derivation of the Equation of Motion

A stationary control volume V is chosen arbitrarily within the fluid medium and one applies the force balance described above, where **n** is the outward-directed

unit normal vector on the surface S which completely surrounds the fluid in V. In simple terms, the force balance states that the time rate of change of fluid momentum must be balanced by all surface-related and body forces acting on the system. Hence, Newton's law for fluid dynamics is written as follows;

$$\begin{aligned}
&\text{rate of accumulation of fluid momentum in } V && \frac{d}{dt}\int_V \rho\mathbf{v}\,dV \\
&= \text{convective forces acting on fluid in } V && \int_S (-\mathbf{n}\cdot\rho\mathbf{v}\mathbf{v})\,dS \\
&+ \text{viscous forces acting on fluid in } V && \int_S (-\mathbf{n}\cdot\tau)\,dS \\
&+ \text{pressure forces acting on fluid in } V && \int_S (-\mathbf{n}p)\,dS \\
&+ \text{external body forces acting on fluid in } V && \int_V \rho\mathbf{g}\,dV
\end{aligned}$$

The total time derivative in the accumulation rate process can be replaced by the partial time derivative because the control volume is stationary and $\mathbf{v}_{\text{surface}} = 0$. Furthermore, it is acceptable to reverse the order of integration with respect to V and partial differentiation with respect to time because the coordinates of V are not functions of time. Gauss's law transforms surface integrals to volume integrals as follows:

$$\begin{aligned}
&\text{Convective forces acting on fluid in } V: && \int_S (-\mathbf{n}\cdot\rho\mathbf{v}\mathbf{v})\,dS = \int_V (-\nabla\cdot\rho\mathbf{v}\mathbf{v})\,dV \\
&\text{Viscous forces acting on fluid in } V: && \int_S (-\mathbf{n}\cdot\tau)\,dS = \int_V (-\nabla\cdot\tau)\,dV \\
&\text{Pressure forces acting on fluid in } V: && \int_S (-\mathbf{n}p)\,dS = \int_V (-\nabla p)\,dV
\end{aligned}$$

Now, all five terms in the vector force balance can be written volumetrically and combined into one volume integral:

$$\int_V \left[\frac{\partial(\rho\mathbf{v})}{\partial t} + \nabla\cdot\rho\mathbf{v}\mathbf{v} + \nabla\cdot\tau + \nabla p - \rho\mathbf{g}\right] dV = 0 \tag{8-22}$$

If one chooses a different control volume within the fluid medium and performs a force balance, the same integral expression is obtained because the original control volume was chosen arbitrarily. However, different limits of integration are needed. There is only one way that (8-22) can be satisfied with several different choices for the integration limits — the integrand must vanish. Hence, the microscopic force balance at the continuum level is

$$\frac{\partial(\rho\mathbf{v})}{\partial t} = -\nabla\cdot\rho\mathbf{v}\mathbf{v} - \nabla\cdot\tau - \nabla p + \rho\mathbf{g} \tag{8-23}$$

In fluid dynamics this is known as the *equation of motion* and applies to all types of fluids in motion or at rest. The only restriction is that gravity represents the external force field for hydrodynamics or hydrostatics. The hydrostatic equation (i.e., $\nabla p = \rho \mathbf{g}$) is obtained by ignoring all terms that contain $\mathbf{v}$ and τ. Each term has units of force per unit volume.

8-4.2 Vector-Tensor Manipulation of the Accumulation Rate Process and Forces Due to Convective Momentum Flux

The product rule of partial differentiation allows one to expand the accumulation term on the left side of the equation of motion:

$$\frac{\partial(\rho \mathbf{v})}{\partial t} = \rho \frac{\partial \mathbf{v}}{\partial t} + \mathbf{v} \frac{\partial \rho}{\partial t} \tag{8-24}$$

Next, a vector-tensor identity is employed to expand the convective momentum flux term in (8-23)

$$\nabla \cdot \rho \mathbf{v}\mathbf{v} = \rho \mathbf{v} \cdot \nabla \mathbf{v} + \mathbf{v} \nabla \cdot \rho \mathbf{v} \tag{8-25}$$

This identity is verified by employing summation notation for $\mathbf{v}$ and the del operator ∇ in rectangular coordinates, because unit vectors δ_x, δ_y, and δ_z are not functions of position. This strategy applies to all vector-tensor identities because all unit vectors in rectangular coordinates can be moved to the left of the derivative operators:

$$\mathbf{v} = \sum_j \delta_j v_j \tag{8-26a}$$

$$\nabla = \sum_i \delta_i \frac{\partial}{\partial x_i} \tag{8-26b}$$

where

$$\delta_1 = \delta_x \qquad \delta_2 = \delta_y \qquad \delta_3 = \delta_z$$
$$x_1 = x \qquad x_2 = y \qquad x_3 = z$$

1. Express $\nabla \cdot \rho \mathbf{v}\mathbf{v}$ in summation notation:

$$\nabla \cdot \rho \mathbf{v}\mathbf{v} = \sum_i \delta_i \frac{\partial}{\partial x_i} \cdot \rho \sum_j \delta_j v_j \sum_k \delta_k v_k \tag{8-27}$$

2. Maintain the order of all unit vectors with respect to the $\cdot$ and move them to the far left side of the summations. Also, maintain the order of all scalars with respect to spatial derivative operators:

$$\nabla \cdot \rho \mathbf{v}\mathbf{v} = \sum_{i,j,k} (\delta_i \cdot \delta_j) \delta_k \frac{\partial}{\partial x_i} \rho v_j v_k \tag{8-28}$$

3. The dot operation contracts two unit vectors that are closest to the $\cdot$. Furthermore,

$$\delta_i \cdot \delta_j = \delta_{ij} \qquad \text{(Kronecker delta)} \tag{8-29}$$

There are 27 terms in the sum, but each term vanishes unless $i = j$. Whenever a Kronecker delta is present and summation occurs over both indicies, equate both indicies and remove the summation over one of the indicies. Hence,

$$\nabla \cdot \rho \mathbf{v}\mathbf{v} = \sum_{i,k} \delta_k \frac{\partial}{\partial x_i} \rho v_i v_k \tag{8-30}$$

4. Apply the product rule of differentiation to the scalars:

$$\nabla \cdot \rho \mathbf{v}\mathbf{v} = \sum_k \delta_k \left[\sum_i \left(\rho v_i \frac{\partial}{\partial x_i} v_k + v_k \frac{\partial}{\partial x_i} \rho v_i \right) \right] \tag{8-31}$$

5. Add the tensorial rank of each cofactor and subtract 2 for the dot operation. Scalars are zeroth-rank tensors and vectors are first-rank tensors. Since the del operator is a vector and convective momentum flux is a second-rank tensor, $\nabla \cdot \rho \mathbf{v}\mathbf{v}$ is a vector. The kth component of $\nabla \cdot \rho \mathbf{v}\mathbf{v}$ is

$$(\nabla \cdot \rho \mathbf{v}\mathbf{v})_k = \sum_i \left(\rho v_i \frac{\partial}{\partial x_i} v_k + v_k \frac{\partial}{\partial x_i} \rho v_i \right) \tag{8-32}$$

6. If a summation is performed over the components of two adjacent vectors or tensors, then the $\cdot$ should be placed between these two quantities. In other words,

$$(\rho \mathbf{v} \cdot \nabla \mathbf{v})_k = \sum_i \rho v_i \frac{\partial}{\partial x_i} v_k \tag{8-33a}$$

$$(\mathbf{v} \nabla \cdot \rho \mathbf{v})_k = \sum_i v_k \frac{\partial}{\partial x_i} \rho v_i \tag{8-33b}$$

Even though this vector-tensor identity was verified using summation notation in rectangular coordinates, it is valid in any coordinate system. It is extremely tedious to verify vector-tensor identities that involve the del operator in curvilinear coordinate systems because the unit vectors exhibit spatial dependence. Now it is possible to combine terms in the equation of motion due to the accumulation rate process and convective momentum flux. Equations (8-24) and (8-25) yield:

$$\begin{aligned} \frac{\partial(\rho \mathbf{v})}{\partial t} + \nabla \cdot \rho \mathbf{v}\mathbf{v} &= \rho \frac{\partial \mathbf{v}}{\partial t} + \mathbf{v} \frac{\partial \rho}{\partial t} + \rho \mathbf{v} \cdot \nabla \mathbf{v} + \mathbf{v} \nabla \cdot \rho \mathbf{v} \\ &= \rho \left(\frac{\partial \mathbf{v}}{\partial t} + \mathbf{v} \cdot \nabla \mathbf{v} \right) + \mathbf{v} \left(\frac{\partial \rho}{\partial t} + \nabla \cdot \rho \mathbf{v} \right) \end{aligned} \tag{8-34}$$

where the terms in the second set of parentheses on the right-hand side of (8-34) cancel via the microscopic form of the overall mass balance for pure or multicomponent fluids (see Problem 8-1). If there are no sources or sinks of overall fluid mass, then this generalized form of the equation of continuity,

$$\frac{\partial \rho}{\partial t} + \nabla \cdot \rho \mathbf{v} = 0 \tag{8-35}$$

is employed to simplify the equation of motion without introducing any additional assumptions. Hence, equation (8-23) reduces to:

$$\rho \left(\frac{\partial \mathbf{v}}{\partial t} + \mathbf{v} \cdot \nabla \mathbf{v} \right) \equiv \rho \frac{D\mathbf{v}}{Dt} = -\nabla \cdot \tau - \nabla p + \rho \mathbf{g} \tag{8-36}$$

where the terms in parentheses correspond to the substantial derivative of $\mathbf{v}$. Equation (8-36) states that the time rate of change of fluid momentum within a control volume that moves at the local fluid velocity is balanced by the sum of viscous, pressure, and gravitational forces that act on the system. This form of the equation of motion applies to all types of fluids (i.e., gases and liquids) in which there are no sources or sinks of overall fluid mass, and gravity represents the only external force. Density ρ is not necessarily constant in (8-36).

8-4.3 Generalized Equation of Motion for Incompressible Liquids

Pressure and gravity forces are combined for liquids with constant density via the introduction of dynamic pressure. This is accomplished by defining a time-independent gravitational potential energy per unit mass of fluid with respect to an arbitrarily chosen horizontal reference plane, $\Phi \equiv gh$, where h is a spatial variable that increases as one moves vertically upward (i.e., opposite to gravity). The gravitational acceleration vector $\mathbf{g}$ is obtained from the gradient of Φ as follows:

$$\mathbf{g} = \delta_h \left(-\frac{\partial \Phi}{\partial h} \right) = -\nabla \Phi \tag{8-37}$$

where the unit vector δ_h is oriented vertically upward. When ρ is approximately constant, pressure and gravity forces in (8-36) are manipulated as follows:

$$-\nabla p + \rho \mathbf{g} = -\nabla p - \rho \nabla \Phi = -\nabla p - \nabla \rho \Phi = -\nabla (p + \rho \Phi) = -\nabla \mathfrak{P} \tag{8-38}$$

where $\mathfrak{P} = p + \rho \Phi$ is defined as dynamic pressure or a combination of gravitational potential energy per unit volume and actual fluid pressure. The generalized equation of motion for incompressible fluids is

$$\rho \left(\frac{\partial \mathbf{v}}{\partial t} + \mathbf{v} \cdot \nabla \mathbf{v} \right) \equiv \rho \frac{D\mathbf{v}}{Dt} = -\nabla \cdot \tau - \nabla \mathfrak{P} \tag{8-39}$$

This is a more generalized form of the Navier–Stokes equation that was derived in 1822 for incompressible Newtonian fluids. Under hydrostatic conditions, $\nabla \mathfrak{P} = 0$ and $\mathfrak{P} =$ constant. This is consistent with the fact that $p = p_{\text{reference}} + \rho g(h_{\text{reference}} - h)$, and the actual pressure increases as one moves downward in a static fluid.

8-4.4 Dimensional Analysis of the Equation of Motion

Dimensional scaling factors for each momentum transfer rate process are generated with the aid of average fluid properties such as density ρ and viscosity μ, and characteristic quantities such as average fluid velocity V and length scale L. The characteristic length L can be the tube diameter, diameter of a sphere or gas bubble, thickness of a falling film, length of a flat plate, and so on. Dimensionless variables with an asterisk are constructed as follows:

Spatial coordinates: $$x^* = \frac{x}{L}, \quad y^* = \frac{y}{L}, \quad z^* = \frac{z}{L}$$

Gradient operator: $$\nabla^* = L\nabla$$

Time variable: $$t^* = \frac{t}{L/V}$$

Fluid velocity: $$\mathbf{v}^* = \frac{\mathbf{v}}{V}$$

Viscous stress: $$\tau^* = \frac{\tau}{\mu V/L}$$

Dynamic pressure: $$\mathfrak{P}^* = \frac{\mathfrak{P}}{\mu V/L}$$

ρV^2 represents another possibility to make dynamic pressure dimensionless, but $\mu V/L$ is preferred for very slow flow where terms that are proportional to V^2 are neglected. Each momentum transfer rate process in the equation of motion is written in terms of dimensionless variables and a dimensional scaling factor that contains the appropriate dimensions. For example,

Accumulation rate process: $$\rho\frac{\partial \mathbf{v}}{\partial t} = \frac{\rho V^2}{L}\frac{\partial \mathbf{v}^*}{\partial t^*}$$

Forces due to convective momentum flux: $$\rho\mathbf{v}\cdot\nabla\mathbf{v} = \frac{\rho V^2}{L}\mathbf{v}^*\cdot\nabla^*\mathbf{v}^*$$

Forces due to viscous momentum flux: $$\nabla\cdot\tau = \frac{\mu V}{L^2}\nabla^*\cdot\tau^*$$

Pressure and gravity forces: $$\nabla\mathfrak{P} = \frac{\mu V}{L^2}\nabla^*\mathfrak{P}^*$$

The equation of motion for a generalized incompressible fluid (8-39) is written in terms of dimensionless variables and dimensional scaling factors:

$$\frac{\rho V^2}{L}\left(\frac{\partial \mathbf{v}^*}{\partial t^*} + \mathbf{v}^* \cdot \nabla^* \mathbf{v}^*\right) = -\frac{\mu V}{L^2}(\nabla^* \cdot \tau^* + \nabla^* \mathfrak{P}^*) \tag{8-40}$$

Notice that the accumulation rate process and convective forces scale as $\rho V^2/L$, whereas viscous, pressure, and gravity forces scale as $\mu V/L^2$. If one takes the ratio of these two dimensional scaling factors, an important dimensionless number is obtained:

$$\frac{\rho V^2/L}{\mu V/L^2} = \frac{\rho V L}{\mu} \equiv \mathrm{Re} \tag{8-41}$$

The Reynolds number (i.e., Re) represents an order-of-magnitude ratio of convective forces to viscous forces, and it appears as the most important dimensionless number on the left-hand side of the dimensionless equation of motion:

$$\mathrm{Re}\left(\frac{\partial \mathbf{v}^*}{\partial t^*} + \mathbf{v}^* \cdot \nabla^* \mathbf{v}^*\right) = -\nabla^* \cdot \tau^* - \nabla^* \mathfrak{P}^* \tag{8-42}$$

If pressure and gravitational forces were not combined via the definition of dynamic pressure, then an additional dimensionless number appears explicitly in the equation of motion. In other words, the ratio of the Reynolds number to the Froude number (i.e., Re/Fr) is required as the coefficient of the gravitational force term in equation (8-36), where $\mathrm{Fr} = V^2/gL$ provides an order-of-magnitude estimate of the ratio of convective forces to gravitational forces. The ratio Re/Fr represents an order-of-magnitude estimate of the ratio of gravitational forces to viscous forces.

8-5 EXACT DIFFERENTIALS

Consider the following differential expression:

$$M\,dx + N\,dy + T\,dz \tag{8-43}$$

where the functions M, N, and T depend on x, y, and z. If (8-43) is an exact differential, then a function $\Phi(x, y, z)$ exists such that

$$M = \left(\frac{\partial \Phi}{\partial x}\right)_{y,z} \qquad N = \left(\frac{\partial \Phi}{\partial y}\right)_{x,z} \qquad T = \left(\frac{\partial \Phi}{\partial z}\right)_{x,y} \tag{8-44}$$

The total differential of the scalar function Φ is

$$d\Phi = \nabla \Phi \cdot d\mathbf{r} = M\,dx + N\,dy + T\,dz \tag{8-45}$$

where $\mathbf{r}$ is the position vector in rectangular coordinates and

$$d\mathbf{r} = \delta_x\, dx + \delta_y\, dy + \delta_z\, dz \tag{8-46}$$

The line integral around an arbitrarily chosen closed path C that surrounds a region R in space,

$$\oint_{\text{closed path } C} d\Phi$$

vanishes because Φ is an exact differential. In other words, changes in Φ depend on the end points along the integration path, not on the actual path that is traversed. Since the initial and final points are identical for a closed path, the line integral of an exact differential is zero. Useful information is obtained by applying Stokes's theorem to line integrals of exact differential functions around closed paths (see Wylie, 1975, pp. 683–684):

$$\begin{aligned}\oint_{\text{closed path } C} d\Phi &= \oint_{\text{closed path } C} \nabla\Phi \cdot d\mathbf{r} \\ &= \iint_{\text{region } R \text{ enclosed by path } C} (\mathbf{n} \cdot \nabla \times \nabla\Phi)\, dS = 0\end{aligned} \tag{8-47}$$

where $\mathbf{n}$ is an outward-directed unit normal vector that emanates from surface S in region R, which is surrounded by closed path C. There are many closed paths in region R, for which the line integral and the corresponding surface integral vanish. This is possible only if (1) Φ is an exact differential and (2) $\mathbf{n} \cdot \nabla \times \nabla\Phi = 0$. Furthermore, $\mathbf{n}$ is specific for each closed path C that surrounds surface S, and condition (2) applies for each choice of $\mathbf{n}$. This suggests that $\nabla \times \nabla\Phi = 0$. Now, the gradient of Φ in rectangular coordinates is

$$\nabla\Phi = \delta_x \frac{\partial\Phi}{\partial x} + \delta_y \frac{\partial\Phi}{\partial y} + \delta_z \frac{\partial\Phi}{\partial z} = \delta_x M + \delta_y N + \delta_z T \tag{8-48}$$

and the curl of the gradient of Φ is

$$\nabla \times \nabla\Phi = \delta_x \left(\frac{\partial}{\partial y}T - \frac{\partial}{\partial z}N\right) + \delta_y \left(\frac{\partial}{\partial z}M - \frac{\partial}{\partial x}T\right) + \delta_z \left(\frac{\partial}{\partial x}N - \frac{\partial}{\partial y}M\right) \tag{8-49}$$

The fact that (8-49) vanishes via Stokes's theorem implies the following three scalar equations:

$$\begin{aligned}\frac{\partial}{\partial y}T - \frac{\partial}{\partial z}N = 0 &\Longrightarrow \frac{\partial}{\partial y}\left(\frac{\partial\Phi}{\partial z}\right) = \frac{\partial}{\partial z}\left(\frac{\partial\Phi}{\partial y}\right) \\ \frac{\partial}{\partial z}M - \frac{\partial}{\partial x}T = 0 &\Longrightarrow \frac{\partial}{\partial z}\left(\frac{\partial\Phi}{\partial x}\right) = \frac{\partial}{\partial x}\left(\frac{\partial\Phi}{\partial z}\right) \\ \frac{\partial}{\partial x}N - \frac{\partial}{\partial y}M = 0 &\Longrightarrow \frac{\partial}{\partial x}\left(\frac{\partial\Phi}{\partial y}\right) = \frac{\partial}{\partial y}\left(\frac{\partial\Phi}{\partial x}\right)\end{aligned} \tag{8-50}$$

Hence, it is acceptable to reverse the order of mixed second partial differentiation of an exact differential without affecting the final result.

8-6 LOW-REYNOLDS-NUMBER HYDRODYNAMICS

In the next 30 pages, we focus on fluid dynamics at vanishingly small Reynolds numbers. This is the *creeping flow regime*, where all terms in the equation of motion that scale as V^2 are neglected at very slow flow rates. In other words, viscous, pressure, and gravity forces are much more important than convective forces, and the entire left side of the equation of motion is neglected. The creeping flow force balance in dimensional form for all fluids is

$$\nabla \cdot \tau + \nabla \mathfrak{P} = 0 \tag{8-51}$$

which reveals that viscous forces are balanced by pressure and gravity forces.

8-6.1 Newton's Law of Viscosity

The generalized form of Newton's law relates τ to linear combinations of velocity gradients with the following restrictions:

1. τ is a symmetric second-rank tensor.
2. Viscous forces should vanish for fluids (a) at rest, (b) in a state of pure translation (i.e., all v_i are constant), and (c) in a state of pure rotation (see Landau and Lifshitz, 1959, p. 48).

To satisfy these conditions, the following linear transport law was constructed for isotropic fluids, where the viscosity μ is a scalar instead of a fourth-rank tensor:

$$\tau = -\mu[\nabla \mathbf{v} + (\nabla \mathbf{v})^{\mathrm{T}}] + \left(\frac{2\mu}{3} - \kappa\right)(\nabla \cdot \mathbf{v}) \sum_i \delta_i \delta_i \tag{8-52}$$

where $(\nabla \mathbf{v})^{\mathrm{T}}$ is the transpose of the velocity gradient tensor and κ is the dilatational viscosity, or second viscosity, which is known from the Chapman–Enskog kinetic theory to be zero for monatomic ideal gases. The sum of the velocity gradient tensor and its transpose in (8-52) is known as the *symmetric rate-of-strain tensor*.

Creeping Flow of an Incompressible Newtonian Fluid. It is reasonable to assume that $\rho \approx$ constant for liquids that are not subjected to large variations in temperature and pressure. This assumption of incompressibility leads to the following form of the equation of continuity (i.e., see 8-35) and Newton's law of viscosity:

$$\nabla \cdot \mathbf{v} = 0 \tag{8-53}$$

$$\tau = -\mu[\nabla \mathbf{v} + (\nabla \mathbf{v})^{\mathrm{T}}] \tag{8-54}$$

Furthermore, the viscous force term in the equation of motion (i.e., see 8-51) undergoes considerable simplification:

$$\nabla \cdot \tau = -\mu[\nabla \cdot \nabla \mathbf{v} + \nabla \cdot (\nabla \mathbf{v})^{\mathrm{T}}] = -\mu \nabla \cdot \nabla \mathbf{v} \tag{8-55}$$

It is necessary to employ summation notation in rectangular coordinates to verify that $\nabla \cdot (\nabla \mathbf{v})^{\mathrm{T}}$ vanishes for incompressible fluids. If

$$\mathbf{v} = \sum_j \delta_j v_j \tag{8-56a}$$

$$\nabla = \sum_i \delta_i \frac{\partial}{\partial x_i} \tag{8-56b}$$

then the velocity gradient tensor and its transpose are represented by

$$\nabla \mathbf{v} = \sum_i \delta_i \frac{\partial}{\partial x_i} \sum_j \delta_j v_j = \sum_{i,j} \delta_i \delta_j \frac{\partial}{\partial x_i} v_j \tag{8-57a}$$

$$(\nabla \mathbf{v})^{\mathrm{T}} = \sum_{i,j} \delta_i \delta_j \frac{\partial}{\partial x_j} v_i \tag{8-57b}$$

The divergence of the transpose of the velocity gradient tensor is

$$\begin{aligned} \nabla \cdot (\nabla \mathbf{v})^{\mathrm{T}} &= \sum_k \delta_k \frac{\partial}{\partial x_k} \cdot \sum_{i,j} \delta_i \delta_j \frac{\partial}{\partial x_j} v_i \\ &= \sum_{i,j,k} (\delta_k \cdot \delta_i) \delta_j \frac{\partial}{\partial x_k} \left(\frac{\partial}{\partial x_j} \right) v_i \\ &= \sum_{i,j} \delta_j \frac{\partial}{\partial x_i} \left(\frac{\partial}{\partial x_j} \right) v_i \end{aligned} \tag{8-58}$$

However complicated the fluid dynamics problem might be, each component of the velocity vector can be solved analytically or numerically. Hence, each v_i exists, it is unique and it is an exact differential. This means that the order of mixed second partial differentiation of each v_i can be reversed without affecting the final result. Now

$$\nabla \cdot (\nabla \mathbf{v})^{\mathrm{T}} = \sum_{i,j} \delta_j \frac{\partial}{\partial x_i} \left(\frac{\partial}{\partial x_j} \right) v_i = \sum_j \delta_j \frac{\partial}{\partial x_j} \left(\sum_i \frac{\partial}{\partial x_i} v_i \right) \tag{8-59}$$

where the final term in parentheses of (8-59) is $\nabla \cdot \mathbf{v}$, and the jth component of the vector $\nabla \cdot (\nabla \mathbf{v})^{\mathrm{T}}$ is

$$[\nabla \cdot (\nabla \mathbf{v})^{\mathrm{T}}]_j = \frac{\partial}{\partial x_j}(\nabla \cdot \mathbf{v}) \tag{8-60}$$

Hence,

$$\nabla \cdot (\nabla \mathbf{v})^{\mathrm{T}} = \nabla(\nabla \cdot \mathbf{v}) = 0 \tag{8-61}$$

for incompressible fluids. The creeping flow equation of motion for incompressible Newtonian fluids is

$$\mu \nabla \cdot \nabla \mathbf{v} = \nabla \mathfrak{P} \tag{8-62}$$

Equation (8-62) generates three coupled linear second-order partial differential equations (PDEs). For complicated two-dimensional flow problems, this force balance and the equation of continuity yield three coupled linear PDEs for two nonzero velocity components and dynamic pressure. In some situations, this complexity is circumvented by taking the curl of the equation of motion:

$$\mu \nabla \times \nabla \cdot \nabla \mathbf{v} = \nabla \times \nabla \mathfrak{P} \tag{8-63}$$

because the curl of the gradient of a scalar such as $\mathfrak{P}$ vanishes if $\mathfrak{P}$ is analytic. In other words,

$$\nabla \times \nabla \mathfrak{P} = 0 \tag{8-64}$$

if $\mathfrak{P}$ is an exact differential. Hence, dynamic pressure is removed from the force balance by taking the curl of the equation of motion. The resulting set of third-order linear PDEs,

$$\nabla \times \nabla \cdot \nabla \mathbf{v} = 0 \tag{8-65}$$

contains only the velocity vector. Another vector-tensor identity,

$$\nabla \times \nabla \cdot \nabla \mathbf{v} = \nabla \cdot \nabla(\nabla \times \mathbf{v}) \tag{8-66}$$

is employed to generate the equation of change for fluid vorticity, where $\frac{1}{2}\nabla \times \mathbf{v}$ is the vorticity vector. Summation notation in rectangular coordinates is required to verify this identity and evaluate each component of the vorticity equation for specific two-dimensional flow problems.

Evaluation of the Curl of the Divergence of the Velocity Gradient. Begin by expressing the velocity gradient tensor using summation notation:

$$\nabla \mathbf{v} = \sum_i \delta_i \frac{\partial}{\partial x_i} \sum_j \delta_j v_j = \sum_{i,j} \delta_i \delta_j \frac{\partial}{\partial x_i} v_j \tag{8-67}$$

The divergence of the velocity gradient tensor is

$$\begin{aligned}\nabla \cdot \nabla \mathbf{v} &= \sum_k \delta_k \frac{\partial}{\partial x_k} \cdot \sum_{i,j} \delta_i \delta_j \frac{\partial}{\partial x_i} v_j \\ &= \sum_{i,j,k} (\delta_k \cdot \delta_i) \delta_j \frac{\partial}{\partial x_k} \left(\frac{\partial}{\partial x_i} \right) v_j \\ &= \sum_{i,j} \delta_j \frac{\partial}{\partial x_i} \left(\frac{\partial}{\partial x_i} \right) v_j \end{aligned} \tag{8-68}$$

Now take the curl of (8-68):

$$\begin{aligned}\nabla \times \nabla \cdot \nabla \mathbf{v} &= \sum_k \delta_k \frac{\partial}{\partial x_k} \times \sum_{i,j} \delta_j \frac{\partial^2}{\partial x_i^2} v_j \\ &= \sum_{i,j,k} (\delta_k \times \delta_j) \frac{\partial}{\partial x_k} \left(\frac{\partial^2}{\partial x_i^2} \right) v_j \end{aligned} \tag{8-69}$$

The cross product of two unit vectors produces another unit vector that is orthogonal to the two original unit vectors:

$$\delta_k \times \delta_j = \sum_m \delta_m \varepsilon_{kjm} \tag{8-70}$$

where ε_{kjm} is the permutation index, which assumes the following values:

$$\varepsilon_{kjm} = \begin{cases} +1 & \text{if } kjm = 123, 231, 312 \\ -1 & \text{if } kjm = 321, 132, 213 \\ 0 & \text{otherwise} \end{cases} \tag{8-71}$$

The final result contains a sum over four different indicies with 81 terms, several of which vanish due to the nature of the permutation index. Equations (8-69) and (8-70) yield:

$$\nabla \times \nabla \cdot \nabla \mathbf{v} = \sum_{i,j,k,m} \delta_m \varepsilon_{kjm} \frac{\partial}{\partial x_k} \left(\frac{\partial^2}{\partial x_i^2} \right) v_j \tag{8-72}$$

Evaluation of the Divergence of the Gradient (i.e., Laplacian) of the Curl of the Velocity Vector. Begin by calculating the curl of the velocity vector with assistance from the permutation index:

$$\nabla \times \mathbf{v} = \sum_k \delta_k \frac{\partial}{\partial x_k} \times \sum_j \delta_j v_j$$

$$= \sum_{j,k} (\delta_k \times \delta_j) \frac{\partial}{\partial x_k} v_j$$

$$= \sum_{j,k,m} \delta_m \varepsilon_{kjm} \frac{\partial}{\partial x_k} v_j \tag{8-73}$$

Now take the gradient of (8-73):

$$\nabla(\nabla \times \mathbf{v}) = \sum_i \delta_i \frac{\partial}{\partial x_i} \sum_{j,k,m} \delta_m \varepsilon_{kjm} \frac{\partial}{\partial x_k} v_j$$

$$= \sum_{i,j,k,m} \delta_i \delta_m \varepsilon_{kjm} \frac{\partial}{\partial x_i} \left(\frac{\partial}{\partial x_k} \right) v_j \tag{8-74}$$

The divergence of (8-74) is

$$\nabla \cdot \nabla(\nabla \times \mathbf{v}) = \sum_p \delta_p \frac{\partial}{\partial x_p} \cdot \sum_{i,j,k,m} \delta_i \delta_m \varepsilon_{kjm} \frac{\partial}{\partial x_i} \left(\frac{\partial}{\partial x_k} \right) v_j$$

$$= \sum_{i,j,k,m,p} (\delta_p \cdot \delta_i) \delta_m \varepsilon_{kjm} \frac{\partial}{\partial x_p} \left(\frac{\partial}{\partial x_i} \right) \left(\frac{\partial}{\partial x_k} \right) v_j$$

$$= \sum_{i,j,k,m} \delta_m \varepsilon_{kjm} \frac{\partial^2}{\partial x_i^2} \left(\frac{\partial}{\partial x_k} \right) v_j \tag{8-75}$$

Vorticity Equation for Creeping Flow of an Incompressible Newtonian Fluid. Since all scalar components of the velocity vector are exact differentials, it is permissible to reverse the order of mixed second partial differentiation without affecting the final result. If this procedure is performed twice, then inspection of summation representations of the following two vector-tensor operations reveals that they are equivalent:

$$\nabla \times \nabla \cdot \nabla \mathbf{v} = \sum_{i,j,k,m} \delta_m \varepsilon_{kjm} \frac{\partial}{\partial x_k} \left(\frac{\partial^2}{\partial x_i^2} \right) v_j \tag{8-76a}$$

$$\nabla \cdot \nabla(\nabla \times \mathbf{v}) = \sum_{i,j,k,m} \delta_m \varepsilon_{kjm} \frac{\partial^2}{\partial x_i^2} \left(\frac{\partial}{\partial x_k} \right) v_j \tag{8-76b}$$

Since the curl of the creeping flow equation of motion for an incompressible Newtonian fluid yields

$$\nabla \times \nabla \cdot \nabla \mathbf{v} = 0 \tag{8-77}$$

it follows that the Laplacian of the vorticity vector must also vanish:

$$\nabla \cdot \nabla(\nabla \times \mathbf{v}) = 0 \tag{8-78}$$

Equation (8-78) is also known as the equation of change for fluid angular velocity in the low-Reynolds-number limit for incompressible Newtonian fluids because $\nabla \times \mathbf{v}$, which is twice the vorticity vector, yields twice the angular velocity vector of a solid that rotates at constant angular velocity. The summation representation of the Laplacian of the vorticity vector,

$$\nabla \cdot \nabla(\nabla \times \mathbf{v}) = \sum_m \delta_m \sum_i \frac{\partial^2}{\partial x_i^2} \sum_{j,k} \varepsilon_{kjm} \frac{\partial}{\partial x_k} v_j = 0 \tag{8-79}$$

provides sufficient detail to analyze each component of this vector equation. Let's consider a rather complicated two-dimensional flow problem in rectangular coordinates where $v_z = 0$ and there is no dependence of v_x and v_y on spatial coordinate z:

$$v_x(x, y)$$
$$v_y(x, y)$$

If one approaches the solution of this problem via the equations of continuity and motion, then it is necessary to solve three coupled linear PDEs (i.e., one first-order PDE and two second-order PDEs) for v_x, v_y, and dynamic pressure. In the low-Reynolds-number limit, it is also possible to attack this problem via the three scalar components of the equation of change for fluid vorticity. For example, if

$$\begin{array}{lll} \delta_1 = \delta_x & \delta_2 = \delta_y & \delta_3 = \delta_z \\ x_1 = x & x_2 = y & x_3 = z \\ v_1 = v_x & v_2 = v_y & v_3 = v_z \end{array}$$

and each scalar component of $\nabla \cdot \nabla(\nabla \times \mathbf{v})$ must vanish, then equation (8-79) yields:

$$m = 1, \ x\text{-component:} \qquad \left(\frac{\partial^2}{\partial x^2} + \frac{\partial^2}{\partial y^2}\right)\left(\frac{\partial}{\partial y} v_z - \frac{\partial}{\partial z} v_y\right) = 0 \quad \text{(trivial)}$$

$$m = 2, \ y\text{-component:} \qquad \left(\frac{\partial^2}{\partial x^2} + \frac{\partial^2}{\partial y^2}\right)\left(\frac{\partial}{\partial z} v_x - \frac{\partial}{\partial x} v_z\right) = 0 \quad \text{(trivial)}$$

$$m = 3, \ z\text{-component:} \qquad \left(\frac{\partial^2}{\partial x^2} + \frac{\partial^2}{\partial y^2}\right)\left(\frac{\partial}{\partial x} v_y - \frac{\partial}{\partial y} v_x\right) = 0$$

At first glance, three coupled linear third-order PDEs must be solved, as illustrated above. However, each term in the x and y components of the vorticity equation is identically zero because $v_z = 0$ and v_x and v_y are not functions of z. Hence, detailed summation representation of the vorticity equation for creeping viscous flow of an incompressible Newtonian fluid reveals that there is a class of two-dimensional flow problems for which it is only necessary to solve one nontrivial component of this vector equation. If flow occurs in two coordinate directions and there is no dependence of these velocity components on the spatial coordinate in the third direction, then one must solve the nontrivial component of the vorticity equation in the third coordinate direction.

8-6.2 Stream Function and Streamlines

Two-Dimensional Planar Flow. A path within a fluid across which no flow occurs is called a *streamline*. In other words, fluid parcels move along streamlines. If $\mathbf{n}$ is an outward-directed unit normal vector from an arbitrary path within a fluid and dl is a differential length along this path, then

$$d\psi \equiv (\mathbf{n} \cdot \mathbf{v})\, dl \tag{8-80}$$

where ψ is the stream function and $\mathbf{v}$ is the fluid velocity vector. $\mathbf{n} \cdot \mathbf{v}$ is the normal component of the fluid velocity that crosses this arbitrary path. If dl is oriented along a streamline, then $\mathbf{n} \cdot \mathbf{v} = 0$ because no flow occurs across a streamline. Hence, $d\psi = 0$ and ψ is a constant for each streamline. Since ψ is analytic, as well as an exact differential, changes in ψ around a closed loop must vanish. In other words,

$$\oint_{\text{closed loop}} d\psi = 0 \tag{8-81a}$$

$$\sum_{\text{closed loop}} d\psi = 0 \tag{8-81b}$$

Consider two-dimensional planar flow in rectangular coordinates [i.e., $v_x(x, y)$ and $v_y(x, y)$] and two adjacent streamlines within the fluid, with stream function values of ψ and $\psi + d\psi$. Point P is located on streamline ψ, and point Q lies on streamline $\psi + d\psi$. As one moves from P to Q, the change in the value of the stream function is $d\psi_{PQ} = d\psi$, and this change is path independent because the stream function is an exact differential. If the straight path from P to Q is not colinear with either the x or y axis, then it should be possible to arrive at point Q via an intermediate point R, where PR is colinear with the x axis and RQ is colinear with the y axis. Consider the first simple path from P to R, which is parallel to the x axis. Either

$$\mathbf{n} = -\delta_y \qquad dl = +dx \qquad d\psi_{PR} = (\mathbf{n} \cdot \mathbf{v})\, dl = -v_y\, dx \tag{8-82a}$$

or

$$\mathbf{n} = -\delta_y \qquad dl = -dx \qquad d\psi_{PR} = (\mathbf{n} \cdot \mathbf{v})\, dl = +v_y\, dx \tag{8-82b}$$

Now, consider the second simple path from R to Q, which is parallel to the y axis. Either

$$\mathbf{n} = +\delta_x \qquad dl = +dy \qquad d\psi_{RQ} = (\mathbf{n} \cdot \mathbf{v})\, dl = +v_x\, dy \tag{8-83a}$$

or

$$\mathbf{n} = -\delta_x \qquad dl = +dy \qquad d\psi_{RQ} = (\mathbf{n} \cdot \mathbf{v})\, dl = -v_x\, dy \tag{8-83b}$$

For the closed triangular loop from $P \to R \to Q \to P$, the line integral of $d\psi$ vanishes because ψ is an exact differential. Hence,

$$d\psi_{PR} + d\psi_{RQ} + d\psi_{QP} = 0 \tag{8-84}$$

$$-d\psi_{QP} = d\psi_{PQ} = d\psi = d\psi_{PR} + d\psi_{RQ} \tag{8-85}$$

Equations (8-82a) and (8-83a) suggest that

$$d\psi = -v_y\, dx + v_x\, dy \tag{8-86}$$

whereas equations (8-82b) and (8-83b) lead to

$$d\psi = +v_y\, dx - v_x\, dy \tag{8-87}$$

Since $\psi(x, y)$ is exact, its total differential is

$$d\psi = \left(\frac{\partial \psi}{\partial x}\right)_y dx + \left(\frac{\partial \psi}{\partial y}\right)_x dy \tag{8-88}$$

Hence, both velocity components for two-dimensional planar flow in rectangular coordinates are related to the stream function in the following manner. Either

$$v_x = +\frac{\partial \psi}{\partial y} \qquad v_y = -\frac{\partial \psi}{\partial x} \tag{8-89a}$$

or

$$v_x = -\frac{\partial \psi}{\partial y} \qquad v_y = +\frac{\partial \psi}{\partial x} \tag{8-89b}$$

The sign convention is not important. Both representations given by (8-89a) and (8-89b) conserve overall mass for two-dimensional flow of an incompressible fluid in rectangular coordinates because $\psi(x, y)$ is exact and the order of mixed second partial differentiation can be reversed without affecting the final result:

$$\nabla \cdot \mathbf{v} = \frac{\partial v_x}{\partial x} + \frac{\partial v_y}{\partial y} = \left(\frac{\partial}{\partial x}\right)\frac{\partial \psi}{\partial y} - \left(\frac{\partial}{\partial y}\right)\frac{\partial \psi}{\partial x} = 0 \tag{8-90}$$

In the low-Reynolds-number limit for incompressible Newtonian fluids, one calculates the stream function from the z-component of the vorticity equation, as described on page 180:

$$\begin{aligned}\left(\frac{\partial^2}{\partial x^2}+\frac{\partial^2}{\partial y^2}\right)\left[\left(\frac{\partial}{\partial x}\right)v_y-\left(\frac{\partial}{\partial y}\right)v_x\right]&=0\\ \left(\frac{\partial^2}{\partial x^2}+\frac{\partial^2}{\partial y^2}\right)\left[\left(\frac{\partial}{\partial x}\right)\frac{\partial\psi}{\partial x}+\left(\frac{\partial}{\partial y}\right)\frac{\partial\psi}{\partial y}\right]&=0\\ \left(\frac{\partial^2}{\partial x^2}+\frac{\partial^2}{\partial y^2}\right)\left(\frac{\partial^2}{\partial x^2}+\frac{\partial^2}{\partial y^2}\right)\psi=(\nabla\cdot\nabla)(\nabla\cdot\nabla\psi)&=0\end{aligned} \tag{8-91}$$

Hence, one linear fourth-order PDE must be solved for the stream function ψ, from which v_x and v_y can be determined. This approach is the method of choice instead of tackling coupled linear first- and second-order PDEs for three unknowns via the equations of continuity and motion. The PDE of interest, given by (8-91), progressed from a second-order equation to a fourth-order equation by taking the curl of the equation of motion to eliminate dynamic pressure, and relating both velocity components to the stream function.

Alternative View of the Relation between Fluid Velocity Components and the Stream Function for Two-Dimensional Flow in Rectangular Coordinates. Conservation of overall mass for an incompressible fluid is prescribed by a simplified form of the equation of continuity when $\rho \approx$ constant:

$$\nabla\cdot\mathbf{v}=0 \tag{8-92}$$

This scalar equation is satisfied for any vector potential $\mathbf{A}$ whose scalar components (i.e., A_x, A_y, and A_z) are exact differentials if

$$\mathbf{v}=\nabla\times\mathbf{A} \tag{8-93}$$

because

$$\nabla\cdot\mathbf{v}=\nabla\cdot\nabla\times\mathbf{A}=0 \tag{8-94}$$

is an identity provided that the order of mixed second partial differentiation of each A_i can be reversed without affecting the final result. If

$$\mathbf{A}=\delta_x A_x+\delta_y A_y+\delta_z A_z \tag{8-95}$$

then the velocity vector is

$$\begin{aligned}\mathbf{v}=\nabla\times\mathbf{A}=\delta_x\left(\frac{\partial}{\partial y}A_z-\frac{\partial}{\partial z}A_y\right)+\delta_y\left(\frac{\partial}{\partial z}A_x-\frac{\partial}{\partial x}A_z\right)\\ +\delta_z\left(\frac{\partial}{\partial x}A_y-\frac{\partial}{\partial y}A_x\right)\end{aligned} \tag{8-96}$$

For two-dimensional planar flow with $v_z = 0$ and no dependence of v_x and v_y on spatial coordinate z, the velocity vector is

$$\mathbf{v} = \delta_x v_x(x, y) + \delta_y v_y(x, y) \tag{8-97}$$

Hence, one makes the following correspondence based on the two previous expressions for $\mathbf{v}$, assuming that each A_i is not a function of z:

$$\begin{aligned} v_x &= +\frac{\partial}{\partial y} A_z \\ v_y &= -\frac{\partial}{\partial x} A_z \\ \frac{\partial}{\partial x} A_y &= \frac{\partial}{\partial y} A_x \end{aligned} \tag{8-98}$$

Hence, one identifies the z-component of the velocity vector potential (i.e., A_z) with the stream function ψ.

Axisymmetric Stream Function in Spherical Coordinates. It is necessary to understand the stream function in sufficient depth because additional boundary conditions are required to solve linear fourth-order PDEs relative to the typical second-order differential equations that are characteristic of most fluid dynamics problems. Consider the following two-dimensional axisymmetric flow problem in which there is no dependence on the azimuthal angle ϕ in spherical coordinates:

$$v_r(r, \theta) \qquad v_\theta(r, \theta) \qquad v_\phi = 0 \tag{8-99}$$

Whereas the stream function for planar flow in rectangular coordinates has units of volumetric flow rate per unit depth, ψ for axisymmetric flow in spherical coordinates has units of volumetric flow rate:

$$\psi \equiv \frac{Q}{2\pi} \tag{8-100}$$

Q is the instantaneous volumetric flow rate downward in the negative z direction which intersects the circle mapped out by one end of a vector that rotates completely around the z axis while the other end is pinned to the z axis at point O. The coordinates of the following points are of interest in developing relations between v_r and v_θ and the stream function:

$$R \text{ at } (r, \theta) \qquad P \text{ at } (r + dr, \theta) \qquad W \text{ at } (r, \theta + d\theta) \tag{8-101}$$

Rotate vectors OR and OP completely around the z axis and calculate the differential volumetric flow rate downward between the two circles mapped out by

points R and P. The velocity component of interest is v_θ, and $2\pi r \sin\theta\, dr$ is the cross-sectional area for flow. Hence,

$$(dQ)_{\text{at constant } \theta} = 2\pi (d\psi)_{\text{at constant } \theta} = v_\theta 2\pi r \sin\theta\, dr \tag{8-102}$$

and

$$v_\theta = \frac{1}{r\sin\theta}\left(\frac{\partial\psi}{\partial r}\right)_{\text{at constant } \theta} \tag{8-103}$$

Now, rotate vectors OR and OW completely around the z axis and calculate the differential volumetric flow rate downward between the two circles mapped out by points R and W when $\theta < \pi/2$. The velocity component of interest is $-v_r$, and $2\pi r^2 \sin\theta\, d\theta$ is the cross-sectional area for flow. In this case,

$$(dQ)_{\text{at constant } r} = 2\pi (d\psi)_{\text{at constant } r} = -v_r 2\pi r^2 \sin\theta\, d\theta \tag{8-104}$$

and

$$v_r = -\frac{1}{r^2\sin\theta}\left(\frac{\partial\psi}{\partial\theta}\right)_{\text{at constant } r} \tag{8-105}$$

The sign convention is arbitrary, provided that one of the two velocity components has a negative sign. These relations between v_r and v_θ and the stream function, given by (8-103) and (8-105), conserve overall mass for an incompressible fluid. When $\rho \approx$ constant, the simplified equation of continuity in spherical coordinates,

$$\nabla \cdot \mathbf{v} = \frac{1}{r^2}\frac{\partial}{\partial r} r^2 v_r + \frac{1}{r\sin\theta}\frac{\partial}{\partial\theta} v_\theta \sin\theta = 0 \tag{8-106}$$

is satisfied because ψ is an exact differential, which implies that

$$\left(\frac{\partial}{\partial r}\right)\frac{\partial\psi}{\partial\theta} = \left(\frac{\partial}{\partial\theta}\right)\frac{\partial\psi}{\partial r} \tag{8-107}$$

Creeping Flow of an Incompressible Newtonian Fluid around a Solid Sphere. This is a classic two-dimensional fluid dynamics problem in spherical coordinates. A stationary solid sphere of radius R is located at the origin of an xyz coordinate system and an incompressible Newtonian fluid with velocity $\delta_z V_{\text{approach}}$ far from the sphere approaches from below. Macroscopic results such as the hydrodynamic drag force and f vs. Re are exactly the same if the sphere falls through a quiescent liquid at terminal velocity given by $-\delta_z V_{\text{solid}}$, where $V_{\text{solid}} = V_{\text{approach}}$. This axisymmetric problem exhibits no swirling motion (i.e., $v_\phi = 0$), and the radial $v_r(r,\theta)$ and polar $v_\theta(r,\theta)$ velocity components exhibit angular symmetry, which implies that there is no functional dependence on azimuthal angle ϕ. Since the approach velocity of the fluid is described best

in rectangular coordinates, it is necessary to determine v_r and v_θ far from the sphere. The scalar (i.e., dot) product is useful in this regard:

$$v_r(r \to \infty) = \delta_r \cdot \delta_z V_{\text{approach}} = V_{\text{approach}} \cos\theta \tag{8-108a}$$

$$v_\theta(r \to \infty) = \delta_\theta \cdot \delta_z V_{\text{approach}} = -V_{\text{approach}} \sin\theta \tag{8-108b}$$

because

$$\delta_z = \delta_r \cos\theta - \delta_\theta \sin\theta + \delta_\phi(0) \tag{8-109}$$

In the low-Reynolds-number limit, the nontrivial ϕ-component of the equation of change for fluid vorticity,

$$\nabla \cdot \nabla(\nabla \times \mathbf{v}) = 0 \tag{8-110}$$

together with

$$v_r(r, \theta) = -\frac{1}{r^2 \sin\theta}\frac{\partial\psi}{\partial\theta} \tag{8-111a}$$

$$v_\theta(r, \theta) = \frac{1}{r \sin\theta}\frac{\partial\psi}{\partial r} \tag{8-111b}$$

yields

$$E^2(E^2\psi) = 0 \tag{8-112}$$

where the E^2 operator in spherical coordinates,

$$E^2 = \frac{\partial^2}{\partial r^2} + \frac{\sin\theta}{r^2}\frac{\partial}{\partial\theta}(\sin\theta)^{-1}\frac{\partial}{\partial\theta} \tag{8-113}$$

is slightly different from the Laplacian operator

$$\nabla \cdot \nabla = \nabla^2 = \frac{1}{r^2}\frac{\partial}{\partial r}\left(r^2\frac{\partial}{\partial r}\right) + \frac{1}{r^2 \sin\theta}\frac{\partial}{\partial\theta}\left(\sin\theta\frac{\partial}{\partial\theta}\right) \tag{8-114}$$

Boundary Conditions and Functional Form of the Stream Function. No slip at the fluid–solid interface requires that the fluid velocity must vanish at $r = R$ if the sphere is stationary. Hence,

$$\left(\frac{\partial\psi}{\partial\theta}\right)_{r=R} = 0 \tag{8-115a}$$

$$\left(\frac{\partial\psi}{\partial r}\right)_{r=R} = 0 \tag{8-115b}$$

These classic no-slip boundary conditions must be modified if the sphere falls through a quiescent liquid, because the liquid in contact with the sphere assumes

the velocity of the solid in the r and θ directions. The remaining boundary conditions are based on the definition of ψ. For example,

$$\psi(r > R, \theta = 0) = 0 \tag{8-115c}$$

$$\psi(r = R, \text{ any } \theta) = 0 \tag{8-115d}$$

if there is no volumetric flow through the circle mapped out by the end of a vector that rotates completely around the z axis when the other end is pinned to the symmetry axis. The cross-sectional area for flow is reduced to a point in (8-115c), and it is completely blocked by the solid in (8-115d). One postulates the functional form of the stream function from the boundary conditions far from the sphere, where the approach velocity is $\delta_z V_{\text{approach}}$, and

$$v_r(r \to \infty) = V_{\text{approach}} \cos\theta = -\frac{1}{r^2 \sin\theta}\frac{\partial\psi}{\partial\theta} \tag{8-115e}$$

$$v_\theta(r \to \infty) = -V_{\text{approach}} \sin\theta = \frac{1}{r \sin\theta}\frac{\partial\psi}{\partial r} \tag{8-115f}$$

Condition (8-115e) is integrated with respect to θ at constant r, which implies that the integration constant could be an unknown function of r. The result yields the functional form of ψ at large r:

$$\psi(r \to \infty, \theta) = -V_{\text{approach}} r^2 \int \sin\theta \cos\theta \, d\theta = -\frac{1}{2} V_{\text{approach}} r^2 \sin^2\theta + f(r) \tag{8-116}$$

Condition (8-115f) indicates that $f(r) =$ constant, because

$$-V_{\text{approach}} \sin\theta = \frac{1}{r \sin\theta}\frac{\partial\psi}{\partial r} = -\frac{V_{\text{approach}} r \sin^2\theta - df/dr}{r \sin\theta} \tag{8-117}$$

$$\frac{df}{dr} = 0 \tag{8-118}$$

and condition (8-115c) reveals that $f(r) = 0$. If one postulates that in general,

$$\psi(r, \theta) = F(r)G(\theta) \tag{8-119}$$

then $G(\theta) = \sin^2\theta$ at large r, and this functional dependence should not change as one moves closer to the sphere at constant θ. Hence,

$$\psi(r, \theta) = F(r) \sin^2\theta$$

and

$$F(r \to \infty) = -\tfrac{1}{2} V_{\text{approach}} r^2 \tag{8-115g}$$

The angular dependence of the stream function represents one of the Legendre polynomials that is unaffected by the E^2 operator for creeping viscous flow in spherical coordinates. In other words,

$$E^2\psi(r,\theta) = E^2[F(r)\sin^2\theta] = \sin^2\theta\left(\frac{d^2}{dr^2} - \frac{2}{r^2}\right)F(r) \tag{8-120}$$

This reassuring observation is left as an exercise for the student to verify.

Analytical Solution of the Vorticity Equation for $\psi(r,\theta)$. Equation (8-120) reveals that

$$E^2[F(r)\sin^2\theta] = H(r)\sin^2\theta \tag{8-121}$$

$$H(r) = \left(\frac{d^2}{dr^2} - \frac{2}{r^2}\right)F(r) \tag{8-122}$$

For creeping viscous flow in spherical coordinates, the ϕ-component of the vorticity equation requires that

$$\begin{aligned} E^2(E^2\psi) = E^2\{E^2[F(r)\sin^2\theta]\} &= E^2[H(r)\sin^2\theta] \\ &= \sin^2\theta\left(\frac{d^2}{dr^2} - \frac{2}{r^2}\right)H(r) = 0 \end{aligned} \tag{8-123}$$

Hence, one arrives at Euler's differential equation for the radial part of the stream function:

$$\left(\frac{d^2}{dr^2} - \frac{2}{r^2}\right)\left(\frac{d^2}{dr^2} - \frac{2}{r^2}\right)F(r) = 0 \tag{8-124}$$

and postulates that

$$F(r) \approx r^n \qquad (\text{or } r^n \ln r \text{ for repeated roots}) \tag{8-125}$$

Upon substitution into Euler's differential equation,

$$[n(n-1)-2][(n-2)(n-3)-2]r^{n-4} = 0 \tag{8-126}$$

one finds four roots (i.e., $n = -1, 1, 2, 4$) that yield the following solution for the stream function:

$$\psi(r,\theta) = \sin^2\theta(A/r + Br + Cr^2 + Dr^4) \tag{8-127}$$

Boundary condition (8-115*c*) is satisfied by the functional form of ψ. Conditions (8-115*e*) to (8-115*g*) require that

$$D = 0 \qquad C = -\tfrac{1}{2}V_{\text{approach}}$$

Conditions (8-115*a*) or (8-115*d*) and (8-115*b*) yield

$$A = -\tfrac{1}{4} V_{\text{approach}} R^3 \qquad B = \tfrac{3}{4} V_{\text{approach}} R$$

The final results are

$$\begin{aligned} \psi(r,\theta) &= V_{\text{approach}} R^2 \sin^2\theta(-\tfrac{1}{4}\eta^{-1} + \tfrac{3}{4}\eta - \tfrac{1}{2}\eta^2) \\ v_r(r,\theta) &= V_{\text{approach}} \cos\theta(1 - \tfrac{3}{2}\eta^{-1} + \tfrac{1}{2}\eta^{-3}) \\ v_\theta(r,\theta) &= -V_{\text{approach}} \sin\theta(1 - \tfrac{3}{4}\eta^{-1} - \tfrac{1}{4}\eta^{-3}) \end{aligned} \tag{8-128}$$

where the dimensionless radial variable $\eta = r/R$. The expression for v_r is employed to calculate the error incurred when the radial term of the equation of continuity in spherical coordinates is simplified:

$$\frac{1}{r^2}\frac{\partial}{\partial r} r^2 v_r \approx \frac{\partial v_r}{\partial r} \tag{8-129}$$

The polar velocity component is linearized within a thin mass transfer boundary layer on the liquid side of the solid–liquid interface to facilitate the development of dimensionless mass transfer correlations.

8-6.3 Integrating Exact Differentials

Consider the following function $P(x, y)$ in which

$$dP = \left(\frac{\partial P}{\partial x}\right)_y dx + \left(\frac{\partial P}{\partial y}\right)_x dy \tag{8-130}$$

is an exact differential. The equation of motion in transport phenomena provides information indirectly about the function P as follows:

$$Q(x, y) = \left(\frac{\partial P}{\partial x}\right)_y \tag{8-131a}$$

$$R(x, y) = \left(\frac{\partial P}{\partial y}\right)_x \tag{8-131b}$$

It is desired to integrate these equations to obtain $P(x, y)$. This task is accomplished as follows:

Step 1. Integrate (8-131*b*) with respect to y (i.e., from y_0 to y) at constant x, realizing that the integration constant can be, at most, a function of x:

$$P(x, y) = \int_{y_0}^{y} R(x, t)\, dt + f(x) \tag{8-132}$$

In practice, integration of R with respect to y is performed using dummy variable t, where t varies from y_0 to y.

Step 2. The unknown integration constant $f(x)$, which corresponds to $P(x, y_0)$, is determined by differentiating (8-132) with respect to x at constant y, and comparing the result with (8-131a):

$$Q(x, y) = \left(\frac{\partial P}{\partial x}\right)_y = \left(\frac{\partial}{\partial x}\int_{y_0}^{y} R(x, t)\, dt\right) + \frac{df}{dx} \tag{8-133}$$

Hence,

$$\frac{df}{dx} = Q(x, y) - \int_{y_0}^{y} \frac{\partial}{\partial x} R(x, t)\, dt \tag{8-134}$$

Step 3. If $f(x)$ and df/dx are only functions of x, then

$$\left(\frac{\partial}{\partial y}\right)\frac{df}{dx} = \frac{\partial Q}{\partial y} - \frac{\partial}{\partial y}\int_{y_0}^{y} \frac{\partial}{\partial x} R(x, t)\, dt = 0 \tag{8-135}$$

This is true if

$$\frac{\partial Q}{\partial y} = \frac{\partial}{\partial y}\int_{y_0}^{y} \frac{\partial}{\partial x} R(x, t)\, dt \tag{8-136}$$

Step 4. The only dependence on y in the integral of (8-136) is found in the upper limit of integration, because y_0 is constant. Hence, the Leibnitz rule for differentiating a one-dimensional integral with variable limits yields:

$$\begin{aligned}\frac{\partial}{\partial y}\int_{y_0}^{y} \frac{\partial}{\partial x} R(x, t)\, dt &= \frac{\partial y}{\partial y}\left(\frac{\partial}{\partial x}\right) R(x, t = y) - \frac{\partial y_0}{\partial y}\left(\frac{\partial}{\partial x}\right) R(x, t = y_0) \\ &= \frac{\partial R}{\partial x}\end{aligned} \tag{8-137}$$

In summary, $P(x, y)$ is determined via (8-132) and $f(x)$ is calculated via integration of (8-134). This methodology is employed below to calculate dynamic pressure. No inconsistencies will develop if (8-136) is satisfied. In other words,

$$\frac{\partial Q}{\partial y} = \frac{\partial R}{\partial x} \tag{8-138}$$

$$\frac{\partial}{\partial y}\left(\frac{\partial P}{\partial x}\right) = \frac{\partial}{\partial x}\left(\frac{\partial P}{\partial y}\right) \tag{8-139}$$

Step 3 is satisfied because P is an exact differential, which implies that the order of mixed second partial differentiation can be reversed without affecting the final result. It might be worthwhile to verify this test for exact differentials, given by (8-139), before embarking on the integrations in steps 1 and 2.

8-6.4 Dynamic Pressure Distribution Via the Equation of Motion

For low-Reynolds-number flow of an incompressible Newtonian fluid, the r and θ-components of the equation of motion are useful to calculate dynamic pressure after the vorticity equation allows one to determine ψ, v_r, and v_θ. Hence,

$$\mu \boldsymbol{\nabla} \cdot \boldsymbol{\nabla} \mathbf{v} = \boldsymbol{\nabla} \mathfrak{P} \tag{8-140}$$

provides information about dynamic pressure in a form that matches equations (8-131a) and (8-131b). It should be obvious that $\mathfrak{P}$ cannot be obtained directly from the vorticity equation because the curl of the equation of motion was performed to eliminate $\boldsymbol{\nabla}\mathfrak{P}$ (i.e., see equations 8-62 through 8-65). In spherical coordinates, with

$$v_r(r, \theta) \qquad v_\theta(r, \theta) \qquad v_\phi = 0 \tag{8-141}$$

the r, θ, and ϕ components of the equation of motion are evaluated explicitly with assistance from equations D, E, and F, and M, N, and O, respectively, in Bird *et al*. (2002), Table A.7-3, p. 836. For example,

$$\begin{aligned}
(\boldsymbol{\nabla}\mathfrak{P})_r &= \frac{\partial \mathfrak{P}}{\partial r} = \mu(\boldsymbol{\nabla} \cdot \boldsymbol{\nabla}\mathbf{v})_r = \mu\left(\nabla^2 v_r - \frac{2v_r}{r^2} - \frac{2}{r^2}\frac{\partial v_\theta}{\partial \theta} - \frac{2}{r^2} v_\theta \cot\theta\right) \\
(\boldsymbol{\nabla}\mathfrak{P})_\theta &= \frac{1}{r}\frac{\partial \mathfrak{P}}{\partial \theta} = \mu(\boldsymbol{\nabla} \cdot \boldsymbol{\nabla}\mathbf{v})_\theta = \mu\left(\nabla^2 v_\theta + \frac{2}{r^2}\frac{\partial v_r}{\partial \theta} - \frac{v_\theta}{r^2 \sin^2\theta}\right) \\
(\boldsymbol{\nabla}\mathfrak{P})_\phi &= \frac{1}{r\sin\theta}\frac{\partial \mathfrak{P}}{\partial \phi} = \mu(\boldsymbol{\nabla} \cdot \boldsymbol{\nabla}\mathbf{v})_\phi = 0
\end{aligned} \tag{8-142}$$

where

$$\nabla^2 \equiv \frac{1}{r^2}\frac{\partial}{\partial r}\left(r^2 \frac{\partial}{\partial r}\right) + \frac{1}{r^2 \sin\theta}\frac{\partial}{\partial \theta}\left(\sin\theta \frac{\partial}{\partial \theta}\right)$$

The following intermediate results are helpful, with $\eta = r/R$:

$$\begin{aligned}
\frac{\partial v_r}{\partial r} &= \frac{3V_{\text{approach}} \cos\theta}{2R}(\eta^{-2} - \eta^{-4}) \\
\frac{\partial v_r}{\partial \theta} &= -V_{\text{approach}} \sin\theta \left(1 - \frac{3}{2}\eta^{-1} + \frac{1}{2}\eta^{-3}\right) \\
\frac{\partial v_\theta}{\partial r} &= -\frac{3V_{\text{approach}} \sin\theta}{4R}(\eta^{-2} + \eta^{-4}) \\
\frac{\partial v_\theta}{\partial \theta} &= -V_{\text{approach}} \cos\theta \left(1 - \frac{3}{4}\eta^{-1} - \frac{1}{4}\eta^{-3}\right) \\
\frac{\partial}{\partial r}\left(r^2 \frac{\partial v_r}{\partial r}\right) &= 3V_{\text{approach}} \eta^{-3} \cos\theta
\end{aligned}$$

$$\frac{\partial}{\partial r}\left(r^2\frac{\partial v_\theta}{\partial r}\right) = \frac{3}{2}V_{\text{approach}}\eta^{-3}\sin\theta$$

$$\frac{\partial}{\partial\theta}\left(\sin\theta\frac{\partial v_r}{\partial\theta}\right) = -2V_{\text{approach}}\sin\theta\cos\theta\left(1-\frac{3}{2}\eta^{-1}+\frac{1}{2}\eta^{-3}\right)$$

$$\frac{\partial}{\partial\theta}\left(\sin\theta\frac{\partial v_\theta}{\partial\theta}\right) = V_{\text{approach}}(\sin^2\theta-\cos^2\theta)\left(1-\frac{3}{4}\eta^{-1}-\frac{1}{4}\eta^{-3}\right) \quad (8\text{-}143)$$

The r and θ components of the equation of motion yield

$$\frac{\partial\mathfrak{P}}{\partial r} = \frac{3\mu V_{\text{approach}}}{R^2}\eta^{-3}\cos\theta \quad (8\text{-}144a)$$

$$\frac{\partial\mathfrak{P}}{\partial\theta} = \frac{3\mu V_{\text{approach}}}{2R}\eta^{-2}\sin\theta \quad (8\text{-}144b)$$

Inspection reveals that dynamic pressure $\mathfrak{P}(r,\theta)$ is an exact differential. Integration of (8-144b) with respect to θ at constant r yields

$$\mathfrak{P}(r,\theta) = \frac{3\mu V_{\text{approach}}}{2R}\eta^{-2}\int\sin\theta\,d\theta + f(r)$$

$$= -\frac{3\mu V_{\text{approach}}}{2R}\eta^{-2}\cos\theta + f(r) \quad (8\text{-}145)$$

The integration constant $f(r)$ in (8-145) is determined from (8-144a):

$$\frac{\partial\mathfrak{P}}{\partial r} = \frac{3\mu V_{\text{approach}}}{R^2}\eta^{-3}\cos\theta = \frac{3\mu V_{\text{approach}}}{R^2}\eta^{-3}\cos\theta + \frac{df}{dr} \quad (8\text{-}146)$$

Hence, $df/dr = 0$ and f is a constant, determined from hydrostatic conditions (i.e., $\mathbf{v} = \delta_z V_{\text{approach}} = \text{constant}$) far from the sphere where $r \to \infty$ and $\mathfrak{P} = \mathfrak{P}_\infty$. The final result for the dynamic pressure distribution is

$$\mathfrak{P}(r,\theta) = \mathfrak{P}_\infty - \frac{3\mu V_{\text{approach}}}{2R}\eta^{-2}\cos\theta \quad (8\text{-}147)$$

8-6.5 Fluid Pressure Distribution

The total force transmitted across the fluid–solid interface requires fluid pressure, not dynamic pressure. Since dynamic pressure is a combination of gravitational potential energy per unit volume and actual fluid pressure, it is rather simple to use equation (8-147) and calculate fluid pressure. The rectangular Cartesian coordinate that increases in the direction opposite to gravity is $z = r\cos\theta$. Hence,

$$\mathfrak{P} = p(r,\theta) + \rho g z = \mathfrak{P}_\infty - \frac{3\mu V_{\text{approach}}}{2R}\eta^{-2}\cos\theta \quad (8\text{-}148)$$

The horizontal plane that intersects the center of the sphere (i.e., $z = 0$, $\theta = \pi/2$) is the reference for the gravitational potential. In this reference plane, dynamic

pressure is $\mathfrak{P}_\infty$ and fluid pressure is p_∞. Furthermore, $\mathfrak{P}_\infty = p_\infty$. The actual fluid pressure is

$$p(r, \theta) = p_\infty - \rho g r \cos\theta - \frac{3\mu V_{\text{approach}}}{2R} \eta^{-2} \cos\theta \tag{8-149}$$

The second term on the right side of (8-149) represents the hydrostatic effect of gravity on fluid pressure, and the third term on the right side represents the hydrodynamic consequence of a blunt object (i.e., the solid sphere) perturbing fluid streamlines in the vicinity of $r \approx R$. The following characteristics of $p(r, \theta)$ are important:

1. Below the xy plane where $\theta > \pi/2$, fluid pressure is greater than p_∞.
2. Directly below the sphere at large r, $p = p_\infty + \rho g r$, which corresponds to hydrostatics because the approach velocity of the fluid is constant.
3. Above the xy plane where $\theta < \pi/2$, fluid pressure is less than p_∞.
4. Directly above the sphere at large r, $p = p_\infty - \rho g r$, which is also a hydrostatic situation.
5. As one moves closer to the sphere at constant θ, the hydrodynamic contribution increases fluid pressure on the front side (i.e., southern hemisphere) and decreases fluid pressure on the back side (i.e., northern hemisphere).
6. The hydrodynamic contribution is more pronounced for higher-viscosity fluids that move faster past smaller spheres.
7. Except for the effect of gravity far from the sphere, fluid pressure is highest on the spherical surface at the stagnation point (i.e., $r = R$, $\theta = \pi$) and lowest on the spherical surface at the separation point (i.e., $r = R$, $\theta = 0$).
8. As one moves along a given streamline, the dynamic contribution to fluid pressure, the magnitude of the tangential velocity component, and the relation between r and θ are illustrated in Table 8-2.
9. If one follows the path of the dimensionless streamline given by $\psi^* = -0.002$ as it approaches the southern hemisphere, the fluid pressure increases from $\theta = 180$ to 155° and the tangential velocity increases as well. From 155 to 90°, the tangential velocity continues to increase and approaches its maximum at 90° while the fluid pressure decreases. From 90 to 25°, the fluid pressure continues to decrease and the tangential velocity decreases slightly. A fluid parcel moving along this streamline experiences no difficulty maintaining these conditions. From 25° to the separation point at $\theta = 0$, the fluid pressure increases while the tangential velocity decreases. This poses a severe demand on fluid parcels attempting to traverse the streamline. This demand is met in the creeping flow regime. However, when turbulent flow is achieved, hydrodynamic increases in fluid pressure on the back side of the sphere along a given streamline are magnified several fold. Consequently, boundary layer separation occurs at $\theta > 0$ because turbulent eddies cannot transfer sufficient momentum from the free stream into the

TABLE 8-2 Numerical Evaluation of the Tangential Velocity Component v_θ and the Dynamic Contribution to Fluid Pressure p (not dynamic pressure $\mathfrak{P}$) as One Traverses a Streamline with $\psi = -0.002$ around a Solid Sphere

$$\psi^* = \frac{\psi}{V_{\text{approach}} R^2} = -0.002 = \left(-\frac{1}{4}\eta^{-1} + \frac{3}{4}\eta - \frac{1}{2}\eta^2\right)\sin^2\theta$$

$$\frac{p(r,\theta) - (p_\infty - \rho g r\cos\theta)}{3\mu V_{\text{approach}}/2R} = -\eta^{-2}\cos\theta$$

$$\frac{v_\theta(r,\theta)}{V_{\text{approach}}} = \left(1 - \frac{3}{4}\eta^{-1} - \frac{1}{4}\eta^{-3}\right)\sin\theta$$

θ	$\eta = r/R$	$-\eta^{-2}\cos\theta$	$v_\theta(r,\theta)/V_{\text{approach}}$
175	1.64	0.37	4.2×10^{-2}
170	1.31	0.57	5.5×10^{-2}
165	1.21	0.67	6.1×10^{-2}
160	1.15	0.71	6.4×10^{-2}
155	1.12	0.72	6.6×10^{-2}
150	1.10	0.71	6.8×10^{-2}
145	1.09	0.69	6.9×10^{-2}
140	1.08	0.66	7.0×10^{-2}
135	1.07	0.61	7.1×10^{-2}
130	1.07	0.56	7.1×10^{-2}
125	1.06	0.51	7.1×10^{-2}
120	1.06	0.45	7.2×10^{-2}
115	1.06	0.38	7.2×10^{-2}
110	1.06	0.31	7.2×10^{-2}
105	1.05	0.23	7.2×10^{-2}
100	1.05	0.16	7.2×10^{-2}
95	1.05	0.08	7.2×10^{-2}
85	1.05	−0.08	7.2×10^{-2}
80	1.05	−0.16	7.2×10^{-2}
75	1.05	−0.23	7.2×10^{-2}
70	1.06	−0.31	7.2×10^{-2}
65	1.06	−0.38	7.2×10^{-2}
60	1.06	−0.45	7.2×10^{-2}
55	1.06	−0.51	7.1×10^{-2}
50	1.07	−0.56	7.1×10^{-2}
45	1.07	−0.61	7.1×10^{-2}
40	1.08	−0.66	7.0×10^{-2}
35	1.09	−0.69	6.9×10^{-2}
30	1.10	−0.71	6.8×10^{-2}
25	1.12	−0.72	6.6×10^{-2}
20	1.15	−0.71	6.4×10^{-2}
15	1.21	−0.67	6.1×10^{-2}
10	1.31	−0.57	5.5×10^{-2}
5	1.64	−0.37	4.2×10^{-2}

fluid boundary layer that hugs the solid, thereby hindering the ability of fluid parcels to penetrate these regions of relatively high pressure. Hence, a low-pressure chaotic eddy current develops behind the sphere, which produces a significant drag force on the solid. The separation point is $\theta \approx 71^\circ$ for laminar boundary layer flow transverse to a solid cylinder, relative to stagnation at $\theta = \pi$ (Schlichting, 1979, p. 171).

8-6.6 Total Vector Force Transmitted across the Fluid–Solid Interface

Interphase momentum transfer is the focus of this section. Macroscopic correlations are based on dynamic forces due to momentum flux that act across the fluid–solid interface, similar to terms of type **2**, **3**, and **4** in the equation of motion. Gravity enters into this discussion via the hydrostatic contribution to fluid pressure, because volumetric body forces are not operative across an interface. The outward-directed unit normal vector from the solid surface into the fluid is **n**. As discussed earlier, forces due to total momentum flux, transmitted in the $-\mathbf{n}$ direction from the fluid to the solid across the interface at $r = R$, are (i.e., see equation 8-20):

$$\mathbf{F}_{\text{fluid-solid}} = -\mathbf{F}_{\text{solid-fluid}} = \int_S [-\mathbf{n} \cdot (\rho \mathbf{v}\mathbf{v} + \tau) - \mathbf{n}p]_{\text{at } r=R}\, dS \tag{8-150}$$

where $\mathbf{F}_{\text{fluid-solid}}$ represents the interfacial force exerted by the fluid on the solid, $\mathbf{F}_{\text{solid-fluid}}$ is the force exerted by the solid on the fluid, and S is the external surface area of the solid sphere. In this example, **n** is given by the unit vector in the r direction (i.e., δ_r). Hence, the vector-tensor dot operations in equation (8-150) yield

$$\mathbf{F}_{\text{fluid-solid}} = -\int_S (\rho v_r \mathbf{v} + \tau_r + \delta_r p)_{\text{at } r=R}\, dS \tag{8-151}$$

where τ_r is a vector viscous force per unit area that acts across a surface at constant r (i.e., the fluid–solid interface). In spherical coordinates, $dS = R^2 \sin\theta\, d\theta\, d\phi$ and

$$\tau_r = \delta_r \tau_{rr} + \delta_\theta \tau_{r\theta} + \delta_\phi \tau_{r\phi} \tag{8-152}$$

Since the fluid velocity vector vanishes on the surface of a stationary sphere and the fluid velocity relative to a moving sphere also vanishes at $r = R$ unless the solid is deformed, the interfacial force is

$$\begin{aligned} \mathbf{F}_{\text{fluid-solid}} &= -R^2 \iint (\tau_r + \delta_r p)_{\text{at } r=R} \sin\theta\, d\theta\, d\phi \\ &= -R^2 \iint [\delta_r(\tau_{rr} + p) + \delta_\theta \tau_{r\theta} + \delta_\phi \tau_{r\phi}]_{\text{at } r=R} \sin\theta\, d\theta\, d\phi \end{aligned} \tag{8-153}$$

This result illustrates that τ_{rr} is a normal viscous stress that acts similarly to pressure forces (i.e., in the direction of **n**). The three scalar components of τ that

represent viscous forces transmitted across the surface at $r = R$ are evaluated with assistance from the two-dimensional velocity profile and Newton's law of viscosity for an incompressible fluid. Equations B.1-15, B.1-18, and B.1-20 in Bird *et al*. (2002, p. 844) are applicable:

$$\tau_{rr}(r = R) = -2\mu \left(\frac{\partial v_r}{\partial r} \right)_{r=R} = -\frac{3\mu V_{\text{approach}}}{R} \cos\theta (\eta^{-2} - \eta^{-4})_{\eta=1} = 0$$

$$\tau_{r\theta}(r = R) = -\mu \left[r \frac{\partial}{\partial r} \left(\frac{v_\theta}{r} \right) + \frac{1}{r} \frac{\partial v_r}{\partial \theta} \right]_{r=R} = \frac{3\mu V_{\text{approach}}}{2R} (\eta^{-4})_{\eta=1} \sin\theta$$

$$\tau_{r\phi} = -\mu \left[\frac{1}{r \sin\theta} \frac{\partial v_r}{\partial \phi} + r \frac{\partial}{\partial r} \left(\frac{v_\phi}{r} \right) \right] = 0 \tag{8-154}$$

Notice that the viscous shear stress $\tau_{r\phi}$ vanishes everywhere throughout the axisymmetric flow field, whereas the normal viscous stress τ_{rr} is zero only at the fluid–solid interface and far from the sphere. The important results from this section are summarized as follows:

$$\mathbf{F}_{\text{fluid-solid}} = -R^2 \iint (\delta_r p + \delta_\theta \tau_{r\theta})_{\text{at } r=R} \sin\theta \, d\theta \, d\phi \tag{8-155}$$

$$p(r = R, \theta) = p_\infty - \left(\rho g R + \frac{3\mu V_{\text{approach}}}{2R} \right) \cos\theta \tag{8-156}$$

$$\tau_{r\theta}(r = R) = \frac{3\mu V_{\text{approach}}}{2R} \sin\theta \tag{8-157}$$

Integration with respect to polar angle θ is performed from 0 to π, and integration with respect to longitudinal angle ϕ is performed from 0 to 2π. In spherical coordinates, δ_r and δ_θ are functions of position and, hence, cannot be removed from the integrals. The general strategy for integrating unit vectors in curvilinear coordinates is to apply trigonometry and re-express these position-dependent unit vectors in terms of rectangular unit vectors δ_x, δ_y, and δ_z, which are not functions of position. The appropriate relations are provided by equations A.6-28 and A.6-29 in Bird *et al*. (2002, p. 828):

$$\delta_r = \delta_x \sin\theta \cos\phi + \delta_y \sin\theta \sin\phi + \delta_z \cos\theta \tag{8-158a}$$

$$\delta_\theta = \delta_x \cos\theta \cos\phi + \delta_y \cos\theta \sin\phi - \delta_z \sin\theta \tag{8-158b}$$

Nine trigonometric integrals are required to evaluate completely the total vector force exerted by the fluid on the solid sphere. However, seven of these integrals vanish because

$$\int \cos\phi \, d\phi = \int \sin\phi \, d\phi = \int \cos\theta \sin\theta \, d\theta = 0 \qquad 0 \le \phi \le 2\pi, \quad 0 \le \theta \le \pi \tag{8-159}$$

The two terms that survive are

$$\mathbf{F}_{\text{fluid-solid}} = \delta_z \left(\rho g R^3 + \frac{3}{2} \mu R V_{\text{approach}} \right) \iint \cos^2 \theta \sin \theta \, d\theta \, d\phi + \delta_z \frac{3}{2} \mu R V_{\text{approach}} \iint \sin^3 \theta \, d\theta \, d\phi \tag{8-160}$$

where the first term represents a contribution from fluid pressure and the second term arises from viscous shear stress. The integrals of interest are evaluated as follows:

$$\iint \cos^2 \theta \sin \theta \, d\theta \, d\phi = \frac{4}{3} \pi \qquad 0 \le \theta \le \pi, \qquad 0 \le \phi \le 2\pi \tag{8-161a}$$

$$\iint \sin^3 \theta \, d\theta \, d\phi = \frac{8}{3} \pi \qquad 0 \le \theta \le \pi, \qquad 0 \le \phi \le 2\pi \tag{8-161b}$$

The source of each contribution to the final expression for $\mathbf{F}_{\text{fluid-solid}}$ is

$$\begin{aligned} \mathbf{F}_{\text{fluid-solid}} = {} & \delta_z \tfrac{4}{3} \pi R^3 \rho g && \text{(hydrostatic effect of gravity on fluid pressure)} \\ & + \delta_z 2\pi \mu R V_{\text{approach}} && \text{(hydrodynamic contribution from fluid pressure)} \\ & + \delta_z 4\pi \mu R V_{\text{approach}} && \text{(hydrodynamic contribution from viscous shear)} \end{aligned} \tag{8-162}$$

8-6.7 Stokes's Law

The final result given by equation (8-162) is generalized for creeping flow of an incompressible Newtonian fluid that impinges on a stationary sphere with constant approach velocity $\mathbf{V}_{\text{approach}}$ from any direction:

$$\mathbf{F}_{\text{fluid-solid}} = -\tfrac{4}{3} \pi R^3 \rho \mathbf{g} + \zeta \mathbf{V}_{\text{approach}} \tag{8-163}$$

The first term on the right side of (8-163) represents a hydrostatic buoyant force due to fluid pressure that acts in the direction opposite gravity. This force remains operative when the fluid is at rest. The second term on the right side of (8-163) represents dynamic contributions from fluid pressure (i.e., 33%) and viscous shear stress (i.e., 67%) which act in the direction of the approach velocity. This dynamic force vanishes under hydrostatic conditions. The friction coefficient ζ, which is the inverse of fluid mobility, is given by

$$\zeta = 6\pi \mu_{\text{fluid}} R_{\text{sphere}} \tag{8-164}$$

if a single spherical object perturbs the fluid streamlines. The Stokes's law dynamic force is $\zeta \mathbf{V}_{\text{approach}}$, which applies for Reynolds number less than 0.5 based on the sphere diameter. The Stokes's law expression for the friction

coefficient, given by equation (8-164), is combined with Einstein's diffusion equation to estimate liquid-phase diffusion coefficients.

Friction Factor/Reynolds Number Correlation for Flow Around Spheres. The magnitude of the dynamic force exerted across the fluid–solid interface provides the basis for macroscopic momentum transfer correlations. The component of this dynamic force in the primary flow direction,

$$(\delta_z \cdot \mathbf{F}_{\text{fluid-solid}})_{\text{dynamic}} = \zeta \delta_z \cdot \mathbf{V}_{\text{approach}} = 6\pi \mu_{\text{fluid}} R_{\text{sphere}} V_{\text{approach}} \equiv \pi R^2 (\tfrac{1}{2} \rho V_{\text{approach}}^2) f \tag{8-165}$$

is useful to define the friction factor f. In (8-165), πR^2 represents a characteristic surface area normal to the bulk fluid flow and $\frac{1}{2}\rho V_{\text{approach}}^2$ is the characteristic kinetic energy per unit volume of fluid. Rearrangement of equation (8-165) yields

$$f = \frac{24}{\text{Re}} \tag{8-166}$$

where

$$\text{Re} = \frac{\rho V_{\text{approach}} (2R)}{\mu} \leq 0.5$$

in the creeping flow regime. The following experimental correlations have been obtained at higher Reynolds numbers, where analytical solution of the equation of motion is much more difficult, if not impossible:

$$f \approx \begin{cases} \dfrac{18.5}{\text{Re}^{0.6}} & 2 < \text{Re} < 500 \\ 0.44 & 500 < \text{Re} < 2 \times 10^5 \end{cases} \tag{8-167}$$

Generalized Interpretation of f vs. Re. When the characteristic velocity and the Reynolds number increase, the friction factor for flow around solid spheres decreases if Re < 500, and f remains approximately constant at 0.44 if Re $>$ 500. However, the dynamic force transmitted across the fluid–solid interface increases at higher Reynolds numbers in all flow regimes. The generalized correlations are

$$(\delta_z \cdot \mathbf{F}_{\text{fluid-solid}})_{\text{dynamic}} = \pi R^2 (\tfrac{1}{2} \rho V_{\text{approach}}^2) f \tag{8-168}$$

$$f = \frac{\text{constant}}{\text{Re}^a} \tag{8-169}$$

where the exponent a is the negative slope of f vs. Re on log-log coordinates. The dependence of $(\delta_z \cdot \mathbf{F}_{\text{fluid-solid}})_{\text{dynamic}}$ on density, viscosity, and approach velocity of the fluid is

$$(\delta_z \cdot \mathbf{F}_{\text{fluid-solid}})_{\text{dynamic}} \approx \mu^a \rho^{1-a} (V_{\text{approach}})^{2-a} \tag{8-170}$$

Intuitively, this interfacial force should increase for fluids with (1) higher viscosity in the creeping flow regime, (2) higher density in the turbulent regime, and (3) higher flow rates in general. Hence, the acceptable range of the exponent a is $0 \leq a \leq 1$. In the creeping flow regime where $a = 1$,

$$(\delta_z \cdot \mathbf{F}_{\text{fluid-solid}})_{\text{dynamic}} \approx \mu V_{\text{approach}} \tag{8-171}$$

At high flow rates around spheres where Re > 500, $a = 0$ and

$$(\delta_z \cdot \mathbf{F}_{\text{fluid-solid}})_{\text{dynamic}} \approx \rho V_{\text{approach}}^2 \tag{8-172}$$

Shortcut Methods for Axisymmetric Creeping Flow in Spherical Coordinates. All the previous results can be obtained rather quickly with assistance from information in Happel and Brenner (1965, pp. 133–138). For example, the general solution for the stream function for creeping viscous flow is

$$\psi(r, \theta) = \sum_{n=z}^{\infty} (A_n r^n + B_n r^{1-n} + C_n r^{2+n} + D_n r^{3-n}) L_n(\cos\theta) \tag{8-173}$$

where the first few Legendre polynomials that describe the angular dependence of ψ are

$$\begin{aligned} L_0(\cos\theta) &= 1 \\ L_1(\cos\theta) &= -\cos\theta \\ L_2(\cos\theta) &= \tfrac{1}{2}\sin^2\theta \\ L_3(\cos\theta) &= \tfrac{1}{2}\sin^2\theta\cos\theta \end{aligned} \tag{8-174}$$

Boundary conditions far from the sphere suggest that only $L_2(\cos\theta)$ is required for Stokes's flow around solid spheres and gas bubbles. Hence, $A_n = B_n = C_n = D_n = 0$ for $n \neq 2$ and

$$\psi(r, \theta) = \frac{1}{2}\sin^2\theta \left(A_2 r^2 + \frac{B_2}{r} + C_2 r^4 + D_2 r \right) \tag{8-175}$$

which agrees with the separation of variables solution given by equation (8-127). Furthermore, the z-component of the dynamic force transmitted across the fluid–solid boundary at $r = R$ for all spherical coordinate axisymmetric problems in any flow regime is given by

$$(\delta_z \cdot \mathbf{F}_{\text{fluid-solid}})_{\text{dynamic}} = 4\pi\mu D_2 \tag{8-176}$$

where D_2 is the coefficient of $\frac{1}{2} r \sin^2\theta$ in the final expression for ψ. Alternatively,

$$(\delta_z \cdot \mathbf{F}_{\text{fluid-solid}})_{\text{dynamic}} = 8\pi\mu \lim_{r\to\infty} \left\{ \frac{\psi(r, \theta) - \psi(r \to \infty, \theta)}{r \sin^2\theta} \right\} \tag{8-177}$$

Verification that both of these prescriptions lead to Stokes's law is left as a problem assignment for the motivated student.

8-6.8 Momentum Boundary Conditions at a Gas–Liquid Interface

Consider two immiscible fluids in contact across a flat interface where surface tension and surface tension gradients are not an issue. Translation of the interface is allowed, but deformation is forbidden. Hence, $(\mathbf{n} \cdot \mathbf{v}_{\text{fluid}})_{\text{at interface}} = 0$, which also implies that there is no mass transfer across the interface. $\mathbf{n}$ is a unit normal vector extending from the interface into one of the phases. Continuity of the velocity vector on each side of the interface yields the following result for contact between a gas and a liquid:

$$(\mathbf{v}_{\text{gas}})_{\text{at interface}} = (\mathbf{v}_{\text{liquid}})_{\text{at interface}} \tag{8-178}$$

If the interface is stationary, or if it translates without accelerating, then a steady-state force balance given by equation (8-180) states that the sum of all surface-related forces acting on the interface must vanish. Body forces are not an issue because the system (i.e., the gas–liquid interface) exhibits negligible volume. The total mass flux vector of an adjacent phase relative to a mobile interface is

$$\rho_{\text{phase}}(\mathbf{v}_{\text{phase}} - \mathbf{v}_{\text{surface}}) \tag{8-179}$$

and $\mathbf{v}_{\text{phase}}$ represents the momentum of that phase per unit mass. These considerations are necessary to construct an expression for surface forces due to convective momentum flux. If $\mathbf{n}$ represents a unit normal vector directed from the interface into the liquid phase, then the force balance at a gas–liquid interface is

$$\int_S \{\mathbf{n} \cdot [\rho_{\text{gas}}\mathbf{v}_{\text{gas}}(\mathbf{v}_{\text{gas}} - \mathbf{v}_{\text{surface}}) + \tau_{\text{gas}}] + \mathbf{n}p_{\text{gas}}\}_{\text{at interface}}\, dS + \int_S \{-\mathbf{n} \cdot [\rho_{\text{liquid}}\mathbf{v}_{\text{liquid}}(\mathbf{v}_{\text{liquid}} - \mathbf{v}_{\text{surface}}) + \tau_{\text{liquid}}] - \mathbf{n}p_{\text{liquid}}\}_{\text{at interface}}\, dS = 0 \tag{8-180}$$

where S is the surface area of the system. The nondeformable nature of the interface, in addition to the fact that there is no mass transfer across it, eliminates contributions from convective momentum flux on both sides of the interface. If the gas is ideal and monatomic and the liquid is incompressible, then Newton's law of viscosity relates viscous stress to velocity gradients in each phase as follows:

$$\tau_{\text{gas}} = -\mu_{\text{gas}}[\nabla\mathbf{v}_{\text{gas}} + (\nabla\mathbf{v}_{\text{gas}})^{\text{T}}] + \frac{2}{3}\mu_{\text{gas}}(\nabla \cdot \mathbf{v}_{\text{gas}}) \sum_i \delta_i\delta_i$$

$$\tau_{\text{liquid}} = -\mu_{\text{liquid}}[\nabla\mathbf{v}_{\text{liquid}} + (\nabla\mathbf{v}_{\text{liquid}})^{\text{T}}] \tag{8-181}$$

Since gas-phase viscosities are typically 100- to 1000-fold smaller than liquid-phase viscosities (i.e., $\mu_{\text{gas}} \ll \mu_{\text{liquid}}$), it is reasonable to neglect viscous forces in the gas phase relative to those in the liquid phase. The simplified force balance, subject to these assumptions, becomes

$$\int_S (\mathbf{n} p_{\text{gas}} - \mathbf{n} \cdot \tau_{\text{liquid}} - \mathbf{n} p_{\text{liquid}})_{\text{at interface}} \, dS = 0 \tag{8-182}$$

The integrand of (8-182) must vanish since there are several choices for the integration limits which define the system. Hence,

$$(\mathbf{n} p_{\text{gas}})_{\text{at interface}} = (\mathbf{n} \cdot \tau_{\text{liquid}} + \mathbf{n} p_{\text{liquid}})_{\text{at interface}} \tag{8-183}$$

If surface tension γ and surface tension gradients $\nabla\gamma$ are important, then the interfacial force balance includes terms that augment the gas-phase pressure:

$$(\mathbf{n} p_{\text{gas}})_{\text{at interface}} = (\mathbf{n} \cdot \tau_{\text{liquid}} + \mathbf{n} p_{\text{liquid}})_{\text{at interface}} + \mathbf{n}\gamma \left(\frac{1}{R_1} + \frac{1}{R_2} \right) + \nabla\gamma \tag{8-184}$$

R_1 and R_2 are the principal radii of curvature of the interface. For bubbles dispersed in a continuous liquid phase, both R_1 and R_2 correspond to the bubble radius. This vector force balance at the gas–liquid interface implies the following scalar results:

1. In the absence of surface tension gradients, which only exist, at most, in coordinate directions that constitute the surface, all shear components of $(\mathbf{n} \cdot \tau_{\text{liquid}})_{\text{at interface}}$ must vanish. This condition is invoked for flow around a gas bubble in the next section. The importance of surface tension gradients could invalidate the use of this boundary condition.
2. The normal component of the interfacial force balance requires that p_{gas} must be balanced by the sum of p_{liquid}, normal viscous stress, and surface tension effects. Under hydrostatic conditions where $\tau = 0$, Laplace's equation for surface phenomena yields

$$p_{\text{gas}} = p_{\text{liquid}} + \frac{2\gamma}{R_{\text{bubble}}} \tag{8-185}$$

where R_{bubble} is the bubble radius. Since the radii of curvature are infinite for a flat interface, (8-185) indicates that p_{gas} and p_{liquid} are equal on both sides of a flat interface under hydrostatic conditions.

Summary of Results for Creeping Viscous Flow Around a Gas Bubble. The shortcut method described above and boundary conditions at a gas–liquid interface are useful to analyze creeping flow of an incompressible Newtonian fluid

around a stationary bubble. The final macroscopic results also apply to nondeformable bubbles that rise slowly through a quiescent liquid. When the bubble is stationary and the fluid moves with velocity $\delta_z V_{\text{approach}}$, boundary conditions at $r \to \infty$ lead to the same functional form of ψ that was adopted for flow around a solid. In other words, the nature of the interface (i.e., gas–liquid or solid–liquid) is not critical in postulating the functional dependence of $\psi(r, \theta)$. Hence, $L_2(\cos\theta)$ is selected to match the boundary conditions far from the bubble. The solution to $E^2(E^2\psi) = 0$ is

$$\psi(r, \theta) = \frac{1}{2}\sin^2\theta\left(A_2 r^2 + \frac{B_2}{r} + C_2 r^4 + D_2 r\right) \tag{8-186}$$

with $C_2 = 0$ and $A_2 = -V_{\text{approach}}$ if the fluid impinges on the southern hemisphere of the bubble (i.e., upward). The other boundary conditions are as follows:

1. There is no volumetric flow through the bubble:

$$\psi(r = R, \theta) = 0$$

2. The bubble is nondeformable:

$$v_r(r = R, \theta) = \frac{-1}{R^2 \sin\theta}\left(\frac{\partial\psi}{\partial\theta}\right)_{r=R} = 0$$

3. The interface is characterized by zero shear stress:

$$\tau_{r\theta}(r = R) = -\mu\left[r\frac{\partial}{\partial r}\left(\frac{v_\theta}{r}\right) + \frac{1}{r}\frac{\partial v_r}{\partial\theta}\right]_{r=R} = 0$$

which lead to $B_2 = 0$ and $D_2 = RV_{\text{approach}}$. Final results for the stream function and both nonzero components of the velocity vector are

$$\begin{aligned}
\psi(r, \theta) &= -\tfrac{1}{2}V_{\text{approach}}R^2\sin^2\theta(\eta^2 - \eta) \\
v_r(r, \theta) &= V_{\text{approach}}\cos\theta(1 - \eta^{-1}) \\
v_\theta(r, \theta) &= -V_{\text{approach}}\sin\theta(1 - \tfrac{1}{2}\eta^{-1})
\end{aligned} \tag{8-187}$$

where $\eta = r/R$. Notice that the bubble does not deform in the r direction, but there is slip at the gas–liquid interface [i.e., $v_\theta(r = R, \theta) \neq 0$]. Similar to the analysis presented earlier, the r and θ components of the equation of motion yield the following exact differential expressions for dynamic pressure in the vicinity of the bubble:

$$\frac{\partial \mathfrak{P}}{\partial r} = \frac{2\mu V_{\text{approach}}}{R^2}\eta^{-3}\cos\theta \tag{8-188a}$$

$$\frac{\partial \mathfrak{P}}{\partial \theta} = \frac{\mu V_{\text{approach}}}{R}\eta^{-2}\sin\theta \tag{8-188b}$$

The final results for dynamic pressure and fluid pressure are

$$\mathfrak{P}(r,\theta) = \mathfrak{P}_\infty - \frac{\mu V_{\text{approach}}}{R}\eta^{-2}\cos\theta \tag{8-189a}$$

$$p(r,\theta) = p_\infty - \rho g r\cos\theta - \left(\frac{\mu V_{\text{approach}}}{R}\right)\eta^{-2}\cos\theta \tag{8-189b}$$

If one applies equation (8-153) to gas–liquid interfaces, the total force exerted by the fluid on the bubble across the nondeformable zero-shear boundary is due exclusively to normal stresses:

$$\begin{aligned}\mathbf{F}_{\text{fluid-bubble}} &= -R^2\iint[\delta_r(\tau_{rr}+p)]_{\text{at } r=R}\sin\theta\,d\theta\,d\phi\\ &= \delta_z\cdot\tfrac{4}{3}\pi R^3\rho g && \text{(Hydrostatic effect of gravity on fluid pressure)}\\ &\quad + \delta_z\cdot\tfrac{4}{3}\pi\mu R V_{\text{approach}} && \text{(Hydrodynamic contribution from fluid pressure)}\\ &\quad + \delta_z\cdot\tfrac{8}{3}\pi\mu R V_{\text{approach}} && \text{(Hydrodynamic contribution from } \tau_{rr})\end{aligned} \tag{8-190}$$

The z-component of the dynamic force transmitted across the gas–liquid boundary at $r = R$ is given by

$$(\delta_z\cdot\mathbf{F}_{\text{fluid-bubble}})_{\text{dynamic}} = 4\pi\mu D_2 = 4\pi\mu_{\text{fluid}} R_{\text{bubble}} V_{\text{approach}} \tag{8-191}$$

due to normal viscous stress τ_{rr} (i.e., 67%) and fluid pressure (i.e., 33%). This is the Stokes's law analog for zero-shear interfaces, whereas results presented earlier in this chapter apply to high-shear liquid–solid interfaces. The dimensionless macroscopic momentum transfer correlation for creeping viscous flow of an incompressible Newtonian fluid around a bubble is $f = 16/\text{Re}$, where $\text{Re} < 0.5$ is based on the bubble diameter.

Creeping Viscous Flow Solutions for Gas Bubbles Which Rise Through Incompressible Newtonian Fluids That Are Stagnant Far from the Submerged Objects. A nondeformable bubble of radius R rises through an incompressible Newtonian fluid such that

$$\mathbf{v}_{\text{bubble}} = \delta_z V_{\text{bubble}} \tag{8-192}$$

This motion of the bubble induces axisymmetric two-dimensional flow in the liquid phase such that creeping viscous flow is appropriate. The Reynolds number for this problem is based on the rise velocity of the bubble, its diameter (i.e., $2R$), and the momentum diffusivity of the liquid. Since the left sides of both the

low-Reynolds-number equation of motion and the ϕ-component of the vorticity equation are neglected, one calculates the stream function from

$$E^2(E^2\psi) = 0 \tag{8-193}$$

The general solution for ψ is

$$\psi(r, \theta) = \sin^2\theta \left(\frac{A}{r} + Br + Cr^2 + Dr^4\right) \tag{8-194}$$

Expressions for the two nonzero velocity components are given by

$$v_r(r, \theta) = -\frac{1}{r^2 \sin\theta}\frac{\partial\psi}{\partial\theta} = -2\cos\theta \left(\frac{A}{r^3} + \frac{B}{r} + C + Dr^2\right) \tag{8-195a}$$

$$v_\theta(r, \theta) = \frac{1}{r \sin\theta}\frac{\partial\psi}{\partial r} = \sin\theta \left(-\frac{A}{r^3} + \frac{B}{r} + 2C + 4Dr^2\right) \tag{8-195b}$$

If one chooses an orthogonal body-fixed coordinate system in which the center of the bubble coincides with the origin of the coordinate system throughout the motion of the bubble, then microscopic results for ψ, v_r, and v_θ are given by equation (8-187), where the bubble and the coordinate system were stationary. In other words, an observer in this translating reference frame sees a stationary bubble and a fluid that moves downward. This is the preferred approach to calculate the steady-state fluid velocity profile and analyze convective mass transfer via boundary layer theory at very large Schmidt numbers. A slightly different analysis that yields the same macroscopic results, but different microscopic results, is based on the following conditions: (1) the bubble achieves its terminal rise velocity to justify steady-state analysis, and (2) calculations are performed when the center of the bubble coincides with the origin of a stationary orthogonal coordinate system. Now the bubble is rising and the fluid is stagnant at large r, according to an observer in this stationary reference frame. The latter analysis, which employs a stationary coordinate system, requires that the following boundary conditions should be invoked to calculate integration constants A, B, C, and D.

1. The fluid is quiescent far from the bubble, which implies that

$$v_r(r \to \infty, \theta) = 0$$
$$v_\theta(r \to \infty, \theta) = 0$$

2. The bubble is nondeformable. Hence, the radial component of the bubble rise velocity must match v_r of the liquid at the gas–liquid interface:

$$v_r(r = R, \theta) = \delta_r \cdot \mathbf{v}_{\text{bubble}} = V_{\text{bubble}} \cos\theta$$

3. The interface is characterized by zero shear stress:

$$\tau_{r\theta}(r = R) = -\mu \left[r \frac{\partial}{\partial r} \left(\frac{v_\theta}{r} \right) + \frac{1}{r} \frac{\partial v_r}{\partial \theta} \right]_{r=R} = 0$$

Condition 1 requires that $C = 0$ and $D = 0$. According to condition 2,

$$-2 \cos\theta \left(\frac{A}{R^3} + \frac{B}{R} \right) = V_{\text{bubble}} \cos\theta \tag{8-196}$$

At any position within this Newtonian fluid, one calculates the $r-\theta$ component of the viscous stress tensor as follows:

$$\begin{aligned} \tau_{r\theta} &= -\mu \left\{ r \sin\theta \left[\frac{d}{dr} \left(-\frac{A}{r^4} + \frac{B}{r^2} \right) \right] + 2 \sin\theta \left(\frac{A}{r^4} + \frac{B}{r^2} \right) \right\} \\ &= -\frac{6\mu A \sin\theta}{r^4} \end{aligned} \tag{8-197}$$

Obviously, integration constant A must be zero to satisfy the zero shear condition 3 at the gas–liquid interface. Now condition 2 is satisfied when $2B = -RV_{\text{bubble}}$. The final results for the stream function and the fluid velocity profile are

$$\begin{aligned} \psi(r, \theta) &= -\tfrac{1}{2} V_{\text{bubble}} R r \sin^2\theta \\ v_r(r, \theta) &= V_{\text{bubble}} \eta^{-1} \cos\theta \\ v_\theta(r, \theta) &= -\tfrac{1}{2} V_{\text{bubble}} \eta^{-1} \sin\theta \end{aligned} \tag{8-198}$$

where $\eta = r/R$. If one multiplies the coefficient of $\frac{1}{2} r \sin^2\theta$ in the expression for ψ by $4\pi\mu_{\text{fluid}}$, then the Stokes's law hydrodynamic drag force exerted by the fluid on the bubble across the interface at $r = R$ is obtained (i.e., $-4\pi\mu_{\text{fluid}} R V_{\text{bubble}}$). This force is negative because it acts (1) in the flow direction of the approaching fluid when the bubble is stationary, (2) in the opposite direction of the motion of the submerged object when the fluid is stationary, or (3) in the direction that describes the relative motion of the fluid with respect to the submerged object. In all of these cases, the hydrodynamic drag force exerted by an incompressible Newtonian fluid on the rising bubble is downward, in the negative z direction.

8-7 POTENTIAL FLOW THEORY

Generalized vector analysis is presented in this section for fluid flow adjacent to zero-shear interfaces in the laminar regime. The following adjectives have been used to characterize potential flow: *inviscid*, *irrotational*, *ideal*, and *isentropic*. Ideal fluids experience no viscous stress because their viscosities are exceedingly small (i.e., $\mu \to 0$). Hence, the $\nabla \cdot \tau$ term in the equation of motion is negligible

even though velocity gradients exist. The irrotational aspect of potential flow provides a convenient mathematical description from which one constructs an expression for the velocity vector. Since irrotational flow implies that there is no vorticity, the defining equation for potential flow at the microscopic level is

$$\nabla \times \mathbf{v} = 0 \tag{8-199}$$

For solid-body rotation at constant angular velocity, the vorticity vector, defined by $\frac{1}{2}(\nabla \times \mathbf{v})$, is equivalent to the angular velocity vector of the solid. For two-dimensional flow in cylindrical coordinates, with $v_r(r, \theta)$ and $v_\theta(r, \theta)$, the volume-averaged vorticity vector,

$$\frac{1}{V}\int_V \frac{1}{2}(\nabla \times \mathbf{v})\, dV = \frac{1}{2\pi R^2 L}\int_V \left\{\delta_r\left(\frac{1}{r}\frac{\partial v_z}{\partial \theta} - \frac{\partial v_\theta}{\partial z}\right) + \delta_\theta\left(\frac{\partial v_r}{\partial z} - \frac{\partial v_z}{\partial r}\right) + \delta_z\left[\frac{1}{r}\frac{\partial (r v_\theta)}{\partial r} - \frac{1}{r}\frac{\partial v_r}{\partial \theta}\right]\right\} r\, dr\, d\theta\, dz \tag{8-200}$$

simplifies considerably to

$$\begin{aligned}\frac{1}{V}\int_V \frac{1}{2}(\nabla \times \mathbf{v})\, dV &= \frac{1}{2\pi R^2}\delta_z \int_0^{2\pi}\int_0^R \left[\frac{1}{r}\frac{\partial (r v_\theta)}{\partial r} - \frac{1}{r}\frac{\partial v_r}{\partial \theta}\right] r\, dr\, d\theta \\ &= \frac{1}{2\pi R^2}\delta_z \left\{\int_0^{2\pi} R v_\theta(r = R, \theta)\, d\theta \right. \\ &\quad \left. - \int_0^R [v_r(r, \theta = 2\pi) - v_r(r, \theta = 0)]\, dr\right\}\end{aligned} \tag{8-201}$$

The second integral of (8-201) vanishes, due to the periodicity of v_r at $\theta = 0$ and 2π. Hence, the volume-averaged vorticity

$$\begin{aligned}\frac{1}{V}\int_V \frac{1}{2}[\nabla \times \mathbf{v}]\, dV &= \frac{1}{2\pi R}\delta_z \int_0^{2\pi} v_\theta(r = R, \theta)\, d\theta \\ &= \frac{\delta_z \langle v_\theta(r = R)\rangle}{R} = \delta_z\, \langle \Omega \rangle\end{aligned} \tag{8-202}$$

is equivalent to the average angular velocity of the fluid $\langle \Omega \rangle$, based on the following definition of the average θ-component of the velocity vector at the outer boundary where $r = R$:

$$\langle v_\theta(r = R)\rangle \equiv \frac{1}{2\pi}\int_0^{2\pi} v_\theta(r = R, \theta)\, d\theta \tag{8-203}$$

Potential flow in liquids implies that there are no rotational tendencies within the fluid, especially near a boundary. The microscopic description of potential flow, given by (8-199), requires that the vorticity vector must vanish. The macroscopic

description of potential flow, given by (8-202), requires that there is no large-scale vorticity, which implies that the volume-averaged vorticity vector must vanish. From a mathematical viewpoint based on the microscopic description, the vorticity vector will vanish if one identifies any scalar velocity potential Φ (not to be confused with the gravitational potential energy per unit mass of fluid), such that $\mathbf{v} = \nabla\Phi$ because $\nabla \times \nabla\Phi = 0$ via Stokes's theorem if Φ is an exact differential. This is true for any multivariable scalar function that is analytic because the order of mixed second partial differentiation can be reversed without affecting the final result. Hence, the requirement of no vorticity at the microscopic level, which is consistent with irrotational flow, suggests that the fluid velocity vector can be expressed as the gradient of a scalar velocity potential. However, the requirement of no vorticity does not provide a unique function for Φ because any scalar that is an exact differential will satisfy $\nabla \times \nabla\Phi = 0$. The unique scalar velocity potential for a particular inviscid flow problem is calculated by invoking incompressibility. Hence,

$$\nabla \cdot \mathbf{v} = \nabla \cdot \nabla\Phi = \nabla^2\Phi = 0 \tag{8-204}$$

which is Laplace's equation. Potential flow solutions in n dimensions (i.e, $1 \leq n \leq 3$) are obtained by solving one second-order partial differential equation (i.e., Laplace's equation) for Φ in terms of n independent spatial variables. This is one of the most straightforward routes to calculate three-dimensional flows. For special classes of two-dimensional flows in which the two important components of the velocity vector are not a function of the spatial coordinate in the no-flow direction, it is also possible to solve potential flow problems rather easily via the stream function ψ. In this case, ψ is constructed to guarantee incompressibility. In other words, the relation between ψ and the two important velocity components automatically satisfies the equation of continuity for any scalar, such as ψ, which is an exact differential. The unique stream function that corresponds to a specific potential flow solution is obtained by invoking no vorticity at the microscopic level. Fluid parcels move along streamlines, where each streamline is defined by a constant value of ψ. Streamlines intersect lines of equipotential (i.e., defined by a constant value of Φ) at right angles. Hence, the complete solution to potential flow problems can be visualized as a web constructed from streamlines and equipotentials. For two-dimensional planar potential flows that do not contain an axis of symmetry, both Φ and ψ satisfy Laplace's equation; $\nabla^2\Phi = 0$ is a consequence of invoking incompressibility, and $\nabla^2\psi = 0$ represents the nontrivial component of the fluid vorticity vector, which must vanish for irrotational flow. Hence, if Φ and ψ represent the scalar velocity potential and stream function, respectively, for a planar potential flow problem, then one can interchange Φ and ψ to generate another planar potential flow solution because these two functions both satisfy Laplace's equation. For two-dimensional axisymmetric flows in cylindrical and spherical coordinates, the nature of the relation between the stream function and the important components of the velocity vector, together with the fact that the vorticity vector must vanish, yields $\mathbf{E}^2\psi = 0$ instead of Laplace's

equation. However, the scalar velocity potential Φ is always calculated from Laplace's equation for all potential flow problems in any coordinate system.

8-7.1 Use of the Potential Flow Equation of Motion to Calculate Dynamic Pressure

The discussion in the preceding section reveals that n-dimensional ideal fluid flow solutions can be obtained without using the equation of motion. Now the generalized vector force balance is manipulated to calculate dynamic pressure. The starting point is the equation of motion for generalized incompressible fluids, given by equation (8-39):

$$\rho\left(\frac{\partial \mathbf{v}}{\partial t} + \mathbf{v}\cdot\nabla\mathbf{v}\right) = -\nabla\cdot\tau - \nabla\mathfrak{P} \tag{8-205}$$

The following assumptions are invoked. Steady-state analysis eliminates the first term on the left side of (8-205). The absence of viscous stress in ideal fluids eliminates the first term on the right side. Hence, the steady-state potential flow equation of motion reduces to

$$\rho\mathbf{v}\cdot\nabla\mathbf{v} = -\nabla\mathfrak{P} \tag{8-206}$$

This represents a balance between forces due to convective momentum flux, fluid pressure, and gravity. The vector-tensor identity presented in Problem 8-7 is used to re-express forces due to convective momentum flux:

$$\mathbf{v}\cdot\nabla\mathbf{v} = \tfrac{1}{2}\nabla(\mathbf{v}\cdot\mathbf{v}) - \mathbf{v}\times(\nabla\times\mathbf{v}) \tag{8-207}$$

Obviously, the second-term on the right side of this identity vanishes for ideal fluid flow in which the vorticity vector vanishes. Hence, for incompressible fluids with constant density,

$$\rho\mathbf{v}\cdot\nabla\mathbf{v} = \nabla(\tfrac{1}{2}\rho\mathbf{v}\cdot\mathbf{v}) = -\nabla\mathfrak{P} \tag{8-208}$$

Rearrangement yields

$$\nabla(\tfrac{1}{2}\rho\mathbf{v}\cdot\mathbf{v} + \mathfrak{P}) = 0 \tag{8-209}$$

Steady-state analysis implies that the combination of fluid kinetic energy per unit volume and dynamic pressure is not time dependent. The potential flow equation of motion suggests that this combination of fluid kinetic energy per unit volume and dynamic pressure is not a function of any independent spatial variable. Consequently,

$$\tfrac{1}{2}\rho\mathbf{v}\cdot\mathbf{v} + \mathfrak{P} = \text{constant} \tag{8-210}$$

This is the ideal isentropic Bernoulli equation, or the ideal mechanical energy balance, which neglects the irreversible dissipation of mechanical energy to thermal

energy. The neglect of friction loss is reasonable for ideal fluids. Equation (8-210) states that the combination of fluid kinetic energy per unit volume, fluid pressure, and gravitational potential energy per unit volume is the same at any point within the fluid. The constant in (8-210) is easiest to evaluate in the horizontal reference plane which corresponds to the zero of potential energy. After the velocity potential, or the stream function, and the nonzero components of the velocity vector have been solved, dynamic and fluid pressure distributions are calculated as follows:

$$\mathfrak{P} = p + \rho g h = \text{constant} - \tfrac{1}{2}\rho \mathbf{v} \cdot \mathbf{v} \tag{8-211}$$

8-7.2 Applications of Potential Flow

In the preceding two sections we described the general methodology for analyzing laminar flow of ideal fluids. In the following sections we present detailed calculations for potential flow around spheres and cylinders. In most cases, it is necessary to put a submerged object into the flow field to distort the streamlines and equipotentials, and generate a challenging problem. However, one must exercise caution when applying the results that are obtained. For example, there is no difference between potential flow solutions around solid spheres and nondeformable gas bubbles. The nature of the interface never influences the solution of Laplace's equation or the boundary conditions because viscous stress is neglected. From a practical viewpoint, potential flow around nondeformable gas bubbles is more realistic and useful than the corresponding flow problems around solid spheres because gas–liquid interfaces are characterized by zero shear and perfect slip. In contrast, solid–liquid interfaces exhibit significant viscous shear and no slip. Since ideal fluids have negligible viscosity, all potential flow solutions reveal significant slip with respect to the velocity component that is parallel to the interface. Consider the following comments about potential flow theory prior to adopting any of the results that emerge from the solution of Laplace's equation.

1. When a nondeformable object is implanted in the flow field and the streamlines and equipotentials are distorted, the nature of the interface does not affect the potential flow velocity profiles. However, the results should not be used with confidence near high-shear no-slip solid–liquid interfaces because the theory neglects viscous shear stress and predicts no hydrodynamic drag force. In the absence of accurate momentum boundary layer solutions adjacent to gas–liquid interfaces, potential flow results provide a reasonable estimate for liquid-phase velocity profiles in the laminar flow regime. Hence, potential flow around gas bubbles has some validity, even though an exact treatment of gas–liquid interfaces reveals that normal viscous stress is important (i.e., see equation 8-190). Unfortunately, there are no naturally occurring zero-shear perfect-slip interfaces with cylindrical symmetry.

2. When forces due to convective and viscous momentum flux are equally important, and neither creeping flow nor potential flow is appropriate, boundary layer theory must be invoked. Coupled solutions to the equation of continuity and the equation of motion require knowledge of the dynamic pressure gradient within the momentum boundary layer. Potential flow theory is employed to calculate the dynamic pressure gradient outside the momentum boundary layer where there are no high-shear solid–liquid interfaces. Hence, $\nabla \mathfrak{P}$ is calculated from the potential flow equation of motion (i.e., equation 8-206), and this dynamic pressure gradient is imposed across the boundary layer. In this manner, two-dimensional momentum boundary layer problems are solved by considering the equation of continuity and the component of the equation of motion in the primary flow direction to calculate the two nonzero components of the fluid velocity vector. Potential flow theory provides useful information for momentum boundary layer problems in a region where there are no solid surfaces. It is difficult to envision why the dynamic pressure gradient in the primary flow direction should be different within the momentum boundary layer than outside the boundary layer.
3. Steady-state heat conduction in pure solids is described by the following thermal energy balance: $\nabla \cdot \mathbf{q} = 0$, where $\mathbf{q}$ represents the molecular flux of thermal energy, and contributions from convective heat transfer are identically zero. If one relates $\mathbf{q}$ to temperature gradients via Fourier's law of heat conduction for an isotropic solid, then the pure-component thermal energy balance with no chemical reactions reduces to

$$\nabla \cdot \mathbf{q} = \nabla \cdot (-k_{\mathrm{TC}} \nabla T) = -k_{\mathrm{TC}} \nabla \cdot \nabla T = -k_{\mathrm{TC}} \nabla^2 T = 0 \qquad (8\text{-}212)$$

   where k_{TC} is the thermal conductivity of the solid. Hence, one obtains temperature profiles in pure solids via the solution of Laplace's equation. This implies that generalized potential flow solutions for the scalar velocity potential are analogous to temperature profiles in solids with the same symmetry. The heat transfer problem is described appropriately as steady-state potential flow of heat in solids.
4. The velocity vector for viscous flow through porous media is described by Darcy's law, $\mathbf{v} = -k \nabla \mathfrak{P}$, where $\nabla \mathfrak{P}$ is the dynamic pressure gradient and k is the conductivity of the medium, which varies inversely with fluid viscosity. This relation between $\mathbf{v}$ and $\nabla \mathfrak{P}$ is reasonable when the particle size is small relative to the dimensions of the system, and the quantities of interest are averaged spatially over the cross section of a macroscopic *unit cell* that captures the periodicity of the porous medium. Darcy's law implies that there is no large-scale volume-averaged vorticity on the unit-cell level. However, the microscopic vorticity vector does not vanish within the momentum boundary layer adjacent to each individual particle. Since the microscopic description of flow through porous media is too difficult to formulate and solve, one relies on expressions for $\mathbf{v}$ and $\mathfrak{P}$ that are averaged spatially over the cross section of each unit cell. If one invokes

incompressibility via the equation of continuity, then dynamic pressure obeys Laplace's equation:

$$\nabla \cdot \mathbf{v} = \nabla \cdot (-k\nabla \mathfrak{P}) = -k\nabla^2 \mathfrak{P} = 0 \tag{8-213}$$

Hence, temperature profiles in pure isotropic solids, the scalar velocity potential for ideal fluid flow, and dynamic pressure profiles for flow through porous media are all based on the solution of Laplace's equation. Whenever the divergence of a vector vanishes and the vector is expressed as the gradient of a scalar, Laplace's equation is required to calculate the scalar profile.

Potential Flow around a Gas Bubble Via the Scalar Velocity Potential. An incompressible fluid with constant approach velocity (i.e., $\delta_z V_{\text{approach}}$) flows upward past a stationary nondeformable gas bubble of radius R. This two-dimensional flow is axisymmetric about the ϕ-axis such that $v_\phi = 0$ and there is no ϕ-dependence of v_r or v_θ. Hence, one must solve Laplace's equation for the scalar velocity potential $\Phi(r, \theta)$ in spherical coordinates because this coordinate system provides the best match with the macroscopic boundary at $r = R$. The appropriate partial differential equation for Φ is

$$\frac{1}{r^2}\frac{\partial}{\partial r}\left(r^2 \frac{\partial \Phi}{\partial r}\right) + \frac{1}{r^2 \sin\theta}\frac{\partial}{\partial \theta}\left(\sin\theta \frac{\partial \Phi}{\partial \theta}\right) = 0 \tag{8-214}$$

The boundary condition at large r is employed to calculate the radial and tangential velocity components, as well as the functional form of the scalar velocity potential. Since the velocity vector far from the bubble is

$$\mathbf{v} = \delta_z V_{\text{approach}} \qquad \text{at } r \to \infty \tag{8-215}$$

vector algebra allows one to determine the components of $\mathbf{v}$ in the r and θ directions. Then this information is coupled with the definition of $\mathbf{v}$ in terms of the gradient of the scalar velocity potential. For example,

$$v_r = \delta_r \cdot \mathbf{v} = (\delta_r \cdot \delta_z) V_{\text{approach}} = V_{\text{approach}} \cos\theta = (\nabla \Phi)_{r\text{-component}} = \frac{\partial \Phi}{\partial r} \tag{8-216}$$

Integration of (8-216) with respect to r at constant θ yields an expression for Φ at large r, realizing that the constant of integration can be a function of θ:

$$\Phi(r \to \infty, \theta) = V_{\text{approach}} r \cos\theta + f(\theta) \tag{8-217}$$

Now, this expression for the scalar velocity potential far from the bubble is compared with the tangential velocity component:

$$v_\theta = \delta_\theta \cdot \mathbf{v} = (\delta_\theta \cdot \delta_z) V_{\text{approach}} = V_{\text{approach}} \cos\left(\frac{\pi}{2} + \theta\right) = -V_{\text{approach}} \sin\theta$$

$$= (\nabla \Phi)_{\theta\text{-component}} = \frac{1}{r}\frac{\partial \Phi}{\partial \theta} \tag{8-218}$$

Information about the integration constant $f(\theta)$ from (8-217) is obtained by using the expression for Φ at large r in equation (8-218):

$$\frac{\partial \Phi}{\partial \theta} = -V_{\text{approach}} r \sin\theta = -V_{\text{approach}} r \sin\theta + \frac{df}{d\theta} \tag{8-219}$$

This indicates that $df/d\theta = 0$, or $f = C_1$ (i.e., constant). It is acceptable to set C_1 to zero because any constant will satisfy Laplace's equation. Furthermore, the value of C_1 does not affect the velocity profile because one calculates the components of the velocity vector from the gradient of Φ, and the gradient of C_1 vanishes. At most, C_1 will affect the magnitude of Φ along an equipotential. Analysis of this problem far from the bubble yields the following expression for the scalar velocity potential:

$$\Phi(r \to \infty, \theta) = V_{\text{approach}} r \cos\theta \tag{8-220}$$

where $\cos\theta$ is one of the Legendre polynomials that represents the solution to the angular part of Laplace's equation for two-dimensional axisymmetric flow in spherical coordinates via *separation of variables*. Hence, if

$$\Phi(r, \theta) = F(r)G(\theta) \tag{8-221}$$

and one moves closer to the bubble at constant θ, then $F(r)$ will change (i.e., terms like $1/r^n$, with $n > 0$, will become important when r is not infinitely large) but $G(\theta)$ should not deviate from its functional form at large r (i.e., $\cos\theta$). In light of this analysis and discussion, one postulates the following functional form for the scalar velocity potential at any position with the incompressible liquid:

$$\Phi(r, \theta) = F(r)\cos\theta \tag{8-222}$$

where $F(r)$ is obtained by solving Laplace's equation. Since the angular dependence of Φ has been determined from the boundary condition far from the bubble, Laplace's equation reduces to a second-order ordinary differential equation for $F(r)$. This is illustrated as follows:

$$\nabla^2\Phi = \frac{\cos\theta}{r^2}\frac{d}{dr}\left(r^2\frac{dF}{dr}\right) + \frac{F(r)}{r^2\sin\theta}\frac{d}{d\theta}\left(\sin\theta\frac{d}{d\theta}\cos\theta\right) = 0 \tag{8-223}$$

Manipulation of the angular (i.e., second) term in the spherical coordinate Laplacian operator reveals $\cos\theta$ dependence, analogous to the radial term. Hence, in operator notation,

$$\nabla^2[F(r)\cos\theta] = \frac{\cos\theta}{r^2}\left[\frac{d}{dr}\left(r^2\frac{d}{dr}\right) - 2\right]F(r) = 0 \tag{8-224}$$

Both terms in brackets in (8-224) will be proportional to r^n if one guesses the trial function $F(r) \approx r^n$. Hence, r^n can be factored and the sum of both coefficients within brackets in (8-225) must vanish to satisfy Laplace's equation. The result is

$$\cos\theta[n(n+1)-2]r^{n-2} = 0 \tag{8-225}$$

which exhibits the following roots: $n = -2, 1$. The general solution for the scalar velocity potential is obtained by adding the solution for each value of n because Laplace's equation is linear in Φ. Hence,

$$\Phi(r,\theta) = \cos\theta\left(Ar + \frac{B}{r^2}\right) \tag{8-226}$$

where the integration constants A and B are determined from the boundary conditions. The solution for $n = 1$ is consistent with the boundary condition far from the bubble, because at large r,

$$\Phi(r \to \infty, \theta) = Ar\cos\theta \tag{8-227}$$

This boundary condition, given by (8-220), reveals that $A = V_{\text{approach}}$. The nondeformable nature of the bubble requires that v_r must vanish at the gas–liquid interface. This boundary condition at $r = R$ translates into

$$v_r(r = R, \theta) = \left(\frac{\partial\Phi}{\partial r}\right)_{r=R} = \cos\theta\left(A - \frac{2B}{R^3}\right) = 0 \tag{8-228}$$

and allows one to solve for the integration constant $B = \frac{1}{2}R^3 V_{\text{approach}}$. The final results for the scalar velocity potential and both components of the velocity vector are

$$\begin{aligned}
\Phi(r,\theta) &= V_{\text{approach}} R\cos\theta\left(\eta + \frac{1}{2}\eta^{-2}\right)\\
v_r(r,\theta) &= \frac{\partial\Phi}{\partial r} = V_{\text{approach}}\cos\theta(1-\eta^{-3})\\
v_\theta(r,\theta) &= \frac{1}{r}\frac{\partial\Phi}{\partial\theta} = -V_{\text{approach}}\sin\theta\left(1 + \frac{1}{2}\eta^{-3}\right)
\end{aligned} \tag{8-229}$$

where $\eta = r/R$. Notice that the tangential velocity component exhibits significant slip at the gas–liquid interface because $v_\theta \neq 0$ at $r = R$, except for $\theta = 0, \pi$. It is relatively straightforward to calculate the dynamic pressure distribution after the two important velocity components have been determined. Application of

$$\mathfrak{P} = p + \rho g h = \text{constant} - \tfrac{1}{2}\rho\mathbf{v}\cdot\mathbf{v} \tag{8-230}$$

yields

$$\mathfrak{P}(r,\theta) = \mathfrak{P}_\infty - \rho V_{\text{approach}}^2 \left[\frac{1}{2}\left(\frac{R}{r}\right)^3 (1 - 3\cos^2\theta) + \frac{1}{8}\left(\frac{R}{r}\right)^6 (1 + 3\cos^2\theta) \right] \tag{8-231}$$

where

$$\mathfrak{P}_\infty + \tfrac{1}{2}\rho V_{\text{approach}}^2 = \text{constant} \tag{8-232}$$

far from the bubble. Fluid pressure is related to dynamic pressure via

$$p(r,\theta) = \mathfrak{P}(r,\theta) - \rho g r \cos\theta \tag{8-233}$$

If the xy plane at $z = 0$ and $\theta = \pi/2$ is chosen as the reference for the gravitational potential, then $\mathfrak{P}_\infty$ is equivalent to the fluid pressure p_∞ in this reference plane far from the bubble. The final result for the fluid pressure distribution is

$$p(r,\theta) = p_\infty - \rho g r \cos\theta - \rho V_{\text{approach}}^2 \left[\frac{1}{2}\left(\frac{R}{r}\right)^3 (1 - 3\cos^2\theta) + \frac{1}{8}\left(\frac{R}{r}\right)^6 (1 + 3\cos^2\theta) \right] \tag{8-234}$$

where the second term on the right side of (8-234) represents the effect of gravity on fluid pressure, and the predominant third term, which vanishes far from the bubble, is due to the fact that the bubble disrupts or perturbs fluid streamlines in its vicinity. The total vector force exerted by the fluid on the bubble across the gas–liquid interface at $r = R$ results solely from pressure forces, because viscous forces are unimportant for ideal fluids. Application of equation (8-153) to ideal fluids with no viscous stress (i.e., $\tau \approx 0$) yields

$$\mathbf{F}_{\text{fluid-bubble}} = -R^2 \int_0^{2\pi} \int_0^{\pi} \delta_r(\theta,\phi)\, p(r = R,\theta) \sin\theta \, d\theta \, d\phi \tag{8-235}$$

The fluid pressure distribution at the gas–liquid interface in the potential flow regime is

$$p(r = R,\theta) = p_\infty - \tfrac{5}{8}\rho V_{\text{approach}}^2 - \rho g R \cos\theta + \tfrac{9}{8}\rho V_{\text{approach}}^2 \cos^2\theta \tag{8-236}$$

where the third term on the right side of (8-236) represents the effect of gravity and the fourth term results from perturbation of fluid streamlines. Symmetry considerations suggest that the first, second, and fourth terms on the right side of (8-236) average to zero over the bubble surface and do not contribute to the total vector force. This can be verified by detailed calculations. The symmetry of the dynamic contribution to fluid pressure (i.e., $\approx \cos^2\theta$), as illustrated by the fourth term on the right side of (8-236), yields no dynamic contribution to the total vector force exerted by the fluid on the bubble. In other words, $\mathbf{F}_{\text{fluid-bubble}}$

for an ideal fluid is the same in any flow regime, provided that the fluid does not deform the bubble, and this force that results from the gravitational contribution to fluid pressure can be calculated from hydrostatics. This statement is verified in the following section via inspection of the stream function for ideal flow around a bubble. The final result for $\mathbf{F}_{\text{fluid-bubble}}$ is

$$\mathbf{F}_{\text{fluid-bubble}} = \rho g R^3 \int_0^{2\pi} \int_0^{\pi} \delta_r(\theta, \phi) \cos\theta \sin\theta \, d\theta \, d\phi = \frac{4}{3}\pi R^3 \rho g \delta_z \quad (8\text{-}237)$$

which corresponds to a buoyant force. Hence, the friction factor f and the friction loss factor e_v are zero for ideal fluids.

Potential Flow around a Gas Bubble Via the Stream Function. The same axisymmetric flow problem in spherical coordinates is solved in terms of the stream function ψ. All potential flow solutions yield an intricate network of equipotentials and streamlines that intersect at right angles. For two-dimensional ideal flow around a bubble, the velocity profile in the preceding section was calculated from the gradient of the scalar velocity potential to ensure no vorticity:

$$\mathbf{v} = \nabla\Phi = \delta_r v_r + \delta_\theta v_\theta = \delta_r \frac{\partial\Phi}{\partial r} + \delta_\theta \frac{1}{r}\frac{\partial\Phi}{\partial\theta} \quad (8\text{-}238)$$

Now, v_r and v_θ are related to the stream function ψ to guarantee incompressibility:

$$v_r = -\frac{1}{r^2 \sin\theta}\frac{\partial\psi}{\partial\theta} \qquad v_\theta = \frac{1}{r\sin\theta}\frac{\partial\psi}{\partial r} \quad (8\text{-}239)$$

The gradient to a streamline in spherical coordinates is

$$\nabla\psi = \delta_r \frac{\partial\psi}{\partial r} + \delta_\theta \frac{1}{r}\frac{\partial\psi}{\partial\theta} = \delta_r v_\theta r \sin\theta - \delta_\theta v_r r \sin\theta \quad (8\text{-}240)$$

If streamlines intersect equipotentials at right angles, then the gradient to a streamline must be perpendicular to the gradient to an equipotential. Hence,

$$\nabla\psi \cdot \nabla\Phi = v_r v_\theta r \sin\theta - v_\theta v_r r \sin\theta = 0 \quad (8\text{-}241)$$

One solves for the stream function by invoking no vorticity at the microscopic level. Since v_r and v_θ are both functions of r and θ, with $v_\phi = 0$, the r and θ components of the vorticity vector are trivially zero. The ϕ-component of $(\nabla \times \mathbf{v})$ yields an equation that must be solved for $\psi(r, \theta)$. Hence, one combines the nontrivial component of the vorticity vector with the relations between v_r, v_θ and ψ, given by (8-239):

$$\begin{aligned}(\nabla \times \mathbf{v})_{\phi\text{-component}} &= \frac{1}{r}\frac{\partial(r v_\theta)}{\partial r} - \frac{1}{r}\frac{\partial v_r}{\partial\theta} \\ &= \frac{1}{r}\frac{\partial}{\partial r}\left(\frac{1}{\sin\theta}\frac{\partial\psi}{\partial r}\right) + \frac{1}{r}\frac{\partial}{\partial\theta}\left(\frac{1}{r^2\sin\theta}\frac{\partial\psi}{\partial\theta}\right) = 0 \end{aligned} \quad (8\text{-}242)$$

Multiplication of (8-242) by $r \sin\theta$ yields

$$\frac{\partial^2 \psi}{\partial r^2} + \frac{\sin\theta}{r^2} \frac{\partial}{\partial \theta} \left(\frac{1}{\sin\theta} \frac{\partial \psi}{\partial \theta} \right) = E^2 \psi = 0 \tag{8-243}$$

Hence, two-dimensional axisymmetric potential flow in spherical coordinates is described by $\nabla^2 \Phi = 0$ for the scalar velocity potential and $E^2 \psi = 0$ for the stream function. Recall that two-dimensional axisymmetric creeping viscous flow in spherical coordinates is described by $E^2(E^2 \psi) = 0$. This implies that potential flow solutions represent a subset of creeping viscous flow solutions for two-dimensional axisymmetric problems in spherical coordinates. Also, recall from the boundary condition far from submerged objects that $\sin^2\theta$ is the appropriate Legendre polynomial for the E^2 operator in spherical coordinates. The methodology presented on pages 186 through 188 is employed to postulate the functional form for ψ:

$$\psi(r, \theta) = F(r) \sin^2\theta \tag{8-244}$$

and calculate its radial dependence via

$$E^2 \psi = E^2[F(r) \sin^2\theta] = \sin^2\theta \left(\frac{d^2}{dr^2} - \frac{2}{r^2} \right) F(r) = 0 \tag{8-245}$$

A power function is appropriate [i.e., $F(r) \approx r^n$], and upon substitution into (8-245),

$$\sin^2\theta [n(n-1) - 2] r^{n-2} = 0 \tag{8-246}$$

The two roots are $n = -1, 2$, which represent a subset of the four roots for the radial function for two-dimensional axisymmetric creeping viscous flow in spherical coordinates (i.e., $n = -1, 1, 2, 4$). One of the roots for the potential flow problem (i.e., $n = 2$) is consistent with the functional form of ψ far from submerged objects. The potential flow solution is

$$\psi(r, \theta) = \sin^2\theta \left(\frac{A}{r} + Br^2 \right) \tag{8-247}$$

Since the coefficient of $\frac{1}{2} r \sin^2\theta$ in (8-247) for the stream function is zero, because $E^2[F(r) \sin^2\theta] = 0$ with $F(r) \approx r^n$ is not satisfied for $n = 1$, there is no dynamic force exerted by the fluid on the bubble across the gas–liquid interface. This claim agrees with calculations of the interfacial vector force from the preceding section. The boundary conditions required to determine A and B in (8-247) are

$$\psi(r \to \infty, \theta) = -\tfrac{1}{2} V_{\text{approach}} r^2 \sin^2\theta \tag{8-248a}$$

$$\psi(r = R, \theta) = 0, \qquad \text{because there is no flow through the bubble} \tag{8-248b}$$

$$v_r(r = R, \theta) = 0, \qquad \text{for a nondeformable bubble} \tag{8-248c}$$

Condition (8-248a) is satisfied when $B = -\frac{1}{2}V_{\text{approach}}$. Conditions (8-248$b$) and (8-248$c$) are redundant because both yield the following value for the integration constant $A = -BR^3$. The final expression for the stream function is

$$\psi(r, \theta) = \tfrac{1}{2}V_{\text{approach}}R^2 \sin^2\theta(\eta^{-1} - \eta^2) \tag{8-249}$$

where $\eta = r/R$. As expected, the stream function vanishes at all positions on the surface of the bubble because there is no flow through this stationary submerged object. It is left as an exercise for the student to verify that v_r and v_θ, calculated from (8-249) for ψ, are exactly the same as those based on the scalar velocity potential from the preceding section (i.e., see equations 8-229).

Potential Flow Solutions for Gas Bubbles Which Rise through Incompressible Fluids That Are Stagnant Far from the Submerged Objects. A nondeformable bubble of radius R rises through an ideal fluid such that

$$\mathbf{v}_{\text{bubble}} = \delta_z V_{\text{bubble}} \tag{8-250}$$

This motion of the bubble induces axisymmetric two-dimensional flow in the liquid phase. In the potential flow regime, one calculates the scalar velocity potential $\Phi(r, \theta)$ via Laplace's equation. The general solution in spherical coordinates is

$$\Phi(r, \theta) = \cos\theta\left(Ar + \frac{B}{r^2}\right) \tag{8-251}$$

and the two nontrivial components of the fluid velocity vector are

$$v_r(r, \theta) = \frac{\partial\Phi}{\partial r} = \cos\theta\left(A - \frac{2B}{r^3}\right) \tag{8-252a}$$

$$v_\theta(r, \theta) = \frac{1}{r}\frac{\partial\Phi}{\partial\theta} = -\sin\theta\left(A + \frac{B}{r^3}\right) \tag{8-252b}$$

The upward motion of the bubble achieves terminal velocity, and one determines the integration constants A and B when the center of the bubble coincides with the origin of a stationary orthogonal coordinate system. The appropriate boundary conditions are described as follows:

1. The fluid is quiescent far from the bubble, which implies that

$$v_r(r \to \infty, \theta) = 0 \qquad v_\theta(r \to \infty, \theta) = 0$$

2. The bubble is nondeformable, which implies that its shape does not change and its radius R remains constant. Hence, the radial component of the bubble rise velocity must match v_r of the liquid at the gas–liquid interface:

$$v_r(r = R, \theta) = \delta_r \cdot \mathbf{v}_{\text{bubble}} = V_{\text{bubble}}\cos\theta$$

Condition 1 implies that $A = 0$. Now, integration constant B is calculated from condition 2, which yields $-2B = R^3 V_{\text{bubble}}$. The final results are

$$\begin{aligned} \Phi(r,\theta) &= -\tfrac{1}{2} V_{\text{bubble}} R \eta^{-2} \cos\theta \\ v_r(r,\theta) &= V_{\text{bubble}} \eta^{-3} \cos\theta \\ v_\theta(r,\theta) &= \tfrac{1}{2} V_{\text{bubble}} \eta^{-3} \sin\theta \end{aligned} \tag{8-253}$$

where $\eta = r/R$.

Potential Flow Transverse to a Long Cylinder Via the Scalar Velocity Potential. The same methodology from earlier sections is employed here when a long cylindrical object of radius R is placed within the flow field of an incompressible ideal fluid. The presence of the cylinder induces v_r and v_θ within its vicinity, but there is no axis of symmetry. The scalar velocity potential for this two-dimensional planar flow problem in cylindrical coordinates must satisfy Laplace's equation in the following form:

$$\nabla \cdot \nabla \Phi = \frac{1}{r}\frac{\partial}{\partial r}\left(r\frac{\partial \Phi}{\partial r}\right) + \frac{1}{r^2}\frac{\partial^2 \Phi}{\partial \theta^2} = 0 \tag{8-254}$$

The cylindrical axis coincides with the z axis of a rectangular Cartesian coordinate system, and fluid approaches the cylinder with constant velocity along the x axis:

$$\mathbf{v} = \delta_x V_{\text{approach}} \qquad \text{at } r \to \infty \tag{8-255}$$

This condition far from the submerged object is used to determine the functional form of the scalar velocity potential. For example, in cylindrical coordinates,

$$v_r = \delta_r \cdot \mathbf{v} = (\delta_r \cdot \delta_x) V_{\text{approach}} = V_{\text{approach}} \cos\theta = (\nabla \Phi)_{r\text{-component}} = \frac{\partial \Phi}{\partial r} \tag{8-256}$$

Integration of (8-256) with respect to r at constant θ yields an expression for Φ at large r, realizing, once again, that the constant of integration can be a function of θ:

$$\Phi(r \to \infty, \theta) = V_{\text{approach}} r \cos\theta + f(\theta) \tag{8-257}$$

Now, consider the tangential velocity component and evaluate $f(\theta)$:

$$\begin{aligned} v_\theta &= \delta_\theta \cdot \mathbf{v} = (\delta_\theta \cdot \delta_x) V_{\text{approach}} = -V_{\text{approach}} \sin\theta \\ &= (\nabla \Phi)_{\theta\text{-component}} = \frac{1}{r}\frac{\partial \Phi}{\partial \theta} = -V_{\text{approach}} \sin\theta + \frac{1}{r}\frac{df}{d\theta} \end{aligned} \tag{8-258}$$

Comparison of these two expressions for v_θ suggests that it is acceptable to neglect $f(\theta)$ (i.e., $f = 0$) and calculate the scalar velocity potential far from the cylinder as follows:

$$\Phi(r \to \infty, \theta) = V_{\text{approach}} r \cos\theta \tag{8-259}$$

Hence, $\cos\theta$ is a good function that satisfies the angular part of Laplace's equation for $\Phi(r, \theta)$ via separation of variables for axisymmetric flow in spherical coordinates, and two-dimensional planar flow transverse to a long cylinder. At any position with the incompressible liquid, one postulates that

$$\Phi(r, \theta) = F(r) \cos\theta \tag{8-260}$$

where $F(r)$ is calculated from Laplace's equation:

$$\nabla^2 \Phi = \frac{\cos\theta}{r} \frac{d}{dr}\left(r \frac{dF}{dr}\right) + \frac{F(r)}{r^2} \frac{d^2}{d\theta^2}(\cos\theta) = 0 \tag{8-261}$$

The fact that $\cos\theta$ is a good function for the angular part of the scalar velocity potential is obvious because both terms in Laplace's equation reveal the same angular dependence. Once again, $F(r) \approx r^n$ is appropriate:

$$\begin{aligned} \nabla^2[F(r)\cos\theta] &= \frac{\cos\theta}{r}\left[\frac{d}{dr}\left(r\frac{d}{dr}\right) - \frac{1}{r}\right] F(r) \\ &= \cos\theta(n^2 - 1) r^{n-2} = 0 \end{aligned} \tag{8-262}$$

Equation (8-262) exhibits roots at $n = \pm 1$. The general solution for Φ is

$$\Phi(r, \theta) = \cos\theta \left(Ar + \frac{B}{r}\right) \tag{8-263}$$

The solution for $n = 1$ is consistent with the boundary condition far from the cylinder, because at large r,

$$\Phi(r \to \infty, \theta) = Ar \cos\theta \tag{8-264}$$

This boundary condition, given by (8-259), reveals that $A = V_{\text{approach}}$. The nondeformable nature of the interface requires that v_r must vanish at $r = R$. Hence,

$$v_r(r = R, \theta) = \left(\frac{\partial \Phi}{\partial r}\right)_{r=R} = \cos\theta \left(A - \frac{B}{R^2}\right) = 0 \tag{8-265}$$

which is satisfied when $B = R^2 V_{\text{approach}}$. The final results for the scalar velocity potential and both components of the velocity vector are

$$\begin{aligned} \Phi(r, \theta) &= V_{\text{approach}} R \cos\theta(\eta + \eta^{-1}) \\ v_r(r, \theta) &= \frac{\partial \Phi}{\partial r} = V_{\text{approach}} \cos\theta(1 - \eta^{-2}) \\ v_\theta(r, \theta) &= \frac{1}{r}\frac{\partial \Phi}{\partial \theta} = -V_{\text{approach}} \sin\theta(1 + \eta^{-2}) \end{aligned} \tag{8-266}$$

where $\eta = r/R$. Once again, slip occurs at the interface because v_θ does not vanish at $r = R$, except for $\theta = 0, \pi$.

Potential Flow Transverse to a Long Cylinder Via the Stream Function. For two-dimensional planar flow in cylindrical coordinates, the radial and polar velocity components are related to the stream function ψ via the following expressions:

$$v_r(r,\theta) = -\frac{1}{r}\frac{\partial \psi}{\partial \theta} \qquad v_\theta(r,\theta) = \frac{\partial \psi}{\partial r} \tag{8-267}$$

It is left as an exercise for the student to verify that these relations between the two nonzero velocity components and ψ conserve overall fluid mass, and that streamlines intersect equipotentials at right angles in cylindrical coordinates. The stream function is obtained by invoking no vorticity at the microscopic level. Only the z-component of the fluid vorticity vector yields nontrivial information about ψ. For example,

$$\begin{aligned}(\boldsymbol{\nabla} \times \mathbf{v})_{z\text{-component}} &= \frac{1}{r}\frac{\partial (r v_\theta)}{\partial r} - \frac{1}{r}\frac{\partial v_r}{\partial \theta} \\ &= \frac{1}{r}\frac{\partial}{\partial r}\left(r\frac{\partial \psi}{\partial r}\right) + \frac{1}{r}\frac{\partial}{\partial \theta}\left(\frac{1}{r}\frac{\partial \psi}{\partial \theta}\right) = \nabla^2 \psi = 0\end{aligned} \tag{8-268}$$

In summary, Laplace's equation must be satisfied by the scalar velocity potential and the stream function for all two-dimensional planar flows that lack an axis of symmetry. The Laplacian operator is replaced by the E^2 operator to calculate the stream function for two-dimensional axisymmetric flows. For potential flow transverse to a long cylinder, vector algebra is required to determine the functional form of the stream function far from the submerged object. This is accomplished from a consideration of v_r and v_θ via equation (8-255):

$$v_r = \delta_r \cdot \mathbf{v} = (\delta_r \cdot \delta_x) V_{\text{approach}} = V_{\text{approach}} \cos\theta = -\frac{1}{r}\frac{\partial \psi}{\partial \theta} \tag{8-269}$$

Integration of (8-269) with respect to θ at constant r yields an expression for ψ at large r. Now, the constant of integration can be a function of r:

$$\psi(r \to \infty, \theta) = -V_{\text{approach}} r \sin\theta + f(r) \tag{8-270}$$

Evaluate $f(r)$ via consideration of the tangential velocity component:

$$\begin{aligned} v_\theta &= \delta_\theta \cdot \mathbf{v} = (\delta_\theta \cdot \delta_x) V_{\text{approach}} = -V_{\text{approach}} \sin\theta \\ &= \frac{\partial \psi}{\partial r} = -V_{\text{approach}} \sin\theta + \frac{df}{dr} \end{aligned} \tag{8-271}$$

Hence, $df/dr = 0$. Once again, the integration constant can be neglected without loss of generality, and the stream function far from the cylinder is

$$\psi(r \to \infty, \theta) = -V_{\text{approach}} r \sin\theta \tag{8-272}$$

One concludes that $\sin\theta$ is a good function which represents the solution to the angular part of Laplace's equation for the stream function in cylindrical coordinates for two-dimensional flow transverse to a long cylinder. This conclusion is verified by postulating the functional form for ψ at any position within the incompressible liquid:

$$\psi(r, \theta) = F(r) \sin\theta \tag{8-273}$$

and demonstrating that both terms in Laplace's equation reveal the same angular dependence. Hence,

$$\begin{aligned} \nabla^2\psi &= \frac{\sin\theta}{r}\frac{d}{dr}\left(r\frac{dF}{dr}\right) + \frac{F(r)}{r^2}\frac{d^2}{d\theta^2}(\sin\theta) \\ &= \frac{\sin\theta}{r}\left[\frac{d}{dr}\left(r\frac{d}{dr}\right) - \frac{1}{r}\right]F(r) = 0 \end{aligned} \tag{8-274}$$

Except for the difference between $\sin\theta$ and $\cos\theta$, notice the similarity between this form of Laplace's equation and (8-262) for the scalar velocity potential Φ. In fact, the general solution for the radial part of the stream function is exactly the same as that for Φ from the preceding section. This is expected because Φ and ψ satisfy the same equation for two-dimensional ideal flows that lack an axis of symmetry. The general solution for ψ is

$$\psi(r, \theta) = \sin\theta\left(Ar + \frac{B}{r}\right) \tag{8-275}$$

Consistency with the boundary condition far from the cylinder, given by (8-272), is obtained when $A = -V_{\text{approach}}$, and the nondeformable nature of the interface requires that

$$v_r(r = R, \theta) = -\frac{1}{R}\left(\frac{\partial\psi}{\partial\theta}\right)_{r=R} = -\cos\theta\left(A + \frac{B}{R^2}\right) = 0 \tag{8-276}$$

which is satisfied when $B = R^2 V_{\text{approach}}$. The final results for the stream function and both nonzero components of the velocity vector are

$$\begin{aligned} \psi(r, \theta) &= -V_{\text{approach}} R \sin\theta(\eta - \eta^{-1}) \\ v_r(r, \theta) &= -\frac{1}{r}\frac{\partial\psi}{\partial\theta} = V_{\text{approach}} \cos\theta(1 - \eta^{-2}) \\ v_\theta(r, \theta) &= \frac{\partial\psi}{\partial r} = -V_{\text{approach}} \sin\theta(1 + \eta^{-2}) \end{aligned} \tag{8-277}$$

where $\eta = r/R$. Notice that (1) both approaches, via Φ or ψ, yield the same results for v_r and v_θ; (2) the stream function vanishes at the cylindrical interface, where $r = R$, because this is a zero-flux boundary in the absence of gas–liquid mass transfer; and (3) the scalar velocity potential is nonzero along the interface.

PROBLEMS

8-1. (a) Derive the equation of continuity in vector form:

$$\frac{\partial \rho}{\partial t} + \nabla \cdot \rho \mathbf{v} = 0$$

via conservation of overall fluid mass within an arbitrary control volume $V(t)$ that moves at the local fluid velocity at each point on its surface $S(t)$.

Answer: The total mass of fluid within an arbitrarily chosen control volume V is

$$\int_V \rho \, dV$$

This is written semi-intensively in terms of the fluid density ρ, but total mass depends on system size via the integration limits which encompass the entire control volume. The final form of the microscopic equation of continuity is intensive because one divides by system volume and simultaneously takes the limit as each coordinate dimension approaches zero. This limiting procedure is not performed explicitly below, but the general methodology can be interpreted in that manner. The rate of accumulation of overall fluid mass within V is expressed in terms of a total time derivative, as follows;

$$\frac{d}{dt}\int_V \rho \, dV = \int_V \frac{\partial \rho}{\partial t} \, dV + \int_S \rho (\mathbf{v}_{\text{surface}} \cdot \mathbf{n}) \, dS \qquad (a)$$

where $\mathbf{n}$ is an outward-directed unit normal vector on surface S that completely surrounds control volume V, and $\mathbf{v}_{\text{surface}}$ is the local velocity of the surface. Equation (a) is facilitated by the Leibnitz rule for differentiating a three-dimensional integral, where both the integrand and the limits of integration are functions of time. This equation represents the left-hand side of the generalized equation of continuity for any type of fluid, and it is equated to the net rate at which overall fluid mass enters the control volume due to mass flux acting across moving surface S. Now, it is necessary to (1) express the total mass flux vector of the fluid with respect to the moving surface, (2) identify the component of this "relative" flux in the direction of the inward unit

normal vector to the surface, $-\mathbf{n}$, and (3) average the normal component of this relative flux over the entire surface S which bounds fluid in control volume V. The results for (1), (2) and (3) are

$$-\int_S \mathbf{n} \cdot \rho(\mathbf{v}_{\text{fluid}} - \mathbf{v}_{\text{surface}})\, dS \tag{b}$$

The balance on overall fluid mass is obtained by equating equations (a) and (b) for an arbitrary control volume that moves independently with respect to the local fluid velocity:

$$\begin{aligned}\frac{d}{dt}\int_V \rho\, dV &= \int_V \frac{\partial \rho}{\partial t}\, dV + \int_S \rho(\mathbf{v}_{\text{surface}} \cdot \mathbf{n})\, dS \\ &= -\int_S \mathbf{n} \cdot \rho(\mathbf{v}_{\text{fluid}} - \mathbf{v}_{\text{surface}})\, dS \end{aligned} \tag{c}$$

It should be obvious that this integral form of the mass balance, with no sources or sinks, adopts the same form for the following three cases:

(a_1)	$\mathbf{v}_{\text{surface}} = 0$	net rate of input due to mass flux $\neq 0$,	open system
(a_2)	$\mathbf{v}_{\text{surface}} \neq \mathbf{v}_{\text{fluid}}$	net rate of input due to mass flux $\neq 0$,	open system
(a_3)	$\mathbf{v}_{\text{surface}} = \mathbf{v}_{\text{fluid}}$	net rate of input due to mass flux $= 0$,	closed system

In each case, equation (c) reduces to

$$\int_V \frac{\partial \rho}{\partial t}\, dV = -\int_S \mathbf{n} \cdot \rho \mathbf{v}_{\text{fluid}}\, dS \tag{d}$$

Application of Gauss's law, or the divergence theorem, transforms the surface integral on the right side of equation (d) to an integral over the entire control volume:

$$\int_V \frac{\partial \rho}{\partial t}\, dV = -\int_V \nabla \cdot \rho \mathbf{v}_{\text{fluid}}\, dV \tag{e}$$

Since there are several choices for this arbitrarily chosen control volume within the fluid, one can change the limits of each three-dimensional integral to coincide with the boundaries of the system. Equation (e) must be satisfied for each choice of integration limits. This is possible only if one equates the integrands, which yields the microscopic or differential form of the equation of continuity.

(b) Does $V(t)$ in part (a) represent an open system or a closed system?

Answer: If $\mathbf{v}_{\text{fluid}} = \mathbf{v}_{\text{surface}}$, then the system is closed because there is no net flux of overall fluid mass that enters or leaves the control volume

across surface S. Otherwise, the system is open and there is a net rate of input or output due to $\mathbf{n} \cdot \rho(\mathbf{v}_{\text{fluid}} - \mathbf{v}_{\text{surface}})$.

8-2. Identify the important dimensionless numbers that appear in the dimensionless equation of continuity for a compressible fluid where the density $\rho = \rho(x, y, z, t)$.

8-3. Evaluate the following tensor double-dot operation explicitly for two-dimensional creeping viscous flow of an incompressible Newtonian fluid around a gas bubble: $[\nabla\mathbf{v}] : \boldsymbol{\delta}$, where $\delta = \sum_i \delta_i\delta_i$ is the unit tensor.

8-4. Begin with the equation of motion in vector-tensor notation for a generalized fluid and briefly describe a strategy to obtain the angular momentum balance. *Hint:* angular momentum is a first-rank tensor.

8-5. Perform vector-tensor manipulation of the equation of motion:

$$\frac{\partial(\rho\mathbf{v})}{\partial t} = -\nabla \cdot \rho\mathbf{v}\mathbf{v} - \nabla \cdot \tau - \nabla p + \rho\mathbf{g}$$

and derive the analog of the Navier–Stokes equation, which must be solved to calculate the velocity vector for laminar viscous flow of a compressible gas that obeys Newton's law of viscosity. Since the flow is compressible, $\nabla \cdot \mathbf{v} \neq 0$. The viscous stress tensor should not appear in your final result. It is not necessary to prove any vector identities using summation notation. It is sufficient to state these identities, use them in the equation of motion, and arrive at the final result in only seven lines of work. *Hint:* Newton's law of viscosity for compressible fluids is

$$\tau = -\mu[\nabla\mathbf{v} + (\nabla\mathbf{v})^{\mathrm{T}}] + (\tfrac{2}{3}\mu - \kappa)(\nabla \cdot \mathbf{v})\delta$$

Some helpful vector-tensor identities are

$$\nabla \cdot (\nabla\mathbf{v})^{\mathrm{T}} = \nabla(\nabla \cdot \mathbf{v})$$
$$\nabla \cdot (\nabla \cdot \mathbf{v})\delta = \nabla(\nabla \cdot \mathbf{v})$$

8-6. The following poem was written by R. B. Bird for W. E. Stewart on the occasion of Stewart's sixtieth birthday. "A student came in to see Warren, and said in a voice quite forlorn, I can't find a path through this quagmire math, these nablas [nablas are del operators] to me are quite foreign. So Warren, who's also called Earl, decided to help this young girl. Without using a book, he unflinchingly took the *Laplacian of grad div curl curl*."

(a) Consider the Laplacian of grad div curl curl of the velocity vector $\mathbf{v}$. Write this operation using condensed vector-tensor notation and determine whether the result yields a vector, a tensor, or a scalar.

(b) Obtain an explicit answer for this vector-tensor operation from part (a) that is appropriate to irrotational (i.e., potential) flow past a stationary gas bubble.

8-7. (a) Prove the following vector-tensor identity:

$$\mathbf{v} \cdot \nabla \mathbf{v} = \tfrac{1}{2}\nabla(\mathbf{v} \cdot \mathbf{v}) - \mathbf{v} \times (\nabla \times \mathbf{v})$$

(b) Use the identity in part (a) to evaluate $\mathbf{v} \cdot (\mathbf{v} \cdot \nabla \mathbf{v})$

8-8. (a) Write the θ component of $\mathbf{v} \cdot \nabla \mathbf{v}$ in cylindrical coordinates.

(b) Write the θ component of $\mathbf{v} \cdot \nabla \mathbf{v}$ in spherical coordinates, where θ is the polar angle.

(c) Which term in the θ component of $\mathbf{v} \cdot \nabla \mathbf{v}$ in spherical coordinates represents a centrifugal force in the θ direction? θ is the polar angle.

(d) Write the z component of $\nabla \cdot \tau$ in cylindrical coordinates.

8-9. The velocity vector for rigid-body rotation of a solid that spins at constant angular velocity is $\mathbf{v} = \boldsymbol{\Omega} \times \mathbf{r}$, where $\boldsymbol{\Omega}$ is the angular velocity vector and $\mathbf{r}$ is the position vector from the axis of rotation. Obtain an expression for the vorticity vector $\frac{1}{2}\nabla \times \mathbf{v}$ for rigid-body rotation in terms of $\boldsymbol{\Omega}$.

8-10. Consider three viscometers described briefly below where slow rotation of a solid surface produces one-dimensional fluid flow in which the nonzero velocity component depends on two spatial coordinates.

(1) For a rotating sphere viscometer, the tangential velocity v_ϕ on the surface of the sphere is $\Omega R \sin\theta$. This reveals the angular dependence of v_ϕ at any radial position, because if one moves into the fluid at larger r and constant θ, and a separation of variables solution to the ϕ-component of the equation of motion is valid, then the $\sin\theta$ dependence shouldn't change. Hence,

$$v_\phi = f(r)g(\theta) = f(r)\sin\theta$$
$$f(r) = \Omega R \qquad \text{at } r = R$$
$$f(r) \to 0 \qquad \text{as } r \to \infty$$

(2) For a parallel disk viscometer (i.e., cylindrical coordinates), the tangential velocity v_θ on the rotating plate is Ωr. This reveals the radial dependence of v_θ at any axial position z between the rotating and stationary plates, because if one moves into the fluid in the z direction from the moving plate at constant r and a separation of variables solution to the θ-component of the equation of motion is valid, then the r

dependence shouldn't change. Hence,

$$v_\theta = f(r)g(z) = rg(z)$$

$$g(z) = \begin{cases} \Omega & \text{on the rotating plate} \\ 0 & \text{on the stationary plate} \end{cases}$$

(3) For a cone-and-plate viscometer (i.e., spherical coordinates), the tangential velocity v_ϕ on the rotating cone is $\Omega r \sin\theta_1$. This reveals the radial dependence of v_ϕ at any angle θ between the rotating cone at θ_1 and the stationary plate at $\theta = \pi/2$, because if one moves into the fluid in the θ direction from the rotating cone toward the stationary plate at constant radial position r, and a separation of variables solution to the ϕ-component of the equation of motion is valid, then the r dependence shouldn't change. Hence,

$$v_\phi = f(r)g(\theta) = rg(\theta)$$

$$g(\theta) = \begin{cases} \Omega \sin\theta_1 & \text{at } \theta = \theta_1 \\ 0 & \text{at } \theta = \pi/2 \end{cases}$$

(a) For each viscometer described above, use the constitutive equations tabulated by Bird *et al.* (2002, p. 844) for incompressible Newtonian fluids to calculate all nonzero components of the viscous stress tensor τ and present your results in matrix form.

(b) Describe qualitatively how the postulated separation-of-variables form of the velocity profile, which conforms to the boundary condition on the rotating surface, simplifies the state of viscous stress in the fluid.

8-11. (a) Consider a parallel disk viscometer as described in Problem 8-10 and write an expression for the vector viscous force per unit area exerted by the rotating plate on a generalized fluid that contacts this plate. Be sure that your answer contains unit vectors.

(b) If the fluid is incompressible and Newtonian, and the profile in Problem 8-10(2) is reasonable [i.e., $v_\theta = rg(z)$], then simplify your expression from part (a) for the vector viscous force per unit area exerted by the rotating plate on the fluid in contact with this plate. Include some unit vectors in your final answer.

(c) Classify your answer in part (b) as a normal force, a shear force, or some combination thereof.

8-12. (a) Use vector notation and express the vector viscous force per unit area exerted by an incompressible Newtonian fluid on the stationary solid plate at $\theta = \pi/2$ in the cone-and-plate viscometer. The flow configuration for this problem in spherical coordinates is illustrated in Bird *et al.* (2002, p. 67). A one-line answer is required. Include unit vectors.

(b) Which term in part (a) provides the most important contribution to the vector viscous force per unit area exerted by the fluid on the stationary plate?

(c) Identify the nontrivial component or components of the low-Reynolds-number equation of change for fluid vorticity which must be analyzed to solve this flow problem via the curl of the equation of motion. A one-line answer is required.

8-13. (a) Use vector notation and express the vector viscous force per unit area exerted by a generalized fluid on the stationary wall of a straight tube (i.e., at $r = R$) with circular cross section. A one-line answer is required. Include unit vectors.

(b) Consider one-dimensional flow of an incompressible Newtonian fluid, $v_z(r)$, and identify the term in part (a) that provides the most important contribution to the vector viscous force per unit area exerted by the fluid on the stationary wall at $r = R$. Classify your answer as (1) a normal stress, (2) a shear stress, or (3) some combination of normal and shear stresses.

(c) Consider one-dimensional flow of a non-Newtonian fluid in the z direction through a straight tube with radius R and circular cross section. Use vector notation and express the vector force per unit area due to bulk fluid flow that is exerted across the exit plane at the tube outlet, where $z = L$. The surface area of interest has magnitude πR^2, but this is not a solid surface. A one-line answer is required, here. Be sure to include unit vectors in your answer. Classify each term as (1) a normal stress, (2) a shear stress, or (3) some combination of normal and shear stresses.

8-14. In the rotating sphere viscometer, a solid sphere of radius R is suspended from a wire and rotates slowly at constant angular velocity Ω about the long axis of the wire in an incompressible Newtonian fluid. The fluid is quiescent far from the sphere.

(a) Use the no-slip boundary condition on the surface of the rotating sphere to postulate the functional form of the fluid velocity profile when rotation is slow enough and centrifugal forces can be neglected.

Answer: Consider rigid-body rotation of a solid sphere about the z axis of a Cartesian coordinate system and calculate the velocity vector at the fluid–solid interface by invoking the no-slip condition

$$\mathbf{v} = (\boldsymbol{\Omega} \times \mathbf{r})_{r=R}$$

The angular velocity vector is oriented in the z direction (i.e., $\boldsymbol{\Omega} = \Omega\delta_z$), and the position vector from the axis of rotation (i.e., along the

wire) to any point on the surface of the solid sphere is

$$\mathbf{r} = R \sin\theta(\delta_r \sin\theta + \delta_\theta \cos\theta)$$

where θ is the polar angle measured from the z axis. Upon taking the cross product, one obtains

$$\mathbf{v} = \Omega R \sin\theta[(\delta_z \times \delta_r)\sin\theta + (\delta_z \times \delta_\theta)\cos\theta]$$

Trigonometric relations between unit vectors in rectangular and spherical coordinates yield the following expression for δ_z (see Bird *et al.*, 2002, p. 828). Hence,

$$\delta_z = \delta_r \cos\theta - \delta_\theta \sin\theta \qquad \delta_z \times \delta_r = \delta_\phi \sin\theta \qquad \delta_z \times \delta_\theta = \delta_\phi \cos\theta$$

If the sphere rotates slowly and centrifugal forces do not induce flow in the radial direction, then one calculates the fluid velocity at the fluid–solid interface via the solid body formalism summarized above. Vector algebra reveals that this problem is described by one-dimensional flow in the ϕ direction, because

$$\mathbf{v} = \Omega R \sin\theta(\delta_\phi \sin^2\theta + \delta_\phi \cos^2\theta) = \delta_\phi \Omega R \sin\theta = \delta_\phi v_\phi$$

This result for v_ϕ at $r = R$ was presented in part (1) of Problem 8-10. At any position within the fluid, a separation-of-variables argument yields the following functional form for the important velocity component, $v_\phi(r, \theta) = f(r)\sin\theta$, where $f(r) = \Omega R$ at the fluid–solid interface.

(b) How many nontrivial components of the equation of change for fluid vorticity must be analyzed to solve this fluid dynamics problem under slow rotation?

Answer: Consult the three scalar components of the vorticity vector shown in Bird *et al.* (2002, p. 836). For one-dimensional flow in the ϕ direction, as described in part (a), one obtains the following result:

$$r\text{-component:} \qquad (\nabla \times \mathbf{v})_r = \frac{1}{r\sin\theta}\frac{\partial}{\partial\theta}(v_\phi \sin\theta) \neq 0$$

$$\theta\text{-component:} \qquad (\nabla \times \mathbf{v})_\theta = -\frac{1}{r}\frac{\partial}{\partial r}(r v_\phi) \neq 0$$

$$\phi\text{-component:} \qquad (\nabla \times \mathbf{v})_\phi = \frac{1}{r}\frac{\partial}{\partial r}(r v_\theta) - \frac{1}{r}\frac{\partial v_r}{\partial\theta} = 0$$

Since there are two nonzero components of the vorticity vector, the r and θ components of the Laplacian of the vorticity vector will yield

nontrivial information about v_ϕ, and both of these expressions must be considered.

(c) Is it better to use (1) the stream function approach via the vorticity equation, or (2) the equation of motion as tabulated in Appendix B of Bird *et al.* (2002, p. 848)?

Answer: Two nontrivial components of the low-Reynolds-number equation of change for fluid vorticity must be analyzed, based on the results in part (b). However, only the ϕ-component of the equation of motion contains useful information to calculate v_ϕ, as illustrated in part (d), and this is the preferred approach.

(d) Calculate the important nonzero components of the fluid velocity vector.

Answer: Use the postulated form of the one-dimensional velocity profile developed in part (a) and neglect the entire left side of the equation of motion for creeping flow conditions at low rotational speeds of the solid sphere. The fact that v_ϕ does not depend on ϕ, via symmetry, is consistent with the equation of continuity for an incompressible fluid. The r and θ components of the equation of motion for incompressible Newtonian fluids reveal that dynamic pressure is independent of r and θ, respectively, when centrifugal forces are negligible. Symmetry implies that $\mathfrak{P}$ does not depend on ϕ, and steady state suggests no time dependence. Hence, dynamic pressure is constant, similar to a hydrostatic situation. Fluid flow is induced by rotation of the solid and the fact that viscous shear is transmitted across the solid–liquid interface. As expected, the ϕ-component of the force balance yields useful information to calculate v_ϕ. The only terms that survive in the ϕ-component of the equation of motion are

$$\frac{1}{r^2}\frac{\partial}{\partial r}\left(r^2\frac{\partial v_\phi}{\partial r}\right)+\frac{1}{r^2}\frac{\partial}{\partial \theta}\left[\left(\frac{1}{\sin\theta}\right)\frac{\partial}{\partial\theta}(v_\phi\sin\theta)\right]=0$$

Now, one calculates $f(r)$ from the preceding equation by letting $v_\phi = f(r)\sin\theta$. For example:

$$\frac{\partial}{\partial\theta}(v_\phi\sin\theta)=2f(r)\sin\theta\cos\theta$$

$$\frac{1}{\sin\theta}\frac{\partial}{\partial\theta}(v_\phi\sin\theta)=2f(r)\cos\theta$$

$$\frac{\partial}{\partial\theta}\left[\frac{1}{\sin\theta}\frac{\partial}{\partial\theta}(v_\phi\sin\theta)\right]=-2f(r)\sin\theta$$

The ϕ-component of the equation of motion reduces to

$$\frac{\sin\theta}{r^2}\left[\frac{d}{dr}\left(r^2\frac{df}{dr}\right)-2f(r)\right]=0$$

If one adopts a trial solution of the form $f(r) \approx r^n$, or $r^n \ln r$ if two values of n are the same, then both terms in brackets in the preceding equation are proportional to r^n. Substitution yields

$$\sin\theta[n(n+1)-2]r^{n-2} = 0$$

and the roots are $n = -2, 1$. The general solution for the ϕ-component of the fluid velocity vector is

$$v_\phi(r,\theta) = \sin\theta\left(Ar + \frac{B}{r^2}\right)$$

The solution for $n = 1$ must be discarded because the fluid is stagnant at large r. Hence, $A = 0$. The boundary condition at the fluid–solid interface yields $B = \Omega R^3$. The creeping viscous flow solution is

$$v_\phi(r,\theta) = \frac{\Omega R^3 \sin\theta}{r^2}$$

(e) Calculate the differential vector force $\mathbf{dF}_{\text{solid on fluid}}$ exerted by the solid on the fluid across the spherical surface at $r = R$.

Answer: Begin by identifying the unit normal vector from the solid to the fluid across the surface at $r = R$; $\mathbf{n} = \delta_r$. Then (1) take the dot product of $\mathbf{n}$ with the total momentum flux tensor, (2) evaluate this vector-tensor operation at the fluid–solid interface, and (3) multiply the result by the differential surface element, $dS = R^2 \sin\theta\, d\theta\, d\phi$, to generate a differential vector force. Hence,

$$\mathbf{dF}_{\text{solid on fluid}} = \mathbf{n} \cdot (\rho\mathbf{vv} + \tau + p\delta)_{r=R}\, dS$$

where δ is the unit tensor. Forces due to convective momentum flux vanish because

$$(\mathbf{n} \cdot \rho\mathbf{vv})_{r=R}\, dS = (\rho v_r \mathbf{v})_{r=R}\, dS = 0$$

since there is no radial flow when the sphere rotates slowly. The final result is

$$\mathbf{dF}_{\text{solid on fluid}} = [\delta_r(\tau_{rr} + p) + \delta_\theta \tau_{r\theta} + \delta_\phi \tau_{r\phi}]_{r=R} R^2 \sin\theta\, d\theta\, d\phi$$

Notice how normal viscous stress τ_{rr} acts in the same coordinate direction as the pressure force. A force transducer implanted within the solid sphere cannot separate the effects due to each type of stress in the radial direction.

(f) What is the normal component of $\mathbf{dF}_{\text{solid on fluid}}$ due to?

Answer: Based on the final result in part (e) for $\mathbf{dF}_{\text{solid on fluid}}$, the normal stress is due to τ_{rr} and fluid pressure. In the absence of centrifugal forces, one calculates fluid pressure from the hydrostatic situation where dynamic pressure is constant throughout the fluid. Hence,

$$p(r = R, \theta) = p_\infty - \rho g R \cos\theta$$

where the xy-plane is the reference for potential energy and p_∞ is the fluid pressure in this reference plane at $z = 0$. Newton's law of viscosity for an incompressible fluid reveals that normal viscous stress vanishes everywhere in the fluid, because

$$\tau_{rr} = -2\mu \frac{\partial v_r}{\partial r} = 0$$

(g) What is/are the shear component(s) of $\mathbf{dF}_{\text{solid on fluid}}$ due to?

Answer: Based on the final result in part (e) for $\boldsymbol{d}\mathbf{F}_{\text{solid on fluid}}$, the shear stresses that must be considered are $\tau_{r\theta}$ and $\tau_{r\phi}$. Newton's law of viscosity for this one-dimensional flow problem reveals that only $\tau_{r\phi}$ is important, because

$$\tau_{r\theta} = -\mu \left[r \frac{\partial}{\partial r} \left(\frac{v_\theta}{r} \right) + \frac{1}{r} \frac{\partial v_r}{\partial \theta} \right] = 0$$

$$\tau_{r\phi}(r = R, \theta) = -\mu \left[r \frac{\partial}{\partial r} \left(\frac{v_\phi}{r} \right) \right]_{r=R} = 3\mu\Omega \sin\theta$$

(h) Calculate the differential vector torque $\mathbf{dT}$ that arises from $\mathbf{dF}_{\text{solid on fluid}}$ acting across the fluid–solid interface at $r = R$.

Answer: The answers to parts (e), (f) and (g) allow one to simplify the differential vector force exerted by the solid sphere on the fluid:

$$\mathbf{dF}_{\text{solid on fluid}} = [\delta_r p(r = R, \theta) + \delta_\phi \tau_{r\phi}(r = R, \theta)] R^2 \sin\theta \, d\theta \, d\phi$$

The corresponding differential torque is

$$\mathbf{dT} = \mathbf{r} \times \mathbf{dF}_{\text{solid on fluid}}$$

where $\mathbf{r}$ is the position vector defined in part (a). Hence,

$$\begin{aligned} \mathbf{dT} &= R \sin\theta (\delta_r \sin\theta + \delta_\theta \cos\theta) \times (\delta_r p + \delta_\phi \tau_{r\phi})_{r=R} R^2 \sin\theta \, d\theta \, d\phi \\ &= (\delta_r \tau_{r\phi} \cos\theta - \delta_\theta \tau_{r\phi} \sin\theta - \delta_\phi p \cos\theta)_{r=R} R^3 \sin^2\theta \, d\theta \, d\phi \end{aligned}$$

(i) Rewrite the three spherical coordinate unit vectors in terms of constant unit vectors in rectangular coordinates, and integrate your expression

from part (h) to calculate the macroscopic torque/angular velocity relation from which the Newtonian viscosity μ can be determined from measurements of torque vs. Ω.

Answer: Before the preceding equation can be integrated to obtain an expression for the macroscopic torque, it is necessary to use trigonometry and re-express the spherical coordinate unit vectors in terms of the set of constant unit vectors in Cartesian coordinates. This information can be found in Bird *et al*. (2002, p. 828). For example:

$$\delta_r = \delta_x \sin\theta\cos\phi + \delta_y \sin\theta\sin\phi + \delta_z \cos\theta$$

$$\delta_\theta = \delta_x \cos\theta\cos\phi + \delta_y \cos\theta\sin\phi - \delta_z \sin\theta$$

$$\delta_\phi = -\delta_x \sin\phi + \delta_y \cos\phi$$

Now the differential torque expression is rewritten in terms of δ_x, δ_y, and δ_z, using explicit results for $\tau_{r\phi}$ and fluid pressure at the fluid–solid interface:

$$\mathbf{dT} = [\delta_r 3\mu\Omega \sin\theta\cos\theta - \delta_\theta 3\mu\Omega \sin^2\theta - \delta_\phi(p_\infty - \rho g R\cos\theta)\cos\theta]R^3 \sin^2\theta\, d\theta\, d\phi$$

Macroscopic torque $\mathbf{T}$ is obtained via integration of the preceding equation over the surface of the solid sphere, where, for example, θ ranges from 0 to π, and ϕ ranges from 0 to 2π. There are no contributions to $\mathbf{T}$ in the x- and y-coordinate directions because, in all cases, one integrates either $\sin\phi$ or $\cos\phi$ over the complete period of these trigonometric functions. Hence, fluid pressure does not contribute to the relation between torque and angular velocity. It is only necessary to consider terms in the z direction due to δ_r and δ_θ. These are:

$$\mathbf{T} = \delta_z 6\pi\mu\Omega R^3 \int (\sin\theta\cos^2\theta + \sin^3\theta)\sin^2\theta\, d\theta$$

$$= \delta_z 6\pi\mu\Omega R^3 \int \sin^3\theta\, d\theta \qquad 0 \le \theta \le \pi$$

The final result is

$$\mathbf{T} = \delta_z \cdot 8\pi\mu\Omega R^3 = 8\pi\mu R^3 \mathbf{\Omega}$$

(j) In which coordinate direction does the macroscopic torque vector act?

Answer: Based on the development in part (i), macroscopic torque is colinear with the angular velocity vector of the solid sphere, and both of these vectors act in the z direction.

(k) Which scalar components of the viscous stress tensor contribute to the macroscopic torque/angular velocity relation?

Answer: Results in part (h) and (i) reveal that $\tau_{r\phi}$ is solely responsible for this macroscopic momentum transfer relation.

(l) Does fluid pressure contribute to the macroscopic torque/angular velocity relation?

Answer: No. See the discussion in part (i).

(m) Determine the parameters a, b, and c in the following scaling relation for the macroscopic torque:

$$\text{magnitude of the torque} \approx \mu^a \Omega^b R^c$$

Answer: Based on the answer to part (i), $a = 1$, $b = 1$, and $c = 3$.

(n) How do your answers in part (m) for a and b relate to the fact that the constitutive relation between viscous stress and velocity gradients is linear via Newton's law of viscosity?

Answer: The values for a and b in this scaling law from part (m) are a direct consequence of the fact that torque is linearly proportional to viscous shear stress, and Newton's law of viscosity is a linear constitutive relation between viscous stress and viscosity (i.e., $a = 1$), and viscous stress and velocity gradients (i.e., $b = 1$), the latter of which can be approximated by the angular velocity Ω of the solid sphere.

(o) Estimate the scaling parameter b in part (m) if the fluid were non-Newtonian with power-law index n in the classic Ostwald–de Waele model as described in Bird *et al.* (2002, p. 241).

Answer: For power-law fluids, viscous stress is proportional to the nth power of the shear rate, which represents the magnitude of the rate-of-strain tensor. Since torque scales linearly with viscous shear stress and shear rate scales linearly with angular velocity, it follows directly that torque scales as the nth power of Ω. Hence, $b = n$.

(p) Calculate the vorticity vector of the fluid, $\frac{1}{2}\nabla \times \mathbf{v}$, at the fluid–solid interface and demonstrate that the fluid vorticity at $r = R$ is different from the vorticity vector of the solid sphere, which undergoes solid body rotation at constant angular velocity Ω.

8-15. (a) Use vector notation and express the vector viscous force per unit area exerted by the rotating solid sphere on an incompressible Newtonian fluid at the fluid–solid interface (i.e., at $r = R$) for a rotating sphere viscometer. A one-line answer is required here. Be sure to include unit vectors in your answer.

Answer: Identify the unit normal vector from the solid sphere to the fluid at the fluid–solid interface (i.e., $\mathbf{n} = \delta_r$). Now, construct the dot

product of this unit normal vector with the viscous stress tensor and evaluate the result at $r = R$. For example,

$$\mathbf{n} \cdot \tau = \tau_r = (\delta_r \tau_{rr} + \delta_\theta \tau_{r\theta} + \delta_\phi \tau_{r\phi})_{r=R}$$

(b) Use the postulated form of the velocity profile for this incompressible Newtonian fluid from part (1) of Problem 8-10 and summarize the state of viscous stress in matrix form. It is not necessary to obtain the exact analytical solution for the velocity profile at low Reynolds numbers to solve this problem.

Answer: The following functional form of the low-Reynolds-number one-dimensional fluid velocity profile is based on solid-body rotation at $r = R$ and conforms to the no-slip boundary condition at the fluid–solid interface:

$$v_\phi(r, \theta) = f(r) \sin\theta$$

Consequently, Newton's law of viscosity reveals that the only nonvanishing components of the viscous stress tensor are the symmetric pair given below:

$$\tau_{r\phi} = \tau_{\phi r} = -\mu r \frac{\partial}{\partial r}\left(\frac{v_\phi}{r}\right) = -\mu r \sin\theta \frac{d}{dr}\left[\frac{f(r)}{r}\right]$$

(c) Is it easier to calculate v_ϕ (1) using the equation of motion, (2) using the stream function approach with the equation of change for fluid vorticity, or (3) are both approaches equally difficult? Choose one of these answers for low Reynolds number flow.

Answer: Approach (i) requires that one must solve the ϕ-component of the equation of motion. Since v_ϕ is a function of both r and θ, there are two nonzero components of $\nabla \times \mathbf{v}$ (i.e., the r and θ components are nontrivial). Hence, approach (ii) requires that one must consider the r and θ components of the Laplacian of the vorticity vector to obtain an expression for the stream function via the low-Reynolds-number equation of change for fluid vorticity. The preferred approach is (1).

(d) At low Reynolds numbers, the solution for one-dimensional flow of an incompressible Newtonian fluid in the rotating sphere viscometer is

$$v_\phi(r, \theta) = \sin\theta \left(Ar + \frac{B}{r^2}\right)$$

Calculate the integration constants A and B.

Answer: The fluid velocity is maximum at the fluid–solid interface and decreases at larger values of r. In particular, v_ϕ tends toward zero

as r approaches infinity. Hence, $A = 0$. Solid-body rotation at $r = R$ yields the following result for integration constant B:

$$v_\phi(r = R, \theta) = \Omega R \sin\theta = \frac{B}{R^2} \sin\theta$$

Therefore, $B = \Omega R^3$.

8-16. A cylindrical fiber is subjected to elongational flow along the fiber axis such that the z-component of the velocity vector is $v_z = Az$, where A is a positive constant that defines the rate of elongational flow. The fiber is isotropic with a Poisson ratio of 0.5, which means that there is no volume change during extensional flow. Newton's law of viscosity is valid to describe this phenomenon.

(a) If the fiber contracts laterally upon extension, then calculate the other important nonzero velocity component.

Answer: Invoke incompressibility because extensional flow occurs at constant volume when Poisson's ratio is $\frac{1}{2}$. In cylindrical coordinates with no flow in the θ direction, the steady-state equation of continuity reduces to

$$\nabla \cdot \mathbf{v} = \frac{1}{r}\frac{\partial}{\partial r}(r v_r) + \frac{\partial v_z}{\partial z} = 0$$

Since $\partial v_z/\partial z = A$, integration of the preceding equation at constant θ and z yields

$$\int d(r v_r) = -\int Ar\, dr$$

Hence,

$$r v_r = -\tfrac{1}{2} A r^2 + g(\theta, z)$$

Integration constant g, which in principle could be a function of θ and z, vanishes when the preceding equation is evaluated at $r = 0$. The radial velocity profile is

$$v_r(r) = -\tfrac{1}{2} A r$$

Since radial flow is negative, or inward, this is consistent with lateral contraction to maintain constant volume when a cylindrical fiber is stretched along its z axis.

(b) Calculate the viscous stress tensor τ and display your results in matrix form.

Answer: Apply Newton's law of viscosity to the following fluid velocity vector field;

$$v_r(r) = -\tfrac{1}{2}Ar \qquad v_\theta = 0 \qquad v_z(z) = Az \qquad \nabla \cdot \mathbf{v} = 0$$

There are no nonzero off-diagonal shear components of τ. The rr and zz components are

$$\tau_{rr} = -2\mu\frac{\partial v_r}{\partial r} = \mu A \qquad \tau_{zz} = -2\mu\frac{\partial v_z}{\partial z} = -2\mu A$$

(c) The elongational viscosity η is defined by the following equation:

$$\tau_{zz} - \tau_{rr} = -\eta\frac{\partial v_z}{\partial z}$$

What is the relation between the elongation viscosity η and the Newtonian viscosity μ?

Answer: Use the results from part (b) for τ_{rr} and τ_{zz} in the defining equation for elongational viscosity, with $\partial v_z/\partial z = A$:

$$\tau_{zz} - \tau_{rr} = -3\mu A = -\eta A$$

Hence, $\eta = 3\mu$.

8-17. Consider the following scalar components of the velocity vector for a viscoelastic liquid in rectangular coordinates:

$$v_x = ax \qquad a > 0$$

$$v_y = by$$

$$v_z = bz$$

(a) Calculate $\nabla \cdot \mathbf{v}$, $\nabla \times \mathbf{v}$, and the rate-of-strain tensor [i.e., $\partial\gamma/\partial t = \nabla\mathbf{v} + (\nabla\mathbf{v})^{\mathrm{T}}$].

(b) What is the relation between the constants a and b?

Answer: Assume that the liquid is incompressible and apply the equation of continuity to this three-dimensional flow field. In rectangular coordinates,

$$\nabla \cdot \mathbf{v} = \frac{\partial v_x}{\partial x} + \frac{\partial v_y}{\partial y} + \frac{\partial v_z}{\partial z} = a + b + b = 0$$

Hence, $b = -\dfrac{1}{2}a < 0$.

(c) Describe this viscoelastic flow field in words.

Answer: This fluid flow description is consistent with elongational flow in the x direction, and simultaneous lateral contraction in the y and z directions, transverse to the primary flow. The process occurs at constant volume and constant density such that Poisson's ratio is $\frac{1}{2}$.

8-18. Consider one-dimensional laminar viscous flow through a straight tube with circular cross section [i.e., $v_z(r)$] and obtain an expression for the axisymmetric stream function ψ at the tube wall, where $r = R$. The average velocity through the tube is $\langle v_z \rangle$.

8-19. Consider one-dimensional viscous flow of an incompressible Newtonian fluid axially (i.e., only v_z) through a straight tube of length L with circular cross section and radius R. The Reynolds number is 500, based on the tube diameter.

(a) Is it possible to use the stream function approach to analyze this flow problem by solving only one nontrivial component of the equation of change for fluid vorticity?

Answer: Even though the flow regime is laminar, not creeping, there are no surviving terms due to the accumulation rate process or convective momentum flux on the left side of any component of the equation of motion. This is a consequence of the fact that there is flow in only one direction, and steady-state analysis of the equation of continuity reveals that v_z is not a function of independent variable z. Hence, the equation of motion is exactly the same for steady-state one-dimensional laminar or creeping flow through a tube, because there is a balance among viscous, pressure, and gravity forces. This problem is a subset of the following class of axisymmetric two-dimensional flows in cylindrical coordinates:

$$v_r(r, z) \text{ and } v_z(r, z) \qquad \text{with } v_\theta = 0$$

where the z axis represents the axis of symmetry and θ is the symmetry variable. It is possible to analyze this laminar flow problem via the stream function, because it is necessary to solve only one nontrivial component of the equation of change for fluid vorticity.

(b) Which nontrivial component(s) of the vorticity equation must be solved to calculate the stream function?

Answer: The θ component. Consider all three components of the vorticity vector in cylindrical coordinates when the velocity vector field is $v_z(r)$;

$$r\text{-component:} \qquad \frac{1}{r}\frac{\partial v_z}{\partial \theta} - \frac{\partial v_\theta}{\partial z} = 0 \qquad \text{(trivial)}$$

$$\theta\text{-component:} \qquad \frac{\partial v_r}{\partial z} - \frac{\partial v_z}{\partial r} \neq 0$$

$$z\text{-component:} \qquad \frac{1}{r}\frac{\partial (r v_\theta)}{\partial r} - \frac{1}{r}\frac{\partial v_r}{\partial \theta} = 0 \qquad \text{(trivial)}$$

(c) On which variables does the stream function ψ depend?

Answer: Since the nonzero velocity component v_z depends on radial position r, so does the stream function ψ. This can be verified by considering the relation between v_z and ψ:

$$v_z(r) = \frac{1}{r}\frac{\partial \psi}{\partial r}$$

Hence, $\psi = \psi(r)$.

(d) What equation must be solved to calculate ψ?

Answer: One must solve the following fourth-order ordinary differential equation for $\psi(r)$:

$$E^4\psi = E^2(E^2\psi) = 0$$

where the E^2 operator for this axisymmetric flow problem in cylindrical coordinates is

$$E^2 = \frac{d^2}{dr^2} - \frac{1}{r}\frac{d}{dr}$$

Recall that the ∇^2 operator must be replaced by the corresponding E^2 operator for axisymmetric flows in cylindrical and spherical coordinates.

(e) If the solution to part (d) is

$$\psi = A + Br^2 + Cr^2 \ln r + Dr^4$$

then write all the boundary conditions that are required to calculate the integration constants A, B, C, and D. It is not necessary to evaluate these integration constants explicitly.

Answer:

(1) There is no flow through a point on the symmetry axis at $r = 0$. Therefore, $\psi(r = 0) = 0$.

(2) There is no slip at the wall at $r = R$. Therefore, $v_z(r = R) = (1/R)(d\psi/dr)_{r=R} = 0$.

(3) If one end of a vector is pinned on the symmetry axis at $r = 0$ and the other end lies somewhere on the lateral surface of the tube at $r = R$, then this vector maps out a circular cross section of πR^2 when it is rotated by 2π radians around the symmetry axis. The volumetric flow rate through this circle is $\pi R^2 \langle v_z \rangle$, where $\langle v_z \rangle$ is the average fluid velocity through the tube. The axisymmetric stream function at $r = R$ is defined by

$$\psi(r = R) = \frac{\pi R^2 \langle v_z \rangle}{2\pi} = \frac{1}{2} R^2 \langle v_z \rangle$$

These three conditions are sufficient to determine all four integration constants. The symmetry condition on v_z at $r = 0$, namely $(dv_z/dr)_{r=0} = 0$, is satisfied by the functional form of $\psi(r)$ and provides no new information to calculate any of the integration constants.

(f) Use one of the boundary conditions at $r = 0$ (i.e., along the centerline of the tube) to simplify the general solution for ψ in part (e).

Answer: Boundary condition (1) in the solution to part (e) indicates that there is no flow through a point on the symmetry axis at $r = 0$. In other words, if both ends of a vector lie on this centerline, then no cross-sectional surface area results from a 360° rotation of this vector around the symmetry axis. Hence, the volumetric flow rate Q and the stream function ψ vanish at $r = 0$. One concludes that $A = C = 0$ and

$$\psi(r) = Br^2 + Dr^4$$

(g) Calculate the velocity profile without performing any tedious algebra to evaluate the integration constants.

Answer: Use the result from part (f) and the relation between v_z and ψ to obtain the velocity profile: for example,

$$v_z(r) = \frac{1}{r}\frac{d\psi}{dr} = 2B + 4Dr^2$$

This is the classic parabolic or quadratic velocity profile for one-dimensional laminar flow of an incompressible Newtonian fluid through a straight tube. The no-slip boundary condition (2) at $r = R$ yields

$$D = -\frac{1}{2}\left(\frac{B}{R^2}\right)$$

Boundary condition (3) yields

$$\psi(r = R) = BR^2 + DR^4 = \tfrac{1}{2}BR^2 = \tfrac{1}{2}R^2\langle v_z \rangle$$

Hence, $B = \langle v_z \rangle$ and

$$v_z(r) = 2\langle v_z \rangle \left[1 - \left(\frac{r}{R} \right)^2 \right]$$

8-20. Calculate the stream function for axisymmetric fully developed creeping viscous flow of an incompressible Newtonian fluid in the annular region between two concentric tubes. This problem is analogous to axial flow on the shell side of a double-pipe heat exchanger. It is not necessary to solve algebraically for all the integration constants. However, you must include all the boundary conditions that allow one to determine a unique solution for ψ. Express your answer for the stream function in terms of:

(1) The appropriate independent variables.

(2) The volumetric flow rate in the direction of flow, Q.

(3) The radius of the outer tube, R.

(4) The radius ratio of the inner tube to the outer tube, $0 < \kappa < 1$.

Sketch the streamlines.

8-21. **(a)** Sketch three fluid streamlines for creeping viscous flow around a stationary solid sphere. Estimate the value of the stream function ψ on each streamline.

(b) Sketch three fluid streamlines within the incompressible liquid phase as a gas bubble rises through an otherwise stationary viscous fluid in the creeping flow regime. Estimate the value of the stream function ψ on each streamline.

(c) Sketch the radial (r) dependence of the fluid pressure distribution at a polar angle $\theta = \pi$ radians for creeping viscous flow of an incompressible Newtonian fluid moving upward past (**i**) a solid sphere, and (**ii**) a gas bubble, both of which are stationary. Include both sketches on one set of axes so that they can be compared qualitatively.

8-22. A solid sphere of radius R falls very slowly with velocity V_{solid} in the negative z direction (i.e., $-\delta_z$) through an incompressible Newtonian liquid that is quiescent far from the sphere.

(a) Calculate the stream function $\psi(r, \theta)$.

Answer: For axisymmetric creeping flow in spherical coordinates, the general solution to the low-Reynolds-number equation of change for fluid vorticity (i.e., $E^4\psi = 0$) is

$$\psi(r, \theta) = \sin^2\theta \left(\frac{A}{r} + Br + Cr^2 + Dr^4 \right)$$

where integration constants A, B, C, and D are determined from the boundary conditions. Since the fluid is stationary far from the submerged object, the fluid velocity vector must vanish as r tends toward infinity. Hence,

$$v_r(r,\theta) = -\frac{1}{r^2 \sin\theta}\frac{\partial \psi}{\partial \theta} = -2\cos\theta\left(\frac{A}{r^3} + \frac{B}{r} + C + Dr^2\right) = 0$$

$$v_\theta(r,\theta) = \frac{1}{r\sin\theta}\frac{\partial \psi}{\partial r} = \sin\theta\left(-\frac{A}{r^3} + \frac{B}{r} + 2C + 4Dr^2\right) = 0$$

when $r \to \infty$. The no-flow condition at large r requires that $C = 0$ and $D = 0$. Now, the two-dimensional velocity profile is

$$v_r = -2\cos\theta\left(\frac{A}{r^3} + \frac{B}{r}\right)$$

$$v_\theta = \sin\theta\left(-\frac{A}{r^3} + \frac{B}{r}\right)$$

From the viewpoint of an observer in a stationary reference frame, one invokes the no-slip condition at the fluid–solid interface when the center of the solid sphere coincides with the center of an xyz coordinate system. Hence, at $r = R$,

$$v_r = \delta_r \cdot [V_{\text{solid}}(-\delta_z)] = -V_{\text{solid}}\cos\theta = -2\cos\theta\left(\frac{A}{R^3} + \frac{B}{R}\right)$$

$$v_\theta = \delta_\theta \cdot [V_{\text{solid}}(-\delta_z)] = V_{\text{solid}}\sin\theta = \sin\theta\left(-\frac{A}{R^3} + \frac{B}{R}\right)$$

These two equations yield the following results for integration constants A and B:

$$A = -\tfrac{1}{4}R^3 V_{\text{solid}} \qquad B = \tfrac{3}{4}RV_{\text{solid}}$$

The final results for the stream function and the two nonzero velocity components are

$$\psi(r,\theta) = \sin^2\theta\left(\frac{A}{r} + Br\right) = V_{\text{solid}}R^2\sin^2\theta\left(\frac{3}{4}\eta - \frac{1}{4}\eta^{-1}\right)$$

$$v_r(r,\theta) = -2\cos\theta\left(\frac{A}{r^3} + \frac{B}{r}\right) = -V_{\text{solid}}\cos\theta\left(\frac{3}{2}\eta^{-1} - \frac{1}{2}\eta^{-3}\right)$$

$$v_\theta(r,\theta) = \sin\theta\left(-\frac{A}{r^3} + \frac{B}{r}\right) = V_{\text{solid}}\sin\theta\left(\frac{3}{4}\eta^{-1} + \frac{1}{4}\eta^{-3}\right)$$

where $\eta = r/R$.

(b) Calculate the hydrodynamic drag force exerted by the fluid on the solid across the spherical interface at $r = R$.

Answer: The coefficient of $\frac{1}{2}r\sin^2\theta$ in the expression for ψ from part (a) is $\frac{3}{2}RV_{\text{solid}}$. Hence, the hydrodynamic force exerted by the fluid on the solid sphere across the fluid–solid interface at $r = R$ is given by the following expression:

$$\begin{aligned}\text{hydrodynamic force} &= 4\pi\mu_{\text{fluid}}(\text{coefficient of } \tfrac{1}{2}r\sin^2\theta \text{ in}\psi)\\ &= 6\pi\mu_{\text{fluid}}RV_{\text{solid}}\end{aligned}$$

which is Stokes's law. This macroscopic relation in fluid dynamics is the same for incompressible Newtonian fluids impinging on stationary solid spheres, or solid spheres falling through stagnant liquids. However, microscopic results for these two problems (i.e., ψ, v_r, and v_θ) are different.

(c) In which direction does this force act?

Answer: Since the answer to part (b) is positive, the hydrodynamic force exerted by the fluid on the solid sphere acts upward in the positive z direction. When the submerged object is stationary and the fluid moves, the hydrodynamic force exerted by the fluid on the solid acts in the primary direction of fluid flow. When the fluid is stationary and the submerged object moves, the hydrodynamic force exerted by the fluid on the solid acts in the opposite direction of the motion of the solid. Hence, the solid sphere falls in the negative z direction, and the hydrodynamic force exerted by the fluid on the solid acts upward.

8-23. Consider creeping viscous flow of an incompressible Newtonian fluid past a stationary gas bubble that is located at the origin of a spherical coordinate system. Do not derive, but write an expression for the tangential velocity component (i.e., v_θ) and then linearize this function with respect to the normal coordinate r within a thin mass transfer boundary layer in the liquid phase adjacent to the gas–liquid interface. *Hint*: Consider the r–θ component of the rate-of-strain tensor:

$$\left(\frac{\partial\gamma}{\partial t}\right)_{r\theta} = r\frac{\partial}{\partial r}\left(\frac{v_\theta}{r}\right) + \frac{1}{r}\frac{\partial v_r}{\partial\theta}$$

evaluated at the gas–liquid interface for the coefficient of the first-order term in the Taylor series that is linear in radial position r.

8-24. **(a)** A gas bubble of radius R rises through a stagnant incompressible Newtonian fluid. The bubble-rise velocity V_0 is constant, and the Reynolds number, $\rho V_0(2R)/\mu$, is approximately 0.15. What boundary conditions are required to calculate the stream function ψ for

axisymmetric two-dimensional flow within the liquid phase when the center of the rising bubble is at the origin of a stationary spherical coordinate system?

(b) Repeat part (a) if a solid sphere of radius R falls vertically at constant velocity V_{solid} through a quiescent liquid.

(c) Calculate the dynamic force exerted by the fluid on the bubble in part (a) and the solid in part (b) across the spherical boundary at $r = R$, and identify the direction in which these forces act.

8-25. A solid sphere of radius R_{sphere} and density ρ_{sphere} falls through an incompressible Newtonian fluid which is quiescent far from the sphere. The viscosity and density of the fluid are μ_{fluid} and ρ_{fluid}, respectively. The Reynolds number is 50, based on the physical properties of the fluid, the diameter of the sphere, and its terminal velocity. The following scaling law characterizes the terminal velocity of the sphere in terms of geometric parameters and physical properties of the fluid and solid:

$$\log v_{\text{terminal}} \approx \alpha \log R_{\text{sphere}} + \beta \log(\rho_{\text{sphere}} - \rho_{\text{fluid}}) + \gamma \log \mu_{\text{fluid}} + \delta \log \rho_{\text{fluid}}$$

(a) Calculate the scaling law parameters α, β, γ, and δ in the equation above. Four numerical answers are required here.

Answer: Since there is no longer any acceleration when submerged objects achieve terminal velocity, the sum of all forces acting on the object must be zero. Hence, there is a balance between buoyancy, gravity, and hydrodynamic drag. The gravity force acts downward, and the buoyant and drag forces act in the opposite direction. Each force is calculated as follows:

Gravitational force:	$\frac{4}{3}\pi R_{\text{sphere}}^3 \rho_{\text{solid}} g$
Buoyant force:	$\frac{4}{3}\pi R_{\text{sphere}}^3 \rho_{\text{fluid}} g$
Hydrodynamic drag force:	$\frac{1}{2}\rho_{\text{fluid}} v_{\text{terminal}}^2 (\pi R_{\text{sphere}}^2) f$

For flow around spheres in any regime, the dimensionless momentum transfer correlation adopts the following form:

$$f = \frac{C_1}{\text{Re}^a} \qquad \text{Re} = \frac{\rho_{\text{fluid}} v_{\text{terminal}} (2R_{\text{sphere}})}{\mu_{\text{fluid}}}$$

Now, the hydrodynamic drag force can be expressed explicitly in terms of physical properties of the fluid and solid:

$$\text{hydrodynamic drag force} = \frac{\pi C_1}{2^{1+a}} (\mu_{\text{fluid}})^a (\rho_{\text{fluid}})^{1-a} (R_{\text{sphere}} v_{\text{terminal}})^{2-a}$$

Rearrangement of the above-mentioned force balance yields the following solution for v_{terminal}:

$$(v_{\text{terminal}})^{2-a} = \frac{(2^{3+a}/3C_1)(R_{\text{sphere}})^{1+a}(\rho_{\text{solid}} - \rho_{\text{fluid}})g}{(\mu_{\text{fluid}})^a(\rho_{\text{fluid}})^{1-a}}$$

Therefore, the scaling law parameters are

$$\alpha = \frac{1+a}{2-a} \qquad \beta = \frac{1}{2-a} \qquad \gamma = \frac{-a}{2-a} \qquad \delta = -\left(\frac{1-a}{2-a}\right)$$

where $a = \frac{3}{5}$ in the intermediate (i.e., laminar) flow regime. With reference to a creeping flow falling sphere viscometer, one measures the terminal velocity of a solid sphere that falls slowly through an incompressible Newtonian fluid. In the creeping flow regime, the dimensionless momentum transfer correlation for solid spheres is $f = 24/Re$, which corresponds to $C_1 = 24$ and $a = 1$. Hence,

$$v_{\text{terminal}} = \frac{\frac{2}{9}R_{\text{sphere}}^2(\rho_{\text{solid}} - \rho_{\text{fluid}})g}{\mu_{\text{fluid}}}$$

One estimates the fluid viscosity by rearranging this equation. This prediction is accurate if the Reynolds number is smaller than 0.5.

(b) A different sphere of the same density with radius $2R_{\text{sphere}}$ falls through the same incompressible Newtonian fluid. Now, the Reynolds number is greater than 50 but less than 500, because the diameter of the sphere has increased by a factor of 2. Does the terminal velocity of the sphere increase, decrease, or remain unchanged?

Answer: Since the scaling law exponent $\alpha > 0$ (i.e., $\alpha = \frac{8}{7}$ when $a = \frac{3}{5}$), one achieves larger terminal velocity if the size of the sphere increases.

(c) By how much, or by what factor, does v_{terminal} change in part (b)? For example, if the terminal velocity of the sphere remains unchanged, then it changes by a factor of 1.

Answer: The scaling law in part (a) can provide both qualitative and quantitative results. If the sphere radius increases by a factor of 2, then v_{terminal} increases by $(2)^{(1+a)/(2-a)}$, which corresponds to $(2)^{8/7}$.

(d) How does the scaling law for terminal velocity change if a nondeformable bubble of radius R_{bubble} rises with constant velocity through the same incompressible Newtonian fluid in the same flow regime (i.e., $50 \leq \text{Re} \leq 500$)?

Answer: First, one must replace R_{sphere} by R_{bubble}, but this is a minor change. Second and most important, the hydrodynamic drag force

acts downward when bubbles rise. Now, the upward buoyant force is counterbalanced by gravity and hydrodynamic drag. Consequently, one must replace $(\rho_{\text{solid}} - \rho_{\text{fluid}})$ by $(\rho_{\text{fluid}} - \rho_{\text{bubble}})$ in the scaling law for v_{terminal}, as presented in part (a).

8-26. We apply here hydrodynamic drag forces via f vs. the Reynolds number to calibrate a rotameter for a test fluid which is different from the original fluid that was used to calibrate the rotameter. A rotameter consists of a vertical conical tube that contains a float of higher density than that of the fluid passing through the meter. The tube diameter is not constant, but it increases linearly as the float moves to higher positions in the conical tube. This feature allows the rotameter to measure a wide range of mass flow rates. When the rotameter is calibrated for a particular fluid, it is very straightforward to measure mass flow rates for that fluid in terms of the height of the float under steady-state conditions. You are given a rotameter calibration curve for water which illustrates that mass flow rate is linearly proportional to float height. However, experiments on a distillation column require that you measure the mass flow rates of alcohols using the rotameter that was calibrated for water.

(a) Devise a strategy and use that strategy to modify the rotameter calibration curve for water so that one can measure the mass flow rate of an alcohol using the same rotameter. Your final answer should include strategies when a log-log plot of friction factor vs. Reynolds number for flow through a conical tube that contains a submerged object (i.e, the float) (1) is a straight line with a slope of -1.0, (2) is a straight line with a slope of -0.5, (3) is a straight line with zero slope.

Answer: Results from Problem 8-25 provide a generalized expression for the terminal velocity of solids or bubbles in stationary fluids. The same results describe the average fluid velocity in the vicinity of a stationary submerged object such as the rotameter float. Of course, the shear area and volume of a solid sphere or gas bubble are well defined in terms of the radius of the submerged object. The corresponding shear area and volume of the rotameter float can be measured, but they cannot be expressed in terms of one simple geometric parameter. Fortunately, these quantities don't change when a different fluid passes through the rotameter. The strategy below, which focuses on the following scaling law for the average fluid velocity in the vicinity of the float,

$$\langle v \rangle_{\text{fluid}} \approx \frac{(\rho_{\text{solid}} - \rho_{\text{fluid}})^{1/(2-a)}}{[(\mu_{\text{fluid}})^{a/(2-a)}(\rho_{\text{fluid}})^{(1-a)/(2-a)}]}$$

reveals that the shear area, float volume, and gravitational acceleration constant do not affect the rotameter correction factor. One obtains the corresponding mass flow rate from the previous scaling law via multiplication by the fluid density and the cross-sectional area. Since the

rotameter correction factor compares mass flow rates for two different fluids when the float height is the same, the flow cross section does not appear in the final result. Hence, it is only necessary to multiply $\langle v \rangle_{\text{fluid}}$ by ρ_{fluid}. Therefore, when the float is at the same position, the mass flow rate of any fluid through the same rotameter scales as

$$\rho_{\text{fluid}} \langle v \rangle_{\text{fluid}} \approx \frac{[\rho_{\text{fluid}}(\rho_{\text{solid}} - \rho_{\text{fluid}})]^{1/(2-a)}}{(\mu_{\text{fluid}})^{a/(2-a)}}$$

The quantity on the right side of this equation must be evaluated for the test fluid and the calibration fluid. This ratio (i.e., test fluid/calibration fluid) represents the calibration factor, which one must multiply by the mass flow rate of the calibration fluid at a given rotameter float height to obtain the mass flow rate of the test fluid when the float is in the same position.

For part (1), $a = 1$ and the mass flow rate for each fluid scales as

$$\text{mass flow rate} \approx \frac{\rho_{\text{fluid}}(\rho_{\text{solid}} - \rho_{\text{fluid}})}{\mu_{\text{fluid}}}$$

For part (2), $a = 0.5$ and the mass flow rate for each fluid scales as

$$\text{mass flow rate} \approx \frac{[\rho_{\text{fluid}}(\rho_{\text{solid}} - \rho_{\text{fluid}})]^{2/3}}{(\mu_{\text{fluid}})^{1/3}}$$

For part (3), $a = 0$ and the mass flow rate for each fluid scales as

$$\text{mass flow rate} \approx [\rho_{\text{fluid}}(\rho_{\text{solid}} - \rho_{\text{fluid}})]^{1/2}$$

(b) At 20°C, the density of water is 1.00 g/cm^3 and the density of methanol is 0.79 g/cm^3. The float density is 3.95 g/cm^3. Compare the mass flow rates of water and methanol through the same rotameter at 20°C when the float rests at the same position in the rotameter. In both cases, the dimensionless momentum transport correlation is $f \approx$ constant in the high-Reynolds-number regime.

Answer: Evaluate the mass flow rate scaling factor for water and methanol via the prescription from part (3) above, because $a = 0$. Then, construct the ratio of these scaling factors to compare the mass flow rates of the two fluids. For example:

(1) Mass flow rate of water $\approx [\rho_{\text{water}}(\rho_{\text{float}} - \rho_{\text{water}})]^{1/2}$

(2) Mass flow rate of methanol $\approx [\rho_{\text{methanol}}(\rho_{\text{float}} - \rho_{\text{methanol}})]^{1/2}$

The ratio of (1) to (2) is 1.09, which indicates that the mass flow rate of water is 9% larger than that of methanol.

(c) How does your comparison of the mass flow rates of water and methanol at 20°C from part (b) change if the float density is only 1.35 g/cm^3?

Answer: Use the scaling laws in part (b) for water and methanol, but reduce the float density from 3.95 g/cm^3 to 1.35 g/cm^3. Now, the ratio of (1) to (2) is 0.89, which indicates that the mass flow rate of water is about 11% less than that of methanol.

(d) In the highly turbulent regime, the mass flow rates of water and methanol will be the same at 20°C when a particular float rests at the same position in the rotameter. What float density is required for this statement to be true?

Answer: Equate the scaling laws in part (b) for water and methanol and solve for ρ_{float}:

$$[\rho_{\text{water}}(\rho_{\text{float}} - \rho_{\text{water}})]^{1/2} = [\rho_{\text{methanol}}(\rho_{\text{float}} - \rho_{\text{methanol}})]^{1/2}$$

$\rho_{\text{float}} = 1.8$ g/cm^3.

8-27. It should be obvious that the terminal velocity of a bowling ball in air is much larger than the terminal velocity of a feather in air. However, in both cases, a steady-state force balance on the object that accounts for buoyancy, gravity, and hydrodynamic drag reveals that $\log(v_{\text{terminal}}) \approx \beta \log(\rho_{\text{solid}} - \rho_{\text{air}})$, where ρ_{solid} corresponds to either the bowling ball or the feather.

(a) What is the value of β if $\text{Re}_{\text{bowling ball}} \approx 200{,}000$?

(b) What is the value of β if $\text{Re}_{\text{feather}} \approx 0.01$?

8-28. (a) By what factor do viscous shear forces at the tube wall increase when the volumetric flow rate through a straight tube is four-fold larger for:

(i) Incompressible Newtonian fluids.

(ii) Incompressible non-Newtonian power-law fluids, with a power-law exponent of 0.5.

In both cases, the flow regime is laminar.

(b) By what factor do normal convective forces increase when the volumetric flow rate through a straight tube is four-fold larger for:

(i) Incompressible Newtonian fluids.

(ii) Incompressible non-Newtonian power-law fluids, with a power-law exponent of 0.5.

In both cases, the flow regime is laminar.

8-29. Laminar flow of an incompressible Newtonian fluid through a straight tube with radius R and length L corresponds to $f = 16/\text{Re}$ and $\log Q \approx$

$\log \Delta\mathfrak{P}$, where f is the friction factor, Re the Reynolds number based on the tube diameter, Q the volumetric flow rate, and $\mathfrak{P}$ the dynamic pressure. Determine the scaling law exponent α for turbulent flow of an incompressible Newtonian fluid through the same tube:

$$\log Q \approx \alpha \log(\Delta\mathfrak{P})$$

where $f = 0.0791/\mathrm{Re}^{1/4}$. *Hint*: The z-component of the dynamic force exerted by the fluid on the wall at $r = R$ is $\pi R^2 \Delta\mathfrak{P}$.

Answer: Prior to solving this problem, it is instructive to consider the underlying fundamentals related to the hint provided above. In terms of the total momentum flux tensor, the total differential vector force exerted by the fluid on the tube wall is

$$\mathbf{dF}_{\text{fluid on solid}} = \mathbf{n} \cdot (\rho \mathbf{vv} + \tau + p\delta)_{r=R}\, dS$$

where $\mathbf{n} = \delta_r$ and the differential lateral surface element is $dS = R\, d\theta\, dz$. Forces due to convective momentum flux vanish because

$$(\mathbf{n} \cdot \rho \mathbf{vv})_{r=R}\, dS = (\rho v_r \mathbf{v})_{r=R}\, dS = 0$$

Both v_r and the total velocity vector vanish at the stationary wall. Now, the differential vector force can be expressed in terms of cylindrical coordinate unit vectors;

$$\mathbf{dF}_{\text{fluid on solid}} = [\delta_r(\tau_{rr} + p) + \delta_\theta \tau_{r\theta} + \delta_z \tau_{rz}]_{r=R} R\, d\theta\, dz \qquad (a)$$

The z-component of $\mathbf{dF}_{\text{fluid on solid}}$ is obvious from expression (a). Rigorously, it is obtained via the following scalar dot-product operation;

$$\delta_z \cdot \mathbf{dF}_{\text{fluid on solid}} = [\tau_{rz}(r = R)] R\, d\theta\, dz \qquad (b)$$

Integration of equation (b) over the complete lateral surface (i.e., $0 \le \theta \le 2\pi$, $0 \le z \le L$) for incompressible Newtonian fluids yields

$$(\mathbf{F}_{\text{fluid on solid}})_{z\text{-component}} = \int (\delta_z \cdot \mathbf{dF}_{\text{fluid on solid}})$$
$$= \iint \left[-\mu \left(\frac{dv_z}{dr} \right)_{r=R} \right] R\, d\theta dz$$

For one-dimensional flow in the z direction, where $v_z(r)$ is a function of radial position only, the final expression for the macroscopic dynamic force

simplifies considerably because τ_{rz} is independent of the lateral surface coordinates. Hence,

$$(\mathbf{F}_{\text{fluid on solid}})_{z\text{-component}} = \left[-\mu\left(\frac{dv_z}{dr}\right)_{r=R}\right] 2\pi RL = \pi R^2 \Delta\mathfrak{P} \qquad (c)$$

This result is verified rather easily for laminar flow in terms of the microscopic fluid velocity gradient at the tube wall. For steady-state one-dimensional flow through a straight tube in any regime, the macroscopic mass and momentum balances yield the same result, as given by equation (c). The solution to this problem begins by employing the macroscopic momentum transfer correlation, which includes the definition of the friction factor, to evaluate the z-component of the dynamic force exerted by the fluid on the tube wall, with shear area given by $2\pi RL$: for example,

$$(\mathbf{F}_{\text{dynamic}})_{z\text{-component}} = \pi R^2 \Delta\mathfrak{P} = \tfrac{1}{2}\rho\langle v_z\rangle^2 (2\pi RL) f$$

Now, use the dimensionless correlation for f vs. Re, where the Reynolds number is defined in terms of the tube diameter:

$$\text{Re} = \frac{\rho\langle v_z\rangle 2R}{\mu}$$

In terms of the scaling law for dynamic force,

$$(\mathbf{F}_{\text{dynamic}})_{z\text{-component}} = \pi R^2 \Delta\mathfrak{P} \approx \mu^a \rho^{1-a} \langle v_z\rangle^{2-a}$$

where $a = \frac{1}{4}$ in the turbulent flow regime. For tube flow, average velocity $\langle v_z\rangle$ and volumetric flow rate Q are related by the cross-sectional area for flow (i.e., πR^2). Hence, the dynamic pressure drop $\Delta\mathfrak{P}$ scales as Q taken to the $(2-a)$ power. In other words,

$$\Delta\mathfrak{P} \approx Q^{2-a}$$

Therefore, the scaling law exponent that relates Q to $\Delta\mathfrak{P}$ is $\alpha = 1/(2-a) = 4/7$. The complete result for laminar or turbulent flow of an incompressible Newtonian fluid through a straight tube of radius R and length L is

$$Q^{2-a} = \frac{2^a \pi^{2-a} R^{5-a} \Delta\mathfrak{P}}{C_1 \rho^{1-a} \mu^a L} \qquad (d)$$

when the dimensionless momentum transfer correlation is $f = C_1/\text{Re}^a$. In the laminar flow regime, where $C_1 = 16$ and $a = 1$, equation (d) reduces to the classic Hagen–Poiseuille law (i.e., $Q = \pi R^4 \Delta\mathfrak{P}/8\mu L$). The solution

to this problem reveals that Q and $\Delta \mathcal{P}$ do not follow a linear relation for turbulent flow of an incompressible Newtonian fluid through a tube.

8-30. **(a)** An incompressible Newtonian fluid undergoes forced-convection laminar flow axially (i.e., in the z direction) through a straight horizontal tube with circular cross section. The tube has radius R and length L. Obtain an expression for the z-component of the dynamic force exerted by the fluid on the stationary inner wall of the tube when $\mathrm{Re} = 500$. Express your answer in terms of fluid properties (i.e., μ and/or ρ), tube dimensions (i.e., R and/or L) and average fluid velocity $\langle v_z \rangle$.

Answer: Use the generalized expression for dynamic force from Problem 8-29:

$$(\mathrm{F}_{\mathrm{dynamic}})_{z\text{-component}} = \tfrac{1}{2}\rho \langle v_z \rangle^2 (2\pi RL) f$$

with $f = C_1/\mathrm{Re}^a$, shear area given by $2\pi RL$, and tube diameter $2R$ as the characteristic length in the definition of the Reynolds number. One obtains

$$(\mathrm{F}_{\mathrm{dynamic}})_{z\text{-component}} = \left(\tfrac{1}{2}\right)^a \pi C_1 R^{1-a} L \rho^{1-a} \mu^a \langle v_z \rangle^{2-a}$$

In the laminar flow regime, $C_1 = 16$ and $a = 1$. Hence,

$$(\mathrm{F}_{\mathrm{dynamic}})_{z\text{-component}} = 8\pi L \mu \langle v_z \rangle$$

(b) By what factor does the dynamic force in part (a) change when the volumetric flow rate is three-fold larger?

Answer: Since volumetric flow rate Q is linearly related to average velocity $\langle v_z \rangle$, a three-fold increase in Q produces a three-fold increase in the dynamic force exerted by the fluid on the tube wall.

8-31. Obtain an expression for the z-component of the dynamic force exerted by the fluid on the stationary inner wall of a hydraulically smooth tube when Re is between 10^4 and 10^5. Express your answer in terms of fluid properties (i.e., μ and/or ρ), tube dimensions (i.e., R and/or L), and average fluid velocity $\langle v_z \rangle$.

Answer: Use the generalized result from part (a) of Problem 8-30:

$$(\mathrm{F}_{\mathrm{dynamic}})_{z\text{-component}} = \left(\tfrac{1}{2}\right)^a \pi C_1 R^{1-a} L \rho^{1-a} \mu^a \langle v_z \rangle^{2-a}$$

For turbulent flow in smooth tubes, $C_1 = 0.0791$ and $a = \frac{1}{4}$. Hence,

$$(\mathrm{F}_{\mathrm{dynamic}})_{z\text{-component}} = 0.21 R^{3/4} L \rho^{3/4} \mu^{1/4} \langle v_z \rangle^{7/4}$$

8-32. Qualitatively rank the magnitudes (i.e., in increasing order) of the z-component of the dynamic force exerted by an incompressible Newtonian fluid on the stationary inner wall of a tube for the following flow conditions:

(a) $\mathrm{Re} = 10^4$ in a hydraulically smooth tube

(b) $\mathrm{Re} = 10^2$

(c) $\mathrm{Re} = 10^7$ in a hydraulically smooth tube

(d) $\mathrm{Re} = 10^3$

(e) $\mathrm{Re} = 10^4$ in a "rough" tube with $k/D \approx 10^{-3}$, where k/D is a dimensionless "roughness" factor

8-33. Consider one-dimensional creeping viscous flow of an incompressible Newtonian fluid in the z direction through a straight horizontal channel that has a square cross section. In rectangular coordinates, x and y represent the independent spatial variables that are perpendicular to the flow direction. Fluid flow is generated by a known pressure drop (i.e., $\Delta p/L$), which is analogous to a pressure gradient in the z direction. Write the nontrivial scalar component or components of the appropriate vector equation that allows one to solve for the nonzero component of the velocity vector. Do not include terms in the equation(s) that are trivially zero. Be sure to include all the necessary boundary conditions.

8-34. Axisymmetric irrotational (i.e., potential) flow of an incompressible ideal fluid past a stationary gas bubble exhibits no vorticity. Hence, $\boldsymbol{\nabla} \times \mathbf{v} = 0$. This problem can be solved using the stream function approach rather than the scalar velocity potential method. Develop the appropriate equation that governs the solution to the stream function ψ for two-dimensional axisymmetric potential flow in spherical coordinates. Which Legendre polynomial describes the angular dependence of the stream function?

8-35. **(a)** Consider two-dimensional axisymmetric potential flow of an incompressible fluid around a nondeformable stationary gas bubble of radius R, as described in Problem 8-34, and calculate the dynamic force exerted by the fluid on the bubble, across the gas–liquid interface, in the primary flow direction. The approach velocity of the fluid far from the bubble is $\delta_z V_{\text{approach}}$ (i.e., upward).

(b) Write an expression for the total vector force exerted by the fluid on the bubble in the potential flow regime. Classify your answer as a normal force, a shear force, or some combination thereof. Be sure to include unit vectors in your final answer.

(c) Use vector notation and simplify your answer from part (b). In other words, what is the final expression for $\mathbf{F}_{\text{fluid on bubble}}$?

8-36. Why doesn't the Froude number appear in the dimensionless equation of motion, given by equation (8-42)? Use one or two sentences to answer this question.

8-37. Indicate whether each statement below is true or false.

(a) In the turbulent flow regime, the terminal velocity of a solid sphere falling through an incompressible Newtonian fluid is larger when the fluid viscosity is lower.

(b) In the turbulent flow regime, the viscous shear force exerted by an incompressible Newtonian fluid on the wall of a straight tube increases four-fold when the volumetric flow rate doubles.

(c) In the creeping flow regime, torque is not linearly proportional to angular velocity in the cone-and-plate viscometer for a power-law fluid with power-law exponent $n = 0.7$.

(d) The scalar velocity potential Φ is an exact differential, which guarantees that the equation of continuity is satisfied for incompressible fluids.

(e) The stream function ψ is an exact differential, which guarantees that the ϕ-component of $\nabla \times \mathbf{v} = 0$ for two-dimensional axisymmetric potential flow of an incompressible fluid around a stationary gas bubble [i.e., $v_r(r, \theta)$ and $v_\theta(r, \theta)$].

Transport Phenomena for Chemical Reactor Design. Laurence A. Belfiore
Copyright © 2003 John Wiley & Sons, Inc.
ISBN: 0-471-20275-4

9

DERIVATION OF THE MASS TRANSFER EQUATION

The following discussion represents a detailed description of the mass balance for any species in a reactive mixture. In general, there are four mass transfer rate processes that must be considered; accumulation, convection, diffusion, and sources or sinks due to chemical reactions. The units of each term in the integral form of the mass transfer equation are moles of component i per time. In differential form, the units of each term are moles of component i per volume per time. This is achieved when the mass balance is divided by the finite control volume, which shrinks to a point within the region of interest in the limit when all dimensions of the control volume become infinitesimally small. In this development, the size of the control volume $V(t)$ is time dependent because, at each point on the surface of this volume element, the control volume moves with velocity $\mathbf{v}_{\text{surface}}$, which could be different from the local fluid velocity of component i, $\mathbf{v}_i$. Since there are several choices for this control volume within the region of interest, it is appropriate to consider an arbitrary volume element with the characteristics described above. For specific problems, it is advantageous to use a control volume that matches the symmetry of the macroscopic boundaries. This is illustrated in subsequent chapters for catalysts with rectangular, cylindrical, and spherical symmetry.

9-1 ACCUMULATION RATE PROCESS

Accumulation of the mass of component i within the control volume is written as a time derivative of a volume integral of the density of component i. In other words, the accumulation rate process is volumetric because it occurs throughout the entire contents of the system. The exact form for the time derivative depends

on the characteristics of the control volume (see Table 8-1 on page 160). For example, if $V(t)$ is stationary with constant spatial coordinates that define its boundaries, then a partial time derivative operator is required. If the control volume is in motion such that at every point on its surface, $\mathbf{v}_{\text{surface}}$ is the same as the local mass-averaged fluid velocity $\mathbf{v}$, then a substantial time derivative operator is needed. When $\mathbf{v}_{\text{surface}}$ is different from the mass-averaged fluid velocity of the mixture, a total time derivative operator allows one to represent the accumulation rate process as $(d/dt)\int \rho_i \, dV$, where the integration is performed over the entire control volume $V(t)$. It should be emphasized that when the control volume is not stationary, the accumulation rate process involves the total time derivative of an integral in which both the integrand ρ_i and the limits $V(t)$ are functions of time. This expression can be manipulated by invoking the Leibnitz rule for differentiating a three-dimensional integral with variable limits:

$$\frac{d}{dt}\int_{V(t)} \rho_i \, dV = \int_{V(t)} \frac{\partial \rho_i}{\partial t} \, dV + \int_{S(t)} \rho_i (\mathbf{n} \cdot \mathbf{v}_{\text{surface}}) \, dS \tag{9-1}$$

where the first two integrals are performed over the entire control volume $V(t)$; the last integral on the right-hand side of (9-1) is performed over the time-varying surface $S(t)$, which completely surrounds the control volume; and $\mathbf{n}$ is the outward-directed unit normal vector at each point on surface $S(t)$. Obviously, the most general form for the control volume has been chosen. If one sets $\mathbf{v}_{\text{surface}} = 0$ for a stationary control volume, then the total time derivative operator reduces to the partial derivative operator, as mentioned above. When $\mathbf{v}_{\text{surface}} = \mathbf{v}$, the Leibnitz rule for the total time derivative operator is equivalent to the substantial time derivative operator. The final form for the microscopic mass transfer equation is independent of the nature of the control volume. It is reassuring to know that our conservation law and the corresponding mathematical description produce the same final result for all three possible choices for the characteristics of the control volume. If the control volume is differentially thick in each coordinate direction, then the mass balance becomes a three-dimensional partial differential equation in any orthogonal coordinate system.

9-2 RATE PROCESSES DUE TO MASS FLUX ACROSS THE SURFACE THAT BOUNDS THE CONTROL VOLUME

This is a surface-related phenomenon based on the mass flux vector of component i and the surface area across which this flux acts. Relative to a stationary reference frame, $\rho_i \mathbf{v}_i$ is the mass flux vector of component i with units of mass of species i per area per time. It is extremely important to emphasize that $\rho_i \mathbf{v}_i$ contains contributions from convective mass transfer and molecular mass transfer. The latter process is due to diffusion. When one considers the mass of component i that crosses the surface of the control volume due to mass flux, the species velocity and the surface velocity must be considered. For example, $\rho_i (\mathbf{v}_i - \mathbf{v}_{\text{surface}})$ is the mass flux vector of component i with respect to the surface

of the control volume that moves with velocity vector $\mathbf{v}_{\text{surface}}$. If the differential surface vector at each point on the surface that bounds the control volume is $\mathbf{n}\,dS$, which is directed outward based on the definition of the unit normal vector $\mathbf{n}$, then the net rate at which the mass of component i enters $V(t)$ due to mass flux is $-\int \rho_i(\mathbf{v}_i - \mathbf{v}_{\text{surface}}) \cdot \mathbf{n}\,dS$. The negative sign is required because $\mathbf{n}$ is an outward-directed unit normal vector and the integral expression represents a net input. The scalar product of the mass flux vector with the differential surface vector is a convenient way of identifying the component of mass flux in the direction of the unit normal vector at each point on the surface. Only the normal component of $\rho_i(\mathbf{v}_i - \mathbf{v}_{\text{surface}})$ is responsible for input or output of the mass of species i across the surface of the control volume. Gauss's law or the divergence theorem is used to relate the surface and volume integrals that appear in the mass transfer equation.

9-3 RATE PROCESSES DUE TO MULTIPLE CHEMICAL REACTIONS

In the most general situation, there are N species in a multicomponent mixture that participate in r chemical reactions. The presence of chemical reaction terms in the mass transfer equation ruin any attempt to invoke analogies between heat transfer and mass transfer, particularly when the chemical kinetics are different from zeroth or first order. In the description below, components are identified by subscript i, and reactions are labeled by subscript j. The stoichiometrically balanced jth chemical reaction is represented generically as $\sum_i \nu_{ij} A_i = 0$, where A_i is a molecular species that participates in the reaction and ν_{ij} is the stoichiometric coefficient of species i in the jth chemical reaction. Stoichiometric coefficients are negative for reactants, positive for products, and zero for inerts. Within the framework of multiple reactions, it is very possible that a particular component could be a product in one reaction and a reactant in a subsequent step. The kinetic rate law for the jth chemical reaction, with units of moles per volume per time, is given by $\mathfrak{R}_j$, and the rate of production of the mass of component i in the jth chemical reaction is $\nu_{ij}(\text{MW}_i)\mathfrak{R}_j$, where MW_i is the molecular weight of the ith component. When one accounts for all of the chemical reactions that occur volumetrically or pseudo-volumetrically within the control volume, the rate of production of the mass of component i with units of mass i per time is $\int[\sum_j \nu_{ij}(\text{MW}_i)\mathfrak{R}_j]\,dV$, where the summation includes all the chemical reactions (i.e., $1 \le j \le r$) and the integration is performed over the entire contents of the control volume. Homogeneous kinetics correspond to a volumetric rate process in the mass transfer equation. Heterogeneous surface-catalyzed kinetics belong in the boundary conditions for a rigorous description of any mass transfer/chemical reaction problem. However, this level of description within a catalytic pellet is too complex to solve. A simplified procedure involves the assumption of homogeneous diffusion within a porous catalyst, where the rate law is written pseudo-volumetrically in the mass transfer equation. The rigorous description of convective diffusion in catalytic reactors, where heterogeneous kinetic rate laws

appear in the boundary conditions for a mathematically well-defined catalytic surface, is reserved for tube-wall reactors in Chapter 23.

9-4 CONSTRUCTING INTEGRAL AND MICROSCOPIC DESCRIPTIONS OF THE MASS TRANSFER EQUATION

The open-system mass balance for component i with units of mass per time is stated qualitatively as $\mathbf{1 = 2 + 3}$ where **1** is the accumulation rate process or the unsteady-state contribution, **2** is the net rate of input due to mass flux acting across the surface that surrounds the control volume, and **3** is the rate of production of component i due to multiple chemical reactions. In mathematical terms;

$$\frac{d}{dt}\int_{V(t)} \rho_i \, dV = \int_{V(t)} \frac{\partial \rho_i}{\partial t} \, dV + \int_{S(t)} \rho_i (\mathbf{n} \cdot \mathbf{v}_{\text{surface}}) \, dS$$

$$= -\int_{S(t)} \rho_i (\mathbf{v}_i - \mathbf{v}_{\text{surface}}) \cdot \mathbf{n} \, dS + \int_{V(t)} \left[\sum_j \nu_{ij} (\text{MW}_i) \mathfrak{R}_j \right] dV \quad (9\text{-}2)$$

This is the integral form of the mass transfer equation within an arbitrary control volume $V(t)$. Notice that there is a term of the form $\int \rho_i (\mathbf{n} \cdot \mathbf{v}_{\text{surface}}) \, dS$ in the accumulation rate process and in the net rate of input due to mass flux acting across the time-varying surface $S(t)$. These terms are present because the surface that bounds the control volume is in motion. The fact that they cancel provides quantitative support for the claim that the final form of the mass transfer equation is independent of the characteristics of the control volume. All surviving terms in the mass balance,

$$\int_{V(t)} \frac{\partial \rho_i}{\partial t} \, dV = -\int_{S(t)} \rho_i (\mathbf{v}_i \cdot \mathbf{n}) \, dS + \int_{V(t)} \left[\sum_j \nu_{ij} (\text{MW}_i) \mathfrak{R}_j \right] dV \quad (9\text{-}3)$$

exhibit no dependence on $\mathbf{v}_{\text{surface}}$. In fact, these surviving terms in the mass balance represent the initial quantitative statement based on $\mathbf{1 = 2 + 3}$, for a stationary control volume. Notice that the accumulation rate process and the rate of production due to homogeneous or pseudo-homogeneous chemical reactions give rise to volume integrals, whereas the net input due to mass flux is expressed as a surface integral. Gauss's law is used to rewrite

$$\int_{S(t)} \rho_i (\mathbf{v}_i \cdot \mathbf{n}) \, dS = \int_{S(t)} (\mathbf{n} \cdot \rho_i \mathbf{v}_i) \, dS \quad (9\text{-}4)$$

in terms of the divergence of the mass flux vector of component i with respect to a stationary reference frame:

$$\int_{S(t)} (\mathbf{n} \cdot \rho_i \mathbf{v}_i) \, dS = \int_{V(t)} (\nabla \cdot \rho_i \mathbf{v}_i) \, dV \quad (9\text{-}5)$$

Now, all terms in the mass balance are expressed as volume integrals. When these three terms are moved to the left-hand side of the mass balance, given by (9-3), the following result is obtained:

$$\int_{V(t)} \left[\frac{\partial \rho_i}{\partial t} + (\nabla \cdot \rho_i \mathbf{v}_i) - \sum_j \nu_{ij} (\mathrm{MW}_i) \mathfrak{R}_j \right] dV = 0 \tag{9-6}$$

The microscopic mass transfer equation is obtained by setting the integrand to zero because there are no severe restrictions on the choice of the volume element, which was placed arbitrarily in a region of interest within the fluid. In other words, if a different volume element is chosen, then the integration limits in the mass balance change but the right-hand side of equation (9-6) is always zero. As a simple illustrative example, $\int x\,dx = 0$ if the sum of the upper and lower integration limits is zero. Hence, the integral will vanish even though the integrand [i.e., $f(x) = x$] is not zero. However, if $\int x\,dx = 0$ for any set of upper and lower limits that do not necessarily sum to zero, then this will be true only when the integrand $f(x) = x \to 0$. The mass transfer equation for component i in a multicomponent mixture with multiple chemical reactions is

$$\frac{\partial \rho_i}{\partial t} + (\nabla \cdot \rho_i \mathbf{v}_i) = \sum_j \nu_{ij} (\mathrm{MW}_i) \mathfrak{R}_j \tag{9-7}$$

No assumptions have been invoked to obtain this result. As illustrated below, the mass flux term with respect to a stationary reference frame, $\nabla \cdot \rho_i \mathbf{v}_i$, contains contributions from bulk fluid flow (i.e., convection) and molecular mass transfer via diffusion. In fact, whenever the divergence of a flux appears in a microscopic balance expression, its origin was a dot product of that flux with the outward-directed unit normal vector on the surface of the control volume, accounting for input and output due to flux across the surface that bounds $V(t)$. The divergence of a flux actually represents a surface-related phenomenon that has been transformed into a volume integral via Gauss's law.

9-5 DIFFUSIONAL FLUXES IN MULTICOMPONENT MIXTURES

Diffusion is defined as the relative motion of a species in a mixture with respect to an average fluid velocity. The average fluid velocity can be chosen as the mass-averaged velocity, molar-averaged velocity, or volume-averaged velocity. The average velocity of the mixture identifies the reference frame for diffusive fluxes. If $\mathbf{v}_i$ is the velocity vector of component i in the mixture, then an average velocity is calculated by summing products of each $\mathbf{v}_i$ and an appropriate normalized weighting factor. The weighting factors are normalized because they sum to unity when the summation includes all components in the mixture. For example, the mass-averaged velocity is obtained when mass fractions or weight fractions represent the weighting factors. Obviously, the molar-averaged velocity is based on mole fraction weighting factors, and the volume-averaged velocity

employs volume fraction weighting factors. The mass-averaged velocity vector of a mixture **v** is a good choice to include in the mass transfer equation because **v** is the velocity vector that appears in the equation of continuity (i.e., the overall mass balance) and the equation of motion (i.e., the momentum balance). Hence, fluid dynamics is typically employed to calculate **v** for a pure fluid and the results are used in the mass transfer equation when the convective mass transfer rate process is important. Diffusion can also be defined as the additive correction factor in the following expression for the mass flux of component i:

$$\rho_i \mathbf{v}_i = \rho_i \mathbf{v} + \mathbf{j}_i \tag{9-8}$$

where $\mathbf{j}_i$ represents the diffusional mass flux of component i with respect to the mass-average velocity of the mixture. There is a simple relation between the diffusional fluxes of all components in the mixture, particularly when one considers (1) diffusional mass fluxes in the mass-averaged reference frame, (2) diffusional molar fluxes in the molar-averaged reference frame, or (3) diffusional volume fluxes in the volume-averaged reference frame. This concept is illustrated with diffusional mass fluxes in the mass-averaged reference frame, where $\mathbf{j}_i$ is defined by equation (9-8). If $\rho_i \mathbf{v}_i = \rho_i \mathbf{v} + \mathbf{j}_i$ is summed over all components in the mixture, then:

$$\sum_i \rho_i \mathbf{v}_i = \mathbf{v} \sum_i \rho_i \tag{9-9}$$

based on definitions of the mass-averaged velocity **v**, mass fraction ω_i, and the total mass density of the mixture ρ,

$$\mathbf{v} = \sum_i \omega_i \mathbf{v}_i \qquad \omega_i = \frac{\rho_i}{\rho} \qquad \rho = \sum_i \rho_i \tag{9-10}$$

Hence, $\sum_i \mathbf{j}_i = 0$, which suggests that the sum of all diffusional mass fluxes in the mixture with respect to the mass-averaged frame is zero. For binary mixtures, this statement is known as *equimolar counterdiffusion*.

With the foregoing definitions of diffusional fluxes in a multicomponent mixture, it is possible to manipulate the mass transfer equation,

$$\frac{\partial \rho_i}{\partial t} + (\nabla \cdot \rho_i \mathbf{v}_i) = \sum_j \nu_{ij} (\mathrm{MW}_i) \mathfrak{R}_j \tag{9-11}$$

without invoking any assumptions for use in Chapter 25. It is convenient to write the mass density of component i (i.e., ρ_i) in terms of the mass fraction of component i and the overall mass density of the mixture. Hence, $\rho_i = \omega_i \rho$. Now, the accumulation rate process in (9-11) can be expanded as a product of two terms:

$$\frac{\partial \rho_i}{\partial t} = \rho \frac{\partial \omega_i}{\partial t} + \omega_i \frac{\partial \rho}{\partial t} \tag{9-12}$$

The net input due to mass flux acting across the surface of the control volume is split into contributions from convection and diffusion via (9-8):

$$\nabla \cdot \rho_i \mathbf{v}_i = \nabla \cdot \rho \omega_i \mathbf{v} + \nabla \cdot \mathbf{j}_i \tag{9-13}$$

The convective mass flux term; $\nabla \cdot \rho\omega_i \mathbf{v}$, is expanded using the product rule for the ∇ operator, which is similar to the product rule for the derivative operator, except for the fact that one must exercise caution in placing the dot between two vectors. It makes no sense to calculate the scalar (i.e., dot) product of a vector and a scalar. If $\rho\omega_i \mathbf{v}$ is viewed as a product of ω_i and $\rho\mathbf{v}$, then:

$$\nabla \cdot \rho\omega_i \mathbf{v} = \nabla \cdot \omega_i \rho\mathbf{v} = \rho\mathbf{v} \cdot \nabla\omega_i + \omega_i \nabla \cdot \rho\mathbf{v} \tag{9-14}$$

The mass transfer equation for component i is

$$\rho\frac{\partial\omega_i}{\partial t} + \omega_i\frac{\partial\rho}{\partial t} + \rho\mathbf{v} \cdot \nabla\omega_i + \omega_i \nabla \cdot \rho\mathbf{v} + \nabla \cdot \mathbf{j}_i = \sum_j \nu_{ij}(\mathrm{MW}_i)\mathfrak{R}_j \tag{9-15}$$

The second and fourth terms on the left-hand side of (9-15) can be combined to reveal the equation of continuity (i.e., the overall mass balance) for the mixture:

$$\omega_i\left(\frac{\partial\rho}{\partial t} + \nabla \cdot \rho\mathbf{v}\right) = 0 \tag{9-16}$$

No approximations have been invoked to eliminate these two terms from the mass transfer equation because

$$\frac{\partial\rho}{\partial t} + \nabla \cdot \rho\mathbf{v} = 0 \tag{9-17}$$

is a microscopic representation of the overall mass balance for pure fluids and multicomponent mixtures provided that there is no generation of overall mass. The final form of the mass transfer equation for component i in a multicomponent mixture with several chemical reactions is

$$\rho\left(\frac{\partial\omega_i}{\partial t} + \mathbf{v} \cdot \nabla\omega_i\right) = -\nabla \cdot \mathbf{j}_i + \sum_j \nu_{ij}(\mathrm{MW}_i)\mathfrak{R}_j \tag{9-18}$$

This equation is not restricted to liquids with constant density, as one might suspect from the fact that the overall mass density ρ appears to the left of the substantial derivative of the mass fraction of component i. Since $\mathbf{v}$ in the mass transfer equation represents the mass-averaged velocity of the mixture,

$$\frac{\partial\omega_i}{\partial t} + \mathbf{v} \cdot \nabla\omega_i \equiv \frac{D\omega_i}{Dt} \tag{9-19}$$

is the substantial derivative of ω_i, written as $D\omega_i/Dt$. It is a measure of the time rate of change of the mass fraction of component i that one would calculate in a control volume which moves along with the mass-averaged velocity at every point on the surface that surrounds $V(t)$. Hence, a concise form for the mass

transfer equation of component i in a multicomponent mixture with multiple chemical reactions is

$$\rho \frac{D\omega_i}{Dt} = -\nabla \cdot \mathbf{j}_i + \sum_j \nu_{ij} (\mathrm{MW}_i) \mathfrak{R}_j \tag{9-20}$$

The only implicit assumption in (9-20) is that overall fluid mass is neither created nor destroyed.

9-6 DIFFUSIONAL FLUXES AND LINEAR TRANSPORT LAWS IN BINARY AND PSEUDO-BINARY MIXTURES

When there are only two components in the mixture, diffusional fluxes are written in terms of a driving force and a binary molecular diffusion coefficient via Fick's first law. For example, if the diffusional mass flux with respect to a reference frame that translates at the mass-averaged velocity of the mixture is based on a mass fraction driving force, then Fick's first law for component A is

$$\mathbf{j}_\mathrm{A} = \rho_\mathrm{A} (\mathbf{v}_\mathrm{A} - \mathbf{v}) = -\rho \mathfrak{D}_\mathrm{AB} \nabla \omega_\mathrm{A} \tag{9-21}$$

where $\mathfrak{D}_\mathrm{AB}$ is the binary molecular diffusion coefficient. This expression for $\mathbf{j}_\mathrm{A}$ neglects contributions from temperature gradients (i.e., Soret diffusion), pressure gradients, and external forces. It is necessary to consider entropy generation within the framework of irreversible thermodynamics to appreciate all the contributions to diffusional mass flux. This is discussed in Chapter 25. In fact, when there are n components in the mixture, the diffusional mass flux of species A exhibits contributions from $(n-1)$ concentration gradients, including $\nabla \omega_\mathrm{A}$. This complexity is circumvented, to some extent, by writing the diffusional mass flux of component i solely in terms of $\nabla \omega_i$ and the molecular diffusion coefficient of species i in a multicomponent mixture. This is not rigorously correct, but the concept of treating a multicomponent mixture as a pseudo-binary mixture allows one to solve the mass transfer equation, either analytically or numerically, and analyze physicochemical phenomena within the internal pores of a catalytic pellet. Hence, this pseudo-binary assumption permits one to write the diffusional mass flux of component i as follows:

$$\mathbf{j}_i = \rho_i (\mathbf{v}_i - \mathbf{v}) \approx -\rho \, \mathfrak{D}_{i,\mathrm{mix}} \nabla \omega_i \tag{9-22}$$

The actual diffusion coefficient in equation (9-22) depends on (1) whether the equation is written for diffusional mass flux or diffusional molar flux, (2) the reference frame (i.e., with respect to $\mathbf{v}$, for example), and (3) the driving force (i.e., mass fraction gradient or mole fraction gradient). Obviously, there are several combinations of factors 1, 2, and 3, and each requires a different proportionality constant between flux and gradient. Interestingly enough for binary mixtures, the

diffusivity for diffusional mass flux in the mass-averaged reference frame with a mass fraction gradient is the same as the diffusivity for diffusional molar flux in the molar-averaged reference frame with a mole fraction gradient. Furthermore, the molecular diffusion coefficient is a function of temperature, pressure, and composition, as discussed in Chapter 21. When diffusion occurs within the internal pores of a catalytic pellet, it is necessary to consider the pore structure of the catalyst in the final expression for the "effective" diffusion coefficient. In other words, one must include a tortuosity factor because diffusion occurs through tortuous pathways that do not conform to a homogeneous medium, and a porosity factor which is equivalent to a void fraction. Tortuosity and porosity are discussed within the framework of the parallel-pore model in Chapter 21.

9-7 SIMPLIFICATION OF THE MASS TRANSFER EQUATION FOR PSEUDO-BINARY INCOMPRESSIBLE MIXTURES WITH CONSTANT PHYSICAL PROPERTIES

The generalized form of the mass transfer equation,

$$\frac{\partial \rho_i}{\partial t} + (\nabla \cdot \rho_i \mathbf{v}_i) = \sum_j \nu_{ij} (\mathrm{MW}_i) \mathfrak{R}_j \tag{9-23}$$

is combined with an expression for the total mass flux of component i with respect to a stationary reference frame that includes Fick's first law of diffusion. The overall objective is to manipulate the microscopic mass balance for multicomponent incompressible mixtures and generate the classic form of the mass transfer equation that allows one to calculate molar density profiles for reactants and products. The multicomponent mixture is treated as a pseudo-binary mixture and the total mass flux of component i with respect to a stationary reference frame is

$$\rho_i \mathbf{v}_i \approx \rho_i \mathbf{v} - \rho \, \mathfrak{D}_{i,\mathrm{mix}} \nabla \omega_i \tag{9-24}$$

where the diffusional mass flux is expressed with respect to the mass-averaged velocity of the mixture, $\mathbf{v}$. This is convenient because the microscopic form of the overall mass balance (i.e., equation of continuity) for an incompressible mixture is

$$\nabla \cdot \rho \mathbf{v} = \rho \nabla \cdot \mathbf{v} = 0 \quad \text{or} \quad \nabla \cdot \mathbf{v} = 0 \tag{9-25}$$

when the overall fluid density ρ is constant. The incompressibility assumption for diffusion and chemical reaction within the pores of a catalytic pellet is reasonable for isothermal operation when reactants and products are not subjected to large changes in pressure. The diffusional mass flux of component i in the mass-averaged reference frame with a mass fraction gradient can be written as

$$\mathbf{j}_i = -\mathfrak{D}_{i,\mathrm{mix}} \nabla \rho_i \tag{9-26}$$

when the overall density is constant. The divergence of the total mass flux of component i with respect to a stationary reference frame is

$$\nabla \cdot \rho_i \mathbf{v}_i = \nabla \cdot \rho_i \mathbf{v} + \nabla \cdot (-\mathfrak{D}_{i,\text{mix}} \nabla \rho_i) \tag{9-27}$$

The product rule for the divergence operator is applied to both terms on the right-hand side of equation (9-27). In any coordinate system, the divergence of the product of a scalar and a vector is expanded as a product of the scalar and the divergence of the vector plus the scalar (i.e., dot) product of the vector and the gradient of the scalar. This vector identity was employed in equation (9-14). The pseudo-binary mass transfer equation for component i is

$$\frac{\partial \rho_i}{\partial t} + \rho_i \nabla \cdot \mathbf{v} + \mathbf{v} \cdot \nabla \rho_i = \mathfrak{D}_{i,\text{mix}} \nabla \cdot \nabla \rho_i + \nabla \rho_i \cdot \nabla \mathfrak{D}_{i,\text{mix}} + \sum_j \nu_{ij} (\text{MW}_i) \mathfrak{R}_j \tag{9-28}$$

in the presence of multiple chemical reactions. For incompressible mixtures with constant physical properties,

$$\nabla \cdot \mathbf{v} = 0 \quad \text{and} \quad \nabla \mathfrak{D}_{i,\text{mix}} = 0 \tag{9-29}$$

Hence, one term each on the left- and right-hand sides of equation (9-29) is zero. Since the mass density of component i, ρ_i, and the molar density of component i, C_i, are related by molecular weight, division by MW_i produces the final form of the mass transfer equation for incompressible pseudo-binary mixtures with constant physical properties:

$$\frac{\partial C_i}{\partial t} + \mathbf{v} \cdot \nabla C_i = \mathfrak{D}_{i,\text{mix}} \nabla^2 C_i + \sum_j \nu_{ij} \mathfrak{R}_j \tag{9-30}$$

where the Laplacian operator $\nabla^2 = \nabla \cdot \nabla$, the rate law for the jth homogeneous or pseudo-homogeneous chemical reaction has units of moles per volume per time, and $\mathfrak{R}_j$ is expressed most conveniently in terms of molar densities. The first term on the left-hand side of the mass transfer equation, $\partial C_i / \partial t$, is the accumulation or unsteady-state rate process, characterized by a first derivative with respect to time. This term is neglected for steady-state simulations. The second term on the left-hand side of the mass transfer equation, $\mathbf{v} \cdot \nabla C_i$, represents convective mass transfer, characterized by first spatial derivatives of molar density multiplied by the appropriate component of the mass-averaged velocity of the mixture. In general, convective mass transfer occurs in all three coordinate directions. However, for simple one-dimensional flow problems, the only important contribution to convective mass transfer occurs in the primary direction of bulk fluid flow. The first term on the right-hand side of the mass transfer equation, $\mathfrak{D}_{i,\text{mix}} \nabla^2 C_i$ corresponds to molecular mass transfer via diffusion, characterized by second spatial derivatives of molar density and the presence of a molecular

transport property ($\mathfrak{D}_{i,\mathrm{mix}}$) when the balance is written in dimensional form. Be careful when radial diffusion in cylindrical or spherical coordinates is written in dimensionless form and the product rule for differentiation is employed to expand the diffusion term, as illustrated below in these coordinate systems;

$$\text{Cylindrical coordinates:} \qquad \frac{1}{\eta}\frac{d}{d\eta}\left(\eta\frac{d\Psi_i}{d\eta}\right) = \frac{d^2\Psi_i}{d\eta^2} + \frac{1}{\eta}\frac{d\Psi_i}{d\eta}$$

$$\text{Spherical coordinates:} \qquad \frac{1}{\eta^2}\frac{d}{d\eta}\left(\eta^2\frac{d\Psi_i}{d\eta}\right) = \frac{d^2\Psi_i}{d\eta^2} + \frac{2}{\eta}\frac{d\Psi_i}{d\eta}$$

where Ψ_i is the dimensionless molar density of component i and η is a dimensionless independent variable in the radial direction (i.e., $\eta = r/R$). A first spatial derivative appears in the second term on the right-hand side of both equations, and in dimensionless form, the diffusion coefficient does not appear explicitly because it is contained in either the mass transfer Peclet number or the Damkohler number. However, molecular mass transfer via radial diffusion is the rate process that generates all four of these terms, and one must not confuse $(1/\eta)\,d\Psi_i/d\eta$ or $(2/\eta)\,d\Psi_i/d\eta$ with radial convection. In general, diffusion occurs in all three coordinate directions. However, the contribution from molecular mass transfer in the primary flow direction is usually small in comparison with convective mass transfer in the same direction when the product of the Reynolds and Schmidt numbers is large. When mass transfer rate processes due to chemical reactions are operative, the mass transfer equation contains a linear or nonlinear function of molar densities for the various species in the mixture, without derivatives. Linear functions represent zeroth- or first-order chemical kinetics and nonlinear functions correspond to apparent nth-order kinetics or complex rate laws which could exhibit molar densities in the denominator of the reaction rate, similar to the Hougen–Watson models. Hence, one should be able to identify the important mass transfer rate processes for a particular problem by visual inspection of the governing mass transfer equation.

Transport Phenomena for Chemical Reactor Design. Laurence A. Belfiore
Copyright © 2003 John Wiley & Sons, Inc.
ISBN: 0-471-20275-4

10

DIMENSIONAL ANALYSIS OF THE MASS TRANSFER EQUATION

10-1 DIMENSIONAL SCALING FACTORS FOR THE MASS TRANSFER RATE PROCESSES

The objective of this section is to identify the characteristic quantities for a generic mass transfer problem and the physical properties of the fluid (i.e., ρ and $\mathscr{D}_{i,\,\mathrm{mix}}$), which can be combined to represent the dimensions and an order-of-magnitude estimate of each term in the mass transfer equation. The characteristic scalar quantities are the average fluid velocity $\langle v \rangle$, a length scale L, and the inlet molar density of reactant A, C_{A0}.

The molar density of each component in the mixture is dimensionalized via division by C_{A0}. The length scale is well defined for a particular problem. For example, L is the radius of spherical catalytic pellets, the radius of long cylindrical catalysts, or one-half of the thickness of porous wafer catalysts, measured in the thinnest dimension. For the purposes of dimensional analysis in this and the following sections, L represents a generic length scale. Two of the characteristic quantities, $\langle v \rangle$ and L, can be used to construct a characteristic time scale similar to the average residence time for flow reactors (i.e., $L/\langle v \rangle$). The dimensional scaling factor for the accumulation rate process (i.e., $\partial C_i/\partial t$) is constructed by combining the characteristic molar density of key limiting reactant A and the characteristic time scale. Hence,

$$\frac{\partial C_i}{\partial t} \approx \frac{\langle v \rangle C_{\mathrm{A0}}}{L} \tag{10-1}$$

represents an order-of-magnitude estimate for, and contains all the dimensions of (i.e., moles per volume per time), the unsteady-state term. The dimensional

scaling factor for the convective mass transfer rate process (i.e., $\mathbf{v} \cdot \nabla C_i$) is constructed by combining the average fluid velocity and a simple representation of the concentration gradient. Since this gradient implies a spatial rate of change, the units of ∇ are L^{-1} and the concentration gradient is estimated by C_{A0}/L. Hence,

$$\mathbf{v} \cdot \nabla C_i \approx \frac{\langle v \rangle C_{A0}}{L} \tag{10-2}$$

also represents an order-of-magnitude estimate for, and contains all the dimensions of, the convective mass transfer rate process. The dimensional scaling factor for the accumulation rate process is the same as the one for convective mass transfer. Consequently, both of these terms are grouped together on the left-hand side of the mass transfer equation. The dimensional scaling factor for diffusion in the mass transfer equation (i.e., $\mathfrak{D}_{i,\,\mathrm{mix}} \nabla^2 C_i$) is constructed by combining the diffusion coefficient of component i and a simple representation of the Laplacian of molar density. Since the Laplacian operator denotes second spatial derivatives, the units of $\nabla^2 = \nabla \cdot \nabla$ are L^{-2} and $\nabla^2 C_i$ is estimated by C_{A0}/L^2. Hence,

$$\mathfrak{D}_{i,\,\mathrm{mix}} \nabla^2 C_i \approx \frac{\mathfrak{D}_{i,\,\mathrm{mix}} C_{A0}}{L^2} \tag{10-3}$$

represents an order-of-magnitude estimate for, and contains all the dimensions of, the diffusion rate process in the mass transfer equation. Finally, the dimensional scaling factors for rate processes due to multiple chemical reactions (i.e., $\Sigma_j \nu_{ij} \mathfrak{R}_j$) are constructed by writing a simple nth-order rate law for the jth independent chemical reaction as follows: $k_j (C_{A0})^{n_j}$, where k_j is the nth-order kinetic rate constant when the rate law for reaction j is expressed on a volumetric basis using molar densities. Hence, an order-of-magnitude estimate of the rate law for each independent chemical reaction $\mathfrak{R}_j$ contains the apparent kinetic rate constant k_j and the apparent reaction order n_j that are specific to the jth chemical reaction. If a multicomponent mixture contains N components that participate in r independent chemical reactions, then it is possible to calculate $r + 2$ dimensional scaling factors in the mass transfer equation for component i: one for the accumulation rate process and convective mass transfer, one for diffusion, and one for each independent chemical reaction, $1 \leq j \leq r$. As illustrated in the next section, $r + 1$ dimensionless numbers can be constructed from $r + 2$ dimensional scaling factors when all the scaling factors have the same dimensions (i.e., moles per volume per time).

10-2 DIMENSIONLESS FORM OF THE GENERALIZED MASS TRANSFER EQUATION WITH UNSTEADY-STATE CONVECTION, DIFFUSION, AND CHEMICAL REACTION

The objective of this section is to identify the dimensionless transport numbers that appear in the mass transfer equation for component i. Order-of-magnitude estimates of the importance of one mass transfer rate process relative to another

mass transfer rate process are obtained by calculating these dimensionless numbers. Since dimensionless numbers are generated by dividing two different dimensional scaling factors, order-of-magnitude estimates can be obtained from the characteristic quantities of a particular mass transfer problem and the physical properties of the fluid of interest. Furthermore, these order-of-magnitude calculations can be performed at the beginning of a mass transfer problem. It is not necessary to conquer mathematical details and obtain analytical or numerical solutions prior to estimating the relative importance of two different mass transfer rate processes. Obviously, the mathematics can be simplified if order-of-magnitude calculations at the outset reveal that it is reasonable to neglect a particular mass transfer rate process before proceeding to obtain the solution.

The strategy for obtaining the dimensionless mass transfer equation is as follows:

1. Begin with the dimensional form of the mass transfer equation for component i, where all variables have dimensions:

$$\frac{\partial C_i}{\partial t} + \mathbf{v} \cdot \nabla C_i = \mathfrak{D}_{i,\,\mathrm{mix}} \nabla^2 C_i + \sum_j \nu_{ij} \mathfrak{R}_j \tag{10-4}$$

2. Introduce dimensionless variables (i.e., $C_i = C_{\mathrm{A0}} \psi_i$, etc.) and write each mass transfer rate process in terms of these dimensionless variables and the corresponding dimensional scaling factor. This scaling factor contains all the dimensions of, as well as an order-of-magnitude estimate for, the particular mass transfer rate process. For example, the left-hand side of equation (10-4) is written as follows, where all the variables are dimensionless:

$$\frac{\langle v \rangle C_{\mathrm{A0}}}{L} \left(\frac{\partial \psi_i}{\partial t} + \mathbf{v} \cdot \nabla \psi_i \right) \tag{10-5}$$

The diffusion term is expressed as

$$\frac{\mathfrak{D}_{i,\,\mathrm{mix}} C_{\mathrm{A0}}}{L^2} \nabla^2 \psi_i \tag{10-6}$$

where the Laplacian operator and the molar density of component i are dimensionless. The rate of production of the moles of component i via multiple chemical reactions is written as

$$\sum_j \nu_{ij} k_j(T) (C_{\mathrm{A0}})^{n_j} \mathfrak{R}_j^* \tag{10-7}$$

where $k_j(T)$ is the kinetic rate constant for reaction j with units of (volume/mole)$^{n_j - 1}$/time, n_j is the simplified order of the jth reaction even though the rate law might be rather complex, and $\mathfrak{R}_j^*$ is the dimensionless rate law for the jth reaction, written on a volumetric or pseudo-volumetric basis using molar densities. For example, if $\mathfrak{R}_{j,\,\mathrm{HW}}$ is the Hougen–Watson

model for reaction j on the interior surface of a catalytic pellet with units of moles per area per time, S_m is the internal surface area per mass of catalyst, and ρ_{app} is the apparent mass density of the pellet, then the dimensionless Hougen–Watson rate law is defined as

$$\mathfrak{R}_j^* = \frac{S_m \rho_{\text{app}} \mathfrak{R}_{j,\text{HW}}}{k_j(T)(C_{\text{A0}})^{n_j}} \tag{10-8}$$

where the numerator is a pseudo-volumetric representation of the rate law for surface-catalyzed chemical reactions.

3. Divide the entire mass transfer equation by the scaling factor for diffusion (i.e., $\mathfrak{D}_{i,\text{mix}} C_{\text{A0}}/L^2$). This is an arbitrary but convenient choice. Any of the $r+2$ dimensional scaling factors can be chosen for this purpose. When the scaling factor for the diffusion term in the dimensional mass transfer equation is divided by $\mathfrak{D}_{i,\text{mix}} C_{\text{A0}}/L^2$, the Laplacian of the molar density contains a coefficient of unity. When the remaining $r+1$ scaling factors in the dimensional mass transfer equation are divided by $\mathfrak{D}_{i,\text{mix}} C_{\text{A0}}/L^2$, the dimensionless mass transfer equation is obtained. Most important, $r+1$ dimensionless transport numbers appear in this equation as coefficients of each of the dimensionless mass transfer rate processes, except diffusion. Remember that the same dimensionless number appears as a coefficient for the accumulation and convective mass transfer rate processes on the left-hand side of the equation.

As mentioned above, the dimensionless transport numbers in the mass transfer equation are generated from ratios of dimensional scaling factors. If one divides the scaling factor for convective mass transfer by the scaling factor for diffusion, the result is

$$\frac{\langle v \rangle C_{\text{A0}}/L}{\mathfrak{D}_{i,\text{mix}} C_{\text{A0}}/L^2} = \frac{L\langle v \rangle}{\mathfrak{D}_{i,\text{mix}}} = \frac{L\langle v \rangle}{\mu/\rho} \frac{\mu/\rho}{\mathfrak{D}_{i,\text{mix}}} = \text{Re}\cdot\text{Sc} = \text{Pe}_{\text{MT}} \tag{10-9}$$

The product of the Reynolds and Schmidt numbers, which counts as one dimensionless number, is equivalent to the Peclet number for mass transfer, Pe_{MT}. The Peclet number represents the ratio of the convective mass transfer rate process to the diffusion rate process of component i, and it appears on the left-hand side of the dimensionless mass transfer equation for component i. The remaining r dimensionless transport numbers can be treated simultaneously because they represent ratios of scaling factors for the reactant–product conversion rate due to the jth independent chemical reaction relative to the rate of diffusion of component i. Hence,

$$\frac{k_j(T)(C_{\text{A0}})^{n_j}}{\mathfrak{D}_{i,\text{mix}} C_{\text{A0}}/L^2} = \frac{k_j(T) L^2 (C_{\text{A0}})^{n_j - 1}}{\mathfrak{D}_{i,\text{mix}}} = \Lambda_{ij}^2 \tag{10-10}$$

where Λ_{ij}^2 is the Damkohler number for component i in the jth chemical reaction. The Damkohler number represents the ratio of the rate of chemical reaction to the rate of mass transfer via diffusion. Obviously, the Damkohler number is chemical-reaction-specific because the kinetic rate constant $k_j(T)$ depends on the particular reaction under consideration. The Damkohler number is also species specific because the rate of mass transfer by diffusion depends on the diffusion coefficient for component i. The latter concept is particularly important when there are several reactants and products diffusing through the pores of a catalytic pellet. Under these conditions, it is necessary to calculate an effective diffusion coefficient and an intrapellet Damkohler number for each component in the reactive mixture. Theoretical details based on this concept are described in Chapter 19 when it is necessary to relate the molar densities of all species in the mixture to the molar density of the key-limiting reactant. This procedure is required only when the rate law is expressed in terms of the molar density of more than one component. Detailed calculations of the effective intrapellet diffusion coefficient of component i are described in Chapter 21. The Damkohler number for component i is always calculated based on the characteristic molar density of reactant A. C_{A0} is defined either on the external surface of a catalytic pellet, or in the feed stream to a flow reactor. The final form of the dimensionless mass transfer equation for component i in pseudo-binary mixtures with constant physical properties is

$$\mathrm{Re}\cdot\mathrm{Sc}\left(\frac{\partial \psi_i}{\partial t} + \mathbf{v}\cdot\nabla\psi_i\right) = 1\nabla^2\psi_i + \sum_{j=1}^{r} \nu_{ij}\Lambda_{ij}^2 \mathfrak{R}_j^* \tag{10-11}$$

For unsteady-state diffusion into a quiescent medium with no chemical reaction, the mass transfer Peclet number does not appear in the dimensionless mass transfer equation for species i because it is not appropriate to make variable time t dimensionless via division by $L/\langle v\rangle$ if there is no bulk fluid flow (i.e., $\langle v\rangle = 0$). In this case, the first term on each side of equation (10-11) survives, which corresponds to the unsteady-state diffusion equation. However, the characteristic time for diffusion of species i over a length scale L, given by $L^2/\mathfrak{D}_{i,\,\mathrm{mix}}$, replaces $L/\langle v\rangle$ to make variable time t dimensionless. Now, the accumulation and diffusional rate processes scale as $C_{A0}\mathfrak{D}_{i,\,\mathrm{mix}}/L^2$, with dimensions of moles per volume per time. Since both surviving mass transfer rate processes exhibit the same dimensional scaling factor, there are no dimensionless numbers in the mass transfer equation which describes unsteady-state diffusion for species i in nonreactive systems.

10-3 FUNCTIONAL DEPENDENCE OF THE MOLAR DENSITY OF SPECIES *i* VIA DIMENSIONAL ANALYSIS

Consider several overlapping subsets of the dimensionless mass transfer equation from Section 10-2 which correspond to various combinations of convection, diffusion, and chemical reaction that may or may not exhibit transient behavior.

If one constructs the appropriate dimensionless equation that governs the molar density profile ψ_i for component i, then ψ_i depends on all the dimensionless independent variables and parameters in the governing equation and its supporting boundary conditions. Geometry also plays a role in the final expression for ψ_i in each case via the coordinate system that best exploits the summetry of the macroscopic boundaries, but this effect is not as important as the dependence of ψ_i on the dimensionless numbers in the mass transfer equation and its boundary conditions. For example, if convection, diffusion, and chemical reaction are important rate processes that must be considered, then the governing equation for transient analysis

$$\text{Re}\cdot\text{Sc}\left(\frac{\partial \psi_i}{\partial t} + \mathbf{v}\cdot\nabla\psi_i\right) = \nabla^2\psi_i + \sum_j \nu_{ij}\Lambda_{ij}^2\mathfrak{R}_j^* \tag{10-12}$$

suggests that

$$\psi_i = f(t, \boldsymbol{r}; \text{Re}\cdot\text{Sc}, \Lambda_{ij\ (\text{all } j)}^2) \tag{10-13}$$

where t is dimensionless time and $\boldsymbol{r}$ represents the set of dimensionless spatial coordinates. Steady-state convection, diffusion, and chemical reaction in packed catalytic tubular reactors are described by

$$\text{Re}\cdot\text{Sc}(\mathbf{v}\cdot\nabla\psi_i) = \nabla^2\psi_i + \sum_j \nu_{ij}\Lambda_{ij}^2\mathfrak{R}_j^* \tag{10-14}$$

and one concludes that the functional dependence of ψ_i is given by

$$\psi_i = f(\boldsymbol{r}; \text{Re}\cdot\text{Sc}, \Lambda_{ij\ (\text{all } j)}^2) \tag{10-15}$$

where time dependence is absent. For convection and diffusion in nonreactive problems, one does not expect functional dependence of ψ_i on any of the Damkohler numbers because the governing equations:

$$\text{Unsteady state:} \qquad \text{Re}\cdot\text{Sc}\left(\frac{\partial \psi_i}{\partial t} + \mathbf{v}\cdot\nabla\psi_i\right) = \nabla^2\psi_i \qquad \psi_i = f(t, \boldsymbol{r}; \text{Re}\cdot\text{Sc}) \tag{10-16a}$$

$$\text{Steady state:} \qquad \text{Re}\cdot\text{Sc}\ (\mathbf{v}\cdot\nabla\psi_i) = \nabla^2\psi_i \qquad \psi_i = f(\boldsymbol{r}; \text{Re}\cdot\text{Sc}) \tag{10-16b}$$

do not require any information about rates of conversion of reactants to products or the corresponding Λ_{ij}^2. In each of these two examples for nonreactive problems, which include laminar mass transfer boundary layer theory, the mass transfer Peclet number is the only dimensionless number that appears in the final expressions for ψ_i. As mentioned above, the accumulation rate process and molecular mass transfer via diffusion are described by the same dimensional

scaling factor when convective mass transfer is absent. For reactive systems, the governing equations and functional dependencies of ψ_i are provided below for transient and steady-state analyses, without convection:

$$\text{Unsteady state:} \qquad \frac{\partial \psi_i}{\partial t} = \nabla^2 \psi_i + \sum_j \nu_{ij} \Lambda_{ij}^2 \mathfrak{R}_j^* \qquad \psi_i = f(t, \boldsymbol{r}; \Lambda_{ij\ (\text{all } j)}^2) \tag{10-17a}$$

$$\text{Steady state:} \qquad 0 = \nabla^2 \psi_i + \sum_j \nu_{ij} \Lambda_{ij}^2 \mathfrak{R}_j^* \qquad \psi_i = f(\boldsymbol{r}; \Lambda_{ij\ (\text{all } j)}^2) \tag{10-17b}$$

Obviously, the Damkohler numbers are important when chemical reaction occurs, as illustrated by these two examples, which include diffusion and pseudo-homogeneous chemical reaction in porous catalytic pellets. Details of the diffusion equation without convection in nonreactive systems are summarized below for transient and steady-state analyses:

$$\text{Unsteady state:} \qquad \frac{\partial \psi_i}{\partial t} = \nabla^2 \psi_i \qquad \psi_i = f(t, \boldsymbol{r}) \tag{10-18a}$$

$$\text{Steady state:} \qquad 0 = \nabla^2 \psi_i \qquad \psi_i = f(\boldsymbol{r}) \tag{10-18b}$$

Notice that the molar density profiles for these problems are not affected by any dimensionless numbers because either there is only one mass transfer rate process for steady-state analysis, or both rate processes are described by the same dimensional scaling factor. These qualitative trends should be considered before one seeks quantitative information about a particular mass transfer problem.

10-4 MAXIMUM NUMBER OF DIMENSIONLESS GROUPS THAT CAN BE CALCULATED FOR A GENERIC MASS TRANSFER PROBLEM

If N components ($1 \le i \le N$) participate in r independent chemical reactions ($1 \le j \le r$), then the previous discussion illustrates the methodology to generate $r + 1$ dimensionless numbers from $r + 2$ dimensional scaling factors in the mass balance for component i. This process is repeated by analyzing the mass balance for each component in the mixture. The characteristic molar density of key-limiting reactant A, C_{A0}, is employed to make all molar densities in the reactive mixture dimensionless, as follows:

$$\psi_i = \frac{C_i}{C_{A0}} \tag{10-19}$$

Hence, the dimensional scaling factor for convective mass transfer is the same in each mass balance. Similarly, dimensional scaling factors for all of the independent chemical reactions do not change from one mass balance to the next. However, when the $r + 2$ dimensional scaling factors in the mass balance for component i are divided by the dimensional scaling factor for component i's rate of diffusion (i.e., $\mathfrak{D}_{i,\,\text{mix}} C_{A0}/L^2$), one obtains $r + 1$ dimensionless numbers

that are species specific because division was performed using a species-specific diffusion coefficient. This analysis yields $r + 1$ unique dimensionless numbers in each dimensionless mass balance; a mass transfer Peclet number based on the rate of diffusion of component i, and a Damkohler number for component i in each independent chemical reaction. It should be mentioned that Λ_{ij}^2 is not very useful if component i does not participate in the jth independent chemical reaction. In summary, there are a total of $N(r + 1)$ unique dimensionless numbers that can be calculated, where $r + 1$ dimensionless numbers appear in each mass balance. There are N different Peclet numbers, where each is based on a rate of molecular mass transfer for component i, and there are Nr different Damkohler numbers, where each characterizes the reactant–product conversion rate for the jth independent chemical reaction relative to the rate of diffusion for component i. Ratios of diffusivities have not been considered in this analysis, but they are necessary to analyze multicomponent adsorption, diffusion, and heterogeneous chemical reaction within the pores of a catalytic pellet.

PROBLEMS

10-1. Consider a non-Newtonian fluid with power-law index n and consistency index m. Construct appropriate dimensionless representations for the Reynolds, Schmidt, and mass transfer Peclet numbers.

Answer: The product of Re and Sc is the mass transfer Peclet number, $\mathrm{Pe}_{\mathrm{MT}}$, where the important mass transfer rate processes are convection and diffusion. Since the dimensional scaling factors for both of these rate processes do not contain information about the constitutive relation between viscous stress and velocity gradients, one concludes that $\mathrm{Pe}_{\mathrm{MT}}$ is the same for Newtonian and non-Newtonian fluids. Hence, the mass transfer Peclet number for species i in a multicomponent mixture is

$$\mathrm{Pe}_{\mathrm{MT}} = \mathrm{Re}\cdot\mathrm{Sc} = \frac{L\langle v\rangle}{\mathfrak{D}_{i,\,\mathrm{mix}}}$$

in terms of characteristic length L and average velocity $\langle v\rangle$. Since the Reynolds number represents a ratio of dimensional scaling factors for convective momentum flux relative to viscous momentum flux, Re should contain information about the power-law parameters. The dimensional scaling factors (i.e., DSF) for both types of momentum flux and the corresponding terms in the equation of motion (i.e., EOM) are summarized below for power-law fluids.

Momentum Transfer Rate Process	DSF	DSF in EOM
Convective momentum flux, $\rho\mathbf{vv}$	$\rho\langle v\rangle^2$	$\nabla\cdot\rho\mathbf{vv} \approx \rho\langle v\rangle^2/L$
Viscous momentum flux, τ	$m(\langle v\rangle/L)^n$	$\nabla\cdot\tau \approx m\langle v\rangle^n/L^{n+1}$

Division of the dimensional scaling factors for these two momentum transfer rate processes, or the corresponding scaling factors in the equation of motion, yields an expression for the Reynolds number. Hence,

$$\mathrm{Re} = \frac{\rho\langle v\rangle^2}{m(\langle v\rangle/L)^n} = \frac{\rho\langle v\rangle^{2-n}L^n}{m}$$

Since the mass transfer Peclet number is insensitive to the power-law parameters, the Schmidt number must reflect a dependence on m and n to offset these corresponding quantities in Re, such that the product of Re and Sc yields $\mathrm{Pe}_{\mathrm{MT}}$. In other words,

$$\mathrm{Sc}\frac{\rho\langle v\rangle^{2-n}L^n}{m} = \frac{L\langle v\rangle}{\mathfrak{D}_{i,\,\mathrm{mix}}}$$

Classically, the Schmidt number represents a ratio of diffusivities for momentum transfer and mass transfer. The preceding equation suggests that

$$\mathrm{Sc} = \frac{m(\langle v\rangle/L)^{n-1}}{\rho\mathfrak{D}_{i,\,\mathrm{mix}}}$$

where $m(\langle v\rangle/L)^{n-1}$ is the dimensional scaling factor, or order-of-magnitude estimate, for non-Newtonian fluid viscosities via the power-law model.

10-2. What important dimensionless number(s) appear in the dimensionless partial differential mass transfer equation for laminar flow through a blood capillary when the important rate processes are axial convection and radial diffusion?

10-3. Consider two-dimensional steady-state mass transfer in the liquid phase external to a solid sphere at high Schmidt numbers. The particle, which contains mobile reactant A, dissolves into the passing fluid stream, where A undergoes nth-order irreversible homogeneous chemical reaction with another reactant in the liquid phase. The flow regime is laminar, and heat effects associated with the reaction are very weak. Boundary layer approximations are invoked to obtain a locally flat description of this problem.

(a) What mass transfer rate processes must be considered to describe this problem?

(b) What dimensionless numbers appear in the dimensionless mass transfer equation?

The set of independent variables and dimensionless parameters for the functional dependencies in parts (c), (d), and (e) should be chosen from the following:

t^* = dimensionless time variable
x^* = dimensionless spatial coordinate measured parallel to the interface
y^* = dimensionless spatial coordinate measured perpendicular to the interface
n = order of the irreversible chemical reaction
all of the dimensionless numbers from part (b)

(c) What is the functional dependence of the dimensionless molar density of mobile component A in solution, $\psi_A = f(?)$?

(d) What is the functional dependence of the local Sherwood number $Sh_{Local} = g(?)$, which is given by the dimensionless concentration gradient with respect to normal coordinate y^* evaluated at the solid–liquid interface?

$$Sh_{local} = -\left(\frac{\partial \psi_A}{\partial y^*}\right)_{y^*=0}$$

(e) What is the functional dependence of the surface-averaged Sherwood number $Sh_{average} = h(?)$, defined by

$$Sh_{average} = -\iint \left(\frac{\partial \psi_A}{\partial y^*}\right)_{y^*=0} dx^* \, dz^*$$

where z^* is the other dimensionless independent variable measured in the plane of the solid–liquid interface, and integration is performed over macroscopic limits on x^* and z^*?

(f) Compare the mass transfer boundary layer thickness of mobile reactant A in solution, adjacent to the fluid–solid interface, with and without chemical reaction. In other words, how does $(\delta_C)_{\text{with chemical reaction}}$ compare with $(\delta_C)_{\text{no chemical reaction}}$ for species A at the same point along the interface?

Transport Phenomena for Chemical Reactor Design. Laurence A. Belfiore
Copyright © 2003 John Wiley & Sons, Inc.
ISBN: 0-471-20275-4

11

LAMINAR BOUNDARY LAYER MASS TRANSFER AROUND SOLID SPHERES, GAS BUBBLES, AND OTHER SUBMERGED OBJECTS

11-1 BOUNDARY LAYER MASS TRANSFER ANALYSIS

As an incompressible fluid of infinite extent approaches and flows past either a spherical solid pellet or a gas bubble, a mobile component undergoes interphase mass transfer via convection and diffusion from the sphere to the fluid phase. The overall objective is to calculate the mass transfer coefficient and the Sherwood number at any point along the interface (i.e., the local transfer coefficients), as well as surface-averaged transfer coefficients. The results are applicable in the laminar flow regime (1) when the sphere is stationary and the fluid moves, (2) when solid spheres fall or gas bubbles rise through a quiescent medium, and (3) when both the sphere and fluid move in opposite directions. The detailed nature of the solution procedure requires that only one sphere be present, but the final results can be extended to describe interphase mass transfer in packed beds. One of the classic applications of these results is interphase transfer of oxygen from gas bubbles to a well-stirred liquid as the bubbles rise through the continuous fluid phase in a mixed-flow apparatus.

11-1.1 Mass Transfer Equation

Steady-state analysis in the absence of any chemical reactions produces the following mass balance for mobile component A in an incompressible fluid when the control volume is differentially thick in all coordinate directions:

$$\mathbf{v} \cdot \nabla C_{\mathrm{A}} = \mathscr{D}_{\mathrm{A,\,mix}} \nabla \cdot \nabla C_{\mathrm{A}} \tag{11-1}$$

The only assumption is that the physical properties of the fluid (i.e., ρ and $\mathfrak{D}_{A,\,mix}$) are constant. The left-hand side of equation (11-1) represents convective mass transfer in three coordinate directions, and diffusion is accounted for via three terms on the right side. If the mass balance is written in dimensionless form, then the mass transfer Peclet number appears as a coefficient on the left-hand side. Basic information for dimensional molar density C_A will be developed before dimensionless quantities are introduced. In spherical coordinates, the concentration profile $C_A(r, \theta, \phi)$ must satisfy the following partial differential equation (PDE):

$$v_r \frac{\partial C_A}{\partial r} + \frac{v_\theta}{r}\frac{\partial C_A}{\partial \theta} + \frac{v_\phi}{r \sin\theta}\frac{\partial C_A}{\partial \phi} = \mathfrak{D}_{A,\,mix}\left[\frac{1}{r^2}\frac{\partial}{\partial r}\left(r^2\frac{\partial C_A}{\partial r}\right) + \frac{1}{r^2 \sin\theta}\frac{\partial}{\partial \theta}\left(\sin\theta\frac{\partial C_A}{\partial \theta}\right) + \frac{1}{r^2 \sin^2\theta}\frac{\partial^2 C_A}{\partial \phi^2}\right] \tag{11-2}$$

This is a horrendous equation that requires simplification via reasonable engineering approximations before one can derive any meaningful results from an analytical solution. The origin of an xyz Cartesian coordinate system is placed at the center of the sphere, and it remains there throughout the analysis. The fluid approaches the stationary sphere from above and moves downward along the z axis in the negative z direction. Hence, the velocity vector (i.e., approach velocity) of the fluid far from the sphere is

$$\mathbf{v}(r \to \infty) = V_{approach}(-\delta_z) \tag{11-3}$$

When the fluid approaches the sphere from above, the fluid initially contacts the sphere at $\theta = 0$ (i.e., the stagnation point) because polar angle θ is defined relative to the positive z axis. This is convenient because the mass transfer boundary layer thickness δ_C is a function of θ, and $\delta_C = 0$ at $\theta = 0$. In the laminar and creeping flow regimes, the two-dimensional fluid dynamics problem is axisymmetric (i.e., about the z axis) with

$$v_r(r, \theta) \qquad v_\theta(r, \theta) \qquad v_\phi = 0 \tag{11-4}$$

Furthermore, the mass transfer problem exhibits symmetry with respect to azimuthal angle ϕ that spans all the longitudinal time zones on the earth, for example. Hence, $\partial C_A/\partial \phi = 0$ and the three-dimensional mass balance for $C_A(r, \theta, \phi)$ is reduced to two dimensions (i.e., r and θ):

$$v_r \frac{\partial C_A}{\partial r} + \frac{v_\theta}{r}\frac{\partial C_A}{\partial \theta} = \mathfrak{D}_{A,\,mix}\left[\frac{1}{r^2}\frac{\partial}{\partial r}\left(r^2\frac{\partial C_A}{\partial r}\right) + \frac{1}{r^2 \sin\theta}\frac{\partial}{\partial \theta}\left(\sin\theta\frac{\partial C_A}{\partial \theta}\right)\right] \tag{11-5}$$

11-1.2 Order-of-Magnitude Analysis at High-Mass-Transfer Peclet Numbers

It is useful to compare the importance of diffusion relative to convection in the primary flow direction within the mass transfer boundary layer. The primary flow direction corresponds to θ, except at the stagnation point, where $\theta = 0$, and at the separation point, where $\theta = \pi$. Hence, one estimates the importance of tangential diffusion relative to tangential convection, which is represented by the second terms on the right and left sides, respectively, of (11-5). At first glance, this comparison seems to be an impossible task, particularly if one does not know the solution for $C_A(r, \theta)$. However, if one can estimate the magnitude of diffusive mass transfer relative to convective transport in the primary flow direction, then the power of order-of-magnitude analysis becomes apparent if diffusion can be neglected. This engineering approximation allows one to discard transport mechanisms that are unimportant before attempting to tackle an already difficult mathematical problem. For example, tangential diffusion is estimated as follows:

$$\mathfrak{D}_{A,\,mix}\frac{1}{r^2\sin\theta}\frac{\partial}{\partial\theta}\left(\sin\theta\frac{\partial C_A}{\partial\theta}\right) \approx \mathfrak{D}_{A,\,mix}\frac{1}{R^2}\frac{\Delta C_A}{(\Delta\theta)^2} \tag{11-6}$$

In similar fashion, convective mass transfer in the primary flow direction is

$$\frac{v_\theta}{r}\frac{\partial C_A}{\partial\theta} \approx \frac{V_{approach}}{R}\frac{\Delta C_A}{\Delta\theta} \tag{11-7}$$

Since both of these terms in the mass transfer equation have units of moles per volume per time, it should be obvious that the ratio of diffusion to convection is dimensionless. This suggests that the relative importance of the two terms should be expressed as a dimensionless number for mass transfer. The desired ratio is

$$\begin{aligned}\frac{\text{tangential diffusion}}{\text{tangential convection}} &= \mathfrak{D}_{A,\,mix}\frac{1}{R^2}\frac{\Delta C_A/(\Delta\theta)^2}{(V_{approach}/R)(\Delta C_A/\Delta\theta)}\\ &= \frac{\mathfrak{D}_{A,\,mix}}{\pi V_{approach}R} = \frac{2}{\pi\cdot \mathrm{Pe}}\end{aligned} \tag{11-8}$$

where $\Delta\theta$ is replaced by π radians and the mass transfer Peclet number is given by the product of the Reynolds and Schmidt numbers:

$$\begin{aligned}\mathrm{Pe} &= \mathrm{Re}\cdot\mathrm{Sc} = \frac{V_{approach}(2R)}{\mathfrak{D}_{A,\,mix}}\\ \mathrm{Re} &= \frac{V_{approach}(2R)}{\mu/\rho}\\ \mathrm{Sc} &= \frac{\mu/\rho}{\mathfrak{D}_{A,\,mix}}\end{aligned} \tag{11-9}$$

Order-of-magnitude analysis indicates that diffusion is negligible relative to convective mass transfer in the primary flow direction within the concentration boundary layer at large values of the Peclet number. Typically, liquid-phase Schmidt numbers are at least 10^3 because momentum diffusivities (i.e., μ/ρ) are on the order of 10^{-2} cm^2/s and the Stokes–Einstein equation predicts diffusion coefficients on the order of 10^{-5} cm^2/s. Hence, the Peclet number should be large for liquids even under slow-flow conditions. Now, the partial differential mass balance for $C_A(r, \theta)$ is simplified for axisymmetric flow (i.e., $v_\phi = 0$), angular symmetry (i.e., $\partial C_A/\partial\phi = 0$), and high-mass-transfer Peclet numbers (i.e., neglect tangential diffusion):

$$v_r \frac{\partial C_A}{\partial r} + \frac{v_\theta}{r}\frac{\partial C_A}{\partial \theta} = \mathfrak{D}_{A,\,mix}\frac{1}{r^2}\frac{\partial}{\partial r}\left(r^2\frac{\partial C_A}{\partial r}\right) \tag{11-10}$$

Initially, the steady-state mass balance contained six terms: three for convection and three for diffusion. Physically realistic approximations have reduced the analysis to radial and tangential convection and radial diffusion. Three boundary conditions are required to obtain a unique solution to (11-10): one condition on θ and two conditions on r. The boundary condition on θ,

$$C_A = C_{A,\,bulk} \text{ at } \theta = 0 \text{ for all values of } r > R \tag{11-11}$$

is consistent with the fact that tangential diffusion is neglected. Otherwise, it is possible that mobile component A within the concentration boundary layer on the liquid side of the interface could diffuse against the primary flow and reach the stagnation point at $\theta = 0$. If this process occurs, then the liquid-phase concentration of A would be greater than its approach stream value of $C_{A,\,bulk}$ prior to the stagnation point. Hence, this boundary condition is consistent with the mass transfer mechanisms that are included in the mass balance. The two boundary conditions on the radial variable are

$$C_A = C_{A,\,interface} \text{ at } r = R \text{ for all values of } \theta > 0 \tag{11-12a}$$

$$\text{(BLBC)} \qquad C_A \to C_{A,\,bulk} \text{ as } r \to \infty \text{ for all values of } \theta < \pi \text{ (i.e., separation point)} \tag{11-12b}$$

The second condition, given by (11-12*b*), is referred to as the *boundary layer boundary condition* (BLBC). The mass transfer boundary layer is infinitely thick at the separation point where $\theta = \pi$, so, in principle, one could travel an infinite distance away from the spherical interface without measuring the bulk concentration of A that is characteristic of the approach stream. Hence, the separation point is not considered in this discussion. A better statement of the boundary layer boundary condition is

$$C_A \to C_{A,\,bulk} \text{ for } r > R + \delta_C(\theta) \qquad \text{where } \theta < \pi \tag{11-13}$$

The latter condition, given by (11-13), is employed in the von Kármán approach to boundary layer problems.

11-1.3 Thin Boundary Layer Simplification at High Schmidt Numbers

Radial diffusion in spherical coordinates,

$$\mathfrak{D}_{\mathrm{A,\,mix}} \frac{1}{r^2} \frac{\partial}{\partial r} \left(r^2 \frac{\partial C_{\mathrm{A}}}{\partial r} \right) \tag{11-14}$$

which represents an important mechanism in the mass balance, contains factors of $1/r^2$ and r^2 because the surface area normal to radial mass flux is proportional to the square of radial position. In other words, the surface area normal to the radial direction at position r is $4\pi r^2$ at the macroscopic level, and $r^2 \sin\theta \, d\theta \, d\phi$ at the microscopic level. Interfacial curvature in the radial diffusion term is important when the concentration boundary layer in the liquid phase adjacent to the spherical interface is relatively thick. However, when boundary layers are thin at large Schmidt numbers, curvature is unimportant and a locally flat description is appropriate. This simplification is analyzed in detail by applying the product rule to the radial diffusion term and factoring the simple second derivative for a flat interface:

$$\begin{aligned} \frac{1}{r^2} \frac{\partial}{\partial r} \left(r^2 \frac{\partial C_{\mathrm{A}}}{\partial r} \right) &= \frac{\partial^2 C_{\mathrm{A}}}{\partial r^2} + \frac{2}{r} \frac{\partial C_{\mathrm{A}}}{\partial r} \\ &= \frac{\partial^2 C_{\mathrm{A}}}{\partial r^2} \left[1 + \frac{(2/r)\partial C_{\mathrm{A}}/\partial r}{\partial^2 C_{\mathrm{A}}/\partial r^2} \right] \end{aligned} \tag{11-15}$$

The second term in brackets in (11-15) is manipulated as follows if $\beta = \partial C_{\mathrm{A}}/\partial r$:

$$\left(\frac{2}{r} \right) \frac{\partial C_{\mathrm{A}}/\partial r}{\partial^2 C_{\mathrm{A}}/\partial r^2} = \frac{2\beta}{r \partial\beta/\partial r} = \frac{2}{(r/\beta)\partial\beta/\partial r} = \frac{2}{\partial \ln \beta / \partial \ln r} \tag{11-16}$$

Hence,

$$\frac{1}{r^2} \frac{\partial}{\partial r} \left(r^2 \frac{\partial C_{\mathrm{A}}}{\partial r} \right) = \frac{\partial^2 C_{\mathrm{A}}}{\partial r^2} \left(1 + \frac{2}{\partial \ln \beta / \partial \ln r} \right) \tag{11-17}$$

The denominator of the second term in parentheses on the right side of (11-17) cannot be evaluated explicitly until one obtains basic information for the concentration profile. However, the following qualitative analysis is based solely on the fact that the mass transfer boundary layer is much thinner than the corresponding momentum boundary layer at very large Schmidt numbers. Under these conditions, the transfer of component A into the liquid phase is limited to a very thin shell that surrounds the sphere. Rates of interphase mass transfer are

large because the interfacial molar flux of component A normal to the spherical interface is given by Fick's law as

$$N_{Ar}(r = R) = -\mathfrak{D}_{A,\,mix}\left(\frac{\partial C_A}{\partial r}\right)_{r=R} \approx \frac{\mathfrak{D}_{A,\,mix}}{\delta_C(\theta)}(C_{A,\,interface} - C_{A,\,bulk}) \quad (11\text{-}18)$$

Hence, high rates of mass transfer are obtained when $\delta_C(\theta)$ is very small. Tangential convection parallel to the interface is responsible for sweeping away the mobile component as it diffuses radially into the boundary layer. The thin boundary layer simplification proceeds as follows:

$$\frac{\partial \ln \beta}{\partial \ln r} = \frac{\text{fractional change in } \partial C_A/\partial r}{\text{fractional change in } r} \gg 1 \quad (11\text{-}19)$$

In other words, if the mass transfer boundary layer is very thin, then there is a tremendous change in the radial concentration gradient as one moves a very short distance radially outward from the spherical interface. Hence, at large Schmidt numbers where $\delta_C(\theta) \ll R$, the following locally flat approximation is valid for spherical interfaces because curvature within the boundary layer is negligible:

$$\text{Spherical coordinates:} \qquad \frac{1}{r^2}\frac{\partial}{\partial r}\left(r^2\frac{\partial C_A}{\partial r}\right) \approx \frac{\partial^2 C_A}{\partial r^2} \quad (11\text{-}20a)$$

A similar simplification for radial diffusion in cylindrical coordinates is valid at large Schmidt numbers;

$$\text{Cylindrical coordinates:} \qquad \frac{1}{r}\frac{\partial}{\partial r}\left(r\frac{\partial C_A}{\partial r}\right) \approx \frac{\partial^2 C_A}{\partial r^2} \quad (11\text{-}20b)$$

Now the simplified mass transfer equation that accounts for convection normal and parallel to the spherical interface, and radial diffusion into a thin boundary layer, is

$$v_r\frac{\partial C_A}{\partial r} + \frac{v_\theta}{r}\frac{\partial C_A}{\partial \theta} = \mathfrak{D}_{A,\,mix}\frac{\partial^2 C_A}{\partial r^2} \quad (11\text{-}21)$$

Equation of Continuity for Radial and Tangential Velocity Components. If the fluid is incompressible, then the microscopic balance on overall fluid mass provides a relation between the two important velocity components that are required in the mass transfer equation. Since the flow is axisymmetric and $v_\phi = 0$,

$$\nabla \cdot \mathbf{v} = \frac{1}{r^2}\frac{\partial}{\partial r}(r^2 v_r) + \frac{1}{r\sin\theta}\frac{\partial}{\partial \theta}(v_\theta \sin\theta) = 0 \quad (11\text{-}22)$$

Unlike the complete solution to the equation of motion (EOM) for two-dimensional flow around a sphere, it is only necessary to relate v_r and v_θ via the

equation of continuity within the following range of the radial variable:

$$R \le r \le R + \delta_C(\theta) \qquad \text{where } \delta_C(\theta) \ll R \tag{11-23}$$

Once again, the following manipulation is performed on the term in (11-22) that contains the radial velocity component:

$$\begin{aligned}\frac{1}{r^2}\frac{\partial}{\partial r}(r^2 v_r) &= \frac{\partial v_r}{\partial r} + \frac{2}{r}v_r = \frac{\partial v_r}{\partial r}\left[1 + \frac{(2/r)v_r}{\partial v_r/\partial r}\right] \\ &= \frac{\partial v_r}{\partial r}\left(1 + \frac{2}{\partial \ln v_r/\partial \ln r}\right)\end{aligned} \tag{11-24}$$

Now, the denominator of the final term in (11-24) can be evaluated explicitly via exact fluid dynamics solutions for creeping flow around a solid sphere, and for creeping and potential flow around a gas bubble. In the creeping or laminar flow regimes, the momentum boundary layer is not thin. Hence, the following claim:

$$\frac{\partial \ln v_r}{\partial \ln r} = \frac{\text{fractional change in } v_r}{\text{fractional change in } r} \gg 1 \tag{11-25}$$

is probably not true. The worst regime for a thin momentum boundary layer corresponds to creeping flow around a solid sphere, where the tangential velocity component for an incompressible Newtonian fluid is

$$v_\theta(r, \theta) = v_\theta(r \to \infty, \theta)\left(1 - \tfrac{3}{4}\eta^{-1} - \tfrac{1}{4}\eta^{-3}\right) \tag{11-26}$$

and $\eta = r/R$ is the dimensionless radial coordinate, which assumes values that are greater than or equal to unity. If the outer edge of the momentum boundary layer δ_v in the fluid phase is identified where this tangential velocity has achieved a specified fraction κ of the free-stream velocity at the same polar angle θ, then

$$v_\theta(R + \delta_v, \theta) = \kappa v_\theta(r \to \infty, \theta) \tag{11-27}$$

The momentum boundary layer thickness is calculated in terms of the sphere radius by solving the following equation, based on (11-26) and (11-27), which is implicit in δ_v/R:

$$1 - \frac{3}{4}\left(1 + \frac{\delta_v}{R}\right)^{-1} - \frac{1}{4}\left(1 + \frac{\delta_v}{R}\right)^{-3} = \kappa \tag{11-28}$$

When $\kappa = 0.99$, $\delta_v/R = 74$, which implies that gradients in v_θ extend outward for 74 sphere radii into the fluid until the tangential velocity achieves 99% of the free-stream velocity. The momentum boundary layer thickness is not defined

in terms of the radial velocity component v_r. However, the preceding discussion suggests that $\partial \ln v_r / \partial \ln r$ should be rather small. Hence,

$$\frac{1}{r^2}\frac{\partial}{\partial r}(r^2 v_r) = \frac{\partial v_r}{\partial r}\left(1 + \frac{2}{\partial \ln v_r / \partial \ln r}\right) \neq \frac{\partial v_r}{\partial r} \tag{11-29}$$

The curvature correction factor in parentheses in (11-29) is calculated explicitly for creeping flow of an incompressible Newtonian fluid around a solid sphere, where

$$v_r(r, \theta) = v_r(r \to \infty, \theta)\left(1 - \tfrac{3}{2}\eta^{-1} + \tfrac{1}{2}\eta^{-3}\right) \tag{11-30}$$

and the momentum boundary layer is rather large. Relative changes in v_r with respect to relative changes in radial coordinate r are calculated as follows:

$$\frac{\partial \ln v_r}{\partial \ln r} = \frac{r}{v_r}\frac{\partial v_r}{\partial r} = \frac{3\eta^{-1} - 3\eta^{-3}}{2 - 3\eta^{-1} + \eta^{-3}} \tag{11-31}$$

Now, it is possible to predict the curvature correction factor $F(\eta)$ for the radial term in the equation of continuity at any position in the fluid (see Table 11-1):

$$\frac{1}{r^2}\frac{\partial}{\partial r}(r^2 v_r) = F(\eta)\frac{\partial v_r}{\partial r} \tag{11-32}$$

$$F(\eta) = 1 + \frac{2(2 - 3\eta^{-1} + \eta^{-3})}{3\eta^{-1} - 3\eta^{-3}} \tag{11-33}$$

Hence, replacing $(1/r^2)\partial(r^2 v_r)/\partial r$ in the equation of continuity by $\partial v_r / \partial r$ is exact at the fluid–solid interface. As one moves into the fluid,

$$\frac{1}{r^2}\frac{\partial}{\partial r}(r^2 v_r) > \frac{\partial v_r}{\partial r} \qquad \text{when } r > R \quad (\text{i.e., } n > 1) \tag{11-34}$$

TABLE 11-1 Exact Calculations of the Curvature Correction Factor and the Error Embedded in the Radial Term of the Locally Flat Equation of Continuity[a]

η	$\partial \ln v_r / \partial \ln r$	$F(\eta)$	$[F(\eta) - 1]/F(\eta)$ (%)
1	∞	1.00	0
1.05	38.0	1.05	4.8
1.10	19.7	1.10	9.1
1.20	9.7	1.21	16.7

[a]For creeping flow around a stationary solid sphere.

If the mass transfer boundary layer thickness is given by $(\eta - 1)R$ in Table 11-1, then the last column represents the maximum underestimate of $(1/r^2)\partial(r^2 v_r)/\partial r$ in the equation of continuity if the curvature correction is neglected. Hence,

$$\frac{\partial v_r}{\partial r} + \frac{1}{r \sin\theta} \frac{\partial}{\partial \theta}(v_\theta \sin\theta) = 0 \tag{11-35}$$

is used to relate v_r and v_θ within the mass transfer boundary layer, which is quite thin at high Schmidt numbers. There is no need to solve (11-35) outside the mass transfer boundary layer because $C_A(r, \theta)$ is required only within δ_C. Fortuitously, the curvature correction in the equation of continuity is not very important at small distances into the fluid, as dictated by thin mass transfer boundary layers.

Locally Flat Description of Boundary Layer Mass Transfer in Spherical Coordinates. Since the radial coordinate r does not change much as one moves from the fluid–solid interface to the outer edge of the mass transfer boundary layer, it is acceptable to replace r by R in the two-dimensional mass transfer equation and the equation of continuity:

$$v_r \frac{\partial C_A}{\partial r} + \frac{v_\theta}{R} \frac{\partial C_A}{\partial \theta} = \mathscr{D}_{A,\,mix} \frac{\partial^2 C_A}{\partial r^2} \tag{11-36}$$

$$\frac{\partial v_r}{\partial r} + \frac{1}{R \sin\theta} \frac{\partial}{\partial \theta}(v_\theta \sin\theta) = 0 \tag{11-37}$$

The next step is to transform variables from r and θ to y and x such that x is a position variable (i.e., arc length) which increases as one moves along the solid–liquid interface and y increases as one moves normal to the interface and into the fluid phase. Furthermore, since the boundary layer thickness is measured in the y direction, it is convenient to define the interface where $y = 0$. It is important to realize that the mass transfer boundary layer is measured in the y direction, but it is a function of x. In agreement with these requirements,

$$\begin{aligned} y &= r - R \qquad & \frac{\partial y}{\partial r} &= 1 \\ x &= R\theta \qquad & \frac{\partial x}{\partial \theta} &= R \end{aligned} \tag{11-38}$$

The solution to this laminar boundary layer problem must satisfy conservation of species mass via the mass transfer equation and conservation of overall mass via the equation of continuity. The two equations have been simplified for (1) two-dimensional axisymmetric flow in spherical coordinates, (2) negligible tangential diffusion at high-mass-transfer Peclet numbers, and (3) negligible curvature for mass flux in the radial direction at high Schmidt numbers, where the mass transfer

boundary layer, which hugs the surface, is very thin:

$$v_r \frac{\partial C_A}{\partial y} + v_\theta \frac{\partial C_A}{\partial x} = \mathfrak{D}_{A,\,mix} \frac{\partial^2 C_A}{\partial y^2} \tag{11-39}$$

$$\frac{\partial v_r}{\partial y} + \frac{1}{\sin\theta} \frac{\partial}{\partial x}(v_\theta \sin\theta) = 0 \tag{11-40}$$

The mass transfer equation could have been extracted from the rectangular coordinate entry in Table B.11 of Bird *et al.* (2002, p. 851) by setting $v_x = v_\theta$ and $v_y = v_r$. Except for the factor of $\sin\theta$, the equation of continuity could have been extracted from the rectangular coordinate entry in Table B.4 of Bird *et al.* (2002, p. 846) by setting $v_x = v_\theta$ and $v_y = v_r$. Hence, the "locally flat" description of this problem is justified, and the only remaining influence of spherical coordinates is the factor of $\sin\theta$ in the equation of continuity. The boundary conditions for $C_A(y, x)$ are repeated here for completeness:

$$C_A = C_{A,\,bulk} \text{ at } x = 0 \text{ for all values of } y > 0$$

$$C_A = C_{A,\,interface} \text{ at } y = 0 \text{ for all values of } x > 0 \tag{11-41}$$

(BLBC) $$C_A \to C_{A,\,bulk} \text{ as } y \to \infty \text{ for all values of } x < \pi R \text{ (i.e., finite } x)$$

11-2 TANGENTIAL VELOCITY COMPONENT v_θ WITHIN THE MASS TRANSFER BOUNDARY LAYER

This is the most important consideration that governs the final solution and the scaling laws which illustrate the dependence of transfer coefficients (including the Sherwood number) and boundary layer thickness on the Reynolds and Schmidt numbers. There is a fundamental difference between solid–liquid and gas–liquid interfaces. All problems in forced convection heat and mass transfer without chemical reaction can be classified in one of these two categories. The nature of viscous shear at the interface propagates throughout the remainder of these analyses for solid–liquid and gas–liquid interfaces. Hence, it will be obvious that correlations for heat and mass transfer which involve convective transport depend strongly on the tangential velocity profile within the thermal or concentration boundary layer. It is not possible to analyze convective heat and mass transfer without equal consideration of the fluid dynamics problem. The discussion that follows should not be classified as coupled mass and momentum transport because the fluid dynamics solution is obtained prior to consideration of the mass transfer problem. In other words, concentration dependence of physical properties such as density, viscosity, and diffusivity is not included in the models.

11-2.1 Creeping Flow Adjacent to a Solid–Liquid Interface

At very large Schmidt numbers, the mass transfer boundary layer in the fluid phase is very thin and hugs the interface. Since tangential and radial velocity

components are required within the range $0 \leq y \leq \delta_C$, it is not necessary to use the exact fluid dynamics solution for v_θ which exhibits gradients within the range $0 \leq y \leq \delta_v$, where $\delta_v \gg \delta_C$ in the asymptotic limit as $\mathrm{Sc} \to \infty$. In other words, it is acceptable to linearize v_θ with respect to r within δ_C. The equation of continuity is used to calculate v_r such that overall mass is conserved. Three attempts to linearize the tangential velocity profile all produce the same result for creeping flow around a solid sphere. The generalized Taylor series expansion for v_θ as a polynomial in r is

$$v_\theta(r,\theta) = v_\theta(r = R,\theta) + (r - R)\left(\frac{\partial v_\theta}{\partial r}\right)_{r=R} + O(r^2) \tag{11-42}$$

If one employs the $r-\theta$ component of the rate-of-strain tensor in spherical coordinates as the coefficient of the first-order term instead of $(\partial v_\theta/\partial r)_{r=R}$, then the polynomial adopts a slightly different mathematical form:

$$v_\theta(r,\theta) = v_\theta(r = R,\theta) + (r - R)\left[\left(\frac{\partial \gamma}{\partial t}\right)_{r_\theta}\right]_{r=R} + O(r^2) \tag{11-43}$$

where

$$\left[\left(\frac{\partial \gamma}{\partial t}\right)_{r_\theta}\right]_{r=R} = \left[r\frac{\partial}{\partial r}\left(\frac{v_\theta}{r}\right) + \frac{1}{r}\frac{\partial v_r}{\partial \theta}\right]_{r=R}$$
$$= \frac{1}{R}\left[\frac{\partial}{\partial \eta}\left(\frac{v_\theta}{\eta}\right) + \frac{\partial v_r}{\partial \theta}\right]_{\eta=1}$$

There is no contribution from $(\partial v_r/\partial\theta)_{\eta=1}$ to the $r-\theta$ component of the rate-of-strain tensor at the solid–liquid interface because the solid is nondeformable. Creeping flow of an incompressible Newtonian fluid around a stationary solid sphere produces the following expressions for the tangential velocity component:

$$v_\theta(r,\theta) = v_\theta(r \to \infty,\theta)\left(1 - \frac{3}{4}\eta^{-1} - \frac{1}{4}\eta^{-3}\right)$$
$$\frac{v_\theta(r,\theta)}{\eta} = v_\theta(r \to \infty,\theta)\left(\eta^{-1} - \frac{3}{4}\eta^{-2} - \frac{1}{4}\eta^{-4}\right)$$
$$\left(\frac{\partial v_\theta}{\partial r}\right)_{r=R} = \frac{V_{\text{approach}}\sin\theta}{R}\left(\frac{3}{4}\eta^{-2} + \frac{3}{4}\eta^{-4}\right)_{\eta=1} = \frac{3V_{\text{approach}}\sin\theta}{2R}$$
$$\left[\left(\frac{\partial \gamma}{\partial t}\right)_{r_\theta}\right]_{r=R} = \frac{V_{\text{approach}}\sin\theta}{R}\left(-\eta^{-2} + \frac{3}{2}\eta^{-3} + \eta^{-5}\right)_{\eta=1} = \frac{3V_{\text{approach}}\sin\theta}{2R} \tag{11-44}$$

Hence, both methods of calculating the tangential velocity gradient at the solid–liquid interface produce the same result. The leading term in the polynomial

expansion for v_θ vanishes for a no-slip interface with significant viscous shear. The linearized tangential velocity profile is

$$v_\theta(r,\theta) \approx (r-R)\frac{3V_{\text{approach}}\sin\theta}{2R} = \frac{3}{2}(\eta-1)V_{\text{approach}}\sin\theta \tag{11-45}$$

The third approach to linearization focuses on the range of the radial variable:

$$1 \le \eta = \frac{r}{R} = 1+\varepsilon \le 1+\frac{\delta_C}{R} \tag{11-46}$$

which suggests that $\varepsilon = \eta - 1 \ll 1$. Now, linearization of

$$\eta^{-\alpha} = (1+\varepsilon)^{-\alpha} = 1-\alpha\varepsilon + O(\varepsilon^2) \tag{11-47}$$

is employed for the last two terms in the exact expression for v_θ:

$$v_\theta(r,\theta) \approx v_\theta(r\to\infty,\theta)\left[1-\tfrac{3}{4}(1-\varepsilon)-\tfrac{1}{4}(1-3\varepsilon)\right] = \tfrac{3}{2}V_{\text{approach}}\varepsilon\sin\theta \tag{11-48}$$

The generalized form for the linear tangential velocity profile within the mass transfer boundary layer for a no-slip interface is

$$v_\theta(r,\theta) = (r-R)g(\theta) = yg(\theta) \tag{11-49}$$

where $g(\theta)$ is the tangential velocity gradient at the solid–liquid interface. The discussion above indicates that

$$g(\theta) = \left[\left(\frac{\partial\gamma}{\partial t}\right)_{r_\theta}\right]_{r=R} = \left[r\frac{\partial}{\partial r}\left(\frac{v_\theta}{r}\right)\right]_{r=R} = \left(\frac{\partial v_\theta}{\partial r}\right)_{r=R} = \frac{3V_{\text{approach}}\sin\theta}{2R} \tag{11-50}$$

in the creeping flow regime.

11-2.2 Radial Velocity Component Adjacent to a Solid–Liquid Interface

The locally flat description of the equation of continuity,

$$\frac{\partial v_r}{\partial y} + \frac{1}{\sin\theta}\frac{\partial}{\partial x}(v_\theta\sin\theta) = 0 \tag{11-51}$$

is used to calculate $v_r(r,\theta)$, which is consistent with the linearized form of the tangential velocity component. It is not acceptable to attempt a linearization of v_r without considering the proposed functional form of v_θ. Hence,

$$\frac{\partial v_r}{\partial y} = -\frac{1}{\sin\theta}\frac{\partial}{\partial x}[yg(\theta)\sin\theta] = -\frac{y}{\sin\theta}\frac{d}{dx}[g(\theta)\sin\theta] \tag{11-52}$$

Integration of (11-52) from the solid–liquid interface where $v_r = 0$ at $y = 0$ to any position y within the mass transfer boundary layer produces the following result:

$$v_r(r,\theta) = -\frac{1}{\sin\theta}\frac{d}{dx}[g(\theta)\sin\theta]\int_0^y y\,dy = -\frac{y^2}{2\sin\theta}\frac{d}{dx}[g(\theta)\sin\theta]$$

$$v_r(r,\theta) = y^2\xi(\theta) \tag{11-53}$$

$$\xi(\theta) = -\frac{1}{2\sin\theta}\frac{d}{dx}[g(\theta)\sin\theta]$$

The equation of continuity has served its purpose for this two-dimensional flow problem. In fact, momentum boundary layer theory employs the same methodology by postulating the functional form for the velocity component parallel to the interface, and calculating the velocity component in the normal coordinate direction via the equation of continuity. Now v_r and v_θ are incorporated into the mass transfer equation.

11-3 BOUNDARY LAYER SOLUTION OF THE MASS TRANSFER EQUATION

The concentration of mobile component A is expressed in terms of the dimensionless profile:

$$P(r,\theta) = \frac{C_{\text{A, interface}} - C_{\text{A}}(r,\theta)}{C_{\text{A, interface}} - C_{\text{A, bulk}}} \tag{11-54}$$

$P(r,\theta)$ must satisfy

$$y^2\xi(\theta)\frac{\partial P}{\partial y} + yg(\theta)\frac{\partial P}{\partial x} = \mathfrak{D}_{\text{A, mix}}\frac{\partial^2 P}{\partial y^2} \tag{11-55}$$

subject to the following boundary conditions:

$$P = 1 \text{ at } \theta = 0\ (x = 0) \text{ for all values of } r > R\ (y > 0)$$

$$P = 0 \text{ at } r = R\ (y = 0) \text{ for all values of } \theta > 0\ (x > 0) \tag{11-56}$$

(BLBC) $$P \to 1 \text{ as } r \to \infty\ (y \to \infty) \text{ for all values of } \theta < \pi \text{ (finite } x)$$

The boundary layer boundary condition (BLBC) suggests that a combination-of-variables approach should be successful if a new independent variable is defined as

$$\zeta = \frac{r - R}{\delta_C(\theta)} = \frac{y}{\delta_C(\theta)} \tag{11-57}$$

This is a canonical form where the numerator of the combined variable is a linear function of the normal coordinate y. The numerator of ζ must vanish

at the solid–liquid interface. The denominator of ζ is some function (i.e., to be determined) of the position variable measured parallel to the interface. It is acceptable to identify the function in the denominator of ζ as the boundary layer thickness. To be successful, the combination of variables approach must transform the partial differential equation for $P(r, \theta)$ into two uncoupled ordinary differential equations for the dimensionless profile $P(\zeta)$ and the mass transfer boundary layer thickness $\delta_C(\theta)$, and condense three boundary conditions for $P(r, \theta)$ into two conditions on $P(\zeta)$ without neglecting any of the original three conditions. The hierarchy is as follows:

C_A is expressed in terms of P.
P is written in terms of ζ.
ζ is the combined variable which depends on $y = r - R$ and δ_C.
δ_C depends on polar angle θ or arc length $x = R\theta$.

The following partial derivatives of the dimensionless profile must be calculated:

$$\begin{aligned}
\left(\frac{\partial P}{\partial y}\right)_x &= \frac{dP}{d\zeta}\left(\frac{\partial \zeta}{\partial y}\right)_x = \frac{1}{\delta_C}\frac{dP}{d\zeta} \\
\left(\frac{\partial^2 P}{\partial y^2}\right)_x &= \left\{\frac{d[(\partial P/\partial y)_x]}{d\zeta}\right\}\left(\frac{\partial \zeta}{\partial y}\right)_x \\
&= \frac{d[(1/\delta_C)_x dP/d\zeta]}{d\zeta}\left(\frac{\partial \zeta}{\partial y}\right)_x = \left(\frac{1}{\delta_C}\right)^2 \frac{d^2P}{d\zeta^2} \qquad (11\text{-}58) \\
\left(\frac{\partial P}{\partial x}\right)_y &= \left(\frac{dP}{d\zeta}\right)\left(\frac{\partial \zeta}{\partial \delta_C}\right)_y \frac{d\delta_C}{dx} = -\frac{y}{(\delta_C)^2}\frac{d\delta_C}{dx}\frac{dP}{d\zeta} \\
&= -\frac{\zeta}{\delta_C}\frac{d\delta_C}{dx}\frac{dP}{d\zeta}
\end{aligned}$$

Now, the objective is to write the mass transfer equation as a second-order ODE for $P(\zeta)$:

$$y^2\xi(\theta)\frac{1}{\delta_C}\frac{dP}{d\zeta} - yg(\theta)\frac{\zeta}{\delta_C}\frac{d\delta_C}{dx}\frac{dP}{d\zeta} = \mathfrak{D}_{A,\,mix}\left(\frac{1}{\delta_C}\right)^2\frac{d^2P}{d\zeta^2} \qquad (11\text{-}59)$$

Multiplication by $(\delta_C)^2$ and letting $y = \zeta\delta_C$ produces the following result:

$$-\left[g(\theta)(\delta_C)^2\frac{d\delta_C}{dx} - (\delta_C)^3\xi(\theta)\right]\zeta^2\frac{dP}{d\zeta} = \mathfrak{D}_{A,\,mix}\frac{d^2P}{d\zeta^2} \qquad (11\text{-}60)$$

The quantity in brackets on the left side of (11-60) has units of a diffusivity (i.e., length^2/time). Hence, it should be proportional to $\mathfrak{D}_{A,\,mix}$. The first objective will

be achieved if

$$g(\theta)(\delta_C)^2\left(\frac{d\delta_C}{dx}\right) - (\delta_C)^3\xi(\theta) = (\text{constant})\,\mathfrak{D}_{A,\,\text{mix}} \tag{11-61}$$

$$\frac{d^2P}{d\zeta^2} = -(\text{constant})\,\zeta^2\frac{dP}{d\zeta} \tag{11-62}$$

The second objective is achieved because the definition of the combined variable ζ fortuitously condenses three boundary conditions for $P(r, \theta)$ to two conditions for $P(\zeta)$. For example,

$$P = 0 \text{ at } r = R \ (y = 0) \text{ for all values of } \theta > 0 \ (x > 0)$$

is equivalent to $P = 0$ at $\zeta = 0$, and

$$P = 1 \text{ at } \theta = 0 (x = 0) \text{ for all values of } r > R \ (y > 0)$$

$$\text{(BLBC)} \quad P \to 1 \text{ as } r \to \infty \ (y \to \infty) \text{ for all values of } \theta < \pi \text{ (finite } x) \tag{11-63}$$

are equivalent to $P = 1$ at $\zeta \to \infty$ because the mass transfer boundary layer thickness $\delta_C(\theta)$ vanishes at the stagnation point where $\theta = 0$, and δ_C is infinitely large at the separation point where $\theta = \pi$.

11-3.1 Gamma Function Profile

The dimensionless profile P is a function of the combined variable ζ as outlined above. Solution of the second-order ODE,

$$\frac{d^2P}{d\zeta^2} = -(\text{constant})\,\zeta^2\frac{dP}{d\zeta} \tag{11-64}$$

conforms to a standard mathematical function if the constant = 3. Whereas this choice seems to bias the final expression for $P(\zeta)$, one must remember that numerical values of ζ depend on the thickness of the mass transfer boundary layer, which is also affected by the choice of the constant. Hence, the scaling law for δ_C in terms of Re and Sc is valid, but the absolute magnitude of the boundary layer thickness should be interpreted with some skepticism. When final solutions for the dimensionless profile and the boundary layer thickness are viewed as a pair, one's confidence should be restored in the predictions for interfacial molar flux, local transfer coefficients, and the surface-averaged Sherwood number. Hence,

$$\frac{d^2P}{d\zeta^2} = \frac{d}{d\zeta}\left(\frac{dP}{d\zeta}\right) = -3\zeta^2\frac{dP}{d\zeta} \tag{11-65}$$

which leads to

$$\frac{dP}{d\zeta} = C_1 \exp(-\zeta^3) \tag{11-66}$$

$$P(\zeta) = C_1 \int_0^{\zeta} \exp(-x^3)\, dx + P(\zeta = 0) \tag{11-67}$$

where integration is performed over the range $0 \leq x \leq \zeta$, and the integration constant $P(\zeta = 0)$ in (11-67) vanishes as a consequence of the first boundary condition. Integration constant C_1 is calculated via the second boundary condition, $P(\zeta \to \infty) = 1$:

$$C_1 = \frac{1}{\displaystyle\int_0^{\infty} \exp(-x^3)\, dx} = \frac{1}{\Gamma(\frac{4}{3})} \tag{11-68}$$

where $\Gamma(\frac{4}{3})$ is the gamma function for an argument of $\frac{4}{3}$. The final expression for the dimensionless concentration profile of mobile component A is

$$P(\zeta) = \frac{C_{\text{A, interface}} - C_{\text{A}}(r, \theta)}{C_{\text{A, interface}} - C_{\text{A, bulk}}} = \frac{1}{\Gamma(\frac{4}{3})} \int_0^{\zeta} \exp(-x^3)\, dx \tag{11-69}$$

where integration is performed over the range $0 \leq x \leq \zeta$.

Mathematical Definition and Applicable Form of the Gamma Function. Definition of the gamma function for argument $n > 0$ is

$$\Gamma(n) \equiv (n-1)\Gamma(n-1) \equiv (n-1)! \equiv \int_0^{\infty} z^{n-1} \exp(-z)\, dz \tag{11-70}$$

A change of variables from z to x, where

$$z = x^{1/n} \quad \text{or} \quad \log z = \frac{1}{n} \log x \tag{11-71}$$

$$\frac{dz}{dx} = \frac{1}{n}\frac{z}{x} = \frac{1}{n} x^{(1-n)/n} \tag{11-72}$$

allows one to re-express the defining integral for $\Gamma(n)$ in a form that is applicable for the dimensionless concentration profile:

$$\Gamma(n) = \int_0^{\infty} x^{(n-1)/n} \exp(-x^{1/n}) \frac{1}{n} x^{(1-n)/n}\, dx = \frac{1}{n} \int_0^{\infty} \exp(-x^{1/n})\, dx \tag{11-73}$$

When $n = \frac{1}{3}$ in (11-73), the constant C_1 in the dimensionless profile $P(\zeta)$ is calculated as follows:

$$(C_1)^{-1} = \int_0^\infty \exp(-x^3)\,dx = \frac{1}{3}\Gamma\left(\frac{1}{3}\right) = \Gamma\left(\frac{4}{3}\right) = \left(\frac{1}{3}\right)! = 0.89 \quad (11\text{-}74)$$

because $\Gamma(\frac{1}{3}) = 2.68$ (Abramowitz and Stegun, 1965, pp. 255–260). The incomplete gamma function for argument $n > 0$ and variable λ is defined as

$$\mathbb{S}(n, \lambda) \equiv \frac{1}{\Gamma(n)} \int_0^\lambda z^{n-1} \exp(-z)\,dz \qquad 0 \le z \le \lambda \quad (11\text{-}75)$$

where the upper limit of integration is λ. If $\exp(-z)$ is expanded in a Taylor series about $z = 0$, then one obtains

$$\exp(-z) = \sum\nolimits_{k=0}^{\infty} \frac{(-1)^k}{k!} z^k \quad (11\text{-}76)$$

Now the defining expression for the incomplete gamma function can be integrated to yield the following polynomial expansion:

$$\begin{aligned} \mathbb{S}(n, \lambda) &\equiv \frac{1}{\Gamma(n)} \int_0^\lambda \left[\sum\nolimits_{k=0}^{\infty} \frac{(-1)^k}{k!} z^{k+n-1} \right] dz \\ &= \frac{\lambda^n}{\Gamma(n)} \sum\nolimits_{k=0}^{\infty} \frac{(-\lambda)^k}{(k+n)k!} \end{aligned} \quad (11\text{-}77)$$

Hence, numerical values for the incomplete gamma function are obtained rather easily by evaluating a sufficient number of terms in this alternating series until contributions from additional terms are negligible. For the boundary layer mass transfer problems of interest in this chapter, one manipulates the defining expression for the incomplete gamma function such that it can be employed to calculate molar density profiles. For example, integration variable z in (11-75) is changed to x via $z = x^{1/n}$ as illustrated in (11-71), (11-72), and (11-73), and the upper limit on transformed integration variable x is λ^n. One obtains

$$\mathbb{S}(n, \lambda) = \frac{\int \exp(-x^{1/n})\,dx}{n\Gamma(n)} \qquad 0 \le x \le \lambda^n \quad (11\text{-}78)$$

The dimensionless profile for mobile component A within the mass transfer boundary layer can be expressed in terms of the incomplete gamma function

when the argument $n = \frac{1}{3}$, but one must exercise caution in choosing the correct variable that appears as the upper limit of integration. When $n = \frac{1}{3}$,

$$\mathbb{S}(\tfrac{1}{3}, \lambda) = \frac{\int \exp(-x^3)\, dx}{\frac{1}{3}\Gamma(\frac{1}{3})} \qquad 0 \le x \le \lambda^{1/3} \tag{11-79}$$

Hence, the dimensionless concentration profile $P(\zeta)$ is given by the incomplete gamma function when the argument $n = \frac{1}{3}$ and the variable $\lambda = \zeta^3$:

$$\begin{aligned} P(\zeta) = \mathbb{S}(\tfrac{1}{3}, \zeta^3) &= \frac{\int_0^{\zeta} \exp(-x^3)\, dx}{\Gamma(\frac{4}{3})} \\ &= \frac{\zeta}{\Gamma(\frac{1}{3})} \sum_{k=0}^{\infty} \frac{(-\zeta)^{3k}}{\left(k + \frac{1}{3}\right) k!} \end{aligned} \tag{11-80}$$

This corresponds to half of the basic information that is required to predict rates of interphase mass transfer, transfer coefficients, and Sherwood numbers.

11-3.2 Thickness of the Mass Transfer Boundary Layer

It is possible to estimate the thickness of the boundary layer via solution of the following equation:

$$g(\theta)(\delta_C)^2 \frac{d\delta_C}{dx} - (\delta_C)^3 \xi(\theta) = 3\mathcal{D}_{\mathrm{A,\,mix}} \tag{11-81}$$

where $g(\theta)$ represents the $r\theta$ component of the rate-of-strain tensor evaluated at the spherical solid–liquid interface for laminar or creeping flow, and

$$\xi(\theta) = -\frac{1}{2\sin\theta} \frac{d}{dx}[g(\theta)\sin\theta] \tag{11-82}$$

Upon substitution and multiplication by $\sin\theta$, one obtains the following ODE for $\delta_C(\theta)$:

$$g(\theta)\sin\theta(\delta_C)^2 \frac{d\delta_C}{dx} + \frac{1}{2}(\delta_C)^3 \frac{d[g(\theta)\sin\theta]}{dx} = 3\mathcal{D}_{\mathrm{A,\,mix}} \sin\theta \tag{11-83}$$

The left side of (11-83) can be rewritten as

$$\frac{1}{3} g(\theta)\sin\theta \frac{d(\delta_C)^3}{dx} + \frac{1}{2}(\delta_C)^3 \frac{d[g(\theta)\sin\theta]}{dx} \tag{11-84}$$

If the leading factor of the second term were $\frac{1}{3}$ instead of $\frac{1}{2}$, then both terms could be combined as follows:

$$\frac{1}{3}g(\theta)\sin\theta\frac{d(\delta_C)^3}{dx}+\frac{1}{3}(\delta_C)^3\frac{d[g(\theta)\sin\theta]}{dx}$$
$$=\frac{1}{3}\frac{d}{dx}[(\delta_C)^3 g(\theta)\sin\theta]=3\mathfrak{D}_{\mathrm{A,\,mix}}\sin\theta \tag{11-85}$$

Since $dx = Rd\theta$, integration of (11-85), subject to the condition that $\delta_C = 0$ at $\theta = 0$, yields the desired result for the simplified mass transfer boundary layer thickness:

$$[\delta_C(\theta)]_{\mathrm{simplified}}=\left[\frac{9R\mathfrak{D}_{\mathrm{A,\,mix}}(1-\cos\theta)}{g(\theta)\sin\theta}\right]^{1/3} \tag{11-86}$$

which is compared with more accurate calculations of $\delta_C(\theta)$, as described below. If the trivial difference between the factors of $\frac{1}{2}$ and $\frac{1}{3}$ is important in (11-84), then the problem is treated as follows:

$$\frac{1}{3}g(\theta)\sin\theta\frac{d(\delta_C)^3}{dx}+\frac{1}{2}(\delta_C)^3\frac{d[g(\theta)\sin\theta]}{dx}$$
$$=A[g(\theta)\sin\theta]^a\frac{d\{(\delta_C)^3[g(\theta)\sin\theta]^{1-a}\}}{dx}=3\mathfrak{D}_{\mathrm{A,\,mix}}\sin\theta \tag{11-87}$$

with $A = \frac{1}{3}$ and $a = -\frac{1}{2}$ via the product rule of differentiation. This integrating-factor approach allows one to calculate the boundary layer thickness via simple integration:

$$\frac{d\{(\delta_C)^3[g(\theta)\sin\theta]^{3/2}\}}{d\theta}=9R\mathfrak{D}_{\mathrm{A,\,mix}}[g(\theta)\sin^3\theta]^{1/2} \tag{11-88}$$

subject to the condition that $\delta_C = 0$ at the stagnation point where the approaching fluid initially contacts the solid sphere at $\theta = 0$. Hence,

$$(\delta_C)^3[g(\theta)\sin\theta]^{3/2}=9R\mathfrak{D}_{\mathrm{A,\,mix}}\int[g(\sigma)\sin^3\sigma]^{1/2}\,d\sigma \qquad 0\le\sigma\le\theta \tag{11-89}$$

$$\delta_C(\theta)=\frac{\left[9R\mathfrak{D}_{\mathrm{A,\,mix}}\int[g(\sigma)\sin^3\sigma]^{1/2}\,d\sigma\right]^{1/3}}{[g(\theta)\sin\theta]^{1/2}} \qquad 0\le\sigma\le\theta \tag{11-90}$$

which suggests a scaling law of the form $\delta_C \approx \{\mathfrak{D}_{\mathrm{A,\,mix}}\}^m$. The exponent $m = \frac{1}{3}$ for boundary layer theory adjacent to a solid–liquid interface should be compared with the value of $\frac{1}{2}$ for the penetration theory. Also, $m = \frac{1}{2}$ for boundary layer heat or mass transfer adjacent to a zero-shear gas–liquid interface at high Prandtl or Schmidt numbers. If the interfacial velocity gradient is expressed in terms of

dimensionless variables, then the scaling law can be written in dimensionless form. Hence, if $\eta = r/R$ and $v_\theta^* = v_\theta / V_{\text{approach}}$, then:

$$g(\theta) = \left[\left(\frac{\partial \gamma}{\partial t}\right)_{r_\theta}\right]_{r=R} = \left[r\frac{\partial}{\partial r}\left(\frac{v_\theta}{r}\right) + \frac{1}{r}\frac{\partial v_r}{\partial \theta}\right]_{r=R}$$
$$= \frac{V_{\text{approach}}}{R}\left[\eta\frac{\partial}{\partial \eta}\left(\frac{v_\theta^*}{\eta}\right)\right]_{\eta=1} \tag{11-91}$$

because the second term vanishes in the expression for the $r\theta$ component of the rate-of-strain tensor due to the nondeformable nature of the solid–liquid interface. Hence, one defines a dimensionless tangential velocity gradient $g^*(\theta)$ at the solid–liquid interface as

$$g^*(\theta) = \frac{g(\theta)}{V_{\text{approach}}/R} = \left[\frac{\partial}{\partial \eta}\left(\frac{v_\theta^*}{\eta}\right)\right]_{\eta=1} \tag{11-92}$$

Creeping flow of an incompressible Newtonian fluid around a solid sphere corresponds to $g^*(\theta) = \frac{3}{2}\sin\theta$. For any flow regime that does not include turbulent transport mechanisms, the dimensionless boundary layer thickness is

$$\frac{\delta_C(\theta)}{R} = \frac{\left[\dfrac{9\mathfrak{D}_{\text{A, mix}}}{RV_{\text{approach}}}\displaystyle\int [g^*(\sigma)\sin^3\sigma]^{1/2}\,d\sigma\right]^{1/3}}{[g^*(\theta)\sin\theta]^{1/2}} \qquad 0 \le \sigma \le \theta \tag{11-93}$$

If the Reynolds number is based on the sphere diameter, as defined earlier, then the group of terms prior to the integral in (11-93) is proportional to the inverse of the mass transfer Peclet number. The general expression for the mass transfer boundary layer thickness is

$$\frac{\delta_C(\theta)}{R} = \left(\frac{1}{\text{Re}\cdot\text{Sc}}\right)^{1/3}\frac{\left[18\displaystyle\int [g^*(\sigma)\sin^3\sigma]^{1/2}\,d\sigma\right]^{1/3}}{[g^*(\theta)\sin\theta]^{1/2}} \qquad 0 \le \sigma \le \theta \tag{11-94}$$

In dimensionless notation, the generalized expression for the simplified mass transfer boundary layer thickness is

$$\left[\frac{\delta_C(\theta)}{R}\right]_{\text{simplified}} = \left(\frac{1}{\text{Re}\cdot\text{Sc}}\right)^{1/3}\left[\frac{18(1-\cos\theta)}{g^*(\theta)\sin\theta}\right]^{1/3} \tag{11-95}$$

Hence, an equivalent form of the previous scaling law, $\delta_C \approx \{\mathfrak{D}_{\text{A, mix}}\}^m$, is $\delta_C \approx 1/(\text{Re}\cdot\text{Sc})^m$ where $m = \frac{1}{3}$ for boundary layer theory adjacent to a solid–liquid interface in the creeping flow regime, and $m = \frac{1}{2}$ for gas–liquid interfaces. As expected, the boundary layer thickness at any position along the interface decreases at higher flow rates and increases when the diffusivity is larger. Since

$\mathfrak{D}_{A,\,mix}$ in the expressions for δ_C and Sc represents a diffusivity instead of a molecular transport property, one must replace $\mathfrak{D}_{A,\,mix}$ by the thermal diffusivity α ($= k_{TC}/\rho C_p$, where $\rho =$ density, $C_p =$ specific heat, and $k_{TC} =$ thermal conductivity) to calculate the analogous heat transfer boundary layer thickness δ_T and the Prandtl number [i.e., $\text{Pr} = (\mu/\rho)/\alpha$]. In the creeping flow regime, where $g^*(\theta) = \frac{3}{2}\sin\theta$,

$$\frac{\delta_C(\theta)}{2R} = \left(\frac{3}{4}\right)^{1/3}\left(\frac{1}{\text{Re}\cdot\text{Sc}}\right)^{1/3}\frac{\left(\theta - \frac{1}{2}\sin 2\theta\right)^{1/3}}{\sin\theta} \tag{11-96}$$

and θ must be expressed in radians. For comparison, when the simplified mass transfer boundary layer thickness in the creeping flow regime is referenced to the sphere diameter, one obtains

$$\left[\frac{\delta_C(\theta)}{2R}\right]_{\text{simplified}} = \left(\frac{3}{2}\right)^{1/3}\left(\frac{1}{\text{Re}\cdot\text{Sc}}\right)^{1/3}(1+\cos\theta)^{-1/3} \tag{11-97}$$

Figure 11-1 illustrates the angular dependence of $\delta_C(\theta)$ (i.e., not $[\delta_C(\theta)]_{\text{simplified}}$), based on the detailed results provided above for creeping flow.

Practical Example. The physical properties of a 20 wt% aqueous sucrose solution at 20°C are (Weast, 1974–1975, p. D-231; Perry and Chilton, 1973, pp. 3–215, 3–225):

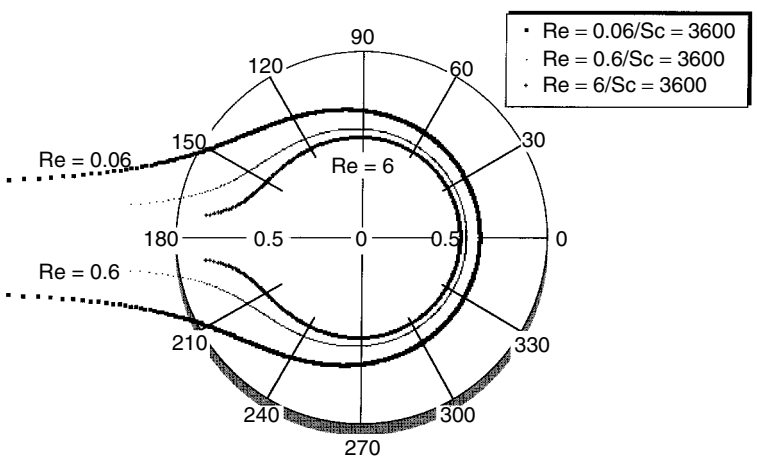

Figure 11-1 Thickness of the mass transfer boundary layer around a solid sphere, primarily in the creeping flow regime. This graph in polar coordinates illustrates $\delta_C(\theta)$ divided by the sphere diameter vs. polar angle θ, and the fluid approaches the solid sphere horizontally from the right. No data are plotted at the stagnation point, where $\theta = 0$.

Density: $\rho = 1.0829$ g/cm^3

Viscosity: $\mu = 1.967 \times 10^{-2}$ g/cm·s

Diffusivity: $\mathfrak{D}_{AB} = 0.50 \times 10^{-5}$ cm^2/s

Hence, the Schmidt number is 3600. If spherical pellets of solid sucrose with a diameter of 1 mm fall through this 20 wt% aqueous solution at a settling velocity of 6.5 cm/min, then the Reynolds number is 0.60, which corresponds to the upper limit of creeping flow. The mass transfer Peclet number is about 2000. The assumptions embedded in the boundary layer model are justified, as sucrose dissolves in solution. At the equatorial position of the pellet where $\theta = \pi/2$ radians,

$$\frac{\delta_C(\theta = \pi/2)}{2R} = \left(\frac{3\pi}{8\,\mathrm{Re}\cdot\mathrm{Sc}}\right)^{1/3} = 8.2 \times 10^{-2}$$

For comparison, the simplified mass transfer boundary layer thickness at the equatorial position is

$$\left[\frac{\delta_C(\theta = \pi/2)}{2R}\right]_{\text{simplified}} = \left(\frac{3}{2\,\mathrm{Re}\cdot\mathrm{Sc}}\right)^{1/3} = 8.9 \times 10^{-2}$$

The former calculation for $\delta_C(\theta = \pi/2)$ yields the maximum value of the dimensionless radial variable (i.e., normal coordinate) at the outer edge of the mass transfer boundary layer:

$$\eta_{\text{maximum}} = \left(\frac{r}{R}\right)_{\text{maximum}} = 1 + \frac{\delta_C(\theta = \pi/2)}{R} \approx 1.16$$

where

$$\frac{\partial \ln v_r}{\partial \ln r} = 12.2 \quad \text{at } \eta_{\text{maximum}}$$

$$\frac{1}{r^2}\frac{\partial (r^2 v_r)}{\partial r} = 1.16\frac{\partial v_r}{\partial r} \quad \text{at } \eta_{\text{maximum}}$$

Hence, neglecting the curvature correction factors of r^2 in the radial term of the equation of continuity corresponds to a 14% underestimate of $(1/r^2)[\partial(r^2 v_r)/\partial r]$ at the outer edge of the mass transfer boundary layer on the equator of the pellet.

11-3.3 Neglecting the Curvature Correction for Radial Diffusion in the Mass Transfer Equation

Results from the practical example in Section 11-3.2 are used to estimate the maximum error incurred by neglecting the effects of curvature in the spherical coordinate microscopic mass balance. For example, it is now possible to

calculate explicitly the importance of the second term on the right side of the following equation:

$$\frac{1}{r^2}\frac{\partial}{\partial r}\left(r^2\frac{\partial C_A}{\partial r}\right) = \frac{\partial^2 C_A}{\partial r^2}\left(1 + \frac{2}{\partial \ln \beta / \partial \ln r}\right) \tag{11-98}$$

where $\beta = \partial C_A/\partial r$. When mass transfer boundary layers are thin at high Schmidt numbers, only the first term on the right side of (11-98) is used to simulate radial diffusion. The error embedded in this approximation is defined as the difference between the exact expression, which includes curvature corrections, and the approximation, which neglects curvature, relative to the exact expression. Hence,

$$\% \text{ error} = 100 \times \left[\frac{\dfrac{1}{r^2}\dfrac{\partial}{\partial r}\left(r^2\dfrac{\partial C_A}{\partial r}\right) - \dfrac{\partial^2 C_A}{\partial r^2}}{\dfrac{1}{r^2}\dfrac{\partial}{\partial r}\left(r^2\dfrac{\partial C_A}{\partial r}\right)}\right]$$

$$= \frac{200}{2 + [\partial \ln \beta / \partial \ln r]} \tag{11-99}$$

The maximum error in equation (11-99) occurs at the outer edge of the mass transfer boundary layer, where $r = R + \delta_C(\theta)$ and $\zeta = (r - R)/\delta_C(\theta) = 1$. The quantity of importance is

$$\left(\frac{\partial \ln \beta}{\partial \ln r}\right)_{\theta,\,\zeta=1} = \frac{[R + \delta_C(\theta)](\partial^2 C_A/\partial r^2)_{\theta,\,\zeta=1}}{(\partial C_A/\partial r)_{\theta,\,\zeta=1}} \tag{11-100}$$

Based on the incomplete gamma function profile for $P(\zeta)$ and the definition of the combined variable ζ, the two partial derivatives of interest on the right side of equation (11-100) are evaluated as follows via the chain rule:

(1) $$\left(\frac{\partial C_A}{\partial r}\right)_\theta = \frac{dC_A}{dP}\left(\frac{dP}{d\zeta}\right)\left(\frac{\partial \zeta}{\partial r}\right)_\theta$$

$$\frac{dC_A}{dP} = -(C_{A,\,\text{interface}} - C_{A,\,\text{bulk}})$$

$$\frac{dP}{d\zeta} = \frac{1}{\Gamma(\frac{4}{3})}\exp(-\zeta^3) \tag{11-101}$$

$$\left(\frac{\partial \zeta}{\partial r}\right)_\theta = \frac{1}{\delta_C(\theta)}$$

$$\left(\frac{\partial C_A}{\partial r}\right)_\theta = -(C_{A,\,\text{interface}} - C_{A,\,\text{bulk}})\frac{1}{\Gamma(\frac{4}{3})}\exp(-\zeta^3)\frac{1}{\delta_C(\theta)}$$

(2) $$\left(\frac{\partial^2 C_A}{\partial r^2}\right)_\theta = \frac{d[(\partial C_A/\partial r)_\theta]}{d\zeta}\left(\frac{\partial \zeta}{\partial r}\right)_\theta$$

$$= (C_{A,\,\text{interface}} - C_{A,\,\text{bulk}})\left[\frac{1}{\delta_C(\theta)}\right]^2\frac{1}{\Gamma(\frac{4}{3})}3\zeta^2\exp(-\zeta^3) \tag{11-102}$$

These expressions are evaluated at the outer edge of the mass transfer boundary layer, where $\zeta = 1$:

$$(1) \qquad \left(\frac{\partial C_A}{\partial r}\right)_{\theta,\,\zeta=1} = -(C_{A,\,\text{interface}} - C_{A,\,\text{bulk}})\frac{e^{-1}}{\Gamma(\frac{4}{3})}\frac{1}{\delta_C(\theta)} \tag{11-103a}$$

$$(2) \qquad \left(\frac{\partial^2 C_A}{\partial r^2}\right)_{\theta,\,\zeta=1} = (C_{A,\,\text{interface}} - C_{A,\,\text{bulk}})\left[\frac{3e^{-1}}{\Gamma(\frac{4}{3})}\right]\left[\frac{1}{\delta_C(\theta)}\right]^2 \tag{11-103b}$$

The curvature correction for radial diffusion is calculated as follows:

$$\left(\frac{\partial \ln \beta}{\partial \ln r}\right)_{\theta,\,\zeta=1} = \frac{[R + \delta_C(\theta)](\partial^2 C_A/\partial r^2)_{\theta,\,\zeta=1}}{(\partial C_A/\partial r)_{\theta,\,\zeta=1}} = -3[1 + R/\delta_C(\theta)] \tag{11-104}$$

and the maximum error associated with neglecting this correction factor is

$$\%\ \text{error} = \frac{200}{2 + (\partial \ln \beta/\partial \ln r)_{\theta,\,\zeta=1}} = -\frac{200(\eta_{\text{maximum}} - 1)}{\eta_{\text{maximum}} + 2} \tag{11-105}$$

where

$$\eta_{\text{maximum}} = \left(\frac{r}{R}\right)_{\text{maximum}} = 1 + \frac{\delta_C(\theta)}{R}$$

At the equatorial position of the solid sucrose pellet, $\eta_{\text{maximum}} = 1.16$ when $\text{Sc} = 3600$ and $\text{Re} = 0.60$. This corresponds to a maximum error of $\approx$10% at η_{maximum} by invoking the following approximation for radial diffusion in the mass transfer equation:

$$\frac{1}{r^2}\frac{\partial}{\partial r}\left(r^2\frac{\partial C_A}{\partial r}\right) \approx \frac{\partial^2 C_A}{\partial r^2} \tag{11-106}$$

which should be compared with a maximum error of $\approx$14% at η_{maximum} by making a similar approximation in the equation of continuity:

$$\frac{1}{r^2}\frac{\partial(r^2 v_r)}{\partial r} \approx \frac{\partial v_r}{\partial r} \tag{11-107}$$

11-4 INTERPHASE MASS TRANSFER AT THE SOLID–LIQUID INTERFACE

The total molar flux of mobile component A with respect to a stationary reference frame $\mathbf{N}_A$ is evaluated at the solid–liquid interface when $\theta > 0$. It is necessary to consider the component of this flux in the normal coordinate (i.e., radial)

direction to develop an expression for the local mass transfer coefficient $k_{C,\,\text{local}}$. $\mathbf{N}_\text{A}$ contains contributions from convection and diffusion. Hence,

$$N_{\text{A}r} = C_\text{A} v_r^* - \mathfrak{D}_{\text{A, mix}} \frac{\partial C_\text{A}}{\partial r} \qquad \text{at } r = R, \theta > 0 \tag{11-108}$$

where v_r^* is the radial component of the molar average velocity $\mathbf{v}^*$, which vanishes at the stationary surface of the spherical solid. In other words, there is no convective contribution to interphase mass transfer at a nonporous solid–liquid interface, even if the interface is mobile. Hence, one calculates $N_{\text{A}r}$ via Fick's law at $r = R$, $y = 0$, $\theta > 0$, $\zeta = 0$ and defines the local mass transfer coefficient as follows:

$$\begin{aligned} N_{\text{A}r}(r = R) = -\mathfrak{D}_{\text{A, mix}} \left(\frac{\partial C_\text{A}}{\partial r}\right)_{r=R} &= -\mathfrak{D}_{\text{A, mix}} \frac{dC_\text{A}}{dP} \left(\frac{dP}{d\zeta}\right)_{\zeta=0} \left(\frac{\partial \zeta}{\partial y}\right)_{\theta>0} \frac{dy}{dr} \\ &\equiv k_{C,\,\text{local}} (C_{\text{A, interface}} - C_{\text{A, bulk}}) \end{aligned} \tag{11-109}$$

Now

$$\begin{aligned} \frac{dC_\text{A}}{dP} &= -(C_{\text{A, interface}} - C_{\text{A, bulk}}) \\ \left(\frac{dP}{d\zeta}\right)_{\zeta=0} &= \frac{1}{\Gamma(\frac{4}{3})} \\ \left(\frac{\partial \zeta}{\partial y}\right)_{y=0,\,\theta>0} &= \frac{1}{\delta_C(\theta)} \\ \frac{dy}{dr} &= 1 \end{aligned} \tag{11-110}$$

The classic result for the local mass transfer coefficient, which depends on polar angle θ along the interface, is

$$k_{C,\,\text{local}}(\theta) = \frac{1}{\Gamma(\frac{4}{3})} \frac{\mathfrak{D}_{\text{A, mix}}}{\delta_C(\theta)} \tag{11-111}$$

where $1/\Gamma(\frac{4}{3})$ is a constant that represents the gradient of the dimensionless concentration profile with respect to the combined variable ζ, evaluated at the solid–liquid interface, $\mathfrak{D}_{\text{A, mix}}$ is a molecular transport property for mass transfer that was introduced via Fick's law to calculate the interfacial molar flux, and $\delta_C(\theta)$ is the mass transfer boundary layer thickness which contains $\mathfrak{D}_{\text{A, mix}}$ as a diffusivity, not a molecular transport property.

It is necessary to replace $\mathfrak{D}_{\text{A, mix}}$ in equation (11-111) for $k_{C,\,\text{local}}$ by the thermal conductivity, which corresponds to the molecular transport property for heat transfer, to calculate the local heat transfer coefficient, by analogy. However, as mentioned above, it is necessary to replace $\mathfrak{D}_{\text{A, mix}}$ in the expression for δ_C by the thermal diffusivity to calculate the analogous thermal boundary layer

thickness. Obviously, the local mass transfer coefficient and the instantaneous rate of interphase mass transfer vary inversely with the boundary layer thickness. High transfer rates are achieved when δ_C is thin at high Schmidt numbers. The boundary layer scaling law $\delta_C \approx (\mathfrak{D}_{A,\,mix})^m$ suggests that

$$k_{C,\,local} \approx (\mathfrak{D}_{A,\,mix})^{1-m} \tag{11-112}$$

Hence, the local mass transfer coefficient scales as the two-thirds power of $\mathfrak{D}_{A,\,mix}$ for boundary layer theory adjacent to a solid–liquid interface, and the one-half power of $\mathfrak{D}_{A,\,mix}$ for boundary layer theory adjacent to a gas–liquid interface, as well as unsteady state penetration theory without convective transport. By analogy, the local heat transfer coefficient follows the same scaling laws if one replaces $\mathfrak{D}_{A,\,mix}$ in the previous equation by the thermal conductivity.

11-4.1 Surface-Averaged Transfer Coefficients for Solid–Liquid Interfaces

Local mass transfer coefficients vary with polar angle θ because of the dependence of $k_{C,\,local}$ on $\delta_C(\theta)$. The predictions above are valid for thin boundary layers, where $\delta_C/R \ll 1$. The sucrose dissolution example problem on page 296 suggests that δ_C grows to ≈8% of the pellet diameter at the equatorial position. Hence, it is recommended to average $k_{C,\,local}$ over the front hemisphere only, where the thin boundary layer approximation is justified. Interphase mass transfer is negligible near the separation point where $\theta = \pi$, because δ_C is very thick. In agreement with these facts, one averages the local mass transfer coefficient as follows:

$$k_{C,\,average} \equiv \frac{\iint k_{C,\,local}(\theta) R^2 \sin\theta \, d\theta \, d\phi}{\iint R^2 \sin\theta \, d\theta \, d\phi} \tag{11-113}$$

where the polar angle θ ranges from 0 to $\pi/2$, and the azimuthal angle ϕ encompasses all the time zones (i.e., $0 \le \phi \le 2\pi$). Since the surface area under investigation is $2\pi R^2$,

$$\begin{aligned} k_{C,\,average} &\equiv \int k_{C,\,local}(\theta) \sin\theta \, d\theta \\ &= \frac{\mathfrak{D}_{A,\,mix}}{\Gamma(\frac{4}{3})} \int \left[\frac{\sin\theta}{\delta_C(\theta)}\right] d\theta \qquad 0 \le \theta \le \pi/2 \end{aligned} \tag{11-114}$$

where $\mathfrak{D}_{A,\,mix}$ is a molecular transport property in (11-114). Hence, the surface-averaged mass transfer coefficient is obtained by averaging the inverse of the boundary layer thickness over the front hemisphere of the solid. Since

$$\frac{\delta_C(\theta)}{2R} = \left(\frac{1}{\mathrm{Re}\cdot\mathrm{Sc}}\right)^{1/3} \frac{\left\{\frac{9}{4}\int [g^*(\sigma)\sin^3\sigma]^{1/2} \, d\sigma\right\}^{1/3}}{[g^*(\theta)\sin\theta]^{1/2}} \tag{11-115}$$

via (11-94), where integration variable σ ranges from 0 to θ, the rather complex expression for $k_{C,\,\text{average}}$ reduces to

$$k_{C,\,\text{average}} = \frac{\mathfrak{D}_{\text{A, mix}}}{2R}(\text{Re}\cdot\text{Sc})^{1/3}\frac{(\frac{4}{9})^{1/3}}{\Gamma(\frac{4}{3})}\int\frac{d\Omega}{\Omega^{1/3}} \tag{11-116}$$

where the integration limits are $\theta = 0$ (i.e., $\Omega = 0$) and $\theta = \pi/2$, and

$$\Omega(\theta) = \int [g^*(\sigma)\sin^3\sigma]^{1/2}\,d\sigma \qquad 0 \le \sigma \le \theta \tag{11-117}$$

The final expression for the surface-averaged mass transfer coefficient is

$$k_{C,\,\text{average}} = \frac{\mathfrak{D}_{\text{A, mix}}}{2R}(\text{Re}\cdot\text{Sc})^{1/3}\frac{(\frac{4}{9})^{1/3}}{\Gamma(\frac{4}{3})}\frac{3}{2}[\Omega(\theta=\pi/2)]^{2/3} \tag{11-118}$$

11-4.2 Dimensionless Mass Transfer Correlation for Solid–Liquid Interfaces

If one divides the average mass transfer coefficient $k_{C,\,\text{average}}$ by the simplest mass transfer coefficient in the absence of convective transport, then the resulting dimensionless ratio is identified as the average Sherwood number. Hence,

$$\begin{aligned}\text{Sh}_{\text{average}} &\equiv \frac{k_{C,\,\text{average}}}{\mathfrak{D}_{\text{A, mix}}/2R} \\ &= (\text{Re}\cdot\text{Sc})^{1/3}\,\frac{(\frac{4}{9})^{1/3}}{\Gamma(\frac{4}{3})}\frac{3}{2}[\Omega(\theta=\pi/2)]^{2/3}\end{aligned} \tag{11-119}$$

The dimensionless tangential velocity gradient at the solid–liquid interface, averaged over the front hemisphere of the solid, exhibits a significant influence on the scaling law between the Sherwood and Reynolds numbers. Since $g^*(\theta)$ is calculated from an analysis of the fluid dynamics problem, it is not a function of the Schmidt number. Hence,

$$\text{Sh}_{\text{average}} = 1.28\ (\text{Re}\cdot\text{Sc})^{1/3}\left\{\int [g^*(\theta)\sin^3\theta]^{1/2}\,d\theta\right\}^{2/3} \qquad 0 \le \theta \le \pi/2 \tag{11-120}$$

reveals the complete scaling law between the Sherwood and Schmidt numbers. In other words, $\text{Sh}_{\text{average}} \approx (\text{Sc})^m$, where $m = \frac{1}{3}$ for boundary layer mass transfer adjacent to a no-slip solid–liquid interface in any flow regime. For a perfect-slip zero-shear gas–liquid interface, the scaling law exponent $m = \frac{1}{2}$, once again, in any flow regime. Hence, the power of the Schmidt number (i.e., $m = \frac{1}{3}$ or $\frac{1}{2}$) in the dimensionless mass transfer correlation identifies the nature of the interface across which interphase transport occurs. By analogy, the surface-averaged

Nusselt number for heat transfer scales at $(\mathrm{Pr})^m$ for solid–liquid and gas–liquid interfaces. The power of the Reynolds number identifies the flow regime: creeping, laminar, or turbulent.

Effect of Flow Regime on the Dimensionless Mass Transfer Correlation. For creeping flow of an incompressible Newtonian fluid around a stationary solid sphere, the tangential velocity gradient at the interface [i.e., $g^*(\theta) = \frac{3}{2}\sin\theta$] is independent of the Reynolds number. This is reasonable because contributions from accumulation and convective momentum transport on the left side of the equation of motion are neglected to obtain creeping flow solutions in the limit where $\mathrm{Re} \to 0$. Under these conditions,

$$\mathrm{Sh}_{\mathrm{average}} = \begin{cases} 1.28\ (\mathrm{Re}\cdot\mathrm{Sc})^{1/3} \left(\sqrt{\tfrac{3}{2}} \int \sin^2\theta d\theta\right)^{2/3} & 0 \le \theta \le \pi/2 \\ 1.25\ (\mathrm{Re}\cdot\mathrm{Sc})^{1/3} & \mathrm{Sc} \gg 1, \mathrm{Re} \to 0 \end{cases} \tag{11-121}$$

When $\mathrm{Sh}_{\mathrm{average}}$ scales as the one-third power of the Reynolds number, this signifies creeping flow adjacent to a solid–liquid interface. By analogy, the average Nusselt number for heat transfer also scales as the one-third power of Re in the creeping flow regime. In the laminar flow regime where viscous and inertial forces are equally important in the momentum boundary layer, the dimensionless tangential velocity gradient (i.e., $r\theta$ component of the rate-of-strain tensor) at the solid–liquid interface,

$$g^*(\theta) = \left[\eta \frac{\partial}{\partial \eta}\left(\frac{v_\theta^*}{\eta}\right)\right]_{\eta=1} = \mathrm{Re}^{1/2}\, f(\text{geometry}) \tag{11-122}$$

scales as the one-half power of the Reynolds number. This result is based on two-dimensional convective transport in the momentum boundary layer adjacent to a locally flat no-slip interface. The dynamic pressure gradient within the momentum boundary layer is not a function of Re because it is calculated in the potential flow regime, far from the solid–liquid interface, and imposed across the momentum boundary layer. Now, the laminar flow factor in the dimensionless mass transfer correlations for high-shear no-slip solid–liquid interfaces provides an additional one-sixth power dependence of Re to the previous scaling laws for $\delta_C(\theta)$, $k_{C,\,\mathrm{local}}(\theta)$, $k_{C,\,\mathrm{average}}$, and $\mathrm{Sh}_{\mathrm{average}}$. For example,

$$\mathrm{Sh}_{\mathrm{average}} \approx \begin{cases} (\mathrm{Re}\cdot\mathrm{Sc})^{1/3} \left\{\displaystyle\int_0^{\pi/2} [\mathrm{Re}^{1/2}\, f(\text{geometry})\ \sin^3\theta]^{1/2}\, d\theta\right\}^{2/3} \\ \mathrm{Re}^{1/2}\ \mathrm{Sc}^{1/3} \\ \mathrm{Sc} \gg 1,\ \mathrm{Re} \text{ is laminar} \end{cases} \tag{11-123}$$

Hence, $\mathrm{Sh}_{\mathrm{average}}$ scales as the one-half power of Re for laminar boundary layer mass transfer across a solid–liquid interface, where $\mathrm{Sc}^{1/3}$ is appropriate. Obviously, the average Nusselt number scales as the one-half power of Re for

completely analogous laminar boundary layer heat transfer across a solid–liquid interface, where the one-third power of the Prandtl number is appropriate to characterize the interface. For turbulent transport across a no-slip interface, $Sh_{average}$ and $Nu_{average}$ scale as Re^{υ}, where the exponent υ ranges from 0.8 to 1.0, and $Sc^{1/3}$ or $Pr^{1/3}$ is appropriate.

11-5 LAMINAR BOUNDARY LAYER MASS TRANSFER ACROSS A SPHERICAL GAS–LIQUID INTERFACE

Mass transfer across a perfect-slip zero-shear interface at high Schmidt numbers is discussed in light of the previous results for no-slip interfaces. The following assumptions are invoked to develop the model:

1. The bubble is stationary and its radius R remains constant during the analysis. Surface stretch is not considered in response to a decrease in fluid pressure that one encounters if, for example, the bubble rises.
2. The fluid is Newtonian and incompressible, and its approach velocity $V_{approach}$ remains constant in the creeping or laminar flow regimes.
3. Analysis is performed at steady state for a nonreactive mixture.
4. All physical properties of the mixture are constant.
5. Tangential diffusion parallel to the interface is neglected at high mass transfer Peclet numbers.
6. The mass transfer boundary layer is very thin relative to the bubble diameter. Hence, a locally flat description is appropriate at high Schmidt numbers. If necessary, analysis is restricted to the front hemisphere of the bubble with respect to the approaching fluid to justify this claim.

In agreement with these assumptions, one arrives at the following locally flat two-dimensional description of the mass transfer equation and the equation of continuity:

$$v_r \frac{\partial C_A}{\partial y} + v_\theta \frac{\partial C_A}{\partial x} = \mathfrak{D}_{A,\,mix} \frac{\partial^2 C_A}{\partial y^2} \tag{11-124}$$

$$\frac{\partial v_r}{\partial y} + \frac{1}{\sin\theta} \frac{\partial (v_\theta \sin\theta)}{\partial x} = 0 \tag{11-125}$$

using the same nomenclature that was introduced above. The boundary conditions on $C_A(y, x)$ are repeated here for completeness:

$C_A = C_{A,\,bulk}$ at $x = 0$ for all values of $y > 0$
$C_A = C_{A,\,interface}$ at $y = 0$ for all values of $x > 0$
$C_A \to C_{A,\,bulk}$ as $y \to \infty$ for all values of $x < \pi R$ (i.e., finite x)

11-5.1 Tangential Velocity Component v_θ within the Mass Transfer Boundary Layer: Creeping and Potential Flow around a Gas Bubble

The similarities between gas–liquid and solid–liquid interfaces end here. Since it is only necessary to adopt the exact fluid dynamics solution for v_θ within the range $0 \le y \le \delta_C$ where $\delta_C/R \ll 1$, if the interface is characterized by perfect-slip and zero-shear, then the first-order term in the polynomial expansion for the tangential velocity component should be identically zero. Hence,

$$v_\theta(r,\theta) = v_\theta(r=R,\theta) + (r-R)\left[\left(\frac{\partial\gamma}{\partial t}\right)_{r\theta}\right]_{r=R} + O(r^2) \qquad (11\text{-}126)$$

$$\left[\left(\frac{\partial\gamma}{\partial t}\right)_{r\theta}\right]_{r=R} = \left[r\frac{\partial}{\partial r}\left(\frac{v_\theta}{r}\right) + \frac{1}{r}\frac{\partial v_r}{\partial\theta}\right]_{r=R} \qquad (11\text{-}127)$$

The second term on the right side of (11-127) vanishes for a nondeformable bubble. Furthermore, creeping flow of an incompressible Newtonian fluid around a stationary gas bubble yields the following expressions for v_θ:

$$\begin{aligned}
v_\theta(r,\theta) &= v_\theta(r\to\infty,\theta)\left(1-\frac{1}{2}\eta^{-1}\right)\\
\frac{v_\theta(r,\theta)}{\eta} &= v_\theta(r\to\infty,\theta)\left(\eta^{-1}-\frac{1}{2}\eta^{-2}\right)\\
\left(\frac{\partial v_\theta}{\partial r}\right)_{r=R} &= \frac{1}{R}\left(\frac{\partial v_\theta}{\partial\eta}\right)_{\eta=1} = \frac{V_{\text{approach}}\sin\theta}{R}\left(\frac{1}{2}\eta^{-2}\right)_{\eta=1} \neq 0\\
\left[\left(\frac{\partial\gamma}{\partial t}\right)_{r\theta}\right]_{r=R} &= \frac{1}{R}\left[\eta\frac{\partial}{\partial\eta}\left(\frac{v_\theta}{\eta}\right)\right]_{\eta=1} = \frac{V_{\text{approach}}\sin\theta}{R}\left(-\eta^{-2}+\eta^{-3}\right)_{\eta=1} = 0
\end{aligned} \qquad (11\text{-}128)$$

Unlike creeping flow about a solid sphere, the $r\theta$ component of the rate-of-strain tensor vanishes at the gas–liquid interface, as expected for zero shear, but the simple velocity gradient $(\partial v_\theta/\partial r)_{r=R}$ is not zero. The fluid dynamics boundary conditions require that $[(\partial\gamma/\partial t)_{r\theta}]_{r=R} = 0$. The leading term in the polynomial expansion for v_θ, given by (11-126), is most important for flow around a bubble, but this term vanishes for a no-slip interface when the solid sphere is stationary. For creeping flow around a gas bubble, the tangential velocity component within the mass transfer boundary layer is approximated as

$$v_\theta(\theta) \approx v_\theta(r=R,\theta) = \tfrac{1}{2}V_{\text{approach}}\sin\theta \qquad \text{Re} \ll 1 \qquad (11\text{-}129)$$

If turbulent transport mechanisms are neglected, then high-Reynolds-number flow around a gas bubble (i.e., in the laminar regime) can be approximated by potential flow, where viscous forces vanishes. Now, the tangential velocity component for

an incompressible fluid is

$$v_\theta(r,\theta) = v_\theta(r\to\infty,\theta)\left(1+\frac{1}{2}\eta^{-3}\right)$$

$$\frac{v_\theta(r,\theta)}{\eta} = v_\theta(r\to\infty,\theta)\left(\eta^{-1}+\frac{1}{2}\eta^{-4}\right)$$

$$\left(\frac{\partial v_\theta}{\partial r}\right)_{r=R} = \frac{1}{R}\left(\frac{\partial v_\theta}{\partial \eta}\right)_{\eta=1} = \frac{V_{\text{approach}}\sin\theta}{R}\left(-\frac{3}{2}\eta^{-4}\right)_{\eta=1} \neq 0$$

$$\left[\left(\frac{\partial \gamma}{\partial t}\right)_{r\theta}\right]_{r=R} = \frac{1}{R}\left[\eta\frac{\partial}{\partial\eta}\left(\frac{v_\theta}{\eta}\right)\right]_{\eta=1} = \frac{V_{\text{approach}}\sin\theta}{R}(-\eta^{-2}-2\eta^{-5})_{\eta=1} \neq 0 \tag{11-130}$$

Neither the $r\theta$ component of the rate-of-strain tensor nor the simple velocity gradient $\partial v_\theta/\partial r$ vanishes at the gas–liquid interface. This is expected for inviscid flow because viscous stress is not considered, even in the presence of a significant velocity gradient. Once again, the leading term in the polynomial expansion for v_θ, given by (11-126), is used to approximate the tangential velocity component for flow of an incompressible fluid adjacent to a zero-shear interface:

$$v_\theta(\theta) \approx v_\theta(r=R,\theta) = \tfrac{3}{2}V_{\text{approach}}\sin\theta \qquad \text{Re is laminar} \tag{11-131}$$

Notice that $v_\theta(r=R)/V_{\text{approach}}$ within the mass transfer boundary layer is three-fold larger for potential flow relative to creeping flow.

11-5.2 Radial Velocity Component Adjacent to a Gas–Liquid Interface

The locally flat description of the equation of continuity,

$$\frac{\partial v_r}{\partial y} + \frac{1}{\sin\theta}\frac{\partial(v_\theta\sin\theta)}{\partial x} = 0 \tag{11-132}$$

is used to calculate $v_r(r,\theta)$, which is consistent with the zeroth-order polynomial approximation for the tangential velocity component. Hence, integration of the equation of continuity from the gas–liquid interface at $y=0$ to any position y within δ_C produces the following result:

$$v_r(r,\theta) = -\frac{1}{\sin\theta}\frac{d[v_\theta(r=R,\theta)\sin\theta]}{dx}\int dy = -\frac{y}{\sin\theta}\frac{d[v_\theta(r=R,\theta)\sin\theta]}{dx}$$

$$v_r(r,\theta) = y\psi(\theta) = (r-R)\psi(\theta) \tag{11-133}$$

$$\psi(\theta) = -\frac{1}{\sin\theta}\frac{d}{dx}[v_\theta(r=R,\theta)\sin\theta]$$

Now, v_r and v_θ are incorporated into the mass transfer equation.

11-6 BOUNDARY LAYER SOLUTION OF THE MASS TRANSFER EQUATION AROUND A GAS BUBBLE

The concentration of mobile component A is expressed in terms of the dimensionless profile $P(r, \theta)$, which must satisfy the following partial differential equation:

$$y\psi(\theta)\frac{\partial P}{\partial y} + v_\theta(r = R, \theta)\frac{\partial P}{\partial x} = \mathfrak{D}_{\mathrm{A,\,mix}}\frac{\partial^2 P}{\partial y^2} \tag{11-134}$$

subject to the same boundary conditions for solid–liquid interfaces. In terms of the combined variable $\zeta = y/\delta_C(\theta)$, the mass transfer equation is written as a second-order ODE for $P(\zeta)$:

$$y\psi(\theta)\frac{1}{\delta_C}\frac{dP}{d\zeta} - v_\theta(r = R, \theta)\frac{\zeta}{\delta_C}\frac{d\delta_C}{dx}\frac{dP}{d\zeta} = \mathfrak{D}_{\mathrm{A,\,mix}}\left(\frac{1}{\delta_C}\right)^2\frac{d^2P}{d\zeta^2} \tag{11-135}$$

Multiplication by $(\delta_C)^2$ and letting $y = \zeta\delta_C$ produces the following result:

$$-\left[v_\theta(r = R, \theta)\delta_C\frac{d\delta_C}{dx} - \psi(\theta)(\delta_C)^2\right]\zeta\frac{dP}{d\zeta} = \mathfrak{D}_{\mathrm{A,\,mix}}\frac{d^2P}{d\zeta^2} \tag{11-136}$$

The quantity in brackets on the left side of (11-136) has units of a diffusivity (i.e., length^2/time). Hence, it should be proportional to $\mathfrak{D}_{\mathrm{A,\,mix}}$. The two ODEs that must be solved are

$$v_\theta(r = R, \theta)\delta_C\frac{d\delta_C}{dx} - \psi(\theta)(\delta_C)^2 = (\text{constant})\cdot\mathfrak{D}_{\mathrm{A,\,mix}} \tag{11-137}$$

$$\frac{d^2P}{d\zeta^2} = -(\text{constant})\cdot\zeta\frac{dP}{d\zeta} \tag{11-138}$$

where the fortuitous choice of the constant is 2, which leads to an error function solution for the dimensionless profile $P(\zeta)$.

11-6.1 Error Function Profile

The dimensionless profile P can be expressed in terms of the error function when the constant in the following equation is 2:

$$\frac{d^2P}{d\zeta^2} = -(\text{constant})\cdot\zeta\frac{dP}{d\zeta} \tag{11-139}$$

Once again, this choice of the constant does not bias this analysis of mass transfer boundary layer theory when the concentration profile and the boundary layer thickness are viewed as a pair. Hence,

$$P(\zeta) = C_1\int \exp(-x^2)\,dx \qquad 0 \le x \le \zeta \tag{11-140}$$

Integration constant C_1 is calculated via the boundary condition, $P(\zeta \to \infty) = 1$:

$$C_1 = \frac{1}{\int \exp(-x^2)\,dx} = \frac{2}{\Gamma(\frac{1}{2})} = \frac{1}{\Gamma(\frac{3}{2})} = \frac{2}{\sqrt{\pi}} \qquad 0 \le x \le \infty \tag{11-141}$$

where $\Gamma(\frac{3}{2})$ is the gamma function for an argument of $\frac{3}{2}$. The final expression for the dimensionless concentration profile of mobile component A is

$$P(\zeta) = \frac{C_{\text{A, interface}} - C_{\text{A}}(r,\theta)}{C_{\text{A, interface}} - C_{\text{A, bulk}}} = \frac{2}{\sqrt{\pi}} \int \exp(-x^2)\,dx = \text{erf}(\zeta) \tag{11-142}$$

where integration is performed over the range $0 \le x \le \zeta$. It is also possible to express the dimensionless concentration profile $P(\zeta)$ in terms of the incomplete gamma function when the argument $n = \frac{1}{2}$ and the variable $\lambda = \zeta^2$:

$$P(\zeta) = \text{S}\left(\frac{1}{2}, \zeta^2\right) = \frac{\int \exp(-x^2)\,dx}{\Gamma(\frac{3}{2})} \qquad 0 \le x \le \zeta \tag{11-143}$$

11-6.2 Thickness of the Mass Transfer Boundary Layer around a Gas Bubble

It is possible to estimate the boundary layer thickness via solution of the following equation:

$$v_\theta(r = R, \theta)\delta_C \frac{d\delta_C}{dx} - \psi(\theta)(\delta_C)^2 = 2\mathcal{D}_{\text{A, mix}} \tag{11-144}$$

$$\psi(\theta) = -\frac{1}{\sin\theta}\frac{d}{dx}[v_\theta(r = R, \theta)\sin\theta] \tag{11-145}$$

Upon substitution for $\psi(\theta)$ in (11-144) and multiplication by $\sin\theta$, one obtains the following ODE for $\delta_C(\theta)$:

$$v_\theta(r = R, \theta)(\sin\theta)\delta_C \frac{d\delta_C}{dx} + (\delta_C)^2 \frac{d}{dx}[v_\theta(r = R, \theta)\sin\theta] = 2\mathcal{D}_{\text{A, mix}}\sin\theta \tag{11-146}$$

The left side of (11-146) can be rewritten as

$$\frac{1}{2}v_\theta(r = R, \theta)(\sin\theta)\frac{d(\delta_C)^2}{dx} + (\delta_C)^2 \frac{d}{dx}[v_\theta(r = R, \theta)\sin\theta]$$
$$= A[v_\theta(r = R, \theta)\sin\theta]^a \frac{d}{dx}\{(\delta_C)^2[v_\theta(r = R, \theta)\sin\theta]^{1-a}\} = 2\mathcal{D}_{\text{A, mix}}\sin\theta \tag{11-147}$$

with $A = \frac{1}{2}$ and $a = -1$. Now, the boundary layer thickness can be calculated via simple integration:

$$\frac{d}{d\theta}\{(\delta_C)^2[v_\theta(r = R, \theta)\sin\theta]^2\} = 4R\mathfrak{D}_{\mathrm{A,\,mix}}v_\theta(r = R, \theta)\sin^2\theta \qquad (11\text{-}148)$$

subject to the condition that $\delta_C = 0$ at the stagnation point where the approaching fluid contacts the gas bubble initially at $\theta = 0$. Hence,

$$(\delta_C)^2[v_\theta(r = R, \theta)\sin\theta]^2 = 4R\mathfrak{D}_{\mathrm{A,\,mix}}\int_0^\theta v_\theta(r = R, \sigma)\sin^2\sigma\, d\sigma \qquad (11\text{-}149)$$

$$\delta_C(\theta) = \frac{\left[4R\mathfrak{D}_{\mathrm{A,\,mix}}\displaystyle\int_0^\theta v_\theta(r = R, \sigma)\sin^2\sigma\, d\sigma\right]^{1/2}}{v_\theta(r = R, \theta)\sin\theta} \qquad (11\text{-}150)$$

which confirms the scaling law $\delta_C \approx (\mathfrak{D}_{\mathrm{A,\,mix}})^m$, with $m = \frac{1}{2}$ for boundary layer mass transfer adjacent to a zero-shear gas–liquid interface at high Schmidt numbers. If the tangential fluid velocity at the gas–liquid interface is written as

$$v_\theta(r = R, \theta) = V_{\mathrm{approach}}v_\theta^*(\eta = 1, \theta) \qquad (11\text{-}151)$$

with $\eta = r/R$, then the dimensionless velocity component v_θ^* reduces to $\frac{1}{2}\sin\theta$ for creeping flow and $\frac{3}{2}\sin\theta$ for potential flow around the bubble. The dimensionless boundary layer thickness is

$$\frac{\delta_C(\theta)}{R} = \frac{\left\{\dfrac{4\mathfrak{D}_{\mathrm{A,\,mix}}}{RV_{\mathrm{approach}}}\displaystyle\int_0^\theta v_\theta^*(\eta = 1, \sigma)\sin^2\sigma\, d\sigma\right\}^{1/2}}{v_\theta^*(\eta = 1, \theta)\sin\theta} \qquad (11\text{-}152)$$

Since the Reynolds number is based on the bubble diameter, the general expression for the dimensionless mass transfer boundary layer thickness is

$$\frac{\delta_C(\theta)}{R} = \left(\frac{1}{\mathrm{Re}\cdot\mathrm{Sc}}\right)^{1/2}\frac{\left[8\displaystyle\int_0^\theta v_\theta^*(\eta = 1, \sigma)\sin^2\sigma\, d\sigma\right]^{1/2}}{v_\theta^*(\eta = 1, \theta)\sin\theta} \qquad (11\text{-}153)$$

which confirms the scaling law $\delta_C \approx 1/(\mathrm{Re}\cdot\mathrm{Sc})^m$, with $m = \frac{1}{2}$ for gas–liquid interfaces. In the creeping flow regime, where $v_\theta^* = \frac{1}{2}\sin\theta$,

$$\frac{\delta_C(\theta)}{2R} = \left(\frac{4}{\mathrm{Re}\cdot\mathrm{Sc}}\right)^{1/2}\frac{(\frac{1}{3}\cos^3\theta - \cos\theta + \frac{2}{3})^{1/2}}{\sin^2\theta} \qquad \mathrm{Re} \ll 1 \qquad (11\text{-}154)$$

This function [i.e., $\delta(\theta)/2R$] given by (11-154) is illustrated in Figure 11-2 for creeping flow of an incompressible Newtonian fluid around a gas bubble at high

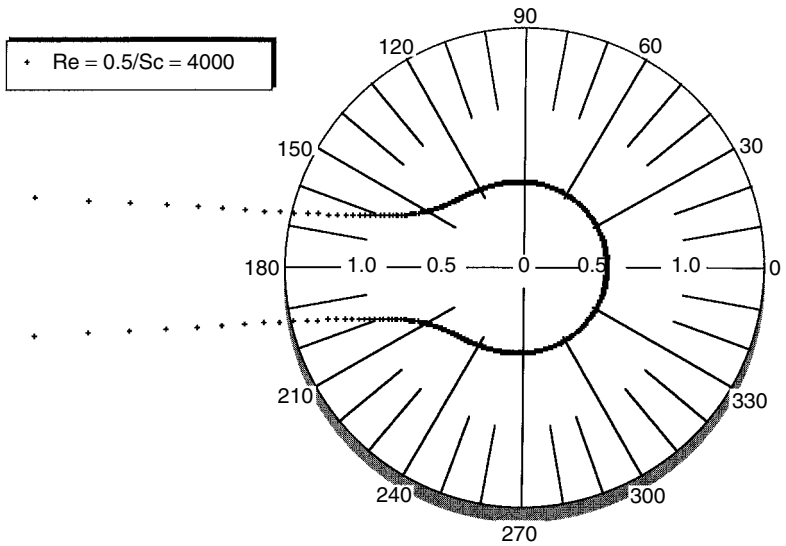

Figure 11-2 Thickness of the mass transfer boundary layer around a gas bubble in the creeping flow regime. This graph in polar coordinates illustrates $\delta_C(\theta)$ divided by the sphere diameter vs. polar angle θ, and the fluid approaches the bubble horizontally from the right. No data are plotted at the stagnation point, where $\theta = 0$.

Schmidt numbers. The fluid approaches the bubble from the right and the boundary layer develops from the stagnation point at $\theta = 0$.

In the potential flow regime, where $v_\theta^* = \frac{3}{2}\sin\theta$ and Re is much larger, but the flow remains laminar, the dimensionless mass transfer boundary layer thickness is

$$\frac{\delta_C(\theta)}{2R} = \left(\frac{4}{3\,\mathrm{Re}\cdot\mathrm{Sc}}\right)^{1/2} \frac{\left(\frac{1}{3}\cos^3\theta - \cos\theta + \frac{2}{3}\right)^{1/2}}{\sin^2\theta} \tag{11-155}$$

θ can be expressed in degrees or radians in (11-154) and (11-155) for $\delta_C(\theta)$. Comparison of liquid-phase mass transfer boundary layer thicknesses for creeping and potential flow of an incompressible Newtonian fluid around a stationary gas bubble reduces to

$$[\delta_C(\theta)]_{\text{creeping flow}} = \kappa\sqrt{(3)}[\delta_C(\theta)]_{\text{potential flow}} \tag{11-156}$$

where

$$\kappa = \left(\frac{\mathrm{Re}_{\text{potential flow}}}{\mathrm{Re}_{\text{creeping flow}}}\right)^{1/2} \gg 1$$

Comparison of $\delta_C(\theta)$ for creeping flow of an incompressible Newtonian fluid around stationary gas bubbles and solid spheres, where the boundary layer adjacent to a no-slip high-shear interface is

$$\frac{[\delta_C(\theta)]_{\text{solid sphere}}}{2R} = \left(\frac{3}{4}\right)^{1/3} \left(\frac{1}{\text{Re}\cdot\text{Sc}}\right)^{1/3} \frac{(\theta - \frac{1}{2}\sin 2\theta)^{1/3}}{\sin\theta} \tag{11-157}$$

reveals that

$$[\delta_C(\theta)]_{\text{solid sphere}} > [\delta_C(\theta)]_{\text{gas bubble}} \qquad \text{Re} \ll 1 \tag{11-158}$$

from the stagnation point at $\theta = 0$ to polar angles slightly greater than 2.5 radians. This result is reasonable because the perfect-slip zero-shear problem maintains a larger convective mass transfer contribution parallel to the interface at $r = R$, which has the effect of sweeping away mobile component A as it diffuses across the interface and into the liquid phase.

Practical Example. The physical properties of water with trace amounts of dissolved oxygen are (Bird *et al.*, 2002, p. 14; Geankoplis, 1983, p. 391; Perry and Chilton, 1973, pp. 3–225).

$T = 20°\text{C}$ viscosity $\mu = 1.00 \times 10^{-2}$ g/cm·s
$T = 25°\text{C}$ viscosity $\mu = 0.92 \times 10^{-2}$ g/cm·s
$T = 40°\text{C}$ viscosity $\mu = 0.65 \times 10^{-2}$ g/cm·s
$T = 20°\text{C}$ momentum diffusivity $\dfrac{\mu}{\rho} = 1.0037 \times 10^{-2}$ cm^2/s
$T = 25°\text{C}$ diffusion coefficient $\mathfrak{D}_{\text{AB}} = 2.41 \times 10^{-5}$ cm^2/s

(a) Calculate the Schmidt number for oxygen transport in water at 20°C.
(b) Oxygen bubbles 2 mm in diameter rise through 20°C water with a velocity of 10 m/min. How thick is the mass transfer boundary layer at the equatorial position of the bubble?
(c) How important is the curvature correction in the equation of continuity at the equatorial position of the bubble?
(d) How important is the curvature correction in the mass transfer equation at the equatorial position of the bubble?

SOLUTION. (a) The Stokes–Einstein diffusion equation, which is applicable for creeping flow of an incompressible Newtonian fluid around spherical particles (i.e., solids or bubbles) at extremely low particle concentrations, reveals that liquid-phase binary molecular diffusion coefficients exhibit the following temperature dependence:

$$\mathfrak{D}_{\text{AB}} \approx \frac{T}{\mu}$$

The diffusivity at 20°C is obtained from the tabulated value at 25°C by employing the appropriate temperature and viscosity ratios at these two temperatures. Hence, $\mathfrak{D}_{AB} = 2.18 \times 10^{-5}$ cm^2/s and $Sc = (\mu/\rho)/\mathfrak{D}_{AB} \approx 460$ at 20°C.

(b) The Reynolds number is 332, and the mass transfer Peclet number is 1.5×10^5. Under these conditions, it is reasonable to neglect tangential diffusion, and potential flow is appropriate. At the equatorial position of the pellet where $\theta = \pi/2$ radians,

$$\frac{\delta_C(\theta = \pi/2)}{2R} = \left(\frac{8}{9\,\mathrm{Re}\cdot\mathrm{Sc}}\right)^{1/2} = 2.4 \times 10^{-3}$$

Hence, the thin boundary layer approximation is justified, and the locally flat description of the equation of continuity and the mass transfer equation is valid.

(c) The maximum value of the dimensionless radial variable (i.e., normal coordinate) at the outer edge of the mass transfer boundary layer is

$$\eta_{\text{maximum}} = \left(\frac{r}{R}\right)_{\text{maximum}} = 1 + \frac{\delta_C\left(\theta = \dfrac{\pi}{2}\right)}{R} \approx 1.0048$$

Corrections for curvature are most important at η_{maximum}. In the potential flow regime,

$$v_r(r, \theta) = -V_{\text{approach}} \cos\theta (1 - \eta^{-3})$$

$$\frac{\partial v_r}{\partial r} = \frac{1}{R}\frac{\partial v_r}{\partial \eta} = -\frac{V_{\text{approach}} \cos\theta}{R} 3\eta^{-4}$$

$$\frac{\partial \ln v_r}{\partial \ln r} = \frac{r}{v_r}\frac{\partial v_r}{\partial r} = \frac{3}{\eta^3 - 1} = 206 \qquad \text{at } \eta_{\text{maximum}}$$

$$\frac{1}{r^2}\frac{\partial (r^2 v_r)}{\partial r} = \frac{\partial v_r}{\partial r}\left(1 + \frac{2}{\partial \ln v_r / \partial \ln r}\right) \approx 1.01 \frac{\partial v_r}{\partial r} \qquad \text{at } \eta_{\text{maximum}}$$

Hence, neglecting the curvature correction factors of r^2 in the radial term of the equation of continuity corresponds to a ≈1.0% underestimate of $(1/r^2)\partial(r^2 v_r)/\partial r$ at the outer edge of the mass transfer boundary layer on the equator of the bubble. Within $\delta_C(\theta)$, the error is much less than 1%. The locally flat description of the equation of continuity is excellent for this application.

(d) Once again, corrections for curvature are most important at the outer edge of the mass transfer boundary layer, where $\eta_{\text{maximum}} = 1.0048$ and $\zeta = 1$. Now the error function profile is used to determine the importance of the second term on the right side of the following equation:

$$\frac{1}{r^2}\frac{\partial}{\partial r}\left(r^2 \frac{\partial C_A}{\partial r}\right) = \frac{\partial^2 C_A}{\partial r^2}\left(1 + \frac{2}{\partial \ln \beta / \partial \ln r}\right)$$

where $\beta = \partial C_A/\partial r$. The error associated with neglecting the second term on the right side of the preceding equation is

$$\% \text{ error} = 100 \times \left[\frac{\dfrac{1}{r^2}\dfrac{\partial}{\partial r}\left(r^2 \dfrac{\partial C_A}{\partial r}\right) - \dfrac{\partial^2 C_A}{\partial r^2}}{\dfrac{1}{r^2}\dfrac{\partial}{\partial r}\left(r^2 \dfrac{\partial C_A}{\partial r}\right)} \right]$$

$$= \frac{200}{2 + (\partial \ln \beta / \partial \ln r)}$$

where

$$\left(\frac{\partial \ln \beta}{\partial \ln r}\right)_{\theta,\, \zeta=1} = [R + \delta_C(\theta)] \frac{(\partial^2 C_A/\partial r^2)_{\theta,\, \zeta=1}}{(\partial C_A/\partial r)_{\theta,\, \zeta=1}}$$

The error function profile for $P(\eta)$ in the liquid phase adjacent to a perfect-slip zero-shear interface is

$$P(\zeta) = \frac{C_{A,\,\text{interface}} - C_A(r,\theta)}{C_{A,\,\text{interface}} - C_{A,\,\text{bulk}}} = \frac{2}{\sqrt{\pi}} \int_0^{\zeta} \exp(-x^2)\, dx = \text{erf}(\zeta)$$

which allows one to evaluate the first and second partial derivatives of C_A with respect to radial position r, as follows:

(1) $$\left(\frac{\partial C_A}{\partial r}\right)_{\theta} = -\left(C_{A,\,\text{interface}} - C_{A,\,\text{bulk}}\right) \frac{2}{\sqrt{\pi}} \exp(-\zeta^2) \frac{1}{\delta_C(\theta)}$$

(2) $$\left(\frac{\partial^2 C_A}{\partial r^2}\right)_{\theta} = \frac{d[(\partial C_A/\partial r)_{\theta}]}{d\zeta} \left(\frac{\partial \zeta}{\partial r}\right)_{\theta}$$

$$= (C_{A,\,\text{interface}} - C_{A,\,\text{bulk}}) \frac{2}{\sqrt{\pi}} 2\zeta \exp(-\zeta^2) \left[\frac{1}{\delta_C(\theta)}\right]^2$$

These expressions are evaluated at the outer edge of the mass transfer boundary layer, where $\zeta = 1$:

(1) $$\left(\frac{\partial C_A}{\partial r}\right)_{\theta,\, \zeta=1} = -(C_{A,\,\text{interface}} - C_{A,\,\text{bulk}}) \frac{2e^{-1}}{\sqrt{\pi}} \frac{1}{\delta_C(\theta)}$$

(2) $$\left(\frac{\partial^2 C_A}{\partial r^2}\right)_{\theta,\, \zeta=1} = (C_{A,\,\text{interface}} - C_{A,\,\text{bulk}}) \frac{4e^{-1}}{\sqrt{\pi}} \left[\frac{1}{\delta_C(\theta)}\right]^2$$

The curvature correction for radial diffusion is

$$\left(\frac{\partial \ln \beta}{\partial \ln r}\right)_{\theta,\, \zeta=1} = [R + \delta_C(\theta)] \frac{(\partial^2 C_A/\partial r^2)_{\theta,\, \zeta=1}}{(\partial C_A/\partial r)_{\theta,\, \zeta=1}} = -2\left[1 + \frac{R}{\delta_C(\theta)}\right]$$

and the maximum error associated with neglecting this correction factor is

$$\% \text{ error} = \frac{200}{2 + (\partial \ln \beta / \partial \ln r)_{\theta,\, \zeta=1}} = -100(\eta_{\text{maximum}} - 1)$$

where

$$\eta_{\text{maximum}} = \left(\frac{r}{R}\right)_{\text{maximum}} = 1 + \frac{\delta_C(\theta)}{R}$$

At the equatorial position of the gas bubble, $\eta_{\text{maximum}} = 1.0048$ when $\text{Sc} = 460$ and $\text{Re} = 332$ at 20°C. This corresponds to a maximum error of ≈0.5% at η_{maximum} by invoking the following approximation for radial diffusion in the mass transfer equation:

$$\frac{1}{r^2}\frac{\partial}{\partial r}\left(r^2\frac{\partial C_{\text{A}}}{\partial r}\right) \approx \frac{\partial^2 C_{\text{A}}}{\partial r^2}$$

which should be compared with a maximum error of ≈1.0% at η_{maximum} by making a similar approximation in the equation of continuity:

$$\frac{1}{r^2}\frac{\partial(r^2 v_r)}{\partial r} \approx \frac{\partial v_r}{\partial r}$$

It should be emphasized that the error associated with the neglect of curvature is proportional to $(\text{Re}\cdot\text{Sc})^{-1/2}$ for gas–liquid interfaces, and $(\text{Re}\cdot\text{Sc})^{-1/3}$ for solid–liquid interfaces. Hence, the error is much less for potential flow around an oxygen bubble relative to creeping flow around a solid sucrose pellet, which was discussed on pages 296–298.

11-7 INTERPHASE MASS TRANSFER AT THE GAS–LIQUID INTERFACE

The radial component of the diffusional molar flux of mobile component A, $N_{\text{A}r}$, is evaluated at the solid–liquid interface (i.e., at $r = R$, $y = 0$, $\theta > 0$, $\zeta = 0$) to calculate the local mass transfer coefficient $k_{C,\,\text{local}}$:

$$\begin{aligned} N_{\text{A}r} &= -\mathfrak{D}_{\text{A, mix}}\frac{\partial C_{\text{A}}}{\partial r} = -\mathfrak{D}_{\text{A, mix}}\frac{dC_{\text{A}}}{dP}\frac{dP}{d\zeta}\left(\frac{\partial \zeta}{\partial y}\right)\left(\frac{dy}{dr}\right) \\ &\equiv k_{C,\,\text{local}}(C_{\text{A, interface}} - C_{\text{A, bulk}}) \end{aligned} \tag{11-159}$$

The classic result for $k_{C,\,\text{local}}$ is

$$k_{C,\,\text{local}}(\theta) = \frac{2}{\sqrt{\pi}}\frac{\mathfrak{D}_{\text{A, mix}}}{\delta_C(\theta)} \tag{11-160}$$

where $2/\sqrt{\pi}$ is a constant that represents the gradient of the dimensionless concentration profile with respect to the combined variable ζ, evaluated at the solid–liquid interface (i.e., at $\zeta = 0$), $\mathfrak{D}_{\text{A, mix}}$ is the molecular transport property for mass transfer that was introduced via Fick's law to calculate the interfacial

molar flux, and $\delta_C(\theta)$ is the mass transfer boundary layer thickness which contains $\mathfrak{D}_{A,\,mix}$ as a diffusivity, not a molecular transport property. The boundary layer scaling law $\delta_C \approx (\mathfrak{D}_{A,\,mix})^m$ suggests that $k_{C,\,local} \approx (\mathfrak{D}_{A,\,mix})^{1-m}$ and $m = \frac{1}{2}$ for boundary layer theory adjacent to a gas–liquid interface.

11-7.1 Surface-Averaged Transfer Coefficients for Gas–Liquid Interfaces

Local mass transfer coefficients vary with polar angle θ because of the inverse relation between $k_{C,\,local}$ and $\delta_C(\theta)$. Once again, it is recommended to average $k_{C,\,local}$ or $\delta_C(\theta)$ over the front hemisphere only, where the thin boundary layer approximation is justified, particularly for creeping flow. Hence,

$$k_{C,\,average} \equiv \frac{\iint k_{C,\,local}(\theta) R^2 \sin\theta\, d\theta\, d\phi}{\iint R^2 \sin\theta\, d\theta\, d\phi} \equiv \int k_{C,\,local}(\theta) \sin\theta\, d\theta$$

$$= \frac{2}{\sqrt{\pi}} \mathfrak{D}_{A,\,mix} \int \frac{\sin\theta}{\delta_C(\theta)}\, d\theta \qquad 0 \le \theta \le \pi/2, 0 \le \phi \le 2\pi \tag{11-161}$$

where $\mathfrak{D}_{A,\,mix}$ is a molecular transport property in (11-161). At high Schmidt numbers, the mass transfer boundary layer thickness in the liquid phase adjacent to a zero-shear interface is

$$\frac{\delta_C(\theta)}{2R} = \left(\frac{2}{\mathrm{Re}\cdot\mathrm{Sc}}\right)^{1/2} \frac{\left[\int v_\theta^*(\eta = 1, \sigma) \sin^2\sigma\, d\sigma\right]^{1/2}}{v_\theta^*(\eta = 1, \theta)\sin\theta} \qquad 0 \le \sigma \le \theta \tag{11-162}$$

and the rather complex expression for $k_{C,\mathrm{average}}$ reduces to

$$k_{C,\,average} = \sqrt{\frac{2}{\pi}} \frac{\mathfrak{D}_{A,\,mix}}{2R} (\mathrm{Re}\cdot\mathrm{Sc})^{1/2} \int \Xi^{-1/2}\, d\Xi \tag{11-163}$$

where the integration limits are $\theta = 0$ (i.e., $\Xi = 0$) and $\theta = \pi/2$, and

$$\Xi(\theta) = \int v_\theta^*(\eta = 1, \sigma) \sin^2\sigma\, d\sigma \qquad 0 \le \sigma \le \theta \tag{11-164}$$

The final expression for the surface-averaged mass transfer coefficient is

$$k_{C,\,average} = \sqrt{\frac{8}{\pi}} \frac{\mathfrak{D}_{A,\,mix}}{2R} (\mathrm{Re}\cdot\mathrm{Sc})^{1/2} [\Xi(\theta = \pi/2)]^{1/2} \tag{11-165}$$

11-7.2 Dimensionless Mass Transfer Correlation for Gas–Liquid Interfaces

The average Sherwood number is obtained by constructing the ratio of the average mass transfer coefficient $k_{C,\,average}$ to the simplest mass transfer coefficient in the

absence of convective transport (i.e., $\mathfrak{D}_{A,\,mix}/2R$). Hence,

$$\begin{aligned} \mathrm{Sh}_{\text{average}} &\equiv \frac{k_{C,\,\text{average}}}{\mathfrak{D}_{A,\,mix}/2R} \\ &= \sqrt{\frac{8}{\pi}}(\mathrm{Re}\cdot\mathrm{Sc})^{1/2}\left[\Xi\left(\theta=\frac{\pi}{2}\right)\right]^{1/2} \end{aligned} \tag{11-166}$$

The dimensionless tangential velocity component at the gas–liquid interface is independent of the Reynolds and Schmidt numbers for creeping and potential flow. The final expression for the surface-averaged Sherwood number in any flow regime where turbulent mass transfer mechanisms are absent is

$$\mathrm{Sh}_{\text{average}} = \sqrt{\frac{8}{\pi}}(\mathrm{Re}\cdot\mathrm{Sc})^{1/2}\left[\int v_\theta^*(\eta=1,\theta)\sin^2\theta\,d\theta\right]^{1/2} \qquad 0\le\theta\le\pi/2 \tag{11-167}$$

which reveals the complete scaling law between the Sherwood number and the mass transfer Peclet number. In other words, $\mathrm{Sh}_{\text{average}} \approx \mathrm{Pe}^m$, where $m = \frac{1}{2}$ for boundary layer mass transfer adjacent to a perfect-slip zero-shear interface. The $\frac{1}{2}$ power of Sc in $\mathrm{Sh}_{\text{average}}$ is characteristic of gas–liquid interfaces, but $\mathrm{Re}^{1/2}$ is insensitive to the flow regime. This is illustrated below for creeping and potential flow.

For creeping flow of an incompressible fluid around a gas bubble, the dimensionless tangential velocity component at the gas–liquid interface is

$$v_\theta^*(\eta=1,\theta) = \frac{v_\theta(\eta=1,\theta)}{V_{\text{approach}}} = \frac{1}{2}\sin\theta \tag{11-168}$$

Hence,

$$\mathrm{Sh}_{\text{average}} = \begin{cases} \sqrt{\dfrac{4}{\pi}}(\mathrm{Re}\cdot\mathrm{Sc})^{1/2}\left(\displaystyle\int \sin^3\theta\,d\theta\right)^{1/2} & 0\le\theta\le\pi/2 \\ \sqrt{\dfrac{8}{3\pi}}(\mathrm{Re}\cdot\mathrm{Sc})^{1/2} & \mathrm{Sc}\gg 1,\ \mathrm{Re}\to 0 \end{cases} \tag{11-169}$$

For potential flow of an incompressible fluid around a gas bubble, the dimensionless tangential velocity component at the gas–liquid interface is

$$v_\theta^*(\eta=1,\theta) = \frac{v_\theta(\eta=1,\theta)}{V_{\text{approach}}} = \frac{3}{2}\sin\theta \tag{11-170}$$

Hence,

$$\mathrm{Sh}_{\text{average}} = \begin{cases} \sqrt{\dfrac{12}{\pi}}(\mathrm{Re}\cdot\mathrm{Sc})^{1/2}\left(\displaystyle\int \sin^3\theta\,d\theta\right)^{1/2} & 0\le\theta\le\pi/2 \\ \sqrt{\dfrac{8}{\pi}}(\mathrm{Re}\cdot\mathrm{Sc})^{1/2} & \mathrm{Sc}\gg 1,\ \text{Re is laminar} \end{cases} \tag{11-171}$$

11-7.3 Boundary Layer Mass Transfer across a Mobile Gas–Liquid Interface

Objectives and Assumptions. In an effort to complement developments from earlier sections, mass transfer across a gas–liquid interface into a quiescent liquid is considered here. This problem differs slightly from the classic unsteady-state penetration theory analysis because the bubble radius $R(t)$ depends on time, for example, due to the fact that the bubble contracts or expands. The overall objectives are to predict the following quantities:

1. Concentration profile of solubilized gas A in the liquid phase, $C_{\mathrm{A}}(r, t)$
2. Time-dependent mass transfer boundary layer thickness, $\delta_C(t)$
3. Total local molar flux of species A across the gas–liquid interface:

$$N_{\mathrm{A}r}[r = R(t), t] \approx \frac{\mathfrak{D}_{\mathrm{A,\,mix}}}{\delta_C(t)}(C_{\mathrm{A,\,interface}} - C_{\mathrm{A,\,bulk}}) \tag{11-172}$$

   where all of the notation is essentially the same as that which has been discussed above
4. Local mass transfer coefficient, based on item 3
5. Total number of moles of species A that has been transported across the gas–liquid interface, based on an unsteady–state macroscopic mass balance

One invokes the following assumptions:

1. A liquid-phase mixture, which contains mobile component A, exhibits constant physical properties, such as ρ and $\mathfrak{D}_{\mathrm{A,\,mix}}$.
2. The problem is axisymmetric with respect to the azimuthal angle ϕ in spherical coordinates.
3. One must consider unsteady-state radial diffusion in spherical coordinates with no chemical reaction. Tangential diffusion in the polar coordinate direction θ is neglected.
4. There is no flow past the bubble. Hence, mass transfer by convection in the polar coordinate direction θ is absent.
5. The mobile nature of the gas–liquid interface induces radial convection in the liquid phase. The velocity of the liquid is, in general, different from that of the interface, except at $r = R(t)$.
6. The diffusional molar flux of component A is expressed via Fick's law in terms of the concentration gradient of A, only. Coupling between the diffusional mass flux of one species and all the independent mass fractions in the liquid phase is avoided by modeling this multicomponent diffusion problem as if it were a pseudobinary mixture.

Mass Transfer Equation. The generalized mass transfer equation in vector form for nonreactive systems

$$\frac{\partial C_A}{\partial t} + \mathbf{v} \cdot \nabla C_A = \mathfrak{D}_{A,\,mix} \nabla \cdot \nabla C_A \tag{11-173}$$

reduces to the following time-dependent partial differential equation, which is consistent with these six assumptions:

$$\frac{\partial C_A}{\partial t} + v_r \frac{\partial C_A}{\partial r} = \mathfrak{D}_{A,\,mix} \frac{1}{r^2} \frac{\partial}{\partial r} \left(r^2 \frac{\partial C_A}{\partial r} \right) \tag{11-174}$$

One seeks the concentration profile of mobile component A within the liquid-phase mass transfer boundary layer during the early stages of this process when $\delta_C(t)$ is small relative to the local radius of curvature of the bubble. Hence, the important range of the independent variable in the radial direction is

$$R(t) \leq r \leq R(t) + \delta_C(t) \tag{11-175}$$

Locally Flat Description. Analogous to the discussion on pages 279–280, one invokes the thin boundary layer approximation for either short contact times or small diffusivities and arrives at a locally flat description of the mass transfer equation for $C_A(r, t)$:

$$\left(\frac{\partial C_A}{\partial t} \right)_r + v_r \left(\frac{\partial C_A}{\partial r} \right)_t \approx \mathfrak{D}_{A,\,mix} \left(\frac{\partial^2 C_A}{\partial r^2} \right)_t \tag{11-176}$$

To assist with the construction of a combined variable ζ that has a magnitude of zero at the gas–liquid interface for $t > 0$, it is necessary to redefine the radial coordinate as $y = r - R(t)$. The hierarchy can be summarized as follows: C_A depends on y and t, y depends on r and t, and R depends only on t. If C_A depends on y and t, then its total differential is

$$dC_A = \left(\frac{\partial C_A}{\partial y} \right)_t dy + \left(\frac{\partial C_A}{\partial t} \right)_y dt \tag{11-177}$$

and the partial derivatives of interest in the mass transfer equation, given by (11-176), are calculated via the chain rule:

$$\left(\frac{\partial C_A}{\partial r} \right)_t = \left(\frac{\partial C_A}{\partial y} \right)_t \left(\frac{\partial y}{\partial r} \right)_t = \left(\frac{\partial C_A}{\partial y} \right)_t \tag{11-178a}$$

$$\left(\frac{\partial^2 C_A}{\partial r^2} \right)_t = \left[\frac{\partial}{\partial r} \left(\frac{\partial C_A}{\partial y} \right)_t \right]_t = \left[\frac{\partial}{\partial y} \left(\frac{\partial C_A}{\partial y} \right)_t \right]_t \left(\frac{\partial y}{\partial r} \right)_t = \left(\frac{\partial^2 C_A}{\partial y^2} \right)_t \tag{11-178b}$$

$$\left(\frac{\partial C_A}{\partial t}\right)_r = \left(\frac{\partial C_A}{\partial y}\right)_t \left(\frac{\partial y}{\partial t}\right)_r + \left(\frac{\partial C_A}{\partial t}\right)_y = \left(\frac{\partial C_A}{\partial y}\right)_t \left(-\frac{dR}{dt}\right) + \left(\frac{\partial C_A}{\partial t}\right)_y \tag{11-178c}$$

Now the boundary layer mass transfer equation [i.e., (11-176)] for $C_A(y, t)$ becomes

$$\left(\frac{\partial C_A}{\partial t}\right)_y + \left(v_r - \frac{dR}{dt}\right)\left(\frac{\partial C_A}{\partial y}\right)_t = \mathfrak{D}_{A,\,\mathrm{mix}} \left(\frac{\partial^2 C_A}{\partial y^2}\right)_t \tag{11-179}$$

where the convective mass transfer term [i.e., the second term on the left side of (11-179)] contains the radial fluid velocity with respect to movement of the gas–liquid interface.

Radial Velocity Profile. The equation of continuity is employed to calculate v_r for one-dimensional flow in spherical coordinates. Incompressibility is a reasonable assumption because the fluid density is not expected to change much as oxygen, for example, diffuses across the gas–liquid interface. If v_θ and v_ϕ are negligible, one must solve

$$\nabla \cdot \mathbf{v} = \frac{1}{r^2}\frac{\partial}{\partial r}(r^2 v_r) = 0 \tag{11-180}$$

Hence, the product of r^2 and v_r is not a function of radial position in the liquid phase. Symmetry of this boundary layer problem with respect to both angular coordinates suggests that the product of r^2 and v_r is, at most, a function of time but not position. In other words, one should obtain the same function of time for the product of r^2 and v_r at any position in the liquid. This is summarized as follows:

$$r^2 v_r = [R(t)]^2 v_r[r = R(t)] = f(t) \tag{11-181}$$

where the fluid velocity at the gas–liquid interface is dR/dt. Time dependence of v_r is reasonable if one seeks the solution to this problem during the early stages of bubble growth, when its spherical shape exhibits stability in the liquid. The liquid-phase radial velocity component is

$$v_r = \left[\frac{R(t)}{r}\right]^2 \frac{dR}{dt} \tag{11-182}$$

and the important velocity term in the mass transfer equation for $C_A(y, t)$ is

$$v_r - \frac{dR}{dt} = \left\{\left[\frac{R(t)}{r}\right]^2 - 1\right\}\frac{dR}{dt} = \left[\left(1 - \frac{y}{r}\right)^2 - 1\right]\frac{dR}{dt}$$
$$= \left[-2\frac{y}{r} + \left(\frac{y}{r}\right)^2\right]\frac{dR}{dt} \tag{11-183}$$

If analysis of the mass transfer equation is performed during short contact times, then all of the following statements apply because $\delta_C(t)$ is small relative to $R(t)$:

$$\begin{aligned} \frac{\delta_C(t)}{R(t)} &\ll 1 \\ \frac{r}{R(t)} &\approx 1 \\ \frac{y}{R(t} &) \ll 1 \\ \left[1 + \frac{y}{R(t)}\right]^n &= 1 + n\left[\frac{y}{R(t)}\right] + \frac{1}{2!}n(n-1)\left[\frac{y}{R(t)}\right]^2 + \cdots \end{aligned} \tag{11-184}$$

The Taylor series in the final equation in (11-184) is employed to evaluate y/r and $(y/r)^2$, with truncation after the linear term. Hence,

$$\frac{y}{r} = y[R(t) + y]^{-1} = \varepsilon(1+\varepsilon)^{-1} \approx \varepsilon(1 - \varepsilon + \cdots) \tag{11-185a}$$

$$\left(\frac{y}{r}\right)^2 = y^2[R(t) + y]^{-2} = \varepsilon^2(1+\varepsilon)^{-2} \approx \varepsilon^2(1 - 2\varepsilon + \cdots) \tag{11-185b}$$

$$-2\frac{y}{r} + \left(\frac{y}{r}\right)^2 \approx -2\varepsilon + 3\varepsilon^2 - 2\varepsilon^3 + \cdots \tag{11-186}$$

where $\varepsilon = y/R(t)$. Truncation after the linear term of (11-186) yields the following expression for the radial fluid velocity with respect to the movement of the gas–liquid interface:

$$v_r - \frac{dR}{dt} \approx -2\frac{y}{R(t)}\frac{dR}{dt} \tag{11-187}$$

which can be rewritten in terms of the time-varying surface area of the bubble, $S(t)$. For example,

$$\begin{aligned} S(t) &= 4\pi[R(t)]^2 \\ \frac{dS}{dt} &= 8\pi R(t)\frac{dR}{dt} \\ \frac{d}{dt}\ln S(t) &= \frac{2}{R(t)}\frac{dR}{dt} \end{aligned} \tag{11-188}$$

Dimensionless Molar Density. The final form of the mass transfer equation for $C_A(y, t)$, which will be used to calculate the concentration profile and boundary layer thickness of species A in the liquid phase, is

$$\left(\frac{\partial C_A}{\partial t}\right)_y - y\frac{d}{dt}\ln S(t)\left(\frac{\partial C_A}{\partial y}\right)_t = \mathfrak{D}_{A,\,mix}\left(\frac{\partial^2 C_A}{\partial y^2}\right)_t \tag{11-189}$$

Now define a dimensionless concentration variable P (i.e., for the molar density profile) for mobile component A, such that

$$P(y,t) \equiv \frac{C_{\text{A, interface}} - C_{\text{A}}(y,t)}{C_{\text{A, interface}} - C_{\text{A, bulk}}} \tag{11-190}$$

where $C_{\text{A, interface}}$ represents the liquid-phase molar density of component A at the gas–liquid interface, assuming that interfacial equilibrium is established much faster than any of the important mass transfer rate processes occurs, and $C_{\text{A, bulk}}$ represents the molar density of component A in the bulk liquid phase, outside the mass transfer boundary layer. Since each important term in the mass transfer equation is linear in the molar density of mobile component A, it follows directly that each term is proportional to the overall concentration driving force, $C_{\text{A, interface}} - C_{\text{A, bulk}}$. Hence, one solves for $P(y,t)$ from

$$\left(\frac{\partial P}{\partial t}\right)_y - y\frac{d}{dt}\ln S(t)\left(\frac{\partial P}{\partial y}\right)_t = \mathfrak{D}_{\text{A, mix}}\left(\frac{\partial^2 P}{\partial y^2}\right)_t \tag{11-191}$$

subject to three boundary conditions:

$$C_{\text{A}} = C_{\text{A, interface}} \text{ (i.e., } P = 0) \qquad \text{at } r = R(t) \text{ (i.e., } y = 0) \text{ for all } t > 0 \tag{11-192a}$$

$$C_{\text{A}} = C_{\text{A, bulk}} \text{ (i.e., } P = 1) \qquad \text{at } t = 0 \text{ for all } r > R(t) \text{ (i.e., } y > 0) \tag{11-192b}$$

$$C_{\text{A}} = C_{\text{A, bulk}} \text{ (i.e., } P = 1) \qquad \text{at finite time when } r \to \infty \text{ (i.e., } y \to \infty) \tag{11-192c}$$

Condition (11-192c) is analogous to the boundary layer boundary condition given by (11-12b), because component A will not diffuse infinitely far into the quiescent liquid during analysis over a finite time scale.

Combination of Variables. Condition (11-192c) and the reconstruction of the independent variable measured normal to the gas–liquid interface [i.e., $y = r - R(t)$] suggest that a combination-of-variables approach will be advantageous in solving for the concentration profile of species A and the mass transfer boundary layer thickness. The overall objective is to reduce the second-order partial differential mass transfer equation for $P(y,t)$, given by (11-191), to a second-order ordinary differential equation for $P(\zeta)$ in which the three boundary conditions given by (11-192) are equivalent to two conditions without discarding any information about the system. In the process, one identifies a first-order ODE for the mass transfer boundary layer thickness. The combined independent variable ζ is constructed in terms of the coordinate measured normal to the gas–liquid interface and the mass transfer boundary layer thickness. Furthermore, the coordinate measured normal to the interface should have a magnitude of zero at the interface. Hence,

$$\zeta = \frac{r - R(t)}{\delta_C(t)} = \frac{y}{\delta_C(t)} \tag{11-193}$$

Now, the hierarchy is summarized once again: C_A depends on P, P depends on ζ, ζ is a function of y and δ_C, and δ_C depends on t. One should not consider that independent variable y depends on r and t, because this was done previously, leading to a convective mass transfer term that contains the radial fluid velocity with respect to the motion of the interface. The appropriate partial derivatives of interest in the mass transfer equation are expressed in terms of P, ζ, and δ_C. Detailed calculations are exactly the same as those provided by equations (11-58):

$$\left(\frac{\partial P}{\partial y}\right)_t = \frac{1}{\delta_C}\frac{dP}{d\zeta}$$
$$\left(\frac{\partial^2 P}{\partial y^2}\right)_t = \left(\frac{1}{\delta_C}\right)^2 \frac{d^2P}{d\zeta^2} \tag{11-194}$$
$$\left(\frac{\partial P}{\partial t}\right)_y = -\frac{\zeta}{\delta_C}\frac{d\delta_C}{dt}\frac{dP}{d\zeta}$$

Upon substitution into the mass transfer equation for $P(y, t)$, given by (11-191), with $y = \zeta\delta_C$, one obtains

$$-\frac{\zeta}{\delta_C}\frac{d\delta_C}{dt}\frac{dP}{d\zeta} - \zeta\delta_C\frac{d\ln S(t)}{dt}\frac{1}{\delta_C}\frac{dP}{d\zeta} = \mathfrak{D}_{A,\,mix}\left(\frac{1}{\delta_C}\right)^2\frac{d^2P}{d\zeta^2} \tag{11-195}$$

Multiplication of (11-195) by $(\delta_C)^2$ yields

$$-\left[\delta_C\frac{d\delta_C}{dt} + (\delta_C)^2\frac{d\ln S(t)}{dt}\right]\zeta\frac{dP}{d\zeta} = \mathfrak{D}_{A,\,mix}\frac{d^2P}{d\zeta^2} \tag{11-196}$$

Since the quantity in brackets on the left side of (11-196) is written completely in terms of time-dependent quantities and has dimensions of a diffusivity, it is removed from the mass transfer equation and set equal to $2\mathfrak{D}_{A,\,mix}$ to assist the combination-of-variables approach in achieving its objectives. In other words,

$$-2\zeta\frac{dP}{d\zeta} = \frac{d^2P}{d\zeta^2} \tag{11-197a}$$

$$\delta_C\left(\frac{d\delta_C}{dt}\right) + (\delta_C)^2\frac{d\ln S(t)}{dt} = 2\mathfrak{D}_{A,\,mix} \tag{11-197b}$$

where $\mathfrak{D}_{A,\,mix}$ represents a diffusivity in (11-197b), because the corresponding heat transfer problem contains the thermal diffusivity α on the right side of (11-197b). The dimensionless molar density profile of mobile component A is obtained from (11-197a), and the mass transfer boundary layer thickness is calculated from (11-197b). The initial condition for the boundary layer thickness is $\delta_C = 0$ at $t = 0$. The three conditions on $P(\zeta)$ are (in the same order that they

were presented above via 11-192):

$$P = 0 \qquad \text{at } r = R(t), \text{ (i.e., } y = 0) \text{ for all } t > 0, \zeta = 0 \tag{11-198a}$$

$$P = 1 \qquad \text{at } t = 0 \text{ for all } r > R(t) \text{ (i.e., } y > 0), \zeta \to \infty \tag{11-198b}$$

$$P = 1 \qquad \text{at finite time when } r \to \infty \text{ (i.e., } y \to \infty), \zeta \to \infty \tag{11-198c}$$

Error Function Molar Density Profile. The fact that conditions (11-198*b*) and (11-198*c*) are the same provides some support for the combination-of-variables approach. The solution of (11-197*a*) for the concentration profile, subject to conditions (11-198*a*) to (11-198*c*), was described in Section 11-6.1 for steady-state boundary layer mass transfer across a zero-shear stationary gas–liquid interface. The final result for mobile component A is

$$P(\zeta) = \frac{C_{\text{A, interface}} - C_{\text{A}}(y,t)}{C_{\text{A, interface}} - C_{\text{A, bulk}}} = \frac{2}{\sqrt{\pi}} \int \exp(-x^2)\, dx = \text{erf}(\zeta) \tag{11-199}$$

where integration is performed over the range $0 \le x \le \zeta$.

Mass Transfer Boundary Layer Thickness. When equation (11-197*b*) is multiplied by $[S(t)]^2$, integration of the ODE for $\delta_C(t)$ is simplified considerably:

$$[S(t)]^2 \delta_C \frac{d\delta_C}{dt} + (\delta_C)^2 S(t) \frac{dS}{dt} = \frac{d}{dt}\left[\frac{1}{2}(\delta_C S)^2\right] = 2\mathcal{D}_{\text{A, mix}}[S(t)]^2 \tag{11-200}$$

Using t as the independent time variable and t' as the integration variable, where t' ranges from 0 to t, (11-200) is integrated to yield an expression for the mass transfer boundary layer thickness:

$$\frac{1}{2}[\delta_C(t) S(t)]^2 = 2\mathcal{D}_{\text{A, mix}} \int_0^t [S(t')]^2\, dt' \tag{11-201}$$

Rearrangement reveals the effect of a time-varying interfacial surface area, in general:

$$\delta_C(t) = \left\{ 4\mathcal{D}_{\text{A, mix}} \left[\frac{1}{S(t)}\right]^2 \int_0^t [S(t')]^2\, dt' \right\}^{1/2} \tag{11-202}$$

This result reduces to the classic penetration theory of mass transfer for unsteady-state diffusion across a stationary interface into a stagnant liquid when $S(t)$ is constant [i.e., $S(t) = S(t') = \text{constant}$]. Under these conditions, (11-202) for δ_C becomes

$$\delta_C(t) = \sqrt{4\mathcal{D}_{\text{A, mix}} t} \tag{11-203}$$

For mobile or stationary interfaces, the mass transfer boundary layer thickness scales as the one-half power of $\mathfrak{D}_{\mathrm{A,\,mix}}$, which represents the diffusivity for mass transfer. One must replace the mass diffusivity by the thermal diffusivity,

$$\alpha = \frac{k_{\mathrm{TC}}}{\rho C_{\mathrm{p}}} \tag{11-204}$$

to calculate the thermal boundary layer thickness for unsteady-state heat transfer across mobile or stationary gas–liquid interfaces.

Local Interfacial Molar Flux. Results for $P(\zeta)$ and $\delta_C(t)$ via (11-199) and (11-202), respectively, represent basic information from which interphase mass transfer correlations can be developed. Gas–liquid mass transfer of mobile component A occurs because it is soluble in the liquid phase, and there is a nonzero radial component of the total molar flux of A, evaluated at $r = R(t)$. Even though motion of the interface induces convective mass transfer in the radial direction, there is no relative velocity of the fluid with respect to the interface at $r = R(t)$. It should be emphasized that a convective contribution to interphase mass transfer in the radial direction occurs only when motion of the interface differs from v_r of the liquid at $r = R$. Hence, Fick's first law of diffusion is sufficient to calculate the molar flux of species A normal to the interface at $r = R(t)$ when $t > 0$:

$$\begin{aligned} N_{\mathrm{A}r}[r = R(t)] &= -\mathfrak{D}_{\mathrm{A,\,mix}} \left(\frac{\partial C_{\mathrm{A}}}{\partial r}\right)_{r=R(t)} \\ &= -\mathfrak{D}_{\mathrm{A,\,mix}} \frac{dC_{\mathrm{A}}}{dP} \left(\frac{dP}{d\zeta}\right)_{\zeta=0} \left(\frac{\partial \zeta}{\partial y}\right)_{t>0} \left(\frac{\partial y}{\partial r}\right)_{t} \\ &\equiv k_{C,\,\mathrm{local}}(t)(C_{\mathrm{A,\,interface}} - C_{\mathrm{A,\,bulk}}) \end{aligned} \tag{11-205}$$

where $\mathfrak{D}_{\mathrm{A,\,mix}}$ represents a molecular transport property in Fick's law and the local mass transfer coefficient $k_{C,\,\mathrm{local}}$ is time dependent for this unsteady-state analysis. The appropriate derivatives of interest are evaluated as

$$\begin{aligned} \frac{dC_{\mathrm{A}}}{dP} &= -(C_{\mathrm{A,\,interface}} - C_{\mathrm{A,\,bulk}}) \\ \left(\frac{dP}{d\zeta}\right)_{\zeta=0} &= \frac{2}{\sqrt{\pi}} \\ \left(\frac{\partial \zeta}{\partial y}\right)_{t>0} &= \frac{1}{\delta_C(t)} \\ \left(\frac{\partial y}{\partial r}\right)_{t} &= 1 \end{aligned} \tag{11-206}$$

These results are similar to those for interphase mass transfer across solid–liquid interfaces, given by (11-109) and (11-110). Hence, the penetration theory for

gas–liquid mass transfer across a mobile interface yields the following expression for the local mass transfer coefficient:

$$k_{C,\,\text{local}}(t) = \frac{2}{\sqrt{\pi}} \frac{\mathfrak{D}_{\text{A, mix}}}{\delta_C(t)} \tag{11-207}$$

where $\mathfrak{D}_{\text{A, mix}}$ represents a molecular transport property in (11-207), but one must remember that δ_C contains $\mathfrak{D}_{\text{A, mix}}$ as a diffusivity. This distinction between molecular transport properties and diffusivities is necessary to construct the corresponding local heat transfer coefficient by analogy. In other words, $\mathfrak{D}_{\text{A, mix}}$ in (11-207) must be replaced by the thermal conductivity k_{TC}, which is the molecular transport property for heat transfer via Fourier's law, but the thermal boundary layer thickness requires the thermal diffusivity α. The previous result for $k_{C,\,\text{local}}$, given by (11-207), should be compared with the earlier one for steady-state boundary layer mass transfer across a stationary spherical gas–liquid interface, given by (11-160). The primary difference is that this penetration theory analysis generates time-dependent expressions for $k_{C,\,\text{local}}$ and δ_C, whereas steady-state boundary layer analysis with two-dimensional flow within δ_C reveals that $k_{C,\,\text{local}}$ and δ_C are functions of independent variable θ, which is measured parallel to the gas–liquid interface. If one adopts equation (11-202) for the mass transfer boundary layer thickness, then the final expression for the local mass transfer coefficient is

$$k_{C,\,\text{local}}(t) = \frac{(\mathfrak{D}_{\text{A, mix}}/\pi)^{1/2} S(t)}{\left\{ \displaystyle\int_0^t [S(t')]^2 \, dt' \right\}^{1/2}} \tag{11-208}$$

Time-Averaged Properties. The unsteady-state macroscopic mass balance for mobile component A is applied to the quiescent liquid, where the rate of interphase mass transfer via equation (11-205) is interpreted as an input term due to diffusion across the gas–liquid interface. There are no output terms, sources, sinks, or contributions from convective mass transfer in the macroscopic mass balance. Hence, the accumulation rate process is balanced by the rate of interphase mass transfer across time-varying surface $S(t)$, where both terms have dimensions of moles per time:

$$\frac{d[\text{moles}]_{\text{A}}}{dt} = S(t) N_{\text{A}r}[r = R(t)] = k_{C,\,\text{local}}(t) S(t) (C_{\text{A, interface}} - C_{\text{A, bulk}}) \tag{11-209}$$

This expression is integrated from $t'' = 0$, when gas–liquid contact initially occurs, to present time t to calculate the total number of moles of species A that has been transported across the interface. The integration variable in the following equation is t'', which varies from 0 to t:

$$[\text{moles}(t)]_{\text{A}} = \int_0^t d[\text{moles}]_{\text{A}} = (C_{\text{A, interface}} - C_{\text{A, bulk}}) \times \int_0^t S(t'') k_{C,\,\text{local}}(t'') \, dt'' \tag{11-210}$$

$$k_{C,\,\text{local}}(t'') = \frac{(\mathfrak{D}_{\text{A, mix}}/\pi)^{1/2} S(t'')}{\left\{\int_0^{t''} [S(t')]^2\, dt'\right\}^{1/2}} \tag{11-211}$$

This time-averaged calculation is presented below in terms of Ω, which is defined by

$$\Omega(t'') = \int_0^{t''} [S(t')]^2\, dt' \tag{11-212}$$

Hence,

$$[\text{moles}(t)]_{\text{A}} = \left(\frac{\mathfrak{D}_{\text{A, mix}}}{\pi}\right)^{1/2} (C_{\text{A, interface}} - C_{\text{A, bulk}}) \int_0^t [\Omega(t'')]^{-1/2}\, d\Omega \tag{11-213}$$

where the Leibnitz rule for differentiating $\Omega(t'')$ with respect to t'' is employed. In general, if the following integral expression for $h(t)$ exhibits time dependence in the integrand and both limits of integration:

$$h(t) = \int g(x, t)\, dx \qquad a(t) \le x \le b(t) \tag{11-214}$$

then

$$\frac{dh}{dt} = g[b(t), t]\frac{db}{dt} - g[a(t), t]\frac{da}{dt} + \int_{a(t)}^{b(t)} \left(\frac{\partial g}{\partial t}\right)_x dx \tag{11-215}$$

Based on the defining equation for $\Omega(t'')$, all the functional dependence of Ω on t'' appears in the upper limit of integration. Therefore, only the first term on the right side of (11-215) (i.e., Leibnitz's rule) is required to calculate $d\Omega/dt''$, after one associates surface area S with the generic integrand g. The result is

$$\frac{d\Omega}{dt''} = [S(t'')]^2 \tag{11-216}$$

The total number of moles of species A that has been transported across the gas–liquid interface at time t is

$$\begin{aligned}[\text{moles}(t)]_{\text{A}} &= 2\left(\frac{\mathfrak{D}_{\text{A, mix}}}{\pi}\right)^{1/2} (C_{\text{A, interface}} - C_{\text{A, bulk}})\{[\Omega(t)]^{1/2} - [\Omega(t=0)]^{1/2}\} \\ &= 2\left(\frac{\mathfrak{D}_{\text{A, mix}}}{\pi}\right)^{1/2} (C_{\text{A, interface}} - C_{\text{A, bulk}}) \left\{\int_0^t [S(t')]^2\, dt'\right\}^{1/2}\end{aligned} \tag{11-217}$$

Generic Example. Consider a simple nth-order power function that describes the time-dependent volume of an oxygen bubble, $V(t)$. The bubble expands into

an incompressible liquid, according to

$$V(t) = \tfrac{4}{3}\pi[R(t)]^3 = \beta t^n \tag{11-218}$$

where β is a positive constant. It is desired to obtain expressions for (a) the mass transfer boundary layer thickness, (b) the local mass transfer coefficient, and (c) the total number of moles of O_2 that has been transported across the gas–liquid interface into the quiescent liquid.

SOLUTION. Expression (11-218) for $V(t)$ allows one to calculate the time-dependent radius $R(t)$ and surface area $S(t)$ of the bubble. Hence,

$$R(t) = \left(\frac{3\beta}{4\pi}\right)^{1/3} t^{n/3}$$

$$S(t) = 4\pi[R(t)]^2 = C_1 t^{2n/3}$$

where the constant C_1 is given by $4\pi(3\beta/4\pi)^{2/3}$. All the desired quantities in parts (a), (b), and (c) contain the following integral of $S(t)$:

$$\int_0^t [S(t')]^2\,dt' = (C_1)^2 \int_0^t (t')^{4n/3}\,dt' = \frac{3(C_1)^2}{4n+3} t^{(4n/3)+1}$$

(a) Mass transfer boundary layer thickness:

$$\delta_C(t) = \left\{ 4\mathfrak{D}_{\mathrm{A,\,mix}} \left[\frac{1}{S(t)}\right]^2 \int_0^t [S(t')]^2\,dt' \right\}^{1/2} = \sqrt{\frac{4\mathfrak{D}_{\mathrm{A,\,mix}} t}{\kappa}} \tag{11-219}$$

where $\kappa = (4n/3) + 1$. Notice that δ_C scales as the one-half power of the product of $\mathfrak{D}_{\mathrm{A,\,mix}}$ and time. The classic penetration theory analysis for unsteady state radial diffusion across a stationary gas–liquid interface into a stagnant liquid is obtained by letting $n = 0$ and $\kappa = 1$. Relative to a stationary interface, the mass transfer boundary layer thickness is thinner when the interface expands. This is obvious in (11-219) because $\kappa > 1$ when $n > 0$.

(b) Local mass transfer coefficient:

$$k_{C,\,\mathrm{local}}(t) = \frac{(\mathfrak{D}_{\mathrm{A,\,mix}}/\pi)^{1/2} S(t)}{\left\{ \int_0^t [S(t')]^2\,dt' \right\}^{1/2}} = \sqrt{\frac{\kappa \mathfrak{D}_{\mathrm{A,\,mix}}}{\pi t}}$$

This transfer coefficient, which varies inversely with the resistance to mass transfer, scales as the one-half power of the quotient of $\mathfrak{D}_{\mathrm{A,\,mix}}$ and time. Since the

resistance is smaller when the interface expands, relative to the stationary interface, one predicts larger mass transfer coefficients and larger rates of interphase mass transfer when surface stretch is operative. Notice how these results for δ_C and $k_{C,\,\text{local}}$ depend on the exponent n in the power function for $V(t)$, but not the parameter β.

(c) Total number of moles of O_2 transported across the gas–liquid interface:

$$[\text{moles}(t)]_A = 2\left(\frac{\mathfrak{D}_{A,\,\text{mix}}}{\pi}\right)^{1/2}(C_{A,\,\text{interface}} - C_{A,\,\text{bulk}})\left\{\int_0^t [S(t')]^2\,dt'\right\}^{1/2}$$

$$= 2C_1\left(\frac{\mathfrak{D}_{A,\,\text{mix}}}{\pi}\right)^{1/2}(C_{A,\,\text{interface}} - C_{A,\,\text{bulk}})\left(\frac{t^\kappa}{\kappa}\right)^{1/2}$$

The classic penetration theory of gas–liquid mass transfer across a stationary interface (i.e., $n = 0$, $\kappa = 1$) reveals $\sqrt{t}$ dependence for the total number of moles of O_2 that has been transported into the quiescent liquid. In general, the functional dependence of $[\text{moles}(t)]_A$ on time scales as $t^{(2n/3)+1/2}$. The volume of the bubble must increase according to $t^{3/4}$, or its radius must increase as $t^{1/4}$ to realize a linear increase in $[\text{moles}(t)]_A$ vs. time throughout the duration of the process.

Addition of Resistances for Bubbles That Translate (i.e., Rise) and Expand in a Quiescent Liquid. Consider the addition of mass transfer resistances when gas bubbles translate and expand simultaneously. The simplest analysis of this rather complex problem focuses on each process separately, such that the mass transfer boundary layer thickness depends on polar coordinate θ due to translation and time t due to surface stretch. These two processes do not occur sequentially, or in series. The fact that they occur simultaneously suggests that they should be modeled in parallel, where the overall resistance is obtained from the inverse sum of resistances law. Since mass transfer coefficients represent the inverse of a resistance, and one must add resistances inversely for processes that occur in parallel, the overall mass transfer coefficient for this problem is obtained by adding the local mass transfer coefficient for each individual process. Hence,

$$k_{C,\,\text{overall}}(\theta, t) = k_{C,\,\text{translation}}(\theta) + k_{C,\,\text{expansion}}(t) \tag{11-220}$$

The steady-state result for $k_{C,\,\text{translation}}(\theta)$, which accounts for two-dimensional flow within δ_C, is given by equation (11-160), and the corresponding boundary layer thickness in the potential flow regime is given by equation (11-155). Transient analysis for $k_{C,\,\text{expansion}}(t)$ is provided by equation (11-208). The fixed bubble radius R for steady-state analysis is replaced by the instantaneous radius of the growing bubble $R(t)$ from the modified penetration theory problem. The dimensionless numbers (i.e., Re·Sc) in equation (11-153) for $\delta_C(\theta)$ should be evaluated using a time-varying bubble diameter [i.e., $2R(t)$]. There is no rigorous justification for employing variable radius $R(t)$ in the steady-state analysis of $k_{C,\,\text{translation}}(\theta)$. Hence, one should realize that this strategy only yields a first approximation for $k_{C,\,\text{overall}}(\theta, t)$.

PROBLEMS

11-1. Use one sentence and qualitatively explain why factors of $1/r^2$ and r^2 appear in mass transfer equation B.10-3 in Bird *et al.* (2002, p. 850) for radial transport in spherical coordinates.

11-2. What important dimensionless number(s) appear in the dimensionless partial differential mass transfer equation for laminar flow through a blood capillary when the important rate processes are axial convection, radial diffusion, and nth-order irreversible chemical reaction?

11-3. The following information is provided for flow around a spherical submerged object with interphase mass transfer into the passing fluid stream:

$$C_{\mathrm{A,\,equilibrium}} = \text{molar density of component A at the interface}$$

$$C_{\mathrm{A,\,bulk}} = \text{molar density of component A within the approaching fluid stream}$$

$$\theta = \frac{\pi}{2} \text{ at the equatorial position of the submerged object}$$

$$\frac{\delta_C(\theta = \pi/2)}{R} = 0.20, \text{ thickness of the mass transfer boundary layer}$$

$$\frac{r}{R} = 1.10, \text{ radial position within the mass transfer boundary layer}$$

Write a sequence of three logical steps that is required to calculate a numerical value for the molar density C_A of mobile component A at position r and θ, indicated above, within the liquid phase for:

(a) Laminar flow of an incompressible Newtonian fluid around a solid sphere of radius R.

(b) Potential flow of an incompressible fluid around a gas bubble of radius R.

11-4. Obtain analytical expressions for the liquid-phase mass transfer boundary layer thickness for **(a)** creeping flow, and **(b)** potential flow around a gas bubble of radius R. In which case will the boundary layer thickness be larger at the same relative position along the surface of the bubble?

11-5. Compare mass transfer boundary layer thicknesses for creeping flow of identical fluids around **(a)** a solid sphere, and **(b)** a gas bubble at the same value of the Reynolds number. In which case is the boundary layer thickness greater?

11-6. **(a)** Calculate the mass transfer boundary layer thickness at the equatorial position (i.e., $\theta = 90^\circ = \pi/2$) of a sucrose pellet in aqueous solution. The sucrose pellets are spherical with a diameter of 1 mm, and the

approach velocity of the aqueous phase is 6.5 cm/min. For a 20 wt% sucrose solution, the physical properties of interest are

$$\text{density} = 1.0829 \text{ g/cm}^3 \text{ at } 20^\circ\text{C}$$

$$\text{viscosity} = 1.967 \times 10^{-2} \text{ g/cm·s at } 20^\circ\text{C}$$

$$\text{binary molecular diffusion coefficient} = 0.50 \times 10^{-5} \text{ cm}^2\text{/s at } 25^\circ\text{C}$$

(b) Calculate the maximum error at the equatorial position of the pellet due to the neglect of curvature in the radial term of the equation of continuity.

11-7. Air bubbles rise through a cylindrical column that is filled with water and a small amount of pyrene butyric acid [i.e., PBA, $R-(CH_2)_3COOH$, where R represents a diamondlike pattern of four aromatic rings that share common sides]. The Reynolds number is 230, based on a bubble diameter of 1 mm, and the Schmidt number for dissolved oxygen in the aqueous phase is 475. PBA is an excellent indicator of dissolved oxygen concentration in water and biological tissues. The fluorescence lifetime of PBA is about 165 ns at ambient temperature. When oxygen diffuses across the gas–liquid interface and interacts with PBA, the fluorescence lifetime (i.e., 65 ns) and the fluorescence intensity decrease at higher oxygen concentrations. A nitrogen laser, which emits 6 mJ of energy at 337 nm during each 10-ns pulse, induces fluorescence excitation of PBA, and a CCD (i.e., charge-coupled device) camera measures the fluorescence emission of PBA/O_2. These types of laser-induced fluorescence experiments are useful to measure the thickness of the mass transfer boundary layer on the liquid side of the gas–liquid interface and the oxygen concentration profile throughout the boundary layer. See, for example, Roy, S; "Laser-induced fluorescence studies of gas transfer at bubble surfaces", PhD thesis, Auburn University (2001). The dissolved oxygen concentration is $\approx$9 mg/L at the air–water interface and about four orders of magnitude smaller in the bulk liquid phase.

(a) Estimate the thickness of the mass transfer boundary layer in the liquid phase at the equatorial position where $\theta = \pi/2$. The bubble diameter is 1 mm.

(b) What is the maximum error introduced at the equatorial position of the bubble by invoking the thin mass transfer boundary layer approximation in the mass transfer equation?

$$\frac{1}{r^2}\frac{\partial}{\partial r}\left(r^2\frac{\partial C_A}{\partial r}\right) \approx \frac{\partial^2 C_A}{\partial r^2}$$

(c) Which concentration profile should be used to compare theory with experimental data from the laser-induced fluorescence technique?

11-8. (a) Oxygen bubbles rise through a quiescent liquid (i.e., water) that is incompressible and Newtonian. Sketch the molar density profile of oxygen $C_A(r, \theta = \pi/4)$ at 25°C in the liquid-phase mass transfer boundary layer as a function of radial position r for the following Reynolds numbers: Re = 0.1, 10, and 200. Put C_A on the vertical axis and r on the horizontal axis. Include three curves on one set of axes and label each curve with the appropriate value of the Reynolds number.

(b) When Re = 10, sketch C_A vs. r at $\theta = \pi/4$ under isothermal conditions when the temperature T is 25 and 37°C. In each case, the bulk molar density of O_2 in the liquid phase outside the mass transfer boundary layer is approximately zero. Put C_A on the vertical axis and r on the horizontal axis. Include two curves on one set of axes and label each curve with the appropriate temperature. Remember that the equilibrium solubility of gases in liquids decreases at higher temperature.

11-9. (a) Oxygen bubbles rise through stagnant water. Calculate the dimensionless molar density of solubilized O_2 [i.e., $P(\zeta)$] at position $r/R = 1.02$ and $\theta = \pi/2$ within the liquid-phase mass transfer boundary layer for oxygen transport into water at 20°C when Re = 10 and Sc = 460. Given; $\Gamma(\frac{1}{2}) = \sqrt{\pi} = \pi^{1/2}$ and $\Gamma(\frac{1}{3}) = 2.679$. The incomplete gamma function for argument $n > 0$ and variable λ,

$$\mathbb{S}(n, \lambda) \equiv \frac{\int_0^\lambda z^{n-1} \exp(-z)\, dz}{\Gamma(n)} \qquad 0 \le z \le \lambda$$

can be expressed in terms of the following polynomial expansion:

$$\mathbb{S}(n, \lambda) \equiv \frac{\int_0^\lambda \left[\sum_{k=0}^{\infty} (-1)^k z^{k+n-1}/k!\right] dz}{\Gamma(n)}$$

$$= \frac{\lambda^n}{\Gamma(n)} \sum_{k=0}^{\infty} \frac{(-\lambda)^k}{k!(k+n)}$$

Include three terms in the series (i.e., $k = 0, 1, 2$) to calculate $P(\zeta)$ for O_2 transport into water at $r/R = 1.02$ and $\theta = \pi/2$.

Answer: In the potential flow regime, the mass transfer boundary layer thickness at the equatorial position of the bubble is calculated as follows via equation (11-155):

$$\frac{\delta_C(\theta = \pi/2)}{R} = 2\left(\frac{8}{9\text{Re}\cdot\text{Sc}}\right) = 2.8 \times 10^{-2}$$

As one moves into the fluid, normal to the gas–liquid interface at the equatorial position such that $r/R = 1.02$, the value of the combined variable ζ is

$$\zeta = \frac{r - R}{\delta_C(\theta = \pi/2)} = 0.72$$

This allows one to calculate the dimensionless molar density profile $P(\zeta)$ for O_2 transport in water at the particular values of r and θ mentioned above. Since the gas–liquid interface is characterized by zero shear and perfect slip, $P(\zeta)$ is obtained from the incomplete gamma function when the argument $n = \frac{1}{2}$ and the variable $\lambda = \zeta^2$. The first three terms of the infinite series yield the following result:

$$\begin{aligned} P(\zeta = 0.72) &= \frac{C_{\text{A, equilibrium}} - C_{\text{A}}(r/R = 1.02, \theta = \pi/2)}{C_{\text{A, equilibrium}} - C_{\text{A, bulk}}} \\ &= \mathbb{S}\left(n = \frac{1}{2}, \lambda = \zeta^2\right) \\ &= \frac{\zeta}{\Gamma\left(\frac{1}{2}\right)} \sum_{k=0}^{\infty} \frac{(-\zeta^2)^k}{k!\left(k + \frac{1}{2}\right)} \\ &= \frac{\zeta}{\Gamma\left(\frac{1}{2}\right)} \left\{2 - \tfrac{2}{3}\zeta^2 + \tfrac{1}{5}\zeta^4 - \cdots\right\} = 0.69 \end{aligned}$$

(b) Calculate the maximum error in this mass transfer analysis at $r = R + \delta_C$ if the effect of curvature is neglected in the radial term of the equation of continuity.

Answer: The radial component of the fluid velocity vector for potential flow around a stationary nondeformable bubble is

$$v_r(r, \theta) = V_{\text{approach}} \cos\theta (1 - \eta^{-3})$$

Hence,

$$\frac{\partial \ln v_r}{\partial \ln r} = \frac{3}{\eta^3 - 1}$$

The curvature correction factor $F(\eta)$ for the radial term in the equation of continuity is calculated as follows:

$$\frac{1}{r^2}\frac{\partial(r^2 v_r)}{\partial r} = F(\eta)\frac{\partial v_r}{\partial r}$$

where

$$F(\eta) = 1 + \frac{2}{\partial \ln v_r / \partial \ln r} = 1 + \frac{2}{3}(\eta^3 - 1)$$

The maximum error that is obtained by neglecting the effects of curvature in the equation of continuity, and approximating $(1/r^2)\,\partial(r^2 v_r)/\partial r$ by $\partial v_r/\partial r$, occurs at the outer edge of the mass transfer boundary layer, where $\eta_{\text{maximum}} = 1 + \delta_C(\theta)/R$. At the equatorial position of the bubble in this analysis, $\eta_{\text{maximum}} = 1.028$. Hence,

$$F(\eta_{\text{maximum}}) = 1.058$$

$$\text{maximum error } (\%) = 100\left(\frac{F(\eta_{\text{maximum}}) - 1}{F(\eta_{\text{maximum}})}\right) = 5.4\%$$

One should realize that these calculations are based on an expression for v_r which corresponds to potential flow past a stationary nondeformable bubble, as seen by an observer in a stationary reference frame. However, this analysis rigorously requires the radial velocity profile for potential flow in the liquid phase as a nondeformable bubble rises through an incompressible liquid that is stationary far from the bubble. When submerged objects are in motion, it is important to use liquid-phase velocity components that are referenced to the motion of the interface for boundary layer mass transfer analysis. This is accomplished best by solving the flow problem in a body-fixed reference frame which translates and, if necessary, rotates with the bubble such that the center of the bubble and the origin of the coordinate system are coincident. Now the problem is equivalent to one where an ideal fluid impinges on a stationary nondeformable gas bubble of radius R. As illustrated above, results for the latter problem have been employed to estimate the maximum error associated with the neglect of curvature in the radial term of the equation of continuity.

(c) Calculate the maximum error in this mass transfer analysis at $r = R + \delta_C$ if the effect of curvature is neglected in the radial term of the mass transfer equation.

Answer: For boundary layer mass transfer in an incompressible liquid that contacts a zero-shear interface, a previous example problem on pages 311 and 312 reveals that the relative importance of the second term on the right side of the spherical coordinate expression for radial diffusion,

$$\frac{1}{r^2}\frac{\partial}{\partial r}\left(r^2\frac{\partial C_A}{\partial r}\right) = \frac{\partial^2 C_A}{\partial r^2}\left(1 + \frac{2}{\partial \ln \beta/\partial \ln r}\right)$$

is

$$\%\text{ error} = \frac{200}{2 + (\partial \ln \beta/\partial \ln r)_{\theta,\zeta=1}} = -100(\eta_{\text{maximum}} - 1)$$

where $\beta = \partial C_A/\partial r$, and

$$\eta_{\text{maximum}} = \left(\frac{r}{R}\right)_{\text{maximum}} = 1 + \frac{\delta_C(\theta)}{R}$$

At the equatorial position of the gas bubble, $\eta_{\text{maximum}} = 1.028$, which corresponds to a maximum error of 2.8% at η_{maximum} by invoking the following approximation for radial diffusion in the mass transfer equation:

$$\frac{1}{r^2}\frac{\partial}{\partial r}\left(r^2\frac{\partial C_{\text{A}}}{\partial r}\right) \approx \frac{\partial^2 C_{\text{A}}}{\partial r^2}$$

11-10. We explore here mass transfer coefficients in terms of the stream function. Write an expression for the surface-averaged dimensionless mass transfer coefficient for laminar flow of an incompressible Newtonian fluid around a stationary gas bubble in terms of the appropriate dimensionless numbers and the dimensionless stream function Ψ^*. Use the approach velocity of the fluid and the radius of the bubble to construct a characteristic volumetric flow rate to make Ψ dimensionless.

Answer: When the local mass transfer coefficient is averaged over the front hemisphere of the bubble, the Sherwood number can be written as follows via (11-167):

$$\text{Sh}_{\text{average}} = \sqrt{\frac{8}{\pi}}(\text{Re}\cdot\text{Sc})^{1/2}\left[\int v_\theta^*(\eta = 1, \theta)\sin^2\theta\, d\theta\right]^{1/2} \qquad 0 \le \theta \le \pi/2$$

The tangential velocity component in spherical coordinates is expressed in terms of the stream function Ψ for two-dimensional axisymmetric flow as

$$v_\theta(r, \theta) = V_{\text{approach}} v_\theta^*(\eta, \theta) = \frac{1}{r\sin\theta}\left(\frac{\partial \Psi}{\partial r}\right)_\theta$$

The stream function Ψ and radial coordinate r are written in terms of dimensionless variables Ψ^* and η as follows:

$$\Psi = V_{\text{approach}} R^2 \Psi^* \qquad r = R\eta$$

Hence,

$$V_{\text{approach}} v_\theta^*(\eta, \theta) = \frac{1}{R\eta\sin\theta}\left[\frac{\partial(V_{\text{approach}} R^2\Psi^*)}{\partial(R\eta)}\right]_\theta$$

$$v_\theta^*(\eta, \theta) = \frac{1}{\eta\sin\theta}\left(\frac{\partial \Psi^*}{\partial \eta}\right)_\theta$$

At the gas–liquid interface, the dimensionless tangential velocity in the liquid phase is

$$v_\theta^*(\eta = 1, \theta) = \frac{1}{\sin\theta}\left(\frac{\partial \Psi^*}{\partial \eta}\right)_{\eta=1}$$

The final expression for the surface-averaged Sherwood number in terms of the dimensionless stream function for laminar flow around a bubble is

$$\mathrm{Sh}_{\mathrm{average}} = \sqrt{\frac{8}{\pi}}(\mathrm{Re}\cdot\mathrm{Sc})^{1/2}\left[\int\left(\frac{\partial\Psi^*}{\partial\eta}\right)_{\eta=1}\sin\theta\,d\theta\right]^{1/2} \qquad 0 \le \theta \le \pi/2$$

11-11. Consider low-Reynolds-number viscous flow of an incompressible Newtonian fluid transverse to a long solid cylinder of radius R and length L. The approach velocity of the fluid, far from the cylinder, is $\delta_x V_{\mathrm{approach}}$ in the x direction, not in the z direction. The fluid–solid interface is characterized by high shear and no slip, and the temperature at the outer edge of the solid cylinder T_{solid} is much higher than the temperature of the approaching fluid T_∞. The fluid dynamics solution to this two-dimensional creeping flow problem is provided by Bird *et al.*, (2002, p. 108, Prob. 3B.9).

(a) Identify 10 key steps, in logical order, which must be implemented to analyze boundary layer heat transfer in the fluid phase adjacent to the submerged object, and calculate the local heat transfer coefficient h_{local}. Write 10 qualitative statements that do not contain any equations.

Answer:

1. Write the steady-state thermal energy balance for an incompressible fluid which includes transport by convection and conduction. Neglect viscous dissipation.

2. Neglect thermal energy transport by conduction in the θ direction when the Peclet number for heat transfer is large.

3. Simplify the radial conduction term, $(1/r)(\partial/\partial r)(r\,\partial T/\partial r)$, at large Prandtl numbers when the thermal boundary layer thickness is small relative to the radius of the cylinder. This is the locally flat approximation.

4. Define a new independent variable in the radial direction (i.e., $y = r - R$) which assumes a value of zero at the solid–liquid interface.

5. Focus on convective transport of thermal energy parallel to the solid–liquid interface. Begin with the exact expression for $v_\theta(r, \theta)$ in the creeping flow regime and linearize this velocity profile with respect to position variable r or y, measured normal to the interface.

6. Use a locally flat description of the equation of continuity and obtain an expression for the radial velocity component v_r, which is consistent with the linear approximation for v_θ.

7. Construct a combined independent variable in terms of y and θ and analyze the thermal energy balance via the method of combination of variables.

8. Independently solve for the temperature profile in terms of the incomplete gamma function, and the thermal boundary layer thickness in terms of the tangential velocity gradient at the solid–liquid interface.

9. Use Fourier's law to calculate the molecular flux of thermal energy in the radial direction, specifically at $r = R$.

10. Equate the result in step 9 to the product of h_{local} and the overall temperature driving force, $T_{\text{solid}} - T_\infty$. This allows one to calculate the local heat transfer coefficient.

(b) Under steady-state conditions, what partial differential equation must be solved to calculate the fluid temperature profile $T(r, \theta)$ within the thermal boundary layer? Do not include any terms in your answer that are not important.

Answer: At large Prandtl and heat transfer Peclet numbers, the fluid temperature must satisfy the following simplified thermal energy balance:

$$v_r \frac{\partial T}{\partial r} + \frac{v_\theta}{R} \frac{\partial T}{\partial \theta} = \alpha \frac{\partial^2 T}{\partial r^2}$$

where α is the thermal diffusivity.

(c) What is the final expression for the fluid temperature profile $T(r, \theta)$ within the thermal boundary layer?

Answer: Since the interface is characterized by high shear and no slip, and the tangential velocity component v_θ varies linearly with normal coordinate r within the thermal boundary layer, one should expect an incomplete gamma function profile given by

$$P(\zeta) \equiv \frac{T_{\text{solid}} - T(r, \theta)}{T_{\text{solid}} - T_\infty} = \frac{1}{\Gamma(\frac{4}{3})} \int_0^\zeta \exp(-z^3)\, dz$$

(d) Write an expression for the local heat transfer coefficient h_{local} in terms of the appropriate molecular transport property and the thermal boundary layer thickness δ_T. Be sure to indicate the important independent variable(s) that h_{local} depends upon.

Answer: Use Fourier's law to calculate the molecular flux of thermal energy in the radial direction at $r = R$. Then, equate this energy flux

to the product of h_{local} and the overall temperature driving force. In other words,

$$-k_{\text{TC}}\left(\frac{\partial T}{\partial r}\right)_{r=R} = h_{\text{local}}(T_{\text{solid}} - T_\infty)$$

Upon evaluating the radial temperature gradient in Fourier's law via the profile in part (c), one obtains the following result for h_{local}:

$$h_{\text{local}}(\theta) = \frac{k_{\text{TC}}}{\Gamma(\frac{4}{3})\delta_T(\theta)}$$

(e) What is the scaling law for the thermal boundary layer thickness δ_T in the creeping flow regime? Be sure to include some important dimensionless numbers in your final answer.

Answer: For creeping flow around high-shear no-slip solid–liquid interfaces,

$$\delta_T \approx (k_{\text{TC}})^{1/3} \approx (\text{Re}\cdot\text{Pr})^{-1/3}$$

(f) What is the scaling law for the local Nusselt number, Nu_{local}, defined by

$$\text{Nu}_{\text{local}} = \frac{h_{\text{local}}2R}{k_{\text{TC}}}$$

where k_{TC} is the thermal conductivity of the fluid. Be sure to include some important dimensionless numbers in your final answer.

Answer: Based on the answers to parts (d) and (e), for creeping flow around high-shear no-slip solid–liquid interfaces,

$$\text{Nu}_{\text{local}}(\theta) = \frac{2R}{\Gamma(\frac{4}{3})\delta_T(\theta)} \approx (\text{Re}\cdot\text{Pr})^{1/3}$$

(g) What is the lower limit of numerical values for the Nusselt number if heat transfer is operative. Obviously, a numerical answer is required, here. *Hint*: Consider the following expression:

$$\text{Nu}_{\text{local}} = \frac{h_{\text{local}}2R}{k_{\text{TC}}} = \frac{h_{\text{local}}(T_{\text{solid}} - T_\infty)}{(k_{\text{TC}}/2R)(T_{\text{solid}} - T_\infty)}$$

Answer: $\text{Nu}_{\text{local}} \geq 1$ or 2, depending on the choice for the characteristic length (i.e., R or $2R$). This lower limit for the Nusselt number corresponds to thermal energy transport exclusively by conduction, with no enhancement from convection parallel to the interface. In general, the Nusselt number, which is a dimensionless heat transfer coefficient, represents a ratio of the total rate of interphase heat

transfer by all mechanisms that are operative for a particular set of conditions, to the rate of interphase heat transfer exclusively by conduction. Hence, if heat transfer occurs due to the presence of a temperature gradient only, then, by definition, the Nusselt number has a lower limit of unity (i.e., when the cylindrical radius corresponds to the characteristic length in this particular problem).

11-12. (a) Derive explicit expressions for the local heat and mass transfer coefficients as a function of surface coordinate θ for boundary layer heat and mass transfer in the liquid phase adjacent to a stationary zero-shear cylindrical surface. Far from the cylinder, the direction of flow of the approaching fluid is transverse (i.e., perpendicular) to the cylindrical axis, and the value of independent variable θ is zero at the stagnation point. The Reynolds number (based on the radius of the cylinder) is 100, the Schmidt and Prandtl numbers are 2500, and the cylinder has a length-to-diameter (L/D) ratio of 50. *Hint*: Consider potential flow transverse to a long cylinder, where the approach velocity of the fluid far from the cylinder is in the negative x direction. The tangential velocity component in the polar coordinate direction is

$$v_\theta(r, \theta) = V_{\text{approach}} \sin\theta(1 + \eta^{-2})$$

where $\eta = r/R$. The negative sign in the preceding expression is omitted when fluid approaches the cylinder in the opposite direction, relative to the problem discussed in Chapter 8 on pages 218–221.

Answer: Begin with the equation of continuity and the mass transfer equation in cylindrical coordinates with two-dimensional flow (i.e., v_r and v_θ) in the mass transfer boundary layer and no dependence of C_A on z because the length of the cylinder exceeds its radius by a factor of 100. Heat transfer results will be generated by analogy with the mass transfer solution. The equations of interest for an incompressible fluid with constant physical properties are

$$\frac{1}{r}\frac{\partial}{\partial r}(r v_r) + \frac{1}{r}\frac{\partial v_\theta}{\partial \theta} = 0$$

$$v_r \frac{\partial C_A}{\partial r} + \frac{v_\theta}{r}\frac{\partial C_A}{\partial \theta} = \mathfrak{D}_{A,\,\text{mix}}\left[\frac{1}{r}\frac{\partial}{\partial r}\left(r\frac{\partial C_A}{\partial r}\right) + \frac{1}{r^2}\frac{\partial^2 C_A}{\partial \theta^2}\right]$$

The corresponding heat transfer problem contains the thermal diffusivity $\alpha = k_{TC}/\rho C_p$, instead of the mass diffusivity, on the right side of the second equation, which becomes the thermal energy balance when C_A is replaced by fluid temperature T. The equation of continuity is the same for either heat or mass transfer. Asymptotic results at large Schmidt and mass transfer Peclet numbers in the laminar regime are obtained by (i) neglecting tangential diffusion in

the θ direction, (2) simplifying radial diffusion in the mass transfer equation via the thin boundary layer approximation, (3) performing a similar simplification of the radial term in the equation of continuity for potential flow transverse to a long cylinder, and (4) replacing $1/r$ on the left side of both equations by $1/R$, because $R \leq r \leq R + \delta$ and $\delta/R \ll 1$, where δ represents the thermal or concentration boundary layer thickness. Now one must solve

$$\frac{\partial v_r}{\partial r} + \frac{1}{R}\frac{\partial v_\theta}{\partial \theta} = 0$$

$$v_r \frac{\partial C_A}{\partial r} + \frac{v_\theta}{R}\frac{\partial C_A}{\partial \theta} = \mathfrak{D}_{A,\,mix}\frac{\partial^2 C_A}{\partial r^2}$$

The analogous heat transfer solution is valid at large Prandtl and thermal Peclet numbers. Independent variables r and θ are replaced by y and x, respectively, such that

$$y = r - R \qquad x = R\theta \qquad v_r = v_y \qquad v_\theta = v_x$$

The dimensionless molar density profile for mobile component A is defined with respect to its liquid-phase molar densities at the solid–liquid interface (i.e., $C_{A,\,equilibrium}$) and in the bulk fluid (i.e., $C_{A,\,bulk}$), such that

$$P(x, y) \equiv \frac{C_{A,\,equilibrium} - C_A(x, y)}{C_{A,\,equilibrium} - C_{A,\,bulk}}$$

The corresponding temperatures at the solid–liquid interface and in the bulk fluid are $T_{interface}$ and T_{bulk}, respectively. Since each term in the mass transfer equation is linear with respect to C_A, the concentration driving force (i.e., $C_{A,\,equilibrium} - C_{A,\,bulk}$) does not appear in the partial differential equation for the dimensionless profile:

$$v_y \frac{\partial P}{\partial y} + v_x \frac{\partial P}{\partial x} = \mathfrak{D}_{A,\,mix}\frac{\partial^2 P}{\partial y^2}$$

If $T_{interface}$ and T_{bulk} replace $C_{A,\,equilibrium}$ and $C_{A,\,bulk}$, respectively, in the definition of the dimensionless profile P, and the thermal diffusivity replaces $\mathfrak{D}_{A,\,mix}$, then the preceding equation represents the thermal energy balance from which temperature profiles can be obtained. The tangential velocity component v_x within the mass transfer boundary layer is calculated from the potential flow solution for v_θ if the interface is characterized by zero shear and the Reynolds number is in the laminar flow regime. Since the concentration and thermal boundary layers are thin for large values of the Schmidt and Prandtl

numbers, respectively, and viscous shear is negligible at the interface, one approximates the tangential velocity component by evaluating v_θ at $r = R$ and truncating the Taylor series expansion for v_θ after the leading zeroth-order term. Hence,

$$v_x(x) = v_\theta(r = R, \theta) = V_{\text{approach}} \sin\theta (1 + \eta^{-2})_{\eta=1}$$
$$= 2V_{\text{approach}} \sin\theta \neq f(y)$$

Realize that $(\partial v_\theta / \partial r)_{r=R}$ and $[(\partial \gamma / \partial t)_{r\theta}]_{r=R}$ are nonzero for potential flow around a cylinder and that the first-order term in the polynomial expansion for v_θ does not vanish, but this first-order term is small relative to the leading zeroth-order term. Now the locally flat description of the equation of continuity allows one to calculate the radial velocity component. For example, integration from the nondeformable solid–liquid interface at $y = 0$, where $v_y = 0$, to any position y within the thin mass transfer boundary layer produces the following result:

$$v_y(x, y) = -\int_0^y \frac{dv_x}{dx}\, dy' = -y\frac{dv_x}{dx} = -2V_{\text{approach}}(\eta - 1)\cos\theta$$

The mass transfer equation for the dimensionless molar density profile of mobile component A is

$$-y\frac{dv_x}{dx}\frac{\partial P}{\partial y} + v_x(x)\frac{\partial P}{\partial x} = \mathfrak{D}_{\text{A, mix}}\frac{\partial^2 P}{\partial y^2}$$

and the analogous thermal energy balance for the dimensionless temperature profile is obtained by replacing $\mathfrak{D}_{\text{A, mix}}$ with the thermal diffusivity. The appropriate boundary conditions here are the same as those employed earlier in this chapter for steady-state boundary layer mass transfer in the liquid phase adjacent to solid spheres and gas bubbles [i.e., see p. 278, (11-41), and (11-56)]. Hence, a combination of variables approach should be successful to obtain the molar density profile and the mass transfer boundary layer thickness. If the combined variable is defined as $\zeta = y/\delta(\theta)$, then the formalism described earlier in the chapter allows one to re-express the mass transfer equation for $P(\zeta)$ as

$$-\left(\delta^2\frac{dv_x}{dx} + v_x\delta\frac{d\delta}{dx}\right)\zeta\frac{dP}{d\zeta} = \mathfrak{D}_{\text{A, mix}}\frac{d^2P}{d\zeta^2}$$

Once again, the quantity in parentheses on the left side of the preceding equation, which depends completely on position variable x measured parallel to the interface, is removed from the mass transfer

equation and set equal to $2\mathfrak{D}_{A,\,mix}$ since it has dimensions of length squared per time. Hence,

(1) $\delta^2\, dv_x/dx + v_x\delta\, d\delta/dx = 2\mathfrak{D}_{A,\,mix}$

(2) $d^2P/d\zeta^2 = -2\zeta\, dP/d\zeta$

The second-order ODE for $P(\zeta)$ yields the error function profile

$$P(\zeta) = \frac{2}{\sqrt{\pi}} \int_0^{\zeta} \exp(-z^2)\, dz = \text{erf}(\zeta)$$

for either dimensionless temperature or molar density of species A. This profile is typical for zero-shear interfaces, where the velocity component parallel to the interface is not considered to be a function of the independent variable measured perpendicular to the interface within a thin mass or heat transfer boundary layer. Further manipulation of the left side of the first-order ODE for the boundary layer thickness is required before obtaining an expression for $\delta(\theta)$. For example,

$$\delta^2 \frac{dv_x}{dx} + v_x\delta \frac{d\delta}{dx} = A(v_x)^a \frac{d}{dx}[\delta^2 (v_x)^{1-a}]$$

Expansion of the right side of the preceding equation reveals that $A = \frac{1}{2}$ and $a = -1$. This allows one to integrate equation (1) above via separation of variables:

$$\frac{1}{2}(v_x)^{-1} \frac{d}{dx}(\delta v_x)^2 = 2\mathfrak{D}_{A,\,mix}$$

subject to the boundary condition where $\delta = 0$ at the stagnation point (i.e., $\theta = 0$ or $x = 0$). One estimates the thickness of the thermal δ_T or concentration δ_C boundary layers from the following equation, where $\mathfrak{D}_{A,\,mix}$ is interpreted as a diffusivity for mass transfer in the expression for δ_C, and must be replaced by the thermal diffusivity α to calculate δ_T:

$$\delta(\theta) = \frac{1}{v_\theta(r = R, \theta)} \left[4R\mathfrak{D}_{A,\,mix} \int_0^{\theta} v_\theta(r = R, w)\, dw \right]^{1/2}$$

Now, calculate the normal component of the total local molar flux of species A at the nondeformable zero-shear interface. Since the radial component of the fluid velocity vector vanishes at $r = R$, species A is transported across the interface exclusively via concentration diffusion (i.e., Fick's law). Then, the diffusional flux of species A in the radial direction, evaluated at the interface, is equated to the product of a local mass transfer coefficient and the overall concentration driving force for mass transfer (i.e., $C_{A,\,equilibrium} - C_{A,\,bulk}$). The

analogous expressions for uncoupled mass and heat transfer across the interface are

$$-\mathfrak{D}_{\mathrm{A,\,mix}}\left(\frac{\partial C_{\mathrm{A}}}{\partial r}\right)_{r=R} \equiv k_{C,\,\mathrm{local}}(\theta)(C_{\mathrm{A,\,equilibrium}} - C_{\mathrm{A,\,bulk}})$$

$$-k_{\mathrm{TC}}\left(\frac{\partial T}{\partial r}\right)_{r=R} \equiv h_{\mathrm{HTC,\,local}}(\theta)(T_{\mathrm{interface}} - T_{\mathrm{bulk}})$$

where $\mathfrak{D}_{\mathrm{A,\,mix}}$ and k_{TC} on the left sides of the previous two equations represent molecular transport properties in Fick's first law of diffusion and Fourier's law of heat conduction for pure fluids, respectively. The local transfer coefficients, $k_{C,\,\mathrm{local}}$ and $h_{\mathrm{HTC,\,local}}$, are functions of independent variable θ measured parallel to the interface. These coefficients decrease as one travels from the stagnation point toward the separation point, in the direction of increasing θ, because the boundary layer thickness increases. If one calculates the temperature and concentration gradients on the left side of the preceding two equations via the dimensionless profile P and the combined independent variable ζ, then the results for $k_{C,\,\mathrm{local}}$ and $h_{\mathrm{HTC,\,local}}$ in terms of δ_C and δ_T are exactly the same as those obtained for steady-state boundary layer mass transfer across a stationary gas–liquid interface, given by equation (11-160). Of course, expressions for the boundary layer thickness differ for zero-shear interfaces with cylindrical and spherical symmetry. One obtains

$$k_{C,\,\mathrm{local}}(\theta) = \frac{2}{\sqrt{\pi}}\frac{\mathfrak{D}_{\mathrm{A,\,mix}}}{\delta_C(\theta)}$$

$$h_{\mathrm{HTC,\,local}}(\theta) = \frac{2}{\sqrt{\pi}}\frac{k_{\mathrm{TC}}}{\delta_T(\theta)}$$

Once again, it should be emphasized that $\mathfrak{D}_{\mathrm{A,\,mix}}$ and k_{TC} in these equations represent molecular transport properties (i.e., mass diffusivity and thermal conductivity, respectively). However, the physical properties for mass and heat transfer in the expressions for boundary layer thickness δ should be interpreted as diffusivities. The molecular transport property in Fick's first law of diffusion is the same as the diffusivity for mass transfer. For heat transfer in pure fluids, thermal conductivity is the molecular transport property in Fourier's law of heat conduction, and $\alpha = k_{\mathrm{TC}}/\rho C_p$ is the thermal diffusivity. Specific calculations for potential flow transverse to a long cylinder are obtained by setting $v_\theta(r = R, \theta) = 2V_{\mathrm{approach}} \sin\theta$ in the equation on page 340 for the boundary layer thickness. Integration yields

$$\delta(\theta) = \left(\frac{2R\mathfrak{D}_{\mathrm{A,\,mix}}}{V_{\mathrm{approach}}}\right)^{1/2} \frac{(1 - \cos\theta)^{1/2}}{\sin\theta}$$

This result can be written in terms of the important dimensionless numbers for mass and heat transfer. A completely dimensionless expression is obtained via division of the boundary layer thickness by the cylindrical radius R. If the Reynolds number is defined using R as the characteristic length, instead of the cylindrical diameter, then

$$\frac{\delta_C(\theta)}{R} = \left(\frac{2}{\text{Re}\cdot\text{Sc}}\right)^{1/2}(1+\cos\theta)^{-1/2}$$

$$\frac{\delta_T(\theta)}{R} = \left(\frac{2}{\text{Re}\cdot\text{Pr}}\right)^{1/2}(1+\cos\theta)^{-1/2}$$

Notice that $\cos\theta$ is symmetric about the x axis, which is defined by $\theta = 0$ and π in cylindrical coordinates, whereas $\sin\theta$ is antisymmetric about this axis. This is important because the useful range of θ is from 0 to π as fluid passes above or below the cylinder. The dependence of δ on θ is the same if one follows a path above the cylinder from 0 to π, or below the cylinder from 2π to π. By definition, the boundary layer thickness vanishes at the stagnation point (i.e., $\theta = 0$). Explicit evaluation of the two preceding equations does not support this claim, even though δ is smallest at $\theta = 0$, because the tangential velocity component also vanishes at the stagnation point. The preceding analysis is not justified quantitatively at the separation point, where $\theta = \pi$, because the assumption that $\delta/R \ll 1$ is invalid. However, the two preceding equations reveal that δ is extremely large at the separation point, which suggests that the resistance to heat or mass transfer is very large and the rates of interphase transfer are vanishingly small. The corresponding results for the local transfer coefficients follow directly from the preceding expressions for δ_C and δ_T. Hence,

$$k_{C,\,\text{local}}(\theta) = \frac{\mathfrak{D}_{\text{A, mix}}}{R}\left(\frac{2\,\text{Re}\cdot\text{Sc}}{\pi}\right)^{1/2}(1+\cos\theta)^{1/2}$$

$$h_{\text{HTC, local}}(\theta) = \frac{k_{\text{TC}}}{R}\left(\frac{2\,\text{Re}\cdot\text{Pr}}{\pi}\right)^{1/2}(1+\cos\theta)^{1/2}$$

Once again, $\mathfrak{D}_{\text{A, mix}}$ and k_{TC} represent molecular transport properties on the right sides of these equations, but the analogy between Sc and Pr, as well as between the mass and heat transfer Peclet numbers (i.e., Re·Sc vs. Re·Pr) is based on diffusivities.

(b) How much error is incorporated in the equation of continuity by neglecting the factors $1/r$ and r in the radial term? Obtain a numerical answer at $\theta = \pi/2$ (i.e., 90°) when the Reynolds number is 100, based on the cylindrical radius, and the Schmidt and Prandtl numbers are 2500.

Answer: The answer to this question focuses on the radial velocity component for potential flow transverse to a long cylinder. Neglecting the negative sign in v_r when the fluid approaches the cylinder in the negative x direction, the result for v_r from equation (8-266) is

$$v_r(r, \theta) = V_{\text{approach}} \cos\theta (1 - \eta^{-2})$$

Since $(1/r)\partial(rv_r)/\partial r$ is replaced by $\partial v_r/\partial r$ in the equation of continuity when analysis is required only within a thin boundary layer, the relative error based on this approximation is

$$\begin{aligned} \%\ \text{error} &\equiv 100\left[\frac{(1/r)\partial(rv_r)/\partial r - \partial v_r/\partial r}{(1/r)\partial(rv_r)/\partial r}\right] \\ &= \frac{100}{1 + \partial \ln v_r/\partial \ln r} \\ &= 100\left(\frac{\eta^2 - 1}{\eta^2 + 1}\right) \end{aligned}$$

The approximation in the equation of continuity introduces no error at the cylindrical interface, where $r = R$ and $\eta = 1$. This error increases as one moves farther away from the interface, because curvature becomes more important at larger r, yet the approximation under consideration neglects the effect of curvature. Hence, the maximum error introduced into the Equation of Continuity occurs at the outer edge of the mass and heat transfer boundary layers, where $r_{\text{maximum}} = R + \delta$ and $\eta_{\text{maximum}} = 1 + \delta/R$. At $\theta = \pi/2$, $\delta/R = 2.8 \times 10^{-3}$, $\eta_{\text{maximum}} = 1.0028$, and the maximum error in the equation of continuity is only 0.28%. Larger error is incurred at slower flow rates because the boundary layer thickness increases as the Reynolds number decreases.

11-13. We explore here analogies between heat and mass transfer boundary layer theory for high-shear no-slip interfaces at high Schmidt and Prandtl numbers. An incompressible fluid at temperature T_{bulk} and composition $C_{\text{A, bulk}}$ flows past a submerged streamlined object with approach velocity V_{approach} in the laminar regime. At the nondeformable fluid–solid interface, the temperature is T_{surface} and the equilibrium molar density of component A in the fluid phase is $C_{\text{A, surface}}$. There is no chemical reaction or irreversible degradation of mechanical energy to thermal energy within the fluid. At high Schmidt and Prandtl numbers, the mass and heat transfer boundary layers (i.e., δ_C and δ_T) are very thin, and a locally flat description is appropriate. Consider two-dimensional flow (i.e., v_x and v_y) within δ_C and δ_T. If the boundary layers are thin relative to the local radius of curvature of the interface, then the tangential velocity component v_x depends linearly on spatial coordinate y, which is measured normal to the interface. No slip is a reasonable assumption at $y = 0$.

(a) Calculate the mass transfer boundary layer thickness for an incompressible fluid with constant physical properties. If δ and the tangential velocity gradient with respect to normal coordinate y, evaluated at the interface [i.e., $(\partial v_x/\partial y)_{y=0}$], are only functions of position x, measured parallel to the interface, then the following hint is helpful:

$$g(x) \equiv \left(\frac{\partial v_x}{\partial y}\right)_{y=0}$$

$$g(x)\delta^2\frac{d\delta}{dx} + \left(\frac{1}{2}\right)\delta^3\frac{dg}{dx} = A[g(x)]^a\frac{d}{dx}(\delta^3 g^{1-a})$$

Answer: Begin with the steady-state mass transfer equation for species A in an incompressible fluid with no chemical reaction. In vector form,

$$\mathbf{v}\cdot\nabla C_{\mathrm{A}} = \mathfrak{D}_{\mathrm{A,\,mix}}\nabla\cdot\nabla C_{\mathrm{A}}$$

In the corresponding thermal energy balance, one replaces $\mathfrak{D}_{\mathrm{A,\,mix}}$ by the thermal diffusivity α, and C_{A} by temperature T. The preceding equation is written in rectangular coordinates because the problem conforms to a locally flat description. If $v_z = 0$ and neither C_A nor T depends on z,

$$v_x\frac{\partial C_{\mathrm{A}}}{\partial x} + v_y\frac{\partial C_{\mathrm{A}}}{\partial y} = \mathfrak{D}_{\mathrm{A,\,mix}}\left(\frac{\partial^2 C_{\mathrm{A}}}{\partial x^2} + \frac{\partial^2 C_{\mathrm{A}}}{\partial y^2}\right)$$

If the heat and mass transfer Peclet numbers are large, then it is reasonable to neglect molecular transport relative to convective transport in the primary flow direction. However, one should not invoke the same type of argument to discard molecular transport normal to the interface. Hence, diffusion and conduction are not considered in the x direction. Based on the problem description, the fluid velocity component parallel to the interface is linearized within a thin heat or mass transfer boundary layer adjacent to the high-shear interface, such that

$$v_x(x, y) \approx v_x(x, y = 0) + yg(x) + \cdots$$

with $v_x(x, y = 0) = 0$. This is reasonable for no-slip interfaces. The equation of continuity for incompressible fluids,

$$\frac{\partial v_x}{\partial x} + \frac{\partial v_y}{\partial y} = 0$$

is employed to calculate v_y. For a nondeformable interface, which implies that $v_y = 0$ at $y = 0$, the equation of continuity yields

$$v_y(x, y) = -\int_0^y y'\frac{dg}{dx}\,dy' = -\left(\frac{1}{2}\right)y^2\frac{dg}{dx}$$

Now the mass transfer equation for species A becomes

$$yg(x)\frac{\partial C_A}{\partial x} - \left(\frac{1}{2}\right) y^2 \frac{dg}{dx}\frac{\partial C_A}{\partial y} = \mathfrak{D}_{A,\,mix}\frac{\partial^2 C_A}{\partial y^2}$$

As mentioned above, the preceding equation is also useful to calculate fluid temperature profiles via boundary layer heat transfer if one replaces C_A by T and $\mathfrak{D}_{A,\,mix}$ by thermal diffusivity α. The dimensionless profile for mass transfer is constructed as follows:

$$P(x, y) = \frac{C_{A,\,surface} - C_A(x, y)}{C_{A,\,surface} - C_{A,\,bulk}}$$

It is acceptable to replace the molar density of species A by P in the mass transfer equation because each term exhibits linear dependence on C_A. Analogously, temperature T is replaced by P in the thermal energy balance. Hence,

$$yg(x)\frac{\partial P}{\partial x} - \left(\frac{1}{2}\right) y^2 \frac{dg}{dx}\frac{\partial P}{\partial y} = \mathfrak{D}_{A,\,mix}\frac{\partial^2 P}{\partial y^2}$$

The boundary conditions for mass transfer are as follows:

(1) $C_A = C_{A,\,surface}$ or $P = 0$ when $y = 0$, for all $x > 0$.

(2) $C_A = C_{A,\,bulk}$ or $P = 1$ when $x = 0$, for all $y > 0$.

(3) $C_A = C_{A,\,bulk}$ or $P = 1$ when $y \to \infty$, for finite x.

The corresponding boundary conditions for heat transfer are obtained by replacing C_A with T, $C_{A,\,surface}$ with $T_{surface}$, and $C_{A,\,bulk}$ with T_{bulk}. Condition 3 represents the boundary layer boundary condition and suggests a combination-of-variables approach with independent dimensionless variable ζ, given by

$$\zeta = \frac{y}{\delta(x)}$$

The hierarchy is as follows:

C_A depends on P.
P depends on ζ.
ζ depends on y and δ.
δ depends on x.

The appropriate partial derivatives in the mass transfer equation are

$$\frac{\partial P}{\partial y} = \frac{1}{\delta}\frac{dP}{d\zeta}$$
$$\frac{\partial^2 P}{\partial y^2} = \frac{1}{\delta^2}\frac{d^2P}{d\zeta^2}$$
$$\frac{\partial P}{\partial x} = -\frac{\zeta}{\delta}\frac{d\delta}{dx}\frac{dP}{d\zeta}$$

Combination of variables will be successful if the mass transfer equation can be written exclusively in terms of ζ. For example, if one substitutes the three previous partial derivatives of the dimensionless molar density profile into the mass transfer equation for species A, then the following equation is obtained after multiplication by δ^2:

$$-\left[g(x)\delta^2\frac{d\delta}{dx} + \left(\frac{1}{2}\right)\delta^3\frac{dg}{dx}\right]\zeta^2\frac{dP}{d\zeta} = \mathfrak{D}_{\mathrm{A,\,mix}}\frac{d^2P}{d\zeta^2}$$

Since the quantity in brackets in this equation has dimensions of a diffusivity, one arrives at two separate ordinary differential equations for $\delta(x)$ and $P(\zeta)$,

(1) $g(x)\delta^2(d\delta/dx) + (\frac{1}{2})\delta^3(dg/dx) = 3\mathfrak{D}_{\mathrm{A,\,mix}}$.

(2) $d^2P/d\zeta^2 = -3\zeta^2\,dP/d\zeta$.

The first of these two equations, together with the hint provided in the problem description, allows one to calculate the boundary layer thickness δ. This is accomplished as follows:

$$g(x)\delta^2\frac{d\delta}{dx} + \left(\frac{1}{2}\right)\delta^3\frac{dg}{dx} = A[g(x)]^a\frac{d}{dx}(\delta^3 g^{1-a})$$
$$= 3A[g(x)]\delta^2\frac{d\delta}{dx} + (1-a)A\delta^3\frac{dg}{dx}$$

Hence, $3A = 1$ and $(1-a)A = \frac{1}{2}$, which yield $A = \frac{1}{3}$ and $a = -\frac{1}{2}$. With assistance from this integrating factor technique, both terms on the left side of (1) are combined, and a rather simple ODE is obtained for $\delta(x)$:

$$\frac{1}{3}[g(x)]^{-1/2}\frac{d}{dx}(\delta^3 g^{3/2}) = 3\mathfrak{D}_{\mathrm{A,\,mix}}$$

Since the boundary layer thickness vanishes at the stagnation point (i.e., $x = 0$), the preceding equation is integrated to produce the following generalized expression for δ:

$$\delta(x) = \frac{\left\{9\mathfrak{D}_{\mathrm{A,\,mix}} \int_0^x [g(x')]^{1/2}\, dx'\right\}^{1/3}}{[g(x)]^{1/2}}$$

Since $\mathfrak{D}_{\mathrm{A,\,mix}}$ appears everywhere in part (a) as a diffusivity, not a molecular transport property, the corresponding heat transfer boundary layer thickness is calculated from the preceding equation via replacement of $\mathfrak{D}_{\mathrm{A,\,mix}}$ by α.

(b) Calculate the dimensionless molar density profile for component A:

$$P(\zeta) = \frac{C_{\mathrm{A,\,surface}} - C_{\mathrm{A}}(x, y)}{C_{\mathrm{A,\,surface}} - C_{\mathrm{A,\,bulk}}}$$

where $\zeta \equiv y/\delta_C(x)$.

Answer: One must solve the following second-order ordinary differential equation for $P(\zeta)$ from (2) on the preceding page:

$$\frac{d^2P}{d\zeta^2} = -3\zeta^2 \frac{dP}{d\zeta}$$

subject to the three boundary conditions mentioned in part (a). Fortuitously, those three conditions for $P(x, y)$ are equivalent to two conditions for $P(\zeta)$, without neglecting any information. For example,

(1) $C_{\mathrm{A}} = C_{\mathrm{A,\,surface}}$ or $P = 0$ when $y = 0$, for all $x > 0$, implies that $P(\zeta = 0) = 0$.

(2) $C_{\mathrm{A}} = C_{\mathrm{A,\,bulk}}$ or $P = 1$ when $x = 0$, for all $y > 0$, implies that $P(\zeta \to \infty) = 1$.

(3) $C_{\mathrm{A}} = C_{\mathrm{A,\,bulk}}$ or $P = 1$ when $y \to \infty$, for finite x, also implies that $P(\zeta \to \infty) = 1$.

If $S(\zeta) \equiv dP/d\zeta$, then the dimensionless mass transfer equation reduces to

$$\frac{d^2P}{d\zeta^2} = \frac{dS}{d\zeta} = -3\zeta^2 S$$

Hence,

$$S(\zeta) = \frac{dP}{d\zeta} = C_1 \exp(-\zeta^3)$$

Boundary condition (1) is employed for the lower integration limit in the following expression, and elements of the Leibnitz rule for differentiating an integral with variable upper limits are invoked to change the integration variable from ζ to z. One obtains

$$P(\zeta) = C_1 \int_0^{\zeta} \exp(-z^3)\, dz$$

Boundary conditions (2) and (3) reveal that integration constant $C_1 = 1/\Gamma(\frac{4}{3})$, via equations (11-73) and (11-74), because

$$\frac{1}{C_1} = \int_0^{\infty} \exp(-z^3)\, dz = \frac{1}{3}\Gamma\left(\frac{1}{3}\right) = \left(\frac{1}{3}\right)! = 0.89$$

In summary, the dimensionless molar density and temperature profiles are described by the incomplete gamma function. This conclusion is expected for high-shear no-slip interfaces in which the fluid velocity component parallel to the interface (i.e., v_x) varies linearly with independent variable y, measured normal to the solid–liquid interface, within a thin mass transfer boundary layer.

(c) Calculate the local rate of interphase mass transfer into the fluid, with units of moles per area per time.

Answer: The mass transfer calculation is based on the normal component of the total molar flux of species A, evaluated at the solid–liquid interface. Convection and diffusion contribute to the total molar flux of species A. For thermal energy transfer in a pure fluid, one must consider contributions from convection, conduction, a reversible pressure work term, and an irreversible viscous work term. Complete expressions for the total flux of species mass and energy are provided in Table 19.2-2 of Bird *et al*. (2002, p. 588). When the normal component of these fluxes is evaluated at the solid–liquid interface, where the normal component of the mass-averaged velocity vector vanishes, the mass and heat transfer problems require evaluations of Fick's law and Fourier's law, respectively. The coefficients of proportionality between flux and gradient in these molecular transport laws represent molecular transport properties (i.e., $\mathfrak{D}_{\mathrm{A,\,mix}}$ and k_{TC}). In terms of the mass transfer problem, one focuses on the solid–liquid interface for $x > 0$:

$$-\mathfrak{D}_{\mathrm{A,\,mix}}\left(\frac{\partial C_{\mathrm{A}}}{\partial y}\right)_{y=0} = -\mathfrak{D}_{\mathrm{A,\,mix}}\frac{dC_{\mathrm{A}}}{dP}\left(\frac{dP}{d\zeta}\right)_{\zeta=0}\left(\frac{\partial \zeta}{\partial y}\right)_x$$

Each of the three derivatives on the right side of this equation is evaluated separately, where the Leibnitz rule for differentiating an integral with variable limits is employed for $(dP/d\zeta)_{\zeta=0}$. For example,

(1) $dC_A/dP = -(C_{A,\,surface} - C_{A,\,bulk})$.

(2) $(dP/d\zeta)_{\zeta=0} = 1/\Gamma(\frac{4}{3})$.

(3) $(\partial\zeta/\partial y)_x = 1/\delta_C(x)$.

The final result for mass transfer is

$$-\mathfrak{D}_{A,\,mix}\left(\frac{\partial C_A}{\partial y}\right)_{y=0} = \frac{\mathfrak{D}_{A,\,mix}(C_{A,\,surface} - C_{A,\,bulk})}{\Gamma(\frac{4}{3})\delta_C(x)}$$

The completely analogous result for heat transfer is

$$-k_{TC}\left(\frac{\partial T}{\partial y}\right)_{y=0} = \frac{k_{TC}(T_{surface} - T_{bulk})}{\Gamma(\frac{4}{3})\delta_T(x)}$$

Once again, mass diffusivity $\mathfrak{D}_{A,\,mix}$ and thermal conductivity k_{TC} in these expressions represent molecular transport properties via Fick's and Fourier's law, respectively. However, the fluid properties that appear in δ_C and δ_T should be interpreted as diffusivities, not molecular transport properties. In terms of the analogies between heat and mass transfer, sometimes $\mathfrak{D}_{A,\,mix}$ represents a diffusivity, and other times it represents a molecular transport property. This ambiguity does not exist in the corresponding expressions for heat transfer. In general, $\mathfrak{D}_{A,\,mix}$ represents a diffusivity in the mass transfer equation and in expressions for the boundary layer thickness δ_C.

(d) Calculate the local mass transfer coefficient $k_{C,\,local}(x)$, defined by

$$J_{Ay}(y=0) = -\mathfrak{D}_{A,\,mix}\left(\frac{\partial C_A}{\partial y}\right)_{y=0} \equiv k_{C,\,local}(x)(C_{A,\,surface} - C_{A,\,bulk})$$

where J_{Ay} is the y component of the diffusional molar flux of species A with respect to the molar average reference frame.

Answer: Based on the local rate of interphase mass transfer from part (c), one obtains

$$k_{C,\,local}(x) = \frac{\mathfrak{D}_{A,\,mix}}{\Gamma(\frac{4}{3})\delta_C(x)}$$

Analogously, the local heat transfer coefficient $h_{local}(x)$ is defined in terms of the local rate of interphase thermal energy transfer:

$$-k_{TC}\left(\frac{\partial T}{\partial y}\right)_{y=0} \equiv h_{local}(x)(T_{surface} - T_{bulk})$$

Hence,

$$h_{\text{local}}(x) = \frac{k_{\text{TC}}}{\Gamma(\frac{4}{3})\delta_T(x)}$$

(e) Calculate the surface-averaged mass transfer coefficient, $k_{C,\,\text{average}}$, defined by

$$k_{C,\,\text{average}} \equiv \frac{1}{L}\int_0^L k_{C,\,\text{local}}(x')dx'$$

where L is the length of the streamlined object in the primary flow direction (i.e., x direction).

Answer: Based on results from part (d), one obtains

$$k_{C,\,\text{average}} \equiv \frac{\mathfrak{D}_{\text{A, mix}}}{L\Gamma(\frac{4}{3})}\int_0^L \frac{dx'}{\delta_C(x')}$$

Now it is necessary to average the inverse of the mass transfer boundary layer thickness over the total length L of the solid–liquid interface. Hence,

$$\int_0^L \frac{dx'}{\delta_C(x')} = \frac{1}{(9\mathfrak{D}_{\text{A, mix}})^{1/3}}\int_0^L \frac{\sqrt{g(x')}\,dx'}{\left[\int_0^{x'}\sqrt{g(x'')}\,dx''\right]^{1/3}}$$

Once again, the Leibnitz rule is useful, because if one defines

$$\aleph(x') \equiv \int_0^{x'} [g(x'')]^{1/2}\,dx''$$

then

$$\frac{d\aleph}{dx'} = [g(x')]^{1/2}$$

via the dependence of $\aleph$ on x' in the upper limit of integration, only. The averaging process proceeds as follows:

$$\int_0^L \frac{dx'}{\delta_C(x')} = \frac{1}{(9\mathfrak{D}_{\text{A, mix}})^{1/3}}\int_0^L \frac{d\aleph}{\aleph^{1/3}}$$

$$= \left(\frac{3}{2}\right)\frac{[\aleph(x'=L)]^{2/3}}{(9\mathfrak{D}_{\text{A, mix}})^{1/3}}$$

Finally, the surface-averaged mass transfer coefficient becomes

$$k_{\text{C, average}} = \frac{3}{9^{1/3} \cdot 2L\Gamma(\frac{4}{3})}[\mathfrak{D}_{\text{A, mix}}\aleph(x' = L)]^{2/3}$$

$$= \frac{0.81}{L}\left\{\mathfrak{D}_{\text{A, mix}}\int_0^L \left[\left(\frac{\partial v_x}{\partial y}\right)_{y=0}\right]^{1/2} dx\right\}^{2/3}$$

One must exercise caution in constructing an analogous expression for the surface-averaged heat transfer coefficient because the presence of $\mathfrak{D}_{\text{A, mix}}$ in the final result for $k_{C,\text{ average}}$ represents a combination of diffusivities and molecular transport properties, both of which are the same for mass transfer. In other words,

$$h_{\text{average}} \equiv \frac{k_{\text{TC}}}{L\Gamma(\frac{4}{3})}\int_0^L \frac{dx'}{\delta_T(x')}$$

$$\delta_T(x) = \frac{\left\{9\alpha\int_0^x [g(x')]^{1/2}\,dx'\right\}^{1/3}}{[g(x)]^{1/2}}$$

where the difference between molecular transport properties (i.e., k_{TC}) and diffusivities (i.e., α) for heat transfer is obvious. Detailed calculations for h_{average} are exactly the same as those for $k_{\text{C, average}}$. The final result for heat transfer is

$$h_{\text{average}} = \frac{0.81k_{\text{TC}}}{L\alpha^{1/3}}\left\{\int_0^L \left[\left(\frac{\partial v_x}{\partial y}\right)_{y=0}\right]^{1/2} dx\right\}^{2/3}$$

(f) Calculate the surface-averaged Sherwood number, $\text{Sh}_{\text{average}}$, defined by

$$\text{Sh}_{\text{average}} \equiv \frac{k_{C,\text{ average}}}{\mathfrak{D}_{\text{A, mix}}/L}$$

Express your result in terms of the Reynolds number,

$$\text{Re} \equiv \frac{LV_{\text{approach}}}{\mu/\rho}$$

the Schmidt number,

$$\text{Sc} \equiv \frac{\mu/\rho}{\mathfrak{D}_{\text{A, mix}}}$$

a geometric factor, and a dimensionless hydrodynamic factor.

Answer: In an effort to present the final result for $\mathrm{Sh}_{\text{average}}$ in dimensionless form, one must introduce dimensionless variables and construct a dimensionless velocity gradient at the solid–liquid interface. For example, if $v_x' = v_x / V_{\text{approach}}$, $\eta = y/L$, and $\xi = x/L$, then,

$$\left(\frac{\partial v_x}{\partial y}\right)_{y=0} = \frac{V_{\text{approach}}}{L}\left(\frac{\partial v_x'}{\partial \eta}\right)_{\eta=0}$$

Now begin with the final result from part (e) for $k_{C,\,\text{average}}$ and construct an expression for the average Sherwood number:

$$\frac{k_{C,\,\text{average}} L}{\mathfrak{D}_{\text{A, mix}}} = 0.81\left(\frac{L V_{\text{approach}}}{\mathfrak{D}_{\text{A, mix}}}\right)^{1/3}\left\{\int_0^1 \left[\left(\frac{\partial v_x'}{\partial \eta}\right)_{\eta=0}\right]^{1/2} d\xi\right\}^{2/3}$$

Since the product of Re and Sc is $L V_{\text{approach}}/\mathfrak{D}_{\text{A, mix}}$, the preceding expression for the average Sherwood number reduces to

$$\mathrm{Sh}_{\text{average}} = 0.81(\mathrm{Re}\cdot\mathrm{Sc})^{1/3}\left\{\int_0^1 \left[\left(\frac{\partial v_x'}{\partial \eta}\right)_{\eta=0}\right]^{1/2} d\xi\right\}^{2/3}$$

The geometric factor of 0.81 originates from $3/[9^{1/3}\cdot 2\Gamma(\frac{4}{3})]$, and the dimensionless hydrodynamic factor, based on the tangential velocity gradient at the solid–liquid interface, is

$$\left\{\int_0^1 \left[\left(\frac{\partial v_x'}{\partial \eta}\right)_{\eta=0}\right]^{1/2} d\xi\right\}^{2/3} = f(\mathrm{Re})$$

Whereas this hydrodynamic factor is independent of the Reynolds number for creeping flow, it scales as $\mathrm{Re}^{(1/6)}$ for laminar flow because

$$\left(\frac{\partial v_x'}{\partial \eta}\right)_{\eta=0} \approx \mathrm{Re}^{1/2}$$

The analogous result for the surface-averaged Nusselt number is

$$\mathrm{Nu}_{\text{average}} \equiv \frac{L h_{\text{average}}}{k_{\text{TC}}} = 0.81(\mathrm{Re}\cdot\mathrm{Pr})^{1/3}\left\{\int_0^1 \left[\left(\frac{\partial v_x'}{\partial \eta}\right)_{\eta=0}\right]^{1/2} d\xi\right\}^{2/3}$$

where the Prandtl number is defined by $\mathrm{Pr} = (\mu/\rho)/\alpha$.

11-14. Consider the locally flat description of heat transfer by convection and conduction from a hot plate to an incompressible fluid at high Peclet numbers with two-dimensional laminar flow in the heat transfer boundary layer adjacent to the hot surface. The tangential fluid velocity component v_x is only a function of position x parallel to the interface.

(a) What is the final expression for the surface-averaged heat transfer coefficient? Answer this question by analogy and express your answer in terms of:

(1) Thermal conductivity k_{TC} of the fluid.

(2) Fluid density ρ.

(3) Specific heat of the fluid C_p.

(4) Length L of the hot plate.

(5) Tangential velocity component $v_x(x)$.

The Chilton–Colburn j-factor for heat transfer is defined by

$$j_{\text{heat transfer}} = \frac{\text{Nusselt number}}{\text{Pr}^{0.33} \cdot \text{Re}}$$

(b) Write the analogous j-factor for mass transfer.

(c) Write the analogous j-factor for momentum transfer.

11-15. In (a), (b), and (c) below, the mass flow rate changes within the same flow regime, as hot water at 40°C flows past solid spherical sucrose pellets packed in a cylindrical tube and sucrose dissolves into the passing fluid stream. For each case, indicate whether the surface-averaged rate of interphase mass transfer increases, decreases, or does not change. Then, calculate the factor by which the surface-averaged rate of interphase mass transfer changes in each case. Note: A factor of 1 indicates no change.

(a) *Creeping flow:* mass flow rate increases by a factor of 3.

(b) *Laminar flow:* mass flow rate increases by a factor of 2.

(c) *Turbulent flow:* mass flow rate decreases by a factor of 4.

(d) In the problem described above, is the surface-averaged rate of interphase mass transfer larger, smaller, the same, or too complex to determine if the temperature of the passing fluid stream decreases from 40°C to 20°C?

(e) *True or False:* If the mass flow rate remains constant but temperature changes cause the diffusion coefficient to increase, then the Schmidt number decreases, the Sherwood number decreases, and the surface-averaged mass transfer coefficient decreases.

11-16. What is the slope of each of the following log-log graphs, where the first quantity appears on the vertical axis and the second quantity appears on the horizontal axis? In all cases, the properties are evaluated in the incompressible Newtonian fluid phase.

(a) Liquid-phase mass transfer boundary layer thickness δ_C adjacent to a gas bubble vs. liquid phase flow rate q in the creeping flow regime.

(b) Local mass transfer coefficient $k_{C,\,\text{local}}$ for dissolution of a solid vs. liquid phase flow rate q in the laminar flow regime.

(c) Local Sherwood number Sh_{local} vs. liquid-phase mass transfer boundary layer thickness δ_C adjacent to a gas bubble in the creeping flow regime.

(d) Local Nusselt number Nu_{local} vs. liquid-phase heat transfer boundary layer thickness δ_T for laminar flow transverse to a long solid cylinder.

(e) Surface-averaged rate of interphase mass transfer across a gas–liquid interface vs. liquid-phase flow rate q at high Reynolds numbers in the absence of any turbulent transport.

11-17. Consider boundary layer mass transfer of species A across a spherical gas–liquid interface in the creeping flow regime. The stagnation point is at $\theta = 0$. By what factor does each of the following properties change when the molecular diffusion coefficient $\mathfrak{D}_{\text{A, mix}}$ increases by a factor of 2? A factor greater than 1 corresponds to an increase, less than 1 represents a decrease, and 1 corresponds to no change.

(a) Mass transfer boundary layer thickness δ_C at $\theta = 90^\circ$

(b) Local mass transfer coefficient $k_{C,\,\text{local}}$ at $\theta = 45^\circ$

(c) Average Sherwood number

(d) Local rate of interphase mass transfer at $\theta = 60^\circ$

(e) By what factor do the mass transfer properties in parts (a) through (d) change when the molecular diffusion coefficient $\mathfrak{D}_{\text{A, mix}}$ increases by a factor of 2 in the laminar flow regime?

11-18 Tabulate the scaling law exponents x, y, and z for the mass transfer boundary layer thickness δ_C and the local mass transfer coefficient $k_{C,\,\text{local}}$ in the following correlations for mobile component A:

$$\log \delta_C \approx x \log \mathfrak{D}_{\text{A, mix}}$$

$$\log k_{C,\,\text{local}} \approx y \log \mathfrak{D}_{\text{A, mix}} + z \log (\text{mass flow rate})$$

Provide numerical values of x, y, and z for each of the five conditions listed below in parts (a) through (e). A total of 15 answers is required.

(a) Solid spheres that fall slowly (i.e., creeping flow) through a liquid.

Answer: For boundary layer mass transfer across solid–liquid interfaces, $x = \frac{1}{3}$ and $y = \frac{2}{3}$. In the creeping flow regime, $z = \frac{1}{3}$. This problem is analogous to one where the solid sphere is stationary and a liquid flows past the submerged object at low Reynolds numbers.

(b) Bubbles that rise (i.e., laminar flow) through a liquid.

Answer: For boundary layer mass transfer across gas–liquid interfaces, $x = \frac{1}{2}$ and $y = \frac{1}{2}$. In the laminar flow regime, $z = \frac{1}{2}$. This problem is analogous to one where the bubble is stationary and a liquid flows past the submerged object at intermediate Reynolds numbers.

(c) Bubbles that expand into a stagnant liquid.

Answer: For unsteady-state mass transfer across expanding gas–liquid interfaces via the penetration theory, $x = \frac{1}{2}$ and $y = \frac{1}{2}$. Since there is no convective mass transfer parallel to the interface, $z = 0$.

(d) Laminar flow of an incompressible liquid past stationary solid spheres.

Answer: For boundary layer mass transfer across solid–liquid interfaces, $x = \frac{1}{3}$ and $y = \frac{2}{3}$. In the laminar flow regime, $z = \frac{1}{2}$.

(e) Unsteady-state diffusion across a stationary gas–liquid interface into a stagnant liquid (i.e., the classic penetration theory).

Answer: For unsteady-state mass transfer across stationary gas–liquid interfaces via the classic penetration theory, $x = \frac{1}{2}$ and $y = \frac{1}{2}$. Since there is no convective mass transfer parallel to the interface, $z = 0$.

11-19. Describe a detailed method of data analysis to determine the coefficient C_1 and the powers α and β from mass transfer experimental data that is typically correlated in the following manner for streamline flow adjacent to a no-slip interface;

$$\text{Sherwood no.} = 2.0 + C_1(\text{Reynolds no.})^{\alpha}(\text{Schmidt no.})^{\beta}$$

(a) What kind of data should be measured? (give a very brief description.)

(b) What quantities should be plotted on what type of axes?

(c) Explain how one should calculate C_1, α, and β from the graphical analysis.

11-20. **(a)** How should you quantitatively describe radial conduction of thermal energy within the heat transfer boundary layer δ_T adjacent to the wall of a tube at high Prandtl numbers? Provide a mathematical expression to answer this question. A one-line answer is required, here.

(b) How should your locally flat expression for radial conduction of thermal energy within δ_T from part (a) be modified when temperature gradients exist throughout the entire cross section of the tube and $\delta_T/R \approx 1$, where R is the tube radius? In other words, what correction is required when the curvature of the wall is important? A one- or two-line mathematical answer is required, here.

11-21. Your experimental apparatus consists of a two-phase column in which mobile component A is transported from a stationary solid phase to a moving liquid phase that flows through the column. How should you quantify the average rate of interphase mass transfer, with units of moles per time, from very simple experimental measurements? Your analytical device is not sophisticated enough to measure any concentrations within the column, but you do have experimental data that characterize the inlet stream at $z = 0$ and the outlet stream at $z = L$.

Answer: Rate of interphase mass transfer = $Q[C_A(z = L) - C_A(z = 0)]$.

11-22. In an effort to analyze Problem 11-21 in more detail, you focus on the instantaneous rate of interphase mass transfer across a high-shear no-slip interface at axial position z within the column and construct the following quasi-macroscopic steady-state mass balance on mobile component A in the liquid phase. The flow regime is laminar and the size of the liquid-phase control volume, CV, is $\varepsilon_p \pi (R_{\text{column}})^2\, dz$:

$$QC_A(z) + C_1 \frac{\mathfrak{D}_A}{d_{\text{pellet}}} \text{Re}^{\xi} \cdot \text{Sc}^{\omega} (C_{A,\text{ interface}} - C_A) A_V \varepsilon_p \pi R_{\text{column}}^2\, dz = QC_A(z + dz)$$

where

C_A = molar density of mobile component A in the liquid phase at position z

$C_{A,\text{ interface}}$ = equilibrium molar density of A in the liquid phase at the solid–liquid interface

Q = volumetric flow rate of the liquid phase through the column

d_{pellet} = diameter of the solid pellets in the stationary phase of the column

$\mathfrak{D}_A$ = diffusion coefficient of mobile component A in the liquid phase

R_{column} = radius of the column

A_V = interfacial area for mass transfer per unit volume of the liquid phase

z = axial coordinate that increases in the direction of flow of the liquid phase

L = length of the column in the primary flow direction (i.e., $0 \leq z \leq L$)

$\mathrm{Sc} = (\mu/\rho)/\mathfrak{D}_{\mathrm{A}}$ is the Schmidt number

$\mathrm{Re} = \rho\langle v_z\rangle_{\text{interstitial}}\, d_{\text{pellet}}/\mu$ is the particle-based Reynolds number that employs the interstitial fluid velocity $\langle v_z\rangle_{\text{interstitial}}$ through the column

$\langle v_z\rangle_{\text{interstitial}} = Q/[\varepsilon_p \pi (R_{\text{column}})^2]$ is the interstitial fluid velocity through the packed bed, which is larger than the superficial velocity through an empty column at the same volumetric flow rate

ε_p = interpellet porosity of the packed column

C_1 = constant in the boundary layer correlation for the interphase mass transfer coefficient [C_1 contains $\Gamma(\frac{4}{3})$]

(a) If $C_{\mathrm{A}}(z = 0) = C_{\mathrm{A0}}$ in the feed stream to the column, then predict the molar density of mobile component A in the exiting liquid stream at $z = L$.

Answer: For laminar flow adjacent to a solid–liquid interface, the Sherwood correlations for boundary layer mass transfer suggest that $\xi = \frac{1}{2}$ and $\omega = \frac{1}{3}$. Hence, the surface-averaged mass transfer coefficient is

$$k_{C,\,\text{average}} = C_1 \frac{\mathfrak{D}_{\mathrm{A}}}{d_{\text{pellet}}} \mathrm{Re}^{1/2} \cdot \mathrm{Sc}^{1/3}$$

because the surface-averaged Sherwood number for mass transfer is defined as

$$\mathrm{Sh}_{\text{average}} = \frac{k_{C,\,\text{average}}\, d_{\text{pellet}}}{\mathfrak{D}_{\mathrm{A}}} \approx C_1 \cdot \mathrm{Re}^{1/2}\, \mathrm{Sc}^{1/3}$$

where the pellet diameter is the characteristic length. Rearrangement of the quasi-macroscopic mass balance yields the following ordinary differential equation for the molar density of species A as a function of axial position z:

$$Q\left\{\frac{C_{\mathrm{A}}(z + dz) - C_{\mathrm{A}}(z)}{dz}\right\} = Q\frac{dC_{\mathrm{A}}}{dz}$$
$$= k_{C,\,\text{average}} A_V \varepsilon_p \pi (R_{\text{column}})^2 (C_{\mathrm{A,\,interface}} - C_{\mathrm{A}})$$

Separation of variables allows one to determine C_A in the exit stream:

$$\frac{dC_A}{C_{A,\,\text{interface}} - C_A} = \frac{k_{C,\,\text{average}} A_V \varepsilon_p \pi (R_{\text{column}})^2 \, dz}{Q}$$

The lower integration limit is $C_A = C_{A0}$ at $z = 0$, and the upper limit is $C_A = C_{AL}$ at $z = L$. Hence,

$$\ln \frac{C_{A,\,\text{interface}} - C_{A0}}{C_{A,\,\text{interface}} - C_{AL}} = \frac{k_{C,\,\text{average}} A_V L}{\langle v_z \rangle_{\text{interstitial}}}$$

The predicted outlet molar density of mobile component A is

$$C_A(z = L) = C_{AL} = C_{A,\,\text{interface}} - (C_{A,\,\text{interface}} - C_{A0}) \times \exp\left(\frac{-k_{C,\,\text{average}} A_V L}{\langle v_z \rangle_{\text{interstitial}}}\right)$$

(b) Calculate numerical values for α, β, and ζ in the following scaling law:

$$\frac{C_{A,\,\text{interface}} - C_A(z = L)}{C_{A,\,\text{interface}} - C_A(z = 0)} \approx \exp(-L^{\alpha} \cdot \text{Re}^{\beta} \cdot \text{Sc}^{\zeta})$$

Be sure that your answers agree with the following trends: The outlet molar density of mobile component A, C_A (at $z = L$), approaches $C_{A,\,\text{interface}}$ for long columns and high diffusivities, but it approaches C_{A0} at high flow rates.

Answer: Rearrangement of the answer to part (a) yields

$$\frac{C_{A,\,\text{interface}} - C_{AL}}{C_{A,\,\text{interface}} - C_{A0}} = \exp\left(\frac{-k_{C,\,\text{average}} A_V L}{\langle v_z \rangle_{\text{interstitial}}}\right)$$

which conforms to the scaling law provided in part (b). Detailed analysis of the exponential argument allows one to determine α, β, and ζ.

$$\frac{k_{C,\,\text{average}} A_V L}{\langle v_z \rangle_{\text{interstitial}}} = \frac{C_1 (\mathfrak{D}_A / d_{\text{pellet}}) \cdot \text{Re}^{1/2} \cdot \text{Sc}^{1/3} \cdot A_V L}{\langle v_z \rangle_{\text{interstitial}}}$$

The mass transfer Peclet number, which appears as a coefficient of the convective rate process in the dimensionless mass balance when convection and diffusion occur, is found in the denominator of the exponential argument. In other words,

$$\text{Pe}_{\text{MT}} = \text{Re} \cdot \text{Sc} = \frac{\langle v_z \rangle_{\text{interstitial}} \, d_{\text{pellet}}}{\mathfrak{D}_A}$$

Hence,

$$\frac{k_{C,\,\text{average}} A_V L}{\langle v_z \rangle_{\text{interstitial}}} = \frac{C_1 \cdot \text{Re}^{1/2} \cdot \text{Sc}^{1/3} \cdot A_V L}{\text{Re} \cdot \text{Sc}}$$

$$= C_1 A_V L \cdot \text{Re}^{-1/2} \cdot \text{Sc}^{-2/3}$$

$$\frac{C_{\text{A, interface}} - C_{AL}}{C_{\text{A, interface}} - C_{\text{A0}}} = \exp(-C_1 A_V L \cdot \text{Re}^{-1/2} \cdot \text{Sc}^{-2/3})$$

and $\alpha = 1$, $\beta = \frac{-1}{2}$, and $\zeta = \frac{-2}{3}$.

11-23. (a) Sketch the molar density of mobile component A in the liquid phase C_A vs. axial position z in a packed column at Reynolds numbers of 1, 20, and 400. Interphase mass transfer of species A is operative from a stationary solid particulate phase to an incompressible liquid phase which undergoes laminar flow through the void space in the column. Put C_A on the vertical axis and axial position z (i.e., cylindrical coordinates) within the packed column on the horizontal axis. The inlet and outlet streams are described by $z = 0$ and $z = L$, respectively. Include three curves on one set of axes and label each curve with the appropriate value of the Reynolds number for laminar flow.

(b) Develop a relation between the initial slope of your graph in part (a), $(dC_A/dz)_{z=0}$ and the Reynolds number for laminar flow. In other words,

$$\left(\frac{dC_A}{dz}\right)_{z=0} = f(\text{Re})$$

Calculate this function of the Reynolds number.

Answer: The quasi-macroscopic mass balance from Problem 11-22 reveals that

$$Q\frac{dC_A}{dz} = k_{C,\,\text{average}} A_V \varepsilon_p \pi (R_{\text{column}})^2 (C_{\text{A, interface}} - C_A)$$

and the surface-averaged mass transfer coefficient for laminar flow adjacent to a high-shear no-slip solid–liquid interface is correlated as follows:

$$k_{C,\,\text{average}} = C_1 \frac{\mathfrak{D}_A}{d_{\text{pellet}}} \text{Re}^{1/2} \cdot \text{Sc}^{1/3}$$

Hence,

$$\frac{dC_A}{dz} = C_1 \frac{\mathfrak{D}_A}{\langle v_z \rangle_{\text{interstitial}} d_{\text{pellet}}} \text{Re}^{1/2} \cdot \text{Sc}^{1/3} \cdot A_V (C_{\text{A, interface}} - C_A)$$

When this axial concentration gradient is evaluated near the inlet to the packed column at $z = 0$, one obtains

$$\left(\frac{dC_A}{dz}\right)_{z=0} = C_1 A_V \cdot \mathrm{Re}^{-1/2} \cdot \mathrm{Sc}^{-2/3}(C_{A,\,\text{interface}} - C_{A0})$$

which indicates that $(dC_A/dz)_{z=0}$ scales at $\mathrm{Re}^{-1/2}$.

(c) If the Reynolds number increases from 1 to 400 and fluid flow within the packed column remains in the laminar regime, then obtain a quantitative estimate of the change in $(dC_A/dz)_{z=0}$. Does the magnitude of $(dC_A/dz)_{z=0}$ increase, decrease, remain unchanged, or is it too complex to determine how the magnitude of this initial slope changes when the Reynolds number increases by a factor of 400?

Answer: If fluid flow between the particles in the packed column remains in the laminar regime as Re increases from 1 to 400, then the axial concentration gradient near the inlet decreases by a factor of 20, since $(dC_A/dz)_{z=0}$ scales at $\mathrm{Re}^{-1/2}$.

Transport Phenomena for Chemical Reactor Design. Laurence A. Belfiore
Copyright © 2003 John Wiley & Sons, Inc.
ISBN: 0-471-20275-4

12

DIMENSIONAL ANALYSIS OF THE EQUATIONS OF CHANGE FOR FLUID DYNAMICS WITHIN THE MASS TRANSFER BOUNDARY LAYER

The primary focus of this chapter is to analyze the dimensionless equation of motion in the laminar flow regime and predict the Reynolds number dependence of the tangential velocity gradient at a spherical fluid–solid interface. This information is required to obtain the complete dependence of the dimensionless mass transfer coefficient (i.e., Sherwood number) on the Reynolds and Schmidt numbers. For easy reference, the appropriate correlation for mass transfer around a solid sphere in the laminar flow regime, given by equation (11-120), is included here:

$$\mathrm{Sh}_{\mathrm{average}} = 1.28(\mathrm{Re}\cdot\mathrm{Sc})^{1/3}\left\{\int [g^*(\theta)\sin^3\theta]^{1/2}d\theta\right\}^{2/3} \qquad 0 \le \theta \le \pi/2 \tag{12-1}$$

where $g^*(\theta)$ represents the dimensionless $r-\theta$ component of the rate-of-strain tensor evaluated at a spherical solid–liquid interface with solid radius R and fluid approach velocity V_{approach}. If dimensionless variables are defined as $\eta = r/R$ (i.e., $\eta \ge 1$) and $v_\theta^* = v_\theta / V_{\mathrm{approach}}$, then

$$\begin{aligned} g(\theta) &= \left[\left(\frac{\partial \gamma}{\partial t}\right)_{r\theta}\right]_{r=R} = \left[r\frac{\partial}{\partial r}\left(\frac{v_\theta}{r}\right) + \frac{1}{r}\frac{\partial v_r}{\partial \theta}\right]_{r=R} \\ &= \left[r\frac{\partial}{\partial r}\left(\frac{v_\theta}{r}\right)\right]_{r=R} = \frac{V_{\mathrm{approach}}}{R}\left[\eta\frac{\partial}{\partial \eta}\left(\frac{v_\theta^*}{\eta}\right)\right]_{\eta=1} \end{aligned} \tag{12-2}$$

and one defines the dimensionless tangential velocity gradient $g^*(\theta)$ at the solid–liquid interface as

$$g^*(\theta) = \frac{g(\theta)}{V_{\mathrm{approach}}/R} = \left[\frac{\partial}{\partial \eta}\left(\frac{v_\theta^*}{\eta}\right)\right]_{\eta=1} \tag{12-3}$$

12-1 GENERALIZED DIMENSIONLESS FORM OF THE EQUATION OF MOTION FOR INCOMPRESSIBLE FLUIDS UNDERGOING LAMINAR FLOW

As illustrated in Chapter 8 via equation (8-42), if dynamic pressure $\mathfrak{P}$ is dimensionalized using a characteristic viscous momentum flux (i.e., $\mu V/L$), then $\mathfrak{P} = (\mu V/L)\mathfrak{P}^*$ and one obtains the following form of the dimensionless equation of motion for laminar flow:

$$\mathrm{Re}\left(\frac{\partial \mathbf{v}^*}{\partial t^*} + \mathbf{v}^* \cdot \nabla^* \mathbf{v}^*\right) = -\nabla^* \cdot \tau^* - \nabla^* \mathfrak{P}^* \tag{12-4}$$

where all variables and parameters are dimensionless.

12-2 INCOMPRESSIBLE NEWTONIAN FLUIDS IN THE CREEPING FLOW REGIME

In the limit of vanishingly small Reynolds numbers, forces due to convective momentum flux are negligible relative to viscous, pressure, and gravity forces. Equation (12-4) is simplified considerably by neglecting the left-hand side in the creeping flow regime. For fluids with constant μ and ρ, the dimensionless constitutive relation between viscous stress and symmetric linear combinations of velocity gradients is

$$\tau^* = -\nabla^* \mathbf{v}^* - (\nabla^* \mathbf{v}^*)^T \tag{12-5}$$

Viscous forces in the equation of motion are treated as follows:

$$-\nabla^* \cdot \tau^* = \nabla^* \cdot \nabla^* \mathbf{v}^* \tag{12-6}$$

because

$$\nabla^* \cdot (\nabla^* \mathbf{v}^*)^T = 0 \tag{12-7}$$

for incompressible fluids in which $\nabla^* \cdot \mathbf{v}^* = 0$. The dimensionless creeping flow equation of motion for incompressible Newtonian fluids is

$$\nabla^* \cdot \nabla^* \mathbf{v}^* = \nabla^* \mathfrak{P}^* \tag{12-8}$$

in which both viscous forces per unit volume and dynamic pressure forces per unit volume scale as $\mu V/L^2$. Since dynamic pressure is an exact differential and the curl of the gradient of any scalar must vanish if the scalar is analytic, $\mathfrak{P}$ is removed from equation (12-8) by taking the curl (i.e., $\nabla \times$) of the creeping flow equation of motion. Hence, in dimensionless form,

$$\nabla^* \times \nabla^* \cdot \nabla^* \mathbf{v}^* = 0 \tag{12-9}$$

Without introducing the stream function or solving this third-order partial differential vector equation for $\mathbf{v}^*$, it should be obvious that the dimensionless velocity vector is a function of spatial coordinates and the specific geometry of the flow problem. However, $\mathbf{v}^*$ is not a function of the Reynolds number because Re does not appear in (12-9). The generic creeping flow solution is written as

$$\mathbf{v}^* = \mathbf{v}^*(\boldsymbol{r}^*; \text{geometry}) \tag{12-10}$$

where $\boldsymbol{r}^*$ represents a generic position vector that accounts for all three spatial coordinates in any orthogonal coordinate system. Based on the absence of Re in the dimensionless creeping flow equation of motion together with (12-10) for the generic velocity profile, it is also true that dynamic pressure $\mathfrak{P}^*$ depends on spatial coordinates and the specific geometry of the flow problem via equation (12-8), but not the Reynolds number. These claims are justified by comparing the functional form of the generic solutions in this chapter with exact analytical solutions for creeping flow of incompressible Newtonian fluids around solid spheres and gas bubbles, as presented in Chapter 8. For two-dimensional axisymmetric creeping flow around a solid sphere, the θ component of (12-10) yields

$$g^*(\theta; \text{geometry}) = \left[\frac{\partial}{\partial \eta}\left(\frac{v_\theta^*}{\eta}\right)\right]_{\eta=1} \neq f(\text{Re}) \tag{12-11}$$

The dimensionless mass transfer correlation, given by (12-1), reveals the complete dependence of the surface-averaged Sherwood number on the Reynolds and Schmidt numbers:

$$\text{Sh}_{\text{average}} = (\text{Re} \cdot \text{Sc})^{1/3} f(\text{geometry}) \tag{12-12}$$

where

$$f(\text{geometry}) = 1.28 \left\{ \int [g^*(\theta; \text{geometry}) \sin^3 \theta]^{1/2} \, d\theta \right\}^{2/3} \qquad 0 \leq \theta \leq \pi/2$$

12-3 LOCALLY FLAT MOMENTUM BOUNDARY LAYER PROBLEM FOR LAMINAR FLOW AROUND SOLID SPHERES

The tangential component of the dimensionless equation of motion is written explicitly for steady-state two-dimensional flow in rectangular coordinates. This locally flat description is valid for laminar flow around a solid sphere because it is only necessary to consider momentum transport within a thin mass transfer boundary layer at sufficiently large Schmidt numbers. The polar velocity component v_θ is written as v_x parallel to the solid–liquid interface, and the x direction accounts for arc length (i.e., $x = R\theta$). The radial velocity component v_r is written

as v_y, and the coordinate measured normal to the interface is $y = r - R$. The dimensionless independent variables are

$$x^* = \frac{x}{R} = \theta \qquad y^* = \frac{y}{R} = \eta - 1 \tag{12-13}$$

In the primary flow direction, parallel to the interface, within the mass and momentum boundary layers, molecular transport of x momentum in the x direction (i.e., $\mu \partial^2 v_x / \partial x^2$) is neglected relative to convective transport of x momentum in the x direction (i.e., $\rho v_x \partial v_x / \partial x$). Hence, when convective, viscous, and dynamic pressure forces are equally important, the x component of the dimensionless equation of motion is

$$\mathrm{Re}\left(v_x^* \frac{\partial v_x^*}{\partial x^*} + v_y^* \frac{\partial v_x^*}{\partial y^*}\right) = \frac{\partial^2 v_x^*}{\partial y^{*2}} - \frac{\partial \mathfrak{P}^*}{\partial x^*} \tag{12-14}$$

if dynamic pressure is dimensionalized using a characteristic viscous momentum flux (i.e., $\mu V/L$). If dynamic pressure is dimensionalized using ρV^2, then the dynamic pressure gradient scales similarly to the two terms on the left side of (12-14). Hence,

$$\mathrm{Re}\left(v_x^* \frac{\partial v_x^*}{\partial x^*} + v_y^* \frac{\partial v_x^*}{\partial y^*}\right) = \frac{\partial^2 v_x^*}{\partial y^{*2}} - \mathrm{Re}\left(\frac{\partial \mathfrak{P}^*}{\partial x^*}\right) \tag{12-15}$$

The latter approach is adopted because dynamic pressure gradients are calculated in the potential flow regime, outside the momentum boundary layer and far from the solid–liquid interface, where $\mu \to 0$ and viscous forces are negligible. Then, $\partial \mathfrak{P}^* / \partial x^*$ is imposed across the boundary layer. This is standard practice for momentum boundary layer problems. Hence, if $\mathbf{v}_P^*$ represents the dimensionless velocity vector in the potential flow regime, then the steady-state dimensionless equation of motion is

$$\mathbf{v}_P^* \cdot \nabla^* \mathbf{v}_P^* = -\nabla^* \mathfrak{P}^* \tag{12-16}$$

There are no dimensionless numbers in this potential flow equation because convective forces per unit volume and dynamic pressure forces per unit volume both scale as $\rho V^2/L$. Furthermore, potential flow theory provides the formalism to calculate $\mathbf{v}_P^*$ and the dimensionless scalar velocity potential Φ^* such that the vorticity vector vanishes and overall fluid mass is conserved for an incompressible fluid. Hence,

$$\mathbf{v}_P^* = -\nabla^* \Phi^*. \tag{12-17a}$$

$$\nabla^* \times \mathbf{v}_P^* = 0. \tag{12-17b}$$

$$\nabla^* \cdot \mathbf{v}_P^* = -\nabla^{*2} \Phi^* = 0. \tag{12-17c}$$

One concludes from (12-17*a*) and (12-17*c*) that neither Φ^* nor $\mathbf{v}_P^*$ is a function of the Reynolds number because Re does not appear in either equation. Consequently, dynamic pressure and its gradient in the x direction are not functions of the Reynolds number because Re does not appear in the dimensionless potential flow equation of motion, given by (12-16), from which $\partial \mathfrak{P}^*/\partial x^*$ is calculated. In summary, two-dimensional momentum boundary layer problems in the laminar flow regime (1) focus on the component of the equation of motion in the primary flow direction, (2) use the equation of continuity to calculate the other velocity component transverse to the primary flow direction, (3) use potential flow theory far from a fluid–solid interface to calculate the important component of the dynamic pressure gradient, and (4) impose this pressure gradient across the momentum boundary layer. The following set of dimensionless equations must be solved for Φ^*, $\mathbf{v}_P^*$, $\mathfrak{P}^*$, v_x^*, and v_y^* in sequential order. The first three equations below are solved separately, but the last two equations are coupled:

$$\nabla^{*2}\Phi^* = 0 \qquad \Phi^* \neq f(\mathrm{Re}) \tag{12-18a}$$

$$\mathbf{v}_P^* = -\nabla^*\Phi^* \qquad \mathbf{v}_P^* \neq f(\mathrm{Re}) \tag{12-18b}$$

$$-\nabla^*\mathfrak{P}^* = \mathbf{v}_P^* \cdot \nabla^*\mathbf{v}_P^* \qquad \mathfrak{P}^* \neq f(\mathrm{Re}) \tag{12-18c}$$

$$\frac{\partial v_x^*}{\partial x^*} + \frac{\partial v_y^*}{\partial y^*} = 0 \tag{12-18d}$$

$$\mathrm{Re}\left(v_x^*\frac{\partial v_x^*}{\partial x^*} + v_y^*\frac{\partial v_x^*}{\partial y^*} + \frac{\partial \mathfrak{P}^*}{\partial x^*}\right) = \frac{\partial^2 v_x^*}{\partial y^{*2}} \tag{12-18e}$$

Based on the dimensionless equation of continuity [i.e., eq. (12-18*d*)] and the x component of the dimensionless equation of motion [i.e., eq. (12-18*e*)] in the laminar flow regime, one concludes that both v_x^* and v_y^* are functions of dimensionless spatial coordinates x^* and y^*, as well as the Reynolds number and the geometry of the flow configuration. Unfortunately, the previous set of equations does not reveal the specific dependence of v_x^* and v_y^* on Re.

12-4 RENORMALIZATION OF THE DIMENSIONLESS VARIABLES REVEALS EXPLICIT DEPENDENCE OF g^* ON Re

Momentum boundary layer problems in the laminar flow regime, particularly (12-18*d*) and (12-18*e*), are revisited after a new set of dimensionless variables is introduced. This strategy will be successful if one redefines dimensionless independent spatial coordinates (i.e., x' and y') and the x and y components of the dimensionless velocity vector (i.e., v_x' and v_y') such that v_x' and v_y' do not depend explicitly on the Reynolds number, based on simultaneous solution of (12-18*d*) and (12-18*e*). The appropriate definitions are

$$x' = x^* \qquad y' = y^*\sqrt{\mathrm{Re}} \qquad v_x' = v_x^* \qquad v_y' = v_y^*\sqrt{\mathrm{Re}} \tag{12-19}$$

The following partial derivatives are required to re-express equations (12-18*d*) and (12-18*e*) in terms of these new variables:

$$\begin{aligned} \frac{\partial v_x^*}{\partial x^*} &= \frac{\partial v_x'}{\partial x'} \qquad \frac{\partial v_x^*}{\partial y^*} = \mathrm{Re}^{1/2}\,\frac{\partial v_x'}{\partial y'} \\ \frac{\partial v_y^*}{\partial y^*} &= \frac{\partial v_y'}{\partial y'} \qquad \frac{\partial}{\partial y^*}\left(\frac{\partial v_x^*}{\partial y^*}\right) = \mathrm{Re}\left(\frac{\partial^2 v_x'}{\partial y'^2}\right) \end{aligned} \tag{12-20}$$

The dimensionless equation of continuity looks exactly the same when the old variables are replaced by the new ones:

$$\text{Renormalized (12-18}d\text{):} \qquad \frac{\partial v_x'}{\partial x'} + \frac{\partial v_y'}{\partial y'} = 0 \tag{12-21}$$

However, the Reynolds number does not appear explicitly in the renormalized form of the dimensionless equation of motion:

$$\text{Renormalized (12-18}e\text{):} \qquad v_x'\frac{\partial v_x'}{\partial x'} + v_y'\frac{\partial v_x'}{\partial y'} + \frac{\partial \mathfrak{P}^*}{\partial x'} = \frac{\partial^2 v_x'}{\partial y'^2} \tag{12-22}$$

The new set of dimensionless variables has transformed the equations of continuity and motion into two coupled partial differential equations for v_x' and v_y' with no explicit dependence on the Reynolds number because Re does not appear in either (12-21) or (12-22). Remember that $\mathfrak{P}^*$ is calculated from potential flow theory via (12-18*c*), exhibiting no dependence on Re, and x' is the same as x^*. Hence, renormalization has no effect on the dimensionless dynamic pressure gradient in the x direction. One concludes from (12-21) and (12-22) that

$$v_x' = v_x'(x', y'; \text{geometry}) \neq f(\mathrm{Re}) \tag{12-23}$$

$$v_y' = v_y'(x', y'; \text{geometry}) \neq f(\mathrm{Re}) \tag{12-24}$$

However, these two dimensionless velocity components depend implicitly on the Reynolds number, because Re is embedded in the dimensionless independent variable y' measured normal to the fluid–solid interface. Now, the dimensionless velocity gradient of interest at the fluid–solid interface is

$$g^*(\theta) = \left[\frac{\partial}{\partial \eta}\left(\frac{v_\theta^*}{\eta}\right)\right]_{\eta=1} = \left\{\frac{\partial[v_x^*/(1+y^*)]}{\partial y^*}\right\}_{y^*=0} = \sqrt{\mathrm{Re}}\left\{\frac{\partial[v_x'/(1+y^*)]}{\partial y'}\right\}_{y'=0} \tag{12-25}$$

which reduces to

$$g^*(\theta) = \sqrt{\mathrm{Re}}\left(\frac{\partial v_x'}{\partial y'}\right)_{y'=0} - v_x'(y'=0) \tag{12-26}$$

Hence, for a high-shear no-slip interface in which the tangential velocity component v_x' vanishes at the solid surface (i.e., $y' = 0$), the dimensionless velocity gradient of interest exhibits the following dependence on the Reynolds number:

$$g^*(\theta) = \sqrt{\mathrm{Re}}\left(\frac{\partial v_x'}{\partial y'}\right)_{y'=0} = \sqrt{\mathrm{Re}}\,\chi(\theta; \text{geometry}) \tag{12-27}$$

where polar angle $\theta = x^* = x'$. This result is used to obtain the complete functional dependence of $\mathrm{Sh}_{\text{average}}$ on the Reynolds and Schmidt numbers via (12-1):

$$\mathrm{Sh}_{\text{average}} = 1.28(\mathrm{Re}\cdot\mathrm{Sc})^{1/3}\left\{\int_0^{\pi/2}\left[\sqrt{\mathrm{Re}}\,\chi(\theta; \text{geometry})\sin^3\theta\right]^{1/2} d\theta\right\}^{2/3} \tag{12-28}$$

Hence, the appropriate scaling law is

$$\mathrm{Sh}_{\text{average}} = \mathrm{Re}^{1/2}\cdot\mathrm{Sc}^{1/3}\,\Xi(\text{geometry}) \tag{12-29}$$

where

$$\Xi(\text{geometry}) = 1.28\left\{\int[\chi(\theta; \text{geometry})\sin^3\theta]^{1/2}\,d\theta\right\}^{2/3} \qquad 0 \le \theta \le \pi/2$$

depends on specific details of the flow geometry within the mass transfer boundary layer. As mentioned previously, the fact that $\mathrm{Sh}_{\text{average}}$ scales as $\mathrm{Sc}^{1/3}$ signifies a high-shear no-slip interface where the tangential velocity profile exhibits linear dependence on the independent variable measured normal to the interface. The

TABLE 12-1 Effect of Flow Regime and the Nature of the Interface on Dimensionless Correlations for the Surface-Averaged Sherwood Number via Steady-State Mass Transfer Boundary Layer Theory in Nonreactive Systems

	Nature of the Interface	
Flow Regime	Solid–Liquid, High Shear, No Slip	Gas–Liquid, Zero Shear, Perfect Slip
Creeping flow	$\mathrm{Sh}_{\text{average}} \approx (\mathrm{Re}\cdot\mathrm{Sc})^{1/3}$	$\mathrm{Sh}_{\text{average}} \approx (\mathrm{Re}\cdot\mathrm{Sc})^{1/2}$
Laminar flow	$\mathrm{Sh}_{\text{average}} \approx \mathrm{Re}^{1/2}\cdot\mathrm{Sc}^{1/3}$	$\mathrm{Sh}_{\text{average}} \approx (\mathrm{Re}\cdot\mathrm{Sc})^{1/2}$
Turbulent flow	$\mathrm{Sh}_{\text{average}} \approx \mathrm{Re}^a\cdot\mathrm{Sc}^{1/3}$, $0.8 \le a \le 1$	Not possible without significant interfacial deformation

$\frac{1}{2}$-power dependence of the dimensionless mass transfer coefficient on Re reveals that the flow regime is laminar. Turbulent mass transfer across high-shear no-slip interfaces also scales as $Sh_{average} \approx Sc^{1/3}$, but the exponent of Re in this correlation is somewhere between 0.8 and 1. All of these dimensionless scaling laws for interphase mass transfer are summarized in Table 12-1 for solid–liquid and gas–liquid interfaces.

Transport Phenomena for Chemical Reactor Design. Laurence A. Belfiore
Copyright © 2003 John Wiley & Sons, Inc.
ISBN: 0-471-20275-4

13

DIFFUSION AND CHEMICAL REACTION ACROSS SPHERICAL GAS–LIQUID INTERFACES

13-1 MOLAR DENSITY PROFILE

Reactant gases such as chlorine and oxygen, which are soluble in common liquids, can diffuse into the liquid phase across a spherical interface and react with other species in the liquid mixture. The objective of this chapter is to illustrate how chemical reaction provides an enhancement factor for mass transfer coefficients in the liquid phase when interfacial curvature cannot be neglected. The results are applicable when gases are dispersed in a liquid via sparger/impeller designs that maximize the surface-to-volume ratio to increase interphase mass transfer. The chemical reaction enhancement factor for curved interfaces reduces to the one for flat interfaces when the radius of curvature of the interface is infinitely large, which is equivalent to a thin mass transfer boundary layer relative to the bubble diameter at very high Damkohler numbers.

In spherical coordinates, the dimensional mass transfer equation with radial diffusion and first-order irreversible chemical reaction exhibits an analytical solution for the molar density profile of reactant A. If the kinetics are not zeroth-order or first-order, then the methodology exists to find the best pseudo-first-order rate constant to match the actual rate law and obtain an approximate analytical solution. The concentration profile of reactant A in the liquid phase must satisfy

$$\mathfrak{D}_{\mathrm{A,\,liq.\ mix.}}\nabla^2 C_{\mathrm{A}} + \sum_j \nu_{\mathrm{A}j}\mathfrak{R}_j = 0 \tag{13-1}$$

This mass balance with diffusion and chemical reaction is written explicitly in spherical coordinates when reactant A is consumed by one first-order irreversible reaction:

$$\mathfrak{D}_{\text{A, liq. mix.}} \frac{1}{r^2} \frac{d}{dr} \left(r^2 \frac{dC_\text{A}}{dr} \right) - k_1 C_\text{A} = 0 \tag{13-2}$$

where r is the position variable measured normal to the gas–liquid interface with origin at the center of the bubble, $\mathfrak{D}_{\text{A, liq. mix.}}$ is an ordinary molecular diffusion coefficient of component A in the liquid mixture, and k_1 is a pseudo-first-order kinetic rate constant for a homogeneous rate law. The boundary conditions are

$$\begin{aligned} C_\text{A} &= C_{\text{A}i} \qquad \text{at } r = R_\text{bubble} \\ C_\text{A} &\longrightarrow 0 \qquad \text{at } r = R_\text{bubble} + \text{MTBLT}_\text{liquid} \end{aligned} \tag{13-3}$$

where $C_{\text{A}i}$ is the interfacial molar density of species A in the liquid phase and $\text{MTBLT}_\text{liquid}$ is the mass transfer boundary layer thickness on the liquid side of the interface. The canonical transformation

$$C_\text{A}(r) = \frac{\Psi_\text{A}(r)}{r} \tag{13-4}$$

allows one to express the radial contribution to the spherical-coordinate Laplacian of molar density in a form that essentially eliminates complications from the fact that the surface area normal to radial mass flux increases as r^2 when reactant A diffuses into the surrounding liquid. Now, it is necessary to calculate

$$\frac{dC_\text{A}}{dr} = \frac{1}{r} \frac{d\Psi_\text{A}}{dr} - \frac{\Psi_\text{A}}{r^2} \tag{13-5a}$$

$$r^2 \frac{dC_\text{A}}{dr} = r \frac{d\Psi_\text{A}}{dr} - \Psi_\text{A} \tag{13-5b}$$

$$\frac{d}{dr} \left(r^2 \frac{dC_\text{A}}{dr} \right) = r \frac{d^2\Psi_\text{A}}{dr^2} + \frac{d\Psi_\text{A}}{dr} - \frac{d\Psi_\text{A}}{dr} = r \frac{d^2\Psi_\text{A}}{dr^2} \tag{13-5c}$$

Hence, the radial contribution to the spherical-coordinate Laplacian of molar density is

$$(\nabla \cdot \nabla C_\text{A})_{r\text{-contribution}} = \frac{1}{r^2} \frac{d}{dr} \left(r^2 \frac{dC_\text{A}}{dr} \right) = \frac{1}{r} \frac{d^2\Psi_\text{A}}{dr^2} \tag{13-6}$$

Now the mass transfer equation for $\Psi_\text{A}(r)$ with radial diffusion and chemical reaction exhibits a flat description in spherical coordinates:

$$\mathfrak{D}_{\text{A, liq. mix.}} \frac{1}{r} \frac{d^2\Psi_\text{A}}{dr^2} = \frac{k_1 \Psi_\text{A}}{r} \tag{13-7}$$

However, the transformation from C_A to Ψ_A via equation (13-4) does not simplify the corresponding mass transfer problem in cylindrical coordinates. The boundary conditions on Ψ_A become

$$\begin{aligned} \Psi_A &= R_{bubble} C_{Ai} \qquad \text{at } r = R_{bubble} \\ \Psi_A &\longrightarrow 0 \qquad\quad \text{at } r = R_{bubble} + \text{MTBLT}_{liquid} \end{aligned} \tag{13-8}$$

The radial variable r is dimensionalized to isolate the Damkohler number in the mass balance. It is important to emphasize that dimensional analysis on the radial coordinate must be performed after implementing the canonical transformation from C_A to Ψ_A. If the surface area factors of r^2 and $1/r^2$ are written in terms of η, as defined by equation (13-9), prior to introducing the canonical transformation given by equation (13-4), then the mass transfer problem external to the spherical interface retains variable coefficients. If diffusion and chemical reaction are considered inside the gas bubble, then the order in which the canonical transformation and dimensional analysis are performed is unimportant. Hence,

$$\eta = \frac{r - R_{bubble}}{\text{MTBLT}_{liquid}} \tag{13-9}$$

Now the dimensionless mass transfer equation for $\Psi_A(\eta)$ exhibits constant coefficients:

$$\frac{d^2\Psi_A}{d\eta^2} = \Lambda^2 \Psi_A \tag{13-10}$$

where the Damkohler number for reactant A is defined by

$$\Lambda^2 = \frac{k_1 (\text{MTBLT}_{liquid})^2}{\mathfrak{D}_{A,\,liq.\,mix.}} \tag{13-11}$$

The final set of boundary conditions for $\Psi_A(\eta)$ is

$$\begin{aligned} \Psi_A &= R_{bubble} C_{Ai} \qquad \text{at } \eta = 0 \\ \Psi_A &\longrightarrow 0 \qquad\quad \text{at } \eta = 1 \end{aligned} \tag{13-12}$$

These boundary conditions are particularly convenient to evaluate the integration constants, as illustrated below. The mass transfer equation corresponds to a second-order linear ordinary differential equation with constant coefficients. The analytical solution for Ψ_A is

$$\Psi_A(\eta) = A \exp(\Lambda\eta) + B \exp(-\Lambda\eta) = C \sinh(\Lambda\eta) + D \cosh(\Lambda\eta) \tag{13-13}$$

The boundary condition at $\eta = 0$ reveals that $D = R_{bubble} C_{Ai}$ and the fact that Ψ_A vanishes at the outer edge of the mass transfer boundary layer (i.e., at $\eta = 1$) gives $C = -D/\tanh\Lambda$. The molar density profile of reactant A in terms of hyperbolic functions is

$$C_A(r) = \frac{1}{r}\Psi_A(\eta) = C_{Ai} \frac{R_{bubble}}{r} \left(\cosh\Lambda\eta - \frac{\sinh\Lambda\eta}{\tanh\Lambda} \right) \tag{13-14}$$

This solution is applicable within the mass transfer boundary layer external to the gas–liquid interface where $0 \leq \eta \leq 1$.

13-2 MOLAR FLUX ANALYSIS

Now that one has obtained the basic information for the molar density of reactant A within the liquid-phase mass transfer boundary layer, it is necessary to calculate the molar flux of species A normal to the gas–liquid interface at $r = R_{\text{bubble}}$, and define the mass transfer coefficient via this flux. Since convective mass transfer normal to the interface was not included in the mass transfer equation with liquid-phase chemical reaction, it is not necessary to consider the convective mechanism at this stage of the development. Fick's first law of diffusion is sufficient to calculate the flux of A in the r direction at $r = R_{\text{bubble}}$. Hence,

$$\begin{aligned} N_{Ar}(r = R_{\text{bubble}}) &\approx -\mathfrak{D}_{\text{A, liq. mix.}} \left(\frac{dC_{\text{A}}}{dr}\right)_{r=R_{\text{bubble}}} \\ &= -\mathfrak{D}_{\text{A, liq. mix.}} \left\{ -\frac{\Psi_{\text{A}}(\eta = 0)}{(R_{\text{bubble}})^2} + \frac{1}{R_{\text{bubble}}} \left(\frac{d\Psi_{\text{A}}}{d\eta}\right)_{\eta=0} \frac{d\eta}{dr} \right\} \\ &= \frac{\mathfrak{D}_{\text{A, liq. mix.}}}{R_{\text{bubble}}} \left[\frac{\Psi_{\text{A}}(\eta = 0)}{R_{\text{bubble}}} - \frac{(d\Psi_{\text{A}}/d\eta)_{\eta=0}}{\text{MTBLT}_{\text{liquid}}} \right] \\ &\equiv k_{\text{A, liquid}}(C_{Ai} - 0) \end{aligned} \tag{13-15}$$

where $C_{\text{A}} \to 0$ at $r = R_{\text{bubble}} + \text{MTBLT}_{\text{liquid}}$ is used to construct the concentration driving force in the expression for interphase mass transfer. If one uses the bubble diameter as the characteristic length to define the Sherwood number, then

$$\text{Sh} \equiv \frac{k_{\text{A, liquid}}(2R_{\text{bubble}})}{\mathfrak{D}_{\text{A, liq. mix.}}} = \frac{2}{C_{Ai}} \left[\frac{\Psi_{\text{A}}(\eta = 0)}{R_{\text{bubble}}} - \frac{(d\Psi_{\text{A}}/d\eta)_{\eta=0}}{\text{MTBLT}_{\text{liquid}}} \right] \tag{13-16}$$

Since $\Psi_{\text{A}} = R_{\text{bubble}} C_{Ai}$ at $\eta = 0$, and

$$\begin{aligned} \frac{d\Psi_{\text{A}}}{d\eta} &= \Lambda(C \cosh \Lambda\eta + D \sinh \Lambda\eta) \\ \left(\frac{d\Psi_{\text{A}}}{d\eta}\right)_{\eta=0} &= C\Lambda = \frac{-\Lambda R_{\text{bubble}} C_{Ai}}{\tanh \Lambda} \end{aligned} \tag{13-17}$$

the final expression for the mass transfer coefficient enhancement factor in the presence of first-order irreversible chemical reaction is

$$\text{Sh} \equiv \frac{k_{\text{A, liquid}}(2R_{\text{bubble}})}{\mathfrak{D}_{\text{A, liq. mix.}}} = 2\left(1 + \frac{R_{\text{bubble}}}{\text{MTBLT}_{\text{liquid}}} \frac{\Lambda}{\tanh \Lambda}\right) \tag{13-18}$$

The appropriate mass transfer coefficient in the boundary layer on the liquid side of spherical interfaces with first-order or pseudo-first-order irreversible chemical reaction predominantly in the liquid phase is

$$k_{\mathrm{A,\,liquid}} = \frac{\mathfrak{D}_{\mathrm{A,\,liq.\ mix.}}}{R_{\mathrm{bubble}}}\left(1 + \frac{R_{\mathrm{bubble}}}{\mathrm{MTBLT}_{\mathrm{liquid}}}\frac{\Lambda}{\tanh\Lambda}\right) \tag{13-19}$$

The mass transfer boundary layer thickness on the liquid side of the interface is very thin at large Damkohler numbers. Hence,

$$1 + \frac{R_{\mathrm{bubble}}}{\mathrm{MTBLT}_{\mathrm{liquid}}}\frac{\Lambda}{\tanh\Lambda} \approx \Lambda\frac{R_{\mathrm{bubble}}}{\mathrm{MTBLT}_{\mathrm{liquid}}} \tag{13-20}$$

when $\Lambda^2 \gg 1$. Under these conditions in the diffusion-limited regime (i.e., $\tanh\Lambda \to 1$),

$$k_{\mathrm{A,\,liquid}} \approx \frac{\mathfrak{D}_{\mathrm{A,\,liq.\ mix.}}}{\mathrm{MTBLT}_{\mathrm{liquid}}}\Lambda \to \sqrt{k_1\mathfrak{D}_{\mathrm{A,\,liq.\ mix.}}} \tag{13-21}$$

Illustrative Problem. Consider a spherical solid pellet of pure A, with mass density ρ_A, which dissolves into stagnant liquid B exclusively by concentration diffusion in the radial direction and reacts with B. Since liquid B is present in excess, the homogeneous kinetic rate law which describes the chemical reaction is pseudo-first-order with respect to the molar density of species A in the liquid phase. Use some of the results described in this chapter to predict the time dependence of the radius of this spherical solid pellet, $R(t)$, **(a)** in the presence of rapid first-order irreversible liquid-phase chemical reaction in the diffusion-limited regime, and **(b)** when no reaction occurs between species A and B. The molecular weight of species A is $\mathrm{MW_A}$.

SOLUTION. The steady-state molar density profile of reactant A, given by (13-14) in the presence of a first-order irreversible chemical reaction, is employed to calculate the r component of the molar flux of A at the solid–liquid interface [i.e., $r = R(t)$]. Then, one constructs an unsteady-state macroscopic mass balance on the solid pellet where no chemical reaction occurs, and the steady-state interfacial flux at $r = R(t)$ is viewed as an output term. If the system is defined as the shrinking volume of the solid pellet, then the unsteady-state macroscopic mass balance is

$$\text{rate of accumulation} = \text{rate of input} - \text{rate of output} + \text{rate of production}$$

Each term in this balance, with dimensions of the moles of A per time, is evaluated separately:

$$\text{rate of accumulation} = \frac{d}{dt}\left(\frac{\frac{4}{3}\pi R^3\rho_{\mathrm{A}}}{\mathrm{MW_A}}\right) = \frac{\rho_{\mathrm{A}}}{\mathrm{MW_A}}4\pi R^2\frac{dR}{dt}$$

$$\text{rate of input} = 0$$

$$\text{rate of output} = 4\pi R^2 \left[-\mathfrak{D}_{\text{A, liq. mix.}} \left(\frac{dC_\text{A}}{dr} \right)_{r=R} \right]$$
$$= 4\pi R^2 k_{\text{A, liquid}} (C_{\text{A}i} - 0)$$
$$\text{rate of production} = 0$$

Hence, one calculates the time dependence of the pellet radius from the following equation:

$$\rho_\text{A} \frac{dR}{dt} = \mathfrak{D}_{\text{A, liq. mix.}} (\text{MW}_\text{A}) \left(\frac{dC_\text{A}}{dr} \right)_{r=R}$$

The first approach employs steady-state results for diffusion with first-order irreversible chemical reaction external to a gas bubble, as discussed in this chapter, to evaluate the radial concentration gradient at the interface. No correction factor is required to account for the fact that, in this chapter, we address diffusion and chemical reaction in an incompressible liquid that surrounds a bubble, whereas the unsteady-state mass balance described by the preceding equation requires the radial concentration gradient adjacent to a solid–liquid interface. If solid A is slightly soluble in liquid B and its radius $R(t)$ doesn't decrease too much during the time span of the analysis, then the liquid-phase mass transfer boundary layer thickness should remain relatively constant. This is a convenient assumption because the Damkohler number and the dimensionless radial variable are defined in terms of $\text{MTBLT}_\text{liquid}$, as given by equations (13-9) and (13-11). A zeroth-order approximation to the effect of convective mass transfer on all the results presented in this chapter is obtained by decreasing $\text{MTBLT}_\text{liquid}$ at higher liquid-phase flow rates. A second approach (1) uses the pellet radius to define the Damkohler number and the dimensionless independent radial variable, (2) considers that the mass transfer boundary layer which surrounds the solid pellet is infinitely thick, and (3) accounts for changes in the Damkohler number as R decreases. In reality, the mass transfer boundary layer increases at longer times because species A diffuses radially outward and reacts with B while the radius of the solid pellet simultaneously shrinks. The steady-state liquid-phase concentration gradient of reactant A at the solid–liquid interface, based on the first approach, is obtained from the Sherwood number correlation given by equations (13-15) and (13-18):

$$\text{Sh} \equiv \frac{k_{\text{A, liquid}} \ (2R)}{\mathfrak{D}_{\text{A, liq. mix.}}} = -\frac{2R}{C_{\text{A}i}} \left(\frac{dC_\text{A}}{dr} \right)_{r=R}$$
$$= 2 \left(1 + \frac{R}{\text{MTBLT}_\text{liquid}} \frac{\Lambda}{\tanh \Lambda} \right)$$

Hence,

$$- \left(\frac{dC_\text{A}}{dr} \right)_{r=R} = \frac{C_{\text{A}i}}{R} \left(1 + \frac{R}{\text{MTBLT}_\text{liquid}} \frac{\Lambda}{\tanh \Lambda} \right)$$

where the pellet radius R decreases with time, but $\text{MTBLT}_{\text{liquid}}$ and Λ are treated as constants in the following analysis. The unsteady-state mass balance on the solid spherical pellet becomes

$$\rho_{\text{A}} \frac{dR}{dt} = -\mathfrak{D}_{\text{A, liq. mix.}}(\text{MW}_{\text{A}}) \frac{C_{\text{A}i}}{R} \left(1 + \frac{R}{\text{MTBLT}_{\text{liquid}}} \frac{\Lambda}{\tanh \Lambda}\right)$$

and one must integrate the following expression to calculate $R(t)$, subject to the initial condition that $R = R_0$ at $t = t_0$:

$$\int_{R_0}^{R(t)} \frac{R'}{1 + (R'/\text{MTBLT}_{\text{liquid}})(\Lambda/\tanh \Lambda)} \, dR' = \frac{-\mathfrak{D}_{\text{A, liq. mix.}}(\text{MW}_{\text{A}}) C_{\text{A}i}(t - t_0)}{\rho_{\text{A}}}$$

Integral tables yield the following result, which can be applied to the preceding equation:

$$\int \frac{x}{a + bx} \, dx = \frac{x}{b} - \frac{a}{b^2} \ln(a + bx)$$

$$a = 1$$

$$b = \frac{\Lambda}{\text{MTBLT}_{\text{liquid}} \tanh \Lambda} = \frac{(k_1/\mathfrak{D}_{\text{A, liq. mix.}})^{1/2}}{\tanh \Lambda}$$

Hence, one determines $R(t)$ implicitly from

$$[R(t) - R_0] \tanh \Lambda \sqrt{\frac{\mathfrak{D}_{\text{A, liq. mix.}}}{k_1}} + \left(\frac{1}{\rho_{\text{A}}}\right) \mathfrak{D}_{\text{A, liq. mix.}}(\text{MW}_{\text{A}}) C_{\text{A}i}(t - t_0)$$

$$= \frac{\mathfrak{D}_{\text{A, liq. mix.}}}{k_1} (\tanh \Lambda)^2 \ln \left\{ \frac{\tanh \Lambda + R(t)\sqrt{k_1/\mathfrak{D}_{\text{A, liq. mix.}}}}{\tanh \Lambda + R_0 \sqrt{k_1/\mathfrak{D}_{\text{A, liq. mix.}}}} \right\}$$

Diffusion-Limited Regime. There are two limiting cases of the preceding equation which predicts the time dependence of the decreasing radius of the spherical solid pellet, $R(t)$. For example, in the diffusion-limited regime where the rate of chemical reaction is much faster than the rate of diffusion of species A into liquid B, the Damkohler number Λ is large and the thickness of the mass transfer boundary layer $\text{MTBLT}_{\text{liquid}}$ is much smaller than the pellet radius. Now, the hyperbolic tangent of Λ approaches unity; the second term in the denominator on the left side of the integral equation for $R(t)$ is much more important than the first term:

$$1 + \frac{R'}{\text{MTBLT}_{\text{liquid}}} \frac{\Lambda}{\tanh \Lambda} \approx \frac{R'\Lambda}{\text{MTBLT}_{\text{liquid}}} \qquad R(t) \le R' \le R_0$$

and $R(t)$ is calculated from

$$\int_{R_0}^{R(t)} \frac{\text{MTBLT}_{\text{liquid}}}{\Lambda}\, dR' = \left(\frac{\mathfrak{D}_{\text{A, liq. mix.}}}{k_1}\right)^{1/2} [R(t) - R_0]$$
$$= \frac{-\mathfrak{D}_{\text{A, liq. mix.}}(\text{MW}_\text{A})C_{\text{A}i}(t - t_0)}{\rho_\text{A}}$$

This is analogous to neglecting the logarithmic term in the implicit expression for $R(t)$ when $k_1 \gg \mathfrak{D}_{\text{A, liq. mix.}}$. Therefore, the final result for $R(t)$ is

$$R(t) = R_0 - \left(\frac{1}{\rho_\text{A}}\right)\sqrt{k_1 \mathfrak{D}_{\text{A, liq. mix.}}}(\text{MW}_\text{A})C_{\text{A}i}(t - t_0)$$

during the early stages of the process. For brevity, if one sets $t_0 = 0$ and extrapolates this result to long times to calculate the time required for complete dissolution of the spherical pellet (i.e., $t_{\text{dissolution}}$), then $R(t_{\text{dissolution}}) = 0$ and

$$t_{\text{dissolution}} = \frac{\rho_\text{A} R_0}{(k_1 \mathfrak{D}_{\text{A, liq. mix.}})^{1/2}(\text{MW}_\text{A})C_{\text{A}i}}$$

which suggests that the dissolution time scales linearly with the initial radius of the spherical solid pellet when fast chemical reaction occurs and the process is limited by radial diffusion of species A into the liquid phase.

No Chemical Reaction in the Liquid Phase. This is the other limiting case where one calculates the time dependence of the radius of the spherical solid pellet when the Damkohler number approaches zero. Hence, species A dissolves into stagnant liquid B and the mass transfer boundary layer thickness grows with the square root of time according to the classic penetration theory. In other words,

$$\text{MTBLT}_{\text{liquid}} \approx [4\mathfrak{D}_{\text{A, liq. mix.}}(t - t_0)]^{1/2}$$

A time-varying mass transfer boundary layer thickness is consistent with the transient aspects of this analysis. When chemical reaction is absent, one must evaluate the following ratio in the limit of vanishingly small Damkohler numbers via l'Hôpital's rule:

$$\lim_{\Lambda \to 0} \left\{\frac{\Lambda}{\tanh \Lambda}\right\} = 1$$

Numerical integration of the following equation yields $R(t)$ in the absence of any liquid-phase chemical reaction, once again subject to the condition that $R = R_0$ at $t = t_0$:

$$\rho_\text{A}\frac{dR}{dt} = -\mathfrak{D}_{\text{A, liq. mix.}}(\text{MW}_\text{A})\frac{C_{\text{A}i}}{R}\left(1 + \frac{R}{\text{MTBLT}_{\text{liquid}}}\right)$$

The long-time behavior of $R(t)$ can be treated analytically, because species A diffuses a significant distance into liquid B and the sphere radius R shrinks considerably, such that

$$\frac{\text{MTBLT}_{\text{liquid}}}{R} \gg 1$$

$$1 + \frac{R}{\text{MTBLT}_{\text{liquid}}} \approx 1$$

Hence,

$$R\frac{dR}{dt} = \frac{-\mathscr{D}_{\text{A, liq. mix.}}(\text{MW}_{\text{A}})C_{\text{A}i}}{\rho_{\text{A}}}$$

and integration from t_0 to time t yields

$$[R(t)]^2 = [R(t_0)]^2 - \frac{2\mathscr{D}_{\text{A, liq. mix.}}(\text{MW}_{\text{A}})C_{\text{A}i}(t - t_0)}{\rho_{\text{A}}}$$

This result for $R(t)$ is useful to estimate the time required for complete dissolution of the spherical solid pellet. Hence, one sets $t_0 = 0$ and solves for $t_{\text{dissolution}}$ such that $R(t_{\text{dissolution}}) = 0$. The result is

$$t_{\text{dissolution}} = \frac{\rho_{\text{A}}[R(t_0)]^2}{2\mathscr{D}_{\text{A, liq. mix.}}(\text{MW}_{\text{A}})C_{\text{A}i}}$$

which suggests that dissolution times scale as the square of the initial radius of the spherical pellet when chemical reaction does not occur.

Alternative Approach in the Absence of Liquid-Phase Chemical Reaction. The previous scaling law for the dissolution of spherical solid particles in a surrounding quiescent liquid can be addressed by performing an unsteady-state macroscopic mass balance on the liquid solution, with volume V_{liquid}. The accumulation of species A is balanced by the rate of interphase mass transfer (MT) when no chemical reaction occurs. Hence,

$$\text{rate of accumulation} = \text{rate of input due to interphase mass transfer}$$

With dimensions of moles per time, each term in this unsteady-state balance is evaluated separately:

$$\text{rate of accumulation} = V_{\text{liquid}}\frac{dC_{\text{A}}}{dt}$$

$$\text{rate of input due to MT} = 4\pi R^2 N_{\text{particles}} k_{C,\text{ liquid}}(C_{\text{A}i} - C_{\text{A}})$$

where C_{A} is the liquid-phase molar density of species A and $N_{\text{particles}}$ represents the total number of spherical solid particles that are present. The time dependence

of the bulk molar density of species A in the liquid phase is calculated from the following ordinary differential equation:

$$\frac{dC_{\mathrm{A}}}{dt} = \frac{C_{\mathrm{A}i} - C_{\mathrm{A}}}{\lambda}$$

subject to the initial condition that $C_{\mathrm{A}} = 0$ at $t = t_0$. The mass transfer time constant for the dissolution process is defined by

$$\lambda = \frac{V_{\mathrm{liquid}}}{4\pi R^2 N_{\mathrm{particles}} k_{C,\,\mathrm{liquid}}}$$

and $C_{\mathrm{A}}(t)$ is given by

$$C_{\mathrm{A}}(t) = C_{\mathrm{A}i}\left[1 - \exp\left(-\frac{t - t_0}{\lambda}\right)\right]$$

Now, it is instructive to re-analyze the unsteady-state macroscopic mass balance on an isolated solid pellet of pure A with no chemical reaction. The rate of output due to interphase mass transfer from the solid particle to the liquid solution is expressed as the product of a liquid-phase mass transfer coefficient $k_{C,\,\mathrm{liquid}}$, a concentration driving force $(C_{\mathrm{A}i} - C_{\mathrm{A}})$, and the surface area of one spherical pellet, $4\pi R^2$. The unsteady-state mass balance on the solid yields an ordinary differential equation for the time dependence of the radius of the pellet. For example,

$$\frac{\rho_{\mathrm{A}}}{\mathrm{MW}_{\mathrm{A}}}\, 4\pi R^2 \frac{dR}{dt} = -4\pi R^2 k_{\mathrm{A,\,liquid}}(C_{\mathrm{A}i} - C_{\mathrm{A}})$$

and the unsteady-state mass balance on the liquid solution suggests that the concentration driving force is

$$C_{\mathrm{A}i} - C_{\mathrm{A}} = C_{\mathrm{A}i} \exp\left(-\frac{t - t_0}{\lambda}\right)$$

Hence $R(t)$ is calculated from

$$\rho_{\mathrm{A}} \frac{dR}{dt} = -k_{\mathrm{A,\,liquid}}(\mathrm{MW}_{\mathrm{A}}) C_{\mathrm{A}i} \exp\left(-\frac{t - t_0}{\lambda}\right)$$

In the absence of any chemical reaction, the Damkohler number vanishes and the steady-state Sherwood number correlation, given by equation (13-18), reduces to

$$\mathrm{Sh} \equiv \frac{k_{\mathrm{A,\,liquid}}(2R)}{\mathfrak{D}_{\mathrm{A,\,liq.\ mix.}}} = 2\left(1 + \frac{R}{\mathrm{MTBLT}_{\mathrm{liquid}}}\right)$$

which suggests that the liquid-phase mass transfer coefficient adopts the following form:

$$k_{\mathrm{A,\,liquid}} = \mathfrak{D}_{\mathrm{A,\,liq.\ mix.}}\left(\frac{1}{R} + \frac{1}{\mathrm{MTBLT}_{\mathrm{liquid}}}\right)$$

Once again, the long-time behavior of $R(t)$ can be treated analytically because

$$\text{MTBLT}_{\text{liquid}} \gg R$$

and

$$k_{\text{A, liquid}} \approx \frac{\mathfrak{D}_{\text{A, liq. mix.}}}{R}$$

Integration of the following equation yields a reasonable estimate of $R(t)$:

$$\int_{R_0}^{R(t)} R'\, dR' = -\frac{\mathfrak{D}_{\text{A, liq. mix.}}(\text{MW}_\text{A})C_{\text{A}i}}{\rho_\text{A}} \int_{t_0}^{t} \exp\left(-\frac{t' - t_0}{\lambda}\right) dt'$$

Hence,

$$[R(t_0)]^2 - [R(t)]^2 = \frac{2\lambda\mathfrak{D}_{\text{A, liq. mix.}}(\text{MW}_\text{A})C_{\text{A}i}}{\rho_\text{A}} \left[1 - \exp\left(-\frac{t - t_0}{\lambda}\right)\right]$$

If one lets $t_0 = 0$ and calculates the dissolution time such that $R(t_{\text{dissolution}}) = 0$, then

$$t_{\text{dissolution}} = -\lambda \ln\left\{1 - \frac{\rho_\text{A}[R(t_0)]^2}{2\lambda\mathfrak{D}_{\text{A, liq. mix.}}(\text{MW}_\text{A})C_{\text{A}i}}\right\}$$

$$\approx \frac{\rho_\text{A}[R(t_0)]^2}{2\mathfrak{D}_{\text{A, liq. mix.}}(\text{MW}_\text{A})C_{\text{A}i}}$$

This result, which agrees with the one on page 377, is valid only if the dissolution time is much shorter than the time constant λ for the overall process (i.e., $t_{\text{dissolution}} \ll \lambda$), such that $\ln(1 - x) \approx -x$ for small values of x. Hence, the expression for $t_{\text{dissolution}}$ here is not realistic because complete dissolution probably requires at least five time constants (i.e., $t_{\text{dissolution}} \approx 5\lambda$) to achieve more than 99% of the new equilibrium or steady state, where the solid particle no longer exists. Another strategy considers that complete dissolution requires an infinite amount of time because the surface area for mass transfer becomes infinitesimally small as the pellet radius shrinks toward zero. Now, one sets $R = 0$ as $t \to \infty$ in the integrated expression for $R(t)$ and solves for the time constant λ. The final result is

$$t_{\text{dissolution}} \approx 5\lambda = \frac{5\rho_\text{A}[R(t_0)]^2}{2\mathfrak{D}_{\text{A, liq. mix.}}(\text{MW}_\text{A})C_{\text{A}i}}$$

which agrees with the scaling law on page 377 when no chemical reaction occurs. However, this estimate of $t_{\text{dissolution}}$ from the preceding equation yields a dissolution time that is five-fold longer than the result on page 377.

Transport Phenomena for Chemical Reactor Design. Laurence A. Belfiore
Copyright © 2003 John Wiley & Sons, Inc.
ISBN: 0-471-20275-4

PART III

KINETICS AND ELEMENTARY SURFACE SCIENCE

Transport Phenomena for Chemical Reactor Design. Laurence A. Belfiore
Copyright © 2003 John Wiley & Sons, Inc.
ISBN: 0-471-20275-4

14

KINETIC MECHANISMS AND RATE EXPRESSIONS FOR HETEROGENEOUS SURFACE-CATALYZED CHEMICAL REACTIONS

14-1 CONVERTING REACTANTS TO PRODUCTS

The overall objectives of this chapter are to develop the methodology of postulating reasonable mechanisms by which reactants are converted to products on a solid catalytic surface, generate kinetic rate laws based on the proposed mechanisms, and use experimental data to determine if the kinetic model is adequate for reactor design. Seven steps are outlined below which provide an overview of the factors that must be considered in the design of heterogeneous catalytic reactors. Kinetic mechanisms and the corresponding rate laws are based on steps 3 through 6.

Step 1. Reactants enter a packed catalytic tubular reactor, and they must diffuse from the bulk fluid phase to the external surface of the solid catalyst. If external mass transfer limitations provide the dominant resistance in this sequence of diffusion, adsorption, and chemical reaction, then diffusion from the bulk fluid phase to the external surface of the catalyst is the slowest step in the overall process. Since rates of interphase mass transfer are expressed as a product of a mass transfer coefficient and a concentration driving force, the apparent rate at which reactants are converted to products follows a first-order process even though the true kinetics may not be described by a first-order rate expression. Hence, diffusion acts as an intruder and falsifies the true kinetics. The chemical kineticist seeks to minimize external and internal diffusional limitations in catalytic pellets and to extract kinetic information that is not camouflaged by rates of mass transfer. The reactor design engineer must identify the rate-limiting step that governs the reactant $\rightarrow$ product conversion rate.

Step 2. Reactants must diffuse into the central core of the porous catalyst. A quantitative description of this diffusion process requires knowledge of the tortuosity factor of the pellet, which accounts for the tortuous pathway that strongly influences diffusion. The reactor design engineer seeks numerical values for the intrapellet Damkohler number and the effectiveness factor to characterize intrapellet diffusion in an isolated catalytic pellet.

Step 3. Reactant gas molecules within the internal pores of the pellet adsorb on catalytically active surface sites. This chemical adsorption process is called *chemisorption* because the interatomic forces of attraction between adsorbed gas molecules and the active sites are similar to the strength of chemical bonds.

Step 4. Adsorbed gas molecules or fragments form an intermediate complex on active surface sites. This short-lived intermediate, called the *transition state*, represents the point of no return for reactants along the reaction pathway.

Step 5. The intermediate complex forms adsorbed products on catalytically active sites.

Step 6. Products desorb from active sites on the interior catalytic surface. This desorption process generates vacant sites that are available to participate in a catalytic cycle.

Step 7. Gaseous products diffuse out of the catalytic pores and into the bulk fluid stream that passes through the packed reactor.

14-2 ISOTHERMS

14-2.1 Langmuir Adsorption Isotherms

In the absence of chemical reaction between adsorbed species, it is instructive to analyze adsorption/desorption equilibria via steps 3 and 6. The overall objective here is to develop expressions between the partial pressure p_A of gas A above a solid surface and the fraction of active sites Θ_A on the catalyst that are occupied by this gas when it adsorbs. The phenomenon of chemisorption and the relation between p_A and Θ_A apply to a unimolecular layer of adsorbed molecules on the catalytic surface. This is typically referred to as a *monolayer*, where the intermolecular forces of attraction between adsorbed molecules and active surface sites are characteristic of chemical bonds. When complete monolayer coverage of the surface exists, subsequent adsorption on this saturated surface corresponds to physisorption, which is analogous to condensation of a gas on a cold substrate. The enthalpy change for chemisorption is exothermic with values between 10 and 100 kcal/mol. The Langmuir adsorption isotherm, first proposed in 1918 (see Langmuir, 1918), is based on the following reversible elementary step that simulates single site adsorption on a catalytic surface when there is only one adsorbate (i.e., gas A) present:

$$A + \sigma \longleftrightarrow A\sigma \tag{14-1}$$

with forward rate constant $k_{A,\,\text{adsorption}}$ (units of mol/area·time·atm) for the adsorption step and backward rate constant $k_{A,\,\text{desorption}}$ (units of mol/area·time) for the

desorption step. A represents a gas molecule, σ is a vacant active site on the catalytic surface, and Aσ corresponds to a surface site that is occupied by an adsorbed molecule of the gas. Since the proposed model consists of elementary steps, the reaction order with respect to each reactant is given by the magnitude of its stoichiometric coefficient. Hence, the forward rate of adsorption is second order and the backward rate of desorption is first order. Instead of using molar densities to construct the rate law, the adsorption rate is written in terms of p_A and Θ_V, where $\Theta_V = 1 - \Theta_A$ represents the fraction of vacant active sites. The desorption rate is expressed in terms of Θ_A. The net rate of adsorption, with units of moles per area per time for this surface-related phenomenon, is

$$\mathfrak{R}_{\text{adsorption}} = k_{\text{A, adsorption}}\, p_A \Theta_V - k_{\text{A, desorption}} \Theta_A \tag{14-2}$$

The principle of microscopic reversibility applies at equilibrium, which states that the rate of chemisorption equals the rate of desorption. It is important to emphasize that individual rates of the forward and backward steps are not zero at equilibrium but that these rates are nonzero and equal to each other. Adsorption isotherms predict surface coverage at equilibrium where $\mathfrak{R}_{\text{adsorption}} = 0$. Hence,

$$k_{\text{A, adsorption}}\, p_A \Theta_V = k_{\text{A, desorption}} \Theta_A \tag{14-3}$$

If one identifies the ratio of $k_{\text{A, adsorption}}$ to $k_{\text{A, desorption}}$ as an adsorption/desorption equilibrium constant, $K_A = k_{\text{A, adsorption}} / k_{\text{A, desorption}}$, with units of inverse pressure, then the Langmuir adsorption isotherm reduces to

$$\Theta_A = \frac{K_A p_A}{1 + K_A p_A} \tag{14-4}$$

If molecules adsorb without dissociating, then chemisorption is an exothermic process in which the adsorbate forms a chemical bond with a preferred active site on the catalytic surface. Hence, the activation energy for adsorption is smaller than the activation energy for desorption, and the adsorption/desorption equilibrium constant decreases at higher temperature. At 323 K, methane exhibits Langmuir-type adsorption on activated carbon with an equilibrium constant (i.e., K_A) of $\approx 10^{-1}$ atm^{-1} (Payne *et al.*, 1968). At 373 K, isobutane adsorption on a zeolite molecular sieve is described by the Langmuir isotherm, with $K_A \approx 28$ atm^{-1} (Hyun and Danner, 1982). Larger adsorption/desorption equilibrium constants imply that fractional surface coverage Θ_A exhibits a steeper initial increase vs. gas pressure p_A (i.e., $d\Theta_A / dp_A = K_A$ as $p_A \to 0$). There is a wealth of experimental data for adsorption of pure gases on various high-surface-area solids in Valenzuela and Myers, (1989). The specific examples for isobutane adsorption on a zeolite molecular sieve, and methane adsorption on activated carbon can be found on pages 38 and 130, respectively, in Valenzuela and Myers.

Functional Form and Limiting Behavior. The functional form of the Langmuir isotherm can be rationalized by calculating the partition function of N indistinguishable molecules adsorbed on a solid surface, where the internal degrees of

freedom of both species are not affected by the adsorption process. At equilibrium, one equates statistical mechanical expressions of the chemical potential for molecules in an ideal gas state and in an adsorbed state. The adsorption/desorption equilibrium constant K_A is proportional to $(1/T)\exp(-E/kT)$, where k is Boltzmann's constant and E is the interaction energy between adsorbed molecule and active site. For more discussion of the statistical mechanics problem, consult Ben-Naim (1992). Limiting behavior of the Langmuir isotherm is analyzed by considering surfaces that are sparsely covered and almost saturated. When the surface is sparsely covered, it is reasonable to assume that the vacant active site fraction Θ_V is close to unity. Under these conditions,

$$\begin{aligned} k_{\text{A, adsorption}}\, p_A &\approx k_{\text{A, desorption}}\, \Theta_A \\ \Theta_A &\approx K_A p_A \qquad \text{(sparsely covered)} \end{aligned} \tag{14-5}$$

which suggests that surface coverage increases linearly with gas pressure. When the surface is almost saturated with a monolayer of gas A, Θ_A is close to unity and

$$\begin{aligned} k_{\text{A, adsorption}}\, p_A \Theta_V &\approx k_{\text{A, desorption}} \\ \Theta_V &\approx \frac{1}{K_A p_A} \qquad \text{(nearly saturated)} \end{aligned} \tag{14-6}$$

which suggests that the vacant-site fraction varies inversely with gas pressure. A significant increase in the apparent surface coverage by gas A at high pressures might indicate that the surface is saturated with a complete monolayer, chemisorption has ceased, and physisorption has begun. Capillary condensation describes this sequence of events. The crossover from chemisorption to physisorption in response to an increase in gas pressure is useful to identify the volume of gas required for complete monolayer coverage when all active sites on the surface are occupied.

Experimental Verification of Adsorption Isotherms and Linear Least-Squares Analysis. If gas A is exposed to a very high surface area solid catalyst (i.e., $\approx$100 m^2/g) in a closed chamber, then a sensitive electronic balance should provide measurements of the increase in catalyst mass at a given gas pressure p_A as active sites become occupied. A flow control valve is necessary to maintain constant pressure p_A while measurements are made, because adsorption of gas molecules on the catalytic surface will cause a decrease in gas pressure if additional gas is not introduced into the system. Knowledge of the gas density at STP conditions and the additional mass of gas from the flow control valve required to maintain constant pressure p_A allows one to calculate the volume of adsorbed gas per initial mass of catalyst, v_A. Experiments are repeated at different gas pressures. The raw data correspond to $p_A - v_A$ pairs that can be modeled via the Langmuir isotherm to extract two important parameters of the adsorption process.

The fractional surface coverage by gas A is defined as follows:

$$\Theta_A \equiv \frac{v_A}{v_{A,\,\text{monolayer}}} \tag{14-7}$$

where $v_{A,\,\text{monolayer}}$ represents the volume of adsorbed gas A per initial mass of catalyst that corresponds to complete monolayer coverage. In principle, one can determine $v_{A,\,\text{monolayer}}$ experimentally by monitoring the increase in catalyst mass at the chemisorption/physisorption crossover, where capillary condensation occurs initially. The linear least-squares procedure described below treats $v_{A,\,\text{monolayer}}$ as a parameter that provides the best match with p_A–v_A data pairs prior to capillary condensation, where chemisorption is predominant. If the Langmuir isotherm applies, then the data are modeled as follows:

$$\Theta_A \equiv \frac{v_A}{v_{A,\,\text{monolayer}}} = \frac{K_A p_A}{1 + K_A p_A} \tag{14-8}$$

Upon rearrangement,

$$\frac{p_A}{v_A} = \frac{1}{K_A v_{A,\,\text{monolayer}}} + \frac{p_A}{v_{A,\,\text{monolayer}}} \tag{14-9}$$

Hence, p_A/v_A varies linearly with gas pressure p_A. Linear least-squares modeling via a first-order polynomial (i.e., $y = a_0 + a_1 x$) employs p_A/v_A as the dependent variable y and p_A as the independent variable x. The zeroth-order coefficient a_0 in the model (i.e., the intercept) is given by

$$\text{intercept} = a_0 = \frac{1}{K_A v_{A,\,\text{monolayer}}} \tag{14-10}$$

and the first-order coefficient a_1 (i.e., slope) is

$$\text{slope} = a_1 = \frac{1}{v_{A,\,\text{monolayer}}} \tag{14-11}$$

Consequently, measuring p_A–v_A data pairs and correlating p_A/v_A vs. p_A in linear fashion allows one to determine $v_{A,\,\text{monolayer}}$ via the slope, which can be verified experimentally at the chemisorption/physisorption crossover. The adsorption/desorption equilibrium constant for gas A is calculated as follows:

$$K_A = \frac{a_1}{a_0} = \frac{\text{slope}}{\text{intercept}} \tag{14-12}$$

14-2.2 Classic BET Isotherm

Brunauer *et al*. (1938) proposed the following isotherm, which accounts for the effects of temperature and pressure on equilibrium surface coverage:

$$\Theta_A \equiv \frac{v_A}{v_{A,\,\text{monolayer}}} = \frac{\beta\xi}{(1-\xi)[1 + (\beta - 1)\xi]} \tag{14-13}$$

where $\beta(T)$ is a temperature-dependent parameter that decreases at higher temperature because it is related to the difference between the heats of chemisorption and physisorption, and $\xi = p_A/P_{A,\,saturation}(T)$. $P_{A,\,saturation}$ is the vapor pressure of pure gas A at the experimental temperature. The derivation of the BET isotherm is presented in Adamson and Gast (1997, pp. 618–620). This isotherm is applicable to multilayer adsorption, where Langmuir-type adsorption applies to each layer. The first layer is chemisorbed and all successive layers are physisorbed. For example, Θ_0 represents the fraction of uncovered surface, whereas Θ_n (i.e., $n \geq 1$) corresponds to the fraction of the surface covered by n layers of adsorbed molecules. The rate of adsorption onto the nth layer, to generate the $(n+1)$st layer, depends on the partial pressure of the adsorbate p_A and the fraction of the surface covered by n layers. Hence,

$$\text{rate of adsorption onto the } n\text{th layer} = k_{\text{adsorption},\,n}\, p_A \Theta_n \tag{14-14}$$

The rate of desorption from the $(n+1)$st layer depends on the fraction of the surface covered by $(n+1)$ layers:

$$\text{rate of desorption from the } (n+1)\text{st layer} = k_{\text{desorption},\,n+1}\Theta_{n+1} \tag{14-15}$$

Since the $(n+1)$st layer is generated by adsorption onto the nth layer and depleted via desorption from the $(n+1)$st layer, one equates (14-14) and (14-15) at equilibrium, as dictated by the principle of microscopic reversibility. There is no generation term due to desorption from the $(n+2)$nd layer, or depletion term due to physisorption onto the $(n+1)$st layer, because the $(n+2)$nd layer does not exist until the previous ones have equilibrated. Hence,

$$k_{\text{adsorption},\,n}\, p_A \Theta_n = k_{\text{desorption},\,n+1}\Theta_{n+1} \tag{14-16}$$

The fractions of the surface covered by adjacent layers are related by

$$\Theta_{n+1} = \kappa_n \Theta_n \tag{14-17}$$

where

$$\kappa_n = p_A \left\{ \frac{k_{\text{adsorption},\,n}}{k_{\text{desorption},\,n+1}} \right\} \qquad n = 0, 1, 2, 3, \ldots$$

Since chemisorption occurs on the first layer and physisorption occurs on all subsequent layers, one assumes that the adsorption and desorption kinetic rate constants, as well as κ_n, are not strongly dependent on the physisorbed layer under consideration. Hence, κ_n is independent of n, for $n > 0$. If this is valid, then

$$\Theta_{n+1} = \kappa\Theta_n = \kappa^2\Theta_{n-1} = \kappa^3\Theta_{n-2} = \cdots = \kappa^n\Theta_1 \tag{14-18}$$

For the chemisorbed layer (i.e., $n = 0$), κ_0 differs from κ on all of the physisorbed layers because adsorption/desorption kinetic rate constants for chemisorption differ from those for physisorption. Hence, let $\kappa_0 = \beta\kappa$. This yields the following

expression for all the surface coverage fractions by various layers of adsorbed molecules in terms of the fraction of uncovered surface:

$$\begin{aligned}\Theta_1 &= \kappa_0\Theta_0 = \beta\kappa\Theta_0 \\ \Theta_{n+1} &= \kappa^n\Theta_1 = \beta\kappa^{n+1}\Theta_0\end{aligned} \tag{14-19}$$

At a given partial pressure of adsorbate p_A, the volume of adsorbed gas per initial mass of catalyst v_A equals the product of the volume of a complete monolayer per initial mass of catalyst $v_{A,\,\text{monolayer}}$, and a weighted sum of the various layers (i.e., n) of adsorbed molecules, where $\Theta_n / \sum_{j=0}^{\infty} \Theta_j$, represents the weighting factor when n layers are stacked upon each other. Consider a region of the catalytic surface where three layers of adsorbed molecules are stacked upon each other. The contribution to v_A from this region is given by

$$3v_{A,\,\text{monolayer}} \frac{\Theta_3}{\sum_{j=0}^{\infty} \Theta_j} \tag{14-20}$$

It is important to realize that Θ_1 and Θ_2 do not account for adsorbed molecules on the first and second layers in this region, where three layers are stacked upon each other. The complete expression for v_A is given by

$$v_A = v_{A,\,\text{monolayer}} \sum_{n=1}^{\infty} n \frac{\Theta_n}{\sum_{j=0}^{\infty} \Theta_j} \tag{14-21}$$

It is necessary to introduce the sum of all surface coverage fractions, including the fraction of uncovered surface in (14-20) and (14-21), because the Θ_n's are not normalized. In other words, $\sum_{n=0}^{\infty} \Theta_n \neq 1$, but

$$\sum_{n=0}^{\infty} \frac{\Theta_n}{\sum_{j=0}^{\infty} \Theta_j} = 1 \tag{14-22}$$

Hence, $\Theta_n / \sum_{j=0}^{\infty} \Theta_j$ is a normalized weighting factor. The fraction of the catalytic surface covered by gas A (i.e., Θ_A) is

$$\Theta_A = \frac{v_A}{v_{A,\,\text{monolayer}}} = \frac{\sum_{n=1}^{\infty} n\Theta_n}{\sum_{n=0}^{\infty} \Theta_n} \tag{14-23}$$

Numerator and denominator on the far right side of (14-23) are evaluated separately:

$$\sum_{n=1}^{\infty} n\Theta_n = \beta\Theta_0 \sum_{n=1}^{\infty} n\kappa^n = \frac{\beta\Theta_0\kappa}{(1-\kappa)^2} \tag{14-24}$$

$$\sum_{n=0}^{\infty} \Theta_n = \Theta_0 + \sum_{n=1}^{\infty} \Theta_n = \Theta_0 + \beta\Theta_0 \sum_{n=1}^{\infty} \kappa^n = \Theta_0 \left(1 + \frac{\beta\kappa}{1-\kappa}\right) \tag{14-25}$$

Equation (14-24) and (14-25) are based on algebraic equivalents of infinite power series. For example,

$$\sum_{n=1}^{\infty} \kappa^n = \frac{\kappa}{1-\kappa}$$
$$\sum_{n=1}^{\infty} n\kappa^n = \frac{\kappa}{(1-\kappa)^2} \tag{14-26}$$

when $\kappa < 1$, which implies that p_A must be less than $P_{A,\,\text{saturation}}$. These results can be obtained by (1) expansion of the series, (2) multiplication by κ to generate a modified series, (3) subtraction of the modified series from the original series, both of which look very similar, and (4) solution of the algebraic equation. The ratio of v_A to $v_{A,\,\text{monolayer}}$, which easily exceeds unity when physisorption occurs, is calculated as follows:

$$\begin{aligned}\frac{v_A}{v_{A,\,\text{monolayer}}} &= \frac{\sum_{n=1}^{\infty} n\Theta_n}{\sum_{n=0}^{\infty} \Theta_n} \\ &= \frac{\beta\Theta_0\kappa/(1-\kappa)^2}{\Theta_0[1+\beta\kappa/(1-\kappa)]} \\ &= \frac{\beta\kappa}{(1-\kappa)[1+(\beta-1)\kappa]}\end{aligned} \tag{14-27}$$

This matches the functional form of the BET isotherm when the parameter κ is given by the ratio of adsorbate partial pressure p_A to its saturation vapor pressure at the experimental temperature T, $P_{A,\,\text{saturation}}(T)$. Let's consider the parameter β, which was defined above as the ratio of κ_0 to κ. If the adsorption and desorption kinetic rate constants for chemisorption follow Arrhenius temperature dependence, then κ_0 for chemisorption on the bare surface is expressed as

$$\begin{aligned}\kappa_0 = p_A \left(\frac{k_{\text{adsorption}}}{k_{\text{desorption}}}\right)_{\text{chemisorption}} &\approx p_A \exp\left[\frac{-(E_{\text{act, adsorb. C}} - E_{\text{act, desorb. C}})}{RT}\right] \\ &\approx p_A \exp\left(\frac{-\Delta H_{\text{chemisorption}}}{RT}\right)\end{aligned} \tag{14-28}$$

The enthalpy change for chemisorption $\Delta H_{\text{chemisorption}}$, which is negative, is given by the difference between activation energies for adsorption onto the bare surface $E_{\text{act, adsorb. C}}$ and desorption from the first chemisorbed layer $E_{\text{act, desorb. C}}$. Similarly, the temperature dependence of κ for each physisorbed layer is obtained by expressing the kinetic rate constants for physisorption in Arrhenius form. The result is

$$\kappa = p_A \left(\frac{k_{\text{adsorption}}}{k_{\text{desorption}}}\right)_{\text{physisorption}} \approx p_A \exp\left(\frac{-\Delta H_{\text{physisorption}}}{RT}\right) \tag{14-29}$$

where the enthalpy change for physisorption $\Delta H_{\text{physisorption}}$, which is negative and equivalent to the enthalpy change for condensation of a gas onto a cold surface, is given by the difference between activation energies for adsorption onto the nth layer $E_{\text{act, adsorb. P}}$ and desorption from the $(n+1)$st layer $E_{\text{act, desorb. P}}$. Equations (14-28) and (14-29) allow one to calculate the temperature dependence of β:

$$\beta(T) = \frac{\kappa_0(T)}{\kappa(T)} \approx \exp\left[\frac{-(\Delta H_{\text{chemisorption}} - \Delta H_{\text{physisorption}})}{RT}\right] \tag{14-30}$$

Furthermore, the expression for $\kappa(T)$, given by equation (14-29), justifies the claim that it represents the ratio of p_{A} to $P_{\text{A, saturation}}(T)$:

$$\begin{aligned}\kappa(T) &\approx p_{\text{A}} \exp\left(\frac{-\Delta H_{\text{physisorption}}}{RT}\right)\\ &\approx p_{\text{A}} \exp\left(\frac{-\Delta H_{\text{condensation}}}{RT}\right)\\ &\approx \frac{p_{\text{A}}}{\exp\left(-\Delta H_{\text{vaporization}}/RT\right)}\end{aligned} \tag{14-31}$$

because

$$P_{\text{A, saturation}}(T) = (\text{constant}) \exp\left(\frac{-\Delta H_{\text{vaporization}}}{RT}\right) \tag{14-32}$$

via the Clausius–Clapeyron equation.

Linear Least-Squares Analysis. Rearrangement of the BET isotherm, given by equation (14-13), suggests a method of analysis to extract $v_{\text{A, monolayer}}$ and β from p_{A}–v_{A} data pairs:

$$\frac{\xi}{v_{\text{A}}(1-\xi)} = \frac{1}{\beta v_{\text{A, monolayer}}}[1 + (\beta - 1)\xi] \tag{14-33}$$

The linear least-squares procedure is summarized as follows:

1. Measure the increase in mass of a high-surface-area catalyst at gas pressure p_{A} and calculate the volume of adsorbed gas per initial mass of catalyst, v_{A}. Correlate p_{A}–v_{A} data pairs via a first-order polynomial, $y = a_0 + a_1 x$.
2. The independent variable x is $p_{\text{A}}/P_{\text{A, saturation}}$ (i.e., ξ).
3. The dependent variable y is $(p_{\text{A}}/v_{\text{A}})/(P_{\text{A, saturation}} - p_{\text{A}})$.
4. The zeroth-order coefficient (i.e., intercept) is $a_0 = 1/\beta v_{\text{A, monolayer}}$.
5. The first-order coefficient (i.e., slope) is $a_1 = (1 - 1/\beta)/v_{\text{A, monolayer}}$.
6. The volume of adsorbed gas A per initial mass of catalyst that corresponds to complete monolayer coverage is $v_{\text{A, monolayer}} = 1/(a_0 + a_1)$.
7. The empirical temperature-dependent parameter is $\beta = (a_1/a_0) + 1$.

14-3 SINGLE-SITE ADSORPTION OF EACH COMPONENT IN A MULTICOMPONENT MIXTURE

In an effort to predict fractional surface coverage of component i in a mixture of reactants and products, it is necessary to analyze adsorption and desorption when several components are present. Each component adsorbs without preference on a single active surface site. Hence, the available vacant sites σ are the same in each reaction. The sequence of reversible elementary steps is

$$\begin{aligned} \mathrm{A} + \sigma &\longleftrightarrow \mathrm{A}\sigma \\ \mathrm{B} + \sigma &\longleftrightarrow \mathrm{B}\sigma \\ \mathrm{C} + \sigma &\longleftrightarrow \mathrm{C}\sigma \\ \mathrm{D} + \sigma &\longleftrightarrow \mathrm{D}\sigma \quad \text{etc.} \end{aligned} \tag{14-34}$$

As a prelude to the development of kinetic rate expressions for heterogeneous chemical reactions, if A reacts with B, for example, then the next step in the mechanism is $\mathrm{A}\sigma + \mathrm{B}\sigma$, forming an activated complex on the surface. Each reversible step in the sequence above is characterized by a forward rate constant $k_{i,\,\text{adsorption}}$ for adsorption, with units of mol/area·time·atm, and a backward rate constant $k_{i,\,\text{desorption}}$ for desorption, with units of mol/area·time. The ratio of these rate constants $k_{i,\,\text{adsorption}}/k_{i,\,\text{desorption}}$ defines the adsorption/desorption equilibrium constant for species i, K_i, with units of inverse atmospheres. The net rate of adsorption for component i, with units of moles per area per time, is

$$\mathfrak{R}_{i,\,\text{adsorption, w/o preference}} = k_{i,\,\text{adsorption}}\, p_i \Theta_V - k_{i,\,\text{desorption}} \Theta_i \tag{14-35}$$

If the adsorption process is species specific such that the fraction of vacant active sites $\Theta_{V\mathrm{A}}$ available to gas A is different from those $\Theta_{V\mathrm{B}}$ available to gas B, and so on, then the net rate of adsorption for component i must be modified as follows:

$$\mathfrak{R}_{i,\,\text{adsorption, w/ preference}} = k_{i,\,\text{adsorption}}\, p_i \Theta_{Vi} - k_{i,\,\text{desorption}} \Theta_i \tag{14-36}$$

where Θ_{Vi} represents the fraction of vacant sites on the surface that are available to molecules of species i. Once again, the adsorption isotherm predicts surface coverage fractions Θ_i at equilibrium by equating the rates of adsorption and desorption, or by stipulating that the net rate of adsorption must vanish for each component. Hence, for each component i in the mixture, one writes:

$$\Theta_i = K_i\, p_i \Theta_{Vi}.$$

An additional condition requires that all vacant-site fractions and coverage fractions must sum to unity. If no active sites on the surface are available to more than one species, then:

$$\Theta_V = \sum_i \Theta_{Vi} \qquad i \text{ includes all components that adsorb}$$

$$\sum_i (\Theta_i + \Theta_{Vi}) = \sum_i (K_i p_i + 1)\Theta_{Vi} = 1 \qquad i \text{ includes all components that adsorb} \tag{14-37}$$

For a gas mixture that contains N components which adsorb preferentially with no overlap among active sites, there are $2N + 1$ unknowns (i.e., Θ_i, Θ_{Vi} and Θ_V), but only $N + 2$ equations as illustrated above. Hence, the system exhibits $N - 1$ degrees of freedom, and no solution is possible until additional constraints are identified. If adsorption occurs without preference, then there are $N + 1$ unknowns (i.e., Θ_i and Θ_V) and $N + 1$ equations:

$$\Theta_i = K_i p_i \Theta_V \qquad 1 \le i \le N$$

$$\Theta_V + \sum_i \Theta_i = \Theta_V \left(1 + \sum_i K_i p_i\right) = 1 \qquad i = \text{all components that adsorb} \tag{14-38}$$

Now, it is possible to generate analytical expressions for the total vacant-site fraction:

$$\Theta_V = \frac{1}{1 + \sum_j K_j p_j} \qquad 1 \le j \le N \tag{14-39}$$

and the fraction of active surface sites that are occupied by component i:

$$\Theta_i = \frac{K_i p_i}{\left\{1 + \sum_j K_j p_j\right\}} \qquad 1 \le j \le N \tag{14-40}$$

where the summations in (14-39) and (14-40) include all components that adsorb. The limiting behavior of this generalized Langmuir isotherm proceeds as follows. The total vacant-site fraction Θ_V approaches unity for a sparsely covered surface. Under these conditions, $\Theta_i \approx K_i p_i$ (sparsely covered), which suggests that fractional coverage by component i varies linearly with its partial pressure. This result for multicomponent adsorbing mixtures is exactly the same as the result for a pure gas, given by equation (14-5), if the total pressure of the pure gas is replaced by its partial pressure in the mixture. Limiting behavior of the Langmuir isotherm for sparsely covered surfaces is analogous to Henry's law, which states that the equilibrium solubility of gases in liquids is proportional to gas-phase partial pressures. Henry's law provides accurate predictions at low solute solubilities and partial pressures, when temperatures are well below the critical temperature of the solvent (see Prausnitz *et al.*, 1999, pp. 586–588). When most of the active sites are occupied and the surface is nearly saturated,

$$\sum_i \Theta_i \gg \Theta_V$$

$$\Theta_V + \sum_i \Theta_i \approx \sum_i \Theta_i = \Theta_V \sum_i K_i p_i = 1 \tag{14-41}$$

$$\Theta_V \approx \frac{1}{\sum_i K_i p_i} \qquad 1 \le i \le N \quad \text{(nearly saturated)}$$

and the total vacant-site fraction varies inversely with a weighted sum of partial pressures of the components that adsorb. This result for mixtures reduces to $\Theta_V \approx 1/p_A$ if only gas A is exposed to the surface, which agrees with equation (14-6).

14-4 DUAL-SITE ADSORPTION OF SUBMOLECULAR FRAGMENTS

This concept is illustrated best by considering the elementary steps involved when diatomic gas A_2 dissociates and adsorbs atomically on two adjacent active sites. Two possibilities exist:

$$\begin{aligned} A_2 &\longleftrightarrow 2A \\ 2A + 2\sigma &\longleftrightarrow 2A\sigma \end{aligned} \tag{14-42a}$$

or

$$\begin{aligned} A_2 + 2\sigma &\longleftrightarrow A\text{–}A\sigma + \sigma \\ A\text{–}A\sigma + \sigma &\longleftrightarrow 2A\sigma \end{aligned} \tag{14-42b}$$

In (14-42*a*), diatomic A_2 dissociates in the gas phase and then each atomic fragment adsorbs on a single site. There is no requirement that both sites must be adjacent to each other. In (14-42*b*), one end of diatomic A_2 adsorbs on a single site. Then, dissociation occurs and the other atomic fragment adsorbs on an adjacent site. Both possibilities can be represented as follows if atomic A adsorbs on a single site:

$$A_2 + 2\sigma \longleftrightarrow 2A\sigma \tag{14-43}$$

Examples of dual-site adsorption of submolecular fragments are mentioned below, where each fragment adsorbs on a single site.

1. Diatomic gases such as H_2, N_2, or Cl_2 adsorb atomically. For example, when one molecule of N_2 and three molecules of H_2 form two molecules of ammonia via the Haber–Bosch process on an iron catalyst, at some stage during the reaction, three H−H single bonds and one N≡N triple bond must dissociate to form three N−H single bonds per molecule of NH_3. There are no H−H or N≡N bonds in the final product. If each atomic fragment occupies a single active site on the catalytic surface, then eight sites are required to produce two molecules of ammonia. Alternatively, N_2

dissociates and adsorbs atomically on two sites. Then, H_2 dissociates and attacks adsorbed N from the gas phase, requiring only one active site per molecule of NH_3.

2. The methanol synthesis from carbon monoxide and hydrogen represents an example where diatomic reactants produce a polyatomic product that contains only one bond that was present originally in the reactants. One molecule of C≡O chemisorbs on the catalytic surface via the carbon atom and two molecules of H_2 must dissociate before forming three C−H bonds and one O−H bond.
3. Methane CH_4 could fragment and undergo dual site adsorption as a methyl radical $\cdot CH_3$ and a hydrogen radical ·H. Ammonia NH_3 could fragment as $\cdot NH_2$ and ·H and adsorb on two active sites.

The isotherm for dissociative adsorption of pure diatomic gas A_2, where each fragment occupies a single site, is based on the following reversible elementary step:

$$A_2 + 2\sigma \longleftrightarrow 2A\sigma \tag{14-44}$$

One A−A bond must be cleaved and two bonds are formed between atomic A and the preferred site on the catalytic surface. The reaction is exothermic only if the strength of the bond between atomic A and the active site is larger than one-half of the A−A bond energy. Otherwise, the adsorption process is endothermic. The rate of adsorption is third-order because one molecule of A_2 and two active sites participate in the forward step. Desorption is second-order because two sites occupied by atomic A are required to generate one molecule of diatomic gas A_2 via the backward step. The net rate of adsorption is

$$\mathfrak{R}_{\text{dual-site adsorption}} = k_{\text{A, adsorption}}\, p_{\text{A}} (\Theta_V)^2 - k_{\text{A, desorption}} (\Theta_{\text{A}})^2 \tag{14-45}$$

where p_{A} is the pressure of diatomic gas A_2. Since the forward and backward rates are the same at equilibrium, the fraction of active sites occupied by atomic A is

$$\Theta_{\text{A}} = \Theta_V (K_{\text{A}} p_{\text{A}})^{1/2} \tag{14-46}$$

where, once again, the adsorption/desorption equilibrium constant is

$$K_{\text{A}} = \frac{k_{\text{A, adsorption}}}{k_{\text{A, desorption}}} \tag{14-47}$$

with units of inverse pressure. K_{A} increases at higher temperature if the strength of the bond between atomic A and the active site is smaller than one-half of the A−A bond energy, because this corresponds to endothermic adsorption. The limiting behavior of the isotherm for dissociative adsorption is described as follows:

1. *Sparsely covered surfaces*, $\Theta_V \approx 1$: $\Theta_A \approx (K_A p_A)^{1/2}$ which suggests that the fractional coverage by atomic A varies with the square root of gas pressure.
2. *Nearly saturated surfaces*, $\Theta_A \approx 1$: $\Theta_V \approx 1/(K_A p_A)^{1/2}$ suggesting that the fraction of vacant sites varies with the inverse square root of gas pressure.

Since the vacant-site fraction Θ_V and the surface coverage fraction Θ_A must sum to unity, the consequence of stipulating that the net rate of adsorption must vanish is

$$\Theta_A = (1 - \Theta_A)(K_A p_A)^{1/2} \tag{14-48}$$

which produces the final form of the isotherm for dual-site adsorption:

$$\Theta_A = \frac{(K_A p_A)^{1/2}}{1 + (K_A p_A)^{1/2}} \tag{14-49}$$

Example: Adsorption in a Four-Component Mixture. Gases A, B_2, C, and D adsorb on a solid catalyst with no preference for specific active sites. A and D experience single-site adsorption, B_2 dissociates and each fragment (i.e., atomic B) adsorbs on a single site, and C undergoes triple-site adsorption, with each fragment C′ adsorbing on a single site. Develop expressions for the adsorption isotherm that predict the fractional surface coverage by each gas at equilibrium.

SOLUTION. The reversible elementary steps that simulate adsorption and desorption of each component in the mixture are

$$\begin{aligned} A + \sigma &\longleftrightarrow A\sigma \\ B_2 + 2\sigma &\longleftrightarrow 2B\sigma \\ C + 3\sigma &\longleftrightarrow 3C'\sigma \\ D + \sigma &\longleftrightarrow D\sigma \end{aligned}$$

The previous discussion of adsorption/desorption equilibria in this chapter allows one to calculate fractional surface coverage by gases A and D as follows:

$$\Theta_i = \Theta_V K_i p_i \qquad i = \text{A and D}$$

For dual-site dissociative adsorption of diatomic B_2,

$$\Theta_B = \Theta_V (K_B p_B)^{1/2}$$

The net rate of adsorption for gas C, which dissociates into three submolecular fragments, is

$$\mathfrak{R}_{\text{triple-site adsorption}} = k_{C,\,\text{adsorption}} p_C (\Theta_V)^3 - k_{C,\,\text{desorption}} (\Theta_{C'})^3$$

The adsorption isotherm for gas C is achieved when $\mathfrak{R}_{\text{triple-site adsorption}} = 0$. Hence,

$$\Theta_{C'} = \Theta_V (K_C p_C)^{1/3}$$

In general, the adsorption isotherm for component i that dissociates into γ submolecular fragments, with each fragment occupying one active site on the catalytic surface, is

$$\Theta_i = \Theta_V (K_i p_i)^{1/\gamma}$$

The vacant-site fraction Θ_V is calculated from the requirement that all surface fractions must sum to unity. Hence, the population balance is

$$\Theta_V + \sum_i \Theta_i = \Theta_V \left[1 + \sum_i (K_i p_i)^{1/\gamma_i} \right] = 1 \qquad i = \text{A, B}_2\text{, C, and D}$$

where γ_i is the number of active sites required for one molecule of component i to adsorb on the surface, after dissociation occurs. The final expression for the adsorption isotherm of component i is

$$\Theta_i = \frac{(K_i p_i)^{1/\gamma_i}}{1 + \sum_j (K_j p_j)^{1/\gamma_j}} \qquad j = \text{A, B}_2\text{, C, and D}$$

14-5 SUMMARY OF ADSORPTION ISOTHERMS FOR PURE GASES

The following relations between fractional surface coverage and gas pressure are useful for correlating experimental data on chemisorption. In most cases, there is theoretical justification for the functional form of the isotherm based on rates of adsorption and desorption. Langmuir (1918) and Sips (1948, 1950) proposed the following relation between Θ_A and p_A:

$$\Theta_A = \frac{C(p_A)^{1/\gamma}}{1 + C(p_A)^{1/\gamma}} \tag{14-50}$$

Previous examples in this chapter indicate that γ should be interpreted as the number of sites required for one molecule of A to adsorb, after dissociation. Langmuir identifies C as $(K_A)^{1/\gamma}$, where K_A is a temperature-dependent adsorption/desorption equilibrium constant. Equation (14-50) can be rearranged to express p_A in terms of Θ_A:

$$p_A = \left[\frac{\Theta_A}{C(1 - \Theta_A)} \right]^{\gamma} \tag{14-51}$$

This represents the starting point for the Fowler–Guggenheim modification (1939), which includes ionic interactions between adsorbed species. If one site is required for one molecule of A to adsorb (i.e., $\gamma = 1$), then:

$$p_A = \frac{\Theta_A}{K_A(1 - \Theta_A)} \exp\left(\frac{z\Theta_A \omega}{kT} \right) \tag{14-52}$$

where ω represents an interaction energy between adsorbed species, z accounts for the charge on each species, and k is Boltzmann's constant.

The Freundlich isotherm (see Freundlich, 1926, 1932) can be rationalized as follows:

$$\text{rate of adsorption} = k_{\text{A, adsorption}}\, p_{\text{A}} \left(\frac{1}{\Theta_{\text{A}}}\right)^{\alpha} \tag{14-53a}$$

$$\text{rate of desorption} = k_{\text{A, desorption}} (\Theta_{\text{A}})^{\beta} \tag{14-53b}$$

where α and β are positive exponents. When the fractional coverage of A on the surface is larger, the adsorption rate is hindered and the desorption rate is accelerated, as expected. According to the principle of microscopic reversibility, which applies at equilibrium, the net rate of adsorption vanishes. Hence,

$$\begin{aligned} k_{\text{A, adsorption}}\, p_{\text{A}} \left(\frac{1}{\Theta_{\text{A}}}\right)^{\alpha} &= k_{\text{A, desorption}} (\Theta_{\text{A}})^{\beta} \\ (\Theta_{\text{A}})^{\alpha+\beta} &= \frac{k_{\text{A, adsorption}}}{k_{\text{A, desorption}}} p_{\text{A}} \\ \Theta_{\text{A}} &= (K_{\text{A}} p_{\text{A}})^{1/n} \qquad \text{(Freundlich)} \end{aligned} \tag{14-54}$$

where $n = \alpha + \beta$ and K_{A} is the temperature-dependent adsorption/desorption equilibrium constant. The Langmuir and Sipps isotherms reduce to the Freundlich isotherm when the surface is sparsely covered. The number of sites required for one molecule of A to adsorb is given by n.

The Slygin–Frumkin (1935) and Temkin (1940) isotherms can be explained by the following rate expressions:

$$\text{rate of adsorption} = k_{\text{A, adsorption}}\, p_{\text{A}} \exp(-\alpha \Theta_{\text{A}}) \tag{14-55a}$$

$$\text{rate of desorption} = k_{\text{A, desorption}} \exp(+\beta \Theta_{\text{A}}) \tag{14-55b}$$

where α and β are positive temperature-dependent parameters. Once again, the dependence of these rate laws on Θ_{A} is consistent with expected trends. At equilibrium,

$$\begin{aligned} k_{\text{A, adsorption}}\, p_{\text{A}} \exp(-\alpha \Theta_{\text{A}}) &= k_{\text{A, desorption}} \exp(+\beta \Theta_{\text{A}}) \\ \exp[(\alpha + \beta)\Theta_{\text{A}}] &= \frac{k_{\text{A, adsorption}}}{k_{\text{A, desorption}}} p_{\text{A}} \\ \Theta_A &= \frac{1}{n} \ln(K_{\text{A}} p_{\text{A}}) \qquad \text{(Slygin–Frumkin and Temkin)} \end{aligned} \tag{14-56}$$

where $n = \alpha + \beta$ and K_{A} is the temperature-dependent adsorption/desorption equilibrium constant.

14-6 HOUGEN–WATSON KINETIC MODELS

14-6.1 Langmuir–Hinshelwood Mechanisms for Surface-Catalyzed Reactions

This mechanism, which was developed in 1940, employs Langmuir isotherms to describe adsorption/desorption equilibria of all reactants and products. Chemical reaction on the catalytic surface is the rate-limiting step, which governs the overall rate of reaction. Each component adsorbs without preference on one active site. The five-step sequence of elementary steps is

$$\begin{aligned} \mathrm{A} + \sigma &= \mathrm{A}\sigma \\ \mathrm{B} + \sigma &= \mathrm{B}\sigma \\ \mathrm{A}\sigma + \mathrm{B}\sigma &\leftrightarrow \mathrm{C}\sigma + \mathrm{D}\sigma \\ \mathrm{C}\sigma &= \mathrm{C} + \sigma \\ \mathrm{D}\sigma &= \mathrm{D} + \sigma \end{aligned} \tag{14-57}$$

The fractional surface coverage by each component follows the Langmuir isotherm for single-site adsorption. Hence,

$$\Theta_i = K_i p_i \Theta_V = \frac{K_i p_i}{1 + \sum_j K_j p_j} \tag{14-58}$$

where the summation in the denominator of (14-58) includes all components in the mixture (i.e., A, B, C, and D) that adsorb on the catalyst. The rate of reaction with units of mol/area·time, based on the slowest step in the mechanism (i.e., $\mathrm{A}\sigma + \mathrm{B}\sigma \leftrightarrow \mathrm{C}\sigma + \mathrm{D}\sigma$), is

$$\mathfrak{R}_{\text{surf. Rx}} = k_{\text{forward, surf. Rx}} \Theta_\mathrm{A} \Theta_\mathrm{B} - k_{\text{backward, surf. Rx}} \Theta_\mathrm{C} \Theta_\mathrm{D} \tag{14-59}$$

where $k_{\text{forward, surf. Rx}}$ and $k_{\text{backward, surf. Rx}}$ are kinetic rate constants for the forward and backward reactions on the catalytic surface, respectively, with the same units as $\mathfrak{R}_{\text{surf. Rx}}$. If one defines an equilibrium constant for the surface-catalyzed reaction based on (14-59) when $\mathfrak{R}_{\text{surf. Rx}} \to 0$,

$$K_{\text{eq, surf. Rx}} \equiv \left(\frac{\Theta_\mathrm{C} \Theta_\mathrm{D}}{\Theta_\mathrm{A} \Theta_\mathrm{B}} \right)_{\text{at equilibrium}} = \frac{k_{\text{forward, surf. Rx}}}{k_{\text{backward, surf. Rx}}} \tag{14-60}$$

and expresses each surface coverage fraction in the rate law as $\Theta_i = K_i p_i \Theta_V$, then:

$$\mathfrak{R}_{\text{surf. Rx}} = k_{\text{forward, surf. Rx}} K_\mathrm{A} K_\mathrm{B} \left(p_\mathrm{A} p_\mathrm{B} - \frac{K_\mathrm{C} K_\mathrm{D}}{K_\mathrm{A} K_\mathrm{B} K_{\text{eq, surf. Rx}}} p_\mathrm{C} p_\mathrm{D} \right) (\Theta_V)^2 \tag{14-61}$$

The dependence of $\mathfrak{R}_{\text{surf. Rx}}$ on $(\Theta_V)^2$ reveals that the rate-limiting step in the mechanism requires two active sites on the catalyst. In general, if n active sites are required for the slowest step in the mechanism, then the reaction rate depends on the nth power of the vacant-site fraction. The combination of equilibrium constants in the backward rate of equation (14-61) is simplified by using the adsorption isotherm (i.e., $\Theta_i = K_i p_i \Theta_V$) to re-evaluate $K_{\text{eq, surf. Rx}}$. Hence,

$$K_{\text{eq, surf. Rx}} \equiv \left(\frac{\Theta_C \Theta_D}{\Theta_A \Theta_B}\right)_{\text{at equilibrium}} = \frac{K_C K_D}{K_A K_B}\left(\frac{p_C p_D}{p_A p_B}\right)_{\text{at equilibrium}}$$
$$= \frac{K_C K_D}{K_A K_B} K_{\text{eq, } p} \tag{14-62}$$

where $K_{\text{eq, } p}$ is the equilibrium constant based on gas-phase partial pressures with units of $(\text{atm})^{\delta}$, and δ is the sum of stoichiometric coefficients for all reactants and products. When the vacant-site fraction Θ_V is evaluated for single-site adsorption of each species in a multicomponent mixture, the final expression for the rate of reaction is

$$\mathfrak{R}_{\text{surf. Rx}} = \frac{k_{\text{forward, surf. Rx}} K_A K_B [p_A p_B - (p_C p_D)/K_{\text{eq, } p}]}{\left(1 + \sum_i K_i p_i\right)^2} \tag{14-63}$$

The summation in the denominator of (14-63) includes all components (i.e., A, B, C, and D) that adsorb on the catalyst. This is the classic Hougen–Watson model for the rate law that corresponds to the Langmuir–Hinshelwood mechanism described by (14-57). Generalized Hougen–Watson models for heterogeneous surface-catalyzed chemical reactions were developed in 1943. They can be summarized generically as follows (see Yang and Hougen, 1950):

$$\mathfrak{R}_{\text{Hougen–Watson}} = \frac{(\text{term A})(\text{term B})}{\text{term C}} \tag{14-64}$$

Term A is a product of kinetic and adsorption/desorption equilibrium constants. The kinetic contribution is given by the forward rate constant of the slowest step. In the example above, equilibrium constants are included only for those reactants that adsorb on the catalytic surface. Term B is written in terms of partial pressures and represents the forward rate minus the backward rate. All reactant partial pressures appear in the forward rate, and all product partial pressures appear in the backward rate, regardless of whether or not each gas adsorbs. The equilibrium constant in the backward rate is based on gas-phase partial pressures. Term C represents the vacant-site fraction on the catalytic surface and includes a contribution from each component that adsorbs. The exponent of this adsorption term in the denominator of the rate law corresponds to the number of active sites that are required in the rate-limiting step.

For example, if a solid catalyst is required to convert reactants A and B to products C and D reversibly but product C does not occupy an active site, then the

previous Hougen–Watson model is modified by excluding $K_C p_C$ in the adsorption term (i.e., denominator). The dual-site chemical reaction rate-controlling step in the mechanism,

$$A\sigma + B\sigma \longleftrightarrow C(g) + D\sigma + \sigma(\text{vacant site}) \tag{14-65}$$

is consistent with the fact that product C volatilizes immediately and does not adsorb on the catalyst. This stoichiometrically balanced rate-limiting step illustrates that it is necessary to maintain a balance on the number of surface sites, occupied and vacant. Hence, a vacant site is generated when products form. The rate of reaction, based on the slowest elementary step, is second-order in the forward direction and third-order in the reverse direction, as illustrated below:

$$\mathfrak{R}_{\text{surf. Rx}} = k_{\text{forward, surf. Rx}} \Theta_A \Theta_B - k_{\text{backward, surf. Rx}} p_C \Theta_D \Theta_V \tag{14-66}$$

and the equilibrium constant for the surface-catalyzed reaction is

$$K_{\text{eq, surf. Rx}} \equiv \left(\frac{p_C \Theta_D \Theta_V}{\Theta_A \Theta_B} \right)_{\text{at equilibrium}} = \frac{K_D}{K_A K_B} K_{\text{eq, } p} \tag{14-67}$$

It is important to understand how the vacant-site fraction Θ_V play a significant role in formulating the backward reaction rate and the equilibrium constant $K_{\text{eq, surf. Rx}}$.

14-6.2 Langmuir–Rideal Mechanism of Catalysis

Reactants A and B reversibly produce C and D via gas–solid kinetics. A and C experience single-site adsorption as characterized by Langmuir isotherms. Reactant B attacks adsorbed A from the gas phase or from a physisorbed layer. In other words, B does not occupy active sites on the catalyst, and neither does product D. Single-site chemical reaction on the surface is the slowest step in the mechanism. Hence,

$$\begin{gathered} A + \sigma = A\sigma \\ A\sigma + B \leftrightarrow C\sigma + D \\ C\sigma = C + \sigma \end{gathered} \tag{14-68}$$

is postulated to construct the Hougen–Watson model via the rate-limiting step (i.e., $A\sigma + B \leftrightarrow C\sigma + D$) as follows:

$$\mathfrak{R}_{\text{surf Rx}} = k_{\text{forward, surf. Rx}} \Theta_A p_B - k_{\text{backward, surf. Rx}} \Theta_C p_D \tag{14-69}$$

The Hougen–Watson kinetic model that is consistent with the Langmuir–Rideal mechanism can be obtained from the rate law in equations (14-63) and (14-64) via the following modification of each generic term:

Term A. The adsorption/desorption equilibrium constant for reactant B is omitted because B does not occupy active sites on the catalyst.

Term B. Identical.

Term C. Adsorption terms $K_i p_i$ are omitted for reactant B and product D, and the exponent of the denominator is 1 because the slowest step requires only one active site.

The kinetic rate law for the Langmuir–Rideal single-site mechanism is

$$\mathfrak{R}_{\text{Hougen–Watson}} = \frac{k_{\text{forward, surf. Rx}} K_A [p_A p_B - (p_C p_D)/K_{\text{eq, } p}]}{1 + K_A p_A + K_C p_C} \tag{14-70}$$

14-6.3 Reactive Intermediates Occupy Active Sites on the Catalytic Surface

The Hougen–Watson model, which accounts for the fact that a kinetically stable intermediate occupies surface sites, consists of two possible elementary steps that can be rate limiting. Furthermore, the adsorption terms in the denominator of the rate law must account for fractional surface coverage by the intermediate. If:

1. The overall chemical reaction is $A + B \leftrightarrow C + D$
2. Each component, including the intermediate AB^*, adsorbs on a single active site
3. Dual-site reaction on the surface is the slowest step

then the six-step sequence of elementary steps is

$$\begin{aligned} A + \sigma &= A\sigma \\ B + \sigma &= B\sigma \\ A\sigma + B\sigma &\leftrightarrow AB^*\sigma + \sigma \\ AB^*\sigma + \sigma &\leftrightarrow C\sigma + D\sigma \\ C\sigma &= C + \sigma \\ D\sigma &= D + \sigma \end{aligned} \tag{14-71}$$

In general, one postulates an N-step mechanism that converts reactants to products. If one of these steps is rate limiting, then this slow step is employed to construct a Hougen–Watson rate law. The remaining $N - 1$ steps, which have equilibrated on the time scale of the slow step, allow one to calculate surface coverage fractions of, at most, $N - 1$ reactive species that adsorb on the catalytic surface. Then, a *population balance*, which requires that all surface coverage and vacant-site fractions must sum to unity, is invoked to calculate the fraction of vacant sites. For example, based on the mechanism proposed above, Langmuir adsorption isotherms for reactants A and B and products C and D are given by

$$\Theta_i = K_i p_i \Theta_V \tag{14-72}$$

Obviously, an expression for fractional surface coverage by the intermediate Θ_{AB^*} is required to calculate the vacant-site fraction Θ_V. If

$$A\sigma + B\sigma \longleftrightarrow AB^*\sigma + \sigma \tag{14-73}$$

is the slowest elementary step in the mechanism, and

$$AB^*\sigma + \sigma = C\sigma + D\sigma \tag{14-74}$$

is equilibrated on the time scale of the rate-limiting step, then Θ_{AB^*} is calculated from the equilibrated step (i.e., 14-74) via the principle of microscopic reversibility. Hence,

$$k_{\text{forward, surf. Rx2}}\Theta_{AB^*}\Theta_V = k_{\text{backward, surf. Rx2}}\Theta_C\Theta_D \tag{14-75}$$

and the fractional surface coverage by AB^* is

$$\Theta_{AB^*} = \frac{\Theta_C\Theta_D}{\Theta_V K_{\text{eq, Rx2}}} \tag{14-76}$$

where equilibrium constant $K_{\text{eq, Rx2}}$ for the equilibrated reaction on the catalytic surface represents the ratio of $k_{\text{forward, surf. Rx2}}$ to $k_{\text{backward, surf. Rx2}}$, which are kinetic rate constants for the forward and backward reactions, respectively. Langmuir adsorption isotherms for products C and D (i.e., $\Theta_i = K_i p_i \Theta_V$) are employed to obtain the final expression for fractional surface coverage by the kinetically stable intermediate:

$$\Theta_{AB^*} = \frac{K_C K_D}{K_{\text{eq, Rx2}}} p_C p_D \Theta_V \tag{14-77}$$

Since surface coverage fractions for all species, including the intermediate, are linearly proportional to the vacant-site fraction, it is straightforward to calculate Θ_V by stipulating that all fractions must sum to unity. Hence,

$$\Theta_{AB^*} + \Theta_V + \sum_{i=\text{A, B, C, D}} \Theta_i = 1 \tag{14-78}$$

$$\Theta_V = \frac{1}{1 + K_A p_A + K_B p_B + (K_C K_D / K_{\text{eq, Rx2}}) p_C p_D + K_C p_C + K_D p_D} \tag{14-79}$$

The kinetic rate law for the six-step mechanism outlined above can be developed by focusing on the slow step (i.e., $A\sigma + B\sigma \leftrightarrow AB^*\sigma + \sigma$):

$$\mathfrak{R}_{\text{surf. Rx1}} = k_{\text{forward, surf. Rx1}}\Theta_A\Theta_B - k_{\text{backward, surf. Rx1}}\Theta_{AB^*}\Theta_V \tag{14-80}$$

When surface coverage fractions are written in terms of partial pressures via the Langmuir isotherm, one arrives at the following rate law:

$$\mathfrak{R}_{\text{surf Rx1}} = k_{\text{forward, surf. Rx1}} K_{\text{A}} K_{\text{B}} \left(p_{\text{A}} p_{\text{B}} - \frac{K_{\text{C}} K_{\text{D}}}{K_{\text{A}} K_{\text{B}} K_{\text{eq, Rx1}} K_{\text{eq, Rx2}}} p_{\text{C}} p_{\text{D}} \right) (\Theta_V)^2 \tag{14-81}$$

where equilibrium constant $K_{\text{eq, Rx1}}$ is a ratio of kinetic rate constants $k_{\text{forward, surf Rx1}}$ and $k_{\text{backward, surf Rx1}}$ in the rate-limiting step. It is important to notice that the rate law is proportional to $(\Theta_V)^2$ because the slow step requires two active sites on the catalytic surface. It is rather straightforward to reduce the combination of equilibrium constants in the backward rate expression to the inverse of the equilibrium constant based on gas-phase partial pressures, $1/K_{\text{eq, }p}$. The following steps accomplish this task:

1. Set $\mathfrak{R}_{\text{surf. Rx1}} \rightarrow 0$ in equation (14-80) and write $K_{\text{eq, Rx1}}$ in terms of surface coverage fractions $\Theta_{\text{AB}^*}\Theta_V/(\Theta_{\text{A}}\Theta_{\text{B}})$ at equilibrium
2. Use Langmuir adsorption isotherms and the fact that the second reaction on the catalytic surface has equilibrated to re-express Θ_{A}, Θ_{B} and Θ_{AB^*} in terms of equilibrium partial pressures to obtain the following result:

$$K_{\text{eq, Rx1}} = \left(\frac{\Theta_{\text{AB}^*}\Theta_V}{\Theta_{\text{A}}\Theta_{\text{B}}} \right)_{\text{at equil}} = \frac{K_{\text{C}} K_{\text{D}}}{K_{\text{A}} K_{\text{B}} K_{\text{eq, Rx2}}} \left(\frac{p_{\text{C}} p_{\text{D}}}{p_{\text{A}} p_{\text{B}}} \right)_{\text{at equil}} \tag{14-82}$$

The final form of the Hougen–Watson model for the six-step mechanism described by (14-71) is

$$\mathfrak{R}_{\text{Hougen–Watson}} = k_{\text{forward, surf. Rx1}} K_{\text{A}} K_{\text{B}} \left\{ p_{\text{A}} p_{\text{B}} - \frac{p_{\text{C}} p_{\text{D}}}{K_{\text{eq, }p}} \right\} (\Theta_V)^2 \tag{14-83}$$

where the vacant-site fraction is

$$\Theta_V = \frac{1}{1 + K_{\text{A}} p_{\text{A}} + K_{\text{B}} p_{\text{B}} + (K_{\text{C}} K_{\text{D}}/K_{\text{eq, Rx2}}) p_{\text{C}} p_{\text{D}} + K_{\text{C}} p_{\text{C}} + K_{\text{D}} p_{\text{D}}} \tag{14-84}$$

14-6.4 Total Pressure Dependence When a Stable Intermediate Occupies Active Sites

If the feed stream to a packed catalytic reactor is stoichiometric in reactants A and B, and the mechanism described by (14-71) applies, then

$$\begin{aligned} p_{\text{A}}(z = 0) &= p_{\text{B}}(z = 0) = \tfrac{1}{2} p_{\text{total}}(z = 0) \\ p_{\text{C}}(z = 0) &= p_{\text{D}}(z = 0) = 0 \end{aligned} \tag{14-85}$$

because products C and D are not present at the inlet. The total pressure dependence of the initial reactant $\rightarrow$ product conversion rate (i.e., at the reactor inlet) is obtained

by simplifying the Hougen–Watson rate law given by equation (14-83). Hence,

$$(\mathfrak{R}_{\text{Hougen-Watson}})_{\text{initial}} = \frac{\frac{1}{4}k_{\text{forward, surf. Rx1}}K_{\text{A}}K_{\text{B}}[p_{\text{total}}(z=0)]^2}{[1+\frac{1}{2}(K_{\text{A}}+K_{\text{B}})p_{\text{total}}(z=0)]^2} \tag{14-86}$$

The initial reactant → product conversion rate approaches zero at very low total pressures, and it approaches a high-pressure asymptote given by

$$(\mathfrak{R}_{\text{Hougen-Watson}})_{\text{initial}} \longrightarrow \frac{k_{\text{forward, surf. Rx1}}K_{\text{A}}K_{\text{B}}}{(K_{\text{A}}+K_{\text{B}})^2} \tag{14-87}$$

If the overall gas-phase chemical reaction is $\text{A} + \text{B} \leftrightarrow \text{C} + \text{D}$, then the total pressure dependence of the initial reactant → product conversion rate is exactly the same for the following two mechanisms:

1. Each component, including the kinetically stable intermediate AB^*, adsorbs on a single active site, and the first of two possible dual-site reactions on the catalytic surface (i.e., $\text{A}\sigma + \text{B}\sigma \leftrightarrow \text{AB}^*\sigma + \sigma$) is rate limiting.
2. Each component adsorbs on a single active site, dual-site reaction on the catalytic surface (i.e., $\text{A}\sigma + \text{B}\sigma \leftrightarrow \text{C}\sigma + \text{D}\sigma$) is rate limiting, and the kinetically stable intermediate AB^* is not considered.

   Hence, the method of initial rates cannot distinguish between these two mechanisms to determine whether surface coverage by an intermediate reactive species is important. However, the total pressure dependence of initial rates can distinguish between either of the mechanisms outlined above and the following scenario:
3. Each component, including the kinetically stable intermediate AB^*, adsorbs on a single active site, and the second of two possible dual-site reactions on the catalytic surface (i.e., $\text{AB}^*\sigma + \sigma \leftrightarrow \text{C}\sigma + \text{D}\sigma$) is rate limiting.

14-6.5 Distinguishable Model Based on Surface Coverage by a Reactive Intermediate

The kinetic rate law of interest in this section is based on the premise that

$$\text{A}\sigma + \text{B}\sigma = \text{AB}^*\sigma + \sigma \tag{14-88}$$

is equilibrated and

$$\text{AB}^*\sigma + \sigma \longleftrightarrow \text{C}\sigma + \text{D}\sigma \tag{14-89}$$

is the slowest step in the mechanism given by (14-71). The first chemical reaction on the catalyst, given by (14-88), is employed to calculate surface coverage by the stable reactive intermediate AB^*, and the second reaction, given by (14-89), is used to develop the Hougen–Watson model. The equilibrium constant for the

first reaction is expressed as a ratio of surface coverage fractions and a ratio of kinetic rate constants for the forward and backward steps, via the principle of microscopic reversibility. Hence,

$$K_{\text{eq, Rx1}} \equiv \left(\frac{\Theta_{\text{AB}^*} \Theta_V}{\Theta_{\text{A}} \Theta_{\text{B}}} \right)_{\text{at equilibrium}} = \frac{k_{\text{forward, surf. Rx1}}}{k_{\text{backward, surf. Rx1}}} \tag{14-90}$$

Langmuir isotherms for reactants A and B (i.e., $\Theta_i = K_i p_i \Theta_V$) allow one to predict surface coverage by AB*:

$$\Theta_{\text{AB}^*} = \frac{K_{\text{eq, Rx1}} \Theta_{\text{A}} \Theta_{\text{B}}}{\Theta_V} = K_{\text{eq, Rx1}} K_{\text{A}} K_{\text{B}} p_{\text{A}} p_{\text{B}} \Theta_V \tag{14-91}$$

All surface coverage fractions are linearly proportional to the vacant-site fraction. Consequently, one obtains an analytical expression for Θ_V by invoking the fact that all fractions must sum to unity (i.e., $\Theta_V + \sum_i \Theta_i = 1$, $i = \text{A, B, AB}^*\text{, C,}$ and D):

$$\Theta_V = \frac{1}{1 + K_{\text{eq, Rx1}} K_{\text{A}} K_{\text{B}} p_{\text{A}} p_{\text{B}} + \sum_{i=\text{A, B, C, D}} K_i p_i} \tag{14-92}$$

The reactant → product conversion rate is formulated via (14-89) as follows:

$$\mathfrak{R}_{\text{surf. Rx2}} = k_{\text{forward, surf. Rx2}} \Theta_{\text{AB}^*} \Theta_V - k_{\text{backward, surf. Rx2}} \Theta_{\text{C}} \Theta_{\text{D}}$$

Once again, Langmuir isotherms for products C and D together with surface coverage by the reactive intermediate AB* reveal that the rate of this slowest step is proportional to $(\Theta_V)^2$, as expected for a catalytic reaction that requires two active sites. Hence,

$$\mathfrak{R}_{\text{Hougen–Watson}} = k_{\text{forward, surf. Rx2}} K_{\text{eq, Rx1}} K_{\text{A}} K_{\text{B}} \left(p_{\text{A}} p_{\text{B}} - \frac{p_{\text{C}} p_{\text{D}}}{K_{\text{eq, } p}} \right) (\Theta_V)^2 \tag{14-93}$$

where the vacant-site fraction Θ_V is calculated from (14-92), and the equilibrium constant based on gas-phase partial pressures $K_{\text{eq, } p}$ conveniently combines (1) the forward and backward kinetic rate constants for the second chemical reaction on the surface, (2) the equilibrium constant for the first surface reaction, and (3) adsorption-desorption equilibrium constants for all reactants and products. In other words,

$$K_{\text{eq, Rx2}} = \frac{k_{\text{forward, surf. Rx2}}}{k_{\text{backward, surf. Rx2}}} = \frac{K_{\text{C}} K_{\text{D}}}{K_{\text{A}} K_{\text{B}}} \frac{K_{\text{eq, } p}}{K_{\text{eq, Rx1}}} \tag{14-94}$$

When the six-step mechanism given by (14-71) provides a reasonable description of the chemical kinetics and the second of two possible dual-site reactions on the catalytic surface is rate limiting, the total pressure dependence of the initial

reactant → product conversion rate is

$$(\mathfrak{R}_{\text{Hougen–Watson}})_{\text{initial}} = \frac{\frac{1}{4}k_{\text{forward, surf. Rx2}}K_{\text{eq, Rx1}}K_{\text{A}}K_{\text{B}}[p_{\text{total}}(z=0)]^2}{\left\{1+\frac{1}{2}(K_{\text{A}}+K_{\text{B}})p_{\text{total}}(z=0)+\frac{1}{4}K_{\text{eq, Rx1}}K_{\text{A}}K_{\text{B}}[p_{\text{total}}(z=0)]^2\right\}^2} \quad (14\text{-}95)$$

if the feed stream to a packed catalytic tubular reactor is stoichiometric in reactants A and B. This initial conversion rate approaches zero at high and low total pressures and, as mentioned above, it is distinguishable from the same six-step mechanism where the first surface reaction is rate limiting. Furthermore, linear least-squares analysis of the total pressure dependence of the initial reactant → product conversion rate is facilitated by (1) dividing (14-95) by $[p_{\text{total}}(z=0)]^2$, (2) inverting the entire expression, and (3) taking its square root. The result is

$$\frac{p_{\text{total}}(z=0)}{[(\mathfrak{R}_{\text{Hougen–Watson}})_{\text{initial}}]^{1/2}} = \frac{2\{1+\frac{1}{2}(K_{\text{A}}+K_{\text{B}})p_{\text{total}}(z=0)+\frac{1}{4}K_{\text{eq, Rx1}}K_{\text{A}}K_{\text{B}}[p_{\text{total}}(z=0)]^2\}}{(k_{\text{forward, surf. Rx2}}K_{\text{eq, Rx1}}K_{\text{A}}K_{\text{B}})^{1/2}}$$

$$= a_0 + a_1 p_{\text{total}}(z=0) + a_2[p_{\text{total}}(z=0)]^2 \quad (14\text{-}96)$$

In Section 14-8, we illustrate how a differential plug-flow mass balance near the inlet of a tubular reactor packed with porous catalytic pellets provides experimental data for quantitative evaluation of $(\mathfrak{R}_{\text{Hougen–Watson}})_{\text{initial}}$ via equation (14-199). Hence, the data pairs include the total pressure dependence of this initial conversion rate. As illustrated by (14-96), a second-order polynomial model is appropriate. Hence,

$$y(x) = a_0 + a_1 x + a_2 x^2 \quad (14\text{-}97)$$

The independent (i.e., x) and dependent (i.e., y) variables are

$$x = p_{\text{total}}(z=0) \quad (14\text{-}98a)$$

$$y = \frac{p_{\text{total}}(z=0)}{[(\mathfrak{R}_{\text{Hougen–Watson}})_{\text{initial}}]^{1/2}} \quad (14\text{-}98b)$$

The parameters of this model (i.e., a_0, a_1, and a_2) are related to some of the kinetic and equilibrium constants in the rate law as follows:

Zeroth-order coefficient: $$a_0 = \frac{2}{(k_{\text{forward, surf. Rx2}}K_{\text{eq, Rx1}}K_{\text{A}}K_{\text{B}})^{1/2}} \quad (14\text{-}99a)$$

First-order coefficient: $$a_1 = \frac{K_{\text{A}}+K_{\text{B}}}{(k_{\text{forward, surf. Rx2}}K_{\text{eq, Rx1}}K_{\text{A}}K_{\text{B}})^{1/2}} \quad (14\text{-}99b)$$

Second-order coefficient: $$a_2 = \frac{1}{2}\left(\frac{K_{\text{eq, Rx1}}K_{\text{A}}K_{\text{B}}}{k_{\text{forward, surf. Rx2}}}\right)^{1/2} \quad (14\text{-}99c)$$

Since there are three equilibrium constants (i.e., K_A, K_B, and $K_{eq,\,Rx1}$) and one kinetic rate constant that one seeks to determine via linear least-squares analysis, it is necessary to have an independent measurement of either K_A or K_B via adsorption studies on the same high-surface-area catalyst in a pulverized state. For example, if this catalyst is exposed to pure gas A and K_A is determined via linear least-squares analysis of its adsorption isotherm, then some of the other temperature-dependent parameters in the Hougen–Watson model are calculated as follows from a_0, a_1 and a_2:

$$K_B = \frac{2a_1}{a_0} - K_A \tag{14-100a}$$

$$k_{\text{forward, surf. Rx2}} = \frac{1}{a_0 a_2} \tag{14-100b}$$

$$K_{eq,\,Rx1} = \frac{4a_2/a_0}{K_A[(2a_1/a_0) - K_A]} \tag{14-100c}$$

where the linear least-squares parameters in the quadratic model have the following dimensions:

$$a_0\ [=]\ \text{atm(mol/area·time)}^{-1/2}$$
$$a_1\ [=]\ \text{(mol/area·time)}^{-1/2}$$
$$a_2\ [=]\ \text{atm}^{-1}\text{(mol/area·time)}^{-1/2}$$

14-6.6 Modification of the Hougen–Watson Model to Correct for Dissociative Adsorption of a Reactant

If diatomic A_2 participates in a catalytic surface reaction by dissociating and adsorbing atomically prior to reacting with B, then the modified Langmuir isotherm that describes surface coverage by atomic A is apparent in the denominator of the kinetic rate law. For example, the overall chemical reaction is

$$A_2 + B \longleftrightarrow C + D \tag{14-101}$$

and single-site adsorption is appropriate for B, C and D. The five-step sequence of elementary steps is

$$\begin{aligned} A_2 + 2\sigma &= 2A\sigma \\ B + \sigma &= B\sigma \\ 2A\sigma + B\sigma &\leftrightarrow C\sigma + D\sigma + \sigma \\ C\sigma &= C + \sigma \\ D\sigma &= D + \sigma \end{aligned} \tag{14-102}$$

The adsorption isotherm for each species is

$$\Theta_i = \Theta_V (K_i p_i)^{1/\gamma_i} \tag{14-103}$$

and the vacant-site fraction is

$$\Theta_V = \frac{1}{1 + \sum_{j=\mathrm{A,\,B,\,C,\,D}} (K_j p_j)^{1/\gamma_j}} \tag{14-104}$$

where $\gamma_\mathrm{A} = 2$ and $\gamma_\mathrm{B} = \gamma_\mathrm{C} = \gamma_\mathrm{D} = 1$. As mentioned previously, γ_j represents the number of catalytically active sites required for one molecule of gas j to adsorb on the surface, where each submolecular fragment occupies a single site if dissociation occurs. Triple-site reaction on the catalytic surface is the rate-limiting step:

$$2\mathrm{A}\sigma + \mathrm{B}\sigma \longleftrightarrow \mathrm{C}\sigma + \mathrm{D}\sigma + \sigma \tag{14-105}$$

with

$$\mathfrak{R}_{\mathrm{Hougen-Watson}} = k_{\mathrm{forward,\,surf.\,Rx}} (\Theta_\mathrm{A})^2 \Theta_\mathrm{B} - k_{\mathrm{backward,\,surf.\,Rx}} \Theta_\mathrm{C} \Theta_\mathrm{D} \Theta_\mathrm{V} \approx (\Theta_V)^3 \tag{14-106}$$

The final expression for the kinetic rate law is

$$\mathfrak{R}_{\mathrm{Hougen-Watson}} = k_{\mathrm{forward,\,surf.\,Rx}} K_\mathrm{A} K_\mathrm{B} \left\{ p_\mathrm{A} p_\mathrm{B} - \frac{p_\mathrm{C} p_\mathrm{D}}{K_{\mathrm{eq},\,p}} \right\} (\Theta_V)^3 \tag{14-107}$$

and the equilibrium constant based on gas-phase partial pressures is

$$K_{\mathrm{eq},\,p} = \left(\frac{p_\mathrm{C} p_\mathrm{D}}{p_\mathrm{A} p_\mathrm{B}} \right)_{\text{at equilibrium}} = \frac{K_\mathrm{A} K_\mathrm{B} k_{\mathrm{forward,\,surf.\,Rx}}}{K_\mathrm{C} K_\mathrm{D} k_{\mathrm{backward,\,surf.\,Rx}}} \tag{14-108}$$

If the feed stream to a tubular reactor packed with porous catalysts is stoichiometric in reactants A_2 and B, then the total pressure dependence of the initial rate of conversion of reactants to products is

$$(\mathfrak{R}_{\mathrm{Hougen-Watson}})_{\mathrm{initial}} = \frac{\frac{1}{4} k_{\mathrm{forward,\,surf.\,Rx}} K_\mathrm{A} K_\mathrm{B} [p_{\mathrm{total}}(z=0)]^2}{\{1 + [\frac{1}{2} K_\mathrm{A} p_{\mathrm{total}}(z=0)]^{1/2} + \frac{1}{2} K_\mathrm{B} p_{\mathrm{total}}(z=0)\}^3} \tag{14-109}$$

This initial rate approaches zero at both low and high total pressure. Quantitative analysis of the total pressure dependence of this initial rate is achieved via algebraic manipulation of (14-109), as follows:

1. Divide the entire initial rate law by $[p_{\mathrm{total}}(z=0)]^2$.
2. Invert the resulting expression and take its cube root.

The result is

$$\left\{\frac{[p_{\text{total}}(z=0)]^2}{(\mathfrak{R}_{\text{Hougen-Watson}})_{\text{initial}}}\right\}^{1/3} = \frac{1+[\frac{1}{2}K_{\text{A}}p_{\text{total}}(z=0)]^{1/2}+\frac{1}{2}K_{\text{B}}p_{\text{total}}(z=0)}{(\frac{1}{4}k_{\text{forward, surf. Rx}}K_{\text{A}}K_{\text{B}})^{1/3}}$$
$$= a_0 + a_1[p_{\text{total}}(z=0)]^{1/2} + a_2 p_{\text{total}}(z=0) \tag{14-110}$$

Hence, linear least-squares analysis of the total pressure dependence of the initial rate of conversion of reactants to products near the inlet of a packed catalytic tubular reactor provides quantitative information about $k_{\text{forward, surf. Rx}}$, K_{A}, and K_{B} via the following procedure:

1. Employ a second-order polynomial $y(x) = a_0 + a_1 x + a_2 x^2$.
2. The independent variable is $x = [p_{\text{total}}(z=0)]^{1/2}$.
3. The dependent variable is $y = \{[p_{\text{total}}(z=0)]^2/(\mathfrak{R}_{\text{Hougen-Watson}})_{\text{initial}}\}^{1/3}$.
4. The zeroth-order coefficient is $a_0 = 1/(\frac{1}{4}k_{\text{forward, surf. Rx}}K_{\text{A}}K_{\text{B}})^{1/3}$.
5. The first-order coefficient is $a_1 = (\frac{1}{2}K_{\text{A}})^{1/2}/(\frac{1}{4}k_{\text{forward, surf. Rx}}K_{\text{A}}K_{\text{B}})^{1/3}$.
6. The second-order coefficient is $a_2 = \frac{1}{2}K_{\text{B}}/(\frac{1}{4}k_{\text{forward, surf. Rx}}K_{\text{A}}K_{\text{B}})^{1/3}$.

In addition to calculating kinetic and equilibrium constants in the Hougen–Watson model via numerical values for a_0, a_1, and a_2, the success of this procedure suggests that the mechanism proposed and the choice of a rate-limiting step are reasonable, based on actual experimental data. For completeness, simultaneous solution of the three equations in steps 4 to 6 yields the following results for the kinetic and adsorption/desorption equilibrium constants in terms of the parameters in the polynomial model:

$$k_{\text{forward, surf. Rx}} = \frac{1}{(a_1)^2 a_2} \qquad K_{\text{A}} = 2\left(\frac{a_1}{a_0}\right)^2 \qquad K_{\text{B}} = \frac{2a_2}{a_0} \tag{14-111}$$

14-6.7 Multisite Adsorption without Dissociation

This example illustrates the difficulty encountered when multisite adsorption occurs without dissociation. If molecular A requires n adjacent surface sites for adsorption, then the elementary steps that describe adsorption/desorption equilibria are

$$\text{A} + n\sigma \longleftrightarrow \text{A}\sigma_n \text{ (i.e., not } n\text{A}'\sigma) \tag{14-112}$$

and the net rate of adsorption is given by

$$\mathfrak{R}_{\text{net, adsorption}} = k_{\text{A, adsorption}}\, p_{\text{A}}(\Theta_V)^n - k_{\text{A, desorption}}\,\Theta_{\text{A}} \tag{14-113}$$

There is a fundamental difference between this desorption step (i.e., $\approx \Theta_{\text{A}}$) and the one that occurs when n submolecular fragments of gas A desorb simultaneously [i.e., $\approx (\theta_{\text{A}'})^n$] and recombine to form a polyatomic molecule of gas

A. The modified Langmuir adsorption isotherm for species A is obtained when $\mathfrak{R}_{\text{net, adsorption}} \rightarrow 0$. Hence,

$$\Theta_{\text{A}} = K_{\text{A}} p_{\text{A}} (\Theta_V)^n \tag{14-114}$$

which applies to any reactant or product gas that requires n adjacent sites for adsorption without dissociation. Obviously, surface coverage fractions are linearly proportional to the vacant-site fraction Θ_V for single-site adsorption (i.e., $n = 1$). If $n > 1$ for one or more species, then it is not possible to generate a simple analytical solution for Θ_V, as illustrated below. The overall chemical reaction is

$$\text{A} + \text{B} \longleftrightarrow \text{C} + \text{D} \tag{14-115}$$

and φ_i indicates the number of adjacent active sites on the catalytic surface that are required for one molecule of species i to adsorb without dissociation. Hence, the modified Langmuir isotherm for species i is

$$\Theta_i = K_i p_i (\Theta_V)^{\varphi_i} \tag{14-116}$$

where $K_i = k_{\text{i, adsorption}} / k_{\text{i, desorption}}$ is the ratio of forward and backward rate constants for adsorption and desorption, respectively. If reactants A and B require more active sites to adsorb on the catalyst, relative to products C and D, then:

$$\varphi_{\text{A}} + \varphi_{\text{B}} - (\varphi_C + \varphi_D) = \varphi_{\text{net}} > 0 \tag{14-117}$$

and vacant sites are generated as reactants are converted to products. The stoichiometrically balanced rate-limiting reversible step on the catalytic surface is written

$$\text{A}\sigma_{\varphi_{\text{A}}} + \text{B}\sigma_{\varphi_{\text{B}}} \longleftrightarrow \text{C}\sigma_{\varphi_{\text{C}}} + \text{D}\sigma_{\varphi_{\text{D}}} + (\varphi_{\text{net}})\sigma \tag{14-118}$$

and the Hougen–Watson kinetic model, based on this slow step, is

$$\mathfrak{R}_{\text{Hougen–Watson}} = k_{\text{forward, surf. Rx}} \Theta_{\text{A}} \Theta_{\text{B}} - k_{\text{backward, surf. Rx}} \Theta_{\text{C}} \Theta_{\text{D}} (\Theta_V)^{\varphi_{\text{net}}} \tag{14-119}$$

Modified Langmuir isotherms are employed to re-express the rate law in terms of partial pressures and the vacant-site fraction:

$$\mathfrak{R}_{\text{Hougen–Watson}} = k_{\text{forward, surf. Rx}} K_{\text{A}} K_{\text{B}} \left\{ p_{\text{A}} p_{\text{B}} - \frac{p_{\text{C}} p_{\text{D}}}{K_{\text{eq, } p}} \right\} (\Theta_V)^{\varphi_{\text{A}} + \varphi_{\text{B}}} \tag{14-120}$$

where the equilibrium constant based on gas-phase partial pressures $K_{\text{eq, } p}$ is given by equation (14-108). The final task involves a calculation of Θ_V which is responsible for the adsorption terms in the denominator of the rate law when all $\varphi_i = 1$. If multisite adsorption of one or more gases without dissociation is operative, then Θ_V satisfies the following nonlinear equation, which is based

on the condition that all surface coverage and vacant-site fractions must sum to unity. Hence,

$$\Theta_V + \sum_{\text{i=A, B, C, D}} \Theta_i = \Theta_V + \sum_i [K_i p_i (\Theta_V)^{\varphi_i}] = 1 \tag{14-121}$$

All the Hougen–Watson models prior to this section have been presented analytically (i.e., in closed form) because solution of equation (14-121) for vacant-site fraction Θ_V is trivial when all $\varphi_i = 1$, which is consistent with the fact that each gas in the reactive mixture exhibits single-site adsorption. Numerical methods are required to calculate Θ_V if one or more gases adsorbs on several adjacent active sites without dissociation.

14-6.8 Surface-Catalyzed Reactions Controlled by Adsorption of a Gas

Dissociative adsorption of N_2 on a promoted iron catalyst, which contains alumina and potassium, is the rate-limiting step in the production of ammonia from a feed of N_2 and H_2 at high temperatures (i.e., $\approx$400°C) and pressures (i.e., 150–300 atm) (see Somorjai, 1994, pp. 465–483). The extremely energetic nitrogen–nitrogen triple bond (i.e., 945 kJ/mol) and the relative inertness of N_2 are responsible for the fact that dissociative adsorption is slow (see Anon *et al.*, 1998). This is an example where

$$N_2 + 2\sigma \longleftrightarrow 2N\sigma \tag{14-122}$$

is the reversible elementary step that allows one to generate a Hougen–Watson kinetic model. The activation energy for adsorption (i.e., $\approx$80 kJ/mol) is considerably less than the strength of the nitrogen–nitrogen triple bond, because N_2 is not completely dissociated in the transition state. Furthermore, the overall adsorption process on certain types of catalytic surfaces could be endothermic, as described by reaction (14-122) (see Problem 14-6). Surface coverage by atomic nitrogen does not follow a classic Langmuir isotherm during the time scale of the other steps in a heterogeneous catalytic mechanism, because the rates of adsorption and desorption are not balanced in reaction (14-122). As an illustrative example where dissociative adsorption does not occur, the overall chemical reaction is

$$A + B \longleftrightarrow C + D \tag{14-123}$$

and the following five-step mechanism is appropriate when adsorption of reactant A on the catalytic surface is the slowest step:

$$\begin{aligned} A + \sigma &\leftrightarrow A\sigma \\ B + \sigma &= B\sigma \\ A\sigma + B\sigma &= C\sigma + D\sigma \\ C\sigma &= C + \sigma \\ D\sigma &= D + \sigma \end{aligned} \tag{14-124}$$

Gases B, C, and D experience single-site adsorption on the catalyst, and surface coverage is described by the classic Langmuir isotherm; $\Theta_i = K_i p_i \Theta_V$. Dual-site chemical reaction on the surface equilibrates on the time scale of the adsorption of reactant A. Hence,

$$\mathfrak{R}_{\text{surf. Rx}} = k_{\text{forward, surf. Rx}} \Theta_A \Theta_B - k_{\text{backward, surf. Rx}} \Theta_C \Theta_D \longrightarrow 0 \qquad (14\text{-}125)$$

which allows one to predict surface coverage of reactant A, if equilibrium surface coverage is appropriate for gases B, C, and D, as indicated in the five-step mechanism. If $K_{\text{eq, surf. Rx}}$ represents the ratio of forward and backward kinetic rate constants for chemical reaction on the catalyst, then the prediction for Θ_A is

$$\begin{aligned} \Theta_A &= \frac{k_{\text{backward, surf. Rx}}}{k_{\text{forward, surf. Rx}}} \frac{\Theta_C \Theta_D}{\Theta_B} \\ &= \frac{K_C K_D}{K_B K_{\text{eq, surf, Rx}}} \frac{p_C p_D}{p_B} \Theta_V \end{aligned} \qquad (14\text{-}126)$$

It should be obvious at this stage of model development that an analytical solution exists for the vacant-site fraction because all surface coverage fractions exhibit linear dependence on Θ_V. Since

$$\Theta_V + \sum_{i=\text{A, B, C, D}} \Theta_i = 1 \qquad (14\text{-}127)$$

one obtains the following closed-form expression for the fraction of vacant sites:

$$\Theta_V = \left(1 + \frac{K_C K_D}{K_B K_{\text{eq, surf. Rx}}} \frac{p_C p_D}{p_B} + \sum_{i=\text{B, C, D}} K_i p_i \right)^{-1} \qquad (14\text{-}128)$$

As mentioned above, the Hougen–Watson kinetic rate law is based on single-site adsorption/desorption of reactant A (i.e., $A + \sigma \leftrightarrow A\sigma$):

$$\mathfrak{R}_{\text{Hougen–Watson}} = k_{\text{A, adsorption}} p_A \Theta_V - k_{\text{A, desorption}} \Theta_A \approx (\Theta_V)^{1.0} \qquad (14\text{-}129)$$

This reactant → product conversion rate is proportional to the first power of Θ_V because only one active site on the catalytic surface is required for gas A to adsorb via the rate-limiting step. If one replaces Θ_A by its expression in (14-126), then the kinetic model reduces to

$$\mathfrak{R}_{\text{Hougen–Watson}} = \left(k_{\text{A, adsorption}} p_A - k_{\text{A, desorption}} \frac{K_C K_D}{K_B K_{\text{eq, surf. Rx}}} \frac{p_C p_D}{p_B} \right) \Theta_V \qquad (14\text{-}130)$$

The adsorption/desorption equilibrium constant for gas A with units of inverse pressure is defined as the ratio of $k_{\mathrm{A,\,adsorption}}$ to $k_{\mathrm{A,\,desorption}}$. Consequently,

$$\mathfrak{R}_{\mathrm{Hougen-Watson}} = k_{\mathrm{A,\,adsorption}} \left(p_{\mathrm{A}} p_{\mathrm{B}} - \frac{K_{\mathrm{C}} K_{\mathrm{D}}}{K_{\mathrm{A}} K_{\mathrm{B}} K_{\mathrm{eq,\,surf.\,Rx}}} p_{\mathrm{C}} p_{\mathrm{D}} \right) \frac{\Theta_V}{p_{\mathrm{B}}} \tag{14-131}$$

and the combination of equilibrium constants in the backward (i.e., desorption) rate of equation (14-131) is equivalent to the inverse of the equilibrium constant based on gas-phase partial pressures, $K_{\mathrm{eq},\,p}$. Hence, the final form of the Hougen–Watson rate law for this adsorption-controlled example is

$$\mathfrak{R}_{\mathrm{Hougen-Watson}} = k_{\mathrm{A,\,adsorption}} \left\{ p_{\mathrm{A}} p_{\mathrm{B}} - \frac{p_{\mathrm{C}} p_{\mathrm{D}}}{K_{\mathrm{eq},\,p}} \right\} \frac{\Theta_V}{p_{\mathrm{B}}} \tag{14-132}$$

and

$$\frac{\Theta_V}{p_{\mathrm{B}}} = \left(p_{\mathrm{B}} + \frac{K_{\mathrm{A}}}{K_{\mathrm{eq},\,p}} p_{\mathrm{C}} p_{\mathrm{D}} + p_{\mathrm{B}} \sum_{i=\mathrm{B,\,C,\,D}} K_i p_i \right)^{-1} \tag{14-133}$$

The total pressure dependence of the initial reactant → product conversion rate near the inlet of a packed catalytic tubular reactor exhibits the following functional form when single-site adsorption of reactant A is the slowest step in the five-step mechanism given by (14-124). The feed stream is stoichiometric in reactants A and B:

$$(\mathfrak{R}_{\mathrm{Hougen-Watson}})_{\mathrm{initial}} = \frac{k_{\mathrm{A,\,adsorption}} p_{\mathrm{total}}(z=0)}{2 + K_{\mathrm{B}} p_{\mathrm{total}}(z=0)} \tag{14-134}$$

This initial rate approaches zero at very low total pressure. The high-pressure asymptote is

$$(\mathfrak{R}_{\mathrm{Hougen-Watson}})_{\mathrm{initial}} \longrightarrow \frac{k_{\mathrm{A,\,adsorption}}}{K_{\mathrm{B}}} \qquad \text{as } p_{\mathrm{total}}(z=0) \to \infty \tag{14-135}$$

Quantitative analysis of the total pressure dependence of the initial rate of conversion of reactants to products is facilitated by algebraic manipulation of the initial rate law given by equation (14-134). One obtains

$$\frac{p_{\mathrm{total}}(z=0)}{(\mathfrak{R}_{\mathrm{Hougen-Watson}})_{\mathrm{initial}}} = \frac{2 + K_{\mathrm{B}} p_{\mathrm{total}}(z=0)}{k_{\mathrm{A,\,adsorption}}} \tag{14-136}$$

The following linear least-squares procedure matches initial rate data to equation (14-136) and extracts information about $k_{\mathrm{A,\,adsorption}}$ and K_{B}:

1. Employ a first-order polynomial $y(x) = a_0 + a_1 x$.
2. The independent variable is $x = p_{\mathrm{total}}(z=0)$.

3. The dependent variable is $y = p_{\text{total}}(z = 0)/(\mathfrak{R}_{\text{Hougen-Watson}})_{\text{initial}}$.
4. The zeroth-order coefficient is $a_0 = 2/k_{\text{A, adsorption}}$.
5. The first-order coefficient is $a_1 = K_{\text{B}}/k_{\text{A, adsorption}}$.

The kinetic rate constant for adsorption of A is calculated from the intercept (i.e., $2/a_0$), and the adsorption/desorption equilibrium constant for reactant B is obtained from the ratio of slope to intercept (i.e., $2a_1/a_0$). If this procedure is successful, then one can be confident that the proposed five-step mechanism given by (14-124) and the choice of single-site adsorption of reactant A as the slow step are reasonable assumptions because the resulting Hougen–Watson model agrees with experimental data.

14-6.9 Heterogeneous Catalytic Rate Laws Controlled by Dual-Site Adsorption of a Reactant

This example illustrates several concepts that have been discussed throughout this chapter. Dissociative adsorption of reactant A_2 is the rate-limiting step, and a stable intermediate A_2B^* occupies a significant fraction of surface sites. The overall chemical reaction is

$$A_2 + B \longleftrightarrow C + D \tag{14-137}$$

Components B, C, D, and A_2B^* experience single-site adsorption, whereas diatomic A_2 undergoes dual-site adsorption. Triple-site chemical reaction on the catalytic surface equilibrates on the time scale of the adsorption of reactant A_2. The modified Langmuir–Hinshelwood mechanism is described by the following sequence of six elementary steps:

$$\begin{aligned} A_2 + 2\sigma &\leftrightarrow 2A\sigma \\ B + \sigma &= B\sigma \\ 2A\sigma + B\sigma &= A_2B^*\sigma + 2\sigma \\ A_2B^*\sigma + \sigma &= C\sigma + D\sigma \\ C\sigma &= C + \sigma \\ D\sigma &= D + \sigma \end{aligned} \tag{14-138}$$

Classic Langmuir isotherms are appropriate to describe surface coverage by B, C, and D. Hence,

$$\Theta_i = K_i p_i \Theta_V \qquad i = \text{B, C, D} \tag{14-139}$$

but

$$\Theta_{\text{A}} \neq \Theta_V (K_{\text{A}} p_{\text{A}})^{1/2} \tag{14-140}$$

because the adsorption and desorption rates for reactant A_2 are not balanced on the time scale of the other five elementary steps. The principle of microscopic

reversibility and Langmuir isotherms for products C and D are invoked to predict surface coverage by the stable intermediate via the second chemical reaction on the catalytic surface. Hence,

$$k_{\text{forward, surf. Rx2}}\Theta_{A_2B^*}\Theta_V = k_{\text{backward, surf. Rx2}}\Theta_C\Theta_D \tag{14-141}$$

$$\Theta_{A_2B^*} = \frac{K_C K_D}{K_{\text{eq, surf. Rx2}}} p_C p_D \Theta_V \tag{14-142}$$

where $K_{\text{eq, surf. Rx2}}$ represents the ratio of forward and backward kinetic rate constants for the second chemical reaction. Now, the principle of microscopic reversibility and a Langmuir isotherm for reactant B are employed to calculate fractional surface coverage by reactant A_2 via the first chemical reaction on the catalytic surface:

$$k_{\text{forward, surf. Rx1}}(\Theta_A)^2\Theta_B = k_{\text{backward, surf. Rx1}}\Theta_{A_2B^*}(\Theta_V)^2 \tag{14-143}$$

$$\Theta_A = \Theta_V \left(\frac{K_C K_D}{K_B K_{\text{eq, surf. Rx1}} K_{\text{eq, surf. Rx2}}}\right)^{1/2} \left(\frac{p_C p_D}{p_B}\right)^{1/2} \tag{14-144}$$

Obviously, all surface coverage fractions are linearly related to Θ_V, which is facilitated by the premise that the stable intermediate occupies a single site. The vacant-site fraction exhibits the following analytical solution:

$$\Theta_V + \Theta_{A_2B^*} + \sum_{i=\text{A, B, C, D}} \Theta_i = 1 \tag{14-145}$$

$$\Theta_V = \left[1 + \frac{K_C K_D}{K_{\text{eq, surf. Rx2}}} p_C p_D + \sum_{i=\text{B, C, D}} K_i p_i + \left(\frac{K_C K_D}{K_B K_{\text{eq, surf. Rx1}} K_{\text{eq, surf. Rx2}}}\right)^{1/2} \left(\frac{p_C p_D}{p_B}\right)^{1/2}\right]^{-1} \tag{14-146}$$

The Hougen–Watson model that is consistent with the six-step mechanism given by (14-138) is constructed by focusing on dual-site adsorption of A_2. Hence,

$$\mathfrak{R}_{\text{Hougen–Watson}} = k_{\text{A, adsorption}} p_A (\Theta_V)^2 - k_{\text{A, desorption}}(\Theta_A)^2 \approx (\Theta_V)^2 \tag{14-147}$$

This rate-limiting step is third order in the forward direction (i.e., adsorption) and second order in the reverse direction (i.e., desorption). Since two active sites are required for dual-site adsorption, one predicts that the kinetic model is proportional to the square of the vacant-site fraction. Substitution for Θ_A from (14-144) leads to

$$\mathfrak{R}_{\text{Hougen–Watson}} = k_{\text{A, adsorption}} \left\{p_A p_B - \frac{K_C K_D}{K_A K_B K_{\text{eq, surf. Rx1}} K_{\text{eq, surf. Rx2}}} p_C p_D\right\} \frac{(\Theta_V)^2}{p_B} \tag{14-148}$$

where the combination of equilibrium constants in the desorption step is equivalent to the inverse of the equilibrium constant based on gas-phase partial pressures. This claim is justified by applying the principle of microscopic reversibility to the net rate of adsorption of reactant A_2 at equilibrium, given by equation (14-147). Hence,

$$k_{\mathrm{A,\,adsorption}}\, p_{\mathrm{A}} (\Theta_V)^2 = k_{\mathrm{A,\,desorption}} (\Theta_{\mathrm{A}})^2 \tag{14-149}$$

Upon rearrangement,

$$K_{\mathrm{A}} \equiv \frac{k_{\mathrm{A,\,adsorption}}}{k_{\mathrm{A,\,desorption}}} = \frac{(\Theta_{\mathrm{A}})^2}{p_{\mathrm{A}} (\Theta_V)^2} \tag{14-150}$$

and substitution for Θ_{A} from (14-144) leads to

$$K_{\mathrm{A}} = \frac{K_{\mathrm{C}} K_{\mathrm{D}}}{K_{\mathrm{B}} K_{\mathrm{eq,\,surf.\,Rx1}} K_{\mathrm{eq,\,surf.\,Rx2}}} \left(\frac{p_{\mathrm{C}} p_{\mathrm{D}}}{p_{\mathrm{A}} p_{\mathrm{B}}} \right)_{\text{at equilibrium}} \tag{14-151}$$

Therefore,

$$\frac{K_{\mathrm{C}} K_{\mathrm{D}}}{K_{\mathrm{A}} K_{\mathrm{B}} K_{\mathrm{eq,\,surf.\,Rx1}} K_{\mathrm{eq,\,surf.\,Rx2}}} = \left(\frac{p_{\mathrm{A}} p_{\mathrm{B}}}{p_{\mathrm{C}} p_{\mathrm{D}}} \right)_{\text{at equilibrium}} = \frac{1}{K_{\mathrm{eq},\,p}} \tag{14-152}$$

When dissociative adsorption of diatomic A_2 is slow and the stable intermediate A_2B^* occupies a significant fraction of single sites, the Hougen–Watson kinetic rate law is

$$\mathfrak{R}_{\mathrm{Hougen-Watson}} = k_{\mathrm{A,\,adsorption}} \left(p_{\mathrm{A}} p_{\mathrm{B}} - \frac{p_{\mathrm{C}} p_{\mathrm{D}}}{K_{\mathrm{eq},\,p}} \right) \frac{(\Theta_V)^2}{p_{\mathrm{B}}} \tag{14-153}$$

and the fraction of vacant sites is given by

$$\Theta_V = \left[1 + \frac{K_{\mathrm{C}} K_{\mathrm{D}}}{K_{\mathrm{eq,\,surf.\,Rx2}}} p_{\mathrm{C}} p_{\mathrm{D}} + \left(\frac{K_{\mathrm{A}}}{K_{\mathrm{eq},\,p}} \right)^{1/2} \left(\frac{p_{\mathrm{C}} p_{\mathrm{D}}}{p_{\mathrm{B}}} \right)^{1/2} + \sum_{i=\mathrm{B,\,C,\,D}} K_i p_i \right]^{-1} \tag{14-154}$$

Total pressure analysis of the initial reactant → product conversion rate near the inlet of a tubular reactor packed with porous catalytic pellets proceeds as follows when the feed stream is stoichiometric in reactants A_2 and B:

$$\begin{aligned} p_{\mathrm{A}}(z=0) &= p_{\mathrm{B}}(z=0) = \frac{p_{\mathrm{total}}(z=0)}{2} \\ p_{\mathrm{C}}(z=0) &= p_{\mathrm{D}}(z=0) = 0 \end{aligned} \tag{14-155}$$

Hence,

$$(\mathfrak{R}_{\mathrm{Hougen-Watson}})_{\mathrm{initial}} = \frac{\frac{1}{2} k_{\mathrm{A,\,adsorption}}\, p_{\mathrm{total}}(z=0)}{\left[1 + \frac{1}{2} K_{\mathrm{B}}\, p_{\mathrm{total}}(z=0) \right]^2} \tag{14-156}$$

which suggests that the initial reactant → product conversion rate is vanishingly small at very low and very high total pressure. Quantitative analysis of the total pressure dependence of this initial rate is based on rearrangement of equation (14-156):

$$\left[\frac{p_{\text{total}}(z=0)}{(\mathfrak{R}_{\text{Hougen-Watson}})_{\text{initial}}}\right]^{(1/2)} = \frac{1+\frac{1}{2}K_{\text{B}}p_{\text{total}}(z=0)}{\left(\frac{1}{2}k_{\text{A, adsorption}}\right)^{1/2}} = a_0 + a_1 p_{\text{total}}(z=0) \tag{14-157}$$

The linear least-squares procedure is summarized as follows:

1. Employ a first-order polynomial $y(x) = a_0 + a_1 x$.
2. The independent variable is $x = p_{\text{total}}(z=0)$.
3. The dependent variable is $y = [p_{\text{total}}(z=0)/(\mathfrak{R}_{\text{Hougen-Watson}})_{\text{initial}}]^{1/2}$.
4. The zeroth-order coefficient is $a_0 = 1/\left(\frac{1}{2}k_{\text{A, adsorption}}\right)^{1/2}$.
5. The first-order coefficient is $a_1 = K_{\text{B}}/(2k_{\text{A, adsorption}})^{1/2}$.

Hence, one calculates the kinetic rate constant for dissociative adsorption of reactant A_2 from

$$k_{\text{A, adsorption}} = \frac{2}{(a_0)^2} \tag{14-158}$$

and the adsorption/desorption equilibrium constant for reactant B is

$$K_{\text{B}} = \frac{2a_1}{a_0} \tag{14-159}$$

14-6.10 Surface-Catalyzed Reactions Controlled by Desorption of a Product

In this kinetic mechanism, the Hougen–Watson rate law is based on the desorption of product D. The overall chemical reaction is

$$\text{A} + \text{B} \longleftrightarrow \text{C} + \text{D} \tag{14-160}$$

and the five-step mechanism, which excludes stable reactive intermediates, is

$$\begin{aligned} \text{A} + \sigma &= \text{A}\sigma \\ \text{B} + \sigma &= \text{B}\sigma \\ \text{A}\sigma + \text{B}\sigma &= \text{C}\sigma + \text{D}\sigma \\ \text{C}\sigma &= \text{C} + \sigma \\ \text{D}\sigma &\leftrightarrow \text{D} + \sigma \end{aligned} \tag{14-161}$$

Since each gas experiences single-site adsorption, classic Langmuir isotherms are appropriate to describe surface coverage by A, B, and C (i.e., $\Theta_i = K_i p_i \Theta_V$). If dual-site chemical reaction on the catalytic surface equilibrates on the time scale of the desorption of product D, then this premise is invoked to calculate Θ_D. Hence,

$$k_{\text{forward, surf. Rx}} \Theta_A \Theta_B = k_{\text{backward, surf. Rx}} \Theta_C \Theta_D \tag{14-162}$$

The prediction for surface coverage by product D, which cannot be obtained by equating adsorption and desorption rates in the fifth elementary step of the mechanism, is calculated from equation (14-162):

$$\Theta_D = \frac{\Theta_A \Theta_B}{\Theta_C} K_{\text{eq, surf. Rx}} = \frac{K_A K_B K_{\text{eq, surf. Rx}}}{K_C} \frac{p_A p_B}{p_C} \Theta_V \tag{14-163}$$

where $K_{\text{eq, surf. Rx}}$ is given by the ratio of $k_{\text{forward, surf. Rx}}$ and $k_{\text{backward, surf. Rx}}$. Linear dependence of each surface coverage fraction on Θ_V reveals that an analytical expression for the Hougen–Watson rate law is feasible. The fraction of vacant sites is given by

$$\Theta_V = \left(1 + \frac{K_A K_B K_{\text{eq, surf. Rx}}}{K_C} \frac{p_A p_B}{p_C} + \sum_{i=\text{A, B, C}} K_i p_i \right)^{-1} \tag{14-164}$$

which the reader should verify rather easily. Now, the rate-limiting desorption step (i.e., $D\sigma \leftrightarrow D + \sigma$) is used to generate the kinetic rate law. The forward rate is based on desorption, and the backward rate corresponds to adsorption of gas D. Hence,

$$\mathfrak{R}_{\text{Hougen–Watson}} = k_{\text{D, desorption}} \Theta_D - k_{\text{D, adsorption}} p_D \Theta_V \approx (\Theta_V)^{1.0} \tag{14-165}$$

and linear dependence on Θ_V is expected because single-site desorption of D is rate controlling. The expression for Θ_D from (14-163) is used to rewrite the rate law as

$$\mathfrak{R}_{\text{Hougen–Watson}} = k_{\text{D, desorption}} \left[\frac{K_A K_B K_{\text{eq, surf. Rx}}}{K_C} \frac{p_A p_B}{p_C} - K_D p_D \right] \Theta_V \tag{14-166}$$

where the adsorption/desorption equilibrium constant K_D for gas D is defined as the ratio of $k_{\text{D, adsorption}}$ to $k_{\text{D, desorption}}$. If one sets $\mathfrak{R}_{\text{Hougen–Watson}} \to 0$ in (14-165) and (14-166) via the principle of microscopic reversibility, then the standard relation between equilibrium constants is obtained:

$$K_D = \frac{\Theta_D}{p_D \Theta_V} = \frac{K_A K_B K_{\text{eq, surf. Rx}}}{K_C} \left(\frac{p_A p_B}{p_C p_D} \right)_{\text{at equilibrium}} \tag{14-167}$$

where the equilibrium partial pressure ratio in equation (14-167) is identified as the inverse of $K_{\text{eq},\,p}$. Hence,

$$\mathfrak{R}_{\text{Hougen–Watson}} = k_{\text{D, desorption}}\{K_{\text{D}}K_{\text{eq},\,p}p_{\text{A}}p_{\text{B}} - K_{\text{D}}p_{\text{C}}p_{\text{D}}\}\frac{\Theta_V}{p_{\text{C}}} \tag{14-168}$$

which can be rearranged and presented in final form as

$$\mathfrak{R}_{\text{Hougen–Watson}} = k_{\text{D, adsorption}}K_{\text{eq},\,p}\left\{p_{\text{A}}p_{\text{B}} - \frac{p_{\text{C}}p_{\text{D}}}{K_{\text{eq},\,p}}\right\}\frac{\Theta_V}{p_{\text{C}}} \tag{14-169}$$

with

$$\frac{\Theta_V}{p_{\text{C}}} = \left(p_{\text{C}} + K_{\text{D}}K_{\text{eq},\,p}p_{\text{A}}p_{\text{B}} + p_{\text{C}}\sum_{i=\text{A, B, C}}K_i p_i\right)^{-1} \tag{14-170}$$

When single-site desorption of product D is the slowest step in the five-step mechanism, given by (14-161), the total pressure dependence of the initial reactant → product conversion rate at the inlet to a packed catalytic tubular reactor is independent of total pressure if the feed stream contains stoichiometric proportions of reactants A and B, but no products. This claim should be obvious because

$$\begin{aligned} p_{\text{A}}(z=0) &= p_{\text{B}}(z=0) = \tfrac{1}{2}p_{\text{total}}(z=0) \\ p_{\text{C}}(z=0) &= p_{\text{D}}(z=0) = 0 \end{aligned} \tag{14-171}$$

$$\begin{aligned} (\mathfrak{R}_{\text{Hougen–Watson}})_{\text{initial}} &= \frac{k_{\text{D, adsorption}}K_{\text{eq},\,p}p_{\text{A}}(z=0)p_{\text{B}}(z=0)}{K_{\text{D}}K_{\text{eq},\,p}p_{\text{A}}(z=0)p_{\text{B}}(z=0)} \\ &\rightarrow k_{\text{D, desorption}} \end{aligned} \tag{14-172}$$

The initial reactant → product conversion rate should increase at higher temperature because kinetic rate constants for elementary steps, particularly the desorption of gas D, increase at higher temperature. In summary, there is no total pressure dependence of the initial reactant → product conversion rate when (1) A + B → C + D, (2) single-site adsorption is appropriate for each component, and (3) desorption of one of the products controls the Hougen–Watson kinetic rate law.

14-7 PRESSURE DEPENDENCE OF THE KINETIC RATE CONSTANT VIA ELEMENTS OF TRANSITION STATE THEORY

Ten mechanisms have been presented in this chapter to describe heterogeneous gas–solid reactions on a catalytic surface, and the corresponding Hougen–Watson rate laws were developed using standard principles from chemical kinetics when

the rate-limiting step can be identified. In some cases, the effect of total pressure on the initial reactant → product conversion rate was discussed qualitatively, particularly at very low and very high pressures. Quantitative treatment of the total pressure dependence of the initial reactant → product conversion rate under isothermal conditions allows one to calculate some of the kinetic and equilibrium constants in the rate law when these "constants" are functions of temperature only. Hence, linear least-squares analyses discussed previously in this chapter yield constant slopes and intercepts based on pressure-independent kinetic rate constants for the rate-limiting step. This is reasonable for reactions that occur under subcritical conditions, far from T_C and p_C. However, one must employ nonlinear least-squares analysis of the total pressure dependence of the initial reactant → product conversion rate when heterogeneous chemical reactions occur near the critical point because the kinetic rate constant depends strongly on pressure. If the volume of activation, or the difference between the partial molar volumes of the activated complex and all the reactants, is positive, then kinetic rate constants decrease at higher pressure. This claim is justified by invoking an expression for the forward kinetic rate constant k_{forward} from transition state theory, based on the following sequence of elementary steps which describes a generic chemical reaction;

Step 1. Reactants ↔ activated complex*, via equilibrium constant $K^*_{eq} = k_{1f}/k_{1b}$.
Step 2. Activated complex* → products, via kinetic rate constant k_2.

The forward and backward kinetic rate constants for reaction 1 are given by k_{1f} and k_{1b}, respectively. If one assumes that reversible step 1 between reactants and the activated complex achieves a quasi-equilibrium, then the overall rate of reaction is governed by step 2. No equilibrium is imposed between reactants and final products. Hence,

$$\text{reaction rate} \approx k_2[\text{activated complex}^*] \tag{14-173}$$

where the brackets indicate molar density. Since the activated complex is a rather short-lived species, its concentration in (14-173) can be estimated by the following pseudo-steady-state approximation, which applies to a constant-volume batch reactor with multiple chemical reactions:

$$\frac{d}{dt}[\text{activated complex}^*] = k_{1f}[\text{reactants}] - (k_{1b} + k_2)[\text{activated complex}^*] \approx 0 \tag{14-174}$$

In terms of the equilibrium constant K^*_{eq} based on molar densities of reactants and the activated complex in step 1, (14-174) yields

$$[\text{activated complex}^*] \approx f(T)K^*_{eq}[\text{reactants}] \tag{14-175}$$

Now, it is possible to express the overall rate for this generic reaction in terms of reactant concentrations and an apparent kinetic rate constant, k_{forward}:

$$\text{reaction rate} \approx g(T)K^*_{\text{eq}}[\text{reactants}] \approx k_{\text{forward}}[\text{reactants}] \tag{14-176}$$

where $f(T)$ and $g(T)$ in equations (14-175) and (14-176) are generic functions of temperature only. If a pseudo-thermodynamic formalism is applied to the quasi-equilibrium established between reactants and the activated complex in the first reaction, then the statement of reaction equilibrium implies that

$$\sum_{\text{all species } i} \nu_i \mu_i = \sum_{\text{all species } i} \nu_i [\mu_i^0(T) + RT \ln a_i] = 0 \tag{14-177}$$

where the summation includes all species in the first reaction, μ_i and a_i are the chemical potential and activity, respectively, of species i in the mixture, ν_i is the stoichiometric coefficient of species i in the first reaction, and $\mu_i^0(T)$ represents the chemical potential of pure component i in a reference state at 1 atm total pressure. Since the equilibrium constant K^*_{eq} for the first reaction is constructed in terms of molar densities, not activities, the statement of reaction equilibrium must be manipulated to yield an expression for K^*_{eq}. For example, the activity of species i is written as a product of its mole fraction x_i and activity coefficient γ_i:

$$a_i = \gamma_i x_i = \gamma_i \frac{C_i}{C_{\text{total}}} \tag{14-178}$$

where C_i and C_{total} represent molar densities of species i and the overall mixture, respectively. Hence,

$$\sum_{\text{all species } i} \nu_i [\mu_i^0(T) + RT(\ln \gamma_i + \ln C_i - \ln C_{\text{total}})] = 0 \tag{14-179}$$

Now, the equilibrium constant between reactants and activated complex in reaction 1 is constructed as follows:

$$\begin{aligned} RT \ln K^*_{\text{eq}} &\equiv RT \sum_{\text{all species } i} \nu_i \ln C_i \\ &= - \sum_{\text{all species } i} \nu_i [\mu_i^0(T) + RT(\ln \gamma_i - \ln C_{\text{total}})] \\ &\equiv -\Delta \mathscr{G}^* \end{aligned} \tag{14-180}$$

where the activation free energy $\Delta \mathscr{G}^*$ represents the difference between molar Gibbs free energies of the activated complex and the reactants in their standard states. These standard states are somewhat unusual and exhibit dependence on temperature, pressure, and composition because K^*_{eq} is defined in terms of molar

densities, not activities or ratios of fugacities. For comparison, equilibrium constants based on activities and the corresponding standard-state free-energy change from reactants to products are typically independent of pressure and composition, due to the appropriate choice of reference state (i.e., pure material at a fixed total pressure of 1 atm) for each component in the mixture. Suffice it to say that the activation free energy defined by equation (14-180) can be rewritten in terms of standard-state chemical potentials that depend on temperature, pressure, and composition as follows:

$$\Delta \mathscr{G}^* \equiv \sum_{\text{all species } i} \nu_i \mu_{i,\,\text{standard state}}(T,\, p,\, \text{composition}) \tag{14-181}$$

Now, in terms of Boltzmann's constant $k_{\text{Boltzmann}}$, Planck's constant h_{Planck}, and the gas constant R, the final result from transition-state theory for first-order homogeneous kinetics, where k_{forward} has dimensions of inverse time, is

$$k_{\text{forward}} = g(T) K^*_{\text{eq}} = \frac{k_{\text{Boltzmann}} T}{h_{\text{Planck}}} \exp\left(-\frac{\Delta \mathscr{G}^*}{RT}\right) \tag{14-182}$$

This result corresponds to free translation of the activated complex over the barrier with activation energy denoted by $\Delta \mathscr{G}^*$, or a very low energy vibration of the activated complex due to weak bonding, which causes it to dissociate into products. The pressure dependence of k_{forward} is contained in the activation free energy $\Delta \mathscr{G}^*$. At constant temperature and composition,

$$\begin{aligned} RT\left(\frac{\partial \ln k_{\text{forward}}}{\partial p}\right)_{T,\,\text{composition}} &= -\left(\frac{\partial \Delta \mathscr{G}^*}{\partial p}\right)_{T,\,\text{composition}} \\ &= -\sum_{\text{all species } i} \nu_i \left(\frac{\partial \mu_{i,\,\text{standard state}}}{\partial p}\right)_{T,\,\text{composition}} \end{aligned} \tag{14-183}$$

Since the pressure dependence of this unusual standard-state chemical potential of species i at constant temperature and composition yields the partial molar volume of species i, $\overline{v_i}$, one obtains the final result for the pressure dependence of kinetic rate constants:

$$RT\left(\frac{\partial \ln k_{\text{forward}}}{\partial p}\right)_{T,\,\text{composition}} = -\sum_{\text{all species } i} \nu_i \overline{v_i} \equiv -\Delta v^* \tag{14-184}$$

The volume of activation Δv^* represents the volume change that accompanies the formation of the activated complex in the transition state, and it is defined by the summation in equation (14-184). The definitive work on this subject by Evans and Polanyi (1935, 1936) describes $\overline{v_i}$ as the molal volume of species i. Laidler (1965, pp. 231–237) describes $\overline{v_i}$ simply as the volume of species i. More recently, Reichardt (1988, p. 275) interprets $\overline{v_i}$ as the partial molar volume

of species i. The first and third interpretations of $\overline{v_i}$ are equivalent for either ideal gases or ideal solutions, but one should not formulate models of the transition state based on absolute rate theory in ideal media. For all three interpretations, if the formation of the activated complex is accompanied by an increase in volume (i.e., $\Delta v^* > 0$), then k_{forward} decreases at higher pressure. In the absence of compressibility data for reactants and the activated complex, simple integration of equation (14-184), with a pressure-independent volume of activation, yields

$$\frac{k_{\text{forward}}(p_2)}{k_{\text{forward}}(p_1)} = \exp\left[\frac{-(p_2 - p_1)\Delta v^*}{RT}\right] \tag{14-185}$$

If one interprets the transition state as the point of no return with respect to the reaction coordinate as reactants climb the impending barrier, and a quasi-equilibrium is established between reactants and the activated complex, then the effect of pressure on k_{forward} is analogous to the effect of pressure on the equilibrium conversion of gas-phase chemical reactions via le Châtelier's principle. In other words, the system gravitates toward the state of smaller volume at higher pressure. In the vicinity of the critical point, enormous fluctuations in density or molar volume are possible because materials are infinitely compressible at T_C and p_C. Hence, pressure has a strong influence on rates of chemical reactions near the critical point, not only due to pressure terms in the rate law but due to the pressure dependence of k_{forward}. The volume of activation or Δv^*, which is typically on the order of ± 25 cm^3/mol under subcritical conditions, has a negligible effect on k_{forward} when chemical reactions occur far below T_C and p_C with mild changes in pressure. In these situations, all linear least-squares analyses of the total pressure dependence of initial reactant $\rightarrow$ product conversion rates, as described above, are valid because k_{forward} is essentially pressure independent. For example, if Δv^* assumes its average value of ± 25 cm^3/mol, then equation (14-185) reveals that a pressure change of 1000 atm affects k_{forward} by a factor of 2.8 at 298 K. For more information about the use of supercritical fluids in heterogeneous catalysis, see the April 1999 issue of *Chemical Reviews*.

14-8 INTERPRETATION OF HETEROGENEOUS KINETIC RATE DATA VIA HOUGEN–WATSON MODELS

As a practical example of the interpretation of kinetic rate data to distinguish between more than one reaction mechanism, consider the dehydrogenation of ethanol (i.e., CH_3CH_2OH, [A]) to acetaldehyde (i.e., CH_3CHO, [C]) and hydrogen (i.e., H_2, [D]). The reversible chemical reaction that occurs on a catalytic surface is

$$\text{A} \longleftrightarrow \text{C} + \text{D} \tag{14-186}$$

If each component experiences single-site adsorption and dual-site chemical reaction is the slowest step, then the following four-step mechanism is reasonable:

$$\begin{aligned} A + \sigma &= A\sigma \\ A\sigma + \sigma &\leftrightarrow C\sigma + D\sigma \\ C\sigma &= C + \sigma \\ D\sigma &= D + \sigma \end{aligned} \tag{14-187}$$

The Hougen–Watson model that is consistent with this mechanism is proportional to the square of the vacant-site fraction because two active sites are required in the rate-limiting step. Hence,

$$\mathfrak{R}_{\text{Hougen–Watson(2-site)}} = k_{\text{forward, surf. Rx}} K_A \left(p_A - \frac{p_C p_D}{K_{\text{eq, } p}} \right) (\Theta_V)^2 \tag{14-188}$$

$$\Theta_V = \frac{1}{1 + \sum_{i=A,\,C,\,D} K_i p_i} \tag{14-189}$$

If hydrogen volatilizes immediately upon dehydrogenation of ethanol, and H_2 does not occupy an active site on the catalytic surface, then the following three-step mechanism is more appropriate:

$$\begin{aligned} A + \sigma &= A\sigma \\ A\sigma &\leftrightarrow C\sigma + D \\ C\sigma &= C + \sigma \end{aligned} \tag{14-190}$$

The Hougen–Watson model for this mechanism, in which single-site chemical reaction is rate limiting, is proportional to the first power of Θ_V:

$$\mathfrak{R}_{\text{Hougen–Watson(1-site)}} = k_{\text{forward, surf. Rx}} K_A \left(p_A - \frac{p_C p_D}{K_{\text{eq, } p}} \right) \Theta_V \tag{14-191}$$

$$\Theta_V = \frac{1}{1 + \sum_{i=A,\,C} K_i p_i} \tag{14-192}$$

Total pressure analysis of the initial reactant → product conversion rate can distinguish between these two mechanisms, provided that rates of conversion can be measured at sufficiently high pressure. The rate expressions given by equations (14-188) and (14-191) have units of mol/area·time for surface-catalyzed chemical reactions. However, rate data obtained from heterogeneous catalytic reactors are typically reported in units of mol/time per mass of catalyst. One obtains these units simply by multiplying the kinetic rate law (i.e., mol/area·time) by the internal surface area per mass of catalyst (i.e., S_m), which is usually on the order of 100 m^2/g. If the feed stream to a packed catalytic reactor contains pure ethanol, then the initial reactant → product conversion rate for the four-step mechanism is

$$[\mathfrak{R}_{\text{Hougen–Watson(2-site)}}]_{\text{initial}} = \frac{k_{\text{forward, surf. Rx}} K_A p_{\text{total}}}{(1 + K_A p_{\text{total}})^2} \tag{14-193}$$

The three-step mechanism in which H_2 does not occupy an active site on the catalyst produces the following total pressure dependence of the initial conversion rate:

$$[\Re_{\text{Hougen–Watson(1-site)}}]_{\text{initial}} = \frac{k_{\text{forward, surf. Rx}} K_{\text{A}} p_{\text{total}}}{1 + K_{\text{A}} p_{\text{total}}} \tag{14-194}$$

Both mechanisms predict vanishingly small rates of conversion at very low total pressure. The dual-site mechanism predicts vanishingly small conversion at very high total pressure, whereas the high-pressure asymptote for the single-site mechanism suggests that the initial rate of conversion approaches $S_m k_{\text{forward, surf. Rx}}$, with units of mol/time per mass of catalyst. Hence, total pressure analysis of the initial reactant → product conversion rate can determine whether the single- or dual-site mechanism is most appropriate to describe experimental data. If the dual-site mechanism is best, then the following rearrangement of the Hougen–Watson model at the reactor inlet allows one to calculate the forward kinetic rate constant for chemical reaction on the catalytic surface (i.e., $k_{\text{forward, surf. Rx}}$) and the adsorption/desorption equilibrium constant for ethanol (i.e., K_{A}) via linear least-squares analysis:

$$\left[\frac{p_{\text{total}}}{(\Re_{\text{Hougen–Watson(2-site)}})_{\text{initial}}}\right]^{1/2} = (K_{\text{A}} k_{\text{forward, surf. Rx}})^{-1/2} + \left(\frac{K_{\text{A}}}{k_{\text{forward, surf. Rx}}}\right)^{1/2} p_{\text{total}} \tag{14-195}$$

The strategy to extract $k_{\text{forward, surf. Rx}}$ and K_{A} is (i.e., referred to as C_1 analysis):

1. Measure the incremental conversion of ethanol per mass of catalyst and calculate the initial reactant → product conversion rate with units of moles per area per time as a function of total pressure at the reactor inlet. One calculates this initial rate of conversion of ethanol to products via a differential material balance, unique to gas-phase packed catalytic tubular reactors that operate under plug-flow conditions at high-mass-transfer Peclet numbers. Since axial dispersion in the packed bed is insignificant,

$$dF_{\text{A}} = \nu_{\text{A}} \Re_{\text{Hougen–Watson(2-site)}} S_m \, dW \tag{14-196}$$

where dF_{A} is the differential molar flow rate of ethanol, ν_{A} the stoichiometric coefficient of ethanol in the overall reaction (i.e., -1), and dW the differential increment in the mass of catalyst in the packed reactor. The conversion χ of ethanol to products is defined relative to ethanol's molar flow rate at the reactor inlet (i.e., $F_{\text{A, inlet}}$):

$$\chi \equiv 1 - \frac{F_{\text{A}}}{F_{\text{A, inlet}}} \tag{14-197}$$

Hence,

$$dF_A = -F_{A,\,\text{inlet}}\, d\chi \tag{14-198}$$

and the ethanol material balance at the reactor inlet is expressed as the incremental change in ethanol conversion per mass of catalyst:

$$F_{A,\,\text{inlet}} \left(\frac{d\chi}{dW}\right)_{\text{inlet}} = S_m [\Re_{\text{Hougen–Watson(2-site)}}]_{\text{initial}} \tag{14-199}$$

Since the initial data point is $\chi = 0$ at $W = 0$, the next few data points very close to the inlet allow one to estimate $(d\chi/dW)_{\text{inlet}}$ via finite-difference algebra. The number of terms that are retained in the Taylor series prior to truncation dictates the correctness of the finite-difference calculation and the number of data points required to approximate $(d\chi/dW)_{\text{inlet}}$ via the forward difference. Then, knowledge of the inlet molar flow rate of ethanol (i.e., $F_{A,\,\text{inlet}}$) and the internal surface area per mass of a porous catalytic pellet (i.e., S_m) provides an estimate of $[\Re_{\text{Hougen–Watson(2-site)}}]_{\text{initial}}$.

2. Perform linear least-squares analysis of $[p_{\text{total}}/(\Re_{\text{Hougen–Watson(2-site)}})_{\text{initial}}]^{1/2}$ vs. p_{total} using a first-order polynomial (i.e., $y = a_0 + a_1 x$), where x is total pressure.
3. The coefficient of the first-order term in the polynomial model (i.e., the slope a_1) is $(K_A/k_{\text{forward, surf. Rx}})^{1/2}$ with units of (mol·atm/area·time)$^{-1/2}$.
4. The coefficient of the zeroth-order term in the polynomial model (i.e., the intercept a_0) is $(K_A k_{\text{forward, surf. Rx}})^{-1/2}$ with units of (mol/area·time·atm)$^{-1/2}$.
5. The forward kinetic rate constant for chemical reaction on the catalytic surface, with units of mol/area·time, is $k_{\text{forward, surf. Rx}} = 1/(a_0 a_1)$.
6. The adsorption/desorption equilibrium constant for single-site adsorption of ethanol, with units of inverse atmospheres, is $K_A = a_1/a_0$.

If the single-site mechanism is best, then the following rearrangement of the Hougen–Watson model at the reactor inlet allows one to calculate $k_{\text{forward, surf. Rx}}$ and K_A via linear least-squares analysis using a first-order polynomial:

$$\frac{p_{\text{total}}}{[\Re_{\text{Hougen–Watson(1-site)}}]_{\text{initial}}} = (K_A k_{\text{forward, surf. Rx}})^{-1} + \frac{1}{k_{\text{forward, surf. Rx}}} p_{\text{total}} \tag{14-200}$$

Now, the strategy to calculate $k_{\text{forward, surf. Rx}}$ and K_A via C_1 analysis is as follows:

1. Measure the incremental conversion of ethanol per mass of catalyst and calculate the initial reactant → product conversion rate with units of moles per area per time as a function of total pressure at the reactor inlet via

$$F_{A,\,\text{inlet}} \left(\frac{d\chi}{dW}\right)_{\text{inlet}} = S_m [\Re_{\text{Hougen–Watson(1-site)}}]_{\text{initial}} \tag{14-201}$$

2. Perform linear least-squares analysis of $p_{\text{total}}/[\mathfrak{R}_{\text{Hougen–Watson(1-site)}}]_{\text{initial}}$ vs. p_{total} using a first-order polynomial (i.e., $y = a_0 + a_1 x$), where x is total pressure.
3. The coefficient of the first-order term in the polynomial model (i.e., the slope a_1) is $1/k_{\text{forward, surf. Rx}}$, with units of (mol/area·time)$^{-1}$.
4. The coefficient of the zeroth-order term in the polynomial model (i.e., the intercept a_0) is $(K_{\text{A}} k_{\text{forward, surf. Rx}})^{-1}$, with units of (mol/area·time·atm)$^{-1}$.
5. The forward kinetic rate constant for chemical reaction on the catalytic surface, with units of mol/area·time, is $k_{\text{forward, surf. Rx}} = 1/a_1$.
6. The adsorption/desorption equilibrium constant for single-site adsorption of ethanol, with units of atm^{-1}, is $K_{\text{A}} = a_1/a_0$.

PROBLEMS

14-1. Is the magnitude of $\Delta H_{\text{chemisorption}}$ for chemisorption (1) greater than, (2) less than, or (3) equal to, the magnitude of $\Delta H_{\text{condensation}}$? Remember that the magnitudes of $\Delta H_{\text{condensation}}$ and $\Delta H_{\text{vaporization}}$ are the same. Explain very briefly.

14-2. For a particular gas/solid–catalyst system, the rate of adsorption is given by

$$\mathfrak{R}_{\text{adsorption}} = k_{\text{forward}} p_{\text{A}} \exp(-\alpha \Theta_{\text{A}})$$

and the rate of desorption is given by

$$\mathfrak{R}_{\text{desorption}} = k_{\text{backward}} \exp(+\beta \Theta_{\text{A}})$$

Parameters α and β depend on temperature.

(a) Obtain an expression for the fractional surface coverage by gas A at equilibrium.

(b) Identify the adsorption isotherm by name, which is described by these rates of adsorption and desorption.

(c) Describe the linear least-squares procedures that must be implemented to calculate the adsorption/desorption equilibrium constant $K_{\text{equilibrium, A}}$ and $v_{\text{A, monolayer}}$ for this adsorption isotherm when $\alpha = \beta = 1$.

14-3. Quantitatively describe a linear least-squares procedure based on the Sipps isotherm,

$$\Theta_{\text{A}} = \frac{C(T)(p_{\text{A}})^{1/\gamma}}{1 + C(T)(p_{\text{A}})^{1/\gamma}}$$

to calculate:

(a) The adsorption/desorption equilibrium constant K_A, which is embedded in the temperature-dependent parameter C.

(b) The exponent γ, which should be interpreted as the number of active sites required for one molecule of A to adsorb on the catalytic surface.

The volume of gas A per initial mass of catalyst that is required for complete monolayer surface coverage (i.e., $v_{A,\,\text{monolayer}}$) has been determined from the chemisorption/physisorption crossover on a graph of v_A vs. p_A.

14-4. The three-parameter Toth equation (1962) describes the pressure dependence of the amount of gas A that adsorbs as a monolayer on high-surface-area dispersed solid catalysts:

$$n_A = \frac{m p_A}{[b + (p_A)^t]^{1/t}}$$

where p_A is the partial pressure of gas A, and n_A represents the moles of gas A that experience monolayer adsorption per initial mass of catalyst.

(a) What is the asymptotic value of n_A at very high gas pressure if capillary condensation does not occur?

(b) If $t = 1$, then describe the adsorption isotherm in words.

(c) Obtain an expression for the adsorption/desorption equilibrium constant K_A in terms of the Toth parameters when $t = 1$.

(d) Develop a strategy to calculate the Toth parameters b and t via linear least-squares analysis based on several $n_A - p_A$ data pairs.

Answer: Begin with the empirical relation between n_A and p_A given above, and take the t-power of the Toth equation. Rearrangement yields

$$b(n_A)^t + (n_A p_A)^t = m^t (p_A)^t$$

Now, take the total differential of the previous equation when b, m, and t are constant. The result is

$$bt(n_A)^{t-1}\, dn_A + t(n_A p_A)^{t-1}(n_A\, dp_A + p_A\, dn_A) = tm^t (p_A)^{t-1}\, dp_A$$

Introduce the following differential relations into the preceding equation

$$dn_A = n_A\, d\ln n_A \qquad dp_A = p_A\, d\ln p_A$$

One obtains

$$bt(n_A)^t\, d\ln n_A + t(n_A p_A)^t (d\ln p_A + d\ln n_A) = tm^t (p_A)^t\, d\ln p_A$$

Group terms and calculate $(d\ln p_A / d\ln n_A)_T$ as follows:

$$\left(\frac{d\ln p_A}{d\ln n_A}\right)_T = \frac{(n_A)^t[b + (p_A)^t]}{(p_A)^t[m^t - (n_A)^t]}$$

The Toth isotherm allows one to manipulate both the numerator and denominator on the right side of the preceding equation

$$\left(\frac{d \ln p_A}{d \ln n_A}\right)_T = \frac{m^t}{m^t - (n_A)^t} = \frac{1}{1 - (n_A/m)^t} = 1 + \frac{(p_A)^t}{b}$$

The final form of the Toth equation that can be compared with experimental data via linear least-squares analysis is

$$\ln\left[\left(\frac{d \ln p_A}{d \ln n_A}\right)_T - 1\right] = t \ln p_A - \ln b$$

Polynomial model is $y = a_0 + a_1 x$.

Independent variable is $x = \ln p_A$.

Dependent variable is $y = \ln[(d \ln p_A / d \ln n_A)_T - 1]$.

Intercept or zeroth-order coefficient in the model is $a_0 = -\ln b$.

Slope or first-order coefficient in the model is $a_1 = t$.

14-5. The Haber–Bosch process converts nitrogen (N_2) and hydrogen (H_2) to ammonia (NH_3) via an iron catalyst. How many active sites on the catalyst are required to produce one molecule of ammonia?

14-6. The isotherm for dissociative adsorption of pure diatomic gas N_2 on an iron catalyst is based on the following reversible elementary step:

$$N_2 + 2\sigma \longleftrightarrow 2N\sigma$$

where σ represents a vacant active site. Atomic nitrogen chemisorbs on a single active site on this promoted iron catalyst. Use bond energies, not activation energies, and describe the conditions when dissociative adsorption, as written above, is **(a)** an endothermic process; **(b)** an exothermic process.

14-7. Sketch surface coverage vs. partial pressure of the adsorbed species for the Langmuir and BET isotherms on the same set of axes.

14-8. Briefly describe linear least-squares analysis of adsorption data that conform to the BET isotherm.

14-9. After complete degassing of a high-surface-area catalyst at high temperature and ultrahigh vacuum, one (1) lowers the temperature, (2) measures the increase in catalyst mass when it is exposed to pure gas A (i.e., nitrogen) at pressure p_A, and (3) calculates the volume of adsorbed gas per initial mass of catalyst, v_A. The BET isotherm is employed

to correlate several $p_A - v_A$ data pairs via a first-order polynomial, $y = a_0 + a_1 x$, where

$$x = \frac{p_A}{P_{A,\,\text{saturation}}}$$

$$y = \frac{p_A / v_A}{P_{A,\,\text{saturation}} - p_A}$$

(a) Why must p_A be less than $P_{A,\,\text{saturation}}$ at the temperature of the adsorption measurements? Provide a physical explanation, not a mathematical one.

(b) Linear least-squares analysis yields a slope a_1 and intercept a_0 from which the volume of gas A per mass of catalyst required for complete monolayer surface coverage is calculated via

$$v_{A,\,\text{monolayer}} = \frac{1}{a_0 + a_1}$$

Use this numerical value for $v_{A,\,\text{monolayer}}$ and describe a logical procedure to estimate the total catalytic surface area per initial mass of catalyst. Consider the covalent and van der Waals radii for homonuclear and heteronuclear diatomic gases.

(c) Prove that the BET parameter β decreases at higher temperature if the magnitude of the heat of chemisorption (i.e., without dissociation) is greater than the magnitude of the heat of physisorption.

14-10. **(a)** Consider multilayer adsorption of gas A on a catalytic surface where the first layer is chemisorbed and the second and third layers are physisorbed. Write Langmuir-type expressions for the net rate of production of the second layer and invoke the principle of microscopic reversibility. Unlike the BET isotherm, the third layer occupies a measurable fraction of the catalyst, and desorption or evaporation from this physisorbed layer must be considered.

(b) Invoke the principle of microscopic reversibility and relate three adjacent surface coverage fractions; Θ_1, Θ_2, and Θ_3.

14-11. Derive the Hougen–Watson kinetic rate law for the generic chemical reaction

$$A_2 + B \longleftrightarrow C + D$$

Dissociative adsorption of reactant A_2 on the catalytic surface is the rate-limiting step, and the stable reactive intermediate A_2B^* occupies a significant fraction of surface sites. It is reasonable to assume that reactant B, intermediate A_2B^*, and products C and D experience single-site adsorption. Express your final answer in terms of the partial pressures of

reactants and products in the gas phase. Surface fractions Θ_i should not appear in the final answer.

14-12. Heterogeneous kinetic rate data have been obtained from experiments using a packed catalytic tubular reactor for the following reversible chemical reaction that occurs on the interior surface of a porous catalyst; $A + B \leftrightarrow C + D$, where desorption of product D is the rate-controlling step in the overall mechanism and all species undergo single-site adsorption. The feed stream is stoichiometric in the two reactants. Graph the initial rate of reaction versus total pressure at high temperature and low temperature on the same set of axes. If the surface-catalyzed chemical reaction is irreversible and $K_{\text{eq},\,p}$ based on gas-phase partial pressures is infinitely large, then how does the total pressure dependence of the initial rate of reaction differ from your answer when the reaction is reversible?

14-13. Heterogeneous kinetic rate data have been obtained from experiments using a packed catalytic tubular reactor for the following reversible chemical reaction that occurs on the interior surface of a porous catalyst: $A + B \leftrightarrow C + D$, where all species undergo single-site adsorption, the stable reactive intermediate occupies a significant fraction of surface sites, and chemical reaction on the surface is the slowest step in the mechanism. The feed stream is stoichiometric in the two reactants, A and B. Graph the initial rate of reaction versus total pressure on the same set of axes for the following cases:

(a) $A\sigma + B\sigma$ forming a stable reactive intermediate that occupies one surface site is the slowest step.

(b) The stable reactive intermediate forming chemisorbed products C and D is the slowest step.

(c) The stable reactive intermediate is not considered in the overall mechanism.

(d) Only A and C adsorb on the surface, and the stable reactive intermediate is not considered in the overall mechanism.

14-14. The overall reversible reaction is $A(g) + B(g) \leftrightarrow C(g) + D(g)$, and a stoichiometric feed of reactants A and B enters a packed catalytic tubular reactor. Each component adsorbs on a single active site on the catalytic surface. Sketch the effect of total pressure on the initial rate of reaction when adsorption of reactant A is the slowest step in the overall mechanism and the stable reactive intermediate does not occupy surface sites.

14-15. Consider the Langmuir–Hinshelwood mechanism for a dual-site rate-controlling surface-catalyzed chemical reaction ($A \leftrightarrow B + C$) and describe how C_1 analysis of the initial rate of reaction should be modified if the chemical reaction is reversible, and the equilibrium constant is known from thermodynamic data. The feed contains only reactant A.

14-16. Carbon monoxide (C≡O) and hydrogen (H_2) produce methanol (CH_3OH) on a ruthenium-exchanged zeolite-Y catalyst within a tubular reactor. Propose a mechanism and develop a kinetic rate law which accounts for the fact that a heterogeneous surface-catalyzed reaction occurs within the internal pores of the zeolite catalyst. *Hint:* There are no hydrogen–hydrogen bonds in methanol.

14-17. **(a)** Consider the triple-site chemical reaction rate-controlling mechanism described by (14-102) in which reactant A_2 undergoes dissociative adsorption and atomic A occupies a single site. Gases B, C, and D also occupy single sites, but they do not dissociate. A stoichiometric feed of reactants A_2 and B is present at the inlet to a packed catalytic tubular reactor. Perform linear least-squares analysis of the total pressure dependence of the initial rate of conversion of reactants to products. Your solution to this problem should contain five or six answers.

(b) Sketch the total pressure dependence of the initial rate of conversion of reactants to products.

14-18. Consider the six-step mechanism described by (14-138) in which dual-site adsorption of reactant A_2 is rate controlling. A stoichiometric feed of reactants A_2 and B is present at the inlet to a packed catalytic tubular reactor. Perform linear least-squares analysis of the total pressure dependence of the initial rate of conversion of reactants to products. Your solution to this problem should contain five or six answers.

14-19. Consider the heterogeneous catalytic mechanism described by (14-124) where adsorption of reactant A on a single active surface site is rate controlling in the five-step mechanism. Qualitatively outline a sequence of experiments and calculations that will allow you to determine the equilibrium constant for the chemical reaction on the catalytic surface:

$$K_{\text{eq, surf. Rx}} = \frac{k_{\text{forward, surf. Rx}}}{k_{\text{backward, surf. Rx}}}$$

This chemical reaction (i.e., $A\sigma + B\sigma \leftrightarrow C\sigma + D\sigma$) is equilibrated on the time scale of the adsorption of reactant A. Your solution to this problem should contain at least three logical steps.

14-20. Consider the three-step Langmuir–Rideal mechanism of heterogeneous catalysis:

$$A + B \longleftrightarrow C + D$$

with single-site rate-controlling chemical reaction on the catalytic surface, as described by (14-68). A stoichiometric feed of reactants A and B is present at the inlet to a packed catalytic tubular reactor.

(a) Sketch the total pressure dependence of the initial rate of conversion of reactants to products. Put total pressure on the horizontal axis and describe the high-pressure behavior of this graph in as much detail as possible.

(b) Perform linear least-squares analysis of the Hougen–Watson kinetic model that corresponds to the Langmuir–Rideal mechanism and quantify the total pressure dependence of the initial rate of conversion of reactants to products.

14-21. Nitrogen and hydrogen produce ammonia in a gas-phase adiabatic tubular reactor operating at 5 atm total pressure. A stoichiometric feed of N_2 and H_2 enters the reactor. The reversible elementary chemical reaction is

$$N_2(g) + 3H_2(g) \longleftrightarrow 2NH_3(g)$$

(a) Develop an expression for the homogeneous kinetic rate law $\mathfrak{R}$, which depends on temperature, total pressure, and conversion of nitrogen if a catalyst is not required.

(b) Propose a mechanism in which N_2 undergoes dissociative adsorption on the catalytic surface and H_2 attacks adsorbed atomic nitrogen from the gas phase. How many elementary steps are required?

(c) Develop a heterogeneous surface-catalyzed kinetic rate law in the presence of a catalyst, based on the mechanism in part (b).

Answer: (a) Since the reaction is elementary and reversible, and it occurs in the gas phase, the rate law should be constructed via partial pressures instead of molar densities, particularly if the forward kinetic rate constant has dimensions of mol/volume·time·$(\text{atm})^4$. The order of the reaction with respect to each component is equivalent to the magnitude of its stoichiometric coefficient. Reactant partial pressures appear in the forward rate, and product partial pressures are used for the backward rate. The backward kinetic rate constant is rewritten in terms of the forward rate constant and the equilibrium constant based on gas-phase partial pressures. In agreement with all these statements,

$$\mathfrak{R} = k_{\text{forward, } p}\left[p_{N_2}(p_{H_2})^3 - \frac{(p_{NH_3})^2}{K_{\text{equilibrium, } p}}\right]$$

Dalton's law is used to express partial pressures in terms of mole fractions and total pressure. Total pressure must be expressed in atmospheres if $K_{\text{equilibrium, } p}$ is calculated via the dimensionless thermodynamic equation for $K_{\text{equilibrium, } f}$, which is based on standard-state enthalpies and entropies of reaction at 298 K. Furthermore, the dimensions of $K_{\text{equilibrium, } p}$ are the same as those of $K^{\circ}_{\text{standard state}}$ [i.e., $(\text{atm})^{-2}$ for this problem]. The latter equilibrium constant, which is based on standard-state fugacities of pure components at 1 atm and 298 K, has a magnitude of 1 when total pressure in the kinetic rate law is expressed in atmospheres. Hence,

$$\mathfrak{R} = k_{\text{forward, } p}(p_{\text{total}})^4 \left[y_{N_2}(y_{H_2})^3 - \frac{(p_{\text{total}})^{-2}(y_{NH_3})^2}{K_{\text{equilibrium, } p}} \right]$$

$$K_{\text{equilibrium, } p}(T) = K^{\circ}_{\text{standard state}} \exp\left(A + \frac{B}{T}\right)$$

$$A = \frac{\Delta S^{\circ}_{\text{Rx,298}}}{R} = \frac{2\Delta S^{\circ}_{\text{formation, } NH_3}(298 \text{ K})}{R}$$

$$B = -\frac{\Delta H^{\circ}_{\text{Rx,298}}}{R} = -\frac{2\Delta H^{\circ}_{\text{formation, } NH_3}(298 \text{ K})}{R}$$

The general expression for mole fraction in terms of the conversion of N_2 for gas-phase flow reactors in which moles are not conserved, is based on stoichiometry and the molar flow rate of N_2. The generic result is

$$y_i(\chi) = \frac{\lambda_i + \upsilon_i \chi}{\delta \chi + \sum_j \lambda_j}$$

where $\upsilon_{N_2} = -1$, $\upsilon_{H_2} = -3$, $\upsilon_{NH_3} = 2$, and $\delta = \sum_i \upsilon_i = -2$. For a stoichiometric feed of nitrogen and hydrogen, the lambda parameter for each reactant gas, which characterizes the inlet molar flow rate of component i relative to the inlet molar flow rate of the key limiting reactant (i.e., N_2), is equivalent to the magnitude of reactant i's stoichiometric coefficient. Hence, $\lambda_{N_2} = 1$, $\lambda_{H_2} = 3$, $\lambda_{NH_3} = 0$, and $\sum_i \lambda_i = 4$.

The final expression for each mole fraction is

$$y_{N_2}(\chi) = \frac{1 - \chi}{4 - 2\chi}$$

$$y_{H_2}(\chi) = \frac{3 - 3\chi}{4 - 2\chi}$$

$$y_{NH_3}(\chi) = \frac{2\chi}{4 - 2\chi}$$

If a catalyst is not required, then the total pressure dependence of the initial rate of conversion of reactants to products scales as the fourth power of p_{total}. This result is compared with the dependence of $\mathfrak{R}_{\text{initial}}$ on p_{total} for the heterogeneous catalytic mechanism described below.

(b) It should be obvious from the chemical structures of reactants and products that the highly energetic nitrogen–nitrogen triple bond must dissociate. Furthermore, dissociative adsorption of nitrogen should be the rate-limiting step in the mechanism. Hence,

$$N_2(g) \leftrightarrow 2N(g)$$

$$2N(g) + 2\sigma = 2N\sigma$$

These two steps are combined to generate the slow step upon which the Hougen–Watson model is developed:

$$N_2(g) + 2\sigma \longleftrightarrow 2N\sigma$$

Hydrogen (i.e., H_2) dissociates and attacks adsorbed atomic nitrogen from the gas phase. Since dissociative adsorption of H_2 does not occur,

$$H_2(g) = 2H(g)$$

is not a critical step in the mechanism because it occurs rapidly, relative to N_2 dissociation, and atomic hydrogen does not occupy surface sites. In the absence of any reactive intermediates, the following sequence of five elementary steps:

$$\begin{aligned} N_2(g) &\leftrightarrow 2N(g) \\ 3H_2(g) &= 6H(g) \\ 2N(g) + 2\sigma &= 2N\sigma \\ 2N\sigma + 6H(g) &= 2NH_3\sigma \\ 2NH_3\sigma &= 2NH_3(g) + 2\sigma \end{aligned}$$

is reduced to four steps, with dissociative adsorption of N_2 being rate limiting:

$$\begin{aligned} N_2(g) + 2\sigma &\leftrightarrow 2N\sigma \\ 3H_2(g) &= 6H(g) \\ 2N\sigma + 6H(g) &= 2NH_3\sigma \\ 2NH_3\sigma &= 2NH_3(g) + 2\sigma \end{aligned}$$

or three steps, where the first one is slow:

$$\begin{aligned} N_2(g) + 2\sigma &\leftrightarrow 2N\sigma \\ 2N\sigma + 3H_2(g) &= 2NH_3\sigma \\ 2NH_3\sigma &= 2NH_3(g) + 2\sigma \end{aligned}$$

(c) The Hougen–Watson model is based on the first step in the three- or four-step mechanism:

$$\mathfrak{R}_{HW} = k_{N,\,adsorption}\, p_{N_2} (\Theta_V)^2 - k_{N,\,desorption} (\Theta_N)^2 \approx (\Theta_V)^2$$

A Langmuir isotherm for NH_3 allows one to calculate surface coverage by ammonia via the last step:

$$\Theta_{NH_3} = K_{NH_3} p_{NH_3} \Theta_V$$

Equilibration of the heterogeneous surface-catalyzed chemical reaction, on the time scale of the slow step, allows one to calculate surface coverage by atomic nitrogen. The principle of microscopic reversibility yields

$$k_{\text{forward, surf. Rx}} (\Theta_N)^2 (p_H)^6 = k_{\text{backward, surf. Rx}} (\Theta_{NH_3})^2$$

for the four-step mechanism, and

$$k_{\text{forward, surf. Rx}} (\Theta_N)^2 (p_{H_2})^3 = k_{\text{backward, surf. Rx}} (\Theta_{NH_3})^2$$

for the three-step mechanism. Since dissociation of H_2 to atomic hydrogen equilibrates on the time scale of the rate-limiting step, the partial pressure of atomic hydrogen is related to the partial pressure of hydrogen gas (i.e., H_2) via

$$(p_H)^2 = K_{\text{hydrogen dissociation}} p_{H_2}$$

The Hougen–Watson kinetic model is expressed in terms of the partial pressure of H_2. If H_2 dissociation is an important step that cannot be neglected in the mechanism, then the hydrogen dissociation equilibrium constant (i.e., $K_{\text{hydrogen dissociation}}$) is included in the rate law. Hence,

$$\Theta_N = \frac{\Theta_{NH_3}}{[K_{\text{equilibrium, surf. Rx}} (p_{H_2})^3]^{1/2}} = \frac{K_{NH_3} p_{NH_3} \Theta_V}{[K_{\text{equilibrium, surf. Rx}} (p_{H_2})^3]^{1/2}}$$

Now, the Hougen–Watson model adopts the following form:

$$\mathfrak{R}_{HW} = \left[k_{N, \text{adsorption}} p_{N_2} - \frac{k_{N, \text{desorption}} (K_{NH_3})^2 (p_{NH_3})^2}{K_{\text{equilibrium, surf. Rx}} (p_{H_2})^3} \right] (\Theta_V)^2$$

Upon factoring the adsorption kinetic rate constant for atomic nitrogen, and realizing that

$$\frac{k_{N, \text{desorption}}}{k_{N, \text{adsorption}}} \frac{(K_{NH_3})^2}{K_{\text{equilibrium, surf. Rx}}} = \frac{1}{K_{\text{equilibrium, } p}}$$

when the principle of microscopic reversibility is applied to the rate-limiting step at equilibrium, one obtains

$$\mathfrak{R}_{\mathrm{HW}} = k_{\mathrm{N,\,adsorption}} \left\{ p_{\mathrm{N_2}} - \frac{1}{K_{\mathrm{equilibrium},\,p}} \frac{(p_{\mathrm{NH_3}})^2}{(p_{\mathrm{H_2}})^3} \right\} (\Theta_V)^2$$

A population balance yields the fraction of vacant sites on the catalytic surface as follows:

$$\Theta_{\mathrm{N}} + \Theta_{\mathrm{NH_3}} + \Theta_V = \Theta_V \left[1 + K_{\mathrm{NH_3}} p_{\mathrm{NH_3}} + \left(\frac{K_{\mathrm{N}}}{K_{\mathrm{equilibrium},\,p}} \right)^{1/2} \frac{p_{\mathrm{NH_3}}}{\{p_{\mathrm{H_2}}\}^{3/2}} \right] = 1$$

where the adsorption/desorption equilibrium constant for atomic nitrogen is

$$K_{\mathrm{N}} = \frac{k_{\mathrm{N,\,adsorption}}}{k_{\mathrm{N,\,desorption}}}$$

If the feed stream to a packed catalytic tubular reactor contains stoichiometric proportions of nitrogen and hydrogen on a molar basis (i.e., 1 : 3), then the total pressure dependence of the initial reactant-product conversion rate is evaluated from the results above when

$$p_{\mathrm{N_2}}(z = 0) = 0.25 p_{\mathrm{total}}(z = 0)$$
$$p_{\mathrm{H_2}}(z = 0) = 0.75 p_{\mathrm{total}}(z = 0)$$
$$p_{\mathrm{NH_3}}(z = 0) = 0$$
$$\Theta_V = 1$$

Hence,

$$\mathfrak{R}_{\mathrm{HW,\,initial}} = 0.25 k_{\mathrm{N,\,adsorption}} p_{\mathrm{total}}(z = 0)$$

In summary, when a heterogeneous solid catalyst is required to produce ammonia from nitrogen and hydrogen, the initial reactant–product conversion rate scales linearly with total pressure at the reactor inlet. In the absence of a catalyst, or when a gas-phase catalyst is employed, the initial rate of reaction scales as the fourth power of total pressure.

14-22. Consider the following generic heterogeneous catalytic chemical reaction:

$$\mathrm{A_2} + \mathrm{B} \longleftrightarrow \mathrm{C} + \mathrm{D}$$

where $\mathrm{A_2}$ experiences dissociative adsorption, C, D, and atomic A each occupy single sites on the catalytic surface, and B attacks adsorbed atomic A (i.e., $\mathrm{A}\sigma$) from the gas phase. The rate-limiting step in the mechanism is

surface-catalyzed chemical reaction. The feed stream to a packed catalytic tubular reactor is stoichiometric in A_2 and B (i.e., 1 : 1 ratio).

(a) Sketch the total pressure dependence of the initial rate of conversion of reactants to products.

(b) Write an expression for the forward rate of reaction on the catalytic surface, and identify the units of the forward kinetic rate constant in this expression.

(c) What important information can be obtained from the slope of $\mathfrak{R}_{\text{HW, initial}}$ vs. p_{total} at very high total pressure?

(d) Apply linear least-squares analysis to p_{total} vs. $\mathfrak{R}_{\text{HW, initial}}$ by answering the following questions:

(1) What polynomial model should be used to analyze the data?

(2) What is the independent variable x, based on the raw data?

(3) What is the dependent variable y, based on the raw data?

(4) How should you process the coefficients of the polynomial, which are determined from the regression analysis, to calculate the temperature-dependent kinetic and equilibrium constants?

Answer: (a) The mechanism proceeds as follows when dual-site chemical reaction on the catalytic surface is the rate-controlling step:

$$\begin{aligned} A_2(g) + 2\sigma &= 2A\sigma \\ 2A\sigma + B(g) &\leftrightarrow C\sigma + D\sigma \\ C\sigma &= C(g) + \sigma \\ D\sigma &= D(g) + \sigma \end{aligned}$$

The Hougen–Watson kinetic model is constructed from the second step in the mechanism:

$$\mathfrak{R}_{\text{HW}} = k_{\text{forward}}(\Theta_A)^2 p_B - k_{\text{backward}}\Theta_C\Theta_D \approx (\Theta_V)^2$$

and surface coverage fractions for C, D, and atomic A follow Langmuir isotherms:

$$\Theta_i = \Theta_V(K_i p_i)^{1/\gamma_i}$$

where γ_i represents the number of surface sites required for one molecule of species i to adsorb on the catalyst. Hence, $\gamma_A = 2$, $\gamma_C = \gamma_D = 1$. The final form of the kinetic rate law is

$$\mathfrak{R}_{\text{HW}} = k_{\text{forward}} K_A \left(p_{A_2} p_B - \frac{p_C p_D}{K_{\text{equilibrium, } p}} \right) (\Theta_V)^2$$

and the vacant-site fraction is obtained from a population balance:

$$\Theta_V = \left[1 + \sum_{i=\mathrm{A,\,C,\,D}} (K_i p_i)^{1/\gamma_i} \right]^{-1}$$

For a stoichiometric feed of reactants A_2 and B, the initial rate of conversion of reactants to products is evaluated as follows:

$$p_{A_2,\,\mathrm{initial}} = p_{\mathrm{B,\,initial}} = 0.5 p_{\mathrm{total}}(z=0)$$

$$p_{\mathrm{C,\,initial}} = p_{\mathrm{D,\,initial}} = 0$$

$$\Theta_V = \frac{1}{1 + \sqrt{K_\mathrm{A} p_\mathrm{A}}}$$

Hence, the kinetic rate law near the inlet to a packed catalytic tubular reactor reduces to

$$\mathfrak{R}_{\mathrm{HW,\,initial}} = \frac{0.25 k_{\mathrm{forward}} K_\mathrm{A} [p_{\mathrm{total}}(z=0)]^2}{\left\{ 1 + \sqrt{\tfrac{1}{2} K_\mathrm{A} p_{\mathrm{total}}(z=0)} \right\}^2}$$

At very large total pressure, the initial reactant–product conversion rate approaches the following asymptotic expression:

$$\mathrm{Lim}_{p_{\mathrm{total}}(z=0)\to\infty} \{\mathfrak{R}_{\mathrm{HW,\,initial}}\} = \tfrac{1}{2} k_{\mathrm{forward}} p_{\mathrm{total}}(z=0)$$

(b, c) Hence, the slope of $\mathfrak{R}_{\mathrm{HW,\,initial}}$ vs. $p_{\mathrm{total}}(z=0)$ achieves a constant slope of $0.5 k_{\mathrm{forward}}$ at very large total pressure. Based on the forward rate of reaction on the catalyst [i.e., $k_{\mathrm{forward}}(\Theta_\mathrm{A})^2 p_\mathrm{B}$] with dimensions of mol/area·time, the units of the forward kinetic rate constant for surface-catalyzed chemical reaction are mol/area·time·atm. These dimensions for k_{forward} are consistent with the slope of $\mathfrak{R}_{\mathrm{HW,\,initial}}$ vs. $p_{\mathrm{total}}(z=0)$.

(d) Linear least-squares analysis of $p_{\mathrm{total}}(z=0)$ vs. $\mathfrak{R}_{\mathrm{HW,\,initial}}$ is based on algebraic manipulation of the following expression:

$$\mathfrak{R}_{\mathrm{HW,\,initial}} = \frac{0.25 k_{\mathrm{forward}} K_\mathrm{A} [p_{\mathrm{total}}(z=0)]^2}{\left\{ 1 + \sqrt{\tfrac{1}{2} K_\mathrm{A} p_{\mathrm{total}}(z=0)} \right\}^2}$$

which yields

$$\frac{[p_{\mathrm{total}}(z=0)]^2}{\mathfrak{R}_{\mathrm{HW,\,initial}}} = \frac{\left\{ 1 + \sqrt{\tfrac{1}{2} K_\mathrm{A} p_{\mathrm{total}}(z=0)} \right\}^2}{0.25 k_{\mathrm{forward}} K_\mathrm{A}}$$

One obtains a linearized form for the initial reactant–product conversion rate by taking the square root of both sides of the preceding equation;

$$\frac{p_{\text{total}}(z=0)}{(\Re_{\text{HW, initial}})^{0.5}} = \frac{1+[0.5K_{\text{A}}p_{\text{total}}(z=0)]^{0.5}}{(0.25k_{\text{forward}}K_{\text{A}})^{0.5}}$$

$$= \frac{2}{\sqrt{k_{\text{forward}}K_{\text{A}}}} + \sqrt{\frac{2}{k_{\text{forward}}}}\{p_{\text{total}}(z=0)\}^{1/2}$$

The linear least-squares prescription is as follows:

1. Use a first-order polynomial model: $y = a_0 + a_1 x$.

2. The independent variable is $x = [p_{\text{total}}(z=0)]^{0.5}$.

3. The dependent variable is $y = p_{\text{total}}(z=0)/(\Re_{\text{HW, initial}})^{0.5}$.

4. The zeroth-order coefficient is $a_0 = 2/(k_{\text{forward}}K_{\text{A}})^{0.5}$.

5. The first-order coefficient is $a_1 = (2/k_{\text{forward}})^{0.5}$.

The temperature-dependent kinetic and equilibrium constants, which can be determined from total pressure dependence of the initial reactant–product conversion rate, are

$$k_{\text{forward}} = \frac{2}{(a_1)^2}$$

$$K_{\text{A}} = 2\left(\frac{a_1}{a_0}\right)^2$$

14-23. In a recently published reactor design textbook, a problem begins as follows: The heterogeneous gas-phase catalytic chemical reaction, A + B → C, is carried out in an isothermal isobaric flow reactor. If C_i represents the molar density of species i, then the volume-based kinetic rate expression for the reaction is

$$r = \frac{k(T)C_{\text{A}}C_{\text{B}}}{1 + K_{\text{A}}C_{\text{A}} + K_{\text{B}}C_{\text{B}}}$$

The publisher asks you to review this problem. Make a recommendation about the validity of this rate law by writing a few sentences. In other words, does the rate law seem reasonable, or should it be modified? If modification is required, indicate qualitatively how the modification should proceed. Please don't include too many equations because the publisher must read your review and decide whether a second edition of this textbook should be printed. All the engineering editors are on vacation in Hawaii.

14-24. Describe a detailed heterogeneous catalytic reaction mechanism where the kinetic rate law contains adsorption terms for at least two species in the denominator, with an exponent of one for the entire group of terms in the denominator. In other words, the forward and backward rate expressions are proportional to the first power of the vacant-site fraction Θ_V, and

more than one species in the chemical reaction occupies active sites on the catalytic surface.

14-25. **(a)** Construct a mechanism and develop a kinetic rate law for the irreversible chemical reaction

$$A_2 + 2B \longrightarrow C$$

where

(1) Diatomic A_2 undergoes dissociative adsorption on a heterogeneous catalyst.

(2) B and C undergo single-site adsorption on a heterogeneous catalyst, without dissociation.

(3) Chemical reaction on the catalytic surface is the rate-limiting step.

(4) Surface coverage by each species follows the Freundlich isotherm for chemisorption.

The kinetic rate constant for this irreversible reaction is k_{forward}. Do not use Langmuir isotherms to describe surface coverage fractions by A_2, B, and C.

Answer: In agreement with statements (1) and (2), it is reasonable to propose the following four-step mechanism. Since A_2 requires two sites for adsorption after dissociation, and B requires one site, the catalytic reaction between one molecule of A_2 and two molecules of B involves four sites. Hence, the quadruple-site chemical-reaction-rate controlling pathway is

$$A_2 + 2\sigma = 2A\sigma$$

$$B + \sigma = B\sigma$$

$$2A\sigma + 2B\sigma \rightarrow C\sigma + 3\sigma$$

$$C\sigma = C + \sigma$$

If the Freundlich isotherm is employed to calculate surface coverage fractions, then:

$$\Theta_i = (K_i p_i)^{1/n_i}$$

where n_i represents the number of active sites required for one molecule of species i to adsorb on the catalyst. For this particular problem, $n_A = 2$, $n_B = 1$, and $n_C = 1$. Notice that the vacant-site fraction does not appear in the equation for Θ_i because Freundlich's rate of adsorption is proportional to $1/\Theta_i$ instead of Θ_V. The

Hougen–Watson model for this four-step mechanism is based on the third step, which is irreversible. Hence,

$$\mathfrak{R}_{\text{Hougen-Watson}} = k_{\text{forward}}(\Theta_A)^2(\Theta_B)^2$$
$$= k_{\text{forward}} K_A (K_B)^2 p_A (p_B)^2$$

(b) Sketch the total pressure dependence of the initial rate of conversion of reactants to products for the kinetic rate law that was developed in part (a). A stoichiometric feed (i.e., 1 : 2) of reactants A_2 and B enters a packed catalytic tubular reactor.

Answer: If Dalton's law is applicable, then a stoichiometric feed of reactants A_2 and B is represented by $p_A = \frac{1}{3} p_{\text{total}}$ and $p_B = \frac{2}{3} p_{\text{total}}$ near the reactor inlet at $z = 0$. Under these conditions,

$$\mathfrak{R}_{\text{HW, initial}} = \tfrac{4}{27} k_{\text{forward}} K_A (K_B)^2 (p_{\text{total}})^3$$

Hence, the initial rate of conversion of reactants to products near the inlet scales as the third power of total pressure.

(c) Compare your sketch in part (b) with the total pressure dependence of $\mathfrak{R}_{\text{HW, initial}}$ if Langmuir isotherms were employed to calculate surface coverage fractions in part (a). A stoichiometric feed (i.e., 1 : 2) of reactants A_2 and B enters a packed catalytic tubular reactor.

Answer: If Langmuir-type adsorption is applicable, then the surface coverage fractions are represented by

$$\Theta_i = \Theta_V (K_i p_i)^{1/n_i}$$

where n_i represents the number of active sites required for one molecule of species i to adsorb on the catalyst. Now, the vacant-site fraction Θ_V plays a role in the kinetic rate law, which adopts the same form that was presented in part (a) based on surface coverage fractions:

$$\mathfrak{R}_{\text{Hougen-Watson}} = k_{\text{forward}}(\Theta_A)^2(\Theta_B)^2$$
$$= k_{\text{forward}} K_A (K_B)^2 p_A (p_B)^2 (\Theta_V)^4$$

A population balance yields the following expression for the fraction of vacant sites:

$$\Theta_V = [1 + (K_A p_A)^{1/2} + K_B p_B + K_C p_C]^{-1}$$

Near the reactor inlet, the initial rate of conversion of reactants to products reveals the following dependence on total pressure:

$$\mathfrak{R}_{\text{Hougen-Watson, initial}} = \frac{\frac{4}{27} k_{\text{forward}} K_A (K_B)^2 (p_{\text{total}})^3}{\left[1 + \left(\frac{1}{3} K_A p_{\text{total}}\right)^{1/2} + \frac{2}{3} K_B p_{\text{total}}\right]^4}$$

which scales as the inverse of p_{total} at high total pressure. Hence, the initial rate approaches zero at both very low and very high total pressure.

(d) Perform linear least-squares analysis of the total pressure dependence of the initial rate of conversion of reactants to products when surface coverage fractions in the kinetic rate law from part (a) are expressed in terms of the Freundlich isotherm for chemisorption. A stoichiometric feed (i.e., 1 : 2) of reactants A_2 and B enters a packed catalytic tubular reactor, and one has data for $\mathfrak{R}_{\text{HW, initial}}$ vs. p_{total}.

Answer: If the Freundlich isotherm adequately describes surface coverage of each species and a stoichiometric feed of reactants is present at the reactor inlet, then:

$$\mathfrak{R}_{\text{HW, initial}} = \tfrac{4}{27} k_{\text{forward}} K_{\text{A}} (K_{\text{B}})^2 (p_{\text{total}})^3$$

There are several approaches by which one can perform linear least squares analysis of the previous equation. For example,

Independent variable;	$x = (p_{\text{total}})^3$
Dependent variable;	$y = \mathfrak{R}_{\text{HW, initial}}$
Polynomial model;	$y = a_0 + a_1 x$
Intercept;	$a_0 = 0$
Slope;	$a_1 = \tfrac{4}{27} k_{\text{forward}} K_{\text{A}} (K_{\text{B}})^2$

Hence, one forces the analysis to yield a zero intercept and solves only one equation for the slope:

$$a_1 = \frac{\sum_i x_i y_i}{\sum_i (x_i)^2}$$

where each sum includes all $x_i - y_i$ data pairs. The previous result from linear least-squares analysis provides a numerical value for the third-order kinetic rate constant [i.e., $k_{\text{forward}} K_{\text{A}} (K_{\text{B}})^2$] when the heterogeneous kinetic rate law is based on gas-phase partial pressures.

14-26. Freundlich isotherms describe surface coverage of each species in the following chemical reaction, which occurs on a heterogeneous catalyst:

$$A_2 + 2B \rightarrow C$$

Diatomic A_2 undergoes dissociative adsorption, B and C undergo single-site adsorption without dissociation, and quadruple-site chemical reaction

on the catalytic surface is the rate-limiting step. The answer to Problem 14-25(a) suggests that the following Hougen–Watson kinetic model describes the rate of conversion of reactants to products:

$$\mathfrak{R}_{\text{Hougen-Watson}} = k_{\text{forward}}(\Theta_A)^2(\Theta_B)^2 = k_{\text{forward}}K_A(K_B)^2p_A(p_B)^2$$

This reaction occurs in a packed catalytic tubular reactor and data have been obtained near the inlet to characterize the total pressure dependence of the initial rate, when a stoichiometric feed (i.e., 1 : 2) of reactants A_2 and B is present. At constant temperature T, experiments were performed such that all total pressures p_{total} exist in a narrow range near the critical point of this ternary mixture. Hence, k_{forward} exhibits a significant dependence on total pressure. Employ a linear least-squares procedure and analyze the experimental data (i.e., $\mathfrak{R}_{\text{HW, initial}}$ vs. p_{total}) which have been measured. *Hint:* Identify the dependent (y) and independent (x) variables, and the slope (a_1) and intercept (a_0) for the following polynomial model; $y = a_0 + a_1x$.

Answer: The total pressure dependence of $\mathfrak{R}_{\text{HW, initial}}$ was developed in Problem 14-25(b):

$$\mathfrak{R}_{\text{HW, initial}} = \tfrac{4}{27}k_{\text{forward}}K_A(K_B)^2(p_{\text{total}})^3$$

When experiments are performed near the critical point of this reactive ternary mixture, the pressure dependence of k_{forward} is given by

$$k_{\text{forward}}(T, p) = k_f^*(T, p_0)\exp\left[-\frac{(p - p_0)\Delta v^*}{RT}\right]$$

where $k_f^*(T, p_0)$ contains the standard Arrhenius-type activation energy at ambient pressure. Since all the experiments are performed at the same temperature, the exponential part of k_{forward}, which contains the volume of activation, is most important for this analysis. The complete dependence of $\mathfrak{R}_{\text{HW, initial}}$ on p_{total} is given by

$$\mathfrak{R}_{\text{HW, initial}} = \frac{4}{27}k_f^*(T, p_0)K_A(K_B)^2(p_{\text{total}})^3\exp\left[-\frac{(p_{\text{total}} - p_0)\Delta v^*}{RT}\right]$$

After dividing by $(p_{\text{total}})^3$ and taking the natural logarithm of both sides of the previous equation, one obtains

$$\ln\left[\frac{\mathfrak{R}_{\text{HW, initial}}}{(p_{\text{total}})^3}\right] = \ln\left[\frac{4}{27}k_f^*(T, p_0)K_A(K_B)^2\right] - \frac{(p_{\text{total}} - p_0)\Delta v^*}{RT}$$

The linear least-squares procedure is summarized as follows:

Independent variable:	$x = p_{\text{total}} - p_0$
Dependent variable:	$y = \ln\left[\dfrac{\Re_{\text{HW, initial}}}{(p_{\text{total}})^3}\right]$
Intercept or zeroth-order coefficient:	$a_0 = \ln\left[\frac{4}{27} k_f^*(T, p_0) K_{\text{A}} (K_{\text{B}})^2\right]$
Slope or first-order coefficient:	$a_1 = -\dfrac{\Delta v^*}{RT}$

Hence, one determines the temperature-dependent combination of kinetic and adsorption/desorption equilibrium constants from the intercept when experiments are performed at temperature T:

$$k_f^*(T, p_0) K_{\text{A}} (K_{\text{B}})^2 = \tfrac{27}{4} \exp(a_0)$$

The volume of activation Δv^* is obtained directly from the slope:

$$\Delta v^* = -RT \frac{d}{d\, p_{\text{total}}} \ln\left\{\frac{\Re_{\text{HW, initial}}}{(p_{\text{total}})^3}\right\}$$

If there is a contraction in the volume of the reactants as they achieve the transition state, then the volume of activation is negative, the slope of the linear least-squares analysis is positive, and an increase in pressure accelerates the rate of conversion of reactants to products not only due to pressure terms in the rate law but also due to an increase in the kinetic rate constant at higher pressures in the vicinity of the critical point.

Transport Phenomena for Chemical Reactor Design. Laurence A. Belfiore
Copyright © 2003 John Wiley & Sons, Inc.
ISBN: 0-471-20275-4

PART IV

MASS TRANSFER AND CHEMICAL REACTION IN ISOTHERMAL CATALYTIC PELLETS

Transport Phenomena for Chemical Reactor Design. Laurence A. Belfiore
Copyright © 2003 John Wiley & Sons, Inc.
ISBN: 0-471-20275-4

15

DIFFUSION AND HETEROGENEOUS CHEMICAL REACTION IN ISOTHERMAL CATALYTIC PELLETS

15-1 COMPLEX PROBLEM DESCRIPTIONS WITHOUT INVOKING ANY ASSUMPTIONS

The mass transfer equation described in Chapters 9 and 10 was developed from first principles by considering a generic volume element and accounting for all the mass transfer rate processes that contribute to the mass of component i in this element of volume. The mass balance for component i is written in dimensional and dimensionless form as

$$\frac{\partial C_i}{\partial t} + \mathbf{v} \cdot \nabla C_i = \mathfrak{D}_{i,\,\mathrm{mix}} \nabla^2 C_i + \sum_{j=1}^{r} \nu_{ij} \mathfrak{R}_j \tag{15-1}$$

$$\mathrm{Re}\cdot\mathrm{Sc}\left(\frac{\partial \Psi_i}{\partial t} + \mathbf{v}^* \cdot \nabla \Psi_i\right) = 1 \cdot \nabla^2 \Psi_i + \sum_{j=1}^{r} \nu_{ij} \Lambda_{ij}^2 \mathfrak{R}_j^* \tag{15-2}$$

Even though the species velocity vectors $\mathbf{v}_i$ are nonzero for reactants and products that diffuse toward and away from the internal catalytic surface, it is customary to neglect convective mass transfer within the pores. In other words, the Reynolds number is vanishingly small and diffusion dominates convective transport. Under these conditions, the dimensionless mass transfer equation for component i reduces to

$$\nabla^2 \Psi_i + \sum_{j=1}^{r} \nu_{ij} \Lambda_{ij}^2 \mathfrak{R}_j^* = 0$$

which corresponds to steady-state diffusion and multiple pseudo-homogeneous chemical reactions within a catalytic pellet. When the chemical kinetics are heterogeneous and occur only on the catalytic surface, the rigorous description of this mass transfer/chemical reaction problem stipulates that rate processes due to multiple chemical reactions must appear in the boundary conditions and not in the mass balance. Hence,

$$\nabla^2 \Psi_i = 0 \tag{15-3}$$

is the simplified mass transfer equation for steady-state diffusion within the internal pores, with chemical reaction occurring only on the boundaries of the control volume. This corresponds to a complex problem description because, even though the mass balance has been simplified superficially:

1. Diffusion occurs in more than one coordinate direction due to the tortuous nature of the pores.
2. The description of diffusion and chemical reaction at the boundaries of the control volume is rather complex.

For example, if $\mathbf{n}$ is an outward-directed unit normal vector which originates on the internal catalytic surface and extends into the pore volume, then the complex radiation-type boundary conditions are

$$\mathbf{n} \cdot (-\mathbb{D}_{i,\,\mathrm{mix}} \nabla C_i)_{\text{catalytic surface}} = \sum_{j=1}^{r} \nu_{ij} \mathfrak{R}_{j,\,\mathrm{HW}} \tag{15-4}$$

This is a mathematical expression for the steady-state mass balance of component i at the boundary of the control volume (i.e., the catalytic surface) which states that the net rate of mass transfer away from the catalytic surface via diffusion (i.e., in the direction of $\mathbf{n}$) is balanced by the net rate of production of component i due to multiple heterogeneous surface-catalyzed chemical reactions. The kinetic rate laws are typically written in terms of Hougen–Watson models based on Langmuir–Hinshelwood mechanisms. Hence, $\mathfrak{R}_{j,\,\mathrm{HW}}$ is the Hougen–Watson rate law for the jth chemical reaction on the catalytic surface. Examples of Hougen–Watson models are discussed in Chapter 14. Both rate processes in the boundary conditions represent surface-related phenomena with units of moles per area per time. The dimensional scaling factor for diffusion in the boundary conditions is

$$\frac{D_{i,\,\mathrm{mix}} C_{\mathrm{A0}}}{L} \text{ [=] moles per area per time} \tag{15-5}$$

For heterogeneous surface-catalyzed chemical kinetics, the scaling factor for the jth reaction is

$$k_j(T)(C_{\mathrm{A0}})^{n_j} \text{ [=] moles per area per time} \tag{15-6}$$

where n_j is the order of the jth chemical reaction and k_j is a rate constant for the surface reaction with units of

$$k_j(T) \text{ [=] (volume/mole)}^{n_j-1} \cdot \text{length/time} \tag{15-7}$$

which reduces to the classic reaction velocity constant for first-order surface kinetics when $n_j = 1$. If N components participate in r chemical reactions, then it is possible to generate $r + 1$ dimensional scaling factors for component i via mass transfer rate processes that are operative in the boundary conditions:

1. One scaling factor for diffusion
2. One scaling factor for each of the r chemical reactions, where $1 \leq j \leq r$

Division of these $r + 1$ scaling factors by the scaling factor for diffusion (i.e., $\mathfrak{D}_{i,\,\mathrm{mix}} C_{\mathrm{A0}}/L$) produces r dimensionless numbers for component i in the boundary conditions. All of these dimensionless numbers can be treated simultaneously because they are constructed from the scaling factor for the jth chemical reaction and the scaling factor for diffusion. Hence,

$$\frac{k_j(T)(C_{\mathrm{A0}})^{n_j}}{\mathfrak{D}_{i,\,\mathrm{mix}} C_{\mathrm{A0}}/L} = \frac{k_j(T) L (C_{\mathrm{A0}})^{n_j-1}}{\mathfrak{D}_{i,\,\mathrm{mix}}} = \beta_{ij} \tag{15-8}$$

which defines the form of the Damkohler number that is appropriate for the boundary conditions. The difference between the Damkohler number β_{ij} in the boundary conditions and the Damkohler number $(\Lambda_{ij})^2$ in the mass transfer equation is based on the fact that both dimensional scaling factors used to construct β_{ij} have units of moles per area per time instead of moles per volume per time. In other words:

1. $\mathfrak{D}_{i,\,\mathrm{mix}} C_{\mathrm{A0}}/L$ is the scaling factor for diffusion in the boundary conditions, whereas $\mathfrak{D}_{i,\,\mathrm{mix}} C_{\mathrm{A0}}/L^2$ is the scaling factor for diffusion in the mass transfer equation.
2. The kinetic rate constant k_j corresponds to the kinetics of heterogeneous surface-catalyzed chemical reactions in the boundary conditions, whereas the rate law is written on a pseudo-volumetric basis when chemical reaction terms are included in the mass transfer equation.

The dimensionless form of the boundary conditions for heterogeneous surface-catalyzed chemical reactions is

$$\mathbf{n} \cdot (-\nabla \Psi_i)_{\text{catalytic surface}} = \sum_{j=1}^{r} \nu_{ij} \beta_{ij} \mathfrak{R}_j^* \tag{15-9}$$

where the dimensionless rate law is defined by

$$\mathfrak{R}_j^* = \frac{\mathfrak{R}_{j,\,\mathrm{HW}}}{k_j(T)(C_{\mathrm{A0}})^{n_j}} \tag{15-10}$$

and $k_j(T)$ is the kinetic rate constant for heterogeneous reactions when the rate law, in units of moles per area per time, is expressed using molar densities. As mentioned above, the mass transfer equation is superficially simple for a rigorous description of steady-state diffusion and heterogeneous chemical reactions within the pores of a catalytic pellet. Either two- or three-dimensional diffusion within the pores gives rise to a partial differential mass balance. Furthermore, the boundary conditions require a complex description because the pores are tortuous and the internal catalytic surface is not mathematically simple. This methodology is the technique of choice in Chapter 23 for duct reactors where expensive metal catalyst is coated on the inner walls of the flow channel and the catalytic surface is mathematically simple because it coincides with the macroscopic boundaries of the problem.

15-2 DIFFUSION AND PSEUDO-HOMOGENEOUS CHEMICAL REACTIONS IN ISOTHERMAL CATALYTIC PELLETS

The rigorous description of diffusion and heterogeneous surface-catalyzed chemical reactions in porous catalytic pellets is almost never solved in practice because the partial differential mass balance and the supporting boundary conditions are extremely complex. The approximate solution overlooks intricate details of the pore structure, exploits the symmetry of the macroscopic boundary of one catalytic pellet instead of one of the pores, and invokes the concept of homogeneous diffusion that is not influenced by the orientation of the internal pores.

Most important, heterogeneous surface-catalyzed chemical reaction rates are written in pseudo-homogeneous (i.e., volumetric) form and they are included in the mass transfer equation instead of the boundary conditions. Details of the porosity and tortuosity of a catalytic pellet are included in the effective diffusion coefficient used to calculate the intrapellet Damkohler number. The parameters S_m (i.e., internal surface area per unit mass of catalyst) and ρ_{app} (i.e., apparent pellet density, which includes the internal void volume), whose product has units of inverse length, allow one to express the kinetic rate laws in pseudo-volumetric form, as required by the mass transfer equation. Hence, the mass balance for homogeneous diffusion and multiple pseudo-volumetric chemical reactions in one catalytic pellet is

$$\nabla^2 \Psi_i + \sum_{j=1}^{r} \nu_{ij} \Lambda_{ij}^2 \mathfrak{R}_j^* = 0 \tag{15-11}$$

where the intrapellet Damkohler number for component i in reaction j is expressed as a ratio of two dimensional scaling factors that have units of moles per volume per time. When equation (15-11) is written for key-limiting reactant A in the presence of only one chemical reaction, and the stoichiometric coefficient of reactant A in this reaction is -1, the simplified homogeneous model reduces to

$$\nabla^2 \Psi_{\text{A}} = \Lambda^2 \mathfrak{R}^* \tag{15-12}$$

where Λ^2 is the intrapellet Damkohler number for reactant A, and the dimensionless kinetic rate law is

$$\mathfrak{R}^* = \frac{S_m \rho_{\text{app}} \mathfrak{R}_{\text{HW}}}{k_n (C_{\text{A0}})^n} \tag{15-13}$$

The Hougen–Watson rate law $\mathfrak{R}_{\text{HW}}$, with units of moles per area per time, is written on a pseudo-volumetric basis using the internal surface area per mass of catalyst S_m, and the apparent mass density of the pellet ρ_{app}. k_n is the nth-order kinetic rate constant with units of (volume/mole)$^{n-1}$ per time when the rate law is expressed on a volumetric basis using molar densities.

15-3 PSEUDO-FIRST-ORDER KINETIC RATE EXPRESSIONS THAT CAN REPLACE HOUGEN–WATSON MODELS AND GENERATE LINEARIZED ORDINARY DIFFERENTIAL EQUATIONS FOR THE MASS BALANCE

The mass transfer equation with one-dimensional diffusion and one chemical reaction is linear and can be solved analytically in rectangular, cylindrical, or spherical coordinates if the rate law corresponds to simple zeroth- or first-order kinetics. Numerical solutions are required for complex rate laws and simple nth-order kinetics with $n \neq 0, 1$. The objective of this section is to develop the methodology to linearize the mass transfer equation when the kinetics are different from zeroth or first-order. The rationale for linearizing the mass transfer equation is that the analytical solutions for first-order irreversible kinetics can be used for quick estimates of reactor performance, without implementing numerical techniques to integrate nonlinear second-order ODEs. Obviously, the mass transfer equation can be linearized very crudely by replacing the rate law with a constant, to simulate zeroth-order chemical kinetics. However, linearization and subsequent analytical solutions can also be obtained if the generalized Hougen–Watson model for the rate of chemical reaction is replaced by $k_1 C_{\text{A}}$ to simulate first-order irreversible kinetics where the rate law depends on the molar density of only one reactant, as shown in the following example.

Example. Determine the best value of the pseudo-first-order kinetic rate constant k_1 that provides the closest match between the actual rate law and the first-order irreversible rate law.

SOLUTION. This is an example of linear least-squares analysis (LLSA), where the objective function is continuous. Typically, LLSA is performed on a discrete set of data points and one seeks to minimize the sum of squares of differences between the data and a continuous model function. In this case, we seek to minimize the square of the difference between two continuous functions over the complete range of reactant conversions that are possible (i.e., $0 \leq x \leq 1$ for irreversible reactions). Hence, the sum of squares in the objective function to be

minimized is replaced by an integral of the square of the difference between the two functions. The objective function that must be minimized is

$$\int [S_m \rho_{\text{app}} \mathfrak{R}_{\text{HW}}(T, p, x) - k_1 C_{\text{A0}}(1 - x)]^2 \, dx \qquad 0 \le x \le x_{\text{equilibrium}} \tag{15-14}$$

where minimization is performed with respect to the parameter k_1, and the integration is performed over the complete range of reactant conversion. The Leibnitz rule for differentiating a one-dimensional integral with constant limits is applied to the objective function. The best value of k_1 corresponds to

$$\int_0^{x_{\text{eq}}} \frac{\partial}{\partial k_1} [S_m \rho_{\text{app}} \mathfrak{R}_{\text{HW}}(T, p, x) - k_1 C_{\text{A0}}(1 - x)]^2 \, dx = 0 \tag{15-15}$$

which reduces to

$$2C_{\text{A0}} \int_0^{x_{\text{eq}}} [S_m \rho_{\text{app}} \mathfrak{R}_{\text{HW}}(T, p, x) - k_1 C_{\text{A0}}(1 - x)](1 - x) \, dx = 0 \tag{15-16}$$

The LLSA prescription for the best pseudo-first-order kinetic rate constant is

$$k_1 = \frac{\displaystyle\int_0^{x_{\text{eq}}} S_m \rho_{\text{app}} \mathfrak{R}_{\text{HW}}(T, p, x)(1 - x) \, dx}{\displaystyle\int_0^{x_{\text{eq}}} C_{\text{A0}}(1 - x)^2 \, dx} \tag{15-17}$$

where $S_m \rho_{\text{app}} \mathfrak{R}_{\text{HW}}(T, p, x)$ represents a generalized rate law that is written on a volumetric or pseudo-volumetric basis. The remainder of this section applies only to irreversible kinetic rate laws where the maximum possible reactant conversion is 100% and the upper integration limit is 1. Since

$$\int_0^1 (1 - x)^2 \, dx = \frac{1}{3} \tag{15-18}$$

the best value of the pseudo-first-order kinetic rate constant reduces to

$$k_1 = \frac{3}{C_{\text{A0}}} \int_0^1 S_m \rho_{\text{app}} \mathfrak{R}_{\text{HW}}(T, p, x)(1 - x) \, dx \tag{15-19}$$

For reversible chemical reactions in which 100% conversion of reactants to products cannot be achieved, the upper integration limit is $x_{\text{equilibrium}}$ and the factor of 3 in (15-19) must be replaced by $3/[1 - (1 - x_{\text{equilibrium}})^3]$. Equation (15-19) is evaluated for irreversible nth-order chemical kinetics when the rate law is only a function of the molar density of the key-limiting reactant. Under these conditions,

$$S_m \rho_{\text{app}} \mathfrak{R}_{\text{HW}}(T, p, x) = k_n (C_{\text{A}})^n = k_n (C_{\text{A0}})^n (1 - x)^n \tag{15-20}$$

where the actual kinetic rate constant k_n has units of (volume/mole)$^{n-1}$ per time. Since

$$\int_0^1 (1-x)^{n+1}\,dx = \frac{1}{n+2} \tag{15-21}$$

the best pseudo-first-order kinetic rate constant with units of inverse time in the linearized mass transfer equation is

$$k_1 = \frac{3}{n+2} k_n (C_{A0})^{n-1} \tag{15-22}$$

which reduces to the correct identity (i.e., $k_1 = k_1$) for first-order chemical kinetics. In summary, the methodology described in this section allows one to approximate a complex kinetic rate law or an nth-order rate law by a pseudo-first-order rate expression, with the corresponding formulas given above. When the kinetics are first-order, the mass transfer equation with one-dimensional diffusion and chemical reaction is a second-order linear ODE for which analytical solutions are available. These solutions are described in Chapter 17 for homogeneous mass transfer models within the pores of a catalytic pellet.

Methodology. Pseudo-first-order kinetic rate constants that are consistent with nth-order kinetics and Hougen–Watson models are calculated as follows:

Step 1. Use the integral form of a linear-least squares analysis to determine the best value of the pseudo-first-order kinetic rate constant, k_1, that will linearize the reaction term in the mass transfer equation. It is necessary to apply the Leibnitz rule for differentiating a one-dimensional integral with constant limits to the following expression:

$$\frac{d}{dk_1}\left\{\int_0^{x_{eq}\to 1} [S_m \rho_{app} \mathfrak{R}_{HW}(T, p, x) - k_1 C_{A0}(1-x)]^2\,dx\right\} = 0 \tag{15-23}$$

Derive an expression for the pseudo-first-order volumetric rate constant based on molar densities in the rate law, k_1 with units of inverse time, in terms of a generic nonlinear rate law for irreversible reactions.

Step 2. Use the general expression in step 1 to determine the best value of k_1 in terms of k_n for irreversible nth-order chemical kinetics where the rate law is expressed in terms of the molar density of only one key-limiting reactant.

$$S_m \rho_{app} \mathfrak{R}_{HW}(T, p, x) = k_n C_{A0}^n (1-x)^n \tag{15-24}$$

You should obtain an analytical answer here for k_1 in terms of k_n that can be checked for consistency when $n = 1$.

Step 3. Use the general expression in step 1 to determine the best value of k_1 for the following reaction that occurs on a catalytic surface:

$$A_2 + B \longrightarrow C + D \tag{15-25}$$

The feed stream is stoichiometric in terms of the two reactants. Diatomic A_2 undergoes dissociative adsorption. Components B, C, and D experience single-site adsorption, and triple-site chemical reaction on the catalytic surface is the rate-controlling feature of the overall irreversible process. This Langmuir–Hinshelwood mechanism produces the following Hougen–Watson kinetic model for the rate of reaction with units of moles per area per time:

$$\mathfrak{R}_{\mathrm{HW}} = \frac{k_{\mathrm{forward}} K_{\mathrm{A}} K_{\mathrm{B}} p_{\mathrm{A}} p_{\mathrm{B}}}{\left(1 + K_{\mathrm{B}} p_{\mathrm{B}} + K_{\mathrm{C}} p_{\mathrm{C}} + K_{\mathrm{D}} p_{\mathrm{D}} + \sqrt{K_{\mathrm{A}} p_{\mathrm{A}}}\right)^3} \tag{15-26}$$

The adsorption/desorption equilibrium constant for each component is $K_i = 0.25\ \mathrm{atm}^{-1}$ and k_{forward} is the kinetic rate constant for the forward chemical reaction on the catalytic surface with units of moles per area per time. The reason that k_{forward} has the same units as $\mathfrak{R}_{\mathrm{HW}}$ is because rate laws for heterogeneous catalysis are written in terms of fractional surface coverage by the adsorbed species that participate in the reaction. Langmuir isotherms are subsequently used to express fractional surface coverage of the reacting species in terms of their partial pressures. The best value for the pseudo-first-order kinetic rate constant is calculated from

$$k_1 = \frac{3}{C_{\mathrm{A0}}} \int_0^1 S_m \rho_{\mathrm{app}} \mathfrak{R}_{\mathrm{HW}}(T, p, x)(1 - x)\, dx \tag{15-27}$$

The ideal gas law is employed to calculate the inlet or initial molar density of reactant A_2 when a stoichiometric feed of A_2 and B enters a gas-phase reactor. Hence,

$$C_{\mathrm{A0}} = \frac{N_{\mathrm{A0}}}{V_{\mathrm{total}}} = \frac{p}{\mathrm{RT}} y_{\mathrm{A,initial}} = \frac{p}{2RT} \tag{15-28}$$

Dalton's law is used to replace each partial pressure in the Hougen–Watson model (i.e., p_i) in terms of total pressure and the mole fraction of component i, $y_i(x)$. Since total moles are conserved in the overall chemical reaction, each y_i is linearly related to the fractional conversion x of reactant A_2. For example,

$$\begin{gathered} y_i(x) = \frac{\Theta_i + \nu_i x}{\delta x + \sum_j \Theta_j} \\ \Theta_{\mathrm{A}} = \Theta_{\mathrm{B}} = 1 \qquad \Theta_{\mathrm{C}} = \Theta_{\mathrm{D}} = 0 \\ \nu_{\mathrm{A}} = \nu_{\mathrm{B}} = -1 \qquad \nu_{\mathrm{C}} = \nu_{\mathrm{D}} = 1 \qquad \delta = 0 \\ y_{\mathrm{A}}(x) = y_{\mathrm{B}}(x) = \frac{1 - x}{2} \qquad y_{\mathrm{C}}(x) = y_{\mathrm{D}}(x) = \frac{x}{2} \end{gathered} \tag{15-29}$$

Total pressure dependence of the best value of k_1 for irreversible chemical kinetics is determined from the following integral expression:

$$k_1(p,T) = \frac{6RT}{p}\int_0^1 \frac{S_m \rho_{\text{app}} k_{\text{forward}} K_A K_B \left[\frac{1}{2}p(1-x)\right]^2 (1-x)}{\left[1 + \frac{1}{2}K_B p(1-x) + \frac{1}{2}(K_C + K_D)px + \sqrt{\frac{1}{2}K_A p(1-x)}\right]^3} dx \tag{15-30}$$

Generate a graph of $k_1/(S_m \rho_{\text{app}} k_{\text{forward}} K_A K_B RT)$ with units of atmospheres vs. total pressure in atmospheres. Identify the total system pressure where the pseudo-first-order rate constant exhibits a maximum. From Figure 15-1, the optimum operating pressure is clearly between 2 and 3 atm.

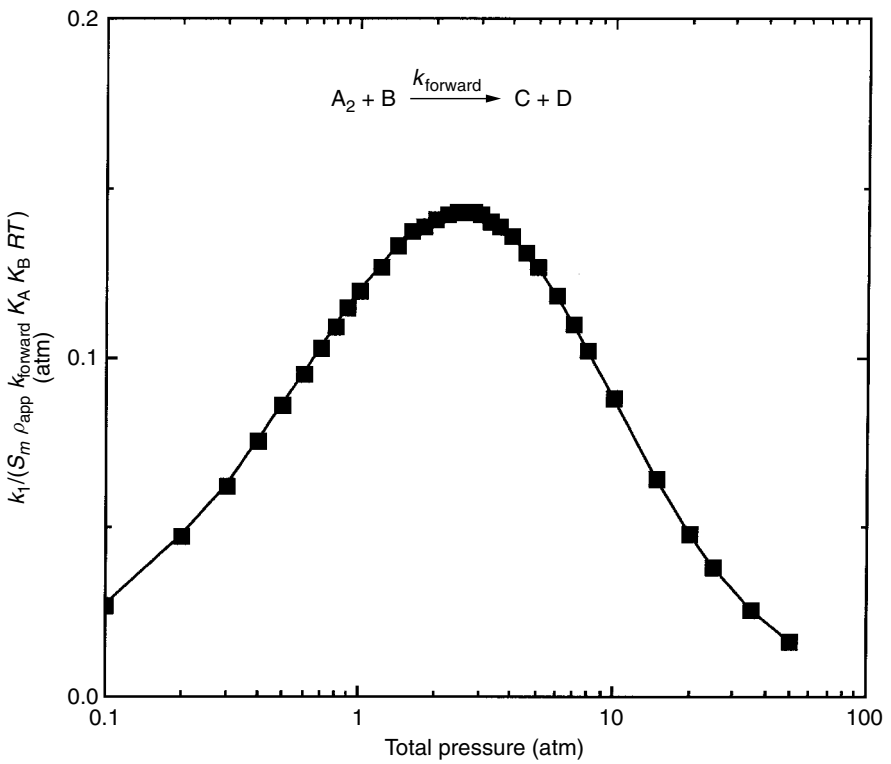

Figure 15-1 Total pressure dependence of the best pseudo-first-order kinetic rate constant when a first-order rate law approximates a Hougen–Watson model for dissociative adsorption of diatomic A_2 on active catalytic sites. Irreversible triple-site chemical reaction between atomic A and reactant B (i.e., $2A\sigma + B\sigma \rightarrow$ products) on the catalytic surface is the rate-limiting step. The adsorption/desorption equilibrium constant for each adsorbed species is 0.25 atm^{-1}.

15-4 DIFFUSION AND HETEROGENEOUS CHEMICAL REACTIONS IN ISOTHERMAL CATALYTIC PELLETS

As indicated by equation (15-12), the simplified homogeneous mass transfer model for diffusion and one chemical reaction within the internal pores of an isolated catalytic pellet is written in dimensionless form for reactant A as

$$\nabla^2 \Psi_A = \Lambda^2 \mathfrak{R}^* \tag{15-31}$$

where the intrapellet Damkohler number for reactant A is defined by

$$\Lambda^2 = \frac{k_n L^2 (C_{A\text{surf}})^{n-1}}{\mathfrak{D}_{A,\text{ effective}}} \tag{15-32}$$

The dimensionless kinetic rate law in the mass balance is defined by

$$\mathfrak{R}^* = \frac{S_m \rho_{\text{app}} \mathfrak{R}_{\text{HW}}}{k_n (C_{A\text{surf}})^n} \tag{15-33}$$

where the characteristic molar density of reactant A is calculated in the vicinity of the external surface of the catalyst, and k_n is an nth-order kinetic rate constant on a volumetric basis when molar densities are used in the rate expression. The units of k_n are (volume/mole)$^{n-1}$ per time. One-dimensional diffusion models represent a further simplification that allows one to obtain basic information for the spatial dependence of reactant molar density by solving ordinary differential equations. Under these conditions,

$$\nabla^2 \Psi_A = \begin{cases} \dfrac{d^2 \Psi_A}{d\eta^2} & \text{for catalysts with rectangular symmetry} \\ \dfrac{1}{\eta} \dfrac{d}{d\eta} \left(\eta \dfrac{d\Psi_A}{d\eta} \right) & \text{for long cylindrical catalysts} \\ \dfrac{1}{\eta^2} \dfrac{d}{d\eta} \left(\eta^2 \dfrac{d\Psi_A}{d\eta} \right) & \text{for catalysts with spherical symmetry} \end{cases} \tag{15-34}$$

The dimensionless spatial coordinate η is measured in the thinnest dimension of rectangular catalysts. For cylindrical and spherical catalysts, η is measured in the radial direction. The characteristic length L which appears in the intrapellet Damkohler number and is required to make the spatial coordinate dimensionless (i.e., η = spatial coordinate/L) is one-half the thickness of catalysts with rectangular symmetry, measured in the thinnest dimension; the radius of long cylindrical catalysts; or the radius of spherical catalysts. Ψ_A is the molar density of reactant A divided by its value in the vicinity of the external surface of the catalyst, $C_{A\text{surf}}$. Hence, by definition, $\Psi_A = 1$ at $\eta = 1$.

PROBLEM

15-1. The following irreversible heterogeneous catalytic reaction is exothermic and it occurs on active sites within the internal pores of a thin wafer:

$$A_2 + B \longrightarrow C$$

Diatomic gas A_2 undergoes dissociative adsorption and gases B and C experience single-site adsorption. Chemical reaction on the catalytic surface is the slowest step. Stoichiometric proportions of A_2 and B are present initially.

(a) Write the Hougen–Watson model for the kinetic rate law $\mathfrak{R}_{HW}$ with units of moles per area per time if the intermediate complex is not included in the mechanism. Remember that reaction on the catalytic surface is rate limiting.

(b) It is desired to approximate the Hougen–Watson model by the best pseudo-volumetric zeroth-order rate law with kinetic rate constant $k_{0,\,\text{pseudovolumetric}}$ such that $S_m \rho_{app} \mathfrak{R}_{HW}$ can be replaced by $k_{0,\,\text{pseudovolumetric}}$. What are the units of $k_{0,\,\text{pseudovolumetric}}$? Derive the equation for $k_{0,\,\text{pseudovolumetric}}$.

Answer: (b) The linear least-squares prescription described in this chapter is used to replace a complex kinetic rate law by a zeroth-order rate law. Hence, the objective function that must be minimized is

$$\int [S_m \rho_{app} \mathfrak{R}_{HW}(T, p, x) - k_0]^2 \, dx \qquad 0 \le x \le x_{equilibrium}$$

where minimization is performed with respect to the parameter k_0, and integration is performed over the complete range of reactant conversion. The best value of k_0 corresponds to

$$\int_0^{x_{eq}} \frac{\partial}{\partial k_0} [S_m \rho_{app} \mathfrak{R}_{HW}(T, p, x) - k_0]^2 \, dx = 0$$

which reduces to

$$-2 \int_0^{x_{eq}} [S_m \rho_{app} \mathfrak{R}_{HW}(T, p, x) - k_0] \, dx = 0$$

The LLSA (i.e., linear least-squares analysis) prescription for the best pseudo-zeroth-order kinetic rate constant is

$$k_0 = \frac{\displaystyle\int_0^{x_{eq}} S_m \rho_{app} \mathfrak{R}_{HW}(T, p, x) \, dx}{\displaystyle\int_0^{x_{eq}} dx}$$

where $S_m \rho_{app} \mathfrak{R}_{HW}(T, p, x)$ represents a generalized rate law that is written on a volumetric or pseudo-volumetric basis. Since the maximum possible reactant conversion is 100% for irreversible chemical reactions, the upper integration limit is 1. Hence, the best value of the pseudo-zeroth-order kinetic rate constant reduces to

$$k_0 = S_m \rho_{app} \int_0^1 \mathfrak{R}_{HW}(T, p, x)\, dx$$

When the kinetics are irreversible, nth order, and only a function of the molar density of key-limiting reactant A_2,

$$S_m \rho_{app} \mathfrak{R}_{HW}(T, p, x) = k_n (C_A)^n = k_n (C_{A0})^n (1 - x)^n$$

the best pseudo-zeroth-order kinetic rate constant, with units of moles per volume per time, is

$$k_0 = k_n (C_{A0})^n \int_0^1 (1 - x)^n\, dx = \frac{1}{n+1} k_n (C_{A0})^n$$

which reduces to the correct identity (i.e., $k_0 = k_0$) for zeroth-order chemical kinetics.

Transport Phenomena for Chemical Reactor Design. Laurence A. Belfiore
Copyright © 2003 John Wiley & Sons, Inc.
ISBN: 0-471-20275-4

16

COMPLETE ANALYTICAL SOLUTIONS FOR DIFFUSION AND ZEROTH-ORDER CHEMICAL REACTIONS IN ISOTHERMAL CATALYTIC PELLETS

16-1 CATALYTIC PELLETS WITH RECTANGULAR SYMMETRY

16-1.1 Irreversible Chemical Reaction

Homogeneous one-dimensional diffusion accompanied by chemical reaction in porous catalysts with rectangular symmetry is described by the following dimensionless mass balance:

$$\frac{d^2\Psi_A}{d\eta^2} = \Lambda^2 \mathfrak{R}^* \tag{16-1}$$

Under isothermal conditions, the kinetic rate constant is truly constant and the dimensionless rate law is

$$\mathfrak{R}^* = \frac{S_m \rho_{app} \mathfrak{R}_{HW}}{k_n (C_{A,\,surface})^n} = (\Psi_A)^n \tag{16-2}$$

for nth-order irreversible chemical kinetics when the reaction rate is only a function of the molar density of reactant A, because

$$S_m \rho_{app} \mathfrak{R}_{HW} = k_n (C_A)^n \tag{16-3}$$

and $\Psi_A = C_A / C_{A,\,surface}$. For zeroth-order kinetics (i.e., $n = 0$), $S_m \rho_{app} \mathfrak{R}_{HW}$ is simply a rate constant on a volumetric basis and $\mathfrak{R}^* = 1$. Hence, the one-dimensional transport/chemical reaction model reduces to

$$\frac{d^2\Psi_A}{d\eta^2} = \Lambda^2 \tag{16-4}$$

This second-order ordinary differential equation given by (16-4), which represents the mass balance for one-dimensional diffusion and chemical reaction, is very simple to integrate. The reactant molar density is a quadratic function of the spatial coordinate η. Conceptual difficulty arises for zeroth-order kinetics because it is necessary to introduce a critical dimensionless spatial coordinate, η_{critical}, which has the following physically realistic definition. When η_{critical}, which is a function of the intrapellet Damkohler number, takes on values between 0 and 1, regions within the central core of the catalyst are inaccessible to reactants because the rate of chemical reaction is much faster than the rate of intrapellet diffusion. The thickness of the dimensionless mass transfer boundary layer for reactant A, measured inward from the external surface of the catalyst, is $1 - \eta_{\text{critical}}$.

The quantitative definition of this critical spatial coordinate is $\Psi_A = 0$ at $\eta = \eta_{\text{critical}}$. Two constants of integration appear when the mass balance is solved for the basic information, $\Psi_A = f(\eta)$. These two integration constants, together with n_{critical}, represent three unknowns that are determined from two boundary conditions and the mathematical definition of the critical spatial coordinate. Hence, the three conditions are:

1. $\Psi_A = 1$ at $\eta = 1$ on the external surface of the catalyst via definitions of the dimensionless molar density of reactant A and the dimensionless spatial coordinate η.
2. (a) $d\Psi_A/d\eta = 0$ at $\eta = \eta_{\text{critical}} \geq 0$ when $\Lambda \geq \Lambda_{\text{critical}}$, or
   (b) $d\Psi_A/d\eta = 0$ at $\eta = 0$ when $\eta_{\text{critical}} < 0$ and $\Lambda < \Lambda_{\text{critical}}$.
3. $\Psi_A = 0$ at $\eta = \eta_{\text{critical}}$.

The latter two conditions indicate that reactant concentration within the catalyst vanishes at the critical spatial coordinate when $0 \leq \eta_{\text{critical}} < 1$, and it does so with a zero slope. Conditions 2a and 3 are reasonable because reactant A will not diffuse further into the catalyst, to smaller values of η, if it exhibits zero flux at η_{critical}. When $\eta_{\text{critical}} < 0$, condition 2b must be employed, which is consistent with the well-known symmetry condition at the center of the catalyst for kinetic rate laws where $\mathfrak{R}^* \neq$ constant. Zeroth-order reactions are unique because they require one to implement a method of "turning off" the rate of reaction when no reactants are present. Obviously, a zeroth-order rate law always produces the same rate of reaction because reactant molar densities do not appear explicitly in the chemical reaction term. Hence, the mass balance for homogeneous one-dimensional diffusion and zeroth-order chemical reaction is solved only over the following range of the independent variable; $\eta_{\text{critical}} \leq \eta \leq 1$, when η_{critical} is between 0 and 1. As illustrated below, the critical spatial coordinate is negative when the intrapellet Damkohler number is smaller than its critical value. Under these conditions, the mass balance is solved for values of η between 0 and 1 when $\Lambda < \Lambda_{\text{critical}}$ and boundary condition 2b is employed. The critical value of the intrapellet Damkohler number is defined mathematically as $\eta_{\text{critical}} = 0$ at $\Lambda = \Lambda_{\text{critical}}$.

In other words, reactants exist everywhere within the pores of the catalyst when the chemical reaction rate is slow enough relative to intrapellet diffusion, and the intrapellet Damkohler number is less than, or equal to, its critical value. These conditions lead to an effectiveness factor of unity for zeroth-order kinetics. When the intrapellet Damkohler number is greater than $\Lambda_{\text{critical}}$, the central core of the catalyst is reactant starved because η_{critical} is between 0 and 1, and the effectiveness factor decreases below unity because only the outer shell of the pellet is used to convert reactants to products. In fact, the dimensionless correlation between the effectiveness factor and the intrapellet Damkohler number for zeroth-order kinetics exhibits an abrupt change in slope when $\Lambda = \Lambda_{\text{critical}}$. Critical spatial coordinates and critical intrapellet Damkohler numbers are not required to analyze homogeneous diffusion and chemical reaction problems in catalytic pellets when the reaction order is different from zeroth-order. When the molar density appears explicitly in the rate law for nth-order chemical kinetics (i.e., $n > 0$), the rate of reaction automatically becomes extremely small when the reactants vanish. Furthermore, the dimensionless correlation between the effectiveness factor and the intrapellet Damkohler number does not exhibit an abrupt change in slope when the rate of reaction is different from zeroth-order.

16-1.2 Critical Dimensionless Spatial Coordinates and Intrapellet Damkohler Numbers

When the mass balance $d^2\Psi_A/d\eta^2 = \Lambda^2$ is integrated twice, subject to the following boundary conditions:

$$(1) \qquad \Psi_A = 1 \quad \text{at } \eta = 1 \tag{16-5a}$$

$$(2a) \qquad \frac{d\Psi_A}{d\eta} = 0 \quad \text{at } \eta = \eta_{\text{critical}} \tag{16-5b}$$

as described above, the following quadratic function is obtained:

$$\Psi_A(\eta;\, \eta_{\text{critical}},\, \Lambda) = 1 + \Lambda^2\eta_{\text{critical}}(1 - \eta) - 0.5\Lambda^2(1 - \eta^2) \tag{16-6}$$

This is the basic information governed by the mass balance, from which the dimensionless correlation between the effectiveness factor and the intrapellet Damkohler number is generated. When

$$\Psi_A(\text{at } \eta = \eta_{\text{critical}};\, \eta_{\text{critical}},\, \Lambda) = 0 \tag{16-7}$$

is implemented to define the critical dimensionless spatial coordinate, a quadratic equation results from (16-6) which can be solved analytically for η_{critical}. The following result is obtained:

$$\eta_{\text{critical}}(\Lambda) = 1 - \frac{\sqrt{2}}{\Lambda} \tag{16-8}$$

where the smaller of the two solutions is chosen to ensure that $\eta_{\text{critical}} < 1$. In agreement with physical reality, η_{critical} increases at higher values of the intrapellet Damkohler number, which implies that a larger fraction of the central core of the catalyst is reactant starved at higher reaction rates, and the mass transfer boundary layer occupies a thinner region near the external catalytic surface. Finally, the critical dimensionless spatial coordinate is zero (i.e., $\eta_{\text{critical}} = 0$) when the intrapellet Damkohler number is $\sqrt{2}$. Hence, $\Lambda_{\text{critical}} = \sqrt{2}$ for zeroth-order chemical kinetics in catalysts with rectangular symmetry (i.e., flat-slab catalysts and wafers). When the intrapellet Damkohler number is less than its critical value, the critical dimensionless spatial coordinate η_{critical} is negative, and boundary condition (2b) must be employed instead of (2a). Under these conditions, the dimensionless molar density profile for reactant A within the catalytic pores is adopted from equation (16-6) by setting η_{critical} to zero. Hence,

$$\Psi_A(\eta; \Lambda) = 1 - 0.5\Lambda^2(1 - \eta^2) \qquad \text{for } \Lambda \leq \Lambda_{\text{critical}} = \sqrt{2} \tag{16-9}$$

Notice that the molar density of reactant A does not decrease to zero at the center of the catalyst, where $\eta = 0$, when the intrapellet Damkohler number is below its critical value. In fact,

$$\Psi_A(\eta = 0; \Lambda) = 1 - 0.5\Lambda^2 > 0 \qquad \text{when } \Lambda < \sqrt{2} \tag{16-10}$$

16-2 LONG, CYLINDRICALLY SHAPED CATALYSTS

16-2.1 Irreversible Chemical Reaction

The homogeneous diffusion model is slightly more complex in cylindrical coordinates relative to the model described above in rectangular coordinates. Additional complexity arises because the radial term of the Laplacian operator ($\nabla \cdot \nabla = \nabla^2$) accounts for the fact that the surface area across which radial diffusion occurs increases linearly with dimensionless coordinate η as one moves radially outward. Basic information for $\Psi_A = f(\eta)$ is obtained by integrating the dimensionless mass balance with radial diffusion and chemical reaction:

$$\frac{1}{\eta}\frac{d}{d\eta}\left(\eta\frac{d\Psi_A}{d\eta}\right) = \Lambda^2 \tag{16-11}$$

subject to two boundary conditions:

$$\text{(1)} \qquad \Psi_A = 1 \qquad \text{at } \eta = 1 \tag{16-12a}$$

$$\text{(2a)} \qquad \frac{d\Psi_A}{d\eta} = 0 \qquad \text{at } \eta = \eta_{\text{critical}} \tag{16-12b}$$

The first integration step produces the following result for the concentration gradient:

$$\eta \frac{d\Psi_A}{d\eta} = 0.5\Lambda^2\eta^2 + C_1 \tag{16-13a}$$

$$\frac{d\Psi_A}{d\eta} = 0.5\Lambda^2\eta + \frac{C_1}{\eta} \tag{16-13b}$$

The second integration generates the molar density profile:

$$\Psi_A = 0.25\Lambda^2\eta^2 + C_1 \ln \eta + C_2 \tag{16-14}$$

where C_1 and C_2 are determined from the two boundary conditions given by equations (16-12). Once again, the dimensionless molar density of reactant A exhibits quadratic dependence on the dimensionless radial coordinate η, but there is an additional logarithmic term that arises because the Laplacian operator in cylindrical coordinates is more complex relative to its analog in rectangular coordinates. Hence, the basic information is

$$\Psi_A(\eta; \eta_{\text{critical}}, \Lambda) = 1 - 0.25\Lambda^2(1 - \eta^2) - 0.5(\Lambda\eta_{\text{critical}})^2 \ln \eta \tag{16-15}$$

16-2.2 Critical Dimensionless Radii and Intrapellet Damkohler Numbers

These critical values are obtained directly from the reactant molar density profile by implementing the condition that $\Psi_A = 0$ at $\eta = \eta_{\text{critical}}$. Hence, the critical dimensionless spatial coordinate is calculated by solving for the appropriate root of the following nonlinear algebraic equation:

$$1 - 0.25\Lambda^2(1 - \eta_{\text{critical}}^2) - 0.5(\Lambda\eta_{\text{critical}})^2 \ln \eta_{\text{critical}} = 0 \tag{16-16}$$

It is only necessary to solve this equation for values of η_{critical} between 0 and 1. Obviously, η_{critical} is a function of the intrapellet Damkohler number, but an explicit analytical function for $\eta_{\text{critical}} = f(\Lambda)$ is not possible. If Λ or Λ^2 is incremented from its critical value to extremely large values in the diffusion-limited regime, then a Newton–Raphson root-finding approach can be implemented to find the realistic root for η_{critical} at each value of the intrapellet Damkohler number (see Table 16-1).

If equation (16-16) is evaluated when $\eta_{\text{critical}} = 0$, then, by definition, one finds that $\Lambda_{\text{critical}} = 2$, which agrees with the first entry in Table 16-1 for long cylindrically shaped catalysts. L'Hôpital's rule confirms that

$$\eta_{\text{critical}}^2 \ln \eta_{\text{critical}} \to 0 \tag{16-17}$$

in the limit when $\eta_{\text{critical}} \to 0$. When the intrapellet Damkohler number is less than its critical value, the critical dimensionless spatial coordinate η_{critical} is negative, and boundary condition 2b must be employed instead of 2a. Under these

TABLE 16-1 Effect of the Intrapellet Damkohler Number on the Critical Dimensionless Radius for Radial Diffusion and Pseudo-Homogeneous Zeroth-Order Chemical Kinetics in Porous Catalysts with Cylindrical Symmetry

Λ	η_{critical}	Λ	η_{critical}
2	0	10	0.86
3	0.47	15	0.90
4	0.62	25	0.94
5	0.70	50	0.97
6	0.75	100	0.986
7	0.79	150	0.991
8	0.82	200	0.993

conditions, the dimensionless molar density profile for reactant A within the catalytic pores is adopted from equation (16-15) by setting η_{critical} to zero. Hence,

$$\Psi_A(\eta;\Lambda) = 1 - 0.25\Lambda^2(1-\eta^2) \qquad \text{for } \Lambda \le \Lambda_{\text{critical}} = 2 \tag{16-18}$$

Notice that the molar density of reactant A does not decrease to zero at the center of the catalyst, where $\eta = 0$, when the intrapellet Damkohler number is less than its critical value. In fact,

$$\Psi_A(\eta = 0;\, \Lambda) = 1 - 0.25\Lambda^2 > 0 \qquad \text{when } \Lambda < 2 \tag{16-19}$$

16-3 SPHERICAL PELLETS

16-3.1 Irreversible Chemical Reaction

The homogeneous diffusion model in spherical coordinates accounts for the fact that the surface area across which radial diffusion occurs increases quadratically with dimensionless coordinate η as one moves radially outward from the center of a spherically shaped catalyst. Once again, basic information for $\Psi_A = f(\eta)$ is obtained by integrating the dimensionless mass balance for reactant A with radial diffusion and chemical reaction

$$\frac{1}{\eta^2}\frac{d}{d\eta}\left(\eta^2\frac{d\Psi_A}{d\eta}\right) = \Lambda^2 \tag{16-20}$$

subject to two boundary conditions:

$$(1) \qquad \Psi_A = 1 \qquad \text{at } \eta = 1 \tag{16-21a}$$

$$(2a) \qquad \frac{d\Psi_A}{d\eta} = 0 \qquad \text{at } \eta = \eta_{\text{critical}} \tag{16-21b}$$

The first integration step produces the following result for the concentration gradient:

$$\eta^2 \frac{d\Psi_A}{d\eta} = \frac{1}{3}\Lambda^2\eta^3 + C_1 \tag{16-22a}$$

$$\frac{d\Psi_A}{d\eta} = \frac{1}{3}\Lambda^2\eta + \frac{C_1}{\eta^2} \tag{16-22b}$$

The second integration generates the molar density profile:

$$\Psi_A = \frac{1}{6}\Lambda^2\eta^2 - \frac{C_1}{\eta} + C_2 \tag{16-23}$$

where C_1 and C_2 are determined from the two boundary conditions given by equations (16-21). Now, the dimensionless molar density of reactant A exhibits quadratic dependence on the dimensionless radial coordinate η, with an additional term that scales as η^{-1} due to the symmetry of the problem in spherical coordinates. Hence, the spatial dependence of the molar density of reactant A is

$$\Psi_A(\eta; \eta_{critical}, \Lambda) = 1 - \frac{1}{6}\Lambda^2(1-\eta^2) - \frac{1}{3}\Lambda^2\eta_{critical}^3\left(1 - \frac{1}{\eta}\right) \tag{16-24}$$

16-3.2 Critical Dimensionless Radii and Intrapellet Damkohler Numbers

Once again, an explicit analytical expression for $\eta_{critical} = f(\Lambda)$ is not possible. If one implements a Newton–Raphson root-finding method to solve equation (16-24) when $\eta = \eta_{critical}$, then:

$$\Psi_A(\text{at } \eta = \eta_{critical}; \eta_{critical}, \Lambda) = 1 - \frac{1}{6}\Lambda^2(1-\eta_{critical}^2) - \frac{1}{3}\Lambda^2\eta_{critical}^3\left(1 - \frac{1}{\eta_{critical}}\right) = 0 \tag{16-25}$$

Table 16-2 illustrates the functional dependence of $\eta_{critical}$ on the intrapellet Damkohler number, Λ. Notice that the numerical results for $\eta_{critical} = f(\Lambda)$ are identical for spheres and cylinders when $\Lambda \geq 15$. For all catalyst shapes, $\eta_{critical} \to 1$ in the diffusion-limited regime when $\Lambda \to \infty$, and the mass transfer boundary layer thickness measured inward from the external surface of the catalyst becomes infinitesimally small. If equation (16-25), which defines $\eta_{critical}$, is solved for Λ^2 instead of $\eta_{critical}$, then:

$$\Lambda^2 = \frac{6}{1 - 3\eta_{critical}^2 + 2\eta_{critical}^3} \tag{16-26}$$

TABLE 16-2 Effect of the Intrapellet Damkohler Number on the Critical Dimensionless Radius for Radial Diffusion and Pseudo-Homogeneous Zeroth-Order Chemical Kinetics in Porous Catalysts with Spherical Symmetry

Λ	η_{critical}	Λ	η_{critical}
$\sqrt{6}$	0	10	0.85
3	0.39	15	0.90
4	0.58	25	0.94
5	0.68	50	0.97
6	0.74	100	0.986
7	0.78	150	0.991
8	0.81	200	0.993

This expression can be evaluated when $\eta_{\text{critical}} = 0$ and, by definition, one finds that $\Lambda_{\text{critical}} = \sqrt{6}$, which agrees with the first entry in Table 16-2 for spherically shaped catalytic pellets.

When the intrapellet Damkohler number is less than its critical value (i.e., $\sqrt{6}$), the critical dimensionless spatial coordinate η_{critical} is negative, and boundary condition 2b must be employed instead of 2a. Under these conditions, the dimensionless molar density profile for reactant A within the catalytic pores is adopted from equation (16-24) by setting η_{critical} to zero. Hence,

$$\Psi_A(\eta; \Lambda) = 1 - \tfrac{1}{6}\Lambda^2(1 - \eta^2) \qquad \text{for } \Lambda \leq \Lambda_{\text{critical}} = \sqrt{6} \tag{16-27}$$

Notice that the molar density of reactant A does not decrease to zero at the center of the sphere, where $\eta = 0$, when the intrapellet Damkohler number is less than its critical value. In fact,

$$\Psi_A(\eta = 0; \Lambda) = 1 - \tfrac{1}{6}\Lambda^2 > 0 \qquad \text{when } \Lambda < \sqrt{6} \tag{16-28}$$

16-4 REDEFINING THE INTRAPELLET DAMKOHLER NUMBER SO THAT ITS CRITICAL VALUE MIGHT BE THE SAME FOR ALL PELLET GEOMETRIES

This is an interesting challange from the standpoint of developing geometry-insensitive universal correlations for all catalyst shapes. As illustrated above, the critical value of the intrapellet Damkohler number is

1. $\Lambda^2_{\text{critical}} = 2$ for catalysts with rectangular symmetry
2. $\Lambda^2_{\text{critical}} = 4$ for long cylindrical catalysts
3. $\Lambda^2_{\text{critical}} = 6$ for spherically shaped catalysts

When the characteristic length L is defined as follows:

1. One-half of the thickness of wafers, measured in the thinnest dimension
2. The radius of long cylinders
3. The radius of a spherical pellet

One common characteristic of these length scales is that the dimensionless spatial coordinate is identically zero at the plane, axis, or point of symmetry, and η reaches its maximum value of unity on the external surface of the catalyst. In terms of a universal correlation, a typical characteristic length scale for all catalyst shapes is $L = V_{\text{catalyst}}/S_{\text{external}}$, where V_{catalyst} is the volume of catalyst and S_{external} is the total external surface area. This definition of L reduces to:

1. One-half of the thickness of wafers, measured in the thinnest dimension
2. One-half of the radius of long cylinders
3. One-third of the radius of a spherical pellet

Detailed calculations of the characteristic length are provided in Chapter 20 for these three simple geometries together with any assumptions of negligible surface area, particularly for rectangles and long cylinders. The overall objective is to determine whether the critical intrapellet Damkohler number for zeroth-order chemical kinetics is insensitive to catalyst shape when the length scale in the definition of Λ^2 is $L = V_{\text{catalyst}}/S_{\text{external}}$. The strategy to test this hypothesis is summarized as follows:

1. Solve the dimensionless mass transfer equation (i.e., the mass balance for reactant A) with homogeneous one-dimensional diffusion and zeroth-order irreversible chemical reaction to obtain an expression for Ψ_A, the dimensionless molar density of reactant A.
2. Use split boundary conditions, $(d\Psi_A/d\eta) = 0$ at $\eta = \eta_{\text{critical}}$ and $\Psi_A = 1$ on the external surface of the catalyst to calculate the integration constants in terms of Λ^2 and η_{critical}. On the external surface, the dimensionless spatial coordinate η has a value of 1 for wafers, 2 for long cylinders, and 3 for spheres.
3. Use the final expression for the dimensionless molar density of reactant A and let $\Psi_A = 0$ when $\eta = \eta_{\text{critical}}$. One obtains a nonlinear equation for η_{critical} in terms of Λ.
4. Calculate the intrapellet Damkohler number when $\eta_{\text{critical}} = 0$, which corresponds to the largest value of Λ that is consistent with the presence of reactant A throughout the catalyst. This is the definition of the critical intrapellet Damkohler number, $\Lambda_{\text{critical}}$. At higher values of Λ, reactant A

does not exist within the central core of the catalyst and the effectiveness factor decreases below its value of unity because the central core is not utilized.

A summary of the final results follows. When $L = V_{\text{catalyst}}/S_{\text{external}}$, critical values of the intrapellet Damkohler number are as follows:

1. $\Lambda^2_{\text{critical}} = 2$ for wafers.
2. $\Lambda^2_{\text{critical}} = 1$ for long cylinders.
3. $\Lambda^2_{\text{critical}} = \frac{2}{3}$ for spheres.

Hence, it is not possible to redefine the characteristic length such that the critical value of the intrapellet Damkohler number is the same for all catalyst geometries when the kinetics can be described by a zeroth-order rate law. However, if the characteristic length scale is chosen to be $V_{\text{catalyst}}/S_{\text{external}}$, then the effectiveness factor is approximately Λ^{-1} for any catalyst shape and rate law in the diffusion-limited regime ($\Lambda \to \infty$). This claim is based on the fact that reactants don't penetrate very deeply into the catalytic pores at large intrapellet Damkohler numbers and the mass transfer/chemical reaction problem is well described by a boundary layer solution in a very thin region near the external surface. Curvature is not important when reactants exist only in a thin shell near $\eta = 1$, and consequently, a locally flat description of the problem is appropriate for any geometry. These comments apply equally well to other types of kinetic rate laws.

PROBLEMS

16-1. What is the critical value of the intrapellet Damkohler number for one-dimensional diffusion and zeroth-order irreversible chemical reaction in catalytic pellets with spherical symmetry? The radius of the sphere is used as the characteristic length in the definition of the Damkohler number.

16-2. Draw the dimensionless molar density profile of reactant A within a porous wafer catalyst for the following values of the intrapellet Damkohler number. The reaction kinetics are zeroth-order and the characteristic length L is one-half of the wafer thickness, measured in the thinnest dimension. Put all five curves on the same set of axes and be as quantitative as possible on both axes. Dimensionless molar density Ψ_A is on the vertical axis and dimensional spatial coordinate η is on the horizontal axis.

(a) $\Lambda^2_{\text{A, intrapellet}} = 1$.

(b) $\Lambda^2_{\text{A, intrapellet}} = 2$.

(c) $\Lambda^2_{\text{A, intrapellet}} = 9.$

(d) $\Lambda^2_{\text{A, intrapellet}} = 25.$

(e) $\Lambda^2_{\text{A, intrapellet}} = 100.$

Answer: See Figure 16-1.

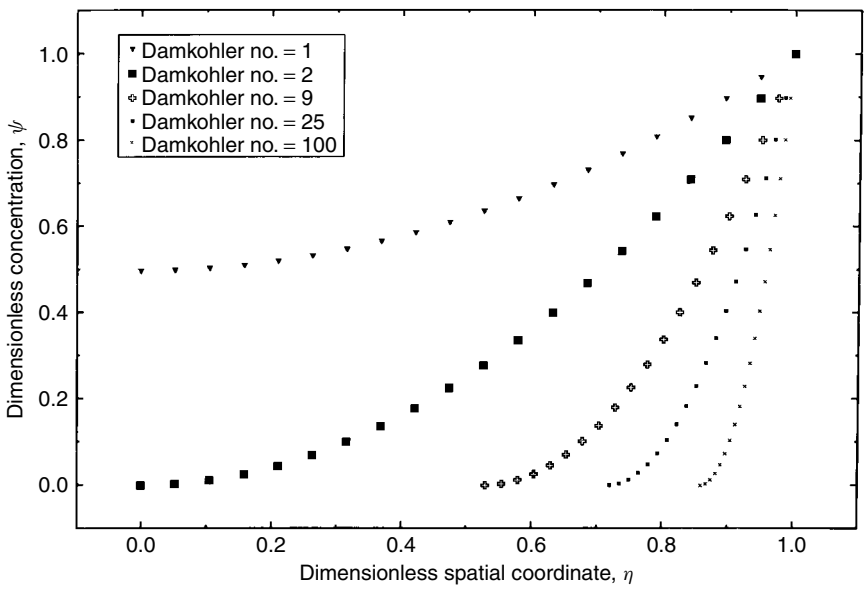

Figure 16-1 Effect of the intrapellet Damkohler number on dimensionless reactant concentration profiles for one-dimensional diffusion and pseudo-homogeneous zeroth-order chemical kinetics in porous catalyst with rectangular symmetry.

Transport Phenomena for Chemical Reactor Design. Laurence A. Belfiore
Copyright © 2003 John Wiley & Sons, Inc.
ISBN: 0-471-20275-4

17

COMPLETE ANALYTICAL SOLUTIONS FOR DIFFUSION AND FIRST-ORDER CHEMICAL REACTIONS IN ISOTHERMAL CATALYTIC PELLETS

17-1 CATALYTIC PELLETS WITH RECTANGULAR SYMMETRY

When the chemical kinetics are first-order and irreversible, the dimensionless reaction rate is

$$\mathfrak{R}^* = \frac{S_m \rho_{\text{app}} \mathfrak{R}_{\text{HW}}}{k_1 C_{\text{A, surface}}} = \Psi_{\text{A}} \tag{17-1}$$

where $S_m \rho_{\text{app}} \mathfrak{R}_{\text{HW}} = k_1 C_{\text{A}}$, and $\Psi_{\text{A}} = C_{\text{A}}/C_{\text{A, surface}}$ is the dimensionless molar density of reactant A. The mass balance with one-dimensional diffusion and chemical reaction in dimensionless form is

$$\frac{d^2 \Psi_{\text{A}}}{d\eta^2} = \Lambda^2 \mathfrak{R}^* = \Lambda^2 \Psi_{\text{A}} \tag{17-2}$$

subject to the following boundary conditions:

$$\Psi_{\text{A}} = 1 \text{ at } \eta = 1 \qquad \text{on the external surface of the catalyst} \tag{17-3a}$$

$$\frac{d\Psi_{\text{A}}}{d\eta} = 0 \text{ at } \eta = 0 \qquad \text{via symmetry at the center of the catalyst} \tag{17-3b}$$

It is not necessary to introduce a critical spatial coordinate because the rate of disappearance of reactant A is extremely small when its molar density approaches zero in the central core of the catalyst at large values of the intrapellet Damkohler number. One-dimensional diffusion and first-order irreversible chemical reaction in rectangular coordinates is described mathematically by a frequently occurring

linear second-order ordinary differential equation with constant coefficients. The complete solution is written in terms of exponential functions:

$$\Psi_A \approx \exp(\zeta \eta) \tag{17-4}$$

When this trial function is substituted into

$$\frac{d^2\Psi_A}{d\eta^2} = \Lambda^2 \Psi_A \tag{17-5}$$

ζ is obtained from the solution of the characteristic equation:

$$\zeta^2 - \Lambda^2 = 0 \tag{17-6}$$

Hence, $\zeta = \pm\Lambda$ and the general solution to the mass balance is given by a linear superposition of both trial functions which correspond to both roots of the characteristic equation:

$$\Psi_A = \alpha \exp(\zeta \eta) + \beta \exp(-\zeta \eta) \tag{17-7}$$

When the roots of the characteristic equation are real, the molar density profile can be written in terms of hyperbolic sines and cosines. Imaginary roots of the characteristic equation lead to trigonometric sines and cosines. Hence,

$$\Psi_A(\eta; \Lambda) = A \cosh \Lambda\eta + B \sinh \Lambda\eta \tag{17-8}$$

where the integration constants, A and B, are determined from the boundary conditions. The symmetry condition at $\eta = 0$ is established if $B = 0$ because the hyperbolic sine is an odd function and the hyperbolic cosine is an even function. In other words, symmetry requires that Ψ_A must be an even function of η. This is equivalent to calculating the concentration gradient from equation (17-8), which must vanish at the center of the catalyst:

$$\frac{d\Psi_A}{d\eta} = A\Lambda \sinh \Lambda\eta + B\Lambda \cosh \Lambda\eta \tag{17-9}$$

$$\left(\frac{d\Psi_A}{d\eta}\right)_{\eta=0} = B\Lambda = 0 \tag{17-10}$$

The boundary condition at the external surface of the catalyst (i.e., $\Psi_A = 1$ at $\eta = 1$) allows one to determine the other integration constant:

$$1 = A \cosh \Lambda \tag{17-11}$$

Hence, the complete solution for the molar density profile within the catalyst is

$$\Psi_A(\eta; \Lambda) = \frac{\cosh \Lambda\eta}{\cosh \Lambda} \tag{17-12}$$

which is normalized and approaches unity on the external surface (i.e., $\eta = 1$) of these porous wafer catalysts.

17-2 LONG, CYLINDRICALLY SHAPED CATALYSTS

Solution of the mass transfer equation in cylindrical coordinates is not as simple as the procedure described above in rectangular coordinates. Radial diffusion and first-order irreversible chemical kinetics in long cylinders produce the following linear second-order ordinary differential equation with variable coefficients:

$$\frac{d}{d\eta}\left(\eta\frac{d\Psi_A}{d\eta}\right) - \Lambda^2\eta\Psi_A = 0 \tag{17-13}$$

The method of attack is to postulate an infinite series solution for Ψ_A in terms of η. When the coefficients of this polynomial solution are calculated from the original differential equation and the two boundary conditions, the classic result is

$$\Psi_A(\eta;\Lambda) = \frac{I_0(\Lambda\eta)}{I_0(\Lambda)} \tag{17-14}$$

where I_0 is the modified or hyperbolic zeroth-order Bessel function of the first kind. An in-depth discussion of Bessel functions can be found in Wylie (1975, pp. 394–412) and Abramowitz and Stegun (1972, pp. 355–494). Actually, the mass transfer equation with radial diffusion and first-order chemical kinetics in cylindrical coordinates is a subset of the following generalized form of second-order ordinary differential equations which have Bessel function solutions:

$$\frac{d}{d\eta}\left(\eta^r\frac{d\Psi_A}{d\eta}\right) + (a\eta^s + b\eta^{r-2})\Psi_A = 0 \tag{17-15}$$

For the particular problem under consideration, described by equation (17-13),

$$r = 1 \qquad s = 1 \qquad a = -\Lambda^2 < 0 \qquad b = 0 \tag{17-16}$$

When the generalized ODE is compared with the mass transfer equation, the following conditions must be satisfied before the basic information for $\Psi_A(\eta)$ can be written in terms of Bessel functions:

$$a \neq 0 \qquad (1-r)^2 \geq 4b \tag{17-17}$$

and

$$b = 0 \quad \text{or} \quad r - 2 < s \tag{17-18}$$

All of these conditions are satisfied. Furthermore, the parameter a governs whether the solution is given by:

1. Bessel functions of the first kind J_ν and the second kind Y_ν when $a > 0$
2. Modified Bessel functions of the first kind I_ν and the second kind K_ν when $a < 0$

Since $a = -\Lambda^2 < 0$, the general solution is

$$\Psi_A(\eta;\Lambda) = \eta^\alpha[C_1 I_\nu(\lambda\eta^\gamma) + C_2 K_\nu(\lambda\eta^\gamma)] \tag{17-19}$$

The parameters α, γ, λ, and ν are defined by (see Wylie, 1975, p. 409)

$$\begin{aligned} \alpha &= \frac{1-r}{2} = 0 \\ \gamma &= \frac{2-r+s}{2} = 1 \\ \lambda &= \frac{2\sqrt{|a|}}{2-r+s} = \Lambda \end{aligned} \tag{17-20}$$

and the order of the Bessel function is

$$\nu = \frac{\sqrt{(1-r)^2 - 4b}}{2-r+s} = 0 \tag{17-21}$$

Hence, the basic information for reactant molar density in long cylindrical pellets is

$$\Psi_A(\eta;\Lambda) = C_1 I_0(\Lambda\eta) + C_2 K_0(\Lambda\eta) \tag{17-22}$$

The modified zeroth-order Bessel function of the second kind approaches infinity in the limit of a zero argument $\lim_{\eta\to 0}(K_0) \to \infty$, which corresponds to the symmetry axis of the cylinder. Hence, one sets the integration constant C_2 to zero and the boundary condition on the external surface of the catalyst is used to calculate $C_1 = 1/I_0(\Lambda)$. The final solution for the basic information is given by equation (17-14).

17-3 SPHERICAL PELLETS

This is a classic chemical engineering problem in a rather difficult coordinate system. The basic information for $\Psi_A(\eta)$ is obtained by solving the one-dimensional mass transfer equation with radial diffusion and simple first-order kinetics in the following form:

$$\frac{1}{\eta^2}\frac{d}{d\eta}\left(\eta^2\frac{d\Psi_A}{d\eta}\right) = \Lambda^2\Psi_A \tag{17-23}$$

From a mathematical viewpoint, the factors of η^2 on the left-hand side of equation (17-23) are the result of calculating the Laplacian (i.e., $\nabla \cdot \nabla\Psi_A = \nabla^2\Psi_A$) via a

transformation from rectangular coordinates to spherical coordinates. In physical terms, the surface area normal to the radial direction, across which radial diffusional flux occurs, scales as the square of radial position. The mass transfer equation is a linear second-order ordinary differential equation with variable coefficients and one might consider a series solution, similar to the approach in cylindrical coordinates. This method of attack is discussed after the classic solution is presented. The radial term of the Laplacian operator in spherical coordinates (i.e., the left-hand side of equation 17-23) can be simplified greatly by introducing a canonical (i.e., conventional) transformation of the basic information from the dimensionless molar density $\Psi_A(\eta)$ to a new function $\Phi(\eta)$ defined by

$$\Psi_A(\eta) = \frac{\Phi(\eta)}{\eta} \tag{17-24}$$

Now, it is necessary to obtain expressions for:

1. $d\Psi_A/d\eta = (1/\eta)\, d\Phi/d\eta - \Phi/\eta^2$
2. $\eta^2 d\Psi_A/d\eta = \eta\, d\Phi/d\eta - \Phi$
3. $d(\eta^2\, d\Psi_A/d\eta)/d\eta = \eta\, d^2\Phi/d\eta^2 + d\Phi/d\eta - d\Phi/d\eta = \eta\, d^2\Phi/d\eta^2$

The mass transfer equation, given by (17-23), is rewritten in terms of the new function $\Phi(\eta)$. Basic information is obtained by solving the following frequently occurring linear second-order ordinary differential equation with constant coefficients:

$$\frac{d}{d\eta}\left(\eta^2 \frac{d\Psi_A}{d\eta}\right) = \eta \frac{d^2\Phi}{d\eta^2} = \Lambda^2\eta^2\Psi_A = \Lambda^2\eta\Phi \tag{17-25}$$

$$\frac{d^2\Phi}{d\eta^2} = \Lambda^2\Phi \tag{17-26}$$

The roots of the characteristic equation are real because $\Lambda^2 > 0$. Hence, the solution to (17-26) is written as a linear combination of hyperbolic sines and cosines:

$$\Phi(\eta;\Lambda) = A \sinh \Lambda\eta + B \cosh \Lambda\eta \tag{17-27}$$

The dimensionless molar density profile is given by

$$\Psi_A(\eta;\Lambda) = \frac{\Phi}{\eta} = \frac{A}{\eta}\sinh \Lambda\eta + \frac{B}{\eta}\cosh \Lambda\eta \tag{17-28}$$

Two boundary conditions are required to calculate the integration constants, A and B:

$$\left(\frac{d\Psi_A}{d\eta}\right)_{\eta=0} = 0 \qquad \text{at the symmetry point in the center of the catalyst.} \tag{17-29a}$$

$$\Psi_A = 1 \text{ at } \eta = 1 \qquad \text{on the external surface of the pellet.} \tag{17-29b}$$

The first boundary condition is equivalent to a finite value of Ψ_A at the symmetry point in spherical coordinates. This condition was invoked in Section 17.2 along the symmetry axis of long cylindrical catalysts to eliminate the modified zeroth-order Bessel function of the second kind, $K_0(\eta = 0)$, from the general solution given by equation (17-22). When the symmetry condition at the center of a spherical pellet is used to evaluate the integration constants, one finds that $B = 0$ in equation (17-28) because:

1. $\lim_{\eta \to 0}(\cosh \Lambda\eta)/\eta \to \infty$.
2. $\lim_{\eta \to 0}(\sinh \Lambda\eta)/\eta = \Lambda$.
3. The hyperbolic cosine is an even function and the hyperbolic sine is odd, but $(\cosh \Lambda\eta)/\eta$ is odd and $(\sinh \Lambda\eta)/\eta$ is even.

Obviously, an even function is required to satisfy the symmetry condition at $\eta = 0$. Hence, B = 0. The integration constant A is calculated from the boundary condition on the external surface, given by (17-29*b*), and the final solution for the basic information is

$$\Psi_A(\eta; \Lambda) = \frac{\sinh \Lambda\eta}{\eta \sinh \Lambda} \tag{17-30}$$

It is rather straightforward to prove that the reactant concentration gradient vanishes at the center of the catalyst, which is consistent with the fact that Ψ_A is an even function of η. However, some insight is required to perform the correct mathematical steps and arrive at the desired result. The product rule is required to calculate the gradient from the basic information given by (17-30):

$$\frac{d\Psi_A}{d\eta} = \frac{1}{\sinh \Lambda}\left(\frac{\Lambda \cosh \Lambda\eta}{\eta} - \frac{\sinh \Lambda\eta}{\eta^2}\right) \tag{17-31}$$

As written, both terms in equation (17-31) for the gradient approach infinity at the center of the catalyst (i.e., $\eta = 0$). However, if one combines these two terms and applies l'Hôpital's rule, the symmetry condition is obvious. The common denominator is η^2. Hence,

$$\frac{d\Psi_A}{d\eta} = \frac{1}{\sinh \Lambda}\left(\frac{\Lambda\eta \cosh \Lambda\eta - \sinh \Lambda\eta}{\eta^2}\right) \tag{17-32}$$

In equation (17-32), the gradient is undefined at $\eta = 0$. One application of l'Hôpital's rule produces the following:

$$\left(\frac{d\Psi_A}{d\eta}\right)_{\eta=0} = \frac{1}{\sinh \Lambda} \frac{\lim_{\eta \to 0}(\Lambda \cosh \Lambda\eta + \Lambda^2\eta \sinh \Lambda\eta - \Lambda \cosh \Lambda\eta)}{\lim_{\eta \to 0}(2\eta)} \tag{17-33}$$

Upon simplification,

$$\left(\frac{d\Psi_A}{d\eta}\right)_{\eta=0} = \frac{1}{\sinh\Lambda}\frac{\lim_{\eta\to 0}(\Lambda^2\eta\sinh\Lambda\eta)}{\lim_{\eta\to 0}(2\eta)} \tag{17-34}$$

$$\left(\frac{d\Psi_A}{d\eta}\right)_{\eta=0} = \left\{\frac{\Lambda^2}{2\sinh\Lambda}\lim_{\eta\to 0}\sinh\Lambda\eta\right\} = 0 \tag{17-35}$$

17-3.1 Bessel Function Solutions

The expanded form of the one-dimensional mass transfer equation with radial diffusion and simple first-order kinetics in spherical coordinates, which is equivalent to (17-23),

$$\eta^2\frac{d^2\Psi_A}{d\eta^2} + 2\eta\frac{d\Psi_A}{d\eta} = \Lambda^2\eta^2\Psi_A \tag{17-36}$$

is a subset of generalized linear second-order ordinary differential equations with variable coefficients that have Bessel function solutions. The generalized form of these differential equations, provided below, looks somewhat different from equation (17-15). However, the final solutions are independent of the generalized ODE that is matched to the mass transfer equation. Bessel functions represent the solution to the following second-order ODE in spherical coordinates (see Wylie, 1975, p. 408):

$$\eta^2\frac{d^2\Psi_A}{d\eta^2} + \eta(a+2b\eta^p)\frac{d\Psi_A}{d\eta} + [c + e\eta^{2q} + b(a+p-1)\eta^p + b^2\eta^{2p}]\Psi_A = 0 \tag{17-37}$$

Correspondence with the mass transfer equation yields

$$a = 2 \qquad b = 0 \qquad c = 0 \qquad e = -\Lambda^2 \qquad q = 1 \qquad p \neq 0 \tag{17-38}$$

The requirements for a Bessel function solution are

$$(1-a)^2 \geq 4c \qquad e \neq 0 \qquad p \neq 0 \qquad q \neq 0 \tag{17-39}$$

Obviously, these requirements are satisfied by the mass transfer equation in spherical coordinates, given by (17-36). The parameter e governs whether the solution is given by:

1. Bessel functions of the first kind J_ν and the second kind Y_ν when $e > 0$
2. Modified Bessel functions of the first kind I_ν and the second kind K_ν when $e < 0$

Since $e = -\Lambda^2 < 0$, the general solution is

$$\Psi_A(\eta;\Lambda) = \eta^\alpha\exp(-\beta\eta^p)[C_1 I_\nu(\lambda\eta^q) + C_2 K_\nu(\lambda\eta^q)] \tag{17-40}$$

The parameters α, β, λ and ν are defined by (see Wylie, 1975, p. 408)

$$\begin{aligned} \alpha &= \frac{1-a}{2} = -0.5 \\ \beta &= \frac{b}{p} = 0 \\ \lambda &= \frac{\sqrt{|e|}}{q} = \Lambda \end{aligned} \tag{17-41}$$

and the order of the Bessel function is

$$\nu = \frac{\sqrt{(1-a)^2 - 4c}}{2q} = 0.5 \tag{17-42}$$

Hence, the basic information for the molar density of reactant A in spherical pellets is

$$\Psi_A(\eta;\Lambda) = \frac{C_1 I_{1/2}(\Lambda\eta)}{\sqrt{\eta}} + \frac{C_2 K_{1/2}(\Lambda\eta)}{\sqrt{\eta}} = \frac{\sinh \Lambda\eta}{\eta \sinh \Lambda} \tag{17-43}$$

PROBLEMS

17-1. Two-dimensional diffusion occurs axially and radially in cylindrically shaped porous catalysts when the length-to-diameter ratio is 2. Reactant A is consumed on the interior catalytic surface by a Langmuir–Hinshelwood mechanism that is described by a Hougen–Watson kinetic model, similar to the one illustrated by equation (15-26). This rate law is linearized via equation (15-30) and the corresponding simulation presented in Figure 15-1. Describe the nature of the differential equation (i.e., the mass transfer model) that must be solved to calculate the reactant molar density profile inside the catalyst.

(a) Is the mass transfer model a partial differential equation (PDE) or an ordinary differential equation (ODE)?

(b) Is the mass transfer model described by a linear or nonlinear differential equation?

(c) Is the mass transfer model a first- or second-order differential equation?

(d) Does the mass transfer model contain constant coefficients or variable coefficients?

(e) Which Bessel functions appear in the final expression for the molar density of reactant A?

(1) Bessel functions of the first kind J_ν.

(2) Bessel functions of the second kind Y_ν.

(3) Modified Bessel functions of the first kind I_ν.

(4) Modified Bessel functions of the second kind K_ν.

17-2. What is the analytical expression for the effectiveness factor vs. the intrapellet Damkohler number that corresponds to one-dimensional diffusion and first-order irreversible chemical reaction in catalytic pellets with cylindrical symmetry? The radius of the cylinder is used as the characteristic length in the definition of the intrapellet Damkohler number.

Answer: See equation (20-54) and Figure 20-1.

Transport Phenomena for Chemical Reactor Design. Laurence A. Belfiore
Copyright © 2003 John Wiley & Sons, Inc.
ISBN: 0-471-20275-4

18

NUMERICAL SOLUTIONS FOR DIFFUSION AND *n*th-ORDER CHEMICAL REACTIONS IN ISOTHERMAL CATALYTIC PELLETS

18-1 KINETIC RATE LAW AND DIFFUSIONAL FLUX

When the chemical kinetics are *n*th-order and irreversible in terms of the molar density of reactant A only, the dimensionless reaction rate is

$$\mathfrak{R}^* = \frac{S_m \rho_{\text{app}} \mathfrak{R}_{\text{HW}}}{k_n (C_{\text{A, surface}})^n} = (\Psi_{\text{A}})^n \tag{18-1}$$

where $S_m \rho_{\text{app}} \mathfrak{R}_{\text{HW}} = k_n (C_{\text{A}})^n$, and $\Psi_{\text{A}} = C_{\text{A}} / C_{\text{A, surface}}$ is the dimensionless molar density of reactant A. The simplified homogeneous mass transfer model for diffusion and one chemical reaction within the internal pores of an isolated catalytic pellet is written in dimensionless form for reactant A as

$$\nabla^2 \Psi_{\text{A}} + \upsilon_{\text{A}} \Lambda_{\text{A}}^2 \mathfrak{R}^* = 0 \tag{18-2}$$

where υ_{A} is the stoichiometric coefficient and Λ_{A}^2 the intrapellet Damkohler number for reactant A, which is defined by

$$\Lambda_{\text{A}}^2 = \frac{k_n L^2 (C_{\text{A, surface}})^{n-1}}{\mathfrak{D}_{\text{A, effective}}} \tag{18-3}$$

The characteristic molar density of reactant A is calculated in the vicinity of the external surface of the catalyst, and k_n is an *n*th-order kinetic rate constant on a volumetric basis when molar densities are used in the rate expression. The units of k_n are (volume/mole)$^{n-1}$/time. One-dimensional diffusion is written in three

important coordinate systems via the Laplacian of molar density, as follows:

$$\nabla^2\Psi_A = \begin{cases} \dfrac{d^2\Psi_A}{d\eta^2} & \text{for catalysts with rectangular symmetry} \\ \dfrac{1}{\eta}\dfrac{d}{d\eta}\left(\eta\dfrac{d\Psi_A}{d\eta}\right) & \text{for long cylindrical catalysts} \\ \dfrac{1}{\eta^2}\dfrac{d}{d\eta}\left(\eta^2\dfrac{d\Psi_A}{d\eta}\right) & \text{for catalysts with spherical symmetry} \end{cases} \tag{18-4}$$

The dimensionless spatial coordinate η is measured in the thinnest dimension of rectangular catalysts. For cylindrical and spherical catalysts, η is measured in the radial direction. The characteristic length L required to make the spatial coordinate dimensionless [i.e., $\eta = \{\text{spatial coordinate}\}/L$] is

1. One-half the thickness of catalysts with rectangular symmetry, measured in the thinnest dimension,
2. The radius of long cylindrical catalysts, or
3. The radius of spherical catalysts

18-2 MASS TRANSFER EQUATION IN THREE COORDINATE SYSTEMS

The dimensionless mass balance with one-dimensional diffusion and *n*th-order irreversible chemical reaction is presented here in three important coordinate systems:

$$\text{Rectangular (i.e., wafers):} \qquad \frac{d^2\Psi_A}{d\eta^2} = \Lambda_A^2(\Psi_A)^n \tag{18-5}$$

$$\text{Long cylinders:} \qquad \frac{1}{\eta}\frac{d}{d\eta}\left(\eta\frac{d\Psi_A}{d\eta}\right) = \Lambda_A^2(\Psi_A)^n \tag{18-6}$$

$$\text{Spherical pellets:} \qquad \frac{1}{\eta^2}\frac{d}{d\eta}\left(\eta^2\frac{d\Psi_A}{d\eta}\right) = \Lambda_A^2(\Psi_A)^n \tag{18-7}$$

subject to the following boundary conditions:

$$\Psi_A = 1 \qquad \text{at } \eta = 1 \text{ on the external surface of the catalyst} \tag{18-8a}$$

$$\frac{d\Psi_A}{d\eta} = 0 \qquad \text{at } \eta = 0 \text{ via symmetry at the center of the catalyst} \tag{18-8b}$$

It is not necessary to introduce a critical spatial coordinate below which the molar density of reactant A vanishes. For *n*th-order irreversible kinetics (i.e., $n > 0$),

the rate of disappearance of reactant A is extremely small when its molar density approaches zero in the central core of the catalyst at large values of the intrapellet Damkohler number.

18-2.1 Numerical Integration of the Mass Transfer Equation with Diffusion and Reaction

The mass balance given by (18-5), (18-6), and (18-7) corresponds to an ordinary differential equation that is second-order due to diffusion and nonlinear when $n \neq 0, 1$ due to the rate of depletion of reactant A via chemical reaction. Numerical integration is required to generate basic information for $\Psi_A(\eta; \Lambda)$, except when $n = 0, 1$. Second-order ODEs are solved numerically by reducing them to a set of two coupled first-order ODEs, which require two boundary conditions for a unique solution. The procedure is illustrated for porous wafers. If the dimensionless gradient of molar density is defined by $d\Psi_A/d\eta = \Omega$, then

$$\frac{d^2\Psi_A}{d\eta^2} = \frac{d\Omega}{d\eta} = \Lambda_A^2(\Psi_A)^n \tag{18-9}$$

These two first-order ODEs for Ψ_A and Ω must be solved simultaneously. The fourth-order Runge–Kutta–Gill numerical integration scheme can be implemented if both boundary conditions (i.e., one for Ψ_A and one for Ω) are known at the same value of the independent variable, either at the center of the catalyst or on its external surface. Notice that the boundary conditions are split because the gradient vanishes by symmetry at the center, and the molar density is known by definition at the external surface. In other words, $\Omega = 0$ at $\eta = 0$, and $\Psi_A = 1$ at $\eta = 1$. These conditions must be satisfied, but they are not sufficient to initiate the numerical algorithm. The two coupled first-order ODEs are solved using trial and error by guessing the molar density of reactant A at the center of the catalyst and accepting the numerical solution when Ψ_A is sufficiently close to 1 at the external surface. Hence, the boundary conditions are $\Omega = 0$ and $\Psi_A =$ guess at $\eta = 0$ for each catalyst geometry.

18-2.2 Effect of Curvature for Cylinders and Spheres

Since

$$\frac{1}{\eta^a}\frac{d}{d\eta}\left(\eta^a \frac{d\Psi_A}{d\eta}\right) = \frac{d^2\Psi_A}{d\eta^2} + \frac{a}{\eta}\frac{d\Psi_A}{d\eta} \tag{18-10}$$

the two coupled first-order ODEs for long cylindrical catalysts (i.e., $a = 1$) are

$$\begin{aligned} \frac{d\Psi_A}{d\eta} &= \Omega \\ \frac{d\Omega}{d\eta} &= \frac{-\Omega}{\eta} + \Lambda_A^2(\Psi_A)^n \end{aligned} \tag{18-11}$$

For spherical catalytic pellets where $a = 2$, the two coupled first-order ODEs are

$$\begin{aligned} \frac{d\Psi_A}{d\eta} &= \Omega \\ \frac{d\Omega}{d\eta} &= \frac{-2\Omega}{\eta} + \Lambda_A^2(\Psi_A)^n \end{aligned} \tag{18-12}$$

18-2.3 Numerical "Nightmare" at the Center of the Catalyst

When the external surface of the catalyst conforms to cylindrical or spherical symmetry, it is not possible to initiate the numerical integration algorithm at the center of the pellet where $\eta = 0$ because the slope of Ω with respect to η is undefined. The singularity at $\eta = 0$ is avoided by starting the integration at $\eta = \varepsilon \approx 10^{-6}$. Hence, the boundary conditions are modified slightly: $\Omega \approx \varepsilon$ and $\Psi_A =$ guess at $\eta = \varepsilon$. One integrates numerically from $\eta = \varepsilon$ to $\eta = 1$, and the correct guess for dimensionless molar density near the center of the pellet is based on the convergence criterion at the external surface. It is not obvious whether to let the dimensionless reactant concentration gradient with respect to η approach zero or ε, when $\eta = \varepsilon$. For example, consider first-order irreversible chemical reactions in spherical catalysts, where the quantity of interest in the mass transfer equation is $-2\Omega/\eta$ at the center of the pellet (i.e., $\eta = 0$). Since analytical solutions are available when the kinetics are first-order and irreversible, (1) begins with the molar density profile given by equation (17-30):

$$\Psi_A(\eta; \Lambda_A) = \frac{\sinh \Lambda_A \eta}{\eta \sinh \Lambda_A} \tag{18-13}$$

(2) calculates the reactant concentration gradient and combines terms:

$$\frac{d\Psi_A}{d\eta} = \frac{\Lambda_A \eta \cosh \Lambda_A \eta - \sinh \Lambda_A \eta}{\eta^2 \sinh \Lambda_A} \tag{18-14}$$

(3) multiplies the previous result by $2/\eta$:

$$\frac{2}{\eta}\frac{d\Psi_A}{d\eta} = \frac{2(\Lambda_A \eta \cosh \Lambda_A \eta - \sinh \Lambda_A \eta)}{\eta^3 \sinh \Lambda_A} \tag{18-15}$$

and (4) evaluates the limit of (18-15) via three applications of l'Hôpital's rule. The final result is

$$\lim_{\eta \to 0} \left(\frac{2}{\eta}\frac{d\Psi_A}{d\eta} \right) = \frac{2\Lambda_A^3}{3 \sinh \Lambda_A} \tag{18-16}$$

Hence, at the center of spherical catalytic pellets, the first term on the right side of the mass transfer equation with diffusion and chemical reaction depends on the intrapellet Damkohler number and adopts a value between zero and $-\frac{9}{5}$ when the

kinetics are first-order and irreversible. The actual choice of $-2\Omega/\eta$ at $\eta = 0$ or $\eta = \varepsilon$ does not have a significant effect on the reactant molar density profile, the concentration gradient at the external surface of the catalyst, or the effectiveness factor. When convergence is achieved at $\eta = 1$, the effectiveness factor E is calculated in terms of the diffusional mass flux of reactant A into the catalytic pellet across its external surface. Hence,

$$E = \frac{\alpha\Omega(\eta = 1)}{\Lambda_A^2} \tag{18-17}$$

where $\alpha = 1$, 2, or 3 for wafers, long cylinders, or spheres, respectively.

18-3 NUMERICAL RESULTS FOR SECOND-ORDER IRREVERSIBLE CHEMICAL KINETICS

Reactant concentrations and effectiveness factors are calculated for diffusion and second-order kinetics in isothermal catalytic pellets via the methodology described above. In each case, convergence is achieved when the dimensionless molar density of reactant A at the external surface is $1 \pm \delta$, where δ is on the order of 10^{-5} or less.

1. *Catalysts with rectangular symmetry* (see Table 18-1). When the intrapellet Damkohler number is larger, (a) the molar density of reactant A at the center of the catalyst is smaller, (b) the concentration gradient at the external surface increases, and (c) the effectiveness factor decreases. These trends are universal.
2. *Long cylindrical catalysts* (see Table 18-1). Effectiveness factors in cylindrical pellets are larger than their counterparts in catalysts with rectangular symmetry, at the same value of the intrapellet Damkohler number (see additional comments below on the relative magnitude of E for catalysts of various geometries).
3. *Spherical catalysts* (see Table 18-1).

At the same value of the intrapellet Damkohler number (i.e., Λ_A^2), the following trend in effectiveness factors is universal for the three catalyst geometries discussed above:

$$E_{\text{spheres}} > E_{\text{long cylinders}} > E_{\text{wafers}} \tag{18-18}$$

when the characteristic length L in the definition of Λ_A^2 is provided in Section 18-1. However, if the characteristic length scale is chosen as $L = V_{\text{catalyst}}/S_{\text{external}}$, where V_{catalyst} and S_{external} are the volume and external surface area of one catalytic pellet, then the effectiveness factor trend given by equation (18-18) must be reversed (see Bird *et al.*, 2002, p. 566). In Section 18-4 we provide examples which illustrate how the definition of the characteristic length L affects the intrapellet Damkohler number and the solution of the mass transfer equation with diffusion and chemical reaction.

TABLE 18-1 Numerical Solution of the Mass Transfer Equation for One-Dimensional Diffusion and Second-Order Irreversible Chemical Kinetics in Porous Catalysts[a]

Λ_A^2	$\Psi_A(\eta = 0)$, guess	$\Psi_A(\eta = 1)$	$\Omega(\eta = 1)$	E
		Rectangular Symmetry		
0.25	0.89707	1.00001	0.22	0.87
0.50	0.82124	1.00001	0.39	0.77
1	0.71281	1.00001	0.65	0.65
2	0.58135	1.00001	1.04	0.52
4	0.443725	1.00001	1.56	0.39
8	0.316935	1.00001	2.27	0.28
16	0.21259	0.999995	3.25	0.20
		Cylindrical Symmetry		
0.10	0.976289	0.999999	0.049	0.98
0.25	0.943559	0.999999	0.12	0.94
0.50	0.89556	1.00001	0.22	0.90
1	0.816461	1.00001	0.41	0.82
2	0.702705	1.00001	0.72	0.72
4	0.563734	1.00001	1.18	0.59
8	0.41914	0.999997	1.87	0.47
10	0.374894	0.999997	2.14	0.43
16	0.289217	0.999993	2.83	0.35
20	0.252885	1.00001	3.22	0.32
50	0.136385	1.00001	5.36	0.21
100	0.080478	1.00001	7.75	0.16
		Spherical Symmetry		
0.10	0.983906	0.999999	0.033	0.99
0.25	0.961072	0.999998	0.081	0.97
0.50	0.92612	1.00001	0.16	0.94
1	0.86525	1.00001	0.30	0.89
2	0.768687	0.999999	0.54	0.82
4	0.63889	1.00001	0.95	0.71
8	0.490571	0.999998	1.58	0.59
10	0.442723	1.00001	1.84	0.55
16	0.3470695	0.999997	2.50	0.47
20	0.305389	0.999998	2.88	0.43
50	0.1676298	0.999999	4.99	0.30
100	0.0995791	0.999995	7.38	0.22

[a]Effectiveness factor is given vs. the intrapellet Damkohler number. Three significant figures are sufficient to guess Ψ_A at, or near, the center of the catalyst.

18-4 EQUIVALENT EXAMPLES WITH DIFFERENT CHARACTERISTIC LENGTH SCALES

Radial diffusion and first-order irreversible chemical reaction in spherical catalysts can be solved analytically or numerically for the effectiveness factor when the

characteristic length is given by $L = V_{\text{catalyst}}/S_{\text{external}} = R/3$. This definition of the characteristic length is useful for nonspherical catalysts that do not conform to any simple geometry. The formalism is illustrated below when the intrapellet Damkohler number (i.e., $\Lambda^2_{V/S}$) is 10, based on this definition of L which is three-fold smaller than the characteristic length for spheres given in Section 18-1. When $L = R/3$, $\Lambda_{V/S}$ is three-fold smaller than Λ_A defined by equation (18-3) with $L = R$. Hence, the analytical solution for the effectiveness factor is obtained by setting $\Lambda_A = 3\Lambda_{V/S}$ and adopting the result given by equation (20-57).

Analytical solution:

$$\Lambda^2_{V/S} = 10$$

$$E = \frac{1}{3\Lambda^2_{V/S}}\{3\Lambda_{V/S} \coth 3\Lambda_{V/S} - 1\} = 0.28$$

Numerical solution:

$$\frac{d\Psi_A}{d\eta} = \Omega$$

$$\frac{d\Omega}{d\eta} = \frac{-2\Omega}{\eta} + \Lambda^2_{V/S}\Psi_A$$

$$\Omega = 10^{-6} \text{ and } \Psi_A = 0.00156265 \text{ at } \eta = 10^{-6}$$

$$\Omega = 2.83 \text{ and } \Psi_A = 1 \text{ at } \eta = 3$$

$$E = \frac{\Omega(\eta = 3)}{\Lambda^2_{V/S}} = 0.28$$

Notice that the geometric factor α is unity in the effectiveness factor calculation given by equation (18-17) for all catalyst geometries when the characteristic length L is $V_{\text{catalyst}}/S_{\text{external}}$. Specifically for spheres, the dimensionless independent spatial variable η ranges from 10^{-6} near the center of the catalyst to 3 at the external surface.

If $L = R$ for spherical pellets, as defined in Section 18-1, then the intrapellet Damkohler number (i.e., Λ^2_A) is nine-fold larger than $\Lambda^2_{V/S}$, and the analytical and numerical solutions for radial diffusion and first-order irreversible chemical reaction proceed as follows. Now, the dimensionless independent spatial variable η ranges from 10^{-6} near the center of the catalyst to 1 at the external surface, and the geometric factor α is 3 for spheres.

Analytical solution:

$$\Lambda^2_A = 90$$

$$E = \frac{3}{\Lambda^2_A}\{\Lambda_A \coth \Lambda_A - 1\} = 0.28$$

Numerical solution:

$$\frac{d\Psi_A}{d\eta} = \Omega$$

$$\frac{d\Omega}{d\eta} = \frac{-2\Omega}{\eta} + \Lambda_A^2 \Psi_A$$

$$\Omega = 10^{-6} \text{ and } \Psi_A = 0.00149036 \text{ at } \eta = 10^{-6}$$

$$\Omega = 8.49 \text{ and } \Psi_A = 1 \text{ at } \eta = 1$$

$$E = \frac{3\Omega(\eta = 1)}{\Lambda_A^2} = 0.28$$

These two example problems are identical, even though the characteristic length differs by a factor of 3. The exact dimensionless molar density of reactant A at the center of the catalyst is obtained from the analytical solution, given by equation (17-30) or (18-13).

$$\Psi_A(\eta = 0) = \lim_{\eta \to 0} \left\{ \frac{\sinh \Lambda_A \eta}{\eta \sinh \Lambda_A} \right\}$$

One application of l'Hôpital's rule yields

$$\Psi_A(\eta = 0) = \frac{\Lambda_A}{\sinh \Lambda_A} = 0.00143904$$

when $\Lambda_A^2 = 90$. This exact result for $\Psi_A(\eta = 0)$ should be compared with the guesses for Ψ_A at $\eta = 10^{-6}$ that are required to initiate the numerical solution of two coupled ODEs for spherical pellets by avoiding the singularity at the center of the catalyst.

Transport Phenomena for Chemical Reactor Design. Laurence A. Belfiore
Copyright © 2003 John Wiley & Sons, Inc.
ISBN: 0-471-20275-4

19

NUMERICAL SOLUTIONS FOR DIFFUSION AND HOUGEN–WATSON CHEMICAL KINETICS IN ISOTHERMAL CATALYTIC PELLETS

In this chapter we present a pseudo-homogeneous model of diffusion and heterogeneous surface-catalyzed chemical reaction within the internal pores of catalytic pellets with rectangular symmetry.

19-1 DIMENSIONLESS KINETIC RATE LAW

The most important characteristic of this problem is that the Hougen–Watson kinetic model contains molar densities of more than one reactive species. A similar problem arises if $S_m \rho_{\text{app}} \mathfrak{R}_{\text{HW}} = k_2 C_{\text{A}} C_{\text{B}}$ because it is necessary to relate the molar densities of reactants A and B via stoichiometry and the mass balance with diffusion and chemical reaction. When adsorption terms appear in the denominator of the rate law, one must use stoichiometry and the mass balance to relate molar densities of reactants and products to the molar density of key reactant A. The actual form of the Hougen–Watson model depends on details of the Langmuir–Hinshelwood-type mechanism and the rate-limiting step. For example, consider the following mechanism:

1. The reaction scheme is $A_2 + B \rightarrow C + D$.
2. Diatomic A_2 undergoes dissociative adsorption.
3. Each of the other gases chemisorbs on a single active site within the internal pores of the catalytic pellet, and all the adsorption/desorption steps have equilibrated.
4. Triple-site chemical reaction on the catalytic surface is rate limiting.
5. The reaction is essentially irreversible.

The heterogeneous rate law with units of moles per area per time can be expressed in terms of partial pressures of each component as follows:

$$\mathfrak{R}_{\mathrm{HW}} = \frac{k_f K_{\mathrm{A}} K_{\mathrm{B}} p_{\mathrm{A}} p_{\mathrm{B}}}{\left(1 + \sqrt{K_{\mathrm{A}} p_{\mathrm{A}}} + K_{\mathrm{B}} p_{\mathrm{B}} + K_{\mathrm{C}} p_{\mathrm{C}} + K_{\mathrm{D}} p_{\mathrm{D}}\right)^3} \tag{19-1}$$

where K_i is an adsorption/desorption equilibrium constant for species i with units of inverse pressure and k_f is the forward kinetic rate constant with units of moles per area per time when the rate law is expressed in terms of fractional surface coverage of reactants A_2 and B. A pseudo-volumetric kinetic rate law is obtained via multiplication of $\mathfrak{R}_{\mathrm{HW}}$ by the internal surface area per mass of catalyst S_m and the apparent density of the porous pellet ρ_{app}. Furthermore, partial pressures in the rate law are replaced by gas-phase molar densities via the ideal gas law:

$$p_i = \left(\frac{N_i}{V_{\mathrm{total}}}\right) RT = C_i RT \tag{19-2}$$

If the dimensionless adsorption terms in the denominator of $\mathfrak{R}_{\mathrm{HW}}$ are not accounted for, then the reaction is irreversible and second-order. Hence, $n = 2$ and

$$\mathfrak{R}^* = \frac{S_m \rho_{\mathrm{app}} \mathfrak{R}_{\mathrm{HW}}}{k_2 (C_{\mathrm{A,\,surface}})^2} \tag{19-3}$$

where k_2 is a second-order kinetic rate constant with units of (volume/mole)/time when the rate law is expressed on a volumetric basis using molar densities. The overall objective here is to compare the effect of Hougen–Watson kinetics and simple nth-order kinetics on the dimensionless mass transfer correlation for isolated catalytic pellets. In this respect, one employs the same definition of the intrapellet Damkohler number for reactant A_2 that was used previously for simple nth-order kinetics, with $n = 2$. Hence,

$$\Lambda_{\mathrm{A}}^2 = \frac{k_2 (C_{\mathrm{A,\,surface}})^2}{\mathfrak{D}_{\mathrm{A,\,effective}} C_{\mathrm{A,\,surface}} / L^2} = \frac{k_2 L^2 C_{\mathrm{A,\,surface}}}{\mathfrak{D}_{\mathrm{A,\,effective}}} \tag{19-4}$$

The dimensionless kinetic rate law, which includes adsorption terms in the denominator, is expressed as

$$\mathfrak{R}^* = \frac{S_m \rho_{\mathrm{app}} k_f K_{\mathrm{A}} K_{\mathrm{B}} (RT)^2 C_{\mathrm{A}} C_{\mathrm{B}} / k_2 (C_{\mathrm{A,\,surface}})^2}{\{1 + \sqrt{K_A RT C_{\mathrm{A}}} + K_{\mathrm{B}} RT C_{\mathrm{B}} + K_{\mathrm{C}} RT C_{\mathrm{C}} + K_{\mathrm{D}} RT C_{\mathrm{D}}\}^3} \tag{19-5}$$

Notice that the rate law becomes dimensionless via division by $k_2 (C_{\mathrm{A,\,surface}})^2$, which is exactly the same as the dimensional scaling factor for irreversible second-order chemical reaction in the numerator of the intrapellet Damkohler

number. The dimensionless molar density of each species in the reactive gas mixture is $\Psi_i = C_i / C_{\text{A, surface}}$ and one must recognize that the forward rate constant k_2 for second-order kinetics with units of (volume/mole)/time is given by

$$k_2 = S_m \rho_{\text{app}} k_f K_{\text{A}} K_{\text{B}} (RT)^2 \tag{19-6}$$

In general, the kinetic rate constant k_n for nth-order kinetics with units of (volume/mole)$^{n-1}$/time is related to the heterogeneous forward rate constant k_f with units of moles per area per time, and details of the porous pellet as follows:

$$k_n = S_m \rho_{\text{app}} k_f K_{\text{A}} K_{\text{B}} K_{\text{C}} \cdots (RT)^n \tag{19-7}$$

where an adsorption/desorption equilibrium constant K_i is required for each reactant that occupies active sites on the interior catalytic surface. The final expression for the dimensionless kinetic rate law is

$$\mathfrak{R}^* = \frac{\Psi_{\text{A}} \Psi_{\text{B}}}{(1 + \sqrt{\theta_{\text{A}} \Psi_{\text{A}}} + \theta_{\text{B}} \Psi_{\text{B}} + \theta_{\text{C}} \Psi_{\text{C}} + \theta_{\text{D}} \Psi_{\text{D}})^3} \tag{19-8}$$

where the dimensionless adsorption/desorption equilibrium constant for species i is $\theta_i = K_i (RT) C_{\text{A, surface}}$.

19-2 MASS BALANCE FOR REACTANT A

The simplified homogeneous mass transfer model for diffusion and Langmuir–Hinshelwood chemical kinetics within the internal pores of an isolated catalytic pellet is written in dimensionless form for reactant A or A_2 (i.e., $\upsilon_{\text{A}} = -1$):

$$\nabla^2 \Psi_{\text{A}} + \upsilon_{\text{A}} \Lambda_{\text{A}}^2 \mathfrak{R}^* = 0 \tag{19-9}$$

One-dimensional diffusion is expressed in terms of the Laplacian of molar density in rectangular coordinates as

$$\nabla^2 \Psi_{\text{A}} = \frac{d^2 \Psi_{\text{A}}}{d\eta^2} \tag{19-10}$$

where the dimensionless spatial coordinate η is measured in the thinnest dimension, and the characteristic length L that appears in the intrapellet Damkohler number (see equation 19-4), and is required to make the spatial coordinate dimensionless [i.e., $\eta =$ (spatial coordinate)$/L$] is one-half the thickness of the pellet, measured in the thinnest dimension.

The basic information for molar density $\Psi_{\text{A}}(\eta)$ is obtained by solving the dimensionless mass balance which includes the appropriate Hougen–Watson model:

$$\frac{d^2 \Psi_{\text{A}}}{d\eta^2} = \frac{\Lambda_{\text{A}}^2 \Psi_{\text{A}} \Psi_{\text{B}}}{(1 + \sqrt{\theta_{\text{A}} \Psi_{\text{A}}} + \theta_{\text{B}} \Psi_{\text{B}} + \theta_{\text{C}} \Psi_{\text{C}} + \theta_{\text{D}} \Psi_{\text{D}})^3} \tag{19-11}$$

subject to the following boundary conditions:

$$\Psi_A = 1 \qquad \text{at } \eta = 1 \text{ on the external surface of the catalyst} \tag{19-12a}$$

$$\frac{d\Psi_A}{d\eta} = 0 \qquad \text{at } \eta = 0 \text{ via symmetry at the center of the catalyst} \tag{19-12b}$$

This second-order ODE for $\Psi_A(\eta)$ with split boundary conditions, given by equations (19-11) and (19-12), cannot be solved numerically until one invokes stoichiometry and the mass balance with diffusion and chemical reaction to relate the molar densities of all gas-phase species within the pores of the catalytic pellet to that of reactant A or A_2.

19-2.1 Stoichiometry and the Steady-State Mass Balance

The dimensionless scaling factor in the mass transfer equation for reactant A with diffusion and chemical reaction is written with subscript j for the jth chemical reaction in a multiple reaction sequence. Hence, Λ_j^2 corresponds to the Damkohler number for reaction j. The only distinguishing factor between all of these Damkohler numbers for multiple reactions is that the nth-order kinetic rate constant in the jth reaction (i.e., k_j) changes from one reaction to another. The characteristic length, the molar density of key-limiting reactant A on the external surface of the catalyst, and the effective diffusion coefficient of reactant A are the same in all the Damkohler numbers that appear in the dimensionless mass balance for reactant A. In other words,

$$\Lambda_j^2 = \frac{k_j L^2 (C_{A,\,\text{surface}})^{n-1}}{\mathfrak{D}_{A,\,\text{effective}}} \tag{19-13}$$

When there are j chemical reactions between i species in a mixture, it is possible to construct a Damkohler number for reaction j that is specific to component i. This is necessary because the effective pore diffusion coefficient within a catalytic pellet depends on molecular size. Hence, if reaction j is described by nth-order irreversible chemical kinetics, then the Damkohler number of component i in the reactive gas mixture is

$$\Lambda_{ij}^2 = \frac{k_j L^2 (C_{A,\,\text{surface}})^{n-1}}{\mathfrak{D}_{i,\,\text{effective}}} \tag{19-14}$$

Notice that the molar density of key-limiting reactant A on the external surface of the catalytic pellet is always used as the characteristic quantity to make the molar density of component i dimensionless in all the species mass balances. $\mathfrak{D}_{i,\,\text{effective}}$ is the effective intrapellet diffusion coefficient of species i. If there is only one chemical reaction, or one rate-limiting step in a multiple reaction sequence, that is characterized by nth-order irreversible kinetics, then the rate constant in the numerator of the Damkohler numbers is the same for each Λ_{ij}^2. Hence, k_j is written as k_n, which signifies that k_n has units of (volume/mole)$^{n-1}$/time for

pseudo-homogeneous kinetics. Now, the subscript on the Damkohler number identifies the particular species in the mixture:

$$\Lambda_i^2 = \frac{k_n L^2 (C_{\mathrm{A,\,surface}})^{n-1}}{\mathfrak{D}_{i,\,\mathrm{effective}}} \tag{19-15}$$

The simplified homogeneous mass transfer model for diffusion and one chemical reaction within the internal pores of an isolated catalytic pellet is written in dimensionless form for component i and includes stoichiometric coefficient υ_i to account for its rate of production (see equation 15-11):

$$\nabla^2 \Psi_i + \upsilon_i \Lambda_i^2 \mathfrak{R}^* = 0 \tag{19-16}$$

Previously, the mass balance was written for reactant A via equation (19-9), whose stoichiometric coefficient υ_{A} is -1. Equation (19-16) is rearranged such that all species-specific quantities are grouped together on the left-hand side of the following equation:

$$\frac{1}{\upsilon_i \Lambda_i^2} \nabla^2 \Psi_i = -\mathfrak{R}^* = \text{same for all components} \tag{19-17}$$

Hence, stoichiometry and the steady-state mass balance with diffusion and one chemical reaction allows one to relate diffusional fluxes as follows:

$$\frac{1}{\upsilon_i \Lambda_i^2} \nabla^2 \Psi_i = \frac{1}{\upsilon_{\mathrm{A}} \Lambda_{\mathrm{A}}^2} \nabla^2 \Psi_{\mathrm{A}} \tag{19-18}$$

Since the Laplacian of a scalar (i.e., dimensionless molar density) is equivalent to the divergence of the gradient of that scalar, (19-18) can be rewritten as

$$\nabla \cdot \frac{1}{\upsilon_i \Lambda_i^2} \nabla \Psi_i = \nabla \cdot \frac{1}{\upsilon_{\mathrm{A}} \Lambda_{\mathrm{A}}^2} \nabla \Psi_{\mathrm{A}} \tag{19-19}$$

when the intrapellet Damkohler numbers are not functions of spatial coordinates. This equation is integrated over an arbitrary gas-phase pore volume within the catalytic pellet:

$$\int_V \nabla \cdot \frac{1}{\upsilon_i \Lambda_i^2} \nabla \Psi_i \, dV = \int_V \nabla \cdot \frac{1}{\upsilon_{\mathrm{A}} \Lambda_{\mathrm{A}}^2} \nabla \Psi_{\mathrm{A}} \, dV \tag{19-20}$$

$$\int_V \nabla \cdot \left(\frac{1}{\upsilon_i \Lambda_i^2} \nabla \Psi_i - \frac{1}{\upsilon_{\mathrm{A}} \Lambda_{\mathrm{A}}^2} \nabla \Psi_{\mathrm{A}} \right) dV = 0 \tag{19-21}$$

Gauss's law is invoked to transform the previous volume integral into an integral over the surface that completely surrounds the chosen pore volume. If $\mathbf{n}$ is an outward-directed unit normal vector that defines the orientation of the surface which completely surrounds the chosen pore volume, then

$$\int_S \mathbf{n} \cdot \left(\frac{1}{\upsilon_i \Lambda_i^2} \nabla \Psi_i - \frac{1}{\upsilon_{\mathrm{A}} \Lambda_{\mathrm{A}}^2} \nabla \Psi_{\mathrm{A}} \right) dS = 0 \tag{19-22}$$

Since there are several choices for pore volume V and the surrounding surface S, and all choices lead to the fact that the integral expressions given by (19-22) must vanish, the integrand of (19-22) must also vanish. Hence,

$$\mathbf{n}\cdot\left(\frac{1}{\upsilon_i\Lambda_i^2}\nabla\Psi_i-\frac{1}{\upsilon_{\mathrm{A}}\Lambda_{\mathrm{A}}^2}\nabla\Psi_{\mathrm{A}}\right)=0 \tag{19-23}$$

If n is the generalized coordinate which increases in the direction of the unit normal vector $\mathbf{n}$, then

$$\mathbf{n}\cdot\nabla\Psi_i=\frac{\partial\Psi_i}{\partial n} \tag{19-24}$$

and

$$\frac{1}{\upsilon_i\Lambda_i^2}\frac{\partial\Psi_i}{\partial n}=\frac{1}{\upsilon_{\mathrm{A}}\Lambda_{\mathrm{A}}^2}\frac{\partial\Psi_{\mathrm{A}}}{\partial n} \tag{19-25}$$

This result is rather general and applies to three-dimensional diffusion within the catalytic pores as well as one-dimensional diffusion that is consistent with the homogeneous model of interest in this chapter. Integration of (19-25) from the external catalytic surface where $\Psi_i=\Psi_{is}$ and $\Psi_{\mathrm{A}}=1$ to an arbitrary position within the pores produces the following relation between dimensionless molar densities that is valid for any component, including reactant A:

$$\Psi_i=\Psi_{is}+\upsilon_i\frac{\Lambda_i^2}{\Lambda_{\mathrm{A}}^2}\,(1-\Psi_{\mathrm{A}}) \tag{19-26}$$

where the stoichiometric coefficient of reactant A is -1. This is the prediction from stoichiometry and the steady-state mass balance with generalized three-dimensional diffusion and one chemical reaction within a porous catalytic pellet of any geometry. It is applicable to one-dimensional diffusion and Langmuir–Hinshelwood kinetics in pellets with rectangular symmetry. Since the development is restricted to one chemical reaction, the numerator of each intrapellet Damkohler number is the same. The distinguishing feature of each Λ_i^2 is the effective intrapellet diffusion coefficient of component i in the denominator of equation (19-15). Hence,

$$\delta_i\equiv\frac{\Lambda_i^2}{\Lambda_{\mathrm{A}}^2}=\frac{\mathfrak{D}_{\mathrm{A,\,effective}}}{\mathfrak{D}_{i,\,\mathrm{effective}}} \tag{19-27}$$

and

$$\Psi_i=\Psi_{is}+\upsilon_i\frac{\mathfrak{D}_{\mathrm{A,\,effective}}}{\mathfrak{D}_{\mathrm{i,\,effective}}}(1-\Psi_{\mathrm{A}}) \tag{19-28}$$

It is important to choose component A as the reactant gas of highest molecular weight. Since the effective pore diffusion coefficient of component i is inversely proportional to the square root of its molecular weight, $\mathfrak{D}_{\mathrm{A,\,effective}}/\mathfrak{D}_{i,\,\mathrm{effective}}<1$

if reactant A is larger than component i. This choice of the key-limiting reactant is designed such that Ψ_i is positive for all other reactants, particularly when Ψ_A is very small. If this strategy produces negative molar densities near the center of the catalyst, then reactant A should be chosen such that the combination of Ψ_{is}, υ_i, and δ_i always yields positive molar densities throughout the catalyst.

19-2.2 Integration of the Mass Transfer Equation with Diffusion and Reaction

The mass balance given by equation (19-11) corresponds to an ordinary differential equation that is second-order due to diffusion and nonlinear due to the rate of depletion of reactant A via chemical reaction. Numerical integration is required to generate basic information for $\Psi_A(\eta; \Lambda_A)$. Second-order ODEs are solved numerically by reducing them to a set of two coupled first-order ODEs, which require two boundary conditions for a unique solution. If the dimensionless gradient of molar density is defined by $d\Psi_A/d\eta = \Omega$, then

$$\frac{d^2\Psi_A}{d\eta^2} = \frac{d\Omega}{d\eta} = \frac{\Lambda_A^2 \Psi_A \Psi_B}{\left(1 + \sqrt{\theta_A \Psi_A} + \theta_B \Psi_B + \theta_C \Psi_C + \theta_D \Psi_D\right)^3} \tag{19-29}$$

These two first-order ODEs for Ψ_A and Ω must be solved simultaneously, with assistance from equation (19-28) for components B, C, and D. The fourth-order Runge–Kutta–Gill numerical integration scheme can be implemented if both boundary conditions (i.e., one for Ψ_A and one for Ω) are known at the same value of the independent variable, either at the center of the catalyst or on its external surface. Notice that the boundary conditions given by (19-12) are split because the gradient vanishes by symmetry at the center, and the molar density is known by definition at the external surface. In other words, $\Omega = 0$ at $\eta = 0$, and $\Psi_A = 1$ at $\eta = 1$. These conditions must be satisfied, but they are not sufficient to initiate the numerical algorithm. The two coupled first-order ODEs are solved using trial and error by guessing the molar density of reactant A at the center of the catalyst and accepting the numerical solution when Ψ_A is sufficiently close to 1 at the external surface. Hence the boundary conditions are $\Omega = 0$ and $\Psi_A =$ guess at $\eta = 0$.

19-3 DIMENSIONLESS CORRELATION FOR THE EFFECTIVENESS FACTOR IN TERMS OF THE INTRAPELLET DAMKOHLER NUMBER

The ratio of reaction rates described below in (1) and (2), with units of moles per time, is defined as the *effectiveness factor:*

(1) The volume-averaged rate of consumption of reactant A in one isolated catalytic pellet, relative to
(2) The rate of consumption of reactant A evaluated using conditions on the external surface of the pellet.

In general, the volume-averaged rate of consumption of reactant A, specified by (1) above, is $\int_V -\upsilon_A \mathfrak{R}(\text{all } C_i)\, dV$ where integration is performed over the entire volume of the catalyst if reactant A exists everywhere throughout the internal pores. A modification of the integration limits on the dimensionless spatial coordinate η is required for zeroth-order kinetics when the intrapellet Damkohler number is larger than its critical value and the central core of the catalyst is void of reactants. The rate of consumption of reactant A based on external surface conditions, specified by (2) above, is $-\upsilon_A \mathfrak{R}(\text{all } C_{i,\,\text{surface}}) V_{\text{catalyst}}$, where V_{catalyst} represents the entire pellet volume. Hence, the general expression for the effectiveness factor is

$$E = \frac{\displaystyle\int_{V_{\text{catalyst}}} [-\upsilon_A \mathfrak{R}(\text{all } C_i)]\, dV}{-\upsilon_A \mathfrak{R}(\text{all } C_{i,\,\text{surface}}) V_{\text{catalyst}}} \tag{19-30}$$

when the kinetics are averaged throughout the volume of one pellet. An equivalent expression for the volume-averaged rate of consumption of reactant A is based on mass flux of reactant A into the pellet across the external surface. Under steady-state conditions, the mass transfer equation for component A with diffusion and one chemical reaction is

$$\mathfrak{D}_{A,\,\text{effective}} \nabla\cdot\nabla C_A + \upsilon_A \mathfrak{R} = \nabla\cdot(\mathfrak{D}_{A,\,\text{effective}} \nabla C_A) + \upsilon_A \mathfrak{R} = 0 \tag{19-31}$$

if $\mathfrak{D}_{A,\,\text{effective}}$ is independent of spatial coordinates. Integration over the entire volume of one catalytic pellet allows one to calculate the volume-averaged rate at which reactant A is consumed by chemical reaction on the interior catalytic surface:

$$\int_{V_{\text{catalyst}}} -\upsilon_A \mathfrak{R}\, dV = \int_{V_{\text{catalyst}}} \nabla\cdot(\mathfrak{D}_{A,\,\text{effective}} \nabla C_A)\, dV \tag{19-32}$$

In other words, if the microscopic mass balance for each component in the reactive mixture must be satisfied at every point within the catalyst, then a volumetric average of this mass balance is also satisfied. If $\mathbf{n}$ is an outward-directed unit normal vector on the external surface of the catalyst, then Gauss's law transforms the volume integral on the right side of (19-32) to an integral over the external catalytic surface:

$$\int_V -\upsilon_A \mathfrak{R}\, dV = \int_V \nabla\cdot(\mathfrak{D}_{A,\,\text{effective}} \nabla C_A)\, dV = \int_S \mathbf{n}\cdot(\mathfrak{D}_{A,\,\text{effective}} \nabla C_A)_{\text{at } S_{\text{external}}}\, dS \tag{19-33}$$

This relation states that the volume-averaged rate of consumption of reactant A via chemical reaction is equivalent to the surface-averaged rate of diffusion of A into the catalyst. Hence, the numerator of the effectiveness factor can be written as

$$\int_S \mathbf{n}\cdot(\mathfrak{D}_{A,\,\text{effective}} \nabla C_A)_{\text{at } S_{\text{external}}}\, dS = \int_S (-\mathbf{n})\cdot(-\mathfrak{D}_{A,\,\text{effective}} \nabla C_A)_{\text{at } S_{\text{external}}}\, dS \tag{19-34}$$

where the right side of this equation corresponds to the diffusional flux of reactant A, given by Fick's law, in the direction of the inward unit normal $-\mathbf{n}$ (i.e., into the pellet) from the external catalytic surface. The effectiveness factor in catalysts of arbitrary geometry and kinetic rate law is

$$E = \frac{\int_S \mathbf{n}\cdot(\mathfrak{D}_{\mathrm{A,\,effective}}\nabla C_{\mathrm{A}})_{\mathrm{at}\ S_{\mathrm{external}}}\, dS}{-\upsilon_{\mathrm{A}}\mathfrak{R}(\mathrm{all}\ C_{i,\,\mathrm{surface}})V_{\mathrm{catalyst}}} \tag{19-35}$$

which seems, at first glance, to be quite complex. However, mass transfer across the external surface is the method of choice to calculate the effectiveness factor when numerical techniques are required to integrate the mass balance with one-dimensional diffusion and chemical reaction. Support for this claim is based on the fact that the concentration gradient, ∇C_{A}, exhibits a nonzero component in only one coordinate direction (i.e., η) due to the one-dimensional nature of diffusional flux in the mass balance. In other words, the reactant molar density is only a function of one spatial coordinate because diffusional flux is assumed to be one-dimensional. This assumption reduces the partial differential mass balance to an ordinary differential equation. In terms of the following dimensionless variables,

$$\Psi_{\mathrm{A}} = \frac{C_{\mathrm{A}}}{C_{\mathrm{A,\,surface}}} \tag{19-36}$$

$$\eta = \frac{\left\{\begin{array}{c}\text{spatial coordinate measured in the}\\ \text{thinnest dimension of a porous wafer}\end{array}\right\}}{L} \tag{19-37}$$

the scalar (i.e., dot) product of the outward directed normal vector $\mathbf{n}$ in equation (19-35) with $\mathfrak{D}_{\mathrm{A,\,effective}}\ \nabla C_{\mathrm{A}}$ reduces to:

$$\mathbf{n}\cdot(\mathfrak{D}_{\mathrm{A,\,effective}}\nabla C_{\mathrm{A}})_{\mathrm{at}\ S_{\mathrm{external}}} = \frac{\mathfrak{D}_{\mathrm{A,\,effective}} C_{\mathrm{A,\,surface}}}{L}\left(\frac{\partial \Psi_{\mathrm{A}}}{\partial \eta}\right)_{\eta=1} \tag{19-38}$$

Since Ψ_{A} is only a function of spatial coordinate η, the partial derivative in (19-38) is replaced by a total derivative, and the dimensionless concentration gradient evaluated at the external surface (i.e., $\eta = 1$) is a constant that can be removed from the surface integral in the numerator of the effectiveness factor. In terms of the Hougen–Watson kinetic model and the dimensional scaling factor for chemical reaction that agree with the Langmuir–Hinshelwood mechanism described at the beginning of this chapter:

$$-\upsilon_{\mathrm{A}}\mathfrak{R}(\mathrm{all}\ C_{i,\,\mathrm{surface}}) = k_2(C_{\mathrm{A,\,surface}})^2\mathfrak{R}^*(\mathrm{all}\ \Psi_{i,\,\mathrm{surface}}) \tag{19-39}$$

where

$$\mathfrak{R}^*(\mathrm{all}\ \Psi_{i,\,\mathrm{surface}}) = \frac{\Psi_{\mathrm{A,\,surf}}\Psi_{\mathrm{B,\,surf}}}{(1+\sqrt{\theta_{\mathrm{A}}\Psi_{\mathrm{A,\,surf}}}+\theta_{\mathrm{B}}\Psi_{\mathrm{B,\,surf}}+\theta_{\mathrm{C}}\Psi_{\mathrm{C,\,surf}}+\theta_{\mathrm{D}}\Psi_{\mathrm{D,\,surf}})^3}$$

The pseudo-volumetric kinetic rate constant for the forward reaction with units of (volume/mole)/time in equation (19-39) is

$$k_2 = S_m \rho_{\text{app}} k_f K_{\text{A}} K_{\text{B}} (RT)^2 \tag{19-40}$$

and the dimensionless molar density of component i on the external surface of the pellet is

$$\Psi_{i,\text{ surface}} = \Psi_{i,\text{ surf}} = \frac{C_{i,\text{ surface}}}{C_{\text{A, surface}}} \tag{19-41}$$

Hence, the effectiveness factor is proportional to the dimensionless concentration gradient at the external surface of the catalyst:

$$E = \frac{\mathfrak{D}_{\text{A, effective}} S_{\text{external}}}{k_2 C_{\text{A, surface}} L V_{\text{catalyst}}} \left(\frac{d\Psi_{\text{A}}}{d\eta} \right)_{\eta=1} \aleph_{\text{surface}} \tag{19-42}$$

The correction factor $\aleph_{\text{surface}}$ in the E vs. Λ_{A} correlation for complex kinetics is given by the inverse of the dimensionless rate law evaluated at the external surface of the catalyst, where the dimensionless molar density of reactant A is unity, by definition. Hence, the correction factor $\aleph_{\text{surface}}$ for the Hougen–Watson model described by equations (19-1) and (19-8) is:

$$\aleph_{\text{surface}} = \frac{1}{\mathfrak{R}^*(\text{all } \Psi_{i,\text{ surface}}} = \frac{(1 + \sqrt{\theta_{\text{A}}} + \theta_{\text{B}} \Psi_{\text{B, surf}} + \theta_{\text{C}} \Psi_{\text{C, surf}} + \theta_{\text{D}} \Psi_{\text{D, surf}})^3}{\Psi_{\text{B, surf}}} \tag{19-43}$$

which accounts for adsorption terms in the denominator of the rate law and the concentration of reactant B in the rate of the forward reaction. For simple nth-order kinetics where the kinetic rate law $\mathfrak{R}$ is only a function of the molar density of reactant A, $\aleph_{\text{surface}} = 1$.

19-4 DIMENSIONLESS CORRELATION FOR POROUS WAFERS WITH RECTANGULAR SYMMETRY

The catalyst has thickness T in the thinnest dimension, which is the coordinate direction defined by η along the unit normal vector $\mathbf{n}$. The lateral surface area, which is linearly proportional to thickness T, is usually neglected relative to the surface area of the flat slabs above and below. If the total external surface area of both flat slabs is S_{external}, then the volume of one catalyst is

$$V_{\text{catalyst}} = \frac{T S_{\text{external}}}{2} \tag{19-44}$$

and

$$\frac{V_{\text{catalyst}}}{S_{\text{external}}} = \frac{T}{2} \tag{19-45}$$

The effectiveness factor contains the following group of terms that is based solely on geometry: $LV_{\text{catalyst}}/S_{\text{external}}$. As mentioned on page 484, the characteristic length L required to make the important spatial variable dimensionless in rectangular coordinates is one-half the thickness of catalysts, measured in the thinnest dimension. Hence,

$$L = \frac{T}{2} \tag{19-46}$$

$$\frac{LV_{\text{catalyst}}}{S_{\text{external}}} = L^2 \tag{19-47}$$

These definitions are consistent with the following properties:

1. $\eta = 1$ on the external surface.
2. $\eta = 0$ along the symmetry plane that slices the catalyst parallel to the flat-slab surfaces and normal to the lateral surface.

In terms of surface-averaged mass transfer across the external surface, the effectiveness factor for Hougen–Watson kinetics in flat-slab catalysts is

$$E = \frac{\mathfrak{D}_{\text{A, effective}}}{k_2 C_{\text{A, surface}} L^2} \left(\frac{d\Psi_{\text{A}}}{d\eta} \right)_{\eta=1} \aleph_{\text{surface}} \tag{19-48}$$

which reduces to

$$E = \frac{1}{\Lambda_{\text{A}}^2} \left(\frac{d\Psi_{\text{A}}}{d\eta} \right)_{\eta=1} \frac{(1 + \sqrt{\theta_{\text{A}}} + \theta_{\text{B}}\Psi_{\text{B, surf}} + \theta_{\text{C}}\Psi_{\text{C, surf}} + \theta_{\text{D}}\Psi_{\text{D, surf}})^3}{\Psi_{\text{B, surf}}} \tag{19-49}$$

The intrapellet Damkohler number is defined by

$$\Lambda_{\text{A}}^2 = \frac{k_2 C_{\text{A, surface}} L^2}{\mathfrak{D}_{\text{A, effective}}} \tag{19-50}$$

and the characteristic length L is defined above as $T/2$.

19-5 NUMERICAL RESULTS FOR $A_2 + B \rightarrow C + D$ IN FLAT-SLAB WAFERS WITH RECTANGULAR SYMMETRY

Effectiveness factor calculations summarized in Tables 19-1 to 19-5 are consistent with Langmuir–Hinshelwood kinetics, as discussed in this chapter. E is larger and approaches 1 asymptotically in the reaction-controlled regime where the intrapellet Damkohler number is small, and E decreases in the diffusion-controlled regime at large values of Λ_{A}. These trends are verified by simulations provided in Table 19-1.

19-5.1 Effect of Product Concentrations Near the External Surface of the Catalyst

The simulations in Table 19-1 represent conditions near the reactor inlet because products C and D are only 10% as abundant as reactants A_2 and B on the external

TABLE 19-1 Numerical Solution of the Mass Transfer Equation for One-Dimensional Diffusion and Hougen–Watson Chemical Kinetics with Dissociative Adsorption of Reactant A_2 in Porous Catalysts with Rectangular Symmetry[a]

	$\theta_A = 0.3$	$\Psi_{B,\,surf} = 1$ $\delta_B = 0.5$ $\theta_B = 0.3$	$\Psi_{C,\,surf} = 0.1$ $\delta_C = 1.2$ $\theta_C = 0.3$	$\Psi_{D,\,surf} = 0.1$ $\delta_D = 0.3$ $\theta_D = 0.3$
Λ_A^2	$\Psi_A(\eta = 0)$, guess	$\Psi_A(\eta = 1)$	$\Omega(\eta = 1)$	E
1	0.934763	0.999999	0.13	0.93
10	0.6009805	0.999999	0.91	0.63
100	0.0869815	1.00001	3.47	0.24

[a]Effectiveness factor is given vs. the intrapellet Damkohler number.

surface of the catalyst. Consequently, most of the active sites are occupied by reactants except when the intrapellet Damkohler number is very large. Farther from the inlet, and closer to the reactor outlet, product concentrations increase in the vicinity of the external surface of the catalyst. Now, most of the active sites are occupied by C and D, because product concentrations are larger within the catalyst than they are on the external surface. This reduces the rate of the forward reaction because it is proportional to fractional surface coverage by A_2 and B. Hence, higher product concentrations could produce reaction-controlled conditions. This is consistent with the fact that the effectiveness factor is larger at the same Λ_A when $\Psi_{C,\,surf}$ and $\Psi_{D,\,surf}$ increase. These concepts are supported by the simulations in Table 19-2.

19-5.2 Effect of Adsorption/Desorption Equilibrium Constants

Reactant equilibrium constants K_A and K_B affect the forward kinetic rate constant, and all K_i's affect the adsorption terms in the denominator of the Hougen–Watson rate law via the θ_i parameters defined on page 493. However, the forward kinetic rate constant does not appear explicitly in the dimensionless simulations because it is accounted for in the numerator of the Damkohler number, and Λ_A^2 is chosen independently to initiate the calculations. Hence, simulations performed at larger adsorption/desorption equilibrium constants and the same intrapellet Damkohler number implicitly require that the forward kinetic rate constant must decrease to offset the increase in reactant equilibrium constants. The vacant-site fraction on the internal catalytic surface decreases when adsorption/desorption equilibrium constants increase. The forward rate of reaction for the triple-site reaction-controlled Langmuir–Hinshelwood mechanism described on page 491 is proportional to the third power of the vacant-site fraction. Consequently, larger K_i's at lower temperature decrease the rate of reactant consumption and could produce reaction-controlled conditions. This is evident in Table 19-3, because the

TABLE 19-2 Numerical Solution of the Mass Transfer Equation for One-Dimensional Diffusion and Hougen–Watson Chemical Kinetics with Dissociative Adsorption of Reactant A_2 in Porous Catalysts with Rectangular Symmetry (*continued*)[a]

		$\Psi_{B,\,surf} = 1$ $\delta_B = 0.5$	$\Psi_{C,\,surf} = 0.5$ $\delta_C = 1.2$	$\Psi_{D,\,surf} = 0.5$ $\delta_D = 0.3$
	$\theta_A = 0.3$	$\theta_B = 0.3$	$\theta_C = 0.3$	$\theta_D = 0.3$
Λ_A^2	$\Psi_A(\eta = 0)$, guess	$\Psi_A(\eta = 1)$	$\Omega(\eta = 1)$	E
1	0.9531372	1.00001	0.096	0.95
10	0.68083	0.999999	0.71	0.70
100	0.143528	0.999999	2.89	0.29

		$\Psi_{B,\,surf} = 1$ $\delta_B = 0.5$	$\Psi_{C,\,surf} = 5$ $\delta_C = 1.2$	$\Psi_{D,\,surf} = 5$ $\delta_D = 0.3$
	$\theta_A = 0.3$	$\theta_B = 0.3$	$\theta_C = 0.3$	$\theta_D = 0.3$
Λ_A^2	$\Psi_A(\eta = 0)$, guess	$\Psi_A(\eta = 1)$	$\Omega(\eta = 1)$	E
1	0.995687	0.999997	0.0087	0.996
10	0.958903	0.999999	0.084	0.96
100	0.709569	0.999998	0.64	0.73

[a]Effectiveness factor is given vs. the intrapellet Damkohler number for different dimensionless product concentrations near the external surface of the catalyst, denoted by $\Psi_{C,\,surf}$ and $\Psi_{D,\,surf}$.

TABLE 19-3 Numerical Solution of the Mass Transfer Equation for One-Dimensional Diffusion and Hougen–Watson Chemical Kinetics with Dissociative Adsorption of Reactant A_2 in Porous Catalysts with Rectangular Symmetry (*continued*)[a]

		$\Psi_{B,\,surf} = 1$ $\delta_B = 0.5$	$\Psi_{C,\,surf} = 0.5$ $\delta_C = 1.2$	$\Psi_{D,\,surf} = 0.5$ $\delta_D = 0.3$
	$\theta_A = 0.05$	$\theta_B = 0.05$	$\theta_C = 0.05$	$\theta_D = 0.05$
Λ_A^2	$\Psi_A(\eta = 0)$, guess	$\Psi_A(\eta = 1)$	$\Omega(\eta = 1)$	E
1	0.82757	1.00001	0.36	0.85
10	0.3057497	0.999999	1.87	0.43
100	0.00729757	0.999998	6.17	0.14

		$\Psi_{B,\,surf} = 1$ $\delta_B = 0.5$	$\Psi_{C,\,surf} = 0.5$ $\delta_C = 1.2$	$\Psi_{D,\,surf} = 0.5$ $\delta_D = 0.3$
	$\theta_A = 1$	$\theta_B = 1$	$\theta_C = 1$	$\theta_D = 1$
Λ_A^2	$\Psi_A(\eta = 0)$, guess	$\Psi_A(\eta = 1)$	$\Omega(\eta = 1)$	E
1	0.992377	0.999999	0.015	0.99
10	0.93095	1.00001	0.14	0.92
100	0.607399	1.00001	0.92	0.59

[a]Effectiveness factor is given vs. the intrapellet Damkohler number for different adsorption/desorption equilibrium constants, denoted by θ_i. In each simulation, θ_i is the same for all four species in the reactive mixture, but θ_i changes from one simulation to the next.

effectiveness factor is considerably larger at the same Λ_A^2 when all K_i's and θ_i's are larger;

19-5.3 Effect of a Stoichiometric Imbalance between Reactants A_2 and B

This is investigated by manipulating the ratio between $C_{A,\,surface}$ and $C_{B,\,surface}$, which is defined by $\Psi_{B,\,surf}$. Effectiveness factors are not very sensitive to a fourfold change in this parameter (i.e., from 0.5 to 2.0), as illustrated in Table 19-4. An excess of reactant B (i.e., $\Psi_{B,\,surf} = 2$) causes A_2 to be depleted at a faster rate relative to the situation when $\Psi_{B,\,surf} = 0.5$. This is reasonable because the probability of finding B on an active site inside the catalyst increases (probably by a factor of 4 in this example) when B is present in excess. Since the rate of the forward reaction depends linearly on active-site surface coverage by reactant B, larger values of $\Psi_{B,\,surf}$ could produce diffusion-controlled conditions. This is marginally obvious in Table 19-4 at $\Lambda_A^2 = 100$, because the effectiveness factor is smaller (i.e., 0.26 vs. 0.32) when reactant B is present in excess.

19-5.4 Effect of Molecular Size of Reactant B

Knudsen and ordinary molecular diffusivities are inversely proportional to the square root of molecular weight. Hence, a fourfold decrease in the molecular

TABLE 19-4 Numerical Solution of the Mass Transfer Equation for One-Dimensional Diffusion and Hougen–Watson Chemical Kinetics with Dissociative Adsorption of Reactant A_2 in Porous Catalysts with Rectangular Symmetry (*continued*)[a]

		$\Psi_{B,\,surf} = 0.5$ $\delta_B = 0.5$	$\Psi_{C,\,surf} = 0.5$ $\delta_C = 1.2$	$\Psi_{D,\,surf} = 0.5$ $\delta_D = 0.3$
	$\theta_A = 0.3$	$\theta_A = 0.3$	$\theta_C = 0.3$	$\theta_D = 0.3$
Λ_A^2	$\Psi_A(\eta = 0)$, guess	$\Psi_A(\eta = 1)$,	$\Omega(\eta = 1)$	E
1	0.97059	1.00001	0.060	0.96
10	0.78958	1.00001	0.46	0.74
100	0.354634	1.00001	2.00	0.32
		$\Psi_{B,\,surf} = 2$ $\delta_B = 0.5$	$\Psi_{C,\,surf} = 0.5$ $\delta_C = 1.2$	$\Psi_{D,\,surf} = 0.5$ $\delta_D = 0.3$
	$\theta_A = 0.3$	$\theta_B = 0.3$	$\theta_C = 0.3$	$\theta_D = 0.3$
Λ_A^2	$\Psi_A(\eta = 0)$, guess	$\Psi_A(\eta = 1)$	$\Omega(\eta = 1)$	E
1	0.937175	1.00001	0.13	0.95
10	0.59074	1.00001	0.92	0.67
100	0.0618387	0.999998	3.55	0.26

[a]Effectiveness factor is given vs. the intrapellet Damkohler number for different stoichiometric imbalances between reactants A_2 and B, denoted by $\Psi_{B,\,surf}$.

TABLE 19-5 Numerical Solution of the Mass Transfer Equation for One-Dimensional Diffusion and Hougen–Watson Chemical Kinetics with Dissociative Adsorption of Reactant A_2 in Porous Catalysts with Rectangular Symmetry (*continued*)[a]

	$\theta_A = 0.3$	$\Psi_{B,\,surf} = 1$ $\delta_B = 0.25$ $\theta_B = 0.3$	$\Psi_{C,\,surf} = 0.5$ $\delta_C = 1.2$ $\theta_C = 0.3$	$\Psi_{D,\,surf} = 0.5$ $\delta_D = 0.3$ $\theta_D = 0.3$
Λ_A^2	$\Psi_A(\eta = 0)$, guess	$\Psi_A(\eta = 1)$	$\Omega(\eta = 1)$	E
1	0.95287	0.999999	0.097	0.96
10	0.67047	1.00001	0.72	0.72
100	0.112525	0.999999	2.99	0.30

[a]Effectiveness factor is given vs. the intrapellet Damkohler number for different molecular sizes of reactant B. This effect is considered by changing the effective intrapellet diffusion coefficient of reactant B, which affects δ_B.

weight of reactant B produces a twofold increase in $\mathfrak{D}_{B,\,effective}$. This is consistent with the fact that δ_B decreases from 0.5 in all the previous simulations, to 0.25 in Table 19-5. Comparison between the simulations in Table 19-2 and Table 19-5 reveals that the molecular size of reactant B has an insignificant effect on E vs. Λ_A.

19-5.5 Summary of Parametric Sensitivity Results on the Effectiveness Factor for Langmuir–Hinshelwood Mechanisms and Hougen–Watson Models

E vs. Λ_A seems to be most sensitive to product concentrations near the external surface of the catalyst and adsorption/desorption equilibrium constants. $\Psi_{C,\,surf}$, $\Psi_{D,\,surf}$, and θ_i directly affect the vacant-site fraction on the interior catalytic surface and the rate of reactant consumption. In the previous simulations, product molar densities near the external surface of the catalyst were varied by a factor of 50 (i.e., from 0.1 to 5), and θ_i was varied by a factor of 20 (i.e., from 0.05 to 1). The effectiveness factor increases significantly when either $\Psi_{C,\,surf}$, $\Psi_{D,\,surf}$ or θ_i is larger. E vs. Λ_A is marginally sensitive to a stoichiometric imbalance between reactants A_2 and B, but $\Psi_{B,\,surface}$ was only varied by a factor of 4 (i.e., from 0.5 to 2). A four-fold decrease in the molecular weight of reactant B, which produces two-fold changes in $\mathfrak{D}_{B,\,effective}$ and δ_B, does not affect E.

PROBLEMS

19-1. Six equations are required to calculate the effectiveness factor for a spherical catalytic pellet when the intrapellet Damkohler number Λ_A^2 is 10. The elementary irreversible chemical reaction is

$$A + 2B \longrightarrow C$$

and the dimensionless kinetic rate law, in terms of dimensionless molar densities, is

$$\mathfrak{R}^* = \Psi_A(\Psi_B)^2$$

(a) Do not linearize the rate law. Write the six equations that a numerical methods software package requires to calculate the effectiveness factor when $\Lambda_A^2 = 10$.

(b) Express the intrapellet Damkohler number for reactant A in terms of the pseudo-volumetric third-order kinetic rate constant k_3.

(c) Obviously, numerical methods are required to calculate the molar density profile of reactant A, and the effectiveness factor vs. intrapellet Damkohler number. If one approximates the third-order kinetic rate law as a first-order chemical reaction, and identifies the best pseudo-first-order rate constant $k_{1,\,\text{pseudovolumetric}}$ via linear least-squares minimization, then analytical solutions can be obtained in spherical pellets for the reactant molar density profile and the effectiveness factor.

(i) How should one calculate $k_{1,\,\text{pseudovolumetric}}$ if a stoichiometric feed (i.e., 1 : 2) of reactants A and B is present initially?

(ii) Express the intrapellet Damkohler number in terms of the best pseudo-first-order kinetic rate constant $k_{1,\,\text{pseudovolumetric}}$.

(iii) What is the analytical solution for the reactant molar density profile Ψ_A?

(iv) What is the analytical solution for the effectiveness factor?

19-2. At relatively low pressures, what dimensionless differential equations must be solved to generate basic information for the effectiveness factor vs. the intrapellet Damkohler number when an isothermal irreversible chemical reaction occurs within the internal pores of flat slab catalysts. Single-site adsorption is reasonable for each component, and dual-site reaction on the catalytic surface is the rate-limiting step for $A + B \rightarrow C + D$. Use the molar density of reactant A near the external surface of the catalytic particles as a characteristic quantity to make all of the molar densities dimensionless. Be sure to define the intrapellet Damkohler number. Include all the boundary conditions required to obtain a unique solution to these ordinary differential equations.

19-3. In this problem, we explore the dimensionless mass transfer correlation between the effectiveness factor and the intrapellet Damkohler number for one-dimensional diffusion and Langmuir–Hinshelwood surface-catalyzed chemical reactions within the internal pores of flat-slab catalysts under isothermal conditions. Perform simulations for E vs. Λ_A^2 which correspond to the following chemical reaction that occurs within the internal pores of catalysts that have rectangular symmetry.

(1) The reaction scheme is $A_2 + 2B \rightarrow C$.

(2) Diatomic A_2 experiences dissociative adsorption whereas the other two components adsorb on single active sites on the internal catalytic surface.

(3) Quadruple-site reaction on the catalytic surface is the slowest step in the overall mechanism.

(4) The reaction is essentially irreversible.

(5) The feed stream to a packed catalytic reactor is stoichiometric (i.e., 1 : 2), in reactants A_2 and B.

The dimensionless adsorption/desorption equilibrium constants are

$$\theta_i = K_i C_{A,\,\text{surface}} RT = 0.3 \qquad i = A_2, B, C$$

for all components. The effective diffusion coefficients are

$$\mathfrak{D}_{B,\,\text{effective}} = 2\mathfrak{D}_{A,\,\text{effective}}$$

$$\mathfrak{D}_{C,\,\text{effective}} = \frac{\mathfrak{D}_{A,\,\text{effective}}}{1.2}$$

In other words, the delta parameters are $\delta_B = 0.5$ and $\delta_C = 1.2$, where δ_i is defined as the ratio of effective diffusion coefficient in the catalytic pores for reactant A_2 relative to the effective diffusion coefficient for component i. Hence,

$$\delta_i = \frac{\mathfrak{D}_{A,\,\text{effective}}}{\mathfrak{D}_{i,\,\text{effective}}} = \left(\frac{\Lambda_i}{\Lambda_A}\right)^2$$

The delta parameters defined above are consistent with the following ranking in molecular size for the two reactants and one product: $C > A_2 > B$. Effective diffusion coefficients and intrapellet Damkohler numbers are species specific because pore diffusion in the gas phase varies inversely with the square root of molecular weight. Hence, larger molecules have smaller diffusivities, larger delta parameters, and larger intrapellet Damkohler numbers. Investigate the sensitivity of E vs. Λ_A^2 to:

(a) Concentration of product C on the external surface of the catalyst.

(b) Adsorption/desorption equilibrium constants for all species that adsorb on the interior catalytic surface.

(c) Stoichiometric imbalance between reactants A_2 and B.

(d) A decrease in the molecular size of reactant B.

Consult the following references for more information about the effect of Langmuir–Hinshelwood kinetics and catalyst shape on the effectiveness factor: Roberts and Satterfield (1965), Knudsen *et al*. (1966), and Hill (1977, pp. 455–456.)

19-4. Consider the Hougen–Watson kinetic model for the production of methanol from CO and H_2, given by equation (22-38). Do not linearize the rate expression. Write the rate law in dimensionless form if the chemical reaction is essentially irreversible (i.e., $K_{\text{eq},p} \rightarrow \infty$).

19-5. Use the kinetic model from Problem 19-4, together with the dimensionless concentration gradient of CO at the external surface of a long porous cylindrical catalyst, and write the appropriate expression for the effectiveness factor. In other words, in cylindrical coordinates, you have chosen a value of the intrapellet Damkohler number, $\Lambda^2_{\text{A, intrapellet}}$, made the correct guess for Ψ_A near the center of the catalyst, solved two coupled ODEs for Ψ_A and $d\Psi_A/d\eta$ with split boundary conditions, and achieved convergence at the external surface of the catalyst, where $\Psi_A = 1$. Now, use the correct value for the dimensionless concentration gradient of CO on the external catalytic surface [i.e., $(d\Psi_A/d\eta)$ at $\eta = 1$] and construct an expression for the effectiveness factor E which is required by numerical analysis software to generate the dimensionless correlation between E and $\Lambda_{\text{A, intrapellet}}$.

Transport Phenomena for Chemical Reactor Design. Laurence A. Belfiore
Copyright © 2003 John Wiley & Sons, Inc.
ISBN: 0-471-20275-4

20

INTERNAL MASS TRANSFER LIMITATIONS IN ISOTHERMAL CATALYTIC PELLETS

20-1 REACTOR DESIGN STRATEGY

The mass balance with homogeneous one-dimensional diffusion and irreversible *n*th-order chemical reaction provides basic information for the spatial dependence of reactant molar density within a catalytic pellet. Since this problem is based on one isolated pellet, the molar density profile can be obtained for any type of chemical kinetics. Of course, analytical solutions are available only when the rate law conforms to simple zeroth- or first-order kinetics. Numerical techniques are required to solve the mass balance when the kinetics are more complex. The rationale for developing a correlation between the effectiveness factor and intrapellet Damkohler number is based on the fact that the reactor design engineer does not want to consider details of the interplay between diffusion and chemical reaction in each catalytic pellet when these pellets are packed in a large-scale reactor. The strategy is formulated as follows:

1. Account for diffusion and chemical reaction in one isolated catalytic pellet and calculate a volumetrically averaged rate of consumption of reactants within the pellet in terms of conditions on the external surface of the catalyst.
2. If concentrations and temperatures on the external catalytic surface are close to the bulk conditions in a packed reactor, then the design engineer can use these bulk conditions to estimate the rate of consumption of reactants within each pellet.
3. The volume-averaged rate of reaction in each catalytic pellet is incorporated into plug-flow mass and thermal energy balances to predict the overall performance of the reactor.

Conditions 2 and 3 are discussed further in Chapters 22 and 30 that focus on packed catalytic tubular reactors. Condition 1 is addressed by defining the effectiveness factor and using basic information from the mass balance to develop a correlation between the effectiveness factor and the intrapellet Damkohler number. The ratio of reaction rates described below in (a) and (b), with units of moles per time, is defined as the *effectiveness factor*.

(a) The volume-averaged rate of consumption of reactants in one isolated catalytic pellet, relative to
(b) The rate of consumption of reactants evaluated using conditions on the external surface of the pellet.

In general, the volume-averaged rate of consumption of reactant A, specified by (a), is $\int -\upsilon_A \mathfrak{R}(C_A)\, dV$, where integration is performed over the entire volume of the catalyst if reactant A exists everywhere within the catalyst. A modification of the integration limits on the dimensionless spatial coordinate η is required for zeroth-order kinetics when the intrapellet Damkohler number is larger than its critical value (i.e., $0 < \eta_{\text{critical}} \leq \eta \leq 1$). The rate of consumption of reactant A based on external surface conditions, specified in (b), is $-\upsilon_A \mathfrak{R}(C_{A,\,\text{surface}}) V_{\text{catalyst}}$ with units of moles of component A per time, where V_{catalyst} represents the entire volume of one pellet. Hence, the general expression for the effectiveness factor in the presence of one chemical reaction, with kinetic rate law $\mathfrak{R}$, is:

$$E = \frac{\displaystyle\int_{V_{\text{catalyst}}} -\upsilon_A \mathfrak{R}(C_A)\, dV}{-\upsilon_A \mathfrak{R}(C_{A,\,\text{surface}}) V_{\text{catalyst}}} \tag{20-1}$$

when the kinetics are averaged throughout the volume of one pellet. An equivalent expression for the volume-averaged rate of consumption of reactant A is based on mass flux of reactant A into the pellet across the external surface. Under steady-state conditions, the mass transfer equation for component A with diffusion and one chemical reaction is

$$\mathfrak{D}_{A,\,\text{effective}} \nabla \cdot \nabla C_A + \upsilon_A \mathfrak{R} = \nabla \cdot (\mathfrak{D}_{A,\,\text{effective}} \nabla C_A) + \upsilon_A \mathfrak{R} = 0 \tag{20-2}$$

Integration of (20-2) over the entire volume of one catalytic pellet allows one to calculate the volume-averaged rate at which reactant A is consumed by chemical reaction on the interior catalytic surface:

$$\int_{V_{\text{catalyst}}} -\upsilon_A \mathfrak{R}(C_A)\, dV = \int_{V_{\text{catalyst}}} \nabla \cdot (\mathfrak{D}_{A,\,\text{effective}} \nabla C_A)\, dV \tag{20-3}$$

In other words, if the microscopic mass balance for each component in the reactive mixture must be satisfied at every point within the catalyst, then a volume average of this mass balance is also satisfied. If $\mathbf{n}$ is an outward-directed unit normal vector on the external surface of the catalyst, then Gauss's law transforms

the volume integral on the right side of (20-3) to an integral over the external catalytic surface:

$$\int_{V_{\text{catalyst}}} -\upsilon_{\text{A}}\mathfrak{R}(C_{\text{A}})\,dV = \int_{V_{\text{catalyst}}} \nabla\cdot(\mathfrak{D}_{\text{A, effective}}\nabla C_{\text{A}})\,dV$$

$$= \int_{S_{\text{external}}} \mathbf{n}\cdot(\mathfrak{D}_{\text{A, effective}}\nabla C_{\text{A}})_{\text{at } S_{\text{external}}}\,dS \qquad (20\text{-}4)$$

This relation states that the volume-averaged rate of consumption of reactant A via chemical reaction is equivalent to the surface-averaged rate of diffusion of A into the catalyst. Hence, the numerator of the effectiveness factor can be written as

$$\int \mathbf{n}\cdot(\mathfrak{D}_{\text{A, effective}}\nabla C_{\text{A}})_{\text{at } S_{\text{external}}}\,dS = \int (-\mathbf{n})\cdot(-\mathfrak{D}_{\text{A, effective}}\nabla C_{\text{A}})_{\text{at } S_{\text{external}}}\,dS \qquad (20\text{-}5)$$

where the right side of (20-5) corresponds to the diffusional flux of reactant A, given by Fick's law, in the direction of the inward unit normal $-\mathbf{n}$ (i.e., into the pellet) from the external catalytic surface. These concepts allow one to write the volume-averaged rate of consumption of reactant A in terms of the surface-averaged diffusional flux of A across the external surface. Hence, an equivalent expression for the effectiveness factor in catalysts of arbitrary geometry and kinetic rate law is

$$E = \frac{\displaystyle\int_{S_{\text{external}}} \mathbf{n}\cdot(\mathfrak{D}_{\text{A, effective}}\nabla C_{\text{A}})_{\text{at } S_{\text{external}}}\,dS}{-\upsilon_{\text{A}}\mathfrak{R}(C_{\text{A, surface}})V_{\text{catalyst}}} \qquad (20\text{-}6)$$

which seems, at first glance, to be more complex. However, mass transfer across the external surface is the method of choice to calculate the effectiveness factor when numerical techniques are required to integrate the mass balance with one-dimensional diffusion and chemical reaction. Support for this claim is based on the fact that the concentration gradient, ∇C_{A}, exhibits a nonzero component in one coordinate direction only (i.e., η), due to the one-dimensional nature of diffusional flux in the mass balance. In other words, the reactant molar density is only a function of one spatial coordinate because diffusional flux is assumed to be one-dimensional. This assumption reduces the partial differential mass balance to an ordinary differential equation. In terms of the following dimensionless variables: $\Psi_{\text{A}} = C_{\text{A}}/C_{\text{A, surface}}$ and $\eta =$ (important spatial coordinate)$/L$, the scalar (i.e., dot) product of the outward-directed normal vector $\mathbf{n}$ with $\mathfrak{D}_{\text{A, effective}}\nabla C_{\text{A}}$ reduces to

$$\mathbf{n}\cdot(\mathfrak{D}_{\text{A, effective}}\nabla C_{\text{A}})_{\text{at } S_{\text{external}}} = \frac{\mathfrak{D}_{\text{A, effective}}C_{\text{A, surface}}}{L}\left(\frac{\partial\Psi_{\text{A}}}{\partial\eta}\right)_{\eta=1} \qquad (20\text{-}7)$$

Since Ψ_A is only a function of spatial coordinate η, the partial derivative in equation (20-7) is replaced by a total derivative, and the dimensionless concentration gradient evaluated at the external surface (i.e., $\eta = 1$) is a constant that can be removed from the surface integral in the numerator of the effectiveness factor (see equation 20-6). For simple nth-order irreversible chemical kinetics in catalytic pellets, where the rate law is a function of the molar density of only one reactant,

$$-\upsilon_A \mathfrak{R}(C_{A,\,\text{surface}}) = k_n (C_{A,\,\text{surface}})^n \tag{20-8}$$

where k_n is an nth-order kinetic rate constant for a volumetric rate law based on gas-phase molar densities. Hence, the generalized form of the effectiveness factor is proportional to the dimensionless concentration gradient at the external surface of the catalyst:

$$E = \frac{\mathfrak{D}_{A,\,\text{effective}} S_{\text{external}}}{k_n (C_{A,\,\text{surface}})^{n-1} L V_{\text{catalyst}}} \left(\frac{d\Psi_A}{d\eta} \right)_{\eta=1} \tag{20-9}$$

The catalytic volume V_{catalyst} and the external surface S_{external} that bounds this volume are calculated explicitly for pellets with rectangular, cylindrical, and spherical symmetry in Section 20-2. The quantity

$$\frac{k_n (C_{A,\,\text{surface}})^{n-1} L V_{\text{catalyst}}}{\mathfrak{D}_{A,\,\text{effective}} S_{\text{external}}} = \frac{\Lambda^2}{\alpha} \tag{20-10}$$

is dimensionless and proportional to the intrapellet Damkohler number for reactant A because

$$\frac{V_{\text{catalyst}}}{S_{\text{external}}} = \frac{L}{\alpha} \tag{20-11}$$

Hence, the generalized form for the dimensionless correlation between the effectiveness factor and the intrapellet Damkohler number is

$$E = \frac{\alpha}{\Lambda^2} \left(\frac{d\Psi_A}{d\eta} \right)_{\eta=1} \tag{20-12}$$

As illustrated below, the gradient of the dimensionless reactant molar density profile is a function of the intrapellet Damkohler number, so the effectiveness factor is only a function of Λ and geometry. Numerical values of α are 1, 2, or 3 for catalysts with rectangular, cylindrical, or spherical symmetry, respectively.

20-2 CORRELATIONS FOR CATALYSTS WITH DIFFERENT MACROSCOPIC SYMMETRY

20-2.1 Porous Catalysts with Rectangular Symmetry

Flat-slab catalysts have the appearance of wafers, and a rectangular coordinate system is most appropriate to exploit the symmetry of the macroscopic boundary. The catalyst has a thickness of T in the thinnest dimension, which is the

coordinate direction defined by η. The lateral surface area, which is linearly proportional to the thickness T, is usually neglected relative to the surface area of the flat slabs above and below. If the total external surface area of both flat slabs is S_{external}, then the volume of one catalyst is

$$V_{\text{catalyst}} = \tfrac{1}{2} T S_{\text{external}} \tag{20-13}$$

and

$$\frac{V_{\text{catalyst}}}{S_{\text{external}}} = \frac{T}{2} \tag{20-14}$$

The effectiveness factor correlation given by equation (20-9) contains the following group of terms that is based solely on geometry: $LV_{\text{catalyst}}/S_{\text{external}}$.

As mentioned previously in this book, the characteristic length L required to make the important spatial variable dimensionless in rectangular coordinates is one-half the thickness of catalysts, measured in the thinnest dimension. Hence,

$$L = \frac{T}{2} \tag{20-15}$$

$$\frac{LV_{\text{catalyst}}}{S_{\text{external}}} = L^2 \tag{20-16}$$

These definitions are consistent with the following properties:

1. $\eta = 1$ on the external surface of the catalyst
2. $\eta = 0$ along the symmetry plane that slices the catalyst parallel to the flat-slab surfaces and normal to the lateral surface.

In terms of surface-averaged mass transfer across the external surface, the effectiveness factor for flat-slab catalysts is

$$E = \frac{\mathfrak{D}_{\text{A, effective}}}{k_n (C_{\text{A, surface}})^{n-1} L^2} \left(\frac{d\Psi_{\text{A}}}{d\eta} \right)_{\eta=1} \tag{20-17}$$

which reduces to

$$E = \frac{1}{\Lambda^2} \left(\frac{d\Psi_{\text{A}}}{d\eta} \right)_{\eta=1} \tag{20-18}$$

as expected if $\alpha = 1$ for rectangular symmetry. The intrapellet Damkohler number for reactant A is defined by

$$\Lambda^2 = \frac{k_n (C_{\text{A, surface}})^{n-1} L^2}{\mathfrak{D}_{\text{A, effective}}} \tag{20-19}$$

where the characteristic length L is defined in (20-15) as $T/2$.

20-2.2 Long Cylindrical Catalysts

These catalysts have a very large length-to-diameter ratio, and the assumption that radial diffusion dominates axial diffusion is appropriate. The pellet

has radius R and length Z. The coordinate direction defined by η is coincident with the radial direction. The external surface area is $S_{\text{external}} = 2\pi RZ$ if one neglects both ends of the long cylinder. The volume of one pellet is $V_{\text{catalyst}} = \pi R^2 Z$. Hence,

$$\frac{V_{\text{catalyst}}}{S_{\text{external}}} = \frac{R}{2} \tag{20-20}$$

The characteristic length L required to make the important spatial coordinate dimensionless is the cylindrical radius R, as mentioned previously in this book. Hence,

$$L = R \tag{20-21}$$

$$\frac{LV_{\text{catalyst}}}{S_{\text{external}}} = \frac{L^2}{2} \tag{20-22}$$

Once again, these definitions are consistent with the following properties:

1. $\eta = 1$ on the external surface of the catalyst
2. $\eta = 0$ along the symmetry axis of the long cylinder.

In terms of surface-averaged mass transfer across the external surface of the catalyst, the effectiveness factor given by equation (20-9) is

$$E = \frac{2\mathfrak{D}_{\text{A, effective}}}{k_n (C_{\text{A, surface}})^{n-1} L^2} \left(\frac{d\Psi_{\text{A}}}{d\eta} \right)_{\eta=1} \tag{20-23}$$

which reduces to

$$E = \frac{2}{\Lambda^2} \left(\frac{d\Psi_{\text{A}}}{d\eta} \right)_{\eta=1} \tag{20-24}$$

as expected if $\alpha = 2$ for long cylindrical pellets. The intrapellet Damkohler number for reactant A is defined by

$$\Lambda^2 = \frac{k_n (C_{\text{A, surface}})^{n-1} L^2}{\mathfrak{D}_{\text{A, effective}}} \tag{20-25}$$

where the characteristic length L is defined in (20-21) as R.

20-2.3 Spherical Catalysts

These catalysts look like porous marbles, and pseudo-homogeneous concentration diffusion occurs exclusively in the radial direction, which coincides with the dimensionless variable η. The pellet has radius R. The total external surface area is $S_{\text{external}} = 4\pi R^2$ and the volume of one pellet is $V_{\text{catalyst}} = \frac{4}{3}\pi R^3$. Hence,

$$\frac{V_{\text{catalyst}}}{S_{\text{external}}} = \frac{R}{3} \tag{20-26}$$

The characteristic length L required to make the important spatial coordinate dimensionless is the pellet radius R, as mentioned previously in this book. Hence,

$$L = R \tag{20-27}$$

$$\frac{LV_{\text{catalyst}}}{S_{\text{external}}} = \frac{L^2}{3} \tag{20-28}$$

Once again, these definitions are consistent with:

1. $\eta = 1$ on the external surface of the catalyst
2. $\eta = 0$ at the symmetry point in the center of the sphere.

In terms of surface-averaged mass transfer across the external surface of the catalyst, the effectiveness factor for spheres is adopted from equation (20-9):

$$E = \frac{3\mathfrak{D}_{\text{A, effective}}}{k_n(C_{\text{A, surface}})^{n-1}L^2}\left(\frac{d\Psi_{\text{A}}}{d\eta}\right)_{\eta=1} \tag{20-29}$$

which reduces to

$$E = \frac{3}{\Lambda^2}\left(\frac{d\Psi_{\text{A}}}{d\eta}\right)_{\eta=1} \tag{20-30}$$

as expected if $\alpha = 3$ for spherical catalysts. The intrapellet Damkohler number for reactant A is defined by

$$\Lambda^2 = \frac{k_n(C_{\text{A, surface}})^{n-1}L^2}{\mathfrak{D}_{\text{A, effective}}} \tag{20-31}$$

where the characteristic length L is defined in (20-27) as R.

20-3 EFFECTIVENESS FACTORS

20-3.1 *n*th-Order Irreversible Chemical Reaction Via Volumetric Averaging of the Kinetic Rate Law

The general expression for the effectiveness factor, given by equation (20-1), is

$$E = \frac{\int_{V_{\text{catalyst}}} -\upsilon_{\text{A}}\mathfrak{R}(C_{\text{A}})\,dV}{-\upsilon_{\text{A}}\mathfrak{R}(C_{\text{A, surface}})V_{\text{catalyst}}} \tag{20-32}$$

when the kinetics are averaged throughout the volume of one pellet. If the kinetics are nth-order, irreversible, and depend only on the molar density of one reactant (i.e., A), then it is possible to manipulate equation (20-32) for catalysts with

rectangular, cylindrical, or spherical symmetry. Hence, $\upsilon_A = -1$, the volumetric kinetic rate law is

$$\mathfrak{R} = S_m \rho_{app} k_{n,surface} (C_A)^n \tag{20-33}$$

and one must integrate the dimensionless molar density profile of reactant A throughout the pellet to calculate the effectiveness factor under isothermal conditions:

$$E = \frac{1}{V_{catalyst}} \int_{V_{catalyst}} \left\{ \frac{C_A}{C_{A,\,surface}} \right\}^n dV \tag{20-34}$$

Flat-Slab or Porous Wafer Catalysts. The nomenclature provided in Section 20-2.1 is employed to evaluate equation (20-34). The catalyst has a thickness of T in the thinnest dimension, which is the coordinate direction defined by $\eta = z/(T/2)$. The lateral surface is neglected, the total external surface area of both flat slabs is $S_{external}$ $(= 2\pi R^2)$, and the volume of one wafer is $V_{catalyst} = T S_{external}/2$. Hence,

$$dV_{catalyst} = dV = \frac{S_{external}}{2} dz \tag{20-35}$$

where z is the dimensional spatial coordinate measured from the symmetry plane (i.e., $z = 0$) to the external surface (i.e., $z = T/2$). One simplifies the effectiveness factor expression given by (20-34) as follows:

$$E = \frac{1}{T} \int_{-T/2}^{T/2} [\Psi_A(\eta; \Lambda)]^n \, dz \tag{20-36}$$

In terms of the dimensionless spatial coordinate η in the thinnest dimension of the wafer, $dz = (T/2)\, d\eta$. Hence,

$$E = \frac{1}{2} \int_{-1}^{1} [\Psi_A(\eta; \Lambda)]^n \, d\eta \tag{20-37}$$

The dimensionless molar density profile of reactant A is symmetric with respect to η about the symmetry plane (i.e., $z = 0$, $\eta = 0$). Consequently, it is only necessary to integrate equation (20-37) from the symmetry plane at the center of the wafer to the external surface, and multiply by 2. The final expression for the effectiveness factor in rectangular coordinates is

$$E = \int_{0}^{1} [\Psi_A(\eta; \Lambda)]^n \, d\eta \tag{20-38}$$

Long Cylindrical Pellets. The nomenclature provided in Section 20-2.2 is employed to evaluate the effectiveness factor. The pellets have radius R and length Z. If r is the dimensional radial variable in cylindrical coordinates, then,

$$V_{catalyst} = \pi R^2 Z \tag{20-39}$$

$$dV_{catalyst} = dV = 2\pi r \, dr Z \tag{20-40}$$

since diffusion occurs primarily in the radial direction. The effectiveness factor given by equation (20-34) is manipulated as follows:

$$E = \frac{1}{V_{\text{catalyst}}} \int_{V_{\text{catalyst}}} [\Psi_A(\eta; \Lambda)]^n \, dV = \frac{2}{R^2} \int_0^R [\Psi_A(\eta; \Lambda)]^n r \, dr \qquad (20\text{-}41)$$

In terms of the dimensionless radial coordinate, $\eta = r/R$, the final expression for the effectiveness factor in cylindrical coordinates is

$$E = 2 \int_0^1 [\Psi_A(\eta; \Lambda)]^n \eta \, d\eta \qquad (20\text{-}42)$$

Spherical Catalysts. Now, the nomenclature provided in Section 20-2.3 is employed to evaluate the effectiveness factor. Each pellet has radius R, and r is the dimensional radial variable in spherical coordinates. Hence,

$$V_{\text{catalyst}} = \tfrac{4}{3}\pi R^3 \qquad (20\text{-}43)$$

$$dV_{\text{catalyst}} = dV = 4\pi r^2 \, dr \qquad (20\text{-}44)$$

since diffusion occurs exclusively in the radial direction. These expressions for catalyst volume are used to simplify the effectiveness factor:

$$E = \frac{1}{V_{\text{catalyst}}} \int_{V_{\text{catalyst}}} [\Psi_A(\eta; \Lambda)]^n \, dV = \frac{3}{R^3} \int_0^R [\Psi_A(\eta; \Lambda)]^n r^2 \, dr \qquad (20\text{-}45)$$

In terms of the dimensionless radial coordinate, $\eta = r/R$, the final expression for the effectiveness factor in spherical coordinates is

$$E = 3 \int_0^1 [\Psi_A(\eta; \Lambda)]^n \eta^2 \, d\eta \qquad (20\text{-}46)$$

20-3.2 Zeroth-Order Chemical Reaction

In the previous section, integral expressions for the effectiveness factor were developed for nth-order irreversible chemical kinetics in which the rate law is only a function of the molar density of one reactant. These results are summarized below:

Rectangular coordinates: $$E = \int_0^1 [\Psi_A(\eta; \Lambda)]^n \, d\eta \qquad (20\text{-}47a)$$

Cylindrical coordinates: $$E = 2 \int_0^1 [\Psi_A(\eta; \Lambda)]^n \eta \, d\eta \qquad (20\text{-}47b)$$

Spherical coordinates: $$E = 3 \int_0^1 [\Psi_A(\eta; \Lambda)]^n \eta^2 \, d\eta \qquad (20\text{-}47c)$$

If the kinetics are not zeroth-order, then these integral expressions are more tedious to use than the ones developed earlier in this chapter based on mass transfer across the external surface of the catalyst. The preferred expressions for the effectiveness factor are summarized below for nth-order irreversible chemical kinetics when the rate law is only a function of the molar density of one reactant:

$$\text{Rectangular coordinates:} \qquad E = \frac{1}{\Lambda^2}\left(\frac{d\Psi_A}{d\eta}\right)_{\eta=1} \tag{20-48a}$$

$$\text{Cylindrical coordinates:} \qquad E = \frac{2}{\Lambda^2}\left(\frac{d\Psi_A}{d\eta}\right)_{\eta=1} \tag{20-48b}$$

$$\text{Spherical coordinates:} \qquad E = \frac{3}{\Lambda^2}\left(\frac{d\Psi_A}{d\eta}\right)_{\eta=1} \tag{20-48c}$$

Equations (20-48) require knowledge of the dimensionless molar density profile to calculate the molar flux of reactant A into the pellet via Fick's law. At first glance, equations (20-47) allow one to calculate the effectiveness factor for zeroth-order kinetics via trivial integration that does not require knowledge of the molar density profile, because $n = 0$. Hence,

$$\text{Rectangular coordinates:} \qquad E = \int_0^1 d\eta = 1 \tag{20-49a}$$

$$\text{Cylindrical coordinates:} \qquad E = 2\int_0^1 \eta\, d\eta = 1 \tag{20-49b}$$

$$\text{Spherical coordinates:} \qquad E = 3\int_0^1 \eta^2\, d\eta = 1 \tag{20-49c}$$

These answers are correct for zeroth-order kinetics only when reactants exist throughout the entire volume of catalyst at small values of the intrapellet Damkohler number. When diffusion of reactants into the central core of the catalyst is the rate-limiting process and $\Lambda > \Lambda_{\text{critical}}$, one should only perform a volumetric average of the kinetic rate law in regions that are not starved of reactants. It is critically important to consider this situation for zeroth-order kinetics because the rate law does not vanish when reactants are depleted. For nth-order kinetics in general, where $n > 0$, the rate law vanishes when reactants are not present, so no errors are introduced by averaging the rate of reactant consumption throughout the entire pellet volume. If the intrapellet Damkohler number is greater than its critical value, then the reactor design engineer manually turns off the rate law in the central core of the catalyst for zeroth-order kinetics by introducing the concept of the critical dimensionless spatial coordinate, η_{critical}. In agreement with previous discussions of η_{critical}, it is necessary to modify the integral expressions for the effectiveness factor, given by equations (20-49), when the kinetics are zeroth-order. This modification restricts the range of integration at

large intrapellet Damkohler numbers (i.e., $\Lambda > \Lambda_{\text{critical}}$):

Rectangular coordinates: $$E = \int_{\eta_{\text{critical}}}^{1} d\eta = 1 - \eta_{\text{critical}} = \frac{\sqrt{2}}{\Lambda} \tag{20-50a}$$

Cylindrical coordinates: $$E = 2\int_{\eta_{\text{critical}}}^{1} \eta\, d\eta = 1 - (\eta_{\text{critical}})^2 \tag{20-50b}$$

Spherical coordinates: $$E = 3\int_{\eta_{\text{critical}}}^{1} \eta^2\, d\eta = 1 - (\eta_{\text{critical}})^3 \tag{20-50c}$$

Obviously, the molar density profile is required to calculate the effectiveness factor for zeroth-order kinetics when $\Lambda > \Lambda_{\text{critical}}$ because $\eta_{\text{critical}} = f(\Lambda)$ is defined by $\Psi_A = 0$.

Problem. Consider zeroth-order chemical kinetics in pellets with rectangular, cylindrical and spherical symmetry. Dimensionless molar density profiles have been developed in Chapter 16 for each catalyst geometry. Calculate the effectiveness factor when the intrapellet Damkohler number is greater than its critical value by invoking mass transfer of reactant A into the pellet across the external surface. Compare your answers with those given by equations (20-50).

20-3.3 First-Order Irreversible Chemical Reaction

Mass flux of reactant A into the catalyst across its external surface is employed to develop analytical expressions for the effectiveness factor in terms of the intrapellet Damkohler number. Reactant molar density profiles for diffusion and first-order irreversible reaction have been developed in three coordinate systems, and these profiles in Chapter 17 represent the starting point to calculate the dimensionless concentration gradient on the external surface of the catalyst. In each case, the reader should verify these effectiveness factor results by volumetrically averaging the dimensionless molar density profile throughout the pellet via equations (20-47) with $n = 1$, realizing that it is not necessary to introduce a critical dimensionless spatial coordinate when the kinetics are first-order.

Flat-Slab or Porous Wafer Catalysts. Basic information for the dimensionless molar density profile of reactant A within these catalyst is (see Section 17-1):

$$\Psi_A(\eta; \Lambda) = \frac{\cosh \Lambda\eta}{\cosh \Lambda} \tag{20-51}$$

The effectiveness factor in rectangular coordinates is calculated using equation (20-48*a*):

$$E = \frac{1}{\Lambda^2}\left(\frac{d\Psi_A}{d\eta}\right)_{\eta=1} = \frac{1}{\Lambda^2}\frac{(\Lambda \sinh \Lambda\eta)_{\eta=1}}{\cosh \Lambda} = \frac{\tanh \Lambda}{\Lambda} \tag{20-52}$$

Long Cylindrical Catalysts. This problem is more difficult because Bessel functions are required to solve the mass transfer equation. The dimensionless molar density profile for reactant A is given by the following classic result (see Section 17-2):

$$\Psi_A(\eta; \Lambda) = \frac{I_0(\Lambda\eta)}{I_0(\Lambda)} \tag{20-53}$$

where I_0 is the modified or hyperbolic zeroth-order Bessel function of the first kind. In cylindrical coordinates, the effectiveness factor is calculated via equation (20-48*b*):

$$E = \frac{2}{\Lambda^2}\left(\frac{d\Psi_A}{d\eta}\right)_{\eta=1} = \frac{2}{\Lambda^2}\left[\frac{\Lambda I_1(\Lambda\eta)}{I_0(\Lambda)}\right]_{\eta=1} = \frac{2}{\Lambda}\left\{\frac{I_1(\Lambda)}{I_0(\Lambda)}\right\} \tag{20-54}$$

where $I_1(\Lambda)$ is the modified or hyperbolic first-order Bessel function of the first kind.

Spherical Catalytic Pellets. Diffusion and first-order chemical reaction in spherical coordinates is a classic chemical engineering problem. Basic information for the dimensionless molar density profile of reactant A is given by (see Section 17-3):

$$\Psi_A(\eta; \Lambda) = \frac{\sinh \Lambda\eta}{\eta \sinh \Lambda} \tag{20-55}$$

The product rule is required to calculate the concentration gradient from (20-55):

$$\frac{d\Psi_A}{d\eta} = \frac{1}{\sinh \Lambda}\left\{\frac{\Lambda \cosh \Lambda\eta}{\eta} - \frac{\sinh \Lambda\eta}{\eta^2}\right\} \tag{20-56}$$

In spherical coordinates, one calculates the effectiveness factor via equation (20-48*c*):

$$\begin{aligned} E = \frac{3}{\Lambda^2}\left(\frac{d\Psi_A}{d\eta}\right)_{\eta=1} &= \frac{3}{\Lambda^2 \sinh \Lambda}\left\{\frac{\Lambda}{\eta}\cosh \Lambda\eta - \frac{1}{\eta^2}\sinh \Lambda\eta\right\}_{\eta=1} \\ &= \frac{3}{\Lambda^2}\left\{\frac{\Lambda}{\tanh \Lambda} - 1\right\} \end{aligned} \tag{20-57}$$

It is rather straightforward to employ numerical methods and demonstrate that the effectiveness factor approaches unity in the reaction-rate-controlled regime, where Λ approaches zero. Analytical proof of this claim for first-order irreversible chemical kinetics in spherical catalysts requires algebraic manipulation of equation (20-57) and three applications of l'Hôpital's rule to verify this universal trend for isothermal conditions in catalytic pellets of any shape.

20-4 DIMENSIONLESS CORRELATION BETWEEN THE EFFECTIVENESS FACTOR AND THE INTRAPELLET DAMKOHLER NUMBER

20-4.1 One-Dimensional Diffusion and Either Zeroth or First-Order Irreversible Chemical Reaction

Catalysts with Cylindrical Symmetry. This analysis is based on the mass transfer equation with diffusion and chemical reaction. Basic information has been obtained for the dimensionless molar density profile of reactant A. For zeroth-order kinetics, the molar density is equated to zero at the critical value of the dimensionless radial coordinate, $\eta_{\text{critical}} = f(\Lambda)$. The relation between the critical value of the dimensionless radial coordinate and the intrapellet Damkohler number is obtained by solving the following nonlinear algebraic equation:

$$4 - \Lambda^2(1 - \eta_{\text{critical}}^2) - 2\Lambda^2\eta_{\text{critical}}^2 \ln \eta_{\text{critical}} = 0 \tag{20-58}$$

which appears initially as equation (16-16). Two different, but equivalent, expressions are used to obtain the relation between the effectiveness factor E and the intrapellet Damkohler number for zeroth-order chemical reactions when the Damkohler number (i.e., Λ) is greater than its critical value of 2 in catalysts with cylindrical symmetry. For Damkohler numbers less than the critical value of 2, the critical dimensionless radial coordinate is negative (i.e., $\eta_{\text{critical}} < 0$). This means that reactant A exists throughout the catalyst and that the effectiveness factor is unity. Hence, this analysis focuses on Damkohler numbers that are larger than the critical value of 2, where the critical value of the dimensionless radial coordinate is between 0 and 1, and there are regions within the central core of the catalyst that are inaccessible to reactant A due to diffusional limitations.

$$\begin{aligned} E(\text{zeroth-order kinetics}) &= 1 - \eta_{\text{critical}}^2 \\ &= \frac{4}{\Lambda^2} - 2\eta_{\text{critical}}^2 \ln \eta_{\text{critical}} \end{aligned} \tag{20-59}$$

Effectiveness factors for diffusion and zeroth-order chemical reaction in long cylindrical catalysts, described by equations (20-58) and (20-59), are illustrated in Figure 20-1 and compared with the results for diffusion and first-order irreversible chemical reaction in the same catalyst geometry, given by

$$E(\text{first-order irreversible kinetics}) = \frac{2}{\Lambda}\left\{\frac{I_1(\Lambda)}{I_0(\Lambda)}\right\} \tag{20-60}$$

where $I_0(\Lambda)$ is the modified or hyperbolic zeroth-order Bessel function of the first kind with argument Λ, and $I_1(\Lambda)$ is the modified or hyperbolic first-order Bessel function of the first kind with argument Λ.

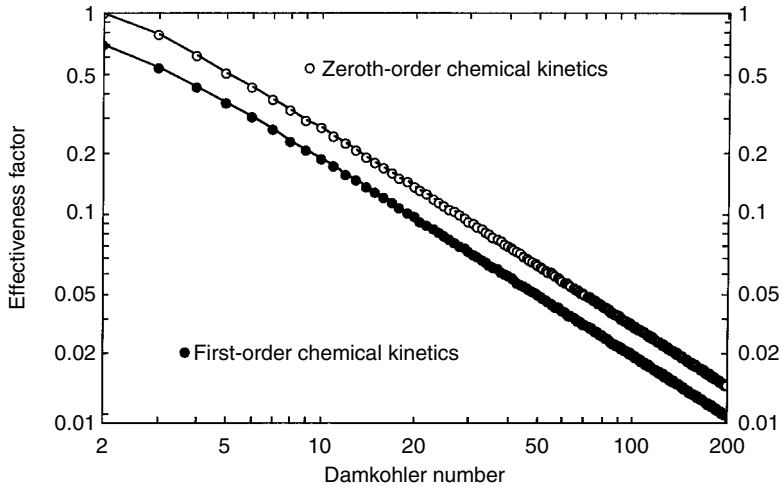

Figure 20-1 Dimensionless correlations between the effectiveness factor and the intrapellet Damkohler number for radial diffusion and *n*th-order irreversible chemical kinetics in long porous cylindrical catalysts (i.e., $n = 0, 1$). The quantity on the horizontal axis is Λ, not Λ^2. The cylindrical radius R is the characteristic length in the definition of Λ.

For more information about Bessel functions, consult Wylie (1975, pp. 394–412) and Abramowitz and Stegun (1972, pp. 355–494).

Catalysts with Spherical Symmetry. This analysis is based on the mass transfer equation with diffusion and chemical reaction in spherical catalysts. For zeroth-order kinetics, the molar density of reactant A is equated to zero at the critical value of the dimensionless radial coordinate, $\eta_{\text{critical}} = f(\Lambda)$. The relation between the critical value of the dimensionless radial coordinate and the intrapellet Damkohler number is obtained by solving the following nonlinear algebraic equation:

$$6 - \Lambda^2(1 - \eta_{\text{critical}}^2) - 2\Lambda^2(\eta_{\text{critical}}^3 - \eta_{\text{critical}}^2) = 0 \qquad (20\text{-}61)$$

which appears initially as equation (16-25). The relation between the effectiveness factor E and the intrapellet Damkohler number for zeroth-order chemical reactions is calculated when the Damkohler number (i.e., Λ) is greater than its critical value of $\sqrt{6}$ in catalysts with spherical symmetry. For Damkohler numbers less than the critical value, the critical dimensionless radial coordinate is negative (i.e., $\eta_{\text{critical}} < 0$). This means that reactants exist throughout the catalyst and that the effectiveness factor is unity. Hence, this analysis focuses on Damkohler numbers that are larger than $\Lambda_{\text{critical}} = \sqrt{6}$, which corresponds to critical values of the dimensionless radial coordinate between 0 and 1, and the internal core of

the catalyst is inaccessible to reactant A due to diffusional limitations.

$$E(\text{zeroth-order kinetics}) = 1 - \eta^3_{\text{critical}} \tag{20-62}$$

Effectiveness factors for diffusion and zeroth-order chemical kinetics in spherical catalysts, described by equations (20-61) and (20-62), are illustrated in Figure 20-2 and compared with the results for diffusion and first-order irreversible chemical kinetics in the same catalyst geometry, given by

$$E(\text{first-order kinetics}) = \frac{3}{\Lambda^2}\left\{\frac{\Lambda}{\tanh \Lambda} - 1\right\} \tag{20-63}$$

20-4.2 One-Dimensional Diffusion and Either Zeroth-, First-, or Second-Order Chemical Reaction in Catalytic Pellets with Rectangular, Cylindrical, or Spherical Geometry

Using log-log coordinates, graphs are provided in Figure 20-3 through Figure 20-6 which illustrate the effectiveness factor versus intrapellet Damkohler number (i.e., Λ) for nth-order irreversible chemical reactions, where $n = 0, 1, 2$. Each graph corresponds to catalysts with different symmetry, and contains data for three different reaction orders. The characteristic length L in the definition of the Damkohler number is:

1. One-half of the thickness of the catalyst in its thinnest dimension for flat-slabs or porous wafers
2. The radius of long cylindrical catalysts
3. The radius of spherical catalysts

The following expressions for the effectiveness factor E have been derived for nth-order irreversible chemical kinetics ($n = \beta$) based on a volumetric average of the rate law and diffusion across the external surface of the catalyst:

$$E = \alpha \int_{\eta_{\text{critical}}}^{1} \eta^{\alpha-1} \Psi_A^{\beta}(\eta; \Lambda)\, d\eta = \frac{\alpha}{\Lambda^2}\left(\frac{d\Psi_A}{d\eta}\right)_{\eta=1} \tag{20-64}$$

where $\alpha = 1, 2, 3$ for catalysts with rectangular, cylindrical, or spherical symmetry, respectively. The intrapellet Damkohler number for reactant A is

$$\Lambda^2 = \frac{k_n (C_{A,\,\text{surface}})^{n-1} L^2}{\mathfrak{D}_{A,\,\text{effective}}} \tag{20-65}$$

k_n [=] (volume/mole)$^{n-1}$/time is an nth-order kinetic rate constant for pseudo-volumetric reactions based on molar densities, and η_{critical} is a function of Λ. The range $0 \le \eta \le \eta_{\text{critical}}$ represents a region in the central core of the catalyst that is inaccessible to reactants for zeroth-order kinetics. For βth-order kinetics

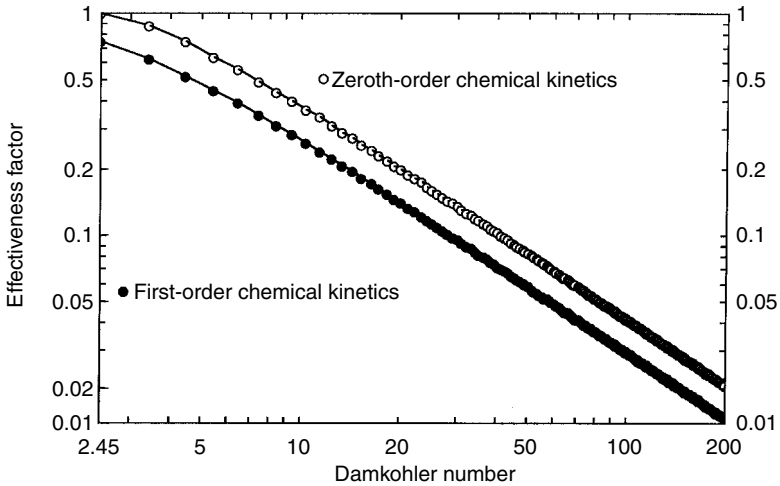

Figure 20-2 Dimensionless correlations between the effectiveness factor and the intrapellet Damkohler number for radial diffusion and *n*th-order irreversible chemical kinetics in porous catalysts with spherical symmetry (i.e., $n = 0, 1$). The quantity on the horizontal axis is Λ, not Λ^2. The spherical radius R is the characteristic length in the definition of Λ.

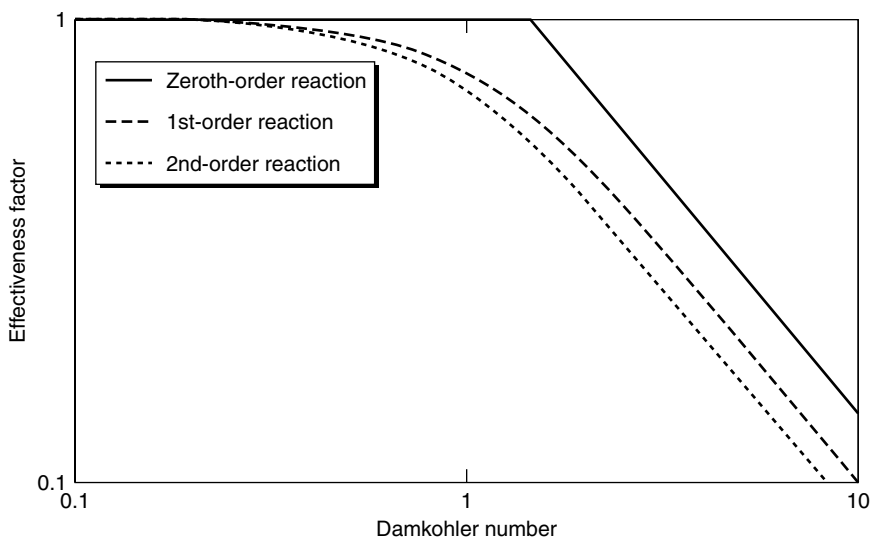

Figure 20-3 Dimensionless correlations between the effectiveness factor and the intrapellet Damkohler number for one-dimensional diffusion and *n*th-order irreversible chemical kinetics in porous catalysts with rectangular symmetry (i.e., $n = 0, 1, 2$). The quantity on the horizontal axis is Λ, not Λ^2. One-half of the thickness of these porous wafer-like catalysts is the characteristic length in the definition of Λ.

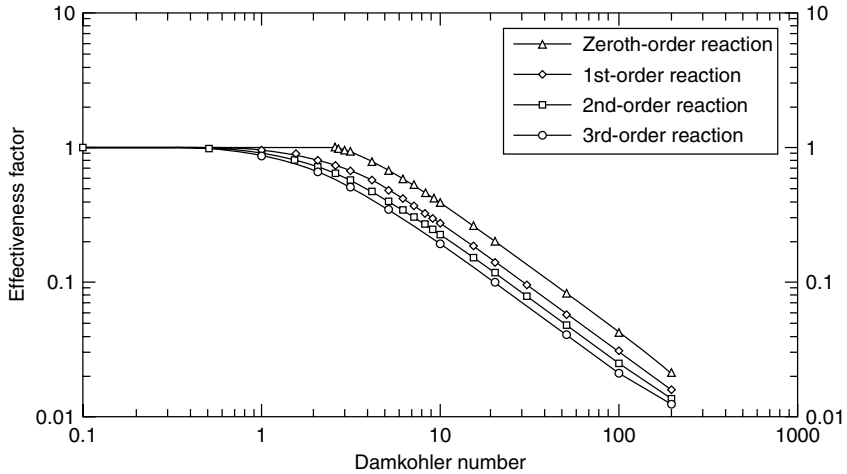

Figure 20-4 Dimensionless correlations between the effectiveness factor and the intrapellet Damkohler number for radial diffusion and nth-order irreversible chemical kinetics in porous catalysts with spherical symmetry (i.e., $n = 0, 1, 2, 3$). The quantity on the horizontal axis is Λ, not Λ^2. The spherical radius R is the characteristic length in the definition of Λ.

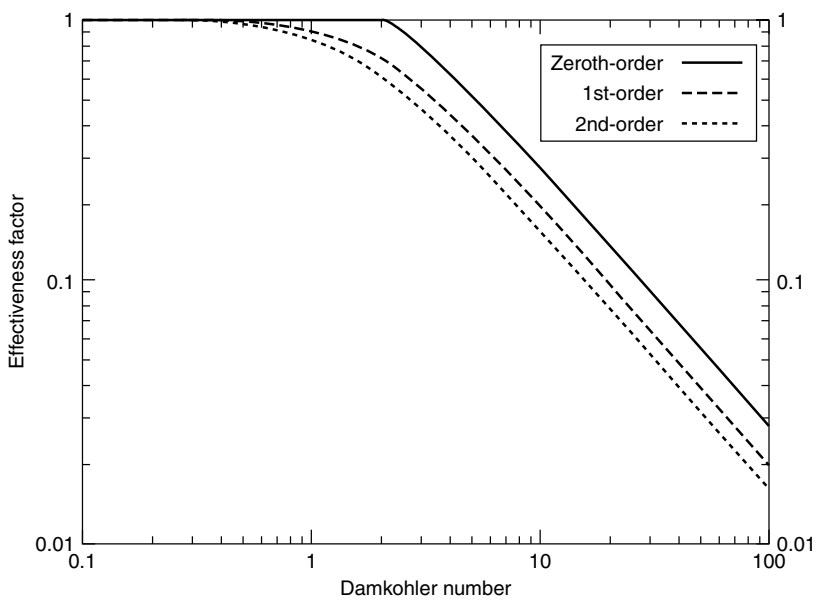

Figure 20-5 Dimensionless correlations between the effectiveness factor and the intrapellet Damkohler number for radial diffusion and nth-order irreversible chemical kinetics in long porous cylindrical catalysts (i.e., $n = 0, 1, 2$). The quantity on the horizontal axis is Λ, not Λ^2. The cylindrical radius R is the characteristic length in the definition of Λ.

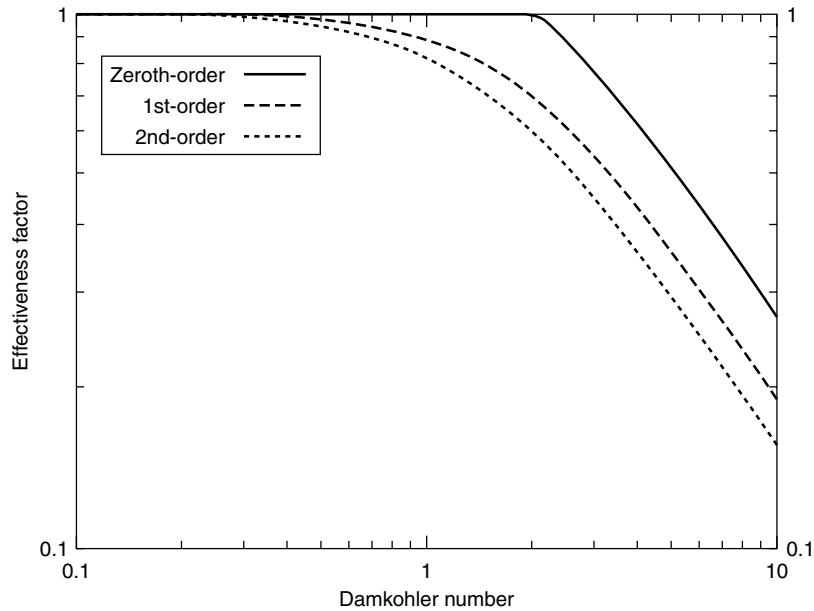

Figure 20-6 Expanded view of the dimensionless correlations between the effectiveness factor and the intrapellet Damkohler number for radial diffusion and nth-order irreversible chemical kinetics in long porous cylindrical catalysts (i.e., $n = 0, 1, 2$). The quantity on the horizontal axis is Λ, not Λ^2. The cylindrical radius R is the characteristic length in the definition of Λ.

when $\beta > 0$, $\eta_{\text{critical}} = 0$. The following problems must be addressed before one can generate effectiveness factor graphs for second-order irreversible chemical kinetics via numerical methods:

1. It is necessary to solve a second-order ordinary differential equation (ODE) with diffusion and chemical reaction. However, most software packages can only solve first-order ODEs.
2. Even though it is possible to convince software packages that second-order ODEs can be solved using techniques for first-order ODEs, all numerical methods require that both boundary condition for a second-order ODE must be known at the starting point. In other words, both boundary conditions must be known at the same value of the spatial coordinate. Split boundary value problems do not conform to this requirement. The mass balance for diffusion and chemical reaction is typically classified as a *split boundary value problem*.
3. In cylindrical and spherical coordinates, the diffusion term in the mass transfer equation includes a factor of $1/r$ when it is expanded. This cannot be evaluated numerically at $r = 0$, which corresponds to the center of the catalyst.

Consult the following references for more information about the effect of catalyst shape on the effectiveness factor: Knudsen *et al.* (1966), and Rester and Aris (1969).

PROBLEMS

20-1. The following irreversible heterogeneous catalytic reaction is elementary and exothermic, and it occurs on active sites within the internal pores of a thin wafer:

$$A_2 + B \longrightarrow C$$

Diatomic gas A_2 undergoes dissociative adsorption and gases B and C experience single-site adsorption. Chemical reaction on the catalytic surface is the slowest step. Stoichiometric proportions of A_2 and B are present initially.

(a) If the intermediate complex occupies three active sites, then how many elementary steps are required to describe this heterogeneous reaction on the catalytic surface, including the adsorption and desorption steps?

(b) Write the Hougen–Watson model for the kinetic rate law $\mathfrak{R}_{HW}$ with units of moles per area per time if the intermediate complex is not included in the mechanism. Remember that reaction on the catalytic surface is rate limiting.

(c) The catalyst is a porous wafer with a thickness of 6 mm in the thinnest dimension. Write an expression for the intrapellet Damkohler number of reactant A_2 based on the Hougen–Watson model in part (b). Be sure that your final answer includes k_{forward} with units of moles per area per time for the surface-catalyzed chemical reaction.

(d) It is desired to approximate the Hougen–Watson model by the best pseudo-volumetric zeroth-order rate law with kinetic rate constant $k_{0,\text{ pseudovolumetric}}$ such that $S_m \rho_{\text{app}} \mathfrak{R}_{HW}$ can be replaced by $k_{0,\text{ pseudovolumetric}}$. What are the units of $k_{0,\text{ pseudovolumetric}}$? Derive the equation for $k_{0,\text{ pseudovolumetric}}$ in five lines of work, or less.

Questions (e) through (k) are based on pseudo-volumetric zeroth-order kinetics.

(e) The catalyst is a porous wafer with a thickness of 6 mm in the thinnest dimension. Write an expression for the intrapellet Damkohler number of reactant A_2 based on the best pseudo-volumetric zeroth-order kinetic rate constant $k_{0,\text{ pseudovolumetric}}$ from part (d).

(f) The intrapellet Damkohler number for reactant A_2 is $\Lambda^2 = 18$, based on your calculation from part (e) using the best pseudo-volumetric zeroth-order kinetic rate constant $k_{0,\text{ pseudovolumetric}}$ from

part (d). Sketch the dimensionless concentration profile of reactant A_2 within the porous wafer as a function of the dimensionless spatial coordinate η measured in the thinnest dimension. Be as quantitative as possible on the horizontal axis, which contains the dimensionless spatial coordinate η.

(g) Write an analytical expression for the molar density profile $\Psi_A(\eta)$ in part (f).

(h) Calculate the effectiveness factor that is consistent with the information in parts (f) and (g). A numerical answer is required here.

(i) The thickness of the porous catalytic wafer is reduced from 6 mm to 2 mm, and the intrapellet Damkohler number is calculated via $k_{0,\,\text{pseudovolumetric}}$ from part (d). Sketch the dimensionless concentration profile of reactant A_2 within the porous wafer as a function of the dimensionless spatial coordinate η measured in the thinnest dimension. Be as quantitative as possible on the horizontal axis, which contains the dimensionless spatial coordinate η.

(j) Write an analytical expression for the molar density profile $\Psi_A(\eta)$ in part (i).

(k) Calculate the effectiveness factor that is consistent with the information in parts (i) and (j). A numerical answer is required here.

The overall objective is to obtain the highest equilibrium conversion of reactants (i.e., $A_2 + B$) to product C.

(l) Should you operate this heterogeneous catalytic reactor at 50 or 75°C?

(m) Should you operate this heterogeneous catalytic reactor at a total pressure of 1 or 2 atm?

20-2. The following irreversible heterogeneous catalytic reaction is elementary and exothermic, and it occurs on active sites within the internal pores of a thin wafer:

$$A_2 + 2B \longrightarrow C$$

Diatomic gas A_2 undergoes dissociative adsorption, gas B does not require an active site on the catalytic surface because it attacks adsorbed atomic A from the gas phase, and gas C experiences single-site adsorption. Chemical reaction on the catalytic surface is rate limiting in the three-step mechanism. Stoichiometric proportions of A_2 and B are present initially (i.e., a 1 : 2 feed of A_2 and B).

(a) The catalyst is a porous wafer with a thickness of 2 mm in the thinnest dimension. Write an expression for the intrapellet Damkohler number of reactant A_2. Be sure that your final answer includes k_{forward} with units of moles per area per time per square atmosphere for the

surface-catalyzed chemical reaction, when the heterogeneous rate law is written in terms of surface coverage fractions.

The Hougen–Watson model is approximated by the best pseudo-volumetric zeroth-order rate law with kinetic rate constant $k_{0,\,\text{pseudovolumetric}}$ such that $S_m \rho_{\text{app}} \Re_{\text{HW}}$ can be replaced by $k_{0,\,\text{pseudovolumetric}}$. The questions below are based on pseudo-volumetric zeroth-order kinetics.

(b) The catalyst is a porous wafer with a thickness of 2 mm in its thinnest dimension. Write an expression for the intrapellet Damkohler number of reactant A_2 based on the best pseudo-volumetric zeroth-order kinetic rate constant $k_{0,\,\text{pseudovolumetric}}$.

(c) The intrapellet Damkohler number for reactant A_2 is $\Lambda_A^2 = 8$, based on your calculation from part (b) using the best pseudo-volumetric zeroth-order kinetic rate constant $k_{0,\,\text{pseudovolumetric}}$. Sketch the dimensionless concentration profile of reactant A_2 within the porous wafer as a function of the dimensionless spatial coordinate η measured in the thinnest dimension. Be as quantitative as possible on the horizontal axis, which contains the dimensionless spatial coordinate η.

(d) Write an analytical expression for the molar density profile $\Psi_A(\eta)$ in part (c).

(e) Calculate the effectiveness factor that is consistent with the information in parts (c) and (d). A numerical answer is required here.

(f) What is the maximum thickness of this porous wafer, in its thinnest dimension, such that reactant A_2 exists everywhere throughout the catalyst? A numerical answer is required here, in millimeters.

20-3. The dimensionless molar density profile of reactant A within a flat-slab porous catalyst is illustrated in Figure 20-7 for the following values of the intrapellet Damkohler number:

$$\Lambda^2_{\text{A, intrapellet}} = 1$$
$$\Lambda^2_{\text{A, intrapellet}} = 2$$
$$\Lambda^2_{\text{A, intrapellet}} = 9$$
$$\Lambda^2_{\text{A, intrapellet}} = 25$$
$$\Lambda^2_{\text{A, intrapellet}} = 100$$

The reaction kinetics are zeroth-order. Dimensionless molar density Ψ_A is on the vertical axis and dimensional spatial coordinate η is on the horizontal axis.

(a) Calculate the effectiveness factor for each value of the intrapellet Damkohler number when the reaction kinetics are irreversible and zeroth-order. Five numerical answers are required here.

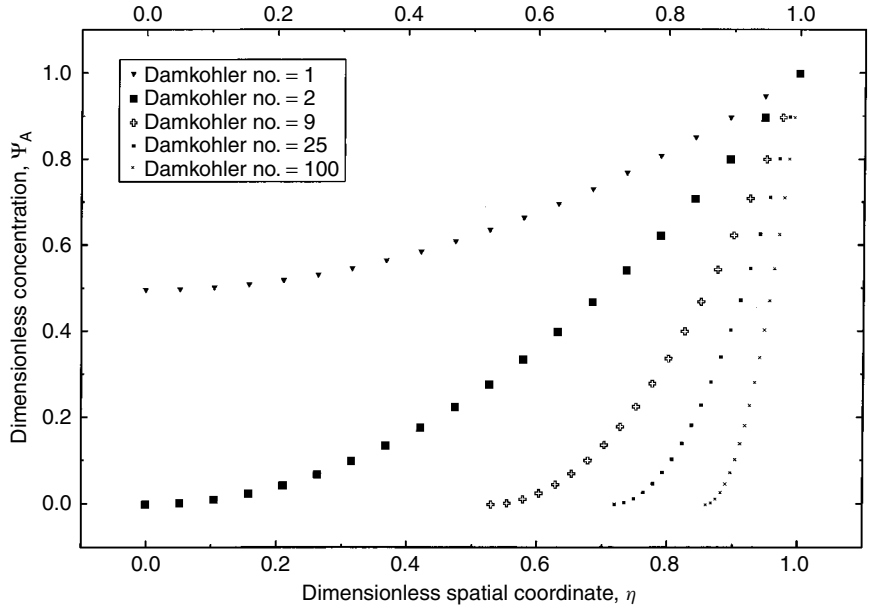

Figure 20-7 Effect of the intrapellet Damkohler number on dimensionless reactant concentration profiles $\Psi_A(\eta)$ for one-dimensional diffusion and pseudo-homogeneous zeroth-order chemical kinetics in porous catalysts with rectangular symmetry.

(b) Calculate the effectiveness factor for each value of the intrapellet Damkohler number when the reaction kinetics are irreversible and first-order. Five numerical answers are required here.

(c) If the reaction kinetics are irreversible and second-order, and the rate law is only a function of the molar density of one reactant, then calculate the gradient of the dimensionless molar density of reactant A at the external surface of the catalyst when $\Lambda^2_{A,\,\text{intrapellet}} = 9$.

20-4. Obtain an analytical expression for the effectiveness factor (i.e., E vs. η_{critical}) in spherical catalysts when the chemical kinetics are zeroth-order and the intrapellet Damkohler number is greater than its critical value. Use the definition of the effectiveness factor that is based on mass transfer via diffusion across the external surface of the catalyst.

20-5. Consider one-dimensional diffusion and zeroth-order chemical reaction in a flat-slab porous wafer-type catalyst. The conditions are approximately isothermal and the intrapellet Damkohler number of reactant A is $\Lambda_{A,\,\text{intrapellet}} = \sqrt{8}$. The mass transfer equation is solved numerically, not analytically.

(a) What set of ordinary differential equations must be solved?

(b) What boundary conditions are required?

(c) What is the numerical value of the effectiveness factor?

20-6. For a particular experiment in a packed catalytic tubular reactor, the chemical kinetics can be approximated by a zeroth-order rate law where the best value for the zeroth-order rate constant is calculated via the formalism on pages 459 and 460. At what value of the intrapellet Damkohler number $\Lambda_{A,\,\text{intrapellet}}$ does reactant A occupy 75% by volume of the catalyst if the porous pellets are **(a)** spherical, **(b)** long cylinders, and **(c)** wafer-like?

(d) Provide a brief explanation of why the intrapellet Damkohler number is not the same for all three catalyst shapes.

(e) Sketch the dimensionless molar density profile of reactant A vs. spatial coordinate η for a long cylindrical catalyst in part (b), and be quantitative on both axes.

20-7. Consider one-dimensional diffusion and nth-order irreversible chemical reaction in a porous catalyst with rectangular symmetry, like a porous wafer. The intrapellet Damkohler number for reactant A is $\Lambda_A^2 = 8$ when the characteristic length is one-half of the thickness of the wafer in its thinnest dimension. Calculate the dimensionless molar density of reactant A at the center of the catalyst (i.e., a numerical answer is required in each case) when

(a) $n = 0$ for zeroth-order chemical kinetics.

(b) $n = 1$ for first-order chemical kinetics.

(c) $n = 2$ for second-order chemical kinetics.

(d) Without using equations, qualitatively describe why the molar density of reactant A at the center of the catalyst increases for larger values of n.

(e) Calculate the effectiveness factor in parts (a), (b), and (c). Three numerical answers are required.

20-8. (a) You are reviewing a manuscript that has been submitted to the *International Journal of Catalysis and Surface Science.* The authors have used the equation below to calculate the dimensionless correlation between the effectiveness factor and the intrapellet Damkohler number for an irreversible second-order chemical reaction that occurs within the internal pores of flat-slab catalysts, where the rate law depends only on the molar density of reactant A.

$$E = \frac{\frac{2}{3}\sqrt{1 - \Psi_A^3(\eta = 0)}}{\displaystyle\int_{\Psi_A(\eta=0)}^{1} \frac{dx}{\sqrt{x^3 - \Psi_A^3(\eta = 0)}}} \qquad \text{where } \Psi_A(\eta = 0) \text{ depends on } \Lambda$$

In the equation above, Ψ_A ($= C_A/C_{A,\,surface}$) is the dimensionless molar density of reactant A, η is the dimensionless spatial coordinate in the thinnest dimension of the catalyst, and $\eta = 0$ defines the midplane of the catalyst. The editor of the journal has asked for your opinion of this research. Should the manuscript be published, or is there an error in the equation above? Provide support for your recommendation. *Hint:* Let $p = (d\Psi_A/d\eta)$, then substitute for the diffusion term in the mass transfer equation:

$$\frac{d^2\Psi_A}{d\eta^2} = \frac{dp}{d\eta} = \frac{dp}{d\Psi_A}\left(\frac{d\Psi_A}{d\eta}\right) = p\frac{dp}{d\Psi_A} = \frac{d(p^2/2)}{d\Psi_A}$$

and solve for p. The effectiveness factor can be written directly in terms of $p(\eta = 1)$.

(b) It should be obvious that the equation under review cannot be evaluated quickly and easily when $\Psi_A(\eta = 0) = 1$. However, the authors have used numerical techniques to generate a graph of the effectiveness factor vs. the intrapellet Damkohler number based on the equation above. What numerical value of the effectiveness factor should you expect to find on the graph when $\Psi_A(\eta = 0) = 1$?

Answer: The dimensionless mass transfer equation in rectangular coordinates with one-dimensional diffusion and *n*th-order chemical reaction represents the starting point for a generic solution to part (a). The dimensionless molar density of reactant A must satisfy

$$\frac{d^2\Psi_A}{d\eta^2} = \Lambda^2(\Psi_A)^n$$

subject to the following split boundary conditions:

$$\frac{d\Psi_A}{d\eta} = 0 \qquad \text{at } \eta = 0$$

$$\Psi_A = 1 \qquad \text{at } n = 1$$

The hint is employed to rewrite the mass balance with Ψ_A as the independent variable because *n*th-order irreversible chemical reaction is expressed in terms of Ψ_A, not η. In other words, it is possible to integrate $(\Psi_A)^n\, d\Psi_A$ without having the final expression for Ψ_A, but $(\Psi_A)^n\, d\eta$ cannot be integrated unless Ψ_A is known as a function of η. Hence,

$$\frac{d\{p^2/2\}}{d\Psi_A} = \Lambda^2(\Psi_A)^n$$

This first-order ordinary differential equation for p as a function of Ψ_A is integrated via separation of variables, subject to

$$p = \frac{d\Psi_A}{d\eta} = 0 \qquad \text{at } \eta = 0$$

Then, the effectiveness factor is calculated by evaluating p at $\eta = 1$ via mass flux of reactant A into the pellet across its external surface. In rectangular coordinates,

$$E = \frac{1}{\Lambda^2}\left(\frac{d\Psi_A}{d\eta}\right)_{\eta=1} = \frac{p(\eta = 1)}{\Lambda^2}$$

Separation of variables yields

$$\int d\left(\frac{p^2}{2}\right) = \Lambda^2 \int (\Psi_A)^n \, d\Psi_A$$

Integration from the center of the catalyst (i.e., $\eta = 0$) yields the following general result for p:

$$p^2 = \frac{2}{n+1}\Lambda^2\{(\Psi_A)^{n+1} - [\Psi_A(\eta = 0)]^{n+1}\}$$

The generalized dimensionless correlation between the effectiveness factor and the intrapellet Damkohler number for nth-order irreversible chemical reaction [i.e., $\Re = k_n(C_A)^n$] is

$$E = \frac{p(\eta = 1)}{\Lambda^2} = \left(\frac{2}{n+1}\right)^{1/2} \frac{1}{\Lambda}\sqrt{1 - [\Psi_A(\eta = 0)]^{n+1}}$$

When the kinetics are second-order and $n = 2$,

$$E = \sqrt{\frac{2}{3}}\frac{1}{\Lambda}\sqrt{1 - \Psi_A^3(\eta = 0)}$$

which is the correct answer, but it doesn't match the one provided in the manuscript. The authors have removed the intrapellet Damkohler number from the preceding expression for the effectiveness factor. Since $p = d\Psi_A/d\eta$, one separates variables and solves for Λ from the generalized solution for p:

$$p = \frac{d\Psi_A}{d\eta} = \Lambda\left(\frac{2}{n+1}\right)^{1/2} \sqrt{(\Psi_A)^{n+1} - [\Psi_A(\eta = 0)]^{n+1}}$$

Separation of variables yields

$$\frac{d\Psi_A}{\{(\Psi_A)^{n+1} - [\Psi_A(\eta = 0)]^{n+1}\}^{1/2}} = \Lambda \left(\frac{2}{n+1}\right)^{1/2} d\eta$$

Integration from the center of the catalyst (i.e., $\eta = 0$) to its external surface (i.e., $\eta = 1$) produces the following result:

$$\Lambda = \left(\frac{n+1}{2}\right)^{1/2} \int_{\Psi_A(\eta=0)}^{1} \frac{dx}{\sqrt{x^{n+1} - [\Psi_A(\eta = 0)]^{n+1}}}$$

Now it is possible to remove the intrapellet Damkohler number from the generalized integral expression for the effectiveness factor:

$$E = \frac{2}{n+1} \frac{\{1 - [\Psi_A(\eta = 0)]^{n+1}\}^{1/2}}{\displaystyle\int_{\Psi_A(\eta=0)}^{1} \frac{dx}{\sqrt{x^{n+1} - [\Psi_A(\eta = 0)]^{n+1}}}}$$

For second-order irreversible chemical kinetics (i.e., $n = 2$), the preceding equation reduces to the one provided by the authors in their manuscript:

$$E = \frac{2}{3} \frac{\{1 - [\Psi_A(\eta = 0)]^3\}^{1/2}}{\displaystyle\int_{\Psi_A(\eta=0)}^{1} \frac{dx}{\sqrt{x^3 - [\Psi_A(\eta = 0)]^3}}}$$

The intrapellet Damkohler number affects the dimensionless reactant molar density at the center of the catalyst, $\Psi_A(\eta = 0)$. In other words, $\Psi_A(\eta = 0)$ is smaller when Λ is larger, as a consequence of diffusional limitations. If one adopts this method of solution for nth-order irreversible chemical kinetics, then the strategy to obtain the dimensionless correlation between the effectiveness factor and the intrapellet Damkohler number is as follows:

1. Choose a value for the intrapellet Damkohler number, Λ.

2. Use trial and error to determine $\Psi_A(\eta = 0)$ that satisfies the following integral equation:

$$\Lambda = \left(\frac{n+1}{2}\right)^{1/2} \int_{\Psi_A(\eta=0)}^{1} \frac{dx}{\sqrt{x^{n+1} - [\Psi_A(\eta = 0)]^{n+1}}}$$

Remember that $0 \leq \Psi_A(\eta = 0) \leq 1$ and $\Psi_A(\eta = 0)$ decreases when Λ is larger.

3. When the correct value for the dimensionless molar density of reactant A is found at the center of the catalyst, one calculates the effectiveness factor as follows:

$$E = \left(\frac{2}{n+1}\right)^{1/2} \frac{1}{\Lambda}\sqrt{1 - [\Psi_A(\eta = 0)]^{n+1}}$$

If $\Psi_A(\eta = 0) = 1$ as indicated in part (b), then diffusion does not hinder the ability of reactants to populate the central core of the catalyst. Furthermore, chemical reaction does not deplete reactant A because its molar density at the center of the catalyst is equivalent to that on the external surface. This situation occurs when $\Lambda \to 0$ and the catalyst operates in the reaction-rate-controlled regime. Hence, the effectiveness factor is unity under isothermal conditions. This result can be obtained mathematically from the integral expression for the effectiveness factor by setting $\Psi_A(\eta = 0) = 1 - \varepsilon$, where $\varepsilon \leq 10^{-5}$.

20-9. Consider the following nine examples of diffusion and chemical reaction in porous catalysts where the irreversible kinetic rate law is only a function of the molar density of reactant A. Identify the problems tabulated below that yield analytical solutions for (a) the molar density of reactant A, and (b) the dimensionless correlation between the effectiveness factor and the intrapellet Damkohler number.

Catalyst Shape	Kinetic Rate Law		
Flat-slab wafers	Zeroth-order	First-order	Second-order
Long cylindrical pellets	Zeroth-order	First-order	Second-order
Spherical pellets	Zeroth-order	First-order	Second-order

20-10. What is the defining expression for the isothermal effectiveness factor in spherical catalysts? Reactant A is consumed by three independent first-order irreversible chemical reactions on the interior catalytic surface. Your final expression should be based on mass transfer via diffusion and include the reactant concentration gradient at the external surface of the catalyst, where $\eta = 1$. Define the intrapellet Damkohler number in your final answer.

20-11. Two expressions are given below to calculate the effectiveness factor E. The first one is exact for nth-order irreversible chemical reaction in catalytic pellets, where α is a geometric factor that accounts for shape via the surface-to-volume ratio. The second expression is an approximation at large values of the intrapellet Damkohler number Λ in the diffusion-limited regime.

(1) $E = (\alpha/\Lambda^2)(d\Psi_A/d\eta)_{\eta=1}$

(2) $E \approx 1/\Lambda$

Is there any inconsistency between these two expressions? In particular, explain why (1) suggests that $E \approx \Lambda^{-2}$, whereas (2) indicates that $E \approx \Lambda^{-1}$.

20-12. **(a)** For a particular chemical reaction that occurs on the internal catalytic surface of a spherical pellet, the kinetics are first-order and irreversible, the chemical reaction time constant is 0.1 s (i.e., $k_1 = 10\ s^{-1}$), and the effective intrapellet diffusivity of reactant A is 0.1 cm^2/s. One requirement is that the effectiveness factor should be greater than 0.3, to obtain reasonable conversion of reactants to products. Calculate the size of each catalytic pellet that will accomplish this task. A numerical answer is required in centimeters. Indicate whether you have calculated the radius or the diameter of the pellet.

(b) Does your calculation in part (a) represent the upper or lower limit on the size of each spherical catalytic pellet?

20-13. What is the most important dimensionless number in mass transfer that is required for isothermal analysis and design of a single porous catalytic pellet?

20-14. *True or False*

(a) At large values of the intrapellet Damkohler number in the diffusion-limited regime, diffusion and chemical reaction in catalytic pellets of any geometry can be described by a boundary layer problem with a very thin mass transfer boundary layer for reactant A, measured inward from the external surface of the catalyst. Hence, for a given kinetic rate law, E vs. Λ is essentially the same for all catalyst geometries at large values of Λ.

(b) In the diffusion-limited regime, if all conditions other than catalyst size are the same, reactants will diffuse further into the central core when the diameter of a spherical pellet is smaller.

(c) For zeroth-order chemical kinetics in long cylindrical catalysts, the rate of conversion of reactants to products is largest when $\Lambda_A^2 = 3$. The cylindrical radius is used as the characteristic length to calculate the intrapellet Damkohler number.

(d) For zeroth-order kinetics, spherical pellets can operate at higher intrapellet Damkohler numbers, relative to long cylinders or wafers, while maintaining the same effectiveness factor because spheres contain most of their volume near the external boundary. The characteristic length is R for spheres and cylinders, and $T/2$ for wafers, where T is the wafer thickness measured in the thinnest dimension.

(e) In the diffusion-limited regime at large values of the intrapellet Damkohler number, the effectiveness factor decreases by a factor of 2 when the volume-to-surface ratio of a single catalytic pellet is doubled. This rule of thumb applies to catalysts of all shapes, and the kinetics can be described by any type of rate law.

Transport Phenomena for Chemical Reactor Design. Laurence A. Belfiore
Copyright © 2003 John Wiley & Sons, Inc.
ISBN: 0-471-20275-4

21

DIFFUSION COEFFICIENTS AND DAMKOHLER NUMBERS WITHIN THE INTERNAL PORES OF CATALYTIC PELLETS

21-1 DEPENDENCE OF INTRAPELLET PORE DIFFUSION ON MOLECULAR SIZE

In Chapter 10, the dimensionless scaling factor in the mass transfer equation with diffusion and chemical reaction was written with subscript j for the jth chemical reaction in a multiple-reaction sequence (see equation 10-10). In the absence of convective mass transfer, the number of dimensionless scaling factors in the mass transfer equation for component i is equal to the number of chemical reactions. Hence, Λ_j^2 corresponds to the Damkohler number for reaction j. The only distinguishing factor between all of these Damkohler numbers for multiple reactions is that the nth-order kinetic rate constant in the jth reaction (i.e., k_j), for a volumetric rate law based on molar densities, changes from one reaction to another. The characteristic length L, the molar density of key-limiting reactant A on the external surface of the catalyst $C_{\text{A, surface}}$, and the effective diffusion coefficient of reactant A, $\mathfrak{D}_{\text{A, effective}}$, are the same in all Damkohler numbers that appear in the dimensionless mass balance for reactant A. In other words,

$$\Lambda_j^2 = \frac{k_j L^2 (C_{\text{A, surface}})^{n-1}}{\mathfrak{D}_{\text{A, effective}}} \tag{21-1}$$

Now, consider the realistic situation where there are j chemical reactions between i species in a mixture. It is possible to construct a Damkohler number for reaction j that is species specific. This is necessary because the effective pore diffusion coefficient within a catalytic pellet is a function of the molecular size of species i. Hence, if reaction j is described by nth-order irreversible chemical kinetics, then the intrapellet Damkohler number of component i, based on the jth chemical

reaction, is

$$\Lambda_{ij}^2 = \frac{k_j L^2 (C_{\text{A, surface}})^{n-1}}{\mathfrak{D}_{i,\text{ effective}}} \tag{21-2}$$

Notice that the molar density of key-limiting reactant A on the external surface of the catalytic pellet is always used as the characteristic quantity to make the molar density of component i dimensionless in all the component mass balances. This chapter focuses on explicit numerical calculations for the effective diffusion coefficient of species i within the internal pores of a catalytic pellet. This information is required before one can evaluate the intrapellet Damkohler number and calculate a numerical value for the effectiveness factor. Hence, $\mathfrak{D}_{i,\text{ effective}}$ is called the *effective intrapellet diffusion coefficient* for species i. When $\mathfrak{D}_{i,\text{ effective}}$ appears in the denominator of Λ_{ij}^2, the dimensionless scaling factor is called the intrapellet Damkohler number for species i in reaction j. When the reactor design focuses on the entire packed catalytic tubular reactor in Chapter 22, it will be necessary to calculate interpellet axial dispersion coefficients and interpellet Damkohler numbers. When there is only one chemical reaction that is characterized by nth-order irreversible kinetics and subscript j is not required, the rate constant in the numerator of equation (21-2) is written as k_n instead of k_j, which signifies that k_n has units of (volume/mole)$^{n-1}$ per time for pseudo-volumetric kinetics. Recall from equation (19-6) on page 493 that second-order kinetic rate constants for a volumetric rate law based on molar densities in the gas phase adjacent to the internal catalytic surface can be written as

$$k_2 = S_m \rho_{\text{app}} k_{f,\text{ surf. Rx}} K_{\text{A}} K_{\text{B}} (RT)^2 \tag{21-3}$$

if reactants A and B undergo single-site adsorption via Langmuir–Hinshelwood mechanisms. Details about the void space within an isolated pellet are required to calculate S_m and ρ_{app}, as described below. The adsorption/desorption equilibrium constants, K_{A} and K_{B} with units of inverse pressure, can be calculated from experimental adsorption isotherms, and $k_{f,\text{ surf. Rx}}$ with units of moles per area per time is the forward rate constant for the heterogeneous surface-catalyzed reaction, where the reaction rate, with units of moles per area per time, is written in terms of surface coverage fractions.

21-1.1 Pore-Size Distribution Functions

The apparent density ρ_{app} of a catalytic pellet is on the order of 1 g/cm^3. The actual definition of ρ_{app} is

$$\rho_{\text{app}} = \frac{\text{pellet mass}}{V_{\text{total}}} \tag{21-4}$$

where V_{total} is the total volume bounded by the external surface of the catalyst. The actual density ρ_{solid} of the solid catalyst, which could be a ceramic, a metal,

a metal alloy, or a metal oxide, is defined as

$$\rho_{\text{solid}} = \rho_{\text{app}} \frac{V_{\text{total}}}{V_{\text{total}} - V_{\text{void}}} = \frac{\rho_{\text{app}}}{1 - \varepsilon_p} \tag{21-5}$$

where V_{void} is the pore volume within the catalyst and ε_p is the intrapellet porosity or void fraction:

$$\varepsilon_p = \frac{V_{\text{void}}}{V_{\text{total}}} = \int_0^\infty f(r)\, dr \tag{21-6}$$

In equation (21-6) for the void fraction ε_p, the pore-size distribution function is given by $f(r)$, and $f(r)\, dr$ represents the fraction of the total volume of an isolated catalytic pellet with pore radii between r and $r + dr$. This is not a normalized distribution function because

$$\int_0^\infty f(r)\, dr = \varepsilon_p \approx 0.50 \tag{21-7}$$

Typically, the pore volume is 40 to 60% of the total volume bounded by the external surface of the catalyst, and $\varepsilon_p \approx 0.50$ is a reasonably good number. The range of pore radii varies from a lower limit of approximately 10 Å to an upper limit slightly above 1 μm (i.e., 10^4 Å). As illustrated below in equation (21-16), smaller pores correspond to a larger internal surface area per volume of catalyst, which is advantageous for converting reactants to products. However, Knudsen diffusion is restricted when the pores are too small because the mean free path of the gas, which varies inversely with gas density, is much larger than the pore diameter.

21-1.2 Evaluating $S_m \rho_{\text{app}}$ Based on Average Pore Radii and Intrapellet Porosity

With the aid of the parallel-pore model, it is possible to calculate the product of ρ_{app} and S_m, which allows one to express heterogeneous kinetic rate laws in pseudo-volumetric form. The parallel-pore model is discussed in greater depth later in this chapter. For the present discussion, it is only necessary to visualize straight cylindrical pores of length L and radius $\langle r_{\text{average}} \rangle$. If Γ represents the total number of pores, then the void volume is

$$V_{\text{void}} = \varepsilon_p V_{\text{total}} = \pi \Gamma \langle r_{\text{average}} \rangle^2 L \tag{21-8}$$

The internal catalytic surface area is $2\pi \Gamma \langle r_{\text{average}} \rangle L$. The mass of an isolated catalytic pellet is $\rho_{\text{app}} V_{\text{total}}$. The internal catalytic surface area per mass of catalyst is given by

$$S_m = \frac{2\pi \Gamma \langle r_{\text{average}} \rangle L}{\rho_{\text{app}} V_{\text{total}}} \tag{21-9}$$

and the void volume per mass of catalyst is

$$V_m = \frac{\varepsilon_p V_{\text{total}}}{\rho_{\text{app}} V_{\text{total}}} = \frac{\varepsilon_p}{\rho_{\text{app}}} = \frac{\pi \Gamma \langle r_{\text{average}} \rangle^2 L}{\rho_{\text{app}} V_{\text{total}}} \tag{21-10}$$

Based on these definitions, the average pore radius is

$$\langle r_{\text{average}} \rangle = \frac{2V_m}{S_m} = \frac{2\varepsilon_p}{S_m \rho_{\text{app}}} \tag{21-11}$$

In general, the average pore radius is defined in terms of the distribution function $f(r)$ as the ratio of the first moment of $f(r)$ to the zeroth moment of $f(r)$, where the nth moment of the distribution is

$$\langle r^n \rangle = \int_0^\infty r^n f(r)\, dr \tag{21-12}$$

The zeroth moment of a normalized distribution function $\varphi(r)$ is unity, by definition, because

$$\int_0^\infty \varphi(r)\, dr = 1 \tag{21-13}$$

However, the pore-size distribution function $f(r)$ is not normalized, so the zeroth moment must be included in the expression for the average pore radius:

$$\langle r_{\text{average}} \rangle = \frac{\displaystyle\int_0^\infty r f(r)\, dr}{\displaystyle\int_0^\infty f(r)\, dr} \tag{21-14}$$

where the denominator on the right side of equation (21-14) is the void fraction. Simple calculations based on straight cylindrical pores reveal that the internal catalytic surface area per mass of catalyst can be estimated from equation (21-11):

$$S_m = \frac{2\varepsilon_p}{\rho_{\text{app}} \langle r_{\text{average}} \rangle} \approx \frac{1}{\langle r_{\text{average}} \rangle} \tag{21-15}$$

Also,

$$S_m \rho_{\text{app}} = \frac{2\varepsilon_p}{\langle r_{\text{average}} \rangle} \approx \frac{1}{\langle r_{\text{average}} \rangle} \tag{21-16}$$

because $\rho_{\text{app}} \approx 1$ g/cm^3 and $\varepsilon_p \approx 0.50$. For example, if the average pore radius is 100 Å and the intrapellet porosity is $\approx 50\%$, then S_m is on the order of 10^6 cm^2 per gram of catalyst (i.e., 100 m^2/g) and $S_m \rho_{\text{app}} \approx 10^6$ cm^{-1}.

21-2 KNUDSEN DIFFUSION IN STRAIGHT CYLINDRICAL PORES

The average pore size within a pellet governs the major contribution to diffusional resistance as reactant and product gases move toward and away from the internal catalytic surface. When ambient temperature and pressure are 300 K and 1 atm, respectively, Knudsen flow provides the major resistance to mass transfer if pore sizes are less than 50 Å. This is a consequence of the fact that the *mean free path of these gases* is larger than the pore diameter, and gas molecules collide with the walls of the channel much more frequently than they collide with other gas molecules. The Knudsen diffusion coefficient of gaseous species i moving through an array of straight cylindrical pores with average radius $\langle r_{\text{average}} \rangle$ is given by the product of the root-mean-square speed of the molecules $\sqrt{\langle v_i^2 \rangle}$ and the average distance that a molecule travels before it collides with the wall of a pore (i.e., this distance is on the order of $2\langle r_{\text{average}} \rangle$). The law of equipartition of energy states that each degree of freedom for translation contributes $k_{\text{Boltzmann}} T/2$ per molecule or $RT/2$ per mole to the total energy of an ideal gas, relative to its ground-state energy. If one interprets the translational contribution to the total energy in terms of the average kinetic energy of an ideal gas, then one obtains the kinetic theory result rather quickly for the root-mean-square speed of molecules that experience three-dimensional motion when molecular velocities follow the Maxwell–Boltzmann distribution. Hence, for one mole of gas i,

$$\tfrac{1}{2}\text{MW}_i \langle v_i^2 \rangle = \tfrac{3}{2} RT \tag{21-17}$$

$$\sqrt{\langle v_i^2 \rangle} = \sqrt{\frac{3RT}{\text{MW}_i}} \tag{21-18}$$

where $k_{\text{Boltzmann}}$ is Boltzmann's constant, R is the gas constant, T is absolute temperature, and MW_i is the molecular weight of species i. This leads to the following expression for the Knudsen diffusion coefficient for species i in a mixture:

$$\mathfrak{D}_{i,\,\text{Knudsen}} = \frac{2}{3}\langle r_{\text{average}} \rangle \sqrt{\frac{3RT}{\text{MW}_i}} \tag{21-19}$$

The factor of $\frac{2}{3}$ appears in equation (21-19) because molecules confined to narrow channels probably collide with the walls of a tube, for example, that are separated by $2\langle r_{\text{average}} \rangle$, and the dimensionality of the system is 3 for random Brownian motion in three dimensions. In many cases, the factor of $\sqrt{3}$ in (21-19) is replaced by the kinetic theory prediction of $\sqrt{8/\pi}$ when $\mathfrak{D}_{i,\,\text{Knudsen}}$ is based on the average speed of the gas molecules (i.e., $\langle v_i \rangle = \sqrt{8RT/\pi \text{MW}_i}$). Now the Knudsen diffusion coefficient is given by 92% of (21-19) (see Moore, 1972, p. 124; Bird *et al.*, 2002, pp. 23, 525; Dullien, 1992, p. 293; and Smith, 1970, p. 405). If the average pore size is expressed in angstroms and the temperature

is in Kelvin, then the Knudsen diffusion coefficient for gas i in cm^2/s is

$$\mathfrak{D}_{i,\,\text{Knudsen}}(\text{cm}^2/\text{s}) = 1.05 \times 10^{-4} \langle r(\text{Å})_{\text{average}} \rangle \left[\frac{T(\text{K})}{\text{MW}_i} \right]^{1/2} \tag{21-20}$$

At 300 K, this diffusivity reduces to

$$\mathfrak{D}_{i,\,\text{Knudsen}}(\text{cm}^2/\text{s}) = 2.6 \times 10^{-4} \langle r(\text{Å})_{\text{average}} \rangle \tag{21-21}$$

when the molecular weight of the gas is 50 Da.

21-3 ORDINARY MOLECULAR DIFFUSION IN BINARY AND PSEUDO-BINARY MIXTURES

The kinetic theory of dilute gases accounts for collisions between spherical molecules in the presence of an intermolecular potential. Ordinary molecular diffusion coefficients depend linearly on the average kinetic speed of the molecules and the mean free path of the gas. The mean free path is a measure of the average distance traveled by gas molecules between collisions. When the pore diameter is much larger than the mean free path, collisions with other gas molecules are most probable and ordinary molecular diffusion provides the dominant resistance to mass transfer. Within this context, ordinary molecular diffusion coefficients for binary gas mixtures are predicted, with units of cm^2/s, via the Chapman–Enskog equation (see Bird *et al*., 2002, p. 526):

$$\mathfrak{D}_{\text{AB}} = \frac{1.86 \times 10^{-3} [T(\text{K})]^{3/2} [(1/\text{MW}_\text{A}) + (1/\text{MW}_\text{B})]^{1/2}}{p(\text{atm}) [\sigma_{\text{AB}}(\text{Å})]^2 \Omega_D \left(\dfrac{kT}{\varepsilon_{\text{AB}}} \right)} \tag{21-22}$$

where σ_{AB} is the collision diameter, or the distance between atomic centers of two dissimilar gas molecules if they collide elastically as hard spheres, Ω_D is a collision integral (i.e., correction factor) that accounts for deviations from the hard-sphere potential, k is Boltzmann's constant, and ε_{AB} is the depth of the potential well, or the Lennard-Jones potential energy of interaction (i.e., actually $-\varepsilon_{\text{AB}}$) between gases A and B when they reside at their equilibrium separation, $r_{\text{equilibrium}} = \sigma_{\text{AB}}(2)^{1/6}$.

If the total pressure p is 1 atm and absolute temperature T is in the vicinity of 298 K, then kinetic theory predicts ordinary molecular diffusivities on the order of 0.1 cm^2/s, which are comparable to Knudsen diffusivities if the average pore radius is 0.1 μm (i.e., 10^3 Å) and molecular weights are about 50 Da. When pore radii are larger than 1 μm, ordinary molecular diffusion provides the dominant resistance to mass transfer in porous catalysts at standard temperature

and pressure. The Lennard-Jones 6-12 intermolecular potential function for pure gas i is

$$\Phi(r) = 4\varepsilon_i \left[\left(\frac{\sigma_i}{r} \right)^{12} - \left(\frac{\sigma_i}{r} \right)^{6} \right] \tag{21-23}$$

where σ_i is the collision diameter between two molecules of gas i, or the diameter of a spherical shell surrounding one molecule of gas i, and ε_i is the depth of the potential function at the equilibrium separation between like molecules (i.e., $d\Phi/dr = 0$). The 6-12 potential is repulsive when $r < r_{\text{equilibrium}}$ and attractive when $r > r_{\text{equilibrium}}$. The collision integral Ω_D is unity for a hard-sphere intermolecular potential. Accurate values of Ω_D for the Lennard-Jones potential can be obtained from the following empirical correlation (see Neufeld *et al.*, 1972):

$$\Omega_D \approx A(T^*)^{-B} + C\exp(-DT^*) + E\exp(-FT^*) + G\exp(-HT^*) \tag{21-24}$$

where

$$T^* = \frac{kT}{\varepsilon_i} \qquad A = 1.06036 \quad B = 0.15610$$
$$C = 0.19300 \quad D = 0.47635 \quad E = 1.03587$$
$$F = 1.52996 \quad G = 1.76474 \quad H = 3.89411$$

For a binary gas mixture of A and B, one estimates the Lennard-Jones parameters that are required to calculate $\mathfrak{D}_{AB}$ via empirical averaging, as follows:

$$\sigma_{AB} = \frac{\sigma_A + \sigma_B}{2} \qquad \varepsilon_{AB} = \sqrt{\varepsilon_A \varepsilon_B} \tag{21-25}$$

If an n-component gas mixture (i.e., $n \geq 2$) can be treated as a pseudo-binary mixture, and the ordinary molecular diffusivity $\mathfrak{D}_{A,\,mix}$ of component A is desired, then the formalism described above is applicable under the following conditions:

1. MW_B is replaced by the average molecular weight MW_{mix} of an $(n-1)$-component mixture, excluding component A:

$$MW_{mix} = \sum_{j=1,\,(j\neq A)}^{n} y_j\, MW_j \tag{21-26}$$

   where y_j is the mole fraction of gas j in an $(n-1)$-component mixture that excludes gas A.

2. Collision diameter σ_{AB} is replaced by $\sigma_{A,\,mix}$, which averages $n-1$ different types of binary collisions that include gas A:

$$\sigma_{A,\,mix} = \frac{1}{n-1} \sum_{j=1,\,(j\neq A)}^{n} \frac{1}{2}(\sigma_A + \sigma_j) \tag{21-27}$$

3. The depth of the potential function ε_{AB} at the equilibrium separation is replaced by a geometric average that includes all n components:

$$\varepsilon_{\text{mix}} = \left(\prod_{j=1}^{n} \varepsilon_j \right)^{1/n} \tag{21-28}$$

Hence,

$$\mathfrak{D}_{\text{A, mix}}(\text{cm}^2/\text{s}) \approx \frac{1.86 \times 10^{-3}[T(\text{K})]^{3/2}[(1/\text{MW}_\text{A}) + (1/\text{MW}_{\text{mix}})]^{1/2}}{p(\text{atm})[\sigma_{\text{A, mix}}(\text{Å})]^2 \Omega_D \left(\dfrac{kT}{\varepsilon_{\text{mix}}} \right)} \tag{21-29}$$

The empirical predictions described above for pseudo-binary mixtures are compared with rigorous calculations for multicomponent mixtures in Section 21-3.3 to justify the pseudo-binary approximation.

21-3.1 Estimating Pure-Component Lennard-Jones Parameters for the 6-12 Intermolecular Potential

The collision diameter σ_i and potential well depth ε_i can be calculated fairly accurately from critical constants or physical properties of a pure gas at its boiling point. For example,

$$\sigma_i(\text{Å}) \approx 0.841[v_{i,\,\text{critical}}(\text{cm}^3/\text{mol})]^{1/3}$$
$$2.44 \left[\frac{T_{i,\,\text{critical}}(\text{K})}{p_{i,\,\text{critical}}(\text{atm})} \right]^{1/3}$$
$$1.18[v_i(T = T_{i,\,\text{boil}})(\text{cm}^3/\text{mol})]^{1/3}$$

For convenience, the potential well depth is divided by Boltzmann's constant because the argument of the collision integral is $kT/\varepsilon_i = T/(\varepsilon_i/k)$:

$$\frac{\varepsilon_i}{k}(\text{K}) \approx 0.77T_{i,\,\text{critical}}(\text{K})$$
$$1.15T_{i,\,\text{boil}}(\text{K})$$
$$1.92T_{i,\,\text{melt}}(\text{K})$$

21-3.2 Addition of Resistances When Knudsen Diffusion and Ordinary Molecular Diffusion Are Operative in Binary and Multicomponent Gas Mixtures

When the average pore radius is between 50 and 10^4 Å, it is necessary to add resistances from Knudsen flow and ordinary molecular diffusion to calculate the net diffusivity of component i in porous pellets. The procedure is (1) illustrated rigorously for binary mixtures, (2) extrapolated to multicomponent mixtures that

can be treated as pseudo-binary mixtures, and (3) stated for multicomponent mixtures without any assumptions or simplifications. Results for binaries are a subset of (2) and (3). In other words, it is easy to verify that (2) and (3) reduce to (1) when mixtures contain only two components. The analysis begins with Fick's first law of diffusion for component A in a binary mixture:

$$\mathbf{j}_A = \rho_A(\mathbf{v}_A - \mathbf{v}) = -\rho\mathfrak{D}_{AB}\nabla\omega_A \tag{21-30}$$

where $\mathbf{j}_A$ is the diffusional mass flux, based on a mass fraction driving force (i.e., $\nabla\omega_A$), with respect to a reference frame that translates at the mass-average velocity of the mixture (i.e., $\mathbf{v}$), ρ is the total mass density of the mixture, and $\mathfrak{D}_{AB}$ is the binary molecular diffusion coefficient. The corresponding expression in terms of molar properties is

$$\mathbf{J}_A^* = C_A(\mathbf{v}_A - \mathbf{v}^*) = -C\mathfrak{D}_{AB}\nabla y_A \tag{21-31}$$

where $\mathbf{J}_A^*$ is the diffusional molar flux, based on a mole fraction driving force (i.e., ∇y_A), with respect to a reference frame that translates at the molar-average velocity of the mixture (i.e., $\mathbf{v}^*$), and C is the total molar density of the mixture. Interestingly enough, the same binary molecular diffusivity is appropriate in both of these flux laws given by equations (21-30) and (21-31). The molar-average velocity of the mixture is defined as a mole-fraction-weighted sum of species velocities for all components. Hence,

$$\mathbf{v}^* = \sum_{i=1}^{n} y_i\mathbf{v}_i \tag{21-32}$$

Since mole fraction y_i is defined as C_i/C, and the molar flux of species i with respect to a stationary reference frame is

$$\mathbf{N}_i = C_i\mathbf{v}_i \tag{21-33}$$

the molar-average velocity of the mixture can be rewritten as

$$\mathbf{v}^* = \frac{\sum_{i=1}^{n}\mathbf{N}_i}{C} = \frac{\mathbf{N}_A + \mathbf{N}_B}{C} \tag{21-34}$$

If one returns to Fick's first law of diffusion on a molar basis, given by (21-31), and substitutes the previous expression for $\mathbf{v}^*$, then

$$\mathbf{J}_A^* = C_A(\mathbf{v}_A - \mathbf{v}^*) = \mathbf{N}_A - y_A(\mathbf{N}_A + \mathbf{N}_B) = -C\mathfrak{D}_{AB}\nabla y_A \tag{21-35}$$

This equation is rearranged and solved for $\mathbf{N}_A$ in the presence of convection and diffusion:

$$\mathbf{N}_A[1 - y_A(1 + \alpha_{BA})] = -C\mathfrak{D}_{AB}\nabla y_A \tag{21-36}$$

where α_{BA} represents the ratio of the magnitudes of the molar flux of B relative to that of component A, both with respect to a stationary reference frame. Hence,

$$\alpha_{BA} = \frac{|\mathbf{N}_B|}{|\mathbf{N}_A|} \tag{21-37}$$

For nonreactive mixtures, Graham's law (proposed in 1831 and documented in 1833; see Graham, 1833) states that

$$\alpha_{BA} = \left(\frac{MW_A}{MW_B}\right)^{1/2} \tag{21-38}$$

suggesting that the molar flux of any component is proportional to the inverse square root of its molecular weight. For reactive mixtures, the stoichiometric condition at the reaction site requires that

$$\alpha_{BA} = \frac{|\upsilon_B|}{|\upsilon_A|} \tag{21-39}$$

When convection and diffusion are operative, the resistance to mass transfer for species A is the inverse of the coefficient of $-C\nabla y_A$ in the following expression for $\mathbf{N}_A$, based on (21-36). Hence,

$$\mathbf{N}_A = -\frac{C\mathfrak{D}_{AB}\nabla y_A}{1 - \beta y_A} \tag{21-40}$$

where $\beta = 1 + \alpha_{BA}$ represents the contribution from convective mass transfer and

$$\text{mass transfer resistance for component A} = \frac{1 - \beta y_A}{\mathfrak{D}_{AB}} \tag{21-41}$$

This resistance is larger when convective mass transfer is negligible relative to diffusion, and $\mathbf{v}^*$ is insignificant. Under these conditions, $\beta \to 0$ and the mass transfer resistance simplifies to $1/\mathfrak{D}_{AB}$. If convective mass transfer is important in a nonreactive mixture of n components which can be treated as a pseudo-binary, then:

$$\beta_{\text{pseudobinary}} = 1 + (n-1)\alpha_{A,\,\text{mix}} \tag{21-42}$$

$$\alpha_{A,\,\text{mix}} = \left(\frac{MW_A}{MW_{\text{mix}}}\right)^{1/2} \tag{21-43}$$

where MW_{mix} is a mole-fraction-weighted sum of molecular weights of $n-1$ components, excluding component A:

$$MW_{\text{mix}} = \sum_{j=1,\,(j\neq A)}^{n} y_j MW_j \tag{21-44}$$

and y_j is the mole fraction of gas j in an $(n-1)$-component mixture that excludes gas A. Now, the mass transfer resistance for component A due to convection and ordinary molecular diffusion in a pseudobinary mixture is

$$\frac{1-[1+(n-1)\alpha_{\mathrm{A,\,mix}}]y_{\mathrm{A}}}{\mathfrak{D}_{\mathrm{A,\,mix}}} \tag{21-45}$$

where $\mathfrak{D}_{\mathrm{A,\,mix}}$ is calculated empirically from equation (21-29). Once again, (21-45) yields a mass transfer resistance of $1/\mathfrak{D}_{\mathrm{A,\,mix}}$, due solely to diffusion, when convective transport is negligible. When $n = 2$, equation (21-45) reduces to equation (21-41) for a binary mixture because $\mathrm{MW}_{\mathrm{mix}} = \mathrm{MW}_{\mathrm{B}}$, $\alpha_{\mathrm{A,\,mix}} = \alpha_{\mathrm{BA}}$, and $\mathfrak{D}_{\mathrm{A,\,mix}} = \mathfrak{D}_{\mathrm{AB}}$. Rigorously, the total mass transfer resistance due to convection and ordinary molecular diffusion for species i in an n-component mixture is

$$\sum_{j=1}^{n} \frac{y_j - \alpha_{ji} y_i}{\mathfrak{D}_{ij}} \tag{21-46}$$

where $\mathfrak{D}_{ij}$ is a binary molecular diffusivity for the $i-j$ gas pair. Only one term in the summation survives when $n = 2$ for binary mixtures, because $y_j - \alpha_{ji} y_i = 0$ when $i = j$.

The net diffusivity of component A within the pores of a catalytic pellet is obtained by adding mass transfer resistances for Knudsen diffusion and ordinary molecular diffusion, where convection reduces the resistance due to ordinary molecular diffusion but Knudsen flow occurs over length scales that are much too small for convective mass transfer to be important. This addition of resistances is constructed to simulate resistances in series, not parallel. Consider the trajectory of a gas molecule that collides with the walls of a channel or other gas molecules. In the pore-size regime where Knudsen and ordinary molecular diffusion are equally probable, these collisions occur sequentially, which suggests that gas molecules encounter each of these resistances in series. Hence, for binary mixtures,

$$\frac{1}{\mathfrak{D}_{\mathrm{A,\,net}}} = \frac{1}{\mathfrak{D}_{\mathrm{A,\,Knudsen}}} + \frac{1-\beta y_{\mathrm{A}}}{\mathfrak{D}_{\mathrm{AB}}} \tag{21-47}$$

Since convective mass transfer is negligible in porous catalytic pellets, it is reasonable to let $\beta = 0$ in (21-47) and add the diffusivities inversely. If the pore diameter is much smaller than the mean free path of the gas, then collisions with the walls are more frequent than collisions with other molecules, and Knudsen diffusion provides the dominant resistance. If the pores are much larger than the mean free path, then collisions with other molecules are more frequent than collisions with the walls of the channel, and ordinary molecular diffusion provides the dominant resistance. Usually, one arrives at a sum of resistances in series by following the trajectory of a single gas molecule within a catalytic pore. It is important to emphasize that one obtains the correct result by tracking a single molecule only if there are no other pathways by which diffusion supplies the

central core of the catalyst with reactants. For example, the sequential process for resistances in series, described above, occurs in parallel with ordinary molecular diffusion if a catalytic pellet exhibits a bimodal distribution of pore sizes, where most of the pore radii are smaller than 1 μm but some pore radii are larger than 1 μm. In other words, the overall objective is to supply the central core of the catalyst with reactants by any mechanism possible. In this case, the net diffusivity, given by equation (21-47) for pores with radii between 50 Å and 1 μm, must be added directly to the ordinary molecular diffusion coefficient for pores with radii that are greater than 1 μm, using the appropriate cross-sectional area weighting factor for pores in each size regime. For mixtures of n components that can be treated as pseudo-binary mixtures, the addition of resistances in series is constructed as follows for pore radii between 50 Å and 1 μm:

$$\frac{1}{\mathfrak{D}_{\mathrm{A,\,net}}} = \frac{1}{\mathfrak{D}_{\mathrm{A,\,Knudsen}}} + \frac{1 - \beta_{\mathrm{pseudobinary}}\, y_{\mathrm{A}}}{\mathfrak{D}_{\mathrm{A,\,mix}}} \tag{21-48}$$

Rigorously, for a mixture of n components, the net diffusivity of component i is calculated via addition of resistances in series in the following manner:

$$\begin{aligned}
\frac{1}{\mathfrak{D}_{i,\,\mathrm{net}}} &= \frac{1}{\mathfrak{D}_{i,\,\mathrm{Knudsen}}} + \sum_{j=1}^{n} \frac{y_j - \alpha_{ji} y_i}{\mathfrak{D}_{ij}} \\
\mathfrak{D}_{ij} &= \frac{1.86 \times 10^{-3} [T(\mathrm{K})]^{3/2} [(1/\mathrm{MW}_i) + (1/\mathrm{MW}_j)]^{1/2}}{p(\mathrm{atm}) [\sigma_{ij}(\mathrm{Å})]^2 \Omega_D (kT/\varepsilon_{ij})} \\
\sigma_{ij} &= \frac{\sigma_i + \sigma_j}{2} \\
\varepsilon_{ij} &= \sqrt{\varepsilon_i \varepsilon_j}
\end{aligned} \tag{21-49}$$

and

$$\alpha_{ji} = \frac{|\mathbf{N}_j|}{|\mathbf{N}_i|} = \begin{cases} \left(\dfrac{\mathrm{MW}_i}{\mathrm{MW}_j}\right)^{1/2} & \text{for nonreactive mixtures} \\ \dfrac{|\upsilon_j|}{|\upsilon_i|} & \text{for reactive mixtures} \end{cases} \tag{21-50}$$

21-3.3 Comparison between Rigorous and Approximate Calculations Based on Ordinary Molecular Diffusion in Nonreactive Multicomponent Gas Mixtures

Consider the four-component nonreactive gas mixture of methane, isobutane, carbon disulfide, and chloromethane. The diffusivity of methane and its total mass transfer resistance due to convection and ordinary molecular diffusion are calculated at 25°C and 1 atm. The data listed in Table 21-1 are available.

TABLE 21-1 Nonreactive Gas Mixture Composition and Pure-Component Lennard-Jones Parameters for the 6-12 Intermolecular Potential

Gas	Potential Well Depth ε_j/k (K)	Molecular Weight (Da)	Mole Fraction in Gas Mixture	Collision Diameter σ_j (Å)
Methane	137	16.04	0.20	3.822
Isobutane	313	58.12	0.45	5.341
CS_2	488	76.14	0.20	4.438
CH_3Cl	855	50.49	0.15	3.375

If one focuses on the three dissimilar binary gas pairs with methane, then it is straightforward to estimate collision diameters, potential well depths and binary molecular diffusivities for each gas pair. For example:

Methane/isobutane:

$$\sigma_{ij} = 4.582 \text{ Å} \quad \frac{\varepsilon_{ij}}{k} = 207 \text{ K} \quad \frac{kT}{\varepsilon_{ij}} = 1.44 \quad \Omega_D = 1.22 \quad \mathfrak{D}_{ij} = 0.105 \text{ cm}^2/\text{s}$$

Methane/carbon disulfide:

$$\sigma_{ij} = 4.130 \text{ Å} \quad \frac{\varepsilon_{ij}}{k} = 259 \text{ K} \quad \frac{kT}{\varepsilon_{ij}} = 1.15 \quad \Omega_D = 1.35 \quad \mathfrak{D}_{ij} = 0.114 \text{ cm}^2/\text{s}$$

Methane/chloromethane:

$$\sigma_{ij} = 3.599 \text{ Å} \quad \frac{\varepsilon_{ij}}{k} = 342 \text{ K} \quad \frac{kT}{\varepsilon_{ij}} = 0.87 \quad \Omega_D = 1.54 \quad \mathfrak{D}_{ij} = 0.138 \text{ cm}^2/\text{s}$$

Graham's law for nonreactive mixtures is employed to calculate α_{ji} for each gas pair, where component $i = 1$ is methane (see Table 21-2).

Notice that isobutane, by virtue of its large collision diameter and high concentration, provides the largest mass transfer resistance for methane in this four-component mixture. The total mass transfer resistance for methane due to convection and ordinary molecular diffusion is 4.49 s/cm^2, obtained by adding resistances in the last column of Table 21-2. The ordinary molecular diffusivity of methane in this four-component mixture is (see equation 18.4–22 in Bird *et al.*, 1960, p. 571; and Hougen and Watson, 1947, pp. 977–979):

$$\mathfrak{D}_{i,\text{mix}} = \frac{1 - y_i \sum_{j=1}^{4} \alpha_{ji}}{\sum_{j=1}^{4} [(y_j - \alpha_{ji} y_i)/\mathfrak{D}_{ij}]} = 0.109 \text{ cm}^2/\text{s} \tag{21-51}$$

when $y_i = y_{\text{methane}} = 0.20$.

Now, the same problem is approached by treating isobutane, carbon disulfide, and chloromethane as a single component in a pseudo-binary mixture with

TABLE 21-2 Individual Mass Transfer Resistances, including Convection and Diffusion, for Methane in a Four-Component Nonreactive Gas Mixture[a]

j	Gas	$\alpha_{ji} = (\mathrm{MW}_i/\mathrm{MW}_j)^{1/2}$	$(y_j - \alpha_{ji} y_i)/\mathfrak{D}_{ij}$ (s/cm^2)
1	Methane	1	0
2	Isobutane	0.53	3.27
3	CS_2	0.46	0.95
4	CH_3Cl	0.56	0.27

[a] The overall composition is provided in Table 21-1; $i = 1$.

methane. When methane is excluded, the remainder of the mixture exhibits the following composition:

$$y_{\text{isobutane}} = y_2 = 0.56 \quad y_{\text{carbondisulfide}} = y_3 = 0.25 \quad y_{\text{chloromethane}} = y_4 = 0.19 \tag{21-52}$$

and the average molecular weight of the remainder of the mixture is

$$\mathrm{MW}_{\text{mix}} = \sum_{j=2}^{4} y_j \, \mathrm{MW}_j = 61.19 \text{ Da} \tag{21-53}$$

Appropriate averaging of the collision diameters and potential well depths produces the following results:

$$\sigma_{1,\,\text{mix}} = \frac{1}{6} \sum\nolimits_{j=2}^{4} (\sigma_1 + \sigma_j) = 4.103 \text{ Å}$$

$$\frac{\varepsilon_{\text{mix}}}{k} = \left[\prod_{j=1}^{4} \left(\frac{\varepsilon_j}{k} \right) \right]^{1/4} = 366 \text{ K} \tag{21-54}$$

At 25°C, $kT/\varepsilon_{\text{mix}} = 0.82$ and the numerical value of the collision integral for diffusion is $\Omega_D = 1.60$. Hence,

$$\mathfrak{D}_{1,\,\text{mix}} \approx \frac{1.86 \times 10^{-3} [T(\text{K})]^{3/2} [(1/\mathrm{MW}_1) + (1/\mathrm{MW}_{\text{mix}})]^{1/2}}{p(\text{atm}) [\sigma_{1,\,\text{mix}}(\text{Å})]^2 \Omega_D (kT/\varepsilon_{\text{mix}})} = 0.100 \text{ cm}^2/\text{s} \tag{21-55}$$

which is ≈8% low relative to the rigorous calculation of 0.109 cm^2/s, provided in (21-51).

Finally, one estimates the total mass transfer resistance for methane due to convection and ordinary molecular diffusion in this pseudo-binary mixture as follows, when $y_{\text{methane}} = y_1 = 0.20$:

$$\frac{1 - y_1 [1 + (4 - 1)(\mathrm{MW}_1/\mathrm{MW}_{\text{mix}})^{1/2}]}{\mathfrak{D}_{1,\,\text{mix}}} = 4.95 \text{ s/cm}^2 \tag{21-56}$$

which is ≈10% high relative to the rigorous calculation of 4.49 s/cm^2.

21-4 ESTIMATING TORTUOSITY FACTORS AND INTRAPELLET POROSITY BASED ON THE DISTRIBUTION IN ORIENTATION AND SIZE OF CATALYTIC PORES VIA THE PARALLEL-PORE MODEL

The parallel-pore model provides an in-depth description of the void volume fraction ε_p and tortuosity factor τ_{or} based on averages over the distribution in size and orientation, respectively, of catalytic pores that are modeled as straight cylinders. These catalyst-dependent structure factors provide the final tools that are required to calculate the effective intrapellet diffusion coefficients for reactants and products, as well as intrapellet Damkohler numbers. The following conditions are invoked:

1. The external surface of the catalyst conforms to a flat-slab geometry.
2. x is the inward coordinate direction measured normal to the macroscopic external surface of the catalyst.
3. z is the coordinate direction that increases along the cylindrical axis of each pore which extends inward from the macroscopic external surface.
4. The pores are oriented at angle θ with respect to the normal.

In other words, the z direction is oriented at angle θ relative to the x direction and $x = z\cos\theta$.

Reactants must diffuse in the x direction to penetrate the central core of the catalyst, but molecules are forced to diffuse in the z direction due to the orientation of the pores. In a plane at constant x within the catalyst, parallel to the macroscopic external surface, $\Phi(r,\theta)\,dr\,d\theta$ is the fraction of the total area in this plane that belongs to pores with angles of inclination between θ and $\theta + d\theta$ and pore radii between r and $r + dr$.

In order to relate the void fraction and tortuosity factor to explicit averages over this distribution function, it is necessary to factor the distribution as follows:

$$\Phi(r,\theta) = h(r)g(\theta) \tag{21-57}$$

This result is valid if the effects of pore size and orientation are uncorrelated. Only the orientation part of this distribution [i.e., $g(\theta)$] is normalized. Similar to the void volume fraction, described by equation (21-6) in terms of the intrapellet porosity, one obtains a void area fraction in each plane at constant x by averaging the distribution function Φ over all possible pore sizes and orientations. Hence,

$$\int_{\theta=0}^{\pi/2}\int_{r=0}^{\infty}\Phi(r,\theta)\,dr\,d\theta = \int_0^{\infty}h(r)\,dr\int_0^{\pi/2}g(\theta)\,d\theta$$
$$= \text{void area fraction} \tag{21-58}$$

The void volume fraction is much easier to relate to experimental measurements via mercury porosimetry, for example, than the void area fraction described by

(21-58). However, the void area fraction is equivalent to the void volume fraction, based on equation (21-76) and the definition of intrapellet porosity ε_p at the bottom of p. 555. Effectiveness factor calculations in catalytic pellets require an analysis of one-dimensional pseudo-homogeneous diffusion and chemical reaction in a coordinate system that exploits the symmetry of the macroscopic boundary of a single pellet. For catalysts with rectangular symmetry as described above, one needs an expression for the average diffusional flux of reactants in the thinnest dimension, which corresponds to the x direction. Hence, the quantity of interest at the local level of description is $J^*_{Ax,\,\text{local}}$, which represents the local diffusional molar flux of reactant A in the x direction with respect to the molar average velocity of the mixture. It should be obvious that

$$J^*_{Ax,\,\text{local}} = \cos\theta\, J^*_{Az,\,\text{local}} \tag{21-59}$$

based on the definitions of the x and z directions within the catalyst. Furthermore, the local diffusional molar flux of reactant A along the z-axis of the cylindrical pores is given by Fick's law:

$$J^*_{Az,\,\text{local}} = -\mathfrak{D}_{A,\,\text{net}} \left(\frac{\partial C_A}{\partial z}\right)_\theta \tag{21-60}$$

where the net intrapellet diffusivity $\mathfrak{D}_{A,\,\text{net}}$ represents a combination of Knudsen and ordinary molecular diffusion via the addition of resistances within the pellet. The chain rule of differentiation allows one to write

$$\left(\frac{\partial C_A}{\partial z}\right)_\theta = \frac{\partial C_A}{\partial x}\left(\frac{\partial x}{\partial z}\right)_\theta = \cos\theta \frac{\partial C_A}{\partial x} \tag{21-61}$$

because $x = z\cos\theta$. Hence, one-dimensional diffusion along the z-axis of the cylindrical pores translates into the following expression for the homogenized local molar diffusional flux normal to the external surface of the catalyst:

$$J^*_{Ax,\,\text{local}} = -(\cos^2\theta)\mathfrak{D}_{A,\,\text{net}} \frac{dC_A}{dx} \tag{21-62}$$

Notice that $J^*_{Ax,\,\text{local}} = J^*_{Az,\,\text{local}}$ and $x = z$ when the cylindrical pores are oriented normal to the external surface (i.e., $\theta = 0$), but reactants cannot diffuse into the central core of the catalyst when the pores are essentially parallel to the external surface (i.e., $\theta = \pi/2$). If $J^*_{Ax,\,\text{local}}$ is averaged over all possible orientations (i.e., $0 \le \theta \le \pi/2$) and pore sizes (i.e., $0 \le r \le \infty$), then the quantity of interest in the mass transfer equation with pseudo-homogeneous one-dimensional diffusion and chemical reaction is obtained. Namely, the average diffusional flux of reactant A in the x direction is

$$J^*_{Ax,\,\text{average}} \equiv \int_{\theta=0}^{\pi/2} \int_{r=0}^{\infty} J^*_{Ax,\,\text{local}}\, \Phi(r,\theta)\, dr\, d\theta \tag{21-63}$$

When the distribution function is factored based on orientation and pore size, as illustrated by equation (21-57),

$$J^*_{\mathrm{A}x,\,\mathrm{average}} = -\int_0^{\pi/2} \{\cos^2\theta\} g(\theta)\, d\theta \left[\int_0^{\infty} \mathfrak{D}_{\mathrm{A,\,net}} h(r)\, dr\right] \frac{dC_{\mathrm{A}}}{dx} \tag{21-64}$$

where the net diffusivity of species A is a function of pore size if Knudsen diffusion is important, but $\mathfrak{D}_{\mathrm{A,\,net}}$ is independent of pore size if ordinary molecular diffusion provides the dominant resistance to mass transfer within the pores. The effective intrapellet diffusion coefficient of reactant A in porous catalysts is defined by

$$J^*_{\mathrm{A}x,\,\mathrm{average}} = -\mathfrak{D}_{\mathrm{A,\,effective}} \frac{dC_{\mathrm{A}}}{dx} \tag{21-65}$$

where

$$\mathfrak{D}_{\mathrm{A,\,effective}} = \int_0^{\pi/2} \{\cos^2\theta\} g(\theta)\, d\theta \left[\int_0^{\infty} \mathfrak{D}_{\mathrm{A,\,net}} h(r)\, dr\right]$$

The tortuosity factor depends on orientation of the cylindrical pores, which is governed by $g(\theta)$. Furthermore, when reactant diffusion into the central core of the catalyst is hindered by pore orientation to a larger extent, the tortuosity is larger. In agreement with these concepts, one defines the tortuosity factor as follows:

$$\frac{1}{\tau_{\mathrm{or}}} \equiv \int_0^{\pi/2} \{\cos^2\theta\} g(\theta)\, d\theta \tag{21-66}$$

Hence,

$$\mathfrak{D}_{\mathrm{A,\,effective}} = \frac{1}{\tau_{\mathrm{or}}} \int_0^{\infty} \mathfrak{D}_{\mathrm{A,\,net}} h(r)\, dr \tag{21-67}$$

When the net intrapellet diffusivity of reactant A is governed by ordinary molecular diffusion, instead of Knudsen diffusion, the net intrapellet diffusivity is not a function of pore size. Hence,

$$\mathfrak{D}_{\mathrm{A,\,effective}} = \frac{\varepsilon_p}{\tau_{\mathrm{or}}} \mathfrak{D}_{\mathrm{A,\,net}} \tag{21-68}$$

where

$$\varepsilon_p \equiv \int_0^{\infty} h(r)\, dr$$

The intrapellet porosity or void volume fraction ε_p is given by an average over the radial part of the distribution function $h(r)$. When all cylindrical pores are oriented parallel to the x direction (i.e., perpendicular to the external surface), the angular part of the distribution function is spiked at $\theta = 0$, which implies that

$$g(\theta) = \delta(\theta - 0) = \delta(\theta) \tag{21-69}$$

where δ represents a delta-function distribution. When delta functions are part of the integrand, integration is performed very quickly by evaluating the remainder of the integrand at the value of the independent variable that makes the argument of the delta function vanish, if this value of the independent variable is within the range of integration. This theorem is based on the fact that delta functions have a numerical value of zero everywhere except where the argument vanishes. At the particular value of the independent variable where the argument of the delta function vanishes, the function exhibits a spike of infinite height and infinitesimal width, with a total area under the curve of unity. Hence, if all pores are oriented in the thinnest dimension of the catalyst, then one-dimensional reactant diffusion into the central core should be equivalent to homogeneous diffusion in the x direction when the catalytic medium is void of tortuous pathways. Under these conditions,

$$\begin{aligned} \frac{1}{\tau_{\text{or}}} &\equiv \int_0^{\pi/2} \{\cos^2\theta\}\delta(\theta)\, d\theta \\ \frac{1}{\tau_{\text{or}}} &= \cos^2(\theta = 0) = 1 \end{aligned} \tag{21-70}$$

which implies that the pore structure does not hinder diffusion in the x direction and $\tau_{\text{or}} = 1$. When all cylindrical pores are oriented perpendicular to the x direction (i.e., essentially parallel to the external surface),

$$g(\theta) = \delta\left(\theta - \frac{\pi}{2}\right) \tag{21-71}$$

and

$$\begin{aligned} \frac{1}{\tau_{\text{or}}} &\equiv \int_0^{\pi/2} \{\cos^2\theta\}\delta\left(\theta - \frac{\pi}{2}\right) d\theta \\ \frac{1}{\tau_{\text{or}}} &= \cos^2\left(\theta = \frac{\pi}{2}\right) = 0 \end{aligned} \tag{21-72}$$

This implies that the nature of the pores does not allow reactants to diffuse into the central core of the catalyst because $\tau_{\text{or}} \to \infty$ and $\mathfrak{D}_{i,\,\text{effective}} \to 0$. If the pore structure is isotropic and random with no preferred orientation, then $g(\theta) = \sigma =$ constant. In this case, it is rather straightforward to evaluate the area under the orientation part of the distribution function, which must be normalized. For example,

$$\int_0^{\pi/2} g(\theta)\, d\theta = \sigma\frac{\pi}{2} = 1 \tag{21-73}$$

which yields $\sigma = 2/\pi$ for random pore orientation. The area under the orientation part of the distribution function, or the strength of $g(\theta)$, is independent of the functional form of $g(\theta)$. Some possibilities for $g(\theta)$ and the corresponding tortuosity factors are summarized in Table 21-3.

TABLE 21-3 Normalized Orientational Part of the Distribution Function in the Parallel-Pore Model for Several Cases and the Corresponding Tortuosity Factors

Orientation of Straight Cylindrical Pores	$g(\theta)$	τ_{or}
Directed along the normal, at $\theta = 0$	$\delta(\theta)$	1
Directed mostly along the normal, with a Gaussian distribution about the normal	$1.16 \exp(-\theta^2)$	1.43
Directed mostly along the normal, with a Lorentzian distribution about the normal	$0.996/(1+\theta^2)$	1.59
Directed mostly along the 45° line, with a Lorentzian distribution about this line	$0.75/[1+(\theta - \pi/4)^2]$	2
No preferred orientation	$\sigma = \dfrac{2}{\pi}$	2
Directed along the external surface, at $\theta = \pi/2$	$\delta\left(\theta - \dfrac{\pi}{2}\right)$	∞

For more information about Lorentzian distributions and Lorentz line shapes, see Fabelinskii (1968, pp. 218–222) and Dicke and Wittke (1960, pp. 275–278).

For randomly oriented pores, the tortuosity factor is evaluated as follows:

$$\frac{1}{\tau_{or}} = \sigma \int_0^{\pi/2} \cos^2\theta \, d\theta = \frac{1}{2}$$
$$\tau_{or} \approx 2 \tag{21-74}$$

This result for τ_{or} is the same if the range of θ includes pores with random orientation on both sides of the unit normal vector, such that one must integrate equation (21-74) from $-\pi/2$ to $+\pi/2$. In this case, σ is reduced to $1/\pi$ to maintain normalization of $g(\theta)$. If most pores are oriented along the normal direction and a Gaussian distribution is employed to describe the fraction of pores with larger orientation angles, then one evaluates the tortuosity factor in the following manner:

$$\frac{1}{\tau_{or}} = 1.16 \int_0^{\pi/2} \{\cos^2\theta\} \exp(-\theta^2) \, d\theta = 0.7$$
$$\tau_{or} \approx 1.43 \tag{21-75}$$

Interestingly enough, void volume fractions and void area fractions are equivalent, if one identifies intrapellet porosity ε_p with an average over the radial part of the distribution function $h(r)$, and the void area fraction is defined by

$$\text{void area fraction} = \int_{\theta=0}^{\pi/2} \int_{r=0}^{\infty} \Phi(r, \theta) \, dr \, d\theta$$
$$= \int_0^{\infty} h(r) \, dr \int_0^{\pi/2} g(\theta) \, d\theta = \varepsilon_p \tag{21-76}$$

The void area fraction in (21-76) is based on the fractional area in a plane at constant x that is available for diffusion into catalysts with rectangular symmetry. A rather sophisticated treatment of the effect of $g(\theta)$ on tortuosity is described by Dullien (1992, pp. 311–312). The tortuosity of a porous medium is a fundamental property of the streamlines or lines of flux within the individual capillaries. Tortuosity measures the deviation of the fluid from the macroscopic flow direction at every point in a porous medium. If all pores have the same constant cross-sectional area, then tortuosity is a symmetric second-rank tensor. For isotropic porous media, the trace of the tortuosity tensor is the important quantity that appears in the expression for the effective intrapellet diffusion coefficient. Consequently, $\tau_{\text{or}} \approx 3$ represents this average value (i.e., trace of the tortuosity tensor) for isotropically oriented cylindrical pores with constant cross-sectional area. Hence,

$$\mathfrak{D}_{i,\,\text{effective}} \approx \frac{1}{3}\varepsilon_p \mathfrak{D}_{i,\,\text{net}} \tag{21-77}$$

Good values for the tortuosity factor range from 2 to 4 for randomly oriented pores, where larger values of τ_{or} correspond to greater intrapellet diffusional resistance. Shrinking pore size, where pore radius is a function of position along the cylindrical axis, and twisted pores are consistent with more diffusional resistance and larger tortuosity factors.

PROBLEMS

21-1. Generate expressions for the effective intrapellet diffusion coefficient of component A in catalytic pellets when (**a**) all pores have radii below 50 Å, and (**b**) all pores have radii that are larger than 1 μm (i.e., 10^4 Å). All pores can be described by straight cylindrical tubes at an angle of inclination of 45° with respect to the thinnest dimension of flat-slab catalysts. The gas mixture contains two components, A and B.

Answer: (**a**) The generalized expression for the intrapellet diffusivity that accounts for resistances to Knudsen and ordinary molecular diffusion is

$$\mathfrak{D}_{\text{A, effective}} = \int_0^{\pi/2} \{\cos^2\theta\} g(\theta)\, d\theta \left[\int_0^{\infty} \mathfrak{D}_{\text{A, net}} h(r)\, dr \right]$$

where the addition of resistances in a multicomponent mixture,

$$\frac{1}{\mathfrak{D}_{\text{A, net}}} = \frac{1}{\mathfrak{D}_{\text{A, Knudsen}}} + \sum_{j=1}^{n} \frac{y_j - \alpha_{j\text{A}} y_{\text{A}}}{\mathfrak{D}_{\text{A}j}}$$

reduces to the result for binary mixtures of A and B when $n = 2$:

$$\frac{1}{\mathfrak{D}_{\text{A, net}}} = \frac{1}{\mathfrak{D}_{\text{A, Knudsen}}} + \frac{1 - (1 + \alpha_{\text{BA}}) y_{\text{A}}}{\mathfrak{D}_{\text{AB}}}$$

When all pore radii are smaller than 50 Å, Knudsen flow provides the dominant resistance to pore diffusion. Hence,

$$\mathfrak{D}_{\mathrm{A,\,net}}(r) \approx \mathfrak{D}_{\mathrm{A,\,Knudsen}}(r) = \frac{2}{3} r \left(\frac{3RT}{\mathrm{MW_A}} \right)^{1/2}$$

where the Knudsen diffusivity is written specifically for a pore with radius r instead of an ensemble of pores with average radius $\langle r_{\mathrm{average}} \rangle$. Since all pores are aligned at an angle of inclination of 45°, the orientation part of the distribution function is spiked at $\theta = \pi/4$ and the effective diffusivity is based solely on Knudsen flow:

$$\mathfrak{D}_{\mathrm{A,\,effective}} = \frac{2}{3} \left(\frac{3RT}{\mathrm{MW_A}} \right)^{1/2} \int_0^{\pi/2} \{\cos^2 \theta\} \delta \left(\theta - \frac{\pi}{4} \right) d\theta \left[\int_0^{\infty} r h(r)\, dr \right]$$

The first moment of the distribution of pore sizes in the preceding equation is, by definition, the product of the zeroth moment and the average pore radius, as given by equation (21-14). Hence,

$$\int_0^{\infty} r h(r)\, dr = \langle r_{\mathrm{average}} \rangle \int_0^{\infty} h(r)\, dr = \varepsilon_p \langle r_{\mathrm{average}} \rangle$$

because the intrapellet porosity ε_p is equivalent to the zeroth moment of the non-normalized distribution of pore sizes. The final expression for the effective intrapellet diffusion coefficient of species A in this micropore model is

$$\mathfrak{D}_{\mathrm{A,\,effective}} = \frac{2}{3} \varepsilon_p \langle r_{\mathrm{average}} \rangle \left(\frac{3RT}{\mathrm{MW_A}} \right)^{1/2} \cos^2 \left(\frac{\pi}{4} \right)$$

which corresponds to a tortuosity factor of 2.

Answer: (**b**) When all pore radii are larger than 1 μm, ordinary molecular diffusion represents the major resistance to mass transfer within the catalytic pores. Hence,

$$\frac{1}{\mathfrak{D}_{\mathrm{A,\,net}}} \approx \sum_{j=1}^{n} \frac{y_j - \alpha_{j\mathrm{A}} y_{\mathrm{A}}}{\mathfrak{D}_{\mathrm{A}j}}$$

which reduces to

$$\mathfrak{D}_{\mathrm{A,\,net}} \approx \frac{\mathfrak{D}_{\mathrm{AB}}}{1 - y_{\mathrm{A}}(1 + \alpha_{\mathrm{BA}})}$$

for binary mixtures of A and B. Now, the net intrapellet diffusivity is independent of both pore size and orientation, and the effective intrapellet diffusion coefficient for component A is given by

$$\mathfrak{D}_{\mathrm{A,\,effective}} = \mathfrak{D}_{\mathrm{A,\,net}} \int_0^{\pi/2} \{\cos^2 \theta\} \delta \left(\theta - \frac{\pi}{4} \right) d\theta \left[\int_0^{\infty} h(r)\, dr \right]$$

The final expression for $\mathfrak{D}_{A,\,\text{effective}}$ in this macropore model is

$$\mathfrak{D}_{A,\,\text{effective}} = \frac{\varepsilon_p \cos^2(\pi/4)\mathfrak{D}_{AB}}{1 - y_A(1 + \alpha_{BA})}$$

which also corresponds to a tortuosity factor of 2.

21-2. Consider the synthesis of methanol from carbon monoxide and hydrogen within the internal pores of catalysts with cylindrical symmetry. The radius of each catalytic pellet is 1 mm, the average intrapellet pore radius is 40 Å, the intrapellet porosity is 0.50, the intrapellet tortuosity factor is 2, and the gas-phase molar density of carbon monoxide in the vicinity of the external surface of the catalytic pellet is 3×10^{-5} g-mol/cm^3. A reasonable Hougen–Watson kinetic rate law is based on the fact that the slowest step in the mechanism is irreversible chemical reaction that requires five active sites on the catalytic surface, due to the postulate that both hydrogen molecules must dissociate and adsorb spontaneously (see Section 22-3.1). *Do not linearize the rate law*. In units of g-mol/cm^3·min·atm^3, the forward kinetic rate constant is

$$k_r(T) = 2 \times 10^4 \exp\left[-\frac{5000}{T(\text{K})}\right]$$

Be sure that the gas constant has units of cm^3·atm/g-mol·K. In other words, $R_g = 82.057$ cm^3·atm/g-mol·K.

(a) The kinetic rate constant k_r given above is useful to construct a rate law in terms of gas-phase partial pressures. Express k_r in terms of kinetic and thermodynamic parameters associated with adsorption, desorption, and heterogeneous chemical reaction on the interior surface of a porous catalyst.

(b) Use your result from part (a) to develop a relation between (**i**) the activation energy for chemical reaction when the kinetic rate law is based on gas-phase partial pressures, $E_{\text{act},\,P}/R = 5000$ K, as indicated above; (**ii**) the enthalpy change for adsorption $\Delta H_{\text{adsorption}}$; and (**iii**) the activation energy for surface-catalyzed chemical reaction when the rate law is expressed in terms of surface coverage fractions.

(c) Calculate the intrapellet Damkohler number of carbon monoxide at 325 K and 0.5 atm total pressure.

(d) What is the numerical value of the effectiveness factor at 325 K and 0.5 atm total pressure?

(e) Is the effectiveness factor larger or smaller when the total gas pressure is increased from 0.5 atm to 1 atm at a constant temperature of 325 K?

(f) Identify the kinetic and thermodynamic parameters that must be considered to determine whether the intrapellet Damkohler number of CO is larger or smaller at higher temperature.

Transport Phenomena for Chemical Reactor Design. Laurence A. Belfiore
Copyright © 2003 John Wiley & Sons, Inc.
ISBN: 0-471-20275-4

PART V

ISOTHERMAL CHEMICAL REACTOR DESIGN

Transport Phenomena for Chemical Reactor Design. Laurence A. Belfiore
Copyright © 2003 John Wiley & Sons, Inc.
ISBN: 0-471-20275-4

22

ISOTHERMAL DESIGN OF HETEROGENEOUS PACKED CATALYTIC REACTORS

A quantitative strategy is discussed herein to design isothermal packed catalytic tubular reactors. The dimensionless mass transfer equation with unsteady-state convection, diffusion, and multiple chemical reactions represents the fundamental starting point to accomplish this task. Previous analysis of mass transfer rate processes indicates that the dimensionless molar density of component i in the mixture Ψ_i must satisfy (i.e., see equation 10-11):

$$\mathrm{Re}\cdot\mathrm{Sc}\left(\frac{\partial\Psi_i}{\partial t}+\mathbf{v}\cdot\nabla\Psi_i\right)=1\cdot\nabla^2\Psi_i+\sum_{j=1}^{r}\nu_{ij}\Lambda_{ij}^2\mathfrak{R}_j^* \tag{22-1}$$

where all variables and parameters are dimensionless. Unsteady-state effects are neglected. This implies that the first term on the left-hand side of the mass transfer equation (i.e., 22-1) is not important after the transient response decays to an indistinguishable fraction of the steady-state behavior. Backmixing due to axial dispersion, and possibly intrapellet diffusion, is accounted for via $\nabla^2\Psi_i$ or residence-time distribution effects when the mass transfer Peclet number (i.e., $\mathrm{Pe}_{\mathrm{MT}}=\mathrm{Re}\cdot\mathrm{Sc}$) is small enough. For example, axial dispersion has an insignificant effect on reactant conversion in the exit stream for second-order irreversible chemical kinetics when the interpellet Damkohler number is 5 and the mass transfer Peclet number is greater than 30. These numerical results for non-ideal reactors are discussed in more detail in Section 22-4.

In a packed catalytic tubular reactor, reactants are converted to products via chemical reaction on the internal surface of the catalyst. This problem was described in detail for a single isolated pellet. At this stage of the design, one seeks an expression for the volume-averaged rate of reactant consumption within

the catalyst. The effectiveness factor appropriate to a specific rate law and catalyst geometry allows one to summarize intrapellet diffusion and chemical reaction within the internal pores in terms of gas-phase conditions near the external surface of the catalyst. When the external resistance to mass transfer in the boundary layer adjacent to the external surface of the catalyst is much smaller than the intrapellet resistance, it is reasonable to calculate the rate of reaction in the vicinity of the external surface of the catalyst using bulk gas-phase concentrations or partial pressures. The average residence time is calculated by solving a plug-flow version of the mass transfer equation which neglects radial variations in molar density, except at the tube wall. The radial concentration gradient vanishes at $r = R_{\text{PFR}}$ if the walls of the reactor are impermeable. A one-dimensional ordinary differential equation is formulated with axial position as the only independent variable. This is illustrated in the next section.

22-1 SIMPLIFICATION OF THE GENERALIZED MASS TRANSFER EQUATION FOR A ONE-DIMENSIONAL PLUG FLOW MODEL

The objective of this section is to begin with the generalized form of the dimensionless mass transfer equation, given by (22-1), and discuss the simplifying assumptions required to reduce this partial differential equation to an ordinary differential design equation for packed catalytic tubular reactors. It should be mentioned that the design equation for tubular reactors, which includes convection and chemical reaction, is typically developed from a mass balance over a differential control volume given by

$$dV_{\text{PFR}} = \pi R_{\text{PFR}}^2 \, dz \tag{22-2}$$

It is not necessary to begin with a generalized form of the mass transfer equation that applies to all fluids with constant physical properties. However, if one compares the dimensionless mass transfer equation presented at the beginning of this chapter with the final form of the differential design equation for plug-flow reactors, then it is possible to identify mass transfer rate processes that are neglected in the design problem. Dimensionless numbers should be calculated to justify the neglect of mass transfer rate processes that are not included in the design of a reactor. Hence, the discussion begins with the dimensionless mass transfer equation and highlights the methodology and assumptions that must be invoked to design a packed catalytic tubular reactor.

Under steady-state conditions in a plug-flow tubular reactor, the one-dimensional mass transfer equation for reactant A can be integrated rather easily to predict reactor performance. Equation (22-1) was derived for a control volume that is differentially thick in all coordinate directions. Consequently, mass transfer rate processes due to convection and diffusion occur, at most, in three coordinate directions and the mass balance is described by a partial differential equation. Current research in computational fluid dynamics applied to fixed-bed reactors seeks a better understanding of the flow phenomena by modeling the catalytic pellets "where they are," instead of averaging or homogenizing

the packed bed (see Nijemeisland and Dixon, 2001). Under the assumption of plug flow with an impermeable tube wall, the three-dimensional mass transfer equation simplifies to a one-dimensional model. In principle, the microscopic axial velocity profile $v_z(r)$, or the z component of the local mass-averaged fluid velocity vector in a packed bed, can be obtained from the extended Brinkman–Forchheimer–Darcy equation (see Vortmeyer and Schuster, 1983) if the effective cross-section-averaged parameters, like fluid viscosity, are available. However, plug flow implies that radial variations in the molar density of reactant A are neglected (except at the tube wall) by expanding the control volume in cylindrical coordinates from $r dr d\theta\, dz$ to $\pi R_{\text{PFR}}^2\, dz$. To maintain consistency with the fact that axial coordinate z is the only independent variable required for this one-dimensional model, it is necessary to replace $v_z(r)$, which depends on radial position in the tube, with a cross-section-weighted average interstitial fluid velocity defined by

$$\langle v_z \rangle = \frac{\displaystyle\int_{\theta=0}^{2\pi} \int_{r=0}^{R_{\text{PFR}}} v_z(r) r\, dr\, d\theta}{\varepsilon_{p,\,\text{interpellet}} \pi R_{\text{PFR}}^2} \tag{22-3}$$

where integration is performed over the entire cross section available for flow and $\varepsilon_{p,\,\text{interpellet}}$ is the interpellet porosity of the packed bed. For spherical catalytic pellets that adopt a hexagonal-close-packed or cubic-close-packed arrangement, the maximum volume fraction of solids is 74% (see Daniels and Alberty, 1975, pp. 621–622). This translates to a minimum interpellet porosity of 26%. The cross-section-weighted average interstitial velocity $\langle v_z \rangle$ is used to make the mass-average fluid velocity dimensionless. Hence, $\langle v_z \rangle$ is required to calculate the Reynolds number. In summary, the convective mass transfer contribution in the primary direction of flow is typically written in terms of $v_z(r)$ for a multi-dimensional description of convection and chemical reaction in tubular reactors. When plug flow is invoked, $v_z(r)$ is replaced by $\langle v_z \rangle$. When the one-dimensional model is written in dimensionless form, $\langle v_z \rangle$ does not appear explicitly in the mass balance because it is contained in the Reynolds number. If reactant A participates in multiple chemical reactions on the catalytic surface, then the one-dimensional mass balance in dimensionless form reduces to the following ordinary differential equation (ODE):

$$\text{Re} \cdot \text{Sc} \frac{d\Psi_{\text{A}}}{d\zeta} = \frac{d^2\Psi_{\text{A}}}{d\zeta^2} + \sum_j \nu_{\text{A}j} \Lambda_{\text{A}j,\,\text{interpellet}}^2 R_j^* \tag{22-4}$$

where the dimensionless axial coordinate in the direction of primary fluid flow is

$$\zeta = \frac{z}{L_{\text{PFR}}} \tag{22-5}$$

L_{PFR} is the length of the tubular reactor, the mass transfer Peclet number is

$$\text{Pe}_{\text{MT}} = \text{Re} \cdot \text{Sc} = \frac{L_{\text{PFR}} \langle v_z \rangle}{\mathfrak{D}_{\text{A,\,interpellet}}} \tag{22-6}$$

the interpellet Damkohler number for species A in the jth reaction is

$$\Lambda^2_{\mathrm{A}j,\,\mathrm{interpellet}} = \frac{k_{n_j} L^2_{\mathrm{PFR}} (C_{\mathrm{A0}})^{n_j - 1}}{\mathfrak{D}_{\mathrm{A,\,interpellet}}} \tag{22-7}$$

C_{A0} is the inlet molar density of reactant A at $z = 0$, $\mathfrak{D}_{\mathrm{A,\,interpellet}}$ is the interpellet diffusion coefficient of species A which accounts for axial dispersion in packed beds, the dimensionless rate of the jth reaction is

$$R^*_j = \frac{S_m \rho_{\mathrm{app}} (1 - \varepsilon_{p,\,\mathrm{interpellet}}) \mathfrak{R}_{\mathrm{HW}j}}{k_{n_j} (C_{\mathrm{A0}})^{n_j}} \tag{22-8}$$

$\mathfrak{R}_{\mathrm{HW}j}$ is the Hougen–Watson rate law for the jth chemical reaction on the catalytic surface with units of moles per area per time, S_m is the internal surface area per mass of catalyst, ρ_{app} is the apparent density of the catalytic pellet, and k_{n_j} is the nth-order kinetic rate constant for the jth reaction with units of (volume/mole)$^{n_j - 1}$ per time when the rate law is written on a volumetric basis using gas-phase molar densities. For second-order kinetics where reactants A and B each adsorb on a single active surface site and dual-site chemical reaction is the rate-limiting step,

$$k_{n_j} = S_m \rho_{\mathrm{app}} k_{j,\,\mathrm{surf\ Rx}} K_{\mathrm{A}} K_{\mathrm{B}} (RT)^2 \tag{22-9}$$

where $k_{j,\,\mathrm{surf\ Rx}}$ is the second-order kinetic rate constant for the jth surface-catalyzed chemical reaction with units of moles per area per time when the rate law is expressed in terms of surface coverage fractions, and K_i is the adsorption/desorption equilibrium constant for single-site adsorption of component i with units of inverse pressure. The factor of $(1 - \varepsilon_{p,\,\mathrm{interpellet}})$ in the dimensionless rate law corresponds to the ratio of pellet volume to total reactor volume. It is required to calculate R^*_j in equation (22-8) because $S_m \rho_{\mathrm{app}} \mathfrak{R}_{\mathrm{HW}j}$ represents a pseudo-volumetric rate of reactant consumption, with units of moles per volume of catalyst per time, and the plug-flow mass balance is based on a differential control volume for the entire packed catalytic tubular reactor (i.e., $dV_{\mathrm{PFR}} = \pi R^2_{\mathrm{PFR}}\, dz$). Hence, the rate of reactant consumption, with units of moles per time, is manipulated as follows:

$$S_m \rho_{\mathrm{app}} \mathfrak{R}_{\mathrm{HW}j}\, dV_{\mathrm{pellet}} = S_m \rho_{\mathrm{app}} \mathfrak{R}_{\mathrm{HW}j} (1 - \varepsilon_{p,\,\mathrm{interpellet}})\, dV_{\mathrm{PFR}} \tag{22-10}$$

since $V_{\mathrm{pellet}} = (1 - \varepsilon_{p,\,\mathrm{interpellet}}) V_{\mathrm{PFR}}$. The product of ρ_{app} and $(1 - \varepsilon_{p,\,\mathrm{interpellet}})$ is equivalent to the density of the entire packed bed. One of the final steps in developing the plug-flow mass balance is division by the size of the differential control volume, dV_{PFR}.

The dimensionless microscopic mass transfer equation presented at the beginning of this chapter has been simplified to obtain the one-dimensional mass balance for reactor design:

$$\mathrm{Re} \cdot \mathrm{Sc} \frac{d\Psi_{\mathrm{A}}}{d\zeta} = \frac{d^2 \Psi_{\mathrm{A}}}{d\zeta^2} + \sum_j \nu_{\mathrm{A}j} \Lambda^2_{\mathrm{A}j,\,\mathrm{interpellet}} R^*_j \tag{22-11}$$

The simplification can be analyzed as follows. The generalized convective mass transfer rate process in dimensional form $\mathbf{v}\cdot\nabla c_A$ becomes

$$\mathbf{v}\cdot\nabla c_A \longrightarrow v_z(r)\frac{\partial C_A}{\partial z} \tag{22-12}$$

if convection occurs predominantly in the primary direction of flow. Under the assumption of plug flow, the mass-average local fluid velocity $v_z(r)$ is replaced by the cross-section-weighted average interstitial velocity $\langle v_z\rangle$. In dimensionless form, $\langle v_z\rangle$ is contained in the Reynolds number and axial convection reduces to

$$\mathbf{v}\cdot\nabla c_A \longrightarrow v_z(r)\frac{\partial C_A}{\partial z} \longrightarrow \frac{d\Psi_A}{d\zeta} \tag{22-13}$$

which is consistent with an ordinary differential design equation. The Reynolds number is based on reactor length L_{PFR} because this is an obvious choice to make the axial coordinate z dimensionless (i.e., $\zeta = z/L_{PFR}$). In both formulations, the mass transfer Peclet number (i.e., $\mathrm{Re}\cdot\mathrm{Sc}$) appears as the dimensionless scaling factor on the left-hand side of the mass balance. The generalized dimensionless form for molecular mass transfer via diffusion, $\nabla\cdot\nabla\Psi_A = \nabla^2\Psi_A$, reduces to $d^2\Psi_A/d\zeta^2$ for a one-dimensional (i.e., ODE) model that accounts for diffusion in the axial direction. The importance of axial diffusion (actually, interpellet axial dispersion, as defined later in this chapter) relative to axial convection is estimated by calculating the mass transfer Peclet number. Backmixing due to axial diffusion is less important when $\mathrm{Pe_{MT}} = \mathrm{Re}\cdot\mathrm{Sc}$ is larger. The contribution from multiple chemical reactions is exactly the same in both forms of the mass transfer equation.

22-2 DIFFERENTIAL FORM OF THE DESIGN EQUATION FOR IDEAL PACKED CATALYTIC TUBULAR REACTORS WITHOUT INTERPELLET AXIAL DISPERSION

If there is only one chemical reaction on the internal catalytic surface, then $\nu_{A1} = -1$ and subscript j is not required for all quantities that are specific to the jth chemical reaction. When the mass transfer Peclet number which accounts for interpellet axial dispersion in packed beds is large, residence-time distribution effects are insignificant and axial diffusion can be neglected in the plug-flow mass balance given by equation (22-11). Under these conditions, reactor performance can be predicted from a simplified one-dimensional model. The differential design equation is

$$\frac{d\Psi_A}{d\zeta} = -\left\{\frac{\Lambda^2_{A,\,\text{interpellet}}}{\mathrm{Re}\cdot\mathrm{Sc}}\right\} R^* \tag{22-14}$$

subject to the boundary condition that $\Psi_A = 1$ at the reactor inlet where $\zeta = 0$. This is a first-order ordinary differential equation because axial diffusion is

neglected. It is instructive to analyze the ratio of the interpellet Damkohler number for reactant A and $\mathrm{Pe}_{\mathrm{MT}}$:

$$\frac{\Lambda^2_{\mathrm{A,\,interpellet}}}{\mathrm{Re}\cdot\mathrm{Sc}} = \frac{k_n L^2_{\mathrm{PFR}} (C_{\mathrm{A0}})^{n-1}/\mathfrak{D}_{\mathrm{A,\,interpellet}}}{L_{\mathrm{PFR}}\langle v_z\rangle/\mathfrak{D}_{\mathrm{A,\,interpellet}}}$$

$$= \frac{L_{\mathrm{PFR}}/\langle v_z\rangle}{1/[k_n (C_{\mathrm{A0}})^{n-1}]} \tag{22-15}$$

The numerator of (22-15) represents the average residence time for convective mass transfer through the reactor:

$$\frac{L_{\mathrm{PFR}}}{\langle v_z\rangle} = \tau \tag{22-16}$$

The denominator of (22-15) corresponds to a characteristic time constant for nth-order irreversible chemical reactions:

$$\frac{1}{k_n (C_{\mathrm{A0}})^{n-1}} = \omega \tag{22-17}$$

This expression for ω is also applicable for reversible chemical kinetics when the forward and backward reactions are both nth-order. In other words, it is acceptable to define the chemical reaction time constant for reversible reactions in terms of the kinetic rate constant for the forward step. The differential design equation given by (22-14) for one-dimensional convection and one chemical reaction in a plug-flow tubular reactor reduces to

$$\frac{d\Psi_{\mathrm{A}}}{d\zeta} = -\left(\frac{\tau}{\omega}\right) R^* \tag{22-18}$$

where the dimensionless rate law R^* accounts for the detailed nature of the chemical kinetics. A simple example of the application of time constants is described by the following scenario. If the chemical kinetics are first-order (i.e., reversible or irreversible) with $n = 1$, then ω is independent of the inlet molar density of reactant A, or the inlet total pressure for gas-phase kinetics. Consequently, reactant conversion depends strongly on residence time τ, but it is not affected by the characteristics of the feed stream. For nth-order kinetics where $n > 1$, an increase in the inlet molar density of reactant A causes ω to decrease, yielding greater conversion of reactants to products without increasing the average residence time. Hence, one should consider the effect that diluting, concentrating or pressurizing the feed stream has on ω if the overall objective is to achieve greater conversion of reactants to products without increasing the length of a tubular reactor.

22-2.1 Relations between Time Constants for Important Mass Transfer Rate Processes and the Dimensionless Numbers in the Mass Balance

The interpellet Damkohler number is a ratio of two mass transfer rate processes; the rate of chemical reaction relative to the rate of mass transfer via interpellet

axial dispersion. The mass transfer Peclet number is also a ratio of two rate processes: the rate of convective mass transfer relative to the rate of mass transfer via interpellet axial dispersion. The denominators of these two dimensionless numbers are the same. Hence,

$$\frac{\Lambda^2_{\text{A, interpellet}}}{\text{Re}\cdot\text{Sc}} = \frac{\tau}{\omega} \tag{22-19}$$

represents the rate of chemical reaction relative to the rate of convective mass transfer. This ratio in equation (22-19) also represents the time constant for convective mass transfer relative to the time constant for nth-order irreversible chemical reaction. In summary, the dimensionless numbers of interest for reactor design can be expressed as ratios of dimensional scaling factors for two mass transfer rate processes, or ratios of time constants for the same two mass transfer rate processes in reverse order. In other words, the dimensional scaling factor for a particular mass transfer rate process is inversely proportional to its time constant. For completeness, the time constant for diffusion is defined as the square of a characteristic length divided by the diffusion coefficient. With respect to the design of a packed catalytic tubular reactor that includes interpellet axial dispersion, the diffusion time constant Θ_D is given by

$$\Theta_D = \frac{L^2_{\text{PFR}}}{\mathfrak{D}_{\text{A, interpellet}}} \tag{22-20}$$

All dimensionless numbers that are required to analyze mass transfer in packed catalytic tubular reactors can be expressed in terms of three time constants: τ, ω, and Θ_{D}. For example, the mass transfer Peclet number is

$$\text{Re}\cdot\text{Sc} = \frac{L_{\text{PFR}}\langle v_z\rangle}{\mathfrak{D}_{\text{A, interpellet}}} = \frac{\Theta_D}{\tau} \tag{22-21}$$

The rate of convective mass transfer relative to the rate of mass transfer via interpellet axial dispersion is equivalent to the ratio of the diffusion time constant relative to the residence time for convective mass transfer. The interpellet Damkohler number for reactant A is

$$\Lambda^2_{\text{A, interpellet}} = \frac{k_n L^2_{\text{PFR}}(C_{\text{A0}})^{n-1}}{\mathfrak{D}_{\text{A, interpellet}}} = \frac{\Theta_D}{\omega} \tag{22-22}$$

The rate of chemical reaction relative to the rate of mass transfer via interpellet axial dispersion is equivalent to the ratio of the diffusion time constant relative to the characteristic time constant for chemical reaction.

22-2.2 Simplified Design Using Effectiveness Factor Correlations Based on Intrapellet Damkohler Numbers

The generalized mass transfer equation has been reduced to the following one-dimensional plug-flow model with axial convection and one chemical reaction in

dimensionless form when the effects of interpellet axial dispersion are negligible:

$$\frac{d\Psi_A}{d\zeta} = -\left(\frac{\tau}{\omega}\right) R^* \tag{22-23}$$

The dimensionless rate of reaction was defined above:

$$R^* = \frac{S_m \rho_{app}(1 - \varepsilon_{p,\,interpellet})\mathfrak{R}_{HW}}{k_n (C_{A0})^n} \tag{22-24}$$

where the Hougen–Watson rate law $\mathfrak{R}_{HW}$ is typically expressed in terms of gas-phase partial pressures or molar densities within the pores of the catalyst. At this stage of the reactor design, the dimensionless rate of chemical reaction is written in terms of dimensionless molar densities near the external surface of a catalytic pellet $\Psi_{i,\,surface}$, and the effectiveness factor, $E(\Lambda_{A,\,intrapellet})$. Hence, the differential design equation, given by (22-23), becomes

$$\frac{d\Psi_A}{d\zeta} = -\left(\frac{\tau}{\omega}\right) E(\Lambda_{A,\,intrapellet}) R^*(\text{all } \Psi_{i,\,surface}) \tag{22-25}$$

The effectiveness factor E is evaluated for the appropriate kinetic rate law and catalyst geometry at the corresponding value of the intrapellet Damkohler number of reactant A. When the resistance to mass transfer within the boundary layer external to the catalytic pellet is very small relative to intrapellet resistances, the dimensionless molar density of component i near the external surface of the catalyst ($\Psi_{i,\,surface}$) is very similar to the dimensionless molar density of component i in the bulk gas stream that moves through the reactor (Ψ_i). Under these conditions, the kinetic rate law is evaluated at bulk gas-phase molar densities, Ψ_i. This is convenient because the convective mass transfer term on the left side of the plug-flow differential design equation ($d\Psi_A/d\zeta$) is based on the bulk gas-phase molar density of reactant A. The one-dimensional mass transfer equation which includes the effectiveness factor,

$$\frac{d\Psi_A}{d\zeta} = -\left(\frac{\tau}{\omega}\right) E(\Lambda_{A,\,intrapellet}) R^*(\text{all } \Psi_i) \tag{22-26}$$

is integrated from the reactor inlet where $\zeta = 0$ and $\Psi_A = 1$ to the outlet where $\zeta = 1$ and $\Psi_A = \Psi_{Afinal} = 1 - \chi_{final}$.

The reactor length required to achieve final conversion χ_{final} is calculated from the average residence time τ as follows:

$$\tau = \frac{L_{PFR}}{\langle v_z \rangle} = \frac{\omega}{E(\Lambda_{A,\,intrapellet})} \int_{\Psi_{A,\,final}}^{1} \frac{d\Psi_A}{R^*(\text{all } \Psi_i)} \tag{22-27}$$

As expected, a shorter reactor is required to achieve the same final conversion when the characteristic chemical reaction time constant ω is smaller and the effectiveness factor E is larger. Since the integral in equation (22-27) that contains the dimensionless kinetic rate law reduces to a constant when the final conversion of

reactant A is specified, the average residence time for a plug-flow tubular reactor is proportional to the chemical reaction time constant and inversely proportional to the effectiveness factor. This relation $\tau \approx \omega/E(\Lambda_{\text{A, intrapellet}})$ can be developed further to generate a scaling law which illustrates how the following factors affect the average residence time required to achieve a specified conversion of reactant A to products:

1. Size of each catalytic pellet, $V_{\text{catalyst}}/S_{\text{external}}$
2. Intrapellet porosity, $\varepsilon_{p,\text{ intrapellet}}$
3. Intrapellet tortuosity factor, τ_{or}
4. Average pore size, $\langle r_{\text{average}} \rangle$
5. Surface-catalyzed kinetic rate constant, $k_{\text{surface Rx}}$
6. Net intrapellet diffusion coefficient, $\mathfrak{D}_{\text{A, net intrapellet}}$

When the intrapellet Damkohler number for reactant A is large enough and the catalyst operates in the diffusion-limited regime, the effectiveness factor is inversely proportional to the Damkohler number (i.e., $\Lambda_{\text{A, intrapellet}}$). Under these conditions, together with a large mass transfer Peclet number which minimizes effects due to interpellet axial dispersion, the following scaling law is valid:

$$\tau \propto \omega\Lambda_{\text{A, intrapellet}} \propto \frac{(V_{\text{catalyst}}/S_{\text{external}})}{\varepsilon_{p,\text{ intrapellet}}} \sqrt{\frac{\tau_{\text{or}}\langle r_{\text{average}} \rangle}{k_{\text{surface Rx}}\mathfrak{D}_{\text{A, net intrapellet}}}} \tag{22-28}$$

This is the focus of Problem 22-10 on p. 608. Hence, the scaling exponents are as follows:

$+1$	for pellet size (i.e., $V_{\text{catalyst}}/S_{\text{external}}$)
-1	for intrapellet porosity, $\varepsilon_{p,\text{ intrapellet}}$
$+0.5$	for intrapellet tortuosity factor, τ_{or}
$+0.5$	for average pore size, $\langle r_{\text{average}} \rangle$
-0.5	for surface-catalyzed kinetic rate constant, $k_{\text{surface Rx}}$
-0.5	for net intrapellet diffusivity, $\mathfrak{D}_{\text{A, net intrapellet}}$

The scaling exponents allow one to estimate how a specified change in one of the six factors described above will affect the average residence time required to achieve the same conversion of reactant A to products, with all other factors remaining unchanged. For example, the average residence time must increase two-fold when the pellet size is doubled because the central core of each catalyst is not used very efficiently. The average residence time must increase two-fold when the average pore size is four-fold larger because the internal surface area per unit volume of catalyst decreases. However, in the micropore regime (i.e., $\langle r_{\text{average}} \rangle < 50$ Å) where Knudsen flow provides the major resistance to intrapellet mass transfer and the net intrapellet diffusivity depends linearly on average pore size, the average residence time is not a function of $\langle r_{\text{average}} \rangle$. For first-order

irreversible chemical kinetics where the characteristic time constant for chemical reaction and the intrapellet Damkohler number do not depend on the molar density of reactant A, if the catalytic pores are large enough and ordinary molecular diffusion provides the major resistance to intrapellet mass transfer, then a four-fold decrease in pressure that produces a four-fold increase in the net intrapellet diffusivity requires a two-fold reduction in the average residence time to achieve the same final conversion of reactant A.

Before one can obtain a numerical value for τ from the integral form of the plug-flow reactor design equation, given by (22-27), it is necessary to focus on the dimensionless kinetic rate law, which could be rather complex.

22-2.3 Generating the Design Correlation between the Average Residence Time for Convective Mass Transfer and the Intrapellet Damkohler Number

Using log-log coordinates, it is possible to generate a linear relation between τ/ω and the intrapellet Damkohler number ($\Lambda_{\text{A, intrapellet}}$) in the diffusion-limited regime for the chemical reaction described below that occurs within the internal pores of catalysts with rectangular symmetry. The overall objective is to achieve 80% conversion of reactant A in the exit stream of the reactor. The time constant for convective mass transfer through the reactor is the average residence time, τ. The time constant for nth-order irreversible chemical reaction is ω. The ratio τ/ω is equivalent to the ratio of the interpellet Damkohler number ($\Lambda^2_{\text{A, interpellet}}$) to the mass transfer Peclet number (i.e., Re ·Sc), where both dimensionless numbers are based on interpellet axial dispersion through the reactor. It is reasonable to neglect residence-time distribution effects because the mass transfer Peclet number is large. The reaction scheme is as follows:

1. $A + B \rightarrow C + D$.
2. Each component adsorbs on a single internal active site within the pores.
3. The activated complex is not considered in the sequence of elementary steps.
4. Dual-site surface reaction is the slowest step in the overall mechanism.
5. The reverse reaction is negligible (i.e., $K_{\text{equilibrium}} \rightarrow \infty$).

The feed stream to the packed catalytic reactor is equimolar, or stoichiometric, in reactants A and B. The dimensionless adsorption/desorption equilibrium constants are

$$\vartheta_i = K_i C_{\text{A, surface}} RT = 0.3 \tag{22-29}$$

for all components. The effective intrapellet diffusion coefficients are

$$\mathfrak{D}_{\text{B, effective}} = 2\mathfrak{D}_{\text{A, effective}} \tag{22-30}$$

$$\mathfrak{D}_{\text{C, effective}} = \frac{\mathfrak{D}_{\text{A, effective}}}{1.2} \qquad \mathfrak{D}_{\text{D, effective}} = \frac{\mathfrak{D}_{\text{A, effective}}}{0.3} \tag{22-31}$$

In other words, the delta parameters are

$$\delta_B = 0.5 \qquad \delta_C = 1.2 \qquad \delta_D = 0.3$$

where δ_i is defined as the ratio of effective intrapellet diffusion coefficients in the catalytic pores for reactant A with respect to component i. Use conditions on the external surface of the catalyst which are representative of pellets near the inlet to the reactor ($\Psi_{B,\,surface} = 1.0$, $\Psi_{C,\,surface} = 0.1$, and $\Psi_{D,\,surface} = 0.1$) to calculate the effectiveness factor at each value of the intrapellet Damkohler number ($\Lambda_{A,\,intrapellet}$).

22-3 DESIGN OF A PACKED CATALYTIC TUBULAR REACTOR FOR THE PRODUCTION OF METHANOL FROM CARBON MONOXIDE AND HYDROGEN

Carbon monoxide and hydrogen produce methanol in a packed catalytic tubular reactor at 2 atm total pressure. The chemical reaction occurs on a high-surface-area catalyst where hydrogen experiences dissociative adsorption and CO adsorbs on a single active site without preference. The overall objective is to calculate the reactor length required to convert a specified fraction of CO to methanol. At sufficiently high mass transfer Peclet numbers, axial dispersion does not affect reactor performance. Hence, a mass transfer/chemical reaction model that includes convective transport and the effectiveness factor should be adequate for reactor design. The catalytic pellets are spherical with an average pore size that favors ordinary molecular diffusion as the primary intrapellet resistance. The reactor design engineer synthesizes the following strategy to obtain a pseudo-analytical solution rather quickly:

1. Postulate a Langmuir–Hinshelwood heterogeneous mechanism for the chemical reaction and develop the corresponding Hougen–Watson kinetic rate law when five-site reaction on the catalytic surface is the slowest step.
2. Linearize the rate of reaction to simulate pseudo-first-order kinetics.
3. Obtain an analytical solution for the effectiveness factor in spherical pellets that is consistent with pseudo-first-order kinetics.
4. Calculate the average residence time for the packed catalytic tubular reactor in terms of the effectiveness factor, and ultimately the intrapellet Damkohler number, without complications due to residence-time distribution effects.

22-3.1 Heterogeneous Catalytic Mechanism

There are no hydrogen–hydrogen bonds in CH_3OH, so it seems reasonable that H_2 must dissociate in the gas phase prior to adsorbing on the catalyst. The carbon–oxygen triple bond in CO reverts to a single bond in the final product. These characteristics of the three components are captured in the four-step modified Langmuir–Hinshelwood mechanism, where chemical reaction is considered to

be rate limiting and, for simplicity, methanol occupies one active site. Hence,

$$\begin{aligned} \mathrm{CO} + \sigma &= \mathrm{CO}\sigma \\ \mathrm{H_2} + 2\sigma &= 2\mathrm{H}\sigma \\ \mathrm{CO}\sigma + 4\mathrm{H}\sigma &\leftrightarrow \mathrm{CH_3OH}\sigma + 4\sigma \\ \mathrm{CH_3OH}\sigma &= \mathrm{CH_3OH} + \sigma \end{aligned} \tag{22-32}$$

Single-site surface coverage by CO and methanol is described by a classic Langmuir isotherm, whereas H_2 requires modification for dual-site dissociative adsorption. Hence,

$$\Theta_i = \Theta_V (K_i p_i)^{1/\gamma_i} \qquad \gamma_{\mathrm{CO}} = 1 \qquad \gamma_{\mathrm{H}} = 2 \qquad \gamma_{\mathrm{MeOH}} = 1 \tag{22-33}$$

Notice that the adsorption/desorption equilibrium constant for H_2 is based on the second equilibrated step in the mechanism, even though $2\mathrm{H_2} + 4\sigma = 4\mathrm{H}\sigma$ is required to produce one molecule of CH_3OH in the third step of (22-32). A population balance leads to the following expression for the vacant-site fraction:

$$\Theta_V = \left\{ 1 + \sum_i (K_i p_i)^{1/\gamma_i} \right\}^{-1} \tag{22-34}$$

If five-site chemical reaction on the catalytic surface is the slowest elementary step, then the Hougen–Watson kinetic rate law is constructed as follows:

$$\begin{aligned} \mathfrak{R}_{\mathrm{Hougen-Watson}} &= k_{\text{forward, surf. Rx}} \Theta_{\mathrm{CO}} (\Theta_{\mathrm{H}})^4 \\ &\quad - k_{\text{backward, surf. Rx}} \Theta_{\mathrm{MeOH}} (\Theta_V)^4 \approx (\Theta_V)^5 \end{aligned} \tag{22-35}$$

This model is expressed in terms of partial pressures by invoking the adsorption isotherms to describe surface coverage by each species:

$$\begin{aligned} \mathfrak{R}_{\mathrm{Hougen-Watson}} &= [k_{\text{forward, surf. Rx}} K_{\mathrm{CO}} p_{\mathrm{CO}} (K_{\mathrm{H}} p_{\mathrm{H}})^2 \\ &\quad - k_{\text{backward, surf. Rx}} K_{\mathrm{MeOH}} p_{\mathrm{MeOH}}] (\Theta_V)^5 \end{aligned} \tag{22-36}$$

The dimensionless equilibrium constant for chemical reaction on the catalytic surface is given by the kinetic rate constant ratio, $k_{\text{forward, surf. Rx}} / k_{\text{backward, surf. Rx}}$. When $\mathfrak{R}_{\mathrm{Hougen-Watson}} \to 0$ in equation (22-36), one arrives at a relation between all of the equilibrium constants:

$$\begin{aligned} K_{\text{eq, surf. Rx}} \equiv \frac{k_{\text{forward, surf. Rx}}}{k_{\text{backward, surf. Rx}}} &= \left[\frac{\Theta_{\mathrm{MeOH}} (\Theta_V)^4}{\Theta_{\mathrm{CO}} (\Theta_{\mathrm{H}})^4} \right]_{\text{at equilibrium}} \\ &= \frac{K_{\text{eq, } p} K_{\mathrm{MeOH}}}{K_{\mathrm{CO}} (K_{\mathrm{H}})^2} \end{aligned} \tag{22-37}$$

where the equilibrium constant based on gas-phase partial pressures $K_{\text{eq, } p}$ has units of $(\mathrm{atm})^{-2}$ and each adsorption/desorption equilibrium constant has units

of $(\text{atm})^{-1}$. The final expression for the rate of reaction, based on the heterogeneous model proposed in (22-32), employs thermodynamic data to calculate the temperature dependence of the equilibrium constant, $K_{\text{eq},\,p}(T)$:

$$\begin{aligned}
\mathfrak{R}_{\text{Hougen-Watson}} &= k_{\text{forward, surf. Rx}} K_{\text{CO}} (K_{\text{H}})^2 \left\{ p_{\text{CO}} (p_{\text{H}_2})^2 - \frac{p_{\text{MeOH}}}{K_{\text{eq},\,p}(T)} \right\} (\Theta_V)^5 \\
\Theta_V &= \left\{ 1 + \sum_i (K_i p_i)^{1/\gamma_i} \right\}^{-1} \\
\ln[K_{\text{eq},\,p}(\text{atm})^{-2}] &= A + \frac{B}{T} \qquad (22\text{-}38) \\
A &= \frac{(\Delta S^\circ)_{\text{Rx, 298}}}{R} = -26.7 \\
B &= -\frac{(\Delta H^\circ)_{\text{Rx, 298}}}{R} = 10,913 \text{ K}
\end{aligned}$$

22-3.2 Linearization of the Hougen–Watson Kinetic Rate Law

It is advantageous to linearize the rate law, given by equations (22-38), because analytical solutions are available for diffusion and chemical reaction within porous catalysts of all geometries when the kinetics are first-order. Consequently, one calculates the effectiveness factor in spherical pellets rather easily after linearization is performed. The best value of the pseudo-first-order kinetic rate constant for irreversible reactions that achieve 100% conversion is

$$k_1 = \frac{3}{C_{\text{A0}}} \int_0^1 S_m \rho_{\text{app}} \mathfrak{R}_{\text{Hougen-Watson}} (1 - x)\, dx \qquad (22\text{-}39)$$

where x corresponds to CO conversion and C_{A0} is the molar density of CO at the reactor inlet. If the feed stream contains CO and H_2 in stoichiometric proportions, then the inlet mole fraction of CO (i.e., y_{A0}) is $\frac{1}{3}$. Hence,

$$C_{\text{A0}} = y_{\text{A0}} \frac{p}{RT} = \frac{p}{3RT} \qquad (22\text{-}40)$$

via the ideal gas law, where p represents total pressure. Dalton's law is used to express each partial pressure p_i in the Hougen–Watson model as a product of total pressure and mole fraction y_i. Hence,

$$\begin{aligned}
p_i &= y_i p \\
y_{\text{CO}} &= \frac{1 - x}{3 - 2x} \\
y_{\text{H}_2} &= \frac{2(1 - x)}{3 - 2x} \qquad (22\text{-}41) \\
y_{\text{MeOH}} &= \frac{x}{3 - 2x}
\end{aligned}$$

and the best pseudo-first-order kinetic rate constant is calculated by evaluating the following integral expression:

$$\frac{k_1}{S_m \rho_{\text{app}} k_{\text{forward, surf. Rx}} K_{\text{CO}} (K_{\text{H}})^2} = 9RTp^2 \int_0^1 \left\{ y_{\text{CO}} (y_{\text{H}_2})^2 - \frac{y_{\text{MeOH}}}{p^2 \exp\left(A + \dfrac{B}{T}\right)} \right\} (\Theta_V)^5 (1 - x)\, dx \tag{22-42}$$

where the upper limit of integration (i.e., $x_{\text{equilibrium}}$) is 100% and the reverse reaction must be neglected. If reversibility is an important consideration in the synthesis of methanol and $x_{\text{equilibrium}} \neq 1$, then the upper integration limit must be reduced from 1 to $x_{\text{equilibrium}}$, and the factor of 9 in (22-42) should be replaced by $9/[1 - (1 - x_{\text{equilibrium}})^3]$, where $x_{\text{equilibrium}}$ depends on temperature and pressure, as appropriate for exothermic reactions that experience a reduction in volume and subsequent decrease in entropy at higher conversion of CO.

22-3.3 Analytical Solution for the Effectiveness Factor

When the kinetics are first-order and irreversible in catalytic pellets with spherical symmetry, the mass transfer/chemical reaction model that focuses on intrapellet diffusion is written in dimensionless form for carbon monoxide as

$$\frac{1}{\eta^2} \frac{d}{d\eta} \left(\eta^2 \frac{d\Psi_{\text{A}}}{d\eta} \right) = \Lambda^2_{\text{intrapellet}} \Psi_{\text{A}} \tag{22-43}$$

with boundary conditions

$$\Psi_{\text{A}} = 1 \qquad \text{at } \eta = 1 \tag{22-44a}$$

$$d\Psi_{\text{A}}/d\eta = 0 \qquad \text{at } \eta = 0 \tag{22-44b}$$

The solution to this linear second-order homogeneous ODE with variable coefficients provides basic information for the dimensionless molar density profile of reactant A (i.e., CO):

$$\Psi_{\text{A}}(\eta;\, \Lambda_{\text{intrapellet}}) = \frac{1}{\eta} \frac{\sinh \Lambda_{\text{intrapellet}} \eta}{\sinh \Lambda_{\text{intrapellet}}} \tag{22-45}$$

The intrapellet Damkohler number $\Lambda_{\text{intrapellet}}$ represents an order-of-magnitude estimate of the rate of chemical reaction relative to the rate of intrapellet diffusion. In terms of the best pseudo-first-order kinetic rate constant k_1 from equation (22-42),

$$\Lambda^2_{\text{intrapellet}} = \frac{k_1 R^2_{\text{pellet}}}{\mathfrak{D}_{\text{CO, intrapellet}}} \tag{22-46}$$

where the effective intrapellet diffusion coefficient for carbon monoxide is based on ordinary molecular diffusion if the catalytic pores are larger than 1 micron.

The effectiveness factor allows one to predict the average rate of consumption of reactants within the internal pores of the catalyst in terms of conditions near the external surface of the pellet, or in the bulk gas stream if external mass transfer resistance is negligible. For spherical geometry and first-order irreversible reaction,

$$E = \frac{3}{\Lambda^2_{\text{intrapellet}}}\left(\frac{d\Psi_A}{d\eta}\right)_{\eta=1} = \int_0^1 3\eta^2\Psi_A(\eta)\,d\eta$$
$$= \frac{3}{\Lambda^2_{\text{intrapellet}}}\left(\frac{\Lambda_{\text{intrapellet}}}{\tanh \Lambda_{\text{intrapellet}}} - 1\right) \tag{22-47}$$

22-3.4 Plug-Flow Design Equation at High Mass Flow Rates

If the mass transfer Peclet number is large enough, then interpellet axial dispersion in packed beds and residence-time distributions do not affect the performance of a tubular reactor. Under these conditions, it is feasible to develop a back-of-the-envelope methodology for prediction of reactor performance via simple integration of the differential design equation given by (22-26), neglecting axial dispersion. Second-order ODEs must be solved when diffusion/dispersion is important. At high Peclet numbers, the following dimensionless first-order ODE accounts for convective mass transfer and chemical reaction:

$$\frac{d\Psi_A}{d\zeta} = -\left(\frac{\tau}{\omega}\right)\mathfrak{R}^* \tag{22-48}$$

where Ψ_A is the dimensionless molar density of CO, ζ the dimensionless axial coordinate in the primary flow direction, τ the average residence time for convective mass transfer, ω the time constant for chemical reaction (i.e., $1/k_{1,\text{ pseudo-first-order}}$), and $\mathfrak{R}^*$ the dimensionless pellet-averaged rate of consumption of reactants that summarizes intrapellet diffusion and chemical reaction within the internal channels of the catalyst by including the effectiveness factor in the rate expression. If the kinetics are first-order and the equilibrium constant is large enough, then

$$\mathfrak{R}^* \approx (1 - \varepsilon_{p,\text{ interpellet}})E(\Lambda_{\text{intrapellet}})\Psi_A(\zeta) \tag{22-49}$$

One calculates the average residence time by integrating the differential design equation, which includes the effectiveness factor:

$$\frac{d\Psi_A}{d\zeta} = -\left(\frac{\tau}{\omega}\right)(1 - \varepsilon_{p,\text{ interpellet}})E(\Lambda_{\text{intrapellet}})\Psi_A(\zeta) \tag{22-50}$$

The integration limits are

$$\Psi_A = \begin{cases} 1 & \text{at } \zeta = 0 \\ 1 - \chi_{\text{final}} & \text{at } \zeta = 1 \end{cases} \tag{22-51}$$

Hence,

$$\tau = \frac{L_{\text{PFR}}}{\langle v_z \rangle_{\text{interstitial}}} = \frac{\omega}{(1 - \varepsilon_{p,\,\text{interpellet}}) E(\Lambda_{\text{intrapellet}})} \ln\left(\frac{1}{1 - \chi_{\text{final}}}\right) \tag{22-52}$$

The effectiveness factor E is expressed in terms of the intrapellet Damkohler number, and the chemical reaction time constant ω is the inverse of the best pseudo-first-order kinetic rate constant. The reactor design engineer employs an integral form of the design equation to predict the length of a packed catalytic tubular reactor L_{PFR} that will achieve a final conversion of CO specified by χ_{final}. The approximate analytical solution, valid at high mass transfer Peclet numbers, is

$$\tau = \frac{\Lambda^2_{\text{intrapellet}} \ln\left(\dfrac{1}{1 - \chi_{\text{final}}}\right)}{3k_1(1 - \varepsilon_{p,\,\text{interpellet}}) \left\{\dfrac{\Lambda_{\text{intrapellet}}}{\tanh \Lambda_{\text{intrapellet}}} - 1\right\}}$$

$$\Lambda^2_{\text{intrapellet}} = \frac{k_1 R^2_{\text{pellet}}}{\mathfrak{D}_{\text{CO, intrapellet}}} \tag{22-53}$$

where k_1 must be evaluated numerically. If the chemical reaction is essentially irreversible over the range of operating temperatures, $K_{\text{eq},\,p} \to \infty$ and the expression for the best pseudo-first-order rate constant reduces to

$$\frac{k_1}{S_m \rho_{\text{app}} k_{\text{forward, surf. Rx}} K_{\text{CO}} (K_{\text{H}})^2 RT} = 9p^2 \int_0^1 y_{\text{CO}} (y_{\text{H}_2})^2 (\Theta_V)^5 (1 - x)\, dx$$

$$y_{\text{CO}} = \frac{1 - x}{3 - 2x} \quad y_{\text{H}_2} = \frac{2(1 - x)}{3 - 2x}$$

$$y_{\text{MeOH}} = \frac{x}{3 - 2x} \quad \Theta_V = \left[1 + \sum_i (K_i y_i p)^{1/\gamma_i}\right]^{-1}$$

$$S_m \rho_{\text{app}} k_{\text{forward, surf. Rx}} K_{\text{CO}} (K_{\text{H}})^2 = 2 \times 10^4 \ \exp[-5000/T(K)] \ \text{g-mol/cm}^3 \cdot \text{min} \cdot \text{atm}^3$$

(22-54)

The pressure dependence of k_1 with units of $(\text{min})^{-1}$ is calculated from 0.03 to 100 atm at 325 K in Figure 22-1 when all adsorption/desorption equilibrium constants are either 0.25 $(\text{atm})^{-1}$ or 2.5 $(\text{atm})^{-1}$. If reversibility is considered in the synthesis of methanol at 325 K and all $K_i = 0.25\ (\text{atm})^{-1}$, then k_1 exhibits a maximum of 15.6 min^{-1} when total pressure is between 5 and 6 atm (i.e., $x_{\text{equilibrium}} \approx 0.98$). For comparison, k_1 exhibits a maximum of 156 min^{-1} at 325 K when total pressure is between 0.5 and 0.6 atm (i.e., $x_{\text{equilibrium}} \approx 0.90$) and all $K_i = 2.5\ (\text{atm})^{-1}$.

If the numerator and denominator of $\tau = L_{\text{PFR}}/\langle v_z \rangle_{\text{interstitial}}$ are multiplied by $\pi R^2_{\text{PFR}} \varepsilon_{p,\,\text{interpellet}}$, then the numerator is equivalent to the reactor void volume, $V_{\text{PFR}} \varepsilon_{p,\,\text{interpellet}}$, and the denominator corresponds to the volumetric flow rate q.

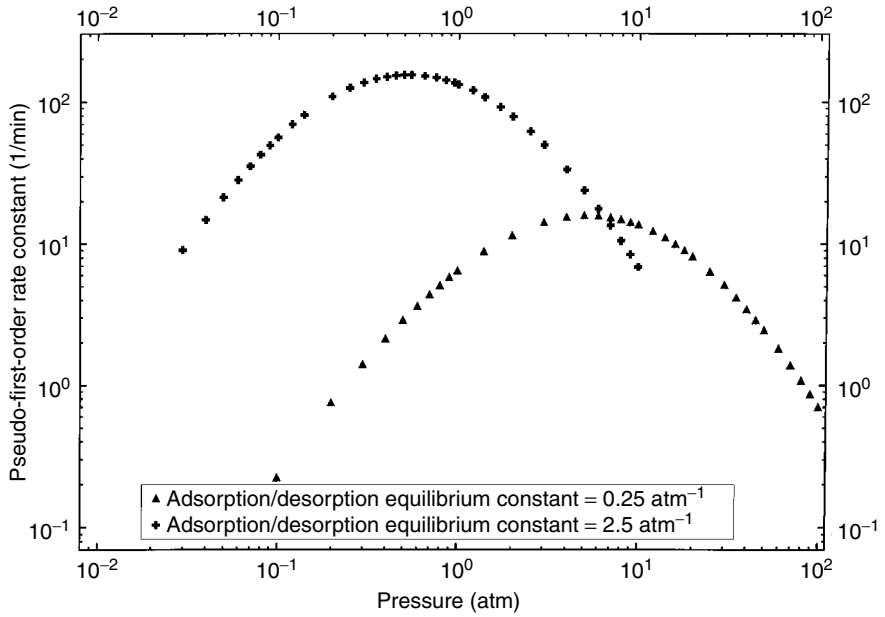

Figure 22-1 Pressure dependence of the best pseudo-first-order kinetic rate constant k_1 with units of min^{-1} is calculated from 0.03 to 100 atm at 325 K for the synthesis of methanol from carbon monoxide and hydrogen. The original heterogeneous catalytic mechanism is postulated as five-site chemical reaction rate controlling, where H_2 undergoes dissociative adsorption and CO and CH_3OH each adsorb on single active sites. In each case, all adsorption/desorption equilibrium constants are either 0.25 or 2.5 atm^{-1}.

The relation between τ and χ_{final}, given by equation (22-52), can be rearranged to calculate final conversion χ_{final} in terms of reactor volume V_{PFR}, where the interpellet porosity is an important design parameter:

$$\chi_{\text{final}} = 1 - \exp\left[\frac{-\varepsilon_{p,\,\text{interpellet}}(1-\varepsilon_{p,\,\text{interpellet}})E(\Lambda_{\text{intrapellet}})V_{\text{PFR}}}{q\omega}\right] \tag{22-55}$$

This result suggests that χ_{final} is optimized when the reactor design engineer achieves a filling factor of 50% (i.e., $\varepsilon_{p,\,\text{interpellet}} = 0.50$) such that one-half of the total reactor volume contains porous catalytic pellets.

22-4 DESIGN OF NON-IDEAL HETEROGENEOUS PACKED CATALYTIC REACTORS WITH INTERPELLET AXIAL DISPERSION

If reactant A participates in one second-order irreversible chemical reaction and its stoichiometric coefficient is -1 in that reaction, then the one-dimensional plug-flow mass balance in dimensionless form, given by (22-11), is described by

the following second-order ordinary differential equation:

$$\mathrm{Re}\cdot\mathrm{Sc}\frac{d\Psi_\mathrm{A}}{d\zeta} = \frac{d^2\Psi_\mathrm{A}}{d\zeta^2} - \Lambda^2_{\mathrm{A,\ interpellet}} E(\Lambda_{\mathrm{A,\ intrapellet}}) R^* \tag{22-56}$$

Subscript j is unnecessary when there is only one chemical reaction. When the kinetics are second-order, irreversible, and only a function of C_A, the dimensionless pseudo-volumetric reaction rate, based on bulk gas-phase concentrations, is

$$\begin{aligned} R^* &= \frac{S_m \rho_{\mathrm{app}} (1 - \varepsilon_{p,\ \mathrm{interpellet}}) \mathfrak{R}_{\mathrm{HW}}}{k_n (C_{\mathrm{A0}})^2} \\ &= \frac{(1 - \varepsilon_{p,\ \mathrm{interpellet}}) k_n (C_\mathrm{A})^2}{k_n (C_{\mathrm{A0}})^2} = (1 - \varepsilon_{p,\ \mathrm{interpellet}})(\Psi_A)^2 \end{aligned} \tag{22-57}$$

because

$$\Psi_\mathrm{A}(\zeta) \equiv \frac{C_\mathrm{A}(z)}{C_\mathrm{A}(z=0)} \tag{22-58}$$

The heterogeneous rate law in (22-57) is dimensionalized with pseudo-volumetric nth-order kinetic rate constant k_n that has units of (volume/mol)$^{n-1}$ per time. k_n is typically obtained from equation (22-9) via surface science studies on porous catalysts that are not necessarily packed in a reactor with void space given by $\varepsilon_{p,\ \mathrm{interpellet}}$. Obviously, when axial dispersion (i.e., diffusion) is included in the mass balance, one must solve a second-order ODE instead of a first-order differential equation. Second-order chemical kinetics are responsible for the fact that the mass balance is nonlinear. To complicate matters further from the viewpoint of obtaining a numerical solution, one must solve a second-order ODE with split boundary conditions. By definition at the inlet to the plug-flow reactor, $\Psi_\mathrm{A} = 1$ at $\zeta = 0$ via equation (22-58). The second boundary condition is $d\Psi_\mathrm{A}/d\zeta \to 0$ as $\zeta \to 1$. This is known classically as the Danckwerts boundary condition in the exit stream (Danckwerts, 1953). For a closed–closed tubular reactor with no axial dispersion or radial variations in molar density upstream and downstream from the packed section of catalytic pellets, Bischoff (1961) has proved rigorously that the Danckwerts boundary condition at the reactor inlet is

$$\Psi_\mathrm{A} - \frac{1}{\mathrm{Re}\cdot\mathrm{Sc}}\left(\frac{d\Psi_\mathrm{A}}{d\zeta}\right) = 1 \qquad \text{at } \zeta = 0 \tag{22-59}$$

which was also employed by Langmuir (1908). Hiby (1962, p. 312) has demonstrated that there is no true back mixing in packed beds, and Wicke (1975) suggests that molecular diffusion across the inlet plane at $\zeta = 0$ is negligible even at small mass transfer Peclet numbers. Hence, it is reasonable to let $\Psi_\mathrm{A} = 1$ at $\zeta = 0$ in packed catalytic tubular reactors, realizing that all possible boundary conditions at the reactor inlet yield similar results at high-mass-transfer Peclet numbers.

The numerical solution of second-order nonlinear ODEs with split boundary conditions requires trial and error integration of two coupled first-order ODEs. If one defines $d\Psi_A/d\zeta = \text{Axial Grad}$, then the one-dimensional plug-flow mass balance with axial dispersion,

$$\frac{d^2\Psi_A}{d\zeta^2} = \text{Re}\cdot\text{Sc}\frac{d\Psi_A}{d\zeta} + \Lambda^2_{A,\,\text{interpellet}}(1-\varepsilon_{p,\,\text{interpellet}})E(\Lambda_{A,\,\text{intrapellet}})(\Psi_A)^2 \tag{22-60}$$

is rewritten as:

$$\frac{d(\text{Axial Grad})}{d\zeta} = \text{Re}\cdot\text{Sc}(\text{Axial Grad}) + \Lambda^2_{A,\,\text{interpellet}}(1-\varepsilon_{p,\,\text{interpellet}})E(\Lambda_{A,\,\text{intrapellet}})(\Psi_A)^2 \tag{22-61}$$

Numerical integration of two coupled first-order ODEs for Ψ_A and Axial Grad requires that both boundary conditions must be known at the same position (i.e., $\zeta = 0$). Since the Danckwerts condition specifies $d\Psi_A/d\zeta$ in the exit stream at $z = L$ (i.e., $\zeta = 1$), it is necessary to (1) guess Axial Grad at $\zeta = 0$, (2) numerically integrate the two ODEs, and (3) monitor the value of Axial Grad at $\zeta = 1$.

Convergence is obtained when the appropriate guess for $d\Psi_A/d\zeta$ at the reactor inlet predicts the correct Danckwerts condition in the exit stream, within acceptable tolerance. To determine the range of mass transfer Peclet numbers where residence-time distribution effects via interpellet axial dispersion are important, it is necessary to compare plug-flow tubular reactor simulations with and without axial dispersion. The solution to the non-ideal problem, described by equation (22-61) and the definition of Axial Grad, at the reactor outlet is $\Psi_A(\zeta = 1,\ \text{RTD})$. The performance of the ideal plug-flow tubular reactor without interpellet axial dispersion is described by

$$\text{Re}\cdot\text{Sc}\frac{d\Psi_A}{d\zeta} = -\Lambda^2_{A,\,\text{interpellet}}(1-\varepsilon_{p,\,\text{interpellet}})E(\Lambda_{A,\,\text{intrapellet}})(\Psi_A)^2$$
$$\Psi_A = 1 \text{ at } \zeta = 0 \tag{22-62}$$

which has the following analytical solution via separation of variables (see equations 22-70 through 22-73):

$$\Psi_A(\zeta) = \frac{1}{1 + [\Lambda^2_{A,\,\text{interpellet}}(1-\varepsilon_{p,\,\text{interpellet}})E(\Lambda_{A,\,\text{intrapellet}})\zeta/\text{Re}\cdot\text{Sc}]} \tag{22-63}$$

In the exit stream of the ideal plug-flow tubular reactor, where $\zeta = 1$,

$$\Psi_A(\zeta = 1, \text{ideal}) = \frac{1}{1 + [\Lambda^2_{A,\,\text{interpellet}}(1-\varepsilon_{p,\,\text{interpellet}})E(\Lambda_{A,\,\text{intrapellet}})/\text{Re}\cdot\text{Sc}]} \tag{22-64}$$

The numerical examples in Sections 22-4.1 and 22-4.2 compare $\Psi_A(\zeta = 1,\ \text{RTD})$ and $\Psi_A(\zeta = 1,\ \text{ideal})$ for several mass transfer Peclet numbers when the kinetics are either first-order or second-order and irreversible.

22-4.1 Numerical Solution of the One-Dimensional Mass Transfer Equation for Second-Order Irreversible Kinetics

When

$$\Lambda^2_{A,\,\text{interpellet}}(1 - \varepsilon_{p,\,\text{interpellet}})E(\Lambda_{A,\,\text{intrapellet}}) = 5$$

ideal and non-ideal plug-flow reactor simulation are provided in Table 22-1 for the following range of mass transfer Peclet numbers: $0.5 \leq \text{Re}\cdot\text{Sc} \leq 15.5$. Reactant conversion in the PFR exit stream is defined by $\chi_{\text{final}} = 1 - \Psi_A(\zeta = 1)$. The Danckwerts condition in the exit stream is considered to be acceptable if $|(d\Psi_A/d\zeta)_{\zeta=1}| < 2 \times 10^{-3}$. Simulations which include interpellet axial dispersion are extremely sensitive to the initial guess for $(d\Psi_A/d\zeta)_{\zeta=0}$. For example, the Danckwerts boundary condition in the exit stream is not satisfied for $\text{Re}\cdot\text{Sc} = 11$ and

$$\Lambda^2_{A,\,\text{interpellet}}(1 - \varepsilon_{p,\,\text{interpellet}})E(\Lambda_{A,\,\text{intrapellet}}) = 5$$

when

$$\left(\frac{d\Psi_A}{d\zeta}\right)_{\zeta=0} = \text{guess} = -0.423$$

because

$$\left(\frac{d\Psi_A}{d\zeta}\right)_{\zeta=1} = 3.76$$

However,

$$\left(\frac{d\Psi_A}{d\zeta}\right)_{\zeta=0} = \text{guess} = -0.423033445$$

which predicts

$$\left(\frac{d\Psi_A}{d\zeta}\right)_{\zeta=1} = -1.20 \times 10^{-4}$$

is acceptable. When the mass transfer Peclet number is larger than 15.5 and this non-ideal reactor problem is solved numerically by incrementing the dimensionless independent spatial variable ζ in the primary flow direction, the two coupled ODEs, given by equation (22-61) and the definition of Axial Grad, exhibit significant instability. In other words, changes in the initial guess for the dimensionless axial gradient at the reactor inlet (i.e., $\zeta = 0$) on the order of 10^{-11} produce enormous fluctuations in reactant concentration profiles such that it is not possible to converge on the Danckwerts boundary condition in the exit stream. At

smaller values of Re·Sc (i.e., <15), the instabilities are not too severe and non-ideal reactor performance can be simulated via the methodology described above. One should realize that this residence-time distribution study is performed in the presence of chemical reaction, but no tracer is employed. It should be obvious from the numerical results summarized in Table 22-1 that one predicts less conversion of reactants to products in the non-ideal reactor relative to the ideal PFR, but reactor performance is almost indistinguishable when the mass transfer Peclet number is greater than ≈15. These simulations provide support for the conservative claim on page 563 which is repeated here: "Axial dispersion has an insignificant effect on reactant conversion in the exit stream for second-order irreversible chemical kinetics when the interpellet Damkohler number, i.e.;

$$\Lambda^2_{\mathrm{A,\ interpellet}}(1-\varepsilon_{p,\ \mathrm{interpellet}})E(\Lambda_{\mathrm{A,\ intrapellet}})=5$$

and the mass transfer Peclet number is greater than 30."

Results from this residence-time distribution simulation are presented graphically in Figure 22-2 as a function of the mass transfer Peclet number. This figure

TABLE 22-1 Numerical Solution of the One-Dimensional Plug Flow Mass Transfer Equation with Convection, Interpellet Axial Dispersion, and Second-Order Irreversible Chemical Kinetics[a]

Re·Sc	$(d\Psi_A/d\zeta)_{\zeta=0}$ (guess)	$(d\Psi_A/d\zeta)_{\zeta=1}$	$\Psi_A(\zeta=1,\ \mathrm{RTD})$	$\Psi_A(\zeta=1,\ \mathrm{ideal})$
0.5	−1.602145	-3.26×10^{-5}	0.424	0.091
1	−1.4582	-1.67×10^{-3}	0.446	0.167
2	−1.22	-4.19×10^{-4}	0.489	0.286
3	−1.03554	$+1.76\times10^{-5}$	0.528	0.375
4	−0.891555	-5.25×10^{-4}	0.562	0.444
5	−0.77787	-2.25×10^{-4}	0.592	0.500
6	−0.6869197	-2.40×10^{-5}	0.620	0.545
7	−0.6131418	-5.69×10^{-5}	0.644	0.583
8	−0.55247335	-9.06×10^{-4}	0.666	0.615
9	−0.50193725	-2.67×10^{-4}	0.685	0.643
10	−0.45933735	$+8.29\times10^{-5}$	0.703	0.667
11	−0.423033445	-1.20×10^{-4}	0.718	0.687
11.01	−0.422697741835	-5.92×10^{-4}	0.719	0.688
12	−0.3917875117	-2.78×10^{-4}	0.733	0.706
13	−0.364653523	-1.54×10^{-4}	0.746	0.722
14	−0.340901636	-5.55×10^{-5}	0.757	0.737
15	−0.3199664314	$+1.02\times10^{-5}$	0.768	0.750
15.5	−0.31039385429	-9.49×10^{-6}	0.773	0.756

[a]Non-ideal simulations satisfy the Danckwerts boundary condition for the outlet concentration gradient. Real and ideal tubular reactor performance at various mass transfer Peclet numbers is compared when the product of the effectiveness factor, the interpellet Damkohler number, and the catalyst filling factor is 5.

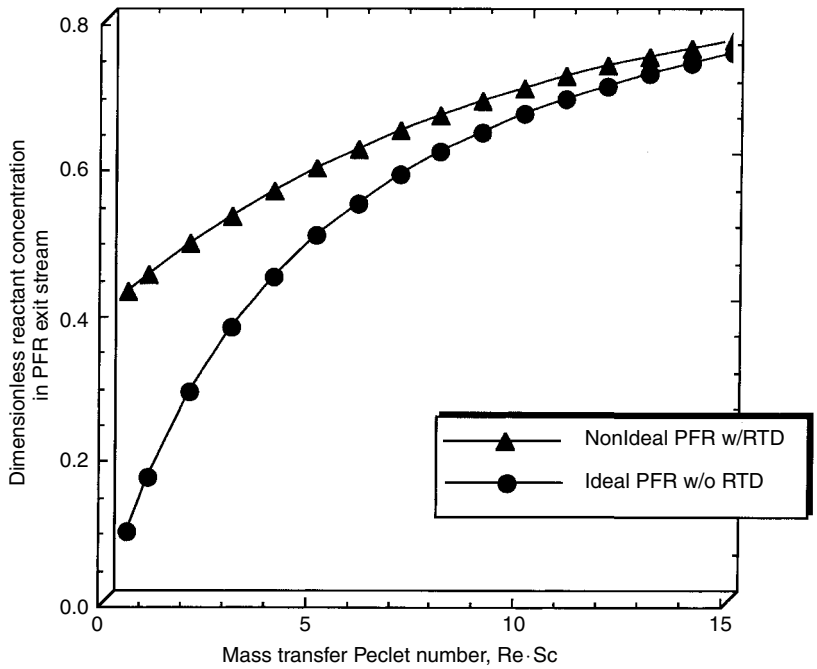

Figure 22-2 Effect of the mass transfer Peclet number on the dimensionless outlet molar density of reactant A for real and ideal tubular reactor performance with second-order irreversible chemical kinetics. The product of the effectiveness factor, the interpellet Damkohler number, and the catalyst filling factor is 5.

compares the dimensionless molar density of reactant A in the exit stream for ideal and non-ideal packed catalytic tubular reactors.

Figure 22-3 illustrates the dimensionless concentration gradient in the inlet stream, which corresponds to the correct guess at $z = 0$ that converges to the Danckwerts boundary condition in the exit stream. Figures 22-2 and 22-3 illustrate the performance of tubular reactors in which convection, interpellet axial dispersion, and chemical reaction represent important mass transfer rate processes that must be considered when the mass transfer Peclet number is small. These simulations provide correct trends when the mass transfer Peclet number is varied numerically, and the interpellet Damkohler number remains constant. However, when tubular reactors are packed with porous catalytic pellets, it is extremely difficult to perform small-scale experiments that can verify these predictions systematically. The difficulty arises because one cannot vary the mass transfer Peclet number experimentally without affecting the interpellet Damkohler number. Hence, it is possible to compare simulation and experiment for a particular combination of $\mathrm{Pe_{MT}}$ and $\Lambda^2_{\mathrm{A,\,interpellet}}$, but experimental design that includes systematic parametric studies in packed catalytic tubular reactors based on these dimensionless numbers is extremely challenging.

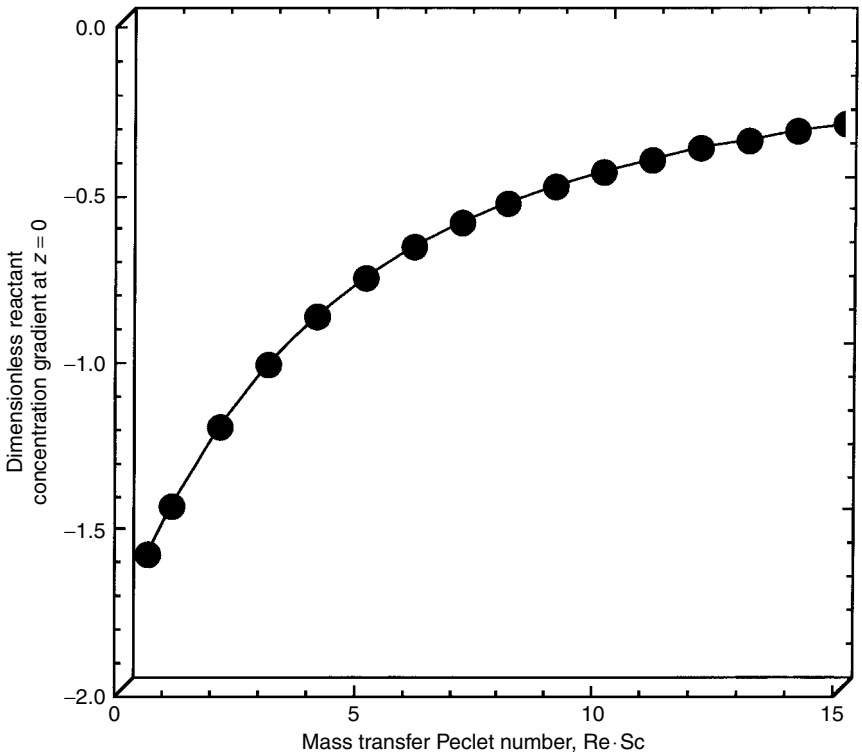

Figure 22-3 Effect of the mass transfer Peclet number on the dimensionless reactant concentration gradient at the inlet to a tubular reactor that converges on the Danckwerts boundary condition in the exit stream for non-ideal performance with second-order irreversible chemical kinetics. The product of the effectiveness factor, the interpellet Damkohler number, and the catalyst filling factor is 5.

22-4.2 Reformulation of the Non-Ideal Tubular Reactor Mass Balance Which Avoids the Instabilities Associated with Stiff Differential Equations

It is possible to avoid some of the instabilities associated with guessing the dimensionless axial concentration gradient at the inlet to a non-ideal tubular reactor by solving the one-dimensional mass transfer equation backwards from outlet to inlet. In practice, it is necessary to introduce a new dimensionless independent spatial variable ξ which increases as one travels backward through the packed catalytic tubular reactor. This stipulation is required by conventional ODE solvers. Hence, if $\xi = 1 - \zeta$, then the two coupled ODEs which represent the mass balance with convection, interpellet axial dispersion, and nth-order irreversible chemical reaction are rewritten as follows:

$$\frac{d\Psi_A}{d\zeta} = \frac{-d\Psi_A}{d\xi} = \text{Axial Grad} \tag{22-65}$$

$$\frac{d^2\Psi_A}{d\zeta^2} = \frac{d(\text{Axial Grad})}{d\zeta} = \frac{-d(\text{Axial Grad})}{d\xi}$$
$$= \text{Re}\cdot\text{Sc}(\text{Axial Grad}) + \Lambda^2_{\text{A, interpellet}}(1-\varepsilon_{p,\text{ interpellet}})E(\Lambda_{\text{A, intrapellet}})(\Psi_A)^n \tag{22-66}$$

The solution to (22-65) and (22-66) is represented by $\Psi_A(\zeta, \text{RTD})$. Now, two boundary conditions in the exit stream are required to initiate the numerical algorithm:

$$\xi = 0 \qquad \text{Axial Grad} = 0 \qquad \Psi_A(\zeta = 1,\ \text{RTD}) = \text{guess}$$

and the correct guess for the dimensionless molar density of reactant A in the exit stream produces convergence at the reactor inlet when $\Psi_A(\xi = 1) = 1 \pm \varepsilon$. The results presented below for $n = 2$ correspond to $\varepsilon \leq 10^{-4}$. Most important, it is possible to extend the range of $\text{Re}\cdot\text{Sc}$ in Table 22-1 for which the performance of ideal and non-ideal reactors can be compared. These numerical results for $\Psi_A(\zeta = 1,\ \text{RTD})$ and analytical results for $\Psi_A(\zeta = 1,\ \text{ideal})$, summarized below in Table 22-2, reveal that the critical value of the mass transfer Peclet number, above which the effect of interpellet axial dispersion is insignificant, is larger when the interpellet Damkohler number increases.

TABLE 22-2 Effect of the Mass Transfer Peclet Number on Real and Ideal Tubular Reactor Performance with Second-Order Irreversible Chemical Kinetics

$\text{Re}\cdot\text{Sc}$	$(d\Psi_A/d\zeta)_{\zeta=0,\text{RTD}}$	$\Psi_A(\zeta = 1,\ \text{RTD})$ (guess)	$\Psi_A(\zeta = 1,\ \text{ideal})$
	$(1-\varepsilon_{p,\text{ interpellet}})E(\Lambda_{\text{A, intrapellet}})\Lambda^2_{\text{A, interpellet}} = 0.5, n = 2$		
1	−0.268	0.856735	0.667
5	−0.096	0.92752	0.9091
10	−0.050	0.9573	0.9524
15	−0.033	0.96996	0.9677
	$(1-\varepsilon_{p,\text{ interpellet}})E(\Lambda_{\text{A, intrapellet}})\Lambda^2_{\text{A, interpellet}} = 1, n = 2$		
1	−0.474	0.76047	0.5
5	−0.186	0.86731	0.833
10	−0.0981	0.91868	0.9091
15	−0.0661	0.94188	0.9375
20	−0.050	0.95487	0.9524
	$(1-\varepsilon_{p,\text{ interpellet}})E(\Lambda_{\text{A, intrapellet}})\Lambda^2_{\text{A, interpellet}} = 5, n = 2$		
1	−1.458	0.447065	0.167
5	−0.778	0.59261	0.5
10	−0.459	0.7033	0.667
15	−0.320	0.76908	0.750
20	−0.244	0.8115	0.8

TABLE 22-2 (***continued***)

Re·Sc	$(d\Psi_A/d\zeta)_{\zeta=0,RTD}$	$\Psi_A(\zeta = 1,\ RTD)$ (guess)	$\Psi_A(\zeta = 1,\ ideal)$
25	−0.197	0.84099	0.833
30	−0.165	0.8626	0.857
50	−0.0996	0.91114	0.9091
	$(1-\varepsilon_{p,\,interpellet})E(\Lambda_{A,\,intrapellet})\Lambda^2_{A,\,interpellet} = 10, n = 2$		
1	−2.212	0.31584	0.09091
5	−1.353	0.439342	0.333
10	−0.861	0.5518	0.5
15	−0.618	0.62992	0.6
20	−0.478	0.68617	0.667
30	−0.326	0.76011	0.75
50	−0.198	0.83735	0.833
	$(1-\varepsilon_{p,\,interpellet})E(\Lambda_{A,\,intrapellet})\Lambda^2_{A,\,interpellet} = 50, n = 2$		
25	−1.764	0.3596	0.3333
30	−1.519	0.3967	0.375
40	−1.182	0.4599	0.4444
50	−0.9634	0.5115	0.5
60	−0.8116	0.5544	0.5455
70	−0.7004	0.5904	0.5833
80	−0.6156	0.6211	0.6154
90	−0.5489	0.6476	0.6429
100	−0.4951	0.6706	0.6667
	$(1-\varepsilon_{p,\,interpellet})E(\Lambda_{A,\,intrapellet})\Lambda^2_{A,\,interpellet} = 75, n = 2$		
40	−1.73	0.3646	0.3478
50	−1.421	0.4131	0.4
60	−1.203	0.4549	0.4444
70	−1.041	0.4913	0.4828
80	−0.9167	0.5232	0.5161
90	−0.8186	0.5514	0.5455
100	−0.7392	0.5765	0.5714
110	−0.6736	0.599	0.5946
120	−0.6187	0.6192	0.6154
130	−0.5719	0.6375	0.6341
	$(1-\varepsilon_{p,\,interpellet})E(\Lambda_{A,\,intrapellet})\Lambda^2_{A,\,interpellet} = 100, n = 2$		
60	−1.585	0.3862	0.375
70	−1.375	0.4211	0.4118
80	−1.214	0.4524	0.4444
90	−1.085	0.4805	0.4737
100	−0.9809	0.5059	0.5
110	−0.8946	0.5289	0.5238
120	−0.8221	0.55	0.5455
130	−0.7604	0.5692	0.5652
140	−0.7072	0.5869	0.5833
150	−0.6609	0.6032	0.6

At seven different values of the interpellet Damkohler number for which real and ideal packed catalytic tubular reactor performance is summarized in Table 22-2, it is possible to identify a critical value of the mass transfer Peclet number $(\mathrm{Re}\cdot\mathrm{Sc})_{\mathrm{critical}}$, above which the effects of interpellet axial dispersion are insignificant for second-order irreversible chemical kinetics. For example, if ideal performance is justified when the outlet conversion of reactants under real and ideal conditions differs by less than 0.5%,

$$\Psi_{\mathrm{A}}(\zeta = 1,\ \mathrm{RTD}) - \Psi_{\mathrm{A}}(\zeta = 1,\ \mathrm{ideal}) \leq 0.005$$

then larger values of $(\mathrm{Re}\cdot\mathrm{Sc})_{\mathrm{critical}}$ are required to achieve ideal performance when the rate of surface catalyzed chemical reaction relative to the rate of mass transfer via interpellet axial dispersion is larger. These trends are summarized in Table 22-3. This trend is reasonable based on the following qualitative analysis. When the time constant for convective mass transfer is several orders of magnitude smaller than the chemical reaction time constant, one should not expect to achieve much conversion of reactants to products in either real or ideal PFRs. Hence, both types of reactors behave similarly, as illustrated in Tables 22-1 and 22-2 when the dimensionless bulk molar density of reactant A is greater than 90% of its inlet value. Now, decrease the chemical reaction time constant at a given value of the time constant for interpellet axial dispersion. This is analogous to increasing the interpellet Damkohler number via equation (22-22). The only way to achieve similar behavior between both types of reactors is to maintain a very small ratio for τ/ω such that very low conversion of reactants to products is obtained. This is accomplished by decreasing the average residence time τ, which is analogous to increasing $\mathrm{Pe}_{\mathrm{MT}}$ via equation (22-21).

For first-order irreversible chemical kinetics in a packed catalytic tubular reactor (i.e., $n = 1$), ideal design strategies are justified if the relative difference

TABLE 22-3 Effect of the Interpellet Damkohler Number on the Critical Value of the Mass Transfer Peclet Number for Second-Order Irreversible Chemical Kinetics in Packed Catalytic Tubular Reactors[a]

$(1 - \varepsilon_{p,\,\mathrm{interpellet}})E(\Lambda_{\mathrm{A,\,intrapellet}})\ \Lambda^2_{\mathrm{A,\,interpellet}}$	$(\mathrm{Re}\cdot\mathrm{Sc})_{\mathrm{critical}}$
0.5	10
1	15
5	30
10	50
50	90
75	105
100	115

[a] Interpellet axial dispersion does not affect reactor performance when the mass transfer Peclet number is above $(\mathrm{Re}\cdot\mathrm{Sc})_{\mathrm{critical}}$.

between real and ideal outlet conversion of reactants differs by less than 0.5%:

$$\frac{\Psi_A(\zeta = 1,\ \text{RTD}) - \Psi_A(\zeta = 1,\ \text{ideal})}{\Psi_A(\zeta = 1,\ \text{RTD})} \leq 0.005$$

Based on this requirement, one obtains the correlation shown in Table 22-4 between the interpellet Damkohler number and the critical value of the mass transfer Peclet number for ideal response. For interpellet Damkohler numbers between 100 and 500 [i.e., $100 < (1 - \varepsilon_{p,\,\text{interpellet}})E(\Lambda_{A,\,\text{intrapellet}})\Lambda^2_{A,\,\text{interpellet}} \leq 500$], a linear relation allows one to predict the critical value of the mass transfer Peclet number, above which ideal reactor performance is guaranteed for first-order irreversible chemical kinetics. Specifically,

$$(\text{Re}\cdot\text{Sc})_{\text{critical}} \approx 111 + 0.72(1 - \varepsilon_{p,\,\text{interpellet}})E(\Lambda_{A,\,\text{intrapellet}})\Lambda^2_{A,\,\text{interpellet}}$$

If one operates a packed catalytic tubular reactor below the critical value of the mass transfer Peclet number where ideal performance is not achieved, then the following empirical linear correlation allows one to predict the dimensionless molar density of reactant A in the exit stream, $\Psi_A(\zeta = 1,\ \text{RTD})$, for first-order irreversible chemical kinetics:

$$\frac{\text{Pe}_{MT}}{(\text{Re}\cdot\text{Sc})_{\text{critical}}}\left\{\frac{\Psi_A(\zeta = 1,\ \text{ideal})}{\Psi_A(\zeta = 1,\ \text{RTD})}\right\} \approx a_0 + a_1\frac{\text{Pe}_{MT}}{(\text{Re}\cdot\text{Sc})_{\text{critical}}} \qquad (22\text{-}67)$$

TABLE 22-4 Effect of the Interpellet Damkohler Number on the Critical Value of the Mass Transfer Peclet Number for First-Order Irreversible Chemical Kinetics in Packed Catalytic Tubular Reactors[a]

$(1 - \varepsilon_{p,\,\text{interpellet}})E(\Lambda_{A,\,\text{intrapellet}})\Lambda^2_{A,\,\text{interpellet}}$	$(\text{Re}\cdot\text{Sc})_{\text{critical}}$
1	15
2	21
4	30
5	34
7	40
10	49
15	61
20	71
25	80
30	89
40	104
50	118
75	149
100	176

[a]Interpellet axial dispersion does not affect reactor performance when the mass transfer Peclet number is above $(\text{Re}\cdot\text{Sc})_{\text{critical}}$.

where the zeroth- and first-order coefficients (i.e., a_0 and a_1) in the previous reactor correlation are weak functions of the interpellet Damkohler number, as illustrated in Table 22-5.

When $n = 1$ for first-order irreversible chemical kinetics, the dimensionless molar density of reactant A in the exit stream of an ideal packed catalytic tubular reactor is given by the following analytical expression at the prevailing value of the actual mass transfer Peclet number, $\mathrm{Pe_{MT}} = \mathrm{Re{\cdot}Sc}$, not $(\mathrm{Re{\cdot}Sc})_{\mathrm{critical}}$:

$$\Psi_{\mathrm{A}}(\zeta = 1,\ \text{ideal}) = \exp\left[\frac{-(1-\varepsilon_{p,\,\text{interpellet}})E(\Lambda_{\mathrm{A,\,intrapellet}})\Lambda^2_{\mathrm{A,\,interpellet}}}{\mathrm{Pe_{MT}}}\right] \tag{22-68}$$

TABLE 22-5 Effect of the Interpellet Damkohler Number on the Zeroth- and First-Order Coefficients in a Linear Empirical Correlation Between Real and Ideal Outlet Conversions[a], Given by Equation (22-67)

$(1-\varepsilon_{p,\,\text{interpellet}})E(\Lambda_{\mathrm{A,\ intrapellet}})\Lambda^2_{\mathrm{A,\,interpellet}}$	a_0	a_1
1	−0.0251	1.0235
2	−0.0277	1.0267
4	−0.0316	1.0296
5	−0.0346	1.0358
7	−0.0370	1.0397
10	−0.0342	1.0313
15	−0.0384	1.0397
20	−0.0350	1.0351
25	−0.0398	1.0426
30	−0.0417	1.0452
40	−0.0461	1.0504
50	−0.0324	1.0309
75	−0.0332	1.0328
100	−0.0393	1.0409
150	−0.0411	1.0356
200	−0.0512	1.0524
250	−0.0598	1.0691
300	−0.0552	1.0554
350	−0.0606	1.0657
400	−0.0543	1.0559
450	−0.0594	1.0653
500	−0.0594	1.0636

[a] Values for first-order irreversible chemical kinetics in packed catalytic tubular reactors that operate at subcritical values of the mass transfer Peclet number.

22-4.3 Replacing the Danckwerts Boundary Condition in the Exit Stream of a Non-Ideal PFR with the Ideal Plug-Flow Reactant Concentration Gradient

This is an unprecedented novel idea that allows one to compare $\Psi_A(\zeta = 1,\ \text{RTD})$ and $\Psi_A(\zeta = 1,\ \text{ideal})$ when both boundary conditions for the non-ideal PFR with interpellet axial dispersion are the same as those for the ideal PFR. In both cases, $\Psi_A = 1$ at the inlet to the reactor (i.e., $\zeta = 0$). The strategy is as follows:

1. Use this boundary condition (i.e., $\Psi_A = 1$ at $\zeta = 0$) to solve the mass balance without interpellet axial dispersion for the ideal plug-flow reactor.
2. Calculate the reactant concentration gradient in the exit stream.
3. Use this condition on $d\Psi_A/d\zeta$ at $\zeta = 1$ from the ideal simulation to replace the Danckwerts boundary condition in the non-ideal simulation which includes interpellet axial dispersion.

As described by equation (22-62), the dimensionless plug-flow mass balance for ideal PFR performance with nth-order irreversible chemical kinetics is

$$\text{Re}\cdot\text{Sc}\frac{d\Psi_A}{d\zeta} = -\Lambda^2_{A,\ \text{interpellet}}(1 - \varepsilon_{p,\ \text{interpellet}})E(\Lambda_{A,\ \text{intrapellet}})(\Psi_A)^n \qquad (22\text{-}69)$$

The analytical solution for n $\neq 1$ is obtained by separating variables and integrating the following expression from $\zeta = 0$ at the reactor inlet to any axial position ζ downstream from the feed:

$$\text{Re}\cdot\text{Sc}\frac{d\Psi_A}{(\Psi_A)^n} = -\Lambda^2_{A,\ \text{interpellet}}(1 - \varepsilon_{p,\ \text{interpellet}})E(\Lambda_{A,\ \text{intrapellet}})d\zeta \qquad (22\text{-}70)$$

$$\Psi_A = 1 \quad \text{at } \zeta = 0$$

which yields

$$\text{Re}\cdot\text{Sc}\left[\left(\frac{1}{\Psi_A}\right)^{n-1} - 1\right] = (n-1)\Lambda^2_{A,\ \text{interpellet}}(1 - \varepsilon_{p,\ \text{interpellet}})E(\Lambda_{A,\ \text{intrapellet}})\zeta \qquad (22\text{-}71)$$

If one defines the following dimensionless parameter:

$$\mu = \frac{\tau}{\omega}(1 - \varepsilon_{p,\ \text{interpellet}})E(\Lambda_{A,\ \text{intrapellet}})$$

$$= \frac{\Lambda^2_{A,\ \text{interpellet}}(1 - \varepsilon_{p,\ \text{interpellet}})E(\Lambda_{A,\ \text{intrapellet}})}{\text{Re}\cdot\text{Sc}} \qquad (22\text{-}72)$$

then the dimensionless reactant molar density profile as a function of axial position ζ through the ideal PFR is

$$\Psi_A(\zeta, \text{ideal}) = \left[\frac{1}{1 + (n-1)\mu\zeta}\right]^{1/(n-1)} \qquad (22\text{-}73)$$

The reactant concentration gradient in the exit stream is calculated from the ideal PFR differential mass balance, given by equation (22-69):

$$\mathrm{Re}\cdot\mathrm{Sc}\left(\frac{d\Psi_A}{d\zeta}\right)_{\zeta=1} = -\Lambda^2_{A,\,\text{interpellet}}(1-\varepsilon_{p,\,\text{interpellet}})E(\Lambda_{A,\,\text{intrapellet}})[\Psi_A(\zeta=1,\ \text{ideal})]^n \tag{22-74}$$

where the reactant concentration in the exit stream is calculated from (22-73):

$$\Psi_A(\zeta=1,\ \text{ideal}) = \left[\frac{1}{1+(n-1)\mu}\right]^{1/(n-1)} \tag{22-75}$$

Hence, the reactant concentration gradient in the ideal PFR exit stream for nth-order irreversible chemical kinetics is

$$\left(\frac{d\Psi_A}{d\zeta}\right)_{\zeta=1} = \frac{-\mu}{[1+(n-1)\mu]^{n/(n-1)}} \tag{22-76}$$

This boundary condition at the reactor outlet should be used in place of the Danckwerts condition to provide a better comparison between ideal and non-ideal PFR simulations of reactant conversion in the PFR exit stream.

Problem. Think about the overall strategy that must be implemented to account for the effect of interpellet axial dispersion on the outlet concentration of reactant A when Langmuir–Hinshelwood kinetics and Hougen–Watson models are operative in a packed catalytic tubular reactor. Residence-time distribution effects are important at small mass transfer Peclet numbers.

22-5 MASS TRANSFER PECLET NUMBERS BASED ON INTERPELLET AXIAL DISPERSION IN PACKED CATALYTIC TUBULAR REACTORS

Results from the previous section in this chapter illustrate how and when interpellet axial dispersion plays an important role in the design of packed catalytic tubular reactors. When diffusion is important, more sophisticated numerical techniques are required to solve second-order ODEs with split boundary conditions to predict non-ideal reactor performance. Tubular reactor performance is non-ideal when the mass transfer Peclet number is small enough such that interpellet axial dispersion cannot be neglected. The objectives of this section are to understand the correlations for effective axial dispersion coefficients in packed beds and porous media and calculate the mass transfer Peclet number based on axial dispersion. Before one can make predictions about the ideal vs. non-ideal performance of tubular reactors, steady-state mass balances with and without axial dispersion must be solved and the reactant concentration profiles from both solutions must be compared. If the difference between these profiles with and without interpellet axial dispersion is indistinguishable, then the reactor operates ideally.

Axial dispersion in packed beds, and Taylor dispersion of a tracer in a capillary tube, are described by the same form of the mass transfer equation. The Taylor dispersion problem, which was formulated in the early 1950s, corresponds to unsteady-state one-dimensional convection and two-dimensional diffusion of a tracer in a straight tube with circular cross section in the laminar flow regime. The microscopic form of the generalized mass transfer equation without chemical reaction is

$$\frac{\partial C_A}{\partial t} + \mathbf{v}\cdot\nabla C_A = \mathfrak{D}_{A,\,\text{ordinary}}\nabla^2 C_A \tag{22-77}$$

for the molar density of a liquid tracer A with constant physical properties. In cylindrical coordinates, if convection occurs primarily in the axial direction and diffusion is important in the radial and axial directions, then the mass balance for tracer A can be written as

$$\frac{\partial C_A}{\partial t} + v_z(r)\frac{\partial C_A}{\partial z} = \mathfrak{D}_{A,\,\text{ordinary}}\left[\frac{1}{r}\frac{\partial}{\partial r}\left(r\frac{\partial C_A}{\partial r}\right) + \frac{\partial^2 C_A}{\partial z^2}\right] \tag{22-78}$$

In the early 1950s, Taylor recognized that this unsteady-state two-dimensional microscopic mass transfer equation for the tracer's molar density, $C_A(r, z, t)$, could be simplified at long times. The strategy involves writing an unsteady-state one-dimensional mass balance for the cross-section-averaged concentration of the tracer, defined by

$$\langle C_A\rangle = f(z,t) = \frac{\displaystyle\int_{\theta=0}^{2\pi}\int_{r=0}^{R} C_A(r,z,t)r\,dr\,d\theta}{\displaystyle\int_{\theta=0}^{2\pi}\int_{r=0}^{R} r\,dr\,d\theta} = \frac{2}{R^2}\int_0^R C_A(r,z,t)r\,dr \tag{22-79}$$

In terms of $\langle C_A\rangle$, the unsteady-state one-dimensional mass balance neglects radial diffusion except at the capillary wall. Hence, if the wall of the capillary is impermeable, which corresponds to zero radial diffusional flux at $r = R$, then the mass balance reduces to

$$\frac{\partial\langle C_A\rangle}{\partial t} + \langle v_z\rangle\frac{\partial\langle C_A\rangle}{\partial z} = \mathfrak{D}_{A,\,\text{eff. axial disp.}}\frac{\partial^2\langle C_A\rangle}{\partial z^2} \tag{22-80}$$

where the ordinary molecular diffusion coefficient in the two-dimensional equation, given by (22-78), is replaced by an effective axial dispersion coefficient in the one-dimensional equation, given by (22-80). The effective axial dispersion coefficient, $\mathfrak{D}_{A,\,\text{eff. axial disp.}}$, is the same as the interpellet diffusion coefficient, $\mathfrak{D}_{A,\,\text{interpellet}}$ in equations (22-6) and (22-7). The experimental correlation for the effective axial dispersion coefficient is based on 175 experimental data points for one-dimensional flow in packed beds and porous media from eight different authors. The particle diameters in these packed beds and porous media range from 0.01 to 0.69 cm.

The following strategy should be used to calculate the interpellet axial dispersion coefficient and the mass transfer Peclet number in packed catalytic tubular reactors (see Dullien, 1992, Chap. 6). Initially, one should calculate a simplified mass transfer Peclet number (i.e., $\mathrm{Pe}_{\mathrm{simple}}$) based on the equivalent diameter of the catalytic pellets, $d_{\mathrm{equivalent}}$, the average interstitial fluid velocity through the packed bed, $\langle v_z \rangle_{\mathrm{interstitial}}$, and the ordinary molecular diffusion coefficient of reactant A, $\mathfrak{D}_{\mathrm{A,\,ordinary}}$.

For catalysts of arbitrary shape, the equivalent diameter is

$$d_{\mathrm{equivalent}} = \frac{6(\text{pellet volume})}{\text{external surface area}} \tag{22-81}$$

This expression for $d_{\mathrm{equivalent}}$ reduces to the actual diameter when the pellets are spherical. The average interstitial fluid velocity is

$$\langle v_z \rangle_{\mathrm{interstitial}} = \frac{q}{\pi R_{\mathrm{PFR}}^2 \varepsilon_{p,\,\mathrm{interpellet}}} \tag{22-82}$$

where q is the volumetric flow rate through the reactor and R_{PFR} is the tube radius. The interpellet porosity $\varepsilon_{p,\,\mathrm{interpellet}}$ is required to determine the actual flow cross section and calculate the average velocity (not the superficial velocity) of the reactive mixture between the catalytic pellets. The prescription to calculate the simplified mass transfer Peclet number for component A is

$$\mathrm{Pe}_{\mathrm{simple}} = \frac{\langle v_z \rangle_{\mathrm{interstitial}} d_{\mathrm{equivalent}}}{\mathfrak{D}_{\mathrm{A,\,ordinary}}} \tag{22-83}$$

The dimensionless quantity Υ, defined by equation (22-84), is equivalent to the ratio of $\mathrm{Pe}_{\mathrm{simple}}$ to the Bodenstein number, as defined by Westerterp *et al.* (1984, pp. 207–211).

$$\Upsilon = \frac{\mathfrak{D}_{\mathrm{A,\,eff.\ axial\ disp.}}}{\mathfrak{D}_{\mathrm{A,\,ordinary}}} \tag{22-84}$$

Empirical and theoretical correlations for Υ are summarized in Table 22-6, and documented for the following range of simplified mass transfer Peclet numbers: $10^{-3} \leq \mathrm{Pe}_{\mathrm{simple}} \leq 3 \times 10^6$. Theoretical correlation (4) in Table 22-6, which has been developed in detail by Deen (1998, pp. 398–404) and Bird *et al.* (2002,

TABLE 22-6 Empirical and Theoretical Correlations between Effective Axial Dispersion Coefficients and the Interstitial Fluid Velocity in Packed Beds and Porous Media

(1)	$\Upsilon \approx 0.67$	when $10^{-3} \leq \mathrm{Pe}_{\mathrm{simple}} < 1$	experimental
(2)	$\Upsilon \approx \mathrm{Pe}_{\mathrm{simple}}$	when $1 < \mathrm{Pe}_{\mathrm{simple}} \leq 100$	experimental
(3)	$\Upsilon \approx 2\mathrm{Pe}_{\mathrm{simple}}$	when $100 < \mathrm{Pe}_{\mathrm{simple}} \leq 3 \times 10^6$	experimental
(4)	$\Upsilon \approx 1 + (\mathrm{Pe}_{\mathrm{simple}})^2/192$	no restriction on $\mathrm{Pe}_{\mathrm{simple}}$	theoretical
(5)	$\Upsilon \approx 0.7[1 + 2.9\mathrm{Pe}_{\mathrm{simple}}^2 (5.8 + \mathrm{Pe}_{\mathrm{simple}})^{-1}]$	spherical packing gaseous fluid	interpolation

pp. 643–646), does not match experimental data very well. Hence, it is recommended that one should use the other four correlations in Table 22-6, which are designed to reproduce the experimental data.

The following comments about the experimental correlations in Table 22-6 provide more insight into the underlying fundamental basis of its existence.

1. Particle size has no explicit effect on the correlations. This is obvious because the correlations are not classified in terms of the equivalent diameters of the packing material used to obtain the experimental data.
2. The effective axial dispersion coefficient, $\mathfrak{D}_{\text{A, eff. axial disp.}}$, is not expressed as a function of the ordinary molecular diffusion coefficient. In other words, the correlations introduced above for $\mathfrak{D}_{\text{A, eff. axial disp.}}/\mathfrak{D}_{\text{A, ordinary}}$ vs. $\text{Pe}_{\text{simple}}$ are exactly the same as those for $\mathfrak{D}_{\text{A, eff. axial disp.}}$ vs. $\langle v_z\rangle_{\text{interstitial}} d_{\text{equivalent}}$. For example, if $\Upsilon \approx \text{Pe}_{\text{simple}}$, as suggested by correlation (2) in Table 22-6, then:

$$\mathfrak{D}_{\text{A, eff. axial disp.}} \approx \langle v_z\rangle_{\text{interstitial}} d_{\text{equivalent}}$$

   If $\Upsilon \approx 2\{\text{Pe}_{\text{simple}}\}$ when the simplified Peclet number is greater than 100, then:

$$\mathfrak{D}_{\text{A, eff. axial disp.}} \approx 2\langle v_z\rangle_{\text{interstitial}} d_{\text{equivalent}}$$

3. When the simplified mass transfer Peclet number is very small (i.e., <1), $\Upsilon \approx 0.67$ instead of unity because the numerator of Υ (i.e., $\mathfrak{D}_{\text{A, eff. axial disp.}}$) is based on unsteady-state pore diffusion without convection, whereas the denominator of Υ (i.e., $\mathfrak{D}_{\text{A, ordinary}}$) is measured in an unrestricted bulk fluid phase. In other words, the diffusivity in the numerator of Υ is reduced by porosity and tortuosity factors.

The differential design equation given by (22-61) or (22-66) for packed catalytic tubular reactors contains the mass transfer Peclet number

$$\text{Pe}_{\text{MT}} = \text{Re}\cdot\text{Sc} = \frac{L_{\text{PFR}}\langle v_z\rangle_{\text{interstitial}}}{\mathfrak{D}_{\text{A, interpellet}}} \tag{22-85}$$

which is based on interpellet axial dispersion, reactor length L_{PFR}, and the average interstitial fluid velocity. The discussion above outlines the strategy to calculate

$$\mathfrak{D}_{\text{A, interpellet}} = \mathfrak{D}_{\text{A, eff. axial disp.}} = \phi_{\text{correlation}}\langle v_z\rangle_{\text{interstitial}} d_{\text{equivalent}} \tag{22-86}$$

where

$$\phi_{\text{correlation}} \approx \begin{cases} 1 & \text{when } 1 < \text{Pe}_{\text{simple}} \le 100 \\ 2 & \text{when } \text{Pe}_{\text{simple}} > 100 \end{cases}$$

Hence, the dimensionless quantity that appears on the left side of the following mass transfer equation with convection, diffusion, and chemical reaction,

$$\text{Re}\cdot\text{Sc}\frac{d\Psi_{\text{A}}}{d\zeta} = \frac{d^2\Psi_{\text{A}}}{d\zeta^2} - \Lambda^2_{\text{A, interpellet}} E(\Lambda_{\text{A, intrapellet}}) R^* \tag{22-87}$$

is the mass transfer Peclet number which accounts for interpellet axial dispersion:

$$\mathrm{Pe_{MT}} = \mathrm{Re}\cdot\mathrm{Sc} = \frac{L_{\mathrm{PFR}}\langle v_z\rangle_{\mathrm{interstitial}}}{\mathfrak{D}_{\mathrm{A,\ interpellet}}} = \frac{L_{\mathrm{PFR}}}{\phi_{\mathrm{correlation}} d_{\mathrm{equivalent}}} \tag{22-88}$$

This dimensionless parameter is required to analyze residence-time distribution effects in packed catalytic tubular reactors, and it corresponds to the quantity on the horizontal axes of Figures 22-2 and 22-3, which compare ideal vs. non-ideal reactor performance.

22-6 APPLICATIONS TO A PACKED CHROMATOGRAPHIC OR ION-EXCHANGE COLUMN

Gas chromatography is a separation technique based on the fact that different components in the mixture exhibit different average residence times due to interactions with the porous packing material. These interactions can be classified as intrapellet diffusion and the column operates similar to a packed catalytic tubular reactor. The important mass transfer mechanisms are convection and diffusion. Hence, it is important to calculate the mass transfer Peclet number that represents an order-of-magnitude ratio of these two mass transfer rate processes. Intrapellet diffusion governs residence times, and interpellet axial dispersion affects the degree to which the output curve is broadened. For axial dispersion in packed columns and packed catalytic tubular reactors,

$$\mathrm{Pe_{MT}} = \frac{L_{\mathrm{PFR}}\langle v_z\rangle_{\mathrm{interstitial}}}{\mathfrak{D}_{\mathrm{eff.\ axial\ disp.}}} \tag{22-89}$$

where $\langle v_z\rangle_{\mathrm{interstitial}}$ is the average interstitial fluid velocity through the packed column, L_{PFR} is the column length, and $\mathfrak{D}_{\mathrm{eff.\ axial\ disp.}}$ is the effective axial dispersion coefficient in a packed column defined by

$$\mathfrak{D}_{\mathrm{eff.\ axial\ disp.}} = \phi_{\mathrm{correlation}}\langle v_z\rangle_{\mathrm{interstitial}} d_{\mathrm{equivalent}} \tag{22-90}$$

where the equivalent diameter of nonspherical packing material is given by

$$d_{\mathrm{equivalent}} = \frac{6V_{\mathrm{pellet}}}{S_{\mathrm{pellet}}} \tag{22-91}$$

which reduces to the pellet diameter for spheres. V_{pellet} and S_{pellet} represent the volume and external surface area, respectively, of one pellet. Hence,

$$\mathrm{Pe_{MT}} = \frac{L_{\mathrm{PFR}}}{\phi_{\mathrm{correlation}} d_{\mathrm{equivalent}}} \tag{22-92}$$

If the mass transfer Peclet number is smaller, then interpellet axial dispersion plays a larger role in influencing the shape of the detector output curve. Small Peclet numbers broaden the detector output curve and reduce the resolution of the separation device. Long columns in a coiled configuration and small packing material are used to design chromatographs with high resolution. This represents a classic example where chromatograph design minimizes effects of residence-time distributions in response to a spike disturbance.

22-7 FACTORS THAT MUST BE CONSIDERED IN THE DESIGN OF A PACKED CATALYTIC TUBULAR REACTOR

The analysis in this section focuses on the appropriate dimensionless numbers that are required to analyze convection, axial dispersion and first-order irreversible chemical reaction in a packed catalytic tubular reactor. The catalytic pellets are spherical. Hence, an analytical solution for the effectiveness factor is employed, based on first-order irreversible chemical kinetics in catalysts with spherical symmetry. It is assumed that the catalytic pores are larger than 1 μm (i.e., $>10^4$ Å) and that the operating pressure is at least 1 atm. Under these conditions, ordinary molecular diffusion provides the dominant resistance to mass transfer within the pores because the Knudsen diffusivity,

$$\mathfrak{D}_{i,\,\text{Knudsen}}(\text{cm}^2/\text{s}) = 1.05 \times 10^{-4} \langle r(\text{Å})_{\text{average}} \rangle \left[\frac{T(\text{K})}{\text{MW}_i} \right]^{1/2} \tag{22-93}$$

is much larger. Hence, the net intrapellet diffusivity is essentially the same as the ordinary molecular diffusion coefficient for reactant A. The strategy is as follows:

Step 1. Calculate the intrapellet Damkohler number for reactant A.

Step 2. Use the analytical expression for first-order kinetics in spheres to calculate the effectiveness factor.

Step 3. Calculate the simple Peclet number based on ordinary molecular diffusion.

Step 4. Use the experimental correlation to calculate the interpellet axial dispersion coefficient.

Step 5. Calculate the mass transfer Peclet number which appears in the mass balance with convection and axial dispersion.

Step 6. Calculate the interpellet Damkohler number, based on axial dispersion, which appears in the mass balance with convection, diffusion, and chemical reaction.

Step 7. Calculate the residence time which represents the time constant for convective mass transfer.

Step 8. Calculate the time constant for first-order irreversible chemical reaction.

Step 9. Calculate the outlet conversion of reactant A in an ideal plug-flow tubular reactor, neglecting residence-time distribution effects.

It is necessary to solve two coupled first-order ODEs with split boundary conditions to estimate the effect of axial dispersion on outlet conversion.

Step 1. Enter the first-order kinetic rate constant for the surface-catalyzed chemical reaction based on gas-phase molar densities. This rate constant has units of cm/min and is known as the *reaction velocity constant*. It is not a pseudo-volumetric rate constant.

$$k_{1,\,\text{surface}} = 5 \times 10^{-4}\ \text{cm/min}$$

Step 2. Enter the diameter of the spherical catalytic pellets in units of centimeters:

$$d_{\text{pellet}} = 1\ \text{cm}$$

Step 3. Enter the intrapellet porosity of a single pellet, which is dimensionless:

$$\varepsilon_{p,\,\text{intrapellet}} = 0.65$$

Step 4. Enter the average intrapellet pore radius in units of micrometers, which must be multiplied by 10^{-4} to convert to centimeters.

$$\langle r_{\text{average}} \rangle = 10\ \mu\text{m}$$

Step 5. Enter the net intrapellet diffusion coefficient of reactant gas A in units of cm^2/s:

$$\mathfrak{D}_{\text{A, net, intrapellet}} = 0.1\ \text{cm}^2/\text{s}$$

Step 6. Enter the intrapellet tortuosity factor, which is dimensionless:

$$\text{tortuosity} = 3$$

Step 7. Enter the total inlet gas-phase volumetric flow rate in units of L/min, which must be multiplied by 10^3 to convert to cm^3/min:

$$\text{gas flow} = 10\ \text{L/min}$$

Step 8. Enter the diameter of the tubular reactor in units of centimeters:

$$2R_{\text{PFR}} = 20\ \text{cm}$$

Step 9. Enter the interpellet porosity of the fixed-bed reactor, which is dimensionless:

$$\varepsilon_{p,\,\text{interpellet}} = 0.50$$

Step 10. Enter the overall reactor length in units of centimeters:

$$L_{\text{PFR}} = 150\ \text{cm}$$

Step 11. Make the kinetic rate constant pseudo-volumetric with units of inverse seconds. The product of S_m and ρ_{apparent} is equivalent to twice the intrapellet porosity divided by the average pore radius. Hence, $k_{1,\text{ pseudo}} = S_m \rho_{\text{apparent}} k_{1,\text{ surface}}$:

$$k_{1,\text{ pseudo}} = \frac{2\varepsilon_{p,\text{ intrapellet}} k_{1,\text{ surface}}}{60\langle r_{\text{average}}\rangle \times 10^{-4}}$$

Step 12. Calculate the intrapellet Damkohler number, where the characteristic length is the radius of the catalytic pellet.

$$\Lambda^2_{\text{intrapellet}} = \frac{k_{1,\text{ pseudo}}(d_{\text{pellet}}/2)^2 \cdot \text{tortuosity}}{\varepsilon_{p,\text{ intrapellet}} \mathfrak{D}_{\text{A, net, intrapellet}}}$$

Step 13. Use the analytical expression for first-order kinetics in spherical pellets to calculate the Effectiveness factor when the characteristic length is the pellet radius.

$$E = \frac{3}{\Lambda^2_{\text{intrapellet}}}\left(\frac{\Lambda_{\text{intrapellet}}}{\tanh \Lambda_{\text{intrapellet}}} - 1\right)$$

Step 14. Calculate the simple Peclet number based on ordinary molecular diffusion and the diameter of the catalytic pellet:

$$\text{Pe}_{\text{simple}} = \left[\frac{\text{gas flow} \times 10^3}{\pi \varepsilon_{p,\text{ interpellet}} R^2_{\text{PFR}}}\right] \frac{d_{\text{pellet}}}{60\mathfrak{D}_{\text{A, ordinary}}}$$

Step 15. Determine the experimental correlation coefficient for interpellet axial dispersion via a conditional IF statement:

$$\phi_{\text{correlation}} = \begin{cases} 1 & \text{if } \text{Pe}_{\text{simple}} \leq 100 \\ 2 & \text{if } \text{Pe}_{\text{simple}} > 100 \end{cases}$$

Step 16. Calculate the mass transfer Peclet number in the mass balance with convection, axial dispersion, and chemical reaction:

$$\text{Pe}_{\text{MT}} = \frac{L_{\text{PFR}}}{\phi_{\text{correlation}} d_{\text{pellet}}}$$

Step 17. Calculate the interpellet axial dispersion coefficient, in units of cm^2/s:

$$\mathfrak{D}_{\text{A, interpellet}} = \phi_{\text{correlation}} d_{\text{pellet}} \left[\frac{\text{gas flow} \times 10^3}{60\pi \varepsilon_{p,\text{ interpellet}} R^2_{\text{PFR}}}\right]$$

Step 18. Calculate the interpellet Damkohler number, where the characteristic length is the overall length of the packed catalytic tubular reactor:

$$\Lambda^2_{\text{interpellet}} = \frac{k_{1,\text{ pseudo}} L^2_{\text{PFR}}}{\mathfrak{D}_{\text{A, interpellet}}}$$

Step 19. Determine the coefficient of the axial concentration gradient in the two coupled ODEs that must be solved to calculate the outlet conversion in a packed catalytic tubular reactor with convection, axial dispersion, and chemical reaction.

$$\text{coeff(Axial Grad)} = \text{Pe}_{\text{MT}}$$

Step 20. Determine the coefficient of the first-order chemical reaction term in the two coupled ODEs that must be solved to calculate the outlet conversion in a packed catalytic tubular reactor with convection, axial dispersion, and chemical reaction.

$$\text{Coeff(chem. Rx)} = E(1 - \varepsilon_{p,\,\text{interpellet}})\Lambda^2_{\text{interpellet}}$$

Step 21. Calculate the time constant for convective mass transfer through the packed catalytic tubular reactor in units of minutes, which is equivalent to the residence time:

$$\tau = \frac{L_{\text{PFR}}}{\langle v_z \rangle_{\text{interstitial}}} = \frac{\pi R^2_{\text{PFR}} L_{\text{PFR}} \varepsilon_{p,\,\text{interpellet}}}{\text{gas flow} \times 10^3}$$

Step 22. Calculate the time constant for first-order irreversible chemical reaction, in units of minutes:

$$\omega = \frac{1}{60 k_{1,\,\text{pseudo}}}$$

Step 23. For internal consistency, be sure that the following ratios are the same:

$$\frac{\tau}{\omega} = \frac{\Lambda^2_{\text{interpellet}}}{\text{Pe}_{\text{MT}}}$$

Step 24. Calculate the outlet conversion of reactant A in an ideal plug-flow tubular reactor with pseudo-volumetric first-order kinetics and no residence-time distribution effects:

$$(\text{final conversion})_{\text{ideal}} = 1 - \exp\left[-\frac{\tau}{\omega} E(1 - \varepsilon_{p,\,\text{interpellet}})\right]$$

Notice that the final conversion for first-order kinetics in an ideal packed catalytic tubular reactor depends on interpellet porosity of the packed bed in the following manner:

$$(\text{final conversion})_{\text{ideal}} \approx 1 - \exp[-\tau(1 - \varepsilon_{p,\,\text{interpellet}})] \tag{22-94}$$

and the average residence time τ is linearly proportional to $\varepsilon_{p,\,\text{interpellet}}$. Hence,

$$(\text{final conversion})_{\text{ideal}} \approx 1 - \exp[-\varepsilon_{p,\,\text{interpellet}}(1 - \varepsilon_{p,\,\text{interpellet}})] \tag{22-95}$$

which exhibits a maximum when the void volume fraction is 50%. One arrives at the same general conclusion by analyzing the dimensionless molar density profile

of reactant A in the exit stream of an ideal packed catalytic tubular reactor when the kinetics are second-order and irreversible, as given by equation (22-75):

$$\Psi_A(\zeta = 1, \text{ideal}) = \frac{1}{1 + [(\tau/\omega)(1 - \varepsilon_{p,\,\text{interpellet}})E(\Lambda_{A,\,\text{intrapellet}})]} \tag{22-96}$$

In other words, $\Psi_A(\zeta = 1, \text{ideal})$ exhibits a minimum in equation (22-96) when the void volume fraction is 50%. These ideal packed catalytic tubular reactor models suggest that it is advantageous to achieve a catalyst filling factor of about 50%.

PROBLEMS

22-1. Carbon monoxide (CO) and hydrogen (H_2) can be converted to methanol (CH_3OH) using a commercial copper/zinc oxide catalyst. Your task as a chemical reaction engineer is to design a packed catalytic tubular reactor that will produce methanol at 500 K and 10 atm total pressure. Under these conditions, the reaction is essentially irreversible. You propose to introduce a stoichiometric feed of the two reactants in the inlet stream. The reactor is packed with catalytic pellets that are spherical in shape. The overall objective is to convert at least 75% of carbon monoxide to methanol. Supervisor A suggests that the mass flow rate should be quite low to achieve 75% conversion in the outlet stream of a reasonably sized reactor. She realizes that the overall design will require a numerical solution and that final answers will not be available for at least one week. Supervisor B is very impatient and wants to see an approximate analytical solution before his business meeting at 12 noon today. He realizes that this answer is only valid at higher mass flow rates and represents an upper limit on the size of the reactor. In both cases, the supervisors do not want to see any derivations because they haven't taken a graduate reactor design course, or any other quantitative course, since the late 1960s. They are interested in your overall strategy, which should be summarized by a series of brief qualitative comments in logical order. Even though derivations are frowned upon, supervisor A would like to see the final expressions before they are submitted to the computer programming department for numerical analysis. Supervisor B wants final results for the approximate analytical solution immediately. He has a pocket calculator and, if necessary, he can insert all of the physicochemical parameters into your final analytical expression and estimate the reactor length during the business meeting today at high noon.

22-2. It is required to convert 65% of reactant A_2 (i.e., a dimer) to products in a packed catalytic tubular reactor. Molecular A_2 is converted irreversibly to products B and C within the internal pores of catalytic pellets

that are spherically symmetric. The important features of this process are as follows:

(1) The overall reaction is $A_2 \rightarrow B + C$.

(2) Molecular A_2 dissociates and spontaneously adsorbs on two active sites.

(3) Products B and C each adsorb on a single active surface site within the catalytic pores.

(4) The activated complex is not included in the series of elementary steps.

(5) Dual-site surface-catalyzed chemical reaction ($2A\sigma \rightarrow B\sigma + C\sigma$) is the slowest step in the overall mechanism, where σ represents an active surface site.

(6) The back reaction is negligible (i.e., $K_{p,\,\text{equilibrium}} \rightarrow \infty$).

(a) Write the kinetic rate law (i.e., Hougen–Watson model) that is required to design the chemical reactor.
Answer: For this irreversible chemical reaction, which occurs on two adjacent catalytically active sites, one expresses the heterogeneous rate law in terms of the surface coverage of A. For example,

$$\mathfrak{R}_{\text{Hougen-Watson}} = k_{f,\,\text{surface Rx}}(\Theta_A)^2$$

with dimensions of moles per internal catalytic surface area per time. If surface coverage of each species follows a Langmuir isotherm, then:

$$\Theta_i = \Theta_V (K_i p_i)^{1/\gamma_i}$$

where γ_i is the number of active sites required for one molecule of species i to undergo chemisorption after dissociation, if necessary (i.e., $\gamma_A = 2$, $\gamma_B = 1$, $\gamma_C = 1$). A population balance yields the following expression for the vacant-site fraction:

$$\Theta_V = \left[1 + \sum_{j=A,B,C} (K_j p_j)^{1/\gamma_j} \right]^{-1}$$

The final expression for the Hougen–Watson kinetic model is

$$\mathfrak{R}_{\text{Hougen-Watson}} = \frac{k_{f,\,\text{surface Rx}} K_A p_A}{\left[1 + \sum_{j=A,B,C} (K_j p_j)^{1/\gamma_j} \right]^2}$$

(b) Write an expression for the intrapellet Damkohler number of reactant A_2 in terms of the forward kinetic rate constant $k_{f,\,\text{surface Rx}}$

that describes the dual-site surface-catalyzed chemical reaction ($2A\sigma \rightarrow B\sigma + C\sigma$). The dimensions of $k_{f,\text{surface Rx}}$ are moles per area per time because the rate law is constructed in terms of fractional surface coverage of A [i.e., $(\Theta_A)^2$].

Answer: The following sequence of steps is required to construct $\Lambda^2_{A,\text{intrapellet}}$:

(1) Make $\mathfrak{R}_{\text{Hougen-Watson}}$ pseudo-volumetric via multiplication by S_m and ρ_{apparent}.

(2) Replace partial pressures with molar densities via the ideal gas law.

(3) Now the numerator of $\mathfrak{R}_{\text{Hougen-Watson}}$, with dimensions of moles per volume per time, resembles a first-order rate expression:

$$(S_m \rho_{\text{apparent}} k_{f,\text{surface Rx}} K_A RT) C_A$$

where the quantity in parentheses has dimensions of a pseudo-volumetric first-order kinetic rate constant (i.e., inverse time) when the rate law is expressed in terms of molar densities.

(4) Use this first-order kinetic rate constant from step 3 in the standard formula for an intrapellet Damkohler number based on simple nth-order kinetics with $n = 1$. For example,

$$\Lambda^2_{A,\text{intrapellet}} = \frac{k_n L^2 (C_{A,\text{surface}})^{n-1}}{\mathfrak{D}_{A,\text{intrapellet}}}$$

$$= \frac{S_m \rho_{\text{apparent}} k_{f,\text{surface Rx}} K_A RT L^2}{\mathfrak{D}_{A,\text{intrapellet}}}$$

The appropriate diffusion coefficient of reactant A_2 must be modified by intrapellet porosity and tortuosity factors which summarize the internal pore structure of each catalytic pellet. For spherical catalysts, the pellet radius R is taken as the characteristic length L.

(c) Use log-log coordinates and sketch the effectiveness factor vs. the intrapellet Damkohler number of reactant A_2. Put numerical values on the vertical and horizontal axes.

(d) At high-mass-transfer Peclet numbers, sketch the average residence time for a plug-flow tubular reactor vs. the intrapellet Damkohler number of reactant A_2 such that 65% conversion of molecular A_2 is achieved in the outlet stream of the reactor.

(e) Economic considerations dictate that the average residence time for this reactor must be less than 5 min when the volumetric

flow rate is 25 L/min. Use your design correlation from part (d) and illustrate how the reactor design engineer should estimate the diameter of spherical catalytic pellets to achieve the desired conversion. Be sure to indicate whether this prediction represents an upper or a lower limit for the diameter of the catalytic pellets.

22-3. Sketch the relation between the length L_{PFR} of a packed catalytic tubular reactor to achieve 80% conversion of reactant A and the radius R of spherical catalytic pellets which are porous and packed within the reactor. Put L_{PFR} on the vertical axis and R on the horizontal axis. The objective is to achieve 80% conversion of reactant A to products at each point on your curve. Include dimensions on both axes and indicate a reasonable range of values for reactor length and catalyst size.

22-4. At high-mass-transfer Peclet numbers, sketch the relation between average residence time divided by the chemical reaction time constant (i.e., τ/ω) for a packed catalytic tubular reactor versus the intrapellet Damkohler number $\Lambda_{A,\,intrapellet}$ for zeroth-, first-, and second-order irreversible chemical kinetics within spherical catalytic pellets. The characteristic length L in the definition of $\Lambda_{A,\,intrapellet}$ is the sphere radius R. The overall objective is to achieve the same conversion in the exit stream for all three kinetic rate laws. Put all three curves on the same set of axes and identify quantitative values for the intrapellet Damkohler number on the horizontal axis.

22-5. The objective of this problem is to calculate reactant conversion in the exit stream of a packed catalytic tubular reactor. The chemical kinetics are irreversible and first-order. The reactor is packed with catalysts that are spherically symmetric. The following data are available. Be careful with units, because the kinetic rate constant and the volumetric flow rate are given in minutes, whereas the net intrapellet diffusivity is given in seconds.

Inlet gas-phase molar density of reactant A, $C_{A0} = 3 \times 10^{-5}$ g-mol/cm^3

First-order kinetic rate constant for the surface-catalyzed chemical reaction based on gas-phase molar densities, $k_{1,\,surface} = 5 \times 10^{-4}$ cm/min (also known as the reaction velocity constant)—this is not a pseudo-volumetric kinetic rate constant

Diameter of spherically shaped catalytic pellets = 1 cm

Intrapellet porosity factor = 65% (i.e., 0.65)

Average intrapellet pore radius = 10 μm = 10^{-5} m = 10^{-3} cm

Net intrapellet diffusion coefficient of reactant A, $\mathscr{D}_{A,net,intrapellet} = 0.1$ cm^2/s

Intrapellet tortuosity factor, $\tau_{or} = 3$

Total gas-phase volumetric flow rate = 10 L/min = 10,000 cm^3/min

Diameter of the tubular reactor = 20 cm

Interpellet porosity of the packed bed = 0.25

Overall reactor length = 1.5 m = 150 cm

Isothermal operation of the reactor at $T = 350$ K

(a) Calculate a numerical value for the effectiveness factor. Be careful in choosing the characteristic length scale for the intrapellet Damkohler number.
Answer: $\Lambda^2_{\text{A, intrapellet}} = 0.125$, effectiveness factor = 0.992.

(b) Evaluate all parameters in the governing ordinary differential equations that describe the solution to this problem. Then, include these parameters in the final form of the coupled ODEs that must be solved to calculate reactant conversion in the exit stream of a packed catalytic tubular reactor.
Answer: $\text{Pe}_{\text{simple}} = 21.2$, $\text{Pe}_{\text{MT}} = 150$, $\Lambda^2_{\text{A, interpellet}} = 115$, and $\Lambda^2_{\text{A, interpellet}}(1 - \varepsilon_{p,\text{ interpellet}})E(\Lambda_{\text{A, intrapellet}}) = 85.4$.

(c) Estimate the final conversion in the exit stream of an ideal plug-flow tubular reactor.
Answer: Residence time $\tau = 1.18$ min, chemical reaction time constant $\omega = 1.54$ min, and $\chi_{\text{final, ideal PFR}} = 0.43$.

(d) Estimate the final conversion in the exit stream of a non-ideal plug-flow reactor that accounts for residence-time distribution effects.
Answer: $\chi_{\text{final, non-ideal PFR}} \approx 0.43$, because $\text{Pe}_{\text{MT}} \approx (\text{Re}\cdot\text{Sc})_{\text{critical}}$.

22-6. Draw a block diagram that illustrates the computer logic required to design a packed catalytic tubular reactor. Your logic should be flexible enough to account for interpellet axial dispersion, if necessary. Do not include any equations.

22-7. (a) How often should your computer program in Problem 22-6 call the Runge–Kutta numerical integration subroutine to calculate the effectiveness factor if

$$A_2 + B \longrightarrow C + D$$

and the Hougen–Watson model for the reactant → product conversion rate is

$$\mathfrak{R}_{\text{Hougen-Watson}} = f(p_A, p_B, p_C, p_D) = \frac{k_f K_A K_B p_A p_B}{(1 + \sqrt{K_A p_A} + \sum_{i=B,C,D} K_i p_i)^\gamma}$$

where p_i is the partial pressure of species i within the internal pores of spherical catalytic pellets.

(b) What is the value of the exponent γ in part (a) for the adsorption terms in the denominator of the Hougen–Watson rate law?

Answer: $\gamma = 3$. Diatomic A_2 undergoes dissociative adsorption, whereas species B, C, and D each require one active site for chemisorption. Triple-site chemical reaction on the catalytic surface is the rate-controlling step, which liberates one active site. Hence,

$$2A\sigma + B\sigma \longrightarrow C\sigma + D\sigma + \sigma$$

For Langmuir-type adsorption, the surface coverage fraction for each species is linearly proportional to the vacant-site fraction, and the Hougen–Watson kinetic rate law scales as $(\Theta_V)^3$. Hence, $\gamma = 3$ reveals that the rate-limiting step requires three active sites on the catalytic surface.

22-8. (a) A rather short tubular reactor packed with spherical porous pellets functions as a catalytic converter in the exhaust system of an automobile. There is not enough space available in the exhaust manifold to increase the length of the reactor. This catalytic muffler converts carbon monoxide and unburned hydrocarbons to carbon dioxide and water vapor. How much conversion of the combustion by-products (i.e., CO and unburned hydrocarbons) should be expected in the exit stream of the catalytic converter under realistic operating conditions, as described below?

Pseudo-first-order kinetic rate constant for the surface-catalyzed chemical reaction based on gas-phase molar densities, $k_{1,\,\text{surface}} = 1.7 \times 10^{-3}$ cm/min ($k_{1,\,\text{surface}}$ is also known as the reaction velocity constant)

Diameter of spherically shaped catalytic pellets = 2 cm

Intrapellet porosity factor = 65% (i.e., 0.65)

Average intrapellet pore radius = 1 μm = 10^{-6} m = 10^{-4} cm

Net intrapellet diffusion coefficient, $\mathfrak{D}_{A,\,\text{net, intrapellet}} = 0.15$ cm^2/s

Intrapellet tortuosity factor, $\tau_{or} = 3$

Total gas-phase volumetric flow rate = 3 L/min = 3000 cm^3/min

Diameter of the catalytic muffler = 7 cm

Interpellet porosity of the packed catalytic reactor = 0.45

Overall length of the catalytic muffler = 15 cm

(b) Your task as a chemical reactor design engineer is to increase the conversion of CO and unburned hydrocarbons to product gases in the exit stream of the catalytic converter. Qualitatively describe two realistic solutions that will achieve higher conversion of combustion by-products to CO_2 and H_2O. Indicate whether each of your realistic solutions affects the mass transfer Peclet number (Pe_{MT}), the effectiveness factor (E), or both Pe_{MT} and E.

22-9. For a given length L_{PFR} of a tubular reactor packed with spherical catalytic pellets, one calculates the following values of five important dimensionless design parameters. The chemical kinetics are first-order and irreversible:

Intrapellet Damkohler number, $\Lambda^2_{\text{A, intrapellet}} = 3$
Effectiveness factor, $E(\Lambda_{\text{A, intrapellet}}) = 0.8$
Mass transfer Peclet number, $\text{Pe}_{\text{MT}} = 75$
Interpellet Damkohler number, $\Lambda^2_{\text{A, interpellet}} = 90$
Interpellet porosity, $\varepsilon_{p,\text{ interpellet}} = 0.5$

Now the reactor length is doubled while maintaining the same pellet packing density.

(a) Recalculate the five important dimensionless design parameters given above. Five numerical answers are required here.
Answer: The mass transfer Peclet number scales as L_{PFR}, and the interpellet Damkohler number scales as L^2_{PFR}. Therefore, $\text{Pe}_{\text{MT}} = 150$ and $\Lambda^2_{\text{A, interpellet}} = 360$. The other three dimensionless numbers are unaffected when the reactor length is doubled.

(b) If the chemical kinetics are first-order and irreversible, then predict the final conversion of reactant A in the exit stream before and after the reactor length is doubled. Assume that interpellet axial dispersion is negligible. Two numerical answers are required here.
Answer: When the chemical kinetics are first-order and irreversible (i.e., $n \neq 1$), with no complications from interpellet axial dispersion, the final conversion of reactants to products in an ideal PFR is

$$1 - \Psi_{\text{A}}(\zeta = 1,\ \text{ideal}) = 1 - \exp\left[\frac{-(1 - \varepsilon_{p,\text{ interpellet}})E(\Lambda_{\text{A, intrapellet}})\Lambda^2_{\text{A, interpellet}}}{\text{Pe}_{\text{MT}}}\right]$$

The required results are:

$$\text{Before}: \quad 1 - \Psi_{\text{A}}(\zeta = 1,\ \text{ideal}) = 38\%$$

$$\text{After}: \quad 1 - \Psi_{\text{A}}(\zeta = 1,\ \text{ideal}) = 62\%$$

(c) Consider second-order irreversible chemical kinetics, use the original and recalculated values of the five important dimensionless design parameters from the problem statement and part (a), and predict the final conversion of reactant A in the exit stream before and after the reactor length is doubled. Assume that interpellet axial dispersion is negligible. Two numerical answers are required here.
Answer: When the chemical kinetics are nth-order and irreversible (i.e., $n \neq 1$), with no complications from interpellet axial dispersion, the final conversion of reactants to products in an ideal PFR is

$$1 - \Psi_A(\zeta = 1,\ \text{ideal}) = 1 - \left[\frac{1}{1 + (n-1)\mu}\right]^{1/(n-1)}$$

where

$$\mu = \frac{(1 - \varepsilon_{p,\,\text{interpellet}})E(\Lambda_{A,\,\text{intrapellet}})\Lambda^2_{A,\,\text{interpellet}}}{\text{Pe}_{MT}}$$

For second-order irreversible kinetics, $n = 2$. Hence,

$$1 - \Psi_A(\zeta = 1,\ \text{ideal}) = \frac{\mu}{1 + \mu}$$

The required results are

$$\text{Before}: \quad 1 - \Psi_A(\zeta = 1,\ \text{ideal}) = 32\%$$

$$\text{After}: \quad 1 - \Psi_A(\zeta = 1,\ \text{ideal}) = 49\%$$

22-10. How does the intrapellet tortuosity factor of a porous catalyst affect the required length of a packed catalytic tubular reactor (i.e., L_{PFR}) to obtain 75% conversion of reactants to products? Use log-log coordinates and illustrate this trend for:

(a) Zeroth-order irreversible chemical kinetics with a reaction time constant of 3 min.

(b) First-order irreversible chemical kinetics with a reaction time constant of 3 min.

The catalytic pellets are spherical with a diameter of 5 mm. Put the intrapellet tortuosity factor on the horizontal axis and cover a reasonable range of values for τ_{or}.

22-11. Consider Taylor dispersion of a tracer in packed beds, mass transfer Peclet numbers based on interpellet axial dispersion coefficients, and the resolution of a chromatograph to explain how the performance of a chromatographic separation device depends on the length of the packed column if all other design parameters, particularly the size of the packing material, remain constant.

22-12. The isothermal plug-flow mass balance for first-order irreversible chemical kinetics in a packed catalytic tubular reactor yields the following functional form for the conversion of reactant A at high-mass-transfer Peclet numbers:

$$\chi_A(\zeta) \approx 1 - \exp\left[\frac{-E(\Lambda_{A,\,\text{intrapellet}})}{w}\zeta f(\varepsilon_{p,\,\text{interpellet}})\right]$$

What is $f(\varepsilon_{p,\,\text{interpellet}})$?

22-13. Various reactor design strategies are summarized below. Indicate whether each of these statements is true or false.

(a) If the average intrapellet pore radius is 10 μm and it is subsequently increased, then reactant → product conversion in the exit stream of a packed catalytic tubular reactor decreases even though the average residence time τ remains constant.

(b) If the average intrapellet pore radius is 10 μm, then an increase in total gas pressure at constant temperature causes the final conversion of reactants to increase in the exit stream of a packed catalytic tubular reactor when the kinetics are irreversible and first-order. The average residence time τ remains constant.

(c) If the kinetics are zeroth-order and the intrapellet Damkohler number $\Lambda^2_{A,\,\text{intrapellet}} = 6$ for spherical catalytic pellets, then a decrease in pellet diameter increases reactant → product conversion in the exit stream of a packed catalytic tubular reactor even though the average residence time τ remains constant.

(d) If interpellet axial dispersion plays a significant role in the design of a packed catalytic tubular reactor, then one should employ a longer residence time under realistic conditions to achieve the final conversion that is predicted by the ideal PFR design equation.

(e) If the length of a packed catalytic tubular reactor increases but the size of the porous catalytic pellets remains constant, then the mass transfer Peclet number is larger and the final conversion of reactants to products decreases under ideal conditions. This is obvious from Figure 22-2, as one moves farther to the right on the horizontal axis.

Transport Phenomena for Chemical Reactor Design. Laurence A. Belfiore
Copyright © 2003 John Wiley & Sons, Inc.
ISBN: 0-471-20275-4

23

HETEROGENEOUS CATALYTIC REACTORS WITH METAL CATALYST COATED ON THE INNER WALLS OF THE FLOW CHANNELS

Steady-state simulations of convection, diffusion, and first-order irreversible heterogeneous chemical reaction are presented in this chapter for catalytic duct reactors with rectangular cross section and nonuniform catalyst activity. Finite-difference results from the microscopic three-dimensional mass transfer equation also satisfy the cross-section-averaged one-dimensional form of the same equation. Comparisons between viscous flow and plug flow in square-cross-section channels suggest how previous inferences of surface-averaged reaction velocity constants from plug-flow simulations should be modified when convective diffusion in the mass transfer boundary layer adjacent to the catalytic surface is modeled correctly. Over a wide range of Damkohler numbers (i.e., 5×10^{-2} to 1×10^{3}), viscous flow in rectangular ducts with intermediate aspect ratios between 2 and 20 can be approximated by the corresponding problem in tubes with the same effective diameter. Over this same range of Damkohler numbers, aspect ratios greater than 100 are required to simulate viscous flow between two parallel plates with catalyst coated on both walls. At low Damkohler numbers where reactant diffusion toward the catalytic surface is not the rate-limiting step, nonuniform activity profiles suggest that most of the catalyst should be deposited in regions that are easily accessible to the reactants. However, this strategy for converting reactants to products is not more effective than uniform deposition in the diffusion-limited regime.

23-1 CONVECTIVE DIFFUSION IN CATALYTIC REACTORS OF NONCIRCULAR CROSS SECTION AND NONUNIFORM CATALYST ACTIVITY

The performance of heterogeneous catalytic reactors in which the catalyst is deposited on the inner walls of the flow channels is the focus of this chapter.

Reactor geometries of this type minimize heat and mass transfer resistances so that chemical kinetics govern the reactant-to-product conversion rate at reasonably small Damkohler numbers. Hence, these duct reactors with noncircular cross section find application at the fundamental level and in industrial situations. From a fundamental standpoint, duct reactors are used to measure the true kinetics of heterogeneous surface-catalyzed chemical reactions, when the rate of reactant diffusion toward the catalytic surface is not the slowest step in the overall process. One important example (Rosner, 1967) is the use of duct reactors to understand the catalytic decomposition of nickel tetracarbonyl, $Ni(CO)_4$. Industrially, duct reactor simulations are used to design antipollution monolithic honeycomb supports such as those that remove carbon monoxide and unburned hydrocarbons from automotive exhaust gases (i.e., catalytic converters). Each channel within a monolithic honeycomb support has a cross section that is either rectangular, triangular, hexagonal, or sinusoidal. Noncircular cross sections are required to pack several channels in a space-filling configuration. In other words, straight channels with circular cross section cannot be bundled together without sacrificing void volume between the channels. This is an undesirable arrangement within a catalytic converter, for example, particularly if the catalyst is coated only on the inner walls of the flow channels because reactant gases that pass between the tubes will not be converted to products. Hence, even though straight channels with noncircular cross section can be packed in a space-filling configuration, they exhibit regions of nonuniform reactant accessibility which are most pronounced in the corners of the flow channels. The reactor design strategy focuses on an optimal deposition of expensive metal catalyst to maximize reactor performance and minimize production costs. The mass transfer equation which includes convection and diffusion in regular polygon ducts is three-dimensional and requires sophisticated numerical techniques to solve partial differential equations. These solutions are compared with plug-flow and viscous-flow two-dimensional solutions in tubular reactors that have the same effective diameter as the regular polygon channel. The numerical complexity required to analyze duct reactors with noncircular cross sections can be simplified from three dimensions to two dimensions if the effective diameter approximation is justified.

Some of the factors affecting reactor performance, in general, are heat and mass transfer limitations, chemical reaction kinetics, and catalyst deposition strategies. One route to eliminate large gas–solid thermal resistances as well as intrapellet mass diffusional resistances in conventional fixed-bed packed catalytic tubular reactors is to deposit expensive metal catalyst as a thin film on the inner walls of the flow channels. The technology required to deposit thin films of metallic catalysts on ceramic surfaces is well-developed (Kolb *et al*., 1993; Cybulski and Moulijn, 1998). The catalytic oxidation of carbon monoxide and hydrocarbons was accomplished using noble metal catalysts (i.e., $PdCl_2$ or $PtCl_2$) dispersed on high-surface-area γ-alumina (i.e., Al_2O_3) coatings in honeycomb-like structures. These high-performance duct reactors can be used to investigate the kinetics of fast heterogeneous reactions because, relative to packed catalytic reactors, duct reactors exhibit improved rates of reactant transport which do not

allow most of the catalytic surface to become starved of reactants. In fact, some duct reactors are limited by chemical kinetics under certain operating conditions. However, the inherent heterogeneities of convective diffusion in most forced-flow systems induce nonuniform local reactant concentration gradients near the catalytic surface. These diffusional heterogeneities might result in the measurement of apparent kinetics of surface reactions which differ drastically from the true kinetics. Fortunately, the falsification of surface reaction kinetics via convective diffusion as an intruder in many well-defined flow systems is predictable. Hence, diffusional effects can be separated from kinetic measurements in the intermediate regime where both mass transfer and chemical kinetics govern the reactant–product conversion rates.

The advantages of duct reactors relative to fixed-bed packed catalytic tubular reactors are as follows:

1. Greater productivity per unit channel cross-sectional area at moderate pressure drops (i.e., clear passageways in a monolithic support minimize frictional energy losses)
2. Higher yield of the desired product at smaller Damkohler numbers
3. Shorter reactor length required to achieve the desired conversion of reactants to products in the exit stream
4. Rapid heating of the catalytic surface, which is essential during the warm-up phase when automotive exhaust contains high concentrations of carbon monoxide and unburned hydrocarbons
5. Versatility of design, particularly with respect to size limitations
6. Vibration resistance of solid monolithic supports that are subjected to severe automotive exhaust environments

Due to the occurrence of nonuniform reactant accessibility in flow channels with noncircular cross section, catalyst deposition strategies become an important factor to consider in the quest for optimal reactor performance.

23-1.1 Assumptions of the Convective Diffusion Model in Regular Polygon Ducts

Heterogeneous catalytic reactor models for ducts with regular polygon cross sections are described within the framework of the following assumptions:

1. Fluid flow with the honeycomb-like channels is steady, laminar, incompressible, and Newtonian. The steady flow assumption is realized in practice by passing the reactive fluid through a geometrically identical channel with inactive walls prior to entering the catalytic reactor. The von Kármán laminar momentum boundary layer approach for estimating the entrance length (L_e) in a parallel plate configuration indicates that $L_e/D \approx \mathrm{Re}/40$, where Re is the Reynolds number based on the spacing D between two parallel plates (Lightfoot, 1974, pp. 102–104).

2. The convective diffusion mass transfer equation is solved for a binary mixture of reactant A and product B.
3. The molar diffusional flux of reactant A toward the catalytic surface is governed by Fick's law with a concentration-independent binary molecular diffusion coefficient. Thermal (Soret), pressure, and forced diffusion are neglected relative to concentration diffusion.
4. Concentration diffusion in the primary direction of flow (i.e., z direction) is negligible compared to convective mass transfer. This assumption is justified at large values of the mass transfer Peclet number.
5. The mass transfer–chemical reaction process occurs isothermally. This critical assumption allows one to neglect energy transport processes within the reactor. Hence, the physical properties of the reactive mixture — overall mass density, viscosity, binary molecular diffusion coefficient, and surface-averaged kinetic rate constant — are treated as constants throughout the reactor.
6. The rate of reaction on the catalytic surface is either first-order or pseudo-first-order with respect to the molar density of reactant A. In the latter case, the pseudo-first-order surface-averaged reaction velocity constant k_1, with units of length per time, is chosen to minimize the following integral in (23-1), as described by equation (15-14). This is actually an integral form of linear least-squares regression to determine the best value of k_1 that will linearize the rate of reactant consumption in the boundary condition at the catalytic surface. It is necessary to apply the Leibnitz rule for differentiating a one-dimensional integral with constant limits to the following expression, where x represents reactant conversion, and C_{A0} is the inlet molar density of reactant A:

$$\frac{d}{dk_1}\left\{\int_0^{x_{eq}\to 1}[\Re_{HW}(T, p, x) - k_1 C_{A0}(1-x)]^2\,dx\right\} = 0 \qquad (23\text{-}1)$$

23-2 FULLY DEVELOPED FLUID VELOCITY PROFILES IN REGULAR POLYGON DUCTS

The microscopic approach to fluid mechanics is employed to calculate velocity profiles for fully developed laminar flow of an incompressible Newtonian fluid. These profiles are obtained by solving the z component (axial) of the equation of motion in rectangular coordinates for one-dimensional flow (i.e., only v_z) due to an imposed pressure gradient ($dp/dz = -\Delta p/L$). It is generally true that honeycomb-like channels in a variety of monolithic supports have cross sections that are either rectangular or triangular. Rectangular ducts are quite common in industrial heat exchangers and fuel cells.

23-2.1 Rectangular Ducts

In this case, the flow cross section is $2a$ in the x direction by $2b$ in the y direction. A series solution has been obtained by Boussinesq (1868) in the following form:

$$\frac{v_z(x^*, y^*)}{\langle v_z \rangle_{\text{avg}}} = \frac{2\left[(1 - y^{*2}) + 4\sum_{n=0}^{\infty}(-1)^{n+1} M_n^{-3} \operatorname{sech} M_n A_r \cosh M_n A_r x^* \cos M_n y^*\right]}{4/3 - (8/A_r)\sum_{n=0}^{\infty} M_n^{-5} \tanh M_n A_r} \tag{23-2}$$

where the dimensionless variables normal to the flow direction are $x^* = x/a$ and $y^* = y/b$. The aspect ratio of the duct is $A_r = a/b$ and the eigenvalues are $M_n = (2n + 1)\pi/2$.

In contrast to one-dimensional laminar flow through a tube, the maximum fluid velocity at the center of a square-cross-section channel is more than twice the average velocity (see Figure 23-1). It is illustrated in Table 23-1 that the following ratio, $v_{z,\max}/\langle v_z \rangle_{\text{avg}}$ at $x^* = y^* = 0$, asymptotically approaches 1.5 at very

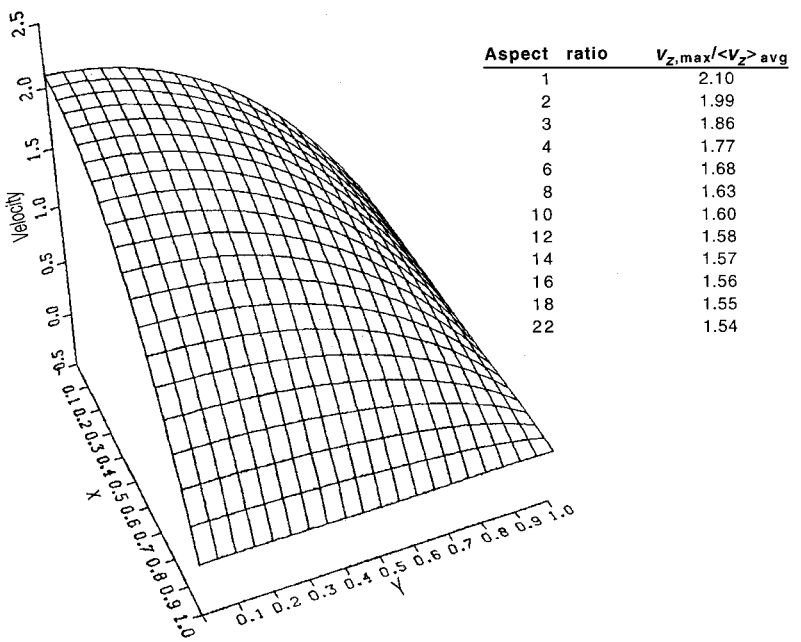

Aspect ratio	$V_{z,max}/\langle V_z \rangle_{avg}$
1	2.10
2	1.99
3	1.86
4	1.77
6	1.68
8	1.63
10	1.60
12	1.58
14	1.57
16	1.56
18	1.55
22	1.54

Figure 23-1 One-dimensional velocity profile for laminar viscous flow in a straight channel with square cross section.

TABLE 23-1 Effect of Aspect Ratio on the Ratio of Maximum to Average Fluid Velocity[a]

Aspect Ratio	$v_{z,\max}/\langle v_z\rangle_{\text{avg}}$	Aspect Ratio	$v_{z,\max}/\langle v_z\rangle_{\text{avg}}$
1	2.10	10	1.60
2	1.99	12	1.58
3	1.86	14	1.57
4	1.77	16	1.56
6	1.68	18	1.55
8	1.63	22	1.54

[a] One-dimensional viscous flow in straight channels with rectangular cross section.

large aspect ratios because the problem is identical to flow between two parallel plates of infinite extent (i.e., see Problem 2B.3 in Bird *et al*., 2002, p. 63).

23-2.2 Triangular Ducts

Consider a straight channel of length L with an equilateral triangular cross section. Fluid flow is bounded by the following planes in rectangular coordinates: $y = H$ and $y = \pm x\sqrt{3}$. Hence, each leg of the equilateral triangle has a length of $2H/\sqrt{3}$. The one-dimensional fluid velocity is given by (Landau and Lifshitz, 1959, p. 58; Bird *et al*., 1977, p. 27),

$$v_z(x, y) = \frac{\Delta p}{4\mu L H}(y - H)(3x^2 - y^2) \tag{23-3}$$

where μ is the fluid viscosity. This problem can be solved using the variational principle of von Helmholtz or the Helmholtz–Korteweg variational principle (see Lamb, 1945, pp. 617–619). Minimization of the following integral expression over the channel cross section S (i.e., $dS = dx\,dy$):

$$\begin{aligned} J &= \iint_{\text{flow cross section } S} \left\{ \mu L \left[\left(\frac{\partial v_z}{\partial x} \right)^2 + \left(\frac{\partial v_z}{\partial y} \right)^2 \right] - 2 v_z \Delta p \right\} dS \\ &= \iint_{\text{flow cross section } S} f\left[x, y, v_z, \left(\frac{\partial v_z}{\partial x} \right), \left(\frac{\partial v_z}{\partial y} \right) \right] dx\,dy \end{aligned} \tag{23-4}$$

where

$$f\left[x, y, v_z, \left(\frac{\partial v_z}{\partial x} \right), \left(\frac{\partial v_z}{\partial y} \right) \right] = \mu L \left[\left(\frac{\partial v_z}{\partial x} \right)^2 + \left(\frac{\partial v_z}{\partial y} \right)^2 \right] - 2 v_z \Delta p$$

is equivalent to solving the corresponding Euler–Lagrange equation in variational calculus (Jenson and Jeffreys, 1977, p. 515, Eqs. 13.69 and 13.71):

$$\frac{\partial f}{\partial v_z} - \frac{\partial}{\partial x}\left[\frac{\partial f}{\partial\,(\partial v_z/\partial x)}\right] - \frac{\partial}{\partial y}\left[\frac{\partial f}{\partial\,(\partial v_z/\partial y)}\right] = 0 \tag{23-5}$$

This Euler–Lagrange equation reduces to the following second-order partial differential equation for $v_z(x, y)$:

$$\frac{\Delta p}{L} + \mu\left(\frac{\partial^2 v_z}{\partial x^2} + \frac{\partial^2 v_z}{\partial y^2}\right) = 0 \tag{23-6}$$

which is identical to the z component of the equation of motion for one-dimensional flow of an incompressible Newtonian fluid in rectangular coordinates. Any trial function for v_z that satisfies the no-slip boundary condition along the three stationary surfaces at $y = H$ and $y = \pm x\sqrt{3}$,

$$v_z(x, y) = (x^2 - m^2 y^2)(y - H)(b + cy + \cdots) \tag{23-7}$$

represents a solution to the viscous flow problem when $m = 1/\sqrt{3}$ and variational parameters b and c are chosen to minimize J. Hence, $\partial J/\partial b = 0$ and $\partial J/\partial c = 0$ generate the following results (Bird *et al.*, 1977, pp. 49–50):

$$\begin{aligned} b &= \frac{7}{2}\frac{\Delta p}{\mu L H}\left\{\frac{17m^2 - 1}{55m^4 + 38m^2 + 3}\right\} \\ c &= -14\frac{\Delta p}{\mu L H}\left\{\frac{3m^2 - 1}{55m^4 + 38m^2 + 3}\right\} \end{aligned} \tag{23-8}$$

Substituting $m = 1/\sqrt{3}$ yields

$$b = \frac{3\Delta p}{4\mu L H} \qquad c = 0 \tag{23-9}$$

which agrees with the velocity profile given by equation (23-3). The average velocity for laminar flow through an isosceles triangular duct bounded by surfaces at $y = H$ and $x = \pm my$ is

$$\begin{aligned} \langle v_z\rangle_{\text{average}} &= \frac{1}{S}\int_{y=0}^{H}\int_{x=-my}^{my} v_z(x, y)\,dx\,dy \\ &= \frac{7}{90}m^3 H^4\frac{\Delta p}{\mu L S}\left\{\frac{27m^2 + 5}{55m^4 + 38m^2 + 3}\right\} \end{aligned} \tag{23-10}$$

The triangular cross section is equilateral when $m = 1/\sqrt{3}$. In this case, the flow cross section $S = H^2/\sqrt{3}$, and the final result for the average velocity is

$$\langle v_z \rangle_{\text{average}} = \frac{\sqrt{3}H^4 \Delta p}{180 \mu L S} = \frac{H^2 \Delta p}{60 \mu L} \tag{23-11}$$

23-2.3 Effective Diameters for Ducts of Noncircular Cross Section

For any type of flow configuration and reactor geometry, the effective diameter is defined in the following manner:

$$d_{\text{effective}} = \frac{4(\text{actual flow cross-sectional area})}{\text{catalytically active perimeter}} \tag{23-12}$$

This effective diameter (or $d_{\text{effective}}/2$) is used as the characteristic length for dimensionless numbers and dimensionless reactor correlations. Ceramic honeycomb supports for automotive exhaust applications (i.e., cordierite, $2MgO \cdot 2Al_2O_3 \cdot 5SiO_2$) typically have effective diameters on the order of 1 mm. Solutions of the three-dimensional mass transfer equation in straight channels with regular polygon cross sections are compared with two-dimensional solutions in tubes that have the same $d_{\text{effective}}$. If these two-dimensional solutions in cylindrical coordinates represent reasonable approximations of the actual performance of duct reactors, in general, then the effective diameter approach offers a considerable reduction in computational time required to generate numerical results. Expressions for $d_{\text{effective}}$ are listed in Table 23-2 for several ducts with regular polygon cross sections. See Rosner (1986, p. 253) for a summary of momentum and heat transfer correlations in straight channels with noncircular cross section.

TABLE 23-2 Effective Diameters for Straight Channels

Cross Section	Description	$d_{\text{effective}}$
Circular	Radius R	$2R$
Annular outside radius R_{out}; radius ratio, $r^* = R_{\text{in}}/R_{\text{out}} < 1$	(a) Inner and outer walls are catalytically active	$2R_{\text{out}}(1 - r^*)$
	(b) Only the inner wall is catalytically active	$2R_{\text{out}}(1 - r^*)(1 + 1/r^*)$
Rectangular	Wall dimensions, $2a$ and $2b$; aspect ratio, $A_r = a/b$	$4a/(1 + A_r)$
Triangular	Equilateral length of each side is $2c$, height is $H = c\sqrt{3}$	$\frac{2}{3}c\sqrt{3} = \frac{2}{3}H$

23-3 MASS TRANSFER EQUATION

Reactor performance is established by calculating the molar density of reactant A from a steady-state mass balance that accounts for axial convection and transverse diffusion. Chemical reaction only occurs on the well-defined catalytic surface which bounds fluid flow in the regular polygon channel. Hence, depletion of reactant A due to chemical reaction appears in the boundary conditions, but not in the mass balance which applies volumetrically throughout the homogeneous flow channel. The mass transfer equation for duct reactors is written in vector form:

$$\mathbf{v} \cdot \nabla C_A = \mathfrak{D}_{A,\,mix} \nabla^2 C_A \tag{23-13}$$

where $\mathbf{v}$ is the mass-average velocity of the reactive mixture, $\mathfrak{D}_{A,\,mix}$ is a concentration-independent molecular diffusion coefficient of reactant A in the gas phase, ∇ is the gradient operator, and ∇^2 is the Laplacian operator for molecular transport. In rectangular coordinates, the molar density of reactant A is a function of all three spatial coordinates, $C_A(x, y, z)$, and one must solve the following second-order, linear, homogeneous, parabolic partial differential equation (i.e., PDE):

$$v_z(x, y) \frac{\partial C_A}{\partial z} = \mathfrak{D}_{A,\,mix} \left(\frac{\partial^2 C_A}{\partial x^2} + \frac{\partial^2 C_A}{\partial y^2} \right) \tag{23-14}$$

The convective contribution on the left side of (23-14) contains variable coefficients due to the viscous nature of the velocity profile. Hence, numerical methods are required to calculate $C_A(x, y, z)$ discretely at selected grid points within the flow channel via finite-difference approximations for first and second derivatives of a continuous function (i.e., see Sections 23-3.5 and 23-5).

23-3.1 Boundary Conditions

Unlike porous pellets, it is mathematically feasible to account for chemical reaction on the well-defined catalytic surfaces that bound the flow regime in regular polygon duct reactors. A qualitative description of the boundary conditions is based on a steady-state mass balance over a differential surface element. Since convective transport vanishes on the stationary catalytic surface, the following contributions from diffusion and chemical reaction are equated, with units of mol/(area·time):

1. Rate of reactant transport toward the catalytic surface via molecular mass transfer
2. Rate of depletion of reactants due to chemical reaction on the catalytic surface

Term 1 requires Fick's first law of diffusion. Hence, one evaluates the reactant molar density gradient, transverse to the flow direction, at the catalytic surface.

Fick's law stipulates that a negative sign is required to calculate the molecular flux of reactants in a positive coordinate direction. Term 2 requires the kinetic rate law for surface-catalyzed chemical reactions. It is not necessary to re-express the rate law pseudo-volumetrically. In other words, the product of S_m and ρ_{apparent} is not appropriate here or in equation (23-1). When term 2 is written as a first-order or pseudo-first-order rate law, the balance between diffusion and chemical reaction at the catalytic surface is recognized canonically as a radiation boundary condition. This is illustrated below for a catalytic duct with rectangular cross section:

$$\begin{aligned} -\mathfrak{D}_{\text{A, mix}} \frac{\partial C_{\text{A}}}{\partial x} &= k_{\text{surface}} C_{\text{A}} \qquad \text{at } x = x_{\text{wall}} \\ -\mathfrak{D}_{\text{A, mix}} \frac{\partial C_{\text{A}}}{\partial y} &= k_{\text{surface}} C_{\text{A}} \qquad \text{at } y = y_{\text{wall}} \end{aligned} \tag{23-15}$$

Symmetry, or zero-flux, is invoked across each nonreactive boundary.

23-3.2 Nonuniform Catalyst Activity

The concept of variable catalyst deposition is included in the boundary conditions along the active surfaces. The kinetic rate constant for surface-catalyzed chemical reactions, k_{surface}, is a function of position along the active surface, but only transverse to the primary flow direction. Hence,

$$k_{\text{surface}}(\text{surface coordinate}) = \langle k_{\text{surface}} \rangle_{\text{average}} F(\text{surface coordinate})$$

where $\langle k_{\text{surface}} \rangle_{\text{average}}$ is the surface-averaged kinetic rate constant, and F is a normalized shape function which describes the nonuniform distribution of catalyst. If $0 \leq y^* \leq 1$ is a dimensionless variable along an active surface at constant x, transverse to the flow direction, and $y^* = 1$ represents a corner region that is not easily accessible to reactants, then

$$\int_0^1 F(y^*)\, dy^* \equiv 1 \tag{23-16}$$

$$\int_0^1 k_{\text{surface}}(y^*)\, dy^* = \langle k_{\text{surface}} \rangle_{\text{average}} \tag{23-17}$$

Several shape functions are presented in Table 23-3. Duct reactor simulations based on these catalyst deposition profiles are discussed in Section 23-6.7.

The objective here is to simulate duct reactor performance with nonuniform catalyst activity and identify optimal deposition strategies when reactant diffusion toward the active surface is hindered, particularly in the corners of the flow channel. Both types of power-function profiles, listed in Table 23-3, are evaluated for $n = 1, 2, 4, 8$. The delta-function distribution has been implemented by Varma (see Morbidelli *et al.*, 1985) to predict optimum catalyst performance in porous pellets with exothermic chemical reaction. Nonuniform activity profiles for catalytic pellets in fixed-bed reactors, in which a single reaction occurs, have been addressed by Szukiewicz *et al.* (1995), and effectiveness factors for

TABLE 23-3 Normalized Catalyst Activity Profiles: Nonuniform Distribution of Catalyst on the Inner Walls of Straight Channels with Rectangular Cross Section[a]

Catalyst Deposition Profile	$F(y^*)$
Uniform activity	1
Potentially optimal distribution of catalyst	$(\pi/2)\cos(y^*\pi/2)$
	$1+\cos(\pi y^*)$
	$[(n+1)/n][1-(y^*)^n]$
Inefficient use of catalyst	$(\pi/2)\cos[(1-y^*)\pi/2]$
	$(n+1)(y^*)^n, n=1, 2, 4, 8$
Delta-function distribution	$\delta(y^*-\alpha), 0 \le \alpha \le 1$
Inactive or severely poisoned catalyst	0

[a]Catalyst activity varies with position along the wall, transverse to the primary flow direction.

zeroth-order chemical reaction in porous catalysts with nonuniform activity have been calculated by Chidambaram (1984). Nonuniform activity profiles have been discussed for hydrodemetallation catalysts that remove contaminant metals from heavy crude oil and prevent poisoning of downstream catalysts (Limbach and Wei, 1988).

23-3.3 Criterion for Optimal Catalyst Activity

The most effective catalyst deposition strategy produces the highest conversion of reactants to products at a given axial position z within the straight channel. This comparison between various shape functions must be performed at identical Damkohler numbers; defined by (23-18):

$$\beta = \frac{\langle k_{n,\,\text{surface}}\rangle_{\text{average}}[C_{\text{Abulk}}(z=0)]^{n-1}(d_{\text{effective}}/2)}{\mathfrak{D}_{\text{A, mix}}} \tag{23-18}$$

which measure the rate of surface-catalyzed chemical reaction relative to the rate of reactant diffusion toward the active surface. In equation (23-18), $\langle k_{n,\,\text{surface}}\rangle_{\text{average}}$ represents the surface-averaged kinetic rate constant for nth-order irreversible chemical reaction on the catalytic surface, with units of $(\text{vol/mol})^{n-1}(\text{length/time})$. The optimal catalyst deposition profile corresponds to the smallest reactant molar density at position z, averaged over the entire cross section S of the channel. One defines the bulk concentration of reactant A as

$$C_{\text{Abulk}}(z) \equiv \frac{\int_S v_z(x, y)C_{\text{A}}(x, y, z)\,dS}{\langle v_z\rangle_{\text{average}}S} \tag{23-19}$$

Hence, two-dimensional numerical integration of the velocity-weighted microscopic concentration profile is required to evaluate the effectiveness of each shape function $F(y^*)$. Duct reactor performance curves are presented as C_{Abulk} vs. z in dimensionless form, as illustrated in Figure 23-2.

23-3.4 Starting Profile

Numerical solution of the mass transfer equation begins at a small nonzero value of $z = z_{\text{start}}$, not at the inlet where $C_{\text{A}}(x, y, z = 0) = C_{\text{A, inlet}}$ for all values of x and y. This is achieved by invoking an asymptotically exact analytical solution for the molar density of reactant A from laminar mass transfer boundary layer theory in the limit of very large Schmidt and Peclet numbers. The boundary layer starting profile is valid under the following condition:

1. Molecular mass transfer in the primary flow direction is negligible relative to convective transport.
2. Interfacial curvature is not an issue.
3. Mass transfer boundary layers are very thin.
4. Boundary layers that grow from adjacent catalytic surfaces do not intersect.

The starting profile for C_{A} is discussed in Problem 23-7. The general philosophy behind this approach is that one should begin the numerical algorithm with assistance from an analytical starting profile that exhibits significant concentration gradients normal to the active walls. It is also desirable to adopt a starting profile at the largest possible value of z_{start}, subject to the following criteria:

1. The maximum thickness of the mass transfer boundary layer adjacent to active surfaces at $x = x_{\text{wall}}$ and $y = y_{\text{wall}}$ must be small relative to the effective diameter of the channel, $d_{\text{effective}}$. This requirement establishes an upper bound on z_{start}.
2. There must be a few interior grid points within the mass transfer boundary layers adjacent to both walls, not including the outer edge of the boundary layer and the active surface. For rectangular ducts, concentration boundary layers are thinnest along the symmetry planes at $x = 0$ and $y = 0$. This requirement establishes a lower bound on z_{start}.
3. The corner region, where boundary layers from adjacent walls overlap, must be acceptably small. This requirement establishes an upper bound on z_{start}.
4. The bulk molar density of reactant A must be acceptably close to $C_{\text{A, inlet}}$. This requirement is consistent with low reactant conversion and establishes an upper bound on z_{start}.
5. Immediately outside the corner region where mass transfer boundary layers from adjacent walls do not overlap or influence each other, the molar density of reactant A at the catalytic surface must be acceptably close to $C_{\text{A, inlet}}$. This requirement establishes an upper bound on z_{start}.

It is also possible to employ the von Kármán–Pohlhausen integral method (see, e.g., Deen, 1998, pp. 353–356) to develop a starting concentration profile for reactant A in the inlet region, subject to the five requirements outlined above. This method conserves mass over the thickness of the mass transfer boundary

layer rather than differentially within the boundary layer. In the corner region, where boundary layers overlap and adjacent walls are equivalent only for square and equilateral triangular cross sections, a smooth interpolation is employed for $C_A(x, y, z_{start})$ as one approaches the active walls.

23-3.5 Second-Order-Correct Finite-Difference Representations of First and Second Derivatives

Nonequispaced data pairs are available for the function $f(x)$ at three values of the independent variable: x_0, x_1, and x_2, where $x_1 - x_0 = h$ and $x_2 - x_1 = j$ (i.e, $h \neq j$). The objective of this summary of numerical analysis is to generate expressions for df/dx and d^2f/dx^2 at $x = x_1$. These results will be used in the numerical algorithms of Sections 23-4 and 23-5 to solve the mass transfer equation. The starting point to develop several formulas in numerical analysis is the Taylor series for $f(x)$, expanded about one of the given data points (i.e., $x = x_1$, for example). nth-order-correct finite-difference expression are obtained by including $n + 1$ terms in the infinite series expansion for $f(x)$. Hence, for second-order correct results (i.e., $n = 2$), three terms are necessary:

$$f(x) = f(x_1) + (x - x_1)f'(x = x_1) + \frac{(x - x_1)^2 f''(x = x_1)}{2!} + \cdots \qquad (23\text{-}20)$$

The two unknown coefficients in equation (23-20) [i.e., $f'(x = x_1)$ and $f''(x = x_1)$] are the quantities of interest. Hence, two equations are required to calculate these unknowns. One generates two independent equations by evaluating $f(x)$ at two different points. Since evaluation of $f(x)$ at $x = x_1$ leads to the trivial result $f(x_1) = f(x_1)$, which is not useful, it seems reasonable that one should evaluate $f(x)$ at the other two points, x_0 and x_2. Hence,

$$\begin{aligned} f(x_0) &= f(x_1) + (x_0 - x_1)f'(x = x_1) \\ &\quad + \frac{(x_0 - x_1)^2 f''(x = x_1)}{2!} + \cdots \\ f(x_2) &= f(x_1) + (x_2 - x_1)f'(x = x_1) \\ &\quad + \frac{(x_2 - x_1)^2 f''(x = x_1)}{2!} + \cdots \end{aligned} \qquad (23\text{-}21)$$

All of the information provided at the beginning of this section has been used. It should be obvious, now, that nth-order-correct finite difference expressions for various derivatives require Taylor series expansions that include $n + 1$ terms with n unknowns, and $n + 1$ known data pairs to determine n unknown derivatives. The function $f(x)$ is expanded about one of the data pairs (i.e., evaluation of the zeroth-order leading term), and the remaining n data pairs are used for nontrivial

evaluation of the truncated series for $f(x)$, generating n equations. As illustrated by equations (23-21) when $n = 2$,

$$f(x_0) = f(x_1) - hf'(x = x_1) + \frac{h^2 f''(x = x_1)}{2!}$$
$$f(x_2) = f(x_1) + jf'(x = x_1) + \frac{j^2 f''(x = x_1)}{2!} \tag{23-22}$$

Solution of equations (23-22) yields second-order-correct finite difference representations for first- and second-derivatives of $f(x)$ at $x = x_1$. These generalized results for nonequispaced data points are:

$$f'(x = x_1) = \frac{\alpha^2 f(x_2) + (1 - \alpha^2) f(x_1) - f(x_0)}{h + \alpha^2 j}$$
$$f''(x = x_1) = \frac{2[\alpha f(x_2) - (1 + \alpha) f(x_1) + f(x_0)]}{j(h + \alpha^2 j)} \qquad \alpha = \frac{h}{j} \tag{23-23}$$

If the three data pairs are equispaced along the x axis, then $h = j$ and $\alpha = 1$, and one obtains the following classic results for second-order correct derivatives:

$$f'(x = x_1) = \frac{f(x_2) - f(x_0)}{2h}$$
$$f''(x = x_1) = \frac{f(x_2) - 2f(x_1) + f(x_0)}{h^2} \tag{23-24}$$

These are central difference expressions because f' and f'' are evaluated at x_1 using information at x_1 and on both sides of x_1. Central differences are useful to calculate slopes in the middle of a set of discrete data points.

23-4 DETAILS OF THE NUMERICAL ALGORITHM

Convective transport of reactant A in the primary flow direction requires evaluation of $\partial C_A/\partial z$. Transverse diffusion of reactant A toward the catalytic surfaces requires evaluation of $\partial^2 C_A/\partial x^2$ and $\partial^2 C_A/\partial y^2$. All three of these partial derivatives can be approximated numerically via finite-difference expressions for f' and f'', given by (23-23) or (23-24). The partial differential mass balance and its boundary conditions are solved for the molar density of reactant A at selected grid points within the flow channel via coupled linear algebraic equations. The algebraic equations that result when finite-difference approximations for first and second derivatives are employed to solve PDEs are similar to the governing equations for some classic problems in chemical engineering (i.e., stagewise calculations in distillation and countercurrent solid–liquid extraction). The numerical algorithm proceeds as follows for equispaced grid points in the x direction (i.e., the spacing is Δx) and the y direction (i.e., the spacing is Δy), such that $\Delta y = \Delta x/A_r$ if the flow cross section is rectangular:

1. At axial position z_k, the molar density of reactant A is known at all x_i and y_j in the flow cross section via the starting profile. The objective is to predict $C_A(x_i, y_j, z_{k+1})$ at the next axial step, z_{k+1}.
2. Convective transport in the primary flow direction is evaluated as a second-order-correct first derivative at the fictitious point, x_i, y_j, and $z_{k+1/2}$, midway between z_k and z_{k+1}:

$$v_z(x, y)\frac{\partial C_A}{\partial z} \approx v_z(x_i, y_j)\frac{\mathbf{C}_A(x_i, y_j, z_{k+1}) - C_A(x_i, y_j, z_k)}{\Delta z} \tag{23-25}$$

   where $\Delta z = z_{k+1} - z_k$.
3. The alternating direction implicit method (i.e., ADI) is employed to calculate transverse diffusion in the x direction via second-order-correct finite differences for a second derivative using unknown molar densities at z_{k+1}. Hence,

$$\mathfrak{D}_{A,\,mix}\frac{\partial^2 C_A}{\partial x^2} \approx \mathfrak{D}_{A,\,mix}\frac{\mathbf{C}_A(x_{i+1}, y_j, z_{k+1}) - 2\mathbf{C}_A(x_i, y_j, z_{k+1}) + \mathbf{C}_A(x_{i-1}, y_j, z_{k+1})}{(\Delta x)^2} \tag{23-26}$$

   where $\Delta x = x_{i+1} - x_i = x_i - x_{i-1}$.
4. When transverse diffusion in the x direction is predicted using unknown molar densities at z_{k+1}, the ADI method estimates transverse diffusion in the y direction via second-order-correct finite differences for a second derivative using known molar densities at z_k. Now,

$$\mathfrak{D}_{A,\,mix}\frac{\partial^2 C_A}{\partial y^2} \approx \mathfrak{D}_{A,\,mix}\frac{C_A(x_i, y_{j+1}, z_k) - 2C_A(x_i, y_j, z_k) + C_A(x_i, y_{j-1}, z_k)}{(\Delta y)^2} \tag{23-27}$$

   where $\Delta y = y_{j+1} - y_j = y_j - y_{j-1}$.
5. At each grid point, x_i and y_j, in the flow cross section, the mass transfer equation (i.e., PDE) is written as a linear algebraic equation in terms of three unknown molar densities at z_{k+1}. In other words,

$$v_z(x, y)\frac{\partial C_A}{\partial z} = \mathfrak{D}_{A,\,mix}\left(\frac{\partial^2 C_A}{\partial x^2} + \frac{\partial^2 C_A}{\partial y^2}\right) \tag{23-28}$$

   is converted to an algebraic equation via second-order-correct finite-difference representations of the appropriate derivatives:

$$\begin{aligned} v_z(x_i, y_j)&\frac{\mathbf{C}_A(x_i, y_j, z_{k+1}) - C_A(x_i, y_j, z_k)}{\Delta z} \\ &= \mathfrak{D}_{A,\,mix}\left[\frac{\mathbf{C}_A(x_{i+1}, y_j, z_{k+1}) - 2\mathbf{C}_A(x_i, y_j, z_{k+1}) + \mathbf{C}_A(x_{i-1}, y_j, z_{k+1})}{(\Delta x)^2}\right. \\ &\quad \left. + \frac{C_A(x_i, y_{j+1}, z_k) - 2C_A(x_i, y_j, z_k) + C_A(x_i, y_{j-1}, z_k)}{(\Delta y)^2}\right] \end{aligned} \tag{23-29}$$

where the three unknown molar densities at z_{k+1} in equation (23-29) are highlighted in boldface.

6. Finite-difference algebraic analogs of the partial differential mass balance, as illustrated by (23-29), are written at each grid point within the flow cross section, excluding the boundaries. Boundary conditions are employed to write algebraic difference equations at the active surfaces, $x = x_{\text{wall}}$ and $y = y_{\text{wall}}$, and at the symmetry planes, $x = 0$ and $y = 0$. If the flow cross section is rectangular, there are N_x grid points in the x direction and N_y grid points in the y direction, excluding the boundaries, then

$$N_x N_y + 2N_x + 2N_y + 4 = (N_x + 2)(N_y + 2) \tag{23-30}$$

linear algebraic equations based on the mass transfer equation and its boundary conditions are written for all unknown molar densities $\mathbf{C}_{\text{A}}(x_i, y_j, z_{k+1})$ at axial position z_{k+1}. On each of the $N_y + 2$ grid lines where y_j is constant, $N_x + 2$ linear algebraic equations are solved for $N_x + 2$ unknown molar densities. In matrix form, each system of equations is written as

$$A_j \mathbf{C}_{\text{A},\, j,k+1} = B_{j,k} \qquad 1 \le j \le N_y + 2 \tag{23-31}$$

A_j is an $N_x + 2$ by $N_x + 2$ square matrix of known coefficients. It has a tridiagonal structure because, at most, only three unknown molar densities at z_{k+1} [i.e., highlighted in boldface print, in (23-29)] appear in each finite-difference equation. A tridiagonal matrix only contains nonzero entries along the major diagonal and the diagonals immediately above and below the major diagonal. $\mathbf{C}_{\text{A},j,k+1}$ is an $N_x + 2$ by 1 column vector which contains all of the unknown molar densities at z_{k+1} along a grid line where y_j is constant. $B_{j,k}$ is an $N_x + 2$ by 1 column vector of known constants based on molar densities at z_k.

7. Matrix algebra is employed to solve $N_y + 2$ systems of linear algebraic equations. However, the problem is simplified when the coefficient matrix A_j is tridiagonal. Under these conditions, the Thomas algorithm (Carnahan *et al.*, 1969, pp. 441–442) provides an efficient solution for all unknown molar densities at z_{k+1} along the grid line where y_j is constant. This procedure is repeated $N_y + 2$ times to calculate all unknown molar densities in the flow cross section at z_{k+1}.
8. Now one takes a jump of size Δz from z_{k+1} to z_{k+2}. Once again, convective transport in the primary flow direction is evaluated as a second-order-correct first derivative at the fictitious point, x_i, y_j, and $z_{k+3/2}$, midway between z_{k+1} and z_{k+2}.
9. The ADI method is employed to calculate transverse diffusion in the y direction using unknown molar densities at z_{k+2}, whereas transverse diffusion in the x direction is estimated using known molar densities at z_{k+1}. Then, steps 5 through 7 are repeated. Notice how transverse diffusion in the x direction is evaluated using unknown molar densities at one

axial position, and then transverse diffusion in the y direction is evaluated using unknown molar densities at the next axial position. This alternation continues until one reaches the reactor outlet.

For example, viscous flow in a square duct with $\beta = 1$ was solved at 289 grid points in the upper right-hand quadrant of the cross section (i.e., $N_x = 15$ and $N_y = 15$).

23-5 SECOND-ORDER CORRECT FINITE-DIFFERENCE EXPRESSIONS FOR FIRST DERIVATIVES ON THE BOUNDARY OF THE FLOW CROSS SECTION

Once again, nonequispaced data pairs are available for the function $f(x)$ at three values of the independent variable; x_0, x_1, and x_2, where $x_1 - x_0 = h$ and $x_2 - x_1 = j$ (i.e, $h \neq j$). The objective of this summary of numerical analysis is to generate expressions for df/dx at $x = x_0$ and $x = x_2$. Whereas the previous exercise in numerical analysis in Section 23-3.5 generated central difference results at $x = x_1$, the discussion in this section focuses on forward and backward differences (see Cutlip and Shacham, 1999, pp. 396–397). These results are employed to generate algebraic difference equations at the lateral boundaries of the control volume.

23-5.1 Forward Difference at $x = x_0$

It is necessary to expand $f(x)$ about x_0 and include three terms in the Taylor series to obtain a second-order correct result for $f'(x = x_0)$. Hence,

$$f(x) = f(x_0) + (x - x_0) f'(x = x_0) + \frac{(x - x_0)^2 f''(x = x_0)}{2!} + \cdots$$

This Taylor series is evaluated at the other two points (i.e., x_1 and x_2) to generate two nontrivial equations for the two unknown coefficients [i.e., $f'(x = x_0)$ and $f''(x = x_0)$]:

$$\begin{aligned} f(x_1) &= f(x_0) + (x_1 - x_0) f'(x = x_0) \\ &\quad + \frac{(x_1 - x_0)^2 f''(x = x_0)}{2!} + \cdots \\ f(x_2) &= f(x_0) + (x_2 - x_0) f'(x = x_0) \\ &\quad + \frac{(x_2 - x_0)^2 f''(x = x_0)}{2!} + \cdots \end{aligned} \tag{23-32}$$

Even though the objective is to obtain an expression for $f'(x = x_0)$, the fact that this expression must be second-order correct requires three terms in the Taylor

series. Consequently, the third term in the series contains the second derivative of $f(x)$, evaluated at $x = x_0$. For nonequispaced data, (23-32) reduces to

$$\begin{aligned} f(x_1) &= f(x_0) + hf'(x = x_0) + \frac{h^2 f''(x = x_0)}{2!} \\ f(x_2) &= f(x_0) + (h + j)f'(x = x_0) + \frac{(h + j)^2 f''(x = x_0)}{2!} \end{aligned} \tag{23-33}$$

Solution of these two equations yields second-order-correct forward difference expressions for first and second derivatives of $f(x)$ at $x = x_0$. The desired result for the first derivative is

$$f'(x = x_0) = \frac{f(x_2) - (1 + 1/\alpha)^2 f(x_1) + [(1 + 1/\alpha)^2 - 1]f(x_0)}{h + j - h(1 + 1/\alpha)^2} \tag{23-34}$$

where $\alpha = h/j$. If the three data pairs are equispaced along the x axis, then $h = j$ and $\alpha = 1$, and one obtains the following second-order correct forward difference expression for a first derivative:

$$f'(x = x_0) = \frac{-f(x_2) + 4f(x_1) - 3f(x_0)}{2h} \tag{23-35}$$

Forward differences are useful to calculate a slope at the initial point of a set of discrete data.

23-5.2 Backward Difference at $x = x_2$

Now, it is necessary to expand $f(x)$ about x_2 and include three terms in the Taylor series to obtain a second-order correct result for $f'(x_2)$. Hence,

$$f(x) = f(x_2) + (x - x_2)f'(x = x_2) + \frac{(x - x_2)^2 f''(x = x_2)}{2!} + \cdots \tag{23-36}$$

This Taylor series is evaluated at the other two points (i.e., x_0 and x_1) to generate two nontrivial equations for the two unknown coefficients [i.e., $f'(x = x_2)$ and $f''(x = x_2)$]:

$$\begin{aligned} f(x_0) &= f(x_2) + (x_0 - x_2)f'(x = x_2) \\ &\quad + \frac{(x_0 - x_2)^2 f''(x = x_2)}{2!} + \cdots \\ f(x_1) &= f(x_2) + (x_1 - x_2)f'(x = x_2) \\ &\quad + \frac{(x_1 - x_2)^2 f''(x = x_2)}{2!} + \cdots \end{aligned} \tag{23-37}$$

The coefficient $f'(x = x_2)$ is of interest in this exercise. For nonequispaced data, equations (23-37) reduce to

$$\begin{aligned} f(x_0) &= f(x_2) - (h + j) f'(x = x_2) + \frac{(h + j)^2 f''(x = x_2)}{2!} \\ f(x_1) &= f(x_2) - j f'(x = x_2) + \frac{j^2 f''(x = x_2)}{2!} \end{aligned} \tag{23-38}$$

Solution of these two equations yields second-order-correct backward difference expressions for first and second derivatives of $f(x)$ at $x = x_2$. The desired result for the first derivative is

$$f'(x = x_2) = \frac{[(1 + \alpha)^2 - 1] f(x_2) - (1 + \alpha)^2 f(x_1) + f(x_0)}{j(1 + \alpha)^2 - (h + j)} \tag{23-39}$$

where $\alpha = h/j$. For equispaced data, one obtains the following second-order correct backward difference expression for a first derivative:

$$f'(x = x_2) = \frac{3 f(x_2) - 4 f(x_1) + f(x_0)}{2h} \tag{23-40}$$

Backward differences are useful to calculate a slope at the final point of a set of discrete data.

23-5.3 Analysis of Boundary Conditions at the Symmetry Plane Via the Central Difference

As mentioned in Section 23-4, step 5, the following algebraic equation, also given by (23-29):

$$\begin{aligned} v_z(x_i, y_j) &\frac{[\mathbf{C}_\mathrm{A}(x_i, y_j, z_{k+1}) - C_\mathrm{A}(x_i, y_j, z_k)]}{\Delta z} \\ &= \mathfrak{D}_{\mathrm{A,\,mix}} \left[\frac{\mathbf{C}_\mathrm{A}(x_{i+1}, y_j, z_{k+1}) - 2\mathbf{C}_\mathrm{A}(x_i, y_j, z_{k+1}) + \mathbf{C}_\mathrm{A}(x_{i-1}, y_j, z_{k+1})}{(\Delta x)^2} \right. \\ &\quad \left. + \frac{C_\mathrm{A}(x_i, y_{j+1}, z_k) - 2C_\mathrm{A}(x_i, y_j, z_k) + C_\mathrm{A}(x_i, y_{j-1}, z_k)}{(\Delta y)^2} \right] \end{aligned} \tag{23-41}$$

represents the finite-difference analog of the partial differential mass balance when transverse diffusion in the x direction is written in terms of unknown molar densities at z_{k+1}, and $\partial^2 C_\mathrm{A}/\partial y^2$ is written in terms of known molar densities at z_k. There are N_x grid points, equally spaced in the x direction (i.e., x_i, $1 \le i \le N_x$), excluding the boundaries. The boundary at the symmetry plane in the center of the channel is identified by grid point $x_0 = 0$, and the boundary at the catalytic surface is identified by grid point $x_{Nx+1} = x_{\mathrm{wall}}$. Equation (23-41) is written at each x_i, y_j ($1 \le i \le N_x$) to generate N_x equations in terms of $N_x + 2$ unknown molar densities at z_{k+1}. There are $N_x + 2$ unknowns because the algebraic difference

equation at grid point x_1, y_j contains unknown molar densities at x_0, x_1, and x_2, and when the mass balance is written at x_{Nx}, y_j, the difference equation contains unknown molar densities at x_{Nx-1}, x_{Nx}, and x_{Nx+1}. Hence, two additional algebraic equations are required before the Thomas algorithm can be employed to solve for the unknown molar densities at z_{k+1}. Since convective transport does not vanish at the symmetry plane, one additional equation is generated by writing the mass balance, given by equation (23-41), at x_0, y_j:

$$v_z(x_0, y_j)\frac{\mathbf{C}_A(x_0, y_j, z_{k+1}) - C_A(x_0, y_j, z_k)}{\Delta z} = \mathfrak{D}_{A,\,mix}\left[\frac{\mathbf{C}_A(x_1, y_j, z_{k+1}) - 2\mathbf{C}_A(x_0, y_j, z_{k+1}) + \mathbf{C}_A(x_{-1}, y_j, z_{k+1})}{(\Delta x)^2} + \frac{C_A(x_0, y_{j+1}, z_k) - 2C_A(x_0, y_j, z_k) + C_A(x_0, y_{j-1}, z_k)}{(\Delta y)^2}\right] \tag{23-42}$$

However, this introduces another unknown molar density at x_{-1} which arises from the second-order correct central difference expression for $\partial^2 C_A/\partial x^2$ at x_0, y_j. The boundary condition at the symmetry plane is used to relate C_A at x_{-1} to C_A at x_1 via a second-order correct central difference expression for a first derivative at $x_0 = 0$:

$$\left(\frac{\partial C_A}{\partial x}\right)_{x_0=0} = \frac{\mathbf{C}_A(x_1, y_j, z_{k+1}) - \mathbf{C}_A(x_{-1}, y_j, z_{k+1})}{2\Delta x} \tag{23-43}$$

which indicates that

$$\mathbf{C}_A(x_1, y_j, z_{k+1}) = \mathbf{C}_A(x_{-1}, y_j, z_{k+1}) \tag{23-44}$$

The final form of the mass balance at grid point x_0, y_j contains two unknown molar densities at x_0 and x_1. One obtains equation (23-45) via substitution of (23-44) into (23-42):

$$v_z(x_0, y_j)\frac{\mathbf{C}_A(x_0, y_j, z_{k+1}) - C_A(x_0, y_j, z_k)}{\Delta z} = \mathfrak{D}_{A,\,mix}\left[\frac{2\mathbf{C}_A(x_1, y_j, z_{k+1}) - 2\mathbf{C}_A(x_0, y_j, z_{k+1})}{(\Delta x)^2} + \frac{C_A(x_0, y_{j+1}, z_k) - 2C_A(x_0, y_j, z_k) + C_A(x_0, y_{j-1}, z_k)}{(\Delta y)^2}\right] \tag{23-45}$$

In a straight channel with annular cross section and no-slip boundaries at the inner and outer walls, the mass balance should not be written at the inner surface (i.e., $x = x_0$). Instead, a second-order correct forward difference expression should be

employed to calculate the transverse concentration gradient at x_0 via one of the boundary conditions. This allows one to relate C_A at x_0 to C_A at x_1 and x_2.

23-5.4 Analysis of Boundary Conditions at the Catalytic Surface Via the Backward Difference

One more algebraic equation is required to solve for all unknown molar densities at z_{k+1}. It is not advantageous to write the mass balance at the catalytic surface (i.e., at x_{Nx+1}) because the no-slip boundary condition at the wall stipulates that convective transport is identically zero. Hence, one relies on the radiation boundary condition to generate equation (23-46). Diffusional flux of reactants toward the catalytic surface, evaluated at the surface, is written in terms of a backward difference expression for a first-derivative that is second-order correct, via equation (23-40). This is illustrated below at $x_{\text{wall}} = x_{Nx+1}$ for equispaced data:

$$
\begin{aligned}
&-\mathfrak{D}_{A,\,\text{mix}}\left(\frac{\partial C_A}{\partial x}\right)_{x=x_{\text{wall}}} \\
&\quad = -\mathfrak{D}_{A,\,\text{mix}}\frac{3\mathbf{C}_A(x_{Nx+1}, y_j, z_{k+1}) - 4\mathbf{C}_A(x_{Nx}, y_j, z_{k+1}) + \mathbf{C}_A(x_{Nx-1}, y_j, z_{k+1})}{2\Delta x} \\
&\quad = k_{1,\text{surface}}\mathbf{C}_A(x_{Nx+1}, y_j, z_{k+1}) \qquad (23\text{-}46)
\end{aligned}
$$

This balance between diffusion and heterogeneous chemical reaction at the catalytic surface allows one to relate C_A at x_{Nx+1} to C_A at x_{Nx} and x_{Nx-1}. Hence, the mass balance at x_{Nx}, y_j contains only two unknown molar densities at z_{k+1}:

$$
\begin{aligned}
&v_z(x_{Nx}, y_j)\frac{\mathbf{C}_A(x_{Nx}, y_j, z_{k+1}) - C_A(x_{Nx}, y_j, z_k)}{\Delta z} \\
&\quad = \mathfrak{D}_{A,\,\text{mix}}\left[\frac{\mathbf{C}_A(x_{Nx+1}, y_j, z_{k+1}) - 2\mathbf{C}_A(x_{Nx}, y_j, z_{k+1}) + \mathbf{C}_A(x_{Nx-1}, y_j, z_{k+1})}{(\Delta x)^2}\right. \\
&\qquad \left. + \frac{C_A(x_{Nx}, y_{j+1}, z_k) - 2C_A(x_{Nx}, y_j, z_k) + C_A(x_{Nx}, y_{j-1}, z_k)}{(\Delta y)^2}\right] \qquad (23\text{-}47)
\end{aligned}
$$

because $\mathbf{C}_A(x_{Nx+1}, y_j, z_{k+1})$ is replaced by $\mathbf{C}_A(x_{Nx}, y_j, z_{k+1})$ and $\mathbf{C}_A(x_{Nx-1}, y_j, z_{k+1})$ via the radiation boundary condition given by equation (23-46).

In summary, boundary conditions at the symmetry plane in the center of the channel and at the catalytic surface provide auxiliary equations for $\mathbf{C}_A(x_{-1}, y_j, z_{k+1})$ and $\mathbf{C}_A(x_{Nx+1}, y_j, z_{k+1})$, respectively. The finite difference analog of the partial differential mass balance is written at $N_x + 1$ grid points (i.e., x_i, y_j; $0 \le i \le N_x$). The balances at x_0, y_j and x_{Nx}, y_j contain two unknowns, whereas the other $N_x - 1$ balances contain three unknowns. This set of $N_x + 1$ linear algebraic equations for $N_x + 1$ unknown molar densities at z_{k+1} is solved via the Thomas algorithm because the coefficient matrix is tridiagonal.

23-6 VISCOUS FLOW

23-6.1 Viscous Flow in a Straight Channel with Square Cross Section

The governing equations in dimensionless form and their numerical solution are discussed for first-order irreversible chemical reaction on a flat surface with uniform catalyst activity [i.e., $F(y^*) = 1$]. The following parameters are appropriate for a straight channel with square cross section:

$$\begin{aligned} &\text{Cross-sectional dimensions, } 2a \times 2b \text{ (i.e., } a = b) \\ &\text{Aspect ratio} = A_r = \frac{a}{b} = 1 \\ &\text{Effective diameter} = d_{\text{effective}} = \frac{4a}{1 + A_r} = 2a \end{aligned} \tag{23-48}$$

The dimensionless independent variables are

$$\begin{aligned} x^* &= \frac{x}{a} \\ y^* &= \frac{y}{b} \\ \xi &= \frac{1}{\text{Pe}_{\text{MT}}} \left(\frac{z}{d_{\text{effective}}} \right) \end{aligned} \tag{23-49}$$

where the mass transfer Peclet number is defined by

$$\text{Pe}_{\text{MT}} = \frac{\langle v_z \rangle_{\text{average}} \, d_{\text{effective}}}{\mathfrak{D}_{\text{A, mix}}} \tag{23-50}$$

The dimensionless bulk molar density of reactant A is calculated by exploiting the symmetry of the rectangular duct and focusing only on one quadrant of the total cross-sectional area (i.e., $0 \le x \le a$, $0 \le y \le b$):

$$\Psi_{\text{Abulk}}(\xi) \equiv \frac{C_{\text{Abulk}}(z)}{C_{\text{Abulk}}(z = 0)} = \int_{x^*=0}^{1} \int_{y^*=0}^{1} v_z^*(x^*, y^*) \Psi_{\text{A}}(x^*, y^*, \xi) \, dx^* \, dy^* \tag{23-51}$$

where

$$v_z^*(x^*, y^*) \equiv \frac{v_z(x, y)}{\langle v_z \rangle_{\text{average}}} \tag{23-52}$$

Notice that the molar density of reactant A at the catalytic surface does not contribute to C_{Abulk} because the weighting factor vanishes at a no-slip boundary. The dimensionless microscopic concentration profile

$$\Psi_{\text{A}}(x^*, y^*, \xi) \equiv \frac{C_{\text{A}}(x, y, z)}{C_{\text{Abulk}}(z = 0)} \tag{23-53}$$

is obtained numerically from the following dimensionless mass transfer equation which includes axial convection and two-dimensional transverse diffusion:

$$v_z^*(x^*, y^*)\frac{\partial \Psi_A}{\partial \xi} = \left(\frac{4}{1+A_r}\right)^2 \left[\frac{\partial^2 \Psi_A}{\partial x^{*2}} + A_r^2 \frac{\partial^2 \Psi_A}{\partial y^{*2}}\right] \tag{23-54}$$

The generalized radiation boundary conditions on the catalytic surfaces are

$$\begin{aligned} -\frac{\partial \Psi_A}{\partial x^*} &= \frac{1+A_r}{2}\beta F(y^*)\Psi_A \qquad \text{at } x^* = 1 \\ -\frac{\partial \Psi_A}{\partial y^*} &= \frac{1+A_r}{2A_r}\beta F(x^*)\Psi_A \qquad \text{at } y^* = 1 \end{aligned} \tag{23-55}$$

and the symmetry conditions along the central planes are

$$\begin{aligned} -\frac{\partial \Psi_A}{\partial x^*} &= 0 \qquad \text{at } x^* = 0 \\ -\frac{\partial \Psi_A}{\partial y^*} &= 0 \qquad \text{at } y^* = 0 \end{aligned} \tag{23-56}$$

By definition, the inlet condition is $\Psi_A = \Psi_{Abulk} = 1$ at $\xi = 0$. However, mass transfer boundary layer theory is employed to generate the following analytical solution near the inlet:

$$\Psi_{Abulk}(\xi_{start}) = 1 - 8\beta\xi_{start} + \cdots \approx 0.9999 \qquad \text{at } \xi_{start} = 1.27 \times 10^{-5}$$

when the Damkohler number is

$$\beta = \frac{\langle k_{1,surface}\rangle_{average}\, d_{effective}}{2\mathfrak{D}_{A,\,mix}} = 1$$

Simulations reveal that $\ln \Psi_{Abulk}$ vs. ξ is linear when $\xi \geq 5 \times 10^{-3}$, and the linear least-squares result when $\beta = 1$ is

$$\Psi_{Abulk}(\xi; \beta = 1) \approx \exp(-\lambda\xi) \qquad \lambda \approx 4.6$$

Self-Consistent Check of the Numerical Solutions

Comparison with Exact Results. It is not unreasonable to suspect that truncation errors in the numerical approximation of first and second derivatives might accumulate in the computational scheme used to integrate the mass transfer equation. One check for accuracy involves a comparison between numerical results and exact analytical solutions. Of course, only a limited number of analytical solutions are available. For example, the following solutions have been obtained analytically for catalytic duct reactors:

1. *Viscous flow between two infinitely wide parallel plates with a very narrow gap separating the two walls*. When one wall is catalytically active, the following solution is applicable (Solbrig and Gidaspow, 1967):

$$\Psi_{\text{Abulk}}(\xi;\beta) = \frac{3}{4}A(\beta)\exp\left[-\frac{128}{3}\lambda(\beta)\xi\right] \tag{23-57}$$

   When both walls are active, numerical solutions for the viscous slot require much less computational time, relative to a rectangular channel with large aspect ratio, because the three-dimensional mass transfer equation is reduced to two dimensions with a very simple velocity profile (see equations 23-77 through 23-79).

2. *Plug flow in a straight channel with square cross section*. If all the walls are catalytically active, then

$$\Psi_{\text{Abulk}}(\xi;\beta) = \left\{\sum_{n=1}^{\infty}\frac{2\beta^2}{\alpha_n^2[\beta(1+\beta)+\alpha_n^2]}\exp(-4\alpha_n^2\xi)\right\}^2 \tag{23-58}$$

   where α_n corresponds to the ordered roots of the transcendental equation $\alpha_n\tan(\alpha_n) = \beta$. Carslaw and Jaeger (1984, p. 491) have tabulated the first six roots (i.e., $1 \le n \le 6$) of this transcendental equation for 38 nontrivial values of the Damkohler number β.

Quasi-Macroscopic Mass Balance. When analytical solutions are not available, the following approach is recommended to verify accuracy of the numerical results. The microscopic mass transfer equation

$$\mathbf{v}\cdot\nabla C_{\text{A}} = \mathfrak{D}_{\text{A, mix}}\nabla^2 C_{\text{A}} \tag{23-59}$$

is integrated over a differential control volume that includes the entire cross section S of the channel (i.e., $dV = S\,dz$). This is analogous to stretching the control volume in the coordinate directions transverse to the flow until one reaches the boundaries of the channel. Since the control volume remains differentially thick in the primary flow direction, one obtains an ordinary differential equation that describes how the bulk molar density of reactant A changes with axial coordinate z. The resulting mass balance corresponds to the differential design equation for a plug-flow reactor with heterogeneous chemical reaction at the catalytic walls. If the control volume were stretched axially from inlet to outlet, encompassing the entire catalytic channel, then the resulting mass balance would resemble that of a continuous-stirred tank reactor. In terms of a plug-flow reactor, development of the differential design equation is illustrated mathematically for an incompressible fluid with constant physical properties, such that $\nabla\cdot\mathbf{v} = 0$. Gauss's law is employed to convert volume integrals to surface integrals, and the unit normal vector $\mathbf{n}$ on each surface that surrounds the control volume is

oriented from the system toward the surroundings. For example,

$$\int_V (\mathbf{v} \cdot \nabla C_A)\, dV = \int_V (\mathbf{v} \cdot \nabla C_A + C_A \nabla \cdot \mathbf{v})\, dV = \int_V (\nabla \cdot C_A \mathbf{v})\, dV$$
$$= \int_S (\mathbf{n} \cdot C_A \mathbf{v})\, dS = \int_S C_A (\mathbf{n} \cdot \mathbf{v})\, dS \tag{23-60}$$

It is only necessary to consider convective mass transfer across surfaces where $\mathbf{n} \cdot \mathbf{v} \neq 0$. There are two surfaces that contribute significantly to the surface integral in (23-60). These surfaces are transverse to the flow at z (i.e., $\mathbf{n} = -\boldsymbol{\delta}_z$, $\mathbf{n} \cdot \mathbf{v} < 0$) and at $z + dz$ (i.e., $\mathbf{n} = +\boldsymbol{\delta}_z$, $\mathbf{n} \cdot \mathbf{v} > 0$). Hence,

$$\int_V (\mathbf{v} \cdot \nabla C_A)\, dV = \int_S C_A (\mathbf{n} \cdot \mathbf{v})\, dS = \int_S (v_z C_A)_{\text{at } z+dz}\, dS - \int_S (v_z C_A)_{\text{at } z}\, dS \tag{23-61}$$

Since

$$C_{A\text{bulk}}(z) \equiv \frac{\int_S v_z(x, y) C_A(x, y, z)\, dS}{\langle v_z \rangle_{\text{average}} S} \tag{23-62}$$

the convective contribution to the quasi-macroscopic mass balance is

$$\int_V (\mathbf{v} \cdot \nabla C_A)\, dV = \langle v_z \rangle_{\text{average}} S \{C_{A\text{bulk}}(z + dz) - C_{A\text{bulk}}(z)\} \tag{23-63}$$

Molecular mass transfer in equation (23-59) is integrated as follows:

$$\int_V (\mathfrak{D}_{A,\text{mix}} \nabla^2 C_A)\, dV = \int_V (\mathfrak{D}_{A,\text{mix}} \nabla \cdot \nabla C_A)\, dV = \int_V (\nabla \cdot \mathfrak{D}_{A,\text{mix}} \nabla C_A)\, dV$$
$$= \int_S (\mathbf{n} \cdot \mathfrak{D}_{A,\text{mix}} \nabla C_A)\, dS$$
$$= \int_S \mathfrak{D}_{A,\text{mix}} (\mathbf{n} \cdot \nabla C_A)\, dS \tag{23-64}$$

It is only necessary to consider diffusional flux across the lateral surface because axial diffusion is insignificant at high mass transfer Peclet numbers. The generalized quasi-macroscopic mass balance for one-dimensional fluid flow through a straight channel with arbitrary cross section and nonzero mass flux at the lateral boundaries is

$$\langle v_z \rangle_{\text{average}} S \{C_{A\text{bulk}}(z + dz) - C_{A\text{bulk}}(z)\} = \int_S \mathfrak{D}_{A,\text{mix}} (\mathbf{n} \cdot \nabla C_A)\, dS \tag{23-65}$$

If this balance is applied to blood vessels or hollow-fiber ultrafiltration membranes with permeable walls, then the contribution from diffusion on the right side of (23-65) is written in terms of a mass transfer coefficient and a concentration driving force. When equation (23-65) is applied to rectangular duct

reactors (i.e., $dS = dx\,dz$ or $dy\,dz$) with first-order irreversible chemical reaction on the catalytic surface, contributions from diffusion are evaluated using the radiation boundary conditions given by (23-15), which account for nonuniform catalyst deposition:

$$-\mathfrak{D}_{\mathrm{A,\,mix}}\frac{\partial C_{\mathrm{A}}}{\partial x} = k_{1,\mathrm{surface}}(y)C_{\mathrm{A}} \qquad \text{at } x = a, \quad \mathbf{n} = +\boldsymbol{\delta}_x, \quad dS = dy\,dz$$

$$-\mathfrak{D}_{\mathrm{A,\,mix}}\frac{\partial C_{\mathrm{A}}}{\partial y} = k_{1,\mathrm{surface}}(x)C_{\mathrm{A}} \qquad \text{at } y = b, \quad \mathbf{n} = +\boldsymbol{\delta}_y, \quad dS = dx\,dz$$

$$k_{1,\mathrm{surface}}(x \text{ or } y) = \langle k_{1,\mathrm{surface}}\rangle_{\mathrm{average}} F(x \text{ or } y) \tag{23-66}$$

Since the control volume (i.e., $dV = S\,dz$) is differentially thick in the z direction, the lateral surfaces across which diffusion occurs are also differentially thick in the z direction. If one focuses only on one quadrant of the total cross-sectional area (i.e., $0 \le x \le a$, $0 \le y \le b$) because all four quadrants behave similarly, then contributions from diffusion in the quasi-macroscopic mass balance are analyzed by integrating with respect to y along the surface at $x = a$, and integrating with respect to x along the surface at $y = b$.

Symmetry conditions at $x = 0$ and $y = 0$ nullify any contributions from molecular mass transfer across these boundaries. Hence,

$$\int_S \mathfrak{D}_{\mathrm{A,\,mix}}(\mathbf{n}\cdot\nabla C_{\mathrm{A}})\,dS = \left[\int_0^b \mathfrak{D}_{\mathrm{A,\,mix}}\left(\frac{\partial C_{\mathrm{A}}}{\partial x}\right)_{x=a} dy\right] dz + \left[\int_0^a \mathfrak{D}_{\mathrm{A,\,mix}}\left(\frac{\partial C_{\mathrm{A}}}{\partial y}\right)_{y=b} dx\right] dz \tag{23-67}$$

Substitution in (23-67) via the radiation boundary conditions given by equations (23-66) yields

$$\int_S \mathfrak{D}_{\mathrm{A,\,mix}}(\mathbf{n}\cdot\nabla C_{\mathrm{A}})\,dS = -\left[\int_0^b k_{1,\,\mathrm{surface}}(y)C_{\mathrm{A}}(x=a,\,y,\,z)\,dy\right] dz - \left[\int_0^a k_{1,\,\mathrm{surface}}(x)C_{\mathrm{A}}(x,\,y=b,\,z)\,dx\right] dz \tag{23-68}$$

The final form of the quasi-macroscopic mass balance, which is applicable to a straight channel with rectangular cross section and first-order irreversible chemical reaction at high mass transfer Peclet numbers, is obtained by combining equations (23-65) and (23-68):

$$\langle v_z\rangle_{\mathrm{average}} S\left(-\frac{dC_{\mathrm{Abulk}}}{dz}\right) = \int_0^b k_{1,\,\mathrm{surface}}(y)C_{\mathrm{A}}(x=a,\,y,\,z)\,dy + \int_0^a k_{1,\mathrm{surface}}(x)C_{\mathrm{A}}(x,\,y=b,\,z)\,dx \tag{23-69}$$

where the flow cross section for one quadrant is $S = ab$. Equation (23-69) is written in dimensionless form as

$$-\frac{d\Psi_{\text{Abulk}}}{d\xi} = \Omega\frac{8\beta}{1+A_r}\left[\int_0^1 F(y^*)\Psi_{\text{A}}(x^*=1, y^*, \xi)\,dy^* + A_r\int_0^1 F(x^*)\Psi_{\text{A}}(x^*, y^*=1, \xi)\,dx^*\right] \tag{23-70}$$

where Ω approaches unity for self-consistency, and the dimensionless deposition profile $F(x^*)$ is the same function of x^* along the active surface at $y = b$ that $F(y^*)$ is in terms of y^* along the surface at $x = a$. Equation (23-70) must be satisfied at each axial position ξ (i.e., $\Omega \to 1$) when a finite-difference solution for $\Psi_{\text{A}}(x^*, y^*, \xi)$ is generated from the microscopic mass transfer equation given by (23-54). This quasi-macroscopic check of the validity of $\Psi_{\text{A}}(x^*, y^*, \xi)$ is tabulated in Table 23-4 for viscous flow in a square duct (i.e., $a = b$) with uniform catalyst activity (i.e., $F = 1$) when the Damkohler number $\beta = 1$ (see also Figure 23-2). Self-consistency (i.e., $\Omega \approx 99\%$) is achieved and maintained after two axial steps in the numerical algorithm. This implies that the finite-difference solution to the microscopic mass transfer equation also satisfies the quasi-macroscopic mass balance discussed in this section.

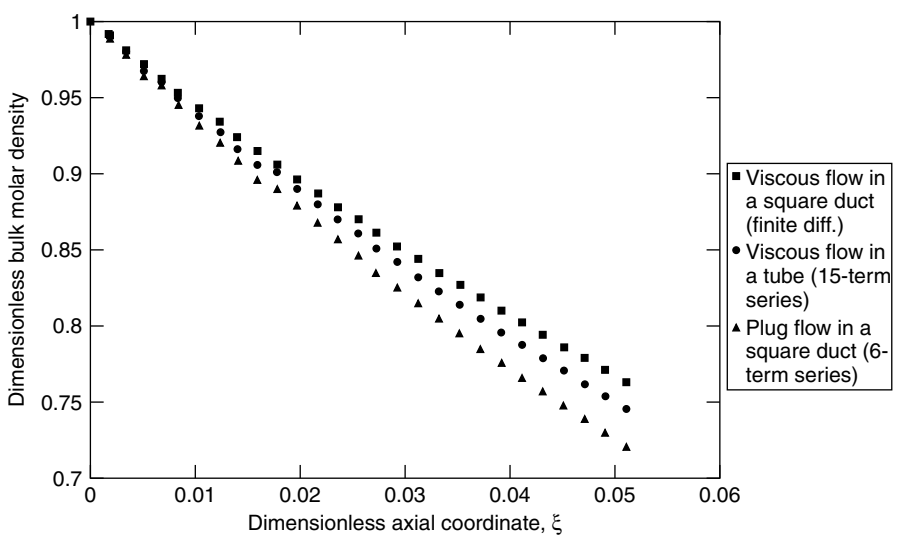

Figure 23-2 Dimensionless correlations between reactant molar density and channel length for viscous flow in square ducts, plug flow in square ducts, and viscous flow in tubes with the same effective diameter for first-order irreversible chemical kinetics and uniform catalyst activity when the Damkohler number is 1.

TABLE 23-4 Reactor Performance Comparisons[a]

Dimensionless Axial Coordinate, ξ	Ω	$\Psi_{A,\,bulk}(\xi)$ Viscous Flow in a Square Duct (finite diff.)	$\Psi_{A,\,bulk}(\xi)$ Plug Flow in a Square Duct (6-term series)	$\Psi_{A,\,bulk}(\xi)$ Viscous Flow in a Tube (15 terms)
1.27×10^{-5}	—	0.9999	—	—
0.0015	1.37	0.991	0.989	0.990
0.003	0.990	0.981	0.978	0.980
0.0047	0.988	0.972	0.964	0.967
0.0064	0.991	0.962	0.958	0.961
0.008	0.994	0.953	0.945	0.950
0.010	0.996	0.943	0.932	0.938
0.012	0.997	0.934	0.920	0.927
0.0137	0.999	0.924	0.908	0.916
0.0156	1.0002	0.915	0.896	0.906
0.0175	1.0008	0.906	0.890	0.901
0.0194	1.001	0.896	0.879	0.890
0.0214	1.0025	0.887	0.868	0.880
0.0233	1.003	0.878	0.857	0.870
0.0253	1.0035	0.870	0.846	0.861
0.027	1.0036	0.861	0.835	0.851
0.029	1.004	0.852	0.825	0.842
0.031	1.0046	0.844	0.815	0.832
0.033	1.005	0.835	0.805	0.823
0.035	1.005	0.827	0.795	0.814
0.037	1.0054	0.819	0.785	0.805
0.039	1.006	0.810	0.776	0.796
0.041	1.0055	0.802	0.766	0.788
0.043	1.006	0.794	0.757	0.779
0.045	1.006	0.786	0.748	0.771
0.047	1.006	0.779	0.739	0.762
0.049	1.0066	0.771	0.730	0.754
0.051	1.0064	0.763	0.721	0.746

[a] Same effective diameter for first-order irreversible chemical kinetics and uniform catalyst activity when the Damkohler number is 1. Validity of the microscopic finite-difference solution for $\Psi_A(x^*, y^*, \xi)$ in the quasi-macroscopic mass balance is also included (i.e., $\Omega \to 1$ for self-consistency).

23-6.2 Viscous Flow vs. Plug flow in Square Ducts

It seems reasonable that one should achieve larger conversion for plug flow, relative to viscous flow, in any type of heterogeneous reactor with catalyst coated on the inner walls. Simulations in Figure 23-2 and Table 23-4 verify this expectation in channels with square cross section, first-order irreversible chemical reaction, uniform catalyst activity, and $\beta = 1$. The corner regions are not problematic in plug-flow simulations because the momentum boundary

layer is nonexistent. Hence, there is sufficient convective transport in the primary flow direction to reduce the thickness of the mass transfer boundary layer and enhance the flux of reactants toward the catalytic surface. If duct reactor simulations are employed to determine the surface-averaged reaction velocity constant (i.e., $\langle k_{1,\text{surface}} \rangle_{\text{average}}$ embedded in the Damkohler number) via experimental measurements of bulk reactant molar density vs. channel length, then the assumption of plug flow leads to an underestimate of $\langle k_{1,\text{surface}} \rangle_{\text{average}}$. This is explained in more detail when effects of the Damkohler number on reactant conversion are understood.

23-6.3 Viscous Flow in Square Ducts and Tubes with the Same Effective Diameter

This comparison focuses on the corner regions in square ducts that are nonexistent in tubes. In both configurations, the momentum boundary layer thickness is substantial (i.e., $\approx d_{\text{effective}}/2$) for fully developed laminar flow. The no-slip boundary condition for viscous flow near the walls increases the mass transfer boundary layer thickness and reduces the flux of reactants toward the catalytic surface relative to plug flow. This effect is significant in the corner regions of the channel with square cross section. Since the entire active surface in heterogeneous tubular reactors is equally accessible to reactants, one predicts larger conversion in tubes via equation (23-71):

$$\Psi_{\text{Abulk}}(\xi;\beta) = \sum_{n=1}^{15} E_n(\beta) \exp[-2\lambda_n(\beta)\xi] \tag{23-71}$$

relative to square ducts (Sideman *et al.*, 1954; Davis and Parkinson, 1970). Simulations in Figure 23-2 and Table 23-4 verify this prediction for first-order irreversible chemical reaction, uniform catalyst activity, and $\beta = 1$. However, differences between C_{Abulk} vs. z for viscous flow in square ducts and tubes with the same $d_{\text{effective}}$ (i.e., third and fifth columns of Table 23-4) are smaller than those between viscous flow and plug flow in square ducts (i.e., third and fourth columns of Table 23-4).

Effect of the Damkohler Number on Conversion in Square Ducts. More conversion is predicted at higher Damkohler numbers because the rate of surface-catalyzed chemical reaction is larger. At a given axial position z, reactant conversion reaches an asymptotic limit in the diffusion-controlled regime, where $\beta \to \infty$. Actual simulations of Ψ_{Abulk} vs. ξ at $\beta = 20$ are almost indistinguishable from those when $\beta = 1000$. The effect of β on bulk reactant molar density is illustrated in Table 23-5 for viscous flow in a square duct at $\xi = 0.20$, first-order irreversible chemical reaction, and uniform catalyst deposition. These results in Table 23-5 for the parameter λ as a function of the Damkohler number β can be predicted via equations (23-80) and (23-81) when $\zeta = \lambda\xi$ and

TABLE 23-5 Effect of the Damkohler Number on Reactant Conversion for Viscous Flow in Square Ducts[a]

β	$[\Psi_{A,\,bulk}(\xi = 0.20; \beta)]_{viscous\ flow}$	λ
0.05	0.93	0.4 ($\xi \geq 0$)
0.5	0.54	3.0 ($\xi \geq 0$)
1	0.37	4.6 ($\xi \geq 0$)
3.33	0.17	8.4 ($\xi \geq 0.03$)
20	0.09	11.2 ($\xi \geq 0.03$)
1000	0.08	12.2 ($\xi \geq 0.03$)

[a]With first-order irreversible chemical kinetics and uniform catalyst activity. $\Psi_{A,\,bulk}(\xi; \beta, A_r) \approx \exp[-\lambda(\beta, A_r)\xi]$.

the asymptotic Nusselt number for mass transfer, Nu in (23-81), is approximately 3 for constant transverse diffusional flux at the catalytic surface.

If the results for plug flow in square ducts are included in Table 23-5, then

$$[\Psi_{Abulk}(\xi = 0.20; \beta)]_{plug\ flow} < [\Psi_{Abulk}(\xi = 0.20; \beta)]_{viscous\ flow} \tag{23-72}$$

As an example, if one measures $\Psi_{Abulk}(\xi = 0.20) = 0.37$, then obviously, $\beta_{viscous\ flow} = 1$ from Table 23-5 if simulations based on viscous flow are used to obtain agreement with experiment. On the other hand, the fact that

$$[\Psi_{Abulk}(\xi = 0.20; \beta = 1)]_{plug\ flow} < 0.37 \tag{23-73}$$

requires that

$$\beta_{plug\ flow} < \beta_{viscous\ flow} = 1 \tag{23-74}$$

if one seeks agreement with experiment based on plug-flow simulations. The inequality (23-74) reveals that

$$[\langle k_{1,surface}\rangle_{average}]_{plug\ flow} < [\langle k_{1,surface}\rangle_{average}]_{viscous\ flow} \tag{23-75}$$

Hence, surface-averaged reaction velocity constants, inferred from plug-flow simulations, are underestimated because convective diffusion in the mass transfer boundary layer adjacent to the catalytic surface is not modeled correctly.

23-6.4 Effect of Aspect Ratio on Conversion in Rectangular Ducts

Higher conversion of reactants is obtained in rectangular ducts when the aspect ratio is larger (see Table 23-6). However, for very small Damkohler numbers (i.e., $\beta \leq 5 \times 10^{-2}$), reactant conversion is independent of aspect ratio (i.e., $1 \leq A_r \leq 20$) because diffusion into the corner regions is not the rate-limiting step. For $\beta > 5 \times 10^{-2}$, the catalytically active walls at $x = \pm a$ become less significant, and the corner regions exert a weaker influence on the overall reactant $\rightarrow$ product conversion rate, when the aspect ratio is larger. These trends are verified by

TABLE 23-6 Effect of Aspect Ratio and Damkohler Number on Reactant Conversion for Viscous Flow in Rectangular Ducts[a]

Aspect Ratio, A_r	$\Psi_{A,\,bulk}(\xi = 0.30;\ \beta = 1)$	λ
1	0.24	4.6 ($\xi \geq 0$)
4	0.21	5.1 ($\xi \geq 0$)
8	0.18	5.4 ($\xi \geq 0$)
20	0.16	6.1 ($\xi \geq 0$)
"Viscous slot" (i.e., $A_r \to \infty$)	0.15	6.4 ($\xi \geq 0$)
Aspect Ratio, A_r	$\Psi_{A,\,bulk}(\xi = 0.10;\ \beta = 1000)$	λ
1	0.25	12.2 ($\xi \geq 0.02$)
4	0.14	18.1 ($\xi \geq 0.01$)
8	0.09	22.8 ($\xi \geq 0.01$)
20	0.06	26.8 ($\xi \geq 0.01$)
"Viscous slot" (i.e., $A_r \to \infty$)	0.05	30.0 ($\xi \geq 0.01$)

[a]With first-order irreversible chemical kinetics and uniform catalyst activity $\Psi_{Abulk}(\xi;\ \beta,\ A_r) \approx \exp[-\lambda(\beta,\ A_r)\xi]$.

TABLE 23-7 Effect of the Damkohler Number on the Aspect Ratio Required to Achieve the Same Reactant Conversion in Rectangular Channels and Tubes[a]

Damkohler Number β	Aspect Ratio Required for Similarity between Tubes and Rectangular Ducts
1000	2.3
20	2.5
3.3	3.5
1	5–6
0.5	8
0.05	>20

[a]With first-order irreversible chemical kinetics and uniform catalyst activity.

simulation in Table 23-6 for viscous flow in channels with rectangular cross section, first-order irreversible chemical reaction, and uniform catalyst deposition.

Smaller aspect ratios exert a stronger influence on reactant conversion when the Damkohler number is larger because the corner regions are critically important in the diffusion-controlled regime, where the rate of reactant consumption is governed by its rate of diffusion toward the active surface (see Table 23-6). When the Damkohler number is 10^3, viscous flow in tubes and rectangular ducts yields comparable graphs of Ψ_{Abulk} vs. ξ when the aspect ratio is ≈ 2.3. However, an

aspect ratio between 5 and 6 is required to produce comparable behavior in tubes and rectangular ducts when $\beta = 1$. In general, smaller aspect ratios are required to produce similarity between viscous flow in tubes and rectangular ducts when the Damkohler number is larger, as summarized in Table 23-7.

23-6.5 Aspect Ratio Required to Achieve Viscous Flow between Two Parallel Plates with a Narrow Gap

Rectangular duct simulations performed over the following range of Damkohler numbers for first-order irreversible chemical reaction:

$$5 \times 10^{-2} \leq \beta = \frac{\langle k_{1,\text{surface}} \rangle_{\text{average}} (d_{\text{effective}}/2)}{\mathfrak{D}_{\text{A, mix}}} \leq 10^{3} \tag{23-76}$$

reveal that an aspect ratio of approximately 100 is required to achieve viscous flow in a slot with catalyst deposited on both walls. Data in Table 23-6 indicate that the presence of four walls and, most important, corner regions, reduces reactant conversion relative to the viscous slot. Diffusion in the x direction, which scales as $1/a^2$, is $(1/A_r)^2$ as important as diffusion in the y direction, which scales as $1/b^2$. Hence, in the asymptotic limit of very large aspect ratio (i.e., $a \to \infty$), the three-dimensional mass transfer equation and its boundary conditions, given by (23-54), (23-55), and (23-56), are reduced to two dimensions for $\Psi_A(y^*, \xi)$ in the viscous slot because the walls at $x = \pm a$ are completely insignificant:

$$v_z^*(y^*) \frac{\partial \Psi_A}{\partial \xi} = 16 \frac{\partial^2 \Psi_A}{\partial y^{*2}} \tag{23-77}$$

$$-\frac{\partial \Psi_A}{\partial y^*} = \begin{cases} \dfrac{1}{2} \beta F(x^*) \Psi_A & \text{at } y^* = 1 \\ 0 & \text{at } y^* = 0 \end{cases} \tag{23-78}$$

In this case, the effective diameter is $4b$, or twice the spacing between the two plates, and the one-dimensional velocity profile for $v_z(y^*)$ is simplified greatly (Bird *et al.*, 2002, Prob. 2B.3, p. 63):

$$v_z^*(y^*) = \frac{3}{2}[1 - (y^*)^2] \tag{23-79}$$

Since the aspect ratio exhibits a weaker influence on reactant conversion when the Damkohler number is smaller, as summarized in Table 23-6, two-dimensional viscous slot simulations provide a better representation of Ψ_{Abulk} vs. ξ at large A_r and small β.

23-6.6 Universal Correlation for Rectangular Ducts with Uniform Catalyst Activity

For all previous examples in this chapter with first-order irreversible chemical kinetics and uniform catalyst activity, the bulk molar density of reactant A can be predicted via the following equation:

$$\Psi_{\text{Abulk}} \approx \exp(-\zeta) \tag{23-80}$$

TABLE 23-8 Effect of Aspect Ratio on the Parameters of a Universal Correlation between Conversion and Reactor Length[a]

A_r	α_1	α_2	α_3
1	2.976	0.054539	0.035116
1.5	3.1225	0.0551617	0.0353119
2	3.392	0.0592472	0.0370348
4	4.439	0.0699285	0.0414517
8	5.597	0.07629185	0.0434312
∞	7.541	0.0235	0.012711

[a]In heterogeneous catalytic rectangular ducts with first-order chemical kinetics and uniform catalyst activity.

where ζ is a transformed axial variable that depends on dimensionless axial variable ξ, Damkohler number β, and aspect ratio A_r (see Hatton and Quarmby, 1962):

$$\zeta(\xi; \beta, A_r) = \frac{8\beta\xi}{1 + \dfrac{2\beta}{\mathrm{Nu}(\xi; A_r)}} \tag{23-81}$$

$$\mathrm{Nu}(\xi; A_r) = \alpha_1(A_r) + \frac{\alpha_2(A_r)}{\xi + \alpha_3(A_r)\xi^m} \tag{23-82}$$

Equal increments in ζ correspond to approximately equal decrements in $\ln \Psi_{\mathrm{Abulk}}$. As illustrated in Table 23-8, α_1, α_2, and α_3 depend on the aspect ratio for rectangular channels. The asymptotic Nusselt number for mass transfer is given by α_1 for constant transverse diffusional flux at the catalytic wall. The exponent m in equation (23-82) is either $\frac{1}{2}$ for plug flow or $\frac{1}{3}$ for viscous flow.

23-6.7 Effect of Catalyst Deposition Profiles on Conversion in Rectangular Ducts

Twelve normalized shape functions presented in Table 23-2 are analyzed at two different Damkohler numbers (i.e., $\beta = 1, 10^3$) and five aspect ratios (i.e., $A_r = 1, 4, 8, 20, 100$). Each nonuniform catalyst activity profile is identified by number, as indicated in Table 23-9.

Simulations in the Diffusion-Limited Regime: $\beta = 10^3$. None of the profiles listed in Table 23-9 is more effective than uniform deposition at any aspect ratio when the Damkohler number $\beta = 10^3$. This is understandable in the diffusion-controlled regime where the rate of chemical reaction on the catalytic surface is not the primary factor that governs the conversion of reactants to products. However, some profiles perform poorly relative to uniform deposition when diffusion of reactants toward the active surface is slow. Differences among the profiles are more pronounced at higher aspect ratios. A qualitative summary at each aspect ratio is provided in Table 23-10. Identification numbers are underlined when

TABLE 23-9 Normalized Catalyst Deposition Profiles for Nonuniform Activity along the Wall of a Rectangular Channel

Identification Number	Catalyst Deposition Profile, $F(y^*)$
1	$(\pi/2)\cos(y^*\pi/2)$
2	$1 + \cos(\pi y^*)$
3	$(\pi/2)\cos[(1 - y^*)\pi/2]$
4	1
5	$2(1 - y^*)$
6	$(3/2)[1 - (y^*)^2]$
7	$(5/4)[1 - (y^*)^4]$
8	$(9/8)[1 - (y^*)^8]$
9	$2y^*$
10	$3(y^*)^2$
11	$5(y^*)^4$
12	$9(y^*)^8$

TABLE 23-10 Comparison of Catalyst Deposition Profiles[a]

$A_r = 100$, $\beta = 10^3$, $0 \le \xi \le 0.20$

Optimum and indistinguishable deposition profiles:
1, 4, 5, 6, 7, 8

Remaining deposition profiles in order of decreasing effectiveness:
$2 >> \underline{3}$ and $\underline{9} > \underline{10} \ggg \underline{11} >> \underline{12}$

$A_r = 20$, $\beta = 10^3$, $0 \le \xi \le 0.20$

Optimum and indistinguishable deposition profiles:
$1, 4, 5, 6, 7, 8 \ge 2$

Remaining deposition profiles in order of decreasing effectiveness:
$2 > 3$ and $9 > \underline{10} \ggg \underline{11} >> \underline{12}$

$A_r = 4$ and 8, $\beta = 10^3$, $0 \le \xi \le 0.24$

Optimum and indistinguishable deposition profiles:
1, 2, 4, 5, 6, 7, 8

Remaining deposition profiles in order of decreasing effectiveness:
3 and $9 > 10 >> \underline{11} >> \underline{12}$

$A_r = 1$, $\beta = 10^3$, $0 \le \xi \le 0.24$

Optimum and indistinguishable deposition profiles:
$1, 2, 4, 5, 6, 7, 8 \ge 3$ and 9

Remaining deposition profiles in order of decreasing effectiveness:
3 and $9 > 10 > 11 > 12$

[a]Based on their ability to convert reactants to products via first-order irreversible chemical kinetics, in rectangular channels with various aspect ratios at large Damkohler numbers (i.e., $\beta = 1000$) in the diffusion-limited regime. Reactant molar density vs. channel length follows a single exponential decay for those deposition profiles that are not underlined.

TABLE 23-11 Comparison of Catalyst Deposition Profiles[a]

$A_r = 100$, $\beta = 1$, $0 \le \xi \le 0.80$
Deposition profiles in order of decreasing effectiveness:
$4 > 8 > \underline{7} > \underline{6} > \underline{1} > \underline{5} > \underline{3} > \underline{9} > \underline{2} > \underline{10} > \underline{11} > \underline{12}$
$A_r = 20$, $\beta = 1$, $0 \le \xi \le 0.80$
Deposition profiles in order of decreasing effectiveness:
$8 > 4 > 7 > \underline{6} > \underline{1} > \underline{5} > \underline{3} > \underline{2} > \underline{9} > \underline{10} > \underline{11} > \underline{12}$
$A_r = 8$, $\beta = 1$, $0 \le \xi \le 0.80$
Deposition profiles in order of decreasing effectiveness:
$7 > 8 > 6 > 1 > 4 > 5 > 2 > \underline{3} > \underline{9} > \underline{10} > \underline{11} > \underline{12}$
$A_r = 4$, $\beta = 1$, $0 \le \xi \le 0.80$
Deposition profiles in order of decreasing effectiveness:
$1 = 6 > 5 = 7 > 8 \ge 2 > 4 > 3 > 9 > 10 > 11 > 12$
$A_r = 1$, $\beta = 1$, $0 \le \xi \le 0.80$
Optimum and indistinguishable deposition profiles:
$1, 5, 6, 7 \ge 8 \ge 2$
Remaining deposition profiles in order of decreasing effectiveness:
$8 \ge 2 > 4 > 3 > 9 > 10 > 11 > 12$

[a]Based on their ability to convert reactants to products via first-order irreversible chemical kinetics, in rectangular channels with various aspect ratios when the Damkohler number is 1. Reactant molar density vs. channel length follows a single exponential decay for those deposition profiles that are not underlined.

$\ln \Psi_{\text{Abulk}}$ vs. ξ deviates considerably from linearity (i.e., a single exponential decay is not sufficient to describe the numerical results). Hence, profiles that are not underlined can be modeled as follows:

$$\Psi_{\text{Abulk}}(\xi; \beta, A_r, \text{deposition}) \approx \exp[-\lambda(\beta, A_r, \text{deposition})\xi] \tag{23-83}$$

Simulations When $\beta = 1$. Now, the rate of reactant diffusion toward the wall is comparable to the rate of reactant consumption via surface-catalyzed chemical reaction. Hence, some of the profiles should be more effective than uniform deposition. This prediction is verified by simulation, but not at the largest aspect ratio (i.e., $A_r = 100$). The effectiveness of nonuniform deposition is more pronounced when the corner regions exert a stronger influence on reactant conversion at smaller aspect ratio. A qualitative summary at each aspect ratio is provided in Table 23-11.

PROBLEMS

23-1. **(a)** At axial positions $\xi = (1/\text{Pe}_{\text{MT}})z/d_{\text{effective}}$ that are far from the inlet to a duct reactor with square cross section, uniform catalyst activity, and catalyst coated on the inner walls of the flow channel, write

a reasonable expression for the dimensionless bulk molar density of reactant A, Ψ_{Abulk}, as a function of the dimensionless axial coordinate ξ. Include some important dimensionless numbers in your final answer. No derivations are required to solve this problem.

(b) Indicate how your answer to part (a) can distinguish between reactor performances for reaction- and diffusion-rate-limited cases.

23-2. Sketch duct reactor performance curves in terms of $\Psi_{\text{Abulk}}(\xi)$ when the flow cross section is rectangular for normalized catalyst activity "shape" profiles given by the following functions: (**a**) $(\pi/2)\cos(0.5\pi y^*)$, and (**b**) $5(y^*)^4$, where y^* is a dimensionless independent variable transverse to the flow direction that assumes a value of zero at the centerline and unity at the wall in the corner region. In both cases, the aspect ratio, Damkohler number, and mass transfer Peclet number are the same. Both graphs should be constructed on the same set of axes.

23-3. Consider the governing equations that describe convection, diffusion, and chemical reaction in tube-wall duct reactors where expensive metal catalyst is coated on the inner walls of the flow channel.

(a) What important dimensionless number(s) appear in the mass balance given by equation (23-14)? Write these dimensionless numbers in terms of characteristic quantities and physical properties of the reactive gas mixture. Be sure to define the appropriate diffusion coefficient, if one appears in the dimensionless numbers.

(b) What important dimensionless number(s) appear in the boundary conditions given by equation (23-15)? Write these dimensionless numbers in terms of characteristic quantities and physical properties of the reactive gas mixture. Be sure to define the appropriate diffusion coefficient, if one appears in the dimensionless numbers.

23-4. The objective of this problem is to choose the best configuration for analysis of true surface-catalyzed kinetic rate data using a miniature laboratory-scale reactor. After data are obtained, linear least-squares analysis of the reaction rate at zero conversion will be performed to calculate the kinetic rate constant, $\langle k_{n,\text{surface}} \rangle_{\text{average}}$, and the adsorption/desorption equilibrium constants. Use numbers from 1 to 8 and identify the best reactor configuration as 1 and the worst configuration as 8. Be sure to use a different number to rank all of the configurations below in terms of their ability to produce true kinetic data. Remember that diffusional heterogeneities in forced-flow channels and diffusional limitations within the pores of catalytic pellets usually result in the measurement of apparent kinetics of surface-catalyzed reactions which differ drastically from the true kinetics.

(a) A packed catalytic tubular reactor with spherically shaped catalysts that are 5 mm in diameter — the intrapellet tortuosity factor is $\tau_{\text{or}} = 4$, and the intrapellet porosity is 50%.

(b) A viscous-flow tube-wall reactor with triangular cross section where the catalyst is coated on the inner walls of the flow channel.

(c) A viscous-flow tube-wall reactor with circular cross section where the catalyst is coated on the inner walls of the flow channel.

(d) A viscous-flow tube-wall reactor with hexagonal cross section where the catalyst is coated on the inner walls of the flow channel.

(e) A viscous-flow tube-wall reactor with square cross section (the aspect ratio $= 1$) where the catalyst is coated on the inner walls of the flow channel.

(f) A packed catalytic tubular reactor with spherically shaped catalysts that are 10 mm in diameter — the intrapellet tortuosity factor is $\tau_{or} = 4$, and the intrapellet porosity is 50%.

(g) A tube-wall reactor with rectangular cross section (the aspect ratio $=$ 20) where the catalyst is coated on the inner walls of the flow channel — the mass flow rate is large enough that the plug-flow assumption is valid.

(h) A packed catalytic tubular reactor with spherically shaped catalysts that are 10 mm in diameter — the intrapellet tortuosity factor is $\tau_{or} = 2$, and the intrapellet porosity is 50%.

23-5. *True or False:* An endothermic heterogeneous catalytic reaction, which converts reactants to products irreversibly, occurs on the inner wall of a well-insulated tube. At any particular axial position within the tubular reactor, the maximum temperature exists at the centerline of the tube.

23-6. Consider a straight tube of radius R with circular cross section and expensive metal catalyst coated in the inner wall. Reactant A is converted to products via first-order irreversible chemical reaction on the catalytic surface at $r = R$. Hence, diffusion of reactant A in the radial direction, toward the catalytic surface, is balanced by the rate of consumption of A due to heterogeneous chemical reaction. The boundary condition at the mathematically well-defined catalytic surface (i.e., $r = R$) is

$$-\mathfrak{D}_{A,\,\text{ordinary}} \left(\frac{\partial C_A}{\partial r} \right)_{r=R} = k_{1,\,\text{surface}} C_{A,\,\text{surface}}$$

where $k_{1,\,\text{surface}}$ is a reaction velocity constant with units of length per time. The surface molar density of reactant A in the kinetic rate law is given by $C_A(r = R, z)$, which depends on axial position z within the tube. However, $C_{A,\,\text{surface}}$ is independent of angular variable θ because there are no problematic corner regions. In other words, all points on the catalytic surface are equally accessible to reactants. Begin with the quasi-macroscopic plug-flow mass balance in a straight channel with rectangular cross section,

variable catalyst activity, and first-order irreversible chemical reaction at high-mass-transfer Peclet numbers, as given by equation (23-69):

$$\langle v_z \rangle_{\text{average}} S \left\{ -\frac{dC_{\text{Abulk}}}{dz} \right\} = \int_0^b k_{1,\,\text{surface}}(y) C_{\text{A}}(x = a, y, z)\, dy + \int_0^a k_{1,\,\text{surface}}(x) C_{\text{A}}(x, y = b, z)\, dx$$

and modify this expression for tubular reactors with uniform catalyst activity.
Answer: The left side of the quasi-macroscopic mass balance, as written above, is the same for all types of catalytic channels with the appropriate description of the flow cross section S. For tubular reactors with radius R, S is given by πR^2. Upon integrating the right side of the preceding equation around the catalytically active perimeter, where the reaction velocity constant and the surface molar density of reactant A are independent of angular coordinate θ, one obtains

$$\langle v_z \rangle_{\text{average}} \pi R^2 \left(-\frac{dC_{\text{Abulk}}}{dz} \right) = k_{1,\,\text{surface}} C_{\text{A, surface}} (2\pi R)$$

If integration is performed along the catalytically active perimeter in one quadrant only (i.e., the xy plane where both x and y are positive), then the complete circumference of the tube on the right side of the preceding equation is replaced by $\pi R/2$, and $S = \pi R^2/4$. However, the final result is unchanged. See Problem 30-7 for a continuation of this analysis and a solution of the quasi-macroscopic plug-flow mass balance in the presence of significant external mass transfer resistence.

23-7. In this problem, we explore boundary layer mass transfer analysis of convective diffusion in heterogeneous catalytic tube-wall reactors, in particular, the asymptotically exact boundary layer solution in the inlet region. An incompressible Newtonian fluid that contains reactant A undergoes steady-state laminar flow through a heterogeneous catalytic reactor with circular cross section. The inner wall of the reactor at radius $r = R$ is coated with expensive metal catalyst. Reactant A is transported by concentration (i.e., Fickian) diffusion toward the wall, where it is depleted by a first-order irreversible heterogeneous chemical reaction on the catalytic surface, which is not porous. This mass transfer–chemical reaction problem is solved numerically via finite-difference methods. However, for reasons that are unique to the numerical method employed, the condition at the reactor inlet, $C_{\text{A}} = C_{\text{A0}}$ at $z = 0$ for all $r < R$, is not used as the initial condition to generate the reactant concentration profile. Instead, boundary layer formalism is implemented to calculate $C_{\text{A}}(r, z_S)$ at some small axial position z_S within the reactor. Hence, the initial reactant concentration profile at $z = z_S$ contains a radial gradient in the starting solution which feeds the catalytic reaction at the tube wall. The numerical approach begins at this small value of z_S for which the boundary layer

solution is valid and proceeds to calculate the reactant concentration profile throughout the reactor. Remember that no reaction occurs within the bulk homogeneous fluid that passes through this tube-wall reactor.

Step 1. Write the mass transfer equation for this problem using vector notation. The physicochemical processes occur at steady state and the physical properties of the fluid (i.e., ρ and $\mathfrak{D}_A$) are constant.

$$\mathbf{v} \cdot \nabla C_A = \mathfrak{D}_A \nabla^2 C_A$$

Step 2. Now, write the mass transfer equation in the appropriate coordinate system [see equation B for cylindrical symmetry in Table 18.2.2 in Bird *et al*. (1960, p. 559).]

Step 3. Invoke the following assumptions and simplify the mass transfer equation:

(a) The mixture flows through the same tube without catalyst coated on the inner surface at $r = R$ prior to entering the reactor. Hence, the axial velocity profile has sufficient opportunity to become fully developed in the presence of an inactive wall.

(b) There is no swirling motion.

(c) There is no convective transport of species A toward the wall.

(d) The reactant concentration profile is angularly symmetric:

$$v_z(r)\frac{\partial C_A}{\partial z} = \mathfrak{D}_A\left[\frac{1}{r}\frac{\partial}{\partial r}\left(r\frac{\partial C_A}{\partial r}\right) + \frac{\partial^2 C_A}{\partial z^2}\right]$$

Step 4. Use an order-of-magnitude analysis to estimate the following ratios:

(a) Axial diffusion with respect to axial convection.

(b) Axial diffusion with respect to radial diffusion.

(c) Radial diffusion with respect to axial convection.

The reactor length L is the characteristic dimension in the axial direction and the tube diameter $2R$ is the characteristic radial dimension. Express your answers in terms of dimensionless numbers and parameters.

Step 5. Use your results from step 4 together with the following assumptions: the mass transfer Peclet number is large, and the tube diameter is much smaller than the overall length of the reactor; to simplify the mass transfer equation.

$$v_z(r)\frac{\partial C_A}{\partial z} = \mathfrak{D}_A\frac{1}{r}\frac{\partial}{\partial r}\left(r\frac{\partial C_A}{\partial r}\right)$$

Step 6. Simplify the radial diffusion term if the Schmidt number is large.

$$\mathfrak{D}_A \frac{1}{r}\frac{\partial}{\partial r}\left(r\frac{\partial C_A}{\partial r}\right) = \mathfrak{D}_A \frac{\partial^2 C_A}{\partial r^2}\left\{1 + \underline{\left[\frac{\partial \ln(\partial C_A/\partial r)}{\partial \ln r}\right]^{-1}}\right\}$$

The underlined term in the preceding equation is negligible when mass transfer boundary layers adjacent to the catalytic surface are very thin at large Schmidt numbers. The locally flat approximation is valid when Sc asymptotically approaches infinity.

Step 7. Write the fully developed axial velocity profile for this flow problem:

$$v_z(r) = 2\langle v_z\rangle\left[1 - \left(\frac{r}{R}\right)^2\right]$$

Step 8. Rewrite the mass transfer equation and the fully developed axial velocity profile in terms of a new radial variable, $s = R - r$, which measures distance from the catalytic surface at $r = R$.

$$v_z(s)\frac{\partial C_A}{\partial z} = \mathfrak{D}_A \frac{\partial^2 C_A}{\partial s^2}$$

$$v_z(s) = 2\langle v_z\rangle\left[2\left(\frac{s}{R}\right) - \left(\frac{s}{R}\right)^2\right]$$

Step 9. Linearize the axial velocity profile within a thin mass transfer boundary layer adjacent to the catalytic surface and incorporate this information in the mass transfer equation for the reactant concentration profile $C_A(s, z)$.

$$v_z(s) \approx 4\langle v_z\rangle\frac{s}{R}$$

$$v_z(s)\frac{\partial C_A}{\partial z} = \mathfrak{D}_A \frac{\partial^2 C_A}{\partial s^2}$$

Step 10. Rewrite the mass transfer equation in terms of the diffusional molar flux of A away from the catalytic surface (i.e., in the s direction). In other words,

$$J_{As} = -\mathfrak{D}_A \frac{\partial C_A}{\partial s}$$

To achieve the desired result, you must perform the following steps in sequential order:

(a) Divide the mass transfer equation from step 9 by s.

(b) Remember that $\mathfrak{D}_A$ is constant and identify J_{As} in the diffusion term.

(c) Differentiate the mass transfer equation with respect to s, remembering that the molar density of reactant A is an exact differential.

Now, the mass transfer equation should appear in the following form:

$$\frac{4\langle v_z\rangle}{R\mathcal{D}_{\mathrm{A}}}\frac{\partial J_{\mathrm{A}s}}{\partial z} = \frac{\partial}{\partial s}\left(\frac{1}{s}\frac{\partial J_{\mathrm{A}s}}{\partial s}\right)$$

Step 11. Write all the boundary conditions that are required to solve this boundary layer problem. It is important to remember that the rate of reactant transport by concentration diffusion toward the catalytic surface is balanced by the rate of disappearance of A via first-order irreversible chemical kinetics (i.e., $k_s C_{\mathrm{A}}$), where k_s is the reaction velocity constant for the heterogeneous surface-catalyzed reaction. At very small distances from the inlet, the concentration of A is not very different from C_{A0} at $z = 0$. If the mass transfer equation were written in terms of C_{A}, then the solution is trivial if the boundary conditions state that the molar density of reactant A is C_{A0} at the inlet, the wall, and far from the wall if z is not too large. However, when the mass transfer equation is written in terms of $J_{\mathrm{A}s}$, the boundary condition at the catalytic surface can be characterized by constant flux at $s = 0$ instead of, simply, constant composition. Furthermore, the constant flux boundary condition at the catalytic surface for small z is different from the values of $J_{\mathrm{A}s}$ at the reactor inlet, and far from the wall. Hence, it is advantageous to rewrite the mass transfer equation in terms of diffusional flux away from the catalytic surface, $J_{\mathrm{A}s}$.

Step 12. Express the mass transfer equation and its boundary conditions in dimensionless form using the following variables:

$$\text{Diffusional molar flux: } \Phi_{\mathrm{A}} \equiv -\frac{J_{\mathrm{A}s}}{k_s C_{\mathrm{A0}}}$$

$$\text{Radial position: } \eta \equiv \frac{s}{R}$$

$$\text{Axial position: } \zeta \equiv \frac{1}{\mathrm{Pe}_{\mathrm{MT}}}\frac{z}{R}$$

where $\mathrm{Pe}_{\mathrm{MT}}$ is the mass transfer Peclet number based on the diameter of the tube.

$$2\frac{\partial \Phi_{\mathrm{A}}}{\partial \zeta} = \frac{\partial}{\partial \eta}\left(\frac{1}{\eta}\frac{\partial \Phi_{\mathrm{A}}}{\partial \eta}\right)$$

where

$$\Phi_{\mathrm{A}} = \begin{cases} 0 & \text{at } \zeta = 0 \text{ and } \eta > 0 \\ 1 & \text{at } \eta = 0 \text{ and } \zeta > 0 \end{cases}$$

$\Phi_{\mathrm{A}} = 0$ at $\eta \to \infty$ and finite ζ (i.e., this is the boundary layer boundary condition).

Step 13. Combine variables as follows:

$$\chi = \frac{\eta}{\delta_{\text{MTBLT}}(\zeta)}$$

and calculate the dimensionless mass transfer boundary layer thickness, $\delta_{\text{MTBLT}}(\zeta)$.

$$\delta_{\text{MTBLT}}(\zeta) = \left(\frac{9\zeta}{2}\right)^{1/3}$$

Step 14. Determine the exponents α, γ, and ε in the following scaling law for the dimensionless mass transfer boundary layer thickness:

$$\log \delta_{\text{MTBLT}} \approx \alpha \log \mathfrak{D}_{\text{A}} + \gamma \log z + \varepsilon \log\langle v_z \rangle$$

Step 15. Let $g(\chi) = (1/\chi)\, d\Phi_{\text{A}}/d\chi$ and calculate the dimensionless molar flux of reactant A, Φ_{A}. Recall that

$$\int_0^\infty t \exp(-t^3)\, dt = \frac{1}{3}\Gamma\left(\frac{2}{3}\right)$$

which can be obtained from equation (11-70) when integration variable $z = t^3$ and $n = 2/3$. The final answer for the dimensionless molar flux of reactant A is

$$\Phi_{\text{A}}(\chi) = -\frac{J_{\text{A}s}(s, z)}{k_s C_{\text{A}0}} = \frac{3}{\Gamma\left(\frac{2}{3}\right)} \int_\chi^\infty t \exp(-t^3)\, dt$$

Step 16. Calculate the dimensionless concentration profile of reactant A, which is defined as follows:

$$W(\chi) = \frac{C_{\text{A}0} - C_{\text{A}}(s, z)}{k_s C_{\text{A}0} R/\mathfrak{D}_{\text{A}}}$$

where $C_{\text{A}0}$ is the molar density of reactant A outside the mass transfer boundary layer (i.e., $\chi \to \infty$). You should arrive at a double integral expression for $W(\chi)$, where integration variable t varies from χ' to ∞, and integration variable χ' ranges from χ to ∞. This expression for $W(x)$ can be evaluated partially by reversing the order of integration, such that χ' varies from χ to t, and t varies from χ to ∞. The final answer for the dimensionless concentration profile of reactant A is

$$W(\chi) = \frac{3\delta_{\text{MTBLT}}(\zeta)}{\Gamma(\frac{2}{3})} \left[\frac{\exp(-\chi^3)}{3} - \chi \int_\chi^\infty t \exp(-t^3)\, dt\right]$$

which is extremely similar to the heat transfer solution of problem 12D.7 in Bird *et al*. (2002, p. 406).

Step 17. If the local diffusional molar flux of reactant A (a) toward the catalytic surface, and (b) evaluated at the surface, is used to define the following local mass transfer coefficient, $k_{c,\text{local}}(z)$:

$$\begin{aligned} J_{\text{A}r}(r = R) &= -J_{\text{A}s}(s = 0) \\ &= k_s C_{\text{A}0} \equiv k_{c,\text{local}}(z)[C_{\text{A}0} - C_{\text{A}}(r = R, z)] \end{aligned}$$

then calculate the local Sherwood number in terms of the dimensionless concentration profile of reactant A, $W(\chi)$. The tube diameter represents the characteristic length in the definition of the Sherwood number:

$$\text{Sh}_{\text{local}}(z) = \frac{k_{c,\text{local}}(z)2R}{\mathfrak{D}_{\text{A}}} = \frac{2}{W(\chi = 0)} = \frac{2\Gamma(\frac{2}{3})}{\delta_{\text{MTBLT}}(\zeta)}$$

Step 18. Determine the exponents a, b, and c in the following scaling law for the local Sherwood number:

$$\log \text{Sh}_{\text{local}} = a \log \text{Re} + b \log \text{Sc} + c \log z + \text{constant}$$

Transport Phenomena for Chemical Reactor Design. Laurence A. Belfiore
Copyright © 2003 John Wiley & Sons, Inc.
ISBN: 0-471-20275-4

24

DESIGNING A MULTICOMPONENT ISOTHERMAL GAS–LIQUID CSTR FOR THE CHLORINATION OF BENZENE TO PRODUCE MONOCHLOROBENZENE

Design a two-phase gas–liquid CSTR that operates at 55°C to accomplish the liquid-phase chlorination of benzene. Benzene enters as a liquid, possibly diluted by an inert solvent, and chlorine gas is bubbled through the liquid mixture. It is only necessary to consider the first chlorination reaction because the kinetic rate constant for the second reaction is a factor of 8 smaller than the kinetic rate constant for the first reaction at 55°C. Furthermore, the kinetic rate constant for the third reaction is a factor of 243 smaller than the kinetic rate constant for the first reaction at 55°C. The extents of reaction for the second and third chlorination steps (ξ_2 and ξ_3) are much smaller than the value of ξ_1 for any simulation (i.e., see Section 1-2.2). Chlorine gas must diffuse across the gas–liquid interface before the reaction can occur. The total gas-phase volume within the CSTR depends directly on the inlet flow rate ratio of gaseous chlorine to liquid benzene, and the impeller speed–gas sparger combination produces gas bubbles that are 2 mm in diameter. Hence, interphase mass transfer must be considered via mass transfer coefficients. The chemical reaction occurs predominantly in the liquid phase. In this respect, it is necessary to introduce a chemical reaction enhancement factor to correct liquid-phase mass transfer coefficients, as given by equation (13-18). This is accomplished via the dimensionless correlation for one-dimensional diffusion and pseudo-first-order irreversible chemical reaction:

$$\text{Sherwood number} = \frac{\Lambda}{\tanh \Lambda} \tag{24-1}$$

where Λ is the square root of the Damkohler number, which provides an order-of-magnitude estimate of the rate of chemical reaction relative to the rate of interphase mass transfer via diffusion.

Use a molecular mechanics program to generate energy-minimized structures and estimate the hydrodynamic radii of benzene and monochlorobenzene. For diatomic molecules, covalent and van der Waals radii are useful to calculate molecular size. From a molecular mechanics viewpoint, space-filling molecular models illustrate the van der Waals radius of each atom in the molecule. Use these hydrodynamic radii to calculate liquid-phase diffusion coefficients via the Stokes–Einstein equation.

Account for the realistic fact that benzene enters the reactor in an undiluted liquid stream, whereas chlorine is actually bubbled through as a gas. Include versatility to dilute the liquid feed stream, if desired. The molar density of pure liquid benzene is $C_{B,\,inlet} = 11.28$ g-mol/L and the kinetic rate constant for the first chlorination reaction is

$$k_r(55^\circ\text{C}) = 8.84 \times 10^{-3}\ \text{L/g-mol·s}$$

The inlet molar flow rate of chlorine gas is κ times the inlet molar flow rate of liquid benzene, and $\kappa = 2$ is a parameter that remains constant for each simulation. The overall objective of this problem is to design a two-phase CSTR that will maximize the rate of production of monochlorobenzene. Economics should be considered from a qualitative viewpoint. Generate graphs of:

1. The total rate of production of the desired product, monochlorobenzene, in both exit streams (i.e., gas and liquid) relative to the inlet molar flow rate of liquid benzene vs. $\log(\tau/\lambda)$
2. The fraction of the desired product C_6H_5Cl that exits as a liquid vs. $\log(\tau/\lambda)$

where τ is the time constant for convective mass transfer in the liquid phase and λ is the time constant for the second-order irreversible chemical reaction in the liquid phase. Identify your operating point on the graph. If too much chlorobenzene exits the CSTR as a gas, then it is necessary to perform a costly liquefaction to recover this desired product as a liquid. Finally, design the CSTR by calculating the volume associated with your operating point if the liquid-phase volumetric flow rate is 10 gal/min. Remember that the CSTR contains dispersed gas bubbles in a continuous liquid phase when you calculate the total volume of the reactor required to perform the task described above.

24-1 STRATEGY TO SOLVE THIS PROBLEM

24-1.1 Practical Considerations

Litz (1985) published an article in *Chemical Engineering Progress* entitled, "A novel gas–liquid stirred tank reactor," from which some key introductory statements are quoted here to emphasize the fact that (1) the liquid-phase reaction is more important than reaction in the gas phase and (2) interphase mass transfer is extremely important. "In most gas–liquid reaction systems, the bulk of the reaction occurs between the liquid, or species dissolved in the liquid phase, and

dissolved gas molecules. However, gases often have very low solubility in liquids. The reactor design strategy must address the question of maximizing the rate of transfer of the gas into the liquid to replace dissolved gas as it is consumed by the reaction."

24-1.2 Parameters and Variables

The homogeneous irreversible chemical reaction that occurs predominantly in the liquid phase of the CSTR is

$$C_6H_6(B) + Cl_2(Cl) \rightarrow C_6H_5Cl(M) + HCl(H) \tag{24-2}$$

where the letters in parentheses are used to denote each component in either phase. The liquid-phase kinetics are second-order and the homogeneous volumetric rate law is written in terms of the molar densities of benzene and dissolved chlorine:

$$\mathfrak{R} = k_r C_B C_{Cl} \tag{24-3}$$

where k_r has units that are appropriate for a second-order volumetric rate law based on molar densities. Several variables and parameters are defined below. The units of each of these quantities are given in the cgs system. The parameters are:

q = total volumetric flow rate of the liquid phase (mL/s)

$C_{B,\,inlet}$ = inlet molar density of liquid benzene (g mol/mL)

$(N_B)^0 = qC_{B,\,inlet}$ = inlet molar flow rate of liquid benzene (g-mol/s)

$(N_{Cl})^0$ = inlet molar flow rate of gaseous chlorine, dispersed as bubbles (g-mol/s)

V_L = total liquid-phase volume within the CSTR (mL)

V_g = total gas-phase volume within the CSTR (mL)

d_{gas} = diameter of gas bubbles rising through the liquid in the CSTR (cm)

a_L = interfacial area for mass transfer per unit volume of the liquid phase (cm^{-1})

k_r = second-order kinetic rate constant for the liquid-phase reaction (mL/g-mol·s)

There are a total of 17 variables that describe the performance of this two-phase CSTR. If the condition of perfect backmixing is achieved, then these unknowns in the outlet liquid and gas streams are the same as the corresponding variables

within the reactor. The variables are as follows (components are denoted by subscript j, interfacial properties are denoted by subscript i):

y_j = bulk gas-phase mole fraction of component j
(j = B,Cl,M,H; 4 unknowns)

y_{ji} = gas-phase mole fraction of component j at the gas–liquid interface
(j = B,Cl,M,H; 4 unknowns)

N_{gas} = total outlet molar flow rate of the exiting gas stream
(g-mol/s; 1 unknown)

C_j = outlet liquid-phase molar density of component j
(j = B,Cl,M,H; g-mol/mL; 4 unknowns)

C_{ji} = liquid-phase molar density of component j at the gas–liquid interface
(j = B,Cl,M,H; g-mol/mL; 4 unknowns)

The next task is to generate 17 equations that relate the 17 unknowns defined above. If this can be done, then the performance of the two-phase CSTR is unique to each set of parameters. Furthermore, if one solves the system of equations described below for a wide range of liquid-phase residence times, then CSTR performance curves can be generated for the outlet flow rate of monochlorobenzene, which is the desired product. For clarity, the 17 coupled algebraic equation are numbered below.

24-2 GAS-PHASE MASS BALANCES WITH INTERPHASE MASS TRANSFER

A gas-phase mass balance can be written for each component because all four components are volatile and exist in both phases. In each case, the control volume contains all gas bubbles in the CSTR. The units of each term in all of the gas-phase mass balances are moles per time. At steady state, the inlet molar flow rate of component j is balanced by the outlet molar flow rate and the rate at which component j leaves the gas phase via interphase mass transfer. The inlet and outlet molar flow rates represent convective mass transfer. Interphase transport is typically dominated by diffusion, but convection can also contribute to the molar flux of component j perpendicular to the gas–liquid interface. All of the gas-phase mass balances can be written generically as

$$(N_j)^0\delta_{j\text{Cl}} = y_j N_{\text{gas}} + k_{j,\,\text{gas}}(y_j - y_{ji})a_L V_L \qquad (1) \rightarrow (4) \qquad (24\text{-}4)$$

where $\delta_{j\text{Cl}}$ is the Kronecker delta, which equals 1 when $j = \text{Cl}$ and 0 otherwise because chlorine is the only component that enters the reactor via the inlet gas stream. The total volume of the continuous liquid phase appears in

these gas-phase balances because the interfacial surface area for mass transfer is defined per unit volume of the liquid phase.

Now, it is necessary to discuss the mass transfer coefficient for component j in the boundary layer on the vapor side of the gas–liquid interface, $k_{j,\,\mathrm{gas}}$, with units of mol/(area·time). The final expression for $k_{j,\,\mathrm{gas}}$ is based on results from the steady-state film theory of interphase mass transfer across a flat interface. The only mass transfer mechanism accounted for in this extremely simple derivation is one-dimensional diffusion perpendicular to the gas–liquid interface. There is essentially no chemical reaction in the gas-phase boundary layer, and convection normal to the interface is neglected. This problem corresponds to a Sherwood number (i.e., Sh) of 1 or 2, depending on characteristic length scale that is used to define Sh. Remember that the Sherwood number is a dimensionless mass transfer coefficient for interphase transport. In other words, Sh is a ratio of the actual mass transfer coefficient divided by the simplest mass transfer coefficient when the only important mass transfer mechanism is one-dimensional diffusion normal to the interface. For each component j in the gas mixture,

$$k_{j,\,\mathrm{gas}} = \frac{c\mathfrak{D}_{j,\,\mathrm{gas\ mix.}}}{\mathrm{MTBLT}_{\mathrm{gas}}} \tag{24-5}$$

where $c(T, p)$ is the total molar density of the gas, $\mathfrak{D}_{j,\,\mathrm{gas\ mix}}$ the molecular diffusion coefficient of component j in the gas mixture, and $\mathrm{MTBLT}_{\mathrm{gas}}$ represents the mass transfer boundary layer thickness on the vapor side of the gas–liquid interface that is difficult, if not impossible, to measure experimentally. However, steady-state mass transfer boundary layer theory, which includes convection and diffusion, suggests that (see equation 11-153):

$$\mathrm{MTBLT}_{\mathrm{gas}} = f((\mathrm{Re}\cdot\mathrm{Sc})_{\mathrm{gas}}) \approx \frac{1}{\sqrt{(\mathrm{Re}\cdot\mathrm{Sc})_{\mathrm{gas}}}} \tag{24-6}$$

is a hydrodynamic factor in the expression for $k_{j,\,\mathrm{gas}}$ that decreases at higher gas flow rates. Hence,

$$k_{j,\,\mathrm{gas}} \approx c\mathfrak{D}_{j,\,\mathrm{gas\ mix.}}\sqrt{(\mathrm{Re}\cdot\mathrm{Sc})_{\mathrm{gas}}} \tag{24-7}$$

but the fact that the gas phase is dispersed could reduce the effect of the gas-phase flow rate on $\mathrm{MTBLT}_{\mathrm{gas}}$ and $k_{j,\,\mathrm{gas}}$. The expressions for $k_{j,\,\mathrm{gas}}$ given by (24-5) and (24-7) are equivalent to equations 18.2-15 and 18.2-16 in Bird *et al.* (2002, p. 548).

24-3 LIQUID-PHASE MASS BALANCES WITH CHEMICAL REACTION, INTERPHASE TRANSPORT, AND REACTION-ENHANCED MASS TRANSFER COEFFICIENTS

The liquid-phase balances with interphase mass transfer and second-order irreversible chemical reaction provide four more equations that relate some of the

unknowns. Now, the control volume corresponds to the total liquid fraction of the CSTR, V_L. Once again, the units of each term in all of the liquid-phase mass balances are moles per time. At steady state, the inlet molar flow rate of component j and its rate of production via chemical reaction are balanced by the outlet molar flow rate and the rate at which component j leaves the liquid phase via interphase mass transfer. In terms of the notation introduced above,

$$(N_j)^0\delta_{j\mathrm{B}} + \upsilon_j \mathfrak{R} V_L = qC_j + k_{j,\,\mathrm{liquid}}(C_j - C_{ji})a_L V_L \qquad (5) \rightarrow (8) \qquad (24\text{-}8)$$

where υ_j is the stoichiometric coefficient of component j; $\delta_{j\mathrm{B}}$ is the Kronecker delta, which accounts for the fact that benzene is the only component of interest that enters the CSTR in the liquid feed stream; and $k_{j,\,\mathrm{liquid}}$ is the mass transfer coefficient on the liquid side of the interface, with units of length per time, that experiences enhancement due to chemical reaction. The stoichiometric coefficients for benzene and dissolved chlorine are -1 and those for monochlorobenzene and hydrogen chloride are $+1$. The first term on each side of the liquid-phase mass balance represents a contribution from convective mass transfer. The last term on the right-hand side accounts for interphase transport. Results from steady-state film theory with one-dimensional diffusion across a flat interface and first-order irreversible chemical reaction allow one to calculate interphase mass transfer coefficients as follows:

$$k_{j,\,\mathrm{liquid}} = \frac{\mathfrak{D}_{j,\,\mathrm{liq.\ mix.}}}{\mathrm{MTBLT}_{\mathrm{liquid}}} \cdot \mathrm{Sh} \qquad (24\text{-}9)$$

which is equivalent to equation 18.4-12 in Bird *et al.* (2002, p. 555). Example 18.4-1 in Bird *et al.* (2002, pp. 555–557) is extremely applicable to this two-phase CSTR problem. Obviously, liquid-phase mass transfer coefficients that allow one to calculate interfacial molar fluxes have units of length per time when the driving force is based on molar densities. $\mathfrak{D}_{j,\,\mathrm{liq.\ mix.}}$ represents the molecular diffusion coefficient of component j in the liquid mixture, $\mathrm{MTBLT}_{\mathrm{liquid}}$ is the mass transfer boundary layer thickness on the liquid side of the interface, and Sh is the Sherwood number for one-dimensional diffusion normal to the interface in the presence of chemical reaction. In the absence of chemical reaction or when reaction rates are extremely slow, the Sherwood number approaches 1 (or 2). When chemical reactions must be considered, the Sherwood number is a function of the Damkohler number, or the Thiele parameter, and the reaction order. Analytical solutions are available for $\mathrm{Sh} = f(\Lambda^2)$, where Λ^2 is the Damkohler number, when the kinetics are zeroth or first-order. Numerical solutions are required for all other forms of the rate law. The following assumptions are invoked to calculate Sh analytically, which can also be interpreted as the gradient of the dimensionless concentration profile of reactant B evaluated at the interface:

1. The interface is locally flat.
2. The kinetic rate law is first-order, or pseudo-first-order, and irreversible.

Obviously, the gas–liquid interface is curved, but $\text{MTBLT}_{\text{liquid}}/d_{\text{gas}} \ll 1$ at very high Schmidt numbers. Under these conditions, the effect of curvature is not important. The steady-state microscopic mass balance for benzene (B) in the liquid phase with one-dimensional diffusion normal to the interface and first-order irreversible chemical reaction is

$$\mathfrak{D}_{\text{B, liq. mix.}} \frac{d^2 C_{\text{B}}}{dx^2} - k_1 C_{\text{B}} = 0 \tag{24-10}$$

where x is a position variable measured normal to the gas–liquid interface and k_1 is a pseudo-first-order kinetic rate constant for a homogeneous rate law. If molar density and spatial position are made dimensionless as follows:

$$\Psi_{\text{B}} = \frac{C_{\text{B}}}{C_{\text{B}i}} \qquad \zeta = \frac{x}{\text{MTBLT}_{\text{liquid}}} \tag{24-11}$$

then the mass balance can be written in dimensionless form as

$$\frac{d^2 \Psi_{\text{B}}}{d\zeta^2} = \Lambda^2 \Psi_{\text{B}} \tag{24-12}$$

where the Damkohler number for benzene is defined by

$$\Lambda^2 = \frac{k_1 (\text{MTBLT}_{\text{liquid}})^2}{\mathfrak{D}_{\text{B, liq. mix.}}} \tag{24-13}$$

The pseudo-first-order kinetic rate constant is defined by

$$k_1 = k_r C_{\text{B}i} \tag{24-14}$$

and to a first approximation, the interfacial molar density of benzene is

$$C_{\text{B}i} \approx C_{\text{B, inlet}} \tag{24-15}$$

The mass balance with diffusion and first-order chemical reaction, given by (24-12), is classified as a frequently occurring second-order linear ordinary differential equation (i.e., ODE) with constant coefficients. It is a second-order equation because diffusion is an important mass transfer rate process that is included in the mass balance. It is linear because the kinetic rate law is first-order or pseudo-first-order, and it is ordinary because diffusion is considered only in one coordinate direction — normal to the interface. The coefficients are constant under isothermal conditions because the physicochemical properties of the fluid don't change

very much, including the concentration dependence of $\mathfrak{D}_{B,\,\text{liq. mix.}}$. The analytical solution for the dimensionless molar density of benzene is obtained as follows:

1. Guess $\Psi_B \approx \exp(m\zeta)$.
2. Substitute this trial function into the mass balance with diffusion and first-order irreversible chemical reaction:

$$\frac{d^2\Psi_B}{d\zeta^2} = \Lambda^2\Psi_B$$

$$m^2\exp(m\zeta) = \Lambda^2\exp(m\zeta)$$

3. Solve the characteristic equation: $m = \pm\Lambda$.

Since $\exp(+\Lambda\zeta)$ and $\exp(-\Lambda\zeta)$ are both solutions to the mass balance, a linear superposition of these solutions also satisfies the mass balance because the ODE is linear. Hence, the general solution is

$$\Psi_B(\zeta) = A\exp(\Lambda\zeta) + B\exp(-\Lambda\zeta) = C\sinh\Lambda\zeta + D\cosh\Lambda\zeta \qquad (24\text{-}16)$$

where the integration constants A and B are different from C and D, and the properties of the hyperbolic sine and cosine allow two possible forms for the same answer, because

$$\sinh\Lambda\zeta = \frac{\exp(\Lambda\zeta) - \exp(-\Lambda\zeta)}{2}$$

$$\cosh\Lambda\zeta = \frac{\exp(\Lambda\zeta) + \exp(-\Lambda\zeta)}{2} \qquad (24\text{-}17)$$

Equation (24-16) is applicable within the mass transfer boundary layer adjacent to the gas–liquid interface where $0 \le x \le \text{MTBLT}_{\text{liquid}}$ and $C_B = C_{Bi}$ at the interface where $x = 0$ (i.e., $\Psi_B = 1$ at $\zeta = 0$). At the other end of the stagnant liquid film, where the boundary layer meets the bulk liquid phase, either:

1. $C_B \approx 0$ (i.e., $\Psi_B \approx 0$ at $\zeta = 1$), which implies that the liquid contains vanishingly small amounts of the mobile component (i.e., this condition is applicable to solubilized gases and volatile liquid-phase products generated by chemical reaction), or
2. $dC_B/dx = 0$ [i.e., $(d\Psi_B/d\zeta)_{\zeta=1} = 0$], which implies that all gradients exist within $\text{MTBLT}_{\text{liquid}}$ (i.e., this condition is more appropriate for liquid-phase components).

At the outer edge of the mass transfer boundary layer where molar densities approach those in the bulk liquid, solubilized chlorine gas is best described

by boundary condition 1, whereas benzene, chlorobenzene and HCl are best described by boundary condition 2. The mass transfer coefficient of interest is defined via the interfacial molar flux of the mobile component evaluated at $x = 0$:

$$N_{Bx}(x=0) = -\mathfrak{D}_{B,\text{ liq. mix.}}\left(\frac{dC_B}{dx}\right)_{x=0} = \frac{\mathfrak{D}_{B,\text{ liq. mix.}}C_{Bi}}{\text{MTBLT}_{\text{liquid}}}\left(\frac{-d\Psi_B}{d\zeta}\right)_{\zeta=0} \equiv k_{B,\text{ liquid}}C_{Bi} \tag{24-18}$$

where condition 1 ($C_B \approx 0$ at $x = \text{MTBLT}_{\text{liquid}}$) is used to construct the concentration driving force in equation (24-18) for interphase mass transfer. Since $\mathfrak{D}_{B,\text{ liq. mix.}}/\text{MTBLT}_{\text{liquid}}$ is the simplest mass transfer coefficient for one-dimensional diffusion with no chemical reaction, as given by equation (24-5), and

$$\text{Sh} \equiv \frac{k_{B,\text{ liquid}}\cdot\text{MTBLT}_{\text{liquid}}}{\mathfrak{D}_{B,\text{ liq. mix.}}} \tag{24-19}$$

it should seem reasonable that the Sherwood number is given by the dimensionless concentration gradient evaluated at the interface under investigation, as suggested by equations (24-18) and (24-19). Hence,

$$\text{Sh} = \left(\frac{-d\Psi_B}{d\zeta}\right)_{\zeta=0} \tag{24-20}$$

If one adopts the solution given by equation (24-16) in terms of hyperbolic sines and cosines, then:

$$\frac{d\Psi_B}{d\zeta} = \Lambda(C\cosh\Lambda\zeta + D\sinh\Lambda\zeta) \tag{24-21}$$

and evaluation of the concentration gradient at the interface where $\zeta = 0$ yields $\text{Sh} = -C\Lambda$. If

$$\Psi_B(\zeta=0) = 1 \qquad \Psi_B(\zeta=1) = 0 \tag{24-22}$$

then

$$D = 1 \qquad C = \frac{-1}{\tanh\Lambda} \tag{24-23}$$

Hence,

$$\text{Sh} = \frac{\Lambda}{\tanh\Lambda} \tag{24-24}$$

represents the mass transfer coefficient enhancement factor in the presence of first-order irreversible chemical reaction, as provided by equation (24-1) in the statement of this design problem. If $(d\Psi_B/d\zeta)_{\zeta=1} = 0$ is employed instead of $\Psi_B(\zeta = 1) = 0$, then

$$D = 1 \qquad C = -\tanh\Lambda \tag{24-25}$$

Now, the enhancement factor is

$$\mathrm{Sh} = \Lambda \tanh \Lambda \tag{24-26}$$

If the rate of chemical reaction is much faster than the rate of mass transfer via diffusion, then $\Lambda \gg 1$ and $\tanh \Lambda \to 1$. Hence, the mass transfer enhancement factor $\mathrm{Sh} \to \Lambda$ in the diffusion-limited regime via equation (24-24) or (24-26). The final form for the liquid-phase mass transfer coefficient of component j in the diffusion-limited regime is

$$k_{j,\,\mathrm{liquid}} = \frac{\mathfrak{D}_{j,\,\mathrm{liq.\ mix.}}}{\mathrm{MTBLT}_{\mathrm{liquid}}}\Lambda = \sqrt{k_r C_{\mathrm{B,\,inlet}} \mathfrak{D}_{j,\,\mathrm{liq.\ mix.}}} \tag{24-27}$$

This is convenient because

$$\mathrm{MTBLT}_{\mathrm{liquid}} \approx \frac{1}{\sqrt{(\mathrm{Re}\cdot\mathrm{Sc})_{\mathrm{liquid}}}} \tag{24-28}$$

which is almost impossible to measure experimentally, does not affect mass transfer coefficients when chemical reaction rates are very fast relative to diffusion. If the curvature of the gas–liquid interface is important, then the Nusselt number for mass transfer based on the bubble diameter can be solved analytically for radial diffusion and first-order irreversible chemical reaction in spherical coordinates. The final result given by equation (13-18) is repeated here for comparison with equation (24-27):

$$\mathrm{Sh} = \frac{k_{j,\,\mathrm{liquid}}\, d_{\mathrm{gas}}}{\mathfrak{D}_{j,\,\mathrm{liq.\ mix.}}} = 2 + \frac{d_{\mathrm{gas}}}{\mathrm{MTBLT}_{\mathrm{liquid}}}\left(\frac{\Lambda}{\tanh \Lambda}\right) \tag{24-29}$$

where the Damkohler number

$$\Lambda^2 = \frac{k_1 (\mathrm{MTBLT}_{\mathrm{liquid}})^2}{\mathfrak{D}_{\mathrm{B,\,liq.\ mix.}}} \tag{24-30}$$

has the same definition as that given by equation (24-13). Furthermore, in the diffusion-limited regime where mass transfer boundary layers are thin and interfacial curvature is negligible:

$$\begin{gathered} \Lambda^2 \gg 1 \\ \tanh \Lambda \to 1 \\ \mathrm{MTBLT}_{\mathrm{liquid}} \ll d_{\mathrm{gas}} \end{gathered} \tag{24-31}$$

the asymptotic expression for the Sherwood number with rapid chemical reaction is

$$\mathrm{Sh} \to 2 + \frac{d_{\mathrm{gas}}}{\mathrm{MTBLT}_{\mathrm{liquid}}}\Lambda \approx d_{\mathrm{gas}} \sqrt{k_r C_{\mathrm{B,\,inlet}} / \mathfrak{D}_{j,\,\mathrm{liq.\ mix.}}} \tag{24-32}$$

This is equivalent to equation (24-27) for the liquid-phase mass transfer coefficient because equations (24-29) and (24-32) yield:

$$k_{j,\,\text{liquid}} = \frac{\mathfrak{D}_{j,\,\text{liq. mix.}}}{d_{\text{gas}}} \cdot \text{Sh} = \sqrt{k_r C_{\text{B, inlet}} \mathfrak{D}_{j,\,\text{liq. mix.}}} \tag{24-33}$$

For reaction-rate-controlled situations when interfacial curvature is important,

$$\Lambda^2 \ll 1 \qquad \tanh \Lambda \to \Lambda \qquad \text{MTBLT}_{\text{liquid}} \gg d_{\text{gas}} \qquad \text{Sh} \to 2 \tag{24-34}$$

24-4 INTERFACIAL EQUILIBRIUM AND EQUALITY OF INTERFACIAL FLUXES

Steady-state mass balances at the gas–liquid interface for each component provide four more equations that describe the performance of the two-phase CSTR. The interface is the control volume, in which there is no accumulation of mass. Hence, the rate at which component j diffuses toward the interface from the bulk gas mixture must be balanced by the rate at which it diffuses away from the interface into the bulk liquid phase. Using the notation above,

$$k_{j,\,\text{gas}}(y_j - y_{ji}) a_L V_L = k_{j,\,\text{liquid}}(C_{ji} - C_j) a_L V_L \qquad (9) \to (12) \tag{24-35}$$

If the interface is thin enough, then the surface area for mass transfer should be the same on both the gas and liquid sides. These interfacial balances are equivalent to the tie-line relations that assist in the graphical solutions for humidification towers and gas absorbers. In other words, whenever interphase mass transfer occurs, interfacial balances provide relations between concentrations at the interface and those in the bulk. Furthermore, equilibrium is typically established at the interface, which provides another set of four equations, one for each component. This brings the total number of equations to 16. Interfacial equilibrium can be addressed by equating the fugacity of component j in both phases. When the gas-phase pressure is not too high, the fugacity of component j is expressed as a product of its mole fraction, fugacity coefficient, and the total pressure of the gas. In the liquid phase, the fugacity of component j is given by a product of its mole fraction, activity coefficient, and the saturation vapor pressure of pure component j at the interfacial temperature. This leads to a relation between vapor- and liquid-phase mole fractions at the interface. For convenience, the gas-phase mole fraction of component j at the interface is written in terms of C_{ji}. The final result is

$$y_{ji} = K_j(T_i,\, p, \text{composition}) C_{ji} \qquad (13) \to (16) \tag{24-36}$$

where K_j represents the product of activity coefficient and saturation vapor pressure of component j divided by the product of fugacity coefficient, total pressure, and total interfacial molar density in the liquid phase. The interfacial temperature T_i represents another unknown that is introduced via the equilibrium

relations $y_{ji} = K_j C_{ji}$. Hence, there are a total of 18 unknowns. The last two equations state that the bulk gas-phase mole fractions must sum to unity:

$$\sum_j y_j = 1 \qquad (17) \tag{24-37}$$

as well as the interfacial gas-phase mole fractions:

$$\sum_j y_{ji} = \sum_j K_j(T_i) C_{ji} = 1 \qquad (18) \tag{24-38}$$

The last restriction defines the interfacial temperature T_i. The performance of the two-phase CSTR is completely defined in terms of 18 equations and 18 unknowns.

24-4.1 Key Assumption: Minimal Gas-Phase Resistance in the Boundary Layer

The following key assumption is invoked prior to solving the system of equations described above. The argument begins by noting that the ratio of diffusion coefficients

$$\frac{\mathfrak{D}_{j,\text{ gas mix.}}}{\mathfrak{D}_{j,\text{ liq. mix.}}} \approx 10^4 \rightarrow 10^5 \tag{24-39}$$

Furthermore, since the mass transfer coefficient in each phase is proportional to the square root of the corresponding diffusivity, as indicated by equations (24-7) and (24-33):

$$\begin{aligned} k_{j,\text{ gas}} &\approx \mathfrak{D}_{j,\text{ gas mix.}} \sqrt{(\text{Re}\cdot\text{Sc})_{\text{gas}}} \\ k_{j,\text{ liquid}} &= \sqrt{k_r C_{\text{B, inlet}} \mathfrak{D}_{j,\text{ liq. mix.}}} \end{aligned} \tag{24-40}$$

it follows that the resistance to interphase mass transfer in the gas phase is more than 100-fold smaller than the corresponding liquid-phase resistance because

$$\frac{k_{j,\text{ gas}}}{k_{j,\text{ liquid}}} \approx \sqrt{\frac{\mathfrak{D}_{j,\text{ gas mix.}}}{\mathfrak{D}_{j,\text{ liq. mix.}}}} \tag{24-41}$$

Hence, the liquid-phase resistance controls interphase mass transfer and, for all practical purposes, $y_j \approx y_{ji}$. This is analogous to drawing horizontal tie-lines between the equilibrium and operating lines during graphical analysis of a gas absorber, where vapor-phase mole fraction is plotted on the vertical axis and liquid-phase mole fraction is on the horizontal axis. This assumption allows one to re-express interphase transport on the liquid side of the gas–liquid interface, $k_{j,\text{ liquid}}(C_j - C_{ji}) a_L V_L$, using the interfacial equilibrium relations given by (24-36):

$$C_{ji} = \frac{y_{ji}}{K_j} \approx \frac{y_j}{K_j} \qquad (13) \rightarrow (16) \tag{24-42}$$

Hence, the interphase transport term in the liquid-phase balances, given by equation (24-8), adopts the following form:

$$k_{j,\,\text{liquid}} \left(C_j - \frac{y_j}{K_j} \right) a_L V_L \tag{24-43}$$

24-4.2 Exact Calculation of the Interfacial Area for Gas–Liquid Mass Transfer

Since the surface area and volume of each gas bubble are well defined in terms of the bubble diameter d_{gas}, it is relatively straightforward to calculate the interfacial area for mass transfer per unit volume of the continuous liquid phase, a_L. The surface area of each bubble is $\pi (d_{\text{gas}})^2$, and the number of bubbles is given by the total gas-phase volume divided by the volume of each bubble, $\pi (d_{\text{gas}})^3/6$. Hence,

$$a_L = \pi (d_{\text{gas}})^2 \left[\frac{V_g}{\pi (d_{\text{gas}})^3/6} \right] \frac{1}{V_L} = \frac{6}{d_{\text{gas}}} \frac{V_g}{V_L} \tag{24-44}$$

The volume fraction of gas bubbles is defined by

$$\beta = \frac{V_g}{V_g + V_L} \tag{24-45}$$

which translates into

$$\frac{V_g}{V_L} = \frac{\beta}{1 - \beta} \tag{24-46}$$

Hence,

$$a_L = \frac{6}{d_{\text{gas}}} \frac{\beta}{1 - \beta} \tag{24-47}$$

24-4.3 Time Constants for Mass Transfer Rate Processes and Dimensionless Numbers

The next objective is to identify a time constant for each important mass transfer rate process and solve the system of equations for the two-phase CSTR in terms of these time constants. This approach allows one to develop generic solutions in dimensionless form. For example, six time constants can be defined for (1) convection in the liquid phase (τ), (2) chemical reaction in the liquid phase (λ), and (3–6) interphase mass transfer for each component (Θ_j, j = B,Cl,M,H). Obviously, these six time constants produce five dimensionless ratios. Remember that time constants represent order-of-magnitude estimates of the time scales of mass transfer rate processes. The time constant for convective mass transfer in the liquid phase is equivalent to the liquid's residence time:

$$\tau = \frac{V_L}{q} \tag{24-48}$$

The time constant for second-order irreversible chemical reaction is

$$\lambda = \frac{1}{k_r C_{\mathrm{B,\,inlet}}} \tag{24-49}$$

The time constant for interphase mass transfer of component j is

$$\Theta_j = \frac{1}{a_L k_{j,\,\mathrm{liquid}}} \tag{24-50}$$

The important dimensionless time constant ratios are

$$\begin{aligned} \rho &= \frac{\tau}{\lambda} = \frac{k_r V_L (C_{\mathrm{B,\,inlet}})^2}{(N_{\mathrm{B}})^0} \\ \frac{1}{\eta_j} &= \frac{\Theta_j}{\lambda} = \frac{k_r C_{\mathrm{B,\,inlet}}}{a_L k_{j,\,\mathrm{liquid}}} \qquad \text{for } j = \mathrm{B,Cl,M,H} \end{aligned} \tag{24-51}$$

Molar density ratios in the liquid phase are defined by

$$x_j = \frac{C_j}{C_{\mathrm{B,\,inlet}}} \tag{24-52}$$

realizing that $\sum_j x_j \neq 1$. Also,

$$K_{j\mathrm{B}} = K_j C_{\mathrm{B,\,inlet}} \tag{24-53}$$

Hence, the interfacial equilibrium relations, given by (24-42), can be rewritten as

$$y_{ji} \approx y_j \approx K_{j\mathrm{B}} x_{ji} \qquad (13) \rightarrow (16) \tag{24-54}$$

24-4.4 Dimensionless Form of the Liquid-Phase Mass Balances

All liquid-phase mass balances, given by equation (24-8):

$$(N_j)^0 \delta_{j\mathrm{B}} + \upsilon_j \mathfrak{R} V_L = q C_j + k_{j,\,\mathrm{liquid}} (C_j - C_{ji}) a_L V_L \qquad (5) \rightarrow (8) \tag{24-55}$$

are written in dimensionless form using the time constants and their ratios introduced in Section 24-4.3. Divide each balance by the inlet molar flow rate of liquid benzene, $(N_{\mathrm{B}})^0 = q C_{\mathrm{B,\,inlet}}$. After rearrangement, one obtains

$$a_L k_{j,\,\mathrm{liquid}} \frac{V_L}{q} \left(\frac{y_j}{K_{j\mathrm{B}}} - x_j \right) = x_j - \delta_{j\mathrm{B}} - \upsilon_j k_r C_{\mathrm{B,\,inlet}} \frac{V_L}{q} x_{\mathrm{B}} x_{\mathrm{Cl}} \qquad (5) \rightarrow (8) \tag{24-56}$$

The term on the left side of (24-56) represents interphase transport. On the right side of the equation, the first term represents convective mass transfer in the outlet stream, the second term represents convective mass transfer for liquid benzene

in the feed stream, and the third term corresponds to the rate of depletion of component j via second-order irreversible chemical reaction. Mass transfer time contants are introduced into equation (24-56) as follows:

$$a_L k_{j,\,\text{liquid}} \frac{V_L}{q} = \frac{\tau}{\Theta_j} = \frac{\tau}{\lambda}\frac{\lambda}{\Theta_j} = \rho\eta_j$$
$$k_r C_{\text{B, inlet}} \frac{V_L}{q} = \frac{\tau}{\lambda} = \rho \tag{24-57}$$

Hence, the final form of the dimensionless liquid-phase mass balances is

$$\frac{\tau}{\Theta_j}\left(\frac{y_j}{K_{j\text{B}}} - x_j\right) = x_j - \delta_{j\text{B}} - \upsilon_j \frac{\tau}{\lambda} x_{\text{B}} x_{\text{Cl}} \qquad (5) \rightarrow (8) \tag{24-58}$$

which can be written for each component j = B,Cl,M,H.

24-4.5 Total Outlet Gas-Phase Flow Rate via the Overall Mass Balance

The overall mass balance is helpful to develop an expression for the total outlet gas-phase flow rate. It is important to realize that there are no restrictions which require that the total outlet gas-phase flow rate be the same as the inlet flow rate of gaseous chlorine. If one adds all four of the liquid-phase mass balances and all four of the gas-phase mass balances, then the result is the overall mass balance, which does not represent another independent equation. It is interesting to note that the sum of the stoichiometric coefficients is zero, which implies that the total number of moles is conserved during the chemical reaction. Furthermore, all interphase transport terms cancel because they represent a redistribution of all four components between the two phases, but there are no input or output contributions from these terms when the control volume corresponds to the total contents of the CSTR. Hence, the overall mass balance is analyzed on a molar basis because the total number of moles is conserved. Each term in the equation has units of moles per time and represents convective mass transfer in either the feed streams or the exit streams. The input terms correspond to the flow rates of liquid benzene and chlorine gas in the two feed streams, $(N_{\text{B}})^0 + (N_{\text{Cl}})^0$. The output terms in the liquid exit stream are $\sum_j qC_j$, and N_{gas} represents convective mass transfer in the outlet gas stream. At steady state,

$$(N_{\text{B}})^0 + (N_{\text{Cl}})^0 = N_{\text{gas}} + \sum_j qC_j \qquad \sum_j [(1) \rightarrow (8)] \tag{24-59}$$

If one defines the following inlet flow rate ratio of gaseous chlorine relative to liquid benzene:

$$\kappa = \frac{(N_{\text{Cl}})^0}{(N_{\text{B}})^0} \tag{24-60}$$

then the steady-state overall mass balance given by (24-59) yields

$$N_{\text{gas}} = (N_{\text{B}})^0 \left(1 + \kappa - \sum_j x_j\right) \qquad \sum_j [(1) \rightarrow (8)] \tag{24-61}$$

24-4.6 Dimensionless Form of the Gas-Phase Mass Balances and Explicit Calculations of the Bulk Gas-Phase Mole Fractions

Simple manipulation of the gas-phase mass balances given by (24-4) allows one to calculate the bulk gas-phase mole fractions. It is necessary to rewrite the interphase transport terms on the gas side of the interface in terms of the corresponding expressions on the liquid side via equation (24-35), because $y_j \approx y_{ji}$. Hence,

$$k_{j,\,\text{gas}}(y_j - y_{ji})a_L V_L = k_{j,\,\text{liquid}}(C_{ji} - C_j)a_L V_L \qquad (9) \rightarrow (12) \tag{24-62}$$

is used to rewrite the last term on the right side of the gas-phase balances:

$$(N_j)^0 \delta_{j\text{Cl}} = y_j N_{\text{gas}} + k_{j,\,\text{gas}}(y_j - y_{ji})a_L V_L \qquad (1) \rightarrow (4) \tag{24-63}$$

Also, interfacial equilibrium via equations (24-36) and (24-42) is invoked to re-express

$$C_{ji} = \frac{y_{ji}}{K_j} \approx \frac{y_j}{K_j} \qquad (13) \rightarrow (16) \tag{24-64}$$

The gas-phase balances are written as follows:

$$(N_j)^0 \delta_{j\text{Cl}} = y_j N_{\text{gas}} + k_{j,\,\text{liquid}} \left(\frac{y_j}{K_j} - C_j\right) a_L V_L \qquad (1) \rightarrow (4) \tag{24-65}$$

Dimensionless equations are generated via division by $qC_{\text{B, inlet}} = (N_{\text{B}})^0$. The ratio of the total outlet gas flow rate to the feed flow rate of liquid benzene is defined by

$$S = \frac{N_{\text{gas}}}{(N_{\text{B}})^0} \tag{24-66}$$

Hence, one solves for the bulk gas mole fractions from

$$\kappa \delta_{j\text{Cl}} = y_j S + a_L k_{j,\,\text{liquid}} \frac{V_L}{q} \left(\frac{y_j}{K_{j\text{B}}} - x_j\right) \qquad (1) \rightarrow (4) \tag{24-67}$$

Since

$$a_L k_{j,\,\text{liquid}} \frac{V_L}{q} = \frac{\tau}{\Theta_j} \tag{24-68}$$

the dimensionless form of these gas-phase balances is

$$\kappa \delta_{j\text{Cl}} = y_j S + \frac{\tau}{\Theta_j} \left(\frac{y_j}{K_{j\text{B}}} - x_j\right) \qquad (1) \rightarrow (4) \tag{24-69}$$

and the bulk gas-phase mole fractions are calculated as follows:

$$y_j = \frac{(\tau/\Theta_j)x_j + \kappa\delta_{j\mathrm{Cl}}}{S + (\tau/\Theta_j K_{j\mathrm{B}})} \tag{24-70}$$

Equation (24-70) is used to calculate three gas-phase mole fractions (j = benzene, chlorobenzene, and HCl). The fourth mole fraction (i.e., chlorine) is obtained from the condition that

$$\sum_j y_j = 1 \qquad (17) \tag{24-71}$$

24-4.7 Summary of Equations That Describe the Two-Phase CSTR Performance

The two-phase CSTR problem has been reduced to the solution of the following nine nonlinear algebraic equations for S, x_j, and y_j, where j = B,Cl,M,H.

Liquid-phase mass balances; j = B,Cl,M,H :

$$\frac{\tau}{\Theta_j}\left(\frac{y_j}{K_{j\mathrm{B}}} - x_j\right) = x_j - \delta_{j\mathrm{B}} - \upsilon_j \frac{\tau}{\lambda} x_{\mathrm{B}} x_{\mathrm{Cl}}$$

Gas-phase mass balances; j = B,M,H :

$$y_j = \frac{(\tau/\Theta_j)x_j + \kappa\delta_{j\mathrm{Cl}}}{S + (\tau/\Theta_j K_{j\mathrm{B}})}$$

Gas-phase mole fraction of chlorine :

$$\sum_j y_j = 1$$

Total outlet gas-phase flow rate :

$$S = 1 + \kappa - \sum_j x_j$$

$$j = \mathrm{B,Cl,M,H}$$

The final task is to identify and calculate some important parameters that are needed to evaluate the time constant ratios λ/Θ_j and the interfacial equilibrium coefficients $K_{j\mathrm{B}}$.

24-5 MOLECULAR DIFFUSION IN LIQUIDS

The Stokes–Einstein equation for binary molecular diffusion coefficients of dilute pseudo-spherical molecules subject to creeping flow through an incompressible Newtonian fluid is (see equation 25-98):

$$\mathfrak{D}_{\mathrm{AB}} = \frac{k_{\mathrm{Boltz}} T}{6\pi\mu_{\mathrm{B}} R_{\mathrm{A}}} \tag{24-72}$$

where T is absolute temperature, $k_{\mathrm{Boltz}} = 1.38 \times 10^{-16}$ g·cm^2/s^2·K is Boltzmann's constant, $\mu_{\mathrm{B}} \approx 0.4$ cp (= 0.004 g/cm·s) is the Newtonian viscosity of the solvent at 55°C, and R_{A} is the effective hydrodynamic radius of a spherical shell

that surrounds a molecule of component A. If a 4-Å-diameter shell is required to surround one molecule of A diffusing through liquid B, then $R_A = 2Å$ and $\mathfrak{D}_{AB} = 1.1 \times 10^{-5}$ cm^2/s at 298 K. Larger molecules have smaller diffusion coefficients, and the temperature dependence is

$$\mathfrak{D}_{AB}(T) \approx \frac{T}{\mu_B(T)} \tag{24-73}$$

where exponential temperature dependence is reasonable for the Newtonian solvent viscosity μ_B. For homonuclear and heteronuclear diatomics, the diameter of an effective spherical shell that surrounds each molecule can be calculated by adding the covalent and van der Waals radii of each atom. Addition of the covalent radii represents the distance between atomic centers, and the van der Waals radius corresponds to the distance from the atomic center to the outer edge of the electron density. Covalent and van der Waals radii are provided in Table 24-1 for hydrogen and chlorine. Hence, the hydrodynamic diameters are 4.19 Å for HCl and 5.58 Å for Cl_2 (Table 24-2), and they are larger than the collision diameter σ or the equilibrium separation between the centers of two molecules, $\sigma(2)^{1/6}$, via the 6–12 Lennard-Jones intermolecular potential. Molecular mechanics software is useful to predict the hydrodynamic diameters of polyatomic molecules like benzene and monochlorobenzene, as summarized in Table 24-2.

TABLE 24-1 Covalent and van der Waals Radii for Atomic H and Cl

Atom	Covalent Radius (Å)	van der Waals Radius (Å)
H	0.30	1.10
Cl	0.99	1.80

TABLE 24-2 Hydrodynamic Diameters of Equivalent Spherical Shells[a]

Molecule	Hydrodynamic Diameter (Å)
C_6H_6	7.2
Cl_2	5.6
HCl	4.2
C_6H_5Cl	8.4

[a] Shells completely surround the diatomic and polyatomic molecules of interest for the chlorination of benzene

24-6 NONLINEAR EQUATION SOLVER PROGRAM

The sequence of equations presented below is required to solve the isothermal gas–liquid CSTR problem for the chlorination of benzene in the liquid phase at 55°C. After some simplifying assumptions, the problem reduces to the solution of nine equations with nine unknowns. Some of the equations are nonlinear because the chemical kinetics are second-order in the liquid phase and involve the molar densities of the two reactants, benzene and chlorine. The problem is solved in dimensionless form with the aid of five time constant ratios that are generated by six mass transfer rate processes: (1) convective mass transfer through the reactor, (2) molecular transport in the liquid phase across the gas-liquid interface for each of the four components, and (3) second-order chemical reaction in the liquid phase.

Inlet molar density of liquid benzene as a pure component, g-mol/mL:

$$C_{\mathrm{B,\,inlet}} = 0.011$$

Factor by which pure liquid benzene is diluted in the liquid feed stream, ≥ 1:

$$\text{dilution factor} = 1 + \frac{\text{molar flow rate of liquid inert}}{\text{molar flow rate of benzene}}$$

Inlet molar density of diluted benzene (g-mol/mL):

$$C_{\mathrm{B,\ dilute}} = \frac{C_{\mathrm{B,\,inlet}}}{\text{dilution factor}}$$

Temperature (K):

$$T = 55 + 273$$

Second-order kinetic rate constant in the liquid phase (mL/g-mol·s):

$$k_r = 8.84$$

Diameter of the gas bubbles that rise through the CSTR's liquid phase (mm):

$$d_{\mathrm{gas}} = 2$$

Interfacial equilibrium coefficient for each component that represents the ratio of the bulk gas-phase mole fraction to the interfacial molar density in the liquid phase, multiplied by the inlet molar density of liquid benzene,

$C_{B,\ \text{dilute}}$. This equilibrium coefficient is larger for components that are more volatile:

$$K_{CB} = \frac{10}{\text{dilution factor}} \quad \text{(for chlorine, which is nonpolar)}$$

$$K_{HB} = \frac{5}{\text{dilution factor}} \quad \text{(for HCl, which is smaller than } Cl_2 \text{ but is strongly polar)}$$

$$K_{BB} = \frac{1.0}{\text{dilution factor}} \quad \text{(for benzene)}$$

$$K_{MB} = \frac{0.50}{\text{dilution factor}} \quad \text{(for } C_6H_5Cl\text{, which is the largest molecule and is polar)}$$

Inlet molar flow rate ratio of gaseous chlorine to liquid benzene:

$$\kappa = 2$$

Gas-phase volume fraction in the CSTR:

$$\beta = \frac{\kappa}{\kappa + \text{dilution factor}}$$

Use the Stokes–Einstein equation to estimate the liquid-phase diffusivity of benzene:

$$k_{\text{Boltz}} = 1.38 \times 10^{-16} (\text{Boltzmann's constant, g·cm}^2/\text{s}^2\text{·K})$$

Viscosity of the liquid mixture at 55°C (cp $= 10^{-2}$ g/cm·s):

$$\text{viscosity} = 0.4$$

Hydrodynamic diameter of benzene (Å):

$$\text{hydro diameter benzene} = 7.2$$

Hydrodynamic diameter of monochlorobenzene (Å):

$$\text{hydro diameter chlorobenzene} = 8.4$$

Hydrodynamic diameter of chlorine (Å):

$$\text{hydro diameter chlorine} = 5.6$$

Hydrodynamic diameter of hydrogen chloride (Å):

$$\text{hydro diameter HCl} = 4.2$$

Liquid-phase diffusivity of benzene at 55°C (cm^2/s):

$$\text{diffusivity benzene} = \frac{k_{\text{Boltz}}(T)}{6\pi(\text{viscosity})(\text{hydro diameter benzene}) \times 10^{-10}/2}$$

Liquid-phase mass transfer coefficient for benzene (cm/s):

$$k_{\text{B, liquid}} = \sqrt{k_r C_{\text{B, dilute}}(\text{diffusivity benzene})}$$

Time constant ratio $(\lambda/\Theta_j) = \eta_j$ for each component that represents the ratio of the time constant for second-order chemical reaction in the liquid phase λ, to the time constant for molecular transport in the liquid phase across the gas–liquid interface Θ_j, which is specific to each component. Molecules with smaller hydrodynamic radii have larger liquid-phase diffusion coefficients via the Stokes–Einstein diffusion equation, and hence their time constant ratio is larger.

$$\eta_{\text{benzene}} = \frac{60}{d_{\text{gas}}}\frac{\beta}{1-\beta}\sqrt{\text{diffusivity benzene}/(k_r C_{\text{B, dilute}})}$$

$$\eta_{\text{chlorobenzene}} = \eta_{\text{benzene}}\sqrt{\text{hydro diameter benzene/hydro diameter chlorobenzene}}$$

$$\eta_{\text{chlorine}} = \eta_{\text{benzene}}\sqrt{\text{hydro diameter benzene/hydro diameter chlorine}}$$

$$\eta_{\text{HCl}} = \eta_{\text{benzene}}\sqrt{\text{hydro diameter benzene/hydro diameter HCl}}$$

Time constant ratio $(\tau/\lambda) = \rho$ for convective mass transfer through the reactor (residence time τ) relative to the time constant for second-order irreversible chemical reaction in the liquid phase λ, where τ is incremented as an important design variable.

Liquid-phase CSTR algebraic equations written in dimensionless form for each component:

$$\eta_{\text{benzene}}\rho\left(\frac{y_{\text{B}}}{K_{\text{BB}}} - x_{\text{B}}\right) = x_{\text{B}} + \rho x_{\text{B}} x_{\text{Cl}} - 1 \quad \text{(mass balance for benzene)}$$

$$\eta_{\text{chlorine}}\rho\left(\frac{y_{\text{Cl}}}{K_{\text{CB}}} - x_{\text{Cl}}\right) = x_{\text{Cl}} + \rho x_{\text{B}} x_{\text{Cl}} \quad \text{(mass balance for chlorine)}$$

$$\eta_{\text{chlorobenzene}}\rho\left(\frac{y_{\text{M}}}{K_{\text{MB}}} - x_{\text{M}}\right) = x_{\text{M}} - \rho x_{\text{B}} x_{\text{Cl}} \quad \text{(mass balance for chlorobenzene)}$$

$$\eta_{\text{HCl}}\rho\left(\frac{y_{\text{H}}}{K_{\text{HB}}} - x_{\text{H}}\right) = x_{\text{H}} - \rho x_{\text{B}} x_{\text{Cl}} \quad \text{(mass balance for HCl)}$$

Outlet gas-phase mole fractions based on the gas-phase mass balances:

$$y_B = \frac{(\eta_{benzene}\rho x_B)}{S + (\eta_{benzene}\rho / K_{BB})}$$

$$y_H = \frac{(\eta_{HCl}\rho x_H)}{S + (\eta_{HCl}\rho / K_{HB})}$$

$$y_M = \frac{(\eta_{chlorobenzene}\rho x_M)}{S + (\eta_{chlorobenzene}\rho / K_{MB})}$$

$$y_{Cl} = 1 - y_B - y_H - y_M$$

Total outlet gas-phase molar flow rate with respect to the inlet molar flow rate of liquid benzene:

$$S = 1 + \kappa - (x_B + x_{Cl} + x_H + x_M)$$

Outlet liquid-phase molar density for each component:

$$C_B = C_{B,\ dilute} x_B \quad \text{(benzene)}$$

$$C_{Cl} = C_{B,\ dilute} x_{Cl} \quad \text{(chlorine)}$$

$$C_M = C_{B,\ dilute} x_M \quad \text{(monochlorobenzene)}$$

$$C_H = C_{B,\ dilute} x_H \quad \text{(hydrogen chloride)}$$

Total outlet flow rate of each component in both phases with respect to the inlet molar flow rate of liquid benzene:

$$\text{total benzene flow} = x_B + y_B S \quad \text{(total } C_6H_6 \text{ flow rate in liquid and gas exit streams)}$$

$$\text{total chlorine flow} = x_{Cl} + y_{Cl} S \quad \text{(total } Cl_2 \text{ flow rate in liquid and gas exit streams)}$$

$$\text{total chlorobenzene flow} = x_M + y_M S \quad \text{(total } C_6H_5Cl \text{ flow rate in liquid and gas exit streams)}$$

$$\text{total HCl flow} = x_H + y_H S \quad \text{(total HCl flow rate in liquid and gas exit streams)}$$

Fraction of the total outlet flow rate for each component that exits the CSTR as a liquid:

$$\text{liq. benzene flow} = \frac{x_B}{x_B + y_B S} \quad \text{(benzene fraction that exits as a liquid)}$$

$$\text{liq. chlorine flow} = \frac{x_{Cl}}{x_{Cl} + y_{Cl} S} \quad \text{(chlorine fraction that exits as a liquid)}$$

$$\text{liq. chlorobenzene flow} = \frac{x_M}{x_M + y_M S} \quad (C_6H_5Cl \text{ fraction that exits as a liquid})$$

$$\text{liq. HCl flow} = \frac{x_H}{x_H + y_H S} \quad (\text{HCl fraction that exits as a liquid})$$

Performance curves for this gas–liquid CSTR, based on the preceding system of equations and parameters, are illustrated in Figure 24-1. A reasonable design corresponds to $10^2 < \tau/\lambda < 10^3$, where the total outlet flow rate of chlorobenzene is between 60 and 93% of the inlet flow rate of liquid benzene, and 45% of the total chlorobenzene product exits the CSTR as a liquid.

24-6.1 Rigorous Trial-and-Error Solution of the Two-Phase CSTR without Assistance from a Nonlinear Algebraic Equation Solver

Further manipulation of the system of equations in Section 24-4.7 that describe the performance of the gas–liquid CSTR:

Liquid-phase mass balances; $j = \text{B,Cl,M,H}$:

$$\frac{\tau}{\Theta_j}\left(\frac{y_j}{K_{j\text{B}}} - x_j\right) = x_j - \delta_{j\text{B}} - \upsilon_j \frac{\tau}{\lambda} x_\text{B} x_\text{Cl}$$

Gas-phase mass balances; $j = \text{B,M,H}$:

$$y_j = \frac{(\tau/\Theta_j)x_j + \kappa\delta_{j\text{Cl}}}{S + (\tau/\Theta_j K_{j\text{B}})}$$

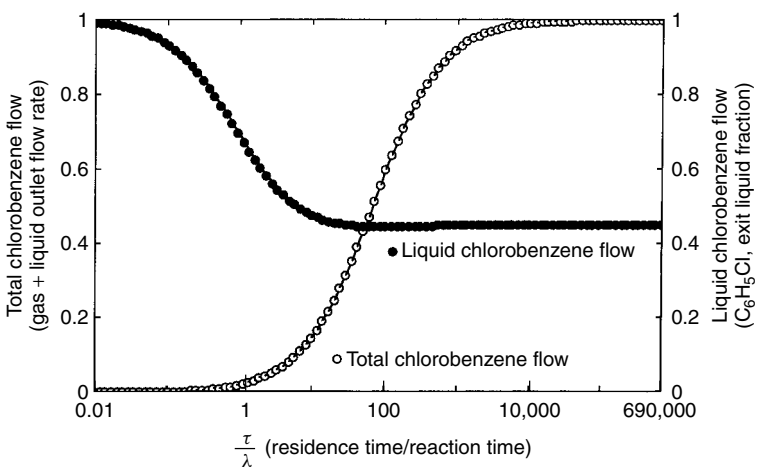

Figure 24-1 CSTR performance curves that illustrate the effect of residence time on the total molar flow rate of chlorobenzene in both the gas and liquid exit streams relative to the inlet molar flow rate of liquid benzene, and the fraction of chlorobenzene that exits the reactor in the liquid phase.

Gas-phase mole fraction of chlorine: $\sum_j y_j = 1$

Total outlet gas phase flow rate: $S = 1 + \kappa - \sum_j x_j$

is required if a nonlinear algebraic equation solver is not available. The appropriate sequence of steps to obtain a unique numerical solution is described below.

Step 1. Use the final expressions for bulk gas-phase mole fractions from the gas phase mass balances:

$$y_j = \frac{(\tau/\Theta_j)x_j + \kappa\delta_{j\mathrm{Cl}}}{S + (\tau/\Theta_j K_{j\mathrm{B}})} \tag{24-74}$$

and substitute for each y_j in the interphase mass transfer contribution of each liquid-phase mass balance:

$$\frac{\tau}{\Theta_j}\left(\frac{y_j}{K_{j\mathrm{B}}} - x_j\right) = x_j - \delta_{j\mathrm{B}} - \upsilon_j \frac{\tau}{\lambda} x_{\mathrm{B}} x_{\mathrm{Cl}} \tag{24-75}$$

Interphase mass transfer on the left side of (24-75) is rearranged as follows:

$$\begin{aligned}\frac{\tau}{\Theta_j}\left(\frac{y_j}{K_{j\mathrm{B}}} - x_j\right) &= \frac{\tau}{\Theta_j}\left[\frac{(\tau/\Theta_j)x_j + \kappa\delta_{j\mathrm{Cl}}}{SK_{j\mathrm{B}} + (\tau/\Theta_j)} - x_j\right] \\ &= \frac{\tau}{\Theta_j}\left[\frac{\kappa\delta_{j\mathrm{Cl}} - SK_{j\mathrm{B}}x_j}{SK_{j\mathrm{B}} + (\tau/\Theta_j)}\right] \\ &= \frac{\tau}{\Theta_j}\left[\frac{(\kappa/K_{j\mathrm{B}})\delta_{j\mathrm{Cl}} - Sx_j}{S + (\tau/\Theta_j K_{j\mathrm{B}})}\right]\end{aligned} \tag{24-76}$$

Hence,

$$\frac{\tau}{\Theta_j}\left[\frac{(\kappa/K_{j\mathrm{B}})\delta_{j\mathrm{Cl}} - Sx_j}{S + (\tau/\Theta_j K_{j\mathrm{B}})}\right] = x_j - \delta_{j\mathrm{B}} - \upsilon_j \frac{\tau}{\lambda} x_{\mathrm{B}} x_{\mathrm{Cl}} \tag{24-77}$$

Step 2. To simplify the liquid-phase mass balances, define the following parameters;

$$\begin{aligned}\alpha_j &\equiv \frac{(\tau/\Theta_j)S}{S + (\tau/\Theta_j K_{j\mathrm{B}})} \qquad j = \mathrm{B,Cl,M,H} \\ \alpha_5 &\equiv \frac{(\tau/\Theta_{\mathrm{Cl}})\kappa}{SK_{\mathrm{CB}} + (\tau/\Theta_{\mathrm{Cl}})}\end{aligned} \tag{24-78}$$

Step 3. Write all of the liquid-phase mass balances in condensed form using the α-parameters defined by equations (24-78):

$$\alpha_5\delta_{j\mathrm{Cl}} - \alpha_j x_j = x_j - \delta_{j\mathrm{B}} - \upsilon_j \frac{\tau}{\lambda} x_{\mathrm{B}} x_{\mathrm{Cl}} \tag{24-79}$$

Step 4. Group all terms and coefficients in equation (24-79) that are specific to component j on one side of the generic liquid-phase mass balance:

$$\frac{(\alpha_j + 1)x_j - \alpha_5\delta_{j\mathrm{Cl}} - \delta_{j\mathrm{B}}}{\upsilon_j} = \frac{\tau}{\lambda}x_{\mathrm{B}}x_{\mathrm{Cl}} \qquad j = \mathrm{B,Cl,M,H} \tag{24-80}$$

where υ_{B} and υ_{Cl} are -1, and υ_{M} and υ_{H} are $+1$. Hence, the left side of (24-80) is the same for all components.

Step 5. Apply stoichiometry from step 4:

$$\frac{(\alpha_j + 1)x_j - \alpha_5\delta_{j\mathrm{Cl}} - \delta_{j\mathrm{B}}}{\upsilon_j} \qquad \text{is the same for each component} \tag{24-81}$$

and obtain relations between the liquid-phase molar density ratios x_j. For example, when the stoichiometric relation is written for three independent pairs of components, one obtains

$$\begin{aligned} j = \mathrm{B} \text{ and } j = \mathrm{H}: &\qquad 1 - (\alpha_{\mathrm{B}} + 1)x_{\mathrm{B}} = (\alpha_{\mathrm{H}} + 1)x_{\mathrm{H}} \\ j = \mathrm{Cl} \text{ and } j = \mathrm{H}: &\qquad \alpha_5 - (\alpha_{\mathrm{Cl}} + 1)x_{\mathrm{Cl}} = (\alpha_{\mathrm{H}} + 1)x_{\mathrm{H}} \\ j = \mathrm{M} \text{ and } j = \mathrm{H}: &\qquad (\alpha_{\mathrm{M}} + 1)x_{\mathrm{M}} = (\alpha_{\mathrm{H}} + 1)x_{\mathrm{H}} \end{aligned} \tag{24-82}$$

Now, the liquid-phase molar density ratios for benzene, chlorine, and monochlorobenzene have been expressed in terms of x_{H}. This is illustrated below using condensed notation via a new set of parameters (i.e., $\omega_1 \rightarrow \omega_5$):

$$\begin{aligned} x_{\mathrm{M}} &= \omega_1 x_{\mathrm{H}} & \omega_1 &\equiv \frac{\alpha_{\mathrm{H}} + 1}{\alpha_{\mathrm{M}} + 1} & & \\ x_{\mathrm{B}} &= \omega_2 - \omega_3 x_{\mathrm{H}} & \omega_2 &\equiv \frac{1}{\alpha_{\mathrm{B}} + 1} & \omega_3 &\equiv \frac{\alpha_{\mathrm{H}} + 1}{\alpha_{\mathrm{B}} + 1} \\ x_{\mathrm{Cl}} &= \omega_4 - \omega_5 x_{\mathrm{H}} & \omega_4 &\equiv \frac{\alpha_5}{\alpha_{\mathrm{Cl}} + 1} & \omega_5 &\equiv \frac{\alpha_{\mathrm{H}} + 1}{\alpha_{\mathrm{Cl}} + 1} \end{aligned} \tag{24-83}$$

Step 6. Write the generic liquid-phase mass balance given by (24-79),

$$\alpha_5\delta_{j\mathrm{Cl}} - \alpha_j x_j = x_j - \delta_{j\mathrm{B}} - \upsilon_j \frac{\tau}{\lambda}x_{\mathrm{B}}x_{\mathrm{Cl}} \tag{24-84}$$

explicitly in terms of the liquid-phase molar density ratio of hydrogen chloride x_{H}:

$$-\alpha_{\mathrm{H}}x_{\mathrm{H}} = x_{\mathrm{H}} - \frac{\tau}{\lambda}x_{\mathrm{B}}x_{\mathrm{Cl}} \tag{24-85}$$

Now, rewrite equation (24-85) using results from step 5, and substitute for x_{B} and x_{Cl} via equations (27-83):

$$(\alpha_{\mathrm{H}} + 1)x_{\mathrm{H}} = \frac{\tau}{\lambda}x_{\mathrm{B}}x_{\mathrm{Cl}} = \frac{\tau}{\lambda}(\omega_2 - \omega_3 x_{\mathrm{H}})(\omega_4 - \omega_5 x_{\mathrm{H}}) \tag{24-86}$$

Step 7. Solve equation (24-86) for x_H, which is written using condensed notation in terms of a new set of parameters (i.e., $\xi_1 \rightarrow \xi_3$):

$$\begin{aligned} \xi_1(x_H)^2 + \xi_2 x_H + \xi_3 &= 0 \\ \xi_1 &= \omega_3\omega_5 \\ \xi_2 &= -\omega_3\omega_4 - \omega_2\omega_5 - \frac{\alpha_H + 1}{\tau/\lambda} \\ \xi_3 &= \omega_2\omega_4 \end{aligned} \tag{24-87}$$

One must consider both roots of the quadratic equation for x_H:

$$x_H = \frac{-\xi_2 \pm \sqrt{(\xi_2)^2 - 4\xi_1\xi_3}}{2\xi_1} \tag{24-88}$$

and choose the correct one. For example,

(a) If $(\xi_2)^2 - 4\xi_1\xi_3 < 0$, then both roots for x_H are imaginary and no realistic solution is available. Since all roots for x_H are real, one concludes that

$$(\xi_2)^2 > 4\xi_1\xi_3 \tag{24-89}$$

(b) If $|[(\xi_2)^2 - 4\xi_1\xi_3]^{1/2}| > |\xi_2|$, which occurs if either ξ_1 or ξ_3 is negative (but both can't be negative simultaneously), then one root for x_H is positive and one is negative. In this case, realistic operation of the two-phase CSTR is governed by the positive root, assuming that x_H is not too large to cause $x_B = \omega_2 - \omega_3 x_H$ or $x_{Cl} = \omega_4 - \omega_5 x_H$ to be negative. This situation will never occur because inspection of (24-78) reveals that all the α-parameters are positive. Hence, all the ω-parameters are positive, as well as ξ_1 and ξ_3. Furthermore,

$$0 < 4\xi_1\xi_3 < (\xi_2)^2 \tag{24-90}$$

(c) If $\xi_2 > 0$ and $|[(\xi_2)^2 - 4\xi_1\xi_3]^{1/2}| < |\xi_2|$, then both roots for x_H are negative and no physically realistic solution exits to simulate the performance of the gas–liquid CSTR. Whereas the latter condition is satisfied because ξ_1 and ξ_3 are positive, inspection of (24-87) reveals that ξ_2 is negative.

(d) Performance of the two-phase CSTR is governed by the following conditions:

$$\begin{aligned} \xi_1 \text{ and } \xi_3 &> 0 \\ \xi_2 &< 0 \\ (\xi_2)^2 &> 4\xi_1\xi_3 \end{aligned} \tag{24-91}$$

Hence, both roots for x_H are positive. The correct root is subject to the following constraints on the total outlet gas-phase flow rate, all of the

bulk gas-phase mole fractions, and the other three liquid-phase molar density ratios:

$$\begin{aligned} S &= 1 + \kappa - \sum_j x_j > 0 && j = \text{B,Cl,M,H} \\ x_j &> 0 && j = \text{B,Cl,M} \\ 0 &< y_j < 1 && j = \text{B,Cl,M,H} \end{aligned} \tag{24-92}$$

Step 8. The trial-and-error calculation procedure is summarized below. Time constants, interfacial equilibrium constants, and the inlet flow rate ratio κ have assigned values.

(a) Estimate the value of $S \approx \kappa$. This is not exact because all liquid-phase molar density ratios do not sum to unity.
(b) Calculate the α's, ω's, and ξ's, as indicated in steps 2, 5, and 7, respectively, based on the initial estimate of S.
(c) Solve the quadratic equation for x_H in (24-88), and choose the correct root that satisfies all the constraints listed in (24-92).
(d) Use the correct root for x_H and calculate the other three liquid-phase molar density ratios, as indicated in step 5.
(e) Recalculate the dimensionless outlet gas-phase flow rate S:

$$S = 1 + \kappa - \sum_{j=\text{B,Cl,M,H}} x_j = 1 + \kappa - \omega_2 - \omega_4 - x_H(1 + \omega_1 - \omega_3 - \omega_5) \tag{24-93}$$

and compare this calculation with the initial estimate of S.
(f) If the two values of S are different, then use the one calculated most recently and return to step 8b.
(g) Repeat these iterative calculations until values of S from the two most recent calculations agree or differ by a relative fraction that is within the tolerance specified.

PROBLEMS

24-1. Design a two-phase gas–liquid CSTR for the chlorination of benzene at 55°C by calculating the total volume that corresponds to an operating point where $\tau/\lambda = 500$ on the horizontal axis of the CSTR performance curve in Figure 24-1. The time constant for convective mass transfer in the liquid phase is τ. The time constant for second-order irreversible chemical reaction in the liquid phase is λ. If the liquid benzene feed stream is diluted with an inert, then λ increases. The liquid-phase volumetric flow rate is 5 gal/min. The inlet molar flow rate ratio of chlorine gas to liquid benzene

is 3, the liquid benzene feed stream is diluted by a factor of 2 on a molar basis using an inert hydrocarbon solvent, and the volume fraction of gas bubbles is 0.60 (i.e., 60%). A numerical answer in gallons is required for this problem. (*Note:* 1 gal = 3785.4 mL.)

24-2. Design a two-phase gas–liquid CSTR for the chlorination of benzene at 55°C by calculating the total volume that corresponds to an operating point where $\tau/\lambda = 1000$. The time constant for convective mass transfer in the liquid phase is τ. The time constant for second-order irreversible chemical reaction in the liquid phase is λ. The liquid-phase volumetric flow rate is 10 gal/min. The inlet molar flow rate ratio of chlorine gas to liquid benzene is 2, the liquid benzene feed stream is diluted by a factor of 2 on a molar basis using an inert hydrocarbon solvent, and the volume fraction of gas bubbles is 0.50 (i.e., 50%). A numerical answer is required for this problem.

24-3. Qualitatively sketch the outlet gas-phase mole fraction of chlorine (i.e., Cl_2) and HCl versus $\log(\tau/\lambda)$ in the two-phase CSTR at a constant value of the inlet molar flow rate ratio of chlorine gas to liquid benzene. Put both curves on the same set of axes.

24-4. Calculate the following ratio of liquid-phase binary molecular diffusion coefficients for hydrogen chloride and chlorobenzene in benzene (solvent) at low concentrations of the solute (hydrogen chloride or chlorobenzene): $\mathfrak{D}_{\text{HCl–benzene}}/\mathfrak{D}_{\text{chlorobenzene–benzene}} = ?$ A numerical answer is required for this problem.

24-5. The Stokes–Einstein equation provides an estimate of the binary diffusivity of dilute mixtures of spherical molecules of A in an incompressible Newtonian solvent B. This correlation is applicable to liquids, not gases:

$$\mathfrak{D}_{AB} = \frac{k_{\text{Boltzmann}} T}{6\pi \mu_B R_A}$$

where $k_{\text{Boltzmann}}$ is Boltzmann's constant, T the absolute temperature, μ_B the viscosity of Newtonian solvent B, and R_A the radius of a hydrodynamic shell that surrounds one molecule of A. Is $\mathfrak{D}_{AB}$ a linear function of temperature? Why or why not? *Answer*: No! $\mathfrak{D}_{AB} \approx T/\mu_B(T) \approx T/\exp(E_{Act}/RT)$, where E_{Act} is the activation energy for viscous transport in the liquid phase.

24-6. Provide three separate definitions of the Sherwood number, without using equation format.

24-7. Draw concentration profiles for solubilized chlorine molecules within the mass transfer boundary layer on the liquid side of the gas–liquid interface:

(a) In the presence of a liquid-phase chemical reaction with benzene when the Damkohler number $\Lambda^2 = 250$.

(b) In the presence of a liquid-phase chemical reaction with benzene when the Damkohler number $\Lambda^2 = 50$.

(c) If no reaction occurs.
Put all three concentration profiles on one set of axes, with Cl_2 concentration on the vertical axis and spatial coordinate normal to the gas–liquid interface on the horizontal axis. Identify the positions of the gas–liquid interface and the bulk liquid phase on the horizontal axis.

(d) Estimate the Sherwood number for mass transfer for each of the three cases described above. Numerical answers are required here.

24-8. In the absence of convective mass transfer and chemical reaction, calculate the steady-state liquid-phase mass transfer coefficient that accounts for curvature in the interfacial region for cylindrical liquid–solid interfaces. An example is cylindrical pellets that dissolve and diffuse into a quiescent liquid that surrounds each solid pellet. The appropriate starting point is provided by equation (B) in Table 18.2-2 on page 559 in Bird *et al.* (1960). For one-dimensional diffusion radially outward, the mass transfer equation in cylindrical coordinates reduces to

$$\mathfrak{D}_{AB}\left[\frac{1}{r}\frac{d}{dr}\left(r\frac{dC_A}{dr}\right)\right] = 0$$

Use the following boundary condition at the outer edge of the mass transfer boundary layer in the liquid phase: $C_A = 0$ at $r = r_2$. At the solid–liquid boundary where $r = r_1$, C_A is given by its equilibrium solubility in the liquid. The thickness of the mass transfer boundary layer is $r_2 - r_1$. *Hint:* Think about your experience with heat transfer coefficients because you have used the solution to this problem several times in the past in other courses that focus on heat transfer.

24-9. Baker's yeast is cultured in a continuous-stirred tank. A yeast inoculum is suspended in the nutrient broth within the reactor. The process requires that oxygen be bubbled through the liquid phase, and mass transfer across the gas–liquid interface is necessary to convert the nutrient substrates to cell mass. The rate of cell growth is described adequately by Monod kinetics. Use the methodology discussed in this chapter and design a strategy to determine if it is cost-effective to increase the stirring speed in the reactor. *Hint:* The slowest process is characterized by the longest mass transfer time constant.

Transport Phenomena for Chemical Reactor Design. Laurence A. Belfiore
Copyright © 2003 John Wiley & Sons, Inc.
ISBN: 0-471-20275-4

PART VI

THERMODYNAMICS AND NONISOTHERMAL REACTOR DESIGN

Transport Phenomena for Chemical Reactor Design. Laurence A. Belfiore
Copyright © 2003 John Wiley & Sons, Inc.
ISBN: 0-471-20275-4

25

CLASSICAL IRREVERSIBLE THERMODYNAMICS OF MULTICOMPONENT MIXTURES

The thermodynamics of irreversible processes begins with three basic microscopic transport equations for overall mass (i.e., the equation of continuity), species mass, and linear momentum, and develops a microscopic equation of change for specific entropy. The most important aspects of this development are the terms that represent the rate of generation of entropy and the linear transport laws that result from the fact that entropy generation conforms to a positive-definite quadratic form. The multicomponent mixture contains N components that participate in R independent chemical reactions. Without invoking any approximations, the three basic transport equations are summarized below.

1. The equation of continuity on page 222 represents a balance on overall fluid mass:

$$\frac{\partial \rho}{\partial t} = -\nabla \cdot \rho \mathbf{v} = -\rho \nabla \cdot \mathbf{v} - \mathbf{v} \cdot \nabla \rho \tag{25-1}$$

or

$$\frac{\partial \rho}{\partial t} + \mathbf{v} \cdot \nabla \rho \equiv \frac{D\rho}{Dt} = -\rho \nabla \cdot \mathbf{v} \tag{25-2}$$

2. The mass balance for a particular component in the mixture, given by (9-20), has been referred to previously as the mass transfer equation because it represents the microscopic starting point for all mass transfer problems:

$$\rho \left(\frac{\partial \omega_i}{\partial t} + \mathbf{v} \cdot \nabla \omega_i \right) \equiv \rho \frac{D\omega_i}{Dt} = -\nabla \cdot \mathbf{j}_i + \sum_{j=1}^{R} \upsilon_{ij} (\mathrm{MW}_i) \mathfrak{R}_j$$

$$= -\nabla \cdot \mathbf{j}_i + r_i \tag{25-3}$$

where $r_i = \mathrm{MW}_i \sum_{j=1}^{R} \upsilon_{ij} \mathfrak{R}_j$ represents the rate of production of the mass of species i due to all chemical reactions.

3. The equation of motion, given by (8-36), represents a vector force balance or a balance on the rate of linear momentum:

$$\rho \left(\frac{\partial \mathbf{v}}{\partial t} + \mathbf{v} \cdot \nabla \mathbf{v} \right) \equiv \rho \frac{D\mathbf{v}}{Dt} = -\nabla p - \nabla \cdot \tau + \sum_{i=1}^{N} \rho \omega_i \mathbf{g}_i \qquad (25\text{-}4)$$

where $\mathbf{g}_i$ is the external force per unit mass that acts specifically on component i in the mixture, and the last term on the right side of equation (25-4) represents the sum of all external forces acting on the fluid (i.e., the summation includes all species in the mixture). In equations (25-2), (25-3), and (25-4), the sum of the unsteady-state and convective contributions is combined into the substantial derivative, D/Dt. This corresponds to the accumulation rate process in a dynamic control volume that moves with the local fluid velocity at every point on the surface of the control volume.

25-1 STRATEGY TO ANALYZE NONEQUILIBRIUM SYSTEMS

Now that the basic tools are available to begin the development of the thermodynamics of irreversible processes, the overall strategy is outlined as follows:

Step 1. Use the equations of continuity and motion to develop an equation of change for kinetic energy.

Step 2. Use the total differential of specific enthalpy in terms of its natural variables, via Legendre transformation of the internal energy from classical thermodynamics, to re-express the pressure gradient in the momentum balance in terms of enthalpy, entropy, and mass fractions. Then, write the equation of change for kinetic energy in terms of specific enthalpy and entropy.

Step 3. Use the first law of thermodynamics in differential form, the equation of continuity, and the mass transfer equation to develop an equation of change for internal energy.

Step 4. Add the equations of change for internal and kinetic energies to obtain the equation of change for total energy.

Step 5. In the equation of change for total energy, identify convective fluxes of internal and kinetic energies, and work terms due to (a) pressure forces, (b) viscous forces, and (c) the external force field. There are no sources or sinks of total energy, even though there is an irreversible exchange between mechanical and thermal energies. Furthermore, since there is no molecular flux of kinetic energy, the remaining terms in the total energy balance are identified as the molecular flux of thermal energy.

Step 6. Rearrange the expression for the molecular flux of thermal energy to obtain the equation of change for specific entropy.

Step 7. Manipulate the equation of change for specific entropy, via definitions of convective and molecular entropy fluxes, to identify all terms that correspond to entropy generation. These terms appear as products of fluxes and forces.

Step 8. Postulate linear relations between these fluxes and forces that obey the Curie restriction, and demonstrate that entropy generation can be expressed as a positive-definite quadratic form.

Step 9. Use matrix concepts for positive-definite quadratic forms and the Onsager reciprocal relations to develop expressions for the diffusional mass flux of component i and the molecular flux of thermal energy in binary mixtures.

Step 10. Use the expression for diffusional mass flux in binary mixtures to derive the Stokes–Einstein diffusion equation for liquid-phase diffusivities.

Step 11. Use the equation of change for internal energy and the molecular flux of thermal energy to develop the appropriate thermal energy balance for multicomponent reactive mixtures.

Step 12. Use the thermal energy and mass balances for multicomponent reactive mixtures to analyze diffusion and chemical reaction in nonisothermal catalytic pellets.

25-2 MICROSCOPIC EQUATION OF CHANGE FOR KINETIC ENERGY

The kinetic energy per unit volume of fluid is

$$\tfrac{1}{2}\rho v^2 = \tfrac{1}{2}\rho \mathbf{v}\cdot\mathbf{v} \tag{25-5}$$

In every equation of change, one of the terms on the left side represents the accumulation rate process based on a stationary volume element. Hence, one seeks an expression for the accumulation of kinetic energy per unit volume of fluid in a stationary control volume:

$$\frac{1}{2}\frac{\partial(\rho\mathbf{v}\cdot\mathbf{v})}{\partial t} = \frac{1}{2}\mathbf{v}\cdot\mathbf{v}\frac{\partial\rho}{\partial t} + \rho\mathbf{v}\cdot\frac{\partial\mathbf{v}}{\partial t} \tag{25-6}$$

where the product rule is applied to the partial time derivative operator. Minor manipulation of (25-6),

$$\frac{1}{2}\frac{\partial(\rho v^2)}{\partial t} = \frac{1}{2}v^2\frac{\partial\rho}{\partial t} + \mathbf{v}\cdot\rho\frac{\partial\mathbf{v}}{\partial t} \tag{25-7}$$

suggests that the accumulation of kinetic energy can be obtained via the equation of continuity and the scalar dot product of the velocity vector with the equation of motion. The appropriate substitutions are

$$\frac{\partial\rho}{\partial t} = -\nabla\cdot\rho\mathbf{v} \qquad \text{(equation of continuity)} \tag{25-8a}$$

$$\rho\frac{\partial \mathbf{v}}{\partial t} = -\rho\mathbf{v}\cdot\nabla\mathbf{v} - \nabla p - \nabla\cdot\tau + \sum_{i=1}^{N}\rho\omega_i\mathbf{g}_i \qquad \text{(equation of motion)} \tag{25-8b}$$

It is necessary to introduce the following vector-tensor identity for convective momentum flux (i.e., $\rho\mathbf{v}\cdot\nabla\mathbf{v}$) in the equation of motion (see Problem 8-7):

$$\mathbf{v}\cdot\nabla\mathbf{v} = \tfrac{1}{2}\nabla v^2 - \mathbf{v}\times(\nabla\times\mathbf{v}) \tag{25-9}$$

Now, one of the terms that must be considered when one constructs the scalar dot product of $\mathbf{v}$ with convective momentum flux in the equation of motion is

$$\mathbf{v}\cdot[\mathbf{v}\times(\nabla\times\mathbf{v})] = 0 \tag{25-10}$$

because the scalar triple product of three vectors vanishes when two of the vectors are identical. The scalar triple product is equivalent to the volume enclosed by six parallelogram planes where three vectors from a common origin coincide with three sides of the three-dimensional structure. When two of these vectors are the same, the structure reduces to one of the parallelogram planes with no volume. Hence, the triple product vanishes, and

$$\mathbf{v}\cdot(\mathbf{v}\cdot\nabla\mathbf{v}) = \tfrac{1}{2}\mathbf{v}\cdot\nabla v^2 \tag{25-11}$$

The equation of change for kinetic energy, which employs the equations of continuity and motion, is

$$\frac{1}{2}\frac{\partial(\rho v^2)}{\partial t} = -\frac{1}{2}v^2\nabla\cdot\rho\mathbf{v} - \frac{1}{2}\rho\mathbf{v}\cdot\nabla v^2 - \mathbf{v}\cdot\nabla p - \mathbf{v}\cdot(\nabla\cdot\tau) + \sum_{i=1}^{N}\rho\omega_i\mathbf{v}\cdot\mathbf{g}_i \tag{25-12}$$

where the first and second terms on the right side of equation (25-12) represent the divergence of the product of $\frac{1}{2}v^2$ and $\rho\mathbf{v}$ via the product rule. When these terms are combined, the equation of change for kinetic energy is

$$\frac{1}{2}\frac{\partial(\rho v^2)}{\partial t} = -\nabla\cdot\rho\mathbf{v}(\tfrac{1}{2})v^2 - \mathbf{v}\cdot\nabla p - \mathbf{v}\cdot(\nabla\cdot\tau) + \mathbf{v}\cdot\sum_{i=1}^{N}\rho\omega_i\mathbf{g}_i \tag{25-13}$$

This completes step 1 in the 12-step strategy outlined in Section 25-1.

25-3 RE-EXPRESSED EQUATION OF CHANGE FOR KINETIC ENERGY

The next task is to replace the pressure gradient in equation (25-13) via the total differential of specific enthalpy dh, where h is written in terms of its natural

thermodynamic variables. These variables are the specific entropy s, pressure p, and $N-1$ mass fractions ω_i for an N-component mixture. The total differential of h is:

$$dh = T\,ds + \frac{1}{\rho}dp + \sum_{i=1}^{N-1} \varphi_i\, d\omega_i \tag{25-14}$$

where the summation includes the first $N-1$ species whose mass fractions represent independent variables, and

$$\varphi_i = \frac{\mu_i}{\mathrm{MW}_i} - \frac{\mu_\mathrm{N}}{\mathrm{MW}_N} \tag{25-15}$$

μ_i is the chemical potential or partial molar Gibbs free energy of species i and MW_i represents its molecular weight. The total differential of specific enthalpy, given by equation (25-14), contains information that is equivalent to the first law of thermodynamics for the total differential of the internal energy. A Legendre transformation from internal energy to enthalpy is performed without loss of thermodynamic information about the system. The coefficient φ_i represents the mass fraction derivative of the specific Gibbs free energy when the following variables remain constant; T, p, and all other mass fractions ω_j, except ω_i and ω_N. Molecular weights are required to convert partial molar properties to partial specific properties. Equation (25-15) represents a classic thermodynamic result when one seeks an expression for the mass fraction derivative of an intensive thermodynamic state function in terms of the mole number derivative of the corresponding extensive state function at constant temperature and pressure (see Section 26-2). If one considers a rectangular coordinate system and adds the following vector quantities:

1. The unit vector in the x direction multiplied by the partial derivative of equation (25-14) with respect to x,
2. The unit vector in the y direction multiplied by the partial derivative of equation (25-14) with respect to y,
3. The unit vector in the z direction multiplied by the partial derivative of equation (25-14) with respect to z,

then the following result is obtained using vector notation:

$$\nabla h = T\nabla s + \frac{1}{\rho}\nabla p + \sum_{i=1}^{N-1} \varphi_i \nabla \omega_i \tag{25-16}$$

In summary, the total differential of any thermodynamic property can be written in vector notation by replacing differentials with gradient operators. This is convenient because one can rearrange (25-16) to solve for the pressure gradient:

$$\nabla p = \rho\nabla h - \rho T\nabla s - \rho \sum_{i=1}^{N-1} \varphi_i \nabla \omega_i \tag{25-17}$$

construct the scalar dot product of $\mathbf{v}$ with ∇p:

$$\mathbf{v} \cdot \nabla p = \rho \mathbf{v} \cdot \nabla h - \rho T \mathbf{v} \cdot \nabla s - \rho \mathbf{v} \cdot \sum_{i=1}^{N-1} \varphi_i \nabla \omega_i \tag{25-18}$$

and substitute (25-18) into the equation of change for kinetic energy, given by (25-13). The final result is

$$\frac{1}{2}\frac{\partial(\rho v^2)}{\partial t} = -\nabla \cdot \rho \mathbf{v}(\tfrac{1}{2})v^2 - \rho \mathbf{v} \cdot \nabla h + \rho T \mathbf{v} \cdot \nabla s + \rho \mathbf{v} \cdot \sum_{i=1}^{N-1} \varphi_i \nabla \omega_i$$

$$- \mathbf{v} \cdot (\nabla \cdot \tau) + \sum_{i=1}^{N} \rho \omega_i \mathbf{v} \cdot \mathbf{g}_i \tag{25-19}$$

It is important to remember that the summation in the fourth term on the right side of (25-19) includes the first $N-1$ components, whereas the summation in the last term on the right side includes all components in the mixture. This completes the second step in the 12-step procedure outlined in Section 25-1.

25-4 MICROSCOPIC EQUATION OF CHANGE FOR INTERNAL ENERGY VIA THE FIRST LAW OF THERMODYNAMICS

The internal energy per unit volume of fluid is ρu, where u is the specific internal energy. Following the methodology in Section 25-2, the left side of the microscopic equation of change for internal energy, with units of energy per volume per time, is

$$\frac{\partial(\rho u)}{\partial t} = \rho \frac{\partial u}{\partial t} + u \frac{\partial \rho}{\partial t} \tag{25-20}$$

where the product rule is applied to the partial time derivative operator. The equation of continuity is used to replace $\partial\rho/\partial t$ in (25-20), and the differential form of the first law,

$$du = T\,ds - p\,d(\tfrac{1}{\rho}) + \sum_{i=1}^{N-1} \varphi_i\,d\omega_i \tag{25-21}$$

is employed to calculate $\partial u/\partial t$ as follows:

$$\frac{\partial u}{\partial t} = T\frac{\partial s}{\partial t} + \frac{p}{\rho^2}\frac{\partial \rho}{\partial t} + \sum_{i=1}^{N-1} \varphi_i \frac{\partial \omega_i}{\partial t} \tag{25-22}$$

Once again, the equation of continuity is used to replace $\partial\rho/\partial t$ in (25-22), and the mass transfer equation for species i replaces $\partial\omega_i/\partial t$. The substitutions are

$$\begin{aligned} \frac{\partial\rho}{\partial t} &= -\nabla\cdot\rho\mathbf{v} \\ \rho\frac{\partial\omega_i}{\partial t} &= -\rho\mathbf{v}\cdot\nabla\omega_i - \nabla\cdot\mathbf{j}_i + r_i \end{aligned} \tag{25-23}$$

The final form of the microscopic equation of change for internal energy is

$$\begin{aligned} \frac{\partial(\rho u)}{\partial t} = \rho T\frac{\partial s}{\partial t} - \frac{p}{\rho}\nabla\cdot\rho\mathbf{v} - \rho\mathbf{v}\cdot\sum_{i=1}^{N-1}\varphi_i\nabla\omega_i \\ - \sum_{i=1}^{N-1}\varphi_i\nabla\cdot\mathbf{j}_i + \sum_{i=1}^{N-1}\varphi_i r_i - u\nabla\cdot\rho\mathbf{v} \end{aligned} \tag{25-24}$$

where all of the summations include the first $N-1$ components in the mixture. This completes step 3 of the 12-step strategy outlined in Section 25-1.

25-5 MICROSCOPIC EQUATION OF CHANGE FOR TOTAL ENERGY

The fourth step of the general strategy in Section 25-1 is to add the microscopic equations of change given by (25-19) and (25-24). The kinetic energy and internal energy equations are repeated here, for comparison:

$$\begin{aligned} \frac{1}{2}\frac{\partial(\rho v^2)}{\partial t} = -\nabla\cdot\rho\mathbf{v}\left(\tfrac{1}{2}\right)v^2 - \rho\mathbf{v}\cdot\nabla h + \rho T\mathbf{v}\cdot\nabla s + \rho\mathbf{v}\cdot\sum_{i=1}^{N-1}\varphi_i\nabla\omega_i \\ - \mathbf{v}\cdot(\nabla\cdot\tau) + \sum_{i=1}^{N}\rho\omega_i\mathbf{v}\cdot\mathbf{g}_i \end{aligned} \tag{25-25}$$

$$\begin{aligned} \frac{\partial(\rho u)}{\partial t} = \rho T\frac{\partial s}{\partial t} - \frac{p}{\rho}\nabla\cdot\rho\mathbf{v} - \rho\mathbf{v}\cdot\sum_{i=1}^{N-1}\varphi_i\nabla\omega_i - \sum_{i=1}^{N-1}\varphi_i\nabla\cdot\mathbf{j}_i \\ + \sum_{i=1}^{N-1}\varphi_i r_i - u\nabla\cdot\rho\mathbf{v} \end{aligned} \tag{25-26}$$

Notice that the fourth term on the right side of (25-25) cancels with the third term on the right side of (25-26). Application of the following vector identity for scalar a and vector $\mathbf{b}$ allows one to combine a few terms in (25-25) and (25-26):

$$\nabla\cdot a\mathbf{b} = a\nabla\cdot\mathbf{b} + \mathbf{b}\cdot\nabla a \tag{25-27}$$

This is the product rule for the divergence of the product of scalar and a vector. The thermodynamic relation between specific enthalpy and specific internal energy via Legendre transformation is $h = u + p/\rho$ (see equation 29-20). Hence, the second term on the right side of (25-25) and the second and sixth terms on the right side of (25-26) can be combined as follows:

$$-\rho\mathbf{v}\cdot\nabla\left(u+\frac{p}{\rho}\right)-\frac{p}{\rho}\nabla\cdot\rho\mathbf{v}-u\nabla\cdot\rho\mathbf{v}=-\nabla\cdot\rho\mathbf{v}\left(u+\frac{p}{\rho}\right)$$
$$=-\nabla\cdot\rho\mathbf{v}u-\nabla\cdot p\mathbf{v} \qquad (25\text{-}28)$$

where the first term on the far right side of (25-28) (i.e., $-\nabla\cdot\rho\mathbf{v}u$) represents the net input of internal energy in a stationary control volume via convective flux, and the second term on the far right side of (25-28), including the negative sign, is the rate of work done on the system by pressure forces. The following vector-tensor identity is useful to isolate the rate of work done on the fluid by viscous forces:

$$\nabla\cdot(\tau\cdot\mathbf{v})=\mathbf{v}\cdot(\nabla\cdot\tau)+\tau\blacklozenge\nabla\mathbf{v} \qquad (25\text{-}29)$$

This is a statement of the product rule for the divergence of the vector dot product of a tensor with a vector, which is valid when the tensor is symmetric. In other words, $\tau = \tau^{\mathrm{T}}$, where τ^{T} is the transpose of the viscous stress tensor. Symmetry of the viscous stress tensor is a controversial topic in fluid dynamics, but one that is invariably assumed. $\blacklozenge$ is short-hand notation for the scalar double-dot product of two tensors. If the viscous stress tensor is not symmetric, then τ must be replaced by τ^{T} in the second term on the right side of the (25-29). The left side of (25-29), with a negative sign, corresponds to the rate of work done on the fluid by viscous forces. The microscopic equation of change for total energy is written in the following form:

$$\frac{\partial[\rho\left(\frac{1}{2}v^2+u\right)]}{\partial t}=-\nabla\cdot\rho\mathbf{v}\left(\tfrac{1}{2}v^2+u\right)-\nabla\cdot p\mathbf{v}-\nabla\cdot(\tau\cdot\mathbf{v})$$
$$+\sum_{i=1}^{N}\rho\omega_i\mathbf{v}\cdot\mathbf{g}_i+\rho T\frac{\partial s}{\partial t}+\rho T\mathbf{v}\cdot\nabla s$$
$$-\sum_{i=1}^{N-1}\varphi_i\nabla\cdot\mathbf{j}_i+\sum_{i=1}^{N-1}\varphi_i r_i+\tau\blacklozenge\nabla\mathbf{v} \qquad (25\text{-}30)$$

Obviously, the left side of this equation represents the accumulation of kinetic and internal energies within a stationary control volume. The first term on the right side of (25-30) corresponds to the net input of kinetic and internal energies via convective flux. Gauss's law states that the volume integral of $-\nabla\cdot$ **vector** is equivalent to $-\mathbf{n}\cdot$ **vector** integrated over the surface that surrounds the control volume, where $\mathbf{n}$ is a unit normal vector on the surface that extends outward or away from the control volume. For the first term on the right side of the total energy equation, the vector is $\rho\mathbf{v}(\frac{1}{2}v^2+u)$, which represents the convective flux

of kinetic and internal energies because $\frac{1}{2}v^2 + u$ are the kinetic and internal energies per unit mass, and $\rho\mathbf{v}$ is the total mass flux vector due solely to convection. Hence, it is always possible to construct the convective flux of any quantity as the product of $\rho\mathbf{v}$ and that quantity per unit mass. Then, the divergence of that flux, including a negative sign, represents the net input across the surface of the control volume via convective transport. The second and third terms on the right side of the total energy equation, given by (25-30), represent the rate of work done on the system by pressure and viscous forces, respectively. The rate of work done on the system by the external field is $\sum_{i=1}^{N} \rho\omega_i \mathbf{v}_i \cdot \mathbf{g}_i$, which includes all components in the mixture. This is related to the fourth term on the right side of (25-30) via the definition of diffusional mass flux $\mathbf{j}_i$ with respect to the mass-average velocity of the mixture $\mathbf{v}$ (see equation 9-8):

$$\mathbf{j}_i = \rho\omega_i(\mathbf{v}_i - \mathbf{v}) \tag{25-31}$$

This relation is employed to re-express $\rho\omega_i\mathbf{v}$ in the fourth term on the right side of (25-30) and isolate the rate of work done on the system by the external field, which, in general, could act differently on each component in the mixture. Equation (25-30) can be written as follows:

$$\begin{aligned}\frac{\partial[\rho(\frac{1}{2}v^2+u)]}{\partial t} &= -\nabla\cdot\rho\mathbf{v}\left(\frac{1}{2}v^2+u\right) - \nabla\cdot p\mathbf{v} - \nabla\cdot(\tau\cdot\mathbf{v}) \\ &\quad + \sum_{i=1}^{N}\rho\omega_i\mathbf{v}_i\cdot\mathbf{g}_i + \rho T\frac{\partial s}{\partial t} + \rho T\mathbf{v}\cdot\nabla s - \sum_{i=1}^{N-1}\varphi_i\nabla\cdot\mathbf{j}_i \\ &\quad + \sum_{i=1}^{N-1}\varphi_i r_i + \tau\blacklozenge\nabla\mathbf{v} - \sum_{i=1}^{N}\mathbf{j}_i\cdot\mathbf{g}_i \end{aligned} \tag{25-32}$$

Now, the equation of change for kinetic and internal energies contains the following elements:

1. The accumulation rate process via the left side of (25-32)
2. The contribution from bulk fluid flow via the convective flux of kinetic and internal energies, which is contained in the first term on the right side of (25-32)
3. The appropriate work-related terms due to pressure forces, viscous forces, and the external force field, the latter being specific to each component in the mixture

25-6 IDENTIFICATION OF THE MOLECULAR FLUX OF THERMAL ENERGY IN THE EQUATION OF CHANGE FOR TOTAL ENERGY

It is implicitly assumed that there are no sources or sinks of the sum of kinetic and internal energies. The second law of thermodynamics states that all of the

kinetic energy which is degraded subsequently appears in the form of thermal (i.e., internal) energy, but the reverse would lead to the existence of a perpetual motion machine of the second kind. Hence, there are interconversions between kinetic and internal energies, and the second law of thermodynamics dictates the path that the system must follow during this energy exchange. There is one transport mechanism that has not been discussed for internal energy via the development presented above. The molecular flux of thermal energy, which is better known as *conductive energy flux*, is a major contributor to the equation of change for internal energy. This is not a concern for kinetic energy because there is no molecular flux of kinetic energy. In any microscopic equation of change, one expects to find a term on the right side that has the form $-\nabla \cdot$ (**molecular flux**) when a molecular flux exists for the property that is being balanced. There are no contributions from molecular flux when the balance is performed on overall fluid mass and kinetic energy. For the internal energy and total energy equations, the contribution from molecular flux can be written very concisely as $-\nabla \cdot \mathbf{q}$, where $\mathbf{q}$ represents the conductive flux of thermal energy in a multicomponent system. One of the objectives of this chapter is to develop an equation for $\mathbf{q}$, where the leading term conforms to Fourier's law of heat conduction (see Section 25-11). The equation of change for total energy,

$$\begin{aligned}\frac{\partial[\rho(\frac{1}{2}v^2+u)]}{\partial t} &= -\nabla\cdot\rho\mathbf{v}\left(\frac{1}{2}v^2+u\right)-\nabla\cdot p\mathbf{v}-\nabla\cdot(\tau\cdot\mathbf{v})\\ &\quad+\sum_{i=1}^{N}\rho\omega_i\mathbf{v}_i\cdot\mathbf{g}_i+\rho T\frac{\partial s}{\partial t}+\rho T\mathbf{v}\cdot\nabla s-\sum_{i=1}^{N-1}\varphi_i\nabla\cdot\mathbf{j}_i\\ &\quad+\sum_{i=1}^{N-1}\varphi_i r_i+\tau\blacklozenge\nabla\mathbf{v}-\sum_{i=1}^{N}\mathbf{j}_i\cdot\mathbf{g}_i \qquad (25\text{-}33)\end{aligned}$$

is rewritten in its final form where the last six terms of (25-33) are identified as the contribution from conductive energy flux in a multicomponent chemically reactive mixture:

$$\begin{aligned}\frac{\partial[\rho(\frac{1}{2}v^2+u)]}{\partial t} &= -\nabla\cdot\rho\mathbf{v}\left(\frac{1}{2}v^2+u\right)-\nabla\cdot p\mathbf{v}-\nabla\cdot(\tau\cdot\mathbf{v})\\ &\quad+\sum_{i=1}^{N}\rho\omega_i\mathbf{v}_i\cdot\mathbf{g}_i-\nabla\cdot\mathbf{q} \qquad (25\text{-}34)\end{aligned}$$

25-7 EQUATION OF CHANGE FOR ENTROPY

The most important aspect of this development of the microscopic equations of change for kinetic, internal, and total energies is the identification of conductive energy flux, which allows one to construct an equation of change for specific

entropy. Since a comparison of equations (25-33) and (25-34) yields:

$$-\nabla \cdot \mathbf{q} = \rho T \frac{\partial s}{\partial t} + \rho T \mathbf{v} \cdot \nabla s - \sum_{i=1}^{N-1} \varphi_i \nabla \cdot \mathbf{j}_i + \sum_{i=1}^{N-1} \varphi_i r_i + \tau \blacklozenge \nabla \mathbf{v} - \sum_{i=1}^{N} \mathbf{j}_i \cdot \mathbf{g}_i \tag{25-35}$$

which satisfies the fifth step in the strategy of Section 25-1, one can rearrange this expression and calculate the substantial derivative of specific entropy as follows:

$$\rho T \left(\frac{\partial s}{\partial t} + \mathbf{v} \cdot \nabla s \right) \equiv \rho T \frac{Ds}{Dt} = -\nabla \cdot \mathbf{q} - \tau \blacklozenge \nabla \mathbf{v} + \sum_{i=1}^{N} \mathbf{j}_i \cdot \mathbf{g}_i + \sum_{i=1}^{N-1} \varphi_i (\nabla \cdot \mathbf{j}_i - r_i) \tag{25-36}$$

where the first summation in equation (25-36) includes all components and the second summation includes the first $N - 1$ components whose mass fractions are included in the group of independent variables for intensive thermodynamic state functions. This expression for Ds/Dt agrees with the principles of classical thermodynamics for multicomponent systems and completes step 6 in Section 25-1.

25-8 RATE OF ENTROPY PRODUCTION IN MULTICOMPONENT SYSTEMS WITH CHEMICAL REACTION

The convective flux of entropy is given by $\rho \mathbf{v} s$, where $\mathbf{v}$ is the mass-average velocity of the mixture. The molecular flux of entropy with respect to $\mathbf{v}$ is defined by

$$\sigma = \frac{1}{T} \left(\mathbf{q} - \sum_{i=1}^{N-1} \varphi_i \mathbf{j}_i \right) \tag{25-37}$$

where the summation includes the first $N - 1$ components. The definition of the rate of entropy production per unit volume, s_G, is

$$\rho \frac{Ds}{Dt} = -\nabla \cdot \sigma + s_G \tag{25-38}$$

Hence, it is necessary to proceed as follows to obtain an expression for s_G:

Step 1. Insert the molecular flux of entropy given by (25-37) into the defining equation for entropy production [i.e., (25-38)]:

$$\rho \frac{Ds}{Dt} = -\nabla \cdot \left[\frac{1}{T} \left(\mathbf{q} - \sum_{i=1}^{N-1} \varphi_i \mathbf{j}_i \right) \right] + s_G \tag{25-39}$$

Step 2. Perform the vector mathematics required in equation (25-39), which involves the divergence of the product of a vector and a scalar:

$$-\nabla \cdot \left(\frac{1}{T}\mathbf{q}\right) = -\frac{1}{T}\nabla \cdot \mathbf{q} + \frac{1}{T^2}\mathbf{q} \cdot \nabla T \tag{25-40}$$

$$\nabla \cdot \left(\frac{1}{T}\sum_{i=1}^{N-1}\varphi_i \mathbf{j}_i\right) = \frac{1}{T}\sum_{i=1}^{N-1}\varphi_i \nabla \cdot \mathbf{j}_i + \frac{1}{T}\sum_{i=1}^{N-1}\mathbf{j}_i \cdot \nabla\varphi_i - \frac{1}{T^2}\nabla T \cdot \sum_{i=1}^{N-1}\varphi_i \mathbf{j}_i \tag{25-41}$$

Step 3. Compare the equation of change for specific entropy, given by (25-36), with equations (25-39), (25-40), and (25-41), after the defining equation for entropy production [i.e., (25-39)] is multiplied by temperature T:

$$\rho T\frac{Ds}{Dt} = \begin{cases} -\nabla \cdot \mathbf{q} - \tau \blacklozenge \nabla \mathbf{v} + \displaystyle\sum_{i=1}^{N}\mathbf{j}_i \cdot \mathbf{g}_i + \sum_{i=1}^{N-1}\varphi_i(\nabla \cdot \mathbf{j}_i - r_i) & \text{(25-42}a\text{)} \\ -\nabla \cdot \mathbf{q} + \dfrac{1}{T}\mathbf{q} \cdot \nabla T + \displaystyle\sum_{i=1}^{N-1}\varphi_i \nabla \cdot \mathbf{j}_i + \sum_{i=1}^{N-1}\mathbf{j}_i \cdot \nabla\varphi_i - \dfrac{1}{T}\nabla T \cdot \displaystyle\sum_{i=1}^{N-1}\varphi_i \mathbf{j}_i + T s_G & \text{(25-42}b\text{)} \end{cases}$$

Step 4. Identify the rate of entropy production per unit volume via comparison of equations (25-42*a*) and (25-42*b*):

$$Ts_G = -\tau \blacklozenge \nabla \mathbf{v} + \sum_{i=1}^{N}\mathbf{j}_i \cdot \mathbf{g}_i - \sum_{i=1}^{N-1}\varphi_i r_i - \frac{1}{T}\mathbf{q} \cdot \nabla T - \sum_{i=1}^{N-1}\mathbf{j}_i \cdot \nabla\varphi_i + \frac{1}{T}\nabla T \cdot \sum_{i=1}^{N-1}\varphi_i \mathbf{j}_i \tag{25-43}$$

This final expression for s_G is divided by temperature T, rearranged, and presented in a classic form that suggests several different products of fluxes and forces:

$$s_G = -\sum_{i=1}^{N-1} r_i \frac{\varphi_i}{T} - \left(\mathbf{q} - \sum_{i=1}^{N-1}\varphi_i \mathbf{j}_i\right) \cdot \frac{1}{T^2}\nabla T - \sum_{i=1}^{N-1}\mathbf{j}_i \cdot \frac{1}{T}\nabla\varphi_i + \left(\sum_{i=1}^{N-1}\mathbf{j}_i \cdot \frac{\mathbf{g}_i}{T}\right) + \mathbf{j}_N \cdot \frac{\mathbf{g}_N}{T} - \tau \blacklozenge \frac{\nabla \mathbf{v}}{T} \tag{25-44}$$

where all of the sums in equation (25-44) include the first $N-1$ components in the mixture. The rate of entropy production per unit volume applies, in general, to multicomponent mixtures with chemical reaction. It can be simplified for pure fluids (i.e., $N=1$) by neglecting all terms in equation (25-44) that contain diffusional mass fluxes and summations that span the range $1 \leq i \leq N-1$. By definition of the mass-average velocity $\mathbf{v}$ of the mixture, the diffusional mass flux of a pure component with respect to $\mathbf{v}$ is zero. Furthermore, $\varphi_i = 0$ when $i=1$ and $N=1$ for pure fluids (i.e., see equation 25-15). Hence, the rate of entropy production per unit volume for a pure fluid is

$$s_G = -\mathbf{q} \cdot \frac{1}{T^2} \nabla T - \tau \blacklozenge \frac{\nabla \mathbf{v}}{T} \tag{25-45}$$

which is the solution to Problem 11D.1 in Bird *et al.* (2002, pp. 372–373). Notice that velocity and temperature gradients, which give rise to molecular fluxes of momentum and thermal energy, lead to entropy generation for irreversible transport processes in pure fluids. For ideal fluids that exhibit no dissipative processes due to vanishingly small viscosity (i.e., $\mu \approx 0$) and thermal conductivity (i.e., k ≈ 0), velocity and temperature gradients do not generate entropy because $\tau = 0$ and $\mathbf{q} = 0$. Since $s_G = 0$ and the molecular flux of entropy vanishes (i.e., $\sigma = 0$), the equation of change for entropy of an ideal fluid is $Ds/Dt = 0$, which implies that there is no change in the entropy of an ideal fluid, from the viewpoint of an observer in a control volume that moves at the local fluid velocity. All of these comments about ideal fluids based on the microscopic description of irreversible thermodynamics are consistent with the steady-state isentropic (i.e., ideal) Bernoulli equation at the macroscopic level.

The definition of diffusional mass flux $\mathbf{j}_i$ with respect to the mass-average velocity $\mathbf{v}$ of the mixture was stated in equation (25-31) as:

$$\mathbf{j}_i = \rho \omega_i (\mathbf{v}_i - \mathbf{v}) \tag{25-46}$$

If this expression is summed over all N components in the mixture, then:

$$\sum_{i=1}^{N} \mathbf{j}_i = \left(\sum_{i=1}^{N} \rho \omega_i \mathbf{v}_i \right) - \rho \mathbf{v} \sum_{i=1}^{N} \omega_i = \rho \left[\left(\sum_{i=1}^{N} \omega_i \mathbf{v}_i \right) - \mathbf{v} \right] = 0 \tag{25-47}$$

based on the definition of the mass-average velocity of the mixture and the fact that all the mass fractions sum to unity (i.e., $\sum \omega_i = 1$). In other words, the mass-average velocity $\mathbf{v}$ is defined such that all of the diffusional mass fluxes with respect to $\mathbf{v}$ sum to zero. This is convenient because

$$\mathbf{j}_N = -\sum_{i=1}^{N-1} \mathbf{j}_i \tag{25-48}$$

where the summation includes the first $N-1$ components in the mixture. Now, the rate of entropy production per unit volume for multicomponent mixtures,

given by equation (25-44), can be re-expressed as;

$$s_G = -\sum_{i=1}^{N-1} r_i \frac{\varphi_i}{T} - \left(\mathbf{q} - \sum_{i=1}^{N-1} \varphi_i \mathbf{j}_i\right) \cdot \frac{1}{T^2} \nabla T$$
$$- \sum_{i=1}^{N-1} \mathbf{j}_i \cdot \frac{1}{T} [\nabla \varphi_i + (\mathbf{g}_N - \mathbf{g}_i)] - \tau \blacklozenge \frac{\nabla \mathbf{v}}{T} \tag{25-49}$$

This is the final expression for s_G and completes objective 7 stated in Section 25-1. The remaining discussion about the thermodynamics of irreversible processes is based on this form for s_G. Obviously, entropy generation is a scalar quantity which can be written generically as

$$s_G = \sum_{i=1}^{2N} (\text{flux})_i (\text{force})_i \tag{25-50}$$

where the driving forces and their corresponding tensorial ranks are summarized in Table 25-1. The first driving force in this table, (ϕ_i / T), which is essentially a chemical potential difference, has a tensorial rank of zero because it is a scalar. The second and third driving forces in Table 25-1 [i.e., temperature gradient, $(1/T^2)\nabla T$, and modified chemical potential gradient in the presence of an external field, $(1/T)(\nabla \varphi_i + (\mathbf{g}_N - \mathbf{g}_i))$] have a tensorial rank of 1 because they are vectors. The fourth driving force, $\nabla \mathbf{v}/T$, has a tensorial rank of 2 because the velocity gradient is a second-rank tensor. For a mixture of N components, there are actually $2N$ different driving forces which generate entropy because the first and third entries in Table 25-1 are written for the first $N - 1$ components. There are $2N$ different fluxes that generate entropy, written below in Table 25-2 in the same order as their corresponding driving forces in Table 25-1.

Entropy generation is a scalar quantity, which is consistent with the following observations:

1. Zeroth-rank tensor (i.e., scalar) fluxes and forces are simply multiplied.

TABLE 25-1 Driving Forces and Their Tensorial Rank[a]

Force		Rank
φ_i / T	$1 \le i \le N-1$	0
$(1/T^2)\nabla T$		1
$(1/T)[\nabla \varphi_i + (\mathbf{g}_N - \mathbf{g}_i)]$	$1 \le i \le N-1$	1
$\nabla \mathbf{v}/T$		2

[a]Forces lead to entropy generation in a chemically reactive mixture of N components.

TABLE 25-2 Fluxes and Their Tensorial Rank[a]

Flux		Rank
$-r_i$	$1 \le i \le N-1$	0
$-\mathbf{q} - \sum_{i=1}^{N-1} \varphi_i \mathbf{j}_i$		1
$-\mathbf{j}_i$	$1 \le i \le N-1$	1
$-\tau$		2

[a]Fluxes lead to entropy generation in a chemically reactive mixture of N components.

2. First-rank tensor (i.e., vector) fluxes and forces are contracted via the scalar dot product $\bullet$.
3. Second-rank tensor fluxes (τ) and forces ($\nabla \mathbf{v}$) are contracted via the double dot product $\blacklozenge$.

25-9 LINEAR RELATIONS BETWEEN FLUXES AND FORCES THAT OBEY THE CURIE RESTRICTION

In this section, we discuss one of the most monumental developments in transport phenomena that all scientists and engineers have followed since the days of Sir Isaac Newton (1643–1727), Jean-Baptiste-Joseph Fourier (1768–1830), and Adolph Eugen Fick (1829–1901). Lars Onsager (1903–1976) is responsible for the development of irreversible phenomena in 1931, which proves that Newton, Fourier, and Fick were correct in postulating linear relations between (1) molecular momentum flux and velocity gradients, (2) molecular flux of thermal energy and temperature gradients, and (3) diffusional flux and concentration gradients. However, the complete expressions for relations 2 and 3 are presented here, where Fourier's and Fick's laws represent one of several contributions to each of the respective fluxes. When the system is not too far removed from equilibrium, *linear laws* are postulated such that each flux is expanded as a linear sum of all the driving forces. Hence,

$$(\text{flux})_i = \sum_{j=1}^{2N} \xi_{ij} (\text{force})_j \tag{25-51}$$

where ξ_{ij}'s represent transport coefficients. For isotropic systems where the transport coefficients are scalars, $(\text{flux})_i$ is coupled to $(\text{force})_j$ and $\xi_{ij} \neq 0$ if the tensorial ranks of $(\text{flux})_i$ and $(\text{force})_j$ are the same or if they differ by an even integer. If the tensorial ranks of $(\text{flux})_i$ and $(\text{force})_j$ differ by ± 1, then $\xi_{ij} = 0$. This classic theorem is known as the *Curie restriction* for isotropic systems (i.e.,

proposed by P. Curie in 1903). As a consequences of this theorem, there are N first-rank tensorial fluxes:

$$\begin{array}{lll} -\left(\mathbf{q} - \displaystyle\sum_{i=1}^{N-1} \varphi_i \mathbf{j}_i\right) & & \text{tensorial rank} = 1 \\ -\mathbf{j}_i & 1 \le i \le N-1 & \text{tensorial rank} = 1 \end{array} \tag{25-52}$$

that are coupled to N first-rank tensorial forces:

$$\begin{array}{lll} \dfrac{1}{T^2}\nabla T & & \text{tensorial rank} = 1 \\ \dfrac{1}{T}[\nabla \varphi_i + (\mathbf{g}_N - \mathbf{g}_i)] & 1 \le i \le N-1 & \text{tensorial rank} = 1 \end{array} \tag{25-53}$$

via linear laws. The Curie theorem suggests that molecular momentum flux τ should be coupled to the chemical potential differences ($\varphi_i/T,\ 1 \le i \le N-1$), and the rates of production of the mass of species i due to chemical reaction ($r_i,\ 1 \le i \le N-1$) should be coupled to the velocity gradient tensor, $\nabla \mathbf{v}$, but these couplings are discarded based on physical rather than mathematical arguments. In other words, it's difficult to rationalize how the presence of a velocity gradient could influence the rate of production of any component in the mixture via chemical reaction. However in some cases, velocity gradients could induce shear stresses that assist mixing and agitation to the extent that chemical reactions are no longer diffusion controlled. Obviously, Curie's theorem suggests that temperature and chemical potential gradients don't generate viscous momentum flux τ. These gradients do affect the density of species i and forces due to the external field that appear in the momentum balance, which represents the starting point for the analysis of free convective heat and mass transfer. More important, velocity gradients don't contribute to diffusional mass flux or molecular flux of thermal energy, even though interphase heat and mass transfer are enhanced at higher shear rates. The latter example does not violate the Curie restriction because higher flow rates that decrease boundary layer thicknesses adjacent to an interface provide a convective enhancement of interphase heat and mass transfer rates. Curie's law applies to molecular fluxes, not convective fluxes.

If the generic form of the rate of entropy production per unit volume,

$$s_G = \sum_{i=1}^{2N} (\text{flux})_i (\text{force})_i \tag{25-54}$$

is combined with the proposed linear relations between $(\text{flux})_i$ and $(\text{force})_j$:

$$(\text{flux})_i = \sum_{j=1}^{2N} \xi_{ij} (\text{force})_j \tag{25-55}$$

then

$$s_G = \sum_{i=1}^{2N} \sum_{j=1}^{2N} \xi_{ij} (\text{force})_i (\text{force})_j \tag{25-56}$$

represents a quadratic form for entropy production. The quadratic form of interest is a second-degree expansion of s_G in terms of products of forces. Furthermore, for irreversible processes,

$$s_G = \sum_{i=1}^{2N} \sum_{j=1}^{2N} \xi_{ij} (\text{force})_i (\text{force})_j > 0 \tag{25-57}$$

which suggests that the quadratic form must be positive definite. The expression for s_G is a positive-definite quadratic form because it is zero only when all the driving forces vanish. The implication of this statement is that there are a few restrictions on the matrix of phenomenological transport coefficients $[\xi_{ij}]$ to ensure that the rate of entropy production is always positive. The necessary and sufficient condition for s_G to be a positive-definite quadratic form is that every principal minor of the matrix of phenomenological transport coefficients must be positive. A principal minor of a square matrix like $[\xi_{ij}]$ is the determinant of any square principal submatrix of $[\xi_{ij}]$, and a principal submatrix has a principal diagonal that is part of the principal diagonal of the original square matrix. For an $N \times N$ square matrix, the sloping line of elements from ξ_{11} to ξ_{NN} is defined as the principal diagonal of $[\xi_{ij}]$. This completes the eighth objective outlined in Section 25-1.

25-10 COUPLING BETWEEN DIFFUSIONAL MASS FLUX AND MOLECULAR FLUX OF THERMAL ENERGY IN BINARY MIXTURES: THE ONSAGER RECIPROCAL RELATIONS

The concepts discussed in Section 25-9 are applied to binary mixtures of A and B with chemical reaction. Now, the Curie restriction states that there are two first-rank tensorial fluxes, $-(\mathbf{q} - \varphi_A \mathbf{j}_A)$ and $-\mathbf{j}_A$, that are coupled to two first-rank tensorial forces, $(1/T^2)\nabla T$ and $(1/T)[\nabla_{\varphi A} + (\mathbf{g}_B - \mathbf{g}_A)]$ via linear laws. Notice that the two fluxes are not simply $\mathbf{q}$ and $\mathbf{j}_A$, but $-(\mathbf{q} - \varphi_A \mathbf{j}_A)$ and $-\mathbf{j}_A$, as dictated by the classical expression for the rate of entropy generation, which is given by equation (25-49) in canonical form. In other words, one must exercise caution in identifying fluxes and forces such that their products correspond to specific terms in the final expression for s_G. The linear laws are

$$\begin{aligned} -\mathbf{j}_A &= \alpha T \frac{1}{T}[\nabla \varphi_A + (\mathbf{g}_B - \mathbf{g}_A)] + \beta T^2 \frac{1}{T^2} \nabla T \\ -(\mathbf{q} - \varphi_A \mathbf{j}_A) &= \delta T \frac{1}{T}[\nabla \varphi_A + (\mathbf{g}_B - \mathbf{g}_A)] + \gamma T^2 \frac{1}{T^2} \nabla T \end{aligned} \tag{25-58}$$

where the phenomenological coupling coefficients are

$$\begin{aligned} \xi_{11} &= \alpha T \qquad \xi_{12} = \beta T^2 \\ \xi_{21} &= \delta T \qquad \xi_{22} = \gamma T^2 \end{aligned} \tag{25-59}$$

In the linear laws given by equations (25-55) or (25-58), it is important that elements on the main diagonal of the matrix of phenomenological transport coefficients represent coupling between associated fluxes and driving forces, as identified by s_{G} in equation (25-49). Notice that factors of T and T^2 are included in the phenomenological coupling coefficients so that the linear laws given by equations (25-58) can be written more concisely as

$$\begin{aligned} -\mathbf{j}_{\mathrm{A}} &= \alpha[\nabla\varphi_{\mathrm{A}} + (\mathbf{g}_{\mathrm{B}} - \mathbf{g}_{\mathrm{A}})] + \beta\nabla T \\ -(\mathbf{q} - \varphi_{\mathrm{A}}\mathbf{j}_{\mathrm{A}}) &= \delta[\nabla\varphi_{\mathrm{A}} + (\mathbf{g}_{\mathrm{B}} - \mathbf{g}_{\mathrm{A}})] + \gamma\nabla T \end{aligned} \tag{25-60}$$

However, the Onsager reciprocal relations and the necessary and sufficient conditions that s_G is a positive-definite quadratic form are based on the ξ_{ij}'s, not α, β, δ, and γ. Onsager applied statistical mechanics to nonequilibrium systems to prove his reciprocal relations in the absence of magnetic fields, $\xi_{ij} = \xi_{ji}$, for the off-diagonal elements in the matrix of phenomenological coefficients. These reciprocal relations have been verified experimentally for particular situations. For the binary system under consideration, the Onsager reciprocal relation is

$$\xi_{12} = \xi_{21} \qquad \beta T^2 = \delta T \qquad \delta = \beta T \tag{25-61}$$

Since the phenomenological transport coefficients can be represented in 2×2 matrix form for binary systems,

$$\begin{matrix} \xi_{11} & \xi_{12} \\ \xi_{21} & \xi_{22} \end{matrix} \tag{25-62}$$

and the principal diagonal extends from ξ_{11} to ξ_{22}, there are three principal submatrices, including the original 2×2 matrix above. The determinants of these principal submatrices must be positive to ensure that s_G is a positive-definite quadratic form, which is equivalent to stating that the rate of entropy generation must be positive for irreversible processes unless all the driving forces vanish. Hence, the three principal minors yield:

$$\begin{aligned} \xi_{11} &> 0 \\ \xi_{22} &> 0 \\ \xi_{11}\xi_{22} - \xi_{12}\xi_{21} &> 0 \end{aligned} \tag{25-63}$$

which translate into the following inequalities:

$$\begin{gathered}\alpha > 0 \qquad \gamma > 0 \\ \alpha\gamma - \beta\delta = \alpha\left(\gamma - \frac{\beta\delta}{\alpha}\right) > 0 \\ \gamma - \frac{\beta\delta}{\alpha} = \gamma - \frac{\beta^2 T}{\alpha} > 0\end{gathered} \tag{25-64}$$

where the Onsager reciprocal relation is used to replace δ in the preceding inequality. Temperature does not appear explicitly in these inequalities because it has been factored, and T must be positive. One of the physical consequences of these matrix requirements for a positive-definite quadratic form for s_G is illustrated in section 25-11 for $\mathbf{q}$.

25-11 IDENTIFICATION OF FOURIER'S LAW IN THE MOLECULAR FLUX OF THERMAL ENERGY AND THE REQUIREMENT THAT THERMAL CONDUCTIVITIES ARE POSITIVE

The linear laws given by equations (25-60) are rearranged to solve for the molecular flux of thermal energy:

$$-\mathbf{q} = -\varphi_A \mathbf{j}_A + \beta T[\nabla\varphi_A + (\mathbf{g}_B - \mathbf{g}_A)] + \gamma\nabla T \tag{25-65}$$

where the Onsager reciprocal relation is used to replace δ in the second term on the right side of (25-65). Furthermore,

$$\nabla\varphi_A + (\mathbf{g}_B - \mathbf{g}_A) = -\frac{1}{\alpha}(\mathbf{j}_A + \beta\nabla T) \tag{25-66}$$

Upon replacing $\nabla\varphi_A + (\mathbf{g}_B - \mathbf{g}_A)$ in the expression for $\mathbf{q}$, one obtains the final form for the molecular flux of thermal energy in binary mixtures:

$$\mathbf{q} = \left(\varphi_A + \frac{\beta T}{\alpha}\right)\mathbf{j}_A - \left(\gamma - \frac{\beta^2 T}{\alpha}\right)\nabla T \tag{25-67}$$

which suggests that diffusional mass flux and temperature gradients give rise to conductive energy flux. Of particular importance in equation (25-67) is the fact that the second term on the right side matches Fourier's law of heat conduction, $\mathbf{q} = -k\nabla T$, with a thermal conductivity k given by

$$k = \gamma - \frac{\beta^2 T}{\alpha} > 0 \tag{25-68}$$

where the inequality in (25-68) stems from the fact that the determinant of the 2×2 matrix of phenomenological transport coefficients must be positive to ensure a positive-definite quadratic form for s_G. Hence,

$$\mathbf{q} = \left(\varphi_A + \frac{\beta T}{\alpha}\right)\mathbf{j}_A - k\nabla T \tag{25-69}$$

25-12 COMPLETE EXPRESSION FOR THE DIFFUSIONAL MASS FLUX OF COMPONENT A IN A BINARY MIXTURE

The linear law for diffusional mass flux in (25-60) that obeys the Curie restriction for coupling between fluxes and forces of the same tensorial rank is

$$\mathbf{j}_A = -\alpha\nabla\varphi_A - \beta\nabla T - \alpha(\mathbf{g}_B - \mathbf{g}_A) \tag{25-70}$$

where φ_A represents a difference between the chemical potentials of components A and B, divided by their respective molecular weights:

$$\varphi_A = \left(\frac{\partial \mathscr{G}}{\partial \omega_A}\right)_{T,p} = \frac{\mu_A}{\mathrm{MW}_A} - \frac{\mu_B}{\mathrm{MW}_B} \tag{25-71}$$

$\mathscr{G}$ is the specific Gibbs free energy of the binary mixture and ω_A is the mass fraction of species A. Since there are three degrees of freedom for a single-phase mixture of two components,

$$\begin{aligned} \mathscr{G} &= \chi(T,\ p,\ \omega_A) \\ \varphi_A &= \left(\frac{\partial \mathscr{G}}{\partial \omega_A}\right)_{T,p} = \psi(T,\ p,\ \omega_A) \end{aligned} \tag{25-72}$$

where χ and ψ represent generic functions for these intensive thermodynamic variables, $\mathscr{G}$ and φ_A. Hence, one writes the total differential of φ_A in terms of temperature, pressure, and mass fraction:

$$d\varphi_A = \left(\frac{\partial \varphi_A}{\partial T}\right)_{p,\,\omega_A} dT + \left(\frac{\partial \varphi_A}{\partial p}\right)_{T,\,\omega_A} dp + \left(\frac{\partial \varphi_A}{\partial \omega_A}\right)_{T,p} d\omega_A \tag{25-73}$$

and performs the same sequence of steps described on page 691 to calculate ∇h in equation (25-16) from the total differential of the intensive enthalpy. The final result indicates that the gradient of φ_A is expressed in terms of temperature, pressure, and concentration gradients, as follows:

$$\nabla\varphi_A = \left(\frac{\partial \varphi_A}{\partial T}\right)_{p,\,\omega_A} \nabla T + \left(\frac{\partial \varphi_A}{\partial p}\right)_{T,\,\omega_A} \nabla p + \left(\frac{\partial \varphi_A}{\partial \omega_A}\right)_{T,p} \nabla\omega_A \tag{25-74}$$

Now, the diffusional mass flux of species A, given by equation (25-70), is written in terms of $\nabla\varphi_A$, ∇T, and the external force field as

$$\mathbf{j}_A = -\alpha\left(\frac{\partial\varphi_A}{\partial\omega_A}\right)_{T,p}\nabla\omega_A - \left[\alpha\left(\frac{\partial\varphi_A}{\partial T}\right)_{p,\omega_A} + \beta\right]\nabla T$$
$$- \alpha\left(\frac{\partial\varphi_A}{\partial p}\right)_{T,\omega_A}\nabla p - \alpha(\mathbf{g}_B - \mathbf{g}_A) \tag{25-75}$$

where the first term on the right side of equation (25-75) corresponds to concentration diffusion (i.e., Fick's law), the second term on the right side represents thermal diffusion (i.e., the Soret effect), the third term on the right side is pressure diffusion, and the fourth term on the right side is identified as forced diffusion in the presence of an external field.

The following transport coefficients are defined:

Binary molecular diffusion: $$\rho\mathfrak{D}_{AB} \equiv \alpha\left(\frac{\partial\varphi_A}{\partial\omega_A}\right)_{T,p} \tag{25-76a}$$

Thermal Soret diffusion: $$\rho\mathfrak{D}_{AB}\frac{k_T}{T} \equiv \alpha\left(\frac{\partial\varphi_A}{\partial T}\right)_{p,\omega_A} + \beta \tag{25-76b}$$

Pressure diffusion: $$\rho\mathfrak{D}_{AB}\frac{k_p}{p} \equiv \alpha\left(\frac{\partial\varphi_A}{\partial p}\right)_{T,\omega_A} \tag{25-76c}$$

These definitions introduce the binary molecular ($\mathfrak{D}_{AB}$), thermal (k_T), and pressure (k_p) diffusion coefficients. The final form for the diffusional mass flux of species A in a binary mixture with respect to the mass-average velocity $\mathbf{v}$ is

$$\mathbf{j}_A = -\rho\mathfrak{D}_{AB}\left\{\nabla\omega_A + k_T\nabla\ln T + k_p\nabla\ln p + \frac{(\mathbf{g}_B - \mathbf{g}_A)}{(\partial\varphi_A/\partial\omega_A)_{T,p}}\right\} \tag{25-77}$$

Since the rate of entropy production per unit volume must be positive for irreversible processes, $\alpha > 0$ is one of the requirements that ensures a positive-definite quadratic form for s_G. Furthermore, $(\partial\varphi_A/\partial\omega_A)_{T,p} > 0$ is one of the three thermodynamic stability criteria that must be satisfied for binary systems to exhibit homogeneous one-phase behavior (see equation 29-130). The thermal and mechanical stability criteria are (1) $c_v > 0$, where c_v is the specific heat at constant volume; and (2) $(\partial p/\partial v)_{T,\text{comp.}} < 0$ along pressure–volume isotherms (see equations 29-63 and 29-66). The requirement for chemical stability, mentioned above in terms of the concentration dependence of the chemical potentials at constant T and p, is also known as the *criterion of diffusional stability* in binary mixtures. If it is violated, then the system splits into two separate phases (i.e., solid–solid or liquid–liquid equilibrium) to reduce the Gibbs free energy of mixing of the composite two-phase system relative to the unstable homogeneous one-phase mixture. Hence, the binary molecular diffusion coefficient $\mathfrak{D}_{AB}$ must be positive for homogeneous single-phase binary mixtures under irreversible conditions. The kinetics of phase separation within the spinodal region at constant

T and p are described by $\mathfrak{D}_{AB} < 0$. Hence, diffusional mass flux occurs in the direction of increasing concentration gradient to assist the system as it splits into two phases. Even though this last statement seems to contradict physical intuition, diffusional mass flux proceeds in the direction of decreasing chemical potential gradient during the kinetics of phase separation as species A, for example, diffuses into a region of higher ω_A to lower the Gibbs free energy of mixing.

25-13 THERMODYNAMIC EVALUATION OF $(\partial\varphi_A/\partial\omega_A)_{T,p}$ IN BINARY MIXTURES

This calculation precludes development of the Einstein diffusion equation for forced diffusion in the presence of a gravitational field. The coefficient of $(\mathbf{g}_B - \mathbf{g}_A)$ in equation (25-77) for the diffusional mass flux of species A can be evaluated via thermodynamics. The extensive Gibbs free energy $\mathfrak{G}$ of a one-phase binary mixture with 3 degrees of freedom requires four independent variables for complete description of this thermodynamic state function. Hence, $\mathfrak{G}(T, p, N_A, N_B)$ is postulated where N_i represents the mole numbers of species i, and the total differential of $\mathfrak{G}$ is

$$d\mathfrak{G} = -S\,dT + V\,dp + \mu_A\,dN_A + \mu_B\,dN_B \tag{25-78}$$

where S and V represent extensive entropy and volume, respectively, of the system. Since $\mathfrak{G}$ is a first-degree homogeneous state function with respect to the molar mass of the system, and N_A and N_B are the only extensive independent variables postulated for $\mathfrak{G}$, Euler's integral theorem for thermodynamic state functions (see equation 29-30d) allows one to calculate the free energy as follows:

$$\mathfrak{G} = N_A\mu_A + N_B\mu_B \tag{25-79}$$

and the corresponding total differential is

$$d\mathfrak{G} = \mu_A\,dN_A + \mu_B\,dN_B + N_A\,d\mu_A + N_B\,d\mu_B \tag{25-80}$$

Comparison of the two differential expressions for $\mathfrak{G}$, given by (25-78) and (25-80), yields the following Gibbs–Duhem relation at constant T and p after division by the total number of moles, $N_A + N_B$:

$$x_A\,d\mu_A + x_B\,d\mu_B = 0 \tag{25-81}$$

where x_i is the mole fraction of species i. At constant T and p, the activity of species A in the mixture is defined by

$$(d\mu_A)_{T,p} \equiv RT(d\ln a_A)_{T,p} \tag{25-82}$$

Differentiation of the Gibbs–Duhem relation (i.e., equation 25-81) by ω_A at constant T and p yields

$$\left(\frac{\partial \mu_B}{\partial \omega_A}\right)_{T,p} = -\frac{x_A}{x_B} RT \left(\frac{\partial \ln a_A}{\partial \omega_A}\right)_{T,p} \tag{25-83}$$

This relation is useful because it allows one to calculate the partial derivative of interest in this section as follows, based on equation (25-71):

$$\begin{aligned}\left(\frac{\partial \varphi_A}{\partial \omega_A}\right)_{T,p} &= \frac{1}{MW_A}\left(\frac{\partial \mu_A}{\partial \omega_A}\right)_{T,p} - \frac{1}{MW_B}\left(\frac{\partial \mu_B}{\partial \omega_A}\right)_{T,p} \\ &= \left[\frac{1}{MW_A} + \frac{x_A}{x_B MW_B}\right] RT \left(\frac{\partial \ln a_A}{\partial \ln x_A}\right)_{T,p} \left(\frac{d \ln x_A}{d\omega_A}\right)_{T,p}\end{aligned} \tag{25-84}$$

Equations M, N, and P′ in Table 17.7-1 of Bird *et al*. (2002, p. 534) provide relations between mole fraction x_A and mass fraction ω_A that allow one to calculate

$$\left(\frac{d \ln x_A}{d\omega_A}\right)_{T,p} = \frac{1}{x_A}\left(\frac{dx_A}{d\omega_A}\right)_{T,p} = \frac{MW_{mixture}}{\omega_A MW_B} \tag{25-85}$$

where the composition-dependent average molecular weight of the binary mixture is defined by

$$\frac{1}{MW_{mixture}} = \frac{\omega_A}{MW_A} + \frac{\omega_B}{MW_B} \tag{25-86}$$

Simple manipulations between mass fractions and mole fractions allow one to arrive at the final expression for the mass fraction (ω_A) derivative of φ_A at constant T and p:

$$\begin{aligned}\left(\frac{\partial \varphi_A}{\partial \omega_A}\right)_{T,p} &= \left[\frac{1}{MW_A} + \frac{x_A}{x_B MW_B}\right] \frac{MW_{mixture}\, RT}{\omega_A MW_B} \left(\frac{\partial \ln a_A}{\partial \ln x_A}\right)_{T,p} \\ &= \frac{MW_{mixture}\, RT}{MW_A MW_B \omega_A \omega_B} \left(\frac{\partial \ln a_A}{\partial \ln x_A}\right)_{T,p}\end{aligned} \tag{25-87}$$

25-14 CONNECTION BETWEEN TRANSPORT PHENOMENA AND THERMODYNAMICS FOR DIFFUSIONAL MASS FLUXES AND DIFFUSIVITIES IN BINARY MIXTURES

Equations (25-77) and (25-87) allow one to express the diffusional mass flux of species A in a homogeneous single-phase binary mixture with respect to the

mass-averaged velocity **v** as

$$\mathbf{j}_A = -\rho \mathfrak{D}_{AB} \left\{ \nabla \omega_A + k_T \nabla \ln T + k_p \nabla \ln p + \frac{\mathrm{MW}_A \, \mathrm{MW}_B \, \omega_A \omega_B (\mathbf{g}_B - \mathbf{g}_A)}{\mathrm{MW}_{\mathrm{mixture}} \, RT \left(\dfrac{\partial \ln a_A}{\partial \ln x_A} \right)_{T,p}} \right\} \tag{25-88}$$

and the binary molecular diffusion coefficient can be calculated from thermodynamic data via equations (25-76*a*) and (25-87):

$$\rho \mathfrak{D}_{AB} = \frac{\alpha \, \mathrm{MW}_{\mathrm{mixture}} \, RT}{\mathrm{MW}_A \, \mathrm{MW}_B \, \omega_A \omega_B} \left(\frac{\partial \ln a_A}{\partial \ln x_A} \right)_{T,p} \tag{25-89}$$

25-15 LIQUID-PHASE DIFFUSIVITIES AND THE STOKES–EINSTEIN DIFFUSION EQUATION FOR BINARY MIXTURES

This classic equation, which combines well-known results from mass transfer and low-Reynolds-number hydrodynamics, is very useful to predict the effect of molecular size on diffusion coefficients. The assumptions that must be invoked to arrive at the Einstein diffusion equation and the Stokes–Einstein diffusion equation are numerous. A single spherical solid particle of species A experiences forced diffusion due to gravity in an infinite medium of fluid B, which is static. Concentration, thermal, and pressure diffusion are neglected with respect to forced diffusion. Hence, the diffusional mass flux of species A with respect to the mass-average velocity **v** is based on the last term in equation (25-88):

$$\mathbf{j}_A = \frac{-\rho \mathfrak{D}_{AB} \, \mathrm{MW}_A \, \mathrm{MW}_B \, \omega_A \omega_B (\mathbf{g}_B - \mathbf{g}_A)}{\mathrm{MW}_{\mathrm{mixture}} \, RT (\partial \ln a_A / \partial \ln x_A)_{T,p}} \tag{25-90}$$

Since there is only one particle of species A in the mixture, the mass fraction of fluid B is essentially unity and $\mathrm{MW}_{\mathrm{mixture}}$ approaches MW_B. The gas constant R is written as the product of Boltzmann's constant and Avogadro's number, and the ratio of MW_A to Avogadro's number is the mass of one molecule of species A, m_A. Hence, the single particle of species A is considered to be one molecule, and if it is a diatomic, then its size can be estimated from the sum of the covalent and van der Waals radii of each atom. If A is a polyatomic molecule, then molecular mechanics is useful to generate an energy-minimized structure, and an effective spherical shell that surrounds the molecule represents the best estimate of molecular size. Now, equation (25-90) reduces to:

$$\mathbf{j}_A = \frac{-\rho \mathfrak{D}_{AB} \, m_A \omega_A (\mathbf{g}_B - \mathbf{g}_A)}{k_{\mathrm{Boltz}} T (\partial \ln a_A / \partial \ln x_A)_{T,p}} \tag{25-91}$$

Thermodynamic activity information is required in the dilute solution regime where Henry's law is applicable. For an ideal mixture, activities are synonymous with mole fractions, and the slope of a_A vs. x_A is unity at infinite dilution. Hence, the thermodynamic derivative in the denominator of equation (25-91) is approximated by unity. Since fluid B is quiescent, the mass-average velocity of the mixture is essentially zero. The consequences of this condition are that $\mathbf{v} \approx 0$ and the pressure gradient balances the gravitational force on fluid B, as expected for a hydrostatic situation. Since there is no acceleration or forced diffusion for the continuum of fluid B, it is reasonable to set $\mathbf{g}_B \approx 0$. Under these conditions, equation (25-91) yields:

$$\mathbf{j}_A = \frac{\rho \mathfrak{D}_{AB} m_A \omega_A \mathbf{g}_A}{k_{Boltz} T} = \rho \omega_A (\mathbf{v}_A - \mathbf{v}) \approx \rho \omega_A \mathbf{v}_A \tag{25-92}$$

Now, a microhydrodynamic force balance is performed on the solid particle of species A that undergoes Brownian motion through static fluid B. The forces of interest are inertial, gravitational, and hydrodynamic drag. Buoyancy is neglected. Under slow-flow conditions, the inertial force is also neglected and the drag force is written as the product of a friction coefficient ζ and the velocity of the particle, $\mathbf{v}_A$. In general, hydrodynamic drag forces scale as $(\mathbf{v}_A)^{2-a}$, where the exponent a represents the slope of a log-log graph of friction factor f vs. the inverse of the Reynolds number. Hence,

$$a = -\left(\frac{d \log f}{d \log \mathrm{Re}}\right) \tag{25-93}$$

For flow around submerged objects, $a = 1$ in the creeping flow regime, and $a = 0$ for turbulent flow. Since the hydrodynamic drag force exerted by fluid B on solid particle A acts in the opposite direction of $\mathbf{v}_A$ when the fluid is stationary, and the gravitational force acts downward, these two forces are balanced:

$$m_A \mathbf{g}_A \approx \zeta \mathbf{v}_A \tag{25-94}$$

These considerations produce the following result for the diffusional mass flux of species A:

$$\mathbf{j}_A = \frac{\rho \mathfrak{D}_{AB} m_A \omega_A \mathbf{g}_A}{k_{Boltz} T} = \rho \omega_A (\mathbf{v}_A - \mathbf{v}) \approx \frac{\rho \omega_A m_A \mathbf{g}_A}{\zeta} \tag{25-95}$$

which reveals that the binary molecular diffusivity for one molecule of species A that experiences forced diffusion in quiescent fluid B is

$$\mathfrak{D}_{AB} = \frac{k_{Boltz} T}{\zeta} \tag{25-96}$$

This is the Einstein diffusion equation, which is not necessarily restricted to liquids. However, if (1) quiescent fluid B is isotropic, incompressible, and Newtonian, and (2) the boundary between particle A and fluid B is a fixed, high-shear,

no-slip interface, then Stokes's law is valid for creeping flow and the friction coefficient is given by

$$\zeta = 6\pi\mu_B R_A \tag{25-97}$$

where R_A is the radius of an effective spherical shell that surrounds molecule A. Hence, the Stokes–Einstein diffusion equation for incompressible liquids is

$$\mathfrak{D}_{AB} = \frac{k_{Boltz}T}{6\pi\mu_B R_A} \tag{25-98}$$

If the interface between particle A and fluid B is better represented by zero-shear rather than no-slip, then the friction coefficient for creeping flow of an incompressible Newtonian fluid around a bubble is

$$\zeta = 4\pi\mu_B R_A \tag{25-99}$$

and the corresponding Stokes–Einstein diffusion equation for incompressible liquids is

$$\mathfrak{D}_{AB} = \frac{k_{Boltz}T}{4\pi\mu_B R_A} \tag{25-100}$$

If there is slip and shear at the boundary between particle A and fluid B, then the friction coefficient for creeping flow of an incompressible Newtonian fluid around this spherical object is given by Happel and Brenner (1965, p. 126) as

$$\zeta = 6\pi\mu_B R_A \left\{\frac{2\mu_B + \kappa R_A}{3\mu_B + \kappa R_A}\right\} \tag{25-101}$$

where κ is the coefficient of sliding friction at the interface. The corresponding Stokes–Einstein diffusion equation is

$$\mathfrak{D}_{AB} = \frac{k_{Boltz}T}{6\pi\mu_B R_A}\left\{\frac{3\mu_B + \kappa R_A}{2\mu_B + \kappa R_A}\right\} \tag{25-102}$$

which reduces to equation (25-98) for a high-shear no-slip interface when $\kappa \to \infty$, and equation (25-100) for a zero-shear perfect-slip interface when $\kappa \to 0$.

PROBLEMS

25-1. Under steady-state conditions, a pure copper wire exhibits a temperature of 50°C at its left end and 200°C at its right end.

(a) Write an expression for the molecular flux of specific entropy.

(b) Draw the wire with temperatures at both ends. Then, draw an arrow that represents the direction in which molecular entropy flux occurs.

(c) Calculate the rate of entropy production per unit volume, s_G.

(d) Is s_G positive or negative?

(e) Use vectors and justify your answer to part (d).

25-2. "Another Way of Looking at Entropy," by Daniel Hershey in *Chemical Engineering Education* (1989, summer, p. 154), discusses entropy and aging. Write an expression for entropy production in the human body that is consistent with the following statement by Hershey: "The internal entropy production in living systems is a consequence of several irreversible chemical reactions which constitute the chemistry of life."

25-3. **(a)** Use the concept of linear laws to write an expression for $\mathbf{j}_A$, the diffusional mass flux of species A with respect to the mass-average velocity $\mathbf{v}$, in a four-component mixture of A, B, C, and D at constant temperature and pressure.

(b) Which phenomenological coupling coefficients in the linear law for $\mathbf{j}_A$ from part (a) are subject to Onsager reciprocal relations?

(c) Identify the type of diffusion that corresponds to each term in your answer to part (a).

(d) Is $\mathbf{q}$, the molecular flux of thermal energy, zero or nonzero for the system described in part (a)?

25-4. Identify 10 assumptions that are consistent with the Stokes–Einstein diffusion equation.

25-5. Identify two reasons why liquid-phase binary molecular diffusion coefficients increase at higher temperature.

25-6. If there is slip and shear at the boundary between particle A and fluid B, then the friction coefficient for creeping flow of an incompressible Newtonian fluid around this spherical object is given by Happel and Brenner (1965, p. 126) as

$$\zeta = 6\pi\mu_B R_A \left\{ \frac{2\mu_B + \kappa R_A}{3\mu_B + \kappa R_A} \right\}$$

where κ is the coefficient of sliding friction at the interface. Use this information to calculate the Stokes–Einstein diffusion coefficient for (**a**) a no-slip solid–liquid interface, and (**b**) a zero-shear gas–liquid interface.

25-7. The Stokes–Einstein equation provides an estimate of the binary molecular diffusion coefficient for dilute mixtures of spherical molecules of A in an incompressible Newtonian solvent B. This correlation is applicable to liquids, not gases. When the interface between solvent B and molecule A is characterized best by no slip and high shear,

$$\mathfrak{D}_{AB} = \frac{k_{\text{Boltzmann}} T}{6\pi\mu_B R_A}$$

where $k_{\text{Boltzmann}}$ is Boltzmann's constant, T the absolute temperature, μ_B the viscosity of Newtonian solvent B, and R_A the hydrodynamic radius of a shell that surrounds one molecule of A. How should you correlate experimental data which reveal that $\mathfrak{D}_{AB}$ is a function of temperature?

Answer: Begin with the Stokes–Einstein diffusion equation and include temperature dependence for the viscosity of the Newtonian solvent. Henry Eyring developed a simple molecular theory for the viscosity of liquids by considering viscous flow as an activated rate process. This is described in Bird *et al.* (2002, pp. 29–31). For example,

$$\mu_B(T) \approx \mu_\infty \exp\left(\frac{E_{\text{activation}}}{RT}\right)$$

where μ_∞ is a pre-exponential factor, or the hypothetical solvent viscosity at very high temperature, and $E_{\text{activation}}$ is the activation energy for viscous transport. This relation correctly predicts a decrease in μ_B at higher temperature, as expected for liquids. Now the temperature dependence of $\mathfrak{D}_{AB}$ is calculated as follows:

$$\begin{aligned}\mathfrak{D}_{AB}(T) &= \frac{k_{\text{Boltzmann}}T}{6\pi R_A \mu_\infty \exp(E_{\text{activation}}/RT)} \\ &= \frac{k_{\text{Boltzmann}}T \exp(-E_{\text{activation}}/RT)}{6\pi R_A \mu_\infty}\end{aligned}$$

Linear least-squares analysis is applied to a set of discrete experimental data for $\mathfrak{D}_{AB}$ vs. T based on this model. In other words, simple manipulation yields

$$\ln\frac{\mathfrak{D}_{AB}}{T} = \ln\frac{k_{\text{Boltzmann}}}{6\pi R_A \mu_\infty} - \frac{E_{\text{activation}}}{RT}$$

Hence, the data should be processed as follows:

(1) Invoke a first-order polynomial, $y(x) = a_0 + a_1 x$.

(2) Identify the independent variable as $x = 1/T$.

(3) Identify the dependent variable as $y = \ln(\mathfrak{D}_{AB}/T)$.

(4) The zeroth-order coefficient in the polynomial model, or the intercept, is

$$a_0 = \ln\frac{k_{\text{Boltzmann}}}{6\pi R_A \mu_\infty}$$

(5) The first-order coefficient in the polynomial model, or the slope, is

$$a_1 = \frac{-E_{\text{activation}}}{R}$$

25-8. The Stokes–Einstein equation for liquid-phase ordinary molecular diffusion coefficients in binary mixtures suggests that the product of $\mathfrak{D}_{AB}$ and the solvent viscosity μ_B should scale linearly with temperature T. Cite references (i.e., equations) from the literature and evaluate the product of $\mathfrak{D}_{AB}$ and μ_B in terms of its scaling-law dependence on temperature for low-density gases. In other words;

$$\mathfrak{D}_{AB}(T)\mu_B(T) \approx T^n$$

Calculate the scaling law exponent n for low-density gases and indicate any important assumptions that you have invoked to obtain your answer.

Answer: At higher temperatures, $\mathfrak{D}_{AB}$ increases and μ_B decreases for liquids, but both $\mathfrak{D}_{AB}$ and μ_B increase for low-density gases. The temperature dependence of these transport coefficients for low-density gases is summarized as follows:

$$\mathfrak{D}_{AB}(T) \approx \frac{T^{3/2}}{\Omega_D(k_{Boltz}T/\varepsilon_{AB})}$$

$$\mu_B(T) \approx \frac{T^{1/2}}{\Omega_V(k_{Boltz}T/\varepsilon_B)}$$

where Ω_D is the collision integral for diffusion in binary mixtures of gases A and B, and Ω_V is the viscosity collision integral for gas B. These collision integrals represent correction factors that account for deviations of the Lennard-Jones 6-12 intermolecular potential energy of interaction from a hard-sphere potential, the latter of which is infinitely repulsive when the centers of mass of two molecules are separated by their collision diameter, but noninteracting at larger separations. When molecules reside at their equilibrium separation distances, the maximum depth of the Lennard-Jones potential well is given by ε_B for pure gas B and ε_{AB} for binary gas mixtures of A and B. Both of these collision integrals are strongly decreasing functions of temperature when $k_{Boltz}T/\varepsilon$ ranges from 0 to 2, but they decrease much more weakly at higher temperatures, where $k_{Boltz}T/\varepsilon$ is larger than 10. The temperature-dependent product of $\mathfrak{D}_{AB}$ and μ_B is

$$\mathfrak{D}_{AB}(T)\mu_B(T) \approx \frac{T^2}{\Omega_D(k_{Boltz}T/\varepsilon_{AB})\Omega_V(k_{Boltz}T/\varepsilon_B)}$$

where the scaling law exponent n is slightly greater than 2. If one neglects temperature dependence of both of the collision integrals, then $n = 2$.

Transport Phenomena for Chemical Reactor Design. Laurence A. Belfiore
Copyright © 2003 John Wiley & Sons, Inc.
ISBN: 0-471-20275-4

26

MOLECULAR FLUX OF THERMAL ENERGY IN BINARY AND MULTICOMPONENT MIXTURES VIA THE FORMALISM OF NONEQUILIBRIUM THERMODYNAMICS

26-1 THREE CONTRIBUTIONS TO q IN BINARY SYSTEMS

For mixtures of A and B, there are two first-rank tensorial fluxes, $-(\mathbf{q} - \varphi_A \mathbf{j}_A)$ and $-\mathbf{j}_A$, that are coupled to two first-rank tensorial forces, $(1/T^2)\nabla T$ and $(1/T)[\nabla\varphi_A + (\mathbf{g}_B - \mathbf{g}_A)]$ via linear transport laws. These fluxes and forces are chosen such that their products correspond to specific terms in the final expression for the rate of entropy generation per unit volume of fluid, s_G. The linear laws are (see equations 25-58):

$$-\mathbf{j}_A = \alpha T \frac{1}{T}[\nabla\varphi_A + (\mathbf{g}_B - \mathbf{g}_A)] + \beta T^2 \frac{1}{T^2}\nabla T \tag{26-1}$$

$$-(\mathbf{q} - \varphi_A \mathbf{j}_A) = \delta T \frac{1}{T}[\nabla\varphi_A + (\mathbf{g}_B - \mathbf{g}_A)] + \gamma T^2 \frac{1}{T^2}\nabla T \tag{26-2}$$

where the phenomenological coupling coefficients are

$$\xi_{11} = \alpha T \qquad \xi_{12} = \beta T^2 \qquad \xi_{21} = \delta T \qquad \xi_{22} = \gamma T^2 \tag{26-3}$$

These linear laws can be written more concisely as

$$-\mathbf{j}_A = \alpha[\nabla\varphi_A + (\mathbf{g}_B - \mathbf{g}_A)] + \beta\nabla T \tag{26-4}$$

$$-(\mathbf{q} - \varphi_A \mathbf{j}_A) = \delta[\nabla\varphi_A + (\mathbf{g}_B - \mathbf{g}_A)] + \gamma\nabla T \tag{26-5}$$

The Onsager reciprocal relation for the 2×2 matrix of phenomenological coupling coefficients is

$$\xi_{12} = \xi_{21} \qquad \delta T = \beta T^2 \qquad \delta = \beta T \tag{26-6}$$

and the following inequalities ensure that s_G is a positive-definite quadratic form:

$$\begin{gathered} \alpha > 0 \qquad \gamma > 0 \\ \alpha\gamma - \beta\delta = \alpha\left(\gamma - \frac{\beta\delta}{\alpha}\right) > 0 \\ \gamma - \frac{\beta\delta}{\alpha} = \gamma - \frac{\beta^2 T}{\alpha} > 0 \end{gathered} \tag{26-7}$$

The molecular flux of thermal energy, given by equation (26-5), is rearranged as follows:

$$-\mathbf{q} = -\varphi_{\mathrm{A}}\mathbf{j}_{\mathrm{A}} + \beta T[\boldsymbol{\nabla}\varphi_{\mathrm{A}} + (\mathbf{g}_{\mathrm{B}} - \mathbf{g}_{\mathrm{A}})] + \gamma\boldsymbol{\nabla}T \tag{26-8}$$

where the Onsager reciprocal relation in (26-6) is used to replace δ in the second term on the right side of equation (26-8). Furthermore,

$$\boldsymbol{\nabla}\varphi_{\mathrm{A}} + (\mathbf{g}_{\mathrm{B}} - \mathbf{g}_{\mathrm{A}}) = -\frac{1}{\alpha}(\mathbf{j}_{\mathrm{A}} + \beta\boldsymbol{\nabla}T) \tag{26-9}$$

represents a rearrangement of the linear law for diffusional mass flux, given by equation (26-4). Upon replacing $\boldsymbol{\nabla}\varphi_{\mathrm{A}} + (\mathbf{g}_{\mathrm{B}} - \mathbf{g}_{\mathrm{A}})$ in equation (26-8), one obtains the final form for the molecular flux of thermal energy in binary mixtures:

$$\mathbf{q} = \left(\varphi_{\mathrm{A}} + \frac{\beta T}{\alpha}\right)\mathbf{j}_{\mathrm{A}} - k\boldsymbol{\nabla}T \tag{26-10}$$

where the thermal conductivity k is identified by the following group of terms:

$$k = \gamma - \frac{\beta^2 T}{\alpha} > 0 \tag{26-11}$$

This inequality in (26-11) stems from the fact that the determinant of the 2×2 matrix of phenomenological transport coefficients $[\xi_{ij}]$ must be positive to ensure a positive-definite quadratic form for s_G. The contribution from thermal Soret diffusion in the final expression for $\mathbf{j}_{\mathrm{A}}$ (see equations 25-76 and 25-77) provides a definition of β in terms of the thermal diffusion coefficient k_T and the temperature dependence of φ_{A}:

$$\rho\mathfrak{D}_{\mathrm{AB}}\frac{k_T}{T} \equiv \alpha\left(\frac{\partial\varphi_{\mathrm{A}}}{\partial T}\right)_{p,\,\omega_{\mathrm{A}}} + \beta \tag{26-12}$$

This relation is rearranged to calculate β as follows:

$$\beta = \rho\mathfrak{D}_{\mathrm{AB}}\frac{k_T}{T} - \alpha\left(\frac{\partial\varphi_{\mathrm{A}}}{\partial T}\right)_{p,\,\omega_{\mathrm{A}}} \tag{26-13}$$

The molecular flux of thermal energy in equation (26-10) is written in terms of the diffusional mass flux of component A and the temperature gradient as

$$\mathbf{q} = \left[\varphi_A + \frac{\rho\mathscr{D}_{AB}}{\alpha}k_T - T\left(\frac{\partial\varphi_A}{\partial T}\right)_{p,\omega_A}\right]\mathbf{j}_A - k\nabla T \tag{26-14}$$

The coefficient of k_T in (26-14) is written in terms of the concentration dependence of φ_A via the definition of the binary molecular diffusivity in equation (25-76*a*):

$$\rho\mathscr{D}_{AB} \equiv \alpha\left(\frac{\partial\varphi_A}{\partial\omega_A}\right)_{T,p} \tag{26-15}$$

Hence;

$$\begin{aligned}
\mathbf{q} &= \left[\varphi_A - T\left(\frac{\partial\varphi_A}{\partial T}\right)_{p,\omega_A} + k_T\left(\frac{\partial\varphi_A}{\partial\omega_A}\right)_{T,p}\right]\mathbf{j}_A - k\nabla T \\
\mathbf{q} &= \mathbf{q}_{\text{interdiffusion}} + \mathbf{q}_{\text{Dufour}} + \mathbf{q}_{\text{Fourier}} \\
\mathbf{q}_{\text{interdiffusion}} &= \left[\varphi_A - T\left(\frac{\partial\varphi_A}{\partial T}\right)_{p,\omega_A}\right]\mathbf{j}_A \\
\mathbf{q}_{\text{Dufour}} &= \left[k_T\left(\frac{\partial\varphi_A}{\partial\omega_A}\right)_{T,p}\right]\mathbf{j}_A \\
\mathbf{q}_{\text{Fourier}} &= -k\nabla T
\end{aligned} \tag{26-16}$$

where the molecular flux of thermal energy is separated into contributions from temperature gradients (i.e., Fourier's law); the diffusion-thermo effect, which is known classically as the Dufour effect; and the interdiffusional flux. The Dufour effect is not the most important coupling between $\mathbf{j}_A$ and $\mathbf{q}$, and it is typically neglected in almost all engineering analyses of heat transfer in multicomponent systems. The most important coupling between diffusional mass flux and conductive energy flux is the interdiffusional flux, and it is discussed in further detail below. One must realize that Fourier's law is not sufficient to describe the molecular flux of thermal energy in systems of more than one component. However, in pure materials where diffusional fluxes vanish, $\mathbf{q}$ is given by Fourier's law.

26-2 THERMODYNAMIC ANALYSIS OF $\varphi_A - T(\partial\varphi_A/\partial T)_{p,\omega_A}$

Recall that the definition of φ_A from equations (25-15) and (25-71) is

$$\varphi_A = \left(\frac{\partial\mathscr{G}}{\partial\omega_A}\right)_{T,p} = \frac{\mu_A}{MW_A} - \frac{\mu_B}{MW_B} \tag{26-17}$$

where $\mathscr{G}$ is the specific Gibbs free energy of the binary mixture and μ_i is the chemical potential of species i. Since there are 3 degrees of freedom for one-phase binary mixtures, $\mathscr{G} = \mathscr{G}(T, p, \omega_A)$ where temperature, pressure, and mass fraction represent three appropriate independent variables. The total differential of the specific Gibbs free energy of the binary mixture is

$$d\mathscr{G} = -s\,dT + \frac{1}{\rho}\,dp + \varphi_A\,d\omega_A \tag{26-18}$$

Since $\mathscr{G}$ is an exact differential, second mixed partial derivatives of $\mathscr{G}$ are independent of the order in which differentiation is performed. This leads to a Maxwell relation between the temperature dependence of φ_A and the mass fraction dependence of specific entropy s. Hence,

$$\left(\frac{\partial \varphi_A}{\partial T}\right)_{p,\,\omega_A} = -\left(\frac{\partial s}{\partial \omega_A}\right)_{T,p} \tag{26-19}$$

The development below calculates the mass fraction dependence of any intensive (i.e., specific) thermodynamic variable, which is written on a per unit mass basis. Of particular importance in this discussion, the thermodynamic variable is either the specific Gibbs free energy or the specific entropy s, and the final result is applicable to binary and multicomponent mixtures.

The extensive Gibbs free energy $\mathfrak{G}$ of a one-phase mixture of N components with $N+1$ degrees of freedom requires $N+2$ independent variables for complete description of this thermodynamic state function. Hence, $\mathfrak{G}(T, p, M_1, M_2, \ldots, M_N)$ is postulated where M_i represents the mass of species i. Mass numbers M_i are used instead of mole numbers N_i because it is necessary to generate mass fractions and the specific Gibbs free energy $\mathscr{G}$ via division by the total mass of the system, $\sum M_i$. The total differential of $\mathfrak{G}$ is

$$d\mathfrak{G} = -S\,dT + V\,dp + \sum_{i=1}^{N} \zeta_i\,dM_i \tag{26-20}$$

where S and V represent extensive entropy and volume, respectively, of the system, the summation includes all components, and ζ_i is a partial specific property instead of a partial molar property because it involves a mass number derivative of the extensive Gibbs free energy $\mathfrak{G}$ when temperature, pressure, and all other mass numbers are held constant. Hence,

$$\begin{aligned}\zeta_i &= \left(\frac{\partial \mathfrak{G}}{\partial M_i}\right)_{T,p,\text{ all } M_j\ (j\neq i)} = \left[\left(\frac{\partial \mathfrak{G}}{\partial N_i}\right)_{T,p,\text{ all } N_j\ (j\neq i)}\right]\left[\left(\frac{\partial N_i}{\partial M_i}\right)_{\text{all } M_j,\ (j\neq i)}\right] \\ &= \frac{\mu_i}{\mathrm{MW}_i}\end{aligned} \tag{26-21}$$

Before proceeding further, it is instructive to summarize some of these partial molar and specific properties that are interrelated. Obviously, μ_i is the chemical

potential of species i, which is equivalent to the mole number derivative of the extensive Gibbs free energy at constant T and p. Equation (26-21) illustrates that ζ_i, which is the mass number derivative of $\mathfrak{G}$ at constant T and p, is directly related to the chemical potential. One of the objectives of the exercise below is to calculate the mass fraction derivative of the intensive (i.e., specific) Gibbs free energy at constant T and p, which is defined as φ_i. At constant T and p, concentration derivatives of the extensive or intensive Gibbs free energy can be expressed in terms of chemical potentials. Since $\mathfrak{G}$ is a first-degree homogeneous state function with respect to the mass of the system, and all $M_i (1 \leq i \leq N)$ represent the extensive independent variables postulated above, Euler's integral theorem for thermodynamic state functions (see equation 29-30d) allows one to calculate the free energy as follows:

$$\mathfrak{G} = \sum_{i=1}^{N} M_i \left(\frac{\partial \mathfrak{G}}{\partial M_i} \right)_{T,p,\text{ all } M_j\ (j \neq i)} = \sum_{i=1}^{N} M_i \zeta_i \tag{26-22}$$

and the corresponding total differential is

$$d\mathfrak{G} = \sum_{i=1}^{N} (\zeta_i \, dM_i + M_i \, d\zeta_i) \tag{26-23}$$

Comparison of the two differential expressions for $\mathfrak{G}$, given by (26-20) and (26-23), yields the following Gibbs–Duhem relation at constant T and p after division by the total system mass, $\sum M_j$:

$$\sum_{i=1}^{N} \omega_i \, d\zeta_i = 0 \tag{26-24}$$

where the mass fraction of species i is defined by

$$\omega_i = \frac{M_i}{\sum_{j=1}^{N} M_j} \tag{26-25}$$

The specific and extensive Gibbs free energies of this N-component mixture are related by total mass. Hence,

$$\mathscr{G} = \frac{\mathfrak{G}}{\sum_{j=1}^{N} M_j} = \sum_{i=1}^{N} \omega_i \zeta_i \tag{26-26}$$

and the total differential of the specific Gibbs free energy is

$$d\mathscr{G} = \sum_{i=1}^{N} (\omega_i \, d\zeta_i + \zeta_i \, d\omega_i) = \sum_{i=1}^{N} \zeta_i \, d\omega_i \tag{26-27}$$

where the Gibbs–Duhem equation at constant T and p, given by (26-24), is used to eliminate the first set of terms in parentheses in equation (26-27). The last term in the summation on the far right side of equation (26-27) (i.e., $\zeta_N\, d\omega_N$) is removed from the summation and $d\omega_N$ is calculated from the following conditions:

1. All mass fractions must sum to unity, $\sum_i \omega_i = 1$, $1 \le i \le N$.
2. All differential mass fractions must sum to zero, $\sum_i d\omega_i = 0$, $1 \le i \le N$.

Hence,

$$d\omega_N = -\sum_{i=1}^{N-1} d\omega_i \tag{26-28}$$

The final expression for the total differential of $\mathscr{G}$ at constant T and p, given by (26-27), is written in terms of $d\omega_i$ for the first $N-1$ components as follows:

$$d\mathscr{G} = \sum_{i=1}^{N-1} (\zeta_i - \zeta_N)\, d\omega_i = \sum_{i=1}^{N-1} \left[\left(\frac{\partial \mathscr{G}}{\partial \omega_i} \right)_{T,p,\text{all } \omega_j\ (j \neq i,N)} \right] d\omega_i \tag{26-29}$$

where it is reasonable to postulate that $\mathscr{G}(T, p, \omega_1, \omega_2, \ldots, \omega_{N-1})$ represents the functional dependence of an intensive thermodynamic variable in a mixture of N components with $N+1$ degrees of freedom. All mass fractions are not independent because they must sum to unity. Consequently, it is not possible to differentiate with respect to ω_i and hold all other mass fractions constant. In other words, at least two mass fractions must change, ω_i and ω_N, where changes in ω_N are equal and opposite to those of ω_i to ensure that all mass fractions sum to unity. For any component i in the mixture whose mass fraction is an independent variable, the following expression is valid, based on equations (26-21) and (26-29):

$$\varphi_i = \left(\frac{\partial \mathscr{G}}{\partial \omega_i} \right)_{T,p,\text{all } w_j,\ (j \neq i,\ N)} = \zeta_i - \zeta_N = \frac{\mu_i}{\text{MW}_i} - \frac{\mu_N}{\text{MW}_N} \tag{26-30}$$

If the specific Gibbs free energy $\mathscr{G}$ is replaced by specific entropy s and the chemical potentials μ_i and μ_N are replaced by partial molar entropies $\mathfrak{s}_i$ and $\mathfrak{s}_N$, then the following result is also valid:

$$\left(\frac{\partial s}{\partial \omega_i} \right)_{T,p,\text{all } \omega_j\ (j \neq i,\ N)} = \frac{\mathfrak{s}_i}{\text{MW}_i} - \frac{\mathfrak{s}_N}{\text{MW}_N} \tag{26-31}$$

Finally, if intensive thermodynamic properties (specific) are replaced by intensive properties on a molar basis, and mass fractions are replaced by mole fractions, then equations (26-30) and (26-31) are valid if the molecular weights are eliminated.

26-3 ANALYSIS OF THE INTERDIFFUSIONAL FLUX OF THERMAL ENERGY IN BINARY MIXTURES AND GENERALIZATION TO MULTICOMPONENT MIXTURES

In this section, we provide further analysis of $\mathbf{q}_{\text{interdiffusion}}$ by combining partial molar Gibbs free energies and partial molar entropies. The interdiffusional flux of thermal energy in a binary mixture was defined in (26-16) as:

$$\mathbf{q}_{\text{interdiffusion}} = \left[\varphi_{\text{A}} - T\left(\frac{\partial \varphi_{\text{A}}}{\partial T}\right)_{p,\,\omega_{\text{A}}}\right]\mathbf{j}_{\text{A}} \tag{26-32}$$

where a Maxwell relation, given by equation (26-19), is used to write the coefficient of $\mathbf{j}_{\text{A}}$ in (26-32) as

$$\begin{aligned}\varphi_A - T\left(\frac{\partial \varphi_A}{\partial T}\right)_{p,\,\omega_{\text{A}}} &= \varphi_{\text{A}} + T\left(\frac{\partial s}{\partial \omega_{\text{A}}}\right)_{T,p} \\ &= \frac{\mu_{\text{A}}}{\text{MW}_{\text{A}}} - \frac{\mu_{\text{B}}}{\text{MW}_{\text{B}}} + T\frac{\mathfrak{s}_{\text{A}}}{\text{MW}_{\text{A}}} - T\frac{\mathfrak{s}_B}{\text{MW}_{\text{B}}} \\ &= \frac{1}{\text{MW}_{\text{A}}}(\mu_{\text{A}} + T\mathfrak{s}_{\text{A}}) - \frac{1}{\text{MW}_{\text{B}}}(\mu_{\text{B}} + T\mathfrak{s}_{\text{B}})\end{aligned} \tag{26-33}$$

The quantities $\mu_i + T\mathfrak{s}_i$ correspond to the partial molar enthalpy $\mathfrak{h}_i$ of each component, since $\mathfrak{G} = H - TS$, and differentiation with respect to the moles of species A at constant T, p and N_{B} produces the following relation between partial molar properties:

$$\left(\frac{\partial \mathfrak{G}}{\partial N_{\text{A}}}\right)_{T,p,\,N_{\text{B}}} = \left(\frac{\partial H}{\partial N_{\text{A}}}\right)_{T,p,\,N_{\text{B}}} - T\left(\frac{\partial S}{\partial N_{\text{A}}}\right)_{T,p,\,N_{\text{B}}} \tag{26-34}$$

$$\mu_{\text{A}} = \mathfrak{h}_{\text{A}} - T\mathfrak{s}_{\text{A}} \tag{26-35}$$

Hence, the interdiffusional flux of thermal energy is written as follows:

$$\mathbf{q}_{\text{interdiffusion}} = \frac{\mathfrak{h}_{\text{A}}}{\text{MW}_{\text{A}}}\mathbf{j}_{\text{A}} - \frac{\mathfrak{h}_{\text{B}}}{\text{MW}_{\text{B}}}\mathbf{j}_{\text{A}} \tag{26-36}$$

By definition of the mass-average velocity $\mathbf{v}$ of the mixture, all diffusional mass fluxes with respect to $\mathbf{v}$ must sum to zero. Hence, $\mathbf{j}_{\text{A}} = -\mathbf{j}_{\text{B}}$ for binary mixtures. The final expression for the molecular flux of thermal energy in binary mixtures, neglecting the diffusion-thermo (i.e., Dufour) effect, is

$$\mathbf{q} = \frac{\mathfrak{h}_{\text{A}}}{\text{MW}_{\text{A}}}\mathbf{j}_{\text{A}} + \frac{\mathfrak{h}_{\text{B}}}{\text{MW}_{\text{B}}}\mathbf{j}_{\text{B}} - k\nabla T \tag{26-37}$$

which reduces to Fourier's law of heat conduction for a pure material. For multicomponent mixtures, generalization of (26-37) leads to

$$\mathbf{q} = -k\nabla T + \sum_{i=1}^{N} \frac{\mathfrak{h}_i}{\mathrm{MW}_i}\mathbf{j}_i \tag{26-38}$$

which represents the starting point for analyses of coupled heat and mass transfer with chemical reaction inside porous catalytic pellets.

PROBLEMS

26.1 In this problem we explore classical irreversible thermodynamics for a multicomponent system, entropy generation, linear laws, and the molecular flux of thermal energy for a ternary system. Consider an N-component system ($1 \leq i \leq N$) in the presence of external force fields and multiple chemical reactions ($1 \leq j \leq R$). $\mathbf{g}_i$ is the external force per unit mass that acts specifically on component i in the mixture, and r_i is the overall rate of production of the mass of component i per unit volume, which is defined by

$$r_i = \mathrm{MW}_i \sum_{j=1}^{R} \nu_{ij}\mathfrak{R}_j$$

where ν_{ij} is the stoichiometric coefficient of component i in reaction j, MW_i the molecular weight of component i, and $\mathfrak{R}_j$ the intrinsic kinetic rate expression on a volumetric basis for reaction j. Obtain an expression for the rate of entropy production per unit volume that conforms to the following generalized pattern:

$$s_G = \sum_{i=1}^{2N} (\mathrm{flux})_i (\mathrm{force})_i$$

where the forces should be identified as

$$\frac{1}{T^2}\nabla T \qquad \frac{1}{T}\nabla \mathbf{v} \qquad \frac{\varphi_i}{T} \qquad (1 \leq i \leq N-1)$$

and

$$\frac{1}{T}[\nabla \varphi_i + (\mathbf{g}_N - \mathbf{g}_i] \qquad (1 \leq i \leq N-1)$$

with

$$\varphi_i = \frac{\mu_i}{\mathrm{MW}_i} - \frac{\mu_N}{\mathrm{MW}_N}$$

and μ_i the chemical potential of component i in the mixture. Extend the definition of the molecular flux of fluid entropy for a binary mixture with

respect to the mass-average fluid velocity **v**, to an N-component system in the following manner:

$$\sigma = \frac{1}{T}\left(\mathbf{q} - \sum_{i=1}^{N-1} \varphi_i \mathbf{j}_i\right)$$

where **q** is the molecular thermal energy flux vector and $\mathbf{j}_i$ is the diffusional mass flux of component i in the mixture with respect to the mass-average velocity.

(a) Construct linear transport laws for all fluxes of tensorial rank = 1. Use summation notation, whenever possible, to condense your answers.

Answer: for $1 \leq i \leq N-1$

$$-\mathbf{j}_i = \sum_{k=1}^{N-1} \xi_{ik} \frac{1}{T} \nabla \varphi_k^* + \xi_{iN} \frac{1}{T^2} \nabla T$$

$$-\left\{\mathbf{q} - \sum_{i=1}^{N-1} \varphi_i \mathbf{j}_i\right\} = \sum_{k=1}^{N-1} \xi_{Nk} \frac{1}{T} \nabla \varphi_k^* + \xi_{NN} \frac{1}{T^2} \nabla T$$

(b) Simplify your result for the diffusional mass flux of component 1 with respect to the mass-average velocity of the mixture if the system is isothermal, isobaric, and contains three components.

Answer: If $N = 3$, $\nabla T = 0$, and $\nabla p = 0$, then:

$$\begin{aligned}
-\mathbf{j}_1 &= \xi_{11} \frac{1}{T} \nabla \varphi_1^* + \xi_{12} \frac{1}{T} \nabla \varphi_2^* \\
&= \left\{ \xi_{11} \frac{1}{T} \left(\frac{\partial \varphi_1}{\partial \omega_1} \right)_{T,p,\omega_2} + \xi_{12} \frac{1}{T} \left(\frac{\partial \varphi_2}{\partial \omega_1} \right)_{T,p,\omega_2} \right\} \nabla \omega_1 \\
&\quad + \left\{ \xi_{11} \frac{1}{T} \left(\frac{\partial \varphi_1}{\partial \omega_2} \right)_{T,p,\omega_1} + \xi_{12} \frac{1}{T} \left(\frac{\partial \varphi_2}{\partial \omega_2} \right)_{T,p,\omega_1} \right\} \nabla \omega_2 \\
&\quad + \xi_{11} \frac{1}{T} (\mathbf{g}_3 - \mathbf{g}_1) + \xi_{12} \frac{1}{T} (\mathbf{g}_3 - \mathbf{g}_2)
\end{aligned}$$

(c) Obtain an expression for the molecular thermal energy flux **q** in this isothermal, isobaric, ternary system. Express your answer in terms of (1) the Onsager coefficients, (2) φ_i where $i = 1, 2$, and (3) $\nabla \varphi_i^* = \nabla \varphi_i + (\mathbf{g}_3 - \mathbf{g}_i)$ where $i = 1, 2$.

Answer: In summation notation for a ternary system at constant temperature:

$$-\mathbf{q} = \sum_{i=1}^{2} \sum_{j=1}^{2} (\varphi_i \xi_{ij} + \delta_{ij} \xi_{ij}) \frac{1}{T} \nabla \varphi_j^*$$

where δ_{ij} is the Kronecker delta.

Transport Phenomena for Chemical Reactor Design. Laurence A. Belfiore
Copyright © 2003 John Wiley & Sons, Inc.
ISBN: 0-471-20275-4

27

THERMAL ENERGY BALANCE IN MULTICOMPONENT MIXTURES AND NONISOTHERMAL EFFECTIVENESS FACTORS VIA COUPLED HEAT AND MASS TRANSFER IN POROUS CATALYSTS

27-1 EQUATION OF CHANGE FOR SPECIFIC INTERNAL ENERGY THAT SATISFIES THE FIRST LAW OF THERMODYNAMICS

For mixtures of N components, the differential form of the first law is written for the specific internal energy u as

$$du = T\,ds - p\,d\left(\frac{1}{\rho}\right) + \sum_{i=1}^{N-1} \varphi_i\,d\omega_i \tag{27-1}$$

This differential expression is consistent with the facts that there are $N+1$ degrees of freedom for a single-phase N-component mixture and that $u(s, \rho, \omega_1, \omega_2, \ldots, \omega_{N-1})$ contains complete information about the system. Equation (27-1) is restricted to Newtonian fluids that cannot store elastic energy (Curtiss and Bird, 1996). For viscoelastic fluids, a work term due to elastic forces must be considered in addition to p-V work, similar to the classical thermodynamic analysis of rubber-like solids. The mass fraction coefficients of the specific internal energy (i.e., φ_i) are related to the chemical potentials μ_i via the development presented in Chapter 26 via equation (26-30). Hence,

$$\varphi_i = \left(\frac{\partial u}{\partial \omega_i}\right)_{s,\rho,\text{ all }\omega_j\ (j\neq i,N)} = \left(\frac{\partial \mathscr{G}}{\partial \omega_i}\right)_{T,p,\text{ all }\omega_j (j\neq i,N)} = \frac{\mu_i}{\mathrm{MW}_i} - \frac{\mu_N}{\mathrm{MW}_N} \tag{27-2}$$

It is permissible to manipulate the differential form of the first law of thermodynamics, as illustrated below, and add the following four equations in rectangular

coordinates:

$$\frac{\partial u}{\partial t} = T\frac{\partial s}{\partial t} - p\frac{\partial(1/\rho)}{\partial t} + \sum_{i=1}^{N-1}\varphi_i\frac{\partial \omega_i}{\partial t} \tag{27-3a}$$

$$v_x\left[\frac{\partial u}{\partial x} = T\frac{\partial s}{\partial x} - p\frac{\partial(1/\rho)}{\partial x} + \sum_{i=1}^{N-1}\varphi_i\frac{\partial \omega_i}{\partial x}\right]$$

where v_x is the x component of the velocity vector (27-3b)

$$v_y\left[\frac{\partial u}{\partial y} = T\frac{\partial s}{\partial y} - p\frac{\partial(1/\rho)}{\partial y} + \sum_{i=1}^{N-1}\varphi_i\frac{\partial \omega_i}{\partial y}\right]$$

where v_y is the y component of the velocity vector (27-3c)

$$v_z\left[\frac{\partial u}{\partial z} = T\frac{\partial s}{\partial z} - p\frac{\partial(1/\rho)}{\partial z} + \sum_{i=1}^{N-1}\varphi_i\frac{\partial \omega_i}{\partial z}\right]$$

where v_z is the z component of the velocity vector (27-3d)

The final result is equivalent to taking the substantial derivative of the first law in any coordinate system. It allows one to generate the equation of change for internal energy by combining the equation of continuity, the mass transfer equation, and the equation of change for specific entropy. Hence, replacing the differential d in the first law by the substantial derivative D/Dt produces the following result after multiplication by the fluid density ρ:

$$\rho\frac{Du}{Dt} = \rho T\frac{Ds}{Dt} + \frac{p}{\rho}\frac{D\rho}{Dt} + \sum_{i=1}^{N-1}\varphi_i\rho\frac{D\omega_i}{Dt} \tag{27-4}$$

The following substitutions are required to obtain the desired result:

1. The equation of change for specific entropy, given by (25-36), replaces the first term on the right side of the internal energy equation:

$$\rho T\frac{Ds}{Dt} = -\nabla\cdot\mathbf{q} - \tau : \nabla\mathbf{v} + \sum_{i=1}^{N}\mathbf{j}_i\cdot\mathbf{g}_i + \sum_{i=1}^{N-1}\varphi_i(\nabla\cdot\mathbf{j}_i - r_i) \tag{27-5}$$

2. The equation of continuity on page 222 replaces the second term on the right of the internal energy equation, given by (27-4):

$$\frac{\partial\rho}{\partial t} + \mathbf{v}\cdot\nabla\rho \equiv \frac{D\rho}{Dt} = -\rho\nabla\cdot\mathbf{v} \tag{27-6}$$

3. The mass transfer equation for component i, given by (9-20), replaces each of the $N-1$ terms in the summation on the right side of the internal

energy equation:

$$\rho\left(\frac{\partial\omega_i}{\partial t}+\mathbf{v}\cdot\nabla\omega_i\right)\equiv\rho\frac{D\omega_i}{Dt}=-\nabla\cdot\mathbf{j}_i+\sum_j \upsilon_{ij}\ \mathrm{MW}_i\ \mathfrak{R}_j$$
$$=-\nabla\cdot\mathbf{j}_i+r_i \tag{27-7}$$

The multicomponent equation of change for specific internal energy, given by (27-4), which is consistent with the first law of thermodynamics and the definition of the molecular flux of thermal energy via the entropy balance, reduces to:

$$\rho\frac{Du}{Dt}=-\nabla\cdot\mathbf{q}-\tau:\nabla\mathbf{v}+\sum_{i=1}^{N}\mathbf{j}_i\cdot\mathbf{g}_i+\sum_{i=1}^{N-1}\varphi_i(\nabla\cdot\mathbf{j}_i-r_i)$$
$$+\frac{p}{\rho}(-\rho\nabla\cdot\mathbf{v})+\sum_{i=1}^{N-1}\varphi_i(-\nabla\cdot\mathbf{j}_i+r_i)$$
$$\rho\frac{Du}{Dt}=-\nabla\cdot\mathbf{q}-p\nabla\cdot\mathbf{v}-\tau:\nabla\mathbf{v}$$
$$+\sum_{i=1}^{N}\mathbf{j}_i\cdot\mathbf{g}_i \tag{27-8}$$

An analysis of each term in the final form of the internal energy equation, given by (27-8), follows:

1. The left side corresponds to the accumulation of internal energy in a control volume that moves at the local fluid velocity at each point on its surface. If the substantial derivative is expanded using vector notation, then there are actually two terms on the left side.

$$\rho\frac{Du}{Dt}=\rho\left(\frac{\partial u}{\partial t}+\mathbf{v}\cdot\nabla u\right)=\frac{\partial(\rho u)}{\partial t}+\nabla\cdot\rho\mathbf{v}u \tag{27-9}$$

The equation of continuity allows one to express the substantial derivative of u (i.e., $\rho\,Du/Dt$) in terms of two contributions on the far right side of (27-9). The accumulation rate process within a stationary control volume is represented by the partial time derivative [i.e., $\rho\,\partial u/\partial t$ or $\partial(\rho u)/\partial t$]. The scalar product of the total mass flux vector with the gradient of internal energy (i.e., $\rho\mathbf{v}\cdot\nabla u$) corresponds to the net rate at which internal energy leaves the control volume due to convective flux acting across the surface of this volume element. The convective flux of internal energy is given by $\rho\mathbf{v}u$. When $\rho\mathbf{v}\cdot\nabla u$ is moved to the right side of the internal energy equation with a negative sign, then $-\rho\mathbf{v}\cdot\nabla u$ corresponds to the net rate at which internal energy enters a stationary control volume due to convective flux.

2. The first term on the right side of the internal energy equation ($-\nabla \cdot \mathbf{q}$) corresponds to the net rate at which internal energy enters the control volume due to molecular flux acting across the surface. For multicomponent mixtures,

$$\mathbf{q} = -k_{\mathrm{TC}} \nabla T + \sum_{i=1}^{N} \frac{\mathfrak{h}_i}{\mathrm{MW}_i} \mathbf{j}_i \tag{27-10}$$

where k_{TC} is the thermal conductivity of the fluid. Fourier's law and the interdiffusional fluxes are considered in equation (27-10), but the diffusion-thermo (i.e., Dufour) effect is neglected.

3. The second term on the right side of the internal energy equation ($-p\nabla \cdot \mathbf{v}$) represents the reversible exchange between internal and kinetic energies. The equations of change for internal and kinetic energies are presented for pure fluids in Bird *et al*. (2002, pp. 81, 336). Of particular importance, the $p\nabla \cdot \mathbf{v}$ term appears with opposite signs in these balances. With the aid of the equation of continuity,

$$-p\nabla \cdot \mathbf{v} = -p\left(-\frac{1}{\rho}\frac{D\rho}{Dt}\right) = p\frac{D\ln\rho}{Dt} \tag{27-11}$$

If work is done on the fluid to compress it, then the density increases in a control volume that moves with the local fluid velocity. This causes an increase in internal energy in the moving control volume. If the fluid expands and does work on the surroundings, then its density decreases, which causes the internal energy to decrease in the moving control volume. These effects of compression and expansion on internal energy are consistent with the first law of thermodynamics.

4. The third term on the right side of the internal energy equation ($-\tau : \nabla\mathbf{v}$) represents the irreversible conversion of kinetic energy to internal energy. This is consistent with the fact that $-(1/T)\tau : \nabla\mathbf{v} > 0$ corresponds to the rate of entropy generation per unit volume due to viscous momentum transport in pure Newtonian fluids with no temperature gradients, via equation (25-45). Obviously, $\tau : \nabla\mathbf{v}$ appears with opposite signs in the equations of change for kinetic and internal energies, as illustrated in Bird *et al*. (2002, pp. 81, 336). Of practical importance, the non-ideal Bernoulli equation for steady flow of an incompressible fluid through a straight horizontal conduit with no change in cross-sectional area reduces to

$$-\int_V (\tau : \nabla\mathbf{v})\, dV = \frac{\text{mass flow rate}}{\rho}\,(p_{\text{upstream}} - p_{\text{downstream}}) > 0 \tag{27-12}$$

Hence, a decrease in fluid pressure (i.e., $p_{\text{upstream}} > p_{\text{downstream}}$) represents the macroscopic consequence of the irreversible degradation of kinetic energy to internal energy via friction loss.

5. The fourth term on the right side of the internal energy equation (i.e., $\sum_i \mathbf{j}_i \cdot \mathbf{g}_i$) arises because the external force field induces diffusional fluxes.

It can be viewed as a work-related term that increases the internal energy of the system, unless diffusion opposes the external force. This contribution vanishes for pure fluids (i.e., $\mathbf{j}_1 = 0$). It also vanishes for multicomponent mixtures when the external force field acts similarly on all components in the mixture (i.e., $\mathbf{g}_i = \mathbf{g}$ for $1 \leq i \leq N$) because the diffusional mass fluxes of all components with respect to the mass-average velocity sum to zero:

$$\sum_{i=1}^{N} \mathbf{j}_i \cdot \mathbf{g}_i = \mathbf{g} \cdot \left(\sum_{i=1}^{N} \mathbf{j}_i \right) = 0 \tag{27-13}$$

27-2 MULTICOMPONENT TRANSPORT IN POROUS CATALYSTS

Steady-state analysis of coupled heat and mass transfer within the pores of catalytic pellets is based on simultaneous solution of the mass transfer equation:

$$-\nabla \cdot \mathbf{j}_i + r_i = -\nabla \cdot \mathbf{j}_i + \sum_j \upsilon_{ij}\ \mathrm{MW}_i\ \mathfrak{R}_j = 0 \tag{27-14}$$

and the thermal energy balance:

$$\nabla \cdot \mathbf{q} = 0 \tag{27-15}$$

when contributions from convective transport are neglected. Irreversible production of thermal energy, reversible exchange between kinetic and internal energies, and effects from external force fields are also neglected in the thermal energy balance. When there is only one chemical reaction on the internal catalytic surface, or if one of the steps in a multistep process is rate limiting, then subscript j is not required and equation (27-14) reduces to:

$$-\nabla \cdot \mathbf{j}_i + \upsilon_i\ \mathrm{MW}_i\ \mathfrak{R} = 0 \tag{27-16}$$

Stoichiometry in the mass balance with diffusion and chemical reaction indicates that

$$\frac{1}{\upsilon_i \mathrm{MW}_i} \nabla \cdot \mathbf{j}_i = \frac{1}{\upsilon_\mathrm{A} \mathrm{MW}_\mathrm{A}} \nabla \cdot \mathbf{j}_\mathrm{A} = \mathfrak{R} \tag{27-17}$$

Equation (27-17) and the thermal energy balance given by (27-15) are integrated over an arbitrary control volume V within the catalytic pores via Gauss's law:

$$\int_V \left[\frac{1}{\upsilon_i \mathrm{MW}_i}\ \nabla \cdot \mathbf{j}_i - \frac{1}{\upsilon_\mathrm{A} \mathrm{MW}_\mathrm{A}} \nabla \cdot \mathbf{j}_\mathrm{A} \right] dV = \int_S \left[\frac{1}{\upsilon_i \mathrm{MW}_i}\, \mathbf{n} \cdot \mathbf{j}_i - \frac{1}{\upsilon_\mathrm{A} \mathrm{MW}_\mathrm{A}}\, \mathbf{n} \cdot \mathbf{j}_\mathrm{A} \right] dS = 0 \tag{27-18}$$

$$\int_V (\nabla \cdot \mathbf{q})\, dV = \int_S (\mathbf{n} \cdot \mathbf{q})\, dS = 0 \tag{27-19}$$

where **n** is a unit normal vector directed outward from the surface of the control volume. Since there are many choices for control volume V and surface S that surrounds this volume element within the catalytic pores, the integrands of the surface integrals in (27-18) and (27-19) must vanish. Hence,

$$\frac{1}{\upsilon_i \mathrm{MW}_i}\,\mathbf{n}\cdot\mathbf{j}_i = \frac{1}{\upsilon_\mathrm{A}\mathrm{MW}_\mathrm{A}}\,\mathbf{n}\cdot\mathbf{j}_\mathrm{A} \qquad 1 \le i \le N \tag{27-20}$$

$$\mathbf{n}\cdot\mathbf{q} = \mathbf{n}\cdot\left(-k_\mathrm{TC}\,\nabla T + \sum_{i=1}^{N}\frac{\mathfrak{h}_i}{\mathrm{MW}_i}\,\mathbf{j}_i\right) = 0 \tag{27-21}$$

These conditions on the diffusional mass flux and the molecular flux of thermal energy, the latter of which includes Fourier's law and the interdiffusional contribution, allow one to relate temperature and reactant molar density within the pellet. If n is the local coordinate measured in the direction of **n**, then equations (27-20) and (27-21) can be combined as follows:

$$\begin{aligned}\mathbf{n}\cdot(k_\mathrm{TC}\,\nabla T) = k_\mathrm{TC}\,\frac{\partial T}{\partial n} &= \sum_{i=1}^{N}(\upsilon_i\mathfrak{h}_i)\frac{1}{\upsilon_i\mathrm{MW}_i}(\mathbf{n}\cdot\mathbf{j}_i)\\ &= \frac{1}{\upsilon_\mathrm{A}\mathrm{MW}_\mathrm{A}}(\mathbf{n}\cdot\mathbf{j}_\mathrm{A})\sum_{i=1}^{N}\upsilon_i\mathfrak{h}_i\end{aligned} \tag{27-22}$$

Since the summation in (27-22) includes all components in the mixture, it represents an exact expression for the enthalpy change due to chemical reaction, $\Delta H_\mathrm{reaction}$, on a molar basis (see Tester and Modell, 1997, pp. 769–770). Intermolecular interactions and non-ideal solution effects are also included in

$$\sum_{i=1}^{N}\upsilon_i\mathfrak{h}_i \equiv \Delta H_\mathrm{reaction} = \Delta H_\mathrm{Rx} \tag{27-23}$$

because $\mathfrak{h}_i$ is the partial molar enthalpy of component i. However, in practice, pure-component molar enthalpies are employed to approximate $\Delta H_\mathrm{reaction}$. This approximation is exact only for ideal solutions because partial molar enthalpies reduce to pure-component molar enthalpies under ideal conditions. Fick's law for $\mathbf{j}_\mathrm{A}$ within the catalytic pores is written in terms of a gas-phase concentration gradient, molecular weight, and the effective intrapellet diffusivity of component A as follows:

$$\begin{aligned}\mathbf{j}_\mathrm{A} &= -\rho\mathfrak{D}_{\mathrm{A,\,effective}}\nabla\omega_\mathrm{A} \approx -\mathfrak{D}_{\mathrm{A,\,effective}}\nabla\rho\omega_\mathrm{A}\\ &= -\mathfrak{D}_{\mathrm{A,\,effective}}\nabla(C_\mathrm{A}\mathrm{MW}_\mathrm{A})\end{aligned} \tag{27-24}$$

$$\frac{1}{\mathrm{MW}_\mathrm{A}}\,\mathbf{n}\cdot\mathbf{j}_\mathrm{A} = -\mathfrak{D}_{\mathrm{A,\,effective}}\,\mathbf{n}\cdot\nabla C_\mathrm{A} = -\mathfrak{D}_{\mathrm{A,\,effective}}\frac{\partial C_\mathrm{A}}{\partial n} \tag{27-25}$$

The stoichiometric coefficient of species A is -1 in the slowest step of the adsorption/reaction/desorption sequence. Hence, equations (27-22), (27-23), and

(27-25) indicate that temperature and reactant molar density are related by

$$k_{\mathrm{TC}} \frac{\partial T}{\partial n} = \mathfrak{D}_{\mathrm{A,\,effective}} \Delta H_{\mathrm{reaction}} \frac{\partial C_{\mathrm{A}}}{\partial n} \tag{27-26}$$

Even though temperature and reactant concentration profiles are solved for one-dimensional diffusion in the thinnest dimension of the pellet (i.e., or radially for long cylinders and spheres), the equations in this section are applicable to multidimensional diffusion and conduction. The coordinate direction denoted by n in (27-26) is not important, because

$$\frac{\partial T/\partial n}{\partial C_{\mathrm{A}}/\partial n} = \frac{\partial T}{\partial C_{\mathrm{A}}} = \frac{\mathfrak{D}_{\mathrm{A,\,effective}} \Delta H_{\mathrm{reaction}}}{k_{\mathrm{TC}}} \tag{27-27}$$

27-3 NONISOTHERMAL EFFECTIVENESS FACTORS IN POROUS CATALYSTS

For a particular catalyst geometry, nonisothermal effectiveness factor calculations via one-dimensional pseudo-homogeneous diffusion and pseudo-volumetric chemical reaction require numerical solutions of coupled mass and thermal energy balances. A good reference that discusses nonisothermal effectiveness factors vs. intrapellet Damkohler numbers with graphical examples and important parameters that govern the shape of the dimensionless correlation is Hill (1977, pp. 458–461). The analysis of coupled thermal energy and mass transfer in multicomponent mixtures in Section 27-2 suggests that the relation between intrapellet temperature and molar density in catalysts of any geometry is obtained by integrating the following ordinary differential equation when C_{A} is one-dimensional and the temperature dependence of the effective intrapellet diffusion coefficient is considered:

$$\frac{\partial T}{\partial C_{\mathrm{A}}} \longrightarrow \frac{dT}{dC_{\mathrm{A}}} = \frac{\mathfrak{D}_{\mathrm{A,\,effective}}(T) \Delta H_{\mathrm{reaction}}}{k_{\mathrm{effective}}} \tag{27-28}$$

The boundary conditions at the external surface of the catalyst are $T = T_{\mathrm{surface}}$ and $C_{\mathrm{A}} = C_{\mathrm{A\ surface}}$, and $k_{\mathrm{effective}}$ is the effective thermal conductivity of the composite catalyst structure (i.e., $\approx 1.6 \times 10^{-3}$ J/cm·s·K for alumina). Initially, the surface temperature and concentration of reactant A in the vicinity of a single isolated catalytic pellet are chosen to match the inlet values to the packed reactor. If external mass and heat transfer resistances are minimal, then bulk gas-phase temperature and reactant concentration at each axial position in the reactor represent the characteristic quantities that should be used to calculate the intrapellet Damkohler number for nth-order chemical kinetics:

$$\Lambda^2_{\mathrm{A,\,intrapellet}} = \frac{k_n(T_{\mathrm{surface}}) L^2 (C_{\mathrm{A,\,surface}})^{n-1}}{\mathfrak{D}_{\mathrm{A,\,effective}}(T_{\mathrm{surface}})}$$

$$k_n(T_{\mathrm{surface}}) = S_m \rho_{\mathrm{app}} k_f (K_{\mathrm{A}} K_{\mathrm{B}} \cdots)(R T_{\mathrm{surface}})^n \ [=]\ (\mathrm{volume/mole})^{n-1}/\mathrm{time} \tag{27-29}$$

where S_m is the internal surface area per mass of catalyst; ρ_{app} is the apparent density of the pellet, including the internal void space; k_f is the forward kinetic rate constant for surface-catalyzed chemical reaction with units of moles per area per time when fractional surface coverage replaces molar density in the rate law; L is the characteristic length for diffusion in the thinnest dimension of the catalyst; and K_i is the adsorption/desorption equilibrium constant for each reactant that adsorbs on the surface with units of inverse atmospheres. The dimensionless rate law in the mass balance with diffusion and chemical reaction must be modified because the dimensional rate law requires $k_n(T)$, and it is dimensionalized via division by $k_n(T_{\text{surface}})(C_{\text{A, surface}})^n$. In other words, the intrapellet Damkohler number is based on $k_n(T_{\text{surface}})$, as illustrated by (27-29). Hence, the ratio $k_n(T)/k_n(T_{\text{surface}})$ survives the dimensional analysis in the mass balance with diffusion and chemical reaction, and this introduces an Arrhenius factor of $\exp[E_{\text{act}}(T - T_{\text{surface}})/RTT_{\text{surface}}]$.

Two coupled ODEs must be solved to calculate temperature and reactant concentration profiles within a catalytic pellet that exhibits rectangular symmetry. The primary contribution to diffusion occurs in the thinnest dimension of the catalyst (i.e., the x direction). Hence, the mass transfer equation with one-dimensional diffusion and nth-order irreversible chemical reaction reduces to

$$-\nabla \cdot \mathbf{j}_i + r_i = -\nabla \cdot [-\mathfrak{D}_{\text{i, effective}} \nabla (C_i \text{MW}_i)] + \upsilon_i \text{MW}_i \mathfrak{R} = 0 \tag{27-30}$$

$$\mathfrak{D}_{\text{i, effective}} \frac{d^2 C_i}{dx^2} + \upsilon_i k_n(T)(C_{\text{A}})^n = 0 \tag{27-31}$$

when the rate law is only a function of the molar density of one reactant. This equation is written in dimensionless form for reactant A (i.e., $\upsilon_{\text{A}} = -1$) whose molar density appears in the kinetic rate law.

$$\mathfrak{D}_{\text{A, effective}}(T) \frac{d^2(\Psi_{\text{A}} C_{\text{A, surface}})}{d\eta^2} = k_n(T_{\text{surface}}) L^2 (\Psi_{\text{A}} C_{\text{A, surface}})^n \frac{k_n(T)}{k_n(T_{\text{surface}})} \tag{27-32}$$

$$\frac{d^2 \Psi_{\text{A}}}{d\eta^2} = \frac{\Lambda^2_{\text{A, intrapellet}} (\Psi_{\text{A}})^n \exp[\gamma(\Theta - 1)/\Theta]}{\varepsilon_{\text{A}}(\Theta)} \tag{27-33}$$

where

$$\eta = \frac{x}{L} \qquad \Psi_{\text{A}} = \frac{C_{\text{A}}}{C_{\text{A, surface}}} \qquad \Theta = \frac{T}{T_{\text{surface}}} \qquad \gamma = \frac{E_{\text{act}}}{RT_{\text{surface}}}$$

$$\varepsilon_{\text{A}}(\Theta) = \frac{\mathfrak{D}_{\text{A, effective}}(T)}{\mathfrak{D}_{\text{A, effective}}(T_{\text{surface}})} = \Theta^{3/2}$$

The three-halves power of dimensionless temperature in the expression for $\varepsilon_A(\Theta)$ is based on the temperature dependence of gas-phase ordinary molecular diffusion coefficients when the catalytic pores are larger than 1 μm. In this pore-size regime, Knudsen diffusional resistance is negligible. The temperature dependence of the collision integral for ordinary molecular diffusion, Ω_D, illustrated in Bird *et al.* (2002, pp. 526, 866), has not been included in $\varepsilon_A(\Theta)$. The thermal energy balance given by equation (27-28), which includes conduction and interdiffusional fluxes, is written in dimensionless form with the aid of one additional parameter, β:

$$\frac{d(\Theta T_{\text{surface}})}{d(\Psi_A C_{A,\ \text{surface}})} = \frac{\mathfrak{D}_{A,\text{ effective}}(T)\Delta H_{\text{reaction}}}{k_{\text{effective}}} \tag{27-34}$$

$$\frac{d\Theta}{d\Psi_A} = -\beta\varepsilon_A(\Theta) \tag{27-35}$$

$$\beta = \frac{\mathfrak{D}_{A,\text{ effective}}(T_{\text{surface}})C_{A,\ \text{surface}}(-\Delta H_{\text{reaction}})}{T_{\text{surface}}\, k_{\text{effective}}} \tag{27-36}$$

Two coupled ODEs are solved with first-order irreversible chemical kinetics, subject to the following split boundary conditions:

1. $\Psi_A = 1$ and $\Theta = 1$ at the external surface of the catalytic pellet, $\eta = 1$.
2. The symmetry condition requires that the gradient $d\Psi_A/d\eta$ must vanish at the center of the catalyst, where $\eta = 0$.

Obviously, numerical methods are required to calculate the effectiveness factor, so the problem is reformulated in terms of three coupled first-order ordinary differential equations. This is required for numerical integration.

$$\frac{d\Psi_A}{d\eta} = \text{gradient} \tag{27-37}$$

$$\frac{d^2\Psi_A}{d\eta^2} = \frac{d(\text{gradient})}{d\eta} = \frac{\Lambda^2_{A,\text{ intrapellet}}(\Psi_A)^n \exp[\gamma(\Theta - 1)/\Theta]}{\varepsilon_A(\Theta)} \tag{27-38}$$

$$\frac{d\Theta}{d\Psi_A} = -\beta\varepsilon_A(\Theta) \tag{27-39}$$

If the numerical algorithm begins at the center of the pellet where $\eta = 0$ and proceeds to the external surface at $\eta = 1$, then only the gradient is known at the outset and one must guess values for dimensionless temperature and molar density at $\eta = 0$. Needless to say, it will be difficult to achieve solutions to this coupled set of equations that match the conditions for Θ and Ψ_A at $\eta = 1$. However, if one begins the numerical integration at the external surface where temperature and molar density are known and proceeds inward, then it is only necessary to guess the gradient at $\eta = 1$ until convergence is obtained, when the

gradient vanishes at the center of the pellet. To implement this procedure, the dimensionless spatial coordinate is redefined as $\zeta = 1 - \eta$ and integration begins at the external surface where $\eta = 1$ and $\zeta = 0$. The three coupled ODEs, given by (27-37) through (27-39), are modified slightly to account for the fact that $d\zeta = -d\eta$.

$$\frac{d\Psi_A}{d\eta} = -\frac{d\Psi_A}{d\zeta} = \text{gradient} \tag{27-40}$$

$$\frac{d(\text{gradient})}{d\eta} = -\frac{d(\text{gradient})}{d\zeta} = \frac{\Lambda^2_{A,\,\text{intrapellet}}(\Psi_A)^n \exp[\gamma(\Theta - 1)/\Theta]}{\varepsilon_A(\Theta)} \tag{27-41}$$

$$\frac{d\Theta}{d\Psi_A} = \frac{d\Theta/d\eta}{d\Psi_A/d\eta} = -\frac{d\Theta/d\zeta}{\text{gradient}} = -\beta\varepsilon_A(\Theta) \tag{27-42}$$

Hence, the final form of the system of equations that describes multicomponent heat and mass transfer in catalytic pellets via pseudo-homogeneous one-dimensional diffusion is

$$\frac{d\Psi_A}{d\zeta} = -\text{gradient} \tag{27-43}$$

$$\frac{d(\text{gradient})}{d\zeta} = -\frac{\Lambda^2_{A,\,\text{intrapellet}}(\Psi_A)^n \exp[\gamma(\Theta - 1)/\Theta]}{\varepsilon_A(\Theta)} \tag{27-44}$$

$$\frac{d\Theta}{d\zeta} = \beta\varepsilon_A(\Theta)(\text{gradient}) \tag{27-45}$$

The boundary conditions at the external surface of the pellet (i.e., $\eta = 1$) are

$$\begin{aligned} \Psi_A(\zeta = 0) &= 1 \\ \Theta(\zeta = 0) &= 1 \\ \text{gradient}(\zeta = 0) &= \text{guess} \end{aligned} \tag{27-46}$$

and the correct guess for the gradient at $\zeta = 0$ is obtained when the gradient vanishes at $\zeta = 1$. Since the macroscopic boundary of each pellet exhibits rectangular symmetry, the effectiveness factor E is given by

$$E = \frac{1}{\Lambda^2_{A,\,\text{intrapellet}}}\left(\frac{d\Psi_A}{d\eta}\right)_{\eta=1} = \frac{\text{gradient}(\zeta = 0)}{\Lambda^2_{A,\,\text{intrapellet}}} \tag{27-47}$$

It is necessary to check for multiple steady-state solutions to equations (27-43), (27-44), and (27-45) for diffusion and chemical reaction within the catalytic pores at constant values of $\Lambda^2_{A,\,\text{intrapellet}}$, β, and γ. This is a difficult task. The thermal

energy generation parameter β is positive for exothermic chemical reactions, and γ is the Arrhenius number. For example, two stable steady states and one unstable steady state exist when

$$0.2 < \Lambda_{\text{A, intrapellet}} < 0.9 \qquad \beta > 0.3 \qquad \gamma = 20 \tag{27-48}$$

for first-order kinetics in catalysts with spherical symmetry. In other words, for each combination of $\Lambda_{\text{A, intrapellet}}$, β, and γ that meets the restrictions in (27-48), there are three solutions for the effectiveness factor. The direction in which steady-state conditions are approached will determine the value of the effectiveness factor for a realistic situation when simulations reveal that multiple stationary states are possible.

27-4 PHYSICOCHEMICAL PROPERTIES OF GASES WITHIN CATALYTIC PELLETS

Gas-phase concentrations in the vicinity of the external surface of the catalyst are calculated using the ideal gas law. Under standard-state conditions, 1 mol of any ideal gas occupies 22.4 L. Furthermore, the ideal gas law suggests that molar density varies inversely with temperature. Hence,

$$C_{\text{A, surface}} \approx 4.5 \times 10^{-5} \frac{298}{T_{\text{surface}}(\text{K})} [=] \text{ mol/cm}^3 \tag{27-49}$$

The temperature dependence of the effective intrapellet diffusion coefficient conforms to the assumption that ordinary molecular diffusion provides the dominant resistance to mass transfer in the pores, relative to Knudsen diffusion. This is valid when the pore diameter is larger than 1 μm. Gas-phase diffusivities are approximately proportional to the three-halves power of absolute temperature. Hence,

$$\mathfrak{D}_{\text{A, effective}}(T_{\text{surface}}) \approx 0.1 \left[\frac{T_{\text{surface}}(\text{K})}{298} \right]^{1.5} [=] \text{ cm}^2/\text{s} \tag{27-50}$$

The enthalpy change for reaction is exothermic and varies from 50 to 80 kJ/mol. The activation energy for the forward reaction varies from 25 to 27 kJ/mol. The temperature at the external surface of the pellet is constant at 350 K. The effective thermal conductivity of alumina catalysts is 1.6×10^{-3} J/cm·s·K. The chemical reaction is first-order and irreversible and the catalysts exhibit rectangular symmetry. When $\varepsilon_{\text{A}}(\Theta) \approx 1$ in the mass transfer equation, simulations in Tables 27-1, 27-2, and 27-3 reveal that the effectiveness factors exceed unity. This is a consequence of the fact that elevated temperatures within the catalyst cause kinetic rate constants to increase exponentially. This increase in $k_n(T)$ outweighs the decrease in reactant molar densities inside the catalyst. Hence, volumetrically averaged reaction rates within the catalyst are greater than the rate of reaction using concentrations and temperatures on the external surface.

TABLE 27-1 Numerical Results for Coupled Heat and Mass Transfer with First-Order Irreversible Exothermic Chemical Reaction in Porous Catalysts with Rectangular Symmetry[a]

$\Lambda_{A,\ intrapellet}$	Effectiveness Factor	$(\text{Gradient})_{\eta=1}$	$(\Theta_{max})_{\eta=0}$	$\Psi_A(\eta = 0)$
0.50	1.39	0.347	1.09	0.81
0.60	1.91	0.687	1.19	0.61
0.65	2.47	1.045	1.33	0.39
0.70	2.71	1.326	1.44	0.24
0.75	2.69	1.512	1.50	0.16
0.80	2.59	1.660	1.53	0.12
0.85	2.48	1.790	1.56	8.4×10^{-2}
0.90	2.36	1.910	1.58	6.3×10^{-2}
0.95	2.25	2.026	1.59	4.7×10^{-2}
1.00	2.14	2.138	1.60	3.6×10^{-2}

[a]Effectiveness factors vs. intrapellet Damkohler numbers when the temperature dependence of effective intrapellet diffusion coefficients is neglected in the mass transfer equation.

TABLE 27-2 Numerical Results for Coupled Heat and Mass Transfer with First-Order Irreversible Chemical Kinetics in Porous Catalysts with Rectangular Symmetry[a]

β	$-\Delta H_{Rx}$ (kJ/mol)	$(\text{Gradient})_{\eta=1}$	$(\Theta_{max})_{\eta=0}$	$\Psi_A(\eta = 0)$
0.44	50	2.13821	1.60	3.6×10^{-2}
0.52	60	2.55677	1.82	7.4×10^{-3}
0.53	61	2.60256	1.85	6.2×10^{-3}
0.54	62	2.64919	1.87	5.2×10^{-3}
0.56	64	2.74502	1.92	3.5×10^{-3}
0.57	66	2.84439	1.97	2.4×10^{-3}
0.61	70	3.05417	2.07	9.9×10^{-4}
0.65	75	3.33814	2.20	2.9×10^{-4}
0.70	80	3.64755	2.35	7.4×10^{-5}

[a]Effect of the enthalpy change for exothermic chemical reaction on the effectiveness factor when the temperature dependence of effective intrapellet diffusion coefficients is neglected in the mass transfer equation.

The effectiveness factor is required to estimate the average rate of consumption of reactants in the catalytic pores based on temperature and molar density at the external surface or in the adjacent bulk gas stream moving through the fixed-bed reactor. Hence, plug-flow design equations presented in Section 27-6 for packed catalytic tubular reactors must include the effectiveness factor in the rate law, even when isothermal operation is a reasonable assumption.

TABLE 27-3 Numerical Results for Coupled Heat and Mass Transfer with First-Order Irreversible Exothermic Chemical Reaction in Porous Catalysts with Rectangular Symmetry[a]

γ	$E_{\text{activation}}$ (kJ/mol)	$(\text{Gradient})_{\eta=1}$	$(\Theta_{\max})_{\eta=0}$	$\Psi_A(\eta = 0)$
8.59	25.0	3.647558	2.35	7.4×10^{-5}
8.76	25.5	3.769966	2.35	4.1×10^{-5}
9.28	27.0	4.167900	2.35	5.8×10^{-6}

[a]Effect of the activation energy for the forward reaction on the effectiveness factor when the temperature dependence of effective intrapellet diffusion coefficients is neglected in the mass transfer equation.

1. *Effect of the intrapellet Damkohler number on the effectiveness factor.* These calculations are summarized in Table 27-1 for the following parametric values:

$$E_{\text{activation}} = 25 \text{ kJ/mol} \qquad \gamma = 8.59$$

$$\Delta H_{\text{Rx}} = -50 \text{ kJ/mol} \qquad \beta = 0.44 \qquad 0.50 \le \Lambda_{\text{A, intrapellet}} \le 1.00$$

2. *Effect of the enthalpy change for reaction and β on the effectiveness factor.* These calculations are summarized in Table 27-2 for the following parametric values:

$$E_{\text{activation}} = 25 \text{ kJ/mol} \quad \gamma = 8.59 \quad \Lambda_{\text{A, intrapellet}} = 1.0$$

$$50 \text{ kJ/mol} \le -\Delta H_{\text{Rx}} \le 80 \text{ kJ/mol} \quad 0.44 \le \beta \le 0.70$$

$$\text{effectiveness factor} = (\text{gradient})_{\eta=1}$$

Detailed information about the entry in Table 27-2 where $\beta = 0.61$, which corresponds to an enthalpy change for chemical reaction of -70 kJ/mol, is provided in Table 27-4.

3. *Effect of the activation energy for the forward reaction and γ on the effectiveness factor.* These calculations are summarized in Table 27-3 for the following parametric values:

$$\Delta H_{\text{Rx}} = -80 \text{ kJ/mol} \quad \beta = 0.70 \quad \Lambda_{\text{A, intrapellet}} = 1.0$$

$$25 \text{ kJ/mol} \le E_{\text{activation}} \le 27 \text{ kJ/mol} \quad 8.59 \le \gamma \le 9.28$$

$$\text{effectiveness factor} = (\text{gradient})_{\eta=1}$$

TABLE 27-4 Computerized Results for Coupled Heat and Mass Transfer with First-Order Irreversible Exothermic Chemical Reaction in Porous Catalysts with Rectangular Symmetry[a]

$d(\Psi)/d(z) = -\text{Gradient}$
$d(\text{Gradient})/d(z) = -(\Lambda^{**}2)^{*}(\Psi^{**}n)^{*}\exp(\gamma^{*}(\Theta - 1)/\Theta)$
$d(\Theta)/d(z) = \beta^{*}\varepsilon^{*}\text{Gradient}$
$\varepsilon = \Theta^{**}(1.5)$
$\gamma = E_{\text{act}}/(8.314^{*}T_{\text{surface}})$
$\beta = D_{\text{eff}}T^{*}_{\text{surf}}C^{*}_{\text{surface}}(-\Delta H_{\text{Rx}})/(T^{*}_{\text{surface}}\text{Thermal } k_{\text{eff}})$
$E_{\text{act}} = 25000$
$D_{\text{eff}}T_{\text{surf}} = 0.1^{*}((T_{\text{surface}}/298)^{**}(1.5))$
$C_{\text{surface}} = 0.000045^{*}(298/T_{\text{surface}})$
$T_{\text{surface}} = 350$
Thermal $k_{\text{eff}} = 0.0016$
$\Delta H_{\text{Rx}} = -70000$
$\Lambda = 1$
Effective = Gradient/$(\Lambda^{**}2)$
$n = 1$

Variable	Nonisothermal Effectiveness Factors, Flat Catalysts			
	Initial Value	Maximum Value	Minimum Value	Final Value
z	0	1	0	1
Ψ	1	1	0.000989142	0.000989142
Gradient	3.05418	3.05418	8.15722e-06	8.15722e-06
Θ	1	2.06732	1	2.06732
ε	1	2.97242	1	2.97242
E_{act}	25000	25000	25000	25000
T_{surface}	350	350	350	350
γ	8.59136	8.59136	8.59136	8.59136
$D_{\text{eff}}T_{\text{surf}}$	0.127285	0.127285	0.127285	0.127285
C_{surface}	3.83143e-05	3.83143e-05	3.83143e-05	3.83143e-05
ΔH_{Rx}	−70000	−70000	−70000	−70000
Thermal k_{eff}	0.0016	0.0016	0.0016	0.0016
β	0.609605	0.609605	0.609605	0.609605
n	1	1	1	1
Λ	1	1	1	1
Effective	3.05418	3.05418	8.15722e-06	8.15722e-06

[a]The temperature dependence of effective intrapellet diffusion coefficients is neglected in the mass transfer equation.

27-5 ESTIMATES OF THE MAXIMUM TEMPERATURE RISE WITHIN CATALYTIC PELLETS FOR EXOTHERMIC CHEMICAL REACTIONS

Gas-phase concentrations in the vicinity of the external surface of the catalyst are calculated using the ideal gas law with the appropriate temperature dependence:

$$C_{\text{A, surface}} \approx 4.46 \times 10^{-5}\frac{298}{T_{\text{surface}}(\text{K})}[=]\ \text{mol/cm}^3 \tag{27-51}$$

The enthalpy change for reaction is exothermic and varies from 50 to 120 kJ/mol. ΔH_{Rx} is probably the most important parameter affecting the temperature within the catalyst. Hence, the effect of ΔH_{Rx}, via the thermal energy generation parameter β, on Θ_{max} is a chemical-reaction-thermodynamic phenomenon. The activation energy for the forward reaction varies from 25 to 30 kJ/mol. $E_{activation}$ is contained in the Arrhenius number γ, which greatly affects the rate of consumption of reactants inside the catalyst, particularly for exothermic reactions that cause the intrapellet temperature to increase. Hence, the effect of the Arrhenius number on the effectiveness factor is purely kinetic in nature. Interestingly, the maximum temperature within the catalyst is not affected by $E_{activation}$ when the central core of the catalyst is starved of reactants. In other words, interior pellet temperatures are governed by the thermal conductivity of the catalyst and the thermodynamics of the chemical reaction, not the kinetics of the reaction. A priori estimates of the maximum temperature rise within the catalyst can be obtained by integrating the temperature–concentration relation, given by equation (27-35):

$$\frac{d\Theta}{d\Psi_A} = -\beta\varepsilon_A(\Theta) \tag{27-52}$$

subject to the following conditions:

1. $\varepsilon_A(\Theta) \approx 1$ when the temperature dependence of the effective diffusion coefficient is neglected.
2. If the intrapellet Damkohler number is large enough, then $\Psi_A \to 0$ at the center of the catalyst where the maximum temperature occurs for exothermic chemical reactions. At smaller values of $\Lambda_{A,\ intrapellet}$, the dimensionless concentration of reactant A at the center of the catalyst is $\Psi_A(\eta = 0)$.
3. $\Psi_A = 1$ when $\Theta = 1$ on the external surface of the catalyst.

Hence, $d\Theta \approx -\beta\, d\Psi_A$. Integration from the external surface to the center of the catalyst yields the following back-of-the-envelope prediction, which does not require numerical simulations:

$$\begin{aligned} \Theta_{max} - 1 &\approx -\beta[\Psi_A(\eta = 0) - 1] \\ \Theta_{max} &\approx 1 + \beta[1 - \Psi_A(\eta = 0)] \end{aligned} \tag{27-53}$$

This simplified calculation reveals why $\Theta_{max} < 1 + \beta$ for exothermic reactions at small values of the intrapellet Damkohler number when the central core of the catalyst is not starved of reactants, and $\Psi_A(\eta = 0) > 0$. In the diffusion-limited regime at larger values of $\Lambda_{A,\ intrapellet}$, the second condition mentioned above yields $\Theta_{max} \approx 1 + \beta$, which translates into

$$\begin{aligned} T_{max} &\approx (1 + \beta)T_{surface} \\ \Delta T_{max} &= T_{max} - T_{surface} \approx \beta T_{surface} \end{aligned} \tag{27-54}$$

If one includes temperature dependence in ε_A and integrates equation (27-52),

$$\frac{d\Theta}{d\Psi_A} = -\beta\varepsilon_A(\Theta) = -\beta\Theta^{3/2} \tag{27-55}$$

subject to the boundary condition on the external surface, where $\Theta = 1$ and $\Psi_A = 1$, then the following dimensionless analytical relation between temperature and reactant molar density is obtained:

$$\Theta = \left[1 - \tfrac{1}{2}\beta(1 - \Psi_A)\right]^{-2} \tag{27-56}$$

For small values of the thermal energy generation parameter β, equation (27-56) is expanded in a Taylor series about $\beta = 0$:

$$\Theta = 1 + \beta(1 - \Psi_A) + \tfrac{3}{4}\beta^2(1 - \Psi_A)^2 + \cdots \tag{27-57}$$

Hence, the maximum temperature at the center of the catalyst in the diffusion-limited regime, where $\Psi_A(\eta = 0) \to 0$, is

$$\Theta_{max} \approx 1 + \beta + \tfrac{3}{4}\beta^2 + \cdots \tag{27-58}$$

which is obviously larger than $1 + \beta$. In general, if ε_A scales as Θ^m, then the maximum temperature at the center of a catalytic pellet with exothermic chemical reaction is

$$(\Theta_{max})^{1-m} = 1 + (1 - m)\beta[1 - \Psi_A(\eta = 0)] \tag{27-59}$$

where $m = 3/2$ if ordinary molecular diffusion provides the dominant resistance to mass transfer within the pores of a catalytic pellet (i.e., macropores with $<r>_{avg}$ larger than 1 μm), and $m = 1/2$ if this resistance is dominated by Knudsen diffusion with average pore sizes smaller than 50 Å (i.e., micropores).

Simulations are presented below in tabular and graphical forms when the temperature at the external surface of the pellet is constant at 350 K. The effective thermal conductivity of alumina catalysts is 1.6×10^{-3} J/cm·s·K. The chemical reaction is first-order and irreversible and the catalysts exhibit rectangular symmetry. Most important in Tables 27-5 to 27-8 and Figures 27-1 to 27-3, the diffusivity ratio $\varepsilon_A(\Theta)$ varies with temperature in the mass transfer equation. This effect was neglected in Tables 27-1 to 27-4. Notice that in all of these tables (i.e., 27-1 to 27-8), numerical simulations reveal that the actual Θ_{max} exceeds $1 + \beta$, except when the intrapellet Damkohler number is small enough and $\Psi_A(\eta = 0) > 0$ because the center of the catalyst is not reactant starved in the chemical-reaction-rate-controlled regime.

1. *Effect of the intrapellet Damkohler number on the effectiveness factor.* These calculations are summarized in Table 27-5 for the following parametric values:

$$E_{activation} = 25 \text{ kJ/mol} \qquad \gamma = 8.59$$

$$\Delta H_{Rx} = -50 \text{ kJ/mol} \qquad \beta = 0.43 \qquad 0.50 \le \Lambda_{A,\,intrapellet} \le 2.00$$

TABLE 27-5 Numerical Results for Coupled Heat and Mass Transfer with First-Order Irreversible Exothermic Chemical Reaction in Porous Catalysts with Rectangular Symmetry[a]

$\Lambda_{A,\,intrapellet}$	Effectiveness Factor	$(\text{Gradient})_{\eta=1}$	$(\Theta_{max})_{\eta=0}$	$\Psi_A(\eta = 0)$
0.50	1.23	0.308	1.07	0.84
0.60	1.40	0.503	1.13	0.73
0.65	1.51	0.639	1.17	0.65
0.70	1.65	0.806	1.22	0.56
0.75	1.77	0.993	1.29	0.45
0.80	1.84	1.174	1.35	0.36
0.85	1.85	1.335	1.40	0.28
0.90	1.82	1.475	1.44	0.22
0.95	1.77	1.600	1.48	0.18
1.00	1.72	1.715	1.50	0.14
2.00	0.89	3.557	1.62	4.4×10^{-3}

[a]Effectiveness factors vs. intrapellet Damkohler numbers when the temperature dependence of effective intrapellet diffusion coefficients is considered in the mass transfer equation. These results should be compared with those in Table 27-1.

TABLE 27-6 Numerical Results for Coupled Heat and Mass Transfer with First-Order Irreversible Chemical Kinetics in Porous Catalysts with Rectangular Symmetry[a]

β	$-\Delta H_{Rx}$ (kJ/mol)	$(\text{Gradient})_{\eta=1}$	$(\Theta_{max})_{\eta=0}$	$\Psi_A(\eta = 0)$
0.43	50	1.7151	1.50	1.4×10^{-1}
0.52	60	1.9875	1.74	6.8×10^{-2}
0.53	61	2.0142	1.76	6.3×10^{-2}
0.54	62	2.0409	1.79	5.8×10^{-2}
0.55	64	2.0943	1.84	4.9×10^{-2}
0.57	66	2.1480	1.89	4.2×10^{-2}
0.60	70	2.2563	2.00	3.0×10^{-2}
0.65	75	2.3945	2.15	2.0×10^{-2}
0.69	80	2.5366	2.30	1.3×10^{-2}
0.73	85	2.6827	2.47	8.2×10^{-3}
0.78	90	2.8325	2.66	5.3×10^{-3}
0.86	100	3.1416	3.08	2.3×10^{-3}
0.95	110	3.4582	3.62	1.0×10^{-3}
1.04	120	3.7754	4.30	5.5×10^{-4}

[a]Effect of the enthalpy change for exothermic chemical reaction on the effectiveness factor when the temperature dependence of effective intrapellet diffusion coefficients is considered in the mass transfer equation. These results should be compared with those in Table 27-2.

TABLE 27-7 Numerical Results for Coupled Heat and Mass Transfer with First-Order Irreversible Exothermic Chemical Reaction in Porous Catalysts with Rectangular Symmetry[a]

γ	$E_{\text{activation}}$ (kJ/mol)	$(\text{Gradient})_{\eta=1}$	$(\Theta_{\max})_{\eta=0}$	$\Psi_A(\eta = 0)$
8.59	25.0	2.5366	2.30	1.3×10^{-2}
8.76	25.5	2.6130	2.31	9.6×10^{-3}
9.28	27.0	2.8595	2.32	3.8×10^{-3}

[a]Effect of the activation energy for the forward reaction on the effectiveness factor when $\Delta H_{\text{Rx}} = -80$ kJ/mol and the temperature dependence of effective intrapellet diffusion coefficients is included in the mass transfer equation. These results should be compared with those in Table 27-3.

TABLE 27-8 Numerical Results for Coupled Heat and Mass Transfer with First-Order Irreversible Exothermic Chemical Reaction in Porous Catalysts with Rectangular Symmetry[a]

γ	$E_{\text{activation}}$ (kJ/mol)	$(\text{Gradient})_{\eta=1}$	$(\Theta_{\max})_{\eta=0}$	$\Psi_A(\eta = 0)$
8.59	25	3.77544139	4.30	5.5×10^{-4}
8.94	26	4.12283872	4.30	1.6×10^{-4}
9.28	27	4.50879163	4.30	3.6×10^{-5}
9.62	28	4.93776970	4.30	6.6×10^{-6}
9.97	29	5.41477412	4.30	8.4×10^{-7}
10.31	30	5.94540484	4.30	1.6×10^{-7}

[a] Effect of the activation energy for the forward reaction on the effectiveness factor when $\Delta H_{\text{Rx}} = -120$ kJ/mol and the temperature dependence of effective intrapellet diffusion coefficients is included in the mass transfer equation.

2. *Effect of the enthalpy change for reaction and β on the effectiveness factor.* These calculations are summarized in Table 27-6 and Figures 27-1 to 27-3 for the following parametric values:

$$E_{\text{activation}} = 25 \text{ kJ/mol} \quad \gamma = 8.59 \quad \Lambda_{\text{A, intrapellet}} = 1.0$$

$$50 \text{ kJ/mol} \leq -\Delta H_{\text{Rx}} \leq 120 \text{ kJ/mol} \quad 0.43 \leq \beta \leq 1.04$$

$$\text{effectiveness factor} = (\text{gradient})_{\eta=1}$$

3. *Effect of the activation energy for the forward reaction and γ on the effectiveness factor.* These calculations are summarized in Table 27-7 for the following parametric values:

$$\Delta H_{\text{Rx}} = -80 \text{ kJ/mol} \quad \beta = 0.69 \quad \Lambda_{\text{A, intrapellet}} = 1.0$$

$$25 \text{ kJ/mol} \leq E_{\text{activation}} \leq 27 \text{ kJ/mol} \quad 8.59 \leq \gamma \leq 9.28$$

$$\text{effectiveness factor} = (\text{gradient})_{\eta=1}$$

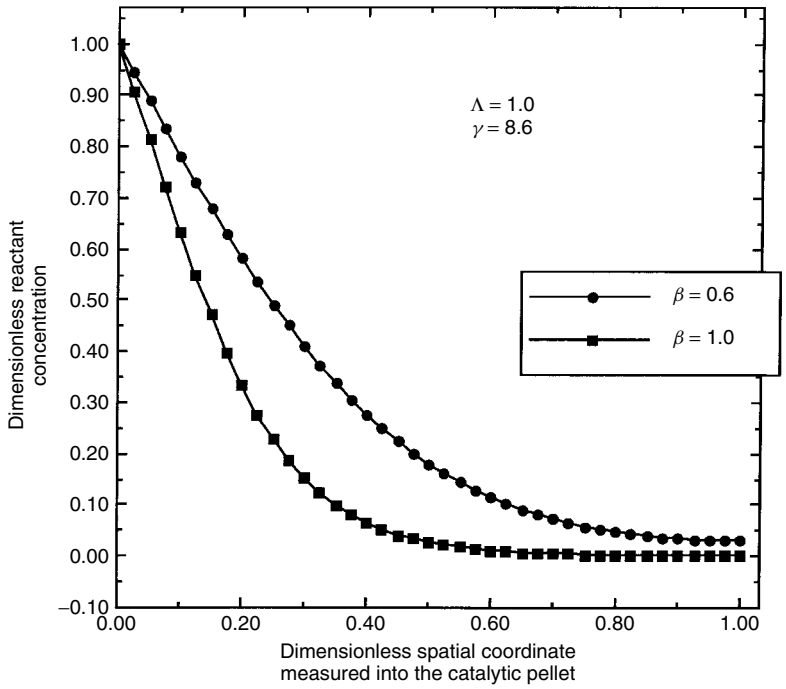

Figure 27-1 Effect of the thermal energy generation parameter β on dimensionless reactant concentration profiles as one travels inward toward the center of a porous catalyst with rectangular symmetry. The chemical kinetics are first-order and irreversible, and the reaction is exothermic. All parameters are defined in Table 27-4. The specific entries for $\beta = 0.6$ and $\beta = 1.0$ are provided in Table 27-6.

4. *Effect of the activation energy for the forward reaction and γ on the effectiveness factor.* These calculations are summarized in Table 27-8 for the following parametric values:

$$\Delta H_{\text{Rx}} = -120 \text{ kJ/mol} \quad \beta = 1.04 \quad \Lambda_{\text{A, intrapellet}} = 1.0$$

$$25 \text{ kJ/mol} \leq E_{\text{activation}} \leq 30 \text{ kJ/mol} \quad 8.59 \leq \gamma \leq 10.31$$

$$\text{effectiveness factor} = (\text{gradient})_{\eta=1}$$

27-6 DESIGN OF A NONISOTHERMAL PACKED CATALYTIC TUBULAR REACTOR

As discussed in Section 22-2.2, it is necessary to include the appropriate effectiveness factor $E(\Lambda_{\text{A, intrapellet}})$ from Section 27-5 in the reaction rate expression which appears in the coupled plug-flow mass and energy balances for

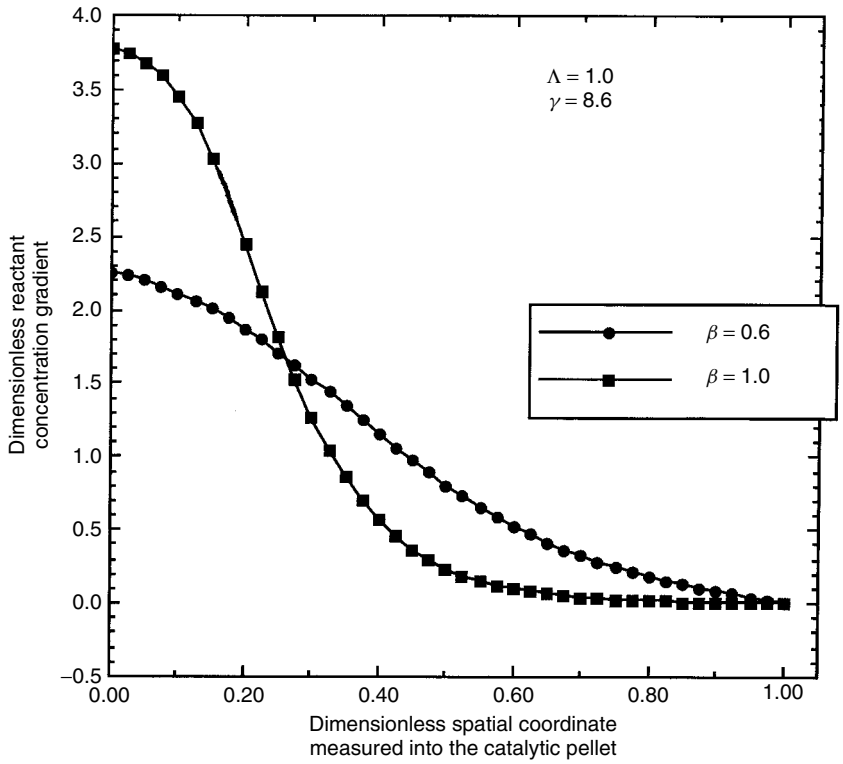

Figure 27-2 Effect of the thermal energy generation parameter β on dimensionless reactant concentration gradient profiles as one travels inward toward the center of a porous catalyst with rectangular symmetry. The chemical kinetics are first-order and irreversible, and the reaction is exothermic. All parameters are defined in Table 27-4. The specific entries for $\beta = 0.6$ and $\beta = 1.0$ are provided in Table 27-6.

the overall packed catalytic reactor. The coupled mass transfer equation (MTE) and thermal energy balance (TEB), summarized in Table 27-9, must be solved numerically.

At each axial step in the numerical solution of the coupled plug-flow mass and energy balances, it is necessary to re-evaluate the nonisothermal effectiveness factor at the appropriate intrapellet Damkohler number. Now, one must use surface concentrations $C_{A,\ surface}$ and temperatures $T_{surface}$ in the vicinity of a single isolated catalytic pellet that match bulk conditions in the reactor at each axial step in the Runge–Kutta numerical algorithm. These continuously changing surface conditions require one to recalculate $\Lambda^2_{A,\ intrapellet}$, β, and γ at each axial step in the numerical solution of the coupled plug-flow MTE and TEB because the effectiveness factor must be recalculated at the current values of these three parameters. This assumes that external resistances to heat and mass transfer are

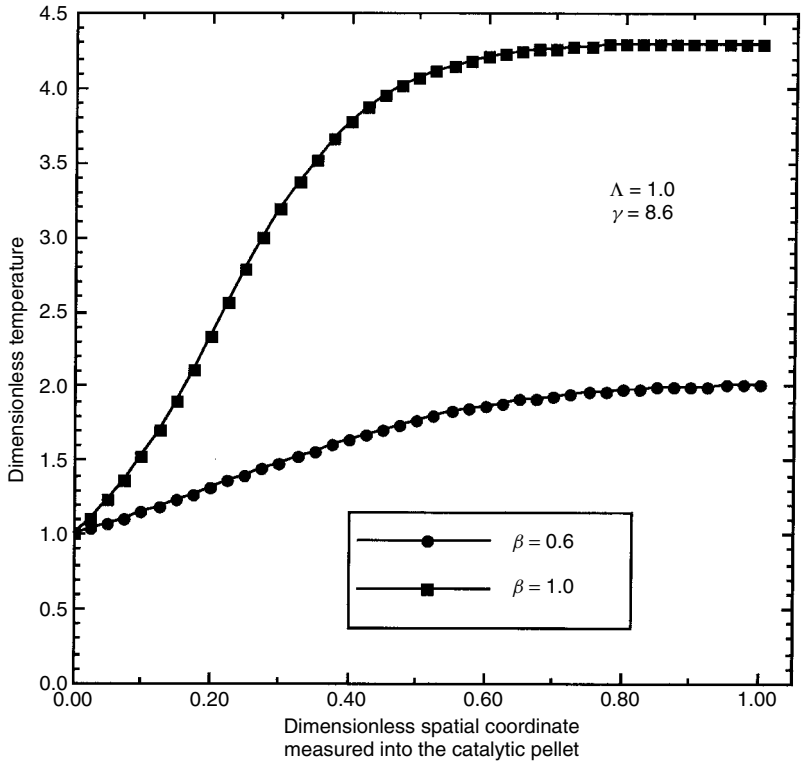

Figure 27-3 Effect of the thermal energy generation parameter β on dimensionless temperature profiles as one travels inward toward the center of a porous catalyst with rectangular symmetry. The chemical kinetics are first-order and irreversible, and the reaction is exothermic. All parameters are defined in Table 27-4. The specific entries for $\beta = 0.6$ and $\beta = 1.0$ are provided in Table 27-6.

TABLE 27-9 System of Equations to Be Analyzed to Design a Packed Catalytic Tubular Reactor That Operates Nonisothermally

nth-order irreversible chemical kinetics: $R(T, x) = k_r(T)[C_{A0}(1 - x)]^n$

Arrhenius model/transition-state theory: $k_r(T) = k_\infty \exp\left(\dfrac{-E_{\text{activation}}}{RT}\right)$

Plug-flow mass balance for reactant A:

$$C_{A0}\frac{dx}{d\tau} = E(\Lambda_{\text{A, intrapellet}})(1 - \varepsilon_{\text{p, interpellet}})R(T, x)$$

Molar density of reactant A: $C_A = C_{A0}(1 - x)$

Plug-flow thermal energy balance for the packed catalytic tubular reactor:

$$\rho\hat{c}_p\frac{dT}{d\tau} = \left(\frac{dQ}{dV_{Rx}}\right)_{\text{thermal energy input}} + (-\Delta H_{Rx})E(\Lambda_{\text{A, intrapellet}})(1 - \varepsilon_{\text{p, interpellet}})R(T, x)$$

minimal so that bulk conditions within the reactor are very close to those that exist near the external surface of the catalyst.

In summary, these predictions of reactor performance, based on the system of equations in Table 27-9, should be accurate at high-mass-transfer Peclet numbers, where it is reasonable to neglect axial dispersion and residence time distribution (RTD) effects on the reactant molar density profile from inlet to outlet. If the heat transfer Peclet number is also large, then it is reasonable to neglect axial conduction of thermal energy. However, without performing a residence time distribution study by including axial dispersion in the plug-flow mass balance for a tubular reactor, it is difficult to know how large the mass transfer Peclet number must be to assume safely that RTDs will not affect reactor performance.

PROBLEMS

27-1. One first-order irreversible chemical reaction occurs within a porous catalyst that exhibits rectangular symmetry. The center of the catalyst corresponds to $\eta = 0$, and the external surface is at $\eta = 1$. The intrapellet Damkohler number for reactant A is 1, and the Arrhenius number is 8.6.

(a) Sketch the dimensionless concentration profile for reactant A, Ψ_A, as a function of dimensionless spatial coordinate η when the thermal energy generation parameter β is 0.6 and 1. Put both profiles on one set of axes and indicate the value of β that corresponds to each curve. *Answer:* See Figure 27-1.

(b) Sketch the dimensionless temperature profile Θ as a function of dimensionless spatial coordinate η when the thermal energy generation parameter β is 0.6 and 1. Put both profiles on one set of axes and indicate the value of β that corresponds to each curve. *Answer:* See Figure 27-3.

27-2. What is the final form of the three dimensionless ODEs that must be solved to analyze coupled heat and mass transfer with second-order irreversible chemical reaction in spherical catalysts? Also, include the final expression that must be used to calculate the effectiveness factor. Remember that in dimensionless form, $\Psi_A = 1$ and $\Theta = 1$ for reactant concentration and temperature, respectively, in the vicinity of the external surface of one porous catalytic pellet. Be sure to include all boundary conditions.

27-3. Estimate the dimensionless concentration gradient on the external surface of the catalyst at $\eta = 1$ or $\zeta = 0$ which yields a zero gradient at the center of the catalyst for the following set of important dimensionless parameters when the chemical kinetics are first-order and irreversible in porous catalysts with rectangular symmetry: $\Lambda_{A,\,\text{intrapellet}} = 2$, $\beta = 0.65$, $\gamma = 8.6$.

Answer: Information from the following tables in this chapter is useful to make an educated guess for the correct dimensionless concentration gradient of reactant A at the external surface of the catalyst. Then, this educated guess is compared with the exact answer, which yields convergence at the center of the pellet.

Table	$\Lambda_{A,\ intrapellet}$	β	γ	Gradient at $\eta = 1$
27-5	2	0.43	8.6	3.56
27-6	1	0.65	8.6	2.39

Tabular data reveal that the dimensionless reactant concentration gradient at the external surface of the catalyst increases at larger values of the intrapellet Damkohler number and the thermal energy generation parameter. The entry above from Table 27-6 suggests that the gradient should be larger than 2.39 when the intrapellet Damkohler number increases to 2. The entry from Table 27-5 suggests that the gradient should be larger than 3.56 when β increases to 0.65. Hence, an educated guess for the gradient at $\eta = 1$ should be between 4 and 5. Computer simulations reveal that the exact value of the gradient at $\eta = 1$ is 4.79, and the corresponding effectiveness factor is 1.2.

27-4. The effectiveness factor is calculated via volumetric averaging of the kinetic rate law for one first-order irreversible chemical reaction in porous catalysts with spherical symmetry. Numerical methods have been employed to solve three coupled first-order ordinary differential equations with split boundary conditions. When the correct guess for the dimensionless reactant concentration gradient at the external surface yields a zero gradient at the center of the pellet, convergence is achieved and one has accurate information about the dimensionless temperature and concentration profiles, $\Theta(\eta)$ and $\Psi_A(\eta)$. Use these dimensionless profiles for Ψ_A and Θ to obtain a dimensionless integral expression for the effectiveness factor based on volumetric averaging of the kinetic rate law.

Answer: Begin with the definition of the effectiveness factor, where the numerator represents a volumetric average of the rate of conversion of reactant A to products and the denominator expresses this rate using conditions on the external surface of the catalyst. For example,

$$E = \frac{\displaystyle\int_V -\upsilon_A k_1(T) C_A(r)\, dV}{-\upsilon_A V_{catalyst} k_1(T_{surface}) C_{A,\ surface}}$$

The following substitutions are employed:

$$\frac{k_1(T)}{k_1(T_{surface})} = \exp\left[\frac{\gamma(\Theta - 1)}{\Theta}\right]$$

$$\frac{C_A(r)}{C_{A,\,\text{surface}}} = \Psi_A(\eta)$$

$$V_{\text{catalyst}} = \tfrac{4}{3}\pi R^3$$

$$dV = 4\pi r^2\, dr$$

$$\eta = \frac{r}{R}$$

The final result in dimensionless notation is

$$E = 3\int_0^1 \Psi_A(\eta) \exp\left[\frac{\gamma(\Theta - 1)}{\Theta}\right] \eta^2\, d\eta$$

27-5. Consider one-dimensional (i.e., radial) diffusion and multiple chemical reactions in a porous catalytic pellet with spherical symmetry. For each chemical reaction, the kinetic rate law is given by a simple *n*th-order expression that depends only on the molar density of reactant A. Furthermore, the thermal energy generation parameter for each chemical reaction, $\beta_j = 0$.

(a) How many coupled first-order ordinary differential equations must be solved with split boundary conditions before one can obtain numerical values for the effectiveness factor?

Answer: Two. The thermal energy balance is not required when the enthalpy change for each chemical reaction is negligible, which causes the thermal energy generation parameters to tend toward zero. Hence, one calculates the molar density profile for reactant A within the catalyst via the mass transfer equation, which includes one-dimensional diffusion and multiple chemical reactions. Stoichiometry is not required because the kinetic rate law for each reaction depends only on C_A. Since the microscopic mass balance is a second-order ordinary differential equation, it can be rewritten as two coupled first-order ODEs with split boundary conditions for C_A and its radial gradient.

(b) Evaluate a volumetric average of the rate of conversion of reactant A to products within each spherical catalytic pellet via consideration of mass transfer across the external surface of the catalyst when multiple chemical reactions occur within the pellet.

Answer: This problem requires information about the numerator of the effectiveness factor. When reactant A participates in each chemical reaction, one must evaluate $\int_V (-\sum_j \upsilon_{Aj} \mathfrak{R}_j)\, dV$, where the kinetic rate law for the jth chemical reaction is given by

$$\mathfrak{R}_j = k_j(T)(C_A)^{n_j}$$

and n_j represents the reaction order. The mass transfer equation allows one to evaluate a volumetric average of the rate of conversion of reactant

A to products by considering mass transfer across the external surface of the catalyst. In the presence of multiple chemical reactions, where each $\mathfrak{R}_j$ depends only on C_A, stoichiometry is not required. Furthermore, the thermal energy balance is not required when $\beta_j = 0$ for each chemical reaction. In the presence of multiple chemical reactions where thermal energy effects must be considered because each $\Delta H_{Rx,j}$ is not insignificant, methodologies beyond those discussed in this chapter must be employed to generate temperature and molar density profiles within catalytic pellets (see Aris, 1975, Chap. 5). In the absence of any complications associated with $\beta_j \neq 0$, one manipulates the steady-state mass transfer equation for reactant A with pseudo-homogeneous one-dimensional diffusion and multiple chemical reactions under isothermal conditions (see equation 27-14):

$$-\nabla \cdot \mathbf{j}_A + MW_A \sum_j \upsilon_{Aj} \mathfrak{R}_j = 0$$

The required volumetric average is

$$\int_V \left(-\sum_j \upsilon_{Aj} \mathfrak{R}_j \right) dV = \int_V \left(-\nabla \cdot \frac{\mathbf{j}_A}{MW_A} \right) dV$$

$$= \int_S \left(-\mathbf{n} \cdot \frac{\mathbf{j}_A}{MW_A} \right)_{\text{external surface}} dS$$

where $\mathbf{n} = \boldsymbol{\delta}_r$, $dS = R^2 \sin\theta \, d\theta \, d\phi$, and Gauss's law or the divergence theorem has been employed. This allows one to evaluate a volumetric average of the rate of conversion of reactant A to products within catalytic pellets in terms of the normal component of diffusional mass flux across the external surface. Since diffusion occurs primarily in the radial direction in catalysts with spherical symmetry, the molar density of reactant A, C_A, and $(\mathbf{n} \cdot \mathbf{j}_A)$ depend only on position variable r, not on the two independent variables that comprise surface element dS. This simplifies the previous surface integral considerably:

$$\int_V \left(-\sum_j \upsilon_{Aj} \mathfrak{R}_j \right) dV = 4\pi R^2 \left(-\boldsymbol{\delta}_r \cdot \frac{\mathbf{j}_A}{MW_A} \right)_{r=R}$$

The final step is to express the diffusional mass flux of reactant A in terms of an effective diffusivity and the gradient of C_A via equations (27-24) and (27-25):

$$\mathbf{j}_A = -\rho \mathfrak{D}_{A,\text{effective}} \nabla \omega_A \approx -\mathfrak{D}_{A,\text{effective}} \nabla \rho \omega_A$$

$$= -\mathfrak{D}_{A,\text{effective}} \nabla (C_A MW_A)$$

$$\left(-\boldsymbol{\delta}_r \cdot \frac{\mathbf{j}_A}{MW_A} \right)_{r=R} = \mathfrak{D}_{A,\text{effective}} (\boldsymbol{\delta}_r \cdot \nabla C_A)_{r=R}$$

$$= \mathfrak{D}_{\mathrm{A,\,effective}} \left(\frac{dC_{\mathrm{A}}}{dr} \right)_{r=R}$$

In conclusion, one solves two coupled first-order ODEs for the molar density profile of reactant A under isothermal conditions, without considering the thermal energy balance. Then, a volumetric average of the rate of conversion of reactant A to products due to multiple chemical reactions is obtained by focusing on the reactant concentration gradient at the external surface of the catalyst:

$$\int_V \left(-\sum_j \upsilon_{\mathrm{A}j} \mathfrak{R}_j \right) dV = 4\pi R^2 \mathfrak{D}_{\mathrm{A,\,effective}} \left(\frac{dC_{\mathrm{A}}}{dr} \right)_{r=R}$$

27-6. **(a)** Identify three physical properties, not dimensionless numbers, of a chemically reacting gas mixture/porous catalyst system that strongly influence the maximum temperature within the catalytic pellet.

(b) Draw a picture of one catalytic pellet and indicate where this maximum temperature occurs if the chemical reaction is endothermic.

(c) Draw a picture of one catalytic pellet and indicate where this maximum temperature occurs if the chemical reaction is exothermic.

(d) Without solving any coupled ODEs, derive a simple expression to estimate the maximum temperature in one catalytic pellet when the chemical reaction is strongly exothermic and the average pore size is greater than 1 μm. *Hint:* Set $C_A \to 0$ at the center of the catalyst.

(e) Calculate the actual maximum temperature rise (i.e., $T_{\mathrm{maximum}} - T_{\mathrm{surface}}$) in a flat-slab alumina catalyst with first-order irreversible chemical reaction when $\Delta H_{\mathrm{Rx}} = -75$ kJ/mol, $\Lambda_{\mathrm{A,\,intrapellet}} = 1$, $T_{\mathrm{surface}} = 350$ K, and $\langle r_{\mathrm{pore}} \rangle_{\mathrm{average}}$ is greater than 1 μm.

27-7. Estimate the maximum temperature at the center of a catalytic pellet at large intrapellet Damkohler numbers in the diffusion-limited regime when the thermal energy generation parameter $\beta = 2$ (i.e., exothermic chemical reaction), the temperature on the external surface of the pellet is $T_{\mathrm{surface}} = 300$ K, and the average pore size is greater than 1 μm.

(a) Invoke the assumption that the temperature-dependent ratio of effective intrapellet diffusivities (i.e., ε_{A}) is approximately equal to unity.

(b) Do not invoke the assumption that $\varepsilon_{\mathrm{A}} \approx 1$ as you did in part (a).

(c) Which estimate for the maximum temperature at the center of the catalyst is more accurate, your answer to part (a) or your answer to part (b)?

27-8. Consider a porous catalytic pellet with exothermic chemical reaction in the diffusion-limited regime at very large values of the intrapellet Damkohler number. Obtain an expression for the maximum temperature

Θ_{max} in terms of the thermal energy generation parameter β when the average pore radii are smaller than 100 Å and Knudsen diffusion provides the dominant resistance to intrapellet mass transfer.

Answer: Let the temperature-dependent ratio of effective intrapellet diffusivities $\varepsilon_A(\Theta)$ be a simple power function of dimensionless temperature Θ. Hence, $\varepsilon_A(\Theta) = \Theta^m$. Now, integrate the thermal energy balance given by equations (27-27) and (27-35) that results from coupled heat and mass transfer in porous catalytic pellets:

$$\frac{d\Theta}{d\Psi_A} = -\beta\varepsilon_A(\Theta) = -\beta\Theta^m$$

subject to the boundary condition on the external surface, where $\Theta = 1$ and $\Psi_A = 1$. The following generalized dimensionless analytical relation between temperature and reactant concentration is obtained:

$$\Theta^{1-m} = 1 + (1-m)\beta(1-\Psi_A)$$

The maximum temperature at the center of a catalytic pellet with exothermic chemical reaction (i.e., $\beta > 0$) is

$$(\Theta_{max})^{1-m} = 1 + (1-m)\beta[1 - \Psi_A(\eta = 0; \Lambda_A)]$$

where $m = \frac{1}{2}$ if Knudsen diffusion provides the dominant resistance to mass transfer within porous catalysts with average pore sizes below 100 Å. In the diffusion-limited regime at very large values of the intrapellet Damkohler number, the molar density of reactant A at the center of the catalyst is essentially zero, and one obtains the following expression for the maximum temperature within adiabatic pellets:

$$\Theta_{max} = (1 + \tfrac{1}{2}\beta)^2$$

27-9. Explain very briefly the following trends that are predicted for coupled heat and mass transfer in porous catalysts when the chemical reaction is first-order and exothermic.

(a) Θ_{max} within the catalyst increases at higher values of β.

(b) Θ_{max} within the catalyst is insensitive to γ.

(c) The effectiveness factor increases when the Arrhenius number γ is larger.

(d) $\Theta_{max} < 1 + \beta$ when the intrapellet Damkohler number is less than 0.9.

(e) $\Theta_{max} > 1 + \beta$ when the intrapellet Damkohler number is larger than 0.9.

27-10. **(a)** For a particular range of intrapellet Damkohler numbers, explain qualitatively why the effectiveness factor can exceed unity (i.e., >1) when the molar density of reactant A within the catalytic pores is much lower than its value on the external surface of the catalyst for exothermic chemical reactions. Use the definition of the effectiveness factor based on volumetric averaging of the kinetic rate law as the basis for your explanation.

(b) Are there any values of the intrapellet Damkohler number where the effectiveness factor exceeds unity (i.e., >1) for endothermic chemical reactions? Consider the definition of the effectiveness factor based on volumetric averaging of the kinetic rate law as the basis for your explanation. *Answer*: No.

(c) For all kinetic rate laws, catalyst geometries, and values of the thermal energy generation parameter β that are positive or negative, explain qualitatively why the effectiveness factor decreases at larger values of the intrapellet Damkohler number in the extreme diffusion-limited regime. In fact, the effectiveness factor scales as $1/\Lambda_{\mathrm{A,\ intrapellet}}$, not $1/\Lambda^2_{\mathrm{A,\ intrapellet}}$.

27-11. Consider the set of coupled ordinary differential equations that must be solved to design a nonisothermal packed catalytic tubular reactor which is not insulated from the surroundings. This information is summarized in Table 27-9.

(a) Is the molecular flux of thermal energy $\mathbf{q}$ zero or nonzero in these equations?

(b) Is the diffusional mass flux of reactant A zero or nonzero in these equations?

27-12. *True or False*.

(a) For strongly exothermic chemical reactions, multiple steady states can occur within a single catalytic pellet. In other words, more than one value of the effectiveness factor corresponds to the same intrapellet Damkohler number. *Answer*: True.

(b) The enthalpy change for chemical reaction, the effective thermal conductivity of the porous solid catalyst, and the specific heat of the reactive gas mixture represent three physical properties of a chemically reacting gas mixture/porous catalyst system that strongly influence the maximum temperature within a catalytic pellet. *Answer*: False.

(c) As illustrated by some of the simulations, nonisothermal effectiveness factors increase above unity over a restricted range of intrapellet Damkohler numbers when the chemical reaction is exothermic. If Λ^2 approaches this restricted range from below and increases smoothly, then the effectiveness factors and the stable operating points of a

catalytic pellet follow a locus of stationary states which differ from the sequence of steady states that are preferred when the intrapellet Damkohler number approaches this restricted range from above and decreases smoothly. This occurs because there are either two or three values of the effectiveness factor that correspond to one value of the intrapellet Damkohler number (i.e., $\Lambda^2 = \Omega$) within this restricted range. Analogous to multiple-steady-state behavior for exothermic reactions in continuous-stirred tank reactors, the actual steady-state conditions within the pellet depend on the previous steady-state operating point of the catalyst and heat and mass transfer dynamics of a single pellet as this particular value of $\Lambda^2 = \Omega$ is approached. This is an example of multiple stationary states and hysteresis loops in catalytic pellets with exothermic chemical reaction. *Answer*: True.

Transport Phenomena for Chemical Reactor Design. Laurence A. Belfiore
Copyright © 2003 John Wiley & Sons, Inc.
ISBN: 0-471-20275-4

28

STATISTICAL THERMODYNAMICS OF IDEAL GASES

28-1 GENERALIZED POSTULATES

The generalized formalism outlined in this section is not limited to ideal gases. It provides the methodology to employ molecular characteristics such as infrared stretching frequencies, thermal wavelengths, and moments of inertia to develop a correspondence between (1) macroscopic thermodynamic state functions such as internal energy U, entropy S, the Helmholtz potential A, chemical potential μ, and equation-of-state information for system pressure; and (2) the microscopic partition function Z, which depends on the energy levels that are available to a single molecule of a pure material. If one expresses Z from a consideration of the energy levels available to a single molecule and the energetic interactions between molecules, then intensive thermodynamic properties are calculated as follows:

Helmholtz free energy: $$A = -kT \ln Z \tag{28-1}$$

Internal energy: $$U = kT^2 \left(\frac{\partial \ln Z}{\partial T} \right)_{V,N} \tag{28-2}$$

Entropy: $$S = k \ln Z + \frac{U}{T} \tag{28-3}$$

Chemical potential: $$\mu = \left(\frac{\partial A}{\partial N} \right)_{T,V} = -kT \left(\frac{\partial \ln Z}{\partial N} \right)_{T,V} \tag{28-4}$$

System pressure: $$p = -\left(\frac{\partial A}{\partial V} \right)_{T,N} = kT \left(\frac{\partial \ln Z}{\partial V} \right)_{T,N} \tag{28-5}$$

where k is Boltzmann's constant, T is temperature, V is total volume, and N represents the number of molecules or moles of a pure material.

28-2 INTRODUCTION TO QUANTUM STATISTICAL MECHANICS

The objective of the following discussion is to calculate the partition function Z of a single molecule that populates several states with a distribution that is appropriate for a canonical ensemble. In the language of quantum mechanics:

1. Each state of a time-varying system is described by a complex time-dependent wavefunction $\psi(\boldsymbol{r}, \text{time})$, where $\boldsymbol{r}$ represents a set of generalized spatial coordinates.
2. ψ satisfies the Schrödinger wave equation:

$$\frac{\partial \psi}{\partial t} = -\frac{2\pi i}{h} \mathscr{H} \psi \tag{28-6}$$

   where h is Planck's constant, $i = \sqrt{-1}$, and $\mathscr{H}$, the Hamiltonian operator for the system, includes contributions from kinetic and potential energies.
3. The time-dependent expectation value of a thermodynamic observable (i.e., property) is illustrated in terms of the Hamiltonian operator. The result provides an estimate of the total energy of the system, whose classical thermodynamic analog is the internal energy;

$$\langle \mathscr{H} \rangle \equiv \int_{\text{all coordinate space}} \psi^* \mathscr{H} \psi \, d\boldsymbol{r} = f(t) \tag{28-7}$$

   where ψ^* is the complex conjugate of the wave function.
4. Equilibrium thermodynamic properties, such as internal energy, are calculated from the time-dependent expectation value of the total system energy as follows:

$$\langle \mathscr{H} \rangle_{\text{equilibrium}} \equiv \lim_{t \to \infty} \left(\frac{1}{t} \int_0^t \langle \mathscr{H} \rangle \, dt' \right) \tag{28-8}$$

5. Analogous to the construction of molecular orbital wavefunctions based on linear combinations of atomic orbitals, ψ for a single molecule is expressed in terms of a set of time-independent orthonormal basis functions $\varphi_i(\boldsymbol{r})$:

$$\psi(\boldsymbol{r}, t) = \sum_i C_i(t) \varphi_i(\boldsymbol{r}) \tag{28-9}$$

   where the summation includes all possible stationary states that are occupied by the molecule at equilibrium. Each φ_i is an eigenfunction of the Hamiltonian operator with stationary-state eigenvalues given by E_i. Hence,

$$\mathscr{H} \varphi_i = E_i \varphi_i \tag{28-10}$$

   For example, see *General Chemistry* by Linus Pauling (1970, App. V), which summarizes hydrogen-like orbitals. These represent the solution to

the time-independent Schrödinger wave equation for a hydrogen-like atom, and form a complete set of orthonormal basis functions denoted by φ_i in equations (28-9) and (28-10).

Density Matrix. As defined by equation (28-7), construct the expectation value of the total energy under dynamic conditions,

$$\langle \mathscr{H} \rangle \equiv \int_{\text{all coordinate space}} \psi^* \mathscr{H} \psi \, d\boldsymbol{r} \tag{28-11}$$

and expand the time-dependent wavefunction ψ in terms of an orthonormal basis set φ_i. The Hamiltonian operates on the basis wavefunctions φ_i, not on the time-dependent weighting factors $C_i(t)$:

$$\begin{aligned}\langle \mathscr{H} \rangle &\equiv \int_{\text{all coordinate space}} \left[\sum_j C_j^*(t) \varphi_j^*(\boldsymbol{r}) \right] \mathscr{H} \left[\sum_i C_i(t) \varphi_i(\boldsymbol{r}) \right] d\boldsymbol{r} \\ &= \sum_{ij} C_i(t) C_j^*(t) \int_{\text{all coordinate space}} \varphi_j^*(\boldsymbol{r}) \mathscr{H} \varphi_i(\boldsymbol{r}) \, d\boldsymbol{r}\end{aligned} \tag{28-12}$$

Products of the complex time-dependent coefficients in the linear expansion of ψ correspond to elements of the density matrix:

$$\rho_{ij}(t) \equiv C_i(t) C_j^*(t) \tag{28-13}$$

Since each φ_i is an eigenfunction of the Hamiltonian operator with eigenvalue E_i, the dynamic expectation value of the total energy reduces to

$$\langle \mathscr{H} \rangle = \sum_{ij} \rho_{ij}(t) E_i \int_{\text{all coordinate space}} \varphi_j{}^*(\boldsymbol{r}) \varphi_i(\boldsymbol{r}) \, d\boldsymbol{r} \tag{28-14}$$

and integration of products of orthonormal basis functions over all coordinate space yields a Kronecker delta:

$$\int_{\text{all coordinate space}} \varphi_j{}^*(\boldsymbol{r}) \varphi_i(\boldsymbol{r}) \, d\boldsymbol{r} \equiv \delta_{ij} \qquad \text{(i.e., 0 if } i \neq j, \text{ 1 if } i = j) \tag{28-15}$$

Hence,

$$\langle \mathscr{H} \rangle = \sum_{ij} \rho_{ij}(t) E_i \delta_{ij} = \sum_i \rho_{ii}(t) E_i \tag{28-16}$$

and diagonal elements of the density matrix, or the density of stationary states, play a key role in calculating dynamic expectation values when orthonormal basis functions are used to construct ψ. At equilibrium, the total energy of a single molecule is

$$\begin{aligned}\langle \mathscr{H} \rangle_{\text{equilibrium}} &\equiv \lim_{t \to \infty} \left[\frac{1}{t} \int_0^t \sum_i \rho_{ii}(t') E_i \, dt' \right] \\ &= \sum_i \left\{ \lim_{t \to \infty} \left[\frac{1}{t} \int_0^t \rho_{ii}(t') \, dt' \right] \right\} E_i\end{aligned} \tag{28-17}$$

The summation includes all possible stationary states with energy E_i that are occupied by the molecule. The equilibrium probability P_i that the molecule populates each of these states is given by a Boltzmann distribution for the canonical ensemble. In other words,

$$P_i \equiv \lim_{t\to\infty}\left[\frac{1}{t}\int_0^t \rho_{ii}(t')\,dt'\right] = A\exp(-\beta E_i) \tag{28-18}$$

and the total energy of the single molecule is

$$\langle \mathscr{H} \rangle_{\text{equilibrium}} = \sum_i P_i E_i = A\sum_i E_i \exp(-\beta E_i) \tag{28-19}$$

Equation (28-19) reveals that the total energy of a single molecule at equilibrium is obtained by weighting the energy of each available stationary state by the occupational probability of that state, which is given by the Boltzmann distribution.

28-3 THE ERGODIC PROBLEM

A canonical ensemble represents a large number of closed systems in thermal contact with each other. Each system in the ensemble occupies stationary states with energy E_i, and P_i describes the occupational probability of each state, as given by equation (28-18). One postulates that $\ln P_i$ is an additive constant of the trajectories of the molecules in each system, where energy, linear momentum, and angular momentum are constants along each trajectory. Since linear and angular momentum vanish at equilibrium, occupational probabilities for stationary states obey the following Boltzmann distribution:

$$\begin{aligned} \ln P_i &\approx \alpha - \beta E_i \\ P_i &= A\exp(-\beta E_i) \end{aligned} \tag{28-20}$$

where α and A are dimensionless, and β has units of reciprocal energy. Since occupational probabilities must sum to unity when all possible states are considered,

$$\sum_i P_i = 1 \tag{28-21}$$

$$A = \frac{1}{\sum_i \exp(-\beta E_i)} = \frac{1}{Z} \tag{28-22}$$

The partition function Z is defined as a sum of Boltzmann factors for discrete stationary states that are available to the canonical ensemble. The partial derivative of Z with respect to the parameter β (i.e., at constant V and N) defines

the internal energy U of the system at equilibrium, in agreement with equation (28-19). Hence,

$$Z = \sum_i \exp(-\beta E_i) \tag{28-23}$$

$$\langle \mathscr{H} \rangle_{\text{equilibrium}} = \frac{1}{Z} \sum_i E_i \exp(-\beta E_i) \tag{28-24}$$

$$\left(\frac{\partial Z}{\partial \beta} \right)_{V,N} = -\sum_i E_i \exp(-\beta E_i) = -Z \langle \mathscr{H} \rangle_{\text{equilibrium}} \equiv -ZU \tag{28-25}$$

$$U \equiv \langle \mathscr{H} \rangle_{\text{equilibrium}} = \sum_i P_i E_i = -\left(\frac{\partial \ln Z}{\partial \beta} \right)_{V,N} \tag{28-26}$$

28-4 $\mathscr{H}$ THEOREM OF STATISTICAL THERMODYNAMICS

In this section, we focus on a relation between entropy and the probability distribution function P_i. If P_i obeys Boltzmann statistics for the canonical ensemble, then one arrives at a correspondence between entropy S and the partition function Z. Equation (28-26) is interpreted within the context of the first law of thermodynamics in differential form:

$$dU = \sum_i (E_i \, dP_i + P_i \, dE_i) = dq + dW \tag{28-27}$$

dU is a path-independent exact differential, whereas heat input dq and work performed on the system dW are inexact differentials. The first-law energy balance states that a path-independent state function U is obtained from the sum of these two path-dependent differentials. Now, it is desired to use the first law and develop correspondences between classical thermodynamic properties, such as dq and dW, and statistical thermodynamic quantities. The basic effect of compressing a system and decreasing its volume (i.e., $dW > 0$) increases the spatial overlap of molecular orbitals that contain electrons. The energy levels of a given electronic configuration can be perturbed by pressure, a phenomenon known as *pressure tuning*. Hence, the following correspondence seems reasonable:

$$dW = -p \, dV = \sum_i P_i \, dE_i \tag{28-28}$$

Furthermore, the addition of thermal energy affects the distribution of molecules among the available stationary states and allows the system to populate states of higher energy. Hence,

$$dq = \sum_i E_i \, dP_i \tag{28-29}$$

In summary, p-V work perturbs the energy levels and heat input perturbs the occupational probabilities of the available equilibrium states. One aspect of the second law identifies $1/T$ as a factor that makes the heat function an exact differential via the entropy state function

$$dS \equiv \frac{1}{T} dq = \frac{1}{T} \sum_i E_i \, dP_i \tag{28-30}$$

The following properties of the probability distribution P_i are invoked:

1. Boltzmann statistics are obeyed:

$$\begin{aligned} P_i &= \frac{1}{Z} \exp(-\beta E_i) \\ \ln P_i &= -\ln Z - \beta E_i \end{aligned} \tag{28-31}$$

2. The Boltzmann distribution is normalized:

$$\begin{aligned} \sum_i P_i &= 1 \\ \sum_i dP_i &= 0 \end{aligned} \tag{28-32}$$

3. The parameter β, as defined in the ergodic problem via equation (28-20), has dimensions of reciprocal energy and is given by $1/kT$. This claim will be justified, and consistency with classical thermodynamics will be demonstrated in Section 28-5.

The differential statement of the second law, given by equation (28-30), is manipulated as follows:

$$\begin{aligned} dS &= \frac{1}{T} \sum_i E_i \, dP_i = k \sum_i \beta E_i \, dP_i = k \sum_i (-\ln Z - \ln P_i) \, dP_i \\ &= -k \ln Z \sum_i dP_i - k \sum_i \ln P_i \, dP_i - k \sum_i dP_i \end{aligned} \tag{28-33}$$

where the first term on the second line of equation (28-33) vanishes because the Boltzmann distribution is normalized, and the last term (which is also zero) is included for convenience. Hence,

$$\begin{aligned} dS &= -k \sum_i \ln P_i \, dP_i - k \sum_i dP_i = -k \sum_i (1 + \ln P_i) \, dP_i \\ &= -d \left(k \sum_i P_i \ln P_i \right) \end{aligned} \tag{28-34}$$

Integration of (28-34) allows one to express entropy in terms of P_i for a canonical ensemble of molecules that obey Boltzmann statistics. The result is exact to within an integration constant that comprises the third law of thermodynamics at absolute zero, where P_i is unity for the state of lowest energy and zero for all higher-energy states. Hence,

$$S = -k \sum_i P_i \ln P_i \tag{28-35}$$

This relation is equivalent to Boltzmann's equation (i.e., $S = k \ln \Omega$) for the microcanonical ensemble, where all quantum states are equally probable and Ω is the thermodynamic multiplicity of states. The correspondence between S and Z is obtained by invoking the Boltzmann distribution for P_i in equation (28-35) using results from (28-31):

$$\begin{aligned} S &= -k \sum_i \frac{1}{Z} \exp(-\beta E_i)(-\ln Z - \beta E_i) \\ &= k \ln Z \left[\frac{1}{Z} \sum_i \exp(-\beta E_i) \right] + k\beta \left[\frac{1}{Z} \sum_i E_i \exp(-\beta E_i) \right] \end{aligned} \tag{28-36}$$

On the second line in equation (28-36), the first term in brackets is unity via (28-23) and the second term is the internal energy U via (28-25). The generalized correspondence between S and Z is

$$S = k \ln Z + k\beta U = k \ln Z - k\beta \left(\frac{\partial \ln Z}{\partial \beta} \right)_{V,N} \tag{28-37}$$

If $k\beta = 1/T$, then

$$S = k \ln Z + \frac{U}{T} \tag{28-38}$$

and the Helmholtz free energy A, obtained via Legendre transformation from $U(S, V, N)$ to $A(T, V, N)$, is

$$A \equiv U - TS = -kT \ln Z \tag{28-39}$$

28-5 CONSISTENCY WITH CLASSICAL THERMODYNAMICS

The extensive internal energy of a pure material is a function of S, V, and N [i.e., $U(S, V, N)$], and the total differential of U is

$$dU = T\,dS - p\,dV + \mu\,dN \tag{28-40}$$

This can be inverted to express entropy as a function of U, V, and N:

$$dS = \frac{1}{T}\,dU + \frac{p}{T}\,dV - \frac{\mu}{T}\,dN \tag{28-41}$$

Equation (28-41) from classical thermodynamics indicates, via the chain rule, that

$$\left(\frac{\partial S}{\partial U}\right)_{V,N} \equiv \frac{1}{T} \tag{28-42}$$

If one employs results from Sections 28-3 and 28-4, and calculates $(\partial S/\partial U)_{V,N}$ from statistical thermodynamics when $\beta \neq$ constant, a relation is obtained between β and T. The independent variables are U, V, and N, and

$$S = k \ln Z + k\beta U \tag{28-43}$$

Hence,

$$\left(\frac{\partial S}{\partial U}\right)_{V,N} = k\left[\left(\frac{\partial \ln Z}{\partial \beta}\right)\left(\frac{\partial \beta}{\partial U}\right)\right]_{V,N} + k\beta + kU\left(\frac{\partial \beta}{\partial U}\right)_{V,N} \tag{28-44}$$

The first and third terms on the right side of (28-44) cancel because (28-26) reveals that:

$$U = -\left(\frac{\partial \ln Z}{\partial \beta}\right)_{V,N} \tag{28-45}$$

Finally,

$$\left(\frac{\partial S}{\partial U}\right)_{V,N} \equiv \frac{1}{T} = k\beta$$

28-5.1 Third Law of Thermodynamics and Degenerate Ground States at Absolute Zero

As illustrated by equation (28-23), the partition function Z represents a sum of Boltzmann factors for all stationary states available to the system. Instead of summing over states, it is possible to sum over all different energy levels provided that each Boltzmann factor is multiplied by the number of states with the same energy. Using summation notation, one obtains the following result:

$$Z = \sum_{i \text{ states}} \exp\left(-\frac{E_i}{kT}\right) = \sum_{j \text{ energy levels}} g_j \exp\left(-\frac{E_j}{kT}\right) \tag{28-46}$$

where g_j is the degeneracy or number of states with energy E_j. If the ground state with energy E_0 and degeneracy g_0 is factored from the sum in (28-46), then the partition function is

$$Z = g_0 \exp\left(-\frac{E_0}{kT}\right)\left[1 + \sum_{j \text{ energy levels}} \frac{g_j}{g_0} \exp\left(-\frac{E_j - E_0}{kT}\right)\right] \tag{28-47}$$

where the summation in equation (28-47) does not include the ground state. Since $\ln Z$ is required to calculate thermodynamic properties, as summarized by equations (28-1) through (28-5), one expands $\ln(1+x) \approx x$, where x represents the population of all higher-energy states relative to the ground state. At extremely low temperature, x is rather small and truncation of the Taylor series after the linear term is justified. Hence,

$$\ln Z = \ln g_0 - \frac{E_0}{kT} + \sum_{j \text{ energy levels}} \frac{g_j}{g_0} \exp\left(-\frac{E_j - E_0}{kT}\right) \tag{28-48}$$

The internal energy of the system, which is consistent with this form of the partition function at low temperatures, is

$$\begin{aligned} U &= -\left(\frac{\partial \ln Z}{\partial \beta}\right)_{V,N} = -\frac{(\partial \ln Z/\partial T)_{V,N}}{(\partial \beta/\partial T)_{V,N}} = kT^2\left(\frac{\partial \ln Z}{\partial T}\right)_{V,N} \\ &= E_0 + \sum_{j \text{ energy levels}} \frac{g_j}{g_0}(E_j - E_0)\exp\left(-\frac{E_j - E_0}{kT}\right) \end{aligned} \tag{28-49}$$

At absolute zero (i.e., $T \to 0$), all molecules occupy the ground state and $U = E_0$. The corresponding entropy is

$$S(T \to 0) = k \ln Z + \frac{U}{T} = k\left(\ln g_0 - \frac{E_0}{kT}\right) + \frac{E_0}{T} = k \ln g_0 \tag{28-50}$$

which indicates that the entropy vanishes at absolute zero only if the degeneracy of the ground state is unity. This is true for perfect crystals because there is only one way to configure molecules in the lowest-energy state. Hence, these statistical results are consistent with the third law of thermodynamics.

28-5.2 Ideal Gas Partition Functions

An ideal gas consists of N indistinguishable molecules that do not interact with each other. The total energy of the ensemble is NE, where E represents the energy of a single molecule. The partition function can be expressed as a product of N single-molecule partition functions because the sum of states includes the same set of stationary states for each molecule. Z for a non-ideal gas cannot be factored as conveniently as Z for an ideal gas. Finally, statistics suggests that it is necessary to divide by $N!$, due to the indistinguishability of N gas molecules. The partition function for the ideal gas ensemble is

$$Z = \frac{Q^N}{N!} \tag{28-51}$$

where Q is the partition function for a single molecule. The energy of a single molecule must account for the electronic ground state, translation, rotation,

and vibration. All internal degrees of freedom are distributed between rotation and vibration. Similar to the factoring that occurred above for Z, it is possible to factor Q with respect to translation, vibration, and rotation. The following subscripts or quantum numbers are used to identify stationary states for various types of motion:

i	translation (actually, i_x, i_y, and i_z in three dimensions)
j	rotation
n	vibration

Hence,

$$Q = \exp\left(-\frac{E_{\text{ground state}}}{kT}\right)\sum_i \exp\left(-\frac{E_i}{kT}\right)\sum_j \exp\left(-\frac{E_j}{kT}\right)\sum_n \exp\left(-\frac{E_n}{kT}\right) \tag{28-52}$$

Translational energies E_i for 3 degrees of freedom are obtained by considering a particle in a three-dimensional box. Vibrational energies are based on the harmonic oscillator, and rotational energies are derived from the rigid rotor.

28-5.3 Translational Motion

A particle of mass m with 1 degree of translational freedom is contained in a box of length L and exhibits the following quantized energy levels:

$$E_{i,\,1-\text{d translation}} = \frac{h^2 i^2}{8mL^2} \tag{28-53}$$

If the particle enjoys 3 degrees of translational freedom in a box with total volume $V = L^3$, then the energy levels are quantized for motion in each coordinate direction. Hence,

$$E_{i,\,3-\text{d translation}} = \frac{h^2(i_x^2 + i_y^2 + i_z^2)}{8mL^2} \tag{28-54}$$

The translational partition function for 3 degrees of freedom can be factored:

$$\begin{aligned} Q_{\text{translation}} &= \sum_{i_x}\sum_{i_y}\sum_{i_z} \exp\left(-\frac{E_{i,\,3-\text{d translation}}}{kT}\right) \\ &= \left[\sum_{i_x}\exp\left(-\frac{h^2 i_x^2}{8mkTL^2}\right)\right]\left[\sum_{i_y}\exp\left(-\frac{h^2 i_y^2}{8mkTL^2}\right)\right]\left[\sum_{i_z}\exp\left(-\frac{h^2 i_z^2}{8mkTL^2}\right)\right] \\ &= \left[\sum_i \exp\left(-\frac{h^2 i^2}{8mkTL^2}\right)\right]^3 \end{aligned} \tag{28-55}$$

The translational partition function can be evaluated by invoking a continuous spectrum of energy levels in the high-temperature limit, where results from quantum mechanics are synonymous with those from classical mechanics. Under these conditions,

$$Q_{\text{translation}} = \left[\int_0^\infty \exp\left(\frac{-h^2x^2}{8mkTL^2}\right) dx\right]^3 = \left(\frac{L}{\lambda_T}\right)^3 = \frac{V}{(\lambda_T)^3} \tag{28-56}$$

where the deBroglie thermal wavelength for a particle of mass m at temperature T is

$$\lambda_T \equiv \frac{h}{\sqrt{2\pi mkT}} \tag{28-57}$$

Integration for $Q_{\text{translation}}$ is based on the fact that

$$\int_0^\infty \exp(-\alpha x^2)\, dx = \frac{1}{2}\sqrt{\frac{\pi}{\alpha}} \tag{28-58}$$

28-5.4 Equation of State

Explicit evaluation of the translational partition function via equation (28-56) allows one to express the complete volume dependence of Z for an ideal gas:

$$\begin{aligned} Z &= \exp\left(\frac{-NE_{\text{ground state}}}{kT}\right)\left[\frac{V}{(\lambda_T)^3}\right]^N \frac{(Q_{\text{rotation}}Q_{\text{vibration}})^N}{N!} \\ \ln Z &= -\ln N! - \frac{NE_{\text{ground state}}}{kT} + N\ln V - 3N\ln\lambda_T \\ &\quad + N\ln(Q_{\text{rotation}}Q_{\text{vibration}}) \end{aligned} \tag{28-59}$$

where the rotational and vibrational partition functions of a single molecule depend on temperature but not total volume V. It is straightforward to calculate the Helmholtz free energy $A(T, V, N)$ for an ideal gas. Furthermore, since

$$dA = -S\,dT - p\,dV + \mu\,dN \tag{28-60}$$

one calculates the gas pressure as follows:

$$p = -\left(\frac{\partial A}{\partial V}\right)_{T,N} = kT\left(\frac{\partial \ln Z}{\partial V}\right)_{T,N} = NkT\left(\frac{\partial \ln Q_{\text{translation}}}{\partial V}\right)_{T,N} = \frac{NkT}{V} \tag{28-61}$$

This equation describes the classic p–V–T behavior of an ideal gas. It reveals a well-known fact that gas pressure is due to the translational kinetic energy of the molecules. The internal degrees of freedom that are distributed between rotational and vibrational motion do not contribute to gas pressure. The equation of state can be written in more conventional form if Boltzmann's constant k is written as the gas constant R divided by Avogadro's number N_{Avo}, and the molar volume of the gas is identified as $v \equiv N_{\text{Avo}}(V/N)$. Hence, $pv = RT$.

28-6 INTERNAL ENERGY AND HEAT CAPACITY OF MONATOMIC IDEAL GASES

Information from Section 28-5 can be used to calculate the internal energy and heat capacity of a monatomic gas because the complete temperature dependence of Z is accounted for by partition functions for translational motion and the electronic ground state. Molecules exhibit 3 degrees of freedom per atom. Hence, there are no internal degrees of freedom for a monatomic gas (i.e., He, Ne, Ar, Kr, Xe) because all 3 degrees of freedom are consumed by translational motion in three different coordinate directions. The internal energy is calculated from equation (28-59):

$$U = kT^2 \left(\frac{\partial \ln Z}{\partial T} \right)_{V,N} = NE_{\text{ground state}} - 3NkT^2 \left(\frac{\partial \ln \lambda_T}{\partial T} \right)_{V,N} + NkT^2 \left(\frac{\partial \ln Q_{\text{rotation}}}{\partial T} \right)_{V,N} + NkT^2 \left(\frac{\partial \ln Q_{\text{vibration}}}{\partial T} \right)_{V,N} \tag{28-62}$$

where the last two terms on the right side of (28-62) contribute only to the internal energy of diatomic and polyatomic gases. The temperature dependence of the thermal wavelength is calculated from equation (28-57):

$$\left(\frac{\partial \ln \lambda_T}{\partial T} \right)_{V,N} = -\frac{1}{2T} \tag{28-63}$$

and the final expression for the internal energy of a monatomic ideal gas is

$$U = NE_{\text{ground state}} + \tfrac{3}{2}NkT \tag{28-64}$$

This is consistent with the *law of equipartition of energy*, which states that each degree of translational motion contributes $\frac{1}{2}kT$ per molecule or $\frac{1}{2}RT$ per mole to the internal energy of an ideal gas, relative to its ground-state energy. The heat capacity at constant volume C_V for molecules that cannot rotate or vibrate is

$$C_V \equiv \left(\frac{\partial U}{\partial T} \right)_{V,N} = \frac{3}{2}Nk = 3\left(\frac{1}{2}Nk \right) \tag{28-65}$$

Each degree of translational motion contributes $\frac{1}{2}R$ per mole to C_V of an ideal gas.

28-7 DIATOMIC GASES

28-7.1 Rotational Motion

The rigid rotor is the simplest model of a diatomic molecule with fixed internuclear distance R_{equil} between two atoms that have masses m_1 and m_2. The

following results from classical mechanics and quantum mechanics are useful to calculate the energy of a diatomic molecule that rotates at angular frequency ω:

Reduced mass: $$\mu_{\text{mass}} = \frac{m_1 m_2}{m_1 + m_2} \tag{28-66a}$$

Moment of inertia: $$I_{\text{moment}} = \mu_{\text{mass}} R_{\text{equil}}^2 \tag{28-66b}$$

Angular momentum: $$M = I_{\text{moment}} \omega \tag{28-66c}$$

Rotational energy: $$E = \frac{1}{2} I_{\text{moment}} \omega^2 = \frac{M^2}{2 I_{\text{moment}}} \tag{28-66d}$$

Quantum mechanics indicates that the square of orbital angular momentum is quantized, with $M^2 = j(j+1)h^2/4\pi^2$. The z component of orbital angular momentum is also quantized, with $M_z = m_z h/2\pi$ and $-j \le m_z \le j$. Hence, there are $2j+1$ quantum states of M_z with the same energy E and squared orbital angular momentum M^2 unless a magnetic field is present. In other words, E and M^2 are functions of j but not of m_z in the absence of a magnetic field. Consequently, the rotational energy levels are also quantized:

$$E_j = \frac{j(j+1)h^2}{8\pi^2 I_{\text{moment}}} \tag{28-67}$$

with a degeneracy of $g_j = 2j+1$. The rotational partition function for a single molecule is

$$\begin{aligned} Q_{\text{rotation}} &= \sum_{j \text{ energy levels}} (2j+1) \exp\left(\frac{-E_j}{kT}\right) \\ &= \sum_{j \text{ energy levels}} (2j+1) \exp\left[\frac{-j(j+1)B}{T}\right] \end{aligned} \tag{28-68}$$

where the characteristic rotational temperature B is given by

$$B \equiv \frac{h^2}{8\pi^2 k I_{\text{moment}}} \tag{28-69}$$

For diatomic molecules, the rotational constant reduces to

$$B \equiv \frac{h^2(m_1 + m_2)}{8\pi^2 k R_{\text{equil}}^2 m_1 m_2} \tag{28-70}$$

Before evaluating Q_{rotation}, it is instructive to calculate B as well as the ratio T/B at normal operating temperatures. The generalized constants of interest are:

Planck's constant: $h = 6.62608 \times 10^{-34}$ J·s

Boltzmann's constant: $k = 1.38066 \times 10^{-23}$ J/K

Avogadro's number: $N_{\text{Avo}} = 6.02214 \times 10^{23}$ molecules/mol

As a specific example, consider carbon monoxide (i.e., C ≡ O):

$$m_1 = \frac{12}{N_{\text{Avo}}} \qquad \text{(i.e., mass of C)}$$

$$m_2 = \frac{16}{N_{\text{Avo}}} \qquad \text{(i.e., mass of O)}$$

$$R_{\text{equil}} = 1.128\text{Å} \qquad \text{(i.e., C ≡O bond length)}$$

Interestingly enough, $B = 2.78$ K for carbon monoxide, and T/B is on the order of 100 at ambient temperature. When T/B is approximately unity, the translational kinetic energy of a molecule is comparable to its rotational energy. Under normal operating conditions, it is reasonable to invoke the high-temperature classical limit for Q_{rotation}, where the summation in equation (28-68) can be replaced by an integral because there is essentially a continuous spectrum of rotational energy levels. Evaluation of Q_{rotation} proceeds as follows:

$$\begin{aligned} Q_{\text{rotation, classical}} &= \int_O^\infty (2j+1) \exp\left[-\frac{j(j+1)B}{T}\right] dj \\ &= \int_O^\infty \exp\left(-\frac{xB}{T}\right) dx = \frac{T}{B} \end{aligned} \tag{28-71}$$

where $x = j(j+1)$ was employed to perform the integration in (28-71).

Contribution of Rotational Motion to the Internal Energy and Heat Capacity. As illustrated by equation (28-62), rotational motion of diatomic and polyatomic nonlinear ideal gases contributes to the internal energy as follows:

$$U_{\text{rotation}} = NkT^2 \left(\frac{\partial \ln Q_{\text{rotation, classical}}}{\partial T}\right)_{V,N} \tag{28-72}$$

Diatomic molecules can rotate independently about two different coordinate axes that are perpendicular to the internuclear bond vector. When the molecule rotates by 90°, for example, about either of these axes, a different set of xyz coordinates is required to describe the positions of the atoms before and after rotation. If the molecule rotates about an axis that is collinear with the internuclear bond vector, then the same set of xyz coordinates describes its atomic positions before and after rotation, regardless of the rotation angle. If a molecule exhibits a degree of freedom due to rotation about a coordinate axis, then, in general, a different set of xyz coordinates is required to describe its atomic positions before and after rotation. For example, Table 28-1 illustrates the number of degrees of freedom

TABLE 28-1 Number of Degrees of Rotational Freedom for Various Classes of Molecules

Class of Molecules	Rotational Degrees of Freedom
Monatomic gases	0
Diatomic molecules	2
Polyatomic nonlinear molecules	3
Polyatomic linear molecules	2
Restricted rotation of diatomic or polyatomic molecules about one coordinate axis	1

consumed by rotation, including restricted rotation if the molecule is hindered by an external barrier.

Equation (28-71) indicates that the rotational motion of diatomic molecules yields $Q_{\text{rotation, classical}} = T/B$, where B is a characteristic rotational temperature that is, at most, a few tens of Kelvin (see Table 28-2). The rotational contribution to the internal energy is

$$U_{\text{rotation}} = NkT^2 \left(\frac{\partial \ln(T/B)}{\partial T} \right)_{V,N} = NkT = 2\left(\frac{1}{2}NkT\right) \tag{28-73}$$

The law of equipartition of energy reveals, once again, that each degree of rotational freedom contributes $\frac{1}{2}kT$ per molecule or $\frac{1}{2}RT$ per mole to the internal energy of a diatomic ideal gas, relative to its ground-state energy. This theorem also applies to polyatomic nonlinear ideal gases, because $Q_{\text{rotation}} \approx T^{1.5}$ and also contains moments of inertia about all three principal rotation axes in the molecule (see equation 28-93). The rotational contribution to the heat capacity at constant volume for a diatomic ideal gas is

$$C_{\text{V, rotation}} \equiv \left(\frac{\partial U_{\text{rotation}}}{\partial T} \right)_{V,N} = Nk = 2\left(\frac{1}{2}Nk\right) \tag{28-74}$$

Each degree of rotational motion contributes $\frac{1}{2}R$ per mole to C_V of an ideal gas, in general.

28-7.2 Vibrational Motion

The harmonic oscillator represents a useful model of the vibrational motion of diatomic molecules. Quantum mechanics reveals that the appropriate energy levels are

$$E_n = h\upsilon \left(n + \tfrac{1}{2}\right) \tag{28-75}$$

with a degeneracy given by $g_n = 1$. The oscillator frequency is υ in cycles per second. If $h\upsilon/2$ is combined with the ground-state electronic energy, then

$$E^*_{\text{ground state}} = E_{\text{ground state}} + \tfrac{1}{2}h\upsilon \tag{28-76}$$

and the vibrational partition function for a single molecule is

$$Q_{\text{vibration}} = \sum_{n \text{ states}} \exp\left(-\frac{h\upsilon n}{kT}\right) = \sum_{n \text{ states}} \exp\left(-\frac{n\Theta}{T}\right) \tag{28-77}$$

The characteristic vibrational temperature in Kelvin is

$$\Theta \equiv \frac{h\upsilon}{k} = \frac{hc\lambda^{-1}}{k} \approx 1.44\lambda^{-1} \tag{28-78}$$

where c is the speed of light in vacuum (i.e., 2.997925×10^{10} cm/s) and λ^{-1} is the vibrational frequency from infrared or Raman spectroscopy in wavenumbers (i.e., cm^{-1}). Once again, it is instructive to calculate Θ prior to evaluating $Q_{\text{vibration}}$. For example, the infrared stretching frequency of carbon monoxide is 2169.5 cm^{-1} in the gas phase, and the characteristic vibrational temperature is 3121.4 K. Hence, the hypothetical translational kinetic energy of C≡O at this temperature is comparable to its vibrational energy. Under normal operating conditions, it is not appropriate to evaluate $Q_{\text{vibration}}$ in the high-temperature classical limit because Θ/T is on the order of 10. Vibrational motion is almost quenched at ambient temperature. Explicit evaluation of $Q_{\text{vibration}}$ proceeds as follows, with $x = \Theta/T$:

$$\begin{aligned} Q_{\text{vibration}} &= \sum_{n \text{ states}} \exp(-nx) = 1 + e^{-x} + e^{-2x} + e^{-3x} + \cdots \\ e^{-x} Q_{\text{vibration}} &= e^{-x} + e^{-2x} + e^{-3x} + \cdots = Q_{\text{vibration}} - 1 \\ Q_{\text{vibration}} &= \frac{1}{1 - \exp(-\Theta/T)} \end{aligned} \tag{28-79}$$

For comparison, the classical expression for $Q_{\text{vibration}}$ at small Θ/T is

$$Q_{\text{vibration, classical}} = \int_O^\infty \exp\left(-\frac{n\Theta}{T}\right) dn = \frac{T}{\Theta} \tag{28-80}$$

which has a form that is similar to $Q_{\text{rotation, classical}}$. $Q_{\text{vibration, classical}}$ can be obtained from $Q_{\text{vibration}}$ in equation (28-79) by expanding $\exp(-\Theta/T)$ in a Taylor series when Θ/T is small, and truncating the series after the linear term. However, $Q_{\text{vibration, classical}}$ is not valid at reasonable temperatures where $T \ll \Theta$.

Contribution of Vibrational Motion to the Internal Energy and Heat Capacity. As illustrated by equation (28-62), vibrational motion of diatomic and polyatomic nonlinear ideal gases contributes to the internal energy as follows:

$$U_{\text{vibration}} = NkT^2 \left(\frac{\partial \ln Q_{\text{vibration}}}{\partial T} \right)_{V,N} \tag{28-81}$$

For diatomic molecules whose infrared stretching vibration is modeled by the harmonic oscillator,

$$U_{\text{vibration}} = -NkT^2 \left\{ \frac{\partial \ln[1 - \exp(-\Theta/T)]}{\partial T} \right\}_{V,N} = \frac{Nk\Theta \exp(-\Theta/T)}{1 - \exp(-\Theta/T)} \tag{28-82}$$

If Θ/T is small, then each vibrational degree of freedom contributes kT per molecule or RT per mole to the internal energy of an ideal gas, relative to the ground state energy given by equation (28-76). However, this is not practical because Θ/T is on the order of 10, vibrational motion is almost quenched at normal operating temperatures, and each vibrational degree of freedom contributes only a small fraction of RT per mole to the internal energy. The vibrational contribution to the heat capacity at constant volume for a diatomic ideal gas is

$$C_{V,\,\text{vibration}} \equiv \left(\frac{\partial U_{\text{vibration}}}{\partial T} \right)_{V,N} = \frac{Nkx^2 e^{-x}}{(1 - e^{-x})^2} \tag{28-83}$$

where $x = \Theta/T$.

Vibrational Motion in Polyatomic Molecules. Normal-mode analysis of vibrational motion in polyatomic molecules is the method of choice when there are several vibrational degrees of freedom. The actual vibrations of a polyatomic molecule are completely disordered, or aperiodic. However, these complicated vibrations can be simplified by expressing them as linear combinations of a set of vibrations (i.e., normal modes) in which all atoms move periodically in straight lines and in phase. In other words, all atoms pass through their equilibrium positions at the same time. Each normal mode can be modeled as a harmonic oscillator. The following rules are useful to determine the number of normal modes of vibration that a molecule possesses:

1. Three degrees of freedom are required to describe the position of each atom in a molecule, such as the x, y, and z coordinates in a rectangular Cartesian system. If N_{atoms} represents the number of atoms in a molecule, then $3N_{\text{atoms}}$ corresponds to the total number of degrees of freedom that the molecule possesses.
2. Motion of the center of mass of the molecule in three orthogonal coordinate directions consumes 3 degrees of freedom for translation. This is true in

all cases unless molecules are confined to motion in two dimensions: for example, on a surface.

3. As described in detail on page 770 and in Table 28-1, nonlinear molecules consume 3 degrees of freedom for rotation, whereas linear molecules exhibit only 2 degrees of rotational freedom. There are several examples where molecules that contain three atoms (i.e., CO_2, CS_2, N_2O) are linear because the bond angle is 180°. Acetylene (i.e., HC≡CH) is a four-atom linear molecule that exhibits only 2 degrees of freedom for rotation. Molecules exhibit fewer rotational degrees of freedom if rotation is hindered.
4. The remaining degrees of freedom are consumed by vibrational motion. Monatomic noble gases exhibit 3 degrees of freedom, and all of them are consumed by translation. There are no contributions from rotation or vibration to the thermodynamic properties of monatomic gases. Diatomic molecules exhibit 6 degrees of freedom: 3 for translation, 2 for rotation, and 1 for its vibrational stretch. In general, linear molecules exhibit $3N_{\text{atoms}} - 5$ degrees of freedom for vibrational motion, and nonlinear molecules exhibit $3N_{\text{atoms}} - 6$.
5. Molecules exhibit a normal mode of vibration for each vibrational degree of freedom. Infrared and Raman spectroscopy are useful tools to measure normal modes of vibration.

The vibrational partition function for polyatomic molecules can be factored with respect to each normal mode of vibration. Since each normal mode is described by a harmonic oscillator with frequency $\upsilon_v = c\lambda_v^{-1}$ and vibrational temperature $\Theta_v = 1.44\lambda_v^{-1}$;

$$\begin{aligned} Q_{\text{vibration}} &= \prod_{v=1}^{3N_{\text{atoms}}-6} \left[1 - \exp\left(\frac{-\Theta_v}{T}\right)\right]^{-1} \\ \ln Q_{\text{vibration}} &= -\sum_{v=1}^{3N_{\text{atoms}}-6} \ln\left[1 - \exp\left(\frac{-\Theta_v}{T}\right)\right] \end{aligned} \tag{28-84}$$

for nonlinear polyatomics. Each normal mode contributes to the internal energy and heat capacity as if its vibrational degree of freedom belongs to a diatomic molecule, and the final results are obtained by summing over all $3N_{\text{atoms}} - 6$ degrees of freedom. Hence,

$$\begin{aligned} U_{\text{vibration}} &= NkT^2 \left(\frac{\partial \ln Q_{\text{vibration}}}{\partial T}\right)_{V,N} \\ &= Nk \sum_{v=1}^{3N_{\text{atoms}}-6} \frac{\Theta_v \exp(-\Theta_v/T)}{1 - \exp(-\Theta_v/T)} \end{aligned} \tag{28-85}$$

The vibrational contribution to the heat capacity at constant volume for nonlinear polyatomic ideal gases is

$$C_{V,\,\text{vibration}} \equiv \left(\frac{\partial U_{\text{vibration}}}{\partial T}\right)_{V,N} = Nk \sum_{v=1}^{3N_{\text{atoms}}-6} \frac{x_v^2 \exp(-x_v)}{[1-\exp(-x_v)]^2} \tag{28-86}$$

where $x_v = \Theta_v / T$. This methodology and a few simplifying assumptions described in Problem 28-2 are employed to calculate the heat capacity of polyatomic gases in packed catalytic tubular reactors when external resistances to heat and mass transfer cannot be neglected (see Section 30-6).

28-7.3 Molecular Parameters for Diatomic and Polyatomic Molecules

Table 28-2 provides useful constants from which characteristic rotational and vibrational temperatures of diatomic molecules have been calculated. These molecular constants were obtained from the *JANAF Thermochemical Tables*, courtesy of Dow Chemical Co., Midland, Michigan, and from Sonntag and Van Wylen (1966, p. 358). Notice that B is smaller for diatomics that contain larger atoms and longer bond lengths, due to the fact that B is inversely proportional to the moment of inertia. This is analogous to the well-known phenomenon that figure skaters spin at lower angular velocity when they extend their arms outward, because angular momentum is conserved. Also, it is possible to stabilize oneself after sudden impact by extending the arms, which increases the moment of inertia. The characteristic vibrational temperature is larger for diatomics that contain smaller atoms with more polar bonds, due to the fact that $\Theta \approx \lambda^{-1}$, and stretching frequencies increase when the reduced mass is smaller or the force constant is larger.

TABLE 28-2 Molecular Parameters and Characteristic Temperatures for Rotation and Vibration of Several Diatomic Molecules

Molecule	R_{equil} (Å)	λ^{-1} (cm^{-1})	B (K)	Θ (K)
N_2	1.0976	2357.6	2.876	3392.0
O_2	1.2074	1580.2	2.080	2273.5
NO	1.1508	1903.6	2.453	2738.8
CO	1.1281	2169.5	2.779	3121.4
H_2	0.7417	4405.3	88.178	6338.2
F_2	1.409	923.1	1.286	1328.1
Cl_2	1.988	561.1	0.346	807.3
Br_2	2.284	323.2	0.116	465.0
I_2	2.667	214.5	0.054	308.6
HF	0.9168	4138.3	30.375	5954.1
HCl	1.2746	2989.6	15.350	4301.3
HBr	1.414	2649.6	12.283	3812.2
HI	1.604	2309.1	9.501	3322.3

TABLE 28-3 Molecular Parameters and Normal Modes of Vibration for Several Polyatomic Molecules

Molecule	Bond Distance (Å)	Bond Angle (deg)	λ^{-1} (cm^{-1})[a]
CO_2	C−O; 1.926	O−C−O; 180	667.3 (2)
(B = 0.561 K)			1342.9
			2349.3
CS_2	C−S; 1.553	S−C−S; 180	396.8 (2)
(B = 0.157 K)			658
			1532.5
N_2O	N−N; 1.1282	N−N−O; 180	589.2 (2)
(B = 0.602 K)	N−O; 1.1842		1276.5
			2223.7
H_2O	O−H; 0.9584	H−O−H; 104.45	1594.6
			3657.1
			3755.8
H_2S	S−H; 1.3455	H−S−H; 93.3	1182.7
			2614.6
			2627.5
NH_2	N−H; 1.025	H−N−H; 103	1550
			3400
			3450
NO_2	N−O; 1.197	O−N−O; 134.25	756.8
			1357.8
			1665.5
CH_4	C−H; 1.091	H−C−H; 109.47	1306 (3)
			1534 (2)
			2916.5
			3018.7 (3)

[a] Numbers in parentheses indicate the degeneracy of each vibrational energy level, as expressed in wavenumbers.

For polyatomic molecules, there are several normal modes of vibration that must be considered, as well as the bond angle that determines whether triatomics are linear or bent. The information in Table 28-3 for seven triatomics and one polyatomic was obtained from the same sources as Table 28-2 for diatomics, as well as Reed and Gubbins (1973, p. 74). Degenerate vibrational energy levels are indicated in parentheses and, in some cases, the characteristic rotational temperature is included under the molecular formula.

28-8 ENTROPY AND CHEMICAL POTENTIAL

28-8.1 Absolute Entropy

All types of motion (i.e., translation, rotation, and vibration) contribute to the entropy of an ideal gas. The following equations that have been discussed in this

chapter are employed to express S in terms of T, p, and N:

$$\begin{aligned}
\ln Z &= -\ln N! - \frac{N E_{\text{ground state}}}{kT} + N \ln V - 3N \ln \lambda_T \\
&\quad + N \ln(Q_{\text{rotation}} Q_{\text{vibration}}) \\
U &= kT^2 \left(\frac{\partial \ln Z}{\partial T} \right)_{V,N} = N E_{\text{ground state}} + \frac{3}{2} NkT \\
&\quad + NkT^2 \left[\frac{\partial \ln(Q_{\text{rotation}} Q_{\text{vibration}})}{\partial T} \right]_{V,N} \\
\lambda_T &\equiv \frac{h}{\sqrt{2\pi mkT}} \\
V &= \frac{NkT}{p} \\
S &= k \ln Z + \frac{U}{T}
\end{aligned} \tag{28-87}$$

Sterling's approximation is useful to simplify the factorial of large numbers with less than 1% error when $N \geq 100$:

$$\begin{aligned}
\ln N! &= \ln[N(N-1)(N-2)\cdots 1] = \sum_{x=1}^{N} \ln x \\
&= \int_1^N \ln x \, dx = [x \ln x - x]_{x=1}^{x=N} \approx N \ln N - N
\end{aligned} \tag{28-88}$$

Obviously, this approximation is excellent when N corresponds to 1 mol of molecules. Molar properties are obtained via division by N, and multiplication by N_{Avo}, where the gas constant $R = kN_{\text{Avo}}$. For diatomic molecules with 2 degrees of freedom for rotation and 1 for vibration,

$$\begin{aligned}
Q_{\text{rotation}} &= \frac{T}{B} \\
Q_{\text{vibration}} &= \left[1 - \exp\left(-\frac{\Theta}{T} \right) \right]^{-1}
\end{aligned} \tag{28-89}$$

The corresponding absolute entropy, with units of R, is

$$\frac{S}{R} = \frac{5}{2} + \ln \frac{(2\pi m)^{3/2} (kT)^{5/2}}{ph^3} + \frac{S_{\text{rotation}}}{R} + \frac{S_{\text{vibration}}}{R} \tag{28-90}$$

$$\frac{S_{\text{rotation}}}{R} = \ln Q_{\text{rotation}} + T \left(\frac{\partial \ln Q_{\text{rotation}}}{\partial T} \right)_{V,N} = 1 + \ln \frac{T}{B} \tag{28-91}$$

$$\frac{S_{\text{vibration}}}{R} = \ln Q_{\text{vibration}} + T\left(\frac{\partial \ln Q_{\text{vibration}}}{\partial T}\right)_{V,N} = -\ln(1 - e^{-x}) + \frac{xe^{-x}}{1 - e^{-x}} \tag{28-92}$$

where $x = \Theta/T$. At 400 K and 1 atm total pressure, the absolute entropy of carbon monoxide is $24.8R$. Below 700 K, entropy calculations for C≡O with and without the contribution from vibrational motion are indistinguishable. In the vicinity of CO's vibrational temperature (i.e., ≈3000 K), vibrational motion contributes approximately 3% to the total absolute entropy. These results are illustrated in Figure 28-1.

For nonlinear polyatomics, the complete vibrational contribution to S is obtained by summing $S_{\text{vibration}}$, as given by equation (28-92), over all $3N_{\text{atoms}} - 6$ vibrational degrees of freedom. However, the complete rotational contribution to S is much more complicated than S_{rotation}, as given by equation (28-91) for diatomics, because

$$Q_{\text{rotation}} = \frac{\pi^{1/2}}{\sigma}\left\{\frac{8\pi^2 I_{\text{moment},\,x}\,kT}{h^2}\;\frac{8\pi^2 I_{\text{moment},\,y}\,kT}{h^2}\;\frac{8\pi^2 I_{\text{moment},\,z}\,kT}{h^2}\right\}^{1/2} \tag{28-93}$$

where three principal moments of inertia are required about a set of coordinate axes whose origin coincides with the molecule's center of mass. The symmetry number σ is 2 for symmetric linear molecules, 1 for asymmetric molecules, and

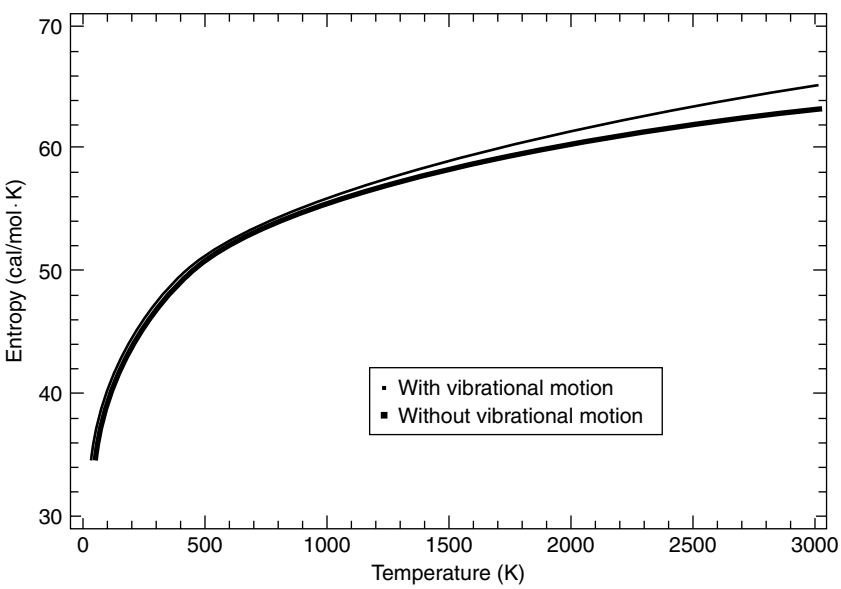

Figure 28-1 Temperature dependence of the absolute entropy of carbon monoxide from 50 to 3000 K at 1 atm total pressure. Ideal gas behavior is assumed throughout. Calculations are performed with and without the contribution from vibrational motion.

12 for methane. σ represents the number of proper rotations in the symmetry group of the molecule, or the number of indistinguishable orientations that a molecule possesses due to rotations about its symmetry axes, excluding the infinite number of possibilities due to rotation about the internuclear bond axis for linear molecules that belong to the $D_{\infty h}$ or $C_{\infty v}$ point groups, if they are symmetric or asymmetric, respectively.

28-8.2 Chemical Potential

If one employs the partition function Z for an ideal gas, as given by equations (28-59) and (28-87), then the Helmholtz free energy and chemical potential are calculated by combining classical and statistical thermodynamics:

$$A = -kT \ln Z \tag{28-94}$$

$$\mu \equiv \left(\frac{\partial A}{\partial N}\right)_{T,V} = -kT \left(\frac{\partial \ln Z}{\partial N}\right)_{T,V} \tag{28-95}$$

where the definition of μ is based on the total differential expression for $A(T, V, N)$:

$$dA = -S\,dT - p\,dV + \mu\,dN \tag{28-96}$$

Since there are N ideal gas molecules, Euler's integral theorem for homogeneous thermodynamic state functions reveals that the chemical potential of a pure material is equivalent to the Gibbs free energy $G(T, p, N)$ on a per molecule basis (see equation 29-30d):

$$\mu = \frac{G}{N} = E_{\text{ground state}} - kT \ln \left\{ \frac{(V/N)\, Q_{\text{rotation}}\, Q_{\text{vibration}}}{(\lambda_T)^3} \right\} \tag{28-97}$$

Expressions for the equation of state, de Broglie thermal wavelength, and rotational and vibrational partition functions for a diatomic molecule, provided by (28-87) and (28-89), as well as multiplication by N_{Avo}, allow one to determine the chemical potential on a molar basis. The final result for μ is consistent with its definition from classical thermodynamics:

$$\mu(T, p) \equiv [\mu^{(0)}(T)]_{\text{ideal gas reference state}} + RT \ln p \tag{28-98}$$

Statistical thermodynamics provides the following result for the chemical potential of a pure diatomic ideal gas in its reference state at 1 atm total pressure:

$$[\mu^{(0)}(T)]_{\text{ideal gas reference state}} = N_{\text{Avo}} E_{\text{ground state}} + RT \ln \left\{ \frac{Bh^3[1 - \exp(-\Theta/T)]}{(2\pi m)^{3/2} k^{5/2} T^{7/2}} \right\} \tag{28-99}$$

PROBLEMS

28-1. In this problem, we compare the temperature dependence of the specific heat of triatomic ideal gases based on statistical thermodynamics and classical/empirical polynomials. Locate the appropriate molecular data for carbon dioxide (CO_2) and nitrogen dioxide (NO_2) that will allow you to compute and graph the specific heat at constant pressure C_p for both gases from 300 to 800 K at atmospheric pressure. The graphs that are generated should be based on calculations from statistical thermodynamics.
Locate the appropriate coefficients that describe empirically the temperature dependence of the specific heat for both carbon dioxide and nitrogen dioxide. The polynomial expression can be written generically in the following form:

$$C_p(T) = \sum_m a_m T^m$$

where the values of m can be positive or negative, and the series is usually truncated after a few terms. Evaluate the specific heat for carbon dioxide from 300 to 800 K based on empirical correlations and display the results on the same graph that contains the calculations from statistical thermodynamics. Repeat the calculations and generate a second graph for nitrogen dioxide. Your solution to this problem should contain the following information.

(1) Molecular parameters for both gases

(2) Polynomial coefficients for both gases

(3) Units of temperature that are required in the polynomial expression

(4) Units of specific heat that are obtained from the polynomial expression

(5) Two graphs of C_p vs. T from 300 to 800 K: one for CO_2 and one for NO_2

Provide a brief explanation for any discrepancies between the statistical results and the classical results.

28-2. In this problem, we correlate the specific heats of normal alkanes from C_1 to C_6 with the number of vibrational degrees of freedom. Locate the appropriate coefficients that describe empirically the temperature dependence of the specific heat for normal alkanes from methane to n-hexane. The polynomial expression can be written generically in the form

$$C_p(T) = \sum_m a_m T^m$$

where the values of m can be positive or negative, and the series is usually truncated after a few terms. For the homologous series under consideration, $m = 0, 1, 2, 3$. Evaluate the specific heat of each gas from 400 to 1500 K

based on empirical correlations and display the results graphically on one set of axes.

Normal alkanes have the general chemical formula given by C_nH_{2n+2}. Hence, the total number of atoms is $3n + 2$ for any alkane defined by the number of carbon atoms (n) in the molecule. The total number of degrees of freedom is $9n + 6$. Since all of the alkanes are nonlinear, $9n$ represents the number of vibrational degrees of freedom per molecule, and these values range from 9 for methane to 54 for n-hexane.

Devise a strategy and follow through with further calculations to provide a detailed analysis of the contribution of vibrational motion to C_p. Make one key assumption to simplify your analysis. Assume that all $9n$ modes of vibration are degenerate for each alkane, and that the nine equal values of Θ for methane are the same as the 18 equal values of Θ for ethane, which, in turn, are the same as the 27 equal values of Θ for propane, and so on. Of course, this assumption is not valid, but it should not interfere much with the thought process. Analyze the empirical temperature polynomials for C_p from a statistical thermodynamic viewpoint.

Answer: At all temperatures investigated, C_p is larger when molecules in this homologous series contain more atoms. Hence, $(\partial C_p/\partial n)_T > 0$. If the data are plotted isothermally as a function of the number of vibrational degrees of freedom, then linear behavior is observed at each temperature:

$$\left[\frac{\partial C_p}{\partial (9n)}\right]_T = f(T) > 0$$

where the slope $f(T)$ increases at higher temperature. The law of equipartition of energy indicates that each degree of translational and rotational freedom contributes $\frac{1}{2}R$ per mole to C_v. If all $9n$ modes of vibration are degenerate for all six alkanes, then the statistical model for nonlinear polyatomic ideal gases yields:

$$C_p = C_v + R = \frac{3}{2}R + \frac{3}{2}R + 9nR\frac{x^2e^{-x}}{(1-e^{-x})^2} + R$$

where $x = \Theta/T$. Manipulation of the preceding two equations allows one to measure the slope $f(T)$ and estimate the average vibrational temperature for all six alkanes:

$$\left[\frac{\partial C_p}{\partial (9n)}\right]_T = f(T) = R\frac{x^2e^{-x}}{(1-e^{-x})^2}$$

via trial and error. If all $9n$ modes of vibration are degenerate for each alkane but $\Theta_{n=1} \neq \Theta_{n=2} \neq \cdots \neq \Theta_{n=6}$, then the analysis described below yields an average vibrational temperature for each gas. Using a nonlinear least-squares approach to minimize the sum of squares of the difference

TABLE 28-4 Approximate Characteristic Temperatures for Vibration of a Homologous Series of Alkanes

Alkane	n	CH bonds	C−C bonds	Θ (K)
Methane	1	4	0	2825
Ethane	2	6	1	2355
Propane	3	8	2	2150
n-Butane	4	10	3	2050
n-Pentane	5	12	4	1995
n-Hexane	6	14	5	1955

[a] All $9n$ degrees of vibrational freedom are degenerate, where n is the number of carbon atoms in the molecule.

between the classical temperature polynomial and the statistical model for C_p, one analyzes the following set of equations separately for each alkane, where the summation includes several discrete temperatures between 400 and 1500 K:

$$\text{error} \equiv \sum_i \left[C_{p,\,\text{classical}}(T_i) - C_{p,\,\text{statistical}}(T_i)\right]^2$$

$$C_{p,\,\text{classical}}(T) = a_0 + a_1 T + a_2 T^2 + a_3 T^3$$

$$C_{p,\,\text{statistical}}(T) = 4R + 9nR\frac{x^2 e^{-x}}{(1-e^{-x})^2}$$

$$\frac{\partial \text{error}}{\partial \Theta} = 0$$

Minimization of the error is performed numerically, and the results are presented in Table 28-4. A lower characteristic vibrational temperature is required in the statistical expression for C_p as n increases. This is consistent with the following facts:

(1) The ratio of CH bonds relative to C−C bonds decreases as the molecular weight of the alkane increases.

(2) The bond energy is larger for CH (i.e., 415 kJ/mol) relative to C−C (i.e., 344 kJ/mol), as obtained from Pauling (1970, p. 913).

(3) The reduced mass is smaller for CH relative to C−C when modeled as a diatomic harmonic oscillator.

(4) The infrared stretching frequency is larger for CH relative to C−C.

28-3. Generate a graph of the temperature dependence of the absolute entropy of carbon monoxide from 50 to 2500 K at 1 atm total pressure. It is reasonable to assume that CO behaves ideally over this temperature range. Do not neglect the contribution from vibrational motion.

28-4. Obtain a complete temperature-dependent expression for the specific heat (C_p) at constant pressure for NO_2 in the gas phase.

28-5. Calculate the entropy change for a nonlinear polyatomic ideal gas that proceeds from state 1 to state 2 at constant volume via (**a**) statistical thermodynamics, and (**b**) classical thermodynamics. Compare your answers.

28-6. Formulate an expression for the (**a**) partition function Z, (**b**) internal energy U, and (**c**) specific heat at constant pressure C_p for 1 mol of chloromethane (CH_3Cl) based on statistical thermodynamics.

28-7. Calculate the entropy of 1 mol of carbon monoxide (CO) at 400 K and 1 atm pressure. It is not necessary to include the contribution from vibrational motion at 2169.5 cm^{-1} because the temperature of the gas (400 K) is more than seven times smaller than the characteristic vibrational temperature (i.e., $1.44\lambda^{-1} = 3121.4$ K). Be careful with units. A few helpful hints are given below based on the gas constant R.

$$82.057 \text{ cm}^3\cdot\text{atm} = 8.314 \text{ J}$$

$$1 \text{ J} = 10^7 \text{ergs} = 10^7 \text{g}\cdot\text{cm}^2/\text{s}^2$$

Transport Phenomena for Chemical Reactor Design. Laurence A. Belfiore
Copyright © 2003 John Wiley & Sons, Inc.
ISBN: 0-471-20275-4

29

THERMODYNAMIC STABILITY CRITERIA FOR SINGLE-PHASE HOMOGENEOUS MIXTURES

Stability criteria are discussed within the framework of equilibrium thermodynamics. Preliminary information about state functions, Legendre transformations, natural variables for the appropriate thermodynamic potentials, Euler's integral theorem for homogeneous functions, the Gibbs–Duhem equation, and the method of Jacobians is required to make this chapter self-contained. Thermal, mechanical, and chemical stability constitute complete thermodynamic stability. Each type of stability is discussed empirically in terms of a unique thermodynamic state function. The rigorous approach to stability, which invokes energy minimization, confirms the empirical results and reveals that $r + 1$ conditions must be satisfied if an r-component mixture is homogeneous and does not separate into more than one phase.

29-1 ENERGY REPRESENTATION OF THE FUNDAMENTAL EQUATION AND EXACT DIFFERENTIALS

Extensive thermodynamic state functions such as the internal energy U depend linearly on mass or mole numbers of each component. This claim is consistent with Euler's theorem for homogeneous functions of the first degree with respect to molar mass. If a mixture contains r components and exists as a single phase, then U exhibits $r + 2$ degrees of freedom and depends on the following natural variables, all of which are extensive:

$$U = U(S, V, N_1, N_2, N_3, \ldots, N_r) \tag{29-1}$$

where S is the entropy, V the volume, and N_i represents the mole numbers of component i. This is the fundamental equation of thermodynamics in the energy

representation. The entropy representation is obtained by interchanging U and S. The differential form of the first law of thermodynamics for open systems, based on the energy representation of the fundamental equation, is

$$dU = \left(\frac{\partial U}{\partial S}\right)_{V,\text{ all } N_i} dS + \left(\frac{\partial U}{\partial V}\right)_{S,\text{ all } N_i} dV + \sum_{i=1}^{r} \left(\frac{\partial U}{\partial N_i}\right)_{S,V,\text{ all } N_j\ [j\neq i]} dN_i \tag{29-2}$$

where the coefficients of U with respect to its natural variables are

$$\begin{aligned} \left(\frac{\partial U}{\partial S}\right)_{V,\text{ all } N_i} &\equiv T \\ \left(\frac{\partial U}{\partial V}\right)_{S,\text{ all } N_i} &\equiv -p \\ \left(\frac{\partial U}{\partial N_i}\right)_{S,V,\text{ all } N_j\ [j\neq i]} &\equiv \mu_i \end{aligned} \tag{29-3}$$

T is temperature, p is pressure, and μ_i is the chemical potential of component i in the mixture. The chemical potential is not a partial molar property of U because S and V are held constant during differentiation instead of T and p, based on the definition of μ in (29-3). The total differential of internal energy

$$dU = T\,dS - p\,dV + \sum_{i=1}^{r} \mu_i\,dN_i \tag{29-4}$$

is an exact differential because U is a thermodynamic state function. The following properties are unique to exact differentials, such as dU:

1. Changes in U are path-independent and depend only on the nature of the initial and final equilibrium states that are linked by the path the system chooses to follow. Different paths that link the same initial and final equilibrium states are characterized by the same change in U.
2. Second mixed partial derivatives of U are independent of the order in which differentiation is performed (i.e., $\partial^2 U/\partial x_i\,\partial x_j = \partial^2 U/\partial x_j\,\partial x_i$). The well-known Maxwell relations are based on this mathematical principle.

One interesting feature of the differential form of the first law of thermodynamics for a pure material which does not exchange mass with its surroundings (i.e., a closed system) is that an exact differential (i.e., dU) is equal to the sum of two path-dependent inexact differentials: heat input to the system (dq) and work performed on the system (dw):

$$dU = dq + dw \tag{29-5}$$

29-2 LEGENDRE TRANSFORMATIONS

As described by equations (29-1) and (29-2), the energy representation of the fundamental equation corresponds to complete thermodynamic information about a multicomponent open system. For example, if

$$U = U(S, V, N_1, N_2, N_3, \ldots, N_r) \tag{29-6}$$

then temperature is obtained from the entropy coefficient of U and pressure is obtained from the volume coefficient of U, as illustrated in (29-3). Equations of state can be developed to correlate information about p, V, and T, where V is one of the natural variables of U. Is it possible to re-express complete thermodynamic information about a system using a different state function that has a different set of independent variables? If possible, then it is important to perform such a transformation without losing any information about the system. As suggested by the title of this section, Legendre transformations are constructed to accomplish this task. A generalized example is based on the function $y(x)$, which hypothetically represents complete information about a system. At position x, the slope is ξ and the y intercept based on a straight line with slope ξ is Ψ. A Legendre transformation maps $y(x)$ into $\Psi(\xi)$, where y the old function or dependent variable, x the old independent variable, Ψ the new function or dependent variable, and ξ the new independent variable. The procedure is based on the *point-slope method*, as follows:

$$\begin{aligned} \xi &= \frac{dy}{dx} = \frac{y - \psi}{x - 0} \\ \Psi &= y - \xi x \end{aligned} \tag{29-7}$$

The total differential of Ψ reveals that the new function depends on ξ:

$$d\Psi = dy - \xi\, dx - x\, d\xi = -x\, d\xi \tag{29-8}$$

because dy and $\xi\, dx$ cancel via the definition of the slope. The following specific example illustrates why information is lost if one re-expresses the old function in terms of the slope. Consider

$$y(x) = A(x - x_0)^2 + B \tag{29-9}$$

where A, B, and x_0 are constants. The slope is

$$\xi = \frac{dy}{dx} = 2A(x - x_0) \tag{29-10}$$

Notice that if y is written in terms of ξ, then information about x_0 is lost in the new representation:

$$y(\xi) = \frac{\xi^2}{4A} + B \tag{29-11}$$

Even though the slope contains information about x_0, via equation (29-10), ξ is the new independent variable in equation (29-11). In other words, ξ can be chosen independently without any knowledge of x_0. Now, if ξ is chosen as the new independent variable and the prescription described by (29-7) for Legendre transformations is employed to calculate a new function Ψ, which is the y intercept of the straight line that corresponds to each slope ξ, then

$$\Psi(\xi) = y - \xi x = B - \xi x_0 - \frac{\xi^2}{4A} \tag{29-12}$$

The new function in (29-12) retains information about all three constants: A, B, and x_0.

Illustrative Problem. Obtain the Legendre transform of the function $Z(x) = A\exp(bx)$, where A and b are constants. Neither Z nor x should appear in the final answer, but the new function should retain information about A and b.

29-2.1 Legendre Transforms of Multivariable Functions

The point-slope formula and the example in the previous section illustrate the methodology to calculate the Legendre transform of a function of one independent variable. Consider the following multivariable function, $y(x_1, x_2, x_3, \ldots, x_n)$, where the associated slopes are

$$\xi_i = \left(\frac{\partial y}{\partial x_i}\right)_{\text{all } x_j \ (j \neq i)} \tag{29-13}$$

The total differential of y is

$$dy = \sum_{i=1}^{n} \xi_i \, dx_i \tag{29-14}$$

If y is a thermodynamic state function, then dy is an exact differential and all the x_i's represent, for example, the natural variables of y. If one performs a Legendre transformation of y with respect to all of its natural variables, then

$$\Psi(\xi_1, \xi_2, \xi_3, \ldots, \xi_n) \equiv y - \sum_{i=1}^{n} \xi_i x_i \tag{29-15}$$

such that all the associated slopes ξ_i assume the role of new natural independent variables for Ψ. This claim is justified by constructing the total differential of Ψ and identifying all differentials on the far right side of equation (29-16) as new independent variables:

$$d\Psi = dy - \sum_{i=1}^{n} (\xi_i \, dx_i + x_i \, d\xi_i) = -\sum_{i=1}^{n} x_i \, d\xi_i \tag{29-16}$$

As a final example, it is not necessary to transform all independent variables of a multivariable function. If Legendre transformation of y is performed with respect to x_1 and x_3, then

$$\Psi(\xi_1, x_2, \xi_3, x_4, x_5, \ldots, x_n) \equiv y - \xi_1 x_1 - \xi_3 x_3 \tag{29-17}$$

Pay particular attention to the set of independent variables for Ψ. If transformation of y is performed with respect to independent variable x_i, then the associated slope ξ_i replaces x_i as a new independent variable.

29-2.2 Thermodynamic State Functions Via Legendre Transformations

Begin with the energy representation of the fundamental equation for a system that contains r components:

$$U = U(S, V, N_1, N_2, N_3, \ldots, N_r) \tag{29-18}$$

where all variables are extensive, and transform U with respect to S. Since the associated slope is defined as temperature T via equation (29-3), the new thermodynamic state function that contains complete information about the system is

$$\Psi = U - TS \equiv A(T, V, N_1, N_2, N_3, \ldots, N_r) \tag{29-19}$$

where A is the Helmholtz free energy. If the internal energy is transformed with respect to V, then the associated slope is $-p$, as defined by equation (29-3), and without loss of information, the new thermodynamic state function is

$$\Psi = U - (-p)V \equiv H(S, p, N_1, N_2, N_3, \ldots, N_r) \tag{29-20}$$

where H is enthalpy. Transformation of U with respect to S and V, with associated slopes given by T and $-p$, respectively, yields the Gibbs free energy G:

$$\Psi = U - TS - (-p)V \equiv G(T, p, N_1, N_2, N_3, \ldots, N_r) \tag{29-21}$$

The best choice among U, A, H, and G to describe a system completely is based on the process under consideration and the natural variables for each thermodynamic state function.

29-2.3 Summary of Legendre Transforms and Thermodynamic State Functions

The Legendre transform of the multivariable function $y(x_1, x_2, x_3, \ldots, x_C, x_{C+1}, x_{C+2}, \ldots, x_n)$ with respect to the first C independent variables (i.e., $x_1 \rightarrow x_C$) is

$$\Psi(\xi_1, \xi_2, \xi_3, \ldots, \xi_C, x_{C+1}, x_{C+2}, \ldots, x_n) = y - \sum_{i=1}^{C} \xi_i x_i \tag{29-22}$$

where ξ_i is the slope of y with respect to x_i. If this methodology is applied to the energy representation of the fundamental equation of thermodynamics, $U(S, V, \text{all } N_i)$, then one generates the following state functions, which represent complete thermodynamic information about a multicomponent system:

Enthalpy: $$H(S, p, \text{all } N_i) \equiv U + pV \tag{29-23a}$$

Helmholtz free energy: $$A(T, V, \text{all } N_i) \equiv U - TS \tag{29-23b}$$

Gibbs free energy: $$G(T, p, \text{all } N_i) \equiv U + pV - TS \tag{29-23c}$$

Exact differential expressions and one coefficient for all four of these thermodynamic state functions are summarized below;

$$dU = T\,dS - p\,dV + \sum_{i=1}^{r} \mu_i\,dN_i \qquad T \equiv \left(\frac{\partial U}{\partial S}\right)_{V, \text{all } N_i} \tag{29-24a}$$

$$dH = T\,dS + V\,dp + \sum_{i=1}^{r} \mu_i\,dN_i \qquad V \equiv \left(\frac{\partial H}{\partial p}\right)_{S, \text{all } N_i} \tag{29-24b}$$

$$dA = -S\,dT - p\,dV + \sum_{i=1}^{r} \mu_i\,dN_i \qquad p \equiv -\left(\frac{\partial A}{\partial V}\right)_{T, \text{all } N_i} \tag{29-24c}$$

$$dG = -S\,dT + V\,dp + \sum_{i=1}^{r} \mu_i\,dN_i \qquad \mu_i \equiv \left(\frac{\partial G}{\partial N_i}\right)_{T, p, \text{all } N_j (j \neq i)} \tag{29-24d}$$

The chemical potential μ_i is a partial molar property of the Gibbs free energy because, as illustrated by the mole number coefficient of G in equation (29-24d), temperature, pressure, and all other mole numbers are held constant during differentiation with respect to N_i.

29-3 EULER'S INTEGRAL THEOREM FOR HOMOGENEOUS FUNCTIONS OF ORDER *m*

Consider the following multivariable function $y(x_1, x_2, x_3, \ldots, x_C, x_{C+1}, x_{C+2}, \ldots, x_n)$ with associated slopes given by

$$\xi_i = \left(\frac{\partial y}{\partial x_i}\right)_{\text{all } x_j \ (j \neq i)} \tag{29-25}$$

The first C independent variables (i.e., $x_1 \rightarrow x_C$) are extensive, whereas the remaining independent variables (i.e., $x_{C+1} \rightarrow x_n$) are intensive. If y is a homogeneous function of order m with respect to its extensive independent variables, then

$$y^*(\lambda x_1, \lambda x_2, \lambda x_3, \ldots, \lambda x_C, x_{C+1}, x_{C+2}, \ldots, x_n) = \lambda^m y(x_1, x_2, x_3, \ldots, x_C, x_{C+1}, x_{C+2}, \ldots, x_n) \tag{29-26}$$

where λ is a constant multiplier. For example, if y is kinetic energy and x_i's represent all of the velocities, then y is a homogeneous function of order $m = 2$ because tripling the velocities (i.e., $\lambda = 3$) yields a kinetic energy that is nine-fold larger than the original function (i.e., $\lambda^m = 3^2$). In general, if the system mass increases by a factor of λ, then all extensive variables increase by this same factor, but the intensive variables (i.e., T, p, and density) remain unaffected because they are not functions of system mass or λ. The dependence on λ of the left side of equation (29-26) for homogeneous functions is

$$\sum_{i=1}^{C} \left[\frac{\partial y^*}{\partial(\lambda x_i)} \right]_{\text{all } x_j \ (j \neq i)} \frac{d(\lambda x_i)}{d\lambda} = \sum_{i=1}^{C} x_i \left[\frac{\partial y^*}{\partial(\lambda x_i)} \right]_{\text{all } x_j \ (j \neq i)} \tag{29-27}$$

The dependence on λ of the right side of equation (29-26) for homogeneous functions is

$$m\lambda^{m-1} y(x_1, x_2, x_3, \ldots, x_C, x_{C+1}, x_{C+2}, \ldots, x_n) \tag{29-28}$$

If one equates (29-27) and (29-28) and lets λ approach unity and $y^* \to y$, then Euler's integral theorem provides the prescription to calculate any homogeneous function in terms of its extensive variables and the associated slopes ξ_i:

$$my(x_1, x_2, x_3, \ldots, x_C, x_{C+1}, x_{C+2}, \ldots, x_n) = \sum_{i=1}^{C} x_i \left(\frac{\partial y}{\partial x_i} \right)_{\text{all } x_j (j \neq i)} = \sum_{i=1}^{C} x_i \xi_i \tag{29-29}$$

All extensive thermodynamic state functions are homogeneous to the first degree with respect to system mass. Hence, $m = 1$ for U, H, A, and G. Integration via Euler's theorem yields the following results, where the extensive natural variables are highlighted in bold:

Internal energy: $$U(\mathbf{S}, \mathbf{V}, \text{all } \mathbf{N}_i) \equiv T\mathbf{S} - p\mathbf{V} + \sum_{i=1}^{r} \mu_i \mathbf{N}_i \tag{29-30a}$$

Enthalpy: $$H(\mathbf{S}, p, \text{all } \mathbf{N}_i) \equiv T\mathbf{S} + \sum_{i=1}^{r} \mu_i \mathbf{N}_i \tag{29-30b}$$

Helmholtz free energy: $$A(T, \mathbf{V}, \text{all } \mathbf{N}_i) \equiv -p\mathbf{V} + \sum_{i=1}^{r} \mu_i \mathbf{N}_i \tag{29-30c}$$

Gibbs free energy: $$G(T, p, \text{all } \mathbf{N}_i) \equiv \sum_{i=1}^{r} \mu_i \mathbf{N}_i \tag{29-30d}$$

Euler's theorem applied to U, H, A, and G is consistent with Legendre transformation of the fundamental equation of thermodynamics in the energy representation to generate defining relations for H, A, and G via equations (29-23). The Gibbs free energy is an example of 'expansions in terms of partial molar

properties' via the chemical potential. If Euler's theorem is applied to intensive thermodynamic state functions which are homogeneous to the zeroth degree (i.e., $m = 0$) with respect to system mass, then one concludes that these intensive functions are independent of total mass or moles. Intensive functions should be addressed by employing Euler's theorem to generate an expression for the corresponding extensive function in terms of its extensive variables, and then dividing the result by total system mass or moles.

Illustrative Problem. Begin with the energy representation of the fundamental equation of thermodynamics $U(S, V, \text{all } N_i)$ for a system of r-components and transform this complete thermodynamic information to a new state function in which entropy S and all mole numbers $N_i (1 \leq i \leq r)$ are not independent variables.

(a) Identify all the new independent variables for this new state function.
(b) Use Euler's theorem to simplify your expression for this new state function, based on classical thermodynamics. *Hint:* In terms of the formalism of statistical thermodynamics, this new state function is given by $-kT \ln X$, where k is Boltzmann's constant and X is the grand partition function.

29-3.1 Rigorous Derivation of Euler's Integral Theorem

If the multiplier λ is treated as a variable, then one should take the total differential of the defining equation for homogeneous functions of the mth order:

$$y^*(\lambda x_1, \lambda x_2, \lambda x_3, \ldots, \lambda x_C, x_{C+1}, x_{C+2}, \ldots, x_n) = \lambda^m y(x_1, x_2, x_3, \ldots, x_C, x_{C+1}, x_{C+2}, \ldots, x_n) \tag{29-31}$$

The total differential of the left side of equation (29-31) is

$$\sum_{i=1}^{C} \left[\frac{\partial y^*}{\partial (\lambda x_i)} \right]_{\text{all } x_j (j \neq i)} d(\lambda x_i) + \sum_{i=C+1}^{n} \left(\frac{\partial y^*}{\partial x_i} \right)_{\text{all } x_j (j \neq i)} dx_i \tag{29-32}$$

where

$$d(\lambda x_i) = x_i \, d\lambda + \lambda \, dx_i$$

The total differential of the right side of equation (29-31) for homogeneous functions is

$$m\lambda^{m-1} y(x_1, x_2, x_3, \ldots, x_C, x_{C+1}, x_{C+2}, \ldots, x_n) \, d\lambda + \lambda^m \sum_{i=1}^{n} \left(\frac{\partial y}{\partial x_i} \right)_{\text{all } x_j (j \neq i)} dx_i \tag{29-33}$$

Upon equating both total differentials in (29-32) and (29-33), one obtains the following result after rearrangement:

$$\sum_{i=1}^{C}\left\{\lambda\left[\frac{\partial y^*}{\partial(\lambda x_i)}\right]_{\text{all } x_j(j\neq i)} - \lambda^m\left(\frac{\partial y}{\partial x_i}\right)_{\text{all } x_j(j\neq i)}\right\} dx_i + \sum_{i=C+1}^{n}\left[\left(\frac{\partial y^*}{\partial x_i}\right)_{\text{all } x_j(j\neq i)} - \lambda^m\left(\frac{\partial y}{\partial x_i}\right)_{\text{all } x_j(j\neq i)}\right] dx_i + \left(\left\{\sum_{i=1}^{C} x_i\left[\frac{\partial y^*}{\partial(\lambda x_i)}\right]_{\text{all } x_j(j\neq i)}\right\} - m\lambda^{m-1}y\right) d\lambda = 0 \qquad (29\text{-}34)$$

Hence, the coefficients of all differentials must vanish to achieve an equality. Of most importance, coefficients on the first and third lines of (29-34) are considered below:

$$\lambda\left[\frac{\partial y^*}{\partial(\lambda x_i)}\right]_{\text{all } x_j(j\neq i)} - \lambda^m\left(\frac{\partial y}{\partial x_i}\right)_{\text{all } x_j(j\neq i)} = 0 \qquad 1 \le i \le C \qquad (29\text{-}35)$$

$$\left\{\sum_{i=1}^{C} x_i\left[\frac{\partial y^*}{\partial(\lambda x_i)}\right]_{\text{all } x_j(j\neq i)}\right\} - m\lambda^{m-1}y = 0 \qquad (29\text{-}36)$$

These two equations are manipulated as follows:

$$\left[\frac{\partial y^*}{\partial(\lambda x_i)}\right]_{\text{all } x_j(j\neq i)} = \lambda^{m-1}\left(\frac{\partial y}{\partial x_i}\right)_{\text{all } x_j(j\neq i)} \qquad 1 \le i \le C \qquad (29\text{-}37)$$

$$m\lambda^{m-1}y = \sum_{i=1}^{C} x_i\left[\frac{\partial y^*}{\partial(\lambda x_i)}\right]_{\text{all } x_j(j\neq i)} = \lambda^{m-1}\sum_{i=1}^{C} x_i\left(\frac{\partial y}{\partial x_i}\right)_{\text{all } x_j(j\neq i)} \qquad (29\text{-}38)$$

The final result for the function y, which is homogeneous in the mth degree with respect to its extensive independent variables, is given in terms of a restricted sum that excludes the intensive independent variables:

$$my = \sum_{i=1}^{C} x_i\left(\frac{\partial y}{\partial x_i}\right)_{\text{all } x_j(j\neq i)} = \sum_{i=1}^{C} x_i\xi_i \qquad (29\text{-}39)$$

One of the most important consequences of Euler's integral theorem, as applied to stability criteria and phase separation, is the expansion of the extensive Gibbs free energy of mixing for a multicomponent mixture in terms of partial molar properties. This result is employed to analyze chemical stability of a binary mixture.

29-4 GIBBS–DUHEM EQUATION

Begin with any of the four extensive state functions (i.e., U, H, A, or G) in terms of the appropriate natural variables such that complete thermodynamic information about a system is known. If the system contains r components in a single phase, then $r + 2$ independent variables are required for a complete description of extensive properties (i.e., apply the phase rule to a single-phase system of r components and add 1 degree of freedom for total system mass). The procedure to generate the Gibbs–Duhem equation is described generically below, using the energy representation of the fundamental equation:

$$U(S, V, \text{all } N_i) = U(x_1, x_2, x_3, \ldots, x_{r+2}) \tag{29-40}$$

where $x_1 = S$, $x_2 = V$, $x_3 = N_1, \ldots, x_j = N_{j-2}$ $(3 \leq j \leq r + 2)$.

Step 1. Calculate the total differential of the extensive thermodynamic state function as a linear sum of differentials that involve the natural variables:

$$dU = \sum_{i=1}^{r+2} \xi_i dx_i \tag{29-41}$$

where the associated slopes are

$$\xi_i = \left(\frac{\partial U}{\partial x_i}\right)_{\text{all } x_j (j \neq i)} \tag{29-42}$$

Hence, $\xi_1 = T$, $\xi_2 = -p$, $\xi_3 = \mu_1, \ldots, \xi_j = \mu_{j-2}$ $(3 \leq j \leq r + 2)$.

Step 2. Use Euler's integral theorem to construct an expression for the extensive thermodynamic state function, which is homogeneous to the first degree with respect to its extensive independent variables. Since all natural variables of U are extensive, the restricted sum in Euler's theorem includes all the variables:

$$U = \sum_{i=1}^{r+2} x_i \xi_i \tag{29-43}$$

Step 3. Calculate the total differential of the function that was constructed via Euler's theorem in step 2:

$$dU = \sum_{i=1}^{r+2} (x_i \, d\xi_i + \xi_i \, dx_i) \tag{29-44}$$

Step 4. The Gibbs–Duhem equation is obtained by comparing total differentials in steps 1 and 3, via (29-41) and (29-44):

$$\sum_{i=1}^{r+2} x_i \, d\xi_i = S \, dT - V \, dp + \sum_{j=1}^{r} N_j \, d\mu_j = 0 \tag{29-45}$$

Step 5. Division by the total number of moles, $N_{\text{total}} = \sum_{j=1}^{r} N_j$, yields

$$-s \, dT + v \, dp = \sum_{j=1}^{r} y_j \, d\mu_j \tag{29-46}$$

where s is molar entropy, v is molar volume, and y_j represents the mole fraction of component j in the mixture.

Step 6. At constant temperature and pressure, the Gibbs–Duhem equation relates all of the activities a_j or activity coefficients γ_j in a multicomponent mixture:

$$\sum_{j=1}^{r} y_j \, d\mu_j = RT \sum_{j=1}^{r} y_j d \ln a_j = RT \sum_{j=1}^{r} y_j d \ln y_j \gamma_j = 0 \tag{29-47}$$

It is only necessary to locate activity coefficient correlations for $r - 1$ components in a mixture of r components, because γ_r can be obtained from, and must satisfy, the Gibbs–Duhem equation.

Illustrative Problem. Begin with the entropy representation of the fundamental equation of thermodynamics for a multicomponent system, $S(U, V, \text{all } N_i)$, and derive the Gibbs–Duhem equation. Does this form differ from equation (29-45) in step 4 above?

29-5 ANALYSIS OF PARTIAL DERIVATIVES VIA JACOBIAN TRANSFORMATIONS

Consider the relation between rectangular coordinates (x, y, z) and cylindrical coordinates (r, θ, z) as defined by the following trigonometric equations:

$$x = r \cos \theta \qquad y = r \sin \theta \qquad z = z \tag{29-48}$$

The Jacobian of the transformation from x, y, z to r, θ, z is denoted by $J_{xyz/r\theta z}$ in the following integration over a differential volume element:

$$\int_V dV = \iiint dx \, dy \, dz = \iiint J_{xyz/r\theta z} \, dr \, d\theta \, dz \tag{29-49}$$

where $J_{xyz/r\theta z} = r$. General expressions for $J_{xyz/r\theta z}$ that yield the same result are derived from the determinant of a 3×3 matrix whose elements systematically portray the dependence of x, y, and z on r, θ, and z. For example,

$$\begin{aligned} J_{xyz/r\theta z} = \frac{\partial(x, y)}{\partial(r, \theta)} &= \left(\frac{\partial x}{\partial r}\right)_\theta \left(\frac{\partial y}{\partial \theta}\right)_r - \left(\frac{\partial y}{\partial r}\right)_\theta \left(\frac{\partial x}{\partial \theta}\right)_r = r \\ J_{xyz/r\theta z} = \frac{\partial(x, y, z)}{\partial(r, \theta, z)} &= \left(\frac{\partial x}{\partial r}\right)_{\theta,z} \left(\frac{\partial y}{\partial \theta}\right)_{r,z} \left(\frac{\partial z}{\partial z}\right)_{r,\theta} \\ &\quad - \left(\frac{\partial y}{\partial r}\right)_{\theta,z} \left(\frac{\partial x}{\partial \theta}\right)_{r,z} \left(\frac{\partial z}{\partial z}\right)_{r,\theta} = r \end{aligned} \tag{29-50}$$

If $y = \theta$, then

$$\begin{aligned} \frac{\partial(x, \theta)}{\partial(r, \theta)} &= \left(\frac{\partial x}{\partial r}\right)_\theta \\ \frac{\partial(x, \theta, z)}{\partial(r, \theta, z)} &= \left(\frac{\partial x}{\partial r}\right)_{\theta,z} \end{aligned} \tag{29-51}$$

which are useful Jacobian representations of a simple partial derivative (see Callen, 1985). Since the defining equations for $J_{xyz/r\theta z}$ in (29-50) can be expressed as a determinant, the following theorem for matrices and determinants provides a useful tool in the analysis of partial differential relations of thermodynamics: If $\partial(x, y)/\partial(r, \theta)$ is expressed as the determinant of a 2×2 matrix, whose elements portray the dependence of x on r and θ, in the first row, and the dependence of y on r and θ, in the second row, then:

1. $\partial(y, x)/\partial(r, \theta)$ is obtained by interchanging the rows of $\partial(x, y)/\partial(r, \theta)$.
2. $\partial(x, y)/\partial(\theta, r)$ is obtained by interchanging the columns of $\partial(x, y)/\partial(r, \theta)$.
3. $\partial(y, x)/\partial(r, \theta) = \partial(x, y)/\partial(\theta, r) = -\partial(x, y)/\partial(r, \theta)$.

If the relation between rectangular and cylindrical coordinates is inverted, then:

$$r = \sqrt{x^2 + y^2} \qquad \theta = \tan^{-1} \frac{y}{x} \qquad z = z \tag{29-52}$$

and the Jacobian of the transformation from r, θ, z to x, y, z is

$$J_{r\theta z/xyz} = \frac{\partial(r, \theta, z)}{\partial(x, y, z)} = \left(\frac{\partial r}{\partial x}\right)_{y,z} \left(\frac{\partial \theta}{\partial y}\right)_{x,z} - \left(\frac{\partial r}{\partial y}\right)_{x,z} \left(\frac{\partial \theta}{\partial x}\right)_{y,z} = \frac{1}{r} \tag{29-53}$$

Hence, results from the illustrative problem above for the transformation from rectangular to cylindrical coordinates, and vice versa, are generalized as follows:

$$\begin{aligned} \frac{\partial(r, \theta, z)}{\partial(x, y, z)} &= \frac{1}{\partial(x, y, z)/\partial(r, \theta, z)} \\ \frac{\partial(r, \theta, z)}{\partial(x, y, z)} \frac{\partial(x, y, z)}{\partial(r, \theta, z)} &= 1 \end{aligned} \tag{29-54}$$

Finally, the chain rule for the Jacobian of the following sequence of transformations:

$$(x, y, z) \longrightarrow (r, \theta, z) \longrightarrow (u, v, z)$$

is

$$J_{xyz/uvz} = \frac{\partial(x, y, z)}{\partial(u, v, z)} = \frac{\partial(x, y, z)}{\partial(r, \theta, z)} \frac{\partial(r, \theta, z)}{\partial(u, v, z)} \tag{29-55}$$

Let's look at thermodynamic relations via the *method of Jacobians*.

Illustrative Problem. Derive an expression for the difference between C_p and C_V when gases do not behave ideally. At constant pressure, $C_p \equiv (\partial H/\partial T)_{p, \text{all } N_i}$, and the specific heat at constant volume is $C_V \equiv (\partial U/\partial T)_{V, \text{all } N_i}$.

SOLUTION. Begin with the total differential of extensive enthalpy of a multicomponent mixture in terms of its natural variables via equation (29-24*b*) and the definition of C_p:

$$\begin{aligned} dH &= T\,dS + V\,dp + \sum_{i=1}^{r} \mu_i\,dN_i \\ C_p &\equiv \left(\frac{\partial H}{\partial T}\right)_{p, \text{all } N_i} = T\left(\frac{\partial S}{\partial T}\right)_{p, \text{all } N_i} \end{aligned} \tag{29-56}$$

The important set of independent variables needed to represent C_p in terms of Jacobians is T, p and all N_i. However, the total differential of extensive internal energy in terms of its natural variables via equation (29-4) and the definition of C_V:

$$\begin{aligned} dU &= T\,dS - p\,dV + \sum_{i=1}^{r} \mu_i\,dN_i \\ C_V &\equiv \left(\frac{\partial U}{\partial T}\right)_{V, \text{all } N_i} = T\left(\frac{\partial S}{\partial T}\right)_{V, \text{all } N_i} \end{aligned} \tag{29-57}$$

suggest that T, V and all N_i are important independent variables for the Jacobian representation of C_V. Hence, one begins with T, p and all N_i for C_p and then switches to T, V and all N_i for C_V:

$$\begin{aligned} C_p &= T\left(\frac{\partial S}{\partial T}\right)_{p, \text{all } N_i} = T\frac{\partial(S, p, \text{all } N_i)}{\partial(T, p, \text{all } N_i)} \\ &= T\frac{\partial(S, p, \text{all } N_i)}{\partial(T, V, \text{all } N_i)} \frac{\partial(T, V, \text{all } N_i)}{\partial(T, p, \text{all } N_i)} \end{aligned} \tag{29-58}$$

The Jacobians in (29-58) are expanded as follows:

$$\begin{aligned} C_p = T &\left[\left(\frac{\partial S}{\partial T}\right)_{V, \text{all } N_i} \left(\frac{\partial p}{\partial V}\right)_{T, \text{all } N_i} - \left(\frac{\partial S}{\partial V}\right)_{T, \text{all } N_i} \left(\frac{\partial p}{\partial T}\right)_{V, \text{all } N_i}\right] \\ &\times \left(\frac{\partial V}{\partial p}\right)_{T, \text{all } N_i} \end{aligned} \tag{29-59}$$

The presence of C_V is obvious in the first term on the right side of (29-59), and with the aid of the following Maxwell relation,

$$\left(\frac{\partial S}{\partial V}\right)_{T,\text{ all } N_i} = \left(\frac{\partial p}{\partial T}\right)_{V,\text{ all } N_i} \tag{29-60}$$

one obtains the final result that relates both heat capacities:

$$C_p = C_V - T\left[\left(\frac{\partial p}{\partial T}\right)_{V,\text{ all } N_i}\right]^2 \left(\frac{\partial V}{\partial p}\right)_{T,\text{ all } N_i} \tag{29-61}$$

The criterion of mechanical stability reveals that $(\partial V/\partial p)_{T,\text{ all } N_i} < 0$, as discussed below in Section 29-6.2. Hence, one concludes that $C_p > C_V$ for any material.

Illustrative Problem

1. Calculate the rate of change of temperature with respect to pressure for an adiabatic compression or expansion. In other words, $(\partial T/\partial p)_S = ?$
2. Prove that the rate of change of pressure with respect to volume is greater in magnitude along an adiabatic path relative to an isothermal path. Use the method of Jacobians and do not restrict your analysis to ideal gases.

29-6 THERMODYNAMIC STABILITY RELATIONS

29-6.1 Thermal Stability via $U(S, V, \text{all } N_i)$

The energy representation of the fundamental equation reveals that $U-S$ diagrams at constant volume and composition provide complete thermodynamic information about a system. Since

$$\left(\frac{\partial U}{\partial S}\right)_{V,\text{ all } N_i} \equiv T > 0 \tag{29-62}$$

it follows that the locus of any sequence of equilibrium states which are plotted on a graph of U vs. S at constant volume and composition must exhibit a positive slope. Furthermore, the curvature condition

$$\left(\frac{\partial^2 U}{\partial S^2}\right)_{V,\text{ all } N_i} = \left(\frac{\partial T}{\partial S}\right)_{V,\text{ all } N_i} = \frac{T}{C_V} > 0 \tag{29-63}$$

is obtained from

$$\begin{aligned} dU &= T\ dS - p\ dV + \sum_{i=1}^{r} \mu_i\ dN_i \\ C_V &\equiv \left(\frac{\partial U}{\partial T}\right)_{V,\text{ all } N_i} = T\left(\frac{\partial S}{\partial T}\right)_{V,\text{ all } N_i} \end{aligned} \tag{29-64}$$

Whereas positive slopes ensure that $T > 0$, positive curvature is consistent with the fact that C_p and C_V are greater than zero. If there is a region of negative curvature between two regions of positive curvature, then phase separation is unavoidable when the equilibrium states are unstable. States are described as unstable if the curvature is negative on a $U-S$ diagram at constant volume and composition. Instability occurs not only where the curvature is negative, but all states are unstable between two points of contact of the common tangent to the $U-S$ curve when a region of negative curvature exists between two regions of positive curvature. States are described as metastable if the curvature is positive and they lie between the points of contact of the common tangent.

Unstable and metastable states split into two phases (i.e., α and β), where each phase is identified by a point of contact of the common tangent to the $U-S$ curve. These two phases are in thermal equilibrium at the same temperature because they have the same slope, as defined by a common tangent. The internal energy $U_\alpha + U_\beta$ and entropy $S_\alpha + S_\beta$ of the two-phase system are obtained from a linear superposition of properties of phases α and β. All properties of the $\alpha + \beta$ two-phase system lie on the common tangent. This ensures that the two-phase system achieves minimum internal energy and maximum entropy at constant volume and composition. In the vicinity of the points of contact of the common tangent, there are many other pairs of states that have the same slope on the $U-S$ diagram, and hence they are at the same temperature. However, the composite properties of any two states near α and β in thermal equilibrium but not on the common tangent are characterized by higher internal energy and lower entropy relative to a linear superposition of states α and β on the common tangent. Hence, energy minimization and/or entropy maximization provide the driving forces for states in the unstable and metastable regions to gravitate toward $\alpha + \beta$.

29-6.2 Mechanical Stability Via $A(T, V, \text{all } N_i)$

Isotherms on an $A-V$ diagram are useful to illustrate the origin of $p-V$ diagrams, superheated liquids and subcooled vapors in metastable states, unstable states between the spinodal points, critical points, and the requirement of mechanical stability. It is reasonable to assume that the slope of A vs. V at constant temperature and composition is negative, because

$$\left(\frac{\partial A}{\partial V}\right)_{T,\,\text{all } N_i} \equiv -p \tag{29-65}$$

However, this is subject to controversy because negative pressure is not disallowed, even though negative absolute temperature is not possible. Several references that add fuel to the fire are: Hayward (1971), Richards and Trevena (1976), and Sedgewick and Trevena (1976).

The curvature condition that ensures single-phase behavior is

$$\left(\frac{\partial^2 A}{\partial V^2}\right)_{T,\,\text{all } N_i} = -\left(\frac{\partial p}{\partial V}\right)_{T,\,\text{all } N_i} > 0 \tag{29-66}$$

When the curvature of $A-V$ isotherms is negative, the criterion for mechanical stability is violated and the system splits into two different states of matter (i.e., solid–liquid equilibrium or vapor–liquid equilibrium). Once again, states between the points of contact of a common tangent to an $A-V$ isotherm can be either metastable or unstable when a region of negative curvature exists between two regions of positive curvature. An analysis of this situation was described in Section 29-6.1, but now the driving force for phase separation is Helmholtz free-energy minimization of two states at the same pressure on the common tangent when the composite isothermal system maintains constant volume. Further analysis of phase behavior is discussed in terms of pressure–volume isotherms at constant composition. These diagrams are generated directly from $A(T, V, \text{all } N_i)$, which contains complete thermodynamic information about the system of interest. The following definitions are appropriate:

1. *Spinodal points:* represent the boundary between positive and negative curvature of $A-V$ isotherms. An equilibrium state on the spinodal curve is defined by $(\partial p/\partial V)_{T,\text{all } N_i} = 0$. Regions between the spinodal points are intrinsically unstable and violate the criterion of mechanical stability.
2. *Binodal points:* represent the points of contact of a common tangent to A vs. V at constant temperature and composition when a region of negative curvature exists between two regions of positive curvature. The locus of binodal points, known as the *binodal curve* or *two-phase envelope*, represents the experimentally observed phase boundary under normal conditions. For example, saturated liquid and saturated vapor represent states on the binodal curve. The binodal region exists between the binodal and spinodal curves, where $(\partial p/\partial V)_{T,\text{all } N_i} < 0$.
3. *Stable states:* defined by positive curvature on the $A-V$ diagram at constant temperature and composition, where $(\partial p/\partial V)_{T,\text{all } N_i} < 0$. Stable equilibrium states exist outside the binodal region where single-phase behavior prevails. Subcooled liquids and superheated vapors represent examples of stable states.
4. *Unstable states:* defined by negative curvature of $A-V$ isotherms, between the spinodal points. In this region, $(\partial p/\partial V)_{T,\text{all } N_i} > 0$. Single-phase equilibrium states of this nature are completely disallowed. Small fluctuations in system properties grow in unrestricted fashion until the system splits into two phases.
5. *Metastable states:* equilibrium states within the binodal region where $(\partial p/\partial V)_{T,\text{all } N_i} < 0$. Superheated liquids and subcooled vapors represent examples of metastable states. They can be isolated and studied because small fluctuations in system properties that normally trigger phase separation are quenched.

At a critical temperature T_{critical}, the binodal and spinodal points coalesce to a single point. This is consistent with the fact that the binodal and spinodal curves are tangent to each other at T_{critical}. From the viewpoint of mechanical

stability, systems are intrinsically stable as one homogeneous phase when the temperature is greater than T_{critical}. Hence, T_{critical} is consistent with the definition of an upper critical solution temperature. Since $(\partial p/\partial V)_{T,\text{ all } N_i} = 0$ at T_{critical}, small changes in pressure produce enormous changes in density near the critical point. This phenomenon is exploited by physical chemists, who perform light-scattering studies near T_{critical}.

29-6.3 Chemical Stability of Binary Mixtures Via $G(T,p,N_1,N_2)$

One of the necessary conditions for miscibility is that the Gibbs free energy of a mixture should be less than a weighted sum of pure component Gibbs free energies. In other words, ΔG_{mixing} must be negative. However, this condition is not sufficient to achieve a single homogeneous phase. In the remainder of this chapter, we focus primarily on the chemical stability of mixtures. Consider N_i moles of pure component i. If each component exists as a pure single phase, then the phase rule suggests that extensive properties such as the Gibbs free energy of pure component i, $G_{i,\text{ pure}}$, enjoy 3 degrees of freedom. If temperature T, pressure p, and mole numbers N_i are chosen as three independent variables for a unique description of $G_{i,\text{ pure}}$, then Euler's integral theorem yields the following result:

$$G_{i,\text{ pure}}(T,\ p,\ N_i) = N_i \mu_{i,\text{ pure}}(T,\ p) \tag{29-67}$$

where the chemical potential of pure component i in its reference state is

$$\mu_{i,\text{ pure}}(T,\ p) = \frac{G_{i,\text{ pure}}(T,\ p,\ N_i)}{N_i} = \left(\frac{\partial G_{i,\text{ pure}}}{\partial N_i}\right)_{T,p} \tag{29-68}$$

Intensive thermodynamic properties such as $\mu_{i,\text{ pure}}$, which is equivalent to the molar Gibbs free energy of pure component i, are homogeneous functions of the zeroth order with respect to molar mass. Hence, Euler's theorem reveals that $\mu_{i,\text{ pure}}$ is not a function of N_i. This is consistent with the phase rule, which predicts that only 2 degrees of freedom are required for a unique description of $\mu_{i,\text{ pure}}$. If an r-component homogeneous mixture contains N_i moles of component i, then the phase rule indicates that $r + 2$ degrees of freedom are required for a unique description of extensive properties, and Euler's integral theorem yields the following expansion in terms of partial molar properties for the Gibbs free energy of the mixture (see equation 29-30*d*):

$$G_{\text{mixture}}(T,\ p,\text{ all } N_i) = \sum_{i=1}^{r} N_i \mu_i(T,\ p,\ \text{composition}) \tag{29-69}$$

where the chemical potential of component i in the mixture is

$$\mu_i(T,\ p,\text{composition}) = \left(\frac{\partial G_{\text{mixture}}}{\partial N_i}\right)_{T,p,N_j(j\neq i)} \tag{29-70}$$

The extensive Gibbs free energy of mixing is constructed from equations (29-67) and (29-69):

$$\Delta G_{\text{mixing}} = G_{\text{mixture}} - \sum_{i=1}^{r} G_{i,\,\text{pure}} = \sum_{i=1}^{r} N_i(\mu_i - \mu_{i,\,\text{pure}}) \tag{29-71}$$

Division by the total number of moles of all components, $N_{\text{total}} = \sum_{j=1}^{r} N_j$, yields the molar Gibbs free energy of mixing:

$$\Delta g_{\text{mixing}} = \frac{\Delta G_{\text{mixing}}}{N_{\text{total}}} = \sum_{i=1}^{r} y_i(\mu_i - \mu_{i,\,\text{pure}}) \tag{29-72}$$

where y_i is the mole fraction of component i in the mixture. With the aid of activity coefficient correlations, (29-72) is useful to generate graphs of Δg_{mixing} vs. mole fraction of either component in binary mixtures at constant temperature and pressure. Chemical stability analysis of these graphs is discussed below.

Shape of Δg_{mixing} vs. Composition. The Gibbs free energy of mixing for binary mixtures is

$$\Delta g_{\text{mixing}} = (1 - y_2)(\mu_1 - \mu_{1,\,\text{pure}}) + y_2(\mu_2 - \mu_{2,\,\text{pure}}) \tag{29-73}$$

and the instantaneous slope of Δg_{mixing} vs. y_2 at constant temperature and pressure is calculated as follows:

$$\left(\frac{\partial \Delta g_{\text{mixing}}}{\partial y_2}\right)_{T,p} = (\mu_2 - \mu_{2,\,\text{pure}}) - (\mu_1 - \mu_{1,\,\text{pure}}) + y_1\left(\frac{\partial \mu_1}{\partial y_2}\right)_{T,p} + y_2\left(\frac{\partial \mu_2}{\partial y_2}\right)_{T,p} \tag{29-74}$$

The last two terms on the right side (29-74) cancel because

$$y_1\, d\mu_1 + y_2\, d\mu_2 = 0 \tag{29-75}$$

at constant temperature and pressure via the Gibbs–Duhem equation (i.e., see 29-47). Hence

$$\left(\frac{\partial \Delta g_{\text{mixing}}}{\partial y_2}\right)_{T,p} = (\mu_2 - \mu_{2,\,\text{pure}}) - (\mu_1 - \mu_{1,\,\text{pure}}) \tag{29-76}$$

If one introduces activities a_i and activity coefficients γ_i such that

$$\begin{aligned} a_i &\equiv y_i\gamma_i \\ \mu_i - \mu_{i,\,\text{pure}} &\equiv RT \ln a_i \qquad \text{at constant } T \text{ and } p \end{aligned} \tag{29-77}$$

then it is possible to evaluate the slope of Δg_{mixing} vs. composition in the concentration limits because

$$\begin{gathered}\left(\frac{\partial \Delta g_{\text{mixing}}}{\partial y_2}\right)_{T,p} = RT \ln \frac{a_2}{a_1} \\ \lim_{y_i \to 1} (a_i) = 1 \\ \lim_{y_i \to 0} (a_i) = 0 \\ \lim_{y_2 \to 1} \left[\left(\frac{\partial \Delta g_{\text{mixing}}}{\partial y_2}\right)_{T,p}\right] = +\infty \\ \lim_{y_2 \to 0} \left[\left(\frac{\partial \Delta g_{\text{mixing}}}{\partial y_2}\right)_{T,p}\right] = -\infty\end{gathered} \tag{29-78}$$

Hence, if Δg_{mixing} is plotted vs. y_2, then the graph begins at pure component 1 with $\Delta g_{\text{mixing}} = 0$ and an infinitely negative slope, and culminates at pure component 2 with $\Delta g_{\text{mixing}} = 0$ and an infinitely positive slope. The consequences of this result are that Δg_{mixing} must be negative near the concentration limits for all mixtures that achieve thermodynamic equilibrium, and these mixtures can separate into phases that are highly concentrated in one of the components, but they can not separate into pure-component phases. These results can be extended to multicomponent mixtures in the following manner:

$$\Delta g_{\text{mixing}} = \sum_{i=1}^{r} y_i (\mu_i - \mu_{i,\,\text{pure}}) = RT \sum_{i=1}^{r} y_i \ln a_i \tag{29-79}$$

If one envisions a multidimensional plot and focuses on the slope of Δg_{mixing} with respect to the mole fraction of component k, then it is necessary to vary the mole fraction of one other component (e.g., y_r). Changes in y_r are not independent, but they are equal and opposite to the changes in y_k to ensure that all mole fractions sum to unity. The following partial derivative is of interest:

$$\begin{aligned}&\left(\frac{\partial \Delta g_{\text{mixing}}}{\partial y_k}\right)_{T,p,\text{ all } y_j (j \neq k,r)} \\ &\quad = RT \sum_{i=1}^{r} \left[\ln a_i \left(\frac{\partial y_i}{\partial y_k}\right)_{T,p,\text{ all } y_j (j \neq k,r)} + y_i \left(\frac{\partial \ln a_i}{\partial y_k}\right)_{T,p,\text{ all } y_j (j \neq k,r)}\right]\end{aligned} \tag{29-80}$$

and the second term in the summation in (29-80) vanishes via the Gibbs–Duhem equation at constant temperature and pressure:

$$\sum_{i=1}^{r} y_i \, d\mu_i = RT \sum_{i=1}^{r} y_i \, d \ln a_i = 0 \tag{29-81}$$

Hence,

$$\left(\frac{\partial \Delta g_{\text{mixing}}}{\partial y_k}\right)_{T,p,\text{ all } y_j(j\neq k,r)} = RT\sum_{i=1}^{r} \ln a_i \left(\frac{\partial y_i}{\partial y_k}\right)_{T,p,\text{ all } y_j(j\neq k,r)} \tag{29-82}$$

and

$$y_k + y_r + \sum_{j(j\neq k,r)} y_j = 1 \tag{29-83}$$

Since all mole fractions in the summation of (29-83) remain constant during differentiation with respect to y_k, one obtains the following result:

$$\left(\frac{\partial \mathbf{y_i}}{\partial \mathbf{y_k}}\right)_{\mathbf{T,p,all\ y_j(j\neq k,r)}} = \begin{cases} 1 & \text{if i = k} \\ -1 & \text{if i = r} \\ 0 & \text{otherwise} \end{cases} \tag{29-84}$$

The concentration dependence of Δg_{mixing} in a multicomponent mixture is

$$\left(\frac{\partial \Delta g_{\text{mixing}}}{\partial y_k}\right)_{T,p,\text{ all } y_j(j\neq k,r)} = RT \ln \frac{a_k}{a_r} \tag{29-85}$$

This slope is infinitely positive in the limit of pure component k (i.e., $y_k \to 1$), and infinitely negative in the limit of extremely dilute mixtures of component k (i.e., $y_k \to 0$). Hence, if phase separation is inevitable and thermodynamic equilibrium is achieved, then multicomponent mixtures will not separate into pure-component phases because a lower Δg_{mixing} can be achieved if the phases are slightly impure.

Intercepts and Common Tangents to Δg_{mixing} vs. Composition in Binary Mixtures. Euler's integral theorem and the Gibbs–Duhem equation provide the tools to obtain expressions for Δg_{mixing} and $(\partial \Delta g_{\text{mixing}}/\partial y_2)_{T,p}$ in binary mixtures. This information allows one to evaluate the tangent at any mixture composition via the point-slope formula. For example, if $\mu_1 = \mu_1^*$ and $\mu_2 = \mu_2^*$ when the mole fraction of component 2 is y_2^*, then equations (29-73) and (29-76) yield:

$$\begin{aligned} \Delta g_{\text{mixing}} &= (1 - y_2^*)(\mu_1^* - \mu_{1,\text{ pure}}) + y_2^*(\mu_2^* - \mu_{2,\text{ pure}}) \\ \left(\frac{\partial \Delta g_{\text{mixing}}}{\partial y_2}\right)_{T,p} &= (\mu_2^* - \mu_{2,\text{ pure}}) - (\mu_1^* - \mu_{1,\text{ pure}}) \end{aligned} \tag{29-86}$$

The Taylor series expansion for the tangent line at y_2^* is truncated after the first-order term without introducing any error:

$$\begin{aligned} \text{tangent}(y_2; y_2^*) &= \Delta g_{\text{mixing}}(y_2^*) + (y_2 - y_2^*)\left[\left(\frac{\partial \Delta g_{\text{mixing}}}{\partial y_2}\right)_{T,p}\right]_{\text{at } y_2^*} \\ &= (1 - y_2^*)(\mu_1^* - \mu_{1,\text{ pure}}) + y_2^*(\mu_2^* - \mu_{2,\text{ pure}}) \\ &\quad + (y_2 - y_2^*)[(\mu_2^* - \mu_{2,\text{ pure}}) - (\mu_1^* - \mu_{1,\text{ pure}})] \end{aligned} \tag{29-87}$$

where tangent(y_2; y_2^*) represents a linear function of y_2 that is tangent to Δg_{mixing} at composition y_2^*. Simplification of (29-87) yields

$$\text{tangent}(y_2;\, y_2^*) = (\mu_1^* - \mu_{1,\,\text{pure}}) + y_2[(\mu_2^* - \mu_{2,\,\text{pure}}) - (\mu_1^* - \mu_{1,\,\text{pure}})] \tag{29-88}$$

Evaluation of the tangent line at the pure-component intercepts provides useful information about the chemical potentials of both components in the mixture at composition y_2^*. For example,

$$\begin{aligned} \text{tangent}(y_2 = 0;\, y_2^*) &= \mu_1^* - \mu_{1,\,\text{pure}} \\ \text{tangent}(y_2 = 1;\, y_2^*) &= \mu_2^* - \mu_{2,\,\text{pure}} \end{aligned} \tag{29-89}$$

Chemical stability of binary mixtures is addressed via the shape of Δg_{mixing} vs. composition. As illustrated below, the tangent line is critical in this analysis because the pure-component intercepts of a common tangent provide the conditions for chemical equilibrium of a two-phase mixture. Homogeneous single-phase behavior occurs at all mixture compositions when both of the following conditions are satisfied:

$$\Delta g_{\text{mixing}} < 0 \tag{29-90a}$$

$$\left(\frac{\partial^2 \Delta g_{\text{mixing}}}{\partial y_2^2}\right)_{T,p} > 0 \tag{29-90b}$$

If condition 1 is violated, then the mixture splits into two phases. However, mixtures that achieve thermodynamic equilibrium will not violate condition 1 near pure-component boundaries because the slope of Δg_{mixing} vs. y_2 is infinitely negative near pure component 1 and infinitely positive near pure component 2. This can occur only if Δg_{mixing} is negative near the pure-component boundaries, since by definition, $\Delta g_{\text{mixing}} = 0$ when $y_2 = 0$ and $y_2 = 1$. The most interesting situations occur when the first condition is satisfied and a region of negative curvature exists between two regions of positive curvature such that $(\partial^2 \Delta g_{\text{mixing}}/\partial y_2^2)_{T,p}$ changes sign smoothly. Under these conditions, the mixture exhibits concentration-dependent miscibility and one must consider stable, metastable, and unstable states, which are separated by binodal and spinodal points, respectively. These terms were defined in Section 29-6.2, but they are redefined here within the context of chemical stability for a binary mixture.

1. *Spinodal points:* represent the boundary between positive and negative curvature of Δg_{mixing} vs. y_2 at constant T and p. An equilibrium state on the spinodal curve is defined by $(\partial^2 \Delta g_{\text{mixing}}/\partial y_2^2)_{T,p} = 0$. Regions between the spinodal points are intrinsically unstable and violate the second criterion of chemical stability, given by equation (29-90b).
2. *Binodal points:* represent the points of contact of a common tangent to Δg_{mixing} vs. y_2 at constant T and p when a region of negative curvature

exists between two regions of positive curvature. If one generates Δg_{mixing} vs. y_2 isothermally, at several different temperatures, then the locus of binodal points is known as the binodal curve on temperature–composition axes or the two-phase envelope, which represents the experimentally observed phase boundary under normal conditions. The binodal region exists between the binodal and spinodal curves, where $(\partial^2 \Delta g_{\text{mixing}}/\partial y_2^2)_{T,p} > 0$.

3. *Stable states:* defined by positive curvature of Δg_{mixing} vs. y_2 at constant T and p, where $(\partial^2 \Delta g_{\text{mixing}}/\partial y_2^2)_{T,p} > 0$. Stable equilibrium states exist outside the binodal region, where both requirements of chemical stability are satisfied and single-phase behavior prevails.
4. *Unstable states:* defined by negative curvature of Δg_{mixing} vs. y_2 at constant T and p, between the spinodal points. In this region, $(\partial^2 \Delta g_{\text{mixing}}/\partial y_2^2)_{T,p} < 0$. Single-phase equilibrium states of this nature are completely disallowed even if the first stability criterion is satisfied.
5. *Metastable states:* equilibrium states that exist within the binodal region, where $(\partial^2 \Delta g_{\text{mixing}}/\partial y_2^2)_{T,p} > 0$.

When a region of negative curvature exists between two regions of positive curvature on the graph of Δg_{mixing} vs. y_2, and concentration-dependent miscibility prevails, the points of contact of the common tangent (i.e., binodal points) identify two different phases, α and β, that are in thermodynamic equilibrium. Since chemical stability is analyzed at constant T and p, these coexisting phases exhibit the same temperature (i.e., $T_\alpha = T_\beta$) and the same pressure (i.e., $p_\alpha = p_\beta$), which are requirements for thermal and mechanical equilibrium. The requirement of chemical equilibrium for a two-phase mixture is

$$\mu_i(\text{phase } \alpha) = \mu_i(\text{phase } \beta) \tag{29-91}$$

Since states α and β correspond to binodal points, and the common tangent, by definition, not only implies that these states have the same slope but also share common intercepts at $y_2 = 0$ and $y_2 = 1$, the requirement for chemical equilibrium is satisfied via equations (29-89). For all metastable and unstable states between two binodal points on the graph of Δg_{mixing} vs. y_2, the single-phase mixture achieves a lower Δg_{mixing} value by splitting into phases α and β. The properties of the two-phase mixture, which lie on the common tangent, are obtained from a linear combination of the properties of α and β. Eubank and Barrufet (1988) discuss algorithms for calculating phase separation in *Chemical Engineering Education*. This publication addresses Δg_{mixing} vs. composition at constant T and p for binary mixtures that exhibit the following properties:

1. Four spinodals, four thermodynamically allowed binodal points, double phase separation (i.e., α/β and γ/δ), and one minimum in Δg_{mixing}
2. Four spinodals, three local minima in Δg_{mixing}, two thermodynamically allowed binodal points, single phase separation (i.e., α/β), and one thermodynamically disallowed binodal point

Tanford (1961, p. 248) illustrates the coalescence of spinodal and binodal points in partially miscible mixtures at the critical temperature, where the spinodal and binodal curves are tangent to each other. If this phenomenon occurs upon raising the temperature, then the critical point is identified as an upper critical solution temperature (i.e., UCST), and homogeneous single-phase behavior exists above the UCST. If coalescence of spinodal and binodal points occurs upon lowering the temperature, then the critical point is identified as a lower critical solution temperature (i.e., LCST), and homogeneous single-phase behavior prevails below the LCST. Olabisi, *et al*. (1979, p. 21) illustrate some interesting temperature–composition phase diagrams that exhibit UCSTs, LCSTs, combinations of these two critical points, and hourglass-shaped phase behavior when the UCST and LCST overlap. van der Put (1998, p. 348) illustrates relations between the concentration dependence of the free energy of mixing and the temperature–composition phase diagram for a binary mixture that exhibits a single eutectic response.

29-6.4 Rigorous Development of Stability Criteria Via Energy Minimization

Euler's integral theorem, the method of Jacobians, Legendre transforms, and positive-definite quadratic forms are employed to address thermodynamic stability. The results identify the limits of stability via spinodal points, not the limits of metastability, points of contact of the common tangent, or binodal regions. Begin with the energy representation of the fundamental equation for an r-component homogeneous mixture. The phase rule requires $r + 2$ independent variables for a complete description of the extensive internal energy:

$$U(S, V, \text{all } N_i) \qquad 1 \leq i \leq r \tag{29-92}$$

The corresponding intensive state function, which enjoys only $r + 1$ degrees of freedom, is obtained via division by the total number of moles, $\sum_{i=1}^{r} N_i = N_{\text{total}}$. Hence,

$$u \equiv \frac{U}{N_{\text{total}}} = u\left(\frac{S}{N_{\text{total}}}, \frac{V}{N_{\text{total}}}, \text{all } \frac{N_i}{N_{\text{total}}}\right) \qquad 1 < i < r - 1 \tag{29-93}$$

where mole fractions are defined by $y_i \equiv N_i/N_{\text{total}}$, molar entropy is $s \equiv S/N_{\text{total}}$, and molar volume is given by $v \equiv V/N_{\text{total}}$. It is not appropriate to include N_{total} in the group of independent variables for u, which is homogeneous to the zeroth degree, because Euler's theorem indicates that

$$\left(\frac{\partial u}{\partial N_{\text{total}}}\right)_{s,v,\text{ all } y_i} = 0 \tag{29-94}$$

All independent variables of u should be intensive. Equation (29-93) is rewritten using a generic set of variables that can be expressed via summation notation

later in this section:

$$u(s, v, y_1, y_2, y_3, \ldots, y_{r-1}) = u(x_0, x_1, x_2, x_3, x_4, \ldots, x_r) \tag{29-95}$$

where $x_0 = s$, $x_1 = v$, and $x_i = y_{i-1}$ $(2 \leq i \leq r)$. Thermodynamic phase behavior was discussed above in terms of thermal stability via $U(S, V, \text{all } N_i)$, mechanical stability via $A(T, V, \text{all } N_i)$, and chemical stability via $G(T, p, \text{all } N_i)$. In each case, the system is driven toward minimum energy when phase separation occurs. If one begins with $u(x_0, x_1, x_2, x_3, x_4, \ldots, x_r)$ and invokes energy minimization, then thermodynamic stability requires that

$$d^2u = \sum_{j=0}^{r} \sum_{k=0}^{r} \frac{\partial^2 u}{\partial x_j \partial x_k} dx_j \, dx_k > 0 \tag{29-96}$$

which conforms generically to a positive-definite quadratic form. In other words, d^2u can be zero only if all fluctuations in its independent variables (i.e., all dx_j) are zero. If fluctuations exist (i.e., some $dx_j \neq 0$), then d^2u must be positive. Notation for the quadratic form is simplified via the following definition:

$$u_{jk} \equiv \frac{\partial^2 u}{\partial x_j \partial x_k} \tag{29-97}$$

Hence,

$$d^2u = \sum_{j=0}^{r} \sum_{k=0}^{r} u_{jk} \, dx_j \, dx_k > 0 \tag{29-98}$$

and stability imposes several requirements on various determinants of the coefficient matrix u_{jk} if the quadratic form must be positive definite. Similar requirements, or restrictions, were imposed on the matrix of phenomenological transport coefficients in Sections 25-9 and 25-10 because the rate of entropy generation for irreversible processes can be expressed as a positive-definite quadratic form. Since the intensive internal energy is a thermodynamic state function, as well as an exact differential, $u_{jk} = u_{kj}$, which represents the starting point to generate Maxwell relations. The following prescription is suggested to analyze the quadratic form given by (29-98).

Step 1. Expand d^2u by accounting for all terms in the summation with $j = 0$ $(0 \leq k \leq r)$ and $k = 0$ $(0 \leq j \leq r)$, realizing that $u_{0k} = u_{k0}$:

$$d^2u = u_{00}(dx_0)^2 + 2 \sum_{k=1}^{r} u_{0k} \, dx_0 \, dx_k + \sum_{j=1}^{r} \sum_{k=1}^{r} u_{jk} \, dx_j \, dx_k > 0 \tag{29-99}$$

Step 2. Construct a new fluctuating independent variable based on a linear combination of fluctuations in the original independent variables for u:

$$dz_0 \equiv dx_0 + \frac{1}{u_{00}} \sum_{k=1}^{r} u_{0k} \, dx_k \tag{29-100}$$

Step 3. Calculate the square of these fluctuations in equation (29-100), which cannot be negative [i.e., $(dz_0)^2 \geq 0$], even though changes in each x_i (i.e., entropy, volume, or composition) can be positive, negative, or zero:

$$(dz_0)^2 = (dx_0)^2 + \frac{2}{u_{00}} \sum_{k=1}^{r} u_{0k}\, dx_0\, dx_k + \left(\frac{1}{u_{00}}\right)^2 \sum_{k=1}^{r} u_{0k}\, dx_k \sum_{j=1}^{r} u_{0j}\, dx_j \tag{29-101}$$

Step 4. Incorporate the result from step 3 into the quadratic form in step 1:

$$d^2u = u_{00}(dz_0)^2 + \frac{1}{u_{00}} \sum_{j=1}^{r} \sum_{k=1}^{r} (u_{00}u_{jk} - u_{0j}u_{0k})\, dx_j\, dx_k > 0 \tag{29-102}$$

Step 5. Use the method of Jacobians to simplify the coefficient of the quadratic form in (29-102). Since $\xi_i \equiv (\partial u/\partial x_i)_{\text{all } x_j (j \neq i)}$:

$$\begin{aligned} u_{00}u_{jk} - u_{0j}u_{0k} = u_{00}u_{jk} - u_{j0}u_{0k} &= \frac{\partial \xi_0}{\partial x_0}\frac{\partial \xi_k}{\partial x_j} - \frac{\partial \xi_0}{\partial x_j}\frac{\partial \xi_k}{\partial x_0} \\ &= \frac{\partial(\xi_0, \xi_k)}{\partial(x_0, x_j)} = \frac{\partial(\xi_0, \xi_k, \text{all } x_i)}{\partial(x_0, x_j, \text{all } x_i)} \qquad (i \neq 0, j) \end{aligned} \tag{29-103}$$

Also,

$$u_{00} = \frac{\partial^2 u}{\partial x_0^2} = \frac{\partial \xi_0}{\partial x_0} = \frac{\partial(\xi_0, x_j, \text{all } x_i)}{\partial(x_0, x_j, \text{all } x_i)} \qquad (i \neq 0, j) \tag{29-104}$$

Step 6. Use the last two general properties of Jacobians given by equations (29-54) and (29-55) to simplify the following ratio:

$$\begin{aligned} &\frac{u_{00}u_{jk} - u_{0j}u_{0k}}{u_{00}} \\ &= \frac{\partial(\xi_0, \xi_k, \text{all } x_i)/\partial(x_0, x_j, \text{all } x_i)}{\partial(\xi_0, x_j, \text{all } x_i)/\partial(x_0, x_j, \text{all } x_i)} \\ &= \frac{\partial(\xi_0, \xi_k, \text{all } x_i)}{\partial(\xi_0, x_j, \text{all } x_i)} = \frac{\partial \xi_k}{\partial x_j} \text{ at constant } \xi_0 \text{ and all } x_i (i \neq 0, j) \end{aligned} \tag{29-105}$$

Legendre Transformation. The previous result from equation (29-105),

$$\frac{u_{00}u_{jk} - u_{0j}u_{0k}}{u_{00}} = \frac{\partial \xi_k}{\partial x_j} \text{ at constant } \xi_0 \text{ and all } x_i (i \neq 0, j) \tag{29-106}$$

is best interpreted by performing a Legendre transformation from u to the intensive Helmholtz free energy:

$$\begin{aligned} a &= u - x_0\xi_0 \\ du &= \sum_{k=0}^{r} \xi_k \, dx_k \\ da &= -x_0 \, d\xi_0 + \sum_{k=1}^{r} \xi_k \, dx_k \end{aligned} \tag{29-107}$$

where $x_0 = s$ and $\xi_0 = T$. The total differential of a is useful to define ξ_k in equations (29-106) and (29-107). Hence,

$$\begin{aligned} \xi_k &\equiv \frac{\partial a}{\partial x_k} \text{ at constant } \xi_0 \text{ and all } x_i (i \neq 0, k) \\ \frac{\partial \xi_k}{\partial x_j} &= \frac{\partial^2 a}{\partial x_j \, \partial x_k} \equiv a_{jk} \text{ at constant } \xi_0 \text{ and all } x_i (i \neq 0, j, k) \end{aligned} \tag{29-108}$$

Step 7. Continue the step-by-step methodology by rewriting the quadratic form in (29-102) using information about the Helmholtz free energy:

$$d^2u = u_{00}(dz_0)^2 + \sum_{j=1}^{r} \sum_{k=1}^{r} a_{jk} \, dx_j \, dx_k > 0 \tag{29-109}$$

Step 8. Expand the quadratic form by accounting for all terms in the summation with $j = 1$ $(1 \leq k \leq r)$ and $k = 1$ $(1 \leq j \leq r)$. Remember that $a_{1k} = a_{k1}$ because thermodynamic state functions, such as the Helmholtz free energy, are exact differentials:

$$d^2u = u_{00}(dz_0)^2 + a_{11}(dx_1)^2 + 2\sum_{k=2}^{r} a_{1k} \, dx_1 \, dx_k + \sum_{j=2}^{r} \sum_{k=2}^{r} a_{jk} \, dx_j \, dx_k > 0 \tag{29-110}$$

Step 9. Define another new fluctuation variable, dw_1, based on a linear combination of original fluctuating independent variables, except ds:

$$dw_1 \equiv dx_1 + \frac{1}{a_{11}} \sum_{k=2}^{r} a_{1k} \, dx_k \tag{29-111}$$

Step 10. Calculate the square of dw_1, which cannot be negative even though all dx_i can be positive, negative, or zero:

$$(dw_1)^2 = (dx_1)^2 + \frac{2}{a_{11}} \sum_{k=2}^{r} a_{1k} \, dx_1 \, dx_k + \left(\frac{1}{a_{11}}\right)^2 \sum_{j=2}^{r} a_{1j} \, dx_j \sum_{k=2}^{r} a_{1k} \, dx_k \tag{29-112}$$

Step 11. Incorporate the result from step 10 into the quadratic form in step 8:

$$d^2u = u_{00}(dz_0)^2 + a_{11}(dw_1)^2 + \frac{1}{a_{11}}\sum_{j=2}^{r}\sum_{k=2}^{r}[(a_{11}a_{jk} - a_{1j}a_{1k})]\,dx_j\,dx_k > 0 \tag{29-113}$$

Step 12. Use the method of Jacobians to simplify the coefficient of the quadratic form in (29-113). Since $\xi_k \equiv (\partial a/\partial x_k)$ at constant ξ_0, all $x_i (i \neq 0, k)$:

$$\begin{aligned} a_{11}a_{jk} - a_{1j}a_{1k} = a_{11}a_{jk} - a_{j1}a_{1k} &= \frac{\partial\xi_1}{\partial x_1}\frac{\partial\xi_k}{\partial x_j} - \frac{\partial\xi_1}{\partial x_j}\frac{\partial\xi_k}{\partial x_1} \\ &= \frac{\partial(\xi_1, \xi_k)}{\partial(x_1, x_j)} = \frac{\partial(\xi_0, \xi_1, \xi_k, \text{all } x_i)}{\partial(\xi_0, x_1, x_j, \text{all } x_i)}\,(i \neq 0, 1, j) \end{aligned} \tag{29-114}$$

Also,

$$a_{11} = \frac{\partial^2 a}{\partial x_1^2} = \frac{\partial\xi_1}{\partial x_1} = \frac{\partial(\xi_0, \xi_1, x_j, \text{all } x_i)}{\partial(\xi_0, x_1, x_j, \text{all } x_i)}\,(i \neq 0, 1, j) \tag{29-115}$$

Step 13. Use the last two general properties of Jacobians given by equations (29-54) and (29-55) to simplify the following ratio:

$$\begin{aligned} &\frac{a_{11}a_{jk} - a_{1j}a_{1k}}{a_{11}} \\ &= \frac{\partial(\xi_0, \xi_1, \xi_k, \text{all } x_i)/\partial(\xi_0, x_1, x_j, \text{all } x_i)}{\partial(\xi_0, \xi_1, x_j, \text{all } x_i)/\partial(\xi_0, x_1, x_j, \text{all } x_i)} \\ &= \frac{\partial(\xi_0, \xi_1, \xi_k, \text{all } x_i)}{\partial(\xi_0, \xi_1, x_j, \text{all } x_i)} \\ &= \frac{\partial\xi_k}{\partial x_j} \text{ at constant } \xi_0, \xi_1 \text{ and all } x_i (i \neq 0, 1, j) \end{aligned} \tag{29-116}$$

Legendre Transformation. The previous result from equation (29-116),

$$\frac{a_{11}a_{jk} - a_{1j}a_{1k}}{a_{11}} = \frac{\partial\xi_k}{\partial x_j} \text{ at constant } \xi_0, \xi_1 \text{ and all } x_i (i \neq 0, 1, j) \tag{29-117}$$

is best interpreted by performing a Legendre transformation from u to the intensive Gibbs free energy of the mixture:

$$\begin{aligned} g_{\text{mixture}} &= u - x_0\xi_0 - x_1\xi_1 \\ du &= \sum_{k=0}^{r}\xi_k\,dx_k \\ dg_{\text{mixture}} &= -x_0\,d\xi_0 - x_1\,d\xi_1 + \sum_{k=2}^{r}\xi_k\,dx_k \end{aligned} \tag{29-118}$$

where $x_0 = s$, $\xi_0 = T$, $x_1 = v$, and $\xi_1 = -p$. The total differential of g_{mixture} is useful to define ξ_k in equations (29-117) and (29-118). Hence,

$$\xi_k \equiv \frac{\partial g_{\text{mixture}}}{\partial x_k} \qquad \text{at constant } \xi_0, \xi_1 \text{ and all } x_i (i \neq 0, 1, k)$$

$$\frac{\partial \xi_k}{\partial x_j} = \frac{\partial^2 g_{\text{mixture}}}{\partial x_j \partial x_k} \equiv (g_{\text{mixture}})_{jk} \qquad \text{at constant } \xi_0, \xi_1 \text{ and all } x_i (i \neq 0, 1, j, k) \tag{29-119}$$

Step 14. Continue the step-by-step methodology by rewriting the quadratic form in (29-113) using information about the Gibbs free energy of the mixture:

$$d^2u = u_{00}(dz_0)^2 + a_{11}(dw_1)^2 + \sum_{j=2}^{r}\sum_{k=2}^{r}(g_{\text{mixture}})_{jk}\, dx_j\, dx_k > 0 \tag{29-120}$$

The cyclic methodology was repeated twice in the preceding 14 steps. After each cycle, the leading term in the summation for d^2u is isolated and another quadratic form remains. After repeating the cycle r times for an r-component mixture, the final expression for d^2u has $r + 1$ terms, where each term contains the square of a linear combination of original fluctuating independent variables. Fluctuations in the original independent variables [i.e., ds, dv, all $dy_i (1 \leq i \leq r - 1)$] can be positive, negative, or zero. However, the square of a linear combination of these fluctuations [i.e., $(dz_0)^2$, $(dw_1)^2$, etc.] must be positive unless all $dx_i = 0$. Energy minimization is achieved by requiring that the coefficient of the square of each linear combination of original fluctuating independent variables be positive. If an r-component mixture is homogeneous and does not exhibit phase separation, then $r + 1$ conditions must be satisfied if $d^2u > 0$. There are also $r + 1$ degree of freedom for any intensive thermodynamic state function. One condition corresponds to thermal stability, another condition represents mechanical stability, and the remaining $r - 1$ conditions define the criteria for chemical or diffusional stability.

29-6.5 Thermodynamic Stability in Binary Mixtures Via Energy Minimization

Results from Section 29-6.4 are analyzed explicitly for a binary mixture, and criteria are identified that must be satisfied if single-phase behavior is favored. Energy minimization given by equation (29-120) is written when $r = 2$:

$$d^2u = u_{00}(dz_0)^2 + a_{11}(dw_1)^2 + (g_{\text{mixture}})_{22}(dy_1)^2 > 0 \tag{29-121}$$

where $x_2 = y_1$ is the mole fraction of component 1, and

$$\begin{aligned} dz_0 &\equiv ds + \frac{u_{01}}{u_{00}}\, dv + \frac{u_{02}}{u_{00}}\, dy_1 \\ dw_1 &\equiv dv + \frac{a_{12}}{a_{11}}\, dy_1 \end{aligned} \tag{29-122}$$

Three conditions must be satisfied if $d^2u > 0$:

$$u_{00} = \frac{\partial^2 u}{\partial x_0^2} = \left(\frac{\partial^2 u}{\partial s^2}\right)_{v,\,\text{composition}} > 0 \tag{29-123a}$$

$$a_{11} = \frac{\partial^2 a}{\partial x_1^2} = \left(\frac{\partial^2 a}{\partial v^2}\right)_{T,\,\text{composition}} > 0 \tag{29-123b}$$

$$(g_{\text{mixture}})_{22} = \frac{\partial^2 g_{\text{mixture}}}{\partial x_2^2} = \left(\frac{\partial^2 g_{\text{mixture}}}{\partial y_1^2}\right)_{T,p} > 0 \tag{29-123c}$$

These are the positive curvature conditions that were discussed empirically for each type of stability. In other words, (1) thermal stability requires that u vs. s must exhibit positive curvature at constant volume and composition, (2) mechanical stability requires that a vs. v must exhibit positive curvature at constant temperature and composition, and (3) chemical stability requires that g_{mixture} (or Δg_{mixing}) vs. mole fraction must exhibit positive curvature at constant T and p.

Thermal Stability. Condition (29-123a) requires that $u_{00} > 0$. This implies that the specific heat at constant volume and composition (C_V) must be positive. Furthermore, the thermodynamic identity given by equation (29-61) via the method of Jacobians,

$$C_p = C_V - T\left[\left(\frac{\partial p}{\partial T}\right)_{V,\,\text{composition}}\right]^2 \left(\frac{\partial V}{\partial p}\right)_{T,\,\text{composition}} = C_V + \frac{\alpha^2 V T}{\kappa} > 0 \tag{29-124}$$

reveals that C_p, which is always greater than C_V, must be positive. In equation (29-124), α represents the coefficient of thermal expansion and κ is isothermal compressibility, defined as

$$\begin{aligned} \alpha &\equiv \left(\frac{\partial \ln V}{\partial T}\right)_{p,\,\text{composition}} \\ \kappa &\equiv -\left(\frac{\partial \ln V}{\partial p}\right)_{T,\,\text{composition}} \end{aligned} \tag{29-125}$$

Mechanical Stability. Condition (29-123b) requires that $a_{11} > 0$. Hence, pressure must decrease at larger volume along a $p-V$ isotherm; otherwise, the system splits into two different states of matter.

Chemical Stability. Condition (29-123c) requires that $(g_{\text{mixture}})_{22} > 0$. Euler's integral theorem for a multicomponent mixture yields (i.e., see equation 29-69):

$$g_{\text{mixture}} = \sum_{i=1}^{r} y_i \mu_i \tag{29-126}$$

This reduces to

$$g_{\text{mixture}} = y_1\mu_1 + (1 - y_1)\mu_2 \tag{29-127}$$

for binary mixtures. Hence,

$$\left(\frac{\partial g_{\text{mixture}}}{\partial y_1}\right)_{T,p} = \mu_1 - \mu_2 + y_1\left(\frac{\partial \mu_1}{\partial y_1}\right)_{T,p} + (1 - y_1)\left(\frac{\partial \mu_2}{\partial y_1}\right)_{T,p} \tag{29-128}$$

The last two terms on the right side of (29-128) cancel via the Gibbs–Duhem equation. In other words,

$$\left(\frac{\partial \mu_2}{\partial y_1}\right)_{T,p} = \frac{-y_1}{1 - y_1}\left(\frac{\partial \mu_1}{\partial y_1}\right)_{T,p} \tag{29-129}$$

This rearrangement of the Gibbs–Duhem equation in (29-129) is useful to simplify the curvature requirement for g_{mixture} vs. y_1 at constant T and p:

$$\left(\frac{\partial^2 g_{\text{mixture}}}{\partial y_1^2}\right)_{T,p} = \left(\frac{\partial \mu_1}{\partial y_1}\right)_{T,p} - \left(\frac{\partial \mu_2}{\partial y_1}\right)_{T,p} = \left(1 + \frac{y_1}{1 - y_1}\right)\left(\frac{\partial \mu_1}{\partial y_1}\right)_{T,p}$$

$$= \frac{1}{1 - y_1}\left(\frac{\partial \mu_1}{\partial y_1}\right)_{T,p} > 0 \tag{29-130}$$

One arrives at the same result by analyzing the curvature of Δg_{mixing} vs. composition via equation (29-76). Since $1 - y_1 > 0$, chemical stability in a binary mixture requires that the chemical potential (and activity) of each component must increase as the system becomes more concentrated with respect to the same component at constant T and p. If the condition, $(\partial \mu_1/\partial y_1)_{T,p} > 0$, is violated, then the mixture splits into two phases of different composition (i.e., either liquid–liquid or solid–solid equilibrium). At constant T and p, chemical potentials and activities are related by (see equation 29-77):

$$\mu_1(T, p, y_1) = \mu_{1,\,\text{pure}}(T, p) + RT \ln a_1(T, p, y_1) \tag{29-131}$$

Now, the criterion for chemical stability can be expressed in terms of the concentration dependence of activities. For example,

$$\left(\frac{\partial \mu_1}{\partial y_1}\right)_{T,p} = RT\left(\frac{\partial \ln a_1}{\partial y_1}\right)_{T,p} > 0 \tag{29-132}$$

Illustrative Problem. The intensive Gibbs free energy of a binary mixture g_{mixture} is expressed as a function of temperature, pressure, and mole fraction y_1 in equation (29-133):

$$g_{\text{mixture}}(T, p, y_1) = [\alpha y_1 + \beta(1 - y_1)]p^2 - [\gamma y_1 + \delta(1 - y_1)]T^4 - \epsilon y_1(1 - y_1) \tag{29-133}$$

where α, β, γ, δ, and ϵ are nonzero constants.

(a) Obtain an expression for Δg_{mixing}.

(b) What restrictions must be placed on α, β, γ, δ, and ε if the mixture is homogeneous and does not exhibit phase separation?

29-6.6 Chemical Stability of Polymer–Solvent Mixtures

Statistical analysis of the placement of polymer chains and solvent molecules on a three-dimensional lattice yields the following expression for the solvent activity in dilute polymer solutions:

$$\begin{aligned}\ln a_{\text{solvent}} &= \frac{1}{RT}\left(\frac{\partial \Delta G_{\text{mixing}}}{\partial N_{\text{solvent}}}\right)_{T,p,N_{\text{polymer}}} \\ &= \ln(1-\varphi_{\text{polymer}}) + \left(1-\frac{1}{m}\right)\varphi_{\text{polymer}} + \chi(\varphi_{\text{polymer}})^2 \end{aligned} \tag{29-134}$$

where φ_{polymer} is the polymer volume fraction, m is the molar volume ratio of polymer to solvent, and χ is the concentration-independent dimensionless Flory–Huggins interaction free energy of mixing. χ is analogous to the one-constant symmetric Margules coefficient K for energetic effects in non-ideal solutions (see Flory, 1953, p. 512 and Chap. 12). Chemical stability of homogeneous polymer solutions requires that

$$\begin{aligned}\left(\frac{\partial \mu_{\text{solvent}}}{\partial y_{\text{solvent}}}\right)_{T,p} &= RT\left(\frac{\partial \ln a_{\text{solvent}}}{\partial y_{\text{solvent}}}\right)_{T,p} \\ &= RT\left(\frac{\partial \ln a_{\text{solvent}}}{\partial \varphi_{\text{polymer}}}\right)_{T,p}\left(\frac{d\varphi_{\text{polymer}}}{d\varphi_{\text{solvent}}}\right)\left(\frac{d\varphi_{\text{solvent}}}{d y_{\text{solvent}}}\right) > 0 \end{aligned} \tag{29-135}$$

Since the solvent volume fraction φ_{solvent} increases when y_{solvent} is higher, but the polymer volume fraction decreases at higher concentrations of solvent (i.e., $\varphi_{\text{polymer}} = 1 - \varphi_{\text{solvent}}$), chemical stability is reformulated in terms of activities:

$$\left(\frac{\partial \ln a_{\text{solvent}}}{\partial \varphi_{\text{polymer}}}\right)_{T,p} = \frac{-1}{1-\varphi_{\text{polymer}}} + \left(1-\frac{1}{m}\right) + 2\chi\varphi_{\text{polymer}} < 0 \tag{29-136}$$

There is an upper limit for the Flory–Huggins thermodynamic interaction parameter χ if the polymer solution is homogeneous:

$$\chi < \frac{1-(1-1/m)(1-\varphi_{\text{polymer}})}{2\varphi_{\text{polymer}}(1-\varphi_{\text{polymer}})} \tag{29-137}$$

For very high molecular weight polymers (i.e., $m \to \infty$) at infinite dilution (i.e., $\varphi_{\text{polymer}} \to 0$), χ must be less than $\frac{1}{2}$ to avoid phase separation.

29-6.7 Chemical Stability of Regular Solutions Via the Margules Model

Euler's theorem for the intensive Gibbs free energy of mixing of an r-component mixture is expressed in terms of activities and activity coefficients as follows:

$$\Delta g_{\text{mixing}} = \sum_{i=1}^{r} y_i(\mu_i - \mu_{i,\,\text{pure}}) = RT \sum_{i=1}^{r} y_i \ln a_i = RT \sum_{i=1}^{r} y_i(\ln y_i + \ln \gamma_i) \tag{29-138}$$

where the summation on the far right side of (29-138) contains contributions from ideal and non-ideal mixing. If the non-ideal contribution to Δg_{mixing} in binary mixtures (i.e., $r = 2$) is given by the one-constant symmetric expression:

$$(\Delta g_{\text{mixing}})_{\text{nonideal}} = RT \sum_{i=1}^{r} y_i \ln \gamma_i = RT(y_1 \ln \gamma_1 + y_2 \ln \gamma_2) = K RT y_1(1 - y_1) \tag{29-139}$$

then the Margules activity coefficient models are

$$\begin{aligned} \ln \gamma_1 &= K(1 - y_1)^2 \\ \ln \gamma_2 &= K(y_1)^2 \end{aligned} \tag{29-140}$$

Miscibility in binary mixtures of small molecules imposes the following restriction on the Margules parameter K, which is concentration independent:

$$\begin{aligned} \left(\frac{\partial \ln a_1}{\partial y_1}\right)_{T,p} = \left[\frac{\partial(\ln y_1 + \ln \gamma_1)}{\partial y_1}\right]_{T,p} &> 0 \\ \frac{1}{y_1} - 2K(1 - y_1) &> 0 \\ K &< \frac{1}{2y_1(1 - y_1)} \end{aligned} \tag{29-141}$$

Even though K depends only on temperature and pressure, it has an upper limit imposed by chemical stability that varies with composition. The minimum upper limit of K occurs for an equimolar mixture where $y_1 = y_2 = \frac{1}{2}$. Hence, complete miscibility in regular solutions is consistent with $K < 2$ (see Tester and Modell, 1997, p. 359).

29-6.8 Chemical Stability of Regular Solutions Via the van Laar Model

This model employs the following expression for the non-ideal Gibbs free energy of mixing in binary solutions:

$$(\Delta g_{\text{mixing}})_{\text{nonideal}} = RT(y_1 \ln \gamma_1 + y_2 \ln \gamma_2) = \frac{RT\alpha\beta y_1 y_2}{\alpha y_1 + \beta y_2} \tag{29-142}$$

The van Laar activity coefficients that are consistent with this model are

$$\ln \gamma_1 = \frac{\alpha}{(1 + \alpha y_1/\beta y_2)^2}$$
$$\ln \gamma_2 = \frac{\beta}{(1 + \beta y_2/\alpha y_1)^2} \tag{29-143}$$

Chemical stability, $(\partial \ln a_i/\partial y_i)_{T,p} > 0$ ($i = 1$ or 2), imposes the following restriction on the van Laar parameters α and β if homogeneous single-phase behavior is favored:

$$2\alpha^2\beta^2 y_1 y_2 < (\alpha y_1 + \beta y_2)^3 \tag{29-144}$$

This inequality becomes an equality at the spinodal points. Since the van Laar model reduces to the one-constant symmetric Margules model when $\alpha = \beta$, inequality (29-144) yields $\alpha = \beta < 2$ for complete miscibility at any mixture composition, which agrees with results from Section 29-6.7.

Examples of Liquid–Liquid Phase Separation in Regular Solutions. van Laar parameters at ambient pressure are provided in Table 29-1 for three binary mixtures that exhibit concentration-dependent miscibility. The corresponding graphs of Δg_{mixing} vs. composition at constant T and p are provided in Figures 29-1 and 29-2. There is a range of compositions where

$$2\alpha^2\beta^2 y_1 y_2 > (\alpha y_1 + \beta y_2)^3 \tag{29-145}$$

These binary mixtures exhibit phase boundaries on temperature–composition phase diagrams, as summarized in Table 29-2. Data are available which indicate that methyl acetate ($T_{\text{boil}} = 57^0$C) and water ($T_{\text{boil}} = 100^0$C) exhibit a minimum-boiling azeotrope at 56.1^0C when the mole fraction of methyl acetate is 0.95 (*Handbook of Chemistry and Physics*, 1974-1975, p. D-30). Since the two-phase

TABLE 29-1 Parameters of the van Laar Activity Coefficient Model

Component	Temperature (^{0}C)	α	β
1. *n*-Hexane 2. Ethanol	59.3–78.3	1.57	2.58
1. Methyl acetate 2. Water	57–100	2.99	1.89
1. Isobutane 2. Furfural	37.8 51.7	2.62 2.51	3.02 2.83

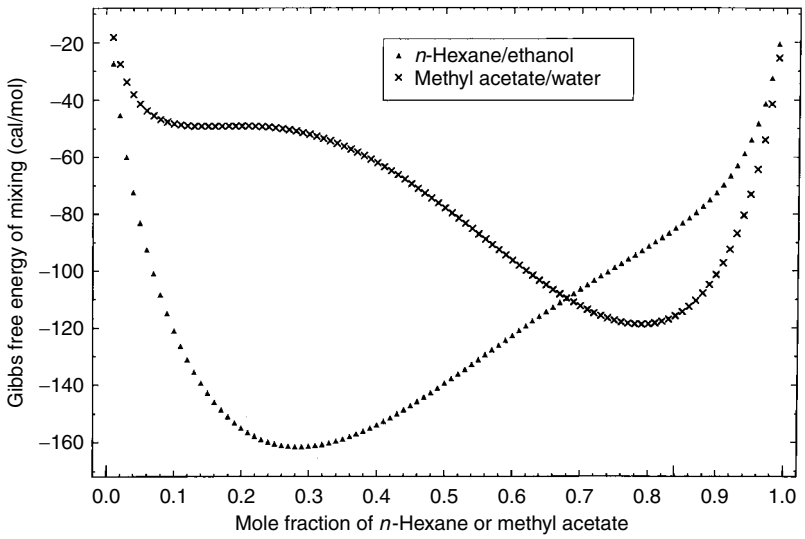

Figure 29-1 Concentration dependence of the Gibbs free energy of mixing at 70°C for regular solutions of *n*-hexane and ethanol, and methyl acetate and water. Non-Ideal effects are based on the van Laar model. Negative curvature [i.e., $(\partial^2 \Delta g_{\text{mixing}}/\partial y_1^2)_{T,p} < 0$] within the spinodal region exists for *n*-hexane mole fractions between 0.57 and 0.76, and methyl acetate mole fractions between 0.17 and 0.56.

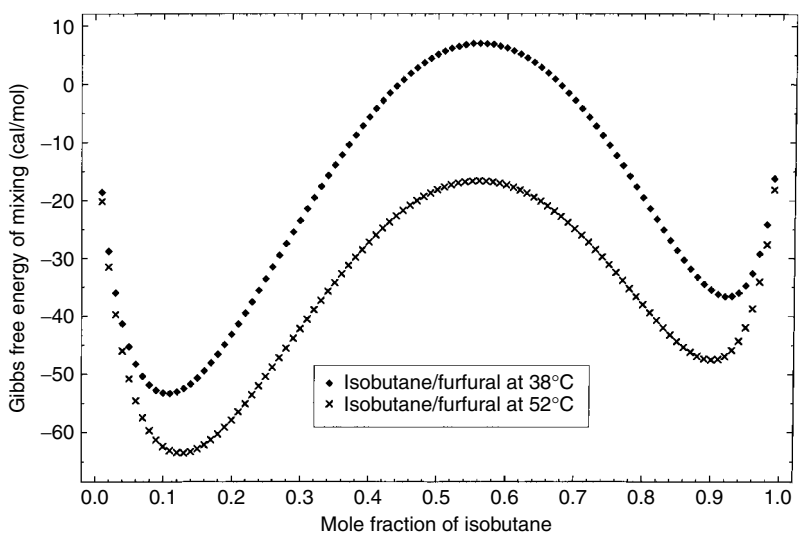

Figure 29-2 Concentration dependence of the Gibbs free energy of mixing at 38 and 52°C for regular solutions of isobutane and furfural. Non-Ideal effects are based on the van Laar model. Negative curvature [i.e., $(\partial^2 \Delta g_{\text{mixing}}/\partial y_1^2)_{T,p} < 0$] within the spinodal region exists for isobutane mole fractions between 0.27 and 0.81 at 38°C, and between 0.29 and 0.78 at 52°C. This binary system exhibits upper critical solution phenomena.

TABLE 29-2 Binodal and Spinodal Points on the Temperature–Composition Phase Diagram for Three Binary Mixtures[a]

Component	Temperature (^{0}C)	Binodal Points, y_1		Spinodal Points, y_1	
1. *n*-Hexane 2. Ethanol	59.3–78.3	0.47	0.81	0.57	0.76
1. Methyl acetate 2. Water	57–100	0.09	0.73	0.17	0.56
1. Isobutane 2. Furfural	37.8	0.12	0.93	0.27	0.81
1. Isobutane 2. Furfural	51.7	0.14	0.91	0.29	0.78

[a]Based on the van Laar activity coefficient parameters in Table 29-1.

envelope (i.e., between the binodal points) at 57^0C extends from methyl acetate mole fractions of 0.09 to 0.73, as indicated in Table 29-2 and illustrated in the upper curve of Figure 29-1, one concludes that the azeotrope is homogeneous because only one liquid phase is in equilibrium with a vapor at the same composition.

Transport Phenomena for Chemical Reactor Design. Laurence A. Belfiore
Copyright © 2003 John Wiley & Sons, Inc.
ISBN: 0-471-20275-4

30

COUPLED HEAT AND MASS TRANSFER IN PACKED CATALYTIC TUBULAR REACTORS THAT ACCOUNT FOR EXTERNAL TRANSPORT LIMITATIONS

When the thermal and mass transfer boundary layers on the outside of a catalytic pellet provide significant resistances to heat and mass transfer between the pellet and the bulk gas stream moving through a packed bed, it is necessary to modify the reactor design formalism described in Chapter 22. Additional equations are required to relate temperature and concentration in the bulk gas to their counterparts on the external surface of the catalytic pellets. It is important to remember that the volumetrically averaged rate of reactant consumption throughout the catalyst can be predicted in terms of the effectiveness factor and the kinetic rate law, which employs temperature and concentration on the external surface of the pellet. The methodology discussed below allows one to calculate temperature and species concentrations in the bulk gas stream, on the external surface of the catalytic pellet, and near the center of the pellet to determine the relative importance of intrapellet and external transport resistances. Since convective transport is negligible within a catalytic pellet, stoichiometric relations between diffusional mass fluxes are employed extensively throughout this chapter. For each component, continuity of total mass flux is invoked normal to the gas/porous-solid interface. Interphase transport coefficients are introduced when fluxes are evaluated at the pellet surface.

It might be possible to neglect the external gas phase resistance to mass transfer relative to intrapellet diffusional resistance through a tortuous pathway. An increase in the gas stream flow rate reduces the external mass transfer resistance further. Remember that diffusion coefficients and mass transfer coefficients increase as one progresses from solids to liquids to gases. Hence, gas-phase mass transfer resistances are small, but the intrapellet gas-phase diffusional resistances should be significant, particularly when the intrapellet Damkohler number is quite large. In contrast, thermal conductivities and heat transfer coefficients increase

as one progresses from gases to liquids to solids. Consequently, the heat transfer resistance in the gas-phase boundary layer external to the pellet is important, particularly if there is a significant resistance to heat transfer inside the composite metal oxide or ceramic catalyst. In this case, an increase in the gas stream flow rate will decrease the thermal boundary layer thickness outside the pellet and reduce external heat transfer limitations.

The dilemma can be summarized as follows. Plug-flow mass and thermal energy balances in a packed catalytic tubular reactor are written in terms of gas-phase concentrations and temperature of the bulk fluid phase. However, the volumetrically averaged rate of reactant consumption within catalytic pellets is calculated via concentrations and temperature on the external surface of the pellets. When external transport resistances are negligible, design of these reactors is simplified by equating bulk gas-phase conditions to those on the external catalytic surface. In this chapter, we address the dilemma when bulk gas-phase conditions are different from those on the external surface of the pellet. The logical sequence of calculations is as follows:

1. Estimate the intrapellet resistance to mass transfer for any component by invoking stoichiometry and the mass balance with diffusion and chemical reaction from the external surface to the central core of the catalyst.
2. Estimate the external resistance to mass transfer by invoking continuity of the normal component of intrapellet fluxes at the gas/porous-solid interface. Then use interphase mass transfer coefficients within the gas-phase boundary layer surrounding the pellets to evaluate interfacial molar fluxes.
3. Analyze coupled mass and thermal energy balances with chemical reaction in an isolated pellet to estimate the intrapellet resistance to heat transfer. Results from step 1 are used to simplify the thermal energy balance.
4. Manipulate the multicomponent thermal energy balance in the gas-phase boundary layer that surrounds each catalytic pellet. Estimate the external resistance to heat transfer by evaluating all fluxes at the gas/porous-solid interface, invoking continuity of the normal component of intrapellet mass flux for each component at the interface, and introducing mass and heat transfer coefficients to calculate interfacial fluxes.

As illustrated in Sections 30-1 and 30-2, all intrapellet resistances can be expressed in terms of $C_{\mathrm{A,\,surface}} - C_{\mathrm{A,\,intrapellet}}$, and $C_{\mathrm{A,\,intrapellet}}$ approaches zero near the central core of the catalyst when the intrapellet Damkohler number is very large. For small values of the intrapellet Damkohler number, effectiveness factor calculations within an isolated pellet allow one to predict $C_{\mathrm{A,\,intrapellet}}$ in terms of $C_{\mathrm{A,\,surface}}$ via the dimensionless molar density profile. All external transport resistances can be expressed in terms of $C_{\mathrm{A,\,bulk\ gas}} - C_{\mathrm{A,\,surface}}$, and integration of the plug-flow mass balance allows one to calculate the bulk gas-phase concentration of reactant A. The critical step involves determination of $C_{\mathrm{A,\,surface}}$ via effectiveness factor formalism. Finally, a complete reactor design strategy is

provided which combines important results discussed below with methodologies from earlier chapters.

30-1 INTRAPELLET AND BULK SPECIES CONCENTRATIONS

30-1.1 Porous Catalytic Pellet

Since contributions from convective transport are negligible in a porous catalyst, one begins with the steady-state mass transfer equation that includes diffusion and multiple chemical reactions for component i (i.e., see equations 9-18 and 27-14):

$$-\nabla \cdot \mathbf{j}_{i,\,\text{pellet}} + r_i = -\nabla \cdot \mathbf{j}_{i,\,\text{pellet}} + \sum_j \upsilon_{ij}\,\text{MW}_i\,\mathfrak{R}_j = 0 \tag{30-1}$$

where $\mathbf{j}_{i,\,\text{pellet}}$ represents the diffusional mass flux of species i with respect to a reference frame that translates at the mass-average velocity of the mixture. If there is only one chemical reaction on the internal catalytic surface or if one of the steps in a multistep process is rate limiting, then subscript j is not required. Hence, the mass balance given by equation (30-1) is simplified slightly:

$$-\nabla \cdot \mathbf{j}_{i,\,\text{pellet}} + \upsilon_i\,\text{MW}_i\,\mathfrak{R} = 0 \tag{30-2}$$

and stoichiometry indicates that

$$\frac{1}{\upsilon_i\,\text{MW}_i}\nabla \cdot \mathbf{j}_{i,\,\text{pellet}} = \frac{1}{\upsilon_\text{A}\,\text{MW}_\text{A}}\nabla \cdot \mathbf{j}_{\text{A},\,\text{pellet}} = \mathfrak{R} \tag{30-3}$$

Equation (30-3) is integrated over an arbitrary control volume V within the catalytic pores via Gauss's law:

$$\int_V \left[\frac{1}{\upsilon_i\,\text{MW}_i}\nabla \cdot \mathbf{j}_{i,\,\text{pellet}} - \frac{1}{\upsilon_\text{A}\,\text{MW}_\text{A}}\nabla \cdot \mathbf{j}_{\text{A},\,\text{pellet}}\right] dV$$
$$= \int_S \left[\frac{1}{\upsilon_i\,\text{MW}_i}\mathbf{n} \cdot \mathbf{j}_{i,\,\text{pellet}} - \frac{1}{\upsilon_\text{A}\,\text{MW}_\text{A}}\mathbf{n} \cdot \mathbf{j}_{\text{A},\,\text{pellet}}\right] dS = 0 \tag{30-4}$$

where $\mathbf{n}$ is a unit normal vector directed outward from the surface of the control volume. Since there are many choices for control volume V and surface S that surrounds this volume element, the integrand of the surface integral in equation (30-4) must vanish. Hence,

$$\frac{1}{\upsilon_i\,\text{MW}_i}\mathbf{n} \cdot \mathbf{j}_{i,\,\text{pellet}} = \frac{1}{\upsilon_\text{A}\,\text{MW}_\text{A}}\mathbf{n} \cdot \mathbf{j}_{\text{A},\,\text{pellet}} \tag{30-5}$$

Fick's law for diffusional mass flux $\mathbf{j}_{i,\,\text{pellet}}$ within the catalytic pores is written in terms of a concentration gradient, molecular weight, and the effective diffusivity

of component i as follows (see equation 27-24):

$$\begin{aligned} \mathbf{j}_{i,\text{ pellet}} &= -\rho \mathfrak{D}_{i,\text{ effective}} \nabla \omega_i \approx -\mathfrak{D}_{i,\text{ effective}} \nabla \rho \omega_i \\ &= -\mathfrak{D}_{i,\text{ effective}} \nabla (C_i \,\text{MW}_i) \\ \frac{1}{\text{MW}_i} \mathbf{n} \cdot \mathbf{j}_{i,\text{ pellet}} &= -\mathfrak{D}_{i,\text{ effective}}\ \mathbf{n} \cdot \nabla C_i = -\mathfrak{D}_{i,\text{ effective}} \frac{\partial C_i}{\partial n} \end{aligned} \tag{30-6}$$

where n is the local coordinate measured in the direction of $\mathbf{n}$. The stoichiometric relation given by equation (30-5) reduces to

$$\frac{1}{\upsilon_i} D_{i,\text{ effective}} \frac{\partial C_i}{\partial n} = \frac{1}{\upsilon_\text{A}} \mathfrak{D}_{\text{A, effective}} \frac{\partial C_\text{A}}{\partial n} \tag{30-7}$$

and the stoichiometric coefficient of reactant A is -1 in the slowest step of the adsorption/reaction/desorption sequence. Equation (30-7) is integrated from the central core of the catalyst, where the molar densities are $C_{i,\text{ intrapellet}}$ and $C_{\text{A, intrapellet}}$, to the external surface, where the appropriate conditions are $C_{i,\text{ surface}}$ and $C_{\text{A, surface}}$. Hence, one calculates the molar density of any species within the catalyst as follows:

$$C_{i,\text{ intrapellet}} - C_{i,\text{ surface}} = \frac{\upsilon_i \mathfrak{D}_{\text{A, effective}}}{\mathfrak{D}_{i,\text{ effective}}} (C_{\text{A, surface}} - C_{\text{A, intrapellet}}) \tag{30-8}$$

The intrapellet mass transfer resistance for component i is directly proportional to the molar density difference on the left side of (30-8). It should be emphasized that the stoichiometric relations given by (30-5) and (30-8) are applicable throughout the entire volume of the pellet when one chemical reaction governs the rate of conversion of reactants to products.

30-1.2 Bulk Gas Phase

When the stoichiometric relation given by (30-5) is evaluated at the external surface of the catalyst, it is possible to invoke continuity across the gas/porous-solid interface and introduce mass transfer coefficients to evaluate interfacial fluxes. Diffusion and chemical reaction within the catalytic pores are consistent with the following stoichiometric relation between diffusional mass fluxes:

$$\frac{1}{\upsilon_i \,\text{MW}_i} \mathbf{n} \cdot \mathbf{j}_{i,\text{ pellet}} = \frac{1}{\upsilon_\text{A} \,\text{MW}_\text{A}} \mathbf{n} \cdot \mathbf{j}_{\text{A, pellet}} \tag{30-9}$$

as illustrated in Section 30-1.1. These fluxes are evaluated on the pellet side of the gas/porous-solid interface, where $\mathbf{n}$ represents the outward-directed unit normal vector from the external surface of the catalyst into the bulk gas phase:

$$\frac{1}{\upsilon_i} \left(\mathbf{n} \cdot \frac{\mathbf{j}_{i,\text{ pellet}}}{\text{MW}_i} \right)_{\text{ext. surface}} = \frac{1}{\upsilon_\text{A}} \left(\mathbf{n} \cdot \frac{\mathbf{j}_{\text{A, pellet}}}{\text{MW}_\text{A}} \right)_{\text{ext. surface}} \tag{30-10}$$

At steady state, continuity of the normal component of mass flux (i.e., $\mathbf{n} \cdot \rho_i \mathbf{v}_i$) on both sides of the interface is invoked for each component. Hence,

$$(\mathbf{n} \cdot \mathbf{j}_{i,\,\text{pellet}})_{\text{ext. surface}} = (\mathbf{n} \cdot \mathbf{j}_{i,\,\text{bulk gas}})_{\text{ext. surface}} \tag{30-11}$$

because convective contributions in the normal coordinate direction are negligible in both phases at the interface. One introduces bulk gas-phase concentrations by evaluating the normal component of these interfacial fluxes in terms of a mass transfer coefficient $k_{i,\,\text{MTC}}$ and a concentration driving force, which is standard procedure for interphase transport. Hence,

$$\left(\mathbf{n} \cdot \frac{\mathbf{j}_{i,\,\text{bulk gas}}}{\text{MW}_i}\right)_{\text{ext. surface}} \equiv k_{i,\,\text{MTC}}(C_{i,\,\text{surface}} - C_{i,\,\text{bulk gas}}) \tag{30-12}$$

Now, the stoichiometric relation at the gas/porous-solid interface, given by (30-10), is expressed in terms of bulk gas-phase concentrations:

$$\frac{1}{\upsilon_i} k_{i,\,\text{MTC}}(C_{i,\,\text{surface}} - C_{i,\,\text{bulk gas}}) = \frac{1}{\upsilon_\text{A}} k_{\text{A},\,\text{MTC}}(C_{\text{A},\,\text{surface}} - C_{\text{A},\,\text{bulk gas}}) \tag{30-13}$$

Since the stoichiometric coefficient of reactant A is -1 in the slowest elementary step, it is possible to relate molar densities on the external surface of the catalyst to those in the bulk gas phase as follows:

$$C_{i,\,\text{surface}} - C_{i,\,\text{bulk gas}} = \frac{\upsilon_i k_{\text{A},\,\text{MTC}}}{k_{i,\,\text{MTC}}}(C_{\text{A},\,\text{bulk gas}} - C_{\text{A},\,\text{surface}}) \tag{30-14}$$

This equation correctly predicts that $C_{i,\,\text{surface}} - C_{i,\,\text{bulk gas}}$ is positive for products and negative for reactants, because $C_{\text{A},\,\text{bulk gas}} > C_{\text{A},\,\text{surface}}$ for reactant A. The kinetic rate law is evaluated on the external surface of the pellet, and the effectiveness factor is employed to predict the average rate of reactant consumption on the internal surface of the catalyst. When molar densities on the external surface are required in the rate law, (30-14) should be employed to re-express $C_{i,\,\text{surface}}$ in terms of bulk gas-phase conditions. This is advantageous because the plug-flow mass balance for species i is written in terms of $C_{i,\,\text{bulk gas}}$.

30-2 INTRAPELLET AND BULK GAS TEMPERATURE

30-2.1 Porous Catalytic Pellet

Steady-state analysis of coupled heat and mass transfer with multiple chemical reactions in the pores of a catalytic pellet is based on simultaneous solution of the mass transfer equation:

$$\rho \mathbf{v} \cdot \nabla \omega_i = -\nabla \cdot \mathbf{j}_{i,\,\text{pellet}} + \sum_j \upsilon_{ij}\,\text{MW}_i\,\mathfrak{R}_j \tag{30-15}$$

and the multicomponent thermal energy balance, which is written in terms of specific internal energy u via equation (27-8):

$$\rho \mathbf{v} \cdot \nabla u = -\nabla \cdot \mathbf{q} - p \nabla \cdot \mathbf{v} - \tau \blacklozenge \nabla \mathbf{v} + \sum_{i=1}^{N} \mathbf{j}_{i,\,\text{pellet}} \cdot \mathbf{g}_i \tag{30-16}$$

where the molecular flux of thermal energy in multicomponent mixtures is

$$\mathbf{q} = -k_{\text{eff. pellet}} \nabla T + \sum_{i=1}^{N} \frac{\mathfrak{h}_i}{\text{MW}_i} \mathbf{j}_{i,\,\text{Pellet}} \tag{30-17}$$

Fourier's law and the interdiffusional fluxes are considered, but the diffusion-thermo (i.e., Dufour) effect is neglected in (30-17). Since contributions from convective transport are insignificant at extremely low Peclet numbers for heat and mass transfer within the catalytic pores, the previous balances reduce to

$$\begin{aligned} 0 &= -\nabla \cdot \mathbf{j}_{i,\,\text{pellet}} + \sum_j \upsilon_{ij}\, \text{MW}_i\, \mathfrak{R}_j \\ 0 &= \nabla \cdot \mathbf{q} \end{aligned} \tag{30-18}$$

Irreversible production of thermal energy (i.e., $-\tau \blacklozenge \nabla \mathbf{v}$), reversible exchange between kinetic and internal energies (i.e., $p \nabla \cdot \mathbf{v}$), and effects from external force fields (i.e., $\sum_{i=1}^{N} \mathbf{j}_{i,\,\text{pellet}} \cdot \mathbf{g}_i$) are also neglected in the thermal energy balance. When there is only one chemical reaction on the internal catalytic surface, or if one of the steps in a multistep process is rate limiting, then subscript j is not required:

$$-\nabla \cdot \mathbf{j}_{i,\,\text{pellet}} + \upsilon_i\, \text{MW}_i\, \mathfrak{R} = 0 \tag{30-19}$$

and stoichiometry in the mass balance with diffusion and chemical reaction indicates that

$$\frac{1}{\upsilon_i\, \text{MW}_i} \nabla \cdot \mathbf{j}_{i,\,\text{pellet}} = \frac{1}{\upsilon_\text{A}\, \text{MW}_\text{A}} \nabla \cdot \mathbf{j}_{\text{A},\,\text{pellet}} = \mathfrak{R} \tag{30-20}$$

Equation (30-20) and the thermal energy balance in (30-18) are integrated over an arbitrary control volume V within the catalytic pores via Gauss's law:

$$\begin{aligned} &\int_V \left[\frac{1}{\upsilon_i\, \text{MW}_i} \nabla \cdot \mathbf{j}_{i,\,\text{pellet}} - \frac{1}{\upsilon_\text{A}\, \text{MW}_\text{A}} \nabla \cdot \mathbf{j}_{\text{A},\,\text{pellet}} \right] dV \\ &\quad = \int_S \left[\frac{1}{\upsilon_i\, \text{MW}_i} \mathbf{n} \cdot \mathbf{j}_{i,\,\text{pellet}} - \frac{1}{\upsilon_\text{A}\, \text{MW}_\text{A}} \mathbf{n} \cdot \mathbf{j}_{\text{A},\,\text{pellet}} \right] dS = 0 \end{aligned} \tag{30-21}$$

$$\int_V (\nabla \cdot \mathbf{q})\, dV = \int_S (\mathbf{n} \cdot \mathbf{q})\, dS = 0 \tag{30-22}$$

where $\mathbf{n}$ is a unit normal vector directed outward from the surface of the control volume. Since there are many choices for control volume V and surface S that surrounds this volume element, the integrands of the surface integrals in equations (30-22) vanish. Hence,

$$\frac{1}{\upsilon_i \, \mathrm{MW}_i} \mathbf{n} \cdot \mathbf{j}_{i,\,\mathrm{pellet}} = \frac{1}{\upsilon_\mathrm{A} \, \mathrm{MW}_\mathrm{A}} \mathbf{n} \cdot \mathbf{j}_{\mathrm{A},\,\mathrm{pellet}} \tag{30-23}$$

$$\mathbf{n} \cdot \mathbf{q} = \mathbf{n} \cdot \left[-k_{\mathrm{eff.\ pellet}} \nabla T + \sum_{i=1}^{N} \frac{\mathfrak{h}_i}{\mathrm{MW}_i} \mathbf{j}_{i,\,\mathrm{pellet}} \right] = 0 \tag{30-24}$$

where $k_{\mathrm{eff.\ pellet}}$ is the effective thermal conductivity of the porous catalyst and $\mathfrak{h}_i$ is the partial molar enthalpy of species i. These conditions on diffusional mass flux and the molecular flux of thermal energy, the latter of which includes Fourier's law and the interdiffusional contribution, allow one to relate temperature and concentration at any position within the pellet. If n is the local coordinate measured in the direction of $\mathbf{n}$, then (30-23) and (30-24) can be combined as follows:

$$\begin{aligned} \mathbf{n} \cdot (k_{\mathrm{eff.\ pellet}} \nabla T) = k_{\mathrm{eff.\ pellet}} \frac{\partial T}{\partial n} &= \sum_{i=1}^{N} \upsilon_i \mathfrak{h}_i \frac{1}{\upsilon_i \, \mathrm{MW}_i} (\mathbf{n} \cdot \mathbf{j}_{i,\,\mathrm{pellet}}) \\ &= \frac{1}{\upsilon_\mathrm{A} \, \mathrm{MW}_\mathrm{A}} (\mathbf{n} \cdot \mathbf{j}_{\mathrm{A},\,\mathrm{pellet}}) \sum_{i=1}^{N} \upsilon_i \mathfrak{h}_i \end{aligned} \tag{30-25}$$

Since the summation in equation (30-25) includes all components in the mixture, it is an exact representation of the enthalpy change for reaction, $\Delta H_{\mathrm{reaction}}$, on a molar basis (see Tester and Modell, 1997, pp. 769–770). Intermolecular interactions and non-ideal heats of solution are also included in

$$\sum_{i=1}^{N} \upsilon_i \mathfrak{h}_i \equiv \Delta H_{\mathrm{reaction}} \tag{30-26}$$

because $\mathfrak{h}_i$ is the partial molar enthalpy of component i. In practice, one estimates $\Delta H_{\mathrm{reaction}}$ using literature values for pure-component molar enthalpies. This approximation is exact for ideal solutions because partial molar enthalpies reduce to pure-component molar enthalpies under ideal conditions. Fick's law for $\mathbf{j}_{\mathrm{A,\,pellet}}$ within the catalytic pores is written in terms of a concentration gradient, molecular weight, and the effective diffusivity of component A as follows:

$$\begin{aligned} \mathbf{j}_{\mathrm{A,\,pellet}} &= -\rho \mathfrak{D}_{\mathrm{A,\,effective}} \nabla \omega_\mathrm{A} \approx -\mathfrak{D}_{\mathrm{A,\,effective}} \nabla \rho \omega_\mathrm{A} \\ &= -\mathfrak{D}_{\mathrm{A,\,effective}} \nabla \{C_\mathrm{A} \, \mathrm{MW}_\mathrm{A}\} \end{aligned} \tag{30-27}$$

$$\frac{1}{\mathrm{MW}_\mathrm{A}} \mathbf{n} \cdot \mathbf{j}_{\mathrm{A,\,pellet}} = -\mathfrak{D}_{\mathrm{A,\,effective}} \, \mathbf{n} \cdot \nabla C_\mathrm{A} = -\mathfrak{D}_{\mathrm{A,\,effective}} \frac{\partial C_\mathrm{A}}{\partial n} \tag{30-28}$$

The stoichiometric coefficient of species A is -1 in the slowest step of the adsorption/reaction/desorption sequence. Hence, temperature and molar density are related by

$$k_{\text{eff. pellet}} \frac{\partial T}{\partial n} = \mathfrak{D}_{\text{A, effective}} \Delta H_{\text{reaction}} \frac{\partial C_{\text{A}}}{\partial n} \tag{30-29}$$

via equations (30-25), (30-26), and (30-28). Even though temperature and reactant concentration profiles are solved for one-dimensional diffusion in the thinnest dimension of the pellet (i.e., or radially for long cylinders and spheres) in Chapter 27, equation (30-29) is applicable to multidimensional diffusion and conduction. The coordinate direction denoted by n in (30-29) is not important. Hence,

$$k_{\text{eff. pellet}}\, dT = \mathfrak{D}_{\text{A, effective}} \Delta H_{\text{reaction}}\, dC_{\text{A}} \tag{30-30}$$

is integrated from the central core of the catalyst, where the conditions are $T_{\text{intrapellet}}$ and $C_{\text{A, intrapellet}}$, to the external surface, where T_{surface} and $C_{\text{A, surface}}$ are appropriate. The final result allows one to predict intrapellet temperatures in terms of the intrapellet molar density of reactant A via

$$T_{\text{intrapellet}} - T_{\text{surface}} = \frac{\mathfrak{D}_{\text{A, effective}}(-\Delta H_{\text{reaction}})}{k_{\text{eff. pellet}}}(C_{\text{A, surface}} - C_{\text{A, intrapellet}}) \tag{30-31}$$

Equation (30-31) is equivalent to (27-53) when physicochemical properties within porous catalysts are independent of temperature. For exothermic chemical reactions (i.e., $\Delta H_{\text{reaction}} < 0$), equation (30-31) correctly reveals that $T_{\text{intrapellet}} > T_{\text{surface}}$ because $C_{\text{A, surface}} > C_{\text{A, intrapellet}}$ for reactant A.

30-2.2 Bulk Gas Phase

Multicomponent heat transfer in the thermal boundary layer external to the pellet is described by (i.e., see equation 27-8):

$$\begin{aligned}\rho \frac{Du}{Dt} = \rho\left(\frac{\partial u}{\partial t} + \mathbf{v}\cdot\nabla u\right) &= \frac{\partial(\rho u)}{\partial t} + \nabla\cdot\rho\mathbf{v}u \\ &= -\nabla\cdot\mathbf{q} - p\nabla\cdot\mathbf{v} - \tau\blacklozenge\nabla\mathbf{v} + \sum_{i=1}^{N}\mathbf{j}_{i,\text{ bulk gas}}\cdot\mathbf{g}_i\end{aligned} \tag{30-32}$$

prior to invoking any assumptions. Steady-state analysis under conditions where the following mechanisms are negligible:

1. Reversible exchange between internal and kinetic energies (i.e., $p\nabla\cdot\mathbf{v} \approx 0$)
2. Irreversible conversion of kinetic energy to internal energy (i.e., $\tau\blacklozenge\nabla\mathbf{v} \approx 0$)
3. External force field effects (i.e., $\sum_{i=1}^{N}\mathbf{j}_{i,\text{ bulk gas}}\cdot\mathbf{g}_i \approx 0$)

allows one to simplify this rather complicated balance:

$$\nabla\cdot(\rho\mathbf{v}u + \mathbf{q}) = 0 \tag{30-33}$$

when contributions from convective transport are not neglected. The thermal energy balance given by equation (30-33) is integrated over an arbitrary control volume V within the external heat transfer boundary layer via Gauss's law;

$$\int_V \left[\nabla \cdot (\rho \mathbf{v} u + \mathbf{q})\right] dV = \int_S \left[\mathbf{n} \cdot (\rho \mathbf{v} u + \mathbf{q})\right] dS = 0 \tag{30-34}$$

where $\mathbf{n}$ is a unit normal vector directed outward from the surface of the control volume. Since there are many choices for control volume V and surface S that surrounds this volume element in the thermal boundary layer, the integrand of the surface integral vanishes in equation (30-34). Hence,

$$\mathbf{n} \cdot (\rho \mathbf{v} u + \mathbf{q}) = \mathbf{n} \cdot \left(\rho \mathbf{v} u - k_{\text{gas phase}} \nabla T + \sum_{i=1}^{N} \frac{\mathfrak{h}_i}{\text{MW}_i} \mathbf{j}_{i,\text{ bulk gas}} \right) = 0 \tag{30-35}$$

where $k_{\text{gas phase}}$ is the thermal conductivity of the gas-phase medium surrounding each pellet. Equation (30-35) is evaluated on the external surface of the catalyst, where $\mathbf{n}$ represents the unit normal vector directed into the pellet and convective transport is negligible. In other words, the bulk gas-phase velocity in the normal coordinate direction (i.e., $\mathbf{n} \cdot \mathbf{v}$) is neglected on the external surface of the catalyst, where molecular fluxes provide the dominant contributions to heat and mass transfer. The mass flux of component i normal to the external gas/porous-solid interface must be continuous. Hence, $\mathbf{n} \cdot \mathbf{j}_i$ is the same on each side of the interface when convective transport is unimportant. When (30-35) is evaluated on the external surface of the pellet and $\mathbf{n} \cdot \mathbf{j}_{i,\text{ bulk gas}}$ in the external boundary layer is replaced by its counterpart in the porous catalyst, it is possible to invoke stoichiometry within the pellet:

$$\frac{1}{\upsilon_i \text{MW}_i} \mathbf{n} \cdot \mathbf{j}_{i,\text{ pellet}} = \frac{1}{\upsilon_\text{A} \text{MW}_\text{A}} \mathbf{n} \cdot \mathbf{j}_{\text{A, pellet}} \tag{30-36}$$

as described by equation (30-5). The result is;

$$\begin{aligned}
(\mathbf{n} \cdot k_{\text{gas phase}} \nabla T)_{\text{ext. surface}} &= \sum_{i=1}^{N} \left[\upsilon_i \mathfrak{h}_i \frac{1}{\upsilon_i \text{MW}_i} (\mathbf{n} \cdot \mathbf{j}_{i,\text{ bulk gas}})_{\text{ext. surface}} \right] \\
&= \sum_{i=1}^{N} \left[\upsilon_i \mathfrak{h}_i \frac{1}{\upsilon_i \text{MW}_i} (\mathbf{n} \cdot \mathbf{j}_{i,\text{ pellet}})_{\text{ext. surface}} \right] \\
&= \frac{1}{\upsilon_\text{A}} \left(\mathbf{n} \cdot \frac{\mathbf{j}_{\text{A, pellet}}}{\text{MW}_\text{A}} \right)_{\text{ext. surface}} \sum_{i=1}^{N} \upsilon_i \mathfrak{h}_i
\end{aligned} \tag{30-37}$$

where the stoichiometric coefficient of reactant A is -1, and the summation on the third line of (30-37) is an exact representation of the enthalpy change for

chemical reaction $\Delta H_{\text{reaction}}$. Hence,

$$(\mathbf{n} \cdot k_{\text{gas phase}} \nabla T)_{\text{ext. surface}} = -\Delta H_{\text{reaction}} \left(\mathbf{n} \cdot \frac{\mathbf{j}_{\text{A, pellet}}}{\text{MW}_{\text{A}}} \right)_{\text{ext. surface}}$$
$$= -\Delta H_{\text{reaction}} \left(\mathbf{n} \cdot \frac{\mathbf{j}_{\text{A, bulk gas}}}{\text{MW}_{\text{A}}} \right)_{\text{ext. surface}} \tag{30-38}$$

The external resistance to heat transfer is incorporated in reactor design simulations by expressing the normal component of interfacial flux in terms of a transfer coefficient and a driving force, the latter of which is sensitive to the direction of the unit normal vector **n** and the fact that Fourier's law and Fick's law require a negative sign to calculate the flux in a particular coordinate direction. These considerations produce the following expressions for the conductive energy flux:

$$(\mathbf{n} \cdot k_{\text{gas phase}} \nabla T)_{\text{ext. surface}} \equiv h_{\text{HTC}} (T_{\text{surface}} - T_{\text{bulk gas}}) \tag{30-39}$$

and the diffusional molar flux of reactant A with respect to the mass-average reference frame:

$$\left[\mathbf{n} \cdot \left(\frac{\mathbf{j}_{\text{A, bulk gas}}}{\text{MW}_{\text{A}}} \right) \right]_{\text{ext. surface}} \equiv k_{\text{A, MTC}} (C_{\text{A, bulk gas}} - C_{\text{A, surface}}) \tag{30-40}$$

normal to the gas/porous-solid interface, where **n** is the unit normal vector directed into the catalyst. Equations (30-38), (30-39), and (30-40) allow one to estimate the temperature difference between the external surface of the catalytic pellet and the bulk gas stream as follows:

$$T_{\text{surface}} - T_{\text{bulk gas}} = \frac{-\Delta H_{\text{reaction}} k_{\text{A, MTC}} (C_{\text{A, bulk gas}} - C_{\text{A, surface}})}{h_{\text{HTC}}} \tag{30-41}$$

which predicts that $T_{\text{surface}} > T_{\text{bulk gas}}$ for exothermic chemical reactions (i.e., negative $\Delta H_{\text{reaction}}$) because $C_{\text{A, bulk gas}} > C_{\text{A, surface}}$ for reactant A. Heat and mass transfer coefficients in the external boundary layers (i.e., h_{HTC} and $k_{\text{A, MTC}}$) are enhanced by convective transport parallel to the gas/porous-solid interface, so they are functions of the Reynolds and Prandtl or Schmidt numbers (i.e., see Table 12-1).

30-3 EVALUATION OF $C_{\text{A,surface}}$ VIA THE EFFECTIVENESS FACTOR: COMPLETE STRATEGY FOR PACKED CATALYTIC TUBULAR REACTORS

Important results from earlier sections are summarized here to develop reactor design strategies when external resistances to heat and mass transfer cannot be neglected. Intrapellet resistances require information about

$C_{A,\,surface} - C_{A,\,intrapellet}$:

$$T_{intrapellet} - T_{surface} = \frac{\mathfrak{D}_{A,\,effective}(-\Delta H_{reaction})}{k_{eff.\ pellet}}(C_{A,\,surface} - C_{A,\,intrapellet})$$

$$C_{i,\,intrapellet} - C_{i,\,surface} = \frac{\upsilon_i \mathfrak{D}_{A,\,effective}}{\mathfrak{D}_{i,\,effective}}(C_{A,\,surface} - C_{A,\,intrapellet}) \tag{30-42}$$

whereas external resistances are based on $C_{A,\,bulk\ gas} - C_{A,\,surface}$:

$$T_{surface} - T_{bulk\ gas} = \frac{-\Delta H_{reaction} k_{A,\,MTC}(C_{A,\,bulk\ gas} - C_{A,\,surface})}{h_{HTC}}$$

$$C_{i,\,surface} - C_{i,\,bulk\ gas} = \frac{\upsilon_i k_{A,\,MTC}}{k_{i,\,MTC}}(C_{A,\,bulk\ gas} - C_{A,\,surface}) \tag{30-43}$$

The latter concentration driving force (i.e., $C_{A,\,bulk\ gas} - C_{A,\,surface}$) is used to construct an expression for the flux of reactant A into the pellet via interphase mass transfer. One employs equation (20-1) for the definition of the effectiveness factor E:

$$E(\Lambda_{A,\,intrapellet}) = \frac{\displaystyle\int_{V_{catalyst}} -\upsilon_A \mathfrak{R}\, dV}{-\upsilon_A \mathfrak{R}(C_{A,\,surface}) V_{catalyst}} \tag{30-44}$$

where $\mathfrak{R}(C_{A,\,surface}) = S_m \rho_{app} \mathfrak{R}_{surface}$ is a pseudo-volumetric kinetic rate law evaluated on the external surface of the catalyst and $\upsilon_A = -1$ for reactant A. The numerator of equation (30-44) represents a volumetric average of the rate of reactant consumption throughout the pellet, which is equivalent to the surface-averaged diffusional molar flux of reactant A into the catalyst across its external surface, via Fick's law. In other words, application of Gauss's law to an integral form of the microscopic mass balance for reactant A with diffusion and one chemical reaction yields the following expression, which is analogous to equation (20-4):

$$\int_V -\upsilon_A \mathfrak{R}\, dV = \int_V -\nabla \cdot \frac{\mathbf{j}_{A,\,pellet}}{MW_A}\, dV = \int_S \left[-\mathbf{n} \cdot \left(\frac{\mathbf{j}_{A,\,pellet}}{MW_A}\right)\right]_{ext.\ surface} dS \tag{30-45}$$

where $\mathbf{n}$ is an outward-directed unit normal vector from the external surface of the catalyst into the bulk gas phase. For one-dimensional problems that are characteristic of diffusion and chemical reaction in catalytic pellets, the molar density of reactant A, its gradient, and its molar flux are not functions of the surface coordinates that comprise the differential surface element dS. Hence, integration on the far right side of (30-45) is trivial, which allows one to replace the numerator of the effectiveness factor in equation (30-44):

$$\left[-\mathbf{n} \cdot \left(\frac{\mathbf{j}_{A,\,pellet}}{MW_A}\right)\right]_{ext.\ surface} S_{catalyst} = E(\Lambda_{A,\,intrapellet}) \mathfrak{R}(C_{A,\,surface}) V_{catalyst} \tag{30-46}$$

where V_{catalyst} and S_{catalyst} represent the volume and external surface area, respectively, of one catalytic pellet. At steady state, continuity of the normal component of mass flux (i.e., $\mathbf{n} \cdot \rho_A \mathbf{v}_A$) on both sides of the gas/porous-catalyst interface is invoked for reactant A:

$$\left[-\mathbf{n}\cdot\left(\frac{\mathbf{j}_{A,\text{ pellet}}}{MW_A}\right)\right]_{\text{ext. surface}} = \left[-\mathbf{n}\cdot\left(\frac{\mathbf{j}_{A,\text{ bulk gas}}}{MW_A}\right)\right]_{\text{ext. surface}} \equiv k_{A,\text{MTC}}(C_{A,\text{ bulk gas}} - C_{A,\text{ surface}}) \tag{30-47}$$

where all fluxes in (30-47) account for transport into the catalyst and convection normal to the interface is negligible. Hence, equations (30-46) and (30-47) yield:

$$k_{A,\text{MTC}}(C_{A,\text{ bulk gas}} - C_{A,\text{ surface}})S_{\text{catalyst}} = E(\Lambda_{A,\text{ intrapellet}})\mathfrak{R}(C_{A,\text{ surface}})V_{\text{catalyst}} \tag{30-48}$$

which states that the rate of interphase mass transfer of reactant A from the bulk gas phase to the external surface of the catalyst is balanced by a volumetric average of the rate of consumption of reactant A within the pellet. The presence of the effectiveness factor on the right side of (30-48) indicates that the rate of consumption of reactant A is averaged volumetrically throughout the pellet. It is not sufficient to evaluate the kinetic rate law on the external surface of a porous catalyst without including the effectiveness factor. Complex kinetic rate laws contain the molar densities of several reactants and products, as well as temperature-dependent rate constants, reaction equilibrium constants, and adsorption–desorption equilibrium constants. If the molar density of species i appears in $\mathfrak{R}$, then evaluation of this rate law on the external surface of the catalyst requires the following substitution for $C_{i,\text{ surface}}$ via equation (30-14):

$$C_{i,\text{ surface}} = C_{i,\text{ bulk gas}} + \frac{\upsilon_i k_{A,\text{MTC}}}{k_{i,\text{MTC}}}(C_{A,\text{ bulk gas}} - C_{A,\text{ surface}}) \tag{30-49}$$

where $C_{i,\text{ bulk gas}}$ is related to $C_{A,\text{ bulk gas}}$ via stoichiometry and the differential plug-flow mass balance with convection and chemical reaction via equation (4-5):

$$\frac{dC_{A,\text{ bulk gas}}}{\upsilon_A} = \frac{dC_{i,\text{ bulk gas}}}{\upsilon_i} \tag{30-50}$$

Integration of this stoichiometric relation from the feed stream (i.e., $z = 0$) to any downstream position z within the packed catalytic reactor allows one to calculate $C_{i,\text{ bulk gas}}$ as follows:

$$C_{i,\text{ bulk gas}} = C_{i,\text{ bulk gas}}(z = 0) + \upsilon_i[C_{A,\text{ bulk gas}}(z = 0) - C_{A,\text{ bulk gas}}] \tag{30-51}$$

If nonisothermal operation is an important consideration and the temperature of the bulk gas stream varies significantly in the primary flow direction (i.e., z), then

evaluation of $\mathfrak{R}$ on the external surface of a catalyst pellet requires substitution for $T_{surface}$ via equation (30-41):

$$T_{surface} = T_{bulk\ gas} - \frac{\Delta H_{reaction} k_{A,\,MTC}(C_{A,\,bulk\ gas} - C_{A,\,surface})}{h_{HTC}} \tag{30-52}$$

Now, all of the tools required to calculate the molar density of reactant A on the external surface of the catalyst are available to the reactor design engineer. It is important to realize that $C_{A,\,surface}$ is the characteristic molar density, or normalization factor, for all molar densities within the catalyst. Hence, $C_{A,\,surface}$ only appears in the expression for the intrapellet Damkohler number (i.e., excluding first-order kinetics) when isolated pellets are analyzed. Furthermore, intrapellet Damkohler numbers are chosen systematically to calculate effectiveness factors via numerical analysis of coupled sets of dimensionless differential equations. Needless to say, it was never necessary to obtain numerical values for $C_{A,\,surface}$ in Part IV of this textbook. Under realistic conditions in a packed catalytic reactor, it is necessary to (1) predict $C_{A,\,surface}$ and $T_{surface}$, (2) calculate the intrapellet Damkohler number, (3) estimate the effectiveness factor via correlation, (4) predict the average rate of reactant consumption throughout the catalyst, and (5) solve coupled ODEs to predict changes in temperature and reactant molar density within the bulk gas phase. The complete methodology is as follows:

Step 1. Use bulk conditions at the reactor inlet, $C_{A,\,bulk\ gas}(z = 0)$ and $T_{bulk\ gas}$ $(z = 0)$, to estimate the intrapellet Damkohler number $\Lambda^2_{A,\,intrapellet}$ and the corresponding effectiveness factor E via dimensionless correlations that account for catalyst geometry and the appropriate kinetic rate law (i.e., nth-order kinetics).

Step 2. Since $C_{i,\,bulk\ gas}(z = 0)$ is known via the nature of the feed stream, one should obtain an iterative solution to the following set of algebraic equations to predict $C_{A,\,surface}$, $C_{i,surface}$ and $T_{surface}$ near the reactor inlet:

$$k_{A,\,MTC}[C_{A,\,bulk\ gas}(z = 0) - C_{A,\,surface}]S_{catalyst} = E(\Lambda_{A,\,intrapellet})\mathfrak{R}(C_{A,\,surface})V_{catalyst}$$

$$C_{i,\,surface} = C_{i,\,bulk\,gas}(z = 0) + \frac{\upsilon_i k_{A,\,MTC}}{k_{i,\,MTC}}[C_{A,\,bulk\ gas}(z = 0) - C_{A,\,surface}]$$

$$T_{surface} = T_{bulk\ gas}(z = 0) - \frac{\Delta H_{reaction} k_{A,\,MTC}[C_{A,\,bulk\ gas}(z = 0) - C_{A,\,surface}]}{h_{HTC}}$$

$$\Lambda^2_{A,\,intrapellet} = \frac{k_{n,\,pseudovolumetric}(T_{surface})L^2(C_{A,\,surface})^{n-1}}{\mathfrak{D}_{A,\,effective}}$$

$$E = f(\Lambda^2_{A,\,intrapellet};\, n,\, \text{catalyst geometry})$$

$$k_{i,\mathrm{MTC}} \text{ from } \begin{cases} \mathrm{Sh}_{\mathrm{average}} = 2.0 + 1.25(\mathrm{Re}\cdot\mathrm{Sc})^{1/3} & \mathrm{Sc} \gg 1, \mathrm{Re} \longrightarrow 0 \\ \mathrm{Sh}_{\mathrm{average}} \approx 2.0 + 0.6\,\mathrm{Re}^{1/2}\cdot\mathrm{Sc}^{1/3} & \mathrm{Sc} \gg 1, \mathrm{Re\ is\ laminar} \end{cases}$$

$$h_{\mathrm{HTC}} \text{ from } \begin{cases} \mathrm{Nu}_{\mathrm{average}} = 2.0 + 1.25(\mathrm{Re}\cdot\mathrm{Pr})^{1/3} & \mathrm{Pr} \gg 1, \mathrm{Re} \longrightarrow 0 \\ \mathrm{Nu}_{\mathrm{average}} \approx 2.0 + 0.6\,\mathrm{Re}^{1/2}\cdot\mathrm{Pr}^{1/3} & \mathrm{Pr} \gg 1, \mathrm{Re\ is\ laminar} \end{cases}$$

Each iteration requires a recalculation of the intrapellet Damkohler number and the effectiveness factor at prevailing values of $C_{\mathrm{A,\,surface}}$ and T_{surface}.

Step 3. When convergence is obtained for $C_{\mathrm{A,\,surface}}$ and T_{surface} near the reactor inlet, it is possible to (a) use the current value of the effectiveness factor, (b) predict the volumetric rate of consumption of reactant A throughout the pellets, (c) employ numerical methods like the Runge–Kutta–Gill fourth-order correct integration algorithm to solve coupled mass and thermal energy balances in a gas-phase PFR:

$$q(z=0)C_{\mathrm{A,\,bulk\ gas}}(z=0)\frac{d\chi}{dV_{\mathrm{PFR}}} = (1-\varepsilon_{\mathrm{inter}})E(\Lambda_{\mathrm{A,\,intrapellet}})S_m\rho_{\mathrm{app}}\mathfrak{R}_{\mathrm{surface}}(C_{\mathrm{A,\,surface}})$$

$$q\rho_{\mathrm{total}}\langle C_{p,\,\mathrm{mixture}}\rangle\frac{dT_{\mathrm{bulk\ gas}}}{dV_{\mathrm{PFR}}} = \frac{dQ}{dV_{\mathrm{PFR}}} + (-\Delta H_{\mathrm{Rx}})(1-\varepsilon_{\mathrm{inter}}) \times E(\Lambda_{\mathrm{A,\,intrapellet}})S_m\rho_{\mathrm{app}}\mathfrak{R}_{\mathrm{surface}}(C_{\mathrm{A,\,surface}})$$

$$V_{\mathrm{PFR}} = \pi R_{\mathrm{PFR}}^2 z \qquad \chi = \frac{\omega_{\mathrm{A,\,inlet}} - \omega_{\mathrm{A}}}{\omega_{\mathrm{A,\,inlet}}} \qquad \omega_{\mathrm{A}} = \frac{\mathrm{MW_A}\,C_{\mathrm{A,\,bulk\ gas}}}{\rho_{\mathrm{total}}}$$

Boundary conditions at the reactor inlet:

$$\chi(z=0) \equiv 0, \qquad T_{\mathrm{bulk\ gas}}(z=0) = T_{\mathrm{bulk\ gas,\,inlet}}$$

and (d) calculate $C_{\mathrm{A,\,bulk\ gas}}(z=\varepsilon)$ and $T_{\mathrm{bulk\ gas}}(z=\varepsilon)$ at a small distance ε downstream from the current values of $C_{\mathrm{A,\,bulk\ gas}}$ and $T_{\mathrm{bulk\ gas}}$. This form of the dimensional PFR balances suggests that the superficial fluid velocity (i.e., $q(z=0)/\pi R_{\mathrm{PFR}}^2$) is required for heterogeneous packed catalytic tubular reactor design. However, the discussion in Chapter 22, particularly equation (22-3), favors the interstitial fluid velocity. The interpellet porosity of the packed bed is $\varepsilon_{\mathrm{inter}}$, which is equivalent to $\varepsilon_{p,\,\mathrm{interpellet}}$. The factor of $(1-\varepsilon_{\mathrm{inter}})$ must be included in the reaction rate term in both balances because:

(i) $E S_m \rho_{\mathrm{app}} \mathfrak{R}_{\mathrm{surface}}$ represents an average, over the volume of each catalytic pellet, of the rate of reactant consumption using conditions on the external surface of the pellet, with units of moles per pellet volume per time.

(ii) The plug-flow mass and thermal energy balances are based on a differential control volume for the entire packed catalytic tubular reactor (i.e., $dV_{\mathrm{PFR}} = \pi R_{\mathrm{PFR}}^2\,dz$).

(iii) Hence, the average rate of reactant consumption, with units of moles per time, is manipulated as follows:

$$E S_m \rho_{\mathrm{app}} \mathfrak{R}_{\mathrm{surface}}\,dV_{\mathrm{pellet}} = E S_m \rho_{\mathrm{app}} \mathfrak{R}_{\mathrm{surface}}(1-\varepsilon_{\mathrm{inter}})\,dV_{\mathrm{PFR}}$$

since $V_{\text{pellet}} = (1 - \varepsilon_{\text{inter}})V_{\text{PFR}}$. One of the final steps in developing the appropriate plug-flow balances is division by the size of the differential control volume, dV_{PFR}.

Step 4. As a first approximation, use values for $C_{\text{A, surface}}$ and T_{surface} based on convergence during the previous iteration in step 2, which includes the most up-to-date values of the intrapellet Damkohler number $\Lambda^2_{\text{A, intrapellet}}$ and the effectiveness factor E, and obtain an iterative solution to the following set of algebraic equations to predict $C_{\text{A, surface}}$, $C_{i,\text{surface}}$, and T_{surface} slightly downstream from their previous values:

$$k_{\text{A, MTC}}[C_{\text{A, bulk gas}}(\varepsilon) - C_{\text{A, surface}}]S_{\text{catalyst}} = E(\Lambda_{\text{A, intrapellet}})\mathfrak{R}(C_{\text{A, surface}})V_{\text{catalyst}}$$

$$C_{i,\text{ surface}} = C_{i,\text{ bulk gas}}(\varepsilon) + \frac{\upsilon_i k_{\text{A, MTC}}}{k_{i,\text{ MTC}}}[C_{\text{A, bulk gas}}(\varepsilon) - C_{\text{A, surface}}]$$

$$C_{i,\text{ bulk gas}}(\varepsilon) = C_{i,\text{ bulk gas}}(z = 0) + \upsilon_i[C_{\text{A, bulk gas}}(z = 0) - C_{\text{A, bulk gas}}(\varepsilon)]$$

$$T_{\text{surface}} = T_{\text{bulk gas}}(\varepsilon) - \frac{\Delta H_{\text{reaction}} k_{\text{A, MTC}}[C_{\text{A, bulk gas}}(\varepsilon) - C_{\text{A, surface}}]}{h_{\text{HTC}}}$$

$$\Lambda^2_{\text{A, intrapellet}} = \frac{k_{n,\text{ pseudovolumetric}}(T_{\text{surface}})L^2(C_{A,\text{ surface}})^{n-1}}{\mathfrak{D}_{\text{A, effective}}}$$

$$E = f(\Lambda^2_{\text{A, intrapellet}}; n, \text{catalyst geometry})$$

$$k_{i,\text{MTC}} \text{ from } \begin{cases} \text{Sh}_{\text{average}} = 2.0 + 1.25(\text{Re}\cdot\text{Sc})^{1/3} & \text{Sc} \gg 1, \text{Re} \longrightarrow 0 \\ \text{Sh}_{\text{average}} \approx 2.0 + 0.6\,\text{Re}^{1/2}\cdot\text{Sc}^{1/3} & \text{Sc} \gg 1, \text{Re is laminar} \end{cases}$$

$$h_{\text{HTC}} \text{ from } \begin{cases} \text{Nu}_{\text{average}} = 2.0 + 1.25(\text{Re}\cdot\text{Pr})^{1/3} & \text{Pr} \gg 1, \text{Re} \longrightarrow 0 \\ \text{Nu}_{\text{average}} \approx 2.0 + 0.6\,\text{Re}^{1/2}\cdot\text{Pr}^{1/3} & \text{Pr} \gg 1, \text{Re is laminar} \end{cases}$$

Once again, each iteration requires a recalculation of the intrapellet Damkohler number and the effectiveness factor at prevailing values of $C_{\text{A, surface}}$ and T_{surface}.

Step 5. Repeat steps 3 and 4 in typical Runge–Kutta–Gill fashion and march through the packed catalytic tubular reactor from inlet to outlet.

30-4 REACTOR DESIGN

30-4.1 Ideal Isothermal Packed Catalytic Tubular Reactors with First-Order Irreversible Chemical Kinetics When the External Resistance to Mass Transfer Cannot Be Neglected

If the enthalpy change due to chemical reaction is insignificant and temperature changes throughout the reactor can be neglected, then the design strategy discussed above is simplified greatly because the thermal energy balance is not required. Furthermore, the only molar density of interest is C_{A}, which appears in the plug-flow mass balance and the kinetic rate law. At high-mass-transfer

Peclet numbers, where interpellet axial dispersion is negligible, the equations of interest are

$$q(z=0)C_{\text{A, bulk gas}}(z=0)\frac{d\chi}{dV_{\text{PFR}}} = (1-\varepsilon_{\text{inter}})E(\Lambda_{\text{A, intrapellet}})S_m\rho_{\text{app}}\mathfrak{R}_{\text{surface}}(C_{\text{A, surface}})$$
$$\chi = \frac{\omega_{\text{A, inlet}}-\omega_{\text{A}}}{\omega_{\text{A, inlet}}} \qquad \omega_{\text{A}} = \frac{\text{MW}_{\text{A}}\,C_{\text{A, bulk gas}}}{\rho_{\text{total}}} \qquad \chi(V_{\text{PFR}}=0)\equiv 0 \tag{30-53}$$

Integration of the plug-flow mass balance is not possible until one equates the rate of mass transfer of reactant A from the bulk fluid phase toward the external surface of the catalyst and the volumetrically averaged rate of reactant consumption within the porous pellet via equation (30-48):

$$k_{\text{A, MTC}}(C_{\text{A, bulk gas}}-C_{\text{A, surface}})S_{\text{catalyst}} = E(\Lambda_{\text{A, intrapellet}})\mathfrak{R}(C_{\text{A, surface}})V_{\text{catalyst}} \tag{30-54}$$

This provides a relation between bulk gas and surface molar densities of reactant A. If the kinetics are first-order and irreversible, then:

$$\mathfrak{R}(C_{\text{A, surface}}) = S_m\rho_{\text{app}}\mathfrak{R}_{\text{surface}}(C_{\text{A, surface}}) = S_m\rho_{\text{app}}k_{1,\text{ surface}}C_{\text{A, surface}} \tag{30-55}$$

where $k_{1,\text{ surface}}$ is a reaction velocity constant with dimensions of length/time. Hence, one uses equations (30-54) and (30-55) to calculate $C_{\text{A, surface}}$ in terms of $C_{\text{A, bulk gas}}$ and then expresses the kinetic rate law in terms of $C_{\text{A, bulk gas}}$ prior to integration of the plug-flow mass balance in (30-53). The first step is accomplished as follows:

$$k_{\text{A, MTC}}(C_{\text{A, bulk gas}}-C_{\text{A, surface}})S_{\text{catalyst}} = E\,S_m\rho_{\text{app}}k_{1,\text{ surface}}C_{\text{A, surface}}V_{\text{catalyst}} \tag{30-56}$$

Since the kinetics are first-order, a simple analytical solution to equation (30-56) is obtained for $C_{\text{A, surface}}$:

$$C_{\text{A, surface}} = \phi C_{\text{A, bulk gas}} \qquad \phi = \frac{1}{1+\beta}$$
$$\beta = \frac{E(\Lambda_{\text{A, intrapellet}})S_m\rho_{\text{app}}k_{1,\text{ surface}}V_{\text{catalyst}}}{k_{\text{A, MTC}}S_{\text{catalyst}}} \tag{30-57}$$

Notice that $\beta \to 0$, $\phi \to 1$, and $C_{\text{A, surface}} \to C_{\text{A, bulk gas}}$ in the reaction-controlled regime, where

$$E(\Lambda_{\text{A, intrapellet}})S_m\rho_{\text{app}}k_{1,\text{ surface}}V_{\text{catalyst}} \ll k_{\text{A, MTC}}S_{\text{catalyst}} \tag{30-58}$$

This suggests that external mass transfer resistance is not very important for (1) low rates of reactant conversion, (2) small catalytic pellets with large external surface-to-volume ratios, and (3) high gas-phase flow rates through the packed

bed. Since bulk and surface molar densities of all species are dimensionalized by the inlet molar density of reactant A, $C_{A,\,inlet}$,

$$\Psi_{A,\,surface} = \frac{C_{A,\,surface}}{C_{A,\,inlet}}$$
$$\Psi_{A,\,bulk\ gas} = \frac{C_{A,\,bulk\ gas}}{C_{A,\,inlet}} \tag{30-59}$$

the one-dimensional mass transfer equation given by (30-53), which neglects interpellet axial dispersion at high-mass-transfer Peclet numbers, is written completely in terms of $\Psi_{A,\,bulk\ gas}$. The dimensionless equations for first-order chemical kinetics are essentially the same as (22-19), (22-24), (22-25), and (30-57):

$$\begin{aligned} \mathrm{Re}\cdot\mathrm{Sc}\frac{d\Psi_{A,\,bulk\ gas}}{d\zeta} &= -\Lambda^2_{A,\,interpellet}(1-\varepsilon_{p,\,interpellet})E(\Lambda_{A,\,intrapellet})\Psi_{A,\,surface} \\ \Psi_{A,\,surface} &= \phi\Psi_{A,\,bulk\ gas} \\ \Psi_{A,\,bulk\ gas}(\zeta=0) &= 1 \end{aligned} \tag{30-60}$$

Separation of variables provides the analytical solution to this first-order ODE given by (30-60). When the external resistance to mass transfer is significant, the following result allows one to predict reactant conversion in the exit stream as a function of important design parameters based on isolated pellets as well as the entire packed catalytic tubular reactor:

$$\chi_{final} \equiv 1 - \Psi_{A,\,bulk\ gas}(\zeta=1) = 1 - \exp(-\kappa)$$

where

$$\kappa = \frac{(1-\varepsilon_{inter})\phi\Lambda^2_{A,\,interpellet}E(\Lambda_{A,\,intrapellet})}{\mathrm{Re}\cdot\mathrm{Sc}} \tag{30-61}$$

Parametric changes that increase κ lead to higher conversion of reactant gas A without increasing the reactor volume, if residence time τ remains constant. As ϕ approaches unity, equation (30-61) correctly predicts greater conversion of reactants to products when external mass transfer resistance is minimized. This is reasonable because a volumetric average of the rate of reactant consumption throughout the pellets is evaluated using the effectiveness factor and the kinetic rate law based on conditions near the external catalytic surface. As the external resistance to mass transfer decreases, reactant molar densities near the external catalytic surface increase and approach those in the bulk gas phase. In most cases, when kinetic rate laws are evaluated at higher reactant molar densities, one achieves greater reactant-to-product conversion rates.

30-4.2 Ideal and Non-Ideal Packed Catalytic Tubular Reactors under Isothermal Conditions with Second-Order Irreversible Chemical Kinetics When the External Resistance to Mass Transfer Is Significant

If the kinetics are nth-order and irreversible in terms of the molar density of reactant A only, then equation (30-54) and a slight modification of (30-55) must

be solved to relate $C_{\text{A, surface}}$ and $C_{\text{A, bulk gas}}$:

$$\beta(C_{\text{A, surface}})^n + C_{\text{A, surface}} - C_{\text{A, bulk gas}} = 0 \tag{30-62}$$

where

$$\beta = \frac{E(\Lambda_{\text{A, intrapellet}})S_m \rho_{\text{app}} k_{n,\text{ surface}} V_{\text{catalyst}}}{k_{\text{A, MTC}} S_{\text{catalyst}}}$$

The parameter β has dimensions of (volume/mol)$^{n-1}$ because $S_m \rho_{\text{app}} k_{n,\text{ surface}}$ is a pseudo-volumetric nth-order kinetic rate constant with units of (volume/mol)$^{n-1}$/time. In dimensionless notation, equation (30-62) yields the following nonlinear polynomial that relates the molar densities of reactant A in the bulk gas stream and at the external surface of the catalyst:

$$\alpha(\Psi_{\text{A, surface}})^n + \Psi_{\text{A, surface}} - \Psi_{\text{A, bulk gas}} = 0 \tag{30-63}$$

where $\alpha = \beta(C_{\text{A, inlet}})^{n-1}$. For example, when $n = 2$, application of the quadratic formula yields the following solution to equation (30-63):

$$\Psi_{\text{A, surface}} = \frac{-1 + \sqrt{1 + 4\alpha\Psi_{\text{A, bulk gas}}}}{2\alpha} \tag{30-64}$$

which reduces to $\Psi_{\text{A, surface}} = \Psi_{\text{A, bulk gas}}$ via l'Hôpital's rule if the external resistance to mass transfer is negligible (i.e., $\alpha = 0$ and $\beta = 0$). Equation (30-64) for $\Psi_{\text{A, surface}}$ is needed in the ideal and non-ideal PFR design equations to calculate the rate of conversion of reactants to products via molar densities on the external surface of the catalyst, together with the effectiveness factor. The methodology and results are presented below in Tables 30-1 and 30-2 at various mass transfer Peclet numbers. The performance of an ideal plug-flow tubular reactor with second-order irreversible chemical kinetics and significant external mass transfer resistance is described by

$$\begin{aligned}
&\text{Re}\cdot\text{Sc}\frac{d\Psi_{\text{A, bulk gas, ideal}}}{d\zeta} \\
&\quad = -\Lambda^2_{\text{A, interpellet}}(1 - \varepsilon_{p,\text{ interpellet}})E(\Lambda_{\text{A, intrapellet}})(\Psi_{\text{A, surface, ideal}})^2 \\
&\Psi_{\text{A, surface, ideal}} = \frac{-1 + \sqrt{1 + 4\alpha\Psi_{\text{A, bulk gas, ideal}}}}{2\alpha} \\
&\Psi_{\text{A, bulk gas, ideal}} = 1 \text{ at } \zeta = 0
\end{aligned} \tag{30-65}$$

When interpellet axial dispersion is important at low-mass-transfer Peclet numbers, the following set of coupled first-order ODEs must be analyzed together with the supporting explicit algebraic equation for $\Psi_{\text{A, surface}}$:

$$\frac{d\Psi_{\text{A, bulk gas, real}}}{d\zeta} = Z$$

$$\frac{dZ}{d\zeta} = \text{Re}\cdot\text{Sc}\cdot Z + \Lambda^2_{\text{A, interpellet}}(1 - \varepsilon_{p,\text{ interpellet}})E(\Lambda_{\text{A, intrapellet}})(\Psi_{\text{A, surface, real}})^2$$

$$\Psi_{\text{A, surface, real}} = \frac{-1 + \sqrt{1 + 4\alpha\Psi_{\text{A, bulk gas, real}}}}{2\alpha} \tag{30-66}$$

$$\Psi_{\text{A, bulk gas, real}} = 1 \text{ at } \zeta = 0$$

$$d\Psi_{\text{A, bulk gas, real}}/d\zeta \to 0 \text{ at } \zeta \to 1$$

In a closed–closed tubular reactor with no axial dispersion or radial variations in molar density upstream and downstream from the packed section of catalytic pellets, Bischoff (1961) has proved rigorously that the Danckwerts boundary condition (Danckwerts, 1953) at the reactor inlet is

$$\Psi_{\text{A, bulk gas, real}} - \frac{1}{\text{Re}\cdot\text{Sc}}\left(\frac{d\Psi_{\text{A, bulk gas, real}}}{d\zeta}\right) = 1 \qquad \text{at } \zeta = 0 \tag{30-67}$$

which was also employed by Langmuir (1908). Hiby (1962, p. 312) has demonstrated that there is no true back mixing in packed beds, and Wicke (1975) suggests that molecular diffusion across the inlet plane at $\zeta = 0$ is negligible even at low-mass-transfer Peclet numbers. Hence, it is reasonable to let $\Psi_{\text{A, bulk gas, real}} = 1$ at $\zeta = 0$ in packed catalytic tubular reactors, realizing that all possible boundary conditions at the reactor inlet yield similar conversion in the exit stream at high-mass-transfer Peclet numbers. As illustrated in Section 22-4.1, instabilities arise during numerical integration of the two coupled ODEs that describe steady-state convection, interpellet axial dispersion, and nth-order irreversible chemical reaction for certain combinations of the interpellet Damkohler number and the mass transfer Peclet number. Hence, it might be best to guess the outlet bulk molar density of reactant A and integrate the non-ideal plug-flow mass transfer equation backwards, from outlet to inlet, until convergence is obtained at $\zeta = 0$, where $\Psi_{\text{A, bulk gas, real}} = 1$. This is accomplished in practice by defining a new independent spatial variable $\xi = 1 - \zeta$, which increases as one moves toward the reactor inlet, and introducing a negative sign in each term on the right side of both coupled first-order ODEs in (30-66) that represent the one-dimensional mass balance.

The important dimensionless parameter that determines the significance of external mass transfer resistance for nth-order irreversible chemical kinetics in packed catalytic tubular reactors was introduced in equation (30-63) as $\alpha = \beta(C_{\text{A, inlet}})^{n-1}$. Simple algebraic manipulation allows one to relate α to the interpellet Damkohler number, the effectiveness factor, the mass transfer Peclet number, and a few other dimensionless parameters. For example, let the coefficient of the chemical reaction term in the dimensionless mass transfer equation be defined as follows:

$$\text{chem. Rx coeff.} \equiv \Lambda^2_{\text{A, interpellet}}(1 - \varepsilon_{p,\text{ interpellet}})E(\Lambda_{\text{A, intrapellet}}) \tag{30-68}$$

The numerator of α contains $S_m\rho_{\text{app}}k_{\text{n, surface}}(C_{\text{A, inlet}})^{n-1}$, which also appears in the numerator of the interpellet Damkohler number, as defined by equation (22-7):

$$\Lambda^2_{\text{A, interpellet}} = \frac{S_m\rho_{\text{app}}k_{n,\text{ surface}}(C_{\text{A, inlet}})^{n-1}L^2_{\text{PFR}}}{\mathfrak{D}_{\text{A, interpellet}}} \tag{30-69}$$

Hence,

$$\alpha = \frac{V_{\text{catalyst}}}{S_{\text{catalyst}}} \frac{E(\Lambda_{\text{A, intrapellet}})\Lambda^2_{\text{A, interpellet}}\mathfrak{D}_{\text{A, interpellet}}}{k_{\text{A, MTC}}L^2_{\text{PFR}}} \tag{30-70}$$

In terms of the coefficient of the chemical reaction term in the dimensionless mass transfer equation, which represents one of the independent parameters that strongly influences the simulation of non-ideal packed catalytic tubular reactors:

$$\alpha = \frac{V_{\text{catalyst}}}{S_{\text{catalyst}}} \frac{\{\text{chem. Rx coeff.}\}\mathfrak{D}_{\text{A, interpellet}}}{k_{\text{A, MTC}}L^2_{\text{PFR}}(1-\varepsilon_{p,\text{interpellet}})} \tag{30-71}$$

The interphase mass transfer coefficient of reactant A (i.e., $k_{\text{A, MTC}}$), in the gas-phase boundary layer external to porous solid pellets, scales as $\text{Sc}^{1/3}$ for flow adjacent to high-shear no-slip interfaces, where the Schmidt number (i.e., Sc) is based on ordinary molecular diffusion. In the creeping flow regime, $k_{\text{A, MTC}}$ is calculated from the following Sherwood number correlation for interphase mass transfer around solid spheres (see equation 11-121 and Table 12-1):

$$\text{Sh}_{\text{average}} \equiv \frac{k_{\text{A, MTC}}(6V_{\text{catalyst}}/S_{\text{catalyst}})}{\mathfrak{D}_{\text{A, ordinary}}} \approx 2 + C_1(\text{Pe}_{\text{simple}})^{1/3} \tag{30-72}$$

where the coefficient C_1 is very close to unity, the leading term (i.e., 2) from stagnant film theory is negligible relative to the flow-related term, both $\text{Sh}_{\text{average}}$ and $\text{Pe}_{\text{simple}}$ are based on ordinary molecular diffusion, and the characteristic length in both of these dimensionless numbers is the equivalent diameter of a single porous pellet, defined by $d_{\text{equivalent}} = 6V_{\text{catalyst}}/S_{\text{catalyst}}$. For laminar flow, the exponent of the Reynolds number in equation (30-72) is $\frac{1}{2}$, and this exponent increases to 0.8 to 1 for turbulent flow. The following expression for α in (30-74) and (30-76) is exact in the creeping flow regime only. Reactor length L_{PFR} in equation (30-71) is replaced by the mass transfer Peclet number, which accounts for interpellet axial dispersion (see equation 22-88):

$$\text{Pe}_{\text{MT}} = \frac{L_{\text{PFR}}}{\phi_{\text{correlation}}\, d_{\text{equivalent}}} \tag{30-73}$$

These substitutions yield

$$\alpha = \frac{\{\text{chem. Rx coeff.}\}(\mathfrak{D}_{\text{A, interpellet}}/\mathfrak{D}_{\text{A, ordinary}})}{6\phi^2_{\text{correlation}}(1-\varepsilon_{p,\text{interpellet}})(\text{Pe}_{\text{simple}})^{1/3}(\text{Pe}_{\text{MT}})^2} \tag{30-74}$$

Analysis of experimental data for interpellet axial dispersion in packed beds has generated the following empirical correlation, as described by equation (22-84) and Table 22-6:

$$\frac{\mathfrak{D}_{\text{A, interpellet}}}{\mathfrak{D}_{\text{A, ordinary}}} \approx \phi_{\text{correlation}}\text{Pe}_{\text{simple}} \tag{30-75}$$

where $\phi_{\text{correlation}}$ is either 1 or 2, depending on the magnitude of $\text{Pe}_{\text{simple}}$. Hence,

$$\alpha = \frac{\{\text{chem. Rx coeff.}\}(\text{Pe}_{\text{simple}})^{2/3}}{6\phi_{\text{correlation}}(1-\varepsilon_{p,\text{interpellet}})(\text{Pe}_{\text{MT}})^2} \tag{30-76}$$

Simulations are provided below as a function of Pe_{MT}, when the chemical reaction coefficient and $\text{Pe}_{\text{simple}}$ remain constant. The importance of interpellet axial dispersion and external mass transfer resistance decreases at higher mass transfer Peclet numbers. Simulations for real and ideal PFRs are presented in Table 30-1. These results illustrate how the outlet conversion in ideal and non-ideal packed catalytic tubular reactors with significant external mass transfer resistance is governed by competing effects, both of which depend on the mass transfer Peclet number. For example, in Table 30-1, the dimensionless outlet molar density of reactant A decreases as Pe_{MT} increases from 0.5 to 6, when the interpellet Damkohler number remains constant and $\alpha \neq 0$. When Pe_{MT} is greater than 6, the molar density of reactant A in the exit stream increases. The ratio of $\Lambda^2_{\text{A, interpellet}}$ to Pe_{MT} is equivalent to τ/ω, which decreases as one moves from left to right in Table 30-1. Under these conditions in the absence of external mass transfer resistance, one achieves less conversion of reactants to products because the residence time decreases. This trend is observed for the dimensionless outlet molar density of reactant A in ideal and non-ideal tubular reactors for all mass transfer Peclet numbers when $\alpha = 0$. However, the external resistance to mass

TABLE 30-1 Effect of the Mass Transfer Peclet Number on Dimensionless Reactant Molar Densities in the Bulk Fluid Phase and Near the External Surface of the Catalytic Pellets in Real and Ideal Heterogeneous Packed Catalytic Tubular Reactors[a]

chem. Rx coeff. $= \Lambda^2_{\text{A, interpellet}}(1-\varepsilon_{p,\text{interpellet}})E(\Lambda_{\text{A, intrapellet}}) = 5$

$\text{Pe}_{\text{simple}} = \dfrac{\langle v_z\rangle_{\text{interstitial}} d_{\text{equivalent}}}{\mathfrak{D}_{\text{A, ordinary}}} = 50 \qquad (\text{Re}\cdot\text{Sc})_{\text{critical}} = 30$

$\phi_{\text{correlation}} = 1 \qquad \varepsilon_{p,\text{interpellet}} = 0.5 \qquad n = 2$

	$\text{Re}\cdot\text{Sc} = \text{Pe}_{\text{MT}}$						
	0.5	1	2	3	6	8	10
$\alpha = \beta C_{\text{A, bulk gas}}(z=0)$	90.48	22.62	5.655	2.513	0.628	0.353	0.226
$\Psi_{\text{A, surface}}(\zeta=0)$	0.0997	0.189	0.341	0.462	0.696	0.783	0.840
$\Psi_{\text{A, surface, ideal}}(\zeta=1)$	0.0947	0.172	0.287	0.370	0.523	0.588	0.638
$\Psi_{\text{A, bulk gas, ideal}}(\zeta=1)$	0.905	0.837	0.754	0.713	0.694	0.710	0.730
$\Psi_{\text{A, bulk gas, ideal}}(\zeta=1;\alpha=0)$	0.091	0.167	0.286	0.375	0.545	0.615	0.667
$-(d\Psi_{\text{A, bulk gas, real}}/d\zeta)_{\zeta=0}$	0.0385	0.1086	0.2316	0.3061	0.3689	0.3576	0.3341
$\Psi_{\text{A, surface, real}}(\zeta=1)$	0.0986	0.183	0.311	0.400	0.554	0.615	0.661
$\Psi_{\text{A, bulk gas, real}}(\zeta=1)$	0.979	0.937	0.856	0.801	0.747	0.749	0.760
$\Psi_{\text{A, bulk gas, real}}(\zeta=1;\alpha=0)$	0.424	0.447	0.489	0.528	0.620	0.666	0.703

[a] With and without significant external mass transfer resistance. The chemical kinetics are second-order and irreversible.

transfer cannot be neglected at low values of Pe_{MT}. The rather large difference between reactant molar densities in the bulk gas stream and those on the external surface of the catalytic pellets supports this claim.

Reactor performance is extremely poor at low values of Pe_{MT} because kinetic rate laws are evaluated at low surface molar densities of the reactants. This problem in the design of packed catalytic tubular reactors is corrected somewhat when Pe_{MT} increases, because α decreases and the external resistance to mass transfer becomes less significant. Hence, one achieves higher conversion of reactants to products at shorter residence times, over a restricted range of Pe_{MT}, because α scales as $(Pe_{MT})^{-2}$, whereas τ/ω scales as $(Pe_{MT})^{-1}$. As one moves from left to right in Table 30-1 at low values of Pe_{MT}, the external resistance to mass transfer decreases more abruptly than τ/ω decreases, and the thickness of the gas-phase mass transfer boundary layer governs the performance of a packed catalytic tubular reactor. At larger values of Pe_{MT} where α is small and external resistance is not very important, reactor performance is governed by the convective mass transfer rate process. Now, the primary consequence of an increase in Pe_{MT} is that τ/ω decreases, and one achieves less conversion of reactants to products.

The highest conversion of reactants to products is achieved in an ideal PFR with no external mass transfer resistance. However, all simulations in Table 30-1 for ideal tubular reactors are not justified because one is operating at mass transfer Peclet numbers that are three- to sixty-fold smaller than $(Re{\cdot}Sc)_{critical}$. The only valid simulations in Table 30-1 are those which include interpellet axial dispersion and significant external mass transfer resistance, because $Pe_{MT} < (Re{\cdot}Sc)_{critical}$ and reactant molar densities near the external surface of the catalytic pellets are less than those in the bulk fluid phase. In general, external resistance to mass transfer reduces reactant molar densities on the catalytic surface, decreases the rate of conversion of reactants to products, and requires longer PFRs to achieve the same final conversion relative to the case where $\alpha = 0$.

30-5 MAXIMUM CONVERSION IN NON-IDEAL PACKED CATALYTIC TUBULAR REACTORS UNDER ISOTHERMAL CONDITIONS

Quantitative results in Table 30-1 reveal that one achieves maximum conversion of reactants to products in ideal (i.e., 30%) and non-ideal (i.e., 25%) packed catalytic tubular reactors when the mass transfer Peclet number is approximately 6 for second-order irreversible chemical kinetics with an interpellet porosity of 50%. Specific values for Pe_{MT} and the corresponding maximum conversion are sensitive to the simple mass transfer Peclet number and the chemical reaction coefficient, where the latter is defined by the product of the effectiveness factor, the interpellet Damkohler number, and the catalyst filling factor. For example, when Pe_{simple} is 50 and the chemical reaction coefficient is 5 for second-order irreversible chemical kinetics, the critical value of Pe_{MT} [i.e., $(Re{\cdot}Sc)_{critical}$] is approximately 30, whereas maximum conversion is obtained when Pe_{MT} is only 6. Hence, one concludes that the ideal simulations in Table 30-1 with $\alpha \neq 0$,

which yield a maximum conversion of 30%, are not justified because one must operate above $(\text{Re}\cdot\text{Sc})_{\text{critical}}$ to achieve ideal performance. Hence, optimum reactor performance, which yields maximum conversion of reactants to products, might occur under non-ideal conditions when external mass transfer resistance is significant. One observes empirically that the simulations presented in Table 30-1 are not influenced much by reaction order n for simple nth-order kinetics. Results presented in Table 30-2 summarize the dependence of Pe_{MT} on the simple mass transfer Peclet number and the chemical reaction coefficient for first-order irreversible chemical kinetics, such that one achieves maximum conversion of reactants to products. In each case, the critical value of the mass transfer Peclet number is included in Table 30-2 to emphasize the fact that values of Pe_{MT}

TABLE 30-2 Combinations of $\text{Pe}_{\text{simple}}$, Pe_{MT}, and the Chemical Reaction Coefficient That Yield Maximum Conversion of Reactants to Products in Non-Ideal Packed Catalytic Tubular Reactors[a]

chem. Rx coeff. $= \Lambda^2_{\text{A, interpellet}}(1 - \varepsilon_{p,\text{ interpellet}})E(\Lambda_{\text{A, intrapellet}})$

$\text{Pe}_{\text{simple}} = \dfrac{\langle v_z\rangle_{\text{interstitial}} d_{\text{equivalent}}}{\mathfrak{D}_{\text{A, ordinary}}}$ $\qquad$ $\text{Pe}_{\text{MT}} = \dfrac{L_{\text{PFR}}}{\phi_{\text{correlation}} d_{\text{equivalent}}}$

$\varepsilon_{p,\text{ interpellet}} = 0.5 \qquad n = 1$

$\text{Pe}_{\text{simple}}$	$\phi_{\text{correlation}}$	Pe_{MT}	Maximum Conversion (%)	α
	chem. Rx coeff. $= 1$		$(Re\cdot Sc)_{\text{critical}} = 15$	
1	1	1.5	23	0.15
10	1	2.0	18	0.39
50	1	3.2	14	0.44
100	1	3.7	12	0.52
250	2	4.7	10	0.30
500	2	5.7	8	0.32
	chem. Rx coeff. $= 20$		$(Re\cdot Sc)_{\text{critical}} = 71$	
1	1	5	85	0.27
10	1	8	73	0.48
50	1	11	59	0.75
100	1	14	52	0.73
250	2	18	43	0.41
500	2	22	37	0.43
	chem. Rx coeff. $= 100$		$(Re\cdot Sc)_{\text{critical}} = 176$	
1	1	10	99	0.33
10	1	18	95	0.48
50	1	24	87	0.79
100	1	27	82	0.99
250	2	28	83	0.84
500	2	48	65	0.46

[a]With first-order irreversible chemical kinetics and significant external mass transfer resistance.

where maximum conversion occurs are subcritical. This is consistent with the inclusion of interpellet axial dispersion in these simulations. Furthermore, the volumetrically averaged rate of conversion of reactants to products must be calculated using molar densities near the external surface of the catalytic pellets, not molar densities in the bulk fluid phase, because $\alpha \neq 0$.

As mentioned above, all 18 examples in Table 30-2 reveal that maximum conversion is obtained under non-ideal conditions, where interpellet axial dispersion must be included in the design simulations. Maximum conversion increases at larger chemical reaction coefficients and smaller simple Peclet numbers. The corresponding value of Pe_{MT}, which yields maximum conversion, increases at larger chemical reaction coefficients and larger values of Pe_{simple}. These trends are illustrated in Figures 30-1, 30-2, and 30-3. When the chemical reaction coefficient remains constant, the presence of both interpellet axial dispersion and external mass transfer resistance in tubular reactor simulations reveals that higher conversion of reactants to products is achieved at shorter residence times, over a restricted range of mass transfer Peclet numbers. Furthermore, non-ideal reactors perform better than ideal reactors, based on the conditions required to achieve maximum conversion, because the ideal reactor simulations are not valid at subcritical mass transfer Peclet numbers. These nontraditional results are attributed to the analysis of external mass transfer resistance in packed catalytic tubular reactors. For example, if external mass transfer resistance is neglected, then reactor performance is predicted from the simulations in Figure 22-2, which should be compared with the more accurate results in Figures 30-1, 30-2, and 30-3.

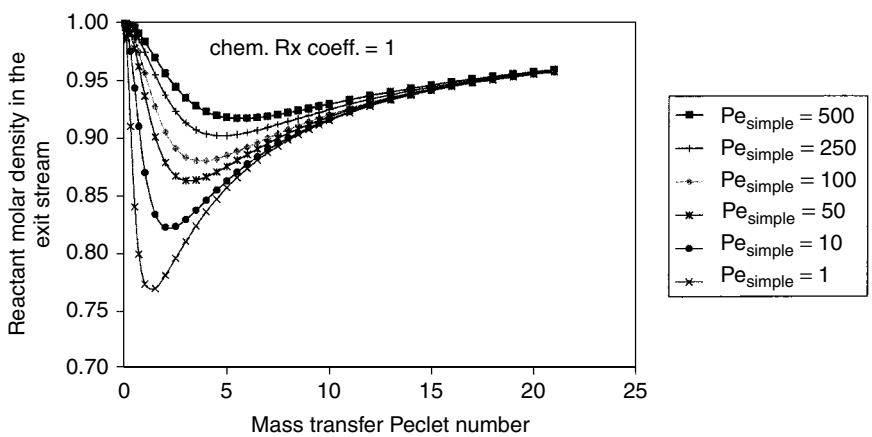

Figure 30-1 Effect of the mass transfer Peclet number and Pe_{simple} on dimensionless reactant molar density in the exit stream of a non-ideal packed catalytic tubular reactor with first-order irreversible chemical kinetics and significant external mass transfer resistance. The product of the interpellet Damkohler number, the effectiveness factor, and the catalyst filling factor is 1.

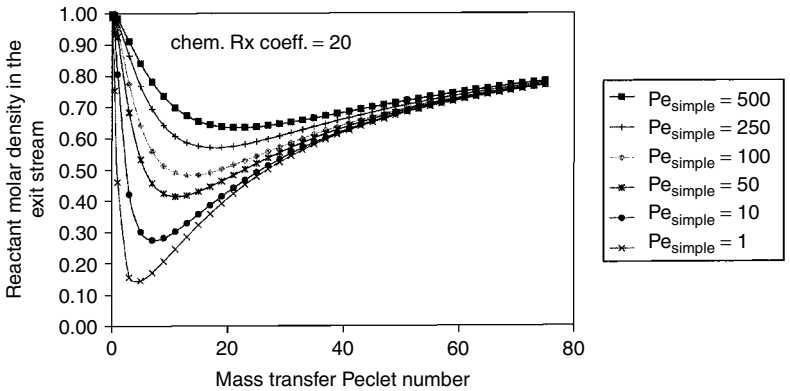

Figure 30-2 Effect of the mass transfer Peclet number and Pe_{simple} on dimensionless reactant molar density in the exit stream of a non-ideal packed catalytic tubular reactor with first-order irreversible chemical kinetics and significant external mass transfer resistance. The product of the interpellet Damkohler number, the effectiveness factor, and the catalyst filling factor is 20.

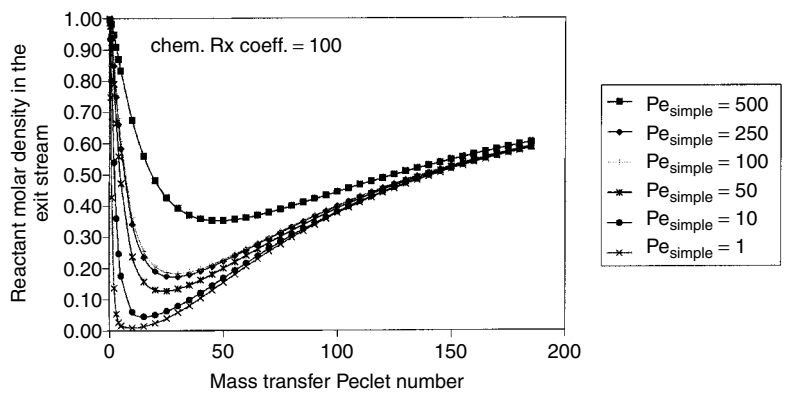

Figure 30-3 Effect of the mass transfer Peclet number and Pe_{simple} on dimensionless reactant molar density in the exit stream of a non-ideal packed catalytic tubular reactor with first-order irreversible chemical kinetics and significant external mass transfer resistance. The product of the interpellet Damkohler number, the effectiveness factor, and the catalyst filling factor is 100.

30-6 ANALYSIS OF FIRST-ORDER IRREVERSIBLE CHEMICAL KINETICS IN IDEAL PACKED CATALYTIC TUBULAR REACTORS WHEN THE EXTERNAL RESISTANCES TO HEAT AND MASS TRANSFER CANNOT BE NEGLECTED

This example summarizes all the tools (i.e., ODEs and supporting algebraic equations) that are required to design a plug-flow reactor at high mass and heat

transfer Peclet numbers when reactants are consumed by first-order irreversible kinetics on the internal surface of spherical catalytic pellets. The calculations presented below are specific to the production of methanol from a stoichiometric feed of CO and H_2. Carbon monoxide is chosen as reactant gas A. Linearization of the reversible kinetic rate law via the methodology on pages 575–576 yields a pseudo-volumetric first-order kinetic rate constant of $\approx 7\ \text{min}^{-1}$ at 325 K and 30 atm total pressure when all adsorption/desorption equilibrium contants are $0.25(\text{atm})^{-1}$. For simplicity, the effectiveness factor is calculated analytically via the classic isothermal expression in spherical coordinates. The reactor is not insulated from the surroundings. The cgs system of units is employed for all these calculations.

$$R_{\text{PFR}} = 10\ \text{cm}\ (\text{radius of the packed catalytic reactor})$$

$$V_{\text{PFR}} = \pi R_{\text{PFR}}^2 z\ (\text{volume of the packed catalytic reactor, cm}^3)$$

$$R_{\text{pellet}} = 0.5\ \text{cm}\ (\text{radius of each porous catalytic pellet})$$

$$S_{\text{catalyst}} = 4\pi R_{\text{pellet}}^2\ (\text{external surface area of each spherical catalytic pellet, cm}^2)$$

$$V_{\text{catalyst}} = \tfrac{4}{3}\pi R_{\text{pellet}}^3\ (\text{volume of each spherical catalytic pellet, cm}^3)$$

$$\langle r_{\text{average}} \rangle = 10^{-6}\ \text{cm}\ (\text{average pore radius, } 1\ \mu\text{m} = 10^{-4}\ \text{cm})$$

$$\varepsilon_{\text{intra}} = 0.6\ (\text{intrapellet porosity or void volume fraction for each catalytic pellet, dimensionless})$$

$$\varepsilon_{\text{inter}} = 0.35\ (\text{interpellet porosity, void volume fraction for the entire packed reactor, dimensionless})$$

$$S_m \rho_{\text{app}} = \frac{2\varepsilon_{\text{intra}}}{\langle r_{\text{average}} \rangle}\ (\text{internal catalytic surface area/volume of pellet, cm}^{-1})$$

$$\tau_{\text{or}} = 2\ (\text{tortuosity factor for randomly oriented pores, dimensionless})$$

$$\omega_{\text{A, inlet}} = 0.875\ (\text{inlet mass fraction of carbon monoxide for a stoichiometric feed of CO and } H_2\text{, dimensionless})$$

$$\chi_{\text{initial}} = 0\ (\text{inlet condition for the conversion of CO to products, dimensionless})$$

$$\omega_{\text{A}} = \omega_{\text{A, inlet}}(1 - \chi)\ (\text{relation between mass fraction and conversion of CO})$$

$$\text{MW}_{\text{A}} = 28\ \text{da.}\ (\text{molecular weight of CO})$$

$\mathrm{MW_B} = 2$ da. (molecular weight of H_2)

$\mathrm{MW_C} = 32$ da. (molecular weight of CH_3OH)

$\omega_B = 0.125\,(1 - \chi)$ (mass fraction of H_2 via equation 3-10)

$\omega_C = \chi$ (mass fraction of CH_3OH via equation 3-10)

$1/\mathrm{MW_{mix}} = \sum_{i=\mathrm{A,B,C}} (\omega_i/\mathrm{MW}_i)$ (average molecular weight of the mixture)

$T_{\mathrm{inlet}} = 510$ K (inlet condition for the temperature of the bulk gas)

$T_{\mathrm{ambient}} = 295$ K (ambient temperature outside of the packed catalytic reactor)

$\sigma = 3.6$ Å (Lennard-Jones collision diameter for CO with $\mathrm{MW_A} = 28$)

$p = 30$ atm (total gas pressure)

$R_{\mathrm{gas}} = 82.057\ \mathrm{cm^3{\cdot}atm/mol{\cdot}K} = 1.987\ \mathrm{cal/mol{\cdot}K} = 8.3144 \times 10^7\ \mathrm{g{\cdot}cm^2/s^2{\cdot}mol{\cdot}K}$

$$\rho_{\mathrm{gas}} = \frac{p\mathrm{MW_{mix}}}{R_{\mathrm{gas}} T_{\mathrm{bulk\ gas}}}$$ (ideal gas density via equation of state, $\mathrm{g/cm^3}$)

$$C_{\mathrm{A,\ bulk\ gas}} = \frac{\rho_{\mathrm{gas}}\omega_{\mathrm{A}}}{\mathrm{MW_A}}$$ (molar density of ideal reactant gas A, $\mathrm{mol/cm^3}$)

$$\rho_{\mathrm{gas,\ inlet}} = \frac{p\mathrm{MW_{mix}}}{R_{\mathrm{gas}} T_{\mathrm{inlet}}}$$ (ideal gas density at reactor inlet, $\mathrm{g/cm^3}$)

$$C_{\mathrm{A,\ bulk\ gas,\ inlet}} = \frac{\rho_{\mathrm{gas,\ inlet}}\omega_{\mathrm{A,\ inlet}}}{\mathrm{MW_A}}$$ (inlet molar density of reactant A, $\mathrm{mol/cm^3}$)

$$\mu_{\mathrm{gas}} = \frac{2.6693 \times 10^{-5}\sqrt{T_{\mathrm{bulk\ gas}}\,\mathrm{MW_{mix}}}}{\sigma^2}\ \mathrm{(g/cm{\cdot}s)}$$ (bulk viscosity of an ideal gas via Chapman–Enskog kinetic theory)

$C_{p,i}(T) =$ temperature dependence of pure-component specific heats via Table 3-1 and page 135, cal/g·K

$C_{p,\text{gas}} = \sum_{i=\text{A,B,C}} \omega_i C_{p,i}$ (specific heat of the mixture via equation 3-12, cal/g·K)

$$k_{\text{TC, gas}} = \mu_{\text{gas}} \left(C_{p,\text{ gas}} + \frac{1.25 R_{\text{gas}}}{\text{MW}_{\text{mix}}} \right)$$ (Eucken formula for the thermal conductivity of a polyatomic gas, cal/cm·s·K)

$$\text{Re} = \frac{\rho_{\text{gas}} q (2R_{\text{pellet}})}{\mu_{\text{gas}} \varepsilon_{\text{inter}} \pi R_{\text{PFR}}^2}$$ (Reynolds number for interstitial gas flow through the packed catalytic reactor)

$q = 100$ cm^3/s (volumetric flow rate of the bulk gas through the packed catalytic reactor, 6 L/min)

$$\text{Pr} = \frac{\mu_{\text{gas}} C_{p,\text{ gas}}}{k_{\text{TC, gas}}}$$ (Prandtl number for bulk gas)

$$\mathfrak{D}_{\text{A, gas}} = \frac{1.8583 \times 10^{-3} (T_{\text{bulk gas}})^{3/2}}{p(\text{MW}_{\text{A}}^{1/2})\sigma^2}$$ (bulk gas-phase diffusivity of CO, cm^2/s)

$$\mathfrak{D}_{\text{A, surface}} = \frac{1.8583 \times 10^{-3} (T_{\text{surface}})^{3/2}}{p(\text{MW}_{\text{A}}^{1/2})\sigma^2}$$ (gas diffusivity of CO, at catalyst surface, cm^2/s)

$$\text{Sc} = \frac{\mu_{\text{gas}}}{\rho_{\text{gas}} \mathfrak{D}_{\text{A, gas}}}$$ (Schmidt number for CO in bulk gas)

$$\text{Sh} = \frac{k_{\text{A, MTC}} (2R_{\text{pellet}})}{\mathfrak{D}_{\text{A, gas}}} = 2 + 0.6\text{Re}^{1/2} \cdot \text{Sc}^{1/3}$$ (External gas-phase mass transfer coefficient $k_{\text{A, MTC}}$, laminar flow around a sphere, cm/s)

$$\text{Nu} = \frac{h_{\text{HTC}} (2R_{\text{pellet}})}{k_{\text{TC, gas}}} = 2 + 0.6\text{Re}^{1/2} \cdot \text{Pr}^{1/3}$$ (External gas-phase heat transfer coefficient h_{HTC}, laminar flow around spheres, cal/cm^2·s·K)

$k_{1,\text{surface}} = 1 \times 10^{-7}$ cm/s (reaction velocity contant at 325 K, optimized at 30 atm via linear least squares analysis when all adsorption/desorption equilibrium constants are 0.25 atm^{-1})

$E_{\text{activation}} = 1 \times 10^4$ (Arrhenius activation energy for kinetic rate constant, cal/mol)

$$k_1 = S_m \rho_{\text{app}} k_{1,\text{ surface}} \exp\left[\frac{-E_{\text{activation}}}{R_{\text{gas}}}\left(\frac{1}{T_{\text{surface}}} - \frac{1}{325\text{K}}\right)\right]$$
(pseudo-volumetric rate constant at temperature T_{surface} for first-order irreversible reaction, s^{-1})

$$\Lambda^2_{\text{intra}} = \frac{k_1 R^2_{\text{pellet}}}{\mathfrak{D}_{\text{A, effective}}}$$ (intrapellet Damkohler number for CO)

$$\mathfrak{D}_{\text{A, Knudsen}} = \frac{2}{3}\langle r_{\text{average}}\rangle \left(\frac{3R_{\text{gas}}T_{\text{surface}}}{\text{MW}_{\text{A}}}\right)^{1/2}$$ (Knudsen diffusivity for CO, cm^2/s)

$$\frac{1}{\mathfrak{D}_{\text{A, net}}} = \frac{1}{\mathfrak{D}_{\text{A, Knudsen}}} + \frac{1}{\mathfrak{D}_{\text{A, surface}}}$$ (addition of diffusional resistances in pores)

$$\mathfrak{D}_{\text{A, effective}} = \frac{\varepsilon_{\text{intra}}\mathfrak{D}_{\text{A, net}}}{\tau_{\text{or}}}$$ (effective diffusivity of CO in pores, cm^2/s)

$$E = \frac{3}{\Lambda^2_{\text{intra}}}\left(\frac{\Lambda_{\text{intra}}}{\tanh \Lambda_{\text{intra}}} - 1\right)$$ (analytical correlation for the effectiveness factor, spherical pellets, first-order reaction)

$$\mathfrak{R} = k_1 C_{\text{A, surface}}$$ (pseudo-volumetric first-order rate law on the external catalytic surface, mol/vol·time)

$$T_{\text{surface}} = T_{\text{bulk gas}} + \frac{(-\Delta H_{\text{Rx}})k_{\text{A, MTC}}(C_{\text{A, bulk gas}} - C_{\text{A, surface}})}{h_{\text{HTC}}}$$ (coupled heat and mass transfer in a multicomponent mixture at steady state)

$$\Delta H_{\text{Rx}} = -2.2 \times 10^4$$ (enthalpy change for the exothermic chemical reaction at 298 K, cal/mol)

$$E\mathfrak{R}V_{\text{catalyst}} = k_{\text{A, MTC}}(C_{\text{A, bulk gas}} - C_{\text{A, surface}})S_{\text{catalyst}}$$ (implicit calculation of $C_{\text{A, surface}}$, mol/cm^3)

$$\frac{d\chi}{dz} = \frac{(1-\varepsilon_{\text{inter}})E\mathfrak{R}\pi R^2_{\text{PFR}}}{qC_{\text{A, bulk gas, inlet}}}$$ (right-hand side of plug-flow mass balance at high Peclet numbers, no axial dispersion)

$$\chi = \chi_{\text{initial}} + \int \frac{d\chi}{dz}dz$$ (calculate the conversion of CO by integrating the plug-flow mass balance)

$U_{\text{overall}} = 5 \times 10^{-4}$ cal/cm^2·sec·K [free convective heat transfer in the gas-phase boundary layer adjacent to the outside wall of the reactor provides the dominant resistance to heat transfer and limits heat removal to the surroundings (this is the only cooling mechanism for the exothermic chemical reaction), overall heat transfer coeffcient across lateral surface, 20 kcal/m^2·hr·K]

$$\frac{dT_{\text{bulk gas}}}{dz} = \frac{(\text{heat generation} - \text{heat removal})\pi R_{\text{PFR}}^2}{q\rho_{\text{gas, inlet}} C_{p,\text{ gas}}}$$ (right-hand side of the plug-flow thermal energy balance at high Peclet numbers, no axial conduction)

$$\text{heat generation} = -\Delta H_{\text{Rx}}(1 - \varepsilon_{\text{inter}})E\mathfrak{R}$$

$$\text{heat removal} = \frac{2U_{\text{overall}}}{R_{\text{PFR}}}(T_{\text{bulk gas}} - T_{\text{ambient}})$$

$$T_{\text{bulk gas}} = T_{\text{inlet}} + \int \frac{dT_{\text{bulk gas}}}{dz}$$ (calculate the temperature of the bulk gas stream by integrating the plug-flow thermal energy balance)

30-6.1 Importance of External Resistance to Mass Transfer

If the external resistance to mass transfer is large, then the molar density of reactant A near the external surface of the catalyst is much smaller than its bulk gas-phase molar density. Equation (30-57) for first-order irreversible kinetics in an isothermal packed catalytic tubular reactor predicts that:

$$\beta = \frac{E S_m \rho_{\text{app}} k_{1,\text{ surface}} V_{\text{catalyst}}}{k_{\text{A, MTC}} S_{\text{catalyst}}} \gg 1$$

$$\phi = \frac{1}{1+\beta} \longrightarrow 0 \qquad (30\text{-}77)$$

$$C_{\text{A, surface}} = \phi C_{\text{A, bulk gas}}$$

in the diffusion-limited regime. The assumption of isothermal behaviour is most critical here, because it is usually possible to replace a complex kinetic rate law with a first-order function (i.e., $S_m \rho_{\text{app}} k_{1,\text{ surface}} C_{\text{A, surface}}$) via the methodology in Sections 15-3 and 22-3.2. For a generalized rate law under nonisothermal conditions, comparison of internal and external mass transfer resistances is based on molar density differences inside and outside the catalyst. For component i,

equations (30-8) and (30-14) yield:

$$\frac{C_{i,\,\text{surface}} - C_{i,\,\text{bulk gas}}}{C_{i,\,\text{intrapellet}} - C_{i,\,\text{surface}}} = \frac{k_{\text{A, MTC}}/\mathfrak{D}_{\text{A, effective}}}{k_{i,\text{MTC}}/\mathfrak{D}_{i,\text{effective}}} \frac{C_{\text{A, bulk gas}} - C_{\text{A, surface}}}{C_{\text{A, surface}} - C_{\text{A, intrapellet}}} \tag{30-78}$$

If this ratio is large, then the external resistance to mass transfer is significant and one introduces considerable error into a design strategy that equates molar densities on the external catalytic surface to those in the bulk fluid phase. Non-isothermal effectiveness factor calculations in an isolated pellet allow one to predict $C_{\text{A, intrapellet}}$ in terms of $C_{\text{A, surface}}$, and the methodology described earlier in Section 30-6 (i.e., see pages 846–850) generates an average profile for $C_{\text{A, surface}}$ and $C_{\text{A, bulk gas}}$ from reactor inlet to outlet. At very large intrapellet Damkohler numbers in the diffusion-limited regime, the molar density of reactant A decreases rapidly as one moves toward the central core of the catalyst. Hence, $C_{\text{A, intrapellet}} \to 0$ and equation (30-78) reduces to:

$$\frac{C_{i,\,\text{surface}} - C_{i,\,\text{bulk gas}}}{C_{i,\,\text{intrapellet}} - C_{i,\,\text{surface}}} = \frac{k_{\text{A, MTC}}/\mathfrak{D}_{\text{A, effective}}}{k_{i,\,\text{MTC}}/\mathfrak{D}_{i,\,\text{effective}}} \left(\frac{C_{\text{A, bulk gas}}}{C_{\text{A, surface}}} - 1 \right) \tag{30-79}$$

which avoids the necessity to recall isolated pellet calculations for $C_{\text{A, intrapellet}}$ near the central core.

30-6.2 Importance of External Resistance to Heat Transfer

During each iteration of the numerical algorithm described on pages 846–850, it is instructive to use the current values of $C_{\text{A, bulk gas}}$ and $C_{\text{A, surface}}$, estimate temperature differences inside and outside of the pellet, and determine the importance of the external resistance to heat transfer in packed catalytic tubular reactors. For example, equations (30-31) and (30-41) suggest that if the chemical reaction is exothermic and the following ratio is large:

$$\frac{T_{\text{surface}} - T_{\text{bulk gas}}}{T_{\text{intrapellet}} - T_{\text{surface}}} = \frac{k_{\text{A, MTC}}/\mathfrak{D}_{\text{A, effective}}}{h_{\text{HTC}}/k_{\text{eff. pellet}}} \frac{C_{\text{A, bulk gas}} - C_{\text{A, surface}}}{C_{\text{A, surface}} - C_{\text{A, intrapellet}}} \tag{30-80}$$

then external heat transfer limitations are significant. At very large intrapellet Damkohler numbers, $C_{\text{A, intrapellet}} \to 0$ and equation (30-80) reduces to:

$$\frac{T_{\text{surface}} - T_{\text{bulk gas}}}{T_{\text{intrapellet}} - T_{\text{surface}}} = \frac{k_{\text{A, MTC}}/\mathcal{D}_{\text{A, effective}}}{h_{\text{HTC}}/k_{\text{eff. pellet}}} \left(\frac{C_{\text{A, bulk gas}}}{C_{\text{A, surface}}} - 1 \right) \tag{30-81}$$

PROBLEMS

30-1. Identify 11 or 12 logical steps, in sequence, which are required for complete design of a packed catalytic tubular reactor that operates isothermally. One-line statements are sufficient. Do not include any equations. The beginning of the first word of the first step is indicated below;

(1) Pro. . .

30-2. The isothermal plug-flow mass balance for first-order irreversible chemical kinetics in an ideal packed catalytic tubular reactor with significant external mass transfer resistance yields the following functional form for the conversion of reactant A at high mass transfer Peclet numbers:

$$\chi_{\text{A}} \approx 1 - \exp\left[-f(\varepsilon_{p,\text{ interpellet}}) \frac{E(\Lambda_{\text{A, intrapellet}})}{\omega} \right]$$

What is $f(\varepsilon_{p,\text{ interpellet}})$?

30-3. Describe how the conversion of reactant A in the exit stream of an ideal packed catalytic tubular reactor with significant external mass transfer resistance is affected (i.e., increases, decreases, does not change, too complex to determine) when each of the following parameters decreases.

(a) $C_{\text{A, inlet}}$, inlet molar density of reactant A when the kinetics are irreversible and second-order.

(b) $\langle r_{\text{pore}} \rangle_{\text{average}}$, average pore size of a single spherical catalytic pellet in the micropore regime where Knudsen flow provides the dominant resistance to intrapellet mass transfer.

(c) $\langle r_{\text{pore}} \rangle_{\text{average}}$, average pore size of a single spherical catalytic pellet in the macropore regime where ordinary molecular diffusion provides the dominant resistance to intrapellet mass transfer.

(d) $\varepsilon_{\text{intrapellet}}$, intrapellet porosity for a single pellet.

(e) τ_{or}, tortuosity factor that describes pore orientation within a single pellet.

(f) $\varepsilon_{p,\text{ interpellet}}$, interpellet porosity of the entire packed catalytic tubular reactor.

(g) Size, or diameter, of a single spherical catalytic pellet.

30-4. Sketch the molar density of reactant A on the external surface of porous catalytic pellets ($C_{A,\,surface}$) as a function of reactor volume (V_{PFR}) for an ideal PFR with significant external mass transfer resistance when the chemical kinetics are:

(a) First-order and irreversible.

(b) Second-order and irreversible

Put both curves on the same set of axes. The effectiveness factor, interpellet porosity, and time constants for convective mass transfer and chemical reaction are the same in both cases.

30-5. **(a)** What is the exact analytical expression for $C_{A,\,surface}$ vs. V_{PFR} for first-order irreversible chemical kinetics in an ideal packed catalytic tubular reactor with significant external mass transfer resistance?

(b) If thermal energy effects due to chemical reaction are negligible in part (a), then how does the intrapellet Damkohler number of reactant A ($\Lambda^2_{A,\,intrapellet}$) change (i.e., increase, decrease, does not change, too complex to determine) from the inlet stream to the outlet stream of the PFR?

30-6. **(a)** What is the final expression that must be integrated to obtain the dimensionless molar density of reactant A in the bulk fluid stream [$\Psi_{A,\,bulk\ gas}(\zeta)$] for an ideal packed catalytic tubular reactor with second-order irreversible chemical kinetics and significant external mass transfer resistance? Be sure that this equation is written in terms of $\Psi_{A,\,bulk\ gas}(\zeta)$ only.

(b) If thermal energy effects due to chemical reaction are negligible in part (a), then how does the intrapellet effectiveness factor change (i.e., increase, decrease, does not change, too complex to determine) from the inlet stream to the outlet stream of the PFR?

30-7. Consider a straight tube of radius R with circular cross section and expensive metal catalyst coated in the inner wall. Reactant A is converted to products via first-order irreversible chemical reaction on the catalytic surface at $r = R$. Hence, diffusion of reactant A in the radial direction, toward the catalytic surface, is balanced by the rate of consumption of A due to heterogeneous chemical reaction. The boundary condition at the mathematically well-defined catalytic surface (i.e., $r = R$) is

$$-\mathfrak{D}_{A,\,ordinary}\left(\frac{\partial C_A}{\partial r}\right)_{r=R} = k_{1,\,surface}C_{A,\,surface}$$

where $k_{1,\,surface}$ is a reaction velocity constant with units of length per time. The surface molar density of reactant A in the kinetic rate law is given by $C_A(r = R, z)$, which depends on axial position z within the tube. However, $C_{A,\,surface}$ is independent of angular variable θ because

there are no problematic corner regions. In other words, all points on the catalytic surface are equally accessible to reactants.

(a) Begin with the quasi-macroscopic plug-flow mass balance in a straight channel with rectangular cross section, variable catalyst activity and first-order irreversible chemical reaction at high mass transfer Peclet numbers, as given by equation (23-69):

$$\langle v_z \rangle_{\text{average}} S \left(-\frac{dC_{\text{A, bulk}}}{dz} \right) = \int_0^b k_{1,\,\text{surface}}(y) C_{\text{A}}(x = a, y, z)\, dy + \int_0^a k_{1,\,\text{surface}}(x) C_{\text{A}}(x, y = b, z)\, dx$$

and modify this expression for tubular reactors with uniform catalyst activity.

Answer: The left side of the quasi-macroscopic mass balance, as written above, is the same for all types of catalytic channels with the appropriate description of the flow cross section S. For tubular reactors with radius R, S is given by πR^2. Upon integrating the right side of the preceding equation around the catalytically active perimeter (i.e., $R\, d\Theta$), where the reaction velocity constant and the surface molar density of reactant A are independent of angular coordinate Θ, one obtains

$$\langle v_z \rangle_{\text{average}} \pi R^2 \left(-\frac{dC_{\text{A, bulk}}}{dz} \right) = k_{1,\,\text{surface}} C_{\text{A, surface}} (2\pi R)$$

If integration is performed along the catalytically active perimeter in one quadrant only (i.e., the xy plane where both x and y are positive), then the complete circumference of the tube on the right side of the preceding equation is replaced by $\pi R/2$, and $S = \pi R^2/4$. The final result is unchanged.

(b) Consider the formalism of external mass transfer resistance and relate $C_{\text{A, surface}}$ to $C_{\text{A, bulk}}$. Remember that (1) the tube is not packed with porous catalytic pellets, (2) the effectiveness factor is unity, and (3) it is not necessary to make the reaction velocity constant pseudo-volumetric because the balance between diffusion and reaction at the catalytic surface is based on two rate processes which have dimensions of moles per area per time. *Hint:* Use a mass transfer coefficient $k_{\text{A, MTC}}$ and a concentration driving force to evaluate the rate of diffusion of reactant A toward the catalytic surface.

Answer: Employ the radiation boundary condition at the mathematically well-defined catalytic surface (i.e., at $r = R$):

$$-\mathcal{D}_{\text{A, ordinary}} \left(\frac{\partial C_A}{\partial r} \right)_{r=R} = k_{1,\,\text{surface}} C_{\text{A, surface}}$$

In the preceding expression, Fick's law is used to evaluate the flux of reactant A toward the catalytic surface. Now, re-express this flux as

$$-\mathcal{D}_{\mathrm{A,\,ordinary}}\left(\frac{\partial C_A}{\partial r}\right)_{r=R} = k_{\mathrm{A,\,MTC}}(C_{\mathrm{A,\,bulk}} - C_{\mathrm{A,\,surface}})$$

The two preceding equations yield a relation for the molar density of reactant A on the catalytic surface in terms of its bulk fluid-phase molar density:

$$C_{\mathrm{A,\,surface}} = \phi C_{\mathrm{A,\,bulk}}$$

$$\phi = \frac{k_{\mathrm{A,\,MTC}}}{k_{\mathrm{A,\,MTC}} + k_{1,\,\mathrm{surface}}}$$

(c) What is the limiting value of $C_{\mathrm{A,\,surface}}$ when $k_{\mathrm{A,\,MTC}}$ is much greater than the reaction velocity constant, $k_{1,\,\mathrm{surface}}$? Notice that both $k_{\mathrm{A,\,MTC}}$ and $k_{1,\,\mathrm{surface}}$ have the same dimensions (i.e., length/time).

Answer: The dimensionless parameter ϕ approaches unity, and $C_{\mathrm{A,\,surface}}$ approaches $C_{\mathrm{A,\,bulk}}$ in the reaction-rate-limited regime.

(d) What is the limiting value of $C_{\mathrm{A,\,surface}}$ when $k_{\mathrm{A,\,MTC}}$ is much smaller than the reaction velocity constant, $k_{1,\,\mathrm{surface}}$?

Answer: Now, the dimensionless parameter ϕ approaches $k_{\mathrm{A,\,MTC}}/k_{1,\,\mathrm{surface}}$, and

$$C_{\mathrm{A,\,surface}} \rightarrow \frac{k_{\mathrm{A,\,MTC}}}{k_{1,\,\mathrm{surface}}} C_{\mathrm{A,\,bulk}}$$

which asymptotically approaches zero in the diffusion-limited regime, where the rate of mass transfer toward the catalytic surface governs the reactant-product conversion rate.

(e) Use the quasi-macroscopic mass balance from part (a) and obtain an expression for $C_{\mathrm{A,\,bulk}}$ as a function of residence time τ, where τ is defined by

$$\tau \equiv \frac{z}{\langle v_z \rangle_{\mathrm{average}}}$$

It is necessary to integrate an ODE subject to the boundary condition $C_{\mathrm{A,\,bulk}} = C_{\mathrm{A,\,inlet}}$ at $z = 0$.

Answer: Combine the results from parts (a) and (b) as follows:

$$\langle v_z \rangle_{\mathrm{average}}\left(-\frac{dC_{\mathrm{A,\,bulk}}}{dz}\right) = \frac{2}{R} k_{1,\,\mathrm{surface}} \phi C_{\mathrm{A,\,bulk}}$$

Then, separate variables and integrate the ODE for $C_{\mathrm{A,\,bulk}}$ as a function of axial position z through the tubular duct:

$$C_{\mathrm{A,\,bulk}}(z) = C_{\mathrm{A,\,inlet}} \exp\left[-\frac{(2/R)k_{1,\,\mathrm{surface}}\phi z}{\langle v_z \rangle_{\mathrm{average}}}\right]$$

(f) Sketch $C_{A,\,bulk}$ vs. axial coordinate z, not residence time τ, for two different values of the reaction velocity constant, $k_{1,\,surface} = 0.1$ and 0.5 cm/s. Put both curves on one set of axes and be sure to label the curves.

Answer: Reactants are converted to products at a faster rate when the reaction velocity constant is larger. Hence, at the same axial position z, there is a greater reduction in $C_{A,\,bulk}$ relative to its inlet value when $k_{1,\,surface}$ is larger. Both curves follow single exponential decay.

(g) Sketch $C_{A,\,bulk}$ vs. axial coordinate z, not residence time τ, for two different values of the Reynolds number in the laminar flow regime, Re = 500 and 1000. Put both curves on one set of axes and be sure to label the curves. The Reynolds number increases by a factor of 2 because the volumetric flow rate, or the average fluid velocity, is doubled. The Reynolds number for tube flow is defined by

$$\mathrm{Re} = \frac{\rho \langle v_z \rangle_{\mathrm{average}} (2R)}{\mu}$$

For laminar flow adjacent to a high-shear no-slip solid–liquid interface, with one-dimensional flow in the mass transfer boundary layer, the mass transfer coefficient $k_{A,\,MTC}$ is obtained from the following Sherwood number correlation (see steps 17 and 18 of Problem 23-7 an page 653, particularly the scaling law exponents a and b):

$$\mathrm{Sh} = \frac{k_{A,\,MTC}(2R)}{\mathfrak{D}_{A,\,ordinary}} \approx C_1 \cdot \mathrm{Re}^{1/3} \cdot \mathrm{Sc}^{1/3}$$

where the Schmidt number Sc is based on ordinary molecular diffusion.

(h) Is the following expression for the dimensionless molar density of reactant A correct?

$$\Psi_{A,\,bulk}(z) = \frac{C_{A,\,bulk}(z)}{C_{A,\,inlet}} = \exp\left\{ -10\phi \frac{\Lambda_A^2}{\mathrm{Pe}_{MT}} \frac{z}{d_{effective}} \right\}$$

where the effective diameter of the channel is $d_{effective} = 2R$, the mass transfer Peclet number for reactant A is:

$$\mathrm{Pe}_{MT} = \mathrm{Re} \cdot \mathrm{Sc} = \frac{\langle v_z \rangle_{average}\, d_{effective}}{\mathfrak{D}_{A,\,ordinary}}$$

the Damkohler number for reactant A is:

$$\Lambda_A^2 = \frac{k_{1,\,surface} R}{\mathfrak{D}_{A,\,ordinary}}$$

and the dimensionless parameter ϕ is defined by:

$$\phi = \frac{k_{\text{A, MTC}}}{k_{\text{A, MTC}} + k_{\text{1, surface}}}$$

Answer: Begin with the final result in part (e):

$$C_{\text{A, bulk}}(z) = C_{\text{A, inlet}} \exp\left[-\frac{(2/R)k_{\text{1, surface}}\phi z}{\langle v_z \rangle_{\text{average}}}\right]$$

and manipulate the argument of the exponential, algebraically, using the parameters defined above. For example,

$$\begin{aligned} &-\frac{(2/R)k_{\text{1, surface}}\phi z}{\langle v_z \rangle_{\text{average}}} \\ &= -\frac{4}{d_{\text{effective}}} \frac{\Lambda_{\text{A}}^2 \mathcal{D}_{\text{A, ordinary}}}{R} \frac{\phi z}{\langle v_z \rangle_{\text{average}}} \\ &= -8\phi \frac{\Lambda_{\text{A}}^2}{\text{Pe}_{\text{MT}}} \frac{z}{d_{\text{effective}}} \end{aligned}$$

Hence, the proposed answer is not correct, because the factor of 10 should be replaced by 8. Otherwise, the proposed functional dependence is correct.

30-8. Consider convection, interpellet axial dispersion, and Hougen–Watson chemical kinetics in a non-ideal isothermal packed catalytic tubular reactor with significant external mass transfer resistance.

(a) The system of two coupled first-order ODEs for reactant molar density is solved numerically from the reactor inlet at $\zeta = 0$ to the outlet at $\zeta = 1$. In this mode, there could be significant instabilities in the shooting method. When the mass transfer Peclet number is 25 and the interpellet Damkohler number is 20, the appropriate guess for the dimensionless axial concentration gradient at $\zeta = 0$ is $(d\Psi_{\text{A}}/d\zeta) = -0.7$, which yields convergence of the Danckwerts boundary condition at the reactor outlet, where $\zeta = 1$. Estimate the appropriate guess for $(d\Psi_{\text{A}}/d\zeta)$ at $\zeta = 0$ when the mass transfer Peclet number is increased to 27 and the interpellet Damkohler number remains unchanged.

(b) The system of two coupled first-order ODEs for reactant molar density is solved numerically from the reactor outlet at $\zeta = 1$ to the inlet at $\zeta = 0$. The numerical instabilities described in part (a) should be reduced somewhat when integration is performed backwards. When the mass transfer Peclet number is 25 and the interpellet Damkohler number is 20, the appropriate guess for the dimensionless molar density of reactant A at $\zeta = 1$ is $\Psi_A = 0.5$, which yields convergence of

the Danckwerts boundary condition at the reactor inlet, where $\zeta = 0$. Estimate the appropriate guess for Ψ_A at $\zeta = 1$ when the mass transfer Peclet number is increased to 27 and the interpellet Damkohler number remains unchanged.

30-9. Identify the important dimensionless number in each case.

(a) External mass transfer resistance in packed catalytic tubular reactors is negligible at very large values of this dimensionless number.
Answer: Reynolds number, mass transfer Peclet number, or the Sherwood number.

(b) Under isothermal conditions, porous catalytic pellets operate in the diffusion-limited regime at very large values of this dimensionless number.
Answer: Intrapellet Damkohler number.

(c) Under isothermal conditions, porous catalytic pellets operate in the diffusion-limited regime at very small values of this dimensionless number.
Answer: Effectiveness factor.

(d) Interpellet axial dispersion is very important in packed catalytic tubular reactors at very small values of this dimensionless number.
Answer: Mass transfer Peclet number.

(e) When the chemical kinetics are second-order and irreversible, external mass transfer resistance in packed catalytic tubular reactors is negligible at very small values of this dimensionless number.
Answer:

$$\alpha = \beta C_{A,\,\text{inlet}} = \frac{C_{A,\,\text{inlet}} E(\Lambda_{A,\,\text{intrapellet}}) S_m \rho_{\text{app}} k_{n,\,\text{surface}} V_{\text{catalyst}}}{k_{A,\,\text{MTC}} S_{\text{catalyst}}}$$

$$= \frac{\Lambda^2_{A,\,\text{interpellet}} E(\Lambda_{A,\,\text{intrapellet}}) (\text{Pe}_{\text{simple}})^{2/3}}{6\phi_{\text{correlation}} (\text{Pe}_{\text{MT}})^2}$$

30-10. **(a)** Write all of the dimensionless equations which must be solved to design an ideal isothermal packed catalytic tubular reactor when the kinetic rate law is zeroth-order and irreversible. Interpellet axial dispersion is negligible, but external mass transfer resistance should be included in your analysis.

(b) Obtain an analytical expression for the dimensionless outlet molar density of reactant A, $\Psi_{A,\text{bulk}}(\zeta = 1)$, as a function of the average residence time τ.

Consider the following parameters in the design of this packed catalytic tubular reactor, which contains porous spherical pellets. The kinetic rate

law is zeroth-order and irreversible. $\Lambda_{A,\,intrapellet}$ is based on the radius of one catalytic pellet.

Intrapellet Damkohler number of reactant A; $\Lambda_{A,\,intrapellet} = 5$
Interpellet porosity of the packed bed; $\varepsilon_{p,\,interpellet} = 0.50$
Time constant for zeroth-order irreversible chemical reaction; $\omega = 1$ minute

Calculate the conversion of reactant A in the exit stream of this packed catalytic tubular reactor for the residence times τ given below:

(c) $\tau = 2$ minutes. A numerical answer is required here.

(d) $\tau = 5$ minutes. A numerical answer is required here.

30-11. Use the following data to analyze the performance of a packed catalytic tubular reactor that contains porous spherical pellets. The heterogeneous kinetic rate law is pseudo-first-order and irreversible such that $R_{surface}$, with units of moles per area per time, is expressed in terms of the partial pressure of reactant A, only (i.e., $R_{surface} = k_{1,\,surface}\,p_A$), and $k_{1,\,surface}$ has dimensions of moles per area per time per atmosphere. $k_{1,\,surface}$ is not a pseudo-volumetric kinetic rate constant. Remember that the kinetic rate constant in both the intrapellet and interpellet Damkohler numbers must correspond to a pseudo-volumetric rate of reaction, where the rate law is expressed in terms of molar densities, not partial pressures.

Isothermal temperature of operation; $T = 375$ K
$k_{1,\,surface} = 5.25 \times 10^{-13}$ moles/(cm^2–sec–atmosphere) at 375 K
Molecular weight of reactant A; $MW_A = 100$ daltons $= 100$ g/mol
Ordinary molecular diffusion coeff. of reactant A at 375 K; $\mathfrak{D}_{A,\,ordinary} = 0.1$ cm^2/sec
Average pore radius; $\langle r_{pore}\rangle_{average} = 40$ Å (i.e.,1 Å $= 10^{-8}$ cm)
Intrapellet porosity of each catalytic pellet; $\varepsilon_{p,\,intrapellet} = 0.50$
Tortuosity factor; $\tau_{or} = 2$
Diameter of each porous catalytic pellet; $d_{pellet} = 2$ cm
Radius of the tubular reactor; $R_{PFR} = 10$ cm
Length of the tubular reactor; $L_{PFR} = 190$ cm
Interpellet porosity of the packed bed; $\varepsilon_{p,\,interpellet} = 0.30$
Volumetric flowrate; $q = 15$ Liters/min $= 250$ cm^3/sec

Hint: Universal gas constant in the appropriate units, as required to make the kinetic rate constant pseudo-volumetric; $R_{gas} = 82.057$ cm^3–atmosphere/(mol-K)

(a) Calculate the conversion of reactant A in the exit stream of an ideal reactor with no external mass transfer resistance.

(b) Calculate the conversion of reactant A in the exit stream of an ideal reactor in which external mass transfer resistance is considered.

(c) Estimate the critical value of the mass transfer Peclet number.

(d) Predict the outlet conversion of reactant A when interpellet axial dispersion is considered, but external mass transfer resistance is neglected.

(e) Predict the outlet conversion of reactant A when interpellet axial dispersion and external mass transfer resistance are considered.

Transport Phenomena for Chemical Reactor Design. Laurence A. Belfiore
Copyright © 2003 John Wiley & Sons, Inc.
ISBN: 0-471-20275-4

REFERENCES

Abramowitz, M., and I. A. Stegun (1972). *Handbook of Mathematical Functions*. New York: Dover Publications.

Adamson, A. W., and A. P. Gast (1997). *Physical Chemistry of Surfaces*, 6th ed. New York: Wiley.

Anon. (1998). *Chemical & Engineering News*, June 22, p. 29.

Aris, R. (1975). *The Mathematical Theory of Diffusion and Reaction in Permeable Catalysts: The Theory of the Steady State*, Vol. 1. New York: Oxford University Press.

Ben-Naim, A. (1992). *Statistical Thermodynamics for Chemists and Biochemists*. New York: Plenum Press.

Bilous, O., and N. R. Amundson (1956). *AIChE Journal*, **2**(1), 117.

Bird, R. B., R. C. Armstrong, and O. Hassager (1977). *Dynamics of Polymeric Liquids*, Vol. 1, *Fluid Mechanics*. New York: Wiley.

Bird, R. B., W. E. Stewart, and E. N. Lightfoot (1960). *Transport Phenomena*. New York: Wiley.

_____ (2002). *Transport Phenomena*, 2nd ed. New York: Wiley.

Bischoff, K. B. (1961). *Chemical Engineering Science*, **16**, 131.

Boussinesq, J. V. (1868). *Journal de Mathématiques Pures et Appliquées*, Ser. 2, **13**, 377–424.

Brunauer, S., P. H. Emmett, and E. Teller (1938). *Journal of the American Chemical Society*, **60**, 309.

Callen, H. B. (1985). *Thermodynamics and an Introduction to Thermostatics*. New York: Wiley.

Carnahan, B., H. A. Luther, and J. O. Wilkes (1969). *Applied Numerical Methods*. New York: Wiley.

Carslow, H. S., and J. C. Jaeger (1984). *Conduction of Heat in Solids*, 2nd ed. New York: Oxford University Press.

Chidambaram, M. (1984). *Hungarian Journal of Industrial Chemistry*, **12**(2), 245.

Churchill, S. (1979a). *The Interpretation and Use of Rate Data: The Rate Concept*. New York: Hemisphere Publishing.

_____ (1979b). In *Proc. 17th Symposium on Combustion*. Pittsburgh, PA., Combustion Institute.

_____ (1984). *AIChE Symposium Series 87*.

_____ (1985). *Industrial and Engineering Chemistry Process Design and Development*, **24**, 542.

Curtiss, C. F., and R. B. Bird (1996). *Advances in Polymer Science*, **125**, 1–100.

Cutlip, M. B., and M. Shacham (1999). *Problem Solving in Chemical Engineering with Numerical Methods*. Upper Saddle River, NJ: Prentice Hall.

Cybulski, A., and J. A. Moulijn (1998). *Structured Catalysts and Reactors*. New York: Marcel Dekker.

Danckwerts, P. V. (1953). *Chemical Engineering Science*, **2**, 1.

Daniels, F., and R. A. Alberty (1975). *Physical Chemistry*, 4th ed. New York: Wiley.

Davis, H. R., and G. V. Parkinson (1970). *Applied Science Research*, **22**, 20.

Deen, W. M. (1998). *Analysis of Transport Phenomena*. New York: Oxford University Press.

Dicke, R. H., and J. P. Wittke (1960). *Introduction to Quantum Mechanics.* Reading, MA: Addison-Wesley Publishing.

Dullien, F. A. L. (1992). *Porous Media, Fluid Transport and Pore Structure*, 2nd ed. San Diego, CA: Academic Press.

Eubank, P. T., and M. A. Barrufet (1988). *Chemical Engineering Education*, Winter.

Evans, M. G., and M. Polanyi (1935). *Transactions of the Faraday Society*, **31**, 875.

_____ (1936). *Transactions of the Faraday Society*, **32**, 1333.

Fabelinskii, I. L. (1968). *Molecular Scattering of Light*, translated from Russian by R. T. Beyer. New York: Plenum Press.

Felder, R. M., and R. W. Rousseau (2000). *Elementry Principles of Chemical Processes*, 3rd ed. New York: Wiley.

Flory, P. J. (1953). *Principles of Polymer Chemistry*. Ithaca, N.Y.: Cornell University Press.

Fogler, S. (1998). *Elements of Chemical Reaction Engineering*, 3rd ed. Upper Saddle River, NJ: Prentice Hall.

Fowler, R. H., and E. A. Guggenheim (1939). *Statistical Thermodynamics*. New York: Cambridge University Press.

Freundlich, H. (1926). *Colloid and Capillary Chemistry*. London: Methuen.

_____ (1932). *Transactions of the Faraday Society*, **28**, 195.

Frumkin, A., and A. Slygin (1935). *Acta Physicochim.*, **3**, 791.

Geankoplis, C. J. (1973). *Momentum, Heat and Mass Transport Processes*. New York: McGraw-Hill.

Graham, T. (1833). On the Law of Diffusion of Gases, *Philosophical Magazine*, **175** (reprinted in *Chemical and Physical Research*, pp. 44–70, Edinburgh University Press, 1876).

Happel, J., and H. Brenner (1965). *Low Reynolds Number Hydrodynamics*. Englewood Cliff, NJ: Prentice Hall.

Hatton, A. P., and A. Quarmby (1962). *International Journal of Heat and Mass Transfer*, **5**, 973–980.

Hayward, A. T. J. (1971). *American Scientist*, **59**, 434.

Hershey, D. (1989). *Chemical Engineering Education*.

Hiby, J. W. (1962). *Interactions between Fluids and Solids*. London: Institute of Chemical Engineers.

Hill, C. G., Jr. (1977). *An Introduction to Chemical Engineering Kinetics and Reactor Design*. New York: Wiley.

Hougen, O. A., and K. M. Watson (1947). *Chemical Process Principles*, Vol. 3. New York: Wiley.

Hyun, S. H., and R. P. Danner (1982). *Journal of Chemical Engineering Data*, **27**, 196.

Jenson, V. G., and G. V. Jeffreys (1977). *Mathematical Methods in Chemical Engineering*, 2nd ed. San Diego, CA: Academic Press.

Knudsen, C. W., G. W. Roberts, and C. N. Satterfield (1966). *Industrial Engineering Chemistry Fundamentals*, **5**(3), 325.

Kolb, W. B., A. A. Papadimitriou, R. L. Cerro, D. D. Leavitt, and J. C. Summers (1993). *Chemical Engineering Progress*, Feb., p. 61.

Laidler, K. J. (1965). *Chemical Kinetics*. New York: McGraw-Hill.

Lamb, H. (1945). *Hydrodynamics*. New York: Dover Publications.

Landau, L. D., and E. M. Lifshitz (1959). *Fluid Mechanics: Course of Theoretical Physics*, Vol. 6. Reading, MA: Addison-Wesley.

Langmuir, I. (1908). *Journal of the American Chemical Society*, **30**, 1742.

_____ (1918). *Journal of the American Chemical Society*, **40**, 1361.

Lightfoot, E. N. (1974). *Transport Phenomena and Living Systems: Biomedical Aspects of Momentum and Mass Transport*. New York: Wiley.

Limbach, K. W., and J. Wei (1988). *AIChE Journal*, **34**(2), 305.

Litz, L. M. (1985). *Chemical Engineering Progress*, **81**(11), 36.

Moore, W. J. (1972). *Physical Chemistry*, 4th ed. Englewood Cliffs, NJ: Prentice-Hall.

Morbidelli, M., A. Servida, S. Carra, and A. Varma (1985). *Industrial and Engineering Fundamentals*, **24**, 116.

Neufeld, P. D., A. R. Janzen, and R. A. Aziz (1972). *Journal of Chemical Physics*, **57**, 1100.

Nijemeisland, M., and A. G. Diyon (2001). *Chemical Engineering Journal*, **82**, 231.

Olabisi, O., L. M. Robeson, and M. T. Shaw (1979). *Polymer–Polymer Miscibility*. San Diego, CA: Academic Press.

Pauling, L. (1970). *General Chemistry*, 3rd ed. San Francisco: W.H. Freeman.

Payne, H. K., G. A. Studervant, and T. W. Leland (1968). *Industrial and Engineering Chemistry Fundamentals*, **7**, 363.

Pedernera, M., D. O. Borio, and J. A. Porras (1997). *AIChE Journal*, **43**(1), 127.

Perry, R., and C. Chilton (1973). *Chemical Engineers' Handbook*, 5th ed. New York: McGraw-Hill.

Prausnitz, J. M., R. N. Lichtenthaler, and E. Gomes de Azevedo (1999). *Molecular Thermodynamics of Fluid-Phase Equilibria*, 3rd ed. Upper Saddle River, NJ: Prentice Hall.

Reed, T. M., and K. E. Gubbins (1973). *Applied Statistical Mechanics: Thermodynamic and Transport Properties of Fluids*. Woburn, MA: Butterworth-Heinemann.

Reichardt, C. (1988). *Solvents and Solvent Effects in Organic Chemistry*, 2nd ed. Basel, Switzerland: VCH.

Rester, S., and R. Aris (1969). *Chemical Engineering Science*, **24**, 793.

Richards, B. E., and D. H. Trevena (1976). *Journal of Physics*, **D9**, 123.

Roberts, G. W., and C. N. Satterfield (1965). *Industrial Engineering Chemistry Fundamentals*, **4**(3), 288.

Rosner, D. E. (1967). In *Proc. 11th International Symposium on Combustion*. Pittsburgh, PA.: Combustion Institute, pp. 181–196.

_____ (1986). *Transport Processes in Chemically Reacting Flow Systems*. Woburn, MA: Butterworth.

Schlichting, H. (1979). *Boundary Layer Theory*, 7th ed. New York: McGraw-Hill.

Sedgewick, S. A., and D. H. Trevena (1976). *Journal of Physics*, **D9**, 1983.

Sideman, S., D. Luss, and R. E. Peck (1954). *Applied Science Research*, **A14**, 157.

Sips, R. (1948). *Journal of Chemical Physics*, **16**, 490.

_____ (1950). *Journal of Chemical Physics*, **18**, 1024.

Slygin, A., and A. Frumkin (1935). *Acta Physicochim.* USSR, **3**, 791.

Smith, J. M. (1970). *Chemical Engineering Kinetics*, 2nd ed. New York: McGraw-Hill.

Smith, J. M., and H. C. Van Vess (1987). *Introduction to Chemical Engineering Thermodynamics*, 4th ed. New York: McGraw-Hill.

Solbrig, C. W., and D. Gidaspow (1967). *Canadian Journal of Chemical Engineering*, **45**, 35.

Somorjai, G. A. (1994). *Introduction to Surface Chemistry and Catalysis*. New York: Wiley.

Sonntag, R. E., and G. J. Van Wylen (1966). *Fundamentals of Statistical Thermodynamics*. New York: Wiley.

Szukiewicz, M., K. Kaczmarski, and R. Petrus (1995). *Hungarian Journal of Industrial Chemistry*, **23**(2), 87.

Tanford, C. (1961). *Physical Chemistry of Macromolecules*. New York: Wiley.

Temkin, M. (1940). *Acta Physicochim.* USSR, **12**, 327.

Tester, J. W., and M. Modell (1997). *Thermodynamics and Its Applications*, 3rd ed. Upper Saddle River, NJ: Prentice Hall.

Toth, J. (1962). *Acta Chim. Acad. Sci. Hung.*, **30**, 1.

Valenzuela, D. P., and A. L. Myers (1989). *Adsorption Equilibrium Data Handbook*. Upper Saddle River, NJ: Prentice Hall.

Van der Put, P. J. (1998). *The Inorganic Chemistry of Materials: How to Make Things Out of Elements*. New York: Plenum Press.

Vortmeyer, D., and J. Schuster (1983). *Chemical Engineering Science*, **38**, 1691.

Weast, R. C. (1974–1975). *CRC Handbook of Chemistry and Physics*, 55th ed. Boca Raton, FL: CRC Press.

Westerterp, K. R., W. P. M. van Swaaij, and A. A. C. M. Beenackers (1984). *Chemical Reactor Design and Operation*, 2nd ed. New York: Wiley.

Wicke, E. (1975). *Chemie Ingenieur Technik*, **47**, 547.

Wylie, C. R. (1975). *Advanced Engineering Mathematics*, 4th ed. New York: McGraw-Hill.

Yang, K. H., and O. A. Hougen (1950). *Chemical Engineering Progress*, **46**(3), 146.

Transport Phenomena for Chemical Reactor Design. Laurence A. Belfiore
Copyright © 2003 John Wiley & Sons, Inc.
ISBN: 0-471-20275-4

INDEX

Accumulation rate process:
  fluid dynamics, 159–160, 168, 172
  mass balance, 253–254
  time derivatives, 160, 168, 254
Activated complex, 421
Activation energy, effectiveness factors, 739, 744–745
Activation free energy, 422–423
Activity, 422, 708–711, 795, 802–804, 814–816
  stability requirements for, 814–817
Activity coefficient, 422, 795, 802, 816–817
Addition of diffusional resistances, 546–552, 666, 849
Addition of resistances, rising/expanding bubbles, 327
Adiabatic reactor:
  temperature rise, 72
  temperature vs. conversion, 55–56, 72
Adiabatic temperature rise, 130, 138, 740–742
  porous catalysts, 740–742, 752–753
Adjoint matrix, 44
Adsorption-controlled chemical reactions, 412–418, 435–438
Adsorption/desorption equilibrium constant, 385, 395
  dimensionless, 493, 507
Adsorption isotherms, 384–391, 397–398
  linear least squares analysis, 387, 391, 428–430
Adsorption rate, 398, 428
  BET isotherm, 388
Advantages of catalytic duct reactors, 613
Alkanes, specific heat, 780–782
Alternating direction implicit (ADI) method, 624–627
Alumina catalysts, thermal conductivity, 733, 737
Ammonia production:
  catalytic mechanism, 435–436
  total pressure analysis, 146–148, 434–438
  total pressure dependence, 438
Analogies, heat/mass transfer, 337–352
Angular momentum balance, 224
Angular momentum, rotational motion, 769, 775
Annular flow, stream function, 240
Apparent density of catalyst, 540
Arrhenius number, 734–737
Aspect ratio:
  effect on conversion in rectangular ducts, 640–643
  rectangular ducts, 615, 632
Average concentration, 593, 621, 632, 635
Average molecular weight, mixtures, 709, 847
Average pore radius, 542
Average velocity, triangular ducts, 617–618
Avogadro's number, 770
Axial dispersion:
  coefficients, 595–596, 599
  in catalytic reactors, 579–601

Axial dispersion: (*Continued*)
experimental correlations, 593–595, 840–841
Axisymmetric stream function, 184–185, 199, 202, 215–217, 240–241
Azeotrope, minimum-boiling, 817, 819

Backward difference, first derivative, 628–629, 631
Basis functions, 758–759
Batch reactor:
adiabatic operation, 130
digital control, 128
mass balance, total pressure, 141, 145–148
multiple reactions, 129, 137–138
nonisothermal design equations, 131–136
thermal energy removal, 136
Benzene chlorination:
problem statement, 13–14, 655–656
strategy, 656–658
Benzene-cyclohexane, thermodynamic data, 62
Benzene hydrogenation, 62–63
Bernoulli equation, 155, 208–209, 699, 730
Bessel functions, 475–476, 479–480, 520, 521–522
BET isotherm:
derivation, 387–391
linear least squares analysis, 391, 431
Binary mixture:
Gibbs free energy of mixing, 802–806, 813–819
thermodynamic stability, 812–819
Binodal curve, 800, 806–807, 818–819
Binodal points, 800, 805–807, 818–819
Blood capillary, mass transfer equation, 328, 635
Bodenstein number, 594
Body-fixed reference frame, rising bubbles, 204, 332
Body forces, gravity, 166–167, 171
Boltzmann:
distribution, canonical ensemble, 760–763
constant, 674, 770
equation for entropy, 763
Bond energies, 147
C-H vs. C-C, 782
nitrogen, 412
Bond lengths, diatomic and triatomic gases, 775–776
Boundary conditions:
constant flux, 651
catalytic duct reactors, 619–620, 633, 636, 853
Damkohler number, 451, 621, 633
Danckwerts, 580–581, 591–592, 839
dimensional scaling factors, 450–451
split, 96, 484–485, 494, 497, 526, 580, 735, 857–858
stream function, 238–239
Boundary layer boundary condition, mass transfer, 278, 284, 287, 289, 303, 320
Boundary layer heat transfer, transverse to long cylinder, 334–343
Boundary layer mass transfer:
bubbles, 303–327
mobile gas-liquid interface, 316–327
transverse to long cylinder, 337–343
Boundary layer separation:
solid cylinder, 195
solid sphere, 193–195
Boundary layer theory:
heat transfer coefficient, 341–342, 834–835
high-shear interface, 343–352
starting concentration profile, 622, 648–653
zero-shear interface, 303–327
Boundary layer thickness:
around gas bubble, 309, 322, 330–331, 659
creeping flow, 295–296, 308–309
creeping vs. potential flow, 309, 328
dimensionless, 294–295, 308, 342, 652
expanding bubble, 322, 326
fluid dynamics, 281
mass transfer, 274, 292–296, 307–311, 340–342, 652, 659, 664
potential flow, 309–311
practical example, 295–296, 310–313
solid sphere vs. gas bubble, 310, 328
Bubbles:
addition of resistances, 327
translating/expanding, 327
Bulk concentration, velocity-weighted, 621, 632, 635
Bulk gas phase concentration, stoichiometry, 824–825, 832
Bulk gas phase temperature vs. concentration, 830, 833, 849
Buoyant force, 243

Calculus of variations, 616–617
Canonical ensemble, 760–763
Canonical transformation, spherical coordinates, 370, 477
Capillary condensation, 386–387
Carbon monoxide:
absolute entropy, 778, 783
bond length, 770
collision diameter, 847
intrapellet Damkohler number, 560, 578
Catalyst activity, nonuniform, 620–621, 643–646

Catalyst design, effectiveness factor, 536
Catalysts:
  apparent density, 540
  average pore radius, 542
  coupled heat/mass transfer, 731–755, 825–830
  intrapellet porosity, 541–542, 553–558
  multiple stationary states, 736–737, 754–755
  numerical results for diffusion/second-order kinetics, 487–488
  parallel-pore model, 541–542, 553–558
  pore-size distribution function, 540–542, 553–557
  surface area per unit mass, 542
  temperature vs. concentration, 733–736, 741–742, 828
  thermal energy balance, 731–736, 825–830
  void area fraction, 553–558
  void volume, 541–542, 553–557
Catalytic converter, 612, 618
Catalytic duct reactors:
  assumption, 613–614
  asymptotic Nusselt number, 643
  boundary conditions, 619–620, 633, 636, 853
  exact solutions, 633–634, 639
  external resistance, 853–857
  mass transfer equation, 619, 633, 649–650
  overview, 611–613
  plug flow, 634
  plug flow vs. viscous flow, 637–639
  quasi-macroscopic mass balance, 634–637, 647–648, 854–855
  square cross-section, 632–640
  universal correlation, 642–643
Catalytic ducts:
  effect of aspect ratio on conversion, 640–643
  effect of Damkohler number on conversion, 639–640, 856–857
Catalytic mechanism:
  adsorption-controlled reactions, 412, 415
  ammonia production, 435–436
  desorption-controlled reactions, 418
  dissociative adsorption, 408–410, 439, 442
  multisite adsorption, 410–412
  with reactive intermediates, 402–408
Catalytic pellets:
  characteristic length, 469, 484
  concentration profiles, first-order kinetics, 473–480, 576
  concentration profiles, zeroth-order kinetics, 463–468, 471, 528–530
  critical spatial coordinate, 462–463, 466, 468, 518–519
  equivalent diameter, 594, 596
  homogeneous model, 452–453, 458, 493–494
  mass balance with diffusion/*n*th-order kinetics, 484–486, 532–533
  numerical integration of mass balance, 485–487, 497, 501–505
  numerical singularity, 486–487, 526
  radiation boundary conditions, 450–451
  rigorous description, 449–452
Catalytic reactor design:
  interpellet porosity, 579, 600–601
  numerical example, 604–608, 859–860
  scaling law, 571–572, 600
  via intrapellet Damkohler number, 603–604
  via tortuosity, 571, 608
  with axial dispersion, 579–601
  with effectiveness factors, 569–572, 577–579, 600–604, 833–835
Catalytic reactors:
  design strategy, 597–600, 609, 833–835, 852
  ducts vs. porous pellets, 646–647
  ideal vs. real performance, 583–592, 837–842
  methanol production, 573–579, 601
  residence time, 568, 600
  square ducts vs. tubes, 637–639
  zeroth-order kinetics, 858–859
Center of catalyst, numerical singularity, 486–487, 526
Central difference, first and second derivative, 623–624, 629–630
Chapman-Enskog equation, 544
Characteristic lengths:
  catalytic pellets, 469, 484
  first-order kinetics in catalysts, 488–490
Chemical equilibrium, requirement, 57, 422, 806
Chemical potential, 57, 422–423, 757, 779, 801, 814–815
  classical vs. statistical, 779
  stability requirement for, 814–815
Chemical reaction coefficient, definition, 839, 841, 843
Chemical stability, requirements for, 801–807, 813–819
Chemisorption, heat of, 384, 390, 428, 560
Chilton-Colburn j-factor, 353
Chlorination of benzene:
  CSTR performance curves, 16
  design equations, 15–16, 671
  kinetic data, 13–14, 656
  multiple reactions, 13

Chlorination of benzene: (*Continued*)
problem statement, 13–14, 655–656
strategy, 656–658
Chromatographic column, 596–597, 608
Classical partition function:
for rotation, 770
for vibration, 772
Closed system, equation of continuity, 223–224
Collision diameter:
carbon monoxide, 847
gas mixture, 545, 551–552
Collision integral for diffusion, 545, 715
Combination of variables, boundary layer theory, 287–289, 306, 320–321, 345–347, 652
Common tangent, stability analysis, 799–800, 804–806
Complex kinetics, effectiveness factors, 497–505, 508
Composition dependence of Δg_{mixing}, 802–805
Composition relations, mass vs. mole fraction, 709
Computational fluid dynamics, 564
Concentration profile:
error function, 306–307, 322, 331
first-order kinetics, 473–480, 576–579, 590, 608, 637–638, 855–857
gamma function, 289–292, 307, 330–331, 652–653
nonisothermal catalysts, 745–746, 748
*n*th-order kinetics, 591–592
packed column, 358
scaling law, 358–360
second-order kinetics, 581
spherical interface, 370–371
unsteady state, 378
zeroth-order kinetics, 463–468, 471, 528–530, 858–859
Concentration, cross-section averaged, 593, 621, 632
Conductive energy flux, reactive mixture, 695–697, 705–706, 717–719, 723–725, 730, 826
Conductive heat transfer, lateral surface of tube, 71
Cone-and-plate viscometer, 226–227
Constant flux boundary condition, 651
Continuous functions, linear least squares, 454, 459–460
Contribution from *j*th reaction, 7, 12
Convective flux:
any quantity, 695
internal energy, 694–695, 729
Convective forces, 161–163, 168, 172
Convective momentum flux, 161–163, 169–170, 172
forces due to, 163, 168, 172
matrix representation, 162
Conversion:
batch reactor, 126
batch reactor, effect of reactor volume, 127
effect of aspect ratio, rectangular ducts, 640–643
effect of Damkohler number, square ducts, 639–640
flow reactor, 50, 66, 426
Conversion vs. time:
batch reactor, 128, 134–135
second-order kinetics, 151
Cordierite, catalytic converter, 618
Correlation coefficient, axial dispersion, 595, 599
Countercurrent cooling, temperature profiles in PFRs, 101–103
Coupled heat/mass transfer:
batch reactor, 127–128
constant wall temperature, 73–76
differential reactor, 54–56, 70–71, 833–835
PFRs, 87–90
PFRs, countercurrent cooling, 98
porous catalysts, 731–755, 825–830
Coupled ODEs, nonisothermal catalysts, 734–736, 748
Coupling between heat/mass transfer, 703–707, 710, 717–719, 723–725
Covalent radius, hydrodynamic shell, 672, 710
Cramer's rule, 144–145
Creeping flow, 175
incompressible Newtonian fluids, 175–179
Newtonian fluid, solid sphere, 185–189
pressure distribution, 192–195, 203
rotating sphere viscometer, 229–230
solid sphere, analytical solution, 188–189
Critical constants, 148
Critical Damkohler number, catalytic pellets, 464, 465, 468–470, 521–522
Critical Peclet number:
non-ideal reactors, 586–590, 841–843, 860
Critical point, 424, 445–446, 800–801
Critical spatial coordinate, catalytic pellets, 462–463, 466, 468, 518–519
CSTR:
multiple reactions, complex kinetics, 17–18
nonlinear algebraic solution, 677–681
strategy for multiple chemical reactions, 11
unsteady state mass balance, 11, 33
CSTR design strategies, 23–25

CSTR train:
multiple reactions, design equations, 22
multiple reactions, unrestricted optimization, 20–23, 26
restricted optimization, variable temperature, 29–30
steady state solution, 40–41, 45
unrestricted optimization, isothermal, 26
Cubic-close-packed, interpellet porosity, 565
Curie restriction, linear transport laws for isotropic media, 701–703, 725
Curl:
of the divergence of the velocity gradient, 177–178, 362
of the gradient, 174
Curvature correction, mass transfer equation, 296–298, 311–313, 650
Cylinder:
boundary layer heat transfer transverse to, 334–343
boundary layer mass transfer transverse to, 337–343
creeping flow transverse to, 334
effectiveness factors, 513–514, 516–517, 520–522, 525–526
potential flow transverse to, 218–222, 337
Cylindrical catalysts:
concentration profiles, zeroth-order kinetics, 464–466
critical Damkohler number, 465, 468–470, 521
critical radius, 466
first-order kinetics, 475–476, 520
Cylindrical coordinates, radial conduction, 355–356
Cylindrical interface, zero-shear heat/mass transfer, 337–343

Dalton's law, 5, 140–141, 575
Damkohler number, 268–269, 371, 451, 458, 483, 492, 494, 539–540, 599, 621, 633, 733
boundary conditions, 451, 621, 633
carbon monoxide, 560, 578
critical values, 464, 465, 468–470, 521–522
effect on conversion, square ducts, 639–640
interpellet, 566, 599, 839
Danckwerts boundary conditions, 580–581, 591–592, 839
Darcy's law, 210
de Broglie thermal wavelength, 767
Degenerate ground states, 764–765
Degradation of kinetic energy, 730
Degrees of freedom:
for rotation, 770–771
for vibration, 773–774
Del operator, 169, 176
Delta function distribution, catalyst activity, 620–621
Delta functions, tortuosity, 555–556
Density matrix, 759–760
Design equations:
chlorination of benzene, 15–16, 671
gas-liquid CSTR, 671, 673–677
ideal reactor, 567–579, 833–835, 846–850
multiple reactions, tubular reactors, 8
nonisothermal tubular reactor, 745–748
with axial dispersion, 579–601
with effectiveness factors, 569–572, 577–579, 600–601, 846–850
Design strategy, packed catalytic reactors, 833–835, 852
Desorption-controlled chemical reactions, 418–420
Desorption rate, 398, 428
BET isotherm, 388
Determinant, 703, 704, 796
Differential method, reaction rate data analysis, 150–151
Differential reactor, ideal design, 567–579, 833–835
Differential scanning calorimeter, 123
Diffusion:
radially in cylinders/spheres, 484–486
reference frames for, 257–258, 260–261
Diffusion coefficients:
catalysts, 540, 543–560
intrapellet, 540, 543–560
macropore model, 559–560
micropore model, 558–559
ordinary molecular, 544–552, 675, 682, 707, 710–715, 719
via thermodynamic data, 709–710
Diffusion, collision integral, 545, 715
Diffusion/Hougen-Watson kinetics, 493–497
numerical results, 501–505
Diffusion in external force field, 707, 725, 730–731, 826, 828
Diffusion-limited regime:
effectiveness factor, 535–537, 741–742, 754
interphase mass transfer, 375–376, 664–665
Diffusion/*n*th-order kinetics, mass balance, 484–486, 532–533
Diffusion/reaction:
mass transfer equation, 271, 452, 458, 493–498, 510, 661, 823, 826
stoichiometry, 494–497, 731–733, 823–829

Diffusion/reaction, flat interface, 660–664
Diffusion/second-order kinetics, numerical results, 487–488
Diffusion-thermo effect, Dufour effect, 719, 730, 826
Diffusion time constant, 269, 379, 569, 668
Diffusional fluxes, 257–261
Diffusional mass flux, 260, 547, 695, 699, 706–708, 710–711, 725, 732, 824, 827
  continuity at interface, 825, 829–830, 832
Diffusional molar flux, 313, 323, 372, 547, 554–555, 663
Diffusional resistances, addition of, 546–552, 666, 849
Diffusional stability, requirement for, 707, 801–807, 813–819
Dilution factor, gas-liquid CSTR, 673
Dimensional analysis, equation of motion, 172–173
Dimensional scaling factors:
  boundary conditions, 450–451
  equation of motion, 172
  mass transfer equation, 265–268
Dimensionless:
  adsorption/desorption equilibrium constant, 493, 507
  concentration gradient, Sherwood number, 663
  equation of motion, 362–366
  equations, external mass transfer resistance, 836–841, 850–851
  kinetic rate law, 268, 451, 453, 458, 461, 473, 483, 491–493, 566
  mass balances, gas-liquid CSTR, 668–671, 675–678
  mass transfer correlation, 301–303, 314–315, 834–835
  mass transfer correlation, gas-liquid interface, 315, 663–664
  mass transfer equation, 269–270, 449, 563, 633, 642
  numbers, equation of continuity, 224
  numbers for mass transfer, 271–272, 632–633, 858
  numbers, via time constants, 568–569, 600
  variables, renormalized, 365–366
Dissociative adsorption, 394–396, 408–410
  catalytic mechanism, 408–410, 439, 442
  total pressure analysis, 439–444
Dissolution of solid pellets, 373–379
  no chemical reaction, 376–379
Dissolution time constant, 379
Dissolution time, scaling law, 376–379
Distribution functions:
  moments, 542, 559
  porous catalysts, 540–542, 553–557
Double dot product, notation, 694
Double-pipe reactors:
  countercurrent cooling, 95–103
  endothermic cocurrent cooling fluid, 87–93
  flow rate ratio, 80
  manipulating cooling fluid flow rate, 81–83
  nonadiabatic, 91–94
  radius ratio, 80
  surface-to-volume ratio, 81
Driving forces, entropy generation, 700, 724
Dual-site adsorption, 394–396
  limiting behavior, 396
Duct reactors:
  assumptions, 613–614
  asymptotic Nusselt number, 643
  boundary conditions, 619–620, 633, 636, 853
  exact solutions, 633–634, 639
  mass transfer equation, 619, 633, 649–650
  overview, 611–613
  plug flow vs. viscous flow, 637–639
  quasi-macroscopic mass balance, 634–637, 647–648, 854–855
  universal correlation, 642–643
Dufour effect, diffusion-thermo effect, 719, 730, 826
Dynamic expectation value, 758–759
Dynamic force, creeping flow, solid sphere, 198–199
Dynamic pressure, 171, 208–209, 213–214
  potential flow, 208–211, 213–214, 364–365
  via creeping flow equation of motion, 191–192, 202–203, 362

Effective diameter:
  noncircular cross-section channel, 618, 632
  square ducts vs. tubes, 637–639
Effectiveness factors:
  activation energy, 739, 744–745
  adsorption equilibrium constants, 502–503, 506–508
  catalyst design, 536
  complex kinetics, 497–505, 508
  cylinders, 513–514, 516–517, 520–522, 525–526
  definition, 497–498, 510–512, 749, 831
  diffusion-limited regime, 535–537, 741–742, 754
  enthalpy of reaction, 738–739, 743–747
  first-order kinetics, 519–526, 531, 576–577, 599, 849
  flat plates, 512–513, 516, 519, 524, 736

in design equations, 569–572, 577–579, 600–601, 846–850
molecular size of reactants, 504–505, 506–508
multiple reactions, 750–752
nonisothermal, 733–755
parametric sensitivity, 505
product concentrations, 501–503, 506–508
second-order kinetics, 487–488, 523–526, 531–535
spheres, 514–515, 517, 520, 522–525, 576–577, 599, 750–752, 849
stoichiometric imbalance, 504, 506–508
third-order kinetics, 525
volumetric average of rate law, 515–519, 523, 749–752
zeroth-order kinetics, 517–519, 521–526, 531
Eigenfunctions, 758–759
Einstein diffusion equation, 711
Electric forces, 167
Elongational:
flow, 235–237
viscosity, 236
Energy levels/rigid rotor, 769
Energy minimization for stability criteria, 807–812
Enhancement factor:
diffusion-limited regime, 373, 664–665
mass transfer coefficient, 369–373, 660–664
Enthalpy change/chemical reaction, 55, 71, 732, 827, 829
Enthalpy of reaction, effectiveness factors, 738–739, 743–747
Entrance length, fully developed flow, 613
Entropy:
equation of change, 696–698, 728
rotational contribution, 777
via statistical thermodynamics, 757, 762–765, 776–779
vibrational contribution, 778
Entropy flux, molecular, 697, 712, 724
Entropy generation:
driving forces, 700, 724
fluxes for, 701
pure fluid, 699
quadratic form, 702–703
reactive mixtures, 697–703, 713, 724
E^2 operator:
cylindrical coordinates, 238
spherical coordinates, 186, 188, 207, 216
Equation of change:
entropy, 696–698, 728
fluid angular velocity, 180
internal energy, 692–693, 727–731, 826
kinetic energy, 689–692
total energy, 693–696
Equation of continuity, 171, 222–223, 259, 280
closed system, 223–224
curvature correction, 282, 296, 311, 313, 331–332, 343
dimensionless numbers, 224
elongational flow, 235–236
flat approximation, spherical coordinates, 281–283, 303
open system, 223–224
radial velocity, 286–287, 305
spherical coordinates, 185, 280
Equation of motion, 167–173, 362
creeping flow, dynamic pressure distribution, 191–192
dimensional analysis, 172–173
dimensionless, 362–366
incompressible liquids, 171, 208, 362
incompressible Newtonian fluid, creeping flow, 177, 362
summary for mass and momentum, 687–688
vector-tensor derivation, 167–168
vector-tensor manipulation, 169–171
Equation of state, ideal gas, 767
Equilibrium constant:
for adsorption, 385, 395
fugacity ratio, 58
standard state, 58
temperature dependence, 59–60, 107, 118–119, 133, 147, 435
Equilibrium distance, Lennard-Jones potential, 544, 672
Equilibrium, gas-liquid interface, 665, 674
Equimolar counterdiffusion, 258
Equipartition of energy, 543, 768, 771
Equipotential lines, 207, 209
perpendicular to streamlines, 207, 215
Equivalent diameter, catalytic pellet, 594, 596
Ergodic problem, statistical thermodynamics, 760–761
Error function:
boundary layer theory, 306–307, 322
concentration profile, 306–307, 322
Eucken equation, thermal conductivity, 848
Euler's differential equation, 188, 212–213, 216, 219, 221
Euler's integral theorem:
for Gibbs free energy, 708, 721, 791, 801, 813–814, 816
homogeneous functions, 790–794, 807, 816
Euler-Lagrange equation, 616–617

Eutectic phase behavior, 807
Exact differentials, 173–174, 176, 182, 185, 207, 252, 761, 786
  integration of, 189–190
Exact solutions, catalytic duct reactors, 633–634, 639
Exothermic adsorption, 395, 430
Expanding bubble:
  boundary layer thickness, 322, 326
  mass transfer coefficient, 323–324, 326
  mass transfer equation, 317–318, 319–320
  radial velocity, 318–319
  scaling laws, 326–327
  time-averaged properties, 324–325
Expectation value, quantum mechanics, 758–760
Extent of reaction:
  differential reactors, 6
  for molar flow rate, gas-phase reactor, 9, 29
  multiple reactions, CSTR train, 19–20
  steady state CSTR analysis, 12
External forces, gravity, 166–167, 171
External heat/mass transfer resistance, 845–850
  dimensionless equations, 836–841, 850–851
  scaling law, 842
External resistance:
  catalytic duct reactor, 853–857
  nonideal reactors, numerical results, 841–845
  heat transfer, 851–852
  mass transfer, 850–851
  overview and strategy, 821–822
  summary of, 831, 850–852

Fick's first law of diffusion, 260, 280, 299, 313, 323, 341, 348, 372, 547, 620, 707, 732, 824, 827, 830
Final conversion with external resistance, 837, 852
Finite difference calculus, 151–152, 623–625, 627–631
  alternating direction implicit method, 624–627
  second-order correct, 623–625,627–631
First law of thermodynamics, 123–124, 692, 727–728, 761, 763, 786
  open system, 52, 68, 692, 727–728, 786
  via substantial derivative operators, 728
First-order kinetics:
  catalysts, characteristic lengths, 488–490
  concentration profiles, 473–480, 576, 608, 637–638, 855–857
  cylindrical catalysts, 475–476, 520
  effectiveness factors, 519–526, 531, 576–577, 599, 849
  ideal reactor, 577–579, 590, 599–600, 607
  porous wafers, 473–474, 519
  spherical catalysts, 476–480, 520
First-order rate constants:
  linear least squares, 453–457, 506, 575–579, 846
  pressure dependence, 457
Flory-Huggins interaction parameter, stability requirements for, 815
Flow rate vs. pressure drop, turbulent flow, 248–250
Fluctuations, phase separation, 800
Fluid dynamics:
  accumulation rate process, 159–160, 168, 172
  physical properties, 156–158
Fluorescence emission, laser-induced, 329
Fluxes, entropy generation, 701
Force balance, 158–167
Forced diffusion, 707
Forward difference, 427
  first derivative, 627–628
Fourier's law of heat conduction, 348–349, 705–706, 718–719, 723–724, 730, 826, 830
Fowler-Guggenheim isotherm, 397
Free energy of activation, 422–423
Freundlich isotherm, 398, 442–446
Friction coefficient:
  gas bubble, 197, 203, 712
  solid sphere, 197, 712
Friction factor, 155
  generalized interpretation, 198–199
  solid sphere, 198–199
Friction loss, 730
Froude number, 173, 251
Fugacity, 148
  coefficients, pure components, 148
Fully developed flow, entrance length, 613
Fundamental equation, thermodynamics, 785–786

Gamma function:
  boundary layer theory, 289–292, 307, 652–653
  concentration profile, 289–292, 307, 652–653
  incomplete, 291–292, 307, 330–331, 652
Gas bubbles:
  creeping flow, 201–205
  momentum boundary conditions, 202, 203–205
  potential flow, 211–218, 251
  rising, 203–205, 217–218
  volume fraction, 667, 674

Gas-liquid CSTR:
calculation procedure, 681
dimensionless mass balances, 668–671, 675–678
gas-phase mass balances, 658–659, 669–671
gas-phase resistance, 666
interphase mass transfer, 658–667
liquid-phase mass balances, 659–660, 668–669, 675
nonlinear algebraic solution, 677–681
nonlinear program, 673–677
performance curves, 677, 682
problem statement, 655–656
strategy, 656–658
Gas-liquid interface:
boundary conditions, 200–201
mass transfer coefficients, 313–314, 372–373, 659, 660, 663–665
Sherwood numbers, 315, 367, 372, 659, 663–664
spherical, 370–373
Gas-liquid mass transfer, interfacial area, 667
Gas-phase mass balances, gas-liquid CSTR, 658–659, 669–671
Gas-phase resistance, gas-liquid CSTR, 666
Gauss' law, 168, 223, 256, 495, 498, 510–511, 635, 694, 751, 823, 826, 829, 831
Gaussian distribution, tortuosity, 557
Gibbs-Duhem equation, 708–709, 721, 794–795, 802–803, 814
Gibbs free energy, differential expression for, 708, 720–722
Gibbs free energy change, chemical reaction, 57
Gibbs free energy of mixing, 802–806, 813–819
nonideal contribution, 816
Gradient operator, 169, 176
dimensional analysis, 172
Gradients of thermodynamic functions, 691–692, 706
Graham's law, 548, 550
Grand partition function, 792
Gravitational forces, 166–167, 243
Gravitational potential energy, 171

$\mathcal{H}$-theorem, statistical thermodynamics, 761–763
Haber-Bosch process, 394, 430
Hagen-Poiseuille law, 249
Half-time, kinetic analysis, 151
Hamiltonian operator, 758–761
Harmonic oscillator, diatomic gases, 771–772
Heat flux:
constant across lateral surface of tube, 72–73, 104
constant wall temperature of tube, 73–76
Heat function, statistical thermodynamics, 761–762
Heat/mass transfer, external resistance, 845–850
Heat of chemisorption, 384, 390, 428, 560
Heat of physisorption, 390–391, 428
Heat transfer:
boundary layer thickness, 295, 323, 336
coefficient, boundary layer theory, 341–342, 834–835
coefficient, high-shear interface, 349–351, 834–835
coefficient, zero-shear interface, 341–342
external resistance, 851–852
physical properties, 157–158
Helmholtz free energy, 757, 763, 767, 779, 789–791, 799–800, 809–811
Helmholtz-Korteweg variational principle, 616–617
Henry's law, 393
Heterogeneities, ducts vs. packed catalytic reactors, 646–647
Hexagonal-close-packed, interpellet porosity, 565
High-shear interface:
boundary layer theory, 343–352
heat transfer coefficient, 349–351, 834–835
mass transfer coefficient, 349–352, 834–835
Homogeneous:
function, Euler's integral theorem, 790–793, 807, 816
model, catalytic pellets, 452–453, 458, 493–494
Honeycomb monolithic exhaust devices, 612, 618
Hougen-Watson:
kinetic models, 399–420, 424–426, 456, 491–493, 574–575, 602
kinetics, diffusion, numerical results, 501–505
model, intrapellet Damkohler number, 602–603
Hydrodynamic diameter, spherical shell, 672, 674, 710
Hydrodynamic drag force, 198–199, 203, 205, 242, 243, 245, 711
Hydrodynamics, low-Reynolds-number, 175–205
Hydrostatics, 156

Hyperbolic functions, solution to differential equations, 371, 474, 477, 662

Ideal design:
  scaling law, 571–572, 600
  with external resistance, 835–838, 841
  with effectiveness factors, 569–572, 577–579, 600–601, 833–835, 846–850
Ideal flow, 205, 699
Ideal gas:
  chemical potential, 779
  entropy, via statistical thermodynamics, 776–779
  equation of state, 767
  partition functions, 765–767
Ideal reactor:
  design equations, 567–579, 833–835, 846–850
  first-order kinetics, 577–579, 590, 599–600, 607
  *n*th-order kinetics, 591–592, 608
  second-order kinetics, 581, 607–608
Incomplete gamma function, 291–292, 307, 330–331, 652
Incompressible liquids, equation of motion, 171, 208, 362
Incompressible Newtonian fluids, creeping flow, 175–179
Independent chemical reaction, 7, 12
Infrared vibrational frequencies, 775–776
Initial rate method, kinetic analysis, 152
Initial rates:
  linear least squares analysis, 407–410, 414–418, 427–428, 440–441, 444
  total pressure dependence of, 404–405, 407–410, 414–418, 425–428, 432
Instability, nonideal catalytic reactors, 582, 585–586, 839
Integral method, reaction rate data analysis, 149–151
Intercepts, Δg_{mixing} vs. composition, stability analysis, 805–806
Interdiffusional flux, linear transport laws, 719, 723–724, 730, 732, 826–827
Interfacial area, gas-liquid mass transfer, 667
Interfacial equilibrium, 665, 674
Interfacial force:
  fluid-solid interface, 195–197, 214–215, 248–249
  gas bubble, 203, 251
  hydrodynamic effect, 197, 203
  hydrostatic effect, 197, 203, 215
  potential flow, 214–215, 251
  rotating sphere viscometer, 230–231
  vector-tensor expression, 195
Interfacial molar flux, 323, 372, 663
Internal energy, 124–126, 129–131, 138, 692–693, 727–731, 757, 761–765, 768, 771, 773, 774, 785–786, 789–791, 794, 798–799, 807–812
  change for chemical reaction, 125, 129, 138
  convective flux of, 694–695, 729
  equation of change, 692–693, 727–731, 826
  ground state, 765
  rotational contribution, 770–771
  translational contribution, 768
  vibrational contribution, 773–774
Interpellet axial dispersion:
  experimental correlations, 593–595, 840–841
  in nonideal reactors, 579–601, 838–845
Interpellet Damkohler number, 566, 599, 839
Interpellet porosity:
  cubic-close-packed, 565
  hexagonal-close-packed, 565
  optimal reactor design, 579, 600–601
Interphase mass transfer:
  diffusion-limited regime, 375–376, 664–665
  effect of flow rate, 353, 359–360
  expanding bubble, 323–324
  gas-liquid CSTR, 658–667
  solid-liquid, 298–303, 356–360, 373–379
Interstitial fluid velocity, 565, 594, 834
Intrapellet:
  diffusion coefficients, 494, 496, 507, 540, 543–560
  porosity, catalysts, 541–542, 553–558
  resistances, summary of, 831
  temperature vs. concentration, 828
Intrapellet concentrations, stoichiometry, 496, 824
Intrapellet Damkohler number:
  carbon monoxide, 560, 578
  catalytic reactor design, 603–604
  Hougen-Watson model, 602–603
Inviscid flow, 205
Ion-exchange column, 596–597
Irreversible:
  exchange, kinetic/internal energies, 730, 826, 828
  thermodynamics, strategy for analysis, 688–689
Irrotational flow, 205
Isentropic flow, 205, 699

Isothermal compressibility, 125, 131, 813
Isothermal vs. nonisothermal analysis, 4

Jacobian transformations, 795–798

Kinetic energy:
  degradation, 730
  equation of change, 689–692
Kinetic rate constant:
  Arrhenius form, 107, 734, 849
  pressure dependence, 420–424, 445–446
  pseudo-volumetric, 493, 540, 566, 599, 733
Kinetic rate law:
  dimensionless, 268, 451, 453, 458, 461, 473, 483, 491–493, 566
  gas phase, reversible, 58, 60, 141, 147
Kinetics:
  of phase separation, 707–708, 800
  true vs. apparent, 646–647
Knudsen diffusion, 543–544, 597, 849
Kronecker delta, 170, 660, 725, 759

Langmuir-Hinshelwood:
  kinetics, intrapellet Damkohler number, 602–603
  mechanism, 399–400, 424–425, 491, 507, 574, 602
Langmuir isotherm, 384–385
  experimental verification, 386–387
  functional form, 385–386
  limiting behavior, 386, 393–394, 396
  linear least squares analysis, 387
Langmuir-Rideal mechanism, 401–402, 425, 433–434
Laplace's equation:
  potential flow, 207, 210–213, 218–221
  surface phenomena, 201
Laplacian:
  of the curl of the velocity vector, 178–179
  operator, dimensional analysis, 266–267
  operator, radial contribution, 370, 458, 476–477, 484
  operator, spherical coordinates, 186, 191, 212, 370
Laser-induced fluorescence emission, 329
le Chatelier's principle, 64, 105, 115, 118, 424
Legendre:
  polynomials, 187–188, 199, 212, 216
  transformation, 691, 787–790, 792, 809–811
Leibnitz rule:
  one-dimensional, 325, 454
  three-dimensional, 159–160, 222, 254
Lennard-Jones 6–12 potential, 545–546, 715
  equilibrium distance, 544, 672
l'Hopital's rule:
  cylindrical catalysts, 467
  spherical catalysts, 478–479, 486, 490, 520
Linear algebraic equations, linear least squares, 143–144
Linear combination of atomic orbitals, 758
Linear least squares analysis, 142–145
  adsorption isotherms, 428–430
  BET isotherm, 391, 431
  continuous functions, 454, 459–460
  first-order rate constants, 453–457, 506, 575–579, 846
  initial rates, 407–410, 414–418, 427–428, 440–441, 444
  Langmuir isotherm, 387
  ordinary molecular diffusion, 714
  supercritical fluids, 445–446
  Toth isotherm, 429–430
  zeroth-order rate constants, 459–460, 527
Linear polynomial, linear least squares analysis, 144–145
Linear transport laws, via irreversible thermodynamics, 701–707, 717–719, 725
Linearization of tangential velocity:
  gas bubble, 304–305
  solid sphere, 285–286
Line integral, 174, 181
Liquid-liquid phase separation, regular solutions, 817–819
Liquid-phase mass balances, gas-liquid CSTR, 659–660, 668–669, 675
Lorentzian distribution, tortuosity, 557
Lower critical solution temperature (LCST), 807
Low-Reynolds-number hydrodynamics, 175–205

Macropore model, diffusion coefficients, 559–560
Macroscopic mass balance, expanding bubble, 324–325
Magnetic forces, 167
Margules model, chemical stability of, 816
Mass balance:
  batch reactor, 125–129, 137, 139
  batch reactor, total pressure, 141, 145–148
  catalysts, numerical integration, 485–487, 497, 501–505
  differential reactor, 65–68, 426–427, 564–570, 834, 836–839, 849
  diffusion, Hougen-Watson kinetics, 493–497
  diffusion, *n*th-order kinetics, 484–486, 532–533

Mass balance: (*Continued*)
gas-liquid interface, 665
gas-phase plug flow reactor, 51–52, 564–570, 834, 836, 849
ideal CSTRs, one chemical reaction, 106
liquid phase differential reactor, 68
multiple reactions, tubular reactor, 5
quasi-macroscopic, 356–360, 634–637, 647–648, 854–855
Mass flux, with respect to moving surface, 222–223, 254–255
Mass transfer:
boundary layer boundary condition, 278, 284, 287, 289, 303, 320
dimensionless numbers for, 271–272, 632–633, 858
effect of flow rate, 353
external resistance, 850–851
gas-liquid interface, 303–327
oxygen bubbles, 310–313
physical properties, 157–158
resistance, 548–552, 666
solid-liquid interface, 298–303
spherical interface, 369–379
time constants, 568–569, 667–668
Mass transfer boundary layer theory:
flat approximation, 280, 283–284, 303, 344
tangential velocity, 284–286, 304–305, 650
Mass transfer boundary layer thickness, 274, 292–296, 307–311, 322, 340–342, 652, 659, 664
dimensionless, 294–295, 308, 342, 652
expanding bubble, 322, 326
penetration theory, 376
scaling law, 293, 294, 308, 323, 652, 659, 664
Mass transfer coefficient:
boundary layer theory, 299–301, 314, 341–342, 834–835
diffusion-limited regime, 373, 664–665
enhancement factor, 369–373, 660–664
expanding bubble, 323–324, 326
gas-liquid interface, 313–314, 372–373, 659, 660, 663–665
high-shear interface, 349–352, 834–835
scaling law, 300, 314, 354–355, 840
surface-averaged, 300–301, 314, 350–352, 834–835
via stream function, 333–334
Mass transfer correlation, dimensionless, 301–303, 314–315, 834–835
Mass transfer equation, 256–257, 619, 633, 649–651, 823, 825
combination of variables, 287–289, 306, 320–321, 345–347, 652
constant physical properties, 261–263, 619, 633, 649, 823, 825
curvature correction, 296–298, 311–313, 332–333, 650
diffusion, reaction, 271, 452, 458, 493–498, 510, 661, 823, 826
dimensional scaling factors, 265–268
dimensionless, 269–270, 449, 563, 633, 642
error function, 306–307, 322
expanding bubble, 317–318, 319–320
gamma function, 289–292, 307, 652–653
hierarchy of variables, 288, 321
large Peclet numbers, 277–278, 619, 633, 649–653
large Schmidt numbers, 279–284, 650–653
order-of-magnitude analysis, 277–278, 649
spherical coordinates, 276
steady state nonreactive, 275–276
thin boundary layers, 279–284, 650–653
Mass-average velocity, 257–258, 547
Maximum:
conversion in non-ideal reactors, 841–845
temperature rise, porous catalysts, 740–742, 752–753
Maxwell relations, 53, 69, 124, 720, 723
Mean free path, 543
Mechanical stability, requirement for, 707, 799–801, 813
Metastable states, 799–800, 805–806
Methanol production:
packed catalytic reactor, 573–579, 601
problem statement, 47, 601
reactor volume vs. conversion, 61–62
reversible kinetic rate law, 60, 575
thermodynamic data, 48
total pressure vs. time, 149
Method of Jacobians, 795–798, 809, 811
Microhydrodynamic force balance, 711
Micropore model, diffusion coefficients, 558–559
Microscopic:
mass balance with multiple chemical reactions, 255–257
reversibility, principle of, 385, 403
Minimum-boiling azeotrope, 817, 819
Mobile gas-liquid interface:
boundary layer mass transfer, 316–327
objectives and assumptions, 316
Molar-average velocity, 299, 547
Molar density:
dimensional analysis, 269–271
functional dependence of, 269–271

Molar density profile:
spherical interface, 370–371
unsteady state, 378
Mole fractions, gas phase, gas-liquid CSTR, 671, 676–678
Molecular flux:
entropy, 697, 712, 724
thermal energy, 695–697, 705–706, 717–719, 723–725, 730, 826
Molecular momentum flux, 156, 163–165
forces due to, 165, 168, 172
matrix representation, 165
Molecular weight, average for mixture, 709, 847
Moment of inertia, 769, 778
Moments of distribution function, 542, 559
Momentum:
boundary conditions, gas-liquid interface, 200–201
boundary layer, strategy, 210
boundary layer thickness, solid sphere, 281
diffusivity, 157
transfer coefficient, 158
transport, fundamental balance, 158–167
Monatomic gases, specific heat, 768
Monolayer, 384
Multicomponent:
diffusion, approximate calculations, 550–552
mixture, Gibbs free energy of mixing, 803–804
mixture, single-site adsorption, 392–394
Multiple reactions:
batch reactor, 129, 137–138
CSTR, variable temperature, 30–31
effectiveness factor, 750–752
mass balance, 255
unrestricted optimization, conjugate gradient method, 21
Multiple stationary states:
CSTRs, 110–117
CSTRs, problem statement, 105–106
porous catalysts, 736–737, 754–755
tubular reactors, 97–103
Multisite adsorption:
catalytic mechanism, 410–412
mixtures, 396–397, 310–411
Multivariable functions, Legendre transforms, 788–790, 792, 809–811

Navier-Stokes equation:
compressible gas, 224
incompressible liquid, 171–172
Negative pressure, 799
Newton's law of viscosity, 175, 200, 224
Nitrogen bond energy, 412
Nonadiabatic reactor volume vs. conversion, 63–64
Noncircular cross-section channel, effective diameter, 618, 632
Nonequilibrium systems, strategy for analysis of, 688–689
Non-equispaced finite difference calculus, 623–624, 627–629
Non-ideal:
catalytic reactor, numerical results, 582–590
conversion, tubular reactor, 583–590
design with external resistance, 838–845
reactor, critical Peclet number, 586–590, 841–843, 860
reactor design, with axial dispersion, 579–601
reactors, maximum conversion, 841–845
Nonisothermal catalysts:
adiabatic temperature rise, 740–742, 752–753
concentration profiles, 745–746, 748
coupled ODEs, 734–736, 748
numerical results, 738–740, 743–747, 749
temperature profiles, 747–748
Nonisothermal CSTR:
design equations, 118–120
effect of flow rate, 114–115
endothermic chemical reactions, 115–117
extinction, 113, 121
hysteresis, 113
ignition, 112–113, 121
inlet temperature of reactive fluid, 114
stable/unstable operating points, 111–112, 117
Nonisothermal effectiveness factors, 733–735
volumetric average of rate law, 749–750
Nonisothermal tubular reactor, design equations, 745–748
Non-Newtonian viscosity, power-law fluid, 273
Nonreactive gas mixture, 551–552
Nonuniform catalyst activity, 620–621, 643–646
Normal:
forces, 160–161, 230–231
modes of vibration, 773
viscous force, solid sphere, 196, 231
*n*th-order kinetics, ideal reactor, 591–592, 608
Numerical:
example, catalytic reactor design, 604–608, 859–860

Numerical: (*Continued*)
instability, nonideal catalytic reactors, 582, 585–586, 839
integration, mass balance for catalysts, 485–487, 497, 501–505
Numerical results:
diffusion, Hougen-Watson kinetics, 501–505
diffusion, second-order kinetics, 487–488
external resistance in nonideal reactors, 841–845
nonisothermal catalysts, 738–740, 743–747, 749
second-order kinetics, 582–588, 607–608
Numerical singularity at center of catalyst, 486–487, 526
Nusselt number:
asymptotic for duct reactors, 643
boundary layer heat transfer, 336–337, 352, 834–835, 848

Onsager reciprocal relations, 703–705, 713, 717
Open system, equation of continuity, 223–224
Optimization:
multiple PFRs in series, 27
multiple reactions in PFRs and CSTRs, 27–28
zeroth-order kinetics in CSTRs, 26–27
Order-of-magnitude analysis, mass transfer equation, 277–278, 649
Ordinary molecular diffusion, 544–552, 671–672, 675, 682, 707, 710–715, 719
temperature dependence, 713–715, 734–735, 737
Orientational distribution functions, tortuosity, 556–557
Oxygen bubbles, 310–313

Packed column, chromatograph, 596–597, 608
Parallel disk viscometer, 225–226
Parallel-pore model, 541–542, 553–558
Parameters for gas-liquid CSTR, 657–658
Parametric sensitivity:
analysis, 83–87, 505
cocurrent cooling fluid flow rate, 85–86
constant PFR wall temperature, 84
countercurrent cooling in PFRs, 99
CSTRs, effect of flow rate, 114–115
CSTRs, inlet cooling fluid temperature, 112–113
CSTRs, inlet temperature of reactive fluid, 114
double-pipe radius ratio, 85–86
effect of activation energy, 87
effectiveness factors, 505
endothermic reactions, cooling fluid flow rate, 89–93
heat transfer time constant, 84–85
Partial molar:
enthalpy, 54, 70, 723–724, 730, 732, 826–827, 829
entropy, 722, 723
internal energy, 125
properties, 54, 70, 125, 423, 720–724, 791–793
volume, 423
Partition function:
ideal gas, 765–767
rotational motion, 769–771, 777
translational motion, 766–767
via statistical thermodynamics, 757, 760–779
vibrational motion, 772, 774, 777
Peclet number:
critical value for non-ideal reactors, 586–590, 841–843, 860
mass transfer, 268, 272, 277, 565, 595–596, 599, 632, 840–845
simplified, 594, 599, 840–841, 843
Penetration theory, boundary layer thickness, 322, 376
Permutation index, 178
Perpetual motion machine, second kind, 696
Phase rule, 52, 68, 720, 794, 801, 812
Phase separation, 707–708, 799–800, 805–808, 815, 817–819
Phenomenological transport coefficients, reciprocal relations, 703–705, 717
Phosphine decomposition, total pressure analysis, 145–146
Physisorption, heat of, 390–391, 428
Planar flow, two-dimensional, 181–183
Planck's constant, 769
Plug flow design:
first-order kinetics, 577–579, 590, 599–600, 607
*n*th-order kinetics, 591–592, 608
scaling law, 571–572, 600
second-order kinetics, 581, 607–608
with axial dispersion, 579–601
with effectiveness factors, 569–572, 577–579, 600–601, 833–835
Plug flow reactor:
cocurrent cooling, 76–83
gas phase, 3
ideal design, 567–579, 833–835
manipulating surface-to-volume ratio, 75–77

manipulating wall temperature, 74–76
thermal energy balance, cocurrent cooling, 78–79
Plug flow, catalytic duct reactor, 634, 854–855
Point-slope method, Legendre transforms, 787
Poisson's ratio, 235
Polymer-solvent mixtures, stability requirements for, 815
Population balance, 392–393, 402–403
Pore-size distribution function, 540–542, 553–557
Porosity:
interpellet, optimal reactor design, 579, 600–601
intrapellet, 541–542, 553–558
Porous media, 210
Positive definite quadratic form, requirements for, 703–705, 718, 808
Potential flow, 205–222, 251
applications, 209–211, 364–365
dynamic pressure, 213–214, 364–365
fluid pressure, 214
gas bubble, boundary conditions, 211–212, 216–217
gas bubbles, 211–218, 251
interfacial force, 214–215, 251
of heat in solids, 210
rising bubbles, 217–218
transverse to cylinders, 218–222, 337
via stream function, 215–217, 220–222, 251
Power series, infinite sum, 390
Power-law fluid:
dimensional scaling factors, 272
dimensionless numbers, 272–273
torque vs. angular velocity, 233
Prandtl number, 157–158, 848
Preferential adsorption, multicomponent mixture, 392–393
Pressure, 156
Pressure dependence:
first-order rate constant, 457
kinetic rate constants, 420–424, 445–446
Pressure diffusion, 707
Pressure distribution:
creeping flow, 192–196, 203
hydrodynamic effect, 193–194, 214
hydrostatic effect, 193, 214
potential flow, 214
Pressure stress, 165–166
forces due to, 166, 168, 172
matrix representation, 165
Pressure tuning, 761
Principal minor and submatrix, quadratic form, 703–704
Principle of microscopic reversibility, 385, 403, 431, 437
Pseudo-steady-state approximation, 28
Pseudo-volumetric, kinetic rate constant, 493, 540, 566, 599
Pure fluid, entropy production, 699

Quadratic:
form, positive definite, 703, 718, 808–812
formula, analysis of roots, 680–681, 838
polynomial, linear least squares, 142–144
Quantum mechanics, 758–760, 766, 769, 771
wave function, 758–759
Quasi-macroscopic mass balance, 356–360, 634–637, 647–648, 854–855

Radial conduction, tube flow, 355–356
Radial diffusion:
cylindrical coordinates, 280, 683
cylinders/spheres, 484–486
cylindrical/spherical coordinates, 263
spherical coordinates, 279–280
Radial velocity:
expanding bubble, 318–319
high-shear interface, 286–287
zero-shear interface, 305
Radiation boundary conditions:
catalytic duct reactors, 619–620, 633, 636, 853–854
catalytic pellets, 450–451
Radius of curvature, 201
Rate-of-strain tensor, 175, 236, 242
Reaction pathway in packed catalytic reactors, 383–384
Reaction rate data analysis:
differential method, 150–151
integral method, 149–151
Reaction:
time constant, effect on conversion, 568
velocity constant, 598
Reactive:
intermediates, catalytic mechanism, 402–408
mixtures, entropy production, 697–703, 713, 724
Reactor:
analysis, via mass transfer time constants, 588
design strategy, 4, 509, 563–564, 573, 597–600, 609, 656–658, 833–835
design, via tortuosity, 571, 608
Reciprocal relations, via Onsager's irreversible thermodynamics, 703–705, 717
Rectangular duct reactors:
asymptotic Nusselt number, 643

Rectangular duct reactors: (*Continued*)
nonuniform catalyst activity, 643–646
universal correlation, 642–643
Rectangular ducts:
aspect ratio, 615
effect of aspect ratio on conversion, 640–643
velocity profile, 615–616
Rectangular symmetry, effectiveness factors, 512–513, 516, 519, 524, 736
Reduced mass, 769, 782
Regular solutions, stability requirements for, 816–819
Renormalized dimensionless variables, 365–366
Residence time optimization:
three CSTRs, 25
two CSTRs, 24
Residence time:
packed catalytic reactor, 568, 600
scaling law, 571–573
Resistance:
series vs. parallel, 549–550
to mass transfer, 548–552, 666
Reversible:
chemical kinetics, liquid phase, 106–107, 149
exchange, kinetic and internal energies, 730, 826, 828
reactions, gas-phase, 56–60, 139
Reynolds number, 173, 848, 856
power-law fluid, 273
Reynolds transport theorem, 159–160
Rigid-body rotation, velocity vector, 225, 227–228
Rising bubbles:
body-fixed reference frame, 204, 332
potential flow, 217–218
Rotameter:
calibration, 245–247
float, 247
Rotating sphere viscometer, 225, 227–235
Rotational:
degrees of freedom, 770–771
motion, diatomic gases, 768–771
partition function, polyatomic molecules, 778
temperature, 769–770, 775–776
Runge-Kutta-Gill numerical integration, 61, 487–490, 497, 501–505, 835

Scalar double dot product, notation, 694
Scalar velocity potential:
analytical solutions, 213, 218, 219
definition, 207
functional form, 211–212
Scaling law:
boundary layer thickness, 293, 294, 308, 323, 354–355, 652, 659, 664
concentration profile, 358–360
dissolution time, 376–379
expanding bubble, 326–327
external mass transfer resistance, 842
hydrodynamic drag force, 198–199, 243, 248–250, 711
mass transfer coefficient, 300, 314, 354–355, 840
packed catalytic reactor, 571–572, 600
Sherwood number, 301–303, 315, 355, 367, 653
velocity gradient, 302, 352, 367
Schmidt number, 158, 848
power-law fluid, 273
Schrödinger wave equation, 758
Second law of thermodynamics, 696, 762
Second-order kinetics:
effectiveness factors, 487–488, 523–526, 531–535
ideal reactor, 581, 607–608
numerical results, 582–588, 607–608
Selectivity, multiple reactions, 17
Separation of variables, 187, 212, 226
Shear forces, 160–161, 231, 247
Sherwood number, 274, 351–352, 361, 363, 367, 372, 374, 378, 653, 655, 663–664, 840
dimensionless concentration gradient, 663
effect of flow regime, 302–303, 315, 367, 834–835, 840
gas-liquid interface, 315, 367, 372, 663–664
scaling laws, 301–303, 315, 355, 367, 653
solid-liquid interface, 301–303, 351–352, 355, 361, 367, 653, 834–835
via stream function, 333–334
Simplified mass transfer Peclet number, 594, 599, 840–841, 843
Single-site adsorption, multicomponent mixture, 392–394
Singularity at center of catalyst, 486–487, 526
Sipps isotherm, 397, 428–429
Slot reactor:
exact solution, 634
numerical solution, 642
Slygin-Frumkin isotherm, 398, 428
Soret effect, thermal diffusion, 707, 718
Specific heat:
alkanes, 780–782
classical vs. statistical, 780–782
C_P vs. C_V, 797–798, 813

multicomponent mixture, 50–51, 67, 125, 797–798, 848
pure component, 48–49, 768, 771, 773, 775, 780–782, 797–798
rotational contribution, 771
temperature polynomial, 49, 135
translational contribution, 768
vibrational contribution, 773, 775, 780–782
Speed of:
gas molecules, 543
light in vacuum, 772
Spheres, effectiveness factors, 514–515, 517, 520, 522–525, 576–577, 599, 750–752, 849
Spherical catalysts:
concentration profiles, zeroth-order kinetics, 466–468
critical Damkohler number, 468–470, 522
critical radius, 468
first-order kinetics, 476–480, 520
Spherical:
coordinates, canonical transformation, 370, 477
gas-liquid interface, 370–373
shell, hydrodynamic diameter, 672, 674, 710
Spinodal:
curve, 805–807, 818–819
points, 800, 805–807, 817–819
Split boundary:
conditions, 96, 484–485, 494, 497, 526, 580, 735, 857–858
value problem, countercurrent flow, 96
Square cross-section channel, catalytic reactor, 632–640
Square ducts:
effect of Damkohler number on conversion, 639–640
plug flow vs. viscous flow, 637–639
Stability:
analysis of PFRs with countercurrent cooling, 103
criteria, rigorous development, 807–812
criteria, summary of, 707, 785
Stable states, 800, 805–806
Stagnation point, boundary layer mass transfer, 295, 309
Starting concentration profile, boundary layer method, 622, 648–653
Start up, five CSTRs, 38–45
Laplace transform analysis, 41
matrix analysis, 42–45
numerical analysis, 39–40
Start up, multiple reactions in two CSTRs, 34–38
Statistical thermodynamics:
ergodic problem, 760–761
generalized postulates, 757
$\mathcal{H}$-theorem, 761–763
summary for ideal gases, 777–778
Sterling's approximation, 777
Stiff differential equations, 582–586
Stoichiometric table, 5, 14, 18, 21, 35
Stoichiometry:
bulk gas phase concentrations, 824–825, 832
diffusion/reaction, 494–497, 731–733, 823–829
intrapellet concentrations, 496, 824
one chemical reaction, 50, 66, 494–497, 731–733, 823–829
total pressure, 140–141
Stokes' flow around:
gas bubbles, 201–205
spheres, 185–189
Stokes' law, solid sphere, 197–200
Stokes' theorem, 174, 207
Stokes-Einstein diffusion equation, 310, 656, 671–672, 675, 682, 710–715
Strategy:
analysis of nonequilibrium systems, 688–689
gas-liquid CSTR, 656–658
ideal/real reactor design, 597–600, 609
packed catalytic reactors, 833–835, 852
Stream function, 181–185
annular flow, 240
axisymmetric, 184–185, 199, 202, 215–217, 240–241
boundary conditions, 238–239
creeping flow, analytical solution, 188–189, 202, 205, 241
potential flow, 215–217, 220–222, 251
solid sphere, functional form via boundary conditions, 186–187
spherical coordinates, 184–185, 199, 202, 215–217
tube flow, 237–240
Streamlines, 181, 207
perpendicular to equipotentials, 207, 215
Subcooled vapors, 800
Submolecular fragments, dual-site adsorption, 394–395
Substantial derivative operator, 160, 259
Sucrose:
pellets, interphase mass transfer, 295–298, 328–329
solutions, physical property data, 329

Summation notation, vector-tensor operations, 169–170, 176–180
Supercritical fluids, 424
  linear least squares analysis, 445–446
Superficial fluid velocity, 834
Superheated liquids, 800
Surface area:
  measurements, 430–431
  per unit mass of catalyst, 542
Surface concentration via effectiveness factor, 830–839, 853
Surface tension:
  forces, 167, 201
  gradients, 201
Symmetry number, 778–779

Tangential velocity:
  bubble , linearization, 304–305
  solid sphere, linearization, 285–286
  within mass transfer boundary layer, 284–286, 304–305, 650
Taylor dispersion in capillaries, 593, 608
Taylor series:
  expansion, tangential velocity, 285, 304
  finite differences, 152, 623, 627, 628
Temkin isotherm, 398, 428
Temperature profiles:
  in PFRs, 76–77. 82, 92–93, 101–103
  nonisothermal catalysts, 747–748
  nonreactive, 95
Temperature vs. concentration:
  bulk gas, 830, 833, 849
  porous catalysts, 733–736, 741–742, 828
Tensor, second-rank, 61–162, 164
Terminal velocity, scaling laws, 243–245, 247, 252
Thermal:
  energy, molecular flux of, 695–697, 705–706, 717–719, 723–725, 730, 826
  expansion coefficient, 53, 69, 125, 131, 813
  runaway, strategies for control, 65–83, 87
  stability, requirement for, 707, 798–799, 813
Thermal conductivity:
  alumina catalysts, 733, 737
  Eucken equation, 848
  Fourier's law, 705–706, 718–719, 723–724, 826–830
Thermal diffusion, Soret effect, 707, 718
Thermal diffusivity, 157
Thermal energy balance:
  batch reactor, 124–126
  CSTR, 107–109
  CSTR cooling fluid, 108–109
  differential reactor, 52–55, 68–71, 834, 850
  in PFRs, countercurrent cooling, 97
  nonreactive, 95
  porous catalysts, 731–736, 825–830
  steady state conduction, 210
Thermal energy generation:
  parameter, 735–737
  CSTR, 108, 110, 116 121
Thermal energy removal:
  batch reactor, 136
  CSTR, 108–110, 116, 121
Thermodynamic:
  functions, gradients of, 691–692, 706
  stability relations, 798–819
Thermodynamics:
  differential relations, 53,59, 69, 124–125, 708–709, 719–722, 786, 790, 796–798
  multicomponent mixtures, 53–54, 69–70, 692, 727
  second law, 696, 762
Thermodynamic state functions via:
  Euler's integral theorem, 791–792
  Legendre transforms, 789–790, 792
Thickness, mass transfer boundary layer, 292–296, 307–311, 322, 340–342, 652, 659
Thin boundary layers, mass transfer equation, 279–284, 650–653
Third law of thermodynamics, 764–765
Third-order kinetics, effectiveness factors, 525
Thomas algorithm, alternating direction implicit method, 626, 631
Time constant for:
  chemical reaction, linear least squares, 128–129
  convective mass transfer, 568–569, 600, 667
  diffusion, 569, 668
  dissolution, 379
  heat transfer, 74, 77, 90, 100
  ideal and real reactor analysis, 588
  irreversible reaction, 128, 568, 600, 668
  mass transfer, 568–569, 667–668
  reversible chemical reactions, 106, 118
Time-dependent concentration profile, 378
Torque, rotating sphere viscometer, 231–233
Tortuosity:
  catalytic reactor design, 571, 608
  parallel-pore model, 555–558
  tensor, 558
Total energy:
  balance, closed system, 123
  equation of change, 693–696
Total momentum flux, forces due to, 166

Total pressure:
analysis, phosphine decomposition, 145–146
dependence of initial rates, 404–405, 407–410, 414–418, 425–428, 432
dissociative adsorption, 439–444
stoichiometry, 140–141
Toth isotherm, 429
Tracer analysis, CSTR, 46
Transition state, 384
theory, 421–423
Translational motion, ideal gas, 766–767
Transport analogies, 157–158
heat/mass, 337–352
Transpose of second-rank tensor, 175–176, 694
Triangular ducts, velocity profile, 616–618
Tridiagonal matrix, 626, 631
Triethanolamine production:
problem statement, 3
reactor volume vs. molar flow rate, 10
Tube flow:
dynamic force, 248–251
force-flow relation, 247–250
friction factor, 247–250
interfacial force, 248–251
Newtonian fluids, 227
radial conduction, 355–356
scaling laws, 249–250
stream function, 237–240
Turbulent flow, flow rate vs. pressure drop, 248–250
Two-phase envelope, 800, 806, 818–819

Universal correlation, catalytic duct reactors, 642–643
Unstable states, 799–800, 805–806
Unsteady state:
concentration profile, 378
mass balance, 373–379
Upper critical solution temperature (UCST), 801, 807, 818

van der Waals radius, hydrodynamic shell, 672, 710
van Laar model, chemical stability of, 816–819
Variables for gas-liquid CSTR, 657–658
Variational calculus, 616–617
Vector, 155–156
potential, 183–184
Vector-tensor:
identities, 169, 177, 208, 224, 225, 690, 694
operations, summation notation, 169–170, 176–180
Velocity:
interstitial, 565, 594, 834
of gas molecules, 543
profiles, regular polygon ducts, 614–618
superficial, 834
Velocity gradient:
tensor, transpose, 175–176
scaling law, 302, 352, 367
Velocity vector, 155–156, 162, 169, 176
rigid-body rotation, 225, 227–228
Velocity-weighted bulk concentration, 621, 632, 635
Vibrational:
degrees of freedom, 773–774
frequencies, infrared, 775–776
temperature, 772, 775, 781–782
Vibrational motion:
diatomic gases, 771–773
polyatomic gases, 773–775
Vibration, normal modes of, 773
Viscoelastic fluids, first law of thermodynamics, 727
Viscometers, 225–235
Viscosity:
liquids/gases, 201
temperature dependence, 714–715
Viscous flow:
slot reactor, 634, 642
square ducts vs. tubes, 637–639
Viscous heating, 730
Viscous momentum flux, 163–165
forces due to, 165, 168, 172
matrix representation, 165
Viscous shear force, solid sphere, 196
Viscous stress, 156, 234
Void:
area fraction, catalysts, 553–558
volume, catalysts, 541–542, 553–557
Volume:
fraction, gas bubbles, 667, 674
of activation, 423–424, 445–446
Volumetric flow rate, axisymmetric, 184
von Helmholtz variational principle, 616–617
von Karman boundary layer:
boundary condition, 278–279
entrance length, 613
von Karman-Pohlhausen boundary layer method, 622–623
Vorticity:
microscopic, 177, 206, 215, 220, 228, 233, 237–238
volume-averaged, 206–207
Vorticity equation, creeping flow, 179–183, 186
solid sphere, analytical solution, 188–189

Wafers:
concentration profiles, zeroth-order kinetics, 463–464, 471
critical Damkohler number, 464, 468–470
critical spatial coordinate, 463, 519
first-order kinetics, 473–474, 519
zeroth-order kinetics, 461–464
Wave function, quantum mechanics, 758–759
Work:
function, statistical thermodynamics, 761–762
terms, total energy equation, 695

Zero-shear heat/mass transfer, long cylinder, 337–343
Zero-shear interface, 200–205, 209
mass transfer coefficients, 313–314, 341–342, 372–373, 659, 660
Sherwood numbers, 315, 367, 372, 659, 663–664
Zeroth-order kinetics:
catalytic reactor, 858–859
concentration profiles, 463–468, 471, 528–530, 858–859
cylindrical catalysts, 464–466
effectiveness factors, 517–519, 521–526, 531
porous wafers, 461–464
spherical catalysts, 466–468
Zeroth-order rate constants, linear least squares, 459–460, 527